DISSERTATION ZUR ERLANGUNG DES DOKTORGRADES

DER FAKULTÄT FÜR CHEMIE UND PHARMAZIE

DER LUDWIG-MAXIMILIANS-UNIVERSITÄT MÜNCHEN

ENERGETIC COORDINATION COMPOUNDS BASED ON NITROGEN-RICH LIGANDS

– ONE CONCEPT, TWO GOALS –

LASER IGNITION AND LEAD-FREE PRIMARY EXPLOSIVES



Norbert Szimhardt

aus

München

2018

Erklärung:

Diese Dissertation wurde im Sinne von § 7 der Promotionsordnung vom 28. November 2011 von Herrn Professor Dr. Thomas M. Klapötke betreut.

Eidesstattliche Versicherung:

Diese Dissertation wurde eigenständig und ohne unerlaubte Hilfe erarbeitet.

München, den 19.07.2018

.....

Norbert Szimhardt

Dissertation eingereicht am:	19.07.2018
1. Gutachter:	Prof. Dr. Thomas M. Klapötke
2. Gutachter:	Prof. Dr. Konstantin Karaghiosoff
Mündliche Prüfung am:	30.08.2018

Danksagung

Mein erster Dank gilt Herrn Prof. Dr. Thomas M. Klapötke, meinem zukünftigen Doktorvater, für die Aufnahme in den Arbeitskreis, die Möglichkeit zu promovieren und die großartige Betreuung. Ich möchte mich für die finanzielle Unterstützung, die Möglichkeit an so vielen unterschiedlichen Konferenzen zu partizipieren sowie die Hilfe bei diversen anderen Problemstellungen bedanken. Er hat ein großes Vertrauen in seine Mitarbeiter und ermöglicht einem so eine ungemeine Forschungs- sowie Publikationsfreiheit. Ich konnte stets auf Sie bauen und möchte mich für die wundervollen gemeinsamen Jahre bedanken.

Zunächst einmal möchte ich Herrn Prof. Dr. Konstantin „Conny“ Karaghiosoff für die Übernahme des Zweitgutachtens danken. Conny hat mir die faszinierende Welt der Kristalle nähergebracht und mich in die Kunst des Messens eingelernt. Ich möchte mich für die unglaubliche Zeit bedanken, die du in diesen Arbeitskreis investierst, sowohl unter der Woche wie auch am Wochenende, an dem ich dir (leider) zu oft Gesellschaft geleistet habe. Du hast stets gute Laune und nimmst dir trotz des ganzen Stresses die Zeit, dich der Probleme anderer anzunehmen. Vielen Dank auch für das Messen und Auswerten diverser ^{15}N NMR Spektren.

Ich möchte mich bei Prof. em. Dr. Wolfang Beck, Prof. Dr. Hans-Christian Böttcher, Prof. i. R. Dr. Ingo-Peter Lorenz und Prof. Dr. Franz Bracher dafür bedanken, dass sie sich bereit erklärt haben, Teil des Prüfungskomitees zu sein.

Ein großer Dank geht an Herrn Dr. Jörg Stierstorfer, einen meiner Mentoren, für die unzähligen Fachgespräche, die guten Ideen, für die Chance sich selbst zu entfalten und die zahlreichen Möglichkeiten, die du mir eröffnet hast. Du hast mir das Lösen von Kristallstrukturen, das Schreiben von schönen und guten Publikationen, das Erstellen von fachlich korrekten Vorträgen und vieles mehr beigebracht. Du warst immer behilflich beim Erstellen von hübschen Bildern und warst stets kritisch beim Schreiben der Paper, wobei du einen während der Korrektur des Öfteren zur Weißglut bringen konntest. Neben der ganzen vielen Arbeit hast du dich dennoch zu einem guten Freund entwickelt, der mich maßgeblich in meiner Entwicklung geprägt hat. Danke für alles!

Dr. Burkhard Krumm sei gedankt für die unzähligen hilfreichen Sicherheitsratschläge, die vielen Scherze über den glorreichen FC Bayern sowie die angenehme gemeinsame Zeit während der Konferenz in Stockholm und beim Spiel 1860 gegen Dortmund (1:0).

Ich möchte mich herzlichst bei Frau Irene Scheckenbach, der heimlichen guten Seele des Arbeitskreises, bedanken. Sie waren mir immer eine große Hilfe im Bürokratendschungel, beim Ausfüllen der unendlichen Reisekostenanträge oder wenn Herr Möbus-Ohly mir mal wieder die Zugangskarte zum Gebäude gesperrt hat. Ich möchte mich bedanken für Ihre und Herrn Prof. Klapötkes wundervolle Art mit Tieren umzugehen, sowie die Möglichkeit Pauli für ein paar Tage mitzunehmen und den liebevollen Umgang mit ihm.

Ein großes Dankeschön geht an meinen ehemaligen F-Praktikanten, Masteranden, Laborkollegen und Freund Maximilian Wurzenberger, der meine Nachfolge antreten wird und diese, der bin ich mir sicher, hervorragend erfüllen wird. Du warst immer wissbegierig, hilfsbereit, hast maßgeblich zur guten Laboratmosphäre beigetragen und warst eine große Unterstützung sowohl auf der chemischen Seite wie auch beim Schreiben der Publikationen. Ich werde unsere gemeinsame Zeit vermissen.

Ich möchte mich bei allen Praktikanten für ihre wahnsinnige Hilfe und Unterstützung beim Anfertigen dieser Arbeit bedanken. Während ich mit Praktikumsbetreuungen, Anfertigen von Publikationen und diversen anderen lästigen Dingen beschäftigt war, habt ihr mir die Arbeit abgenommen. Mein Dank geht dabei an: Manuel Freis, Andreas Beringer, Chantal von der Heide, Maximilian Wurzenberger (2x), Lukas Zeisel, Florian Binder, Alexander Kremsmair, Hannes Reichherzer, Jasmin Lechner, Andreas Hess, Philipp Spieß, Michael Gruhne und Marcus Lommel. Besonders hervorheben möchte ich in diesem Zusammenhang die Herren Lukas Zeisel, Philipp Spieß, Michael Gruhne und Marcus Lommel, die mir ungemein geholfen haben bei der Erstellung und Fertigstellung diverser Publikationen.

Ein besonderer Dank geht an Jasmin Lechner ohne die diese Arbeit absolut nicht vorstellbar gewesen wäre. Sie hat so einen immensen Beitrag mit der Anfertigung von Bildern, Formatierungen und Korrekturlesen geleistet, wofür ich ihr für ewig dankbar sein werde. Ich möchte mich zudem für die wunderbare Unterstützung und Hilfe in diesen stressigen und schwierigen Zeiten bedanken.

Ein weiterer besonderer Dank geht an Herrn Marcus Lommel und Michael Gruhne. Ihr habt mir unglaublich viel geholfen beim Anfertigen der Arbeit, beim Schreiben der Publikationen, beim Bestimmen von Sensivitäten und jeglichen weiteren anfallenden Arbeiten. Ihr teilt eure Faszination und Wissbegierde für energetische Materialien mit uns und seid euch nie zu schade für etwas. Vielen Dank für alles. Ihr seid eine große Bereicherung für den Arbeitskreis und euch gehört die Zukunft!

Ich möchte mich bei Herrn Sven Ruhland von der VOERE GmbH Präzisionstechnik bedanken, der maßgeblichen Anteil zur Entwicklung meines Laserzündungsapparates und anderer kleinerer Erfindungen beigetragen hat. Vielen Dank für die finanzielle und materialtechnische Unterstützung.

Prof. Dr. Jürgen Evers danke ich für die Messung und Auswertung von zahlreichen X-ray Pulverdiffraktogrammen.

Ich bedanke mich bei Herrn Stefan Huber für die hochpräzise Bestimmung unzähliger Sensivitäten, für seine lockere und unbekümmerte Art sowie die stets zeitgenauen Chemikalienbestellungen.

Vielen Dank an Cornelia Unger, die zahlreiche zeitraubende toxikologische Tests mit meinen Verbindungen gemacht hat.

Ich möchte mich bei Herrn Dr. Manuel Joas bedanken für die Einführung in die Chemie der hochenergetischen Materialien, insbesondere die der Primärsprengstoffe und energetischen Übergangsmetallkomplexe. Du warst ein großer Antrieb und Grund für die Ergebnisse dieser Arbeit.

Mein Dank geht an alle vergangenen Laborkollegen Dr. Tobias Herrmann, Josh Bauer, Alicia Dufter, Thomas Reich, Dr. Andreas Preimesser sowie ehemalige Kollegen Dr. Philipp Schmid, Dr. Dennis Fischer, Dr. Daniel Izsak und derzeitige Kollegen besonders Maurus Völkl und Jelena Reinhardt für die angenehme Zeit und unvergesslichen Jahre im Arbeitskreis. Ihr wart eine Bereicherung während der Mittagessen, der gemeinsamen Konferenzen und der vielen zusammen gefeierten Partys. Vielen Dank an Herrn Ivan Gospodinov für die vielen nervigen Unterbrechungen im Laboralltag, wenn er mal wieder durch Gang getingelt ist, sowie unserer schönen und unvergesslichen Zeit während unseres Besuchs der Gordon Research Conference in den USA. Ich bedanke mich bei Frau Stefanie Heimsch für das Befüllen der Kühlschränke und die Einführung von Red Bull.

Zu guter Letzt möchte ich mich bei meinen Eltern Erzsebet und Ferenc für ihre Liebe, ihre Entbehrungen, ihre Unterstützung und einfach alles, was sie für mich getan haben, bedanken! Ein besonderer Dank geht auch an Steffi und Paul für ihre Hilfe und Unterstützung während der letzten Jahre.

CONFIDENTIALITY CLAUSE:

This phD thesis contains confidential data of the research group of Prof. Dr. Thomas M. Klapötke.

This work may only be made available for the reviewers and the examination board. Any publication and duplication of this phD thesis – even in part – is prohibited. An inspection by third parties requires the expressed permission of the author and Prof. Dr. Thomas M. Klapötke.

Table of Contents

1 Introduction 1

1.1 Definition and Classification of Energetic Materials 1

1.1.1 Primary Explosives 2

1.1.2 Secondary Explosives 3

1.1.3 Pyrotechnics 5

1.1.4 Propellants 6

1.2 Primary Explosives: Modern Challenges and Recent Developments 7

1.3 Ignition and Initiation Devices with Primary Explosives 11

1.4 Laser Ignition and Initiation of Energetic Materials 17

1.5 Motivation, Concept and Objectives 24

1.6 References 27

2 Set-Up 33

2.1 Laser Ignition Setup 33

2.1.1 Sample Test Setup 33

2.1.2 Laser Ignition Test Setup 33

2.2 Test Setups for Primary Explosives 34

2.2.1 Hot Plate and Hot Needle Tests 34

2.2.2 Secondary Explosive Initiation Capability Tests 35

2.2.3 Ball Drop Impact Sensitivity Test 37

2.2.4 Priming Mixtures 38

2.3 References 41

3 1,1'-Nitramino-5,5'-bitetrazoles 43

3.1 Introduction 44

3.2 Results and Discussion 45

3.3 Crystal Structures 46

3.4 Physicochemical Properties 48

3.4.1 Thermal Behavior 49

3.4.2 Heats of Formation, Sensitivity and Detonation Parameters 49

3.5 Conclusions 50

3.6 Experimental Section 51

3.7 References 54

4 Metal Salts and Complexes of 1,1'-Dinitramino-5,5'-bitetrazole 57

4.1 Introduction 58

4.2 Results and Discussion 60

4.2.1 Synthesis 60

4.2.2 Crystal Structures 61

4.2.3 Energetic Properties and Laser Initiation 67

4.2.4 Thermal Behavior 69

4.2.5 Sensitivities 69

4.2.6 Hot Plate and Hot Needle Test 70

4.2.7 Laser Initiation 70

4.3 Experimental Section 70

4.4 Conclusions 74

4.5 References 75

5 Potassium *N*-Nitramino-5*H*-tetrazolates — Powerful Green Primary Explosives with High Initiation Capabilities 79

5.1 Introduction 80

5.2 Experimental Section 82

5.3 Results and Discussion 83

5.3.1 Synthesis 83

5.3.2 Crystal Structures 85

5.3.3 Scanning Electron Microscopy (SEM) and Energy-dispersive X-ray Spectroscopy (EDX)….. 87

5.3.4 Physicochemical Properties 88

5.3.5 Toxicity 90

5.4 Conclusions 91

5.5 References 92

6 Methylsemicarbazide as a Ligand in Late 3d Transition Metal Complexes 97

6.1 Introduction 98

6.2 Results and Discussion 100

6.2.1 Synthesis 100

6.2.2 Crystal Structures 102

6.2.3 Sensitivities and Thermal Stability ... 110
6.2.4 Toxicity ... 117
6.2.5 Laser Initiation ... 118
6.2.6 UV-Vis Spectroscopy ... 119
6.3 Conclusions ... 120
6.4 References ... 122
7 Synthesis and Characterization of Tetrahedral Zn(II) Complexes with 3,6,7-Triamino-7*H*-[1,2,4]triazolo[4,3-*b*][1,2,4]triazole as Nitrogen-rich Ligand ... 125
7.1 Introduction ... 126
7.2 Results and Discussion ... 127
7.2.1 Synthesis ... 127
7.2.2 Crystal Structures ... 128
7.2.3 IR Spectroscopy ... 132
7.2.4 Physicochemical and Energetic Properties ... 133
7.3 Conclusions ... 135
7.4 Experimental Section ... 135
7.5 References ... 138
8 Di(1*H*-tetrazol-5-yl)methane as Neutral Ligand in Energetic Transition Metal Complexes ... 141
8.1 Introduction ... 142
8.2 Results and Discussion ... 144
8.2.1 Synthesis ... 144
8.2.2 Crystal Structures ... 148
8.2.3 Sensitivities and Thermal Stability ... 155
8.2.4 Laser Ignition Tests ... 157
8.3 Conclusions ... 159
8.4 Experimental Part ... 160
8.5 References ... 167
9 2,2-Bis(5-tetrazolyl)propane as Ligand in Energetic 3d Transition Metal Complexes…. ... 173
9.1 Introduction ... 174
9.2 Results and Discussion ... 177

9.2.1 Synthesis 177
9.2.2 Crystal Structures 179
9.2.3 Sensitivities and Thermal Stabilities 185
9.2.4 Laser Ignition Experiments 187
9.3 Conclusions 188
9.4 References 189
10 Coordination Chemistry with 1-Methyl-5*H*-tetrazole: Cocrystallization, Laser-ignition, Lead-free Primary Explosives – One Ligand, three Goals 193
10.1 Introduction 194
10.2 Results and Discussion 197
10.2.1 Synthesis 197
10.2.2 Crystal Structures 201
10.2.3 Sensitivities and Thermal Stability 210
10.2.4 Toxicity 216
10.2.5 Laser Initiation 217
10.2.6 UV-Vis Spectroscopy 219
10.3 Conclusions 221
10.4 References 222
11 2-Methyl-substituted Monotetrazoles in Copper(II) Perchlorate Complexes: Manipulating Coordination Chemistry and Derived Energetic Properties 227
11.1 Introduction 228
11.2 Results and Discussion 230
11.2.1 Synthesis 230
11.2.2 Crystal Structures 232
11.2.3 Thermal Properties and Sensitivities 238
11.2.4 Optical Initiation and UV-Vis Spectroscopy 241
11.3 Conclusions 243
11.4 References 244
12 Highly Functional Energetic Complexes: Stability Tuning through Coordination Diversity of Isomeric Propyl-linked Ditetrazoles 247
12.1 Introduction 248
12.2 Results and Discussion 251

12.2.1 Synthesis 251
12.2.2 Crystal Structures 257
12.2.3 Sensitivities and Thermal Stabilities 266
12.2.4 Toxicity Assessment 271
12.2.5 Laser Ignition Tests 272
12.2.6 UV-Vis Spectroscopy 273
12.3 Conclusions 275
12.4 References 276
13 Copper(II) Chlorate Complexes – the Renaissance of a Forgotten and Misjudged Energetic Anion 281
13.1 Introduction 282
13.2 Synthesis 283
13.3 Results and Discussion 285
13.3.1 Crystal Structures 285
13.3.2 Sensitivities, Thermal Stability and UV-Vis Spectroscopy 286
13.3.3 Toxicity 287
13.4 Conclusions 287
13.5 References 288
14 Nitrogen-Rich Copper(II) Bromate Complexes: an Exotic Class of Primary Explosives 291
14.1 Introduction 292
14.2 Results and Discussion 295
14.2.1 Synthesis 295
14.2.2 Crystal Structures 296
14.2.3 Sensitivities and Thermal Stability 302
14.2.4 Laser Ignition Tests und UV-Vis Measurements 304
14.2.5 Toxicity Determination and Mass Spectrometry (MS) of Decomposition Gases 306
14.3 Conclusions 307
14.4 Experimental Section 308
14.5 References 312
15 1-Amino-triazole Transition Metal Complexes as Laser Ignitable and Lead-free Primary Explosives 319

15.1 Introduction 320

15.2 Results and Discussion 323

15.2.1 Synthesis 323

15.2.2 Crystal Structures 328

15.2.3 Scanning Electron Microscopy (SEM) and Energy Dispersive X-ray Spectroscopy (EDX)…… 334

15.2.4 Sensitivities and Thermal Stability 336

15.2.5 Toxicity 342

15.2.6 Laser Initiation 342

15.2.7 UV-Vis Spectroscopy 344

15.3 Conclusions 345

15.4 References 346

16 Maximization of the Energy Capability Level in Transition Metal Complexes through Application of 1-Amino- and 2-Amino-5*H*-tetrazole Ligands 349

16.1 Introduction 350

16.2 Results and Discussion 353

16.2.1 Synthesis 353

16.2.2 Crystal Structures 359

16.2.3 Powder Diffraction 368

16.2.4 Scanning Electron Microscopy (SEM) and Energy Dispersive X-ray Spectroscopy (EDX)…… 369

16.2.5 Sensitivities and Thermal Stability 371

16.2.6 Primary Explosive Suitability Evaluation 376

16.2.7 Toxicity 378

16.2.8 Laser Initiation 379

16.2.9 UV-Vis Spectroscopy 380

16.3 Conclusions 381

16.4 References 383

17 Use of a Copper(II) Azide Complex as a Primary Explosive 387

17.1 Introduction 388

17.2 Synthesis 403

17.3 References 408

17.4 Claims 408

18 Summary and Conclusion 415

18.1 References 424

19 Appendix 427

19.1 Supplementary Information: 1,1'-Nitramino-5,5'-bitetrazoles 427

19.1.1 X-Ray-Diffraction 427

19.1.2 Computations 429

19.1.3 ^{15}N NMR Spectrum of 1,1'-Dinitramino-5,5'-bitetrazole (1) 430

19.1.4 Experimental Part 431

19.1.5 References 432

19.2 Supplementary Information: Metal Salts and Complexes of 1,1'-Dinitramino-5,5'-bitetrazole 434

19.2.1 X-Ray Diffraction 434

19.2.2 Experimental Part 439

19.2.3 IR Spectroscopy of 7a and 7b 441

19.2.4 References 441

19.3 Supplementary Information: Potassium *N*-Nitramino-5*H*-tetrazolates — Powerful Green Primary Explosives with High Initiation Capabilities 443

19.3.1 Experimental Procedure and General Methods 443

19.3.2 IR Spectroscopy 447

19.3.3 X-Ray Diffraction 448

19.3.4 Initiation Capability Tests 450

19.3.5 Hot Needle Tests 453

19.3.6 Heat of Formation Calculations 454

19.3.7 References 455

19.4 Supplementary Information: Methylsemicarbazide as a Ligand in Late 3d Transition Metal Complexes 458

19.4.1 Compound Overview 458

19.4.2 X-ray Diffraction 458

19.4.3 IR Spectroscopy of 11, 12, 15, 18, 20 and 23 469

19.4.4 DTA Plots of 6–8, 11, 12, 15 and 18 471

19.4.5 UV-Vis Spectra of 4–8 472

19.4.6 Experimental Part and General Methods 472

19.4.7 References 486

19.5 Supplementary Information: Di(1*H*-tetrazol-5-yl)methane as Neutral Ligand in Energetic Transition Metal Complexes 488

19.5.1 X-ray Diffraction ... 488
19.5.2 IR Spectroscopy of 11, 12 and 14, 15 ... 494
19.5.3 DTA Plots of 6–8, 11–13 and 15 ... 495
19.5.4 TGA Plot of Compound 12 ... 496
19.5.5 Hot Plate and Hot Needle Tests ... 496
19.5.6 References ... 498

19.6 Supplementary Information: 2,2-Bis(5-tetrazolyl)propane as Ligand in Energetic 3d Transition Metal Complexes ... 499
19.6.1 Compounds Overview ... 499
19.6.2 IR Spectroscopy of 1–15 ... 500
19.6.3 X-ray Diffraction ... 504
19.6.4 DTA Plots of 1–15 ... 511
19.6.5 Hot Plate and Hot Needle Tests ... 514
19.6.6 UV-Vis Spectra of 10, 13 and 14 ... 515
19.6.7 Experimental Part and General Methods ... 516
19.6.8 References ... 524

19.7 Supplementary Information: Coordination Chemistry with 1-Methyl-5*H*-tetrazole: Cocrystallization, Laser-ignition, Lead-free Primary Explosives – One Ligand, three Goals ... 526
19.7.1 Compounds Overview ... 526
19.7.2 X-ray Diffraction ... 527
19.7.3 IR Spectroscopy of 3, 6–9, 12, 17 and 23 ... 544
19.7.4 DTA plots of 1–10, 12–14, 27 and 29–37 ... 547
19.7.5 Thermal Gravimetric Analysis of 4, 9, 17 and 24 ... 551
19.7.6 Column Diagrams of the Complexes 15–26 ... 552
19.7.7 Hot Plate and Hot Needle Tests ... 553
19.7.8 Laser Ignition Tests ... 555
19.7.9 UV-Vis Spectra of 15, 20–27, 31 and 36 ... 557
19.7.10 Experimental Part ... 558
19.7.11 References ... 575

19.8 Supplementary Information: 2-Methyl-substituted Monotetrazoles in Copper(II) Perchlorate Complexes: Manipulating Coordination Chemistry and Derived Energetic Properties… ... 578
19.8.1 Overview of Synthesized Compounds ... 578
19.8.2 Experimental and General Methods ... 578
19.8.3 IR Spectroscopy of 1–7 ... 586
19.8.4 X-ray Diffraction ... 587
19.8.5 DTA Plots of 1–7 ... 591

19.8.6 TGA Plots of 1–4 592
19.8.8 Hot Plate, Hot Needle and Optical Initiation Tests 593
19.8.9 References 594

19.9 Supplementary Information: Highly Functional Energetic Complexes: Stability Tuning through Coordination Diversity of Isomeric Propyl-linked Ditetrazoles 596
19.9.1 Compounds overview 596
19.9.2 IR Spectroscopy of 1–15 597
19.9.3 X-ray Diffraction 602
19.9.4 DTA Plots of 1–3, 10 and 13–15 609
19.9.5 Column Diagrams of the Complexes of 8 and 11–15 611
19.9.6 Hot Plate and Hot Needle Tests 612
19.9.7 Laser Ignition Tests 613
19.9.8 UV-Vis Spectra of 4, 9, 10 and 13–15 615
19.9.9 Experimental Part and General Methods 615
19.9.10 References 625

19.10 Supplementary Information: Copper(II) Chlorate Complexes – the Renaissance of a Forgotten and Misjudged Energetic Anion 627
19.10.1 Experimental Procedure and General Methods 627
19.10.2 Synthesis 632
19.10.3 Crystal structures 633
19.10.4 Sensitivities and Thermal Stability 643
19.10.5 Laser Ignition Tests 646
19.10.6 UV-Vis Spectroscopy 647
19.10.7 Initiation capability tests 649
19.10.8 Toxicity 651
19.10.9 X-ray Diffraction 651
19.10.10 IR Spectroscopy 654
19.10.11 References 656

19.11 Supplementary Information: Nitrogen-Rich Copper(II) Bromate Complexes: an Exotic Class of Primary Explosives 659
19.11.1 X-ray Diffraction 659
19.11.2 IR Spectroscopy of 1–6 662
19.11.3 References 663

19.12 Supplementary Information: 1-Amino-triazole Transition Metal Complexes as Laser Ignitable and Lead-free Primary Explosives 665
19.12.1 Compounds Overview 665

19.12.2 IR Spectroscopy of 1–16 ... 666
19.12.3 X-ray Diffraction ... 670
19.12.4 TGA Plot of the Zinc(II) Perchlorate Complex 13 ... 680
19.12.5 DTA Plots of 1–9 and 14–16 ... 681
19.12.6 Column Diagrams of the Complexes 3–9 ... 684
19.12.7 Hot Plate and Hot Needle Tests ... 685
19.12.8 Laser Ignition Test of Complex 16 ... 690
19.12.9 Experimental Part and General Methods ... 691
19.12.10 References ... 703

19.13 Supplementary Information: Maximization of the Energy Capability Level in Transition Metal Complexes through Application of 1-Amino- and 2-Amino-5*H*-tetrazole Ligands…. ... 705

19.13.1 Compounds Overview ... 705
19.13.2 IR Spectroscopy of 1–9, 12 and 16–23 ... 706
19.13.3 X-ray Diffraction ... 711
19.13.4 TGA Plots of 1 and 2 ... 727
19.13.5 DTA Plots of 1–3, 8, 9, 12 and 16–23 ... 728
19.13.6 Column Diagrams of the Complexes of 18–23 ... 732
19.13.7 Hot Plate and Hot Needle Tests ... 733
19.13.8 Initiation Capability Tests ... 741
19.13.9 Laser Ignition Tests ... 742
19.13.10 UV-Vis Spectra of 18, 19, 21 and 23 ... 744
19.13.11 Experimental Part and General Methods ... 744
19.13.12 References ... 757

19.14 Supplementary Information: Use of a Copper(II) Azide Complex as a Primary Explosive.. ... 759

19.14.1 Crystal Structures and X-ray Powder Diffraction ... 759
19.14.2 Vacuum Stability Tests (VST) ... 761

1 Introduction

1.1 Definition and Classification of Energetic Materials

A definition of energetic materials as "chemical compounds or compositions that contain both fuel and oxidizer and rapidly react to release energy and gas" is given by the *American Society for Testing and Materials*.[1] This definition is relatively inaccurate when seeking to describe the energetic materials presented in this thesis. The majority of compounds in this work are not distinguished by a balanced oxygen content, and many of the most explosive derivatives do not even contain oxygen. Therefore, it is necessary to introduce a more general definition of energetic materials: "Energetic materials are chemical compounds or compositions, which may react rapidly under release of energy and gas." The type of reaction may be a combustion, deflagration or detonation.

Many variations in the classification of chemical energetic materials can be found in the past.[2] The main difference in the classifications is with respect to their chemical nature and their performance and application. Depending on their purpose, energetic materials can be categorized into three main types: explosives, propellants, and pyrotechnics (Figure 1). The output of high explosives such as primaries or secondaries usually results in a detonation, whereas the output of a pyrotechnic produces some sort of audio-visual effect (based on redox reaction of inorganic reducing agents and oxidizer compounds), and propellants serve to accelerate either projectiles, missiles or rockets.[3] However, since this work focuses on the synthesis of new explosives, only these are further subdivided according to their sensitivities.

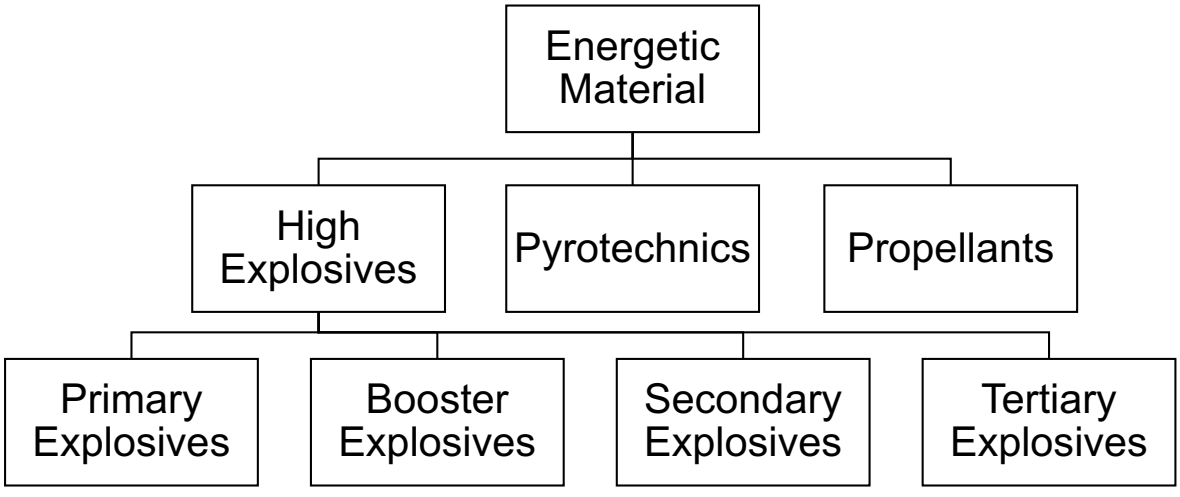


Figure 1. Classification of energetic materials into the four main types.

1.1.1 Primary Explosives

Substances which can be assigned to the class of primary explosives are, in contrast to secondary explosives, compounds that undergo a much faster deflagration-to-detonation transition (DDT) after being initiated by a non-explosive simple initiating impulse (SII). Typically, primary explosives are more sensitive to mechanical, thermal or electrostatic stimuli (impact, friction, heat or ESD) than secondaries and exhibit values of ≤ 4 J toward impact, ≤ 10 N against friction and ≤ 20 mJ toward electrostatic discharge.[3–5] In contrast to this, performance criteria such as detonation velocity (primaries: 3500–5500 ms^{-1}, secondaries: 6500–9000 ms^{-1}) and heat of explosion (primaries: 1000–2000 kJ kg^{-1}, secondaries: 5000–6000 kJ kg^{-1}) of primary explosives are significantly lower than those of secondaries.[3] Primary explosives produce either a large quantity of heat or a shock wave allowing the transfer of detonation to a less sensitive but more powerful secondary explosive, which cannot be initiated as easily. Primaries are therefore incorporated into some kind of initiating device (e.g. detonator, blasting cap, primer) and used as an initiator for propellants, booster explosives or main charges.[3] One primary explosive discovered in the 17th century, is mercury(II) fulminate (MF), which was used by Alfred Nobel to initiate dynamite in metal blasting cap detonators.[6] The most commonly used primary explosives nowadays are lead azide (LA) and lead styphnate (LS; normal and basic) (Chart 1); two compounds that display a high toxic potential toward humans and nature.[7,8] The latter compound has a lower performance than lead azide but is more sensitive to mechanical stress. In the meantime, nitroaromatics like DDNP and KDNBF, which in turn are not without their own disadvantages, are replacing lead styphnate in more and more applications.[9,10] Another primary compound that has a major negative impact on nature is cadmium azide, which is used as a primary in detonators for high-temperature stable special applications where stability is crucial such as deep oil drilling.[3] Depending on the application, it may not be absolutely necessary for the primary explosive to produce a shock wave. In the case of priming charges, for example, the transfer to the propellant charge is not detonative due to the interaction of the pyrotechnic components and the primary explosives lead styphnate and the nitrogen-rich sensitizer tetrazene.[11] Triacetone trioxide, a very sensitive compound discovered in 1895 by the German chemist Richard Wolffenstein, is sadly very popular with terrorists and suicide bombers due to its ease of production from household articles.[12] This very volatile substance is repeatedly responsible for major explosions and accidents due to its high sensitivity.

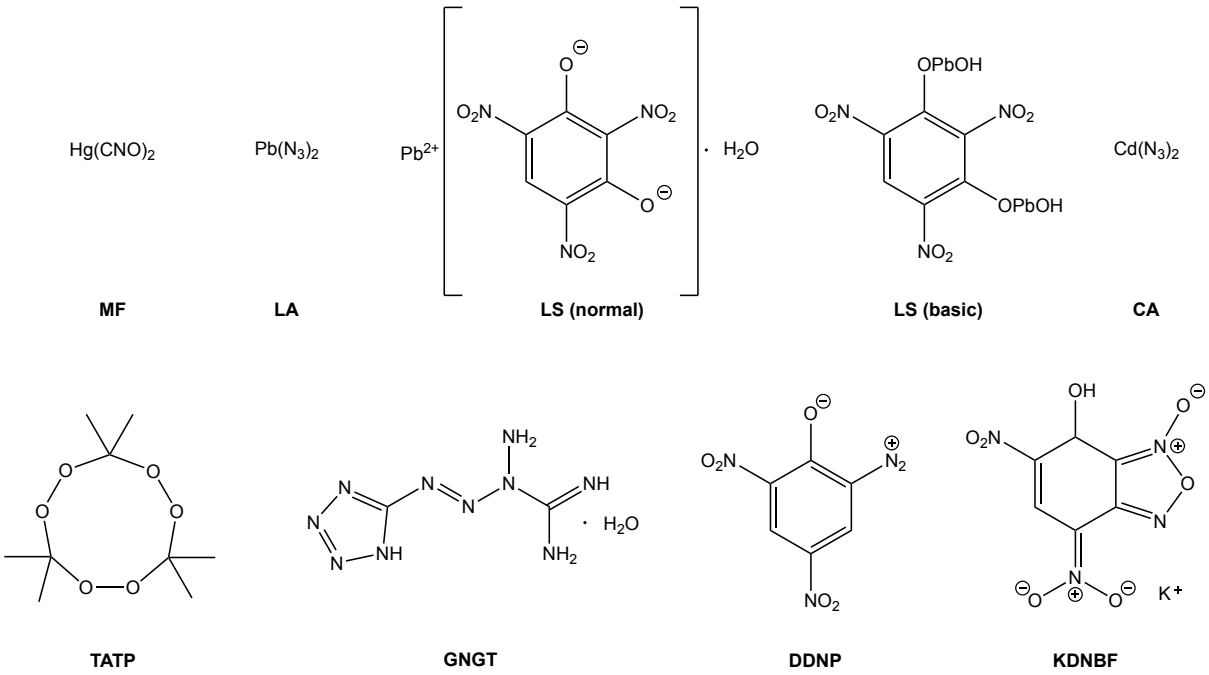


Chart 1. Commonly used primary explosives: mercury fulminate (**MF**), lead azide (**LA**), normal lead styphnate (**LS**), basic lead styphnate (**LS**), cadmium azide (**CA**), triacetone triperoxide (**TATP**), tetrazene (**GNGT**), diazoniumdinitrophenolate (**DDNP**) and potassium dinitrobenzfuroxan (**KDNBF**).

1.1.2 Secondary Explosives

As mentioned above, secondaries have a much slower DDT, are less sensitive to external stimuli (mechanical, thermal, and electrical), and usually achieve better performance (detonation velocity, detonation pressure and heat of explosion) in comparison to primary explosives.[3] The characteristic sensitivity values of conventional secondaries (Chart 2) are generally ≥ 4 J for impact and ≥ 80 N for friction at detonation velocities in the range of 6500-9000 ms^{-1}.[3] Nonetheless, secondary explosives require primaries as initiators, as already mentioned, due to their high stabilities.

Many of the secondary explosives, which are in use today, suffer from numerous drawbacks such as high toxicity, high sensitivity (insensitive munition, IM) or low performance, which makes intensive research into possible replacements necessary.[3,13] In the field of secondary explosives, the widely used hexogen (RDX) and its degradation and decomposition products, are toxic to plants, microorganisms, and microbes.[14] RDX itself is toxic to organisms at the base of the food chain such as earthworms, similar to TNT, whose degradation products also have an acute ecotoxicity.[15] In general, improved physicochemical properties such as detonation parameters and stabilities outperforming the commonly used RDX are desired.

Desirable properties for modern energetic materials include high detonation velocity (> 9000 ms^{-1}), high pressure (380 kbar), and a high heat of explosion.[3, 16] The thermal stability of a newly synthesized material should exceed that of the corresponding benchmark compounds in addition to displaying a high thermal stability for the safe storage of energetic materials.[17] Additionally to the performance properties, the desired criteria for a new material to become widely accepted are insensitivity towards destructive stimuli such as electrostatic discharge, heat, friction, and impact to ensure safe handling and enhance controllability of kinetic energy release.[18] Another significant factor that needs to be considered is the price. This means cheap starting materials, simple synthesis, and no elaborate purification.

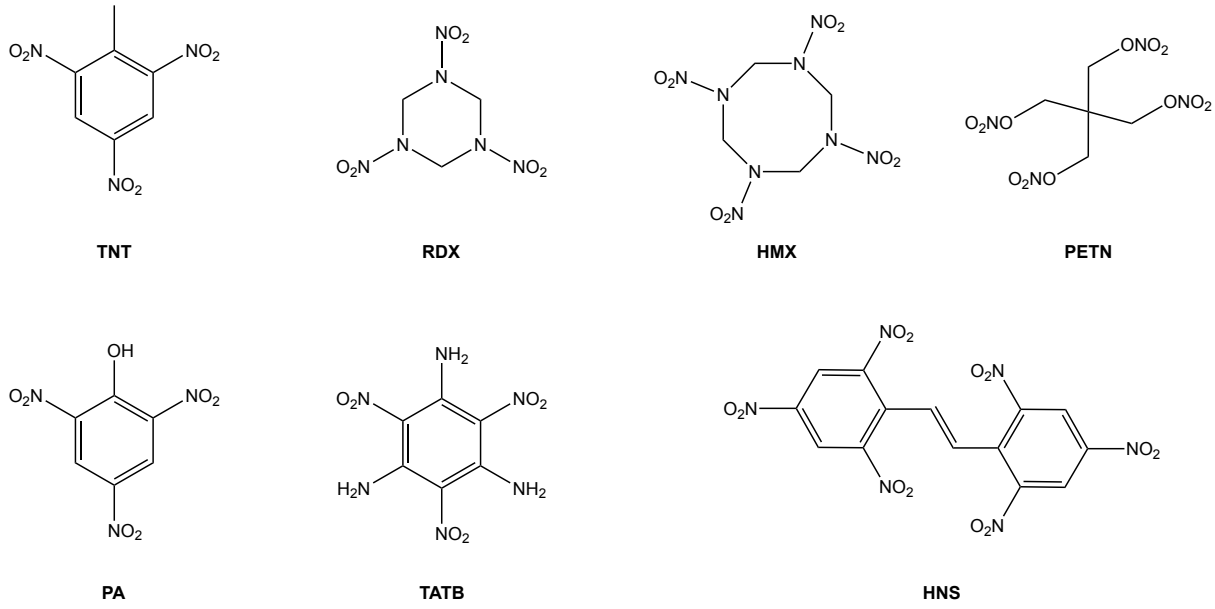


Chart 2. Selected molecular structures of typical secondary explosives: trinitrotoluene (**TNT**), hexogen (**RDX**), octogen (**HMX**), pentaerythritol tetranitrate (**PETN**), picric acid (**PA**), triaminotrinitrobenzene (**TATB**) and hexanitrostilbene (**HNS**).

There are three major methods of introducing potentially explosive energy into a molecule: fuel and oxidizer being contained in the same molecule, compounds possessing ring or cage strain (CL-20, ONC) and a high heat of formation. Classical secondary explosives like the melt castable 2,4,6-trinitrotoluene and nitroglycerine derive all their energy from the oxidation of the carbon backbone. Both compounds exhibit negative heats of formation and hence much lower performance rates than RDX. Hexogen itself also obtains its energy from the oxidation of the carbon backbone and from the formation of dinitrogen due to the N-N bonds in the nitramine moieties. Therefore, a large quantity of gaseous products (CO, CO_2, N_2 etc.) together with a positive heat of formation are generated, which results (along with the higher density) in significantly high-performance values.

In recent years, there has been much research in the field of nitrogen-rich chemistry. In this regard, azoles (e.g. TKX-50)[19] have become favored candidates because they are (generally) highly endothermic compounds (due to the many N-N and C-N bonds), have relatively high densities and have a high nitrogen content which makes them attractive from an environmental point of view. Of particular interest are azoles paired with energetic substituents like nitro ($-NO_2$), nitrato ($-ONO_2$) or nitramine ($-NHNO_2$) functionalities which contribute to a well-balanced oxygen content.[20] In particular polynitroazoles (e.g. BTNPM)[21] have been in focus because of their high performance and low sensitivity to friction and impact.[22] Much research is still being conducted in the field of secondary explosives.[23] Chart 3 shows the molecular structures of some of the recently developed compounds over the last few decades.

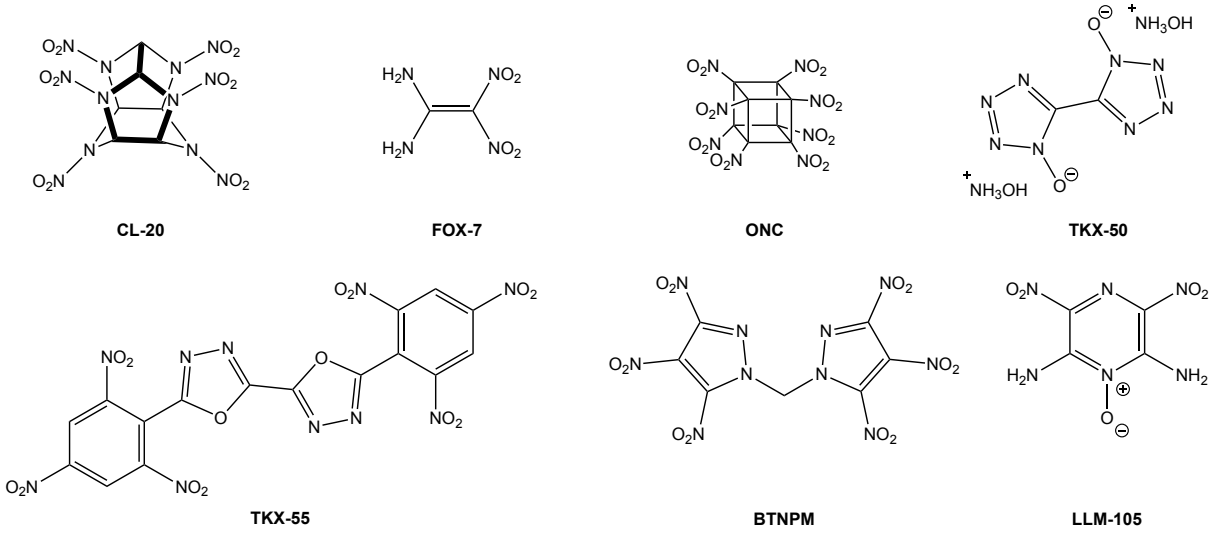


Chart 3. Molecular structures of some of the recently developed secondary explosives: hexanitrohexaazaisowurtzitane (**CL-20**), 1,1-diamino-2,2-dinitro ethene (**FOX-7**), octanitrocubane (**ONC**), dihydroxylammonium 5,5′-bistetrazole-1,1′-diolate (**TKX-50**), 5,5′-bis(2,4,6-trinitrophenyl)-2,2′-bi(1,3,4-oxadiazole) (**TKX-55**), bis(3,4,5-trinitropyrazol-1-yl)methane (**BTNPM**) and 3,5-dinitro-2,6-pyrazinediamine-1-oxide (**LLM-105**).

1.1.3 Pyrotechnics

Pyrotechnics, whose etymology stems from ancient Greek and means "the art of making fire" or "the art of taming fire", basically consists of two components, the oxidizing agent and, the counterpart, the reducing agent or fuel.[3] In contrast to explosives, pyrotechnics are usually compositions, since the oxidizing and reducing parts do not necessarily have to be combined in one molecule. Pyrotechnics are nowadays indispensable for a multitude and have a multitude

of uses. Depending on the application, they can generate light (e.g. flares, fireworks), sound (e.g. firecrackers), heat (e.g. igniter, delay compositions), gas or create a smoke (e.g. cloaking fog) effect or a combination of these.[3,24,25] Especially in combination with primary explosives and other essential additives, they play a fundamental role as initiators and are therefore used in blasting caps, detonators and primers in the form of priming charges.[26] The effect of pyrotechnic devices is produced by a self-sustaining exothermic reaction with reaction velocities between those of propellants and explosives.[3] Typical representatives for oxidizers and reducing agents in pyrotechnic systems are listed in Figure 2.

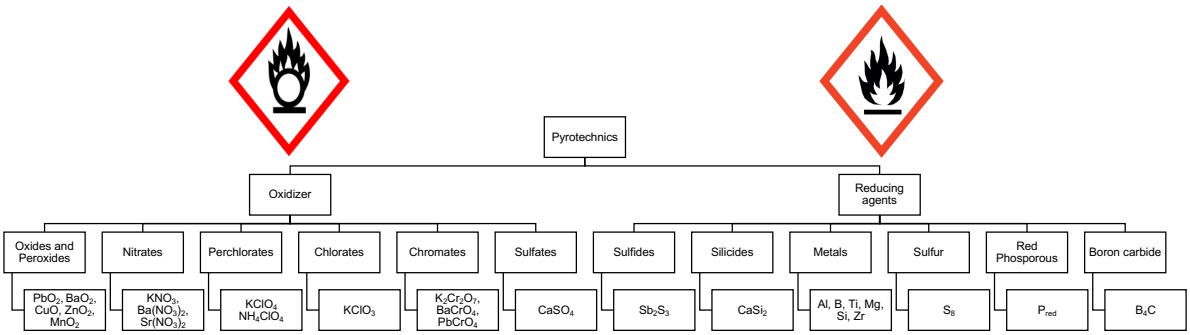


Figure 2. Selected typical representatives for oxidizing and reducing agents in pyrotechnic systems.

1.1.4 Propellants

Propellants can be further divided into gun and the slower burning rocket propellants. The latter can be further subdivided into solid and liquid propellants. The main characteristic of propellants is that they do not have a DDT but ideally burn down in a controlled manner.[3] The most important parameters of propellants are the specific impulse, the combustion temperature and the resulting pressure during combustion. The oldest known propellant charge is black powder, which was discovered by chance in China (~ 220 B.C) and consists of a mixture of potassium nitrate, sulfur, and charcoal dust.[3] Towards the end of the 19th century, black powder met no longer the requirements of modern artillery weapons, and was gradually replaced by smokeless single-based (NC), double-based (NC/NG), or triple-based (NC/NG/NQ) gunpowders (Chart 4).[27] Modern research in this field focusses on the reduction of gun corrosion through integration of energetic nitrogen-rich additives.[3] Solid rocket propellants can be subdivided into double-base and composite types. While the double-base (homogenous) propellants consist mainly of NC/NG, the composite fuels are usually heterogeneous mixtures

of ammonium perchlorate (oxidizer), aluminum (fuel) and a polymeric binder/cure system (hydroxy-terminated polybutadiene (HTPB), diisocyanate).[28] Since the perchlorate anion of the oxidizer has adverse effects on humans and the environment, a massive effort is currently being made to find alternatives. Among the most promising at present is ammonium dinitramide (ADN). A classical representative of a liquid bipropellant system comprises monomethylhydrazine (MMH) and nitrogen tetroxide (NTO) which react on contact hypergol.[29]

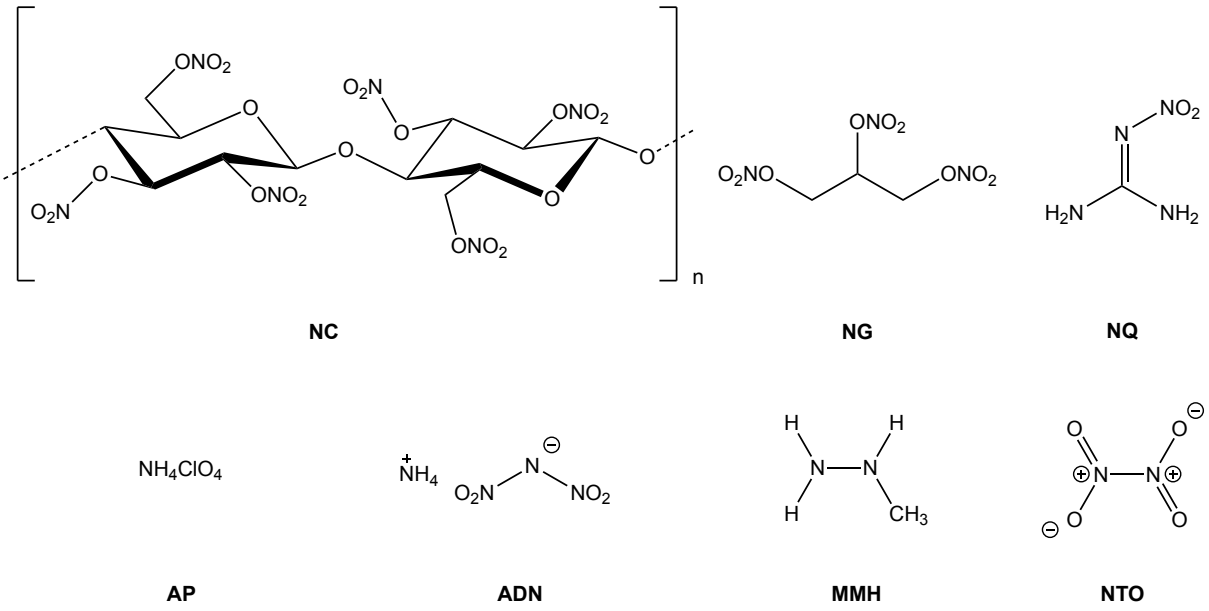


Chart 4. Selected molecular structures or sum formula of: nitrocellulose (**NC**), nitroglycerine (**NG**), nitroguanidine (**NQ**), monomethylhydrazine (**MMH**), nitrogen tetroxide (**NTO**), ammonium perchlorate (**AP**) and ammonium dinitramide (**ADN**).

1.2 Primary Explosives: Modern Challenges and Recent Developments

As already mentioned in chapter 1.1.1 above, mercury fulminate was replaced at the beginning of the 20th century by the only minimally less toxic lead compounds LA and LS.[4,30] Despite their very toxic character, both compounds are still in use as part of priming mixtures and as neat or formulated materials in a large number of applications.[26] The toxic byproducts of lead-based primary explosives can have serious effects on nature and the population. Particularly at risk in this context are people who regularly frequent shooting ranges and military grounds or use a firearm either recreationally or for their occupational work (e.g. police officers, security and military personnel). Several studies in the last decades have proven a significantly increased

blood lead level (BLL) for people using firearms. The increase in BLL and its correlated detrimental health outcomes are directly associated with the number of rounds fired by a person. The negative effects of these compounds are not only limited to military areas but can also affect ammunitions and explosives workers, miners and construction workers.[5] The intake of lead has devastating consequences for the human body, and late-stage lead poisoning can result in seizures, comas, irreparable brain damage and even death.[31] Lead is an acute and chronic poison and can also be responsible for high blood pressure, anemia and problems with the nervous system, kidney, heart and reproductive system.[32,33] Once absorbed by the body, it is difficult to excrete.[3] Even small amounts of lead are toxic and several billion dollars a year are spent in the US alone due to the cost-intensive restoration.[3] Several studies show that chronic lead intake leads to irreversible damage, especially in children and even fetuses.[34] It is responsible for a higher risk of autism, a late onset of puberty (by 6-8 months) and a reduced IQ value of up to 9 points.[35] Due to its profound toxicity, lead (and its compounds) are one of the most highly regulated chemicals in the world. In the USA, various laws such as the Clean Air Act (1963), the Clean Water Act (1972), and regulations by the EPA (2017) have already been passed in an attempt to reduce lead exposure.[5] In Europe, LA and LS have also moved more into focus by the European chemicals agency (ECHA) and their usage is being limited more than ever by a ban due to their inclusion on the REACH (Registration, Evaluation, Authorization, and Restriction of Chemicals) candidate list.[36] This has created a distinct demand for environmentally friendly primary explosives that are capable of replacing both lead azide and lead styphnate. For this reason, scientists from many countries around the world are working intensively on possible alternatives and replacements. Since then, dozens of governmental programs (DoD, SERDP, ESTCP, OEP) have been launched in the USA alone.[5]

In order to be considered as a suitable candidate, a number of independent criteria must be met (Figure 3). First of all, the potential compounds, as well as the degradation products, must be free of toxic components and the waste-stream generated during synthesis should be environmentally compatible. The primary must be able to pass through a DDT instantly, be sufficiently sensitive to impact and friction, and still be safe and predictable to handle. Furthermore, the desired compounds should at least match or, ideally, exceed the performance of the benchmark compounds. The candidate should be thermally (> 150 °C), chemically, and long-term stable (over different temperature ranges). In the case of lead styphnate substitutes for primer applications, the compound should hardly form any residues that could corrode the gun barrel or other structural components. Another important aspect is compatibility with other explosives (RDX, PETN, HMX), with the typical pyrotechnic components of mixtures

(oxidizers, reducing agents, fuels), and with materials of which the respective application consists (aluminum, brass, stainless steel, etc.). To ensure safe synthesis, handling, and storage, the compound should not be water-soluble in order to avoid recrystallization. Last but not least, one of the main exclusion criteria is that the candidate should be able to be prepared in a simple one to a maximum of two-stage synthesis, be easily upscalable and of course be able to be synthesized from easily accessible and affordable starting materials. After looking at this huge list, it becomes clear why, even after more than a century of research, only a few compounds have made it onto the list of potential candidates.

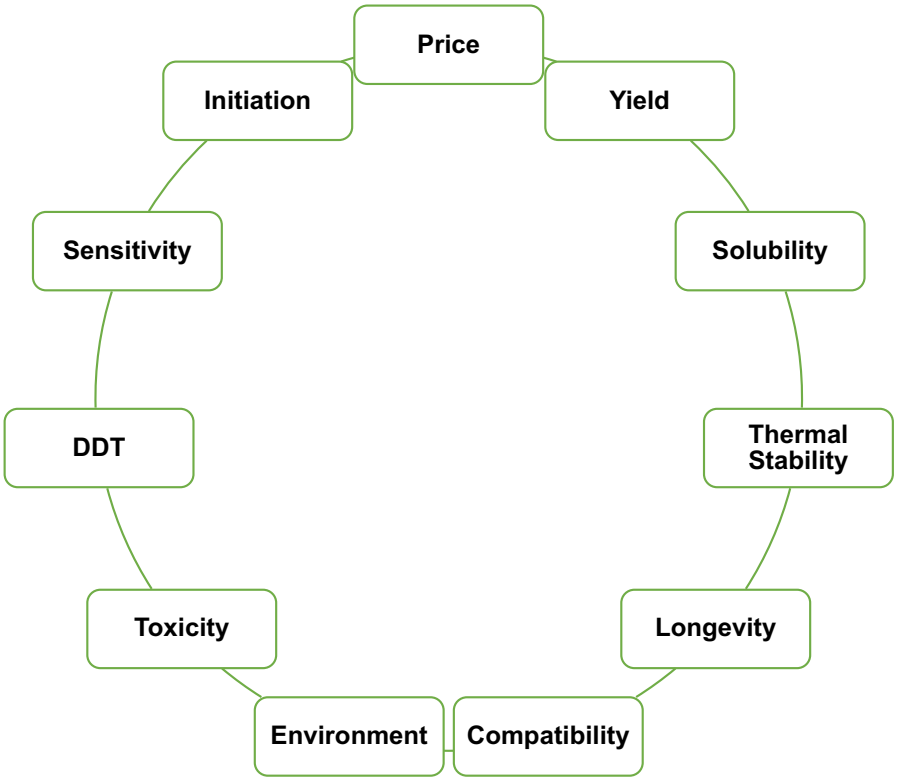


Figure 3. Requirements for potential new primary explosives to be met.

In the last half-century, a number of new primary explosives have been synthesized, characterized, and extensively tested. The most promising, most developed candidates are summarized in Chart 5 and subdivided into a.) LA b.) CA c.) tetrazene, and d.) LS replacements. The possible solution approaches can be roughly categorized into a.) neutral, b.) ionic, c.) energetic coordination compounds (ECC), and nanothermites. Each of the listed compounds has its drawbacks. For example, the limiting factors for silver azide (SA) are the price, the toxicity to freshwater organisms, and the incompatibility with common stab initiation mixtures (tetrazene and Sb_2S_3). DBX-1, the copper(I) salt of nitrotetrazole, shows very promising characteristics as LA drop-in replacement but suffers from an elaborately synthetic pathway as

well as stability and compatibility issues.[37] Another promising compound currently under investigation as a substitute is dipotassium-1,1'-dinitramino-5,5'-bitetrazolate (K_2DNABT).[38] Being a primary explosive with very fast DDT while displaying the performance of a secondary explosive is extraordinary. Nevertheless, the most significant disadvantage remains the long-lasting 7-step synthesis, which is an exclusion criterion as long as no synthesis optimization is carried out on the molecule. Tetrazene, a molecule that does not leave behind any residues during decomposition, is used on a large scale as a sensitizer in priming mixtures (stab and percussion). Without the additive, LS would not ignite so reliably. Unfortunately, the nitrogen-rich molecule is sensitive to hydrolysis, does not have long-term stability, and also has a low thermal decomposition temperature. A compound, that could potentially replace tetrazene and has better stability values, is MTX-1, which was synthesized by Fronabarger *et al.* in 2016.[39] Preliminary tests have already been successfully conducted and have underlined the vast potential of this compound.

The most advanced attempts made to date, concern the use of diazoniumdinitrophenolate (DDNP), and the potassium salts KDNBF or KDNP as a replacement for lead styphnate in primer caps. Unfortunately, DDNP suffers from stability problems (low thermal decomposition temperature, sensitivity to sunlight), causes allergic reactions, and will never fulfill the requirements necessary for a non-civil application.[40] The thermal stability can be compensated by the use of KDBNF or KDNP, but it can be assumed that both compounds may also lead to allergic reactions or other health problems due to their nitroaromatic character. The most promising concepts are based on ionic compounds (higher thermal stability in comparison to neutral molecules) with the environmentally benign alkali metal potassium and nitrogen-rich anions as well as on the strategy of energetic coordination compounds (ECC). In particular, the concept of energetic transition metal complexes has incredible potential in this context. Using interchangeable, environmentally friendly metal centers, endothermic ligands, and anions as building blocks allows fine-tuning of the ECC properties.[41] Hence, regarding the intended application, an energetic complex can be designed by adjusting sensitivities, performance and the atoms involved in order to meet the desired requirements (e.g. being thermally stable, perchlorate-free, insoluble, etc.). Other arguments in support of this strategy are the simple and cheap synthesis and the widely commercially available starting materials. An extraordinary class of coordination compounds is the highly energetic copper(II) azide complexes based on endothermic ligands. Cuprous and copper(II) azide both have excellent initiation capabilities and thermal stabilities, but are clearly too sensitive and unpredictable for potential applications.[4] The concept behind the complexes is to desensitize copper(II) azide through the

implementation of endothermic ligands by maintaining its superior energetic properties. A major part of this work is therefore dedicated to the research and examination of this outstanding and promising class of compounds.

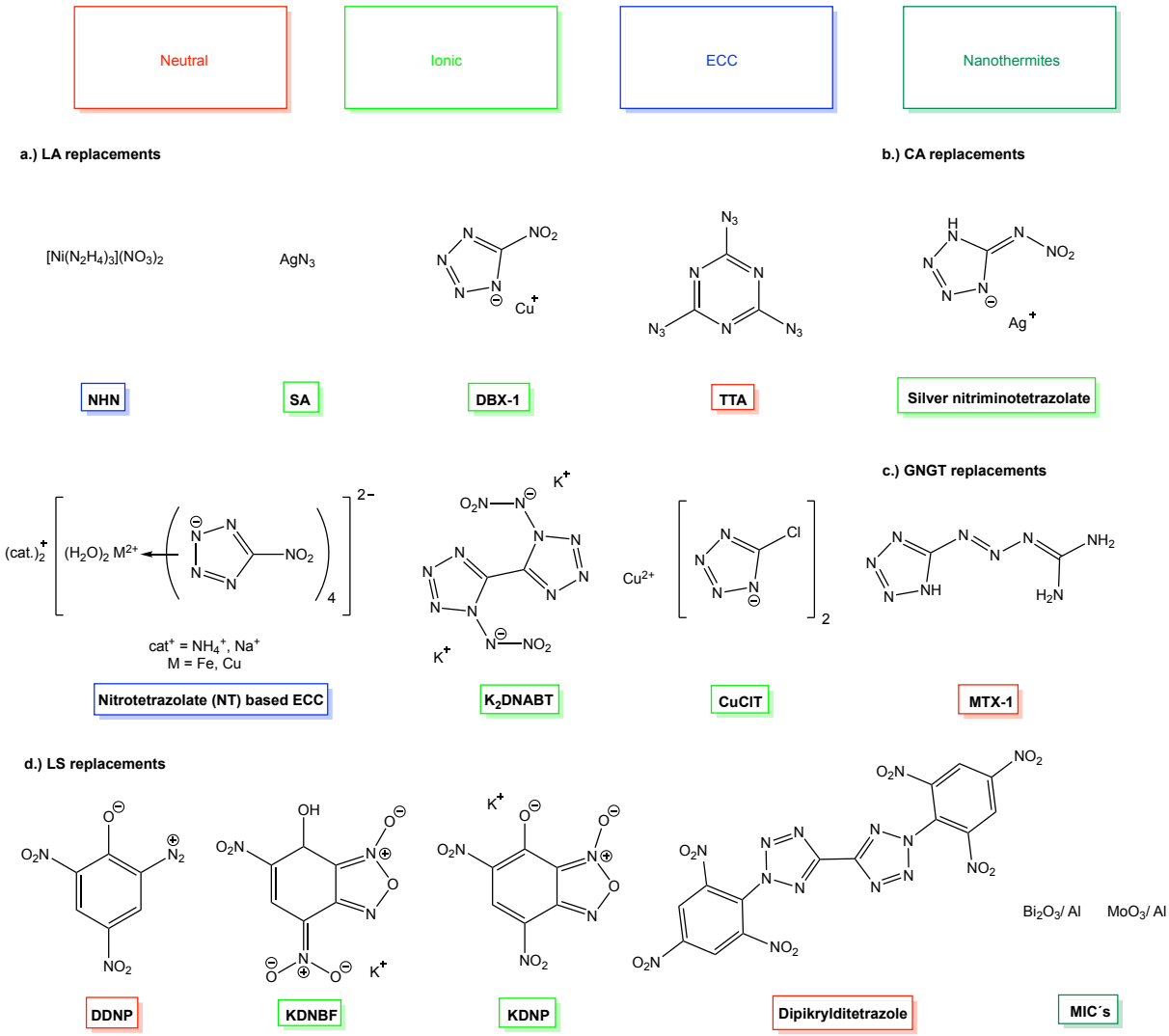


Chart 5. Selected promising candidates for the replacement of a.) lead azide, b.) cadmium azide, c.) tetrazene, and d.) lead styphnate.

1.3 Ignition and Initiation Devices with Primary Explosives

The ignition of energetic materials, as well as the initiation of explosives, can take place via various methods.[26] Figure 4 roughly summarizes and illustrates the most common systems based on flame, heat, friction/impact, shock, and optics. Depending on the output, the initiating system is called a detonator (shock wave) or igniter (flame).[42] The oldest and simplest method is probably the ignition by flame. This method, which has been practiced since the 15th century

with a matchlock to ignite black powder, is still used today in fuse type blasting caps (Figure 4a).[43] The fundamental construction principle is the same for all detonators. A so-called simple initiating impulse (SII) comes in and ignites a pyrotechnic ignition mixture that starts the explosive train, or the primary charge is directly triggered by the SII.[4] In the last step of the ignition chain, the output charge is ignited, which usually consists of a secondary explosive (PETN, RDX, HMX, etc.). Nowadays, there are basically two common types of heat ignition systems (Figure 4b,c), used in mining and demolition.[44] In the first mechanism, the detonation of the primary explosive is facilitated by a thin electrically heated bridgewire which is in direct contact with the primary. With the electric match system, on the other hand, which is now the most frequently used type in the world, a pyrotechnic component is ignited first.[42] Another very common type, encountered in many military systems (warheads, landmines, grenades) is the stab detonator based on mechanical stimuli where, at first, a very friction- and impact-sensitive mixture is ignited by a firing pin and then the ignition chain is started (Figure 4d).[45]

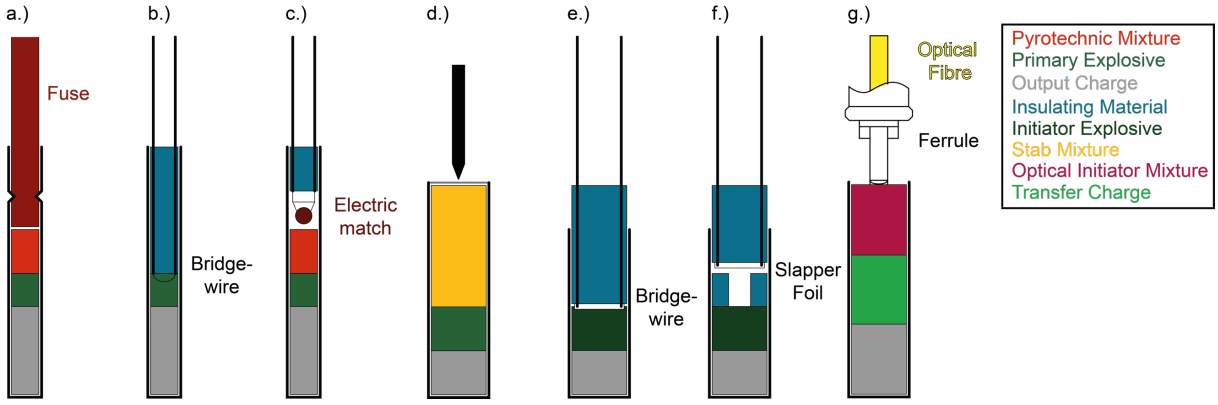


Figure 4. Overview of the main type detonators: a.) flame (fuse); b.) heat (electrecially heated bridgewire); c.) heat (electric match); d.) friction/impact (stab); e.) shock (exploding bridgewire); f.) shock (slapper); g.) optical.

So-called exploding bridge detonators (EBW detonators) are based on the principle of shock wave initiation (Figure 4e).[26] This detonator, well protected from electric fields and found in civilian applications, was originally developed for the fast (microsecond function times) and predictable ignition of nuclear weapons as part of the 1940s Manhattan Project.[46,47] When a high voltage is applied, the electrical resistance causes the wire to heat up so much that it evaporates and finally explodes. This explosion ignites an initiator explosive which is usually the shock-wave-sensitive PETN. Some applications use thin metal foils instead of wires. The second shockwave detonator, an improvement on the EBW detonator, is the so-called slapper detonator, which is currently used in nuclear weapons due to its even greater safety with respect to it disinclination to unintentionally ignite.[26] Instead of using the exploding foil directly to

detonate the initiator explosive, a small circle of insulating material is driven into an additional disc by the electrical evaporation of the foil, at the end of which is a pellet with the initiator explosive. The last increasingly popular method of initiation is the optical ignition by laser. An optical fiber with ferrule transmits a laser pulse directly to the optical initiator explosive (e.g. BNCP with an optical dopant), which in turn ignites the transfer charge (e.g. BNCP and HMX) followed by the output charge (e.g. HMX or TATB). This very attractive method has many advantages over classical systems. The main advantage is the potential use of less sensitive explosives (ideally primary explosive free), which provides greater safety in the synthesis and processing of these initiator materials.[48] In addition, laser ignition systems have shorter function times, better shielding against electrostatic discharge, and greater safety toward accidental initiation by mechanical stimuli.[42]

Lead azide is mainly used as the primary explosive component in detonators and blasting caps, while lead styphnate is predominantly found in priming mixtures (e.g. primer, stab and percussion detonators). Since particle size, morphology, and the presence of additives and coatings can influence the properties of primary explosives which holds true for the other types (secondary explosives, pyrotechnics, propellants), different types of lead azides have been developed since the 1920s.[5] Depending on the application, a rough distinction is made between the following classes: a.) dextrinated lead azide (DLA), b.) service lead azide (SLA), c.) RD1333 and special purpose lead azide (SPLA) and d.) on-demand lead azide (ODLA). Compared to LA, LS is mainly used in priming percussion and stab initiation mixes. Only in special cases, such as the NOL-130 formulation where extreme impact and friction sensitivity are necessary, is lead azide added to the mixture. As already explained, primary explosives are usually part of a kind of initiating device depending on the respective application. The most commonly used include detonators, blasting caps, and primers.

Detonators are often part of a larger ignition apparatus and are used where a strong shock wave is needed to ignite energetic materials (e.g. secondary explosives). Detonators are vital as main components for a variety of military ammunitions such as grenades, mortar grenades, rockets, artillery ammunition, and many more.[5] In addition to the two main types based on the principle of stab (e.g. M55 and M61) and electric ignition (e.g. M100) fuse detonators (e.g. M35, Figure 5) are widely used. A conventional stab detonator, shown in Figure 5, is ignited by a mechanical impulse and usually consists of three separate parts: (i) stab mix; (ii) a transfer charge of RD1333 lead azide, and an (iii) output charge of RDX or HMX. The stab mixture is usually a formulation such as the NOL-130 consisting of basic lead styphnate (40%) and lead azide

(20%) as primary explosives, tetrazene (5%) as sensitizer, barium nitrate (20%) as oxidizer, and antimony trisulfide (15%) as reducing agent and friction agent.[26] During activation of the detonator, the protective layer is perforated by the firing pin and the stab mixture is penetrated. This leads, on the one hand, to friction and, on the other hand, to local heating of the mix at the tip of the pin due to compression.

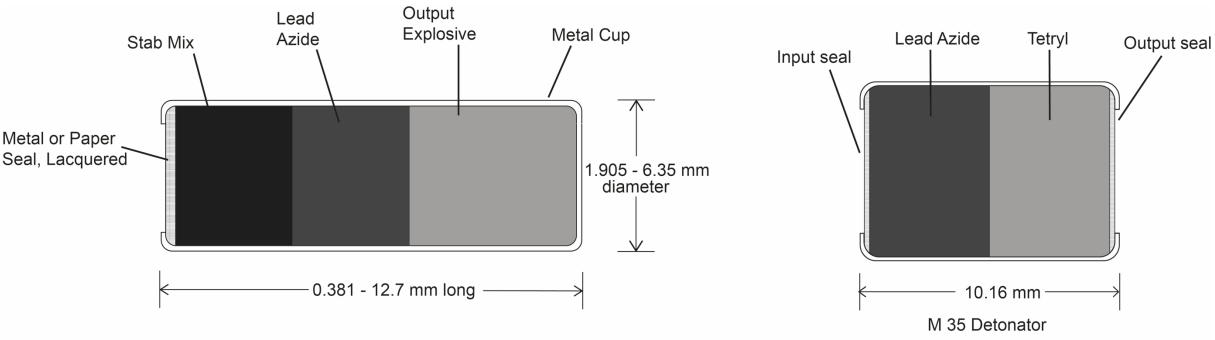


Figure 5. Schematic design of a stab detonator (left) and a typical military flash (fuse) detonator like the M35 (right).[26]

Blasting caps are available in a variety of different types (e.g. electric, non-electric fuse, Figure 5), all of which are very similar in construction to detonators. The main difference is that they are usually larger. Instead of being part of an ignition chain, these are usually used independently to ignite secondary explosives such as plastic explosives and demolition charges.[5] Typically, these blasting caps contain dextrinated lead azide, but lead-free DDNP is also occasionally found.

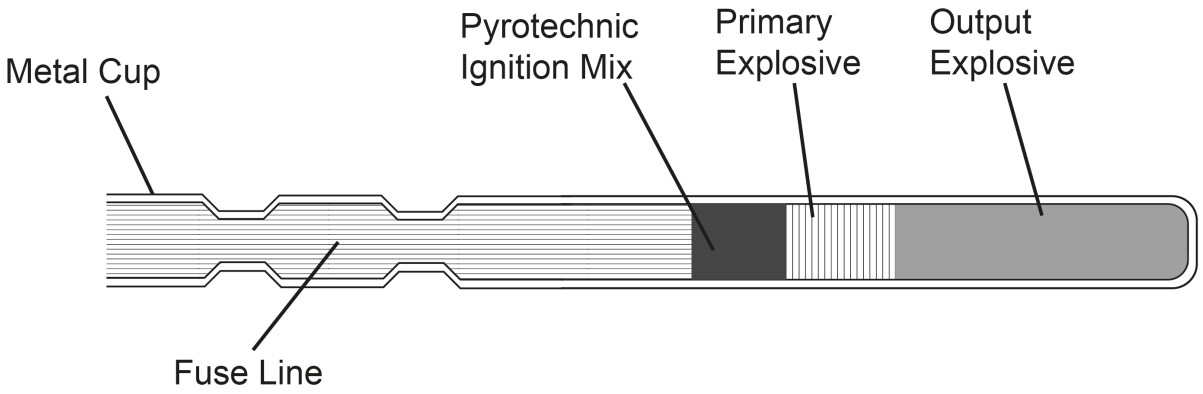


Figure 6. Schematic structure of a commercially available non-electric blasting cap.[26]

About 200 years ago, the percussion lock with a firing pin replaced the earlier flintlock mechanism in guns.[43] Therefore, when firing a bullet, the priming mixture was no longer ignited by a spark, but by the impact of the firing pin. Responsible for this change are **primers**, which have become indispensable nowadays as an integral part of ammunition cartridges

(Figure 7). In particular, percussion primers, where a distinction is made between rimfire and centerfire (Figure 8), are the most common and come in a variety of sizes and configurations depending on the requirements and ammunition size.

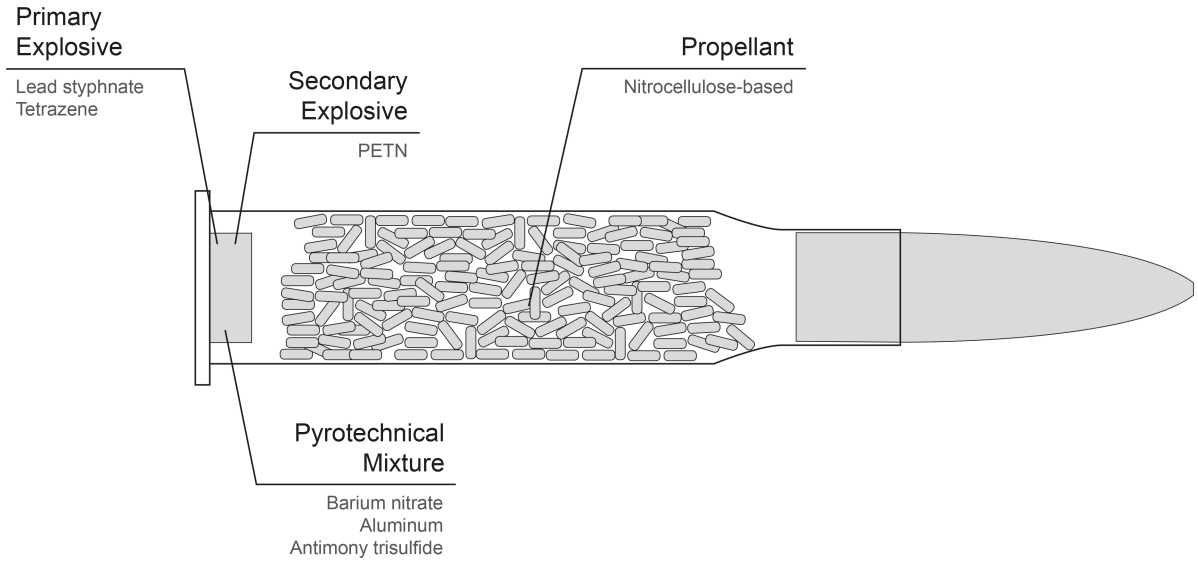


Figure 7. 7.62 mm NATO standard rifle cartridge.

The structure and mechanism of primer design have not changed much until today. The firing pin hits the bottom of the priming cap, which is pressed in and causes friction between it and the bottom of an anvil. The resulting friction ignites the priming mixture. The resulting gases and molten slag ignite the propellant powder, which deflagrates quickly and releases the bullet from the cartridge case.

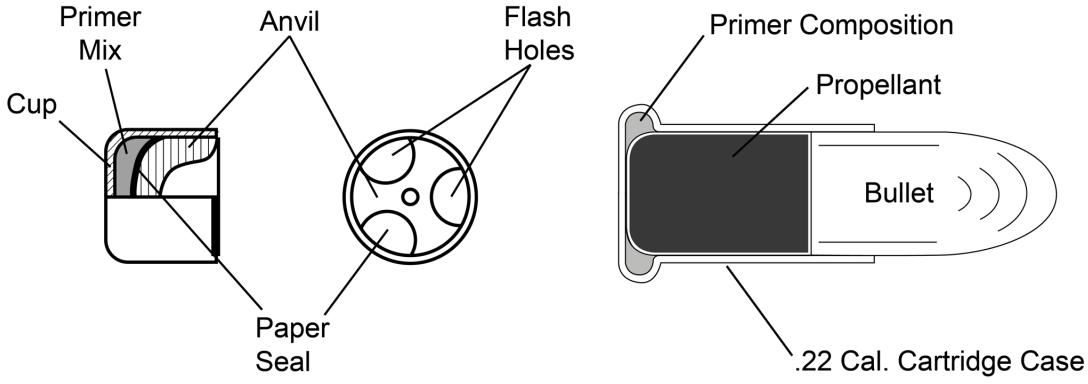


Figure 8. Center fire (left) and rimfire (right) percussion primer.[6]

The priming mixtures are relatively similar to the stab mixture. They are mainly based on lead styphnate and, unlike detonators and blasting caps, are not supposed to generate shock waves but instead generate a large amount of slag-generating heat which ignites the propellant charge without destroying the case.

An overview of various past and current priming mixtures broken down by the five main components can be found in Figure 9.

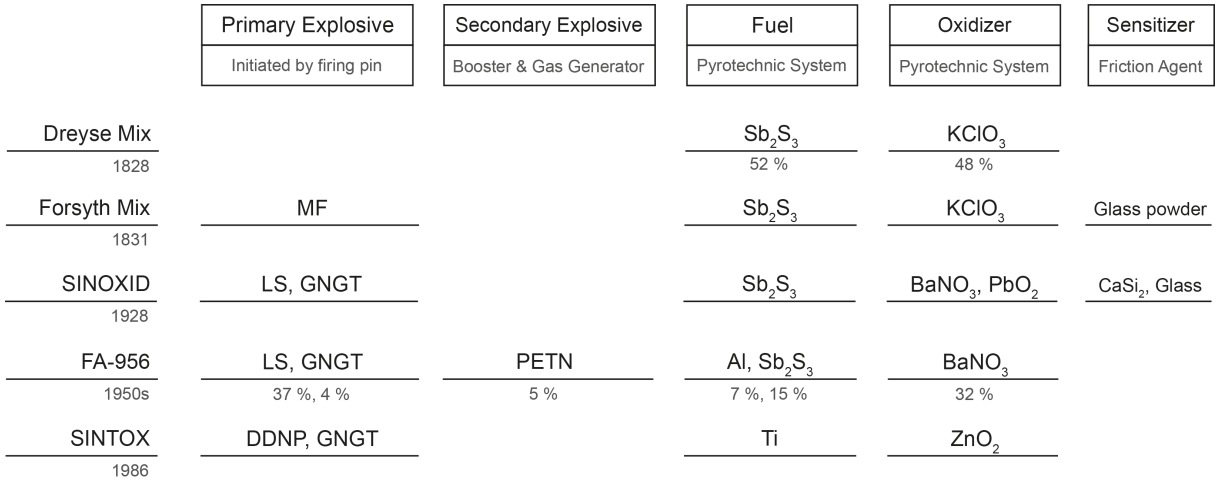


Figure 9. Overview of selected old and new generation priming mixtures.

The first priming mixture based on potassium chlorate was investigated in the early 1800s and led to the invention of the needle-gun by N. Dreyse in 1828.[49] The somewhat less sensitive priming mixture was then doped 1831 by A. J. Forsyth with mercury fulminate as a classical primary explosive and ground glass powder as a sensitizer to increase the friction sensitivity. Mercury fulminate caused health problems and formed undesired amalgams with the upcoming copper and brass priming caps. Furthermore, potassium chlorate caused perceptible corrosion, especially when black powder was replaced with smokeless propellants. From 1898 to 1928, attempts were made to overcome this issue by using lead or copper thiocyanate, mixtures of picric acid, or barium peroxide as replacements.[50] The resulting auspicious and non-corrosive priming composition, SINOXID, was manufactured in Germany by RWS / Dynamit Nobel AG.[9,11] The US company Frankford Arsenal developed a similar priming mixture called FA-956, which can be referred to as a "classical mixture" and is the most popular priming composition today.[51] The subsequently-used primary explosive is lead styphnate, providing a corrosion-free ignition of the applied pyrotechnic mixture, but there are health issues due to its lead content. Furthermore, the usage of lead styphnate is always accompanied by the sensitizer tetrazene, which suffers from storability issues as an auto-catalytic decomposition takes place in a hydrolytic environment or at elevated temperatures.[39] The technology of primer processing has not changed over time, but the requirements regarding environmentally benign and non-toxic substances, especially in the European Union, have. The essential primary explosive lead styphnate appears on the REACH list as a substance of very high concern, leading to the development of novel non-toxic priming mixtures.[36] RWS / Dynamit Nobel AG

tried to accomplish this task with a composition called SINTOX, replacing LS with DDNP. Furthermore, the toxic antimony and barium salts of the pyrotechnic system were also replaced, resulting in a thoroughly "green" mixture. Tetrazene remains as the sensitizer in the priming mixture, but the whole pyrotechnic system, as well as the primary explosive itself, are exchanged with substances of much lower concern.[11] Researchers are currently investigating the application of MIC-based (Metastable Intermolecular Composites, nanothermites) priming mixtures and are also testing encapsulated red phosphorus in primer caps. Interestingly, both attempts cannot meet the sensitivity requirements without being sensitized with the problematic tetrazene.[51] Since the drawbacks of the commonly used non-toxic primary explosives are well-known, there is still an ongoing demand for novel "green" primaries and priming mixtures.

1.4 Laser Ignition and Initiation of Energetic Materials

Each of the initiation systems described above has its drawbacks. Easy initiation through various stimuli (flame, heat, shock, impact/friction, ESD) ensures the reliability of a primary explosive but also increases the risk of accidental ignition during synthesis, transport, and handling of these substances. Not affected by this problem are EBWs and EFIS, which in turn can be susceptible to stray voltages which can damage the electronics of these detonators in the long run.[42] Because of the disadvantages of classical methods, there is still a great need for new, even safer systems. Optical initiation by laser has an extraordinary potential to fill this gap. The application of laser-ignitable explosives, being selectively sensitive to laser irradiation but reasonably insensitive to any other type of external stimuli can be used as insensitive but powerful munitions with reliable and fast detonation to allow much safer handling and to prevent undesired initiation. Other important factors in favor of optical initiation are the shielding against interfering electrical pulses, the extremely short operating times, and the associated higher ignition precision.[42] One of the first ever documented investigations in the field of laser ignition of energetic materials was conducted by Brish *et al.*[52,53] as well as by Menichelli and Yang in the late 60s,[54] whereby the commonly used compounds lead azide, PETN, trinitrophenylmethylnitramine (tetryl), and RDX were successfully initiated. While the first tests were still carried out with the unfavorably large solid-state lasers, current laser ignition tests can now be carried out with diode lasers due to advances in technology.[55] In particular, the compound class of the ECC mentioned above, which are not only excellently suited as lead-free primary explosives, have proven their effectiveness in this context. Research

into laser ignitability began with the cobalt(III) complexes CP and its successor BNCP (Chart 6).[56,57] Notably, a large number of energetic complexes based on different ligands, metals, and partly anions were successfully laser-ignited by Zhilin and Ilyushin in the early 2000s.[58,59] One compound that stood out due to its extremely high laser ignitability was the mercury(II) complex HTMP.[60]

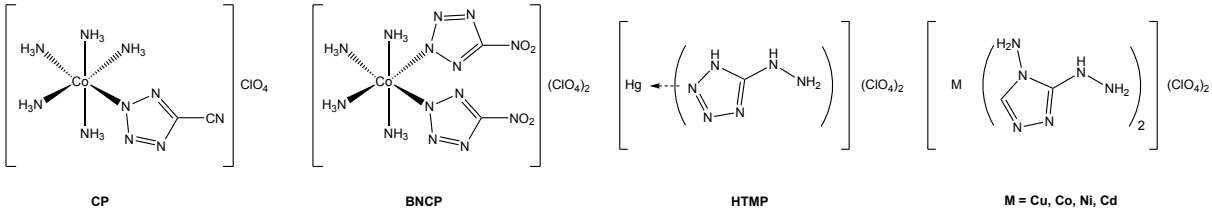


Chart 6. Old generation of laser-ignitable explosives: pentaammine(5-cyano-2*H*-tetrazolato)cobalt(III) perchlorate (**CP**), tetraammine-*cis*-bis-(5-nitro-2*H*-tetrazolato) cobalt(III) perchlorate (**BNCP**), 5-hydrazino-1*H*-tetrazolemercury(II) perchlorate (**HTMP**), 3-hydrazino-4-amino-1,2,4-triazole-based metal(II) perchlorates.

Based on these promising results, several research groups and companies all over the world began to investigate laser-ignitable ECC for future civilian and military applications. In 2005, Talawar *et al.* synthesized nickel(II), copper(II), and zinc(II) analogs to BNCP.[61] Despite the fact that none of these compounds have been evaluated regarding their behavior toward laser irradiation, the sensitivities toward impact and friction, as well as the decomposition temperatures are within the range of BNCP and thus allow an association to their cobalt(III) analogs. In recent years, in particular our research group and Myers *et al.* have been working intensively towards ideal laser-ignitable energetic materials. In 2016, Myers *et al.* focused on several tetrazine complexes containing copper(II) and iron(II) as the respective metal centers (Chart 7).[48,62] The isolated, octahedrally coordinated iron(II) compounds, which consisted of several different tetrazine ligands, showed onset decomposition temperatures of 169–208 °C, and manageable sensitivities toward impact and friction in the range of secondary explosives (IS: 4–12 J, FS: 78–195 N).[48] By rational design of the respective ligand's architecture, the MLCT charge transfer bands of the isolated compounds could be gradually shifted toward the NIR, causing a higher absorption at the Nd:YAG-laser's wavelength (1064 nm). As a result, the new complexes $[Fe(TriTzPyr)_3][ClO_4]_2$ and $[Fe(NH_2TriTzPyr)_3][ClO_4]_2$ could be tailored to the required needs, which could be initiated at an energy density of 4.5 J cm^{-2} (PETN: 6.4 J cm^{-2}). The additionally obtained copper(II) nitrate complexes, which decomposed at temperatures in between 140–228 °C, showed relatively low impact sensitivities (7– >78 J) and were relatively insensitive toward friction (304– > 360 N).[62] Surprisingly, and despite significantly higher

absorption in the NIR in comparison to PETN, none of the investigated copper(II) complexes could be initiated with an Nd:YAG laser at an energy density of 4.5 J cm^{-2}. In addition to these findings, our group obtained several very promising results with regard to laser-sensitive ECC. In 2013, several copper(II) complexes using 5-(1-methylhydrazinyl)-1*H*-tetrazole as ligand and the counterions nitrate, perchlorate, chloride, and dinitramide were synthesized.[63] Most of the compounds received detonated by exposing them to laser irradiation (wavelength: 940 nm, pulse length: 100 µs). The respective chloride complex was not tested, and one complex consisting of non-coordinating nitrate counterions showed no reaction during the laser experiments. The laser-sensitive compounds showed quite high sensitivities (IS: 1–10 J, FS: 5–120 N, ESD: 7–170 mJ) and decomposed in a relatively wide range between 145–217 °C.[63] Subsequent approaches of our group included transition metal(II) complexes with 1,2-bis[5-(1-methylhydrazinyl)tetrazol-1-yl]ethane (bmte; transition metals: Co^{II}, Cu^{II}, Ni^{II}; properties: IS: 1–5 J, FS: 5–30 N, ESD: 15–110 mJ, T_{dec}: 170–239 °C) and 3-amino-1-nitroguanidine (ANQ; transition metals: Ag^{I}, Co^{II}, Cu^{II}; properties: IS: < 1–3 J, FS: < 5–16 N, ESD: 10–500 mJ, T_{dec}: 134–176 °C) as ligands.[64,65] The most promising complexes investigated by our group were probably the 3d metal perchlorate complexes with various alkyl bridged ditetrazoles along with dopants such as carbon black or dyes.[42,66]

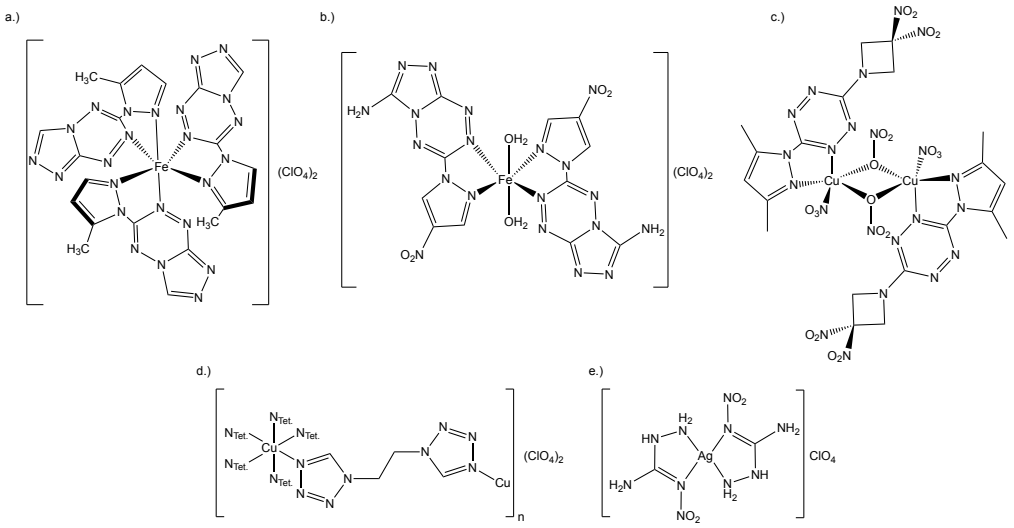


Chart 7. New generation of laser-ignitable explosives: a.) $[Fe(TriTzPyr)_3][ClO_4]_2$, b.) $[Fe(H_2O)_2(H_2NTriTz^{NO_2}Pyr)_2](ClO_4)_2$, c.) $[Cu(\mu\text{-}NO_3)(NO_3)(DNAZTzDMP)_2]$, d.) $[Cu(1,1\text{-}dte)_3](ClO_4)_2$, and e.) $[Ag(ANQ)_2]ClO_4$.

In regard to the large number of promising, laser-ignitable ECC that have been synthesized and characterized in recent years, the question of the specific mechanism of the laser ignition process arises – a topic that has been the subject of controversial discussion. Myers *et al.* for

instance, postulated a direct correlation between the complexes absorption in the NIR and their ability to detonate by laser irradiation.[48] In the course of this investigations in respect to iron(II) tetrazine complexes, the apparent emphasis of the comparatively low sensitivities toward mechanical stimuli indicates the independence of a compound's ability to be initiated by laser irradiation and its mechanical sensitivities. In contrast, subsequent investigation of non-ignitable copper(II) nitrate complexes led to the assumption that the laser initiation process might not depend on NIR-absorption or thermal stability.[62] Despite the indisputably higher absorption of the received complexes than of PETN and their lower thermal stability, none of the copper(II) nitrate complexes detonated upon exposure to laser irradiation. As a result, Myers *et al.* expressed the expectation that generally, nitrate-containing complexes are impossible to initiate via laser beams.[62]

Studies by our group, focusing on transition metal complexes of ANQ, led to similar perceptions regarding the initiation of nitrate complexes and the correlation between the absorption of a compound and its photosensitivity.[65] In addition, the laser ignition process of perchlorate complexes was presumed to be of an electronic nature rather than a thermal one proceeding through a radical mechanism during the initial stages of decomposition.[59] Related research of our group confirmed the supposed initiation mechanism by electron excitation and was even able to synthesize a laser-ignitable copper(II) complex with coordinating nitrate anions.[63] Nevertheless, subsequent investigations again called a thermal initiation mechanism into play, which is allegedly caused by lattice heating in the course of photon absorption of the compound.[64] A conclusive look at the results presented confirms the previously mentioned dividedness in predicting the specific laser initiation mechanism and the subsequent forecasts. For this reason, the following explanations aim at a rather physical and theoretical view taking into account the initiation mechanism of energetic compounds. Scharff *et al.* implemented a series of experimental and computational methods (UV–Vis, evaluation of quantum yields, mass spectrometry, quantum chemical calculations, and dynamic simulations) using the PETN derivative pentaerythritol trinitrate chlorotetrazine (PetrinTzCl) as an example in 2015.[67] The investigations revealed a promising model for understanding the optical initiation process of energetic materials including the photodecomposition of the tetrazine ring by a highly selective two-photon absorption. The latter leads to the excitation of the molecule into mostly unattainable electronic states, followed by an internal conversion of the photon energy to vibrational kinetic energy which finally leads to the decomposition of the molecule.[67] In addition to these results, Kuklja *et al.* carried out measurements with two different lasers (λ_1 = 1060 nm, λ_2 = 530 nm), which led to the observation, that only the 1060 nm laser could ignite

the PETN-sample examined.[68] In accordance with Scharff *et al.*, the initiation mechanism proposed here includes selective photoexcitation of the investigated molecule into an excited triplet state, followed by thermally stimulated dissociation to most likely form active particles like NO_2 radicals. Compared to non-selective initiation modes, this proposed mechanism of a resonance photoinitiation is exceptionally effective, as it dissipates almost all the absorbed energy in the formation of excited states.[68] On the other hand, non-selective initiation modes (e.g. according to the hot spot theory),[3] tend to use the irradiated energy mostly for heating the molecules lattice instead of forming excited states. In summary, Kuklja *et al.* expect the presence of one of these initiation mechanisms (selective resonance or non-selective) to be dependent on the conditions of the experiment– a fact confirmed by Aluker *et al.*.[69] As a result, the non-selective and thus less effective photothermal initiation mode, which has a competitive advantage over the photochemical mechanism, seems to be the more suitable way to initiate energetic materials with low demands on the initiation threshold. Photochemical initiation, on the other hand, requires extensive research to precisely define the ideal initiation parameters of each individual compound but subsequently bears the potential of being carried out at lower thresholds.[8] Finally, it should be mentioned that the initiation process in energetic coordination compounds still requires extensive research to develop credible statements about the influence of the coordination geometry, the ligand, the transition metal, the counterion, and the sensitivity of the respective ECC or its ligands.

The application of optical ignition systems in precision rifles is currently being investigated and has already been made available by VOERE Präzisionstechnik GmbH.[70] An advantage of laser ignition over mechanical ignition is the presence of less vibration and therefore higher precision due to the absence of moving parts that activate the explosive train as soon as the trigger is pulled. In addition, the optical system is claimed to be more resistant to coldness and requires less maintenance. Polycarbonate primers instead of brass are used and the priming mixture is ignited by a laser system integrated into the weapons bolt. The high power (280 W, 240 A) and a relatively long ignition time (> 2500 µs) indicate from the available information that the use of non-corrosive, relatively insensitive ECC would be very well suited to this application.

Reactive armor and active protection systems have played an important role in research and development for decades. The replacement of electric detonators by optical ones is an urgent task and is currently being investigated by several companies (ADS, Dynitec etc.) worldwide.[71] As already described, optical detonators show no losses caused by long wiring, due to the usage of fiber optic cables, and are not affected by the danger of an electromagnetic

pulse (EMP) while maintaining very fast operating times. These companies are already able to ignite BNCP-based formulations with function times of less than 30 µs. Due to the increased sensitivity of BNCP toward various mechanical stimuli, the optical device requires a safety pin to protect the primary explosive from unintentional initiation. In order to remove the requirement for a safety pin in the future, extensive research has been carried out in recent years on laser-ignitable but at the same time less sensitive initiator compounds (sensitivities in the range of booster explosives). Energetic coordination compounds are therefore ideally suited to close this gap with their easily adjustable properties.

The idea of Explosive Reactive Armor (ERA) was initiated by M. Held in 1970 and offers a countermeasure against anti-tank warheads.[72] While passive armor can protect the armored fighting vehicle (AFV) and the crew from regular ballistic threats, they are not impervious to armor-piercing (AP) ammunition, designed for penetrating 300 mm thick of armor steel.[73] The best-known example would be the infamous grenade launcher RPG-7, whose standard warhead PG7 detonates on impact, using the shaped charge effect to penetrate the target (Figure 10). This usually results in a fast-moving jet of the warhead's copper liner, concentrating a high amount of energy in a small area.

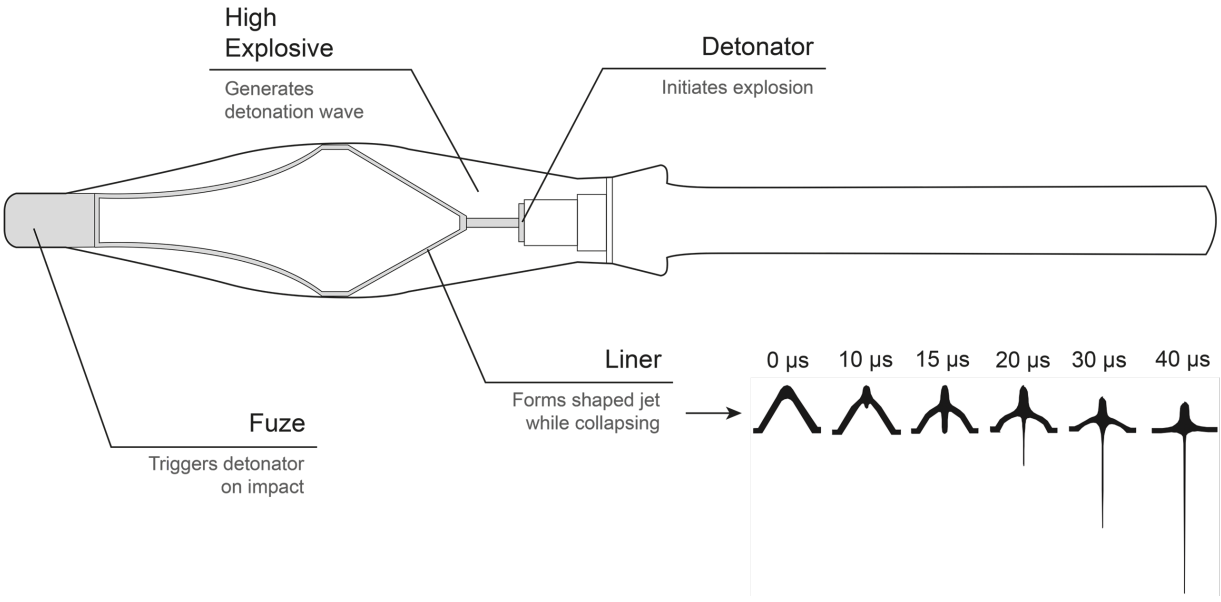


Figure 10. Simplified profile of a PG-7 warhead and the shaped jet formation.

Passive armor has hardly any effect on shape charges, so tests were undertaken with systems based on ERA, which successfully protected against AP ammunition. The first generation of "add-on"-ERA vehicles were equipped with a series of two steel plates (approx. 30 x 30 cm), separated by an explosive layer (Figure 11).

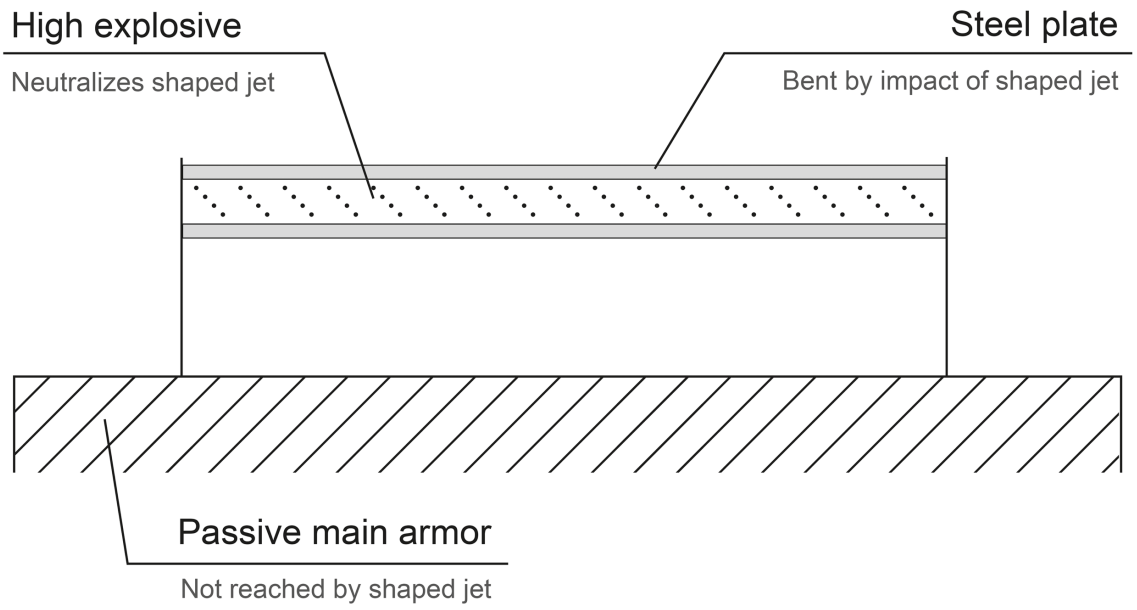


Figure 11. Explosive reactive armor (ERA) cassette on passive main armor.

As soon as the outer steel plate of the ERA sandwich is being penetrated by a shape-charged warhead, the impact of the jet formed compresses and initiates the explosive.[74] As a result, the detonation products and particles defuse the arising jet while disturbing its linearity.[75] Using a RDX-based explosive that intelligently aligns the angles of the plates, it is assumed that the former Soviet Union's ERA was able to minimize the penetration effectiveness of a warhead by up to 98 %. This was possible by expanding the space between the ERA cassette and the passive armoring, maximizing the interaction of material and jet after the explosion, and adjusting the plate thickness.[73–75] The major drawback of such systems is the collateral damage that threatens the infantry. This is reduced by a new generation of Active Protection Systems (APS), called Hard-Kill Defensive Aid Suites (Figure 12). Popular systems called Arena or Trophy have mainly been developed by the former Soviet states and Israel. Their exact functionalities are still highly classified today. These APS are constantly tracking their environment, detecting incoming threats, processing all information, and taking countermeasures if necessary. This can also be achieved by releasing fast-moving fragments or a projectile to intercept the incoming warhead, or preferably, with much less collateral damage, by a directed explosive blast.[73] Assuming that the maximum velocity of a RPG-7 is about 300 m/s, typical response times for a Hard-Kill APS are in the range of 1-2 seconds.[78] Therefore, the application of the much faster and reliable laser ignition as a non-explosive impulse to activate the explosive train is urgently needed and currently under investigation.

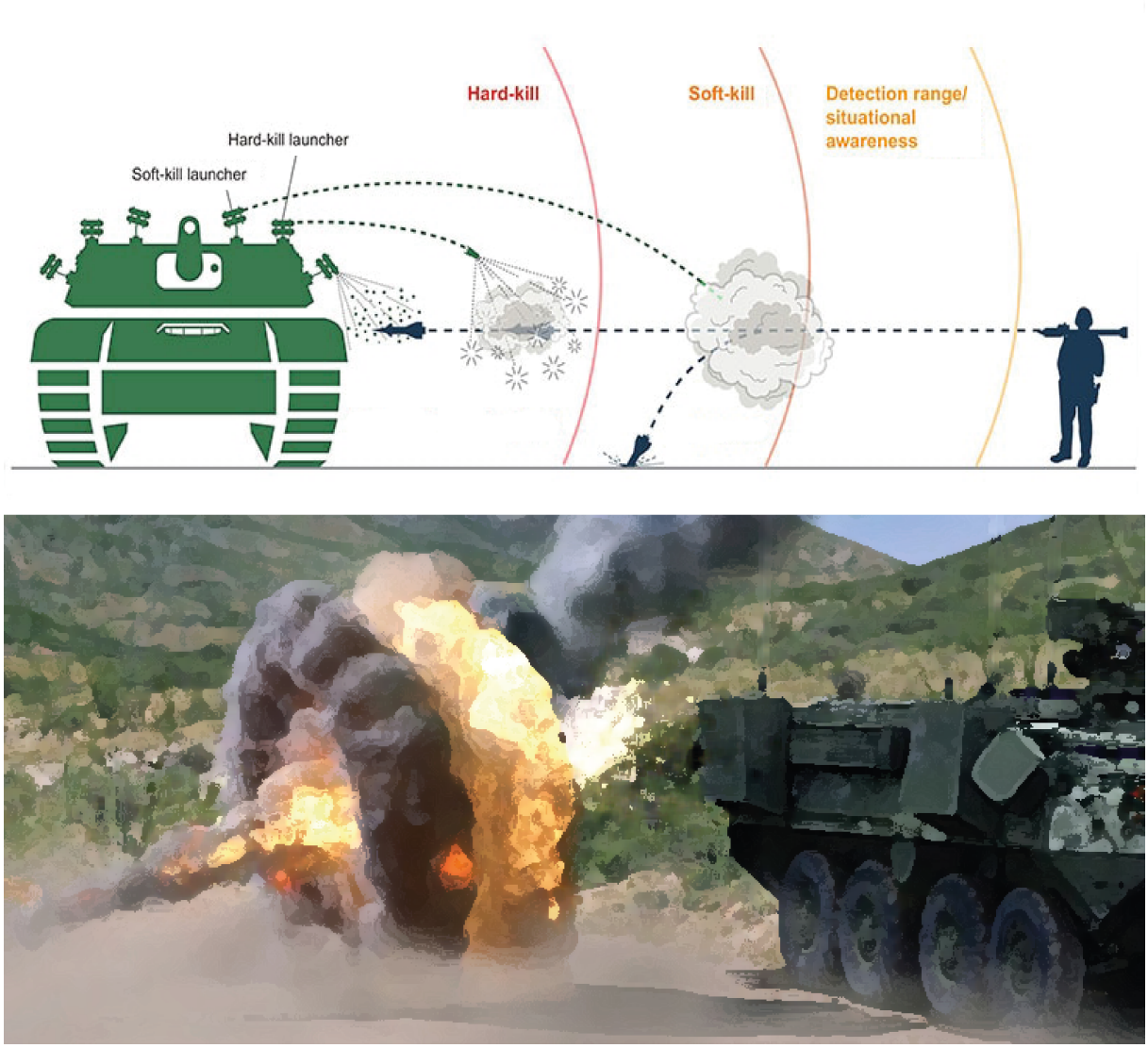


Figure 12. Military active protection systems for vehicles.[76,77]

1.5 Motivation, Concept and Objectives

As the title implies, the goals and motivation of this work were twofold: research into new laser-ignitable materials and the development of new environmentally friendly lead-free primary explosive alternatives. The concept of energetic coordination compounds (ECC) was seen as a possible means of meeting both these objectives. As already shown in various literature reports, this strategy is very well suited to approach and overcome these fundamental challenges.[42,48,58–60,63,79] ECCs usually consist of three building blocks (Figure 13). The first building block is the ligand which mainly functions as a fuel and comes from the family of azoles, chiefly triazoles and tetrazoles. These ligands have a large number of potential coordination sites and possess a

highly endothermic character due to their high nitrogen content and the associated driving force for the formation of molecular nitrogen. The second component is the metal, which, with the exception of silver, mainly comes from the 3d series. The metal center serves as a catalyst, and a matrix that holds all the components together. The last component is the anion, which functions as the oxidizing agent or contributes substantially to the endothermic character of the complex. By variation of the individual building blocks, the chemical and physical properties of the complexes can be tailored to meet the specific requirements. This makes it possible to control various parameters including sensitivity toward mechanical stimuli, thermal stability, performance, solubility, and optical properties like laser ignitibility.

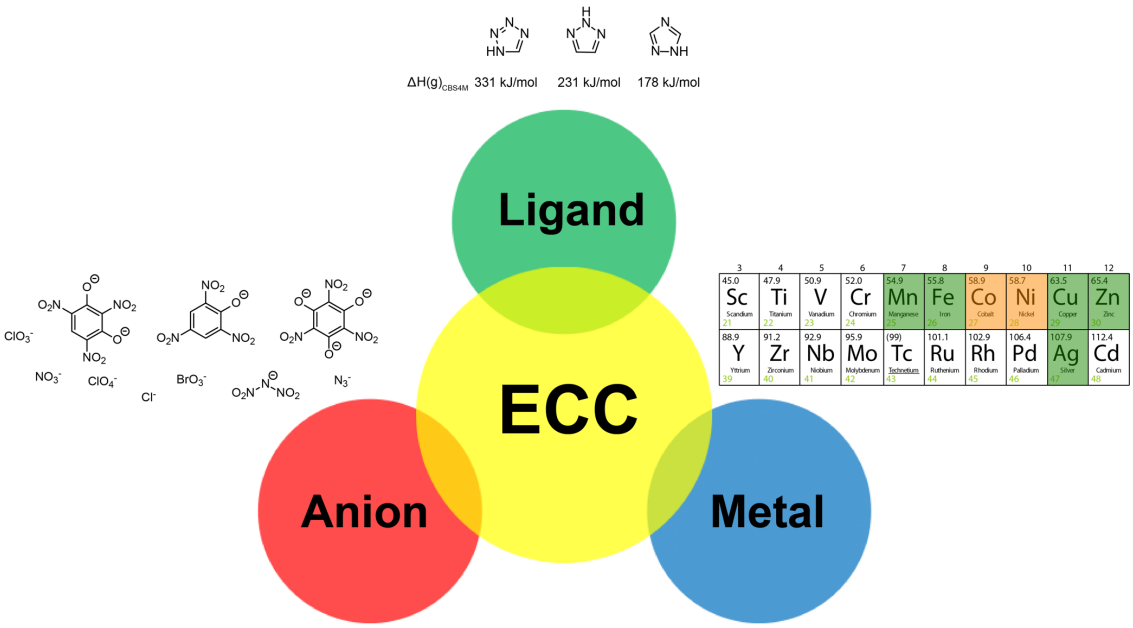


Figure 13. Concept of energetic coordination compounds (ECC).

Based on the influence of the various components, an attempt was made to establish trends and tendencies in the stability and laser ignitability of the complexes. Special attention was paid to the influence of the building blocks on the coordination sphere, which can be significantly modified by altering the respective metal, anions (oxidizing vs. endothermic; bridging ability; dentation; charge; oxophilic character; coordinating vs. non-coordinating), and ligands (bridging ability; acidity; isomers; side chain functionalization, etc.). In the synthesis of the new compounds, all well-known environmentally-friendly aspects and non-toxicities were taken into account. Compounds that do not meet these requirements were synthesized purely out of academic interest for better comparability.

The laser ignition or initiation of energetic materials has been intensively studied in recent years.[42,48,58–60] Nevertheless, the goal of this work was the establishment of a new, faster laser ignition test setup and method (based on a diode laser) as well as the synthesis, characterization, and evaluation of new laser-ignitable materials. In order to identify possible correlations and to gather new information or critical parameters for the laser ignition mechanism, all compounds that could be successfully ignited by laser were additionally analyzed by UV-Vis-NIR spectroscopy. The second focus of this work was placed on the exploration of environmentally benign primary explosives. The majority of the primary explosive-containing applications are still based on the two highly toxic lead compounds LA and LS. Pressure on industry to replace these inexpensive compounds is growing constantly; in particular after both substances were included on the candidate list of substances of very high concern for authorization as part of the REACH registrations and there is a serious risk that both could be banned or restricted.[36] A large number of different criteria must be met for both laser-ignitable compounds and environmentally friendly primary explosives in order to be considered as potential substitutes for these well-established compounds (Figure 14). Ideally, the laser-ignitable compounds should have a short function time, pass the GAP test and meet the requirements and sensitivities of a booster explosive (NATO standard) to replace the currently used BNCP and to increase the safety of the optical primers/detonators.[80] In addition to the ECC concept, efforts were made to address the problem of environmentally-friendly primary explosives with various salts based on the nitraminotetrazole framework; a strategy that has proved to be very promising in the past.[38] In comparison, salts offer many benefits over neutral compounds such as lower sensitivity and higher thermal stability.

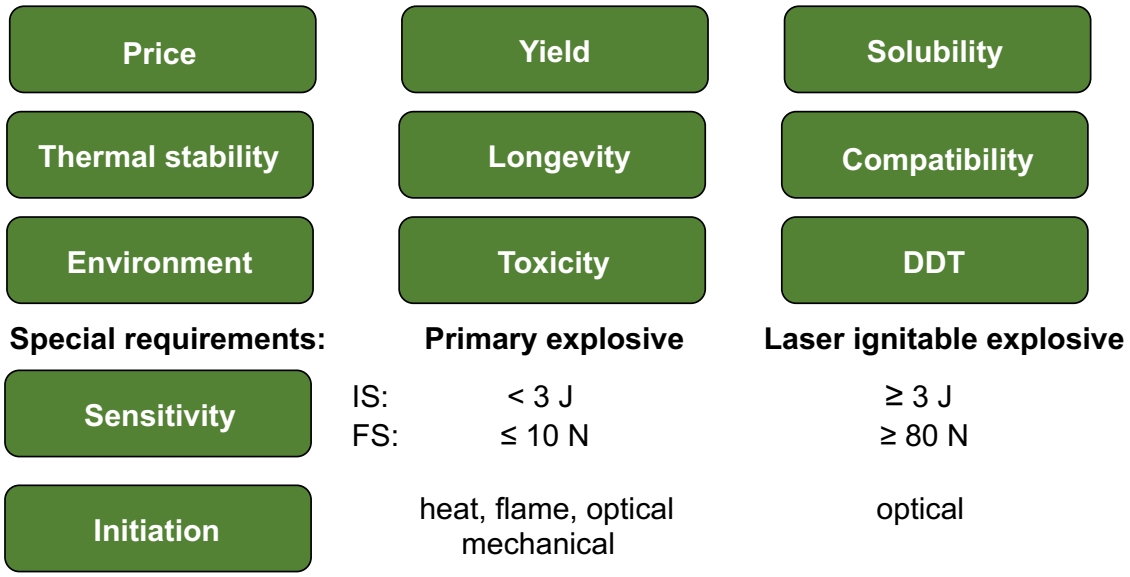


Figure 14. Requirements for new energetic materials depending on the application.

To test the suitability of the newly synthesized primary explosives, several new test methods were established within our working group. These included the initiation capability testing of common secondary explosives in copper shells as well as the testing within the scope of priming mixtures in conventional 7.62 mm primer caps. The primer caps were in turn tested with a firing pin device and a primer ball drop test. In addition to the standard measurement methods, particularly sensitive compounds were tested with the ball drop test. Since both classes of compounds were at their respective sensitivity limits, the majority of the compounds were tested for their suitability as both primary explosives and laser-ignitable materials. Throughout the work, in addition to purely academic basic research, the focus was placed on applicability in industrial processes.

1.6 References

[1] http://www.astm.org/; Accessed June 2018.

[2] J. Akhaven, *The chemistry of explosives*, RSC Paperbacks, Cambridge, **1998**.

[3] T. M. Klapötke, *Chemistry of High-Energy Materials*, 4th ed., Walter De Gruyter, Berlin, Boston, **2017**.

[4] R. Matyás, J. Pachman, *Primary Explosives*, 1st ed., Springer, Heidelberg, New York, Dordrecht, London, **2013**.

[5] T. Brinck, *Green Energetic Materials*, 1st ed., John Wiley & Sons, Chichester, **2014**.

[6] W. Beck, J. Evers, M. Göbel, G. Oehlinger, T. M. Klapötke, *Z. Anorg. Allg. Chem.* **2007**, *633*, 1417–1422.

[7] L. T. Fairhall, W. V. Jenrette, S. W. Jones, E. A. Pritchard, *Public Health Rep.* **1943**, *58*, 607.

[8] D. Gidlow, *Occup. Med.* **2015**, *65*, 348.

[9] U. Brede, R. Hagel, K. H. Redecker, W. Weuter, *Propellants, Explos., Pyrotech.* **1996**, *21*, 113–117.

[10] U. Bley, A. Hoschenko, R. Hagel, P. S. Lechner, Ruag Ammotec GmbH., Germany. **2004**, p. 5 pp.

[11] R. Hagel, K. Redecker, *Propellants, Explos., Pyrotech.* **1986**, *11*, 184–187.

[12] S. Quellen Field, *BOOM! The Chemistry and History of Explosives*, Chicago Review Press Incorporated, Chicago, Illinois, **2017**.

[13] N. V. Latypov, J. Bergman, A. Langlet, U. Wellmar, U. Bemm, *Tetrahedron* **1998**, *54*, 11525–11536.

[14] C. A. McFarland, M. J. Quinn, Jr., M. A. Bazar, L. G. Talent, M. S. Johnson, *Environ. Toxicol. Chem.* **2009**, *28*, 1043–1050.

[15] H. Ek, G. Dave, G. Birgersson, L. Foerlin, *Aquat. Ecosyst. Health Manage.* **2003**, *6*, 415–421.

[16] V. Thottempudi, H. Gao, J. n. M. Shreeve, *J. Am. Chem. Soc.* **2011**, *133*, 6464–6471.

[17] N. Fischer, T. M. Klapötke, D. Piercey, S. Scheutzow, J. Stierstorfer, *Z. Anorg.und Allg. Chem.* **2010**, *636*, 2357–2363.

[18] N. Fischer, K. Karaghiosoff, T. M. Klapötke, J. Stierstorfer, *Z. Anorg.und Allg. Chem.* **2010**, *636*, 735–749.

[19] N. Fischer, D. Fischer, T. M. Klapötke, D. G. Piercey, J. Stierstorfer, *J. Mater. Chem. A* **2012**, *22*, 20418–20422.

[20] N. Fischer, T. M. Klapötke, J. Stierstorfer, *Eur. J. Inorg. Chem.* **2011**, *2011*, 4471–4480.

[21] D. Fischer, J. L. Gottfried, T. M. Klapötke, K. Karaghiosoff, J. Stierstorfer, T. G. Witkowski, *Angew. Chem., Int. Ed.* **2016**, *55*, 16132–16135.

[22] A. R. Katritzky, G. L. Sommen, A. V. Gromova, R. M. Witek, P. J. Steel, R. Damavarapu, *Chem. Heterocycl. Compd.* **2005**, *41*, 111–118.

[23] T. M. Klapötke, T. G. Witkowski, *ChemPlusChem* **2016**, *81*, 357–360.

[24] J. Glück, T. M. Klapötke, T. Küblböck, *New J. Chem.* **2018**, *42*, 10670–10675.

[25] J. Glück, T. M. Klapötke, M. Rusan, J. J. Sabatini, J. Stierstorfer, *Angew. Chem. Int. Ed.* **2017**, *56*, 16507–16509.

[26] P. W. Cooper, *Explosives Engineering*, Wiley-VCH, New York, Chichester, Weinheim, Brisbane, Singapore, Toronto, **1966**.

[27] J. B. Bernadou, *Smokeless Powder, Nitro-Cellulose, and Theory of the Cellulose Molecule*, Triese Publishing, **2017**.

[28] D. Trache, T. M. Klapötke, L. Maiz, M. Abd-Elghany, L. T. DeLuca, *Green Chem.* **2017**, *19*, 4711–4736.

[29] V. Weiser, N. Eisenreich, A. Baier, W. Eckl, *Propellants, Explos., Pyrotech.* **1999**, *24*, 163–167.

[30] T. L. Davis, *The Chemistry of Powder and Explosives*, GSG & Associates, San Pedro CA, **1943**.

[31] National Research Council (U.S.), Committee on Measuring Lead in Critical Populations, *Lead in the Human Environment*, The National Academics Press, Washington D. C, **1980**.

[32] A. T. Grabmann, dissertation, Ludwig-Maximilians Universität München, **2016**.

[33] P. Mühle, dissertation, Ludwig-Maximilians Universität München, **2010**.

[34] A. D. Woolf, R. Goldman, D. C. Bellinger, *Pediatr. Clin. North Am.* **2007**, *54*, 271–294.

[35] National Research Council (U.S.), Committee on Measuring Lead in Critical Populations National Research Council, *Measuring Lead Exposure in Infants, Children, and other Sensitive Populations*, The National Academics Press, Washington D. C, **1993**.

[36] https://echa.europe.eu/candidate-list-table; Accessed June 2018.

[37] J. W. Fronabarger, M. D. Williams, W. B. Sanborn, J. G. Bragg, D. A. Parrish, M. Bichay, *Propellants, Explos., Pyrotech.* **2011**, *36*, 541–550.

[38] D. Fischer, T. M. Klapötke, J. Stierstorfer, *Angew. Chem., Int. Ed.* **2014**, *53*, 8172–8175.

[39] J. W. Fronabarger, M. D. Williams, A. G. Stern, D. A. Parrish, *Cent. Eur. J. Energ. Mater.*, **2016**, *13*, 33–52.

[40] J. J. Sabatini, K. D. Oyler, *Crystals*, **2016**, *6*, 5.

[41] N. Szimhardt, M. H. H. Wurzenberger, A. Beringer, L. J. Daumann, J. Stierstorfer, *J. Mater. Chem. A* **2017**, *5*, 23753–23765.

[42] M. Joas, dissertation, Ludwig-Maximilians Universität München, **2014**.

[43] D. Izsák, dissertation, Ludwig-Maximilians Universität München, **2015**.

[44] http://www.detnet.com/; Accessed July 2018.

[45] N. Mehta, K. Oyler, G. Cheng, A. Shah, J. Marin, K. Yee, *Z. Anorg. Allg. Chem.* **2014**, *640*, 1309–1313.

[46] L. W. Alvarez, *Alvarez: Adventures of a Physicist*, Basic Books, Inc., New York, **1987**.

[47] R. Varosh, *Propellants Explos. Pyrotech.*, **1996**, *21*, 150–154.

[48] T. W. Myers, J. A. Bjorgaard, K. E. Brown, D. E. Chavez, S. K. Hanson, R. J. Scharff, S. Tretiak, J. M. Veauthier, *J. Am. Chem. Soc.*, **2016**, *138*, 4685–4692.

[49] Amtsblatt, Minden, **1828**, 344.

[50] J. Smyth Wallace, *Chemical Analysis of Firearms, Ammunition, and Gunshot Residue*, Vol. 17, CRC Press, **2008**.

[51] C. M. Csernica, in *40th Int. Pyro. Symp.*, Colorado, 114–133.

[52] A. A. Brish, I. A. Galeev, B. N. Zaitsev, E. A. Sbitnev, L. V. Tatarintsev, *Combust. Explo. Shock* **1966**, *2*, 81–82.

[53] A. A. Brish, I. A. Galeev, B. N. Zaitsev, E. A. Sbitnev, L. V. Tatarintsev, *Combust. Explo. Shock* **1966**, *5*, 326–328.

[54] V. J. Menichelli, L. C. Yang, NASA Technical Report 32–1474; Jet Propulsion Lab., California Institute of Tech.; Pasadena, CA, 1970.

[55] E. S. Hafenrichter, B. W. Marshall, K. J. Fleming, *41st Aerospace Sciences Meeting and Exhibit*, Reno, USA, January 6–9, **2003**.

[56] S. C. Kunz, F. J. Salas, *13th International Pyrotechnics Seminar*, Grand Junction, USA, July 11–15, **1988**, 505–532.

[57] J. A. Merson, F. J. Salas, J. G. Harlan, *19th International Pyrotechnics Seminar*, Christchurch, New Zealand, February 21–25, **1994**, 191–206.

[58] A. Y. Zhilin, M. A. Ilyushin, I. V. Tselinksii, A. S. Kozlov, I. S. Lisker, *Russ. J. Appl. Chem.* **2003**, *76*, 572–576.

[59] I. A. Ugryumov, M. A. Ilyushin, I. V. Tselinksii, A. S. Kozlov, *Russ. J. Appl. Chem.* **2003**, *76*, 439–441.

[60] M. A. Ilyushin, I. V. Tselinsii, I. A. Ugryumov, A. Y. Zhilin, A. S. Kozlov, *6th New Trends in Research of Energetic Materials Seminar*, Pardubice, Czech Republic, April 22–24, **2003**, 146–152.

[61] M. B. Talawar, A. P. Agrawal, S. N. Asthana, *J. Hazard Mater.* **2005**, *120*, 25–35.

[62] T. W. Myers, K. E. Brown, D. E. Chavez, R. J. Scharff, J. M. Veauthier, *Eur. J. Inorg. Chem.* **2016**, *2016*, 3178–3183.

[63] M. Joas, T. M. Klapötke, J. Stierstorfer, N. Szimhardt, *Chem. Eur. J.* **2013**, *19*, 9995–10003.

[64] M. Joas, T. M. Klapötke, N. Szimhardt, *Eur. J. Inorg. Chem.* **2014**, *2014*, 493–498.

[65] N. Fischer, M. Joas, T. M. Klapötke, J. Stierstorfer, *Inorg. Chem.* **2013**, *52*, 13791–13802.

[66] M. Joas, U. Deisenroth, IBD Deisenroth Engineering GmbH, Patent Number DE102016120539A1, Germany **2018**, p. 6pp.

[67] M. T. Greenfield, S. D. McGrane, C. A. Bolme, J. A. Bjorgaard, T. R. Nelson, S. Tretiak, R. J. Scharff, *J. Phys. Chem. A* **2015**, *119*, 4846–4855.

[68] E. D. Aluker, A. G. Krechetov, A. Y. Mitrofanov, D. R. Nurmukhametov, M. M. Kuklja, *J. Phys. Chem. C* **2011**, *115*, 6893–6901.

[69] E. D. Aluker, A. S. Zverev, A. G. Krechetov, A. Yu. Mitrofanov, A. O. Terentyeva, A. V. Tupitsyn, *Russ. J. Phys. Ch. B* **2014**, *8*, 687–691.

[70] VOERE, *Projekt Laser Handout*, Kufstein, **2015**.

[71] H. Scholles, R. Schirra, H. Zoellner, *42nd International Pyrotechnics Seminar*, Grand Junction, USA, July 10–15, **2016**, 422–428.

[72] M. Held, Messerschmidt-Bölöw-Blohm GmbH, Patent Number US4368660A, Germany **1980**.

[73] P. J. Hazell, *Armour: Materials, Theory, and Design*, CRC Press, London, New York, **2015**.

[74] M. Held, *Propellants Explos. Pyrotech.* **2004**, *29*, 244–246.

[75] M. Mayseless, *J. Appl. Mech.* **2011**, *78*, 051006-051001-051006-051011.

[76] https://ihsmarkit.com/research-analysis/developments-in-active-protection-system-aps-technologies.html; Accessed July 2018.

[77] https://www.raytheon.com/capabilities/products/aps; Accessed July 2018.

[78] *Tradoc Bulletin 3, Soviet RPG-7 Antitank Grenade Launcher*, U.S. Army Training and Doctrine Command, **1976**.

[79] J.-G. Xu, C. Sun, M.-J. Zhang, B.-W. Liu, X.-Z. Li, J. Lu, S.-H. Wang, F.-K. Zheng, G.-C. Guo, *Chem. Mater.* **2017**, *29*, 9725–9733.

[80] NATO Allied Ordnance Publication 7 – Edition 2, June **2003**.

2 Set-Up

2.1 Laser Ignition Setup

2.1.1 Sample Test Setup

In order to ensure the success of the laser initiation process and to create reproducible conditions, the respective compounds had to be prepared accurately before each experiment. Approximately 15 mg of the carefully pestled complex to be investigated was transferred to a transparent plastic cap (PC), pressed with a pressure force of 1 kN and sealed by a UV-curing adhesive (LUX-TOOLS). To ensure force transmission from the press to the percussion cap (Figure 1), the cap had to be inserted into a purpose-built setup consisting of three metal cylinders and a metal pin.

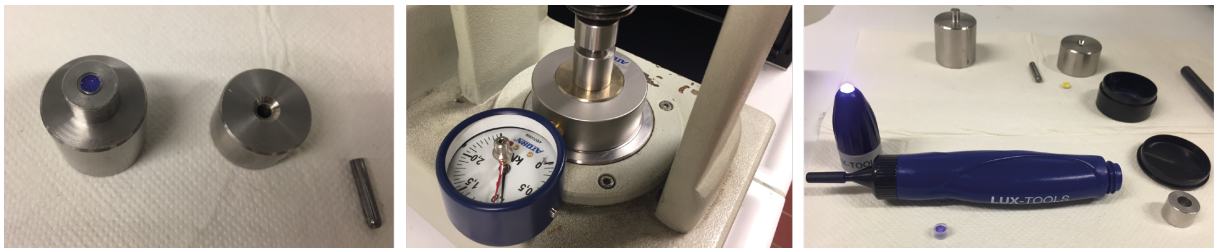


Figure 1. Stepwise preparation of the sample for the laser initiation experiments.

2.1.2 Laser Ignition Test Setup

The laser initiation experiments were performed with a 45 W InGaAs laser diode operating in single-pulsed mode. The operating parameters are summarized in Table 1. The diode was attached to an optical fiber with a core diameter of 400 µm and a cladding diameter of 480 µm. The optical fiber was connected via a SMA type connecter directly to the laser and to a collimator (Figure 2). This collimator was coupled to an optical lens, which was positioned at its focal distance (f = 29.9 mm) from the sample. The lens was shielded from the explosive by a sapphire glass. The confined samples were irradiated at a wavelength of 915 nm, a voltage of 4 V, varying currents of 5 A up to 10 A and pulse lengths of 0.1–15 ms. The combined currents and pulse lengths resulted in an energy output in the range of millijoules.

Table 1. Operating parameters of the laser diode.

Parameter	
Current I [A]	5–10
Voltage U [V]	4
Theoretical maximal output power P_{max} [W]	45
Wavelength λ [nm]	915
Pulse length [ms]	0.1–15
Theoretical energy E_{max} [mJ]	0.15–60

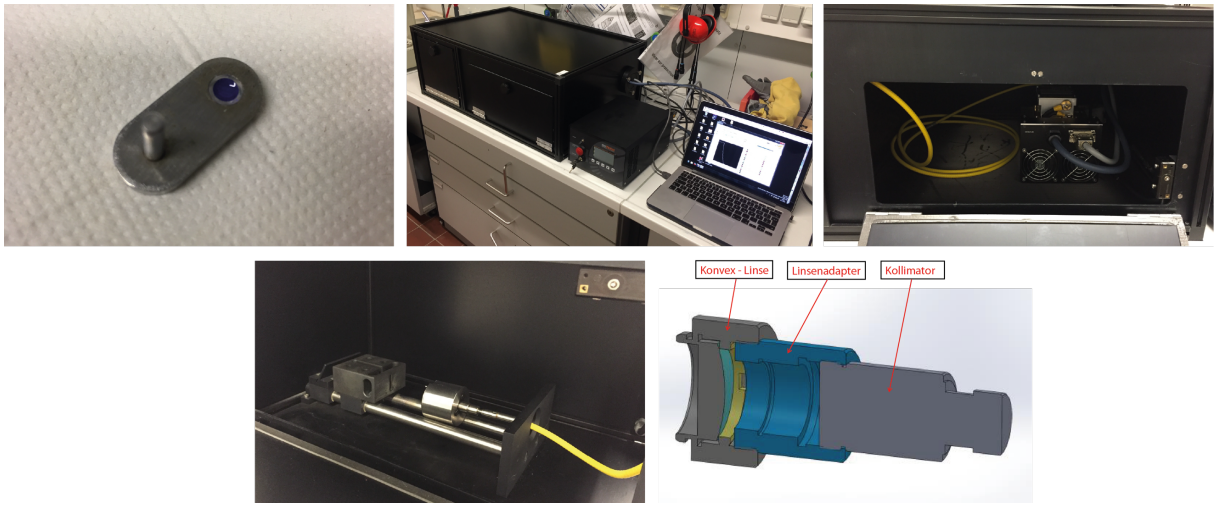


Figure 2. Laser ignition test setup.

2.2 Test Setups for Primary Explosives

2.2.1 Hot Plate and Hot Needle Tests

Hot plate and hot needle tests of the most promising compounds were performed in order to evaluate their initiation capability and suitability as primary explosives (Figure 3/4). The samples were fixed on a copper plate underneath adhesive tape and initiated by a red hot needle. Strong deflagration or detonation of the compound usually indicates a valuable primary explosive. The safe and straightforward hot plate test only showed the behavior of the unconfined sample toward fast heating on a copper plate. It does not necessarily allow any conclusions to be drawn regarding a compound´s suitability as a primary explosive.

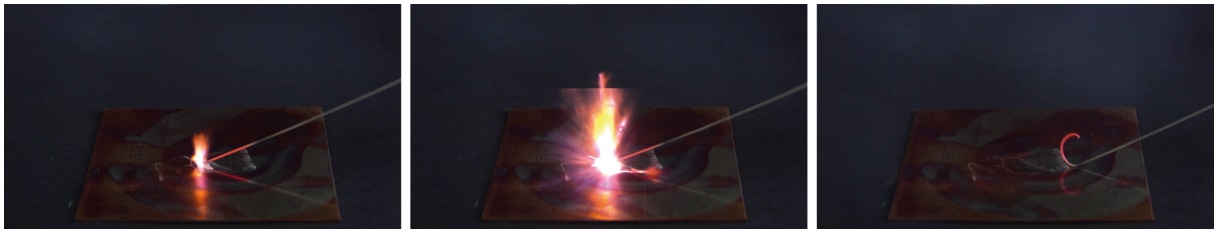


Figure 3. Detonation during the hot needle test of $[Zn(2\text{-}AT)_6](ClO_4)_2 \bullet 2\text{-}AT$ shown as a sequence.

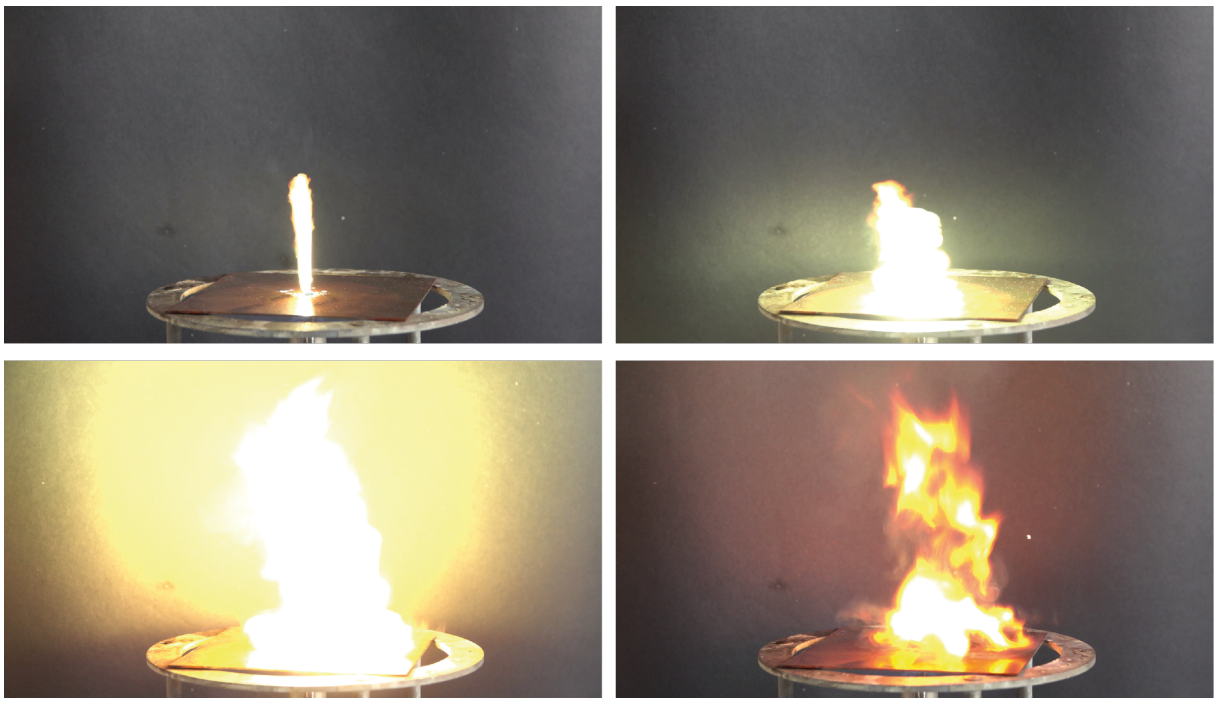


Figure 4. Moment of deflagration during the hot plate test of $[Cu(NO_3)_2(1\text{-}AT)_2]$ shown as a sequence.

2.2.2 Secondary Explosive Initiation Capability Tests

Initiation capability tests (Figure 5) of the newly investigated compounds toward secondary explosives like PETN or RDX were carried out in a copper shell with a diameter of 7 mm and length of 88 mm filled with 200 mg of sieved secondary explosive (grain size < 100 µm). First, the secondary explosive was pressed with a weight of 8 kg, then the primary explosive (5–50 mg) to be investigated was subsequently filled on top of the main charge and pressed with the same pressure force. The shell was sealed by an insulator, placed in a retaining ring, which was soldered to a copper witness plate with a thickness of 1 mm and finally initiated by a type

A electric igniter. A positive test is indicated by a hole in the copper plate and fragmentation of the shell caused by a DDT of the secondary explosive (Figure 6).

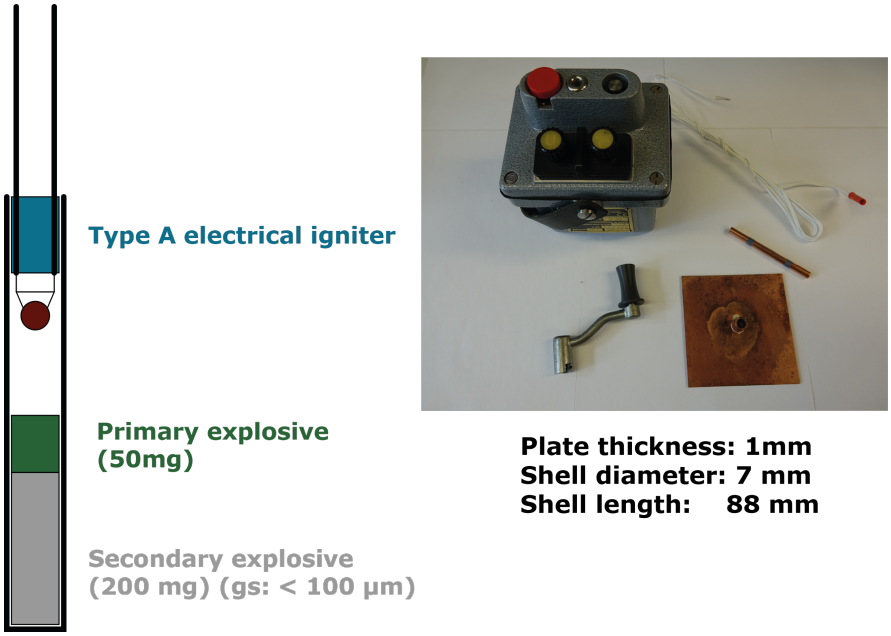


Figure 5. Secondary explosive initiation capability test setup.



Figure 6. Positive PETN initiation test of $[Cu(1\text{-}AT)_6](ClO_4)_2$.

2.2.3 Ball Drop Impact Sensitivity Test

Ball drop impact sensitivities (Figure 7) were determined for selected compounds on an OZM ball drop machine (BIT-132) in accordance with MIL-STD-1751A (method 1016) by dropping a free-falling steel ball onto the explosive compound.[1] A 0.33 mm layer of an approximately 30 mg sample was spread onto a steel block. The steel ball guide was set to the desired height and the loaded impact block positioned underneath. By releasing the ball shield, a 0.50-inch steel ball weighing 8.35 g was allowed to fall onto the sample. Any visual observation of decomposition was regarded as a positive result. If no reaction occurred, the remaining substance was disposed of, and the impact block was loaded with a freshly prepared sample.[2] The impact energy was calculated as the product of the weight of the steel ball and its fall height. The limiting impact energy was determined in conformity with the recommended UN method for testing impact and friction sensitivities (method 1 of 6), according to ST/SG/AC.10/11/Rev.6 (s. 13.4.2.3.3).[3] An initial drop height was chosen, at which an explosion of the sample could be ensured. The impact energy level (ball guide height) was now stepwise decreased until no reaction was observed. At this point, testing was continued up to a total of six trials at this energy level.

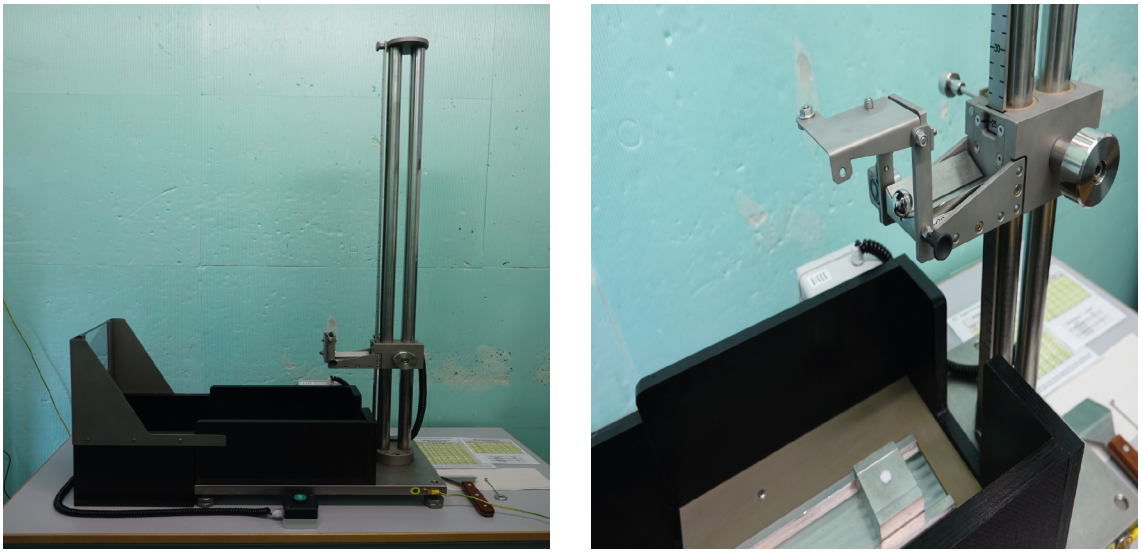


Figure 7. Ball drop impact sensitivity tester.

If an explosion occurred, the procedure was repeated by decreasing the drop height. As soon as six trials at a fixed energy level turned out to be negative, the next higher energy level, where at least one out of at least six trials resulted in an explosion, was determined as the limiting impact energy. The E_{50} impact energy represents the 50 % initiation probability level and was determined by the application of Probit analysis as described by Šelešovský and Pachman.[4]

The probabilities of ignition were calculated at 6 levels of drop height, with 10 trials at each level and transformed into Probit values. The Probit values versus the logarithmic form of impact energies show a linear dependence, which enables a linear regression fit. The regression line was transformed back into the original coordinates (initiation probability vs. impact energy), expressing the whole sensitivity curve. The desired impact energies (E_{50}, all-fire, no-fire) were therefore obtained, as well as the corresponding 95 % confidence intervals according to the linear regression.

2.2.4 Priming Mixtures

The suitability of the newly developed primary explosives was not only investigated as a lead azide substitute in detonators/blasting caps but also as a lead styphnate replacement as part of priming compositions in primer caps. To ensure reproducible results, the inert components of the priming mixtures were passed through a sieve tower with the aid of sieves of various pore sizes before the composition was prepared.

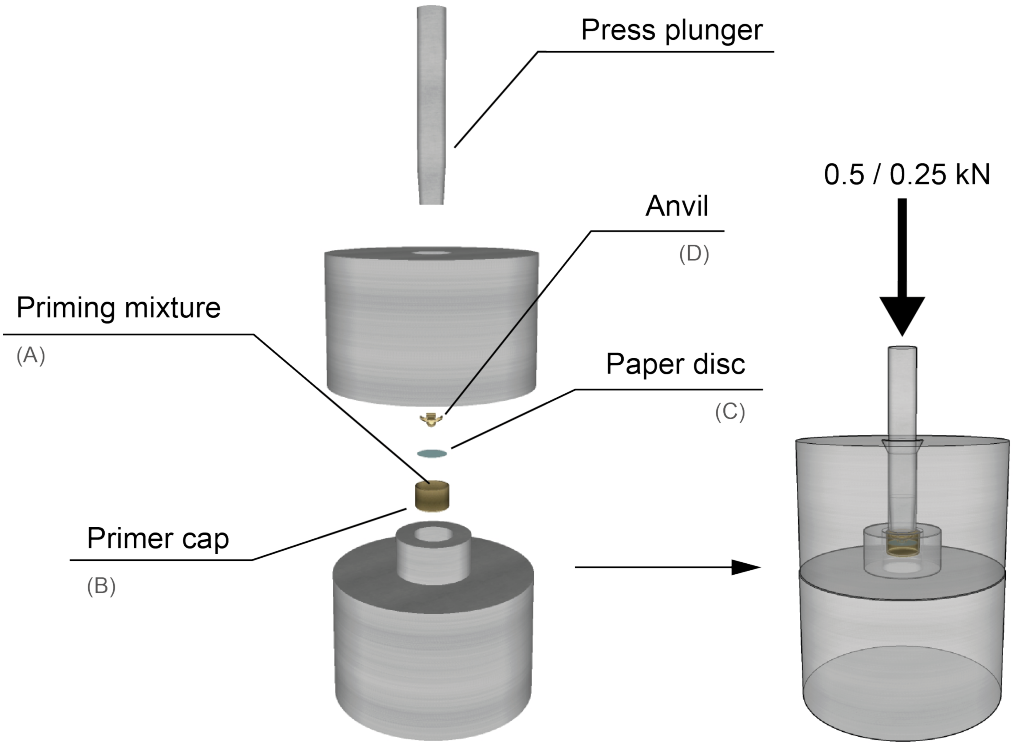


Figure 8. Primer cup processing.

The various components were transferred into a mixing container, weighed and then blended with an overhead mixer for 30 minutes. The commonly used large-rifle (7.62 mm) percussion

primer consists of a brass primer cap (B) and the priming mixture (A) covered by a paper disc (C), which is pressed onto the mixture. Lastly an anvil (D) is pressed on top of the primer (Figure 8). Previous experiments have shown that the optimal priming mixture amount is approximately 23±2 mg. The priming mixture with the paper disc is pressed with a pressure force of 0.5 kN into the cup on which the anvil is pressed with a force of 0.25 kN. The paper disk (C) seals the underlying primer mixture. As soon as the firing pin hits the primer (B), the resulting friction between anvil (D) and the primer bottom ignites the ignition mixture (A). The flame passes through the holes and ignites the propellant (Figure 9), the combustion of which accelerates the projectile by generating thrust.

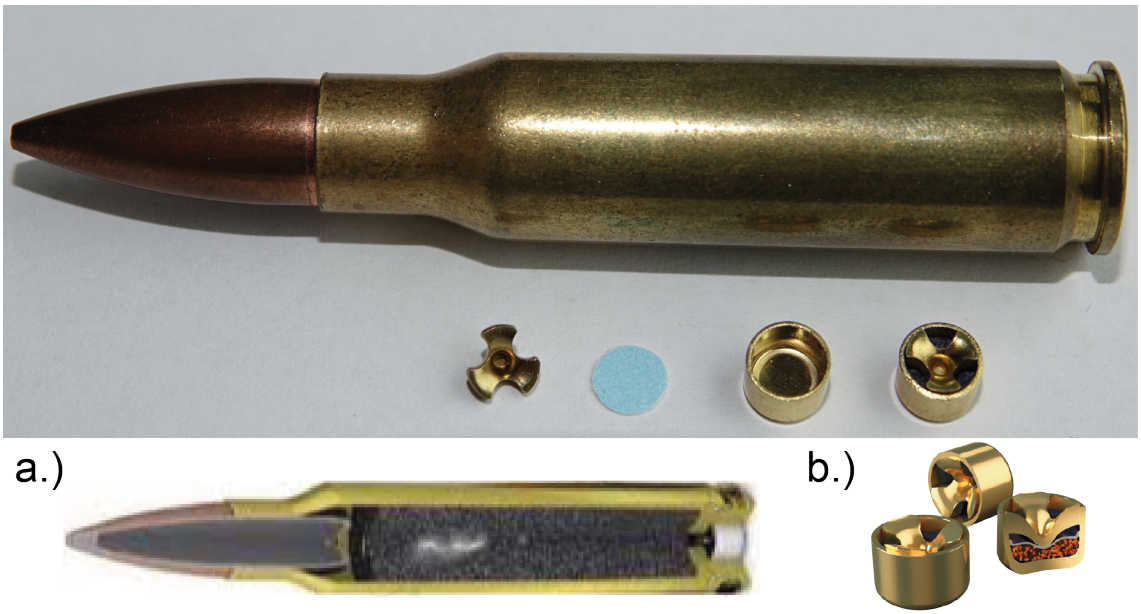


Figure 9. Large rifle (7.62 mm) cartridge components: a.) schematic structure; b.) primer cap.[5,6]

To investigate the flame output, as well as the ignition behavior under realistic conditions, the primer was loaded into a 7.62 mm cartridge shell using a hand primer setting tool. Without propellant and projectile, the primed cartridge was inserted directly into the chamber of the manual cocking unit of a M2 precision rifle built by VOERE (Figure 10). When the trigger was pulled, the firing pin hits the primer with a defined impact energy (610 mJ) causing ignition of the priming mixture. The resulting muzzle flash of a positive test is exemplarily shown in Figure 10.



Figure 10. Manual cocking unit used in the testing procedure.



Figure 11. Muzzle flash of a green priming mixture based on K_2DNABT as primary explosive.

The primer impact sensitivity characteristics were determined by ball drop tests according to NATO requirements (Figure 12).[7] The test ensures that the primers meet the requirements regarding the desired initiation energy range. A processed primer was loaded into the ball drop apparatus and a steel block with a firing pin guide placed above the primer. The firing pin was put into the guide, being in contact with the primer. To perform the test, a steel ball with a specific mass (111.7 g) was dropped onto it, pushing the firing pin into the primer cap (depth: 1.47–1.73 mm). The firing pin thus acts as the percussion impulse and simulates the firing pin of a weapon. The applied impact energy can be adjusted and is calculated as the product of the weight and drop height of the ball. A positive result was achieved by initiation of the priming mixture which could be detected optically or acoustically (Figure 13).



Figure 12. Ball drop impact sensitivity tester for primer caps.

The E_{50} impact energy represents the 50 % initiation probability level and was determined by the application of Bruceton analysis (up-and-down method) with 25–30 trials as described by Dixon and Mood.[8] The impact sensitivity was tested at an initial height. The drop height was increased by a fixed step size if no reaction occurred or decreased if the test result was positive. The less frequent outcome of the entire test set was used to calculate the impact energy E_{50} and the standard deviation. To obtain valid test results, the standard deviation must be within a certain range, depending on the step size. If this criterion is not met, the entire test set must be repeated with an adjusted step size.

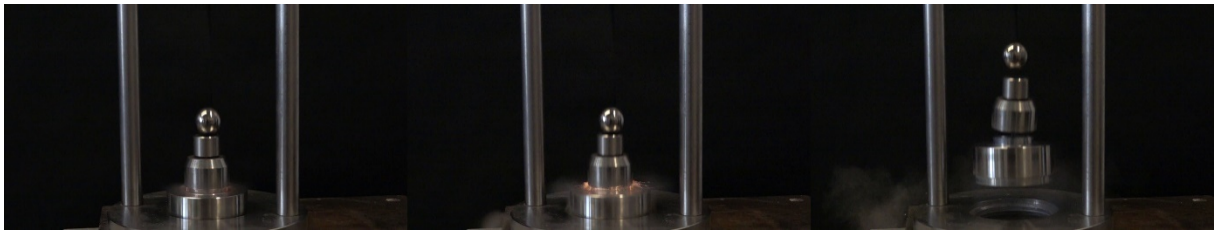


Figure 13. Positive initiation of a primer cap based on a copper(II) azide complex as primary.

2.3 References

[1] Military Standard 1751A (MIL-STD-1751A): safety and performance tests for qualification of explosives (high explosives, propellants and pyrotechnics), method 1016, Dec. 11, 2001.

[2] OZM Research: Ball Drop Impact Test BIT-132, Instruction Manual, Rev. No. 1/17, 2017.

[3] UN Model Regulation: Recommendations on the Transport of Dangerous Goods – Manual of Tests and Criteria, section 13.4.2.3.3, 2015.

[4] J. Šelešovský, J. Pachman, *Cent. Eur. J. Energ. Mater.* **2010**, *7*, 269–278.

[5] www.sellier-bellot.cz/en/product/components/primers/; Accessed July 2018.

[6] www.ruag.com/sites/default/files/media_document/2017-01/RUA0016_Leistungsbroschuere_12s_f2_01_Interactive.pdf; Accessed July 2018.

[7] NATO document PFP(NAAG-LG/3-SG/1)D/(2004)1: Primer Sensitivity Test Procedure, Section 24, 2004.

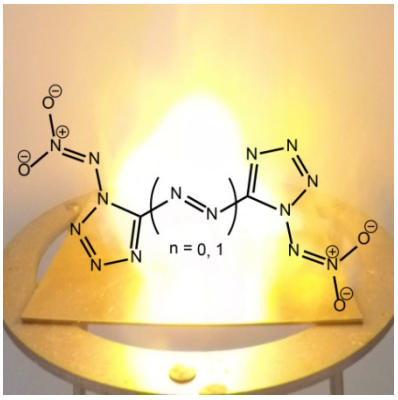
[8] W. J. Dixon, A. M. Mood, *J. Am. Stat. Assoc.* **1948**, *43*, 109-126.

3 1,1’-Nitramino-5,5’-bitetrazoles

Dennis Fischer, Thomas M. Klapötke**,** Jörg Stierstorfer and Norbert Szimhardt

published in *Chemistry A European Journal* **2016**, *22*, 4966–4970

DOI: 10.1002/chem.201600177



1-Nitraminobitetrazoles are a class of very high performing explosive materials with potential application as heavy metal free primary explosives. Even more powerful but also more sensitive are the corresponding 1-nitramino-azobitetrazoles described herein.

Abstract

1,1'-Dinitramino-5,5'-bitetrazole (**1**), and 1,1'-dinitramino-5,5'-azobitetrazole (**2**) were synthesized for the first time. The neutral compounds are extremely sensitive and powerful explosives. Selected nitrogen-rich salts were prepared in order to adjust sensitivity and performance values. The compounds were characterized by low temperature X-ray diffraction, infrared and Raman spectroscopy, multinuclear NMR spectroscopy, elemental analysis, and DTA/DSC. Calculated energetic performances using the EXPLO5 code based on calculated (CBS-4M) heats of formation and X-ray densities support the high energetic performances of the 1,1'-dinitramino-5,5'-bitetrazoles as energetic materials. The sensitivities toward impact, friction and electrostatic discharge were also explored. Most of the compounds show sensitivities in the range of primary explosives and should only be handled with great care!

3.1 Introduction

Modern CHNO explosives consist of a high heat of formation backbone combined with the density enhancing properties of oxidizing building blocks like N-oxides or nitro moieties.[1,2] The introduction of these units into tetrazole chemistry results in the substitution of the acidic protons with hydroxyl or nitramino moieties and is one of the strategies to synthesize highly energetic tetrazole derivatives. Both moieties lead to an increase in explosive performance but only the hydroxyl functionality is decreasing the sensitivity whereas the N-nitramino moiety makes even the anions of the molecules highly sensitive toward impact and friction. A few examples are given in Figure 1.

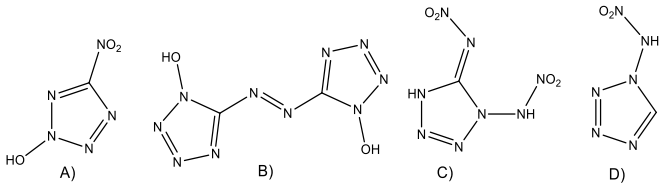


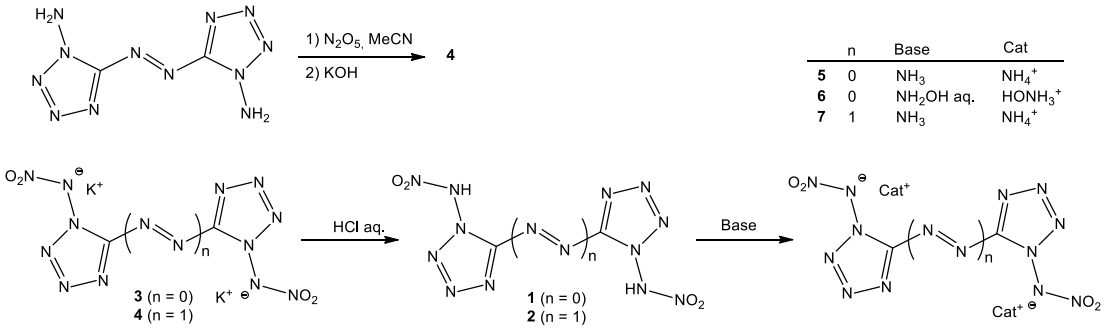
Figure 1. A selection of tetrazoles substituted with hydroxyl or nitramino moieties: A) 2-hydroxy-5-nitrotetrazole,[3] B) 1,1'-dihydroxy-5,5'-azotetrazole,[4] C) 1,5-dinitraminotetrazole,[5] D) 1-nitraminotetrazole.[6]

1-Nitraminotetrazoles are of great interest for the design of heavy metal free primary explosives[7] and other energetic ingredients for which increased sensitivities are desired.

In this contribution 1,1'-dinitramino-5,5'-bitetrazole (**1**) and selected ionic derivatives are presented as consequence of our ongoing research toward 1-nitraminotetrazoles. Furthermore, highly energetic 1,1'-dinitramino-5,5'-azobitetrazole (**2**) was synthesized and its potassium (**4**) and ammonium (**7**) salts were investigated.

3.2 Results and Discussion

The neutral compounds **1** and **2** can be isolated from the potassium salts **3** and **4** by acidification and extraction into organic solvents (ethyl acetate was used here). The synthesis and properties of **3**, which is an outstanding primary explosive has been described recently.[7] Potassium-1,1'-dinitramino-5,5'-azobitetrazolate (**4**) is synthesized by nitration of 1,1'-diamino-5,5'-azobitetrazole[8] and subsequent quenching with KOH. The nitration is carried out with great care in dry acetonitrile below 0 °C with two equivalents of N_2O_5 according to Scheme 1. The addition of the nitrating reagent has to be carried out very slowly since the starting material dissolves not very well in acetonitrile. An excess of nitrating reagent would cause decomposition of the product. Compound **4** is isolated after quenching with aqueous KOH and subsequent filtering of the potassium salt. Salts **5**–**7** derived from **1** and **2** were synthesized by neutralization of the solution of the parent acid with the appropriate base (Scheme 1). Compound **1** was isolated as a solid and characterized whereas compound **2** was only isolated once resulting in a violent detonation



Scheme 1. Synthesis of compounds **1**, **2** as well as **4**–**7**.

3.3 Crystal Structures

During this work the crystal structures of compounds **1** and **4**–**7** were determined by low temperature X-ray diffraction. Selected data of the measurements and the refinements are given in the SI. The crystal structures were deposited in the CSD database.[9]

The parent compound **1**, shown in Figure 2, crystallizes in the monoclinic space group $P2_1/n$ with two molecular moieties in the unit cell. The observed density of 1.967 g cm^{-3} at 173 K is one of the highest ever observed for a CHNO containing tetrazole derivative. Both tetrazole rings are coplanar. The C–C bond length of 1.44 Å is significantly shorter than a typical C–C single bond (1.54 Å). The nitramino group is strongly twisted out of the ring plane (<N2–N1–N5–N6: 111.3°). The nitramine proton is involved in the strong hydrogen bond N5–H5···N3: 0.87(2), 2.16(2), 2.971(2) Å, 155(2)°.

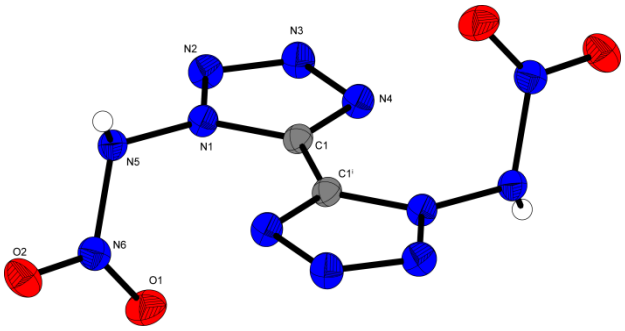


Figure 2. Representation of the molecular unit of 1,1'-dinitramino-5,5'-bitetrazole (**1**), showing the atom-labelling scheme. Thermal ellipsoids for non-hydrogen atoms in all crystal structure plots represent the 50% probability level.

Bis(ammonium) 1,1'-dinitramino-5,5'-bitetrazolate (**5**) crystallizes also in the monoclinic space group $P2_1/c$. The observed density of 1.848 g cm^{-3} (100 K) is lower than that of **1**. However, it is slightly higher compared to ammonium 5,5'-bitetrazolate-dioxide (1.800 g cm^{-3} at 173 K).[10] The nitramino groups again are twisted out from the bitetrazole plane with a torsion angle C1–N1–N5–N6 of 78.5(1)°. Figure 3 shows one molecular anion cation pairing of **5**.

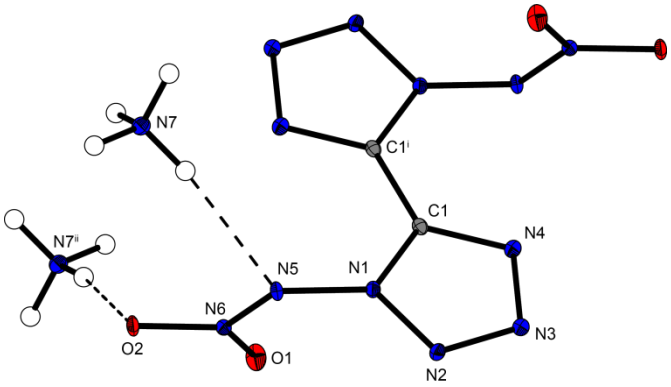


Figure 3. Molecular unit of **5**, showing the atom-labelling scheme. Symmetry codes: (i) 1–x, –y, 1–z (ii) –x, –y, 1–z.

Bis(hydroxylammonium) 1,1'-dinitramino-5,5'-bitetrazolate (**6**) crystallizes also anhydrously from methanol with a slightly higher density of 1.877 g cm^{-3} (173 K) than **6** in the triclinic space group *P*–1. The molecular unit is shown in Figure 4.

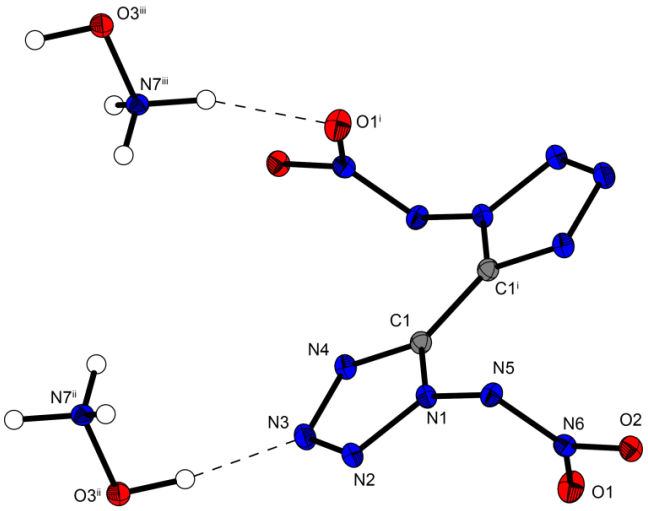


Figure 4. Molecular unit of **6**, showing the atom-labelling scheme. Symmetry codes: (i) –x, 2–y, 1–z (ii) 1–x, 1–y, 1–z (iii) x, 1+y, 1+z.

Dipotassium 1,1'-dinitramino-5,5'-azobitetrazolate (**4**) crystallizes with a density of 2.143 g cm^{-3} at 100 K in the triclinic space group *P*-1 with two molecules in the unit cell. The density is slightly lower than that of potassium 5,5'-azotetrazole-dioxide (2.200 g cm^{-3} at 173 K).[4] Figure 5 illustrates the molecular unit. The two ring planes show a torsion angle of 21.6°. Again the nitramine moieties are twisted out of the ring planes (<C1–N1–N5–N6 = 84.41(3)°, <C2–N9–N13–N14 = 87.27(3)°). The N–N bond lengths of the nitramines are 1.402(8) Å (N1–N5) and 1.395(8) Å (N9–N13).

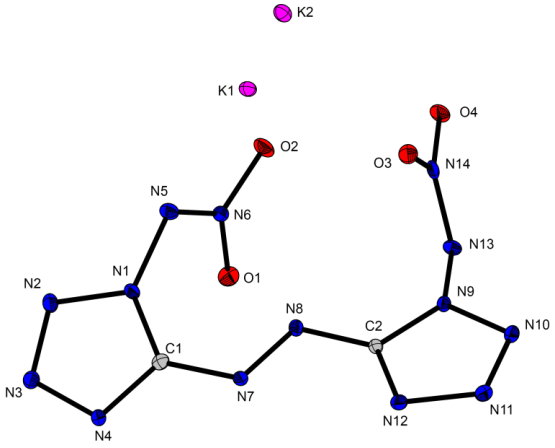


Figure 5. Representation of the molecular unit of **4**, showing the atom-labelling scheme.

The molecular moiety of diammonium 1,1'-dinitramino-5,5'-azobitetrazolate (**7**), which crystallizes in the triclinic space group *P*−1, is depicted in Figure 6. The density of **7** (1.786 g cm^{-3} at 173 K) is smaller than that observed for ammonium salt **5** and also smaller than that of bis(ammonium) 5,5'-azotetrazole-dioxide (1.800 g cm^{-3} at 173 K).[4] The tetrazole rings are not coplanar (<N1–C1–C2–N6: 28.2(2)°). The N=N azo bond has a length of 1.261(2) Å, which is slightly longer than typical N=N double bonds (1.20 Å). In accordance to the structure of **4** both nitramino groups are on one side of the dianion. All protons of the ammonium cations participate in hydrogen bonds.

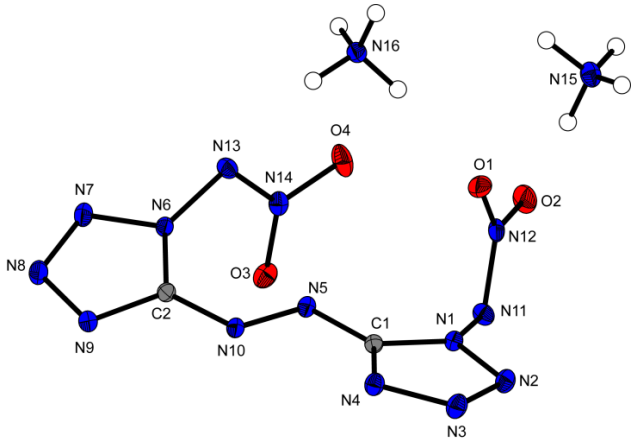


Figure 6. Representation of the molecular unit of **7**, showing the atom-labelling scheme.

3.4 Physicochemical Properties

Since all materials investigated are highly energetic compounds, their physicochemical properties were explored.

3.4.1 Thermal Behavior

The thermal behavior of compound **1** was investigated using DTA (OZM research) showing a violent detonation at 107 °C. Compounds **4**–**8** were investigated on a Linseis PT10 DSC with a heating rate of 5 °C min^{-1} using ~1 mg of material. All 1-nitraminotetrazoles and their salts detonated violently in the DSC, in the case of **4** and **7** with damage to the Pt100 sensor. Compound **2** was too sensitive to measure a DSC curve in a proper way. In general, the salts of 1,1'-dinitramino-5,5'-azobitetrazole are less thermally stable than the ones of 1,1'-dinitramino-5,5'-bitetrazole. Compound **3** decomposes at 200 °C[7] while **4** is only stable up to 180 °C. The same trend occurs with the ammonium salts **5** and **7**. Latter one detonated in the DSC damaging the setup and therefore only a smaller part of the graph could be recorded (Figure 7).

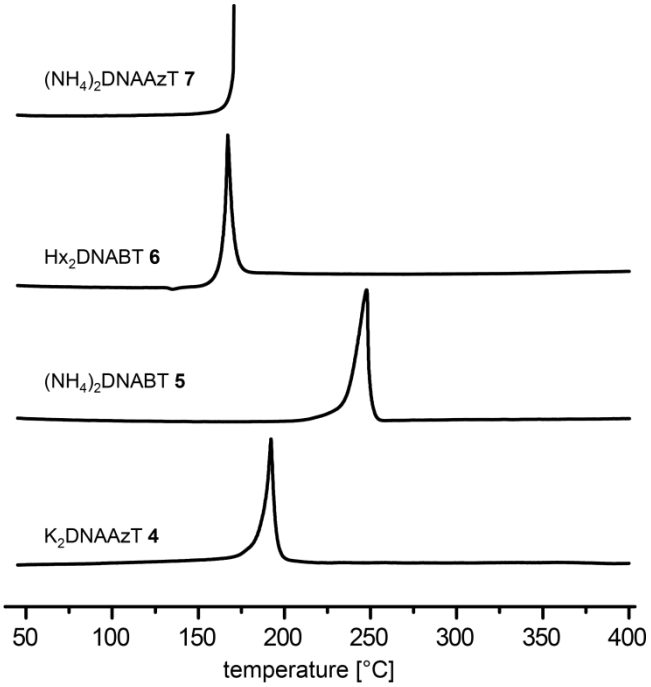


Figure 7. DSC plots of compounds **4**–**7** (exo-up, 5 °C min^{-1}).

3.4.2 Heats of Formation, Sensitivity and Detonation Parameters

The heats of formation were calculated theoretically using the atomization Equation (1) and CBS-4M electronic enthalpies described in the SI. The detonation parameters were calculated with the EXPLO5 6.03 computer code using X-ray densities which were converted to room temperature values according to Equation (2). A coefficient of volume expansion[11] α_v of $1.5 \cdot 10^{-4}$ K^{-1} was used.

$$\Delta_f H°_{(g,M,298)} = H_{(M,298)} - \Sigma H°_{(atoms,298)} + \Sigma \Delta_f H°_{(atoms,298)} \quad (1)$$

$$\rho_{298K} = \rho_T/(1+\alpha_v(298-T_0)) \quad (2)$$

The energetic parameters of compounds **1**, **4**, **5**, **6**, and **7** are summarized in Table 1. All compounds are formed endothermically. The 1-nitraminotetrazoles reach high heat of formations, the highest being 942 kJ mol^{-1} for compound **7**. All compounds are very powerful explosives and also very sensitive. The acids **1** and **2** even exploded during an attempt to gently pick crystals or to measure their sensitivities. Compound **2** was too sensitive for a normal characterization. Looking toward their properties 1-nitraminotetrazoles are typically primary explosives and most of them also detonate in the flame like typical primaries.

Table 1. Energetic performance parameters of **1** as well as **4**–**7**.

	1	**4**	**5**	**6**	**7**
Formula	$C_2H_2N_{12}O_4$	$C_2K_2N_{12}O_4$	$C_2H_8N_{14}O_4$	$C_2H_8N_{14}O_6$	$C_2H_8N_{16}O_4$
***IS*[a] [J]**	< 1	< 1	2	2	< 1
***FS*[b] [N]**	< 5	< 5	< 5	5	< 5
***ESD*[c] [J]**	0.03	0.04	0.2	0.1	0.05
Ω_{CO2}[d] [%]	−6.20	−4.42	−21.90	−9.87	−19.96
$T_{dec.}$[e] [°C]	107	180	210	155	170
ρ[f] [g cm^{-3}]	1.971 (173 K) 1.930 (298 K)	2.143 (100 K) 2.081 (298 K)	1.848 (100 K) 1.795 (298 K)	1.877 (173 K) 1.842 (298 K)	1.786 (173 K) 1.753 (298 K)
$\Delta_f H°$[g] [kJ mol^{-1}]	932.1	625.5	647.7	789.8	941.9
$\Delta_f U°$[h] [kJ kg^{-1}]	3697.1	1788.8	2327.0	2543.3	3050.0
EXPLO5 6.03 values:					
$-\Delta_{ex}H°$[i] [kJ kg^{-1}]	6629	5398	5325	6384	5752
T_{det} [K]	4645	3651	3536	4083	3843
P_{CJ}[j] [kbar]	456	343	361	418	358
V_{det}[k] [m s^{-1}]	10142	8911	9519	9885	9472
V_0[l] [L kg^{-1}]	808	516	908	879	908

[a] Impact sensitivity (BAM drophammer (1 of 6)); [b] Friction sensitivity (BAM friction tester (1 of 6)); [c] Electrostatic discharge device (OZM research); [d] Oxygen balance (Ω = (xO–2yC–1/2zH)M/1600); [e] Start of decomposition temperature from DSC/DTA (β = 5 °C min^{-1}); [f] X-ray density; values for 298 K were recalculated from low temperature X-ray diffraction densities using the formula $\rho_{298K} = \rho_T/(1+\alpha_v(298\text{-}T)$,[13] $\alpha_v = 1.5 \cdot 10^{-4}$ K^{-1}; [g] Calculated enthalpy of formation; [h] Calculated energy of formation; [i] Heat of explosion; [j] Detonation pressure; [k] Detonation velocity; [l] Volume of detonation gases (assuming only gaseous products).

3.5 Conclusions

1,1'-Dinitramino-5,5'-bitetrazole (**1**) was isolated and selected nitrogen-rich salts were synthesized. 1,1'-Dinitramino-5,5'-azobitetrazole (**2**) was synthesized for the first time by the nitration of 1,1'-diamino-5,5'-azobitetrazole and its potassium and ammonium salts were investigated. The synthesis of the 1-nitraminotetrazoles is carried out by nitration of

1-aminotetrazoles or 1-methoxycarbonyl protected 1-aminotetrazoles in dry acetonitrile using N_2O_5 as the nitrating reagent. All 1-nitraminotetrazoles are very powerful and sensitive explosives. They are exclusively in the sensitivity range of primary explosives. The detonation velocity values are calculated with the EXPLO5 V6.03 computer code and found to be all beyond the 9000 m s^{-1} mark for the CHNO compounds. The detonation pressure reaches values beyond 300 kbar and culminate in 456 kbar for compound **1**. The aprotic potassium salts of the 1-nitraminotetrazoles decompose at higher temperatures than their salts with protic cations in general. The salts of **1** are more temperature stable than the salts of **2**. The new compounds were characterized by low temperature X-ray diffraction, NMR, IR, Raman and investigated toward their physicochemical properties using DSC/DTA and BAM standard testing methods.

3.6 Experimental Section

General Procedures

Raman spectra were recorded with a Bruker MultiRAM FT-Raman fitted with a liquid nitrogen cooled germanium detector and a Nd:YAG laser (λ = 1064 nm), infrared spectra were measured with a Perkin–Elmer Spectrum BX-FTIR spectrometer equipped with a Smiths DuraSampl*IR* II ATR device. All spectra were recorded at ambient temperature, the samples were solids. NMR spectra were recorded at 25 °C with a JEOL Eclipse 400 ECX instrument, and chemical shifts were determined with respect to external Me_4Si (^1H, 400.2 MHz; ^{13}C, 100.6 MHz), $MeNO_2$ (^{14}N, 40.7 MHz). Elemental analysis (C/H/N) were performed with an Elementar Vario EL analyzer. Decomposition points were either determined by differential scanning calorimetry (DSC) measurements with a Linseis DSC-PT10, using a heating rate of 5 °C min^{-1} or DTA by using an *OZM Research DTA 552-Ex* instrument with *Meavy 2.1.2* software. Sensitivity data (impact and friction) were performed using a drophammer and friction tester analog to BAM (Bundesanstalt für Materialforschung und Prüfung).[12] The sensitivity toward electrostatic discharge was tested by using an OZM Research electric spark tester ESD 2010 EN.

CAUTION! All investigated compounds are potentially explosive energetic materials. This necessitates additional meticulous safety precautions (earthed equipment, Kevlar® gloves, Kevlar® sleeves, face shield, leather coat, and ear plugs).

1,1'-Dinitramino-5,5'-bitetrazole (1)

Compound **3** (522 mg,1.56 mmol) was dissolved in 60 mL 2 M HCl and extracted six times with ethyl acetate (30 mL each). The combined organic phases were dried over magnesium sulfate and concentrated under reduced pressure without heating, yielding an orange oil. The orange oil was carefully dried under high vacuum affording an ochre colored residue, which was dissolved in a few mL diethyl ether and left to crystallize. Within a few hours, colorless single crystals, which were suitable for X-ray, were obtained in nearly quantitative yield.

DTA (5 °C min^{-1}): 107 °C (dec.); **IR** (atr, cm^{-1}): $\tilde{\nu}$ = 3397 (w), 3092 (m), 3031 (m), 2925 (m), 2854 (m), 2803 (m), 2613 (w), 1712 (w), 1625 (vs), 1460 (w), 1450 (w), 1398 (s), 1316 (s), 1290 (s), 1194 (s), 1116 (s), 1012 (m), 969 (m), 957 (m), 863 (s), 756 (s), 734 (s), 706 (m); **^{1}H NMR** (dmso-d_6, 25 °C, ppm) δ: 5.67; **^{13}C{^{1}H} NMR** (dmso-d_6, 25 °C, ppm) δ: 140.5; **^{14}N NMR** (dmso-d_6, 25 °C, ppm) δ: −5.6 (N6); **^{15}N NMR** (dmso-d_6, 25 °C, ppm) δ: 3.9 (N3), −5.6 (N6), −9.0 (N2), −49.2 (N4), −117.0 (N1), −122.0 (N5); **m/z** (FAB^-): 257.2 [$C_2HN_{12}O_4^-$]; **BAM drophammer**: < 1 J; **friction tester**: < 5 N; **ESD**: 0.03 J.

Dipotassium 1,1'-dinitramino-5,5'-azobitetrazolate (4)

1,1'-diamino-5,5'-azotetrazole[8] (490 mg, 2.5 mmol) was suspended in dry acetonitrile (50 mL). The mixture was cooled on ice and a solution of N_2O_5 (540 mg, 5 mmol) cold acetonitrile (in 30 mL) was added dropwise. The diaminoazotetrazole dissolved and the red color of the product appeared. The reaction was quenched with 7 mL of 2 M KOH. The red precipitate was filtered and dried in air. 550 mg (62 %) of crystalline K_2DNAAzT were obtained.

DSC (5 °C min^{-1}): 180 °C (dec.); **IR** (atr, cm^{-1}): $\tilde{\nu}$ = 1635 (m), 1451 (s), 1434 (s), 1297 (s), 1242 (m), 1226 (w), 1119 (m), 1080 (vs), 1037 (s), 875 (w), 770 (w), 751 (w), 740 (w); **BAM drophammer**: < 1 J; **friction tester**: < 5 N; **ESD**: < 2 mJ.

Diammonium 1,1'-dinitramino-5,5'-bitetrazolate (5)

Compound **3** (1.67 g**,** 5 mmol) was dissolved in HCl (80 mL, 4 M) and extracted four times with ethyl acetate (50 mL). An excess of 2 M NH_3 was added to the organic phase and the mixture was stirred vigorously for 10 min. The aqueous phase was separated and left for crystallization.

Once the remaining liquid between the crystals was getting distinctly viscous a few mL of ice water was added and the crystals were isolated by filtration and washed with little ice water. 850 mg (58 %) of **5** were isolated in the form of colorless, rhombic crystals.

DSC (5 °C min^{-1}): 210 °C (dec.); **IR** (atr, cm^{-1}): $\tilde{\nu}$ = 3187 (w), 3044 (w), 1406 (s), 1369 (m), 1277 (s), 1264 (vs), 1177 (w), 1166 (s), 1124 (m), 1032 (w), 1005 (w), 990 (w), 874 (s), 776 (m); **Raman** (1064 nm, 200 mW, 25 °C, cm^{-1}): $\tilde{\nu}$ = 3134 (2), 1613 (100), 1457 (6), 1279 (30), 1256 (7), 1154 (3), 1085 (19), 1016 (33), 988 (3), 892 (2), 747 (3), 730 (4), 519 (8), 323 (3); **^{1}H NMR** (dmso-d_6, 25 °C, ppm) δ: 7.05; **^{13}C{^{1}H} NMR** (dmso-d_6, 25 °C, ppm) δ: 140.9; **EA** ($C_2H_8N_{14}O_4$, 292.18): calc.: C 8.22, H 2.76, N 67.11 %; found: C 8.85, H 2.71, N 66.62 %; **m/z** (FAB^-): 257 [$C_2HN_{12}O_4^-$]; **BAM drophammer**: 2 J; **friction tester**: < 5 N; **ESD**: 0.2 J.

Dihydroxylammonium 1,1'-dinitramino-5,5'-bitetrazolate (6)

Compound **3** (1.67 g, 5 mmol) was dissolved in HCl (80 mL, 4 M) and extracted four times with 50 mL ethyl acetate. Hydroxylamine (10 mmol, 50% aq.) in water (10 mL) was added and the mixture was stirred vigorously for 10 min. The aqueous phase was separated and left for crystallization. The crystals obtained were put on a filter paper and washed with a minimum amount of EtOH/Et_2O mixture. 939 mg (58 %) of colorless crystals were obtained.

DSC (5 °C min^{-1}): 155 °C (dec.); **IR** (atr, cm^{-1}): $\tilde{\nu}$ = 3073 (w), 2970 (w), 2706 (w), 1617 (w), 1539 (w), 1507 (w), 1369 (s), 1282 (vs), 1268 (s), 1158 (m), 1122 (s), 1011 (m), 870 (m), 816 (w), 778 (m), 723 (w), 712 (w); **Raman** (1064 nm, 200 mW, 25 °C, cm^{-1}): $\tilde{\nu}$ = 3091 (2), 2993 (3), 1613 (100), 1588 (2), 1532 (2), 1460 (5), 1283 (24), 1254 (8), 1149 (7), 1096 (13), 1017 (25), 996 (3), 889 (2), 750 (3), 730 (3), 516 (5); **^{1}H NMR** (dmso-d_6, 25 °C, ppm) δ: 10.02; **^{13}C{^{1}H} NMR** (dmso-d_6, 25 °C, ppm) δ: 141.0; **EA** ($C_2H_8N_{14}O_6$, 324.18): calc.: C 7.41, H 2.49, N 60.49 %; found: C 8.14, H 2.47, N 60.54 %; **BAM drophammer**: 2 J; **friction tester**: 5 N; **ESD**: 0.1 J.

Diammonium 1,1'-dinitramino-5,5'-azobitetrazolate (7)

Compound **4** (905 mg, 2.5 mmol) was dissolved in HCl (30 mL, 4 M) and extracted four times with ethyl acetate (25 mL). An excess of 2 M NH_3 was added to the organic phase and the mixture was stirred vigorously for 5 min. The aqueous phase was separated and left for

crystallization. Once the remaining liquid between the crystals was getting distinctly viscous a few mL of ice water was added and the crystals were isolated by filtration and washed with little ice water. 640 mg (80 %) of **7** were isolated in the form of red crystals.

DSC (5 °C min^{-1}): 170 °C (dec.); **IR** (atr, cm^{-1}): $\tilde{\nu}$ = 3178 (m), 3067 (m), 2853 (w), 1394 (s), 1278 (vs), 1238 (s), 1222 (s), 1154 (w), 1094 (w), 1080 (w), 998 (w), 998 (w), 926 (w), 890 (w), 876 (m), 771 (m), 750 (m), 737 (m), 712 (w), 695 (w), 684 (w); **Raman** (1064 nm, 200 mW, 25 °C, cm^{-1}): $\tilde{\nu}$ = 1490 (2), 1475 (19), 1453 (4), 1429 (100), 1398 (37), 1297 (2), 1244 (39), 1225 (11), 1157 (3), 1095 (30), 1082 (7), 1012 (12), 999 (7), 927 (19), 878 (8), 775 (3), 718 (2), 685 (2), 614 (2), 373 (2), 293 (2); **^{1}H NMR** (dmso-d_6, 25 °C, ppm) δ: 7.07; **^{13}C{^{1}H} NMR** (dmso-d_6, 25 °C, ppm) δ: 157.97; **EA** ($C_2H_8N_{16}O_4$, 320.19): calc.: C 7.50, H 2.52, N 69.99 %; found: C 9.03, H 2.67, N 69.97 %; **BAM drophammer**: < 1 J; **friction tester**: < 5 N; **ESD**: 0.05 J.

Supporting information available in the appendix in **Chapter 19.1** and under:

https://onlinelibrary.wiley.com/action/downloadSupplement?doi=10.1002%2Fchem.201600177&attachmentId=157138355

3.7 References

[1] J. Zhang, J. M. Shreeve, *J. Am. Chem. Soc.*, **2014**, *136*, 4437–4445.

[2] D. E. Chavez, J. C. Bottaro, M. Petrie, D. A. Parrish, *Angew. Chem. Int. Ed.*, **2015**, *54*, 12973–12975.

[3] M. Göbel, K. Karaghiosoff, T. M. Klapötke, D. G. Piercey, J. Stierstorfer, *J. Am. Chem. Soc.,* **2010***, 132,* 17216–17226.

[4] D. Fischer, T. M. Klapötke, D. G. Piercey, J. Stierstorfer, *Chem. Eur. J.* **2013**, *19*, 4602–4613.

[5] a) D. Fischer, T. M. Klapötke, J. Stierstorfer, *Angew. Chem. Int. Ed.* **2015**, *54*, 10299–10302; b) D. Fischer, T. M. Klapötke, J. Stierstorfer, *Angew. Chem.* **2015**, *35*, 10438–10441.

[6] M. A. Ilyushin, A. N. Terpigorev, I. V. Tselinskii, **1999**, *69*, 1645–1657.

[7] a) D. Fischer, T. M. Klapötke, J. Stierstorfer, *Angew. Chem. Int. Ed.* **2014**, *53*, 8172–8175; b) D. Fischer, T. M. Klapötke, J. Stierstorfer, *Angew. Chem*. **2014**, *126*, 8311–8314.

[8] F. Li, X. Cong, Z. Du, C. He, L. Zhao, L. Meng, *New J. Chem*. **2012**, *36*, 1953–1956.

[9] CCDC 1430341 (**1**), 1430338 (**4**), 1430342 (**5**), 1430339 (**6**) and 1430340 (**7**) contain the supplementary crystallographic data for this paper. These data are provided free of charge by The Cambridge Crystallographic Data Centre.

[10] N. Fischer, T. M. Klapoetke, M. Reymann, J. Stierstorfer, *Eur. J. Inorg. Chem.* **2013**, 2167–2180.

[11] C. Xue, J. Sun, B. Kang, Y. Liu, X. Liu, G. Song, Q. Xue, *Propellants, Explos. Pyrotech.* **2010**, *35*, 333–338.

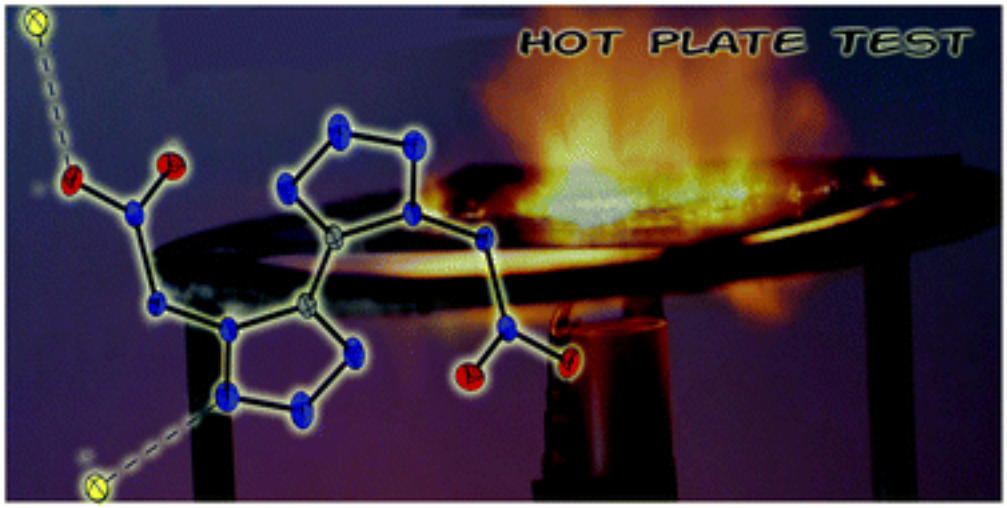
[12] a) Reichel & Partner GmbH, http://www.reichel-partner.de; b) Test methods according to the UN Recommendations on the Transport of Dangerous Goods, Manual of Test and Criteria, fourth revised edition, United Nations Publication, New York and Geneva, 2003, ISBN 92–1-139087–7, Sales No. E.03.VIII.2; 13.4.2 Test 3 a (ii) BAM Fallhammer; c) http://www.bam.de

4 Metal Salts and Complexes of 1,1'-Dinitramino-5,5'-bitetrazole

Norbert Szimhardt, Marc F. Bölter, Maximilian Born, Thomas M. Klapötke, and Jörg Stierstorfer

published in *Dalton Transactions* **2017**, *46,* 5033–5040

DOI: 10.1039/C7DT00536A



The moment of detonation during a hot plate test of highly energetic sodium 1,1'-dinitramino-5,5'-bitetrazolate, the representative of the synthesized alkaline and transition metal salts which are very sensitive toward friction, impact, heat and partly also susceptible to laser irradiation.

Abstract

Potassium 1,1'-dinitramino-5,5'-bitetrazolate is one of the most promising primary explosives which is currently under investigation for different applications. This is due to its high initiation power and the exclusion of heavy metals. To close the gap, the remaining alkali metal salts such as the lithium **6**, sodium **7**, rubidium **8** and cesium **9** salts were synthesized by reaction of the highly soluble ammonium salt **5** with corresponding metal hydroxide solutions. In addition, the highly explosive silver salt **10** as well as several other transition metal(II) amine complexes with nickel(II) **11**, copper(II) **12** and zinc(II) **13** were prepared in a similar manner. The structure of all compounds was determined by X-ray diffraction. The sensitivities toward impact, friction, heat and electrostatic discharge as well as their behavior on laser irradiation of the transition metal complexes was explored.

4.1 Introduction

The research on green energetic materials is still an ongoing project in many research groups worldwide.[1–5] All classes of energetic materials such as explosives, propellants, pyrotechnics contain ingredients or at least decomposition products which are not environmentally benign. Nitrogen-rich derivatives are promising alternatives as energetic materials due to their high heat of formation and the formation of molecular nitrogen as an end product of propulsion or explosion. The most applied primary explosives e.g. in blasting caps are still lead azide and lead styphnate.[6] Lead azide is reliable, cheap, easy to manufacture and shows perfect thermal stability. However they are listed by REACH regulations as "substances of very high concern" and are banned for future applications.[7] Alternatives are strongly needed. In 2015, the dipotassium salt of 1,1'-dinitramino-5,5'-tetrazole (K_2DNABT) gained worldwide interest as a new and promising primary explosive.[8] It showed an extremely short DDT (deflagration to detonation transition)[6] and also high sensitivities toward stimuli such as friction, impact and electrostatic discharge which is desirable for compounds used in initiators. In preliminary tests it showed almost no toxicity in aquatic media (toward the bacteria *Vibrio fischeri*) which makes it to an outstanding candidate for replacement of toxic lead azide. The search for alternatives for lead azide is an ongoing topic to many research groups or companies worldwide.[9] Mostly metal salts of acidic energetic organic molecules were described since they often show higher decomposition temperatures than pure organic salts or the corresponding organic acid.

Examples are KDNP (potassium 4,6-dinitro-7-hydroxybenzofuroxan)[10] or DBX-1 (copper(I) 5-nitrotetrazolate) (Figure 1).[11]

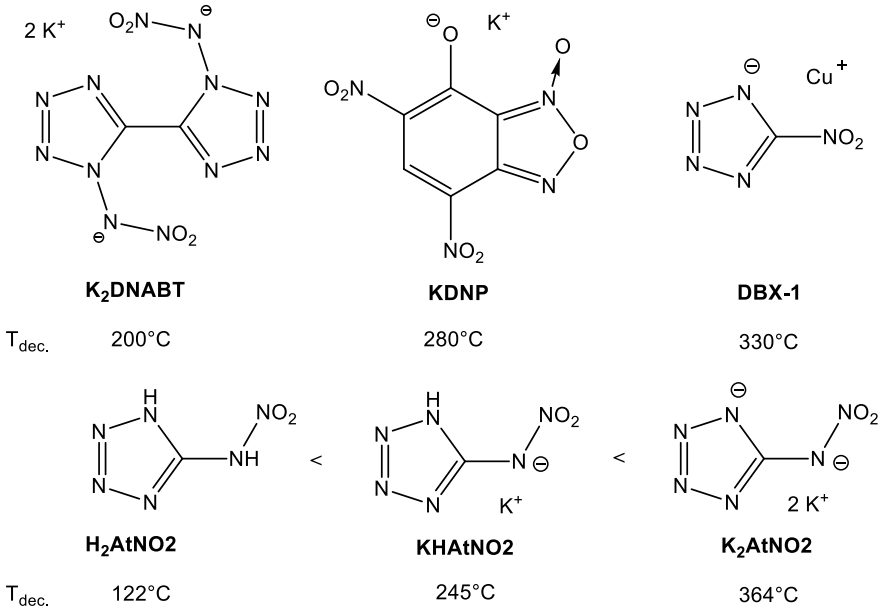


Figure 1. Structural formula of K_2DNABT, KDNP, DBX-1, 5-nitriminotetrazole (H_2AtNO2) and its mono- ($KHAtNO_2$) and di-potassium (K_2AtNO2) salts. Temperatures of decomposition were taken from different references and measured at variable heating rates and methods.

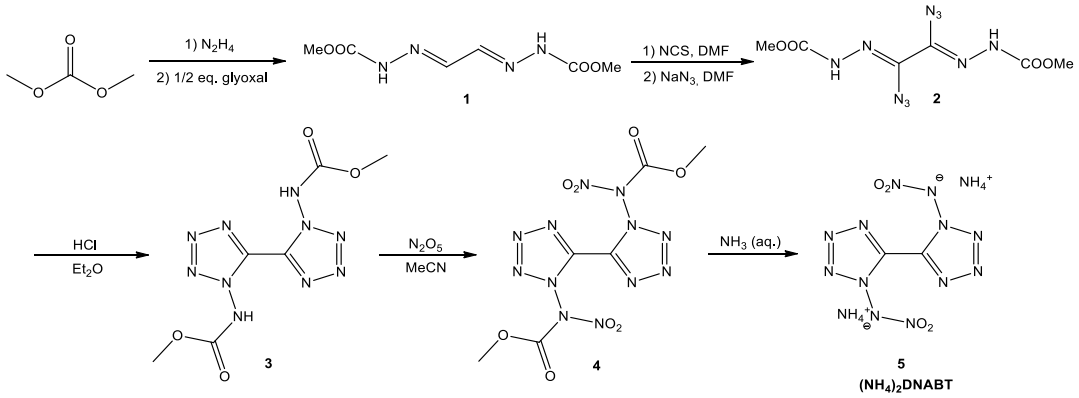
The same trend can be observed for metal free salts of 1,1'-dinitramino-5,5'-nitetrazole such as the ammonium or hydrazinium bitetrazolate salts.[12] They are extremely powerful energetic materials with outstanding detonation velocities, however their high sensitivities and low thermal stabilities will probably prevent any application as secondary explosives.[12] An exceptional high thermal resistance of 223 °C was only found for 4,4',5,5'-tetraamino-3,3'-bi-1,2,4-triazolium 1,1'-dinitramino-5,5'-bitetrazolate.[13] Low thermal stabilities were observed for a huge number of metal-free 1- and 5-nitraminotetrazoles.[1c] The trend of increasing thermal stability by deprotonation and introduction of metal cations can impressively be seen on the following examples: 5-nitrimino-1,4-*H*-tetrazole (H_2AtNO_2, $T_{dec.}$: 122 °C)[14] < potassium 5-nitrimino-1*H*-tetrazolate ($KHAtNO_2$, $T_{dec.}$: 245 °C)[14] < dipotassium 5-nitriminotetrazolate (K_2AtNO_2, $T_{dec.}$: 364 °C).[15] Consequently, in this paper the synthesis and characterization of a large variety of highly energetic (alkali, earth alkali and transition) metal 1,1'-dinitramino-5,5'-bitetrazolates is presented.

4.2 Results and Discussion

4.2.1 Synthesis

Warning (!): Synthesized compounds **5**–**13** (especially **8**–**10**) are extremely powerful and sensitive compounds. Unintentional explosions of **8** and **10** happened during handling. Protective measures are mandatory.

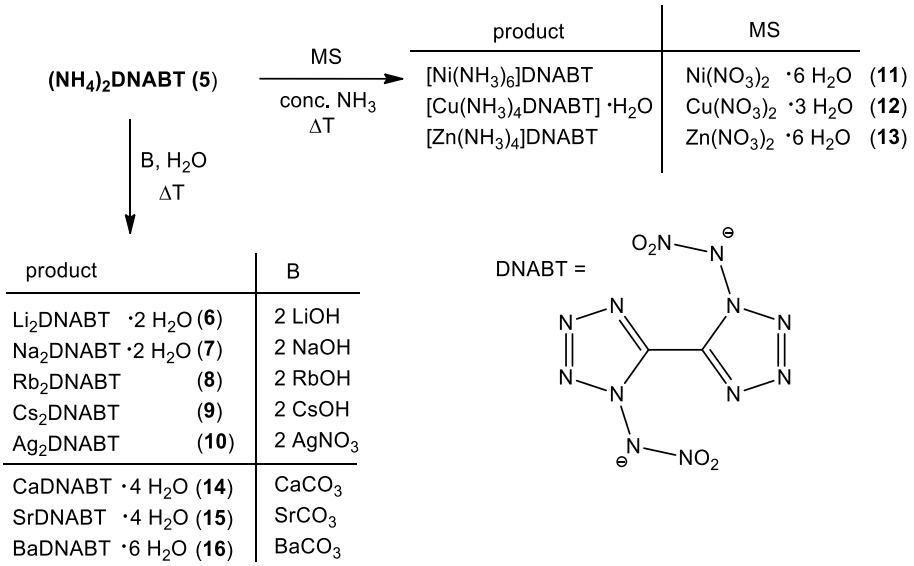
All metal salts were synthesized starting from diammonium 1,1'-dinitramino-5,5'-bitetrazolate (**5**) as precursor.[12] Compound **5** was prepared slightly different in comparison to our previous method illustrated in Scheme 1. During the synthesis of the 1,1'-dinitramino-5,5'-bitetrazolate dianion the diazido compound **3** could be crystallized and the structure determined. Also, the nitrated bitetrazole **4**, which is highly energetic but rather unstable, could be isolated and characterized.



Scheme 1. New synthetic route to compound **5**.

The ammonium salt **5** shows a high solubility in water or concentrated ammonia and was therefore very well suited as starting material. The metal salts/complexes were prepared in straightforward ionic metathesis reactions by combining solutions of compound **5** and metal salts in the corresponding solvent (Scheme 2). Very careful heating of the reaction mixture is required to ensure a complete acid-base reaction. The alkaline earth metal salts **14**–**16** could only be synthesized insufficiently. In contrast to expectations compounds **14**–**16** are highly soluble in water. These solutions could not be stored by exposure to air because of the intake of carbon dioxide which led to the precipitation of Ca- Sr- and $BaCO_3$ again. Therefore **14**–**16** could not be purified in larger quantities. Solely the crystal structures of **15** as tetrahydrate and **16** as hexahydrate could be determined which are shown in the SI. A practical elemental analysis of **14** confirmed the inclusion of four crystal water molecules. In contrast the water-

free alkaline salts K_2DNABT, **8** and **9** as well as the silver salt are hardly soluble in water. The rubidium **8** and cesium salt **9** started to precipitate right after addition of the metal(I) hydroxide solution. In case of **9** a very fast precipitation led to a violent detonation of the reaction mixture and should be avoided. Recrystallization from hot water afforded single crystals suitable for X-ray diffraction. Single crystals of **6**–**9** and **11**–**13** were grown directly from the corresponding reaction media. Two drops of concentrated ammonia were added in order to better the solubility of the silver salt **10**. Single crystals could be isolated from the mother liquor and transferred into perfluorinated oil for XRD. All attempts to dry the silver salt for further characterization failed and led to detonation of the compound! The sodium salt was obtained in two different polymorphs (**7a** and **7b**) with varying physicochemical properties depending on the solvent. H_2O afforded monoclinic **7a**, recrystallization of the compound from EtOH yielded orthorhombic **7b**.



Scheme 2. Synthesis of **6**–**16** based on ionic metathesis reactions.

4.2.2 Crystal Structures

The structures of **2**, **6**–**13** as well as **15** and **16** were determined by low temperature crystal X-ray diffraction. Details on the measurements and refinements are given in the SI. The crystal structures were deposited in the CSD database[16] and can be obtained free of charge with the CCDC Nos. 1502966 (**2**), 1500005 (**6**), 1500002 (**7a**), 1500003 (**7b**), 1500001 (**8**), 1500004 (**9**), 1502967 (**10**), 1510458 (**11**), 1502968 (**12**), 1510459 (**13**), 1524647 (**15**) and 1524646 (**16**).

Azide **2** crystallizes in the form of red rods in the triclinic space group *P*−1 with one formula unit per unit cell and a calculated density of 1.584 g cm^{-3} at 173 K. The molecular unit consists of two asymmetric moieties with a centre of inversion on the C1–C1^{i} bond and is illustrated in Figure 2. The molecule shows an obvious conjugation of the π-electrons and is almost planar. Only the azide chains are marginally twisted out of the plane. All bond lengths in the chain from oxygen atom O2 to O2^{i} are between typical single and double bonds.

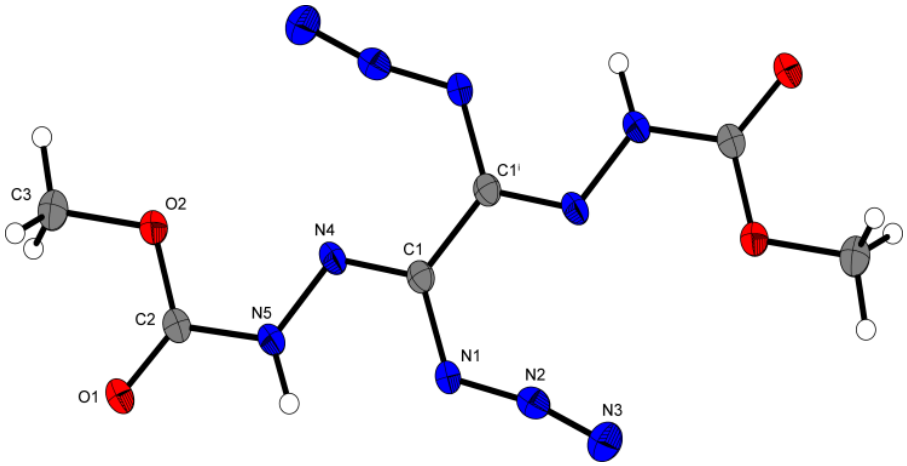


Figure 2. Molecular structure of **2** showing the atom-labelling scheme. Selected bond lengths [Å]: C1–C1^{i} 1.468(4), N1–C1 1.399(3), N1–N2 1.242(2), N2–N3 1.126(3), N4–C1 1.282(3), N4–N5 1.364(2), N5–C2 1.356(3), C2–O1 1.215(3), C2–O2 1.334(2), O2–C3 1.439(3). Selected bond angles [°]: N1–N2–N3 168.7(2), C1–N1–N2 122.5(2). Thermal ellipsoids in all structures represent the 50 % probability level. Hydrogen atoms are shown as small spheres of arbitrary radii. Symmetry code (i) 2−x, 1−y, 1−z.

The bond lengths, bond angles, and torsion angles for the 1,1'-dinitramino-5,5'-bitetrazolate dianion in all metal salts **6**–**13** are in the range of the literature reported neutral parent compound and its potassium salt.[8,12] All four alkaline metal salts crystallize in common space groups (**8**: *P*–1; **6**, **7a**, **9**: $P2_1/c$; **7b**: *Pbca*) with almost increasing densities (**7a**: 1.927 g cm^{-3} (173 K) < **7b**: 1.940 g cm^{-3} (123 K); **6**: 1.949 g cm^{-3} (123 K); **8**: 2.551 g cm^{-3} (173 K) < **9**: 2.829 g cm^{-3} (173 K)) in different coordination spheres (**6**: fivefold; **7a/b**: sixfold; **8**: ninefold; **9**: eightfold). The lithium and sodium salts were the only two alkali metals, which crystallized as dihydrates. Their molecular units are shown in Figure 3 and 4.

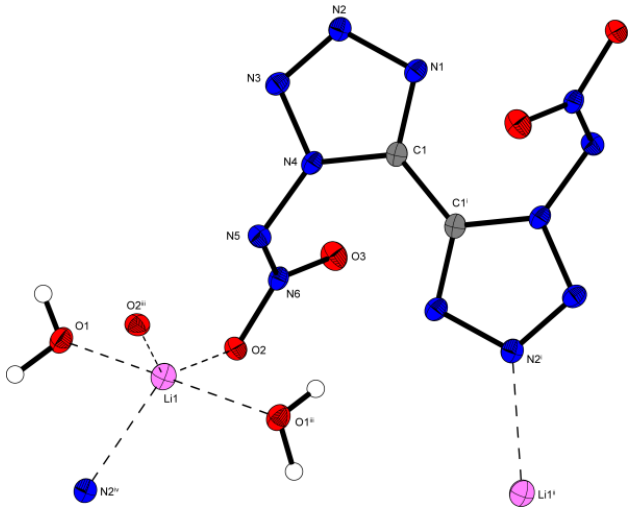


Figure 3. Extended molecular structure of **6** showing the atom-labelling scheme. Selected bond lengths [Å]: O1–Li1 2.047(3), O1^{iii}–Li1 2.114(3), O2–Li1 2.097(3), O2^{iii}–Li1 2.051(3), N2^{iii}–Li1 2.208(4). Symmetry codes (i) 1−x, −y, 1−z; (ii) −x, 0.5+y, 0.5−z; (iii) x, −0.5−y, −0.5+z; (iv) x, −0.5−y, −0.5+z.

The sodium salt **7** crystallizes in two varying polymorphs (Figure 4) depending on the solvent used. Each compound exhibits a different hydrogen bond network that affects their packing. Therefore, both compounds can be clearly distinguished through infrared spectroscopy (Figure S3).

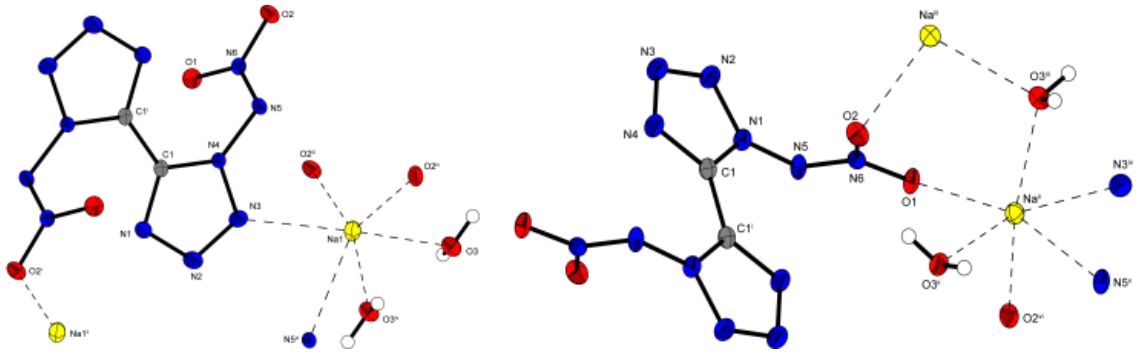


Figure 4. Extended molecular structures of **7a** (left) and **7b** (right) showing the atom-labelling scheme. Selected coordination distances [Å] **7a**: Na1–O3 2.368(2), Na–O3^{v} 2.391(2), Na–N3 2.491(2), Na–N5^{vi} 2.594(2), Na–O2^{iv} 2.454(2), Na–O2^{iii} 2.433(2); **7b**: Na^{ii}–O1 2.378(1), Na^{ii}–O3^{iii} 2.336(1), Na^{ii}–N3^{iv} 2.602(1), Na^{ii}–O2^{vi} 2.377(2), Na^{ii}–N5^{v} 2.543(1), Na^{ii}–O3^{ii} 2.392(1). Symmetry codes **7a**: (i) −x, 1−y, 1−z; (ii) −1+x, y, z; (iii) 1−x, 1−y, 1−z; (iv); 1−x, −0.5+y, 1.5−z; (v) 1−x, −y, 1−z; (vi) x, 0.5−y, −0.5+z. **7b**: (i) −1−x, 1−y, −z; (ii) −0.5−x, 0.5+y, z; (iii) −x, 0.5+y, 0.5−z; (iv) −0.5−x, 1−y, 0.5+z; (v) −1−x, 0.5+y, 0.5−z; (vi) −1.5+x, y, 0.5−z.

The very sensitive heavy metal rubidium **8** and cesium **9** salts crystallize without inclusion of crystal water and are illustrated in Figure 5.

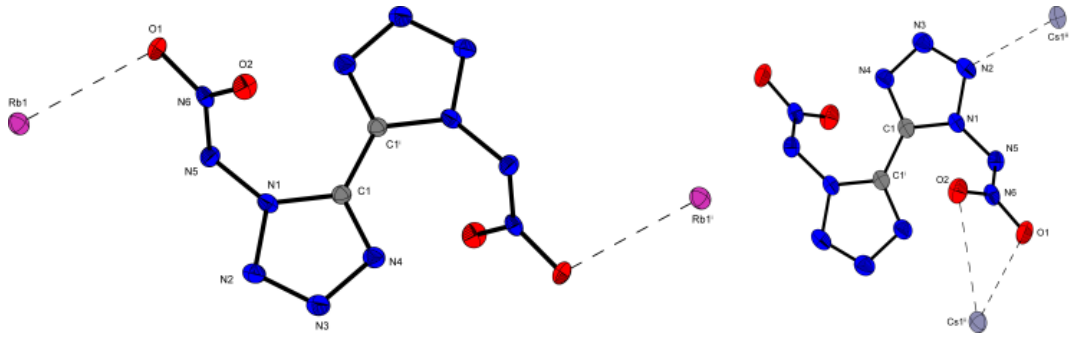


Figure 5. Molecular structures of **8** (left) and **9** (right) showing the atom-labelling scheme. Selected coordination distances lengths [Å] **8**: Rb1–O1 2.872(2); **9**: Cs1^{iii}–N2 3.334(3), Cs1^{ii}–O2 3.335(3), Cs1^{ii}–O1 3.043(2). Symmetry codes **8**: (i) −x, 1−y, 1−z; **9**: (i) x, 0.5−y, 0.5+z; (ii) 1+x, 0.5−y, 0.5+z; (iii) 1−x, −0.5+y, 0.5−z.

The silver salt **10** crystallizes in the form of colorless needles in the monoclinic space group *P*2/*c* with four formula units per unit cell and a calculated density of 3.240 g cm^{-3} at 173 K. Figure 6 displays the extended molecular structure of compound **10** and its labeling scheme. Both silver cations show different surroundings. Silver atom Ag2 is positioned on the crystallographic origin (0,0,0), while atom Ag1 is on (0,0.0140(1),1/4) bearing a rotation axis. Both are strongly linear coordinated (Ag1–N4/N4^{iv} 2.267(7) Å, Ag2–N3/N3^{ii} 2.250(7) Å). Taking into account also weaker coordination distances up to 3 Å, atom Ag1 is coordinated by eight donor atoms, while atom Ag2 is octahedrally coordinated by six donors. The coordination distances are in agreement with values reported for silver 1-methyl-5-nitriminotetrazolate in the literature.[17]

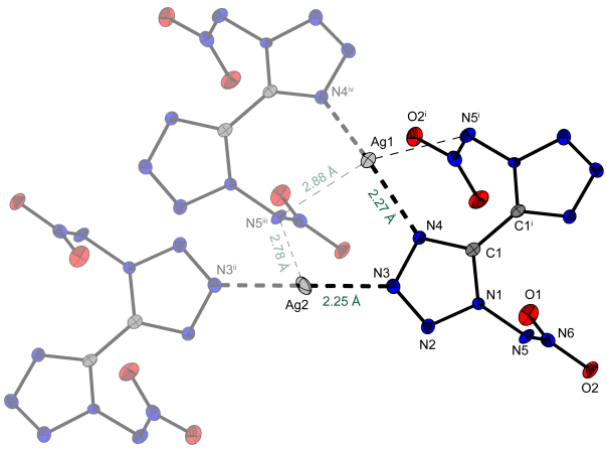


Figure 6. Extended molecular structure of **10**, indicating a strong linear coordination of the silver cations by the nitrogen atoms N4 and N3. Selected bond lengths [Å]: Ag2–N3 2.250(7), Ag2–N5^{ii}

2.776(7), Ag2–O2^{v} 2.680(4), Ag1–N4 2.267(7), Ag1–N5^{iii} 2.883(8), Ag1–O2^{vi} 2.594(4), Ag1–O1^{vi} 2.881(6). Symmetry codes (i): 1−x, y, 0.5−z; (ii) −x, −y, −z; (iii) −1+x, y, z; (iv) −x, y, 0.5−z; (v) 1−x, 1−y, −z; (vi) 1−x, −1+y, 0.5−z.

Compound **11** is, to the best of our knowledge, the first energetic hexamminenickel(II) complex in literature. It crystallizes in the form of clear light purple cylinders in the monoclinic space group $P2_1/c$ with four formula units per unit cell and a calculated density of 1.708 g cm^{-3} at 173 K. The nickel(II) centers are octahedrally coordinated (Figure 7) by six ammine ligands. The DNABT counterion is (in contrast to the other already discussed metal salts) not involved in coordination. All bond lengths between the d^8-metal(II) center and the ligands lie in the same range between 2.09 and 2.16 Å and are in good agreement with values reported in the literature.[18]

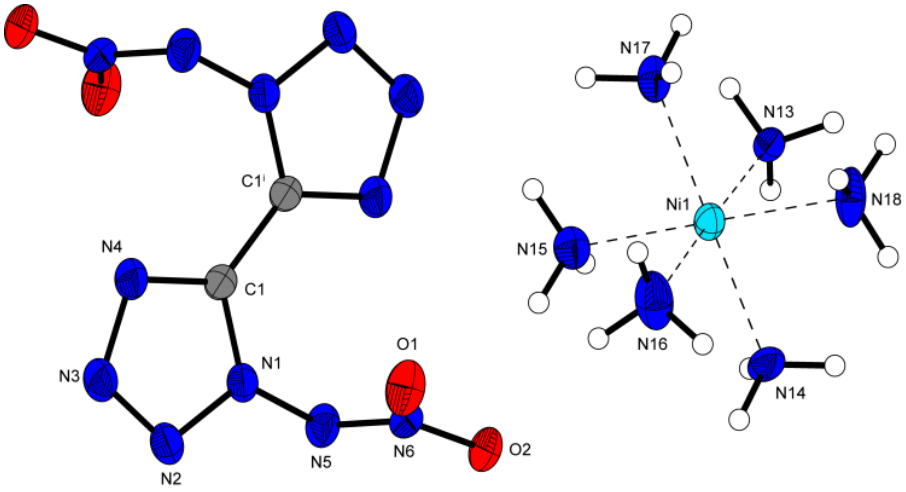


Figure 7. Molecular structure of **11** showing the atom-labelling scheme. Selected bond lengths [Å]: Ni1–N17 2.098(4), Ni1–N13 2.116(3), Ni1–N15 2.119(3), Ni1–N16 2.124(4), Ni1–N14 2.128(4), Ni1–N18 2.154(4). Symmetry code (i): 1−x, 1−y, −z.

Complex **12** crystallizes in the form of blue blocks in the monoclinic space group $C2/c$ with four formula units per unit cell and a calculated density of 1.860 g cm^{-3} at 123 K. The extended molecular structure is illustrated in Figure 8 and shows a Jahn-Teller distorted octahedral coordination sphere of the copper(II) cation. The metal centers are coordinated by four ammine ligands in a plane (Cu1–N7 2.022(7) Å, Cu1–N8 2.008(7) Å) and two longer coordinated nitramine nitrogen atoms N5 of the DNABT in axial positions (Cu1–N5 2.573(2) Å). The coordination octahedron is slightly distorted and deviates partly from 90° (< N5^{i}–Cu1–N8 = 94.83(8)° and < N5^{i}–Cu1–N8^{i} = 85.17(8)°) which might be the sterical influence of the DNABT dianion. The structure (bond lengths and angles) of the complex is comparable to a similar copper(II)-ammine-tetrazolate described in literature.[19] Both compounds crystallize with one

crystal water. In the case of **8** a hydrogen bond to the tetrazole nitrogen atom N3 and the nitrogen atom N7 of one of the ammine ligands is formed. The bidentate DNABT ligand bridges the copper atoms to linear one-dimensional polymeric chains along the *c* axis. The closest Cu-Cu distance is 6.82 Å along *a/b*. Hydrogen bonds between the ammine and tetrazole ligands stabilize the polymeric chains to each other.

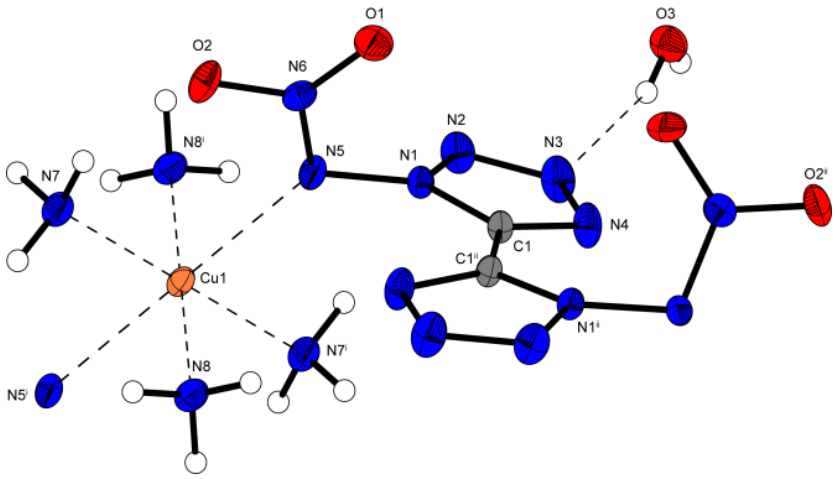


Figure 8. Extended molecular structure of **12** showing the distorted octahedral coordination sphere of the copper(II) cation. Selected bond lengths [Å]: Cu1–N5 2.573(2), Cu1–N7 2.022(2), Cu1–N8 2.008(2). Selected bond angles [°]: $N5^{i}$–Cu1–N8 94.83(8), $N5^{i}$–Cu1–$N8^{i}$ 85.17(8). Symmetry codes (i) −x, −y, −z; (ii) −x, y, 0.5−z.

To the best of our knowledge, tetramminezinc(II) complexes with energetic counter anions have not been reported in literature so far. The zinc(II) DNABT complex **13** crystallizes in the form of colorless rods in the monoclinic space group $P2_1/n$ with four formula units per unit cell and a calculated density of 1.812 g cm^{-3}. In contrast to **9** and **10** the coordination sphere of the zinc(II) metal center (Figure 9) is tetrahedral and consists of four ammine ligands with similar bond distances (Zn–N15 1.995(2) Å, Zn–N16 2.009(2) Å, Zn–N13 2.019(2) Å and Zn–N14 2.016(2) Å). The observed zinc(II) ammine distance values are consistent with the literature data.[21] The tetrahedral coordination sphere only show small divergences (Figure 9 caption) to the perfect angle of 109.4°. This may be due to the large set of hydrogen bonds of the NH_3 ligands formed.

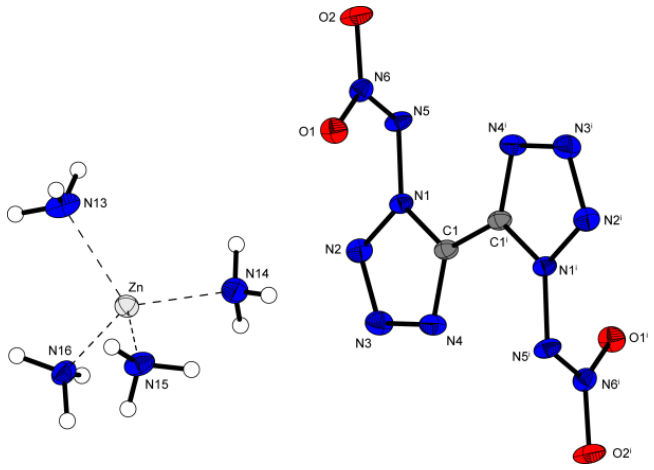


Figure 9. Molecular structure of **13**. Selected bond lengths [Å]: Zn–N15 1.995(2), Zn–N16 2.009(2), Zn–N13 2.019(2), Zn–N14 2.016(2). Selected bond angles [°]: N15–Zn–N16 109.86(9), N14–Zn–N16 106.74(9), N13–Zn–N16 103.44(9). Symmetry code (i) 1−x, −y, −z.

4.2.3 Energetic Properties and Laser Initiation

The sensitivities toward friction, impact and electrostatic discharge for **4** and **6**–**13** were determined according to BAM standards. The compounds have been classified in accordance to the *UN recommendations on the transport of dangerous goods* using the obtained values.[22] In addition, the thermal stabilities were determined by various methods. An overview of the physicochemical properties of **4** and **6**–**13** is given in Table 1.

Table 1. Energetic properties and laser initiation tests of **2**, **6**–**13**.

	2	**6**	**7a**	**7b**	**8**	**9**	**10**	**11**	**12**	**13**
formula	$C_6H_6N_{12}O_8$	$C_2H_4Li_2N_{12}O_6$	$C_2H_4Na_2N_{12}O_6$	$C_2H_4Na_2N_{12}O_6$	$C_2Rb_2N_{12}O_4$	$C_2Cs_2N_{12}O_4$	$C_2Ag_2N_{12}O_4$	$C_2H_{18}NiN_{18}O_4$	$C_2H_{14}CuN_{16}O_5$	$C_2H_{12}ZnN_{16}O_4$
FW/ [g mol^{-1}]	374.2	306.0	338.1	338.1	427.0	512.9	471.8	417.0	405.8	389.7
***IS*/ [J][a]**	< 1	< 1	< 1	< 1	< 1	< 1	n.d.	3	2	1.5
***FS*/ [N][b]**	< 5	< 5	< 5	< 5	< 5	< 5	n.d.	80	10	6
***ESD*/ [J][c]**	0.003	0.020	0.030	0.150	0.020	< 0.020	n.d.	0.130	0.150	0.100
grain size/ [µm]	< 100	< 100	500–1000	500–1000	100–500	100–500	n.d.	100–500	100–500	100–500
***N*/ [%][d]**	44.9	54.9	49.7	49.7	39.4	32.2	35.6	60.5	55.2	57.5
***$T_{dec.}$*/ [°C][e]**	102	239	241	247	186	220	n.d.	167	155	182
***ρ*/ [g cm^{-3}][f]**	1.538	1.911	1.889	1.887	2.501	2.774	3.177	1.675	1.809	1.777
hot needle	n.d.	dec.[h]	dec.[h]	dec.[h]	det.[j]	det.[j]	n.d.	defl.[i]	dec.[h]	defl.[i]
hot plate	n.d.	det.[j]	det.[j]	det.[j]	det.[j]	det.[j]	n.d.	det.[j]	defl.[i]	det.[j]
laser init.[g]	n.d.	n.d.	n.d.	n.d.	n.d.	n.d.	n.d.	det.[j]	det.[j]	n.d.

[a] Impact sensitivity according to the BAM drophammer (method 1 of 6); [b] Friction sensitivity according to the BAM friction tester (method 1 of 6); [c] electrostatic discharge sensitivity (OZM ESD tester); [d] Nitrogen content; [e] Temperature of decomposition according to DSC, DTA or TGA (onset temperatures at a heating rate of 5 °C min^{-1}); [f] X-ray density converted to RT ($\rho_{298K} = \rho_T / (1 + \alpha_V(298 - T_0)$; $\alpha_V = 10^{-4}$ K^{-1}); [g] Laser initiation (λ = 915 nm, τ = 15 ms); [h] Decomposition; [i] Deflagration; [j] Detonation; n.d. = not determined (either not possible or meaningful).

4.2.4 Thermal Behavior

The thermal stabilities of **4** and **6**–**13** were determined either by DSC, DTA or TGA scans at a heating rate of 5 °C min^{-1}. All of the compounds **6**–**13** have the ability to strongly damage the thermal analytical device during their violent decomposition or detonation, respectively. All synthesized DNABT salts and complexes showed a higher thermal stability than the neutral parent compound H_2DNABT of 107 °C.[2] The decomposition temperatures of the investigated metal compounds, given as the extrapolated onset temperatures, range from 186 °C (**8**) up to a 247 °C (**7b** dehydrated) for the metal salts and from 155 °C (**12**) to 182 °C (**13**) for the metal complexes. Compound **4** shows an even lower thermal stability than H_2DNABT (**4**: 102 °C, H_2DNABT: 107 °C). The quite disappointing low thermal stabilities of the complexes **11**–**13** can be explained by the loss of the coordinated ammine ligands, which leads to decomposition of the compound (Cu < Ni < Zn). The thermo plots of compound **6** and **12** show endothermic signals (**6**: 50–70 °C, **12**: 123 °C), which indicates the loss of crystal water. This loss could also be observed in the TGA scans of the sodium salts **7a** and **7b**. Interestingly the two sodium salts show different decomposition temperatures, which can be explained by the different hydrogen bond networks. With 220 °C cesium salt **9** is the most temperature stable of all investigated water-free compounds although being one of the most sensitive.

4.2.5 Sensitivities

All investigated compounds show sensitivities in the range of primary explosives such as lead or silver azide. They are very sensitive toward impact with sensitivities of 1 J (or less) (**2**, **6**–**9**) up to 3 J for the nickel(II) ammine complex (**11**). The friction sensitivities are comparable with values from less than 5 N (**2**, **6**–**9**) up to 80 N for compound **11**. A possible explanation for the low sensitivity of **11** could be the high number of non-energetic ammine ligands. As expected, the silver salt (**10**) is the most sensitive compound, which can even detonate without any external manipulation! The range of sensitivities toward electrostatic discharge range from 0.003 to 0.150 J. Interestingly, polymorph **7b** is significantly less sensitive toward electrostatic discharge than **7a**.

4.2.6 Hot Plate and Hot Needle Test

The ignitibility of metal compounds **6**–**9** and **11**–**13** was further tested through hot needle and hot plate tests. The hot needle test was performed by securing a small amount of sample underneath adhesive tape, followed by penetration with a red heated needle. Except for the rubidium (**8**) and cesium (**9**) salts, which detonated to the extent desired, all tested compounds only decomposed or deflagrated. Detonation of the compound indicates a primary explosive. The practicable hot plate test instead, only shows the behavior of the unconfined sample toward fast heating on a hot copper plate. It does not necessarily allow to draw conclusions on its capability as a primary explosive. All compounds except the copper(II) complex **12** which deflagrated sharply, detonated when reaching their respective ignition temperatures.

4.2.7 Laser Initiation

Approximately 15 mg of **11** and **12** (which are the only colored compounds in this work) were filled into a plastic cap, pressed with 1 kN and sealed by an UV-curing adhesive. The confined samples were then irradiated through an optical lens connected to an optical fibre with a monopulsed diode laser at a wavelength of 915 nm, a pulse length of 15 ms and a current of 7 A. Both investigated complexes **11** and **12** detonated after initiation by laser irradiation and could therefore be used as photosensitive primary explosives in suitable detonation systems.

4.3 Experimental Section

General Methods

All chemicals and solvents were employed as received (Sigma-Aldrich, Fluka, Acros). The synthesis of compounds **1**–**5** can be found in the Supporting Information. ^{1}H, ^{13}C and ^{14}N NMR spectra were recorded with neat solids as samples at ambient temperature using a JEOL Eclipse 270, JEOL EX 400 or a JEOL Eclipse 400 instrument. The chemical shifts quoted in ppm in the text refer to typical standard tetramethylsilane (^{1}H, ^{13}C) and nitromethane (^{14}N) in d_6-DMSO as the solvent. Decomposition temperatures were measured through differential thermal analysis (DTA) with an OZM Research DTA 552-Ex instrument, through differential scanning calorimetry (DSC) with a LINSEIS DSC PT10 or by thermogravimetric analysis (TGA) with a Perkin Elmer TGA4000 instrument. The samples were measured in a range of 25–400 °C at a

heating rate of 5 °C min^{-1}. Infrared spectra were measured with a Perkin–Elmer FT-IR Spectrum BXII instrument equipped with a Smith Dura Samp*IIR* II ATR unit. Mass spectra of the described compounds were measured at a JEOL MStation JMS 700 using FAB technique. Determination of the carbon, hydrogen and nitrogen contents were carried out by combustion analysis using an Elementar Vario El (nitrogen values determined are often lower than the calculated ones due to their explosive behavior. Sensitivity tests are described in the SI.

CAUTION! *All investigated compounds are potentially explosive energetic materials, which show increased sensitivities toward various stimuli (e.g. elevated temperatures, impact, friction or electrostatic discharge). Therefore, proper security precautions (safety glass, face shield, earthed equipment and shoes, leather coat, Kevlar gloves, Kevlar sleeves and ear plugs) have to be applied while synthesizing and handling the described compounds.*

General procedure for the preparation of the DNABT alkali salts (6, 7a, 8–9): An aqueous solution of the ammonium salt **5** (**6**/**7a**: 100 mg, 0.34 mmol; **8**/**9**: 29.0 mg, 0.10 mmol) was treated with the corresponding aqueous metal hydroxide solution (**6**: lithium hydroxide (8.14 mg, 0.34 mmol); **7a**: sodium hydroxide (13.6 mg, 0.34 mmol); **8**: 50 wt.% rubidium hydroxide (20.5 mg, 0.10 mmol); **9**: 50 wt.% cesium hydroxide (30.0 mg, 0.10 mmol)) and stirred mechanically for 10 min at 70 °C. The clear solutions were left to crystallize until a crystalline solid appeared. The products were filtered off, washed with ethanol and dried in air.

Li_2DNABT · 2 H_2O (6): Colorless crystals of compound **6**, which were suitable for X-ray, started to crystallize within several days. Yield: 84.1 mg (0.27 mmol, 80 %).

DSC (5 °C min^{-1}): 50–70 °C (dehydration), 239 °C (dec.); **IR** (atr, cm^{-1}): $\tilde{\nu}$ = 3441 (m), 3293 (m), 3210 (m), 3083 (w), 1652 (m), 1432 (s), 1401 (s), 1373 (s), 1288 (vs), 1271 (vs), 1184 (s), 1129 (s), 1048 (m), 1042 (m), 1020 (m), 1002 (m), 876 (s), 778 (s), 731 (w), 714 (m), 672 (w), 622 (m), 488 (w), 467 (w); **EA** ($C_2H_4Li_2N_{12}O_6$, 306.01): calc.: C 7.85, H 1.32, N 54.93 %; found: C 8.36, H 1.75, N 55.34 %; **BAM drophammer**: < 1 J; **friction tester**: < 5 N; **ESD**: 25 mJ.

Na_2DNABT · 2 H_2O (7a): Compound **7a** was isolated within several days in the form of colorless blocks suitable for X-ray determination. Yield: 95.4 mg (0.28 mmol, 83 %).

TGA (5 °C min^{-1}): 95–105 °C (dehydration), 241 °C (dec.); **IR** (atr, cm^{-1}): $\tilde{\nu}$ = 3568 (m), 3469 (w), 1616 (w), 1430 (m), 1370 (s), 1325 (s), 1299 (vs), 1268 (s), 1177 (m), 1168 (m), 1129 (m), 1037 (m), 1004 (m), 881 (m), 835 (m), 774 (m), 733 (w), 713 (w), 676 (w), 463 (s), 457 (s); **EA** ($C_2H_4Na_2N_{12}O_6$, 338.11): calc.: C 7.10, H 1.19, N 49.71 %; found: C 7.39, H 1.39, N 49.78 %; **BAM drophammer**: < 1 J; **friction tester**: < 5 N; **ESD**: 30 mJ.

Na_2DNABT · 2 H_2O (7b): Colorless blocks of polymorph **7b** were obtained by recrystallization of compound **7a** (42.3 mg, 0.13 mmol) out of ethanol within one day suitable for X-ray determination. Yield: 38.8 mg (0.11 mmol, 92 %).

TGA (5 °C min^{-1}): 112–126 °C (dehydration), 247 °C (dec.); **IR** (atr, cm^{-1}): $\tilde{\nu}$ = 3574 (s), 3399 (m), 1622 (m), 1428 (vs), 1369 (s), 1299 (vs), 1265 (vs), 1166 (m), 1122 (s), 1035 (m), 1018 (m), 995 (m), 883 (s), 776 (m), 733 (w), 714 (w), 675 (w), 614 (w), 531 (m), 492 (m), 457 (m); **EA** ($C_2H_4Na_2N_{12}O_6$, 338.11): calc.: C 7.10, H 1.19, N 49.71 %; found: C 7.37, H 1.23, N 49.45 %; **BAM drophammer**: < 1 J; **friction tester**: < 5 N; **ESD**: 150 mJ.

Rb_2DNABT (8): Suitable crystals for X-ray determination were obtained of compound **8** in a quantitative yield within one day.

DTA (5 °C min^{-1}): 186 °C (dec.); **IR** (atr, cm^{-1}): $\tilde{\nu}$ = 1424 (s), 1394 (m), 1359 (m), 1283 (vs), 1253 (vs), 1170 (m), 1161 (s), 1121 (s), 1031 (s), 1005 (m), 998 (s), 870 (s), 828 (m), 809 (m), 803 (m), 772 (vs), 726 (s), 714 (s), 698 (m), 691 (m), 680 (m), 671 (m), 658 (m); **BAM drophammer**: < 1 J; **friction tester**: < 5 N; **ESD**: 20 mJ.

Cs_2DNABT (9): Compound **9** was isolated in a quantitative yield in form of colorless needles suitable for X-ray determination within a few hours.

DTA (5 °C min^{-1}): 220 °C (dec.); **IR** (atr, cm^{-1}): $\tilde{\nu}$ = 1410 (s), 1360 (m), 1281 (vs), 1254 (s), 1171 (m), 1161 (m), 1128 (s), 1124 (s), 1034 (m), 1000 (m), 868 (s), 774 (m), 723 (w), 715 (m), 672 (w); **BAM drophammer**: < 1 J; **friction tester**: < 5 N; **ESD**: < 20 mJ.

Ag_2DNABT (10): An aqueous solution of compound **5** (50.0 mg, 0.17 mmol) was reacted with an aqueous solution of silver nitrate (28.9 mg, 0.17 mmol). The precipitating colorless silver salt **10** was dissolved in two drops of concentrated ammonia. Colorless crystals suitable for X-ray determination were isolated overnight.

General procedure for the synthesis of metal(II) DNABT amine complexes (11–13):

Compound **5** (**11**: 182 mg, 0.62 mmol; **12**: 35.0 mg, 0.12 mmol; **13**: 189 mg, 0.65 mmol) was dissolved in the least necessary amount of concentrated ammonia and added to a solution of the corresponding metal(II) nitrate (**11**: nickel(II) nitrate hexahydrate (180 mg, 0.62 mmol); **12**: copper(II) nitrate trihydrate (29.0 mg, 0.12 mmol); **13**; zinc(II) nitrate hexahydrate (193 mg, 0.65 mmol)) in concentrated ammonia and stirred mechanically for 1 min at room temperature. The reaction mixtures were left to crystallize until a solid appeared. The products were filtered off and dried at 50 °C overnight.

[$Ni(NH_3)_6$]DNABT (11): Complex **11** was obtained within 30 min in the form of purple cylinders suitable for X-ray determination. Yield: 133 mg (0.32 mmol, 51 %).

DTA (5 °C min^{-1}): 167 °C (dec.); **IR** (atr, cm^{-1}): $\tilde{\nu}$ = 3354 (m), 3282 (m), 1615 (m), 1478 (m), 1415 (s), 1365 (m), 1285 (vs), 1245 (vs), 1161 (s), 1124 (s), 1034 (m), 996 (m), 874 (m), 777 (m), 629 (s); **EA** ($C_2H_{18}NiN_{18}O_4$, 416.98): calc.: C 5.76, H 4.35, N 60.46 %; found: C 6.27, H 4.24, N 57.05 %; **BAM drophammer**: 3 J; **friction tester**: 80 N; **ESD**: 0.13 J.

[$Cu(NH_3)_4$DNABT] · H_2O (12): Compound **12** was isolated within 20 min in the form of blue crystals suitable for X-ray determination. Yield: 32.9 mg (0.08 mmol, 68 %).

DSC (5 °C min^{-1}): 123 °C (dehydration), 155 °C (dec.); **IR** (atr, cm^{-1}): $\tilde{\nu}$ = 3543 (w), 3361 (m), 3342 (m), 3269 (m), 3194 (w), 1618 (m), 1414 (s), 1368 (m), 1290 (s), 1264 (vs), 1247 (vs), 1166 (m), 1151 (m), 1123 (m), 1013 (w), 994 (w), 877 (m), 770 (m), 678 (s), 558 (w), 544 (w); **EA** ($C_2H_{14}CuN_{16}O_5$, 405.79): calc.: C 5.92, H 3.48, N 55.23 %; found: C 6.45, H 3.44, N 54.63 %; **BAM drophammer**: 2 J; **friction tester**: 10 N; **ESD**: 0.15 J.

[Zn(NH$_3$)$_4$]DNABT (13): The tetrammine zinc(II) complex **13** was obtained within several hours in the form of colorless rods suitable for X-ray determination. Yield: 105 mg (0.27 mmol, 41 %).

DTA (5 °C min^{-1}): 182 °C (dec.); **IR** (atr, cm^{-1}): $\tilde{\nu}$ = 3309 (m), 3263 (m), 3252 (m), 3224 (m), 3183 (m), 1620 (w), 1408 (s), 1367 (m), 1280 (vs), 1268 (vs), 1249 (vs), 1160 (m), 1127 (s), 1117 (s), 1032 (w), 999 (w), 872 (m), 773 (m), 692 (s), 674 (s); **EA** ($C_2H_{12}ZnN_{16}O_4$, 389.61): calc.: C 6.17, H 3.10, N 57.52 %; found: C 6.68, H 3.06, N 56.13 %; **BAM drophammer**: 1.5 J; **friction tester**: 6 N; **ESD**: 0.10 J.

4.4 Conclusions

The synthesis and characterization of several new metal salts and complexes of 1,1'-dinitramino-5,5'-bitetrazole (H_2DNABT) is described. Since the potassium salt K_2DNABT is a very promising environmentally benign primary explosive the remaining alkali salts as well as selected alkaline earth and transition metal complexes should be investigated toward their energetic behavior. Within the group of alkali metal salts (Li (**6**), Na (**7**), K_2DNABT, Rb (**8**), Cs (**9**)) the lithium and sodium salts form dihydrates which can reversibly be dehydrated. Two polymorphs of latter one were explored formed by recrystallization from water (**7a**) and ethanol (**7b**), respectively. The rubidium, cesium and silver (**10**) salts are poorly soluble in water. All are highly sensitive showing a superfast "deflagration to detonation" behavior on contact with flame or hot surfaces. The silver salt usually explodes during drying or when touched in the dry state. The alkaline earth metal salts (Ca (**14**), Sr (**15**), Ba (**16**)) are highly soluble in water and could not be purified sufficiently. They are forming tetra- (**14**, **15**) and hexahydrates (**16**) in the solid state. Neat transition metal complexes could only be synthesized with Ni(II) (**11**), Cu(II) (**12**) and Zn(II) (**13**) under addition and coordination of ammonia. The nickel(II) and copper(II) salts could be successfully initiated by laser irradiation. For the first time the cations hexaamminenickel(II) and tetraamminezinc(II) were combined with energetic counterions. The crystal structure of all compounds except for **14** could be determined by low temperature X-ray diffraction, which gave insight in the coordination of the metal centers and hydrogen bond interactions. Sensitivities of the alkaline and transition metal salts were measured showing extremely high values partly much more susceptible. The lowest thermal stability of 155 °C was observed for the tetrammine-copper(II) complex which might be caused by the loss of ammonia. The highest value (247 °C) was observed for the dehydrated sodium salt **7b**. With

respect to potential application in priming charges the potassium salt is still the most promising due to its manageable sensitivities in combination with a thermal stability of 200 °C.

Supporting information available in the appendix in **Chapter 19.2** and under:

http://www.rsc.org/suppdata/c7/dt/c7dt00536a/c7dt00536a1.pdf

4.5 References

[1] a) J. Zhang, S. Dharavath, L. A. Mitchell, D. A. Parrish and J. M. Shreeve, *J. Am. Chem. Soc.* 2016, **138**, 7500; b) P. Yin, D. A. Parrish and J. M. Shreeve, J. *Am. Chem. Soc.*, 2015, **137**, 4778; c) H. Gao and J. M. Shreeve, *Chem. Rev.* 2011, **111**, 7377.

[2] a) K. B. Landenberger, O. Bolton and A. J. Matzger, *J. Am. Chem. Soc.*, 2015, **137**, 5074; b) S. Seth and A. J. Matzger, *Inorg. Chem.*, 2017, **56**, 561–565.

[3] a) D. E. Chavez, D. A. Parrish and L. Mitchell, *Angew. Chem. Int. Ed.* 2016, **55**, 8666; b) D. G. Piercey, D. E. Chavez, B. L. Scott, G. H. Imler and D. A. Parrish, *Angew. Chem. Int. Ed.* 2016, **55**, 15315; c) T. W. Myers, C. J. Snyder, D. E. Chavez, R J. Scharff and J. M. Veauthier, *Chem. Eur. J.* 2016, **22**, 10590; d) D. E. Chavez, J. C. Bottaro, M. Petrie and D. A. Parrish, *Angew. Chem. Int. Ed.* 2015, **54**, 12973.

[4] a) X. X. Zhao, S. H. Li, Y. C. Li, F. Q. Zhao and S. P. Pang, *J. Mater. Chem.* A, 2016, **4,** 5495; b) Y.-C. Li, C. Qi, S.-H. Li, H.-J. Zhang, C.-H. Sun, Y.-Z. Yu and S.-P. Pang, *J. Am. Chem. Soc.*, 2010, **132**, 12172.

[5] a) D. Fischer, J. L. Gottfried, K. Karaghiosoff, T. M. Klapötke, J. Stierstorfer and T. Witkowski, *Angew. Chem. Int. Ed.* 2016, **55**, 16132; b) N.-D. H. Gamage, B. Stiasny, J. Stierstorfer, P. D. Martin, T. M. Klapötke and C. H. Winter, *Chem. Eur. J.* 2016, **22**, 2582; c) D. Fischer, T. M. Klapötke and J. Stierstorfer, *Chem. Commun.* 2016, **52**, 916.

[6] R. Matyas and J. Pachman, Primary Explosives, Springer, 2013.

[7] http://www.speciation.net/News/REACH-Update-List-of-300-chemicals-of-very-high-concern-;~/2008/09/18/3831.html (accessed on 27.12.2016).

[8] a.) D. Fischer, T. M. Klapötke, J. Stierstorfer, *Angew. Chem. Int. Ed.* 2014, **53**, 8172; b) D. Fischer, T. M. Klapötke and J. Stierstorfer, *Angew. Chem.* 2014, **126**, 8311.

[9] S. R. Ahmad and M. Cartwright, Laser Ignition of Energetic Materials, Wiley, 2014, chapter 8, 193.

[10] J. W. Fronabarger, M. D. Williams, W. B. Sanborn, J. G. Bragg, D. A. Parrish and M. Bichay, *Propellants Explos. Pyrotech*. 2011, **36**, 541.

[11] a) J. W. Fronabarger, M. D. Williams, W. B. Sanborn and D. A. Parrish, Magdy Bichay, *Propellants Explos. Pyrotech.* 2011, **36**, 459; b) J. W. Fronaberger; M. D. Williams; M. Bichay and M. Bichay, Joint Armaments Conference, Dallas, TX, 2010 http://www.dtic.mil/ndia/2010armament/Thursday ReunionMichael Williams.pdf (accessed on 27.12.2016).

[12] D. Fischer, T. M. Klapötke, J. Stierstorfer and N. Szimhardt, *Chem. Eur. J.* 2016, **22**, 4966.

[13] T. M. Klapötke, P. C. Schmid and J. Stierstorfer, *J. Mater. Chem. A*, 2015, **3**, 2658.

[14] T. M. Klapötke and J. Stierstorfer, *Helv. Chim. Acta* 2007, **90**, 2132.

[15] S. N. Semenov, A. Yu. Rogachev, S. V. Eliseeva, Y. A. Belousov, A. A. Drozdov and S. I. Troyanov, *Polyhedron*, 2007, **26**, 4899.

[16] J. Stierstorfer, PhD thesis, Ludwig-Maximilians Universität München, 2009, 311.

[17] Crystallographic data for the structure(s) have been deposited with the Cambridge Crystallographic Data Centre. Copies of the data can be obtained free of charge on application to The Director, CCDC, 12 Union Road, Cambridge CB2 1EZ, UK (Fax: int.code_(1223)336-033; e-mail for inquiry: fileserv@ccdc.cam.ac.uk; e-mail for deposition: (deposit@ccdc.cam.ac.uk).

[18] T. M. Klapötke, J. Stierstorfer and A. U. Wallek, *Chem. Mat.* 2008, **20**, 4519.

[19] P. Schwendt, D. Dudasova, J. Chrappova, M. Drabik and J. Marek, *J. Therm. Anal. Calorim.* 2008, **91**, 293.

[20] T. M. Klapötke, J. Stierstorfer and B. Weber, *Inorg. Chim. Acta,* 2009, **362**, 2311.

[21] Y. Qu, Z.-D. Liu, M.-Y. Tan and H.-L. Zhu, *Acta Crystallogr.* 2004, ***E60***, m1343.

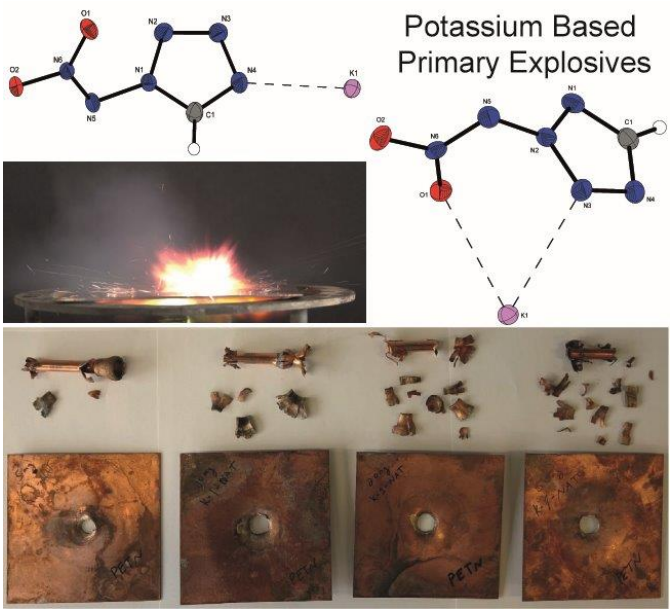
[22] Impact: insensitive > 40 J, less sensitive ≥ 35 J, sensitive ≥ 4 J, very sensitive ≤ 3 J; Friction: insensitive > 360 N, less sensitive = 360 N, sensitive < 360 N and > 80 N, very sensitive ≤ 80 N, extremely sensitive ≤ 10 N, According to: *Recommendations on the Transport of Dangerous Goods, Manual of Tests and Criteria*, 4th edition, United Nations, New York-Geneva, **1999**.

.

5 Potassium *N*-Nitramino-5*H*-tetrazolates — Powerful Green Primary Explosives with High Initiation Capabilities

Norbert Szimhardt, Maximilian H. H. Wurzenberger, Philipp Spieß, Thomas M. Klapötke, and Jörg Stierstorfer

submitted to *Propellants, Explosives, Pyrotechnics*



Green lead-free primary explosive alternatives are still of high interest. Potassium 1- and 2-nitraminotetrazolates show an extraordinary potential, which could be confirmed by their high initiation capabilities.

Abstract

Since the nowadays used lead-based primary explosives, lead azide, picrate and styphnate suffer from various environmental and toxic issues, there is a great need for new green materials. Therefore, two highly promising lead-free primary explosives potassium 1-(*N*-nitramino)-5*H*-tetrazolate (**1**, 1-KNAT**)** and potassium 2-(*N*-nitramino)-5*H*-tetrazolate (**2**, 2-KNAT) have been synthesized and characterized. Both isomers show superior energetic performance, initiation capability and were comprehensively analyzed by low-temperature X-ray diffraction, IR, multinuclear NMR spectroscopy, elemental analysis, and DTA. Sensitivity determinations toward impact, friction, and electrostatic discharge revealed its highly powerful, but also sensitive character. In addition, their potential as lead-free primaries were evaluated in initiation tests of PETN or RDX filled detonators confirming their great suitability as lead-free primary explosives.

5.1 Introduction

In the field of high energy density materials (HEDM), the challenge has always been to find an ideal balance between high performance and molecular stability. By combining synthetic and theoretical studies, various strategies for the design of new energetic materials have become established.[1–4] However, driven by mounting demands for environmental sustainability and superior performance, considerable research is now focused on promoting the generation of eco-friendly and safe HEDM.[2,5,6] At least since the REACH (Registration, Evaluation, Authorization, and Restriction of Chemicals)[7] regulation in 2011, the restriction or even the prohibition of lead azide (LA) and lead styphnate (LS), which have been put on the candidate list, seems very likely in future. During the research for green primary explosives for both military and civilian purposes, metal-organic compounds have received considerable attention.[8–10] The formation of energetic salts seems to be extremely useful for triggering the individual behavior because of a crystal package and a pronounced cation-anion packing.[11] Among the alkali cations, potassium is considered the best as it combines environmental safety, good coordination, high availability, and low costs.[12] Up to now, several promising potassium-based primaries have been reported and investigated as potential substitutes for the commonly used lead-containing primary explosives (Chart 1).[13–17] KDNBF is currently widely used in lead-free primer and igniter systems.[17] With KDNP in comparison, the temperature stability could be further improved, whereby also suitable properties for application as possible LS

alternative could be shown.[13] In 2014, Fischer *et al.* reported K_2DNABT, a highly powerful green primary explosive, which combined good thermal stability and initiation capability, but shows increased sensitivity issues.[14] With the introduction of the nitramino group, the detonation properties and ease of salt formation could be significantly enhanced.[18] Nevertheless, a seven-step synthesis reduces the usability for industrial processes in order to replace the easily accessible lead compounds. From this point of view, a simpler and shorter synthesis would be very desirable.

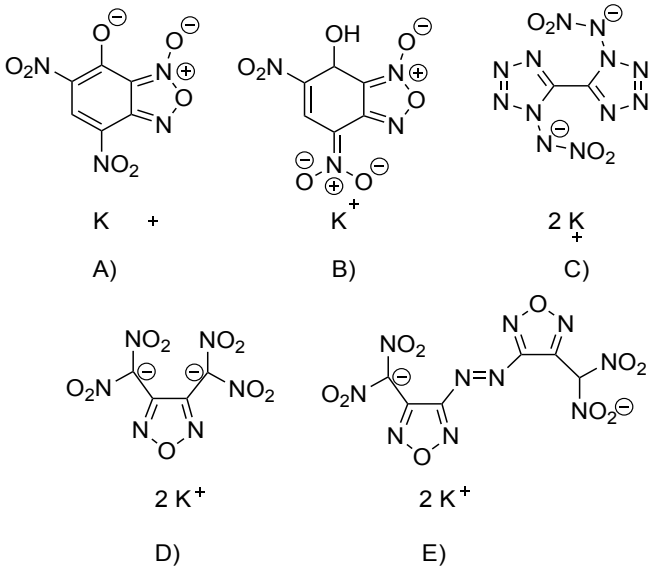


Chart 1. Molecular structures of possible LS and LA substitutes based on potassium-based primaries: A) KDNP, B) KDNBF, C) K_2DNABT, D) potassium 4,5-bis(dinitromethyl)furoxanate, E) potassium 4,4′-bis(dinitromethyl)-3,3′-azofurazanate.

Mentally separating the symmetrical K_2DNABT system into two molecules, leads to a mononitraminotetrazolate, which is noticeably easier to synthesize and shows comparable energetic parameters to the parent dinitraminotetrazolate compound. Almost two decades ago, first approaches to synthesize the silver and ammonium salts of 1-(*N*-nitramino)-5*H*-tetrazolate and 2-(*N*-nitramino)-5*H*-tetrazolate salts have been reported using alkyl nitrates as the nitrating reagent.[19] The salts were hardly characterized and suffer from an extreme lack of data (XRD, NMR spectroscopy, sensitivities, etc.). In order to close this gap and due to the expected enormous sensitivity of the silver salts and the probably undesirable good solubility of the ammonium salts, the previously unknown environmentally friendly potassium salts were selected as target molecules. Therefore, in our continuing efforts toward environmentally benign materials, we have now prepared and characterized the manageable potassium salts 1-KNAT (**1**) and the corresponding isomeric 2-KNAT (**2**) by an alternative synthetic route. Both

compounds show promising energetic and physicochemical properties competitive with those of LA.

5.2 Experimental Section

More information on the general methods and synthesis of the starting compounds can be found in the Supporting Information.

Caution! All investigated compounds are highly powerful energetic materials, which show increased sensitivities toward various stimuli (e.g. elevated temperatures, impact, friction, or electrostatic discharge). Although no hazards occurred, proper security precautions (safety glasses, face shield, earthed equipment and shoes, leather jacket, Kevlar gloves, Kevlar sleeves, and ear plugs) have to be worn while synthesizing and handling the described compounds.

General procedure for the potassium *N*-nitramino-5*H*-tetrazolates **1** and **2**:

Under nitrogen atmosphere, the corresponding amino-5*H*-tetrazole was dissolved in dry acetonitrile and cooled to 0 °C. NO_2BF_4 was added portion wise, and after complete addition, the ice bath was removed. After stirring overnight, acetonitrile was removed under reduced pressure. The obtained residue was dissolved in a small amount of EtOH and one equivalent of KOEt dissolved in EtOH was added under ice cooling. Colorless precipitation was observed, filtered off, and a second equivalent KOEt in EtOH was added to the filtrate under the same cooling conditions. After filtration, the slightly yellow residue was washed with cold EtOH to obtain the corresponding potassium nitramino-5*H*-tetrazolate. The obtained solid material was further dried overnight at 110 °C.

Potassium 1-(*N*-nitramino)-5*H*-tetrazolate (**1**)

Following the general procedure 1-amino-5*H*-tetrazole (0.50 g, 5.80 mmol), dissolved in acetonitrile (20 mL), reacts with NO_2BF_4 (0.85 g, 7.00 mmol) to obtain **1** in form of a colorless solid (0.63 g, 3.80 mmol, 64 %). Single crystals suitable for X-ray diffraction were obtained by recrystallization from acetonitrile.

DTA (5 °C min^{-1}): onset: 180 °C (exothermic decomposition after melting); IR (ATR, cm^{-1}): $\tilde{\nu}$ = 3136 (m), 1676 (w), 1572 (w), 1500 (w), 1480 (vw), 1463 (m), 1410 (m), 1384 (s), 1306

(vs), 1276 (s), 1198 (m), 1176 (m), 1161 (s), 1105 (m), 1092 (s), 1007 (m), 957 (m), 925 (w), 891 (m), 867 (s), 820 (w), 775 (s), 725 (m), 725 (m), 717 (m), 687 (w), 654 (s), 535 (w), 472 (w), 453 (m); ^{1}H NMR (DMSO-d_6, 25 °C, ppm) δ: 9.18 (s, 1H, C-*H*); ^{13}C NMR (DMSO-d_6, 25 °C, ppm) δ: 142.2 (s, 1C, *C*N$_4$); ^{14}N NMR (DMSO-d_6, 25 °C, ppm): δ = 4.2 (N6); ^{15}N NMR (DMSO-d_6, 25 °C, ppm): δ 2.8 (d, $^{3}J_{N–H}$ = 2.8 Hz, N3), –4.9 (s, N6), –14.3 (d, $^{3}J_{N–H}$ = 0.8 Hz, N2), –54.3 (d, $^{2}J_{N–H}$ = 12.2 Hz, N4), –116.1 (d, $^{2}J_{N–H}$ = 8.4 Hz, N1), –122.7 (s, N5); EA: ($CHKN_5O_2$, 167.98) calc.: C 7.14, H 0.60, N 49.98 %; found: C 7.40, H 0.89, N 47.02 %; ball drop impact tester: < 4 mJ; BAM drophammer: < 1 J; friction tester: < 0.1 N; ESD: 0.89 mJ (at grain size < 100 µm).

Potassium 2-(*N*-nitramino)-5*H*-tetrazolate (**2**)

Following the general procedure 2-amino-5*H*-tetrazole (0.82 g, 7.50 mmol) dissolved in 20 mL acetonitrile, reacts with NO_2BF_4 (1.40 g, 10.5 mmol) to obtain **2** as a yellowish solid (0.77 g, 4.60 mmol, 48 %). Single crystals suitable for X-ray diffraction were obtained by recrystallization from acetonitrile.

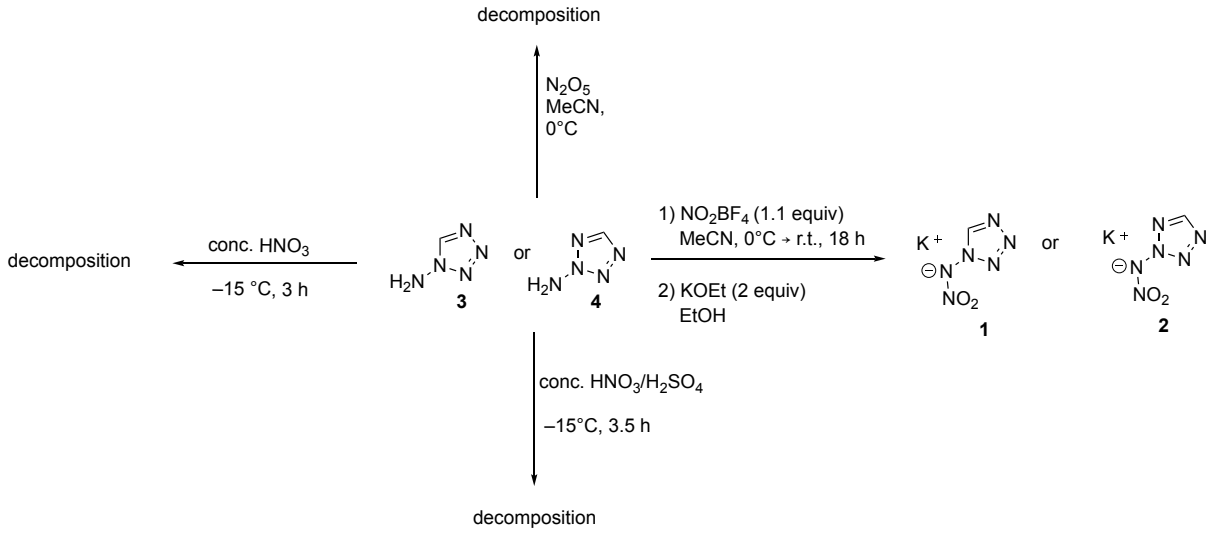
DTA (5 °C min^{-1}): 176 °C (exothermic decomposition after melting); IR (ATR, cm^{-1}): $\tilde{\nu}$ = 3136 (w), 1814 (vw), 1572 (vw), 1505 (vw), 1481 (w), 1423 (s), 1371 (w), 1334 (s), 1272 (vs), 1262 (vs), 1220 (s), 1166 (m), 1130 (s), 1030 (s), 1009 (m), 1006 (m), 1003 (m), 910 (m), 892 (s), 778 (m), 730 (w), 705 (m), 677 (m), 677 (m); ^{1}H NMR (DMSO-d_6, 25 °C, ppm) δ: 8.77 (s, 1H, -C*H*); ^{13}C NMR (DMSO-d_6, 25 °C, ppm) δ: 151.3 (s, 1C, *C*N4); ^{14}N NMR (DMSO-d_6, 25 °C, ppm): δ = –3.1 (N6); ^{15}N NMR (DMSO-d_6, 25 °C, ppm) δ: –4.00 (s, N6), –7.8 (d, $^{3}J_{N–H}$ = 1.5 Hz, N3), –54.4 (d, $^{2}J_{N–H}$ = 12.4 Hz, N4), –76.2 (d, $^{3}J_{N–H}$ = 7.1 Hz, N2), –76.8 (d, $^{2}J_{N–H}$ = 14.4 Hz, N1), –113.1 (s, N5); EA: ($CHKN_5O_2$, 167.98) calc.: C 7.14, H 0.60, N 49.98 %; found: C 7.65, H 0.78, N 45.29 %; ball drop impact tester: < 4 mJ; BAM drophammer: 5 J; friction tester: < 0.1 N; ESD: 8.2 mJ (at grain size < 100 µm).

5.3 Results and Discussion

5.3.1 Synthesis

The starting materials 1-amino-5*H*-tetrazole and 2-amino-5*H*-tetrazole have been synthesized according to literature modified procedures (more details can be found in the SI). Several direct

nitration procedures of 1-amino-5*H*-tetrazole and 2-amino-5*H*-tetrazole with N_2O_5, 100 % nitric acid and mixed acids have been approached in order to synthesize **1** and **2** in a more convenient way but were unfortunately unsuccessful (Scheme 1). During the addition step or further by quenching the acid mixtures, gas evolution could be observed. The gas evolution is a reliable indicator for decomposition of the starting material, which can be attributed to the relatively labile N–N bonds of 1-amino-5*H*-tetrazole and 2-amino-5*H*-tetrazole, which break under these harsh reaction conditions, releasing nitrogen gas. This work deals with the successful nitration with the mild nitration reagent NO_2BF_4, as an alternative method described in the literature.[19] The corresponding salts **1** and **2** were obtained by the stoichiometric addition of potassium ethanolate, after the previous precipitation of KBF_4. Unfortunately, NO_2BF_4 is a relatively expensive reagent and decomposes under hydrolysis fuming on air. This complicates the storage of NO_2BF_4 and practicability. Hence, further research into other nitration methods using inexpensive reagents is highly desirable in order to compete with existing inexpensive lead compounds concerning the production for industrial purposes. By protecting the weak point, the amino group of the aminotetrazoles with a protecting group (e.g. carbamate functionality), harsh nitration conditions might be tolerated without observed decomposition. The addition of an excess of base might cleave the nitrated aminotetrazoles and could give access to the potassium salts. Further research studies in this area should be carried out to make these compounds economically attractive. As the used starting material 1-amino-5*H*-tetrazole is accessible through a selective synthetic route from standard feedstock without distillation or column chromatography, compound **1** indicates a great potential to compete in industrial purposes with existing used primaries.



Scheme 1. Different reaction routes using various nitration reagents starting from 1-amino-5*H*-tetrazole and 2-amino-5*H*-tetrazole.

The structural and molecular composition of **1** and **2** were confirmed by elemental analysis, X-ray diffraction, IR, and multinuclear NMR spectroscopy (^{1}H, ^{13}C, ^{14}N, and ^{15}N). Both isomers can easily be differentiated by NMR and IR analysis (Figure S1). Six nitrogen resonances were observed in each proton coupled ^{15}N NMR spectrum of **1** and **2** (Figure 1).

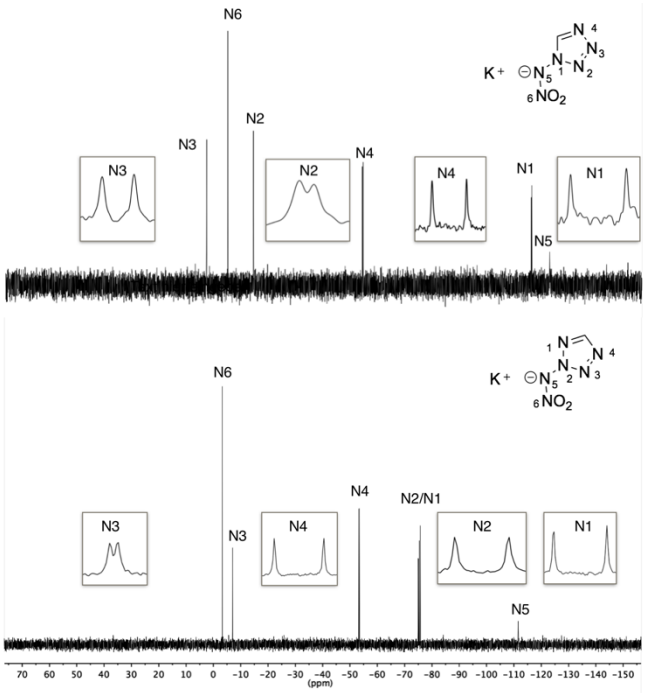


Figure 1. Proton-coupled ^{15}N NMR spectra of compound **1** and **2**.

5.3.2 Crystal Structures

Low-temperature X-ray diffraction was used to characterize **1** and **2**. The crystal structures were uploaded to the CSD database and can be obtained free of charge with the CCDC no. 1849956 (**1**) and 1849957 (**2**). Details to the measurement and refinement data are given in the SI. Compound **1** crystallizes in the form of colorless blocks in the monoclinic space group $P2_1/c$ with a density of 1.973 g cm^{-1}(143 K) and four molecules per unit cell. The molecular structure and coordination environment around the potassium cation of **1** are shown in Figures 2 and 3. The alkali metal is sevenfold coordinated by four different 1-nitraminotetrazolates, which bind with atoms N3, N4, O1, or O2.

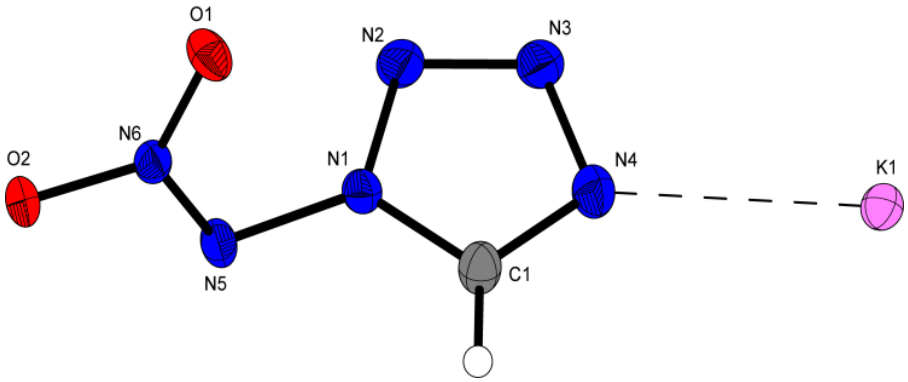


Figure 2. Molecular structure of **1**. Thermal ellipsoids of non-hydrogen atoms in all structures are set to the 50 % probability level. Selected bond lengths (pm): C1–H1 92.8(16), N1–C1 133.0(2), N4–C1 131.5(2), N3–N4 136.65(18), N2–N3 129.8(2), N1–N2 134.70(17), 140.47(19), N5–N6 131.81(18), N1–N5 140.5(19), O1–N6 124.70(15), O2–N6 127.10(17); symmetry codes: (i) 1+x, y, z; (ii) –x, –0.5+y, 0.5–z; (iii) 1–x, –0.5+y, 0.5–z; (iv) x, 0.5–y, –0.5+z; (v) 1+x, 0.5–y, 0.5+z.

Compound **2** is shown in Figure 4 and crystallizes in the form of colorless rods in the orthorhombic space group *Pbca* with eight formula units per unit cell and a calculated density of 1.983 g cm^{-1} (143 K). The densities of both isomers are slightly lower in comparison to K_2DNABT (2.172 g cm^{-3} (100 K)).[14] In both molecules, the nitro groups are twisted by 109.12° (**1**) and 108.06° (**2**) out of the ring plane, while N5 is almost planar to the tetrazole ring. A comparison of the bond lengths shows that the bond length in **1** between N5 and N6 is slightly shorter with 131.8 pm than in **2** (133.4 pm). These values lie between N-N single and double bonds[20], which reflects the electron-withdrawing effect of the nitro group on the amide moiety. The weakest bond in both molecules is between N1-N5 with 140.5 pm (**1**) and 139.4 pm (**2**). Further details on the crystal structure can be found in the Supporting Information.

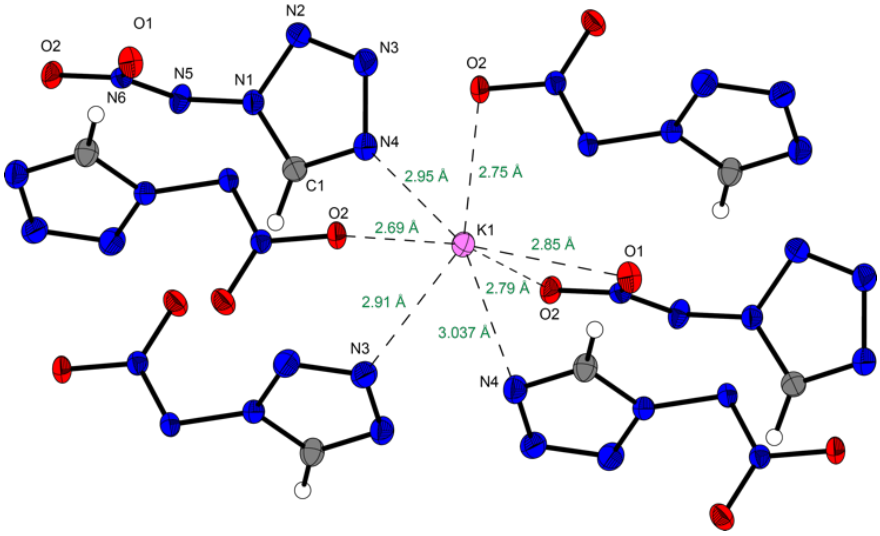


Figure 3. Coordination environment of the potassium cation in **1**.

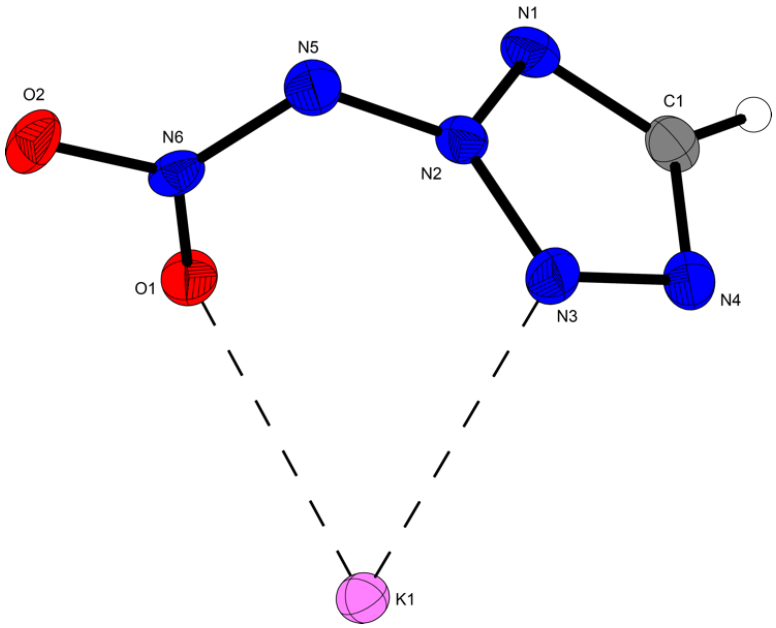


Figure 4. Molecular structure of **2**. Selected bond lengths (pm): C1–H1 94.7(17), N1–C1 132.1(2), N4–C1 134.11(19), N1–N2 132.50(17), N2–N3 131.75(17), N2–N5 139.37 (17), N3–N4 132.14(18), N5–N6 133.40(17), O1–N6 124.94(15), O2–N6 124.46(16); symmetry codes: (i) 0.5–x, 1–y, –0.5+z; (ii)–x, –0.5+y,0.5–z; (iii) 0.5+x, –1+y, 0.5–z; (iv) 0.5+x, y, 0.5–z; (v) 0.5–x, –0.5+y, z; (vi) x, 0.5–y, 0.5+z.

5.3.3 Scanning Electron Microscopy (SEM) and Energy-dispersive X-ray Spectroscopy (EDX)

Scanning electron microscopy in combination with energy dispersive X-ray spectroscopy was used to determine the morphology, grain size and chemical composition, which can strongly influence the observed sensitivities performed. Due to the simpler synthesis, the associated lower costs and the more promising characteristics of compound **1** compared to **2**, only this salt was measured by SEM and EDX. Compound **1** shows the consistency of small tubes with cavities (Figure 5). Aside from insignificant trace amounts of silicon, the EDX spectrum only shows elements which are actually present in the molecular structure. No contamination of fluorine or boron was detected.

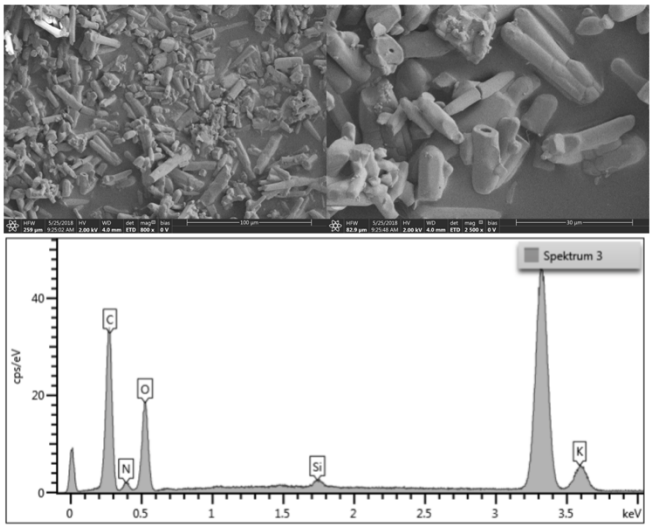


Figure 5. SEM image (800 x magnitude (left) and 2500 x magnitude (right)) and EDX spectrum of compound **1**.

5.3.4 Physicochemical Properties

Since all materials investigated are highly energetic compounds, their physicochemical properties were explored. The thermal behavior of compound **1** and **2** was investigated using DTA (Figure 6). Violent detonations could be observed for **1** at 180 °C, and 176 °C for compound **2**, after melting of both compounds shortly before (the decomposition peak of compound **2** is relatively broad due to the small amount of substance used for the measurement).

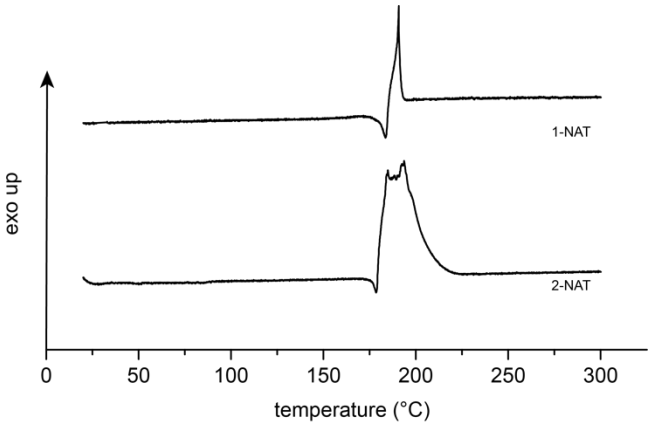


Figure 6. DTA plots of compound **1** and **2**.

To evaluate the potential of **1** and **2** as suitable green primary explosives, the sensitivity toward impact, friction, electrostatic were investigated (Table 1). The friction, impact, and electrostatic sensitivities of **1** and **2** are comparable to those of LA and K_2DNABT.[14] The measured friction

and ball drop impact sensitivities correspond to the lowest possible determinable values for the equipment used, which underlines the highly sensitive nature of these synthesized compounds. Interestingly, and to our surprise, compound **2** was slightly less sensitive toward impact than **1**. The detonation parameters of **1** and **2** were calculated using the latest EXPLO5 6.04 computer code.[21] Both compounds have very high positive heats of formation, as shown in Table 1.

Table 1. Explosive and detonation parameters of **1** and **2** in comparison to K_2DNABT and LA.

	1	**2**	**K_2DNABT**[14]	**$Pb(N_3)_2$**[22]
Formula	$CHKN_6O_2$	$CHKN_6O_2$	$C_2K_2N_{12}O_4$	N_6Pb
***IS*[a] [J]**	< 1	5	1	2.4–4
***FS*[b] [N]**	< 0.1	< 0.1	< 0.1	0.1–1.0
***ESD*[c] [mJ]**	0.9	8.2	3.0	< 5.0
***BDIS* [mJ]**	< 4[o]	< 4[o]	31.1[p]	53.3[q]
Ω_{CO2}[d] [%]	–6.2	–6.2	–4.8	–11.0
$T_{dec.}$[e] [°C]	180	176	200	320–360
δ[f] [g cm^{-3}]	1.928	1.938	2.172	4.80[n]
$\Delta_f H°$[g] [kJ mol^{-1}]	93.4	77.9	326.4	450.1[n]
$\Delta_f U°$[h] [kJ kg^{-1}]	621.7	529.6	1035.6	1574.9[n]
EXPLO5 6.04 values:				
$-\Delta_{ex}H°$[i] [kJ kg^{-1}]	4616	4526	4959	1575
T_{det}[j] [K]	3259	3209	3417	3285
P_{CJ}[k] [GPa]	25.0	25.1	32.5	34.9
V_{det}[l] [ms^{-1}]	7858	7882	8691	6077
V_0[m] [dm^3 kg^{-1}]	410	409	485	252

[a] Impact sensitivity (BAM drop-hammer (1 of 6)). [b] Friction sensitivity (BAM friction tester (1 of 6)). [c] Electrostatic discharge device (OZM research). [d] Oxygen balance (Ω = (xO–2yC–1/2zH)M/1600). [e] Onset temperatures measured by DTA (β = 5 °C min^{-1}). [f] X-ray densities converted to RT. [g] Calculated enthalpy of formation. [h] Calculated energy of formation. [i] Heat of explosion. [j] Temperature of detonation. [k] Detonation pressure. [l] Detonation velocity. [m] Gas volume after detonation (assuming only gaseous products). [n] From EXPLO5 database. [o] Ball drop impact sensitivity determined with the OZM ball drop tester applying the 1 of 6 method in accordance with the MIL-STD 1751A (method 1016). [p] E_{50} ball drop impact sensitivity determined with the OZM ball drop tester applying the Probit method with 10 trials at 6 different heights. [q] E_{50} ball drop impact sensitivity of dextrinated LA.[22]

As expected, the enthalpy of formation and energy of formation values are lower than for the double potassium salt K_2DNABT.[14]

The nitramino-5*H*-tetrazolate isomers outperform easily lead azide in performance parameters such as heat of explosion, detonation velocity and gas volume after detonation.[22] Nevertheless, the values are still below those of K_2DNABT, which can be attributed to the higher density and higher heat of formation. The value for the temperature of detonation is in the range of lead azide. From the point of view of detonation pressure, both isomers exhibit detonation pressures 10 GPa lower than for lead azide and 7.5 GPa lower than for K_2DNABT.

In order to determine the compounds' deflagration to detonation transition (DDT) capability, hot needle (HN) and hot plate (HP) tests were performed (Figure 7). The HN test was performed by the fixation of each compound underneath adhesive tape. The following penetration of **1** and

2 with a red-heated needle resulted in a vast detonation, which indicates their great potential as valuable primary explosives. The safe and straightforward HP test shows the behavior of the unconfined samples toward fast heating. Both compounds detonated also violently during the hot plate test with a slight bending of the plates.

5.3.5 Toxicity

To estimate the potential environmental impact of compound **1** and **2**, toxicity measurements were carried out using the luminesce marine bacterium *Vibrio fischeri*.[23] Our studies show that, after a time period of 30 min 85 % of the bacteria were unaffected at a concentration of 1.60 g L^{-1} (**1**) and 1.61 g L^{-1} (**2**). Due to the extreme non-toxicity of the compounds, no reasonably EC_{50} value could be determined with the dilution series used. Nevertheless, with values clearly over 1.00 g L^{-1}, both compounds can be considered as non-toxic (toxicity level after 30 min incubation: very toxic < 0.10 g L^{-1}, toxic 0.10–1.00 g L^{-1}, non-toxic > 1.00 g L^{-1}).[24]

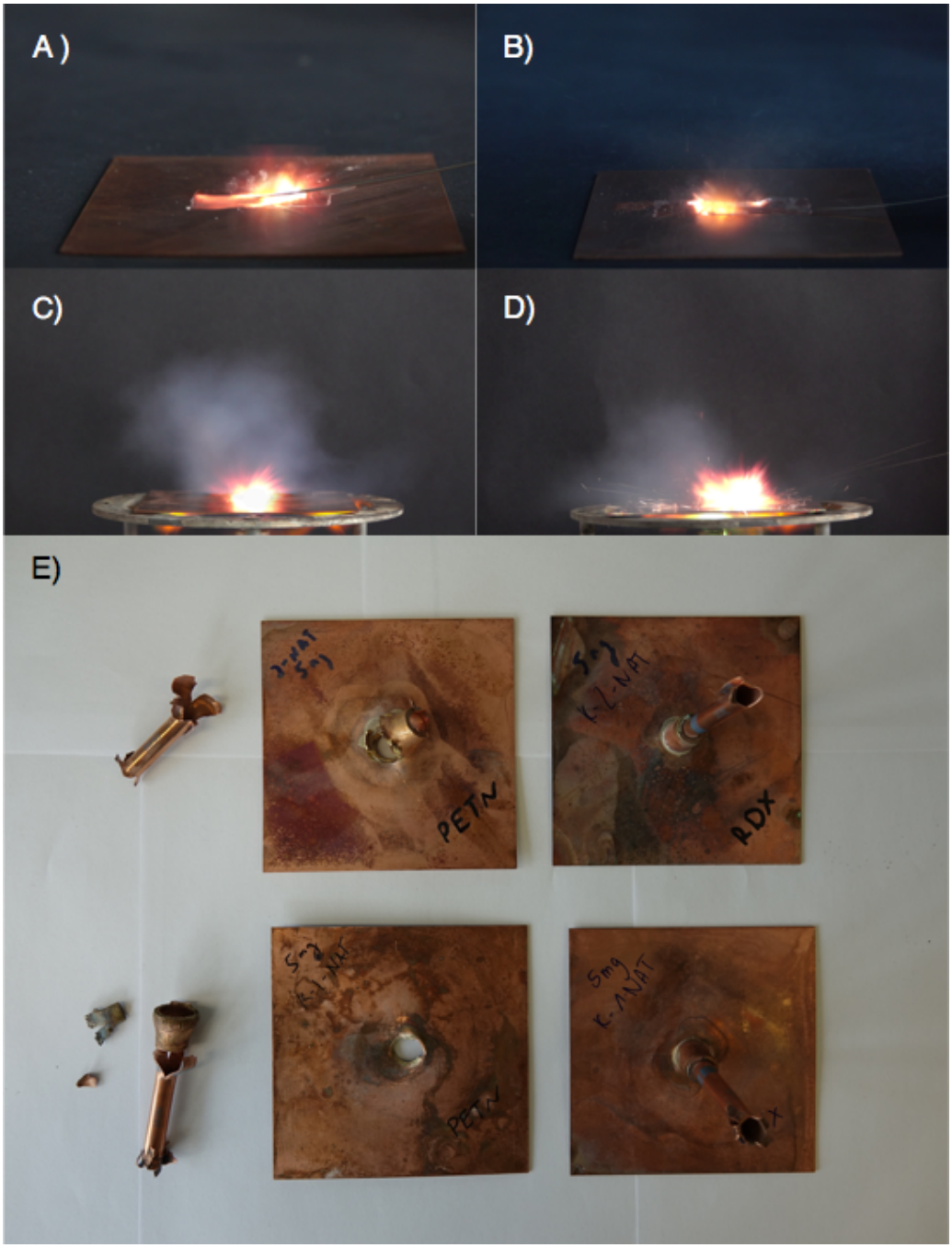


Figure 7. A) and B) HN test of **1** and **2**; C) and D) HP test of **1** and **2**; E) Positive PETN (left) and RDX (right) initiation tests with 5 mg of compound **1** (bottom) and **2** (top).

5.4 Conclusions

Potassium 1-(*N*-nitramino)-5*H*-tetrazolate (**1**, 1-KNAT) and its isomeric counterpart potassium 2-(*N*-nitramino)-5*H*-tetrazolate (**2**, 2-KNAT), two new promising primary explosives, could be synthesized through direct nitration of 1-amino-5*H*-tetrazole and 2-amino-5*H*-tetrazole and

subsequent addition of potassium ethanolate in a one-step reaction. The potassium salts that could be prepared by an alternative route compared to the literature-known ammonium and silver salts represent a good compromise between solubility, sensitivity, performance, and environmental compatibility. Since the compounds known from literature have been very poorly analyzed, this work carries out an extensive analytical study of the two potassium salts in order to close this gap. Both compounds were characterized by low-temperature X-ray diffraction and showed, unfortunately, a slightly lower density compared to K_2DNABT. In addition, the compounds were analyzed by vibrational (IR) and multinuclear NMR spectroscopy, as well as by EA. To identify impurity residues and to investigate the morphology, grain size and crystal habit of **1**, the latter was measured with scanning electron microscopy and energy dispersive X-ray spectroscopy. Thermal stability measurements by DTA showed satisfying exothermic decomposition temperatures around 180 °C. The measured sensitivities toward friction and impact, underline the highly sensitive character of the two isomers while remaining safe to handle. The calculations of the energetic properties of 1-KNAT and 2-KNAT, show their excellent performance in comparison to lead azide, outperforming LA in several important parameters. Easy thermal initiation was proven by hot plate and hot needle tests and an excellent secondary explosive initiation capability was observed. Only 5 mg of the two compounds were sufficient to initiate PETN and RDX reliably. Toxicity measurements using *Vibrio fischeri* showed the non-toxic character of the environmentally benign potassium salts. 1-KNAT can be considered as a promising lead-free green primary explosive for potential future initiation systems due to its simpler synthesis (starting material is more easily accessible) and better sensitivity values compared to **2**.

Supporting information available in the appendix in **Chapter 19.3**.

5.5 References

[1] P. E. Eaton, R. L. Gillardi, M. X. Zhang, Polynitrocubanes: Advanced High-Density, High-Energy Materials, *Adv. Mater.* **2000**, *12*, 1143–1148.

[2] T. M. Klapötke, C. Petermayer, D. G. Piercey, J. Stierstorfer, 1,3-Bis(nitroimido)-1,2,3-triazolate Anion, the N-Nitroimide Moiety, and the Strategy of Alternating Positive and

Negative Charges in the Design of Energetic Materials, *J. Am. Chem. Soc.* **2012**, *134*, 20827–20836.

[3] K. B. Landenberger, O. Bolton, A. J. Matzger, Energetic–Energetic Cocrystals of Diacetone Diperoxide (DADP): Dramatic and Divergent Sensitivity Modifications via Cocrystallization, *J. Am. Chem. Soc.* **2015**, *137*, 5074–5079.

[4] H. Gao, J. M. Shreeve, Azole-Based Energetic Salts, *Chem. Rev.* **2011**, *111*, 7377–7436.

[5] J. Zhang, L. A. Mitchell, D. A. Parrish, J. M. Shreeve, Enforced Layer-by-Layer Stacking of Energetic Salts towards High-Performance Insensitive Energetic Materials, *J. Am. Chem. Soc.* **2015**, *137*, 10532–10535.

[6] T. Yongxing, Y. Hongwei, W. Bo, J. Xuehai, L. Chunxu, C. Guangbin, Synthesis and Characterization of a Stable, Catenated N11 Energetic Salt, *Angew. Chemie Int. Ed.* **2013**, *52*, 4875–4877.

[7] https://echa.europa.eu/de/candidate-list-table (Acessed April 2018).

[8] M. H. V Huynh, M. D. Coburn, T. J. Meyer, M. Wetzler, Green primary explosives: 5-Nitrotetrazolato-N^2-ferrate hierarchies, *Proc. Natl. Acad. Sci.* **2006**, *103*, 10322 LP-10327.

[9] L. Shenghua, W. Yuan, Q. Cai, Z. Xiuxiu, Z. Jichuan, Z. Shaowen, P. Siping, 3D Energetic Metal–Organic Frameworks: Synthesis and Properties of High Energy Materials, *Angew. Chemie Int. Ed.* **2013**, *52*, 14031–14035.

[10] J. Qin, J. Zhang, M. Zhang, D. Du, J. Li, Z. Su, Y. Wang, S. Pang, S. Li, Y. Lan, A Highly Energetic N-Rich Zeolite-Like Metal-Organic Framework with Excellent Air Stability and Insensitivity, *Adv. Sci.* **2015**, *2*, 1500150.

[11] M. Armand, F. Endres, D. R. MacFarlane, H. Ohno, B. Scrosati, Ionic-liquid materials for the electrochemical challenges of the future, *Nat. Mater.* **2009**, *8*, 621.

[12] L. Zhai, X. Fan, B. Wang, F. Bi, Y. Li, Y. Zhu, A green high-initiation-power primary explosive: synthesis, 3D structure and energetic properties of dipotassium 3,4-bis(3-dinitromethylfurazan-4-oxy)furazan, *RSC Adv.* **2015**, *5*, 57833–57841.

[13] J. W. Fronabarger, M. D. Williams, W. B. Sanborn, D. A. Parrish, M. Bichay, KDNP – A Lead Free Replacement for Lead Styphnate, *Propellants Explos. Pyrotech.* **2011**, *36*, 459–470.

[14] D. Fischer, T. M. Klapötke, J. Stierstorfer, Potassium 1,1'-Dinitramino-5,5'-bistetrazolate: A Primary Explosive with Fast Detonation and High Initiation Power, *Angew. Chem. Int. Ed.* **2014**, *53*, 1–5.

[15] Y. Tang, C. He, L. A. Mitchell, D. A. Parrish, J. M. Shreeve, Potassium 4,4′-Bis(dinitromethyl)-3,3′-azofurazanate: A Highly Energetic 3D Metal–Organic Framework as a Promising Primary Explosive, *Angew. Chemie Int. Ed.* **2016**, *55*, 5565–5567.

[16] H. Chunlin, J. M. Shreeve, Potassium 4,5-Bis(dinitromethyl)furoxanate: A Green Primary Explosive with a Positive Oxygen Balance, *Angew. Chemie Int. Ed.* **2015**, *55*, 772–775.

[17] D. E. G. Jones, H. T. Feng, R. C. Fouchard, Kinetic Studies of the Thermal Decomposition of KDNBF, a Primer for Explosives, *J. Therm. Anal. Calorim.* **2000**, *60*, 917–926.

[18] P. Yin, D. A. Parrish, J. M. Shreeve, Energetic Multifunctionalized Nitraminopyrazoles and Their Ionic Derivatives: Ternary Hydrogen-Bond Induced High Energy Density Materials, *J. Am. Chem. Soc.* **2015**, *137*, 4778–4786.

[19] M. A. Ilyushin, A. N. Terpigorev, I. V. Tselinskii, Effect of Isomeric Structure of (*N*-Nitramino)tetrazoles on the Properties of Theirs Salts, *Russ. J. Gen. Chem.* **1999**, *69*, 1645–1657.

[20] A. F. Hollemann, E. Wiberg, *Lehrbuch der Anorganischen Chemie*, 101st Edition, de Gruyter, New York, **1999**.

[21] M.Sućeska, EXPLO5 Version 6.04 Users' Guide. Zagreb, Croatia: OZM; 2018.

[22] a) R. Meyer, J. Köhler, A. Homburg, In *Explosives*, Wiley-VCH: Weinheim, **2002,** p. 196–197; b) Military Standard 1751A (MIL-STD-1751A): safety and performance tests for qualification of explosives (high explosives, propellants and pyrotechnics), method 1016, Dec. 11, 2001.

[23] G. I. Sunahara, S. Dodard, M. Sarrazin, L. Paquet, G. Ampleman, S. Thiboutot, J. Hawari, A. Y. Renoux, *Ecotoxicol. Environ. Saf.*, **1998**, *39*, 185−194.

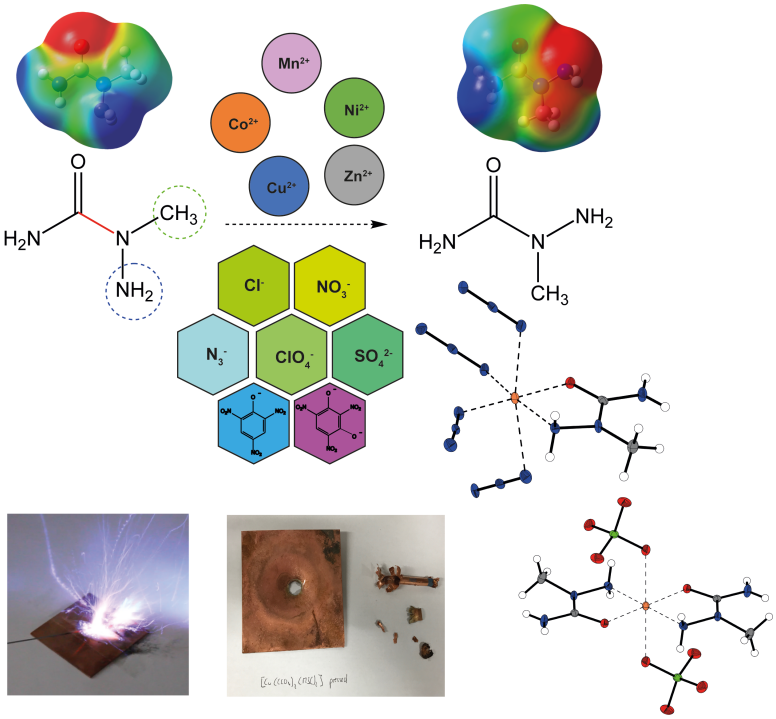
[24] C. J. Cao, M. S. Johnson, M. M. Hurley, T. M. Klapötke, *JANNAF J. Propuls. Energet.* **2012**, *5*, 41–51.

6 Methylsemicarbazide as a Ligand in Late 3d Transition Metal Complexes

Norbert Szimhardt and Jörg Stierstorfer

published in *Chemistry A European Journal* **2018**, *24,* 2687–2698

DOI: 10.1002/chem.201705030



Methylsemicarbazide (MSC) was successfully demonstrated as suitable building block in the formation of 25 new energetic coordination compounds (ECC). The further clever selection of late 3d metals, co-solvents and anions yielded a wide choice of different functional materials partly suitable for laser ignition or as classical primary explosive.

Abstract

Most ignition and initiation systems nowadays still contain poisonous chemicals such as lead styphnate and lead azide but also chromates and other compounds of high concern. Therefore, methylsemicarbazide (**1**, MSC), which can be prepared in a one-step reaction and an extraordinary high yield of 95 %, has been evaluated as ligand in energetic coordination compounds. For the first time 25 new transition metal complexes (Mn^{2+}, Ni^{2+}, Co^{2+}, Cu^{2+}, and Zn^{2+}) using methylsemicarbazide (**1**) as the ligand were prepared and comprehensively analyzed by e.g. XRD, IR, EA, UV/Vis and DSC/DTA/TGA. Many show a strong energetic character, which can be tuned by using different anions such as Cl^-, SO_4^{2-}, NO_3^-, ClO_4^-, picrate or styphnate. Selected compounds were additionally evaluated as lead-free primary explosives in initiation tests (nitropenta filled detonators) and in laser ignition systems. Especially compound **7** showed very promising results during these tests and could be a potential candidate for future applications.

6.1 Introduction

The investigation of energetic coordination compounds (ECC) is one of the most useful strategies in discovering new environmentally benign materials for ignition and initiation mixtures.[1-4] Ignition implies the release and transfer of energy in the form of heat, flame or subsonic shock waves. This is required for many different applications such as ammunition or in gas generators (e.g. airbags, oxygen candles). Igniters mostly contain a complex mixture of an inorganic pyrotechnic mixture or thermite as well as a weak primary explosive (often lead styphnate (LS) or diazodinitrophenol (DDNP)) and a sensitizer (often tetrazene).[5] Owing to their high toxicity and the related pollution of the environment, research into possible replacements is strongly needed.[6-8] Various requirements have to be fulfilled when synthesizing suitable candidates. The compound should not only be non-toxic and environmentally friendly but also be easily produced. Depending on the application, the mixtures can be ignited by impact, friction, light, electric impulses or heat. In contrast, initiation mixtures produce hypersonic shock waves, which are able to set of secondary explosives. Until the early 20th century, mercury fulminate (MF), first applied by Alfred Nobel, was the initiator of choice (Figure 1).[9] Nowadays, usually lead azide (LA) or silver azide are used. Initiation compositions are used e.g. in millions of commercial detonators for the mining industry but also in nearly all military warheads.

The use of late first row transition metals (Mn^{2+}, Fe^{2+}, Co^{2+}, Ni^{2+}, Cu^{2+}, Zn^{2+}) is a good compromise of (i) availability (ii) price (iii) density (iv) toxicity (only for Mn^{2+}, Fe^{2+}, Cu^{2+} and Zn^{2+}) and (v) the coordination ability to nitrogen-rich ligands because of low oxophilicity.

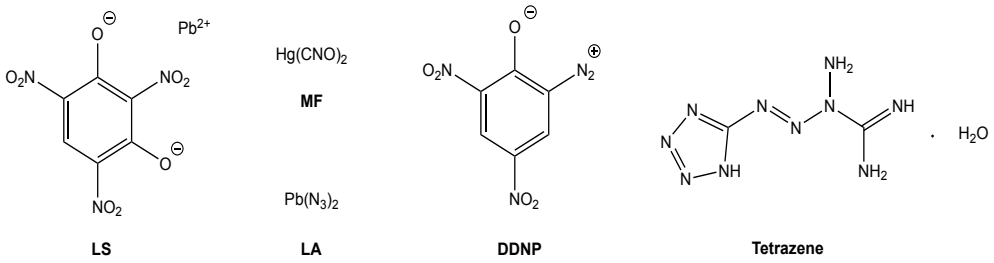


Figure 1. Molecular structures of lead styphnate (**LS**), mercury fulminate (**MF**), lead azide (**LA**), diazoniumdinitrophenolate (**DDNP**) and tetrazene.

Useful ECC contain (a) a metal cation, (b) nitrogen-rich ligands and (c) coordinating or non-coordinating anions (either oxygen-rich such as NO_3^-, ClO_4^-, $N(NO_2)_2^-$ or nitrogen-rich such as N_3^-, tetrazolates or triazolates). Various combinations have been described in the literature.[10] Highly energetic and sensitive complexes are formed by the combination of hydrazine derivatives (hydrazine, monomethylhydrazine, dimethylhydrazine, semicarbazide (SC), carbohydrazide (CHZ) but also N-amino-azoles) as the ligand with nitrate or perchlorate transition metal salts.[11,12] One of the most prominent ECC of this type is NHN (nickel hydrazine nitrate) which has also successfully been tested in detonators but contains very toxic nickel(II).[13]

Carbohydrazide (CHZ), which belongs to the group of carbazides was first synthesized 1894 by Curtius and Heidenreich who obtained the compound by the reaction of diethyl carbonate with hydrazine.[14] Since then, many carbazide-based compounds have been reported (prominent examples in Figure 2a) with manifold uses for example as precursor of drugs[15] and herbicides[16]. Also various coordination compounds were synthesized using carbazide ligands (Figure 2b) which are proposed to be interesting energetic materials[17]. Especially some of them with possible application as primary explosives[18] and partly also ignitable by laser irradiation (Figure 2b).[19] Some of the described CHZ and SC compounds are too sensitive for any potential use. In order to decrease the sensitivity, we synthesized methylsemicarbazide (**1**, MSC) as a new ligand for ECC. MSC has a higher carbon content and has been shown to be an outstanding ligand for the preparation of new energetic material complexes with tunable sensitivities and promising properties.

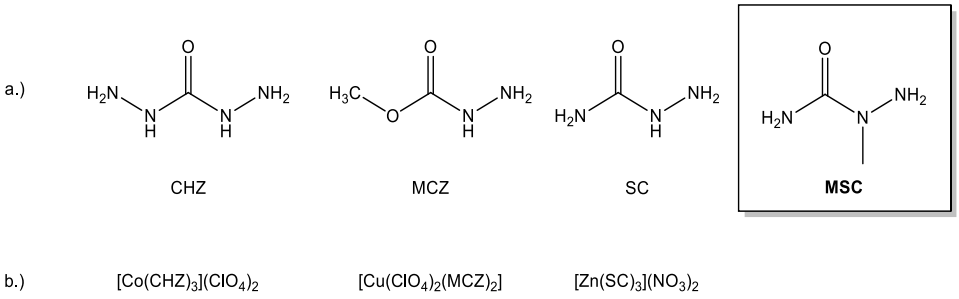
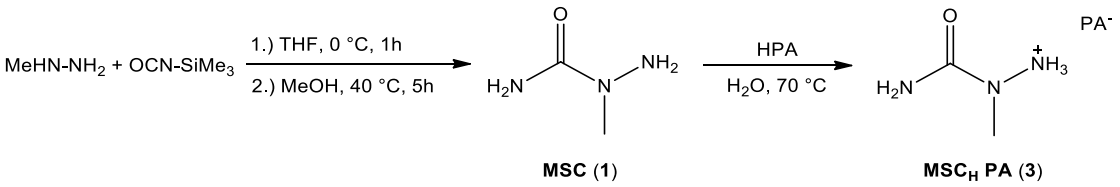


Figure 2. a.) Overview of selected carbazides; b.) energetic coordination compounds (ECC) with different carbazide ligands and transition metals.[20]

6.2 Results and Discussion

6.2.1 Synthesis

The title compound methylsemicarbazide (**1**) can be prepared mainly in two routes starting from different reactants. One way is the reaction of sodium cyanate with methylhydrazine in hydrochloric acid at 0 °C overnight followed by chromatographic purification.[21] Another route is the high-yielding reaction of commercially available trimethylsilylisocyanate with methylhydrazine carried out in dry THF (Scheme 1) at a temperature of 0 °C.[22] Due to the very hygroscopic character of (trimethylsilyl)isocyanate the reaction mixture was held constant under nitrogen atmosphere. Addition of methanol and heating to 40 °C for 5 hours led to the isolation of **1** with a high yield of 95 %. The acid-base reaction of **1** with picric acid in boiling water resulted in X-ray suitable crystals of the protonated picrate salt **3**.



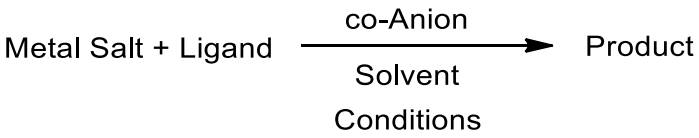
Scheme 1. Applied synthesis of methylsemicarbazide (**1**) and its protonated picrate salt (**3**).

Methylsemicarbazide (**1**) bears no acidic proton, which allows the inclusion of the neutral molecule to form complex cations or neutral metal coordination compounds with endothermic (e.g. azides) or oxidizing anions like nitrates, perchlorates, picrates (PA) or trinitroresorcinates (HTNR). The selective integration of these anions results in energetic coordination compounds with adjustable sensitivity and performance.

The coordination compounds **4**–**28** were prepared by the simple reaction of transition metal(II) salts with corresponding equivalents of methylsemicarbazide (**1**) as ligand in water at room or elevated temperatures (Table 1). Due to the good solubility of the resulting complexes only small quantities of solvents were used. In some cases, specific amounts of co-solvents like ethanol or acid were added to the reaction mixture in order to get better crystallization behavior, improved yields or higher purities. The concentration of acid used as co-solvent is significant for the formation of the complexes. Excessive amounts of acid, especially for the perchlorate complexes can cause protonation of the methyl-hydrazine moiety and associated blocking of a coordination site. In this context methylsemicarbazidium perchlorate (**2**) was observed. Another observation was the hydrolysis of methylsemicarbazide (**1**) in too strongly acidic media, which is detected by decomposition products like ammonium perchlorate. Also, in case of the cobalt(II) chloride complexes, two different species have been observed when using varying concentrations of acid. These are the blue water-free compound (**16**) from concentrated hydrochloric acid and a red diaqua complex (**17**) from diluted 2 M acid.

The synthesis of the zinc(II) perchlorate complexes **11** and **12** strongly depends on the stoichiometry of added ligand and yields two different coordination compounds with two or three ligands coordinating to the zinc(II) metal centre, respectively. The corresponding metal(II) salts for the complexes **19**–**28** were synthesized in situ by reaction of metal(II) carbonates and picric/styphnic acid at 70 °C in water. The colored reaction mixtures were left for crystallization until a solid appeared. All products were filtered off, washed with cold ethanol to remove unreacted starting materials when necessary and dried overnight in air. Most of the compounds were obtained in yields of 28–97 % directly from the mother liquor in form of suitable crystals for X-ray determination within hours or days (details are conducted in the experimental part in the SI). Only complexes **20** and **23** precipitated as amorphous powders after the addition of the ligand and all recrystallization attempts failed. A complex formula based on elemental analysis of $[M^{II}(MSC)_3](PA)_2$ is proposed for compounds **20** and **23**. The majority of the coordination compounds were isolated water-free (without crystal water molecules or aqua ligands) which leads to a higher performance and thermal stability of the compounds. All compounds, except **2** and **16**, could be synthesized and characterized in larger quantities. For the perchlorate salt **2** and the cobalt(II) chlorido complex **16**, unfortunately, only a few single crystals could be picked between unreacted starting material, decomposition products and powder bulk material with unknown constitution. Therefore; only the crystal structures of **2** and **16** could be determined which are shown in the SI. The attempted syntheses of iron(II) and (III) as well as Ag(I) complexes were unsuccessful.

Table 1. Synthesis of transition metal complexes **4**–**28** with methylsemicarbazide.



Metal Salt	Ligand	co-Anion	Solvent	Conditions	Product	No.
$CuSO_4 \cdot 5\ H_2O$	2 MSC		H_2O	RT	$[Cu(H_2O)_2(MSC)_2]SO_4$	(**4**)
$CuCl_2 \cdot 2\ H_2O$	2 MSC		H_2O, 15% HCl	RT	$[CuCl_2(MSC)_2]$	(**5**)
$Cu(NO_3)_2 \cdot 3\ H_2O$	2 MSC		H_2O, EtOH	RT	$[Cu(NO_3)_2(MSC)_2]$	(**6**)
$Cu(ClO_4)_2 \cdot 6\ H_2O$	2 MSC		H_2O, 70% $HClO_4$	RT	$[Cu(ClO_4)_2(MSC)_2]$	(**7**)
$CuSO_4 \cdot 5\ H_2O$	1 MSC	2 NaN_3	H_2O	60 °C, 5 min	$[Cu(N_3)_2MSC]$	(**8**)
$ZnCl_2$	2 MSC		H_2O	RT	$[ZnCl_2(MSC)_2]$	(**9**)
$Zn(NO_3)_2 \cdot 6\ H_2O$	2 MSC		H_2O, EtOH	RT	$[Zn(NO_3)_2(MSC)_2]$	(**10**)
$Zn(ClO_4)_2 \cdot 6\ H_2O$	2 MSC		H_2O	RT	$[Zn(H_2O)_2(MSC)_2](ClO_4)_2$	(**11**)
$Zn(ClO_4)_2 \cdot 6\ H_2O$	3 MSC		H_2O	RT	$[Zn(MSC)_3](ClO_4)_2 \cdot H_2O$	(**12**)
$MnCl_2 \cdot 2\ H_2O$	2 MSC		H_2O	RT	$[MnCl_2(MSC)_2]$	(**13**)
$Mn(NO_3)_2 \cdot 4\ H_2O$	2 MSC		H_2O	RT	$[Mn(NO_3)_2(MSC)_2]$	(**14**)
$Mn(ClO_4)_2 \cdot 6\ H_2O$	2 MSC		H_2O	RT	$[Mn(H_2O)_2(MSC)_2](ClO_4)_2$	(**15**)
$CoCl_2 \cdot 6\ H_2O$	2 MSC		H_2O, conc. HCl	RT	$[CoCl_2(MSC)_2]$	(**16**)
$CoCl_2 \cdot 6\ H_2O$	2 MSC		H_2O, 2M HCl	RT	$[Co(H_2O)_2(MSC)_2]Cl_2$	(**17**)
$Ni(ClO_4)_2 \cdot 6\ H_2O$	3 MSC		H_2O	50 °C, 5 min	$[Ni(MSC)_3](ClO_4)_2$	(**18**)
$CuCO_3$	2 MSC	2 HPA	H_2O	70 °C, 5 min	$[Cu(PA)_2(MSC)_2]$	(**19**)
$ZnCO_3 \cdot 3\ Zn(OH)_2$	12 MSC	2 HPA	H_2O	70 °C, 5 min	$[Zn(MSC)_3](PA)_2$	(**20**)
$MnCO_3$	2 MSC	2 HPA	H_2O	70 °C, 5 min	$[Mn(PA)_2(MSC)_2]$	(**21**)
$CoCO_3 \cdot H_2O$	2 MSC	2 H_2TNR	H_2O	70 °C, 5 min	$[Co(PA)_2(MSC)_2]$	(**22**)
$NiCO_3 \cdot 2\ Ni(OH)_2 \cdot 4\ H_2O$	9 MSC	2 H_2TNR	H_2O	70 °C, 5 min	$[Ni(MSC)_3](PA)_2$	(**23**)
$CuCO_3$	2 MSC	2 H_2TNR	H_2O	70 °C, 5 min	$[Cu(H_2O)_2(MSC)_2](HTNR)_2$	(**24**)
$ZnCO_3 \cdot 3\ Zn(OH)_2$	8 MSC	2 H_2TNR	H_2O	70 °C, 5 min	$[Zn(H_2O)_2(MSC)_2](HTNR)_2$	(**25**)
$MnCO_3$	2 MSC	2 H_2TNR	H_2O	70 °C, 5 min	$[Mn(HTNR)_2(MSC)_2]$	(**26**)
$CoCO_3 \cdot H_2O$	2 MSC	2 H_2TNR	H_2O	70 °C, 5 min	$[Co(H_2O)_2(MSC)_2](HTNR)_2$	(**27**)
$NiCO_3 \cdot 2\ Ni(OH)_2 \cdot 4\ H_2O$	6 MSC	2 H_2TNR	H_2O	70 °C, 5 min	$[Ni(H_2O)_2(MSC)_2](HTNR)_2$	(**28**)

6.2.2 Crystal Structures

The structures of all complexes (except **20** and **23**) were determined by low temperature crystal X-ray diffraction. Details on the crystal structures of compounds **5**, **6**, **9**, **19**, **21**, **24**, **25**, **27** are given in the SI together with the measurement and refinement data. Single crystals of the zinc(II), manganese(II) and nickel(II) perchlorate complexes **11**, **12**, **15** and **18** were measured to give an indication of the most likely composition. An adequate refinement of the data set was not possible because of the strongly disordered moieties, however elemental analysis confirmed its preliminary observed structures. The coordination compounds **11**/**15** and **20**/**23** exhibit the same coordination environment and their infrared absorptions were therefore compared by infrared spectroscopy (Figure S11/12). The crystal structures were deposited to the CSD database[23] and can be obtained free of charge with the CCDC nos. 1534424 (**1**),

1534443 (**2**), 1574510 (**3**), 1534422 (**4**), 1534425 (**5**), 1534426 (**6**), 1534428 (**7**), 1534427 (**8**), 1580445 (**9**), 1534421 (**10**), 1534435 (**13**), 1534440 (**14**), 1534429 (**16**), 1534441 (**17**), 1534429 (**19**), 1574511 (**21**), 1574509 (**22**), 1534442 (**24**), 1534434 (**25**), 1534437 (**26**), 1534420 (**27**), 1534423 (**28**).

Methylsemicarbazide (**1**) crystallizes in the monoclinic space group $P2_1/n$ with four formula units per unit cell and a calculated density of 1.288 g cm^{-3} at 173 K. Selected bond distances and angles of the molecule are given in Figure 3. The C–O (1.249(2) Å), C1–N1 (1.346(2) Å) and N–N (1.414(2) Å)) bonds are comparable to values found in carbohydrazide and urea. Lengthening of the C–O double bond comes along with shorter C–N and N–N single bond distances and confirms the conjugation of these atoms.[24,25] In addition, stabilization of the molecular structure is generated through strong intermolecular hydrogen bonds formed between the carbonyl function and the neighboring amino groups (N1–H1B··O1 0.93(2), 2.02(2), 2.9428(19) Å, 172(17)°; N3–H3A··O1 0.947(18), 2.052(18), 2.9920(19) Å, 171.7(15)°, N3–H3B··O1 0.91(2), 2.25(2), 3.148(2) Å, 172.5(16)°). These observations are consistent with the almost planar geometry of the molecule (< (N3–N2–C1–N1) = −5.8(2)°; < (C2–N2–C1–O1) = 6.9(2)°).

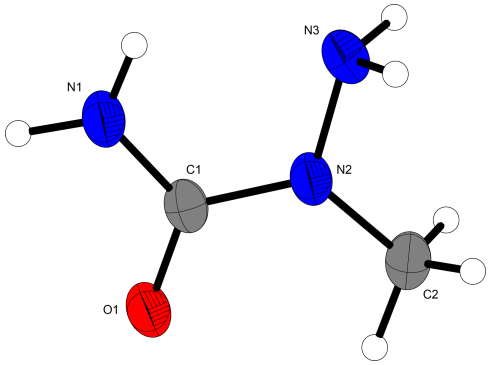


Figure 3. Molecular structure of methylsemicarbazide (**1**). Thermal ellipsoids of non-hydrogen atoms in all structures are set to the 50 % probability level. Selected bond lengths (Å): O1–C1 1.249(2), N1–C1 1.346(2), N2–N3 1.414(2), N2–C1 1.349(2), N2–C2 1.445(2); selected bond angles (°): N3–N2–C1 117.81(2), N1–C1–N2 117.26(2), N3–N2–C2 119.20(2), O1–C1–N1 121.40(2), C1–N2–C2 122.26(2), O1–C1–N2 121.28(2); selected torsion angles (°): N3–N2–C1–N1 −5.8(2), C2–N2–C1–O1 6.9(2).

As described above, parent compound **1** can be protonated under certain acidic conditions. Protonation takes place on the NH_2 group of the methylhydrazine functional group and causes a reorientation of half of the molecule. The salts show significantly higher densities in comparison to the neutral molecule (**2**: 1.734 g cm^{-3} (123 K); **3**: 1.750 g cm^{-3} (143 K) vs. 1.288

g cm^{-3} (173 K) for **1**). The perchlorate compound **2** crystallizes in the monoclinic space group $P2_1/c$ with sixteen formula units per unit cell. On the other hand, the picrate salt **3** crystallizes in the triclinic space group $P\bar{1}$ with two molecules in the unit cell. Structural parameters and the molecular structures of both salts are shown in Figure 4. Salt formation had no significant influence on the bond distances but rather on the planarity of the methysemicarbazinium cation with a torsion angle of < (C2–N2–C1–N3) = −30.1(6)° in **3**.

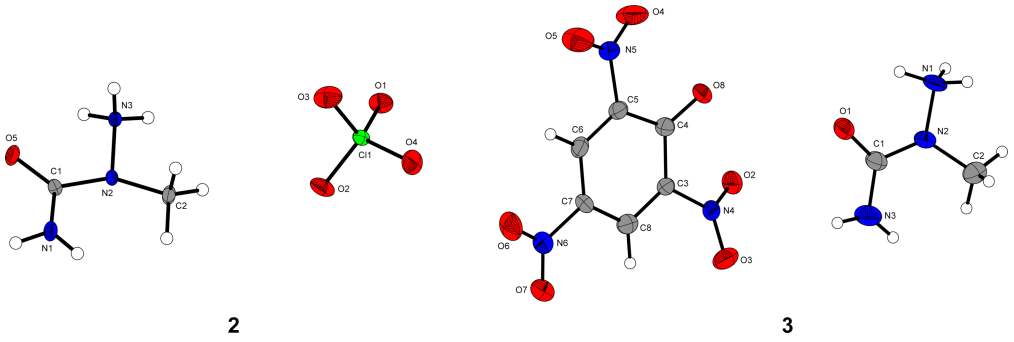


Figure 4. Molecular moieties of the MSC salts **2** (left) and **3** (right). Selected bond lengths (Å): **2**: N1–C1 1.325(4), N2–N3 1.430(3), N2–C2 1.464(4), N2–C1 1.386(4), C1–O5 1.238(4) Cl1–O1 1.438(2); **3**: N1–N2 1.446(5), N2–C1 1.405(5), N2–C2 1.457(6), N3–C1 1.322(6), C1–O1 1.228(6); selected bond angles (°): **2**: N3–N2–C1 111.3(2), N3–N2–C2 112.9(2), C1–N2–C2 124.2(2), O1–C1–N1 125.1(3), O1–C1–N2 118.0(3); **3**: N1–N2–C1 110.5(3), N1–N2–C2 112.9(3), C1–N2–C2 122.9(2), O1–C1–N2 119.7(4), O1–C1–N3 124.3(4); selected torsion angle (°): **3**: C2–N2–C1–N3 −30.1(6).

The bond distances and most angles of the coordinating MSC ligands in the examined coordination compounds are similar to the non-coordinated ligand **1**. The carbazide ligand is therefore not investigated or discussed in more detail in any of the compounds crystal structures outlined below. Methylsemicarbazide (**1**) is bidentate and coordinates through the carbonyl oxygen and amino-methylhydrazine nitrogen atom to the transition metal. A reorientation of the MSC molecule, already described in the salts **2** and **3**, can be observed in the complexes (Figure 5). All complexes show a (more or less) octahedral coordination sphere, which can be explained by the low steric hindrance of the ligand.

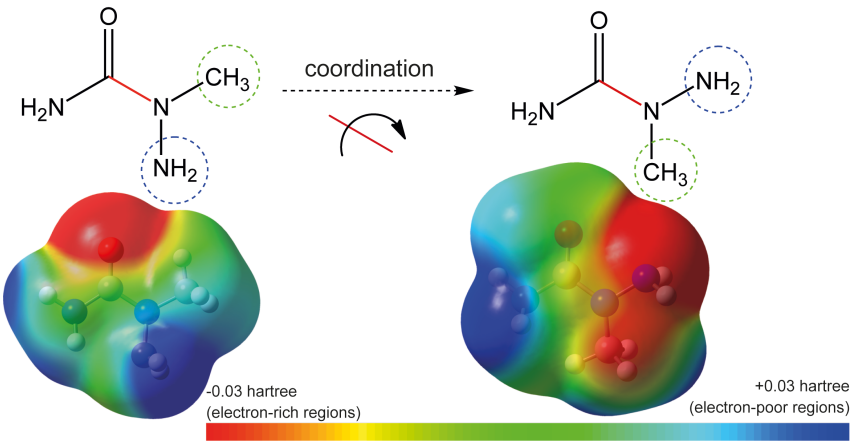


Figure 5. Reorientation of the MSC molecule after coordination or salt formation and depiction of the calculated (B3LYP / 6-31G(d,p)) electrostatic potentials (3D isosurface of electron density) of **1** and its coordinated form.

The copper(II) sulfate complex **4** crystallizes in the form of blue rods in the monoclinic space group $P2_1/c$ with four formula units per unit cell and a calculated density of 1.857 g cm^{-3} at 123 K. The molecular unit shown in Figure 6 consists of a octahedrally surrounded copper(II) center with two aqua ligands along the Jahn-Teller distorted axial axis (Cu1–O8 = 2.495(3) Å) and two bidentaly connected MSC ligands in a plane (Cu1–O5 = 1.934(3) Å, Cu1–N2 = 1.977(4) Å, < (O5—Cu1—N2) = 83.28(1)°, < (O5—Cu1—N2^{i}) = 96.73(12)°). All complexes described here show higher densities than the non-coordinating MSC molecule itself.

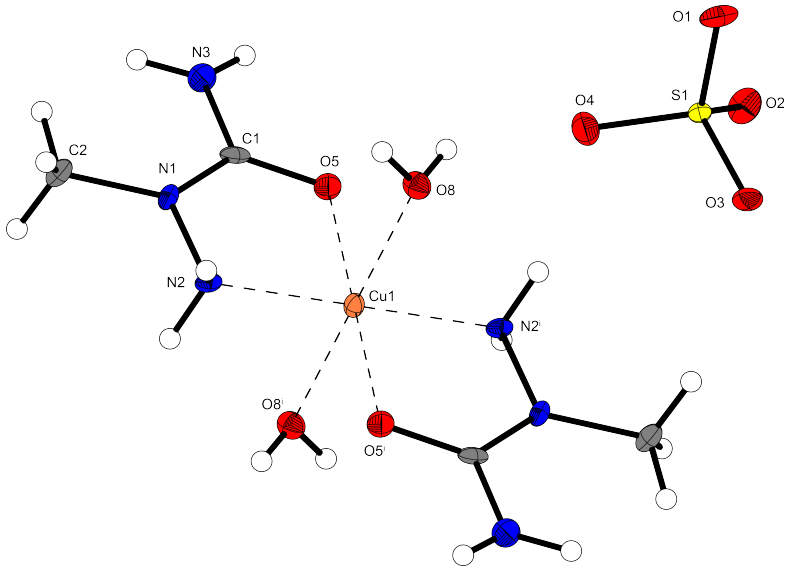


Figure 6. Molecular unit of $[Cu(H_2O)_2(MSC)_2]SO_4$ (**4**). Selected bond lengths (Å): Cu1–O5 1.934(3), Cu1–O8 2.495(3), Cu1–N2 1.977(4), S1–O1 1.467(3); selected bond angles (°): O5–Cu1–O8 88.03(11), O5–Cu1–N2 83.28(12), O8–Cu1–N2 90.26(12), O5–Cu1–O8^{i} 91.97(11), O5–Cu1–N2^{i} 96.73(12), O1–S1–O2 109.77(16). Symmetry code: (i) −x, −y, −z.

Complexes **5** (copper(II), green block, Figure S1), **9** (zinc(II), colorless block, Figure S2) and **16** (cobalt(II), blue block) with coordinating chlorido ligands crystallize in the monoclinic space group $P2_1/c$ with two formula units per unit cell showing similar densities (**5**: 1.838 g cm^{-3} at 123 K; **9**: 1.799 g cm^{-3} and **16**: 1.791 g cm^{-3} at 123 K). The remaining complex **13** with coordinating chlorido ligands and manganese(II) transition metal center (colorless block, Figure S3) also crystallizes in a monoclinic space group ($P2_1/n$) with four formula units per unit cell and exhibits a calculated density of 1.765 g cm^{-3} at 173 K. Every metal(II) center, as illustrated for compound **16** (Figure 7), shows an octahedral surrounding with two chloridos and two methylsemicarbazides. On the contrary, the cobalt(II) chloride complex **17** is composed of two aqua ligands and two MSC ligands. The chlorides act only as counter-anions (Figure 7). It crystallizes in the monoclinic space group $P2_1/n$ with four formula units per unit cell and has a calculated density of 1.735 g cm^{-3} at 123 K.

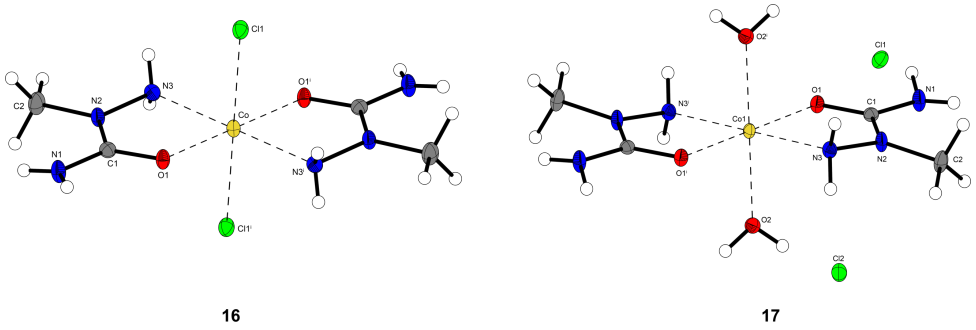


Figure 7. Complex units of compound **16** (left) and **17** (right). Selected coordination distances (Å): **16**: Co–Cl1 2.4935(6), Co1–O1 2.0396(16), Co1–N3 2.140(2); **17**: Co1–O2 2.1016(17), Co1–N3 2.138(2), Co1–O3 2.0505(16); selected bond angles (°): **16**: Cl1–Co–O1 88.48(5), Cl1–Co–N3 91.22(7), Cl1–Co–O1^{i} 91.53(5), Cl1–Co–N3^{i} 88.78(7), O1–Co–N3 78.46(8), O1–Co–N3^{i} 101.54(8); **17**: O2–Co1–O1 91.09(2), O2–Co1–N3 88.67(2), O1–Co1–N3 78.06(2), N3–Co1–O1 101.94(2). Symmetry codes: **16**: (i) 1−x, −y, 1−z; **17**: (i) 1−x, 1−y, 1−z.

The copper(II) and manganese(II) nitrato complexes **6**/**14** crystallize isotypically in the triclinic space group $P\bar{1}$ with one formula unit per unit cell (**6**: blue block, 1.873 g cm^{-3}; **14**: colorless block, 1.752 g cm^{-3} at 173 K). The colorless zinc(II) nitrato compound **10** crystallizes in the monoclinic space group $P2_1$ with two formula units per unit cell and a calculated density of 1.860 g cm^{-3} (123 K). Each metal(II) cation is bonded to two nitrato ligands in axial positions and two MSC ligands in equatorial positions. As expected, the d^9-copper(II) center shows Jahn-Teller distortion (elongation in axial direction). Their molecular motifs are illustrated in Figure 8 and S4.

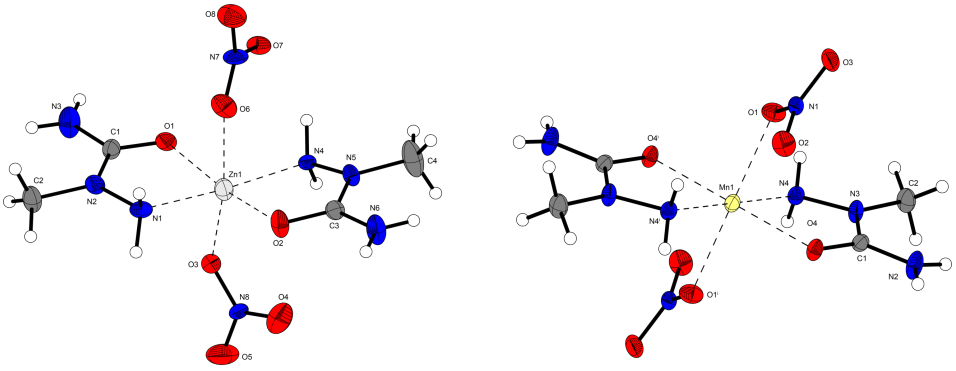


Figure 8. Molecular units of compounds **10** (left) and **14** (right). Selected coordination distances (Å): **10**: Zn1–O1 2.061(6), Zn1–O2 2.046(6), Zn1–O3 2.145(9), Zn1–O6 2.351(9), Zn1–N1 2.073(10), Zn1–N4 2.092(9); **14**: Mn1–O1 2.2176(17), Mn1–N4 2.268(2), Mn1–O4 2.1392(15); selected bond angles (°): **10**: O1–Zn1–O2 169.2(4), O1–Zn1–O3 88.7(3), O1–Zn1–O6 85.8(3), O1–Zn1–N1 78.9(4), O1–Zn1–N4 100.5(3), O2–Zn1–O3 102.0(4), O2–Zn1–O6 83.5(4), O2–Zn1–N1 99.5(4), O2–Zn1–N4 80.3(4), O3–Zn1–O6 172.5(3), O3–Zn1–N1 87.9(4), O3–Zn1–N4 97.1(3), O6–Zn1–N1 86.1(4), O6–Zn1–N4 89.0(3), N1–Zn1–N4 175.0(4); **14**: O1–Mn1–O4 89.53(5), O1–Mn1–N4 83.80(7), O1–Mn1–O4^{i} 90.47(5), O1–Mn1–N4^{i} 96.20(7), O4–Mn1–N4 73.24(6), O4–Mn1–N4^{i} 106.76(6). Symmetry code: **14**: (i) 2−x, −y, 2−z.

From an energetic perspective the most interesting copper(II) perchlorato complex **7** is octahedrally coordinated by two perchlorato ligands in Jahn-Teller distorted axial positions and by two chelating MSC ligands in a plane (Figure 9). It crystallizes in the form of blue blocks in the monoclinic space group $P2_1/c$ with two formula units per unit cell and the highest calculated density of 2.055 g cm^{-3} at 123 K of all complexes described here.

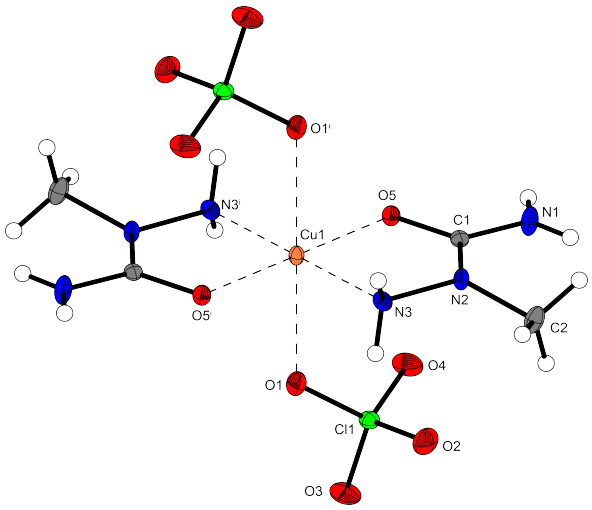


Figure 9. Complex unit of the highly energetic complex [Cu(ClO$_4$)$_2$(MSC)$_2$] (**7**). Selected bond lengths (Å): Cu1–O1 2.4730(16), Cu1–O5 1.9257(15), Cu1–N3 1.994(2), Cl1–O1 1.4472(**16**); selected

bond angles (°): O1–Cu1–O5 91.41(6), O1–Cu1–N3 90.07(7), O1–Cu1–O5i 88.59(6), O1–Cu1–N3i 89.93(7), O5–Cu1–N3 82.83(8), O5–Cu1–N3^{i} 97.17(8), O1–Cl1–O2 108.57(11). Symmetry code: (i) 2−x, −y, 1−z.

Copper(II) azido complex **8** crystallizes in the form of green needles in the monoclinic space group $P2_1/c$ with four formula units per unit cell and a calculated density of 2.016 g cm^{-3} at 123 K. Every copper(II) center is hexa-coordinated by one chelating MSC molecule and four bridging azido ligands forming polymeric chains. It is the only octahedral complex with just one methylsemicarbazide ligand coordinating to the metal(II) center. Due to the d^9-induced Jahn-Teller distortion, elongation along the axial sites can be observed, which are occupied by azido ligands (Cu1–N6^{ii} = 2.636(3) Å, Cu1–N9^{i} = 2.479(2) Å). The coordination environment of the copper(II) cation is depicted in Figure 10a and shows the small deviation of the ideal coordination sphere caused by the fixed structure of the azidos and the MSC ligand (< (O1—Cu1—N3) = 81.52(7)°, < (N3—Cu1—N6^{ii}) = 78.03(10)°). Various coordination and bridging modes of the azido ligands (1,1; 1,3; 1,1,3; 1,1,1 etc.) are possible and known in literature.[26] The azido ligand N4—N5—N6 connects two copper(II) centers through cis 1,3-coordination while trans 1,3-coordination can be observed for the second azido equivalent N7—N8—N9 (Figure 10b). This end-on binding situation causes similar bond lengths and almost linear bond angles within the azido groups (N4–N5 = 1.204(3) Å, N5–N6 = 1.162(3) Å, N7–N8 = 1.195(3) Å, N8–N9 = 1.160(4) Å, < (N4—N5—N6) = 176.4(3)°, < (N7—N8—N9) = 179.6(3)°).

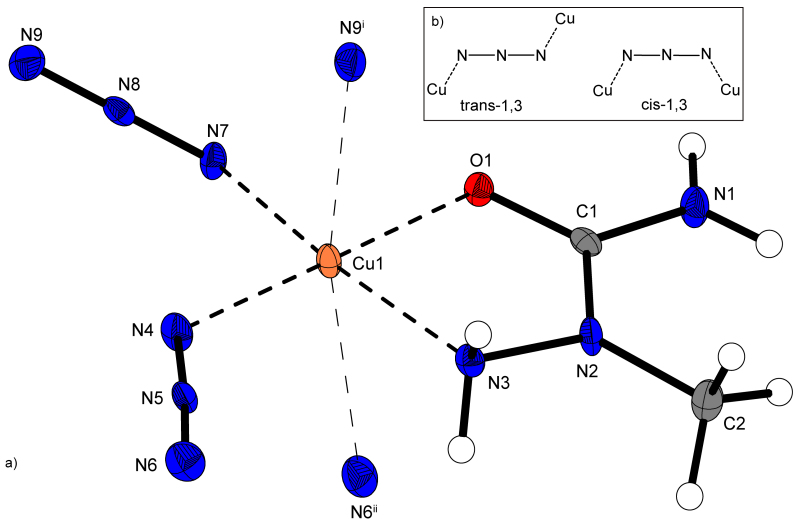


Figure 10. a.) Depiction of the octahedral coordination environment of the copper(II) cation in **8**. Selected bond lengths (Å): Cu1–O1 1.957(2), Cu1–N3 2.012(3), Cu1–N4 1.963(3), Cu1–N7 1.988(2), Cu1–N6^{ii} 2.636(3), Cu1–N9^{i} 2.479(2), N4–N5 1.204(3), N5–N6 1.162(3), N7–N8 1.195(3), N8–N9 1.160(4); selected bond angles (°): O1–Cu1–N3 81.52(9), O1–Cu1–N4 179.24(9), O1–Cu1–N7

88.72(9), O1–Cu1–N6^{ii} 85.14(9), O1–Cu1–N9^{i} 86.59(9), N3–Cu1–N4 99.15(10), N3–Cu1–N7 169.26(10), N3–Cu1–N6^{ii} 78.03(10), N3–Cu1–N9^{i} 92.01(10), N4–Cu1–N7 90.58(10), N4–Cu1–N6^{ii} 94.63(11), N4–Cu1–N9^{i} 93.75(11), N6^{ii}–Cu1–N7 96.77(9), N7–Cu1–N9^{i} 91.88(9), N6^{ii}–Cu1–N9^{ii} 167.88(8), N4–N5–N6 176.4(3), N7–N8–N9 179.6(3). Symmetry codes: (i) 2.5−x, −0.5+y, 0.5−z; (ii) 1.5−x, 0.5+y, 0.5−z; b.) Observed coordination modes of the azido ligand in **8**.

The water-free copper(II) **19** (green block), manganese(II) **21** (yellow block) and cobalt(II) **22** (orange block) picrate complexes crystallize isotypically to each other in the triclinic space group *P*−1 with one formula unit per unit cell exhibiting very similar calculated densities (**19**: 1.885 g cm^{-3} at 123 K; **21**: 1.825 g cm^{-3} and **22**: 1.866 g cm^{-3} at 143 K) and cell dimensions. Their molecular unit consist of two chelating MSC ligands and two picrate ligands in axial positions (Figure S5/6 and 11). The picrate anion binds via its deprotonated phenolate-group to the transition metal(II) in a monodentate way causing shortening of the MSC bond angle due to the steric hindrance of the trinitrobenzene derivative (< (O1—Co1—N3) = 77.42(7)°).

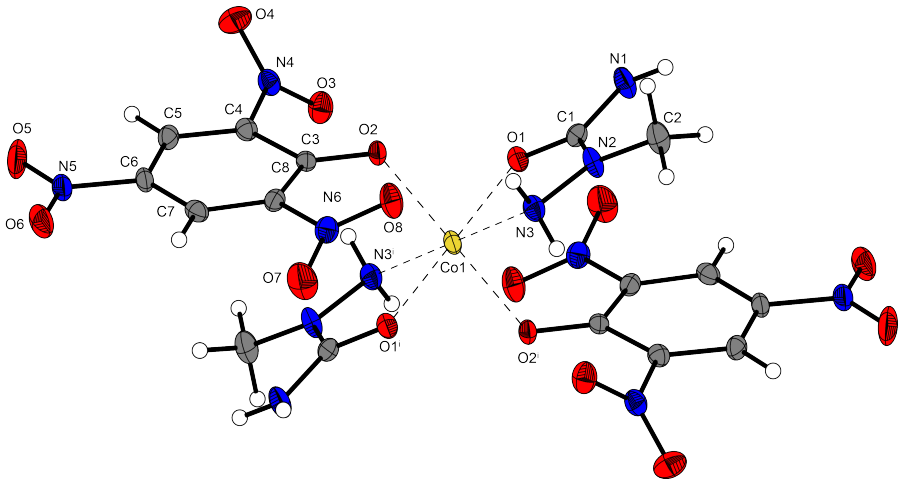


Figure 11. Molecular unit of the cobalt(II) picrate complex **22**. Selected bond lengths (Å): Co1–O1 2.0664(15), Co1–O2 2.1136(13), Co1–N3 2.115(2); selected bond angles (°): O1–Co1–O2 90.36(6), O1–Co1–N3 77.42(7), O1–Co1–O2^{i} 89.64(5), O1–Co1–N3^{i} 102.58(7), O2–Co1–N3 89.26(7), O2–Co1–N3^{i} 90.74(7). Symmetry code: (i) 1−x, 1−y, −z.

In comparison to the picrate compounds discussed so far, the styphnate counter-anions do not coordinate to the transition metals(II) in compounds **24**/**25** and **27**/**28**, which crystallize isotypically in the triclinic space group *P*−1 with one formula unit per unit cell and analogous cell parameters. Their densities increase in the row of Ni^{2+} (1.844 g cm^{-3}; 173 K) < Co^{2+} (1.852 g cm^{-3}; 123 K) < Zn^{2+} (1.866 g cm^{-3}, 123 K) < Cu^{2+} (1.880 g cm^{-3}; 173 K). The molecular unit of the complexes illustrated in Figure 12 and in the SI are built up by two aqua ligands, two MSC ligands and two non-coordinating styphnates. The space group *P*−1 could

also be determined for the water-free manganese(II) picrate complex **26** (1.892 g cm^{-3} at 123 K), which shows a different molecular composition with no aqua ligands, but two coordinating styphnate ligands instead (Figure 12). A similar situation that was found for the picrates with distortion along the MSC bond angle can also be observed for the styphnate coordination compounds. Each copper(II) complex in **19** and **24** show Jahn-Teller distortion with longer axial bond distances.

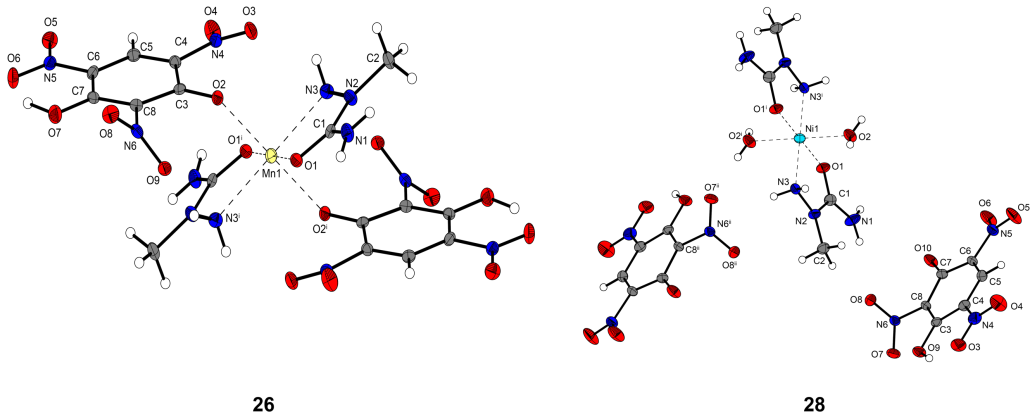


Figure 12. Complex units of compounds **26** (left) and **28** (right). Selected coordination distances (Å): **26**: Mn1–O1 2.1426(15), Mn1–O2 2.1949(15), Mn1–N3 2.266(2); **28**: Ni1–N3 2.060(3), Ni1–O1 1.9923(15), Ni1–O2 2.143(2); selected bond angles (°): **26**: O1–Mn1–O2 90.51(6), O1–Mn1–N3 73.19(7), O1–Mn1–O2^{i} 89.46(6), O1–Mn1–N3^{i} 106.81(7), O2–Mn1–N3 91.45(7), O1^{i}–Mn1–O2 89.49(6), O2–Mn1–N3^{i} 88.55(7); **28**: O1–Ni1–O2^{i} 91.30(8), O1–Ni1–N3^{i} 99.43(8), O2–Ni1–N3 85.23(9), O2–Ni1–N3^{i} 94.78(9), O1^{i}–Ni1–O2^{i} 88.70(8), O1^{i}–Ni1–N3^{i} 80.57(8). Symmetry codes: **26**: (i) 1−x, 1−y, −z; **28**: (i) −x, −y, 1−z; (ii) 1−x, 1−y, 1−z.

6.2.3 Sensitivities and Thermal Stability

Thermal stability measurements of highly sensitive coordination compounds are very challenging since quantities larger than ~2 mg can damage the instrument seriously. On the other hand, endothermic signals such as melting, vaporization, dehydration or loss of ligand may not be detected properly when using an inadequate amount. Approximately 1 mg of the compounds were measured with a heating rate of 5 °C min^{-1} via differential thermal analysis (DTA) and/or by thermal gravimetric analysis (TGA). Critical temperatures are given as onset temperatures and are summarized in Table 2. Additional details on the DTA plots of **6**–**8, 11**, **12**, **15** and **18** are given in the Supporting Information. The majority of the investigated compounds have exothermic decomposition events higher or close to 180 °C. Losses of water or ligands expressed by endothermic decomposition points have been observed partly at lower

temperatures. Methylsemicarbazide (**1**) showed no exothermic decompositon event in the measured range of 25–400 °C but had indeed two endothermic points. Compound **1** first melts (60 °C) and vaporizes afterwards at temperatures above 110 °C, which was determined by constant weight loss during TGA (Figure 13). This behaviour could be a possible explanation for the exceptional endothermic peaks observed for **5**, **9**, **10**, **12**–**14**, **17** and **18** during DTA measurements. Endothermic loss of coordinating MSC molecules could lead to the formation of intermediate species, which decompose in an exothermic manner at later stages. Numerous decomposition paths and mechanisms are possible. Similar phenomena have already been described in the literature.[27-29] The ligand vaporization tendency and the relating bond strengths are strongly influenced by the metal ($Zn(ClO_4)_2$ (**12**) vs. $Ni(ClO_4)_2$ (**18**), Figure S12), anion ($Cu(NO_3)_2$ (**6**) vs. $Cu(ClO_4)_2$ (**19**), Figure S12) and the corresponding coordination environment ($Zn(ClO_4)_2$, (**11**) vs. (**12**)). The copper(II) azido (Figure 13) and nitrato complexes **6** and **8**, which decompose exothermically at low temperatures of 121 °C (**8**) and 147 °C (**6**) showed the lowest thermal stabilities of all investigated coordination compounds. Comparing them to the other complexes bearing different anions, but the same metal ion, the decomposition temperatures increase in the following order: N_3^- (121 °C) < NO_3^- (146 °C) < SO_4^{2-} (156 °C) < Cl^- (166 °C) < PA^- (179 °C) ≈ $HTNR^-$ (179 °C) < ClO_4^- (186 °C). This general trend underlines the importance and correlation of the decomposition temperature with the anion and coordination environment.

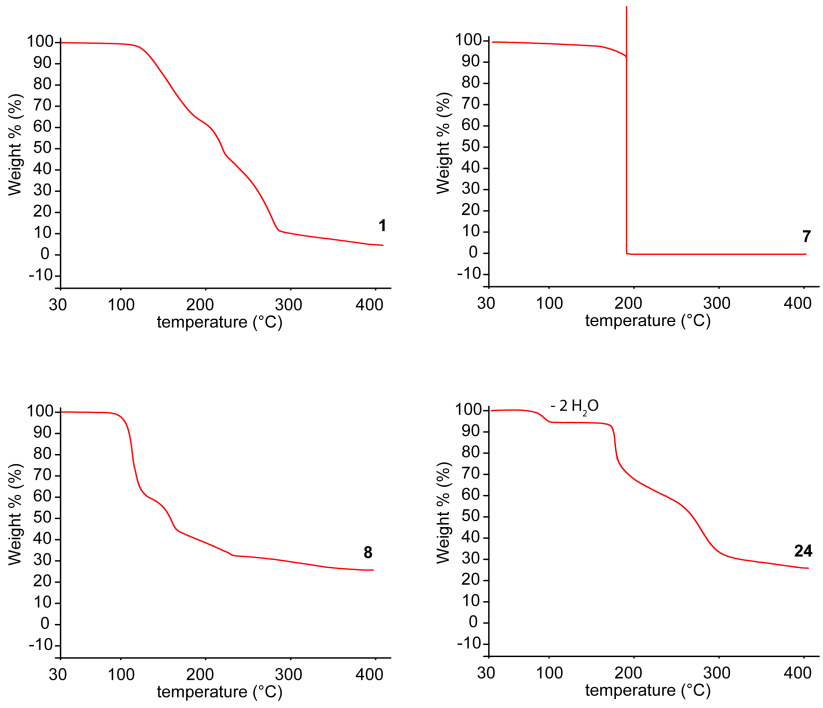


Figure 13. TGA measurements of the free ligand **1** and selected complexes at a heating rate of 5 °C min^{-1}.

The water-free metal(II) MSC picrate coordination compounds showed relatively high thermal stabilities ranging from 179 °C for **19** up to 217 °C for **23** (Figure 14). Their exothermic decomposition temperatures increase in the following order: Cu^{2+} (179 °C) < Zn^{2+} (190 °C) ≈ Mn^{2+} (190 °C) < Co^{2+} (211 °C) < Ni^{2+} (217 °C). For previous complexes analogous trends have been observed.[30]

Table 2. Thermal stability measurements of **1**, **3**–**15** and **17**–**28** by DTA.

	$T_{endo1.}$ (°C)[a]	$T_{endo2.}$ (°C)[a]	$T_{exo.}$ (°C)[b]
MSC (**1**)	60	111	—
MSC_H PA (**3**)	—	—	166
$[Cu(H_2O)_2(MSC)_2]SO_4$ (**4**)	144	—	156
$[CuCl_2(MSC)_2]$ (**5**)	146	—	166
$[Cu(NO_3)_2(MSC)_2]$ (**6**)	—	—	147
$[Cu(ClO_4)_2(MSC)_2]$ (**7**)	—	—	186
$[Cu(N_3)_2(MSC)]$ (**8**)	—	—	121
$[ZnCl_2(MSC)_2]$ (**9**)	171	—	186
$[Zn(NO_3)_2(MSC)_2]$ (**10**)	183	—	208
$[Zn(H_2O)_2(MSC)_2](ClO_4)_2$ (**11**)	114	—	231
$[Zn(MSC)_3](ClO_4)_2 \cdot H_2O$ (**12**)	123	187	333
$[MnCl_2(MSC)_2]$ (**13**)	107	189	209
$[Mn(NO_3)_2(MSC)_2]$ (**14**)	169	—	208
$[Mn(H_2O)_2(MSC)_2](ClO_4)_2$ (**15**)	96	—	234
$[Co(H_2O)_2(MSC)_2]Cl_2$ (**17**)	99	259	266
$[Ni(MSC)_3](ClO_4)_2$ (**18**)	252	—	258
$[Cu(PA)_2(MSC)_2]$ (**19**)	—	—	179
$[Zn(MSC)_3](PA)_2$ (**20**)	—	—	190
$[Mn(PA)_2(MSC)_2]$ (**21**)	—	—	190
$[Co(PA)_2(MSC)_2]$ (**22**)	—	—	211
$[Ni(MSC)_3](PA)_2$ (**20**)	—	—	217
$[Cu(H_2O)_2(MSC)_2](HTNR)_2$ (**24**)	119	—	179
$[Zn(H_2O)_2(MSC)_2](HTNR)_2$ (**25**)	134	—	195
$[Mn(HTNR)_2(MSC)_2]$ (**26**)	—	—	184
$[Co(H_2O)_2(MSC)_2](HTNR)_2$ (**27**)	155	—	205
$[Ni(H_2O)_2(MSC)_2](HTNR)_2$ (**28**)	172	—	193

Onset temperatures at a heating rate of 5 °C min^{-1}. [a] endothermic peak, which indicates melting, vaporization, dehydration or loss of coordinating MSC molecules; [b] exothermic peak, which indicates decomposition.

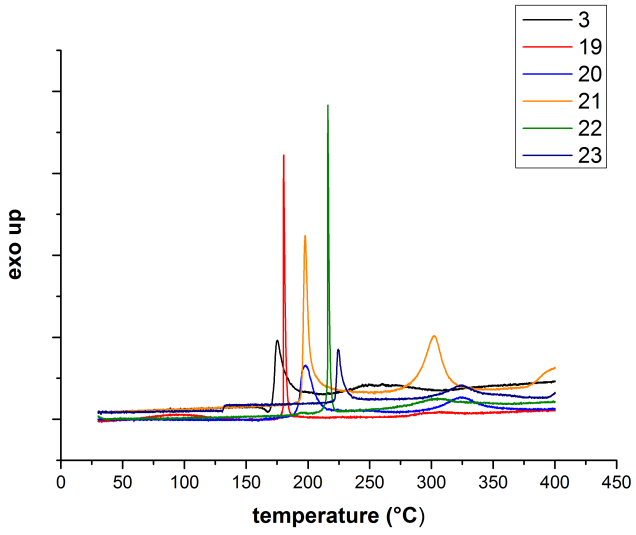


Figure 14. DTA plot (5 °C min^{-1}) comparison of the picrate compounds **3** and **19**–**23**.

Most of the styphnate complexes showed similar thermal stabilities in comparison with the picrates (Figure 16) but crystallized in different complex structures. Instead of coordinating trinitrobenzene derivative ligands, complexes with two aqua molecules were obtained. Dehydration indicated by an endothermic peak in the DTA plots (Figure 15) can be achieved by heating shown through weight loss during the TGA measurements (Figure 13).

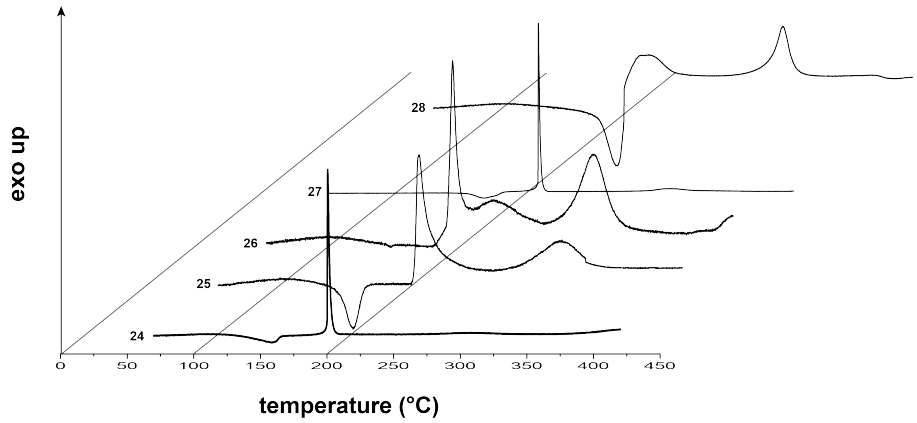


Figure 15. DTA plots (5 °C min^{-1}) of the styphnate complexes **24**–**28**.

The sensitivities toward impact, friction and electrostatic discharge for the compounds were determined according to BAM standards. In addition, the compounds have been classified in accordance to the "UN Recommendations on the Transport of Dangerous Goods" using the measured values. An overview of the sensitivities is given in Table 3. The uncoordinated free ligand **1** can be considered as "insensitive" with values greater than 40 J for impact, greater than 360 N for friction and an ESD value of 1.50 J. For complete energetic categorization of compound **1**, we calculated the enthalpy of formation to be −205 kJ mol^{-1}.[31] So the compound is formed exothermically in contrast to the condensed phase heat of formation of monomethylhydrazine (54.1 kJ mol^{-1}).[32]

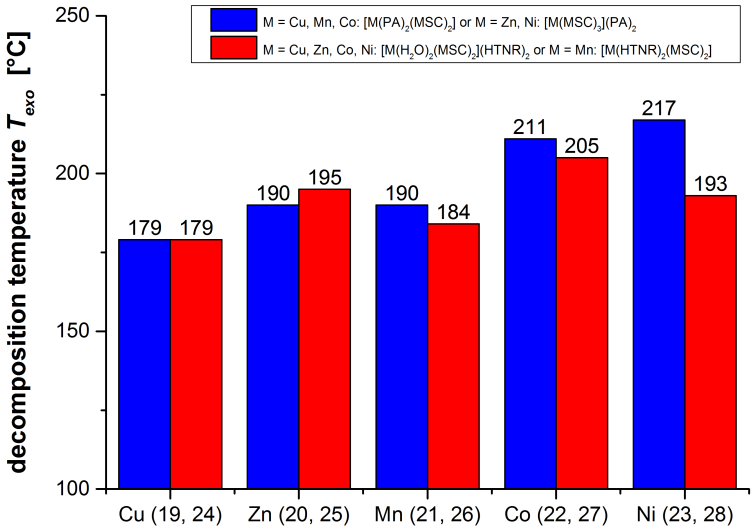


Figure 16. Comparison of the exothermic decomposition temperatures of picrate complexes with styphnate coordination compounds.

Table 3. Sensitivities toward impact, friction and ESD of **1**, **3**–**12**, **14**–**15** and **17**–**28**.

compound	*IS* (J)[a]	*FS* (N)[b]	*ESD* (J)[c]	grain size (µm)
1	> 40	> 360	1.50	< 100
3	> 40	160	0.65	< 100
4	> 40	> 360	1.50	< 100
5	> 40	> 360	1.50	< 100
6	> 40	324	1.50	< 100
7	2	24	0.07	< 100
8	10	> 360	1.50	< 100
9	> 40	> 360	1.50	< 100
10	> 40	> 360	1.50	< 100
11	> 40	160	0.30	< 100
12	25	> 360	0.60	< 100
14	40	> 360	1.25	< 100
15	10	216	1.00	< 100
17	> 40	> 360	1.50	< 100
18	10	< 60	0.10	< 100
19	30	> 360	0.30	< 100
20	10	360	1.00	< 100
21	9	288	0.55	< 100
22	5	288	0.30	< 100
23	10	> 360	0.75	< 100
24	> 40	> 360	0.40	< 100
25	> 40	> 360	1.00	< 100
26	25	324	0.60	< 100
27	> 40	> 360	1.50	< 100
28	> 40	> 360	1.50	< 100

[a] Impact sensitivity according to the BAM drophammer (method 1 of 6); [b] friction sensitivity according to the BAM friction tester (method 1 of 6); [c] electrostatic discharge sensitivity (OZM ESD tester); Impact: insensitive > 40 J, less sensitive ≥ 35 J, sensitive ≥ 4 J, very sensitive ≤ 3 J; Friction: insensitive > 360 N, less sensitive = 360 N, sensitive < 360 N and > 80 N, very sensitive ≤ 80 N, extremely sensitive ≤ 10 N. According to the UN Recommendations on the Transport of Dangerous Goods.

The sulfate, chloride and nitrate complexes are insensitive against impact, friction and ESD (except compound **6**, which is sensitive toward friction). In most cases, substitution of these

anions with perchlorates, azides, picrates or styphnates causes higher sensitivities toward impact, friction and ESD (impact: 2–40 J, friction: 24–360 N; ESD: 0.07–1.50 J). All water-free compounds with coordinating picrates or styphnates are more sensitive toward mechanical stimuli than their aqua ligand-containing analogs. Compound **7**, which behaves like a primary explosive, can be classified as very sensitive toward impact and friction, but it is still safe to handle, which makes it a very suitable initiating substance. The sensitivity toward impact of the $[M^{II}(PA)_2(MSC)_2]/[M^{II}(MSC)_3](PA)_2$ complexes (Figure 17) increases in the order: Cu^{2+} < Zn^{2+} < Ni^{2+} < Mn^{2+} < Co^{2+} and in the following order toward friction: $Cu^{2+} \approx Ni^{2+} < Zn^{2+} < Mn^{2+} < Ni^{2+}$. Incorporation of aqua ligands in the styphnate complexes **24**/**25** and **27**/**28** leads to an increase in stability toward mechanical stimuli but decreases its energetic character compared to the relating water-free picrate complexes (Figure 17).

Hot needle and hot plate tests of the most promising compound **7** showed a sharp deflagration in both tests (Figure 18). The sample was fixed on a copper plate underneath adhesive tape and initiated by a red hot needle. Strong deflagration or detonation of the compound usually indicates a valuable primary explosive. The safe and straightforward hot plate test shows only the behaviour of the unconfined sample toward fast heating on a copper plate. It does not necessarily allow any conclusions on a compound´s capability as a suitable primary explosive.

Based on the positive results of the hot needle and hot plate tests, the initiation capability of compound **7** toward pentaerythritol tetranitrate (PETN) as secondary explosive was investigated. A copper shell with a diameter of 7 mm and length of 88 mm was filled with 200 mg sieved PETN (grain size 100–500 µm) and pressed with a weight of 8 kg. 50 mg of the primary explosive was subsequently loosely filled on top of the main charge. To examine the influence of pressing of the primary explosive on the initiation capability, two experiments were conducted a.) with pressing and b.) without. The shell was sealed by an insulator, placed in a retaining ring, which was soldered to a copper witness plate with a thickness of 1 mm and finally initiated by a type A electrical igniter (Figure 19).

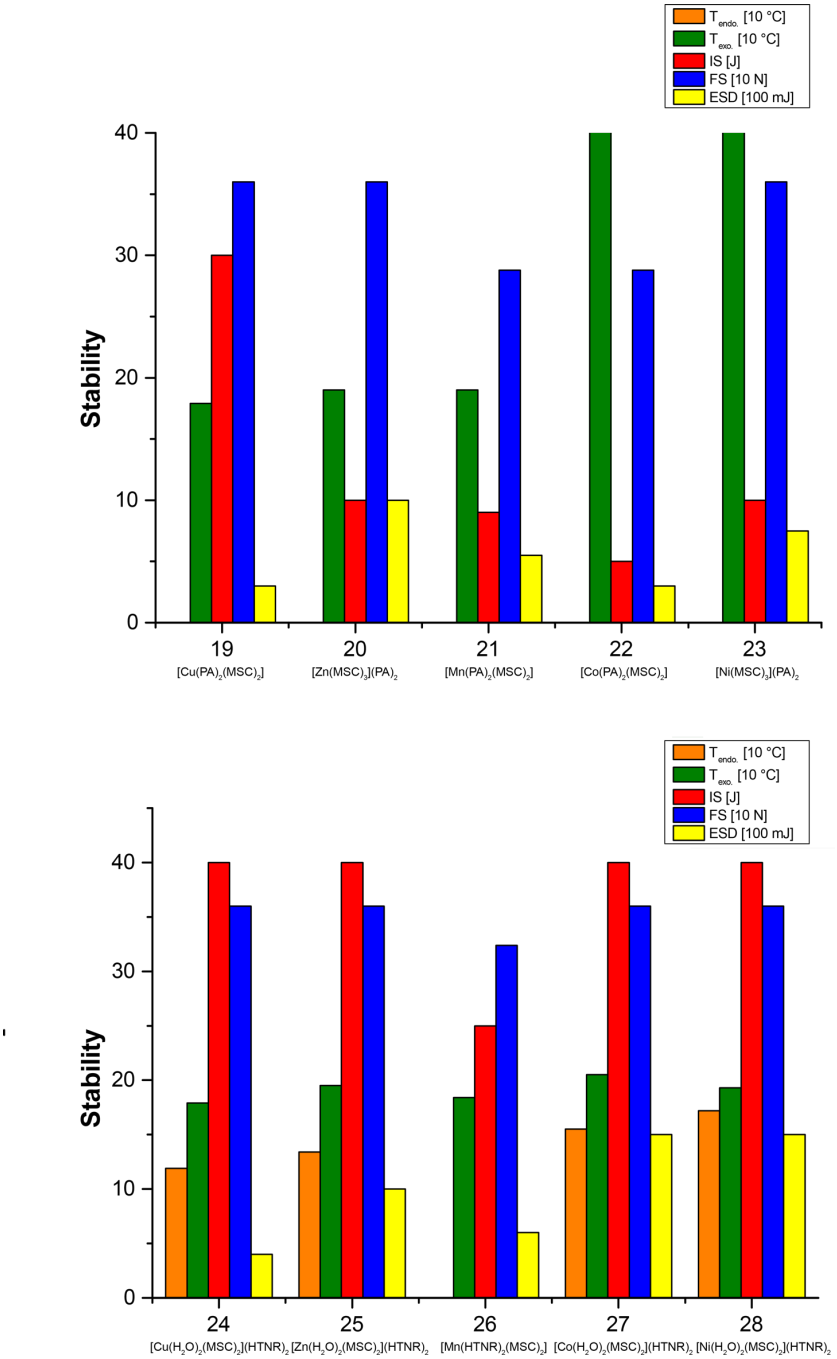


Figure 17. Stabilities of the picrate and styphnate coordination compounds **19**–**28**.

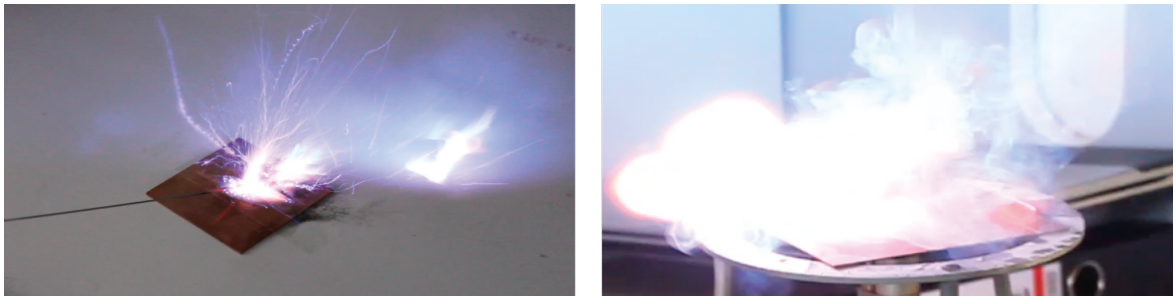


Figure 18. Moment of deflagration of compound **7** during the hot needle test (left) and hot plate test (right).



Figure 19. Schematic test setup (left); copper shell and plate before the initiation capability test (right).

A positive test is indicated by a hole in the copper plate and fragmentation of the shell caused by a deflagration-to-detonation transition (DDT) of the secondary explosive. In the case of compound **7**, two different results are observed depending on the pressing of the sample and the related loading density (Figure 20). A negative test, represented by a nearly undamaged copper plate, was obtained after loosely filling the primary into the shell. Pressing of the sample on top of the main charge led to a positive result and complete detonation of PETN proofed by a hole in the plate.

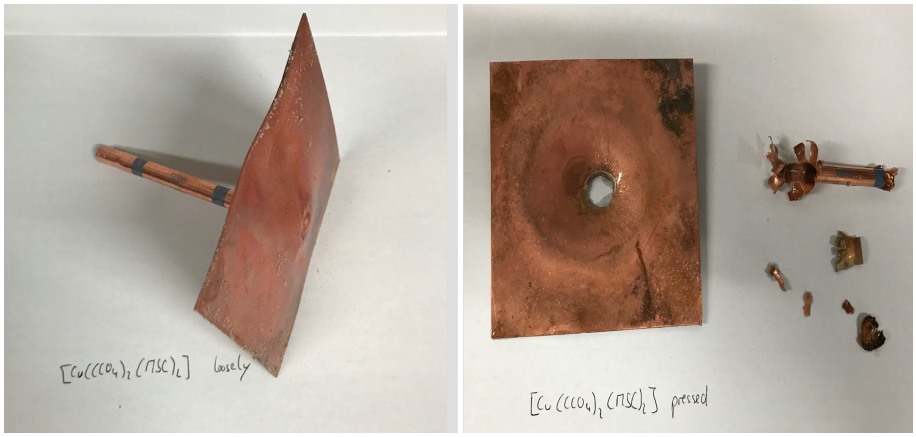


Figure 20. Negative (left) and positive (right) results of the PETN initiation tests.

6.2.4 Toxicity

The toxicity of compound **1** was determined using the known luminescence marine bacterium *Vibrio fischeri* in order to estimate the potential toxicological impact of the corresponding complexes.[33] With a value of 1.48 g L^{-1} for the half maximal effective concentration EC_{50}

after 30 min, the compound can be considered as non-toxic (toxicity level after 30 min incubation: very toxic < 0.10 g L^{-1}; toxic 0.10–1.00 g L^{-1}; non-toxic > 1.00 g L^{-1}).[34]

6.2.5 Laser Initiation

In recent years, more and more research groups all over the world have been working intensively on new laser ignitable energetic materials.[3, 35, 36] The laser initiation shows many advantages compared to conventional methods like mechanical stimuli or heat and investigated compounds do not require high sensitivities toward the customary stimuli. Consequently, laser ignitable explosives with high performance, high thermal stability and no impact on the environment can be used as insensitive but powerful energetic materials to allow much safer handling and prevent undesired initiations. About 15 mg of the carefully pestled complex to be investigated were filled into a transparent plastic cap, pressed with a pressure force of 1 kN and sealed by a UV-curing adhesive. The laser initiation experiments were carried out with a 45 W InGaAs laser diode operating in the single-pulsed mode. The diode was connected to an optical fiber with a core diameter of 400 µm and a cladding diameter of 480 µm. The optical fiber was coupled via a SMA type connecter directly to the laser and to a collimator. This collimator was linked to an optical lens, which was positioned in its focal distance (f = 29.9 mm) to the sample. The lens was protected from the explosive by a sapphire glass. The confined samples were irradiated at a wavelength of 915 nm, a voltage of 4 V and varying parameters regarding pulse length (0.1 ms or 15 ms) and current (8 A or 9 A). The combined current and pulse length result in an approximately energy output of 0.20 mJ (0.1 ms/ 8 A) and 34 mJ (15 ms/ 9 A). Only selected compounds with promising properties (**7**, **8** and **18**) were tested toward laser irradiation and showed different responses depending on the used metal(II) and anion. A summary of the test results is given in Table 4. All investigated complexes could be initiated showing detonations for **7** and **18** (Figure 21) and decomposition for compound **8** under the applied laser parameters.

Table 4. Results of the laser ignition tests.

compound	0.1 ms/ 8 A	15 ms/ 9 A
7	det.	–
8	dec.	–
18	x	det.

(–: not tested, x: no ignition, dec.: decomposition, deflag.: deflagration, det.: detonation). Operating parameters: current I = 8–9 A; voltage U = 4 V; theoretical maximal output power P_{max} = 45 W; theoretical energy E_{max} = 0.20–34 mJ; wavelength λ = 915 nm; pulse length τ = 0.1–15 ms.

Different laser initiation thresholds could be observed for the complexes expressed by varying outcomes and required energy inputs. Copper(II) complex **7** detonated at the lowest possible initiation energy configurable in the settings of the laser device. The compound exhibits slightly increased sensitivities against mechanical stimuli but is still safe to handle and therefore a promising candidate for future laser ignition systems.

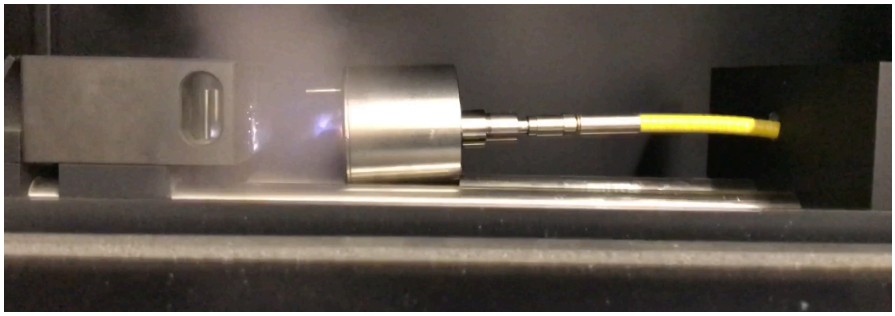


Figure 21. Moment of detonation of compound **7**.

6.2.6 UV-Vis Spectroscopy

In order to get a deeper insight into the laser initiation mechanism of energetic materials solid state UV-Vis spectra for the coordination compounds **7**, **8** and **18** were recorded in the wavelength region 350–1000 nm (Figure 22). In addition, the influence of different anions on the absorption for copper(II) complexes was investigated and compared to each other (Figure S13). An overview of the observed optical properties is given in Table 5.

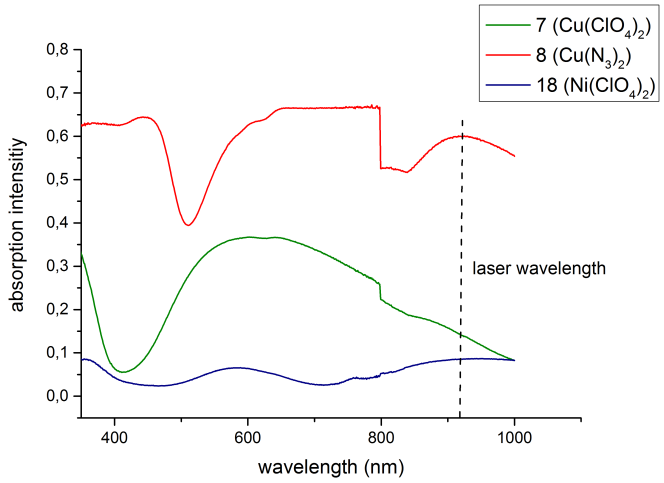


Figure 22. UV-Vis spectra in the solid state of complexes **7**, **8** and **18**. The step in the absorption intensity at 800 nm in the spectra is caused by a detector change. The UV-Vis spectra have only qualitative character.

All analyzed complexes showed characteristic absorptions in the near-infrared, visible and UV region correlating with their observed complementary colors. Depending on the transition metal (Cu^{2+} vs. Ni^{2+}) or coordination environment (blue $Cu(ClO_4)_2$ (**7**) vs. green $Cu(N_3)_2$ (**8**)) different d-d transitions can be found. As expected, the blue copper(II) complexes **4**–**7** differ only minimally from each other, which can be explained by their similar coordination environment.

Table 5. Optical properties of **14**-**27**, **31** and **36**.

compound	M	color	$\lambda_{d\text{-}d}$[a]	$\lambda_{915}/\lambda_{d\text{-}d}$[b]
4	Cu^{II}	blue	646	0.51
5	Cu^{II}	blue	642	0.51
6	Cu^{II}	blue	603	0.46
7	Cu^{II}	blue	602	0.40
8	Cu^{II}	green	786	0.89
18	Ni^{II}	blue	581, 952	0.98

[a] absorption intensity maximum wavelength, which can be assigned to electron d-d excitations in the measured range of 350–1000 nm; [b] quotient of the absorption intensity at the laser wavelength and the intensity at the d-d absorption wavelength.

The nature of the laser ignition process (e.g. thermally, electronically or combined) and the related requirements of compounds to be laser ignitable are still not fully understood.[37] Looking at the absorption intensity of the coordination compounds at the irradiated wavelength of 915 nm (Figure 22), one could possibly derive a direct connection to the performed laser ignition since all complexes could be initiated. However, the laser initiation capability depends not only on the absorption but also on multiple other factors like crystal structure or the coordination environment.[29] It can be concluded that deflagration or detonation of the complexes after exposure to laser irradiation occurs possibly if the compounds possess high mechanical sensitivities. Because of the influence of the metal, anion and ligand on the laser initiation process, as well as the mechanism itself has not been clarified yet, future investigations will be needed to fully understand the laser initiation of energetic materials.

6.3 Conclusions

Methylsemicarbazide (**1**, MSC), a methyl derivative of semicarbazide and member of the prominent carbazide family, was prepared in a facile one-step reaction by treatment of trimethylsilylisocyanate with methylhydrazine in a high yield of 95 %. Toxicity determination showed no toxicity of **1** toward aquatic life, which makes it a suitable candidate as ligand in environmental benign complexes for various applications. In comparison to hydrazine and methylhydrazine as ligands (both show high toxicities), significantly less sensitive compounds

are obtained which might be a reason of the negative heat of formation (−205 kJ mol^{-1}) of **1**. In the present extensive study 25 new coordination compounds, with **1** as the ligand, were synthesized and investigated. Coordination causes intramolecular rotation of the bidentate ligand and leads to an increase in density in comparison to the free compound **1**. Obtained complexes are composed of a 3d transition metal (Mn, Co, Ni, Cu, Zn), methylsemicarbazide and varying anions (SO_4^{2-}, Cl^-, NO_3^-, ClO_4^-, N_3^-, picrates, styphnates). Attempts using Fe(II) and Fe(III) salts failed. The concept of energetic coordination compounds (ECC), which are obtained by including nitrate, perchlorate, nitrophenolates and azide anions, is a brilliant, inexpensive and simple strategy in order to find new laser-ignitable and eco-friendly primary explosives. Energetic and optical properties can be easily adjusted by variation of the building blocks (metal, ligand, anion). Most of the complexes showed exothermic decomposition temperatures higher or close to 180 °C during differential thermal analysis (DTA) measurements. Thermal gravimetric analysis (TGA) of selected compounds gave new insights into possible decomposition pathways at elevated temperatures. Highest stabilities toward temperature were observed for nickel(II) and cobalt(II) complexes, while highest stabilities toward physical stress for manganese(II) and zinc(II) complexes. Additionally, low temperature X-ray structure elucidation for 22 compounds was achieved and allowed the correlation between crystal structure and mechanical stabilities (e.g. the bridging azido ligand in the low-performing copper(II) complex **8** vs. the highly sensitive perchlorato complex **7**). All investigated picrate complexes crystallized water-free and showed higher sensitivities in comparison to their diaqua containing styphnate analogs. Compound **7** has a high thermal stability (186 °C) and shows manageable sensitivities for a primary explosive. Further investigation in a PETN filled copper shell proofed its suitability as lead-free alternative. The successful ignition (observing detonation) of PETN makes copper(II) complex **7** to an interesting candidate for future primary explosive applications. It can be prepared by a simple, low-cost and upscalable reaction. Also, non-classical initiation tests by laser irradiation at a wavelength of 915 nm showed detonation of complex **7** after irradiation at the lowest applicable energy input of the laser setup (0.2 mJ).

Supporting information available in the appendix in **Chapter 19.4** and under:

https://onlinelibrary.wiley.com/action/downloadSupplement?doi=10.1002%2Fchem.201705030&attachmentId=2189752042

6.4 References

[1] T. W. Myers, K. E. Brown, D. E. Chavez, R. J. Scharff, J. M. Veauthier, *Inorg. Chem.* **2017**, *56*, 2297–2303.

[2] S. Seth, K. A. McDonald, A. J. Matzger, *Inorg. Chem.* **2017**, *56*, 10151–10154.

[3] M. Freis, T. M. Klapötke, J. Stierstorfer, N. Szimhardt, *Inorg. Chem.* **2017**, *56*, 7936–7947.

[4] S. Li, Y. Wang, C. Qi, X. Zhao, J. Zhang, S. Zhang, S. Pang, *Angew. Chem., Int. Ed.* **2013**, *52*, 14031–14035.

[5] K. D. Oyler, in *Green Energetic Materials*, Wiley, **2014**, pp. 103–132.

[6] Y. Tang, C. He, L. A. Mitchell, D. A. Parrish, J. M. Shreeve, *Angew. Chem., Int. Ed.* **2016**, *55*, 5565-5567.

[7] D. G. Piercey, D. E. Chavez, B. L. Scott, G. H. Imler, D. A. Parrish, *Angew. Chem., Int. Ed.* **2016**, *55*, 15315–15318.

[8] R. Haiges, K. O. Christe, *Inorg. Chem.* **2013**, *52*, 7249-7260.

[9] R. Matyás, J. Pachman, in *Primary Explosives*, Springer, Heidelberg **2013**.

[10] M. A. Ilyushin, I. V. Tselinsky, I. V. Shugalei, *Cent. Eur. J. Energ. Mater.* **2012**, *9*, 293–327.

[11] M. Joas, T. M. Klapötke, J. Stierstorfer, N. Szimhardt, *Chem. - Eur. J.* **2013**, *19*, 9995–10003.

[12] J. Zhang, Y. Du, K. Dong, H. Su, S. Zhang, S. Li, S. Pang, *Chem. Mat.* **2016**, *28*, 1472–1480.

[13] B. Hariharanath, K. S. Chandrabhanu, A. G. Rajendran, M. Ravindran, C. B. Kartha, *Def. Sci. J.* **2006**, *56/3*, 383–389.

[14] T. Curtius, K. Heidenreich, *Chem. Ber.* **1894**, *27*, 55.

[15] M. B. Labib, P. F. Lamie, *Med. Chem. Res.* **2016**, *25*, 2607–2618.

[16] R. J. W. Cremyln, J. L. Turner, *J. Chem. Soc., C* **1970**, 2629–2631.

[17] W.-C. Tong, J.-C. Liu, Q.-Y. Wang, L. Yang, T.-L. Zhang, *Z. Anorg. Allg. Chem.* **2014**, *640*, 2991–2997.

[18] a.) V. P. Sinditskii, A. E. Fogelz´ang, M. D. Dutov, V. V. Serushkin, S. P. Yarkov, B. S. Svetlov, *Zh. Neorg. Khim.* **1986**, *31*, 1759–1765; b.) V. P. Sinditskii, A. E. Fogelz´ang, M. D. Dutov, V. I. Sokol, V. V. Serushkin, B. S. Svetlov,, M. A. Porai-Koshits, *Zh. Neorg. Khim.* **1987**, *32*, 1944–1949; c.) M. B. Talawar, A. P. Agrawal, J. S. Chhabra, S. N. Asthana, *J. Hazard. Mater.* **2004**, *113*, 57–65.

[19] M. Joas, T. M. Klapötke, *Propellants, Explos., Pyrotech.* **2015**, *40*, 246–252.

[20] C. Sitong, G. Weiming, Z. Bo, Z. Tonglai, Y. Li, *Polyhedron* **2016**, *117*, 110–116.

[21] Fu, X.; He, F.; Li, Y.; Liu, L.; Mi, Y.; Xu, Y.-C.; Xun, G.; Yu, Z.; Zhang, J. Y.; Dai, M. Heterocyclic hydrazone compounds as c-Met tyrosine kinase inhibitors and their preparation and use in the treatment of cancer and inflammation. WO2011018454A1, **2011**.

[22] Shibayama, A.; Kajiki, R.; Kobayashi, M.; Mitsunari, T.; Nagamatsu, A. Preparation of 6-acyl-1,2,4-triazine-3,5-dione derivatives as herbicides. WO2012002096A1, **2012**.

[23] Crystallographic data for the structures have been deposited with the Cambridge Crystallographic Data Centre. Copies of the data can be obtained free of charge on application to The Director, CCDC, 12 Union Road, Cambridge CB2 1EZ, UK (Fax: int.code_(1223)336-033; e-mail for inquiry: fileserv@ccdc.cam.ac.uk; e-mail for deposition: (deposit@ccdc.cam.ac.uk).

[24] P. Domiano, M. A. Pellinghelli, A. Tiripicchio, *Acta Crystallogr., Sect. B* **1972**, *28*, 2495–2498.

[25] J. E. Worsham, Jr., H. A. Levy, S. W. Peterson, *Acta Crystallogr.* **1957**, *10*, 310–323.

[26] A. Cabort, B. Therrien, K. Bernauer, G. Süss-Fink, *Inorg. Chim. Acta* **2003**, *349*, 78–84.

[27] K. C. Patil, *J. Chem. Sci.*, **1986**, *96*, 459–464.

[28] R. A. F. Sherriff and A. K. Galwey, *J. Chem. Soc. A*, **1967**, 1705–1708.

[29] J. Stierstorfer, N. Szimhardt, M. H. H. Wurzenberger, L. Daumann, A. Beringer, *J. Mater. Chem. A*, **2017**, *5*, 23753–23765.

[30] M. Joas, PhD thesis; Ludwig-Maximilians Universität München, **2014**.

[31] a) CBS-4M was applied for the electronic enthalpy; atomization method for conversion to gas phase enthalpy of formation and Trouton's rule for computing the sublimation enthalpy; b) T. Altenburg, T. M. Klapötke, A. Penger, J. Stierstorfer, *Z. Anorg. Allg. Chem*. **2010**, *636,* 463–471.

[32] NIST http://webbook.nist.gov/cgi/cbook.cgi?ID=C302012&Mask=1E9F, Accessed October 2017.

[33] G. I. Sunahara, S. Dodard, M. Sarrazin, L. Paquet, G. Ampleman, S. Thiboutot, J. Hawari, A. Y. Renoux, *Ecotoxicol. Environ. Saf.*, **1998**, *39*, 185−194.

[34] C. J. Cao, M. S. Johnson, M. M. Hurley, T. M. Klapötke, *JANNAF J. Propuls. Energet.*, **2012**, *5*, 41–51.

[35] T. W. Myers, J. A. Bjorgaard, K. E. Brown, D. E. Chavez, S. K. Hanson, R. J. Scharff, S. Tretiak, J. M. Veauthier, *J. Am. Chem. Soc.* **2016**, *138*, 4685−4692.

[36] M. A. Ilyushin, I. V. Tselinksi, Zh. Prikl. Khim. (S.-Petersburg, Russ. Fed.) **2000**, *73*, 1233−1240.

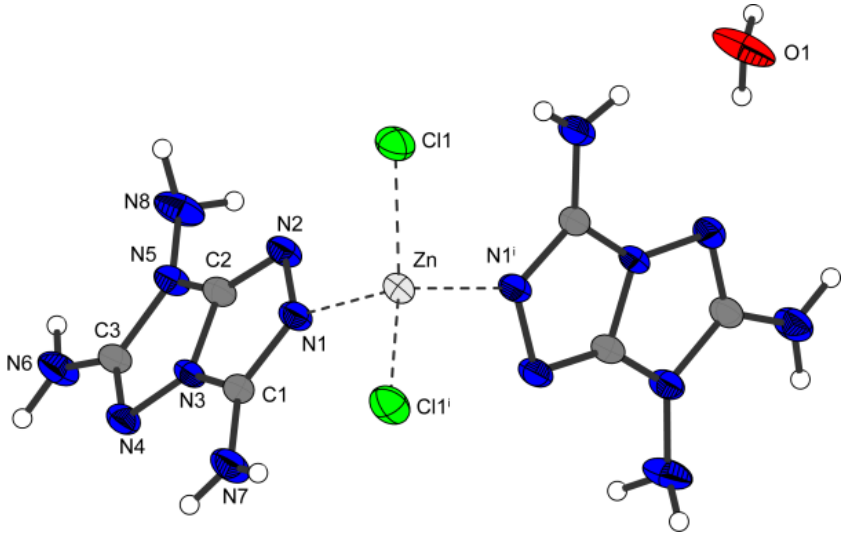
[37] E. D. Aluker, A. G. Krechetov, A. Y. Mitrofanov, D. R. Nurmukhametov, M. M. Kuklja, *J. Phys. Chem. C*, **2011**, *115*, 6893−69.

7 Synthesis and Characterization of Tetrahedral Zn(II) Complexes with 3,6,7-Triamino-7*H*-[1,2,4]triazolo[4,3-*b*][1,2,4]triazole as Nitrogen-rich Ligand

Thomas M. Klapötke, Philipp C. Schmid, Jörg Stierstorfer and Norbert Szimhardt

published in *Zeitschrift für Allgemeine und Anorganische Chemie* **2016**, *642,* 383–389

DOI: 10.1002/zaac.201600006



Synthesis and characterization of tetrahedral Zn(II) complexes with 3,6,7-triamino-7*H*-[1,2,4]triazolo[4,3-*b*][1,2,4]triazole as nitrogen-rich ligand.

Abstract

Triaminotriazolotriazole (**TATOT**) was used as a nitrogen-rich ligand for the formation of the energetic Zn(II)-complexes $[ZnCl_2(TATOT)_2] \cdot H_2O$ (**2**), $[Zn(H_2O)(TATOT)_3](NO_3)_2 \cdot 2\ H_2O$ (**3**) and $[Zn(TATOT)_4](ClO_4)_2 \cdot 2\ H_2O$ (**4**). The zinc(II) species were prepared in a straightforward and inexpensive synthesis. The complexes **2**–**4** were structurally characterized using X-ray diffraction. Additionally, the new compounds were characterized using elemental analysis and infrared (IR) spectroscopy. Finally, the sensitivities toward thermal and mechanical stimuli were determined by differential thermal analysis (DTA) and BAM (Bundesanstalt für Materialforschung und -prüfung) methods.

7.1 Introduction

Within the field of inorganic chemistry, coordination chemistry has a long history and found application in various fields, such as gas storage,[1] homogeneous catalysis,[2] supramolecular chemistry,[3] molecular magnetism,[4] and energetic materials.[5]

In the area of energetic materials, the formation of transition metal complexes is continuously gaining importance.[6] When designing new energetic materials, the desired properties of the explosive need to be customized to specific applications.[7] The main advantage of using transition metal complexes is an inexpensive and straightforward synthesis. In addition, the large number of possible combinations: i) the metal, ii) the ligand, and iii) the anion allow to tailor the desired energetic and optical properties of the target molecule.

Even though many transition metals can be utilized for the formation of energetic coordination compounds (ECC),[8] heavy metals, such as Pb(II), Hg(II), and Cd(II) exhibit a high toxicity and therefore ought to be replaced. In contrast, Zn(II)-complexes indicate a low toxicity,[9] which is a major aspect, when considering environmental issues.

The concept of using nitrogen-rich heterocycles as ligands in energetic transition metal complexes has become popular in the last decade.[10] Prominent examples are 5-(1-methylhydrazinyl)-1*H*-tetrazole,[11] 3-hydrazino-4-amino-1,2,4-triazole,[12] 5,5′-bis(1*H*-tetrazolyl)amine,[13] and 3-amino-6-(3,5-dimethylpyrazole)-tetrazine [14], which are illustrated in Figure 1.

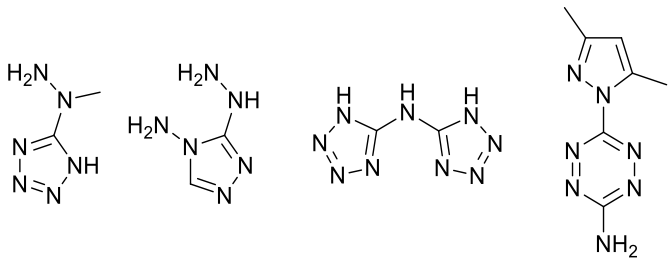


Figure 1. Chemical structure of selected nitrogen-rich ligands (from left to right): 5-(1-methylhydrazinyl)-1*H*-tetrazole, 3-hydrazino-4-amino-1,2,4-triazole, 5,5′-bis(1*H*-tetrazolyl)amine, 3-amino-6-(3,5-dimethylpyrazole)-tetrazine.

Klapötke *et al*. and Shreeve *et al*. introduced, independently of one another, several new nitrogen-rich salts based on the 3,6,7-triamino-7*H*-[1,2,4]triazolo[4,3-*b*][1,2,4]triazolium (TATOT) cation (see Figure 2).[15,16] The energetic TATOT salts showed several desired properties, such as a high stability toward thermal and mechanical stimuli as well as a low toxicity.[15, 16]

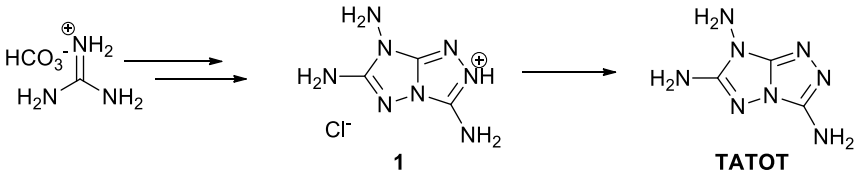


Figure 2. Chemical structure of compound **1** and the ligand TATOT.

In this study, we report on the investigations of TATOT as a neutral, nitrogen-rich ligand. Therefore, selected Zn(II)-complexes have been prepared and characterized by infrared (IR) spectroscopy, elemental analysis and differential thermal analysis (DTA). X-ray elucidation gave insight in the coordination behavior of the nitrogen-rich ligand.

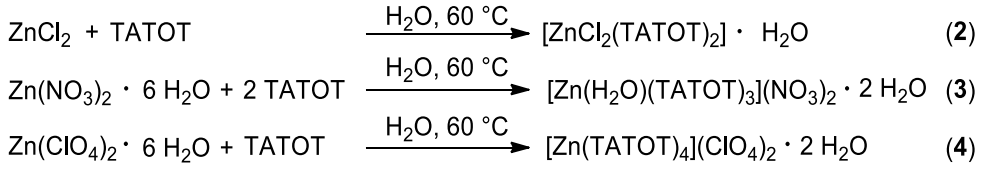
7.2 Results and Discussion

7.2.1 Synthesis

Compound **1**, the precursor hydrochloride salt of the TATOT ligand was obtained in the form of single crystals suitable for X-ray measurements through careful recrystallization of an aqueous solution of **1** (see Figure 2). Approaches toward the formation of Zn(II) complexes under acidic reaction conditions, were not successful and only gave compound **1**. One possible

explanation would be the protonation of the most nucleophilic position in the ligand. Protonation of this nitrogen atom blocks the best coordination-binding site.

The coordination compounds **2**–**4** were synthesized by mixing solutions of TATOT and metal(II) salts in water at 60 °C (Scheme 1). The clear reaction mixtures were slowly cooled down to room temperature and left until a solid precipitated. All products crystallized in the form of single crystals and were obtained in good yields directly from the mother liquor. The complexes **2**–**4** were filtered off and dried in air.



Scheme 1. Synthetic route toward compounds **2**–**4**.

7.2.2 Crystal Structures

The crystal structures of compounds **1**–**4** were determined by low temperature X-ray diffraction. Selected parameters of the X-ray determinations are given in Table S1 in the Supporting Information. The cif files were deposited[17] with the CCDC Nos. 1441526 (**1**), 1429888 (**2**), 1429889 (**3**), and 1429890 (**4**).

The bond lengths, bond angles and torsion angles of the neutral TATOT ligand in the complexes **2**–**4**, and protonated cation in **1**, are in the range of the literature reported neutral TATOT and triazolium molecules.[15]

Compound **1** crystallizes in the triclinic space group *P*−1 with two molecules in the unit cell and a calculated density of 1.724 g cm^{-3} at 173 K. The molecular structure and the geometric parameters of **1** are shown in Figure 3.

Notably, all the zinc(II) transition metals in **2**–**4** show a tetrahedral coordination sphere. The Zn^{II} $3d^{10}$-configuration results in similar ligand field stabilization energies (LFSE) for a tetrahedral and octahedral coordination sphere. Thus, we assume the high steric hindrance and the fixed structure of the TATOT ligands is responsible for the tetrahedral coordination sphere.

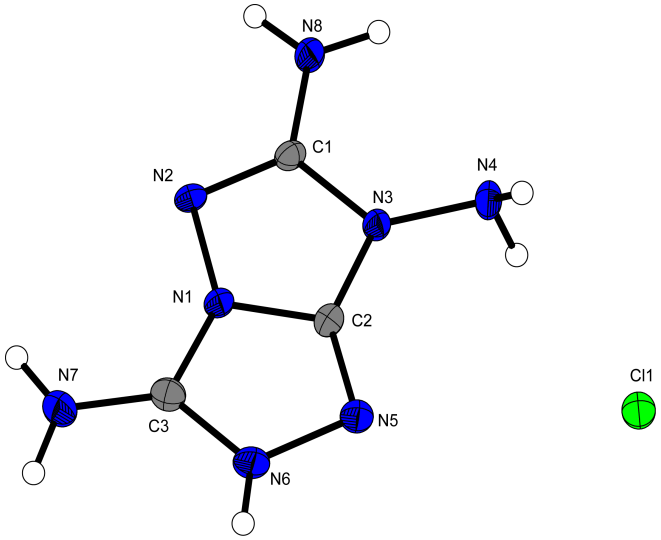


Figure 3. Molecular unit of compound **1**. Selected bond lengths (Å): N1–N2 1.403(2), N1–C2 1.349(2), N1–C3 1.348(2), N2–C1 1.324(2), N3–N4 1.395(2), N3–C1 1.388(2), N3–C2 1.362(2), N5–N6 1.408(2), N5–C2 1.299(3), N6–C3 1.340(3), N7–C3 1.324(2), N8–C1 1.326(2); selected bond angles (°): N2–N1–C2 113.98(2), N2–N1–C3 138.79(2), C2–N1–C3 107.20(2), N1–N2–C1 100.68(2), N4–N3–C1 124.27(2), N4–N3–C2 129.45(2), C1–N3–C2 106.14(2), N6–N5–C2 100.29(2), N5–N6–C3 113.34(2), N2–C1–N3 114.04(2), N2–C1–N8 125.01(2), N3–C1–N8 120.94(2), N3–C2–N5 140.01(2), N1–C2–N3 105.14(2), N1–C2–N5 114.84(2), N1–C3–N7 125.98(2), N6–C3–N7 129.68(2), N1–C3–N6 104.32(2); selected torsion angles (°): N6–N5–C2−N1 –0.07(2).

The zinc(II) chloride complex **2** crystallizes in the form of colorless blocks in the orthorhombic space group *Fddd* with 16 formula units per unit cell and a calculated density of 1.817 g cm^{-3} at 173 K. The molecular unit consists of two asymmetric unit cells. The zinc(II) center is tetrahedrally coordinated (see Figure 4) by two chloride anions and by two monodentate TATOT molecules (Zn1–N1 = 1.997(2) Å). The Zn1–Cl1 bonds are due to the electrostatic repulsion of the chloride anions marginally longer than the zinc-nitrogen bonds (Zn1–Cl1 = 2.256(8) Å). The coordination tetrahedron is slightly distorted and deviates from 109.5° (∢(Cl1–Zn1–N1) = 115.72(7)°, ∢(Cl1–Zn1–Cl1^{i}) = 113.51(3)° and ∢(Cl1–Zn1–N1^{i}) = 104.17(7)°), because of the previously mentioned steric and electrostatic hindrance. The complex monomers are connected to three-dimensional zig-zag analog strengths over various hydrogen bonds forming tube-like cavities along the *a* and *b* axis (Figure 5). The H-bonds were preferably formed between the chlorido ligands and the N-H functionalities of neighboring TATOT ligands. Complex **2** is displayed in Figures 4 and 5.

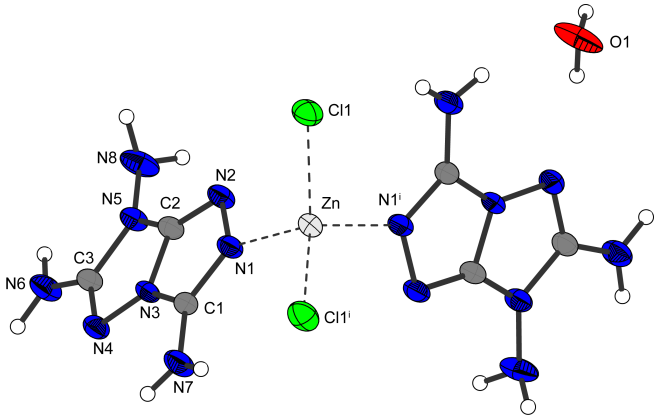


Figure 4. Molecular unit of $[ZnCl_2(TATOT)_2] \cdot H_2O$ (**2**). Selected bond lengths (Å): Zn1–Cl1 2.256(8), Zn1–N1 1.997(2), N1–N2 1.423(3), N1–C1 1.329(3), N2–C2 1.305(3), N3–C2 1.338(4), N3–C1 1.353(4), N3–N4 1.404(3), N4–C3 1.332(4), N5–N8 1.395(4), N5–C2 1.364(4), N5–C3 1.388(3), N6–C3 1.324(4), N7–C1 1.349(4); selected bond angles (°): Cl1–Zn1–N1 115.12(7), Cl1–Zn1–Cl1^{i} 113.51(3), Cl1–Zn1–N1^{i} 104.17(7), N1–Zn1–N1^{i} 104.77(2), Zn1–N1–C1 133.23(2), N2–N1–C1 110.0(2), Zn1–N1– N2 116.37(2), N1–N2–C2 102.6(2), N4–N3–C2 113.8(2), C1–N3–C2 106.8(2), N4–N3–C1 139.3(2), N3–N4–C3 101.4(2), N8–N5–C3 120.0(2), C2–N5–C3 106.7(2), N8–N5–C2 129.2(2), N1–C1–N3 107.1(2), N3–C1–N7 124.7(3), N1–C1–N7 128.3(3), N3–C2–N5 105.4(2), N2–C2–N5 141.0(3), N2–C2–N3 113.6(2), N4–C3–N5 112.8(2), N4–C3–N6 125.4(2), N5–C3–N6 121.8(2); selected torsion angles (°): N1–N2–C2−N3 –0.3(3); symmetry code: (i) −0.25−x, 0.75−y, z.

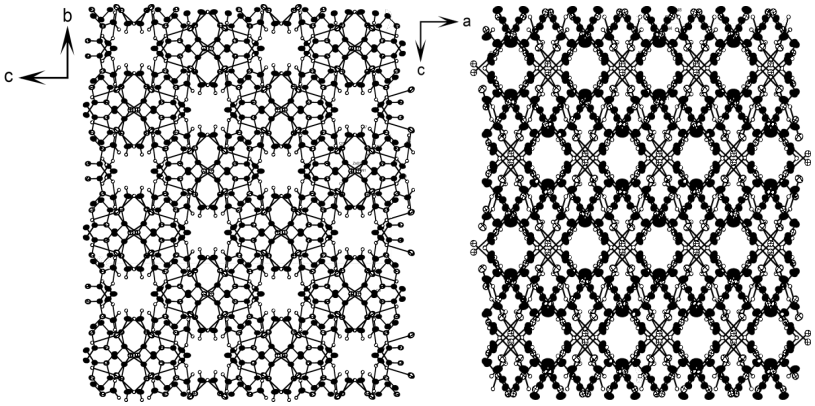


Figure 5. A projection of the structure of **2** along the *a* axis (left), showing the zig-zag analog strengths and along the *b* axis (right).

The zinc(II) nitrate complex **3** crystallizes in the form of colorless blocks in the triclinic space group *P*−1 with two formula units per unit cell and a calculated density of 1.825 g cm^{-3} at 173 K. The zinc(II) center is coordinated by three TATOT molecules and one aqua ligand (Zn1–O1 = 2.047(2) Å, Zn1–N1 = 1.980(2) Å, Zn1–N9 = 1.977(2) Å and Zn1–N17 = 1.925(2) Å; Figure 6), resulting in a strongly distorted tetrahedral coordination sphere (∢(O1–Zn1–N1) = 103.52(9)°, ∢(O1–Zn1–N9) = 95.28(9)° and ∢(O1–Zn1–

N17) = 98.81(9)°). This distortion can be explained by a non-coordinating nitrate anion (see Figure 6). The short distance between the zinc(II) cation and the non-coordinating nitrate anion (Zn1–O4 = 2.882(2) Å) results in angles close to 120° (∢(N1–Zn1–N9) = 118.41(9)°, ∢(N17–Zn1–N1) = 117.28(9)° and ∢(N17–Zn1–N9) = 116.74(9)°), giving an almost pyramidial configuration.

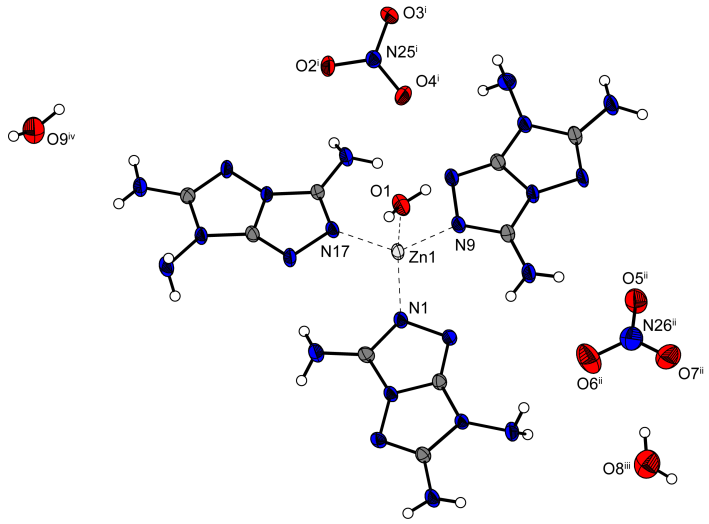


Figure 6. Molecular and asymmetric unit of $[Zn(H_2O)(TATOT)_3](NO_3)_2 \cdot 2\ H_2O$ (**3**). Selected bond lengths (Å): Zn1–O1 2.047(2), Zn1–N1 1.980(2), Zn1–N9 1.977(2), Zn1–N17 1.975(2), $O2^{i}$–$N25^{i}$ 1.243(3), $O3^{i}$–$N25^{i}$ 1.255(3), $O4^{i}$–$N25^{i}$ 1.246(3), $O5^{ii}$–$N26^{ii}$ 1.239(3), $O6^{ii}$–$N26^{ii}$ 1.259(3), $O7^{ii}$–$N26^{ii}$ 1.252(3); selected bond angles (°): O1–Zn1–N1 103.52(9), O1–Zn1–N9 95.28(9), O1–Zn1–N17 98.81(9), N1–Zn1–N9 118.41(9), N1–Zn1–N17 117.28(9), N9–Zn1–N17 116.74(8), $O2^{i}$–$N25^{i}$–$O3^{i}$ 119.6(2), $O2^{i}$–$N25^{i}$–$O4^{i}$ 120.2(2), $O3^{i}$–$N25^{i}$–$O4^{i}$ 120.2(2), $O5^{ii}$–$N26^{ii}$–$O6^{ii}$ 119.8(3), $O6^{ii}$–$N26^{ii}$–$O7^{ii}$ 119.0(3), $O5^{ii}$–$N26^{ii}$–$O7^{ii}$ 121.2(2); selected torsion angles (°): N1–N2–C2–N3 0.0(3); symmetry codes: (i) −x, −y, 1−z; (ii) −x, 1−y, 1−z; (iii) x, y, 1+z; (iv) x, −1+y, z.

The perchlorate coordination compound **4** crystallizes in the form of colorless blocks in the triclinic space group *P*−1 with two formula units per unit cell and a calculated density of 1.829 g cm^{-3} at 173 K. The zinc(II) center has a slightly distorted tetrahedral coordination sphere and is bonded to four TATOT ligands (Zn1–N1 = 2.009(2) Å, Zn1–N9 = 1.983(2) Å, Zn1–N17 = 1.989(2) Å, Zn1–N25 = 1.993(2) Å; (∢(N1–Zn1–N9) = 111.41(8)°, ∢(N1–Zn1–N17) = 108.80(8)° and ∢(N1–Zn1–N25) = 105.41(8)°; Figure 7).

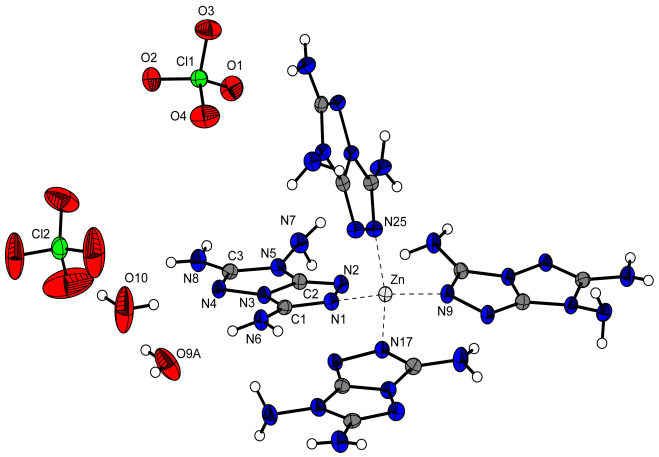


Figure 7. Molecular unit of $[Zn(TATOT)_4](ClO_4)_2 \cdot 2\ H_2O$ (**4**). Selected bond lengths (Å): Zn1–N1 2.009(2), Zn1–N9 1.983(2), Zn1–N17 1.989(2), Zn1–N25 1.993(2), Cl1–O2 1.425(3), Cl1–O3 1.433(2), Cl1–O1 1.428(2), Cl1–O4 1.430(2), Cl2–O7 1.416(3), Cl2–O8 1.414(3), Cl2–O5 1.393(3), Cl2–O6 1.391(4); selected bond angles (°): N1–Zn1–N9 111.41(8), N1–Zn1–N17 108.80(8), N1–Zn1–N25 105.41(8), N9–Zn1–N17 110.84(8), N17–Zn1–N25 109.58(8), O1–Cl1–O2 110.34(2), O1–Cl1–O3 109.71(2), O1–Cl1–O4 108.58(2), O2–Cl1–O4 109.45(2), O3–Cl1–O4 110.79(2), O5–Cl2–O6 109.5(2), O7–Cl2–O8 110.3(2), O6–Cl2–O8 108.2(2), O6–Cl2–O7 109.9(3), O5–Cl2–O7 109.13(2), O5–Cl2–O8 110.0(2); selected torsion angles (°): N1–N2–C2−N3 0.2(2).

7.2.3 IR Spectroscopy

Infrared spectra were recorded for the uncoordinated ligand and the complexes **2–4** (Figure 8). The absorption frequencies were assigned referring to values reported in literature.[15,18] The N–H bond stretching vibration of the free ligand shows strong absorptions in the region between 3500–3100 cm^{-1}. These stretching modes are broadened due to hydrogen bond formation. Moreover, the valence vibrations are partly overlaid by the stretching vibrations of the aqua ligand (**3**) and the crystal water in the spectra of the complexes **2–4**. Further, the spectrum of the uncoordinated ligand shows a typical N–H deformation vibration at 1570 cm^{-1}, a C=N stretching mode at 1619 cm^{-1} and a valence vibration at 1502 cm^{-1}. The according vibrations in the coordination compounds are shifted to higher wavenumbers due to complexation. Other important absorptions in the spectrum of the ligand are the C–N valence vibration mode at 1294 cm^{-1} and the C–NH_2 deformation mode at 1078 cm^{-1}. Further characteristic absorptions can be observed for the nitrate anion in complex **3** at 1338 cm^{-1} and for the perchlorate anion in compound **4** at 1064 cm^{-1}. These values lie in a typical range for non-coordinating anions.[19] In summary, the X-ray structures fit to the measured infrared spectra.

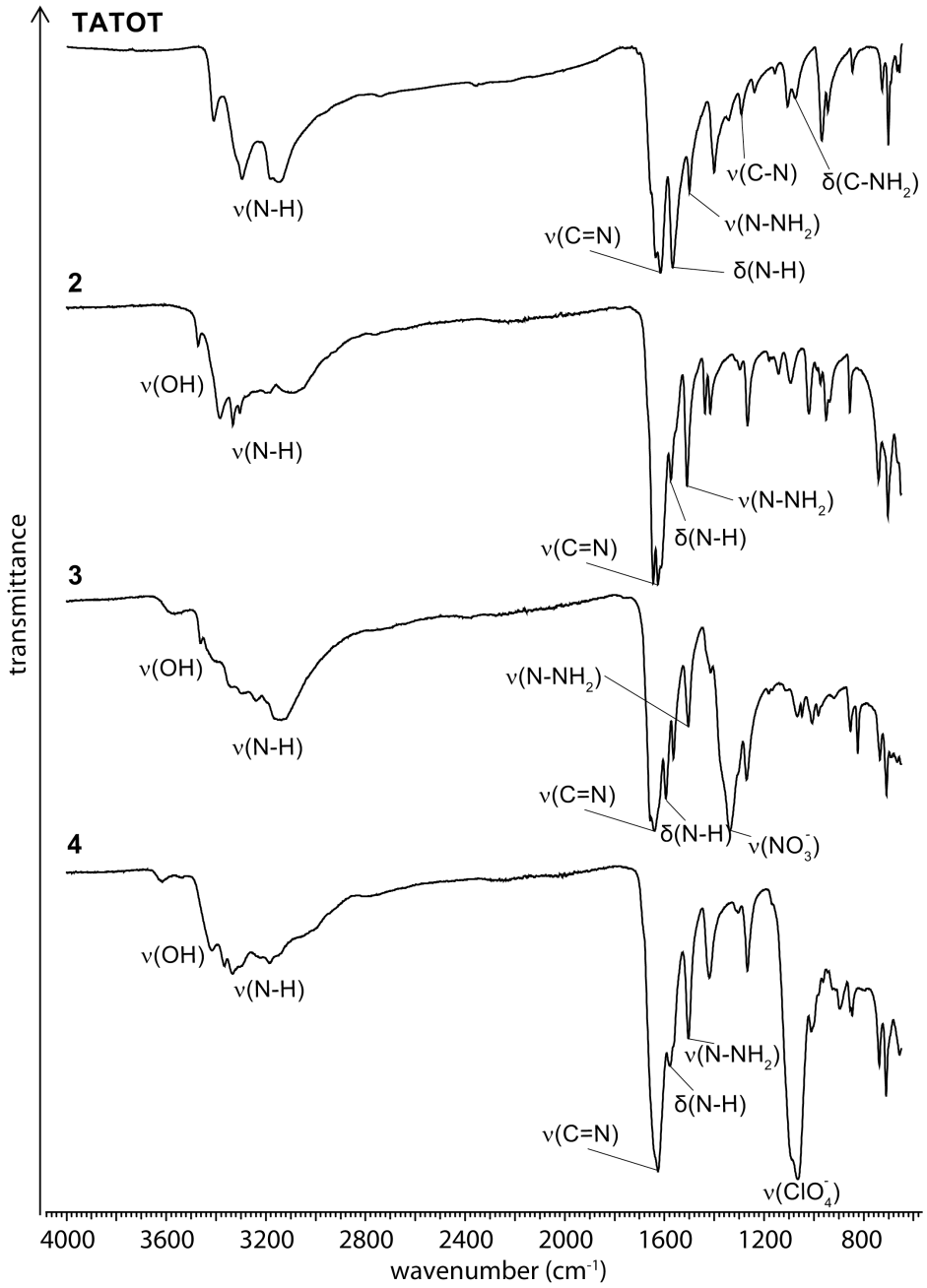


Figure 8. Infrared spectra of the uncoordinated ligand and the complexes **2**–**4**.

7.2.4 Physicochemical and Energetic Properties

The sensitivities toward friction, impact and electrostatic discharge for all the synthesized salts and complexes have been determined according to BAM standards. An overview of the physico-chemical properties of the new compounds **1**–**4** is given in Table 1. All compounds in this report are insensitive to friction. Compounds **2**–**4** can also be classified as insensitive to

electrostatic discharge (1.50 J). Apart from perchlorate **4** (35 J), all compounds are insensitive to impact with values higher than 40 J.

The thermal stabilities of all compounds were determined by DTA scans with a heating rate of β = 5 °C min^{-1}. The decomposition temperatures of the investigated compounds, given as the extrapolated onset temperatures, all lie above 200 °C. The DTA plots of zinc(II) complexes **2**–**4** are displayed in Figure 9. The nitrate complex **3** has the lowest decomposition temperature at 234 °C, whereas chloride **2** and perchlorate **4** decompose at 271 °C and 274 °C, respectively.

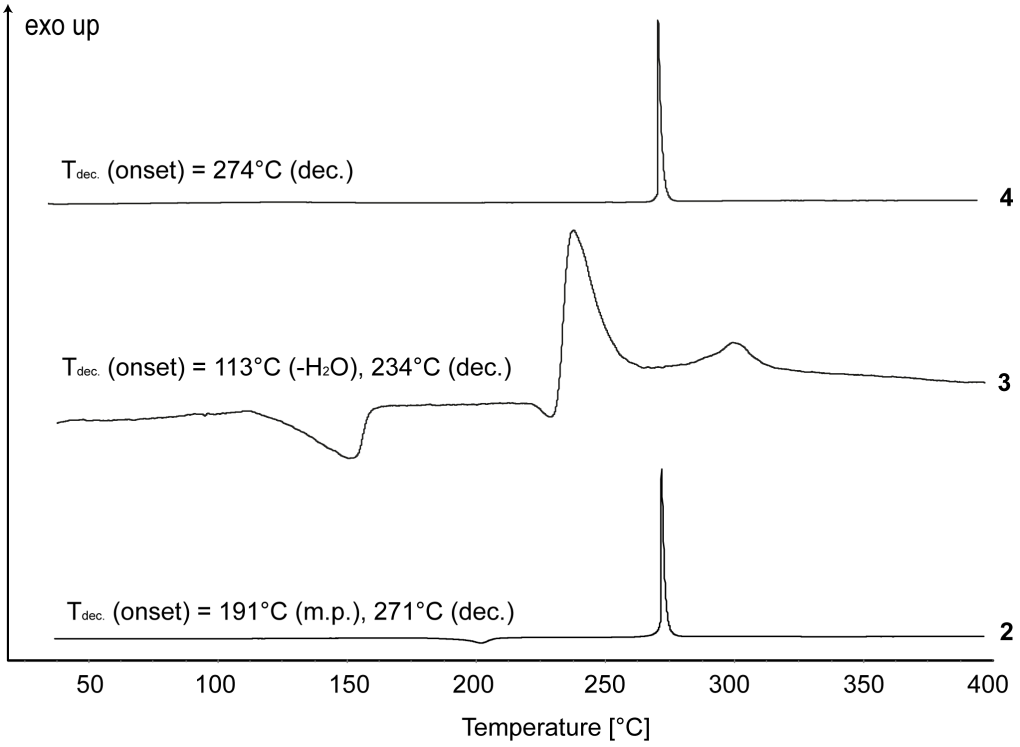


Figure 9. DTA plots of compounds **2**–**4** measured with a heating rate of 5 °C min^{-1}.

Table 1. Physico-chemical properties of **1**–**4**.

	1	**2**	**3**	**4**
Formula	$C_3H_6N_8Cl$	$C_6H_{14}Cl_2ZnN_{36}O$	$C_9H_{24}ZnN_{26}O_9$	$C_{12}H_{28}Cl_2ZnN_{32}O_{10}$
***M* [g mol^{-1}]**	190.62	462.57	705.85	916.85
***IS*[a] [J]**	> 40	> 40	> 40	35
***FS*[b] [N]**	> 360	> 360	> 360	> 360
***ESD*[c] [J]**	1.50	1.50	1.50	1.50
***T*$_{dec}$[d] [°C]**	301	271	234	274
grain size [µm]	100–500	100–500	500–1000	< 100

[a] impact sensitivity (BAM drophammer (1 of 6)); [b] friction sensitivity (BAM friction tester (1 of 6)); [c] electrostatic discharge device (OZM research); [d] start of decomposition temperature from DTA (β = 5 °C min^{-1}).

7.3 Conclusions

For the first time, the nitrogen rich heterocycle 3,6,7-triamino-7*H*-[1,2,4]triazolo[4,3-b][1,2,4]triazole (TATOT) was used as a ligand for the formation of metal complexes. The Zn(II) species $[ZnCl_2(TATOT)_2] \cdot H_2O$ (**2**), $[Zn(H_2O)(TATOT)_3](NO_3)_2 \cdot 2\ H_2O$ (**3**) and $[Zn(TATOT)_4](ClO_4)_2 \cdot 2\ H_2O$ (**4**) were investigated by X-Ray analysis, giving insight in the structural behavior of TATOT. Compounds **2**–**4** show a tetrahedral coordination sphere. In compound $[ZnCl_2(TATOT)_2] \cdot H_2O$ (**2**) the complex monomers were connected to three-dimensional zig-zag analog strengths over various hydrogen bonds forming tube-like cavities. IR spectroscopy could confirm the formation of hydrogen-bonds between the Cl ligand and the transition metal, which were observed in the crystal structures.

7.4 Experimental Section

Caution! *Compounds **2**–**4** are energetic materials with sensitivities toward shock and friction. Therefore, proper security precautions (safety glass, face shield, earthed equipment and shoes, Kevlar gloves and ear plugs) have to be applied while synthesizing and handling the described compounds.*

General Methods

All chemicals and solvents were employed as received (Sigma-Aldrich, Fluka, Acros). ^{1}H and ^{13}C spectra were recorded using a JEOL Eclipse 270, JEOL EX 400 or a JEOL Eclipse 400 instrument. The chemical shifts quoted in ppm in the text refer to the typical standard tetramethylsilane (^{1}H, ^{13}C) in d_6-DMSO as the solvent. Differential thermal analysis (DTA) measurements to determine the decomposition temperatures of compound **1**−**4** were performed at a heating rate of 5 °C min^{-1} with an OZM Research DTA 552-Ex instrument. Infrared spectra were measured with a Perkin–Elmer FT-IR Spectrum BXII instrument equipped with a Smith Dura SamplerIIR II ATR unit. To measure elemental analyses a Netsch STA 429 simultaneous thermal analyzer was employed.

To determine the molecular structures of compounds **1**−**4** in the crystalline state an Oxford Xcalibur3 diffractometer with a Spellman generator (voltage 50 kV, current 40 mA) and a KappaCCD detector was used. The data collection was performed using the CrysAlis CCD software,[20] the data reduction with the CrysAlis RED software.[21] The solution and refinement

of all structures were performed using the programs SIR-92,[22] SHELXS-97[23] and SSHELXL-97[24] implemented in the WinGX software package[25] and finally checked with the PLATON software.[26] In all crystal structures the hydrogen atoms were located and refined. The absorptions were corrected with the SCAL3 ABSPACK multi-scan method.[27]

The impact sensitivity tests were carried out according to STANAG 4489[28] modified instruction[29] using a Bundesanstalt für Materialforschung (BAM) drophammer.[30] The friction sensitivity tests were carried out according to STANAG 4487[31] modified instruction[32] using the BAM friction tester. The classification of the tested compounds results from the 'UN Recommendations on the Transport of Dangerous Goods'.[33] All compounds were tested upon the sensitivity towards electrical discharge using the Electric Spark Tester ESD 2010 EN.[34]

3,6,7-Triamino-7*H*-[1,2,4]triazolo[4,3-*b*][1,2,4]triazolium chloride (1)[15]

Triaminoguanidine hydrochloride (70 g, 500 mmol, 1.00 eq.) was dissolved in 750 mL 2 M hydrochloric acid. Cyanogen bromide (105.9 g, 1000 mmol, 2.00 eq.) was added and the solution was heated under stirring to 60 °C and was then kept at 60 °C for 2 h. After refluxing the reaction mixture for one additional hour the solution was cooled to 0 °C in an ice bath. Reaching a temperature of 0 °C, the solution deposited white platelets of compound (**1**). Yield: 50.3 g, 264 mmol, 53 %. Slow evaporation of an aqueous solution of **4** afforded single crystals suitable for low temperature X-ray measurement.

DTA (5 °C min^{-1}) onset: 301 °C (dec.); **IR** (ATR, cm^{-1}): ν = 3417 (m), 3320 (w), 3239 (m), 3120 (m), 1672 (s), 1659 (v), 1625 (s), 1590 (m), 1552 (m), 1516 (s), 1444 (m), 1417 (m), 1362 (w), 1308 (w), 1170 (m), 1104 (w), 1036 (m), 955 (s), 846 (m), 778 (w), 727 (s), 700 (vs), 677 (m); **^{1}H NMR** (d_6-DMSO, 400 MHz, ppm) δ = 13.33 (br s, 1H, *H*-2), 8.20 (s, 2H, *H*-9), 8.20 (s, 2H, *H*-11), 7.28 (s, 2H, *H*-11), 5.80 (s, 2H, *H*-10); **^{13}C NMR** (d_6-DMSO, 101 MHz, ppm) δ = 160.2 (*C*-6), 147.4 (*C*-8), 141.2 (*C*-3); **MS** *m/z* (FAB^{-}): 35.0 (Cl^{-}), *m/z* (FAB^{+}): 155.2 ($C_3H_6N_8^{+}$); **EA** calc. (%) for $C_3H_7N_8Cl$ (190.62 g mol^{-1}): C 18.91, H 3.70, N 58.79 %; found: C 19.19, H 3.65, N 58.51 %; **IS**: > 40 J; **FS**: > 360 N (at grain size 100–500 µm).

General procedure for the preparation of compounds 2–4:

The ligand TATOT was prepared according to the literature procedure.[15] The stoichiometry of the reaction of TATOT: metal salt was chosen to be 1:1 or 2:1, instead of the stoichiometry found in the crystalline products, because these ratios were found to give the highest yields. The yields of the described reactions are based on the amounts of TATOT used in the corresponding reactions.

A solution of the corresponding metal(II) salt **2**: zinc(II) chloride (68.2 mg, 0.50 mmol); **3**: zinc(II) nitrate hexahydrate (149 mg, 0.50 mmol); **4**: zinc(II) perchlorate hexahydrate (186 mg, 0.50 mmol)) in water (3 mL) was added to a 60 °C warm solution of 3,6,7-triamino-7*H*-[1,2,4]triazolo[4,3-*b*][1,2,4]triazole (**2**, **4**: 77 mg, 0.50 mmol; **3**: 154 mg, 1.00 mmol) in water (10 mL) and stirred for 1 min. The clear reaction mixtures were cooled down to room temperature and left to crystallize until a solid appeared. All products were filtered off and dried in air.

$[ZnCl_2(TATOT)_2] \cdot H_2O$ (2)

Coordination compound **2** was obtained overnight in the form of colorless blocks suitable for X-ray determination. Yield: 96.0 mg (0.21 mmol, 83 %).

DTA (5 °C min^{-1}) onset: 191 °C (m. p.), 271 °C (dec.); **IR** (ATR, cm^{-1}): v = 3472 (w), 3384 (m), 3332 (m), 3304 (m), 3197 (m), 3096 (m), 1645 (vs), 1626 (vs), 1614 (vs), 1574 (s), 1509 (s), 1437 (m), 1416 (m), 1297 (w), 1266 (m), 1180 (w), 1142 (w), 1093 (w), 1020 (m), 988 (w), 974 (w), 951 (m), 937 (m), 856 (m), 740 (s), 703 (s); **EA** calc. (%) for $C_6H_{14}Cl_2ZnN_{36}O$ (462.57 g mol^{-1}): C 15.58, H 3.05, N 48.45 %; found: C 15.67, H 3.02, N 47.53 %; **IS**: > 40 J; **FS**: > 360 N; **ESD**: 1.50 J (at grain size 100–500 µm).

$[Zn(H_2O)(TATOT)_3](NO_3)_2 \cdot 2\ H_2O$ (3)

Coordination compound **3** was obtained overnight in the form of colorless blocks suitable for X-ray determination. Yield: 203 mg (0.29 mmol, 86 %).

DTA (5 °C min^{-1}) onset: 113 °C (loss of water), 234 °C (dec.); **IR** (ATR, cm^{-1}): *v* = 3462 (w), 3398 (w), 3295 (m), 3240 (m), 3139 (m), 1657 (vs), 1640 (vs), 1594 (s), 1564 (s), 1504 (m), 1414 (m), 1338 (vs), 1270 (s), 1181 (m), 1167 (m), 1048 (m), 1007 (m), 982 (m), 919 (m), 853

(m), 824 (s), 804 (m), 735 (s), 708 (s), 691 (s), 665 (s); **EA** calc. (%) for $C_9H_{24}ZnN_{26}O_9$ (705.85 g mol^{-1}): C 15.31, H 3.43, N 51.60 %; found: C 15.51, H 3.56, N 51.68 %; **IS**: > 40 J; **FS**: > 360 N; **ESD**: 1.50 J (at grain size 500–1000 µm).

$[Zn(TATOT)_4](ClO_4)_2 \cdot 2\ H_2O$ (4)

Coordination compound **4** was obtained overnight in the form of colorless blocks suitable for X-ray determination. Yield: 82.0 mg (0.09 mmol, 72 %).

DTA (5 °C min^{-1}) onset: 274 °C (dec.); **IR** (ATR, cm^{-1}): ν = 3417 (w), 3366 (m), 3334 (m), 3183 (m), 1626 (vs), 1504 (m), 1419 (m), 1267 (m), 1064 (vs), 1010 (m), 982 (m), 963 (m), 926 (m), 897 (m), 854 (m), 846 (m), 796 (m), 738 (s), 710 (s), 656 (s); **EA** calc. (%) for $C_{12}H_{28}Cl_2ZnN_{32}O_{10}$ (916.85 g mol^{-1}): C 15.72, H 3.08, N 48.89 %; found: C 15.94, H 3.03, N 48.78 %; **IS**: 35 J; **FS**: > 360 N.

7.5 References

[1] a) S. S. Nagarkar, B. Joarder, A. K. Chaudhari, S. Mukherjee, S. K. Ghosh, *Angew. Chem.* **2013**, *125*, 2953–2957; *Angew. Chem. Int. Ed.* **2013**, *52*, 2881–2885; b) Y. Bae, R. Q. Snurr, Angew. Chem. 2011, 123, 11790–11801; *Angew. Chem. Int. Ed.* **2011**, *50*, 11586–11596; c) C. Wang, D. Liu, W. Lin, J. *Am. Chem. Soc.* **2013**, *135*, 13222–13234.

[2] D. Steinborn, *Grundlagen der metallorganischen Komplexkatalyse*, 2nd ed., Vieweg+Teubner, Wiesbaden, **2010**.

[3] J.-M. Lehn, *Supramolecular Chemistry*, 1st ed., Wiley-VCH, Weinheim, **1995**.

[4] O. Kahn, *Molecular Magnetism*, 1st ed., Wiley-VCH, Weinheim, New York, **1993**.

[5] Q. Zhang, J. M. Shreeve, *Angew. Chem. Int. Ed.* **2014**, *53*, 2540–2542.

[6] O. S. Bushuyev, P. Brown, A. Maiti, R. H. Gee, G. R. Peterson, B. L. Weeks, L. J. Hope-Weeks, *J. Am. Chem. Soc.* **2012**, *134*, 1422–1425.

[7] A. K. Sikder, N. Sikder, *J. Hazard. Mater.* **2004**, *112*, 1–15.

[8] G.-H. Tao, B. Twamley, J. n. M. Shreeve, *Inorg. Chem.* **2009**, *48*, 9918–9923.

[9] W.-C. Tong, J.-C. Liu, Q.-Y. Wang, L. Yang, T.-L. Zhang, *Z. anorg. allg. Chem.* **2014**, *640*, 2991–2997.

[10] S. Li, Y. Wang, C. Qi, X. Zhao, J. Zhang, S. Zhang, S. Pang, *Angew. Chem. Int. Ed.* **2013**, *52*, 14031–14035.

[11] M. Joas, T. M. Klapötke, J. Stierstorfer, N. Szimhardt, *Chem. Eur. J.* **2013**, *19*, 9995–10003.

[12] I. A. Ugryumov, M. A. Ilyushin, I. V. Tselinskii, A. S. Kozlov, *Russ. J. Appl. Chem.* **2003**, *76*, 439–441.

[13] a.) M. Friedrich, J. C. Gálvez-Ruiz, T. M. Klapötke, P. Mayer, B. Weber, J. J. Weigand, *Inorg. Chem.* **2005**, *44*, 8044–8052; b.) D. E. Chavez, M. A. Hiskey, D. L. Naud, *Journal of Pyrotechnics* **1999**, 10, 17–36.

[14] T. W. Myers, D. E. Chavez, S. K. Hanson, R. J. Scharff, B. L. Scott, J. M. Veauthier, R. Wu, *Inorg. Chem.* **2015**, *54*, 8077–8086.

[15] T. M. Klapötke, P. C. Schmid, S. Schnell, J. Stierstorfer, *Chem. Eur. J.* **2015**, *21*, 9219–9228.

[16] P. Yin, J. Zhang, D. A. Parrish, J. n. M. Shreeve, *J. Mater. Chem.* **2015**, *3*, 8606–8612.

[17] Crystallographic data for the structure(s) have been deposited with the Cambridge Crystallographic Data Centre. Copies of the data can be obtained free of charge on application to The Director, CCDC, 12 Union Road, Cambridge CB2 1EZ, UK (Fax: int.code_(1223)336-033; e-mail for inquiry: fileserv@ccdc.cam.ac.uk; e-mail for deposition: deposit-@ccdc.cam.ac.uk).

[18] a) M. Hesse, H. Meier, B. Zeeh, *Spektroskopische Methoden in der Organischen Chemie,* 7th ed., Thieme, Stuttgart, New York, **2005**; b) G. Socrates, *Infrared and Raman Characteristic Group Frequencies: Tables and Charts*, 3rd ed., John Wiley & Sons, Chichester, **2004**.

[19] a) F. A. Miller, C. H. Wilkins, *Anal. Chem.* **1952**, *24*, 1253-1294; b) J. Evers, I. Gospodinov, M. Joas, T. M. Klapötke, J. Stierstorfer, *Inorg. Chem.* **2014**, *53*, 11749–11756.

[20] *CrysAlis CCD*, Version 1.171.27p5 beta, Oxford Diffraction Ltd.

[21] *CrysAlis RED*, Version 1.171.27p5 beta, Oxford Diffraction Ltd.

[22] A. Altomare, G. Cascarano, C. Giacovazzo, A. Guagliardi, Completion and Refinement of Crystal Structures with SIR92, *J. Appl. Crystallogr*. **1993**, *26*, 343–350.

[23] G. M. Sheldrick, SHELXS-97, Program for Crystal Structure Solution, Universität Göttingen, **1997**.

[24] G. M. Sheldrick, SHELXL-97, Program for the Refinement of Crystal Structures, University of Göttingen, Germany, **1994**.

[25] L. Farrugia, *J. Appl. Cryst.* **1999**, *32*, 837–838.

[26] Spek, A. L. Platon, Utrecht University, Utrecht, The Netherlands, **1999**.

[27] SCALE3 ABSPACK-An Oxford Diffraction Program, Oxford Diffraction Ltd., **2005**.

[28] NATO standardization agreement (STANAG) on explosives, *impact sensitivity tests*, no. 4489, 1st ed., Sept. 17, **1999**.

[29] WIWEB-Standardarbeitsanweisung 4-5.1.02, Ermittlung der Explosionsgefährlichkeit, hier der Schlagempfindlichkeit mit dem Fallhammer, Nov. 8, **2002**.

[30] http://www.bam.de

[31] NATO standardization agreement (STANAG) on explosive,*friction sensitivity tests*, no. 4487, 1st ed., Aug. 22, **2002**.

[32] WIWEB-Standardarbeitsanweisung 4-5.1.03, Ermittlung der Explosionsgefährlichkeit oder der Reibeempfindlichkeit mit dem Reibeapparat, Nov. 8, **2002**.

[33] Impact: Insensitive > 40 J, less sensitive ≥35 J, sensitive ≥4 J, very sensitive ≤3 J; friction: Insensitive > 360 N, less sensitive = 360 N, sensitive < 360 N a. > 80 N, very sensitive ≤80 N, extreme sensitive ≤10 N; According to the UN Recommendations on the Transport of Dangerous Goods (+) indicates: not safe for transport.

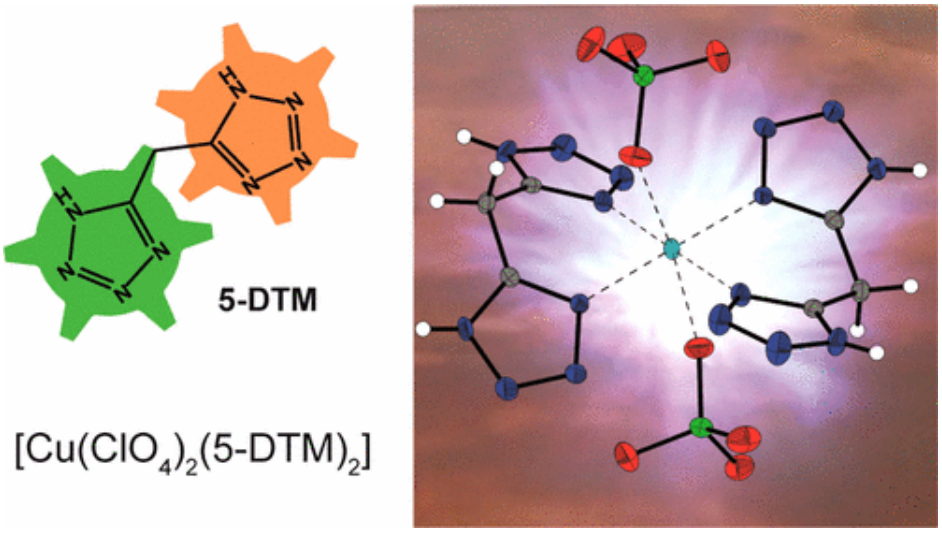
[34] http://www.ozm.cz

8 Di(1*H*-tetrazol-5-yl)methane as Neutral Ligand in Energetic Transition Metal Complexes

Manuel Freis, Thomas M. Klapötke, Jörg Stierstorfer and Norbert Szimhardt

published in *Inorganic Chemistry* **2017**, *56,* 7936–7947

DOI: 10.1021/acs.inorgchem.7b00432



A series of new energetic transition metal (Mn, Co, Ni, Cu, Zn) complexes were synthesized by using di(1*H*-tetrazol-5-yl)methane as neutral chelating ligand. The valuable strategy of choosing between different counteranions enables tuning of the desired physico-chemical properties. Adjacent picture shows detonation of the highly powerful and sensitive copper diperchlorate complex.

Abstract

The synthesis of di(1*H*-tetrazol-5-yl)methane (**1**, 5-DTM), starting from commercially available sodium azide and malononitrile, is described. This tetrazole was characterized and investigated for use as a neutral nitrogen-rich ligand in various energetic transition metal complexes: ($[CuCl_2(5\text{-}DTM)_2] \cdot 2\ H_2O$ (**2**), $[Co(H_2O)_2(5\text{-}DTM)_2]Cl_2$ (**3**), $[Ni(H_2O)_2(5\text{-}DTM)_2]Cl_2$ (**4**), $[Co(H_2O)_2(5\text{-}DTM)_2](NO_3)_2$ (**6**), $[Ni(H_2O)_2(5\text{-}DTM)_2](NO_3)_2$ (**7**), $[Zn(H_2O)_2(5\text{-}DTM)_2](NO_3)_2$ (**8**), $\{[Cu_3(SO_4)_2(5\text{-}DTM_{\text{-H}})_2(H_2O)_4(5\text{-}DTM)_2] \cdot 2\ H_2O\}_\infty$ (**9**), $[Cu(H_2O)_2(5\text{-}DTM)_2](NO_3)_2$ (**11**), $[Cu(NO_3)_2(5\text{-}DTM)_2] \cdot 2\ H_2O$ (**12**), $[Cu(NO_3)_2(5\text{-}DTM)_2]$ (**13**), $[Cu(H_2O)_2(5\text{-}DTM)_2](ClO_4)_2$ (**14**) and $[Cu(ClO_4)_2(5\text{-}DTM)_2]$ (**15**). Obtained coordination compounds were characterized using single crystal X-ray diffraction (except for **7** and **13**), IR spectroscopy, elemental analysis and differential thermal analysis (DTA). The sensitivities to external stimuli (impact, friction, electrostatic discharge) were determined. Complexes **12** and **13** were tested for their ignitability by laser irradiation.

8.1 Introduction

Depending on the field of application, energetic materials are divided into three main types: high explosives, propellants and pyrotechnics. These main types of energetic materials can be further divided into the following classes:[1] (i) primary explosives, (ii) secondary explosives (high explosives), (iii) rocket propellants (propellants), (iv) gun propellants (propellants), (v) detonators and igniters (pyrotechnics), (vi) decoy flares (pyrotechnics), (vii) smoke-generating munitions (pyrotechnics), (viii) light-generating pyrotechnics (pyrotechnics). The ignition and initiation of energetic materials can occur in different ways, for example by flame, heat, mechanical stimuli (friction and impact) or shock.[2] The initiating system is called a detonator (shockwave) or an igniter (flame) depending on the output of the energetic material.[3] Many of the initiating systems that are in use today suffer from manifold drawbacks, such as high toxicity (lead-containing formulations) or sensitivity (risk of unintended initiation by impact, friction or electrostatic discharge), which makes the research into possible replacements necessary.[4-7] In response to the disadvantages of conventional initiator systems, a new ignition and initiation method was developed using laser irradiation as the ignition source. The first published laser initiation experiments were carried out by Russian and American research groups in the late sixties and early seventies by investigating samples of lead azide, RDX, Tetryl and PETN.[8-10] During these investigations two laser-type systems were used: a ruby laser

(λ = 694 nm)[11] and a neodymium glass laser (λ = 1060 nm) operating in the Q-switch mode.[8] Owing to the relatively large size of these solid-state lasers practical applications were limited. New options for the initiation and ignition of energetic materials were achieved through the commercial availability of laser diodes.[11] In 1988, Kunz and Salas published details of one of the first diode laser ignitions of explosives by thermally igniting pentaammine(5-cyano-2*H*-tetrazolate)cobalt(III) perchlorate (CP, Figure 1) and a mixture of Ti/$KClO_4$ with a GaAlAs diode laser.[12]

In contrast to traditional initiation methods (spark, friction, heat, etc.), laser ignition and initiation is probably the most beneficial method. Unintended initiation can be excluded in most cases because of the isolation of the energetic material to electric impulses. Further advantages over classical initiation methods are the short function times and the possible application of less sensitive ignition charges (impact sensitivity ≥ 3 J, friction sensitivity ≥ 80 N, T_{dec} ≥ 180 °C), which increases the safety and handling of these compounds significantly. Recent studies show that energetic coordination compounds (ECC) are highly sensitive to laser irradiation, which makes them to excellent candidates in laser ignitable initiation systems.[13, 14] The investigation of energetic transition metal complexes, with respect to their initiation abilities, started with the previously mentioned CP and its promising replacement tetraammine-*cis*-bis(5-nitro-2*H*-tetrazolato-N^2)cobalt(III) perchlorate (BNCP, Figure 1).[12, 15] BNCP possesses excellent energetic properties with a calculated detonation velocity of 8.1 km s^{-1}.[16] Since then, various coordination compounds with varying ligands and metal centers have been synthesized and tested in applications of laser irradiation.[17–20] Our research group presented a large series of copper(II) based primary explosives using di(1*H*-tetrazol-5-yl)ethane as nitrogen-rich ligand.[17] In order to decrease the carbon content, di(1*H*-tetrazol-5-yl)methane (**1**, 5-DTM) was used in combination with different transition metals such as Mn, Co, Ni, Cu and Zn. The ligand has already been described in its deprotonated form in coordination compounds.[21, 22] For the first time, 5-DTM has been used in its neutral form to generate explosives with a higher performance.

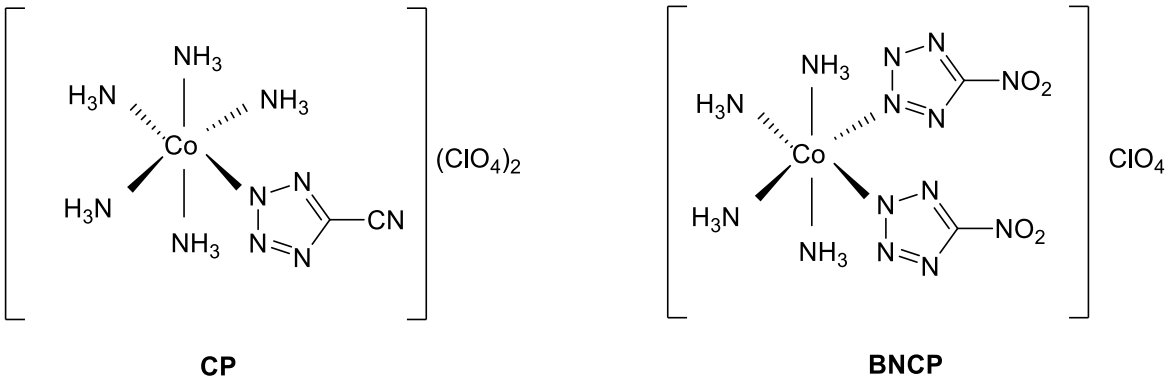
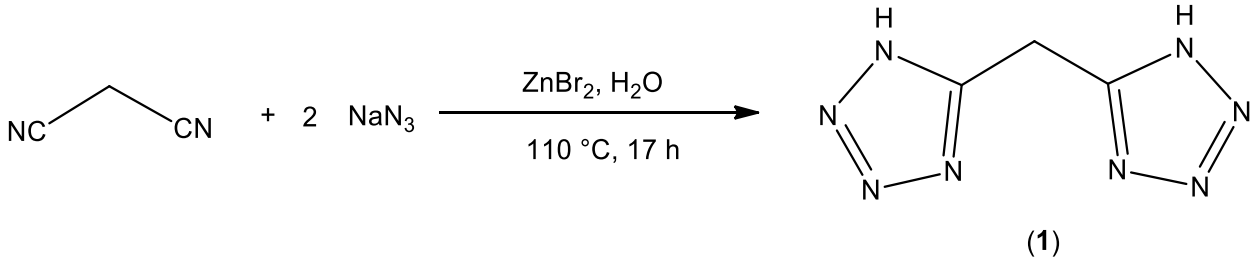


Figure 1. Molecular structures of CP and BNCP.

8.2 Results and Discussion

8.2.1 Synthesis

Di(1*H*-tetrazol-5-yl)methane (**1**, 5-DTM) can be prepared in different ways. One route is the cyclization of malononitrile with sodium azide and dimethylammonium chloride in DMF under reflux. However, purification of the product is complicated.[23] A better route is the [2+3] cycloaddition reaction of sodium azide with malononitrile catalyzed by zinc bromide in water according to a modified literature procedure at temperature of 110 °C (Scheme 1).[24] The temperature of the reaction mixture has to be held constantly at an oil bath temperature of 110 °C, which prevents the possible hydrolysis reaction of one of the nitrile groups of malononitrile when heating at temperatures above 120 °C. Acidification of the reaction mixture with diluted 2 M hydrochloric acid, followed by extraction with ethyl acetate, resulted in the isolation of the product with a yield of 55 %.

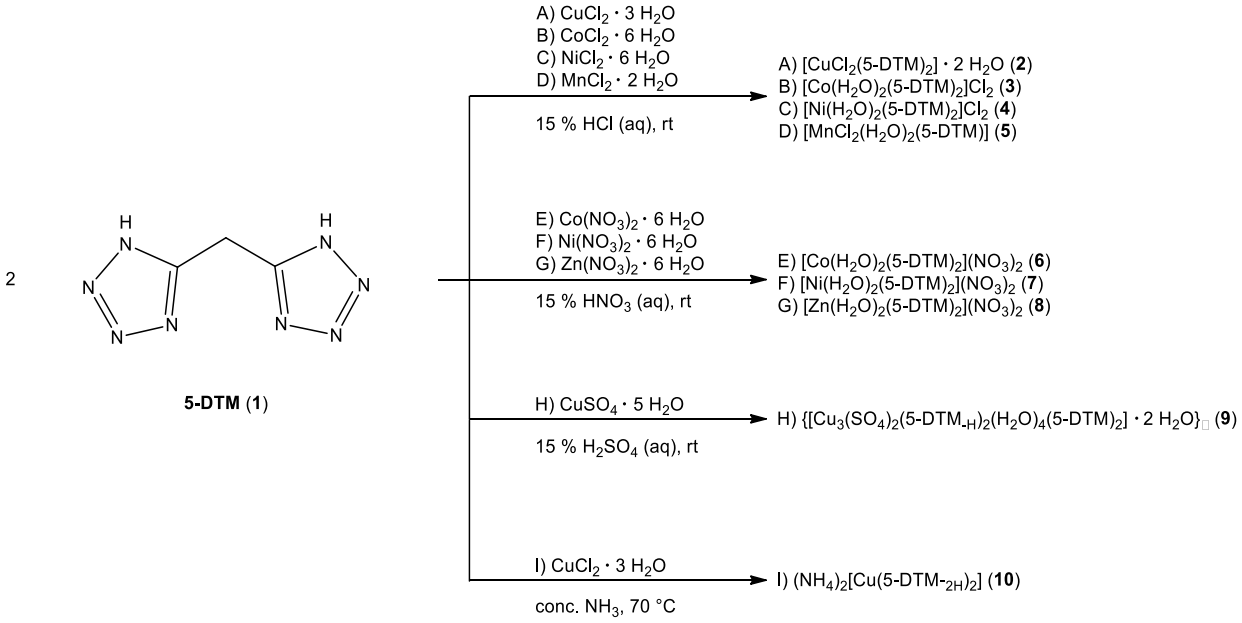


Scheme 1. Synthesis of di(1*H*-tetrazol-5-yl)methane (**1**).

The transition metal(II) complexes **2**–**9** were prepared by combining solutions of di(1*H*-tetrazol-5-yl)methane (**1**) and metal(II) salts in the corresponding acid at room temperature (Scheme 2). Due to the highly acidic character of the ligand (pK_a^1 = 3.42, pK_a^2 = 5.30),[23]

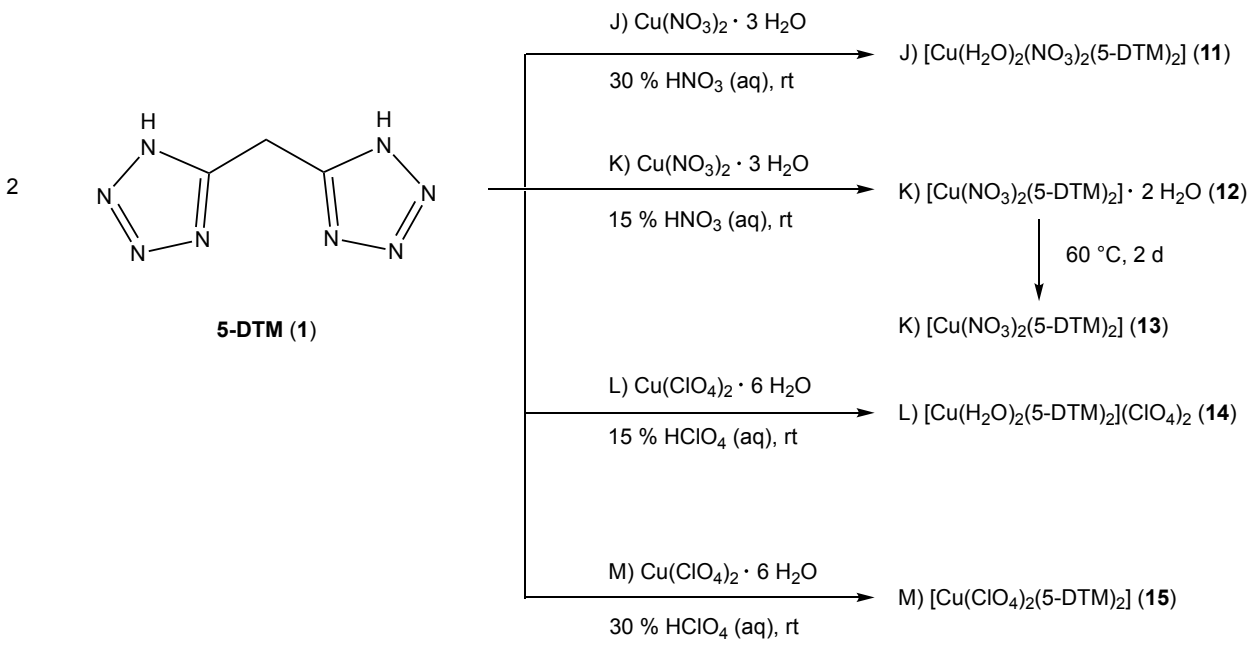
diluted acids were chosen as solvent for the reaction in order to prevent precipitation of the corresponding metal tetrazolate salts. This strategy ensures the incorporation of the neutral nitrogen-rich ligand to build up cationic or neutral complexes with oxidizing anions like nitrates or perchlorates to produce more sensitive energetic materials as possible alternatives for heavy metal free primary explosives.

The colored reaction mixtures were left for crystallization until a solid appeared. Ethanol was added as co-solvent in order to get better crystallization behavior in the synthesis of compound **3**. The products were obtained in yields of 29–100 % directly from the mother liquor as single crystals suitable for X-ray diffraction. Only compound **7** precipitated as a powder and single crystals could not be obtained by recrystallization. The coordination compounds were filtered off, washed with a small amount of ethanol and dried in air. In case of the manganese chloride complex **5** and the anionic copper amine complex **10** only a few single crystals could be picked between powder bulk material with unknown composition. The attempted synthesis of these two complexes in larger quantities failed unfortunately and only the crystal structure of both compounds could be determined which are shown in the SI (Figure S1 and S2).



Scheme 2. Synthesis of selected chloride, nitrate and sulfate-based 5-DTM complexes **2**–**10** with different metal centers.

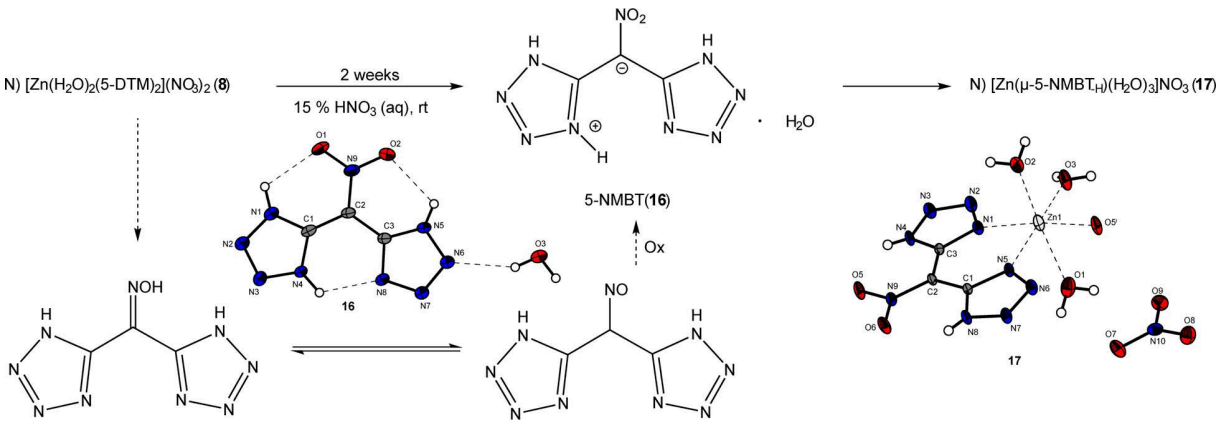
The synthesis of the copper(II) nitrate and perchlorate complexes (nitrate: **11** and **12**; perchlorate: **14** and **15**) strongly depends on the volume and concentration of the acid, and yields in each case two different coordination isomers.



Scheme 3. Synthesis of the coordination isomers **11** and **12** as well as **14** and **15**.

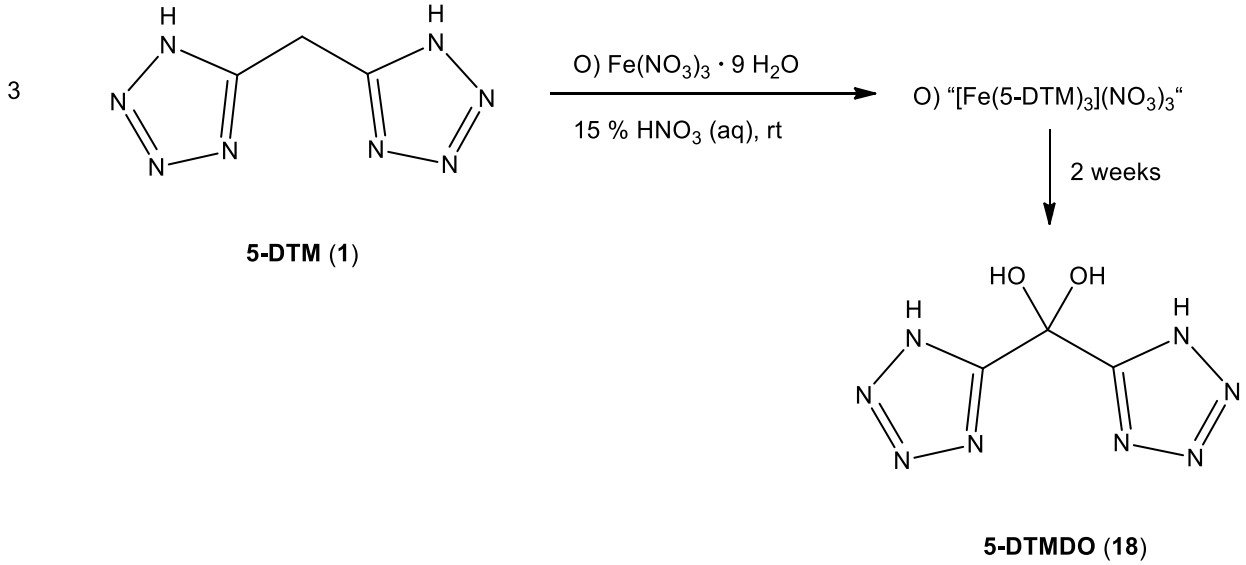
Each complex exhibits a different coordination environment and can therefore be clearly distinguished by infrared spectroscopy (Figure S4). Compound **13** could be obtained by dehydration of **12**. Attempted preparation of the cobalt, manganese, nickel or zinc perchlorate complexes failed due to no precipitation or crystallization of solid material.

Crystals of compound **8** were left for an additional two week's time in the mother liquor (15 % HNO_3). Portions of **8** re-dissolved and two other crystalline species, **16** and **17**, were obtained and investigated by low temperature X-ray diffraction. The methylene bridge of 5-DTM was nitrated and formed a coordination complex with zinc(II) nitrate (Scheme 4). Unfortunately, sufficient amounts of both compounds could not be isolated for further analytics. Both crystal structures are shown in SI (Figure S3 and S4). Compound **16** represents one of the few examples of a nitration under very diluted conditions. Nitration has been shown to also take place in reactions where the NO_2^+ concentration is undetectable by spectroscopic methods.[25] There are different interpretations to explain this reaction. One of them is the dissociation of NO_3^- to NO_2^+ and O^{2-}.[26] The second possibility is a (Lewis acid-assisted) nitrosation mechanism by nitrous acid, which is formed as a result of oxidation-reduction reactions.[27] This nitroso compound would be in equilibrium with the keto-oxime.[28] This nitroso compound could then be oxidized to the nitro compound 5,5′-(nitromethylene)bis(1*H*-tetrazole) (**16**, 5-NMBT), which formed a cationic complex with zinc(II) nitrate.



Scheme 4. Formation of 5,5'-(nitromethylene)bis(1*H*-tetrazole) (**16**, 5-NMBT) and its zinc(II) nitrate complex as well as the molecular structures of **16** and **17** determined by XRD.

The direct synthesis of compound **16** under varying conditions (65 % HNO_3, 100 % HNO_3, liquid NO_2) failed in each case due to many side reactions. However; the keto-oxime was detected by NMR spectroscopy in each case, which further points to the possible nitrosation mechanism described above. Another indication of this mechanism was the isolation of di(1*H*-tetrazol-5-yl)methanediol (**18**, 5-DTMDO) out of an iron(III) nitrate/ 5-DTM batch (Scheme 5), which was characterized by X-ray diffraction (see S3). Unfortunately, no intermediates could be isolated. The reaction of keto-oximes to ketones catalyzed by transition metals is a literature known reaction.[29] In water this ketone is in equilibrium with the geminal diol **18**.



Scheme 5. Formation of di(1*H*-tetrazol-5-yl)methanediol (**18**, 5-DTMDO).

8.2.2 Crystal Structures

All complexes (except **7** and **13**) were characterized using low temperature single crystal X-ray diffraction. Details on the measurement and refinement data are given in the SI. The crystal structures were deposited in the CSD database[30] and can be obtained free of charge with the CCDC nos. 1528237 (**2**), 1528239 (**3**), 1528244 (**4**), 1528241 (**5**), 1528233 (**6**), 1528246 (**8**), 1528236 (**9**), 1528238 (**10**), 1528240 (**11**), 1528243 (**12**), 1528245 (**14**), 1528235 (**15**), 1528234 (**16**), 1528243 (**17**), 1532131 (**18**). The bond lengths and angles of the ditetrazole rings of the compounds **2**–**6**, **8**–**12** as well as **14**, **15** are in the typical range of 5,5'-ditetrazoles and nearly the same as in the non-coordinating ligand **1**.[17, 31]

The copper(II) chloride complex **2** crystallizes in the form of dark blue rhombs in the monoclinic space group *C*2/*c* with four formula units per unit cell and a calculated density of 1.859 g cm^{-3} at 173 K. The molecular unit is built up of two asymmetric unit cells. The copper(II) center is octahedrally coordinated (Figure 2) by two chloride anions in axial positions and by two neutral, chelating 5-DTM molecules in a plane (Cu1–N1 = 1.998(2) Å, Cu1–N5 = 2.008(2) Å and < N5–N5^{i}–N1^{i}–N1 = –0.00(8)°). The axial Cu–Cl1 bond of 2.859(7) Å is a very long and weak coordination bond but still in the range of values given by the literature for copper–chloride coordination bonds.[32] As expected, d^9-copper(II) shows Jahn-Teller distortion in its coordination sphere along the Cu1–Cl1 axis. The coordination octahedron is slightly distorted and deviates from 90° (< (Cl1–Cu1–N1) = 91.76(7)°, < (Cl1–Cu1–N5) = 82.88(7)° and < (N1–Cu1–N5) = 85.99(8)°) because of the fixed structure of the 5-DTM ligand.

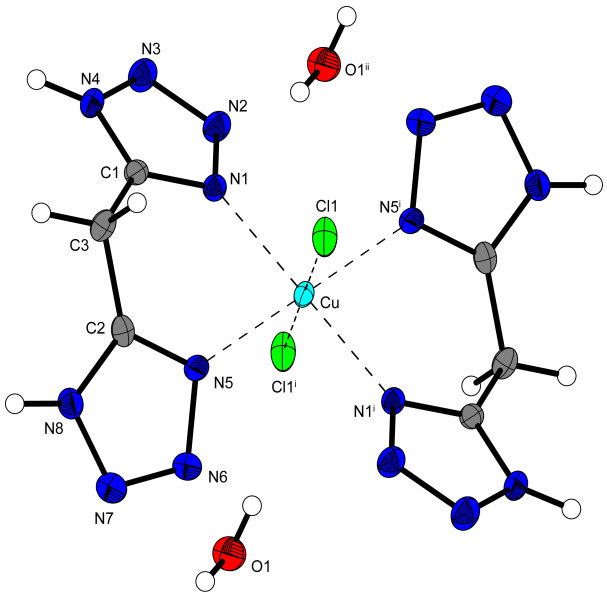


Figure 2. Molecular unit of $[CuCl_2(5\text{-DTM})_2] \cdot 2\ H_2O$ (**2**). Thermal ellipsoids of non-hydrogen atoms in all structures are set to the 50% probability level. Selected bond lengths (Å): Cu1–Cl1 2.859(7),

Cu1–N1 1.998(2), Cu1–N5 2.008(2), N1–N2 1.355(3), N1–C1 1.319(3), N2–N3 1.294(3), N3–N4 1.346(3), N4–C1 1.323(3), N5–N6 1.369(3), N5–C2 1.495(3), N6–N7 1.288(3), N7–N8 1.354(3), N8–C2 1.323(3), C1–C3 1.485(4), C2–C3 1.313(3); selected bond angles (°): Cl1–Cu1–N1 91.76(7), Cl1–Cu1–N5 82.88(7), Cl1–Cu1–N1^{i} 88.24(7), Cl1–Cu1–N5^{i} 97.12(7), N1–Cu1–N5 85.99(8), N1–Cu1–N5^{i} 94.01(8), Cu1–N1–C1 126.91(2), N2–N1–C1 106.85(2), Cu1–N1–N2 125.52(2), N1–N2–N3 109.6(2), N2–N3–N4 106.6(2), N3–N4–C1 109.00(2), Cu1–N5–C2 126.58(2), N6–N5–C2 106.91(2), Cu1–N5–N6 126.46(2), N5–N6–N7 109.21(2), N6–N7–N8 107.16(2), N7–N8–C2 108.92(2), N1–C1–N4 107.9(2), N4–C1–C3 126.4(2), N1–C1–C3 125.7(2), N8–C2–C3 126.7(2), N5–C2–C3 125.5(2), N5–C2–N8 107.80(2), C1–C3–C2 109.6(2); symmetry codes: (i) 0.5−x, 0.5+y, −z; (ii) 0.5−x, 0.5+y, 0.5−z.

The cobalt(II) chloride complex $[Co(H_2O)_2(5\text{-DTM})_2]Cl_2$ (**3**) crystallizes in the form of clear gold colored prisms in the monoclinic space group $P2_1/c$ with two formula units per unit cell and a calculated density of 1.920 g cm^{-3} at 173 K. The cobalt(II) metal center has an octahedral coordination sphere with two aqua ligands and two 5-DTM ligands (Figure 3).

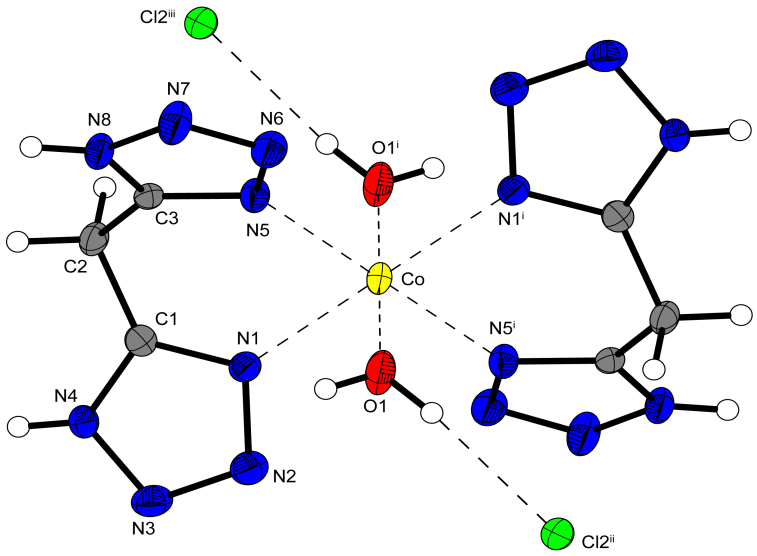


Figure 3. Molecular unit of $[Co(H_2O)_2(5\text{-DTM})_2]Cl_2$ (**3**). Selected bond lengths (Å): Co1–O1 2.056(2), Co1–N1 2.153(2), Co1–N5 2.104(2); selected bond angles (°): O1–Co1–N1 88.69(7), O1–Co1–N5 86.52(7), N1–Co1–N5 84.02(7); selected torsion angles (°): N1–N1^{i}–N5^{i}–N5 −0.00(7); symmetry codes: (i) 2−x, 1−y, 1−z; (ii) x, 0.5−y, 0.5+z; (iii) 2−x, 0.5+y, 0.5−z.

All bond lengths between the d^7-metal(II) center and the ligands are relatively similar and show no significant distortion along the axial axis (Co1–O1 = 2.056(2) Å, Co1–N1 = 2.153(2) Å and Co1–N5 = 2.104(2) Å). When comparing the two chloride 5-DTM coordination compounds **2** and **3**, it can be seen that cobalt has a higher affinity to oxygen than copper, which prefers the coordination of chloride. The same is true for the nickel(II) chloride complex $[Ni(H_2O)_2(5\text{-DTM})_2]Cl_2$ (**4**), which crystallizes in the form of dark blue needles in the monoclinic space

group $P2_1/c$ with two formula units per unit cell and a calculated density of 1.920 g cm^{-3} at 298 K. The nickel(II) center is octahedrally coordinated (Figure 4) by two aqua ligands in axial positions and by two neutral 5-DTM molecules in a plane (Ni1–N1 = 2.108(5) Å, Ni1–N5 = 2.058(2) Å and < N1–N1^{i}–N5^{i}–N5 = –0.00(2)°).

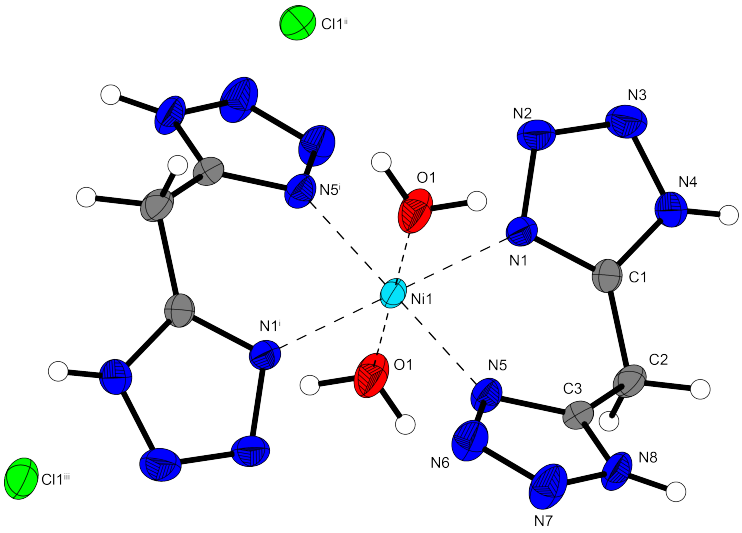


Figure 4. Molecular unit of $[Ni(H_2O)_2(5\text{-DTM})_2]Cl_2$ (**4**). Selected bond lengths (Å): Ni1–O1 2.064(5), Ni1–N1 2.108(5), Ni1–N5 2.058(5); selected bond angles (°): O1–Ni1–N1 89.63(2), O1–Ni1–N5 86.34(2), N1–Ni1–N5 85.74(2); selected torsion angles (°): N1–N1^{i}–N5^{i}–N5 −0.00(2); symmetry codes: (i) 2−x, 1−y, 1−z; (ii) x, 0.5−y, 0.5+z; (iii) 1−x, 1−y, 1−z.

All bond lengths between the d^8-metal(II) center and the ligands lie in the same range and show no distortion along the axis (Ni1–O1 = 2.064(5) Å, Ni1–N1 = 2.108(5) Å and Ni1–N5 = 2.058(5) Å). The coordination octahedron is slightly distorted and deviates from 90° (< O1–Ni1–N1 = 89.63(2)°, < O1–Ni1–N5 = 86.34(2)° and < N1–Ni1–N5 = 85.74(2)°). Similar to cobalt(II) complex **3**, the nickel(II) centers show a higher affinity to oxygen than the copper(II) complex **2**. The molecular structure of $[Co(H_2O)_2(5\text{-DTM})_2](NO_3)_2$ (**6**) is depicted in Figure 5. The cobalt(II) cations in **6**, which crystallize in the orthorhombic space group *Pnma* with four formula units per unit cell and a calculated density of 1.918 g cm^{-3} at 173 K, have a centrosymmetric six-fold coordination sphere. Again, the same situation as in compound **3** can be observed, where all bond lengths between the cobalt(II) center and the ligands are in the same range without distortion (Co1–O1 = 2.071(2) Å, Co1–N4 = 2.123(2) Å and Co1–N8 = 2.162(2) Å). The cobalt(II) complex has the same sum formula as compound **11**, but with a different metal center. However, the nitrate anion in **6**, in contrast to the other nitrates **11** and **12**, has an inversion center that generates the second half of the anion by symmetry.

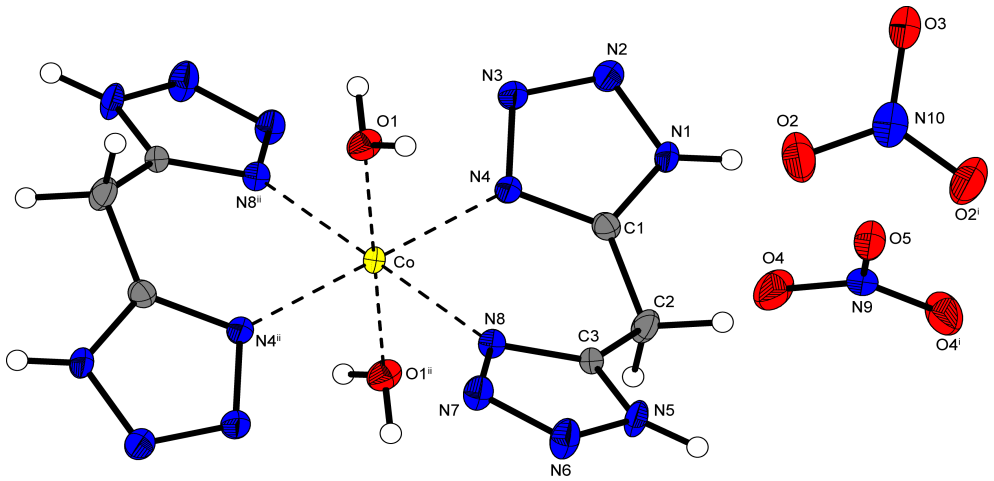


Figure 5. Molecular unit of $[Co(H_2O)_2(5\text{-DTM})_2](NO_3)_2$ (**6**). Selected bond lengths (Å): Co1–O1 2.071(2), Co1–N4 2.123(2), Co1–N8 2.162(2), O2–N10 1.236(3), O3–N10 1.314(4), O4–N9 1.234(3), O5–N9 1.274(4); selected bond angles (°): O1–Co1–N4 90.22(7), O1–Co1–N8 94.22(7), N4–Co1–N8 83.79(7), O2–N10–O3 119.06(2), O4–N9–O5 118.54(2); selected torsion angles (°): N4–N4^{i}–N8^{i}–N8 −0.00(8); symmetry codes: (i) x, 0.5−y, z; (ii) 1−x, −y, 1−z.

The molecular structure of $[Zn(H_2O)_2(5\text{-DTM})_2](NO_3)_2$ (**8**) is shown in Figure 6 and, apart from the different metal center, looks almost identical to **6**. Compound **8** crystallizes in the orthorhombic space group *Pnma* with four formula units per unit cell and a calculated density of 1.928 g cm^{-3} at 173 K. The zinc(II) cation shows an octahedral surrounding and is bonded to four nitrogen atoms of two 5-DTM ligands in the equatorial plane and to two aqua ligands in axial positions (Zn1–O7 = 2.100(2) Å, Zn1–N3 = 2.142(2) Å and Zn1–N7 = 2.174(2) Å).

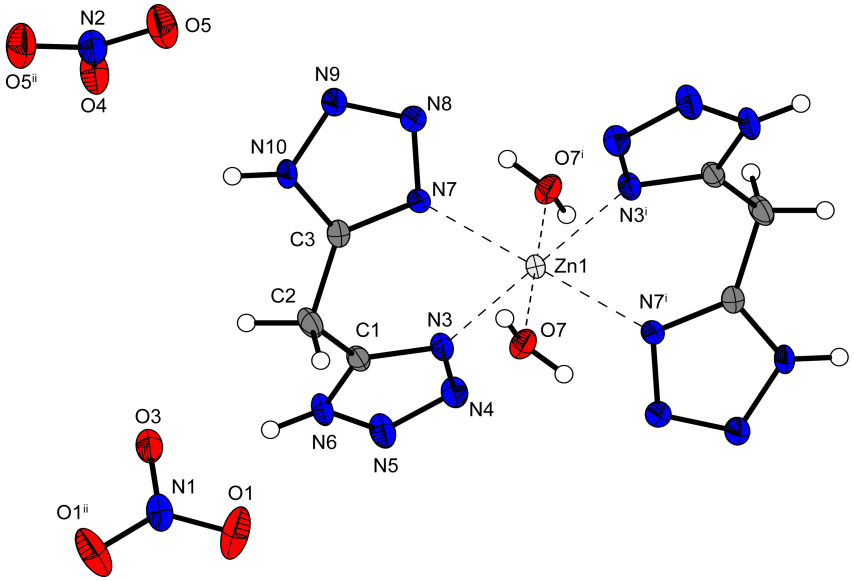


Figure 6. Molecular unit of $[Zn(H_2O)_2(5\text{-DTM})_2](NO_3)_2$ (**8**). Selected bond lengths (Å): Zn1–O7 2.100(2), Zn1–N3 2.142(2), Zn1–N7 2.174(2), O1–N1 1.234(2), O3–N1 1.276(4), O5–N2 1.241(3),

O4–N2 1.308(5); selected bond angles (°): O7–Zn1–N3 89.22(7), O7–Zn1–N7 85.61(7), N3–Zn1–N7 83.49(7), O1–N1–O3 118.28(2), O4–N2–O5 119.33(2); selected torsion angles (°): N3–N3^{i}–N7^{i}–N7 0.00(8); symmetry codes: (i) 1−x, −y, 1−z; (ii) x, 0.5−y, z.

The very interesting polymeric copper(II) sulfate complex **9** crystallizes in the form of blue plates in the triclinic space group *P*−1 with only one formula unit per unit cell and a calculated density of 2.125 g cm^{-3} at 173 K (Figure 7). The coordination compound **9** is built up by three non-equivalent copper(II) centers and four types of ligands (Figure 8). Every copper(II) center has an octahedral coordination sphere with two Jahn-Teller distorted axial ligands. Cu1 is coordinated by two neutral 5-DTM ligands in a plane (Cu1–N9 = 1.973(7) Å, Cu1–N13 = 2.011(6) Å and < N9–N9^{i}–N13^{i}–N13 = –0.0(2)°) and by two additional tetrazole rings (the neutral half of a deprotonated 5-DTM molecule) in axial positions that connect this motif to the Cu2 center (Cu1–N7 = 2.535(7) Å). Cu2 in contrast is surrounded by two mono-deprotonated 5-DTM anions in equatorial positions (Cu2–N1 = 1.993(7) Å, Cu2–N5 = 2.003(7) Å and < N1–N1^{i}–N5^{i}–N5 = 0.0(3)°) and by two axial Jahn-Teller distorted aqua ligands (Cu2–O10 = 2.506(8) Å). The deprotonated part of the ditetrazole ligand connects Cu2 with Cu3 (Cu3–N4 = 2.055(7) Å).

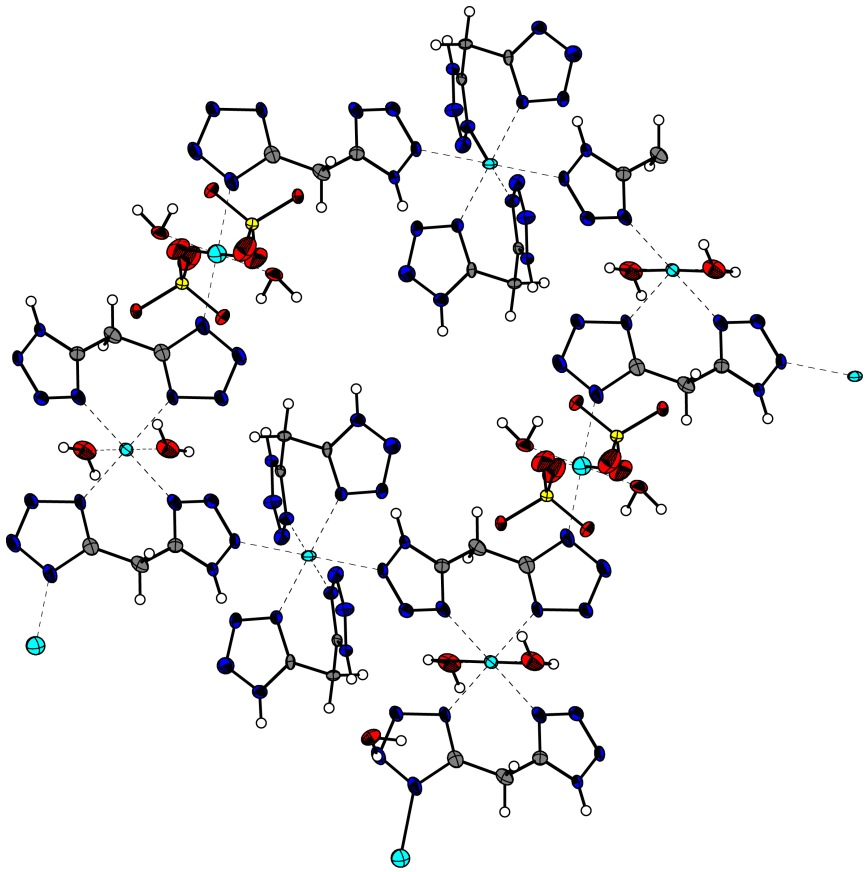


Figure 7. Polymeric structure of compound **9**.

Cu2 in contrast is surrounded by two mono-deprotonated 5-DTM anions in equatorial positions (Cu2–N1 = 1.993(7) Å, Cu2–N5 = 2.003(7) Å and < N1–N1^{i}–N5^{i}–N5 = 0.0(3)°) and by two axial Jahn-Teller distorted aqua ligands (Cu2–O10 = 2.506(8) Å). The deprotonated part of the ditetrazole ligand connects Cu2 with Cu3 (Cu3–N4 = 2.055(7) Å). This coordination moiety also consists of two aqua ligands (Cu3–O7 = 1.941(7) Å) and two sulfate anions in axial positions (Cu3–O4 = 2.404(8) Å). The octahedral coordination spheres only show small divergences to the perfect angle of 90° (< (N7–Cu1–N13) = 87.0(2)°, < (O10–Cu2–N1) = 85.6(3)° and (O4–Cu3–O7) = 85.6(3)°). The bond lengths and angles of the deprotonated 5-DTM molecule are in the same range as the values for the neutral ligand described in the complexes above. The structure and geometry (bond lengths and angles) of the sulfate ligands are comparable to those found in literature.[33]

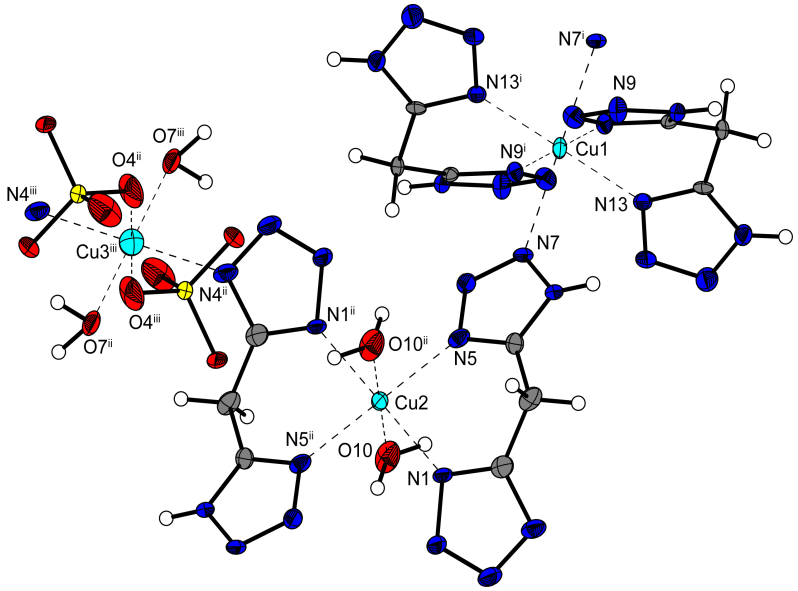


Figure 8. Molecular unit of {[$Cu_3(SO_4)_2$(5-DTM$_{-H}$)$_2$(H_2O)$_4$(5-DTM)$_2$] · 2 H_2O}$_\infty$ (**9**). Selected bond lengths (Å): Cu1–N7 2.535(7), Cu1–N9 1.973(7), Cu1–N13 2.011(6), Cu2–O10 2.506(8), Cu2–N1 1.993(7), Cu2–N5 2.003(7), Cu3–O4 2.404(8), Cu3–O7 1.941(7), Cu3–N4 2.055(7), S1–O1 1.473(6), S1–O2 1.478(7), S1–O3 1.462(8), S1–O4 1.462(8); selected bond angles (°): N7–Cu1–N9 82.9(2), N7–Cu1–N13 87.0(2), N9–Cu1–N13 86.3(3), O10–Cu2–N1 85.6(3), O10–Cu2–N5 97.6(2), N1–Cu2–N5 86.5(8), O4–Cu3–O7 85.6(3), O4–Cu3–N4 83.3(3), O7–Cu3–N4 92.4(3), O1–S1–O2 109.3(4), O1–S1–O3 109.8(4), O2–S1–O3 109.1(4), O2–S1–O4 107.7(4), O3–S1–O4 111.2(5); selected torsion angles (°): N9–N9^{i}–N13^{i}–N13 −0.0(2), N5–N5^{i}–N1^{i}–N1 0.0(3), O4–O4^{i}–N4^{i}–N4 0.0(3); symmetry codes: (i) 2−x, −y, −z; (ii) 1−x, 1−y, −z; (iii) x, y, −1+z.

The diaqua copper(II) nitrate complexes **11** and **12** crystallize as coordination isomers in the space groups $P2_1/c$ (**4**) and $P\bar{1}$ (**5**) and calculated densities of 1.895 g cm^{-3} and 1.957 g cm^{-3} at 173 K. The molecular units are shown in Figure 9. The copper(II) centers have an octahedral

coordination sphere with Jahn-Teller distortion along the axial copper oxygen bonds (Cu1–O1). The nitrate counterions in the structure of compound **12** are in contrast to its coordination isomer **11**, involved in coordination to the transition metal.

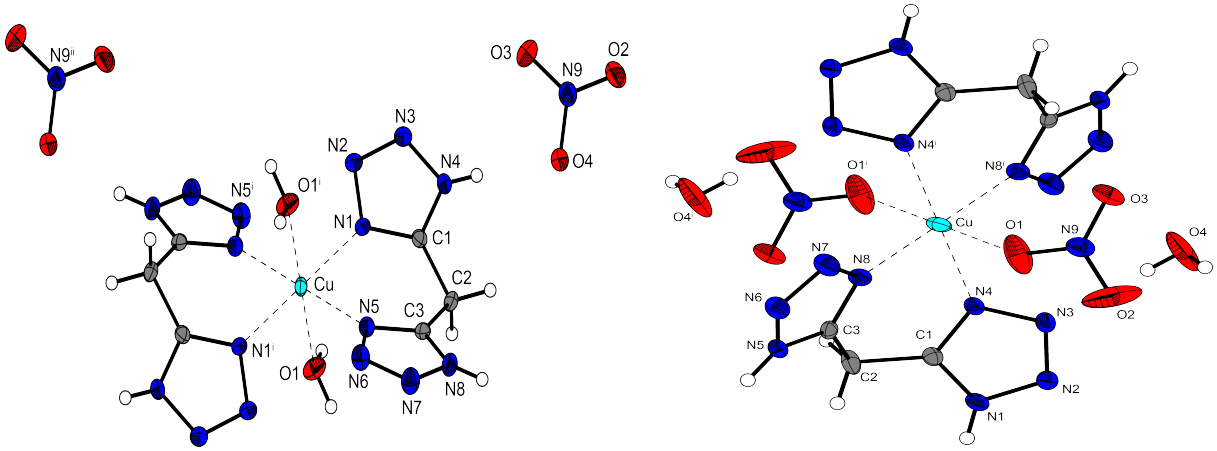


Figure 9. Molecular unit of $[Cu(H_2O)_2(5\text{-DTM})_2](NO_3)_2$ (**11**, left) and $[Cu(NO_3)_2(5\text{-DTM})_2] \cdot 2\ H_2O$ (**12**, right). Selected bond lengths (Å): **11**: Cu1–O1 2.337(2), Cu1–N1 2.008(2), Cu1–N5 2.028(2), O2–N9 1.228(2), O3–N9 1.230(2), O4–N9 1.290(2); **12**: Cu1–O1 2.425(2), Cu1–N4 2.016(2), Cu1–N8 1.983(2), O1–N9 1.239(3), O2–N9 1.241(3), O3–N9 1.214(3); selected bond angles (°): **11**: O1–Cu1–N1 88.95(5), O1–Cu1–N5 92.64(5), N1–Cu1–N5 85.82(5), O3–N9–O4 118.36(2), O2–N9–O3 122.84(2), O2–N9–O4 118.80(2); **12**: O1–Cu1–N4 85.74(7), O1–Cu1–N8 87.35(7), N4–Cu1–N8 86.10(7), O1–N9–O2 115.9(2), O2–N9–O3 121.4(2), O1–N9–O3 122.7(2); symmetry codes: **11**: (i) 0.5−x, 0.5+y, −0.5−z; (ii) 0.5−x, 0.5+y, −0.5−z; **12**: (i) 1−x, −y, −1−z.

The perchlorate complexes $[Cu(H_2O)_2(5\text{-DTM})_2](ClO_4)_2$ (**14**) and $[Cu(ClO_4)_2(5\text{-DTM})_2]$ (**15**) crystallize in the form of dark blue crystals (**14**: orthorhombic, *Pbca,* 2.038 g cm^{-3}; **15**: monoclinic, $P2_1/n$, 2.128 g cm^{-3} (173 K). Both molecular structures are illustrated in Figure 10. Each copper(II) complex is octahedrally coordinated and shows a Jahn Teller distortion along the axial bonds. The extreme sensitivity of compound **15** can be attributed to the direct coordination of the perchlorate ligands, which differ in their dative bond lengths (Cu1–O4 = 2.531(2) Å and Cu1–O8 = 2.379(2) Å).

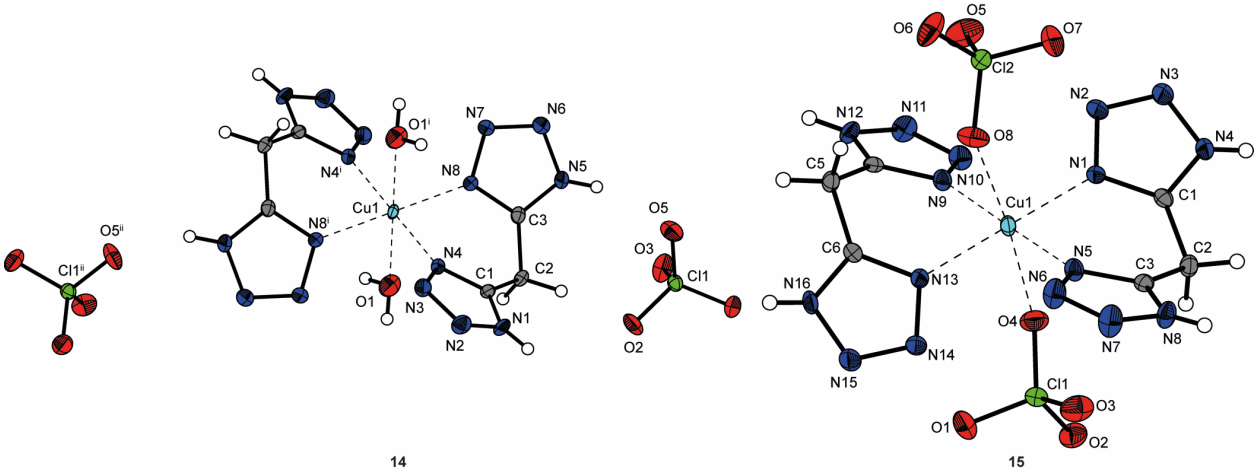


Figure 10. Molecular unit of $[Cu(H_2O)_2(5\text{-DTM})_2](ClO_4)_2$ (**14**, left) and $[Cu(ClO_4)_2(5\text{-DTM})_2]$ (**15**, right). Selected bond lengths (Å): **14**: Cu1–O1 2.397(2), Cu1–N4 1.987(2), Cu1–N8 2.018(2), Cl1–O2 1.435(2), Cl1–O3 1.444(3), Cl1–O4 1.435(2), Cl1–O5 1.439(2); **15**: Cu1–O4 2.531(2), Cu1–O8 2.379(2), Cu1–N1 2.008(2), Cu1–N5 1.977(2), Cu1–N9 1.986(2), Cu1–N13 2.015(2), Cl1–O1 1.428(2), Cl1–O2 1.450(2), Cl1–O3 1.445(2), Cl1–O4 1.436(2), Cl1–O5 1.432(2), Cl1–O6 1.4448(2), Cl1–O7 1.416(2), Cl1–O8 1.443(2); selected bond angles (°): **14**: O1–Cu1–N4 87.66(6), O1–Cu1–N8 91.44(6), N4–Cu1–N8 86.33(6), O2–Cl1–O3 109.33(9), O2–Cl1–O4 110.39(8), O2–Cl1–O5 109.77(8), O3–Cl1–O4 109.43(8), O3–Cl1–O5 108.47(9), O4–Cl1–O5 109.42(8); **15**: O4–Cu1–O8 175.32(6), O4–Cu1–N1 86.03(7), O4–Cu1–N5 93.34(6), O4–Cu1–N9 87.33(9), O4–Cu1–N13 92.70(7), O8–Cu1–N1 97.43(7), O8–Cu1–N5 90.05(7), O8–Cu1–N9 89.31(7), O8–Cu1–N13 83.82(7), N1–Cu1–N5 86.28(8), N1–Cu1–N9 93.19(8), N1–Cu1–N13 178.66(8), N5–Cu1–N9 179.11(8), N5–Cu1–N13 94.23(8), N9–Cu1–N13 86.32(8), O1–Cl1–O2 109.22(2), O1–Cl1–O3 109.56(2), O1–Cl1–O4 110.69(2), O2–Cl1–O3 107.79(2), O2–Cl1–O4 110.56(2), O3–Cl1–O4 108.98(2), O5–Cl2–O6 108.92(2), O5–Cl2–O7 112.10(2), O5–Cl2–O8 109.17(2), O6–Cl2–O7 108.61(2), O6–Cl2–O8 108.32(2), O7–Cl2–O8 109.65(2); selected torsion angles (°): **14**: N4–N4^{i}–N8^{i}–N8 0.00(5); **15**: N13–N1–N9–N5 1.43(8); symmetry codes: **14**: (i) −x, −y, −z; (ii) −0.5+x, 0.5−y, −z.

8.2.3 Sensitivities and Thermal Stability

The sensitivities toward impact, friction and heat were explored precisely. Compound **15** was too sensitive for any measurements. An outline of the decomposition temperatures and the sensitivities toward impact, friction and electrostatic discharge of the coordination compounds **2**–**4**, **6**–**9**, **11**–**15** and the free ligand **1** is given in Table 1. Compound **1** has sensitivities greater than 40 J for impact and greater than 360 N for friction and can therefore be classified as insensitive according to UN standards. The ESD value is 0.30 J. The chloride and sulfate complexes **2**–**4** and **9** are insensitive toward impact and friction. The compounds are also

classified as insensitive toward electrostatic discharge (0.80–1.50 J). As shown in Table 1, substitution of chloride/sulfate by nitrate as anion decreases the stability against impact and friction in most cases (impact: 1–6 J; friction: 160–360 N). Most of the compounds also show higher sensitivities toward electrostatic discharge (0.26–1.50 J). As expected, the introduction of highly oxidizing anions like perchlorate vastly increases the sensitivities. Extra safety precautions should be taken when handling the perchlorate complexes **14** and **15**, which are both classified as primary explosives (IS: < 1 J; FS: < 5 N). Compound **14** also shows the highest sensitivity toward electrostatic discharge (> 100 mJ). In comparison to previously published copper(II) di(1*H*-tetrazol-5-yl)ethane complexes[17] a trend to slightly higher sensitivities was observed.

The thermal stabilities of all coordination compounds were determined by DTA scans with a heating rate of β = 5 °C min^{-1}. All synthesized complexes showed a lower thermal stability than the free ligand **1**. Ditetrazole **1** and nickel(II) chloride complex **4** showed no significant decomposition point (exothermic peak) in the measured range of 25–400 °C. However, in the TGA measurements, **1** and **4** slowly started to lose weight constantly at about 100 °C. The decomposition temperatures of the investigated compounds, given as the extrapolated onset temperatures, range from 85 °C for **14** up to 233 °C (which is quite impressive) for the extremely sensitive water-free perchlorate complex **15** (Figure S5). The low thermal stability of **14** can be explained by the loss of the coordinated aqua ligands, which immediately leads to the detonation of the compound. Only the cobalt chloride complex **3** had a higher decomposition temperature (243 °C). Compound **11** has an endothermic signal at 97 °C which presumably indicates the loss of coordinated aqua ligands (Figure S5). TGA (thermal gravimetric analysis) measurements with a heating rate of β = 2 °C min^{-1} in a nitrogen atmosphere in open Al_2O_3 crucibles with a Perkin Elmer TGA4000 thermogravimetric analyzer have shown that compound **12** loses its crystal water at temperatures lower than 100 °C (Figure S6). Drying of **12** at 60 °C yielded the dehydrated complex **13** without decomposition. A higher heating rate (e.g. 5 °C min^{-1}) leads to decomposition of the complex right after dehydration (Figure S5).

Table 1. Sensitivities and thermal behavior of **1**–**6**, **7**–**9** and **11**–**15**.

compound	*IS* (J)[a]	*FS* (N)[b]	*ESD* (J)[c]	T_{dec} (°C)[d]
1	> 40	> 360	0.30	>100[e]
2	> 40	> 360	1.50	204
3	> 40	> 360	1.00	243
4	> 40	> 360	1.50	>100[e]
6	4	240	0.20	223
7	1	> 360	1.50	142
8	6	252	1.50	158
9	> 40	> 360	0.80	224
11	6	> 360	0.26	144
12	2	160	1.50	141–147
13	2	160	0.25	148
14	< 1	< 5	> 0.10	85
15	< 1	< 5	not tested	233

[a] impact sensitivity according to the BAM drophammer (method 1 of 6); [b] friction sensitivity according to the BAM friction tester (method 1 of 6); [c] electrostatic discharge sensitivity (OZM ESD tester); [d] temperature of decomposition according to DTA (onset temperatures at a heating rate of 5 °C min^{-1}); [e] weight loss in TGA.

Hot plate tests showed a detonation for compound **15** (Figure S7) and deflagrations for **12** and **13** (Figure S8 and S9). Interestingly, dehydration of compound **12** to **13** had no effect on the mechanical sensitivities but instead had an effect on the explosive power and sensitivity toward electrostatic discharge. Compound **13** deflagrated with a louder fulmination during the hot plate test. The ignitability of the perchlorate complex **15** was further tested through a hot needle test (Figure S10). The sample was fixed on an aluminum plate using adhesive tape. Detonation of the compound usually indicates a useful primary explosive. Instead, the practical and safe hot plate test instead only shows the behavior of the unconfined sample toward fast heating on a hot copper plate. It does not necessarily allow drawing conclusions on its capability as a primary explosive.

8.2.4 Laser Ignition Tests

Laser ignition tests in the past showed that copper(II) complexes are capable compounds for laser initiation systems.[16-18] The laser ignition experiments were carried out with a 25 W InGaAs laser diode operating in single-pulsed mode. The diode was directly coupled to an optical fiber with a core diameter of 105 µm, a cladding diameter of 125 µm and a buffer diameter of 250 µm.[3] Approximately 25–50 mg of the carefully pestled compound to be examined were filled into a glass tube (l = 2 cm, d = 3 cm) and relatively tight packed. The optical fiber was linked via a ST type connecter with a 2.5 mm ceramic ferrule directly to the top of the investigated sample (Figure 11). Finally, the ST connector of the optical fiber was fixed with adhesive tape to the glass tube.

In the last step, the optical fiber of the sample was connected with the Laser Firing Unit. Access to the software of the Laser Firing Unit to adapt changes to the laser parameters, such as the current or the pulse length, was provided through a RS-232 serial port.

Only samples of **12** and **13** were tested in laser initiation experiments because of their proper sensitivities. Compounds **14** and **15** are also capable for laser irradiation. However, they are too sensitive for any use. Compounds **12** and **13** were irradiated with a monopulsed diode laser at pulse lengths of 100 µs or 600 µs, at a wavelength of 940 nm and a current of 12 A. An overview of the results is given in Table 2. The two crystal water molecules in **12** cause a higher initiation threshold and therefore no reaction was observed. Only compound **13** could be initiated at the maximum pulse length of τ_{max} 600 µs (Figure 10) showing a discrete deflagration under emission of light. Therefore, compound **13** is a rare example of a perchlorate-free photosensitive energetic complex with manageable sensitivities.

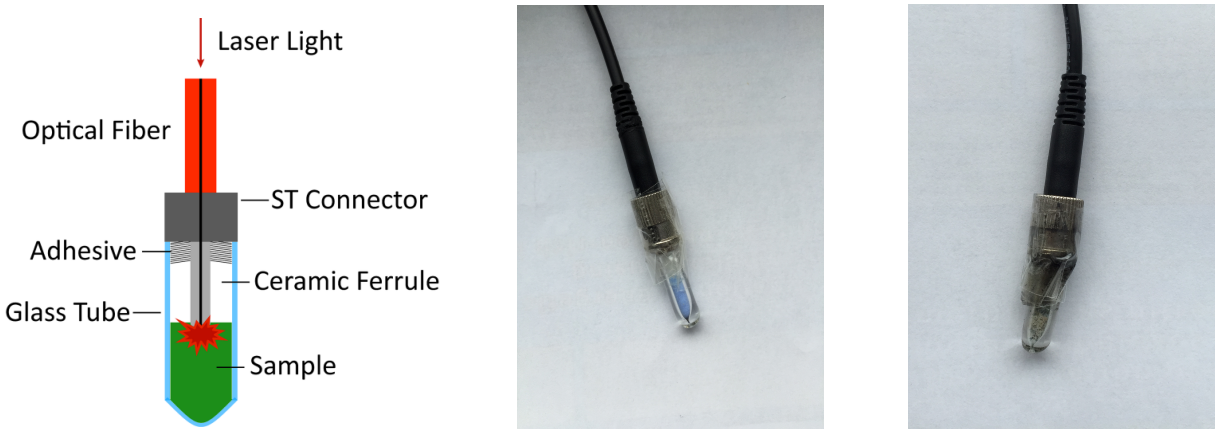


Figure 11. left: Schematic test setup for the laser ignition experiments.[3] middle and right: Picture of the sample before and after laser irradiation.

Table 2. Results of the laser ignition tests.

τ	12	13
100 µs	–	×
600 µs	×	+

(–: not tested, x: no ignition, +: ignition). Operating parameters: current I_{max} = 12 A; voltage U = ~ 5.5 V; theoretical output power P_{max} = 25 W; theoretical energy E_{max} = 15 mJ; experimental energy = 12 mJ (due to the limited capacity of the capacitor, the theoretical maximum energy of the 25 W laser diode could not be achieved); wavelength λ = 940 nm; pulse length τ_{max} = 600 µs.

8.3 Conclusions

The nitrogen-rich ligand di(1*H*-tetrazol-5-yl)methane (**1**, 5-DTM) was prepared in a reasonable yield and high purity in a one-step synthesis starting from commercial available sources. The compound was characterized by multi nuclear NMR spectroscopy (^{1}H, ^{13}C), elemental analysis, vibrational spectroscopy (IR), DTA and sensitivity measurements. In order to develop new photosensitive and environmentally benign primary explosives, various energetic transition metal complexes were synthesized and characterized. Energetic coordination compounds (ECC) consist of nitrogen-rich ligands, oxidizing anions (perchlorate, nitrate) and a transition metal. The synthetic route to these complexes is straightforward, cost-effective and fulfills environmental needs. For the first time, 14 novel coordination compounds based on 5-DTM as chelating neutral ligand were synthesized and extensively characterized by IR spectroscopy, elemental analysis, DTA and sensitivity measurements. In addition, X-ray crystal structures were determined for 13 complexes to get better insights into the interesting and challenging complex units. The 5-DTM chloride complexes **2**–**4** show different coordination spheres depending on the inserted transition metal (copper(II) favors chloride, while cobalt(II) and nickel(II) prefer aqua ligands). The preparation of the 5-DTM copper(II) nitrate and perchlorate complexes (nitrate: **11** and **12**; perchlorate: **14** and **15**) were strongly dependent on the concentration and volume of the solvent, and yielded two different coordination isomers in each case. In addition a polymeric copper(II) sulfate complex **9** was obtained showing a mixed coordination mode of 5-DTM, which is built up by three non-equivalent copper(II) centers and four types of ligands (water, sulfate, neutral and deprotonated 5-DTM molecules). The perchlorate complex **15** is an extremely sensitive (much more sensitive than lead and silver azide) primary explosives and showed heavy detonations during the hot plate and hot needle tests. The compound has an astonishing high thermal stability with a decomposition temperature of 233 °C (the water containing perchlorate complex exploded at a temperature as low as 85 °C). Dehydration of compound **12** to **13** had no effect on the sensitivities but instead had an effect on the explosive power. Compound **13** deflagrated with a more intense fulmination during the hot plate test than compound **12**. The copper(II) nitrate **13** (IS: 2 J, FS: 160 N, T_{dec}: 148 °C) could be successfully initiated by a laser beam with a wavelength of 940 nm at a pulse length of 600 μs. Derivatization (e.g. methylation) of the ligand might be of interest in future works in the field of energetic coordination compounds to increase the stability and decrease the sensitivity of the complexes.

8.4 Experimental Part

All chemicals and solvents were employed as received (Sigma-Aldrich, Fluka, Acros). ^{1}H and ^{13}C NMR spectra were recorded using a JEOL Eclipse 270, JEOL EX 400 or a JEOL Eclipse 400 instrument. The chemical shifts quoted in ppm in the text refer to typical standards such as tetramethylsilane (^{1}H, ^{13}C). To determine the dehydration, melting and decomposition temperatures of the described compounds an OZM Research DTA 552-Ex instrument (heating rate 5 °C min^{-1} in the range of 25–400 °C) was used. Infrared spectra were measured with pure samples on a Perkin-Elmer BXII FT-IR system with a Smith DuraSampler IR II diamond ATR unit or as KBr pellet on a Perkin Elmer Spectrum One FT-IR spectrometer. Determination of the carbon, hydrogen and nitrogen contents were carried out by combustion analysis using an Elementar Vario El (nitrogen values determined are often lower than the calculated ones due to their explosive behavior). Impact sensitivity tests were carried out according to STANAG 4489[34] modified instruction[35] using a BAM (Bundesanstalt für Materialforschung) drophammer.[36] The friction sensitivity tests were carried out according to STANAG 4487[37] modified instruction[38] using the BAM friction tester. The classification of the tested compounds results from the "UN Recommendations on the Transport of Dangerous Goods".[39] Additionally all compounds were tested upon the sensitivity toward electrical discharge using the Electric Spark Tester ESD 2010 EN.[40]

CAUTION! All investigated compounds are potentially explosive energetic materials, which show partly increased sensitivities toward various stimuli (e.g. elevated temperatures, impact, friction or electrostatic discharge). Therefore, proper security precautions (safety glass, face shield, earthed equipment and shoes, leather coat, Kevlar gloves, Kevlar sleeves and ear plugs) have to be applied while synthesizing and handling the described compounds.

Di(1*H*-tetrazol-5-yl)methane (1)

Di(1*H*-tetrazol-5-yl)methane was prepared according to a modified procedure outlined by Z. P. DEMKO and K. B. SHARPLESS[24]: a suspension of sodium azide (14.3 g, 0.22 mol), zinc bromide (22.5 g, 0.10 mol) and malononitrile (6.61 g, 0.10 mol) in water (150 mL) was refluxed for 17 h. After cooling down to room temperature, the suspension was dissolved in 2 M hydrochloric acid (200 mL). The resulting clear solution was extracted three times with ethyl acetate (500 mL each) and the combined organic phases were dried over magnesium sulfate.

The solution was concentrated leaving a colorless powder as product, which was finally dried under vacuum. Yield: 8.42 g (55.4 mmol, 55 %).

TGA (5 °C min^{-1}): weight loss starting above 100 °C; IR (ATR, cm^{-1}): $\tilde{\nu}$ = 2993 (m), 2942 (m), 2922 (m), 2882 (m), 2787 (m), 2723 (m), 2443 (w), 1727 (w), 1558 (s), 1532 (s), 1505 (w), 1431 (w), 1386 (s), 1365 (m), 1317 (m), 1267 (s), 1227 (s), 1102 (w), 1090 (w), 1067 (s), 1033 (s), 1013 (m), 998 (s), 929 (m), 912 (m), 873 (vs), 763 (vs), 742 (m), 725 (w), 700 (w); ^{1}H NMR (DMSO-d_6, 25 °C, ppm) δ: 4.74 (s, 2H, -CH_2); ^{13}C NMR (DMSO-d_6, 25 °C, ppm) δ: 152.7 (CN$_4$), 19.5 (-CH$_2$); EA ($C_3H_4N_8$ 152.12) calc.: C 23.69, H 2.65, N 73.66 %; found: C 24.28, H 2.78, N 72.69 %; BAM drophammer: > 40 J; friction tester: > 360 N; ESD: 0.30 J (at grain size < 100 µm).

[CuCl$_2$(5-DTM)$_2$] • 2 H$_2$O (2)

Di(1*H*-tetrazol-5-yl)methane (**1**, 76.0 mg, 0.50 mmol) was dissolved in diluted hydrochloric acid (15 %, 2 mL) at room temperature. Copper(II) chloride dihydrate (43.0 mg, 0.25 mmol) was dissolved in hydrochloric acid (15 %, 1 mL) and added to the reaction mixture, creating a dark blue solution. This solution was mechanically stirred for one minute and left to crystallize. Within one day, X-ray suitable single crystals were obtained in the form of blue blocks. The crystals were filtered off, washed with a small amount of ethanol and dried in air. Yield: 101 mg (0.21 mmol, 85 %).

DTA (5 °C min^{-1}): 127 °C (loss of crystal water), 139 °C (m.p.), 204 °C (dec.); IR (ATR, cm^{-1}): $\tilde{\nu}$= 3381 (m), 3358 (m), 2278 (m), 1763 (m), 1646 (m), 1575 (s), 1392 (m), 1274 (m), 1093 (s), 1076 (m), 1059 (s), 1022 (s), 997 (s), 926 (s), 896 (vs), 791 (m), 750 (s), 680 (s), 664 (s); EA ($C_6H_{12}Cl_2CuN_{16}O_2$, 473.72): calcd: C 15.18, H 2.55, N 47.21 %; found: C 15.45, H 2.80, N 47.02 %.; BAM drophammer: > 40 J; friction tester: > 360 N; ESD: 1.50 J (at grain size 100–500 µm).

[Co(H$_2$O)$_2$(5-DTM)$_2$]Cl$_2$ (3)

Cobalt(II) chloride hexahydrate (59.5 mg, 0.25 mmol) and 5-DTM (76.0 mg, 0.50 mmol) were dissolved in diluted hydrochloric acid (15 %, 3 mL). After stirring the reaction mixture for 1 minute at room temperature, ethanol (2 mL) was added and the bluish solution left to

crystallize. Clear gold prisms of **3**, which were suitable for X-ray, started to crystallize within 1 h. The crystals were filtered off, washed with ethanol and dried in air. Yield: 112 mg (0.24 mmol, 95 %).

DTA (5 °C min^{-1}): 178 °C (loss of water), 243 °C (dec.); IR (ATR, cm^{-1}): $\tilde{\nu}$= 3267 (m), 2978 (m), 2954 (m), 2923 (m), 2893 (m), 2853 (m), 1664 (w), 1615 (w), 1553 (s), 1540 (s), 1462 (w), 1455 (w), 1444 (w), 1414 (m), 1369 (w), 1344 (m), 1288 (w), 1252 (vs), 1114 (m), 1071 (vs), 1057 (m), 1025 (m), 1015 (m), 938 (m), 831 (s), 796 (m), 777 (s), 752 (s), 725 (s), 710 (s), 688 (s), 650 (s), 621 (m), 610 (m), 601 (m), 590 (m), 583 (m), 576 (m), 569 (m), 561 (m), 552 (m); EA ($C_6H_{12}Cl_2CoN_{16}O_2$, 470.11): calcd: C 15.33, H 2.57, N 47.67 %; found: C 15.55, H 2.66, N 45.94 %; BAM drophammer: > 40 J; friction tester: > 360 N; ESD: 1.00 J (at grain size 100–500 µm).

[Ni(H$_2$O)$_2$(5-DTM)$_2$]Cl$_2$ (4)

Oven-dried (130 °C, 2 h) compound **1** (228 mg, 1.50 mmol) was dissolved in diluted hydrochloric acid (15 %, 1 mL) at room temperature. Nickel(II) chloride hexahydrate (119 mg, 0.50 mmol) was dissolved in hydrochloric acid and added to the reaction mixture, creating a dark blue solution. This solution was mechanically stirred for 1 minute and left to crystallize. Within one day, X-ray suitable single crystals were obtained in the form of dark blue needles. The crystals were filtered off, washed with a small amount of ethanol and dried in air. Yield: 110 mg (0.23 mmol, 46 %).

TGA (5 °C min^{-1}): weight loss starting above 100 °C; IR (ATR, cm^{-1}): $\tilde{\nu}$= 3292 (m), 3222 (m), 2979 (m), 2920 (m), 2894 (m), 2812 (m), 2735 (w), 2685 (w), 2623 (w), 2357 (w), 2343 (w), 1623 (w), 1556 (s), 1542 (s), 1507 (w), 1464 (w), 1457 (w), 1414 (m), 1370 (m), 1344 (m), 1289 (w), 1252 (v), 1190 (w), 1116 (m), 1072 (s), 1060 (s), 1028 (m), 1017 (s), 937 (s), 831 (s), 795 (s), 768 (s), 752 (s), 727 (s), 710 (s), 686 (s), 669 (s), 650 (vs), 627 (m), 620 (m), 614 (m), 606 (s). 598 (m), 590 (s), 577 (s), 563 (s); EA ($C_6H_{12}Cl_2N_{16}NiO_2$, 469.87): calcd: C 15.34, H 2.57, N 47.70 %; found: C 15.98, H 3.09, N 47.25 %; BAM drophammer: > 40 J; friction tester: > 360 N; ESD: 1.00 J (at grain size 100–500 µm).

General procedure for the preparation of metal(II) (5-DTM) nitrate complexes (6–8):

A solution of 5-DTM (76.0 mg, 0.50 mmol) in diluted nitric acid (15 %, 2 mL) was added to a solution of the corresponding metal(II) nitrate (**6:** cobalt(II)nitrate hexahydrate (72.8 mg, 0.25 mmol); **7**: nickel(II)nitrate hexahydrate (72.7 mg, 0.25 mmol); **8**: zinc(II) nitrate hexahydrate (74.4 mg, 0.25 mmol)) in diluted nitric acid (15 %, 3 mL) and stirred mechanically for 1 min at room temperature. The colored reaction mixtures were left to crystallize until solids appeared. The products were filtered off, washed with a small amount of ethanol and dried in air.

$[Co(H_2O)_2(5\text{-DTM})_2](NO_3)_2$ (6)

Compound **6** was obtained within 1 h in the form of orange needles suitable for X-ray determination. Yield: 94.1 mg (0.18 mmol, 72 %).

DTA (5 °C min^{-1}): 223 °C (dec.); IR (ATR, cm^{-1}): $\tilde{\nu}$ = 3282 (w), 2360 (m), 1707 (s), 1657 (m), 1650 (m), 1597 (m), 1549 (m), 1504 (m), 1392 (s), 1291 (s), 1218 (s), 1158 (s), 1099 (s), 1052 (s), 921 (vs), 759 (s), 668 (s), 640 (vs), 620 (vs), 614 (vs), 607 (vs), 594 (vs), 583 (vs), 572 (vs), 560 (vs), 552 (vs); EA ($C_6H_{12}CoN_{18}O_8$, 523.21): calcd: C 13.77, H 2.31, N 48.19 %; found: C 13.70, H 2.14, N 45.05 %; BAM drophammer: 4 J; friction tester: 240 N; ESD: 0.20 J (at grain size < 100 µm).

$[Ni(H_2O)_2(5\text{-DTM})_2](NO_3)_2$ (7)

Complex **7** was obtained within 4 weeks in the form of amorphous purple plates. Yield: 38.0 mg (0.07 mmol, 29 %).

DTA (5 °C min^{-1}): 142 °C (dec.); IR (ATR, cm^{-1}): $\tilde{\nu}$ = 3161 (w), 2996 (m), 2906 (m), 2886 (m), 2728 (m), 2626 (m), 2500 (m), 2350 (w), 2168 (w), 1658 (m), 1650 (m), 1572 (m), 1502 (w), 1396 (s), 1290 (vs), 1111 (s), 1062 (vs), 1017 (s), 932 (s), 890 (s), 819 (s), 759 (vs), 722 (s), 713 (s), 685 (s), 662 (s); EA ($C_6H_{12}NiN_{18}O_8$, 522.97): calcd: C 13.78, H 2.31, N 48.21 %; found: C 14.41, H 2.20, N 47.82 %; BAM drophammer: 1 J; friction tester: > 360 N; ESD: 1.50 J (at grain size 100–500 µm).

$[Zn(H_2O)_2(5\text{-DTM})_2](NO_3)_2$ (8)

Coordination compound **8** was obtained within 2 weeks in the form of colorless plates suitable for X-ray determination. Yield: 91.0 mg (0.17 mmol, 69 %).

DTA (5 °C min^{-1}): 158 °C (dec.); IR (ATR, cm^{-1}): $\tilde{\nu}$= 3436 (w), 3186 (w), 3152 (w), 2981 (w), 2918 (w), 2747 (w), 2711 (w), 2614 (w), 2566 (w), 2465 (w), 2424 (w), 2196 (w), 2148 (w), 1856 (w), 1652 (w), 1577 (m), 1559 (m), 1495 (s), 1468 (s), 1453 (m), 1444 (m), 1402 (m), 1378 (s), 1333 (s), 1297 (s), 1270 (s), 1248 (m), 1233 (m), 1214 (m), 1124 (w), 1108 (w), 1082 (s), 1066 (s), 1042 (m), 1029 (s), 1022 (s), 995 (s), 932 (s), 880 (m), 812 (s), 783 (m), 765 (vs), 713 (s), 704 (s), 654 (s), 626 (s), 621 (s), 604 (s), 598 (s), 574 (s), 566 (s), 554 (s); ^{1}H NMR (DMSO-*d*$_6$, 25 °C, ppm) δ: 4.78 (s, 2H, -C*H*$_2$); ^{13}C NMR (DMSO-*d*$_6$, 25 °C, ppm) δ: 152.1 (*C*N$_4$), 18.9 (-*C*H$_2$); EA ($C_6H_{12}N_{18}O_8Zn$, 529.66): calcd: C 13.61, H 2.28, N 47.60 %; found: C 13.93, H 2.41, N 47.30 %; BAM drophammer: 6 J; friction tester: 252 N; ESD: 1.50 J (at grain size 100–500 µm).

$\{[Cu_3(SO_4)_2(5\text{-DTM}_{-H})_2(H_2O)_4(5\text{-DTM})_2] \bullet 2\ H_2O\}_\infty$ (9)

Solutions of copper(II) sulfate pentahydrate (62.4 mg, 0.25 mmol) and 5-DTM (76.0 mg, 0.50 mmol) in sulfuric acid (15 %, 8 mL) were mixed and stirred for one minute at room temperature. A copper(II) sulfate complex with a mixed coordination mode of 5-DTM was formed. The compound started to crystallize within 1 h as blue microcrystalline plates suitable for X-ray determination. The crystals were filtered off, washed with ethanol and dried in air. Yield: 80 mg (0.07 mmol, 87 %).

DTA (5 °C min^{-1}): 139 °C (loss of water), 224 °C (dec.); IR (ATR, cm^{-1}): $\tilde{\nu}$= 3605 (v), 3452 (w), 3152 (w), 3026 (w), 2983 (w), 2919 (w), 2871 (w), 2713 (w), 2342 (w), 2170 (w), 2103 (w), 2057 (w), 1893 (m), 1608 (m), 1575 (m), 1505 (m), 1449 (w), 1442 (w), 1408 (w), 1392 (m), 1293 (m), 1287 (m), 1269 (w), 1194 (w), 1169 (s), 1128 (m), 1117 (s), 1105 (s), 1082 (s), 1070 (s), 1047 (s), 1018 (s), 979 (s), 962 (s), 938 (s), 923 (s), 790 (s), 751 (s), 743 (vs), 706 (s), 659 (s), 630 (vs), 607 (s), 591 (s), 570 (s); EA ($C_{12}H_{26}Cu_3N_{32}O_{14}S_2$, 1097.39): calcd: C 13.14, H 2.39, N 40.85 %; found: C 13.18, H 2.47, N 40.03 %; BAM drophammer: > 40 J; friction tester: > 360 N; ESD: 0.80 J (at grain size < 100 µm).

$[Cu(H_2O)_2(5\text{-DTM})_2](NO_3)_2$ (11)

Copper(II) nitrate trihydrate (60.0 mg, 0.25 mmol) and 5-DTM (76.0 mg, 0.50 mmol) were dissolved in nitric acid (30 %, 3 mL) and mechanically stirred for 1 minute at room temperature. From this dark blue solution, compound **11** could be isolated in the form of blue blocks suitable for X-ray determination after one week. The crystals were filtered off and dried in air. Yield: 101 mg (0.19 mmol, 77 %).

DTA (5 °C min^{-1}): 97 °C (loss of water), 144 °C (dec.); IR (ATR, cm^{-1}): $\tilde{\nu}$= 3538 (w), 3459 (w), 2985 (w), 2938 (w), 1652 (w), 1630 (w), 1575 (m), 1487 (m), 1457 (m), 1400 (s), 1313 (vs), 1291 (s), 1262 (s), 1120 (m), 1071 (s), 1026 (s), 1000 (s), 935 (vs), 914 (s), 908 (s), 811 (m), 762 (vs), 714 (s), 698 (m), 655 (m), 608 (m), 601 (s), 590 (s), 582 (s), 576 (s), 554 (s); EA ($C_6H_{12}Cu\ N_{18}O_8$, 527.83): calcd: C 13.65, H 2.29, N 47.77 %; found: C 13.11, H 2.24, N 44.74 %; BAM drophammer: 6 J; friction tester: > 360 N; ESD: 0.26 J (at grain size 100–500 µm).

$[Cu(NO_3)_2(5\text{-DTM})_2] \cdot 2\ H_2O$ (12)

5-DTM (76.0 mg, 0.50 mmol) and copper(II) nitrate trihydrate (60.0 mg, 0.25 mmol) were dissolved in nitric acid (15 %, 3 mL) and mechanically stirred for 1 minute at room temperature. From this clear dark blue solution, complex **12** could be isolated in the form of blue rods suitable for X-ray determination after 10 days. The crystals were filtered off, washed with a small amount of ethanol and dried in air. Yield: 103 mg (0.20 mmol, 78 %).

DTA (5 °C min^{-1}): 127 °C (melting followed by decomposition between 141 °C and 147 °C); IR (ATR, cm^{-1}): $\tilde{\nu}$= 3517 (w), 2998 (w), 2911 (m), 2888 (w), 2706 (m), 2614 (m), 2469 (m), 2166 (w), 1922 (w), 1609 (w), 1567 (m), 1543 (m), 1467 (m), 1434 (s), 1392 (s), 1304 (vs), 1296 (vs), 1254 (s), 1192 (m), 1119 (m), 1066 (s), 1049 (s), 1006 (s), 932 (s), 817 (s), 791 (m), 755 (s), 726 (m), 715 (m), 705 (m), 699 (m), 680 (m), 673 (w), 656 (m); EA ($C_6H_{12}CuN_{18}O_8$, 527.83): calcd: C 13.65, H 2.29, N 47.77 %; found: C 13.90, H 2.31, N 47.79%; BAM drophammer: 2 J; friction tester: 160 N; ESD: 1.50 J (at grain size 100–500 µm).

$[Cu(NO_3)_2(5\text{-DTM})_2]$ (13)

Drying of complex **12** (100 mg, 0.19 mmol) at 60 °C in the oven for 48 h yielded 93.5 mg (0.19 mmol, 100 %) of the water-free coordination compound **13**.

DTA (5 °C min^{-1}): 129 °C (m. p.), 148 °C (dec.); IR (ATR, cm^{-1}): $\tilde{\nu}$ = 3521 (v), 3178 (v), 2998 (w), 2909 (w), 2716 (w), 2623 (w), 1568 (m), 1467 (m), 1438 (m), 1386 (m), 1309 (v), 1266 (s), 1118 (m), 1109 (m), 1069 (s), 1049 (m), 1018 (m), 1007 (s), 933 (m), 818 (m), 810 (m), 792 (m), 766 (m), 755 (m), 739 (m), 728 (m), 716 (m), 706 (m), 656 (w), 648 (w), 636 (w), 630 (w), 612 (w), 600 (w), 588 (w), 582 (w), 575 (w), 568 (w); EA ($C_6H_8CuN_{18}O_6$, 491.80): calcd: C 14.65, H 1.64, N 51.27 %; found: C 14.66, H 1.97, N 49.65 %; BAM drophammer: 2 J; friction tester: 160 N; ESD: 0.25 J (at grain size < 100 µm).

$[Cu(H_2O)_2(5\text{-DTM})_2](ClO_4)_2$ (14)

Copper(II) perchlorate hexahydrate (93.0 mg, 0.25 mmol) in perchloric acid (15 %, 1 mL) was added to a solution of 1 (76.0 mg, 0.50 mmol) in diluted perchloric acid (15 %, 2 mL). The resulting blue solution was stirred for 1 minute at room temperature and left to crystallize. Within two weeks, dark blue single crystals suitable for X-ray were obtained. The crystals were filtered off, washed with a small amount of ethanol and dried in air. Yield: 131 mg (0.22 mmol. 87 %).

DTA (5 °C min^{-1}): 85 °C (explosion); IR (ATR, cm^{-1}): $\tilde{\nu}$ = 3619 (w), 3437 (w), 3177 (m), 3098 (m), 3026 (m), 2951 (m), 2833 (w), 2758 (w), 2615 (w), 1732 (w), 1628 (m), 1565 (m), 1547 (m), 1466 (w), 1406 (m), 1373 (w), 1350 (w), 1291 (w), 1269 (w), 1255 (w), 1187 (w), 1127 (s), 1094 (s), 1081 (s), 1069 (vs), 1054 (s), 1028 (vs), 1009 (vs), 934 (s), 802 (m), 749 (s), 721 (s), 709 (m), 690 (s), 656 (m); EA ($C_6H_{12}Cl_2CuN_{16}O_8$, 602.71): calcd: C 11.96, H 2.01, N 37.18 %; found: C 12.11, H 2.07, N 36.76 %; BAM drophammer: < 1 J; friction tester: < 5 N; ESD: > 100 mJ (at grain size 500–1000 µm).

$[Cu(ClO_4)_2(5\text{-DTM})_2]$ (15)

A solution of $Cu(ClO_4)_2 \cdot 6\,H_2O$ (186 mg, 0.50 mmol in 1 mL 15 % perchloric acid) was added to an agitated solution of the nitrogen-rich ligand **1** (152 mg, 1.00 mmol) in perchloric acid

(15 %, 2 mL). After stirring the reaction mixture for 1 minute, the solution was left to crystallize at room temperature. Within two months, the product started to crystallize in the form of blue blocks but only a few crystals were filtered off and dried in air. Due to the extreme sensitivity of the compound, no yield was determined and no elemental analysis and ESD measurements were carried out.

DTA (5 °C min^{-1}): 233 °C (dec.); IR (KBr, cm^{-1}): $\tilde{\nu}$ = 3632 (w), 3424 (vs), 3245 (m), 3103 (m), 3043 (m), 2989 (w), 2928 (m), 2853 (w), 2785 (w), 2635 (w), 1637 (m), 1628 (m), 1575 (m), 1397 (m), 1385 (m), 1300 (w), 1281 (w), 1262 (m), 1160 (m), 1122 (s), 1099 (s), 1080 (s); BAM drophammer: < 1 J; friction tester: < 5 N; ESD: > 100 mJ (at grain size 500–1000 µm).

Supporting information available in the appendix in **Chapter 19.5** and under:

https://pubs.acs.org/doi/suppl/10.1021/acs.inorgchem.7b00432/suppl_file/ic7b00432_si_001.pdf

8.5 References

[1] Klapötke, T. M. Chemistry of High-Energy Materials. 2nd ed., Walter de Gruyter: Berlin, Boston, 2012.

[2] Cooper, P. W. Explosives Engineering. Wiley-VCH: New York, Chichester, Weinheim, Brisbane, Singapore, Toronto, 1996.

[3] Joas, M. *Dissertation*, Ludwig-Maximilians Universität München, 2014.

[4] a) Zhang, J.; Dharavath, S.; Mitchell, L. A.; Parrish, D. A.; Shreeve, J. M. Bridged bisnitramide-substituted furazan-based energetic materials. *J. Am. Chem. Soc.,* **2016**, *138*, 7500−7503; b) Yin, P.; Parrish, D. A.; Shreeve, J. M. Energetic fused triazoles – a promising C-N fused heterocyclic cation. *J. Am. Chem. Soc.,* **2015**, *137*, 4778–4786; c) Gao, H.; Shreeve, J. M. Azole-based energetic salts. *Chem. Rev.,* **2011**, 111, 7377–7436.

[5] Haiges, R; Belanger-Chabot, G.; Kaplan, S. M.; Christe, K. O. Synthesis and structural characterization of 3,5-dinitro-1,2,4-triazolates. *Dalton Trans.,* **2015**, *44*, 2978–2988.

[6] McDonald, K. A.; Seth, S.; Matzger, A. J. Coordination Polymers with High Energy Density: An Emerging Class of Explosives. *Cryst. Growth Des,.* **2015,** *15*, 5963–5972.

[7] a) Wang, S.-H.; Zheng, F.-K.; Wu, M.-F.; Liu, Z-F.; Chen, J.; Guo, G.-C.; Wu, A-Q. Hydrothermal syntheses, crystal structures and physical properties of a new family of energetic coordination polymers with nitrogen-rich ligand *N*-[2-(1*H*-tetrazol-5-yl)ethyl] glycine, *CrysEngComm*, **2013**, *15*, 2616–2623, b) Wang, S.-H.; Zheng, F.-K.; Zhang, M.-J., Liu, Z.-F.; Chen, J.; Xiao, Y.; Wu, A-Qing.; Guo, G.-C.; Huang, J.-S.; Homochiral Zinc(II) Coordination Compounds Based on In-SituGenerated Chiral Amino Acid−Tetrazole Ligands: Circular Dichroism, Excitation Light-Induced Tunable Photoluminescence, and Energetic Performance, *Inorg. Chem.,* **2013**, *52*, 10096−10104.

[8] Brish, A. A.; Galeev, I. A.; Zaitsev, B. N.; Sbitnev, E. A.; Tatarintsev, L. V. Initiation of detonation in condensed explosives by laser-emission. *Fiz. Goreniya Vzryva,* **1966**, 132–133.

[9] Brish, A. A.; Galeev, I. A.; Zaitsev, B. N.; Sbitnev, E. A.; Tatarintsev, L. V. Triggering mechanism of condensed explosives by laser radiation. *Fiz. Goreniya Vzryva,* **1969**, *5*, 475–480.

[10] Yang, L. C.; Menichelli, V. J. Detonation of insensitive high explosives by a Q-switched ruby laser. *Appl. Phys. Lett.,* **1971**, *19*, 473–475.

[11] Hafenrichter, E. S.; Marshall Jr., B.; Fleming, K. J. Fast laser diode ignition of CP and BNCP. *Proceedings of the International Pyrotechnics Seminar,* **2002**, *29th*, 787–793.

[12] Kunz, S. C.; Salas, F. J. Diode laser ignition of high explosives and pyrotechnics. *Proceedings of the International Pyrotechnics Seminar* **1988**, *13th*, 505–523.

[13] Joas, M.; Klapötke, T. M.; Stierstorfer, J.; Szimhardt, N. Synthesis and Characterization of Various Photosensitive Copper(II) Complexes with 5-(1-Methylhydrazinyl)-1*H*-tetrazole as Ligand and Perchlorate, Nitrate, Dinitramide and Chloride as Anions. *Chem. Eur. J.,* **2013**, *19*, 9995–10003.

[14] Myers, T. W.; Bjoorgard, J. A.; Brown, K. E.; Chavez, D. E.; Hanson, S. K.; Scharff, R. J.; Tretiak, S.; Veauthier, J. M. Energetic Chromophores: Low-Energy Laser Initiation in Explosive Fe(II) Tetrazine Complexes. *J. Am. Chem. Soc.,* **2016***, 138*, 4685–4692.

[15] Merson, J. A.; Salas, F. J.; Harlan, J. G. The development of laser ignited deflagration-to-detonation transition (DDT) detonators and pyrotechnic actuators. *Proceedings of the International Pyrotechnics Seminar,* **1994**, *19th*, 191–206.

[16] Zhilin, A. Y.; Ilyushin, M. A.; Tselinskii, I. V.; Kozlov, A. S.; Lisker, I. S. High-energy-capacity cobalt(III) tetrazolates. *Russ. J. Appl. Chem.,* **2003**, *76*, 572–576.

[17] Evers, J.; Gospodinov, I.; Joas, M.; Klapötke, T. M.; Stierstorfer J. Cocrystallization of Photosensitive Energetic Copper(II) Perchlorate Complexes with the Nitrogen-rich Ligand 1,2-Di(1*H*-tetrazol-5-yl)ethane. *Inorg. Chem.,* **2014**, *53*, 11749–11756.

[18] Zhilin, A. Y.; Ilyushin, M. A.; Tselinskii, I. V.; Brykov, A. S. Synthesis of a high-energy-capacity compound, cis-tetraamminebis(5-nitro-2*H*-tetrazolato-N2)cobalt(III)perchlorate. *Russ. J. Appl. Chem.,* **2001**, *74*, 99–102.

[19] Smirnov, A. V.; Ilyushin, M. A.; Tselinskii, I. V. Synthesis of Cobalt(III) Ammine Complexes as Explosives for Safe Priming Charges. *Russ. J. Appl. Chem.,* **2004**, *77*, 794–796.

[20] Myers, T. W.; Brown, K. E.; Chavez, D. E.; Scharff, R. J.; Veauthier, J. M. Correlating the Structural, Electronic, and Explosive Sensitivity Properties of CuII Tetrazine Complexes. *Eur. J. Inorg. Chem.,* **2016***,* 3178–3183.

[21] Bai, M.; Zhang, J.-B.; Cao, L.-H.; Li, Y.-P.; Wang, D.-Z. Zinc(II) and cadmium(II) metal complexes with bis(tetrazole) ligands: synthesis and crystal structures. *J. Chin. Chem. Soc.,* **2011**, *58*, 69–74.

[22] Feng, Y.; Bi, Y.; Zhao, W.; Zhang, T. Anionic metal-organic frameworks lead the way to eco-friendly high-energy-density materials. *J. Mater. Chem. A.,* **2016,** *4*, 7596–7600.

[23] Zubarev, V. Y.; Trifonov, R. E.; Poborchii, V. V.; Ostrovskii, V. A. Polynuclear branched tetrazole systems. 3. Acidity of α,ω-ditetrazol-5-ylalkanes. *Chem. Heterocycl. Compd.,* **2006**, *42*, 469–474.

[24] Demko, Z. P.; Sharpless, K. B. Preparation of 5-Substituted 1H-Tetrazoles from Nitriles in Water. *J. Org. Chem.,* **2001**, *66*, 7945–7950.

[25] Urbanski, T. Chemistry and Technology of Explosives, Pergamon Press-PWN: Oxford-Warsaw, 1964.

[26] Urbanski, T. On the mechanism of nitration with dilute nitric acid. *Bull. Acad. Pol. Sci., Ser. Sci. Chim.,* **1980**, *28*, 609–611.

[27] Veibel, S. Nitration process. I. Nitrosation of phenol. *Ber. Dtsch. Chem. Ges.,* **1930**, *63B*, 1577–1582.

[28] Chand, D.; Parrish, D. A.; Shreeve J. M. Di(1*H*-tetrazol-5-yl)methanone oxime and 5,5-(hydrazonomethylene)bis(1*H*-tetrazole) and their salts: a family of highly useful new tetrazoles and energetic materials. *J. Mater. Chem. A,* **2013**, *1*, 15383–15389.

[29] Quan, N.; Shi, X.-X.; Nie, L.-D.; Dong, J.; Zhu, R.-H. A green chemistry method for the regeneration of carbonyl compounds from oximes by using cupric chloride dihydrate as recoverable promoter for hydrolysis. *Synlett,* **2011**, 1028–1032.

[30] Crystallographic data for the structures have been deposited with the Cambridge Crystallographic Data Centre. Copies of the data can be obtained free of charge on application to The Director, CCDC, 12 Union Road, Cambridge CB2 1EZ, UK (Fax: int.code_(1223)336-033; e-mail for inquiry: fileserv@ccdc.cam.ac.uk; e-mail for deposition: (deposit@ccdc.cam.ac.uk).

[31] Diop, C. A. K.; Mahon, M.F; Molloy, K.C.; Ooi, L.; Raithby, P.R.; Venter, M. M.; Teat, S. J. Supramolecular lattices built from di- and tri-tetrazoles: the structures of 1,3,5-tritetrazol-5-ylbenzene bis-dioxane monohydrate and ditetrazol-5-ylmethane. *CrystEngComm,* **2002**, *4*, 462–466.

[32] Burns, P. C.; Hawthorne, F. C. Tolbachite, copper chloride, the first example of copper ion (2+) octahedrally coordinated by chloride ion (1+). *Am. Mineral.,* **1993**, *78*, 187–189.

[33] Lavrenyuk, H.; Mykhalichko, O.; Zarychta, B.; Olijnyk, V.; Mykhalichko, B. A new copper(II) chelate complex with tridentate ligand: Synthesis, crystal and molecular electronic structure of aqua-(diethylenetriamine-N, N′, N″)-copper(II) sulfate monohydrate and its fire retardant properties. *J. Mol. Struct.,* **2015**, *1095*, 34–41.

[34] NATO standardization agreement (STANAG) on explosives, impact sensitivity tests, no. 4489, 1st ed., Sept. 17, 1999.

[35] WIWEB-Standardarbeitsanweisung 4-5.1.02, Ermittlung der Explosionsgefährlichkeit, hier der Schlagempfindlichkeit mit dem Fallhammer, Nov. 8, 2002.

[36] http://www.bam.de.

[37] NATO standardization agreement (STANAG) on explosive, friction sensitivity tests, no. 4487, 1st ed., Aug. 22, 2002.

[38] WIWEB-Standardarbeitsanweisung 4-5.1.03, Ermittlung der Explosionsgefährlichkeit oder der Reibeempfindlichkeit mit dem Reibeapparat, Nov. 8, 2002.

[39] Impact: insensitive > 40 J, less sensitive ≥ 35 J, sensitive ≥ 4 J, very sensitive ≤ 3 J; Friction: insensitive > 360 N, less sensitive = 360 N, sensitive < 360 N and > 80 N, very sensitive ≤ 80 N, extremely sensitive ≤ 10 N. According to the UN Recommendations on the Transport of Dangerous Goods, (+) indicates not safe for transport.

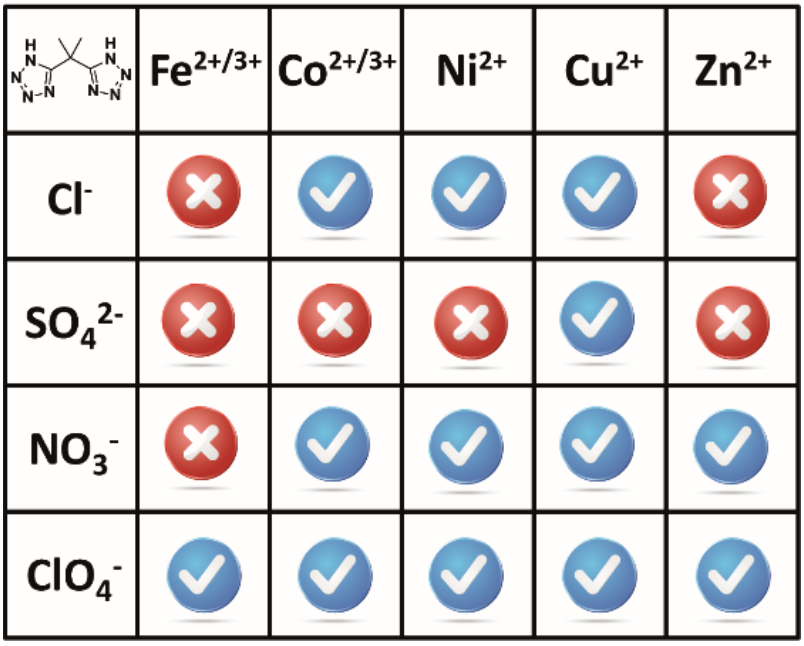
[40] http://www.ozm.cz.

9 2,2-Bis(5-tetrazolyl)propane as Ligand in Energetic 3d Transition Metal Complexes

Norbert Szimhardt, Michael S. Gruhne, Marcus Lommel, Andreas Hess, Maximilian H. H. Wurzenberger, Thomas M. Klapötke and Jörg Stierstorfer

published in *Zeitschrift für Anorganische und Allgemeine Chemie,* ***2018***.

DOI: 10.1002/zaac.201800288



The successful application of 2,2-bis(5-tetrazolyl)propane as a nitrogen-rich ligand in combination with five different metal cations and four different types of anions leads to the formation of 15 new energetic transition metal complexes. A variation of the building blocks, resulted in the formation of compounds possessing different characteristics.

Abstract

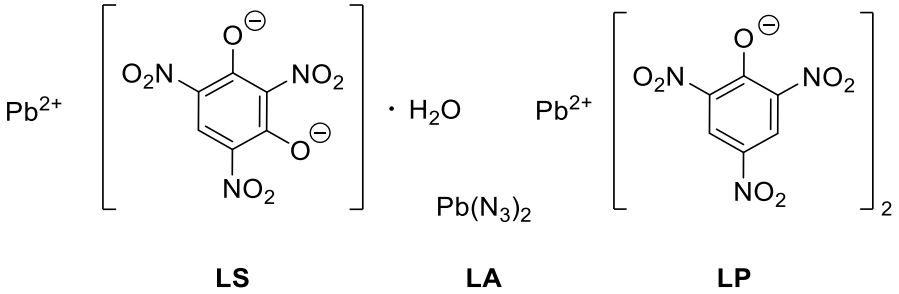
This contribution covers the preparation and characterization of 2,2-bis(5-tetrazolyl)propane (**1**, 5-DTP). The bridged bitetrazole is used as a neutral nitrogen-rich ligand in 3d transition metal(II) based complexes for the first time and can be synthesized via [2+3] cycloaddition from sodium azide and dimethylmalononitrile. The combination with different anions (e.g., perchlorate, nitrate, sulfate, and chloride) yields materials with widely varying physicochemical properties. Obtained coordination compounds were characterized using low-temperature single crystal X-ray diffraction (except **14**), IR spectroscopy, elemental analysis, and DTA (except **16**). The sensitivities toward external stimuli (impact and friction) were determined according to the Bundesamt für Materialforschung und -prüfung (BAM) standard methods together with its sensitivities against electrostatic discharge (except **16**). Complexes **10** and **14** were characterized in laser ignition experiments. For determination of the compounds' deflagration to detonation transition (DDT) capability, hot plate and hot needle tests were performed for the zinc(II) and copper(II) perchlorate complexes.

9.1 Introduction

In the context of high toxicity and increasing environmental hazards, the commonly used primary explosives lead styphnate (**LS**) and lead azide (**LA**) (Chart 1) have been added to the candidate list of authorization (substances of very high concern, Annex XIV) during the REACH (Registration, Evaluation, Authorization and Restriction of Chemicals) regulations in 2011.[1] Consequently, research into lead-free replacements, with lower impact on our environment, is inevitable.

Investigations into coordination compounds, comprising endothermic nitrogen-rich ligands such as tetrazoles and triazoles, a late 3d-transition metal and a coordinating or non-coordinating anion, demonstrated promising properties suitable for a wide range of applications, more particularly as metal-organic frameworks (MOFs),[2] spin crossover systems,[3] and energetic materials.[4] Polynuclear branched tetrazole systems can be considered as analogs to multibasic carboxylic acids concerning the complex-forming activity with metal ions. Investigations into the coordination ability of late 3d transition metals resulted in a preference for the heterocyclic derivatives.[5] Specifically, carboxyl groups are substituted by

tetrazol-5-yl fragments,[6] showing similarities in acidities, abilities to form intermolecular hydrogen bonds, and electron-withdrawing effects.[7]

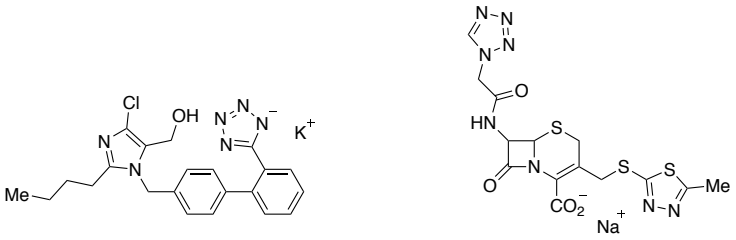


LS **LA** **LP**

Chart 1. Commonly used primary explosives: lead(II) styphnate (**LS**), lead(II) azide (**LA**), and lead(II) picrate (**LP**).

On this basis, the biological activity of tetrazoles was newly interpreted. N-H-unsubstituted and 1,5-disubstituted tetrazole rings are metabolically stable and can serve as bioisostere for amide and carboxy groups in modified amino acids. An increasing use as biologically active oligo- and polypeptides can be found.[8,9] The already mentioned ability to form hydrogen bonds is comparable with those of purine and pyrimidine bases.[10] Involvement of two nitrogen atoms of the heterocycle in intermolecular hydrogen bonding opens up the possibility of multicenter intermolecular interactions, especially with hydrogen atoms of the active site of enzymes.[7]

Therefore, tetrazoles have a strong position in the pharmaceutical market as drugs. With medicinal applications ranging from hypotensive action,[11] antimicrobial, anti-inflammatory,[12] antifungal[13] and antiviral activities.[14,15] Selected pharmaceuticals are exemplarily shown in Chart 2.



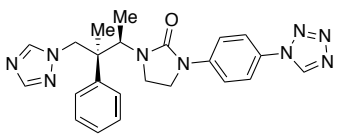


Chart 2. Tetrazole-based pharmaceutical products.

Apart from this, tetrazole derivatives offer tremendous potential as endothermic ligands in environmentally benign energetic coordination compounds (ECC), to some extent ignitable by laser irradiation.[16–17] The first published laser initiation experiments date back to the late sixties by analyzing samples of LA, RDX, Tetryl, and PETN.[18–20] Investigations were performed by utilizing two laser-type systems, more particularly a ruby laser ($\lambda = 694$ nm)[21] and a neodymium laser ($\lambda = 1060$ nm) operating in the Q-switch mode.[20] Owing to the relatively large size of the used solid-state lasers, practical applications were limited. Due to the commercial availability of laser diodes, new options regarding initiation and ignition of energetic materials arose.[21] With common ignition methods (flame, heat, mechanical stimuli, or shock)[22], existing disadvantages like unintended initiation can be excluded by isolation of the energetic material to electric impulses. Nevertheless, shorter function times and the use of less sensitive ignition charges (impact sensitivity ≥ 3 J, friction sensitivity ≥ 80 N, $T_{dec} \geq 180$ °C) increase the safety and handling of these compounds significantly. Recent investigations stated the high sensitivity of energetic coordination compounds toward laser irradiation, which predicts excellent suitability for laser ignitable initiation systems.[16,17] In consideration of initiation abilities, energetic transition metal complexes investigations were started with pentaamine(5-cyano-2*H*-tetrazolate)cobalt(III) perchlorate (CP, Chart 3) and its subsequent replacement tetraamine-cis-bis(5-nitro-2*H*-tetrazolato-*N*2)-cobalt(III) perchlorate (BNCP, Chart 3) applying a GaAlAs diode laser.[23,24] Despite positive initiation by laser ignition, both compounds still suffer from increased sensitivities, restricting their applicability. Since then, several coordination compounds, comprising various ligands and metal centers, have been synthesized and investigated regarding applications in laser ignitable initiation systems.[25–29]

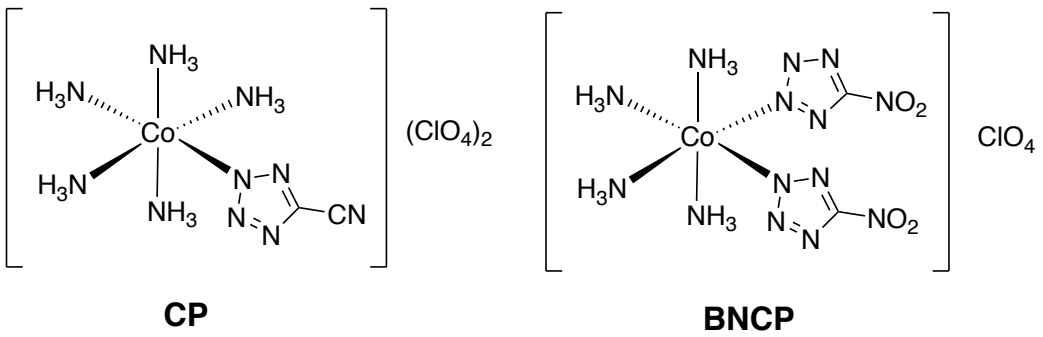


Chart 3. Molecular structures of CP and BNCP.

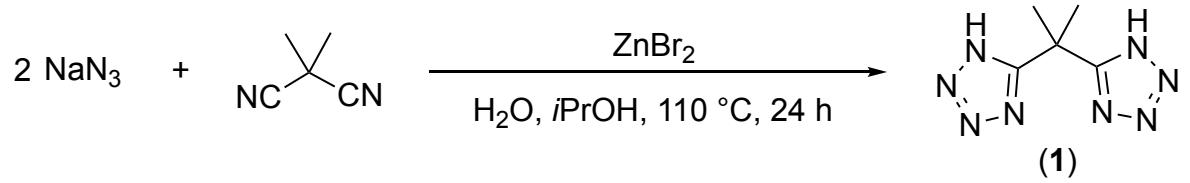
An extensive series of late 3d transition metal(II) based energetic coordination compounds using di(1*H*-tetrazol-5-yl)ethane, and its methylene bridged analog di(1*H*-tetrazol-5-

yl)methane as nitrogen-rich ligands were presented by our research group. Due to the increased sensitivities, derivatization (e.g., alkylation) was of interest in order to increase the stability and decrease the sensitivity of the compounds.[26,30] In this contribution, a large series of energetic complexes consisting of 2,2-bis(5-tetrazolyl)propane (5-DTP), which has been used for the first time in literature, were examined and their physicochemical properties explored. The synthesized complexes consist of a late 3d transition metal(II) as center, 5-DTP as ligand and coordinating or non-coordinating anions (nitrate, perchlorate, chloride or sulfate).

9.2 Results and Discussion

9.2.1 Synthesis

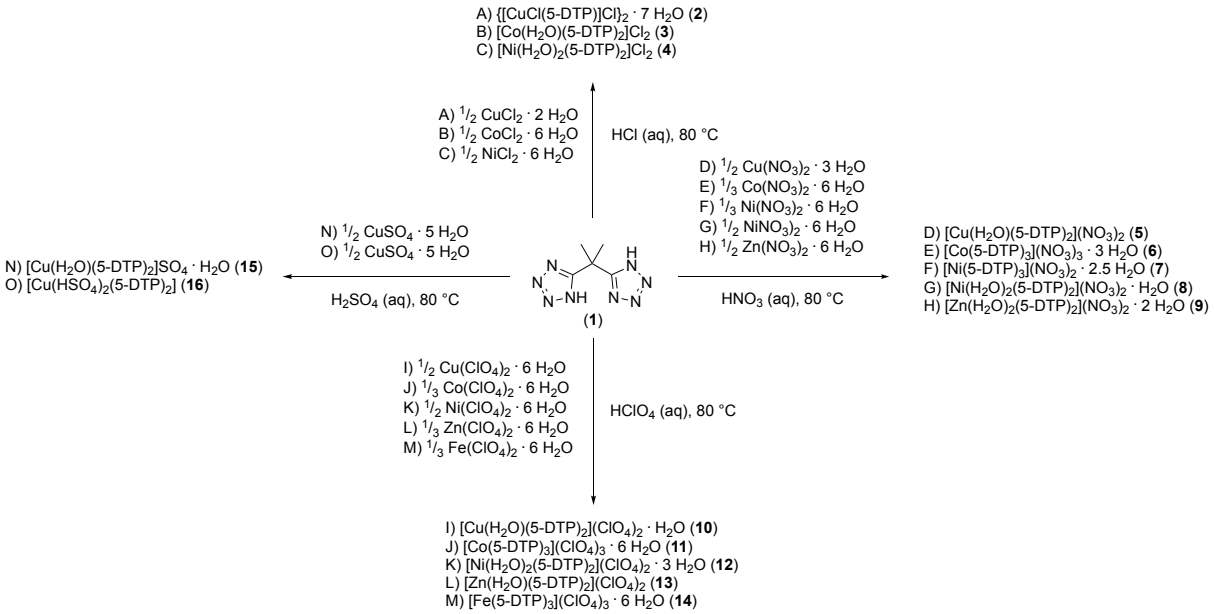
The nitrogen-rich ligand 2,2-bis(5-tetrazolyl)propane (**1**, 5-DTP) could be obtained in a yield of 55 % by [2+3] cycloaddition reaction using dimethylmalononitrile and sodium azide as reactants (Scheme 1). According to a literature procedure,[31] the starting materials and zinc(II) bromide as catalyst were partially dissolved in water, while propan-2-ol was added to increase the solubility. The reaction mixture was refluxed at a constant reaction temperature of 110 °C to prevent decomposition of dimethylmalononitrile at higher temperatures. After 24 hours, the suspension was acidified with 2 M hydrochloric acid to dissolve the precipitate. After extraction with ethyl acetate and recrystallization from water the product was obtained in the form of colorless crystals.



Scheme 1. Synthesis of 2,2-bis(5-tetrazolyl)propane (**1**).

In comparison to the very sensitive copper(II) perchlorate complexes based on 5-DTM as ligand, compounds based on 5-DTP are supposed to show a higher tolerance toward mechanical stimuli.[30] The transition metal(II) complexes **2**–**16** were prepared by combining solutions of stoichiometric amounts of 2,2-bis(5-tetrazolyl)propane (**1**) as ligand and metal(II) salts in the corresponding acid at 80 °C (Scheme 2). Due to the acidic character of the ligand, diluted acids were used as the solvent for the reaction in order to prevent precipitation of the corresponding

metal(II) tetrazolate salts. This strategy ensures the incorporation of the neutral nitrogen-rich ligand to build up cationic or neutral complexes with non-oxidizing anions like chlorides or sulfates and oxidizing ones like nitrates or perchlorates to produce more promising energetic materials as possible alternatives for toxic heavy metal based primary explosives. Metal centers of the complexes **6**, **11**, and **14** were oxidized through perchloric acid, resulting in the oxidation state +III of cobalt and iron.



Scheme 2. Synthesis of 5-DTP complexes **2**–**16** with different metal(II) or metal(III) centers and chloride, nitrate, perchlorate and sulfate as anions.

The reaction mixtures were left for a few days or weeks until crystalline material could be obtained. All compounds could be achieved in the form of X-ray suitable crystals directly from the mother liquor. Unfortunately, only a few single crystals could be picked of complex **16** beside compounds with unknown composition, which allowed no further characterization of the compound. Regarding complexes based on nickel(II) nitrate, two different species could be isolated, depending on the amount of ligand used. The products were filtered off and dried in air.

No further purification step was necessary to get pure products in satisfying to high yields (36–82 %). IR-spectra were measured for every compound except **16** and are available in the supporting information (Figure S1–S4).

9.2.2 Crystal Structures

All complexes were characterized using low-temperature single crystal X-ray diffraction. Finalization of the data set for complexes **6**, **7**, **11**, **12**, and **14** was not possible because of the strongly disordered moieties and the related weak diffractions. Nonetheless, the elemental analysis in combination with infrared spectroscopy validated their temporarily observed structures. Details of the crystal structures of complexes **6**, **11**, and **16** as well as measurement and refinement data are given in the Supporting Information. The crystal datasets were uploaded to the CSD database[32] and can be obtained free of charge with the CCDC no. 1850236 (**1**), 1850244 (**2**), 1850246 (**3**), 1850239 (**4**), 1850243 (**5**), 1850238 (**8**), 1850237 (**9**), 1850245 (**10**), 1850242 (**13**), 1850241 (**15**), 1850240 (**16**).The atomic distances and angles of the coordinating ligand 5-DTP are nearly the same as in the non-coordinating compound and are consequently not discussed.[31]

5-DTP (**1**) crystallizes in the orthorhombic space group *Fdd*2 with eight formula units per unit cell and a calculated density of 1.437 g cm^{-3} at 173 K (Figure 1). The molecular unit is built up by two asymmetric units and shows two planar tetrazole rings (< (N1–N2–N3–N4) = −0.08(18)°, < (C1–N1–N2–N3) = −0.59(18)°) substituted and connected by an isopropane molecule. As expected, the nitrogen-nitrogen and nitrogen-carbon distances lie in a typical range of literature reported tetrazole compounds and are between single and double bonds.[33–34]

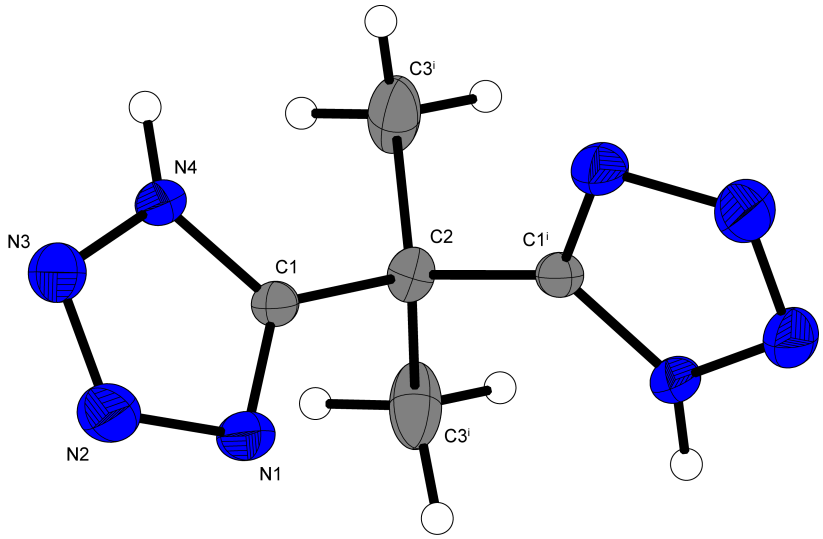


Figure 1. Molecular unit of 2,2-bis(5-tetrazolyl)propane (**1**). Selected bond lengths (Å): C1–C2 1.507(18), C1–N1 1.320(18), N1–N2 1.363(19), N2–N3 1.290(19), N3–N4 1.343(18), N4–C1 1.334(17), C2–C3^{i} 1.532(2); selected bond angles (°): C1–C2–C1^{i} 108.10(14), C3^{i}–C2–C3^{i} 110.20(16),

C1–N1–N2 106.39(12), N1–N2–N3 110.10(14), N2–N3–N4 106.70(12), N3–N4–Cl 109.00(11). Symmetry code: (i) −x, −y, z.

Compound **2** crystallizes in the monoclinic space group $P2_1/n$ with four formula units per unit cell and a calculated density of 1.596 g cm^{-3} at 173 K. The complex has a profoundly distorted trigonal bipyramidal coordination sphere with a chlorido ligand and two coordinating ditetrazoles (Figure 2). The possible reason for the distortion could be the fixed structure of the nitrogen-rich ligand. The distance between the copper(II) center and the chloride is in a typical range for trigonal bipyramidal coordinated chlorido ligands.[35]

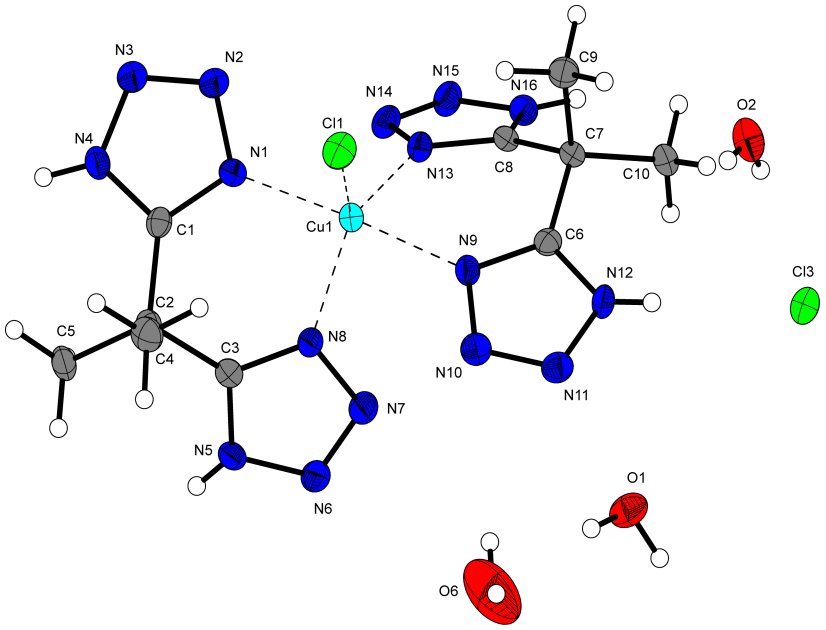


Figure 2. Selection of the molecular unit of $\{[CuCl(5\text{-}DTP)_2]Cl\}_2 \cdot 7\ H_2O$ (**2**). Selected bond lengths (Å): Cu1–N9 1.979(12), Cu1–N1 1.982(4), Cu1–N8 2.050(12), Cu1–N13 2.158(12), Cu1–Cl1 2.293(14); selected bond angles (°): N9–Cu1–N1 175.9(12), N9–Cu1–N8 91.01(5), N1–Cu1–N8 84.97(12), N9–Cu1–N13 84.56(5), N1–Cu1–N13 95.87(11), N8–Cu1–N13 106.5(5), N9–Cu1–Cl1 91.98(5), N1–Cu1–Cl1 91.29(12), N8–Cu1–Cl1 132.9(5), N13–Cu1–Cl1 120.6(5).

he cobalt(II) chloride complex **3**, with a calculated density of 1.678 g cm^{-3} at 173 K, crystallizes in the monoclinic space group *P*2/*c* with two formula units per unit cell. The molecular unit is built up by two asymmetric unit cells (Figure 3). The cobalt(II) center is octahedrally coordinated by two *cis* aqua ligands and two twisted 5-DTP molecules on the opposite side in nearly the same distance from the metal(II). The coordination as well as the bond lengths, and angles are similar to the cobalt(II) chloride complex with di(1*H*-tetrazol-5-yl)methane as ligand instead, however, the aqua ligands are *trans* coordinated.[30]

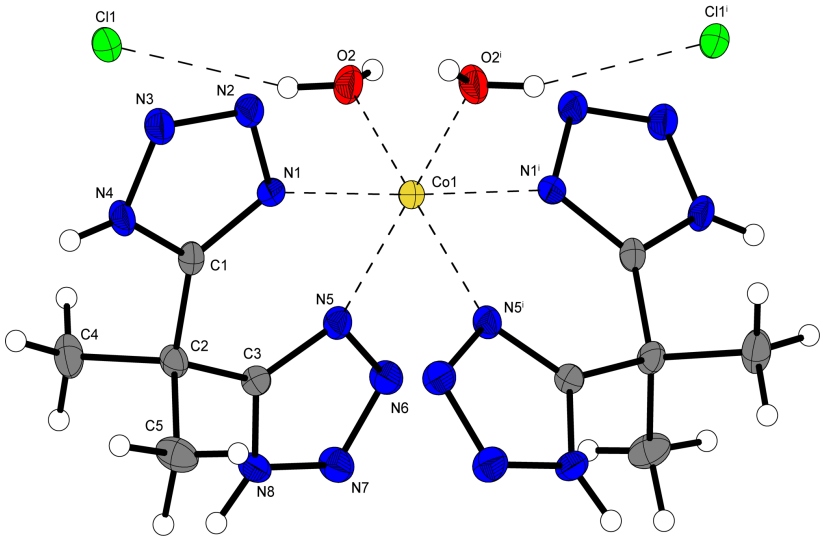


Figure 3. Molecular unit of $[Co(H_2O)_2(5\text{-DTP})_2]Cl_2$ (**3**). Selected bond lengths (Å): Co1–O2 2.072(2), Co1–N1 2.106(2), Co1–N5 2.132(2); selected bond angles (°): $O2^i$–Co1–O2 97.10(9), O2–Co1–$N1^i$ 89.63(8), O2–Co1–N1 88.74(8), $N1^i$–Co1–N1 177.54(7), $O2^i$–Co1–N5 169.26(9), O2–Co1–N5 90.42(9), $N1^i$–Co1–N5 99.00(8), N1–Co1–N5 82.85(8), $O2^i$–Co1–$N5^i$ 90.42(9), O2–Co1–$N5^i$ 169.26(9), N5–Co1–$N5^i$ 83.22(8). Symmetry code: (i) 1−x, y, 0.5−z.

Coordination compound **4** crystallizes in the monoclinic space group *P*2/*n* with four formula units per unit cell and a calculated density of 1.683 g cm^{-3} at 173 K (Figure 4). Complex **4** shows a similar coordination sphere like the cobalt(II) based complex **3** with two asymmetric unit cells per molecular unit and an octahedron built up by two aqua ligands and two chelating 5-DTP's.

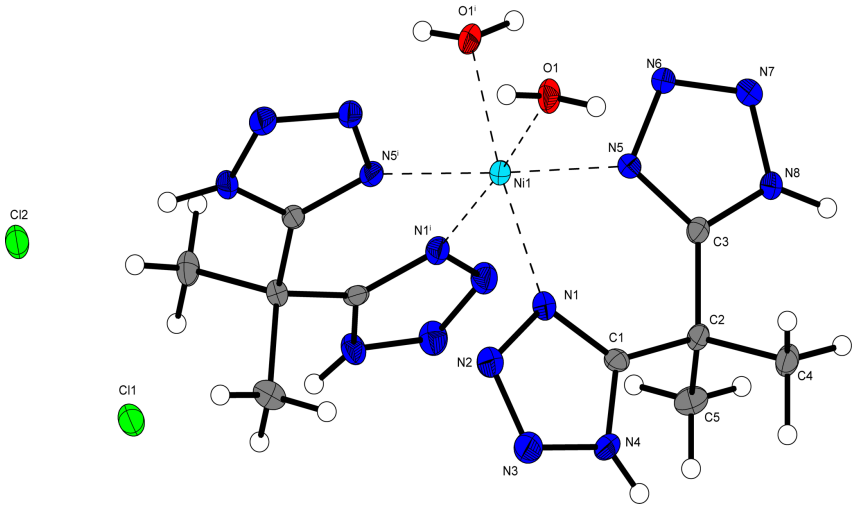


Figure 4. Molecular unit of $[Ni(H_2O)_2(5\text{-DTP})_2]Cl_2$ (**4**). Selected bond lengths (Å): Ni1–N5 2.049 (2), Ni1–O1 2.070(22), Ni1–N1 2.071(22); selected bond angles (°): N5–Ni1–$N5^i$ 177.84(9), N5–Ni1–O1 89.81(10), N5–Ni1–$O1^i$ 88.64(10), O1–Ni1–$O1^i$ 88.15(10), N5–Ni1–N1 85.09(9), $N5^i$–Ni1–N1

96.48(9), O1–Ni1–N1 92.35(10), O1^{i}–Ni1–N1 173.70(10), N5–Ni1–N1^{i} 96.48(9), N1–Ni1–N1^{i} 87.84(10). Symmetry code: (i) 1.5−x, y, 0.5−z.

$[Cu(H_2O)(5\text{-DTP})_2](NO_3)_2$ (**5**) crystallizes in the monoclinic space group $P2_1/c$ with four formula units per unit cell and a calculated density of 1.808 g cm^{-3} at 173 K. The copper(II) metal center is surrounded by one aqua ligand and two 5-DTP's. Compared to the trigonal bipyramidal coordinated copper(II) chloride complex **2**, a distorted square pyramidal structure with an aqua ligand in axial position and 5-DTP's in a plane (Figure 5) can be observed.

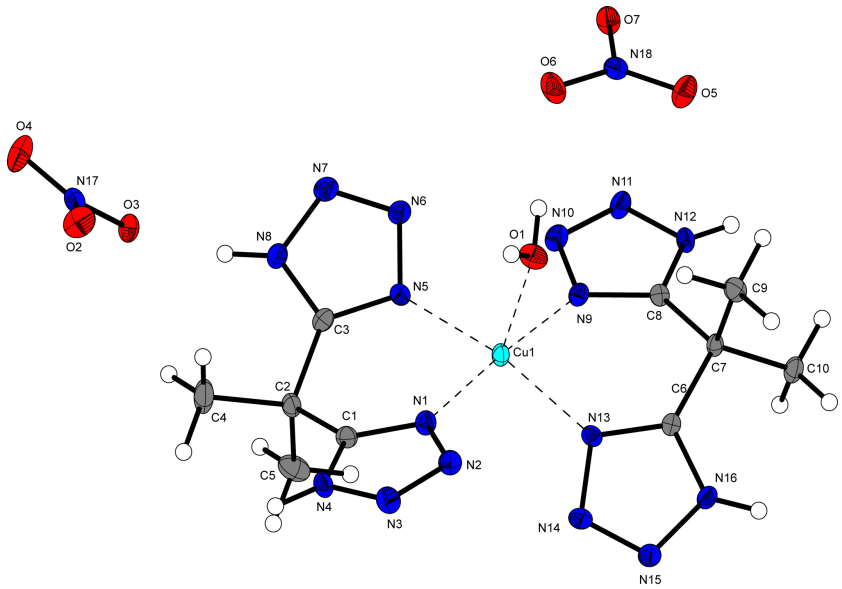


Figure 5. Molecular unit of $[Cu(H_2O)(5\text{-DTP})_2](NO_3)_2$ (**5**). Selected bond lengths (Å): Cu1–N13 1.985(19), Cu1–N5 1.986(19), Cu1–N1 2.002(19), Cu1–N9 2.034(19), Cu1–O1 2.198(2); selected bond angles (°): N13–Cu1–N5 166.20(8), N13–Cu1–N1 92.60(8), N5–Cu1–N1 84.81(8), N13–Cu1–N9 84.59(8), N5–Cu1–N9 97.07(8), N1–Cu1–N9 175.45(8), N13–Cu1–O1 100.87(8), N5–Cu1–O1 92.92(8), N1–Cu1–O1 98.41(8), N9–Cu1–O1 85.66(8).

Two *cis* coordinating aqua ligands and two *cis* chelating 5-DTP's form the octahedral nickel(II) complex **8**, which crystallizes in the monoclinic space group $P2/c$ with four formula units per unit cell and a calculated density of 1.719 g cm^{-3} at 173 K (Figure 6). The molecular unit is built up by two asymmetric unit cells.

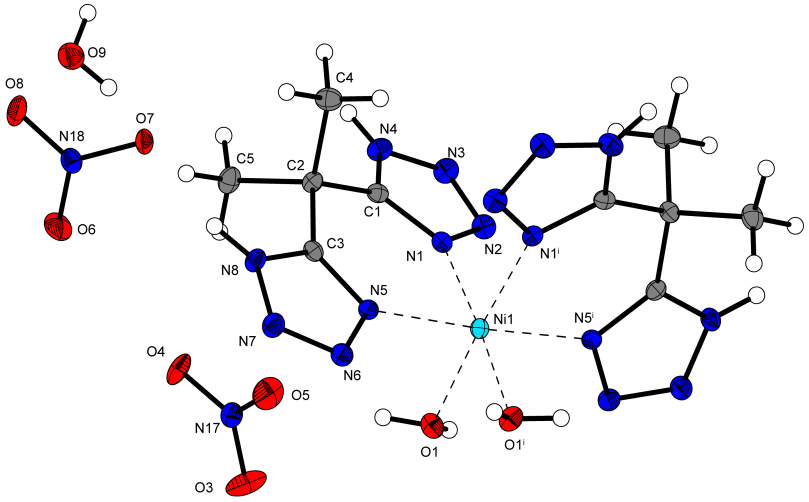


Figure 6. Molecular unit of $[Ni(H_2O)_2(5\text{-DTP})_2](NO_3)_2 \bullet H_2O$ (**8**). Selected bond lengths (Å): Ni1–N5 2.052(18), Ni1–N1 2.075(2), Ni1–O1 2.080(18); selected bond angles (°): $N5^i$–Ni1–N5 176.38(6), $N5^i$–Ni1–N1 92.05(7), N5–Ni1–N1 85.41(7), N5–Ni1–O1 90.22(7), N1–Ni1–O1 91.52(75), N1–Ni1–$N1^i$ 91.05(80), $N5^i$–Ni1–O1 92.42(72), N5–Ni1–O1 90.22(72), N1–Ni1–O1 91.52(8). Symmetry codes: (i) 1−x, y, 0.5−z.

Compound **9** (Figure 7) crystallizes in the form of colorless rods in the triclinic space group *P*–1 with one formula unit per unit cell and a calculated density of 1.736 g cm^{-3} at 173 K. The molecular unit is built up by two asymmetric unit cells. The zinc(II) center is octahedrally surrounded by two aqua ligands, and two chelating 5-DTP's. The analogous zinc(II) complex with di(1*H*-tetrazol-5-yl)methane as ligand instead of 5-DTP, shows nearly the same coordination sphere.[30]

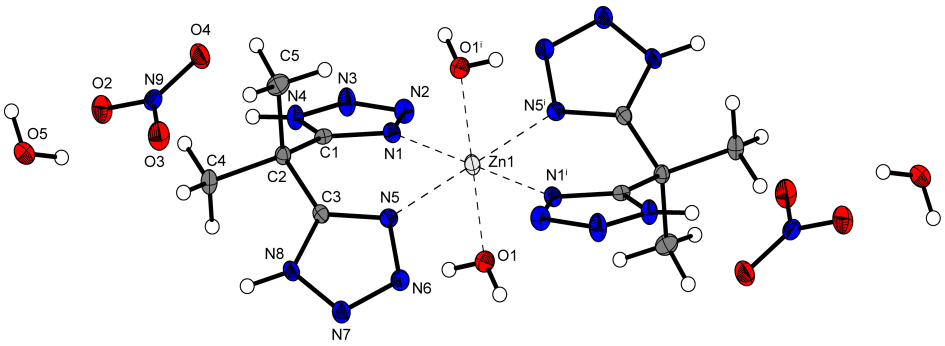


Figure 7. Molecular unit of $[Zn(H_2O)_2(5\text{-DTP})_2](NO_3)_2 \bullet 2\ H_2O$ (**9**). Selected bond lengths (Å): Zn1–N5 2.131(2), Zn1–N1 2.145(19), Zn1–O1 2.149(2); selected bond angles (°): $N5^i$–Zn1–N1 97.13(8), N5–Zn1–N1 82.87(8), N5i–Zn1–O1 91.37(9), N5–Zn1–O1 88.63(9), N1–Zn1–O1 86.85(8), $N1^i$–Zn1–O1 93.15(8). Symmetry code: (i) −x, −y, 2−z.

The perchlorate complex **10** crystallizes in the monoclinic space group *C*2/*c* with eight formula units per unit cell and a calculated density of 1.848 g cm^{-3} at 173 K. An aqua ligand in axial

position, and two 5-DTP's in a plane are forming a distorted square-pyramidal coordination sphere (Figure 8). Independently of the counter anion, copper(II) complexes with 5-DTP prefer penta-coordinated structures, illustrated by compound **2** and **5**, in contrast to di(1*H*-tetrazol-5-yl)methane based complexes, forming octahedral shaped coordination spheres.[30]

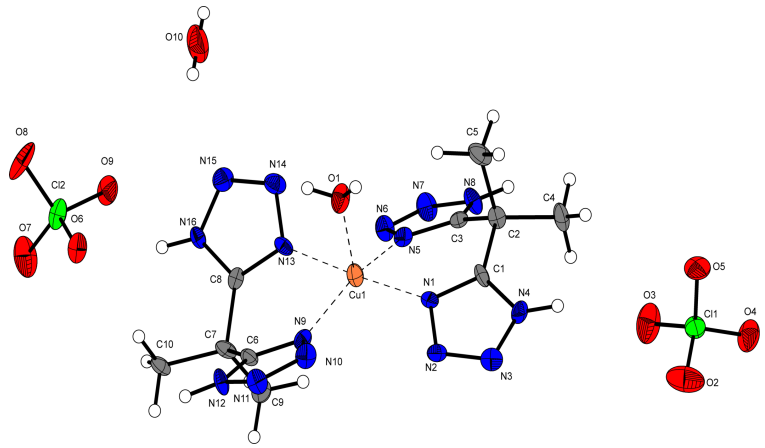


Figure 8. Molecular unit of $[Cu(H_2O)(5\text{-DTP})_2](ClO_4)_2 \bullet H_2O$ (**10**). Selected bond lengths (Å): Cu1–O1 2.254(5), Cu1–N5 1.979(6), Cu1–N1 1.988(7), Cu1–N9 2.024(6), Cu1–N13 1.983(7); selected bond angles (°): N5–Cu1–N1 87.0(3), N1–Cu1–N9 97.7(3), N9–Cu1–N13 86.2(3), N13–Cu1–N5 89.4(3), O1–Cu1–N5 107.8(2), O1–Cu1–N13 89.7(2), N9–Cu1–N5 158.9(3), N1–Cu1–N13 176.1(3).

The zinc(II) complex **13** (Figure 9) crystallizes in the form of colorless rods in the monoclinic space group *I*2 with two formula units per unit cell and a calculated density of 1.807 g cm^{-3} at 173 K. The molecular unit is built up by two asymmetric unit cells. Similar to previously discussed copper(II) complexes, compound **13** shows a penta-coordinated central metal(II). Again, already observed for complex **2**, a trigonal bipyramidal coordination sphere is formed.

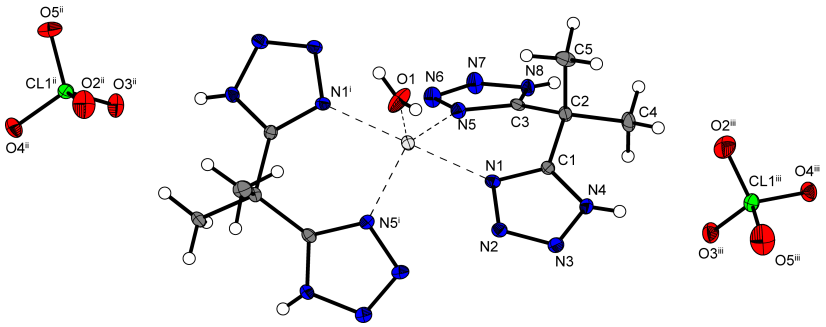


Figure 9. Molecular unit of $[Zn(H_2O)(5\text{-DTP})_2](ClO_4)_2$ (**13**). Selected bond lengths (Å): Zn–N1 2.170(3), Zn–N5 2.024(3), Zn–O1 1.990(4); selected bond angles (°): N1–Zn–N5 84.85(13), N1–Zn–N5^{i} 95.51(13), O1–Zn–N1 89.67(8), O1–Zn–N5 122.79(8), N5^{i}–Zn–N5 114.43(12), N1–Zn–N1^{i} 179.35(12). Symmetry codes: (i) −x, y, 2−z; (ii) −0.5+x, −0.5+y, 0.5+z; (iii) 0.5+x, 0.5+y, −0.5+z.

The penta-coordinated complex **15** crystallizes in the form of blue needles in the monoclinic space group $P2_1/c$ with four formula units per unit cell and a calculated density of 1.776 g cm^{-3} at 133 K (Figure 10). The structure is rather square pyramidal with an aqua ligand in axial position and two 5-DTP ligands in a plane, but could also be treated as highly disordered trigonal bipyramidal with the same configuration observed for complex **13** and copper(II) instead of zinc(II) as transition metal(II).

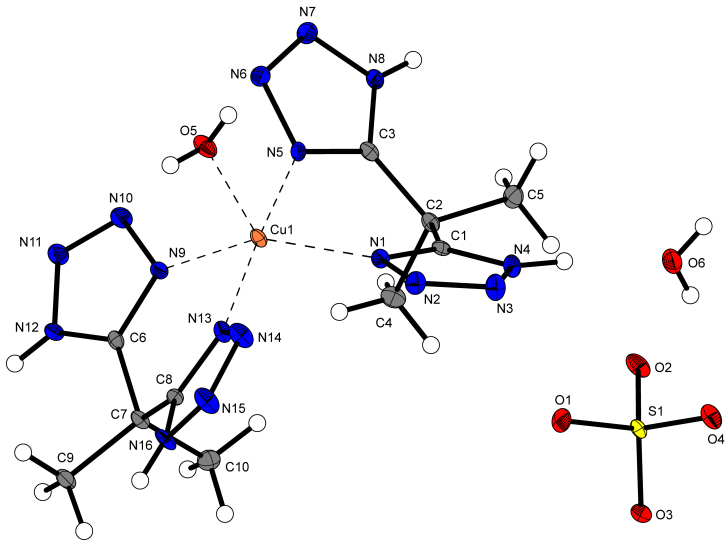


Figure 10. Molecular unit of $[Cu(H_2O)(5\text{-DTP})_2]SO_4 \bullet H_2O$ (**15**). Selected bond lengths (Å): Cu1–N13 1.989(3), Cu1–N5 1.991(3), Cu1–N1 2.022(3), Cu1–N9 2.038(3), Cu1–O5 2.066(3); selected bond angles (°): N13–Cu1–N5 175.12(11), N13–Cu1–N1 92.99(11), N5–Cu1–N1 85.33(11), N13–Cu1–N9 85.09(11), N5–Cu1–N9 93.68(11), N1–Cu1–N9 145.34(11), N13–Cu1–O5 94.54(12), N5–Cu1–O5 90.33(12), N1–Cu1–O5 114.50(11), N9–Cu1–O5 100.14(11).

9.2.3 Sensitivities and Thermal Stabilities

The thermal stabilities of all compounds were determined by differential thermal analysis (DTA) with a heating rate of $\beta = 5$ °C min^{-1} (Table 1). DTA-plots were available in the Supporting Information (Figure S8–S10). Most of the complexes show decomposition temperatures comparable to the free ligand **1** (250 °C) or even higher. Especially, the chloride (**2** and **3**), sulfate (**15**), perchlorate (**10** and **13**), and the nitrate complexes (**5** and **6**) exhibit very high exothermic decomposition temperatures (225–293 °C). The other nitrate and perchlorate compounds (**7**–**9**, **12**, and **14**) are less stable toward heat (163–206 °C).

Table 1. Thermal stability measurements of **1**–**15** by DTA.[a]

compound	$T_{endo1.}$ (°C)[b]	$T_{endo2.}$ (°C)[b]	$T_{exo.}$ (°C)[c]
$C_5H_8N_8$ (1)	235	–	235
2	92	–	259
3	194	–	253
4	207	–	207
5	172	–	293
6	125	–	267
7	–	–	203
8	126	–	163
9	107	–	170
10	138	168	251
11	88	–	206
12	159	–	190
13	–	–	256
14	145	–	176
15	162	188	225

[a] Onset temperature at a heating rate of 5 °C min^{-1}; [b] Endothermic peak, which indicates melting, vaporization, dehydration, or loss of aqua ligands; [c] Exothermic peak, which indicates decomposition.

The sensitivities toward impact, friction, and electrostatic discharge were investigated for all complexes **2**–**15** and the corresponding free ligand **1**. An overview is given in Table 2. The free ligand **1** is, according to UN standards, "insensitive" toward friction and electrostatic discharge with values greater than 360 N for friction and greater than 1.50 J for ESD, but "sensitive" toward impact (25 J).[36] The chloride and sulfate complexes **2**–**4** and **15** with coordinating 5-DTP are "insensitive" toward impact (≥ 40 J), friction (> 360 N) and electrostatic discharge (≥ 0.75 J). Substitution of chloride by nitrate (**5**–**9**) increases the sensitivities. Values of 5–10 J for impact, ≥ 324 N for friction and ≥ 0.15 J for ESD were measured. Replacing nitrate by perchlorate (**10**–**14**) decreases, as expected, the stability toward impact (< 1–12.5 J), friction (10–72 N), and ESD (0.065–0.50 J), whereby some complexes, such as compound **10** and **13**, are very sensitive toward impact, but still practicable without substantial risk.

Table 2. Sensitivities toward impact, friction, and ESD of **1**–**15**.

Compound[a]	*IS*[b] (J)	*FS*[c] (N)	*ESD*[d] (J)
1[b]	30	> 360	1.50
2[b]	> 40	> 360	1.50
3[c]	> 40	> 360	1.50
4[c]	> 40	> 360	1.50
5[a]	8	360	1.50
6[b]	10	> 360	1.50
7[c]	5	324	1.50
8[b]	10	360	0.15
9[b]	40	> 360	0.20
10[c]	3	10	0.065
11[c]	12.5	72	0.50
12[c]	20	216	0.75[g]
13[a]	2	20	0.20
14[b]	< 1	15	0.10
15[b]	> 40	> 360	0.75

[a] Determined at a grain size < 100 µm. [b] Determined at a grain size 100–500 µm. [c] Determined at a grain size 500–1000 µm. [d] Impact sensitivity according to the BAM Drophammer (method 1 of 6). [e] Friction sensitivity according to the BAM friction

tester (method 1 of 6). [f] Electrostatic discharge sensitivity (OZM ESD tester); [g] Electrostatic discharge sensitivity (OZM Electric Spark XSpark10).

Hot plate and hot needle tests of the most promising compounds **10** and **13** were performed to get an insight into the compounds' behavior during fast heating with and without confinement. For both tested compounds, only deflagrations could be observed during hot plate as well as hot needle tests (Figure 11, S11–S12).

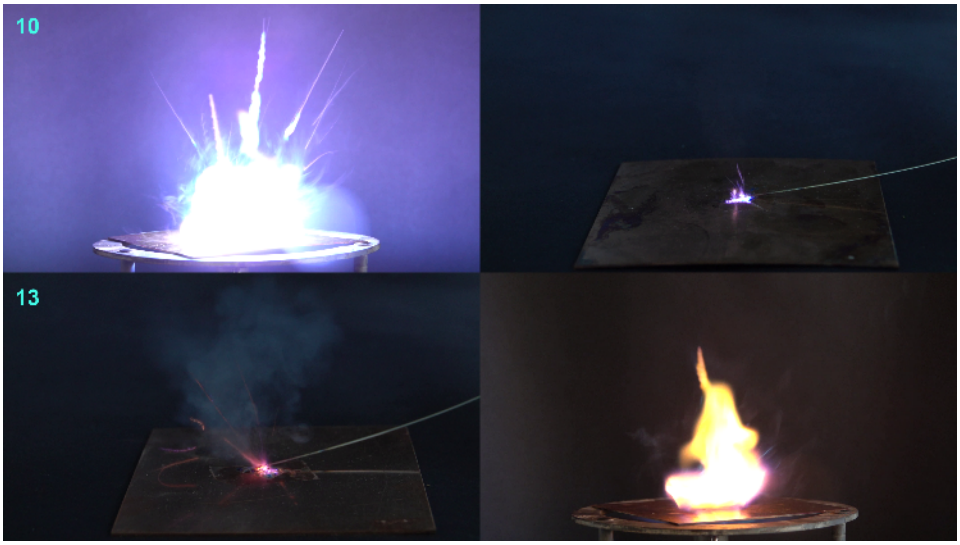


Figure 11. Upper side: moment of deflagration of **10** during the hot plate and hot needle test. Bottom side: deflagration of complex **13** during hot needle and hot needle test.

9.2.4 Laser Ignition Experiments

Laser ignition is a modern way of initiation of energetic materials, which shows various advantages over classical approaches. Cobalt(III) amine complexes have shown good results in laser ignition tests, as well as some copper(II) complexes in the past.[32,37] The confined samples of **10** and **14** were irradiated at a wavelength of 915 nm, a pulse length of 15 ms (1 ms for **10**), a current of 7 A for **10**, 9 A for **14** and a voltage of 4 V which results in an approximately energy output of 0.7–37.5 mJ. Other compounds were not tested due to their low sensitivities toward other initiation impulses and the consequently expected negative laser ignition test. An overview of the results is given in Table 3. UV-Vis-Spectra of **10**, **13** and **14** were measured in liquid in the corresponding acid. Details on the measurement and spectra are available in the Supplementary Information (Figure S13).

Table 3. Results of the laser ignition tests.[a]

compound	*I* (A)	*τ* (ms)	result
10	7	1	det.
10	7	15	det.
14	9	15	deflag.

[a] (deflag.: deflagration, det.: detonation). Operating parameters: current I = 7–9 A, voltage U = 4 V; theoretical output power P_{max} = 45 W; theoretical energy E_{max} = 0.70–37.5 mJ; wavelength λ = 915 nm; pulse length τ = 1–15 ms.

The copper(II) perchlorate complex **10** detonated under both applied energy inputs, while compound **14** showed only a deflagration during the laser ignition experiment (Figure 12). The copper(II) complex is, therefore, a valuable photosensitive energetic coordination compound with manageable sensitivities and holds great promise for possible future applications.

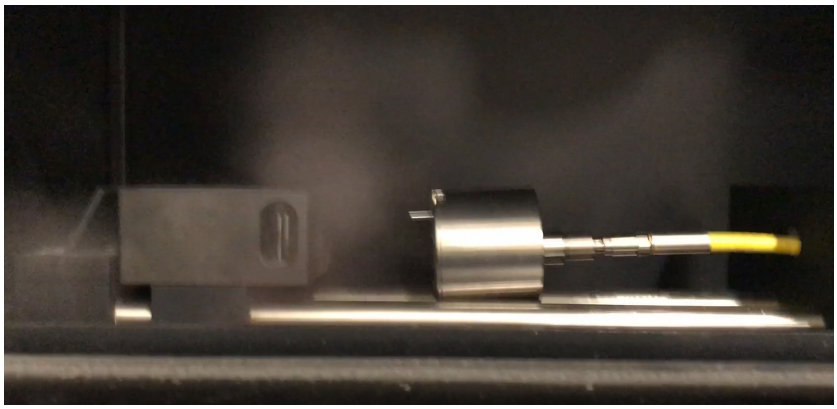


Figure 12. Moment of detonation of complex **10** during the laser initiation experiment.

9.3 Conclusions

The nitrogen-rich ligand 2,2-bis(5-tetrazolyl)propane (**1**, 5-DTP) was synthesized in high purity and characterized by multinuclear NMR spectroscopy (^{1}H, ^{13}C). Furthermore, **1** was investigated by X-ray diffraction, elemental analysis, IR spectroscopy, differential thermal analysis together with its sensitivities toward various stimuli (impact, friction, ESD). The aim of this work was to develop new photosensitive and environmentally friendly primary explosives by combining different transition metal(II) salts with the prepared nitrogen-rich ligand. The synthetic route toward these new energetic coordination compounds is simple, cost-efficient, and environmentally benign. All newly synthesized coordination compounds except **16** were characterized by IR spectroscopy, elemental analysis, DTA and sensitivity measurements. The X-ray crystal structure of 15 complexes could be determined to get an insight into the fascinating coordination behavior. Adjustment of the optical and energetic

properties could be achieved through the variation of the anion (chloride, nitrate, sulfate, or perchlorate) and the late 3d transition metals. The compounds show captivating structures, building distorted coordination spheres caused by the chelating ligand. Most of the complexes show good thermal stabilities. Especially the most interesting coordination compounds **10** and **13** possess very high exothermic decomposition temperatures above 250 °C, while both show manageable sensitivities toward impact, friction, and ESD. Furthermore, copper(II) compound **10** (IS: 3 J, FS: 10 N, ESD: 0.065 J) was successfully initiated in laser experiments with a very low energy input of only 0.7 mJ, making it to a promising candidate as laser ignitable explosive.

Supporting information available in the appendix in **Chapter 19.6** and under:

https://onlinelibrary.wiley.com/action/downloadSupplement?doi=10.1002%2Fzaac.201800288&file=zaac201800288-sup-0001-SupMat.pdf

9.4 References

[1] https://echa.europa.eu/de/candidate-list-table, accessed May 2018.

[2] Q. Jun-Sheng, B. Shao-Juan, L. Peng, X. Wei, D. Dong-Ying, Z. Liang, L. Ya-Qian, S. Zhong-Min, *Chem. Asian J.* **2014**, *9*, 749–753.

[3] A. Rudavskyi, R. W. A. Havenith, R. Broer, C. de Graaf, C. Sousa, *Dalton Trans*. **2013**, *42*, 14702–14709.

[4] L. Shenghua, W. Yuan, Q. Cai, Z. Xiuxiu, Z. Jichuan, Z. Shaowen, P. Siping, *Angew. Chem., Int. Ed*. **2013**, *52*, 14031–14035.

[5] V. Y. Zubarev, E. V. Bezklubnaya, A. K. Pyartman, R. E. Trifonov, V. A. Ostrovskii, *Chem. Heterocycl. Compd*. **2003**, *39*, 1317–1325.

[6] V. Y. Zubarev, R. E. Trifonov, V. V. Poborchii, V. A. Ostrovskii, *Chem. Heterocycl. Compd*. **2006**, *42*, 469–474.

[7] V. A. Ostrovskii, R. E. Trifonov, E. A. Popova, Russ. *Chem. Bull*. **2012**, *61*, 768–780.

[8] G. R. Marshall, D. J. Kuster, Y. Che, *Methods Mol. Biol*. **2009**, *575*, 123–158.

[9] R. J. Herr, Bioorg. *Med. Chem*. **2002**, *10*, 3379–3393.

[10] R. Trifonov, M. Trukhnitskaya, A. Tarkhanova, I. Vikhrova, V. Ostrovskii, Russ. *J. Org. Chem.* **2006**, *42*, 1059–1062.

[11] B. Le Bourdonnec, E. Meulon, S. Yous, J.-F. Goossens, R. Houssin, J.-P. Hénichart, *J. Med. Chem*. **2000**, *43*, 2685–2697.

[12] J. R. Anacona, P. Alvarez, *Transition Met. Chem*. **2002**, *27*, 856–860.

[13] C. N. S. S. P. Kumar, D. K. Parida, A. Santhoshi, A. K. Kota, B. Sridhar, V. J. Rao, *MedChemComm* **2011**, *2*, 486–492.

[14] A. D. Abell, G. J. Foulds, *J. Chem. Soc., Perkin Trans. 1* **1997**, 2475–2482

[15] B. C. H. May, A. D. Abell, *J. Chem. Soc., Perkin Trans*. *1* **2002**, 172–178.

[16] M. Joas, T. M. Klapötke, J. Stierstorfer, N. Szimhardt, *Chem. Eur. J*. **2013**, *19*, 9995–10003.

[17] T. W. Myers, J. A. Bjorgaard, K. E. Brown, D. E. Chavez, S. K. Hanson, R. J. Scharff, S. Tretiak, J. M. Veauthier, *J. Am. Chem. Soc.* **2016**, *138*, 4685–4692.

[18] A. A. Brish, B. N. Zaitsev, E. A. Sbitnev, L. V. Tatarintsev, *Fiz. Goreniya Vzryva* **1966**, *2*, 132–133.

[19] A. A. Brish, B. N. Zaitsev, E. A. Sbitnev, L. V. Tatarintsev, *Fiz. Goreniya Vzryva* **1969**, *5*, 475–480.

[20] L. C. Yang, V. J Menichelli, *Appl. Phys. Lett.* **1971**, *19*, 473–475.

[21] E. S. Hafenrichter, B. Marshall, K. J. Fleming, Fast laser diode ignition of CP and BNCP. In *Proceedings of the 29th International Pyrotechnics Seminar*, Westminster, CO, July 14-19, **2002**; IPSUSA, **2002**; pp 787–793.

[22] P. W. Cooper, *Explosives Engineering*, Wiley-VCH: Weinheim, **1996**.

[23] S. C. Kunz, F. J. Salas, Diode laser ignition of high explosives and pyrotechnics. In *Proceedings of the 13th International Pyrotechnics Seminar*, Grand Junction, CO, July 11-15, 1988; IIT Research Insitute: Chicago, IL, 1988; pp 505–523.

[24] J. A. Merson, F. J. Salas; J. G. Harlan, The development of laser ignited deflagaration-to-detonation transition (DDT) detonators and pyrotechnic actuators. In *Proceedings of the 19th International Pyrotechnics Seminar*, Christchurch, New Zealand, Feb 20-25, 1994; IPS, 1994; pp 191–206.

[25] A. Y. Zhilin, M. A. Ilyushin, I. V. Tselinskii, A. S. Kozlov, I. S. Lisker, *Russ. J. Appl. Chem.* **2003**, *76*, 572–576.

[26] J. Evers, I. Gospodinov, M. Joas, T. M. Klapötke, J. Stierstorfer, *Inorg. Chem.* **2014**, *53*, 11749–11756.

[27] A. Y. Zhilin, M. A. Ilyushin, I. V. Tselinskii, A. S. Brykov, *Russ. J. Appl. Chem.* **2001**, *74*, 99–102.

[28] A. V. Smirnov, M. A. Ilyushin, I. V. Tselinskii, *Russ. J. Appl. Chem.* **2004**, *77*, 794–796.

[29] T. W. Myers, K. E. Brown, D. E. Chavez, R. J. Scharff, J. M. Veauthier, *Eur. J. Inorg. Chem.* **2016**, *2016*, 3178–3183.

[30] M. Freis, T. M. Klapötke, J. Stierstorfer, N. Szimhardt, *Inorg. Chem.* **2017**, *56*, 7936–7947.

[31] Z. P. Demko, K. B. Sharpless, *J. Org. Chem.* **2001**, *66*, 7945–7950.

[32] Crystallographic data for the structures have been deposited with the Cambridge Crystallographic Data Centre. Copies of the data can be obtained free of charge on application to The Director, CCDC, 12 Union Road, Cambridge CB2 1EZ, UK (Fax: int.code_(1223)336-033; e-mail for inquiry: fileserv@ccdc.cam.ac.uk; e-mail for deposition: (deposit@ccdc.cam.ac.uk).

[33] D. Chand, D. A. Parrish, J. M. Shreeve, *J. Mater. Chem.* **2013**, *1*, 15383–15389.

[34] C. A. K. Diop, M. F. Mahon, K. C. Molloy, L. Ooi, P. R. Raithby, M. M. Venter, S. J. Teat, *CrystEngComm* **2002**, *4*, 462–466.

[35] J. Brugger, D. C. McPhail, J. Black, L. Spiccia, *Geochim. Cosmochim. Acta* **2001**, *65*, 2691–2708.

[36] Impact: insensitive > 40 J, less sensitive ≥ 35 J, sensitive ≥ 4 J and very sensitive ≤ 3J; friction: insensitive > 360 N, less sensitive = 360 N, sensitive < 360 N and > 80 N, very

sensitive ≤ 80 N and extremely sensitive ≤ 10 N. According to the UN Recommendations on the Transport of Dangerous Goods

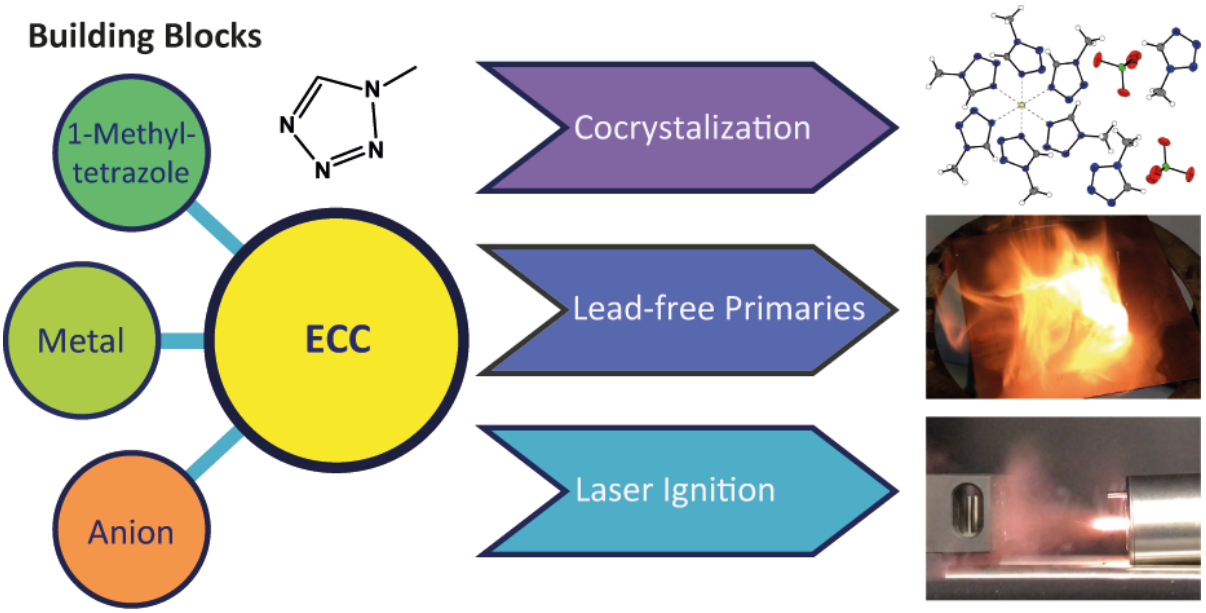
[37] A. Y. Zhilin, M. A. Ilyushin, I. V. Tselinskii, A. S. Kozlov, N. E. Kuz'mina, *Russ. J. Appl. Chem.* **2002**, *75*, 1849–1851.

10 Coordination Chemistry with 1-Methyl-5*H*-tetrazole: Cocrystallization, Laser-ignition, Lead-free Primary Explosives – One Ligand, three Goals

Norbert Szimhardt, Maximilian H. H. Wurzenberger, Andreas Beringer, Lena J. Daumann and Jörg Stierstorfer

published in *Journal of Materials Chemistry A* **2017**, *5,* 23753–23765

DOI: 10.1039/C7TA07780G



Numerous energetic coordination complexes (Mn^{II}, Fe^{II}, Co^{II}, Ni^{II}, Cu^{II}, Zn^{II}, Ag^{I}) using 1-methyl-5*H*-tetrazole as the ligand were synthesized and tuned by different counteranions (e.g. NO_3^-, ClO_4^-, picrate, styphnate). They show great potential of mechanical or optical systems.

Abstract

The synthesis and characterization of 1-methyl-5*H*-tetrazole (**1**, MTZ) from 1,5*H*-tetrazole and methyl iodide is achieved. This neutral ligand was evaluated for its use in energetic transition metal complexes. The formation of complexes is a valuable concept because of the easy synthesis and the large number of possible combinations: i) metal, ii) ligand, and iii) anion. A series of 31 new complexes based on MTZ as the ligand was prepared in order to tune optical properties and sensitivity values by using seven different metals (Mn^{2+}, Fe^{2+}, Co^{2+}, Ni^{2+}, Cu^{2+}, Zn^{2+}, Ag^{+}) and six different anions (chloride, nitrate, perchlorate, cyanodinitromethanide, picrate, styphnate). This variation allows to tailor the energetic properties of the desired molecule toward e.g. suitable primary explosives or laser-ignitable materials. Obtained compounds were characterized by low temperature single crystal X-ray diffraction, IR spectroscopy, elemental analysis and thermal analysis (DTA, DSC and TGA). The sensitivities toward external stimuli (impact, friction and electrostatic discharge) were determined according to the *Bundesamt für Materialforschung und -prüfung* (BAM) standard methods. These complexes have been characterized in laser ignition experiments and as new primary explosives. UV-Vis measurements of selected complexes were carried out to get a possible insight into the laser initiation mechanism. For the first time a large number of compounds with sensitivities ranging from insensitive to very sensitive were synthesized to give a wide range of new materials for different possible applications.

10.1 Introduction

Lead styphnate and lead azide were put on the candidate list of authorization (substances of very high concern, Annex XIV) for the REACH (Registration, Evaluation, Authorization and Restriction of Chemicals)[1] regulations in 2011 due to their high toxicity. Almost certainly, the two compounds will be strictly regulated or banned. Therefore; research into possible lead-free replacements is strongly needed.

The use of endothermic ligands, such as tetrazoles and triazoles, in coordination compounds has been growing over the past few years with multiple uses in the field of inorganic chemistry.[2,3] Specifically, these complexes have applications as metal-organic frameworks (MOFs),[4] spin crossover systems[5] and energetic materials.[6,7]

Crystalline compounds containing two or more different species – including hydrates, solvates, coordinating and non-coordinating ligands – are defined as cocrystals and have an increasing number of applications as molecular semiconductors, advanced pharmaceuticals and optical materials.[8] In the field of energetic materials, cocrystallization can be used for enhancing the density and the detonation/combustion performance or to lower the mechanical sensitivities.[9] Regarding energetic complexes, this concept has recently been described with 1,2-di(1*H*-tetrazol-5-yl)ethane as the ligand.[10] In this work, the neutral ligand itself has been used as a cocrystallized species for the first time to increase the stability of the energetic complexes.

Coordination compounds of iron(II), in particular bearing alkylated tetrazole ligands like 1-methyl-5*H*-tetrazole (**1**), are one of the most investigated compounds in spin crossover systems.[11] The perchlorate and tetrafluoroborate iron(II) alkyltetrazole coordination compounds exhibited two different lattice sites for the central metals with a spin transition from high spin (*hs*) to low spin (*ls*) at a specific temperature.[12] Metastable long-lived *hs* and *ls* states on both sides can be induced through irradiation of green or red light, which makes spin crossover compounds interesting for uses in liquid crystals, gel phases and molecular switches.[13] In terms of energetic materials, transition metal complexes have been proposed for numerous applications.[14] Ordinary used primary explosives, such as lead(II) azide, lead(II) styphnate and, in former times, mercury(II) fulminate (Chart 1), have led to significant contamination of the environment.[15,16] Energetic coordination compounds (ECCs) containing nitrogen-rich tetrazole ligands with high positive heats of formation and low or non-toxic metals like copper, zinc or iron can be used as substitutes for currently used primary explosives containing toxic heavy metals (Chart 2a/b).[6,17-19]

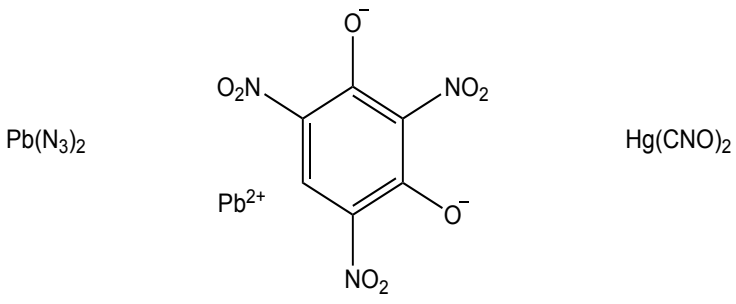


Chart 1. Commonly used primary explosives: lead(II) azide, lead(II) styphnate and mercury(II) fulminate.

The use of laser initiation systems is also becoming more attractive as a strategy for replacing sensitive primary explosives.[20] Instead of using very sensitive compounds for igniting secondary explosives, relatively insensitive energetic materials are ignited directly by laser

irradiation. The ignition can be triggered by using high power lasers or with lower energies by adding small amounts of light absorbing materials to the energetic materials, like carbon black or chemical dyes.[21] However, promising explosive coordination complexes (ECCs), using transition metals as the central atom (for example Cu^{2+}, Co^{2+}, Ni^{2+} or Fe^{2+}) and tetrazole ligands have been reported in literature that are ignitable by laser irradiation without the addition of dyes (Chart 2d).[22,23] The most prominent examples include pentaammine(5-cyano-2*H*-tetrazolate)cobalt(III) perchlorate (CP),[24] tetraammine-*cis*-bis(5-nitro-2*H*-tetrazolato-*N*^{2})cobalt(III) perchlorate (BNCP)[25] and 5-hydrazino-1*H*-tetrazolemercury(II) perchlorate (HTMP, Chart 2c).[26] While they were initiated by laser ignition, they proved to be too sensitive for any application. The research of insensitive replacements is still of interest.

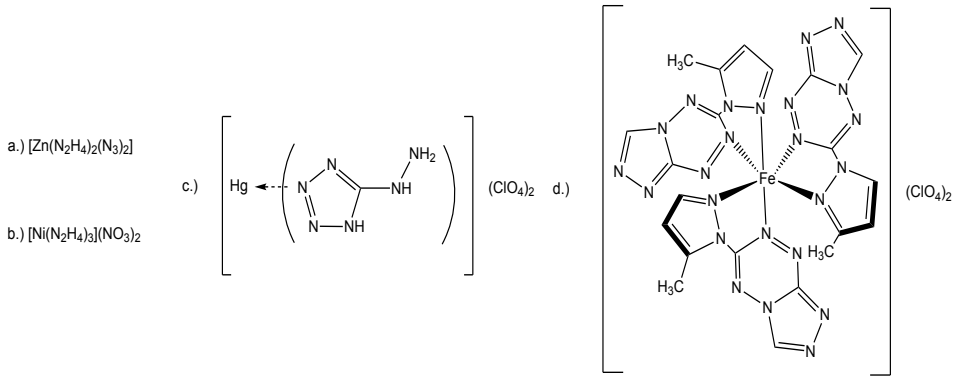


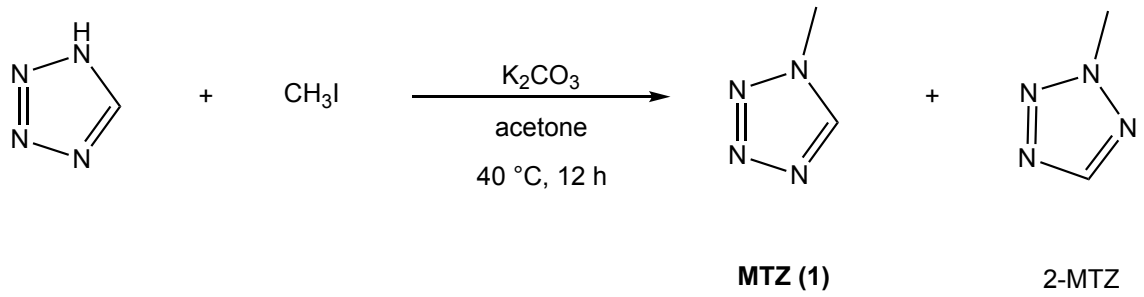
Chart 2. Energetic coordination compounds (ECC): a) $[Zn(N_2H_4)_2(N_3)_2]$[16] and b) $[Ni(N_2H_4)_3](NO_3)_2$[17] as possible replacements for lead containing primaries; c) 5-hydrazino-1*H*-tetrazolemercury(II) perchlorate (old generation of laser ignitable explosives)[25] and d) $[Fe(TriTzPyr)_3](ClO_4)_2$ (new generation of laser ignitable explosives).[22]

1-Methyl-5*H*-tetrazole (**1**) was first synthesized 1910 by reaction of methylisocyanide with hydrazoic acid by *Oliveri-Nandalá*.[27] The ligand has a high nitrogen content of 66.63 % and can be easily synthesized at low cost. The resulting driving force of producing nitrogen gas out of N–N single or N=N double bonds, makes it promising as a ligand in combination with oxidizing anions for ECCs. Until now, the compound has only been described in relation to EPR studies,[28] spin transition complexes[10-12,29] and pyrotechnic/[30] propellant compositions.[31] Therefore, in this paper, efforts have been made to utilize MTZ as a neutral ligand to generate new energetic complexes with promising properties as (laser-ignitable) primary explosives or cocrystallized coordination compounds.

10.2 Results and Discussion

10.2.1 Synthesis

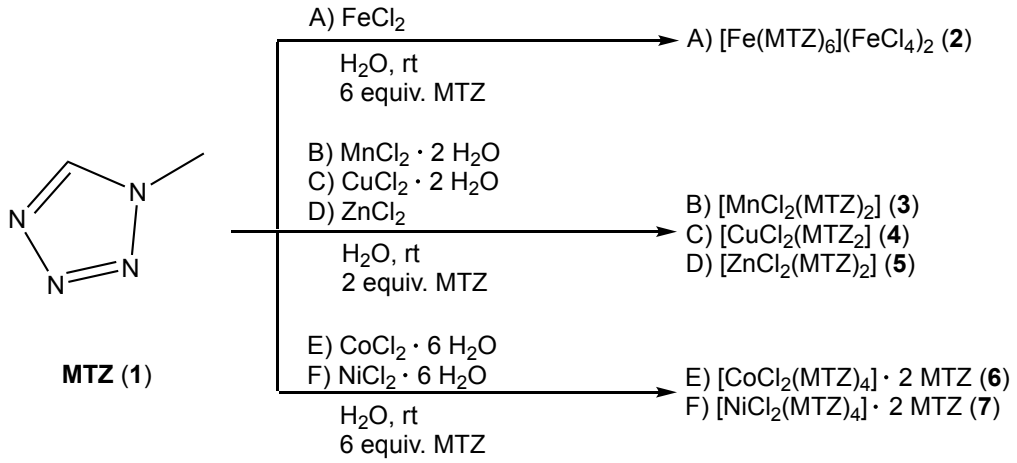
The nitrogen-rich heterocycle 1-methyl-5*H*-tetrazole (**1**, MTZ) can be synthesized in various ways. One route is the cycloaddition reaction of sodium azide with triethyl orthoformate and methylamine in acetic acid under reflux.[32] Another route is the nucleophilic methylation of 1*H*-tetrazole with a methylating agent such as methyl iodide. The methylation reaction reported here was carried out in acetone at 40 °C under reflux using potassium carbonate as base, according to a modified literature procedure (Scheme 1).[33] The methylation leads to an isomeric mixture of 1-methyl-5*H*-tetrazole (**1**) and 2-methyl-5*H*-tetrazole. The desired product can be isolated from this mixture either by flash column chromatography or distillation. Filtration of the reaction mixture followed by distillation (MTZ: 90 °C, 0.01 mbar, 2-MTZ: 40 °C, 12 mbar) of the organic residue resulted in the isolation of the product **1** with a yield of 48 %. The side product 2-methyl-5*H*-tetrazole was obtained with a yield of 23 %.



Scheme 1. Synthesis of 1-methyl-5*H*-tetrazole (**1**, MTZ).

The divalent transition metal complexes **2**–**13** and **15**–**26** were prepared by combining solutions of 1-methyl-5*H*-tetrazole (**1**) and metal(II) salts with the respective stoichiometries at room temperature (Scheme 2–4). Water was chosen as a non-flammable, low-volatile and cheap reaction medium because of the good solubility of both the metal(II) salts and the tetrazole ligand in this solvent. In order to get crystalline materials, a minimal amount of solvent was used. An iron(II) tetrachloridoferrate(III) coordination compound **2** with iron in two different oxidation states was synthesized analogous to the literature known spin crossover tetrabromidoferrate(II) complex of 1-methyl-5*H*-tetrazole.[12] Ethanol was used for recrystallization of **2** and as co-solvent in the synthesis of the perchlorate complexes **15**–**20** to get better crystallization.

Complexes **4** and **5** have already been described in the literature and were synthesized to fill the gaps in the physico-chemical analytics.[34,35] The cobalt(II) and nickel(II) chlorido coordination compounds **6** and **7** crystallized, in contrast to **3**–**5** and the literature reported $CoCl_2$, $NiCl_2$ complexes, with four coordinating and two cocrystallized non-coordinating MTZ molecules. The nickel(II) chlorido complex **7** precipitated as a powder and single crystals could not be obtained by recrystallization. On comparison of the infrared spectra of **3**, **6** and **7**, and elemental analysis a complex formula of $[NiCl_2(MTZ)_4] \cdot 2$ MTZ is proposed for the coordination compound **7** (Figure S20).

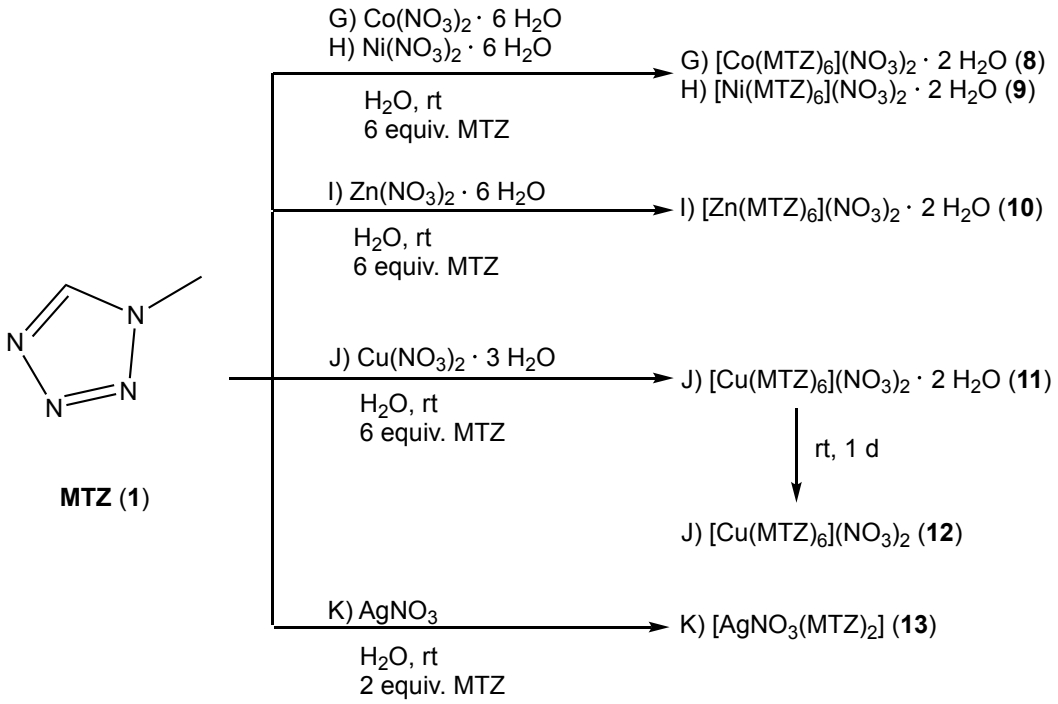


Scheme 2. Synthesis of the metal(II) chloride based MTZ complexes **2**–**7** with different metal centers.

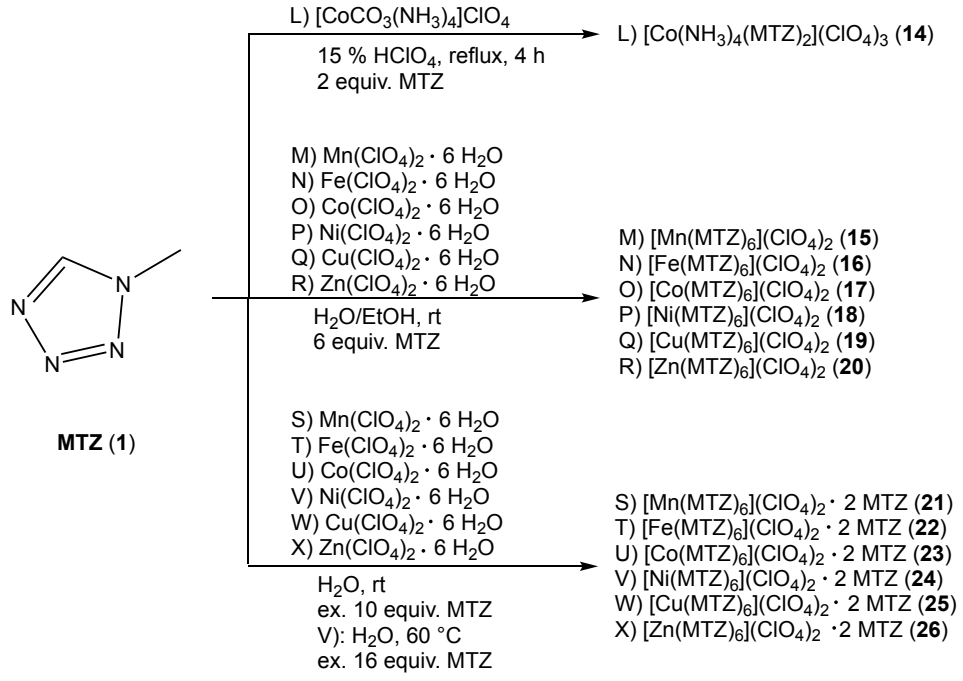
The ligand has no acidic proton, which enables the integration of the neutral tetrazole ligand to assemble cationic or neutral complexes with oxidizing anions like nitrates, perchlorates, cyanodinitromethanides (CDNM), picrates (PA) or trinitroresorcinates (HTNR). The incorporation of these oxidizing anions leads to more sensitive and powerful energetic materials and are possible alternatives for lead free laser ignitable primary explosives.

Compound **11** lost the crystal water molecules and its crystallinity overnight, in contrast to **8**–**10**, and was analyzed in its anhydrous form **12**. The colored reaction mixtures were left for crystallization until a precipitate appeared. The majority of the complexes were obtained in satisfying yields directly from the mother liquor as single crystals suitable for X-ray diffraction within a few hours or days. Unfortunately compound **14** precipitated as an amorphous powder in a low yield of 18 % and despite considerable recrystallization efforts single crystals could not be obtained.

The complex was synthesized by treatment of carbonatotetraaminecobalt(III) perchlorate with two equivalents of **1** in 15 % perchloric acid for 4 hours under reflux according to a modified procedure of an analogous compound.[36] The compound was filtered off, washed with a small amount of ethanol and dried in air.

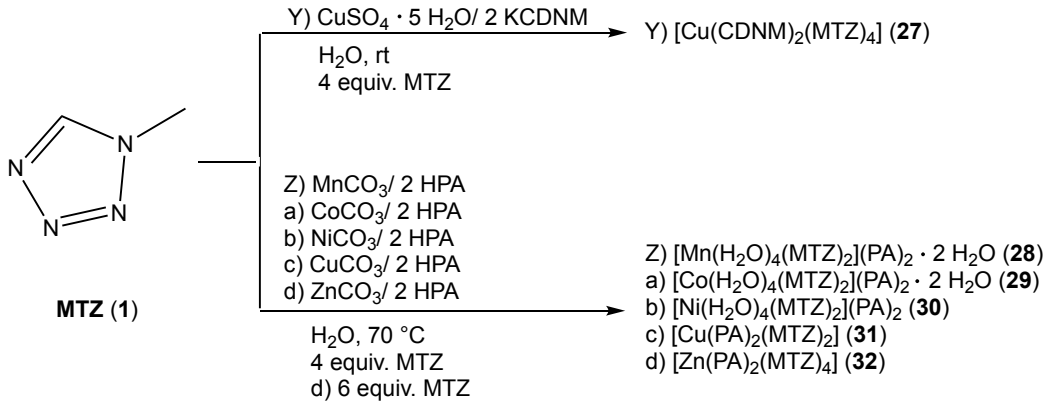


Scheme 3. Synthesis of selected metal nitrate based MTZ complexes **8**–**13** with different metal centers.



Scheme 4. Synthesis of the energetic perchlorate coordination compounds **14**–**26**.

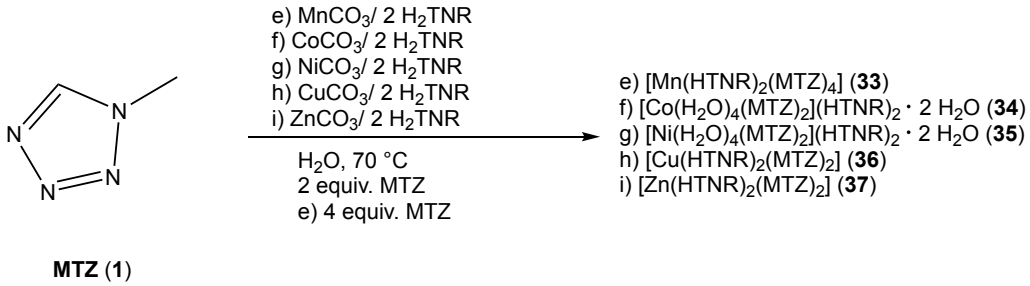
All perchlorate complexes were obtained without inclusion of aqua ligands or water solvent molecules, which results in a higher performance. The synthesis of the perchlorate complexes is strongly dependent on the quantity of the ligand added and yields either a structure where all MTZ ligands are bound to the metal ions (**15**–**20**) or a complex unit with two additional cocrystallized tetrazoles (**21**–**26**) when an excess of the ligand is used. Both species can be clearly distinguished through infrared spectroscopy.[32] This is illustrated exemplarily for the cobalt(II) perchlorate complexes **17** and **23** in Figure S22. In addition to an intense stretching vibration around 1106 cm^{-1} stemming from the perchlorate counter ions, a characteristic ring vibration of the bound MTZ ligand around 965 cm^{-1} is observed in the spectra of both **17** and **23**. The free ligand as well as complex **23** exhibits a stretch in the spectra at around 997 cm^{-1} stemming from in plane ring vibrations in free MTZ.[32] The C-H vibration can be detected at 3100 cm^{-1} in the free ligand and complex **23** spectra, respectively, while the bound MTZ ligand in **23** and **17** does occur at slightly higher wavenumbers (3147 cm^{-1}).



Scheme 5. Formation of the complexes **27**–**32** with varying metal centers and anions.

The corresponding metal(II) precursors for the complexes **27**–**37** were prepared and used *in situ* by simple acid-base reactions between metal(II) carbonates and picric/styphnic acid or metathesis reactions. The aqueous solutions of the corresponding precursors were then reacted with ligand **1** (Schemes 5 and 6). In some cases, non-stoichiometric amounts of the ligand were used to increase the yield or purity of the respective compounds. All complexes crystallized within several minutes (copper(II) picrate and styphnate compounds) or days and were obtained directly from the mother liquor in reasonable yields (60–86 %). Crystals were filtered off, washed with cold ethanol when necessary to remove unreacted starting materials and dried in air, resulting in suitable samples for X-ray diffraction. Due to the high solubility of compound **33** in ethanol, no purification step was performed. In case of the manganese(II) picrate complex **28** unfortunately only a few X-ray suitable single crystals could be picked between unreacted

starting material and powder bulk material with unknown composition. The attempted synthesis of the coordination compound in sufficient amounts failed and only the crystal structure could be determined which is shown in the SI (Figure S13).



Scheme 6. Synthesis of the metal(II) based styphnate complexes **33**–**37**.

10.2.2 Crystal Structures

All complexes (except **4**, **5**, **7**–**9**, **12**, **14** and **16**) were characterized using low temperature single crystal X-ray diffraction. Details on the crystal structures of complexes **3**, **11**, **15**, **17**, **18**, **20**, **21**, **23**–**26**, **28**–**30**, **32** and **34**–**37** are given in the SI together with the measurement and refinement data. The single crystals of the cobalt(II) and nickel(II) nitrate complexes **8** and **9** were measured to give an indication of the most likely structures. Finalization of the data set was not possible because of the strongly disordered moieties and the related weak diffractions. The complexes **8** and **9** exhibit the same coordination environment and were therefore compared with **10** by infrared spectroscopy to confirm its structure (Figure S21). The crystal structures were uploaded to the CSD database[37] and can be obtained free of charge with the CCDC nos. 1566368 (**2**), 1566362 (**3**), 1566371 (**6**), 1566381 (**10**), 1566384 (**11**), 1566379 (**13**), 1566370 (**15**), 1566366 (**17**), 1566363 (**18**), 1566364 (**19**), 1566361 (**20**), 1566359 (**21**), 1566380 (**22**), 1566382 (**23**), 1566385 (**24**), 1566386 (**25**), 1566360 (**26**), 1566378 (**27**), 1566377 (**28**), 1566376 (**29**), 1566372 (**30**), 1566375 (**31**), 1566383 (**32**), 1566373 (**33**), 1566367 (**34**), 1566374 (**35**), 1566365 (**36**), 1566369 (**37**). The bond lengths and angles of the coordinating and non- coordinating MTZ rings in the investigated complexes are in the typical range of tetrazole ligands and similar to the non-coordinating ligand **1**.[38,39] The tetrazole ligand is therefore not discussed in detail in any of the following compounds. Coordination to the metal centers always takes place by the N4 nitrogen atom of 1-methyl-5*H*-tetrazole (**1**). All complexes with MTZ show an octahedral coordination sphere. This can be explained by the low steric hindrance of the ligand.

$[Fe(MTZ)_6](FeCl_4)_2$ (**2**) contains iron in the oxidation states +II and +III. It crystallizes in the form of yellow blocks in the trigonal space group *P*−3 with one formula unit per unit cell and a calculated density of 1.747 g cm^{-3} at 123 K. The molecular unit consists of six asymmetric unit cells with a octahedrally coordinated iron(II) center, which is bonded to six MTZ ligands (Fe1–N1 = 2.010(13) Å, < (N1—Fe1—N1^{i}) = 88.68(6)°). The second iron(III) atom is tetrahedrally coordinated by four chloride ligands (Fe2–Cl1 = 2.203(5) Å, < (Cl2—Fe2—Cl1^{vii}) = 109.49(2)°, (Cl1^{vi}—Fe2—Cl1^{vii}) = 109.46(2)°) forming the tetrachloridoferrate(III) counteranion (Figure 1).

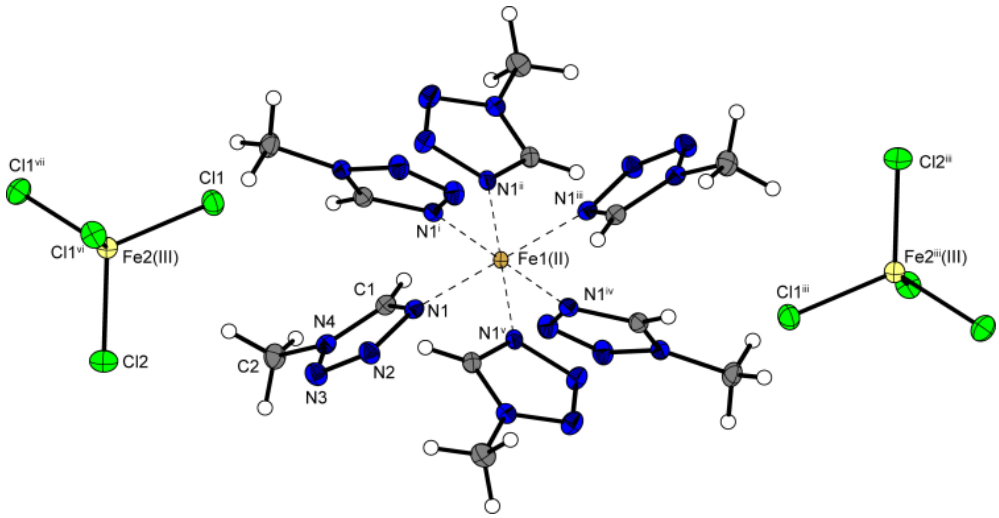


Figure 1. Molecular unit of $[Fe(MTZ)_6](FeCl_4)_2$ (**2**). Thermal ellipsoids of non-hydrogen atoms in all structures are set to the 50% probability level. Selected bond lengths (Å): Fe1–N1 2.010(13), Fe2–Cl2 2.185(8), Fe2–Cl1 2.202(5); selected bond angles (°): N1–Fe1–N1^{i} 88.68(6), N1–Fe1–N1^{ii} 91.32(6), Cl2–Fe2–Cl1^{vi} 109.49(2), Cl1^{vi}–Fe2–Cl1^{vii} 109.46(2). Symmetry codes: (i) y, −x+y, 1−z; (ii) −y, x−y, z; (iii) x−y, x, 1−z; (iv) −x+y, −x, z; (v) −x, −y, 1−z; (vi) −x+y, 1−x, z; (vii) 1−y, 1+x−y, z.

The cobalt(II) chlorido complex $[CoCl_2(MTZ)_4] \bullet 2$ MTZ (**6**) crystallizes in the form of yellow blocks in the monoclinic space group $P2_1/c$ with two formula units per unit cell and a calculated density of 1.617 g cm^{-3} at 123 K. In comparison to literature tetrazole containing complexes, most of the investigated compounds, show low densities, which can be attributed to the low density of MTZ itself.[40] The molecular unit contains two cocrystallized non-coordinating MTZ molecules, which are stabilized by non-covalent interactions and an octahedrally coordinated cobalt(II) cation. The metal(II) center is coordinated (Figure 2) by two chlorido ligands in axial positions and by four MTZ molecules in a plane (Co1–N1 = 2.143(6) Å, Co1–N5 = 2.161(6) Å, Co1–Cl1 = 2.443(2) Å). The deviation of the ideal coordination sphere is marginal (< (N1—Co1—N1) = 89.52(2)°, < (Cl11—Co1—N5) = 90.48(2)°, < (N1—Co1—N5) = 87.7(2)°).

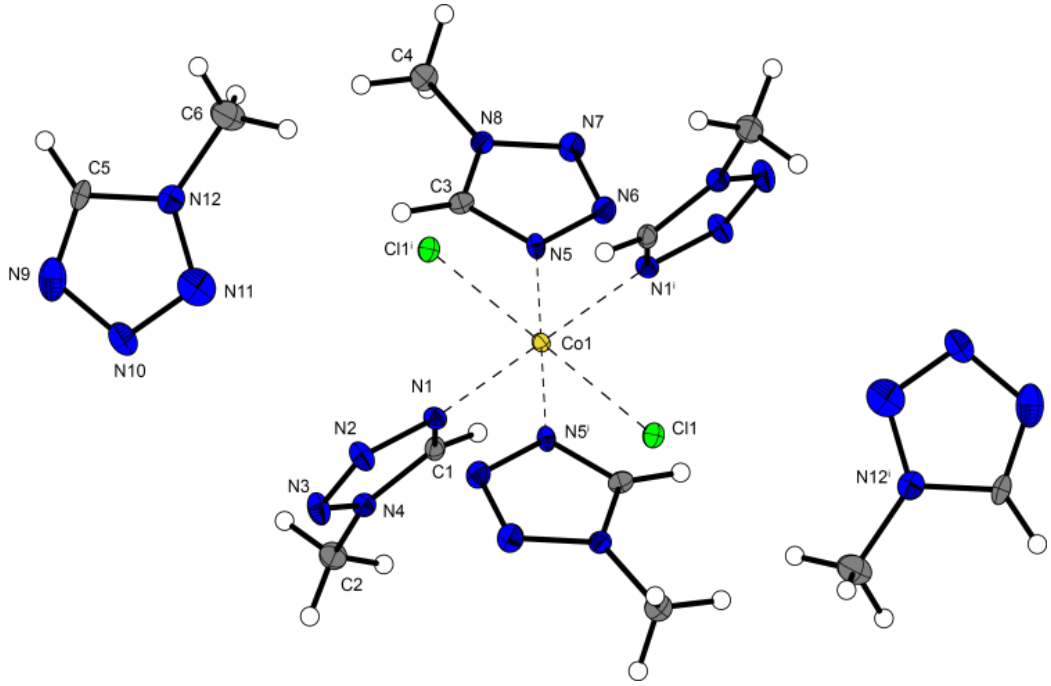


Figure 2. Molecular unit of $[CoCl_2(MTZ)_4]$ • 2 MTZ (**6**). Selected bond lengths (Å): Co1–N1 2.143(6), Co1–N5 2.161(6), Co1–Cl1 2.443(2); selected bond angles (°): Cl1–Co1–N1 89.52(2), Cl1–Co1–N5 90.48(2), N1–Co1–N5 87.7(2). Symmetry code: (i) −x, 1−y, −z.

The complexes **10** (colorless block) and **11** (blue block) with nitrate counterions are crystallizing isotypically in the triclinic space group *P*−1 with two formula units per unit cell showing almost the same metric (see Table S1 in the SI) and densities: **10**: 1.608 g cm^{-3} and **11**: 1.626 g cm^{-3} at 123 K.

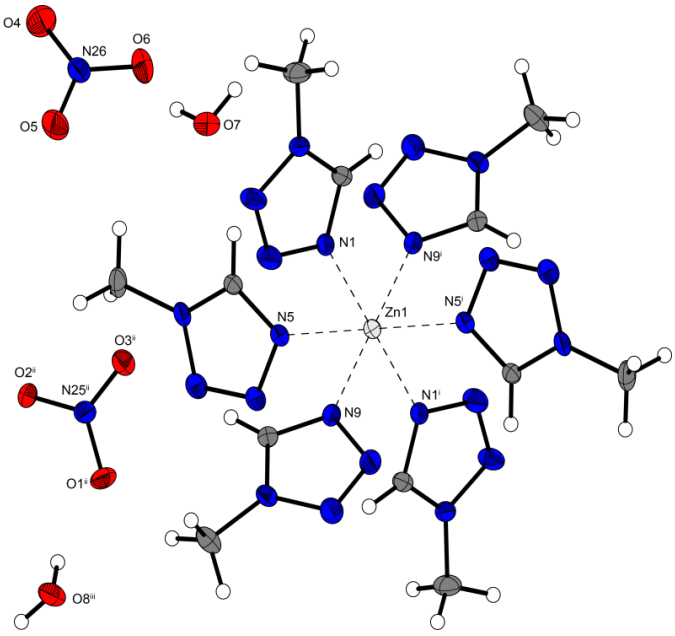


Figure 3. Molecular unit of $[Zn(MTZ)_6](NO_3)_2$ • 2 H_2O (**10**). Selected bond lengths (Å): Zn1–N5 2.139(2), Zn1–N1 2.166(2), Zn1–N9 2.185(2), O2–N25 1.257(3), O3–N25 1.250(3), O4–N26 1.223(4);

selected bond angles (°): N5–Zn1–N1 88.91(8), N5^{i}–Zn1–N1 91.09(8), N5–Zn1–N9^{i} 91.77(8), N5^{i}–Zn1–N9^{i} 88.23(8), N1–Zn1–N9^{i} 89.51(8), N1^{i}–Zn1–N9^{i} 90.49(8), O3–N25–O2 120.0(2), O1–N25–O2 119.8(2), O4–N26–O5 120.6(3), O4–N26–O6 119.8(3), O5–N26–O6 119.5(3). Symmetry codes: (i) 2−x, 2−y, −z; (ii) 2−x, 1−y, 1−z.

Both metal(II) centers have an octahedral coordination sphere with six MTZ ligands (Figure 3 and S2). As expected, the d^{9}-ion copper(II) ion in **11** shows Jahn-Teller distortion along its axial coordination sphere. In comparison, the respective zinc(II) complex exhibits a nearly undistorted coordination sphere and the six surrounding MTZ´s is nearly undistorted (Zn1–N5 = 2.139(2) Å, Zn1–N1 = 2.166(2) Å, < (N5^{i}—Zn1—N9^{i}) = 88.23(8)°, < (N1—Zn1—N9^{i}) = 89.51(8)°).

The silver(I) complex **13** crystallizes in the monoclinic space group $P2_1/c$ with four formula units per unit cell and a calculated density of 2.112 g cm^{-3} at 123 K. Every silver(I) center is penta-coordinated by two MTZ ligands and two bridging nitrates (Figure 4).

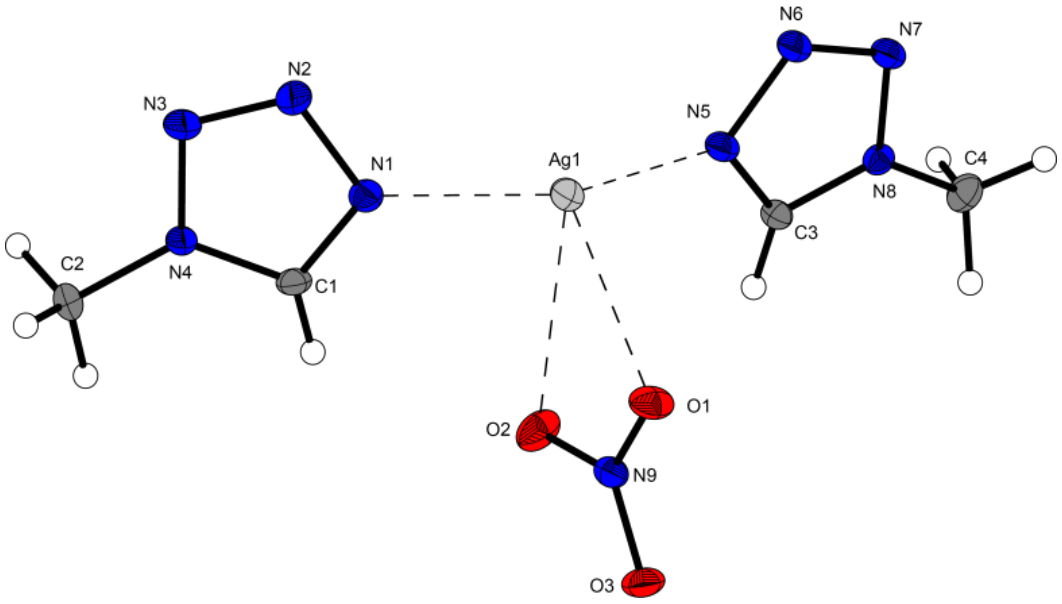


Figure 4. Molecular unit of [AgNO$_3$(MTZ)$_2$] (**13**). The fifth ligand from an adjacent nitrate was omitted for clarity. Selected bond lengths (Å): Ag1–N1 2.233(3), Ag1–N5 2.255(3), Ag1–O1 2.544(3), Ag1–O3^{i} 2.545(3), Ag1–O2 2.719(3), O1–N9 1.251(4), O2–N9 1.257(5), O3–N9 1.252(4); selected bond angles (°): N1–Ag1–N5 137.76(12), N1–Ag1–O1 111.85(11), N5–Ag1–O1 95.09(11), N1–Ag1–O3^{i} 119.23(11), N5–Ag1–O3^{i} 95.82(11), O1–Ag1–O3^{i} 81.30(10), O1–N9–O3 120.7(3), O1–N9–O2 119.6 (3), O3–N9–O2 119.7(3). Symmetry codes: (i) 1+x, y, z; (ii) −1+x, y, z.

The nitrato ligand binds through all of its three oxygen atoms. In addition to a bidentate coordination mode to one silver(I) cation, the nitrato ligand is also bound in a monodentate fashion to a second silver(I) ion, bridging the two cations and forming polymeric chains along

the *a* axis (Figure 5). The distances between silver(I) and oxygen (Ag1–O1 = 2.544(3) Å, Ag1–O3^{i} 2.545(3) Å, Ag1–O2 2.719(3) Å) are longer than the silver(I) nitrogen distances (Ag1–N1 = 2.233(3) Å, Ag1–N5 = 2.255(3) Å).

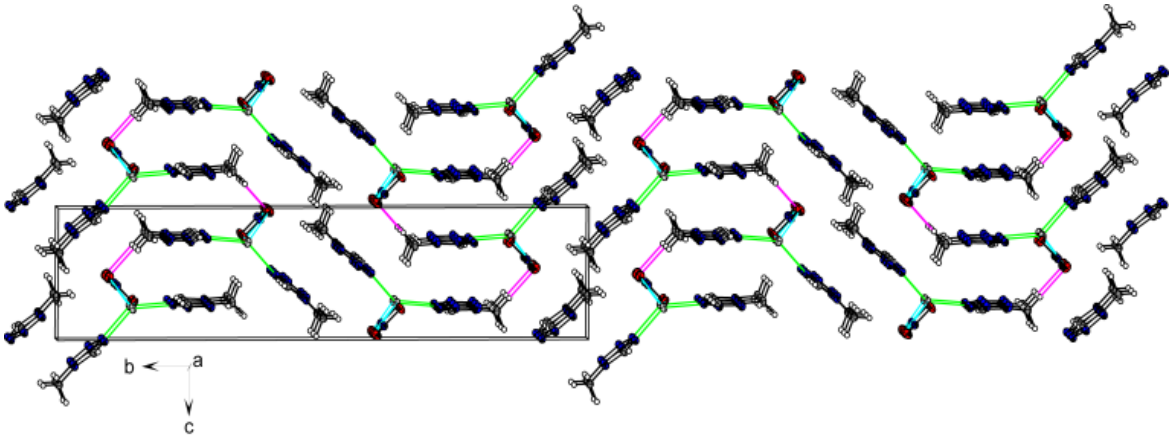


Figure 5. View on the structure of **13** along the *a* axis (Ag–O bonds = cyan; Ag–N bonds = green). Stabilization through non-classical hydrogen bonds (C–H··N and C–H··O; C–H··O hydrogen bonds = purple) and hydrophobic interactions between the methyl groups.

The complexes with perchlorate counterions **15**/**20** and **17**/**18** crystallize isotypically in monoclinic and trigonal space groups (**15**: $P2_1/n$, 1.582 g cm^{-3} (Figure S3); **17**: $R\bar{3}$, 1.614 g cm^{-3} (Figure S4); **18**: $R\bar{3}$, 1.629 g cm^{-3} (Figure S5); **20**: $P2_1/n$, 1.635 g cm^{-3} at 123 K (Figure S6)). The blue copper(II) perchlorate compound **19** is the only complex that crystallizes in the triclinic space group $P\bar{1}$ with two formula units per unit cell and a calculated density of 1.645 g cm^{-3} at 123 K, which is the highest of all perchlorates. Its molecular motif is illustrated in Figure 6. Each metal(II) center contains an octahedral surrounding and is connected to six tetrazole ligands. As already observed in the coordination environment of the cation in **11**, the copper(II) center shows a Jahn-Teller distortion caused by the d^9-configuration (Cu1−N1 2.035(2) Å, Cu1−N5 2.014(2) Å, Cu1−N9 2.401(2) Å).

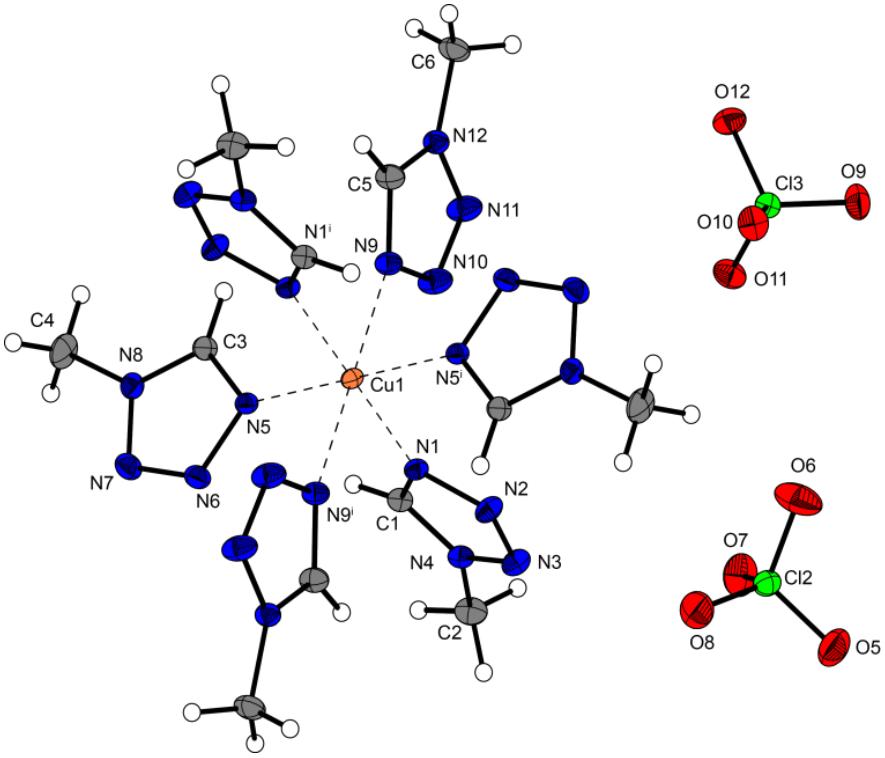


Figure 6. Complex unit of $[Cu(MTZ)_6](ClO_4)_2$ (**19**). Selected bond lengths (Å): Cu1–N1 2.035(2), Cu1–N5 2.014(2), Cu1–N9 2.401(2), Cl2–O5 1.437(2); selected bond angles (°): N1–Cu1–N5 89.83(2), N1–Cu1–N9 91.04(2), N5–Cu1–N9 89.54(2), O5–Cl2–O6 109.32(2). Symmetry codes: (i) −x, 2−y, −z; (ii) 1−x, −y, 1−z; (iii) 1−x, 1−y, 1−z; (iv) −x, 1−y, −z.

New perchlorate species **21**–**26** of the investigated metals(II) were obtained after using an excess of the tetrazole ligand during the synthesis. The complexes with two cocrystallized tetrazoles crystallize isotypically in the triclinic space group *P*−1 with one formula unit per unit cell and similar densities. However, their densities increase in the row of Mn^{2+} (1.590 g cm^{-3}; 123 K) < Fe^{2+} (1.592 g cm^{-3}; 173 K) < Co^{2+} (1.612 g cm^{-3}, 143 K) < Ni^{2+} (1.621 g cm^{-3}; 143 K) < Cu^{2+} (1.623 g cm^{-3}; 143 K) < Zn^{2+} (1.630 g cm^{-3}; 123 K). The molecular structure of complex **22** is shown in Figure 7 and used exemplarily for all complexes. Again, two additional non-coordinating MTZ molecules could be cocrystallized. Six regular tetrazole ligands are surrounding the transition metal(II) centers in octahedral arrangements and interact hydrophobically and through non-classical hydrogen bonds with the cocrystallized compounds.

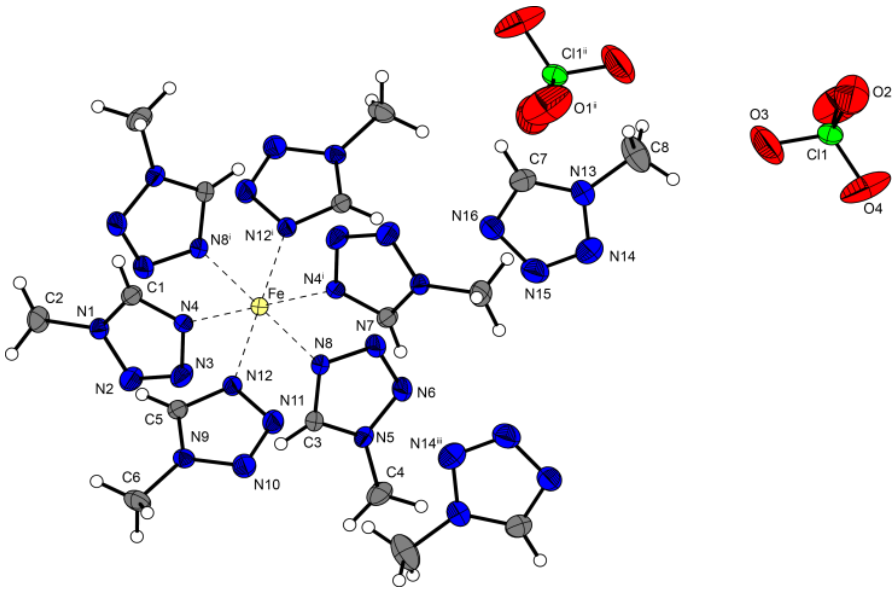


Figure 7. Complex unit of $[Fe(MTZ)_6](ClO_4)_2 \bullet 2$ MTZ (**22**). Selected bond lengths (Å): Fe1–N12 2.181(2), Fe1–N4 2.183(2), Fe1–N8 2.194(2), Cl1–O4 1.405(4); selected bond angles (°): N12–Fe1–N4 89.53(8), $N12^{i}$–Fe1–N4 90.48(8), O1–Cl1–O4 108.1(2), N12– Fe1–$N8^{i}$ 91.61(8), $N12^{i}$–Fe1–$N8^{i}$ 88.39(8), N4–Fe1–$N8^{i}$ 89.63(8), $N4^{i}$–Fe1–$N8^{i}$ 90.37(8), $N12^{i}$–Fe1–N8 91.61(8). Symmetry codes: (i) −x, −y, 1−z; (ii) 1−x, 1−y, −z; (iii) 1−x, 1−y, 1−z.

The cyanodinitromethanide complex **27** crystallizes in the form of blue blocks in the triclinic space group *P*−1 with one formula unit per unit cell and a calculated density of 1.746 g cm^{-3} at 123 K. The molecular unit is built up of two asymmetric unit cells. The octahedral complex (Figure 8), with four MTZ ligands in a plane (Cu1–N8 = 2.002(16) Å, Cu1–N1 = 2.019(19) Å, < ($N8^{i}$–Cu1–$N7^{i}$) = 88.54(6)°, < ($N1^{i}$–Cu1–$N7^{i}$) = 90.72(7)°), shows, elongation along the axial positions, which are occupied by two cyanodinitromethanide anions (Cu1–N7 = 2.412(18) Å). The structure of the CDNM anion is comparable to literature values.[41]

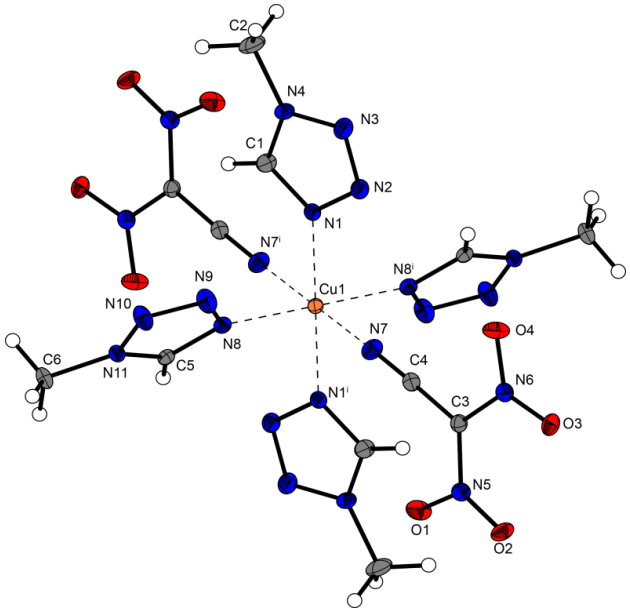


Figure 8. Molecular unit of $[Cu(CDNM)_2(MTZ)_4]$ (**27**). Selected bond lengths (Å): Cu1–N8 2.002(16), N6–C3 1.399(2), N7–C4 1.151(3), Cu1–N1 2.019(19), C3–C4 1.407(3), Cu1–N7 2.412(18), N5–C3 1.394(3), O2–N5 1.238 (2), O4–N6 1.243(3); selected bond angles (°): N8–Cu1–$N1^i$ 91.31(7), $N8^i$–Cu1–$N1^i$ 88.69(7), N8–Cu1–$N7^i$ 91.46(6), $N1^i$–Cu1–$N7^i$ 90.72(7), N1–Cu1–$N7^i$ 89.28(7), N8–Cu1–N7 88.54(6), O3–N6–O4 122.53(17), O3–N6–C3 122.02(18), O4–N6–C3 115.45(16), C1–N1–N2 106.45(18), N5–C3–N6 124.47(17), N5–C3–C4 117.23(16), N7–C4–C3 178.0(2). Symmetry code: (i) 1−x, −y, −z.

The manganese(II) **28** and cobalt(II) **29** picrate complexes crystallize isotypically in the monoclinic space group $P2_1/c$ with two formula units per unit cell and calculated densities of 1.746 g cm^{-3} at 123 K for **28** and 1.786 g cm^{-3} at 173 K for **29**. Their molecular units consist of two MTZ ligands, four aqua ligands, two crystal water and two non-coordinating picrate counteranion (Figure S12/13). The same monoclinic space group $P2_1/c$ could be observed for the nickel(II) picrate complex **30** (1.757 g cm^{-3} at 123 K), which shows a different molecular composition with no crystallized water molecules, two aqua and four MTZ ligands (Figure S14). Among the metal(II) picrate complexes, only the copper(II) **31** and zinc(II) **32** complexes crystallize water-free in monoclinic space groups (**31**: $P2_1/c$; **32**: $P2_1/n$) with two formula units per unit cell and calculated densities of 1.828 g cm^{-3} at 123 K for **31** and 1.724 g cm^{-3} at 173 K for **32**.

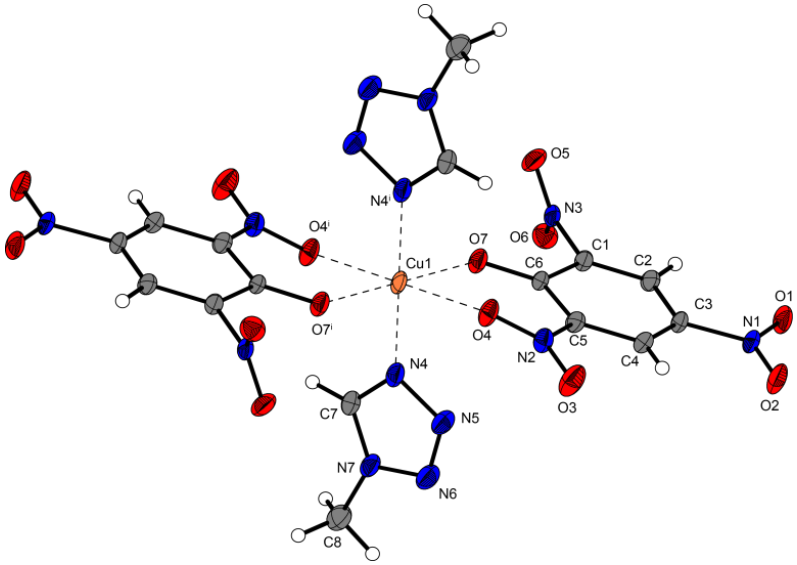


Figure 9. Molecular unit of the copper(II) picrate complex **31**. Selected bond lengths (Å): Cu1–N4 2.001(3), Cu1–O4 2.354(2), Cu1–O7 1.929(2); selected bond angles (°): O4–Cu1–N4 91.63(9), O7–Cu1–N4 91.07(9), O4–Cu1–O7 79.32(9). Symmetry code: (i) 1−x, 1−y, −z.

In comparison to the other picrate compounds discussed so far, the trinitrophenolate counteranions coordinate bidentately to the copper(II) (via the nitro- and deprotonated phenolate-groups) and monodentately to the zinc(II) metal cations in **31**/**32**. The remaining coordination sites of the octahedron are occupied by two methyltetrazole ligands in **31** (Figure 9) and by four tetrazoles in **32** (Figure S15). The octahedral geometry of **31** shows deviations to the ideal 90° angle caused by the fixed structure of the picrate anion and its Jahn-Teller distortion along the O4–Cu1–O4^{i} axis (< (O4–Cu1–N4) = 91.63(9)°, < (O7–Cu1–N4) = 91.07(9)°, < (O4–Cu1–O7) = 79.32(9)°).

The manganese(II) styphnate complex **33** interestingly crystallizes isotypically to the zinc(II) picrate complex **32** with almost the same density (1.732 g cm^{-3} at 123 K) but with different anionic ligands, and is depicted in Figure 10.

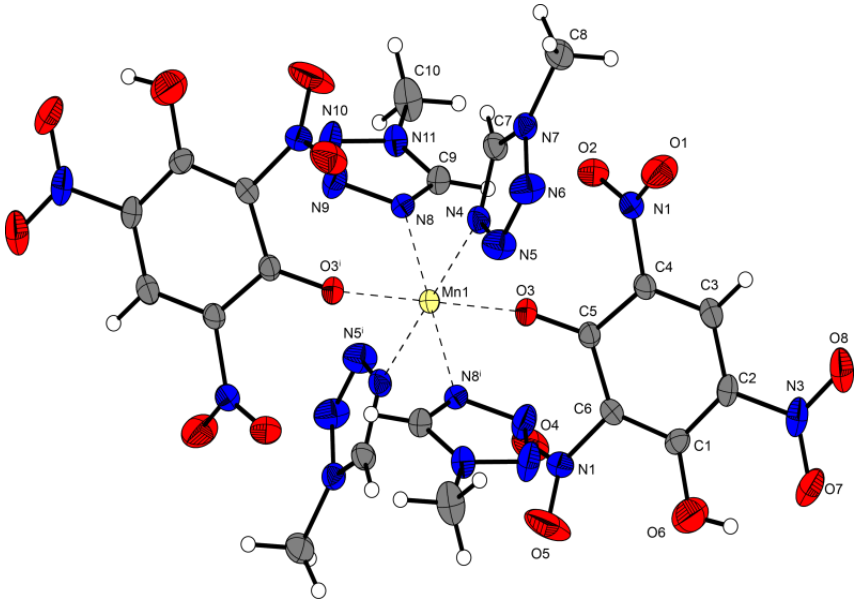


Figure 10. Molecular unit of $[Mn(HTNR)_2(MTZ)_4]$ (**33**). Selected bond lengths (Å): Mn1–O3 2.156(2), Mn1–N4 2.250(3), Mn1–N8 2.239(3); selected bond angles (°): O3–Mn1–N4 93.04(9), O1–Mn1–N8 85.42(11), N4–Mn1–N8 92.18(10). Symmetry code: (i) −x, 2−y, −z.

The cobalt(II) **34** and nickel(II) **35** styphnate complexes (Figures S16 and 17) crystallize isotypically to each other and to the picrate complexes **28**/**29**. A similar situation can be observed for complex **36**, which exhibits a similar coordination sphere like **31** with analogous cell parameters but with styphnates instead of picrates (Figure S18). The zinc(II) complex **37** has the same sum formula as compound **36**, but crystallizes triclinic in the space group *P*−1 and a different metal center (Figure S19).

10.2.3 Sensitivities and Thermal Stability

Thermal measurements of highly energetic and sensitive complexes are very challenging since larger quantities (> 2 mg) can damage the instrument seriously. On the other hand, endothermic signals may not be detected properly when using an insufficient amount. Endothermic events like dehydration, melting or loss of cocrystallized/coordinating MTZ molecules, as well as other critical temperatures of the described compounds were measured with a heating rate of β = 5 °C min^{-1} via differential thermal analysis, differential scanning calorimetry or by thermal gravimetric analysis. The measured onset temperatures are summarized in Tables 1 and 2. Details on the DTA plots of complexes **1**–**10**, **12**–**14**, **27** and **29**–**37** are given in the Supporting Information. Most of the complexes have exothermic decomposition events higher or close to 200 °C, which is in the range of the uncoordinated ligand **1** (T_{exo}: 206 °C).

Table 1. Thermal stability measurements of **1**–**10** and **11**–**20** by DTA.

compound	$T_{endo1.}$ (°C)[a]	$T_{endo2.}$ (°C)[a]	$T_{exo.}$ (°C)[b]
MTZ (**1**)	39	—	206
$[Fe(MTZ)_6](FeCl_4)_2$ (**2**)	—	—	236
$[MnCl_2(MTZ)_2]$ (**3**)	—	—	234
$[CuCl_2(MTZ)_2]$ (**4**)	185	—	199
$[ZnCl_2(MTZ)_2]$ (**5**)	184	—	204
$[CoCl_2(MTZ)_4]$ • 2 MTZ (**6**)	66	—	206
$[NiCl_2(MTZ)_4]$ • 2 MTZ (**7**)	106	—	199
$[Co(MTZ)_6](NO_3)_2$ • 2 H_2O (**8**)	—	—	199
$[Ni(MTZ)_6](NO_3)_2$ • 2 H_2O (**9**)	86	166	194
$[Zn(MTZ)_6](NO_3)_2$ • 2 H_2O (**10**)	50–75[c]	—	196
$[Cu(MTZ)_6](NO_3)_2$ (**12**)	—	—	160
$[AgNO_3(MTZ)_2]$ (**13**)	—	—	119
$[Co(NH_3)_4(MTZ)_2](ClO_4)_3$ (**14**)	—	—	201
$[Mn(MTZ)_6](ClO_4)_2$ (**15**)	—	—	223
$[Fe(MTZ)_6](ClO_4)_2$ (**16**)	—	—	213
$[Co(MTZ)_6](ClO_4)_2$ (**17**)	—	—	253
$[Ni(MTZ)_6](ClO_4)_2$ (**18**)	—	—	271
$[Cu(MTZ)_6](ClO_4)_2$ (**19**)	178	—	211
$[Zn(MTZ)_6](ClO_4)_2$ (**20**)	196	—	221

Onset temperatures at a heating rate of 5 °C min^{-1}; [a] endothermic peak, which indicates melting, dehydration or loss of coordinating/cocrystallized MTZ molecules; [b] exothermic peak, which indicates decomposition; [c] weight loss detected by TGA.

Table 2. Thermal stability measurements of **21**–**27** and **29**–**37** by DTA.

compound	$T_{endo1.}$ (°C)[a]	$T_{endo2.}$ (°C)[a]	$T_{exo.}$ (°C)[b]
$[Mn(MTZ)_6](ClO_4)_2$ • 2 MTZ (**21**)	105	—	216
$[Fe(MTZ)_6](ClO_4)_2$ • 2 MTZ (**22**)	111	—	215
$[Co(MTZ)_6](ClO_4)_2$ • 2 MTZ (**23**)	107	—	210
$[Ni(MTZ)_6](ClO_4)_2$ • 2 MTZ (**24**)	93	—	207
$[Cu(MTZ)_6](ClO_4)_2$ • 2 MTZ (**25**)	78	—	206
$[Zn(MTZ)_6](ClO_4)_2$ • 2 MTZ (**26**)	108	—	212
$[Cu(CDNM)_2(MTZ)_4]$ (**27**)	—	—	201
$[Co(H_2O)_4(MTZ)_2](PA)_2$ • 2 H_2O (**29**)	61[c]	79[c]	248
$[Ni(H_2O)_4(MTZ)_2](PA)_2$ (**30**)	106	—	211
$[Cu(PA)_2(MTZ)_2]$ (**31**)	—	—	226
$[Zn(PA)_2(MTZ)_4]$ (**32**)	92	—	212
$[Mn(HTNR)_2(MTZ)_4]$ (**33**)	141	—	202
$[Co(H_2O)_4(MTZ)_2](HTNR)_2$ • 2 H_2O (**34**)	70	80	200
$[Ni(H_2O)_4(MTZ)_2](HTNR)_2$ • 2 H_2O (**35**)	86	105	227
$[Cu(HTNR)_2(MTZ)_2]$ (**36**)	—	—	231
$[Zn(HTNR)_2(MTZ)_2]$ (**37**)	—	—	214

Onset temperatures at a heating rate of 5 °C min^{-1}; [a] endothermic peak, which indicates melting, dehydration or loss of coordinating/cocrystallized MTZ molecules; [b] exothermic peak, which indicates decomposition; [c] measured by DSC.

However, endothermic decompositions e.g. loss of water or ligand have been observed partly at lower temperatures. Both nitrate complexes **12** and **13**, which decompose exothermically at relatively low temperatures of 160 °C (**12**) and 119 °C (**13**), showed the lowest thermal stabilities of all investigated compounds. Comparing them to the other coordination compounds bearing the same metal ion, but different anions, no general trend regarding their decomposition temperatures could be observed.

Exceptional endothermic events during the DTA measurements could be observed for the complexes (**4**, **5**, **9**, **19**, **20**, **32**, **33**) and were further investigated by thermal gravimetric analysis (Figure 11 and Figure S27). The free ligand **1**, which has a relatively low melting point of 39 °C, shows a continuous weight loss at elevated temperatures until its exothermic decomposition temperature is reached. This fact can be attributed to its high vapor pressure and could be a possible explanation for the observed endothermic peaks in the DTA plots for the above-mentioned complexes. Comparable phenomena have been reported in the literature.[42,43] The endothermic loss of two coordinating MTZ molecules in the complexes **19** and **32** leads most likely to an intermediate species, which decomposes at a later stage exothermically (similar to compounds **20** and **33**). Various decomposition paths and mechanisms are possible. The tendency of vaporization of the ligands and the relating bond strength of the coordinating tetrazoles is strongly dependent on the metal ($MnCl_2$ (**3**) vs. $CuCl_2$ (**4**)/ $ZnCl_2$ (**5**)), anion ($Ni(NO_3)_2$ (**9**) vs $Ni(ClO_4)_2$ (**18**)) and the corresponding coordination environment of the complexes. For example, the monodentate picrate complex **32** disintegrates in two stages (loss of two ligands followed by exothermic event) whereas the bidentate styphnate complex **36** decomposes in only one single stage.

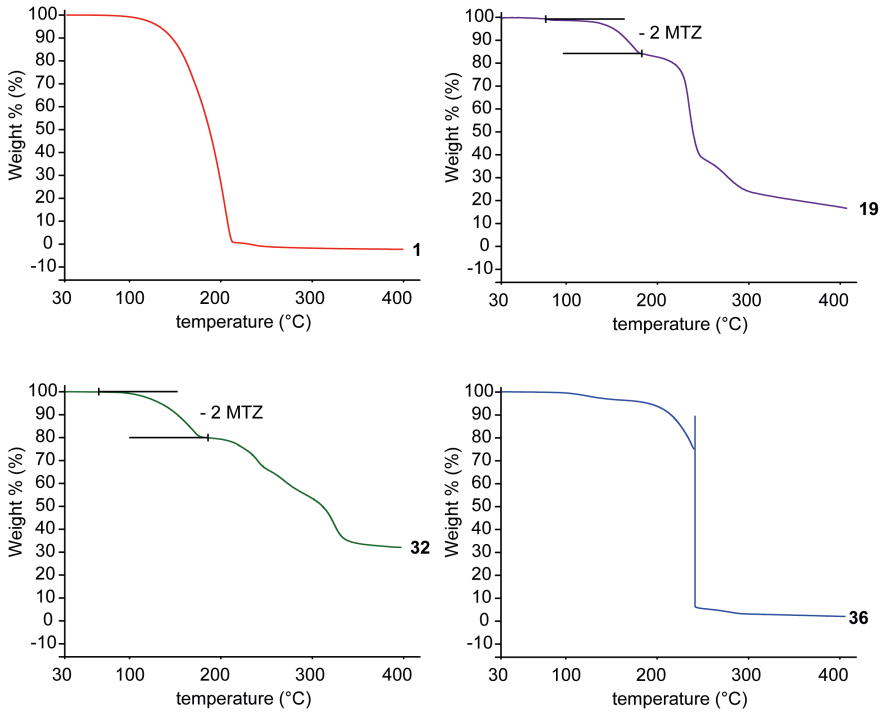


Figure 11. TGA measurements (5 °C min^{-1}) of the selected compounds.

The thermal stability of the metal(II) MTZ perchlorate complexes (Figure 12) increases in the following order: Cu^{2+} (211 °C) < Fe^{2+} (213 °C) < Zn^{2+} (221 °C) < Mn^{2+} (223 °C) < Co^{2+} (253 °C) < Ni^{2+} (271 °C). For previous compounds a similar trend has been reported in

literature.[44] The cocrystal perchlorate complexes **21**–**26** (Figure 13) as well as the chlorides **6**/**7** lose their cocrystallized MTZ molecules in the range between 66–111 °C and are slightly less temperature stable than their corresponding perchlorate compounds **15**–**20**. The aqua ligand and crystal water containing complexes can by dehydrated after heating demonstrated by an endothermic peak in the DTA/DSC plots or by weight loss during the TGA measurements.

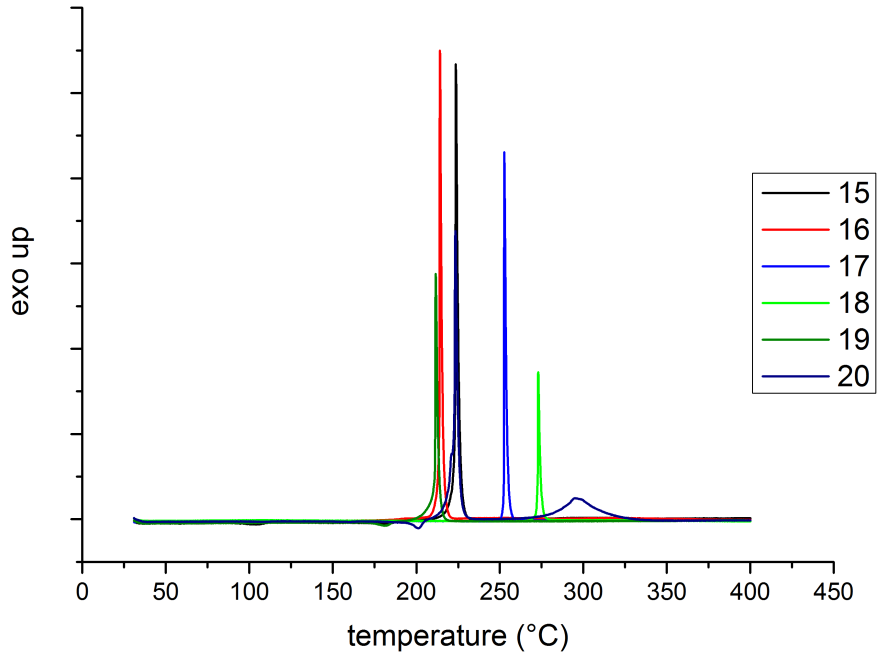


Figure 12. DTA plots (5 °C min^{-1}) of the perchlorate complexes **15**–**20**.

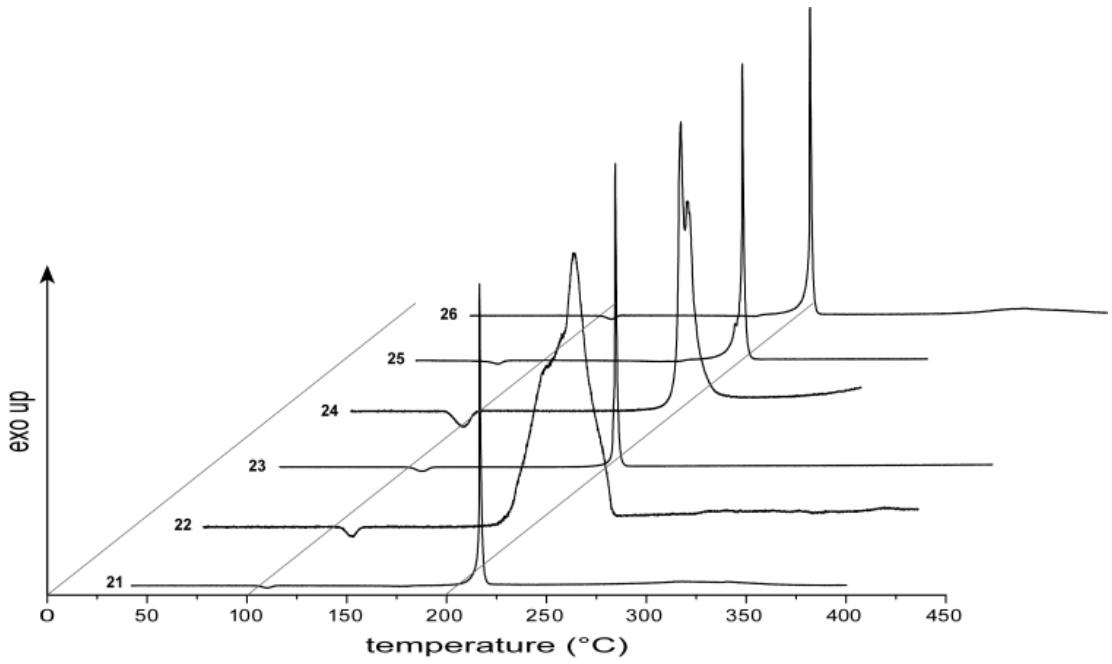


Figure 13. DTA plots (5 °C min^{-1}) of the perchlorate cocrystal compounds **21**–**26**.

The sensitivities toward impact, friction and electrostatic discharge for the compounds were determined according to BAM standards. In addition, the compounds have been classified in accordance to the "UN Recommendations on the Transport of Dangerous Goods" using the measured values. An overview of the sensitivities is given in Table 3. The uncoordinated ligand **1** has sensitivities greater than 40 J, greater than 360 N for friction and an ESD value of 1.50 J and can therefore be classified as insensitive. The chloride complexes **3**–**8** are insensitive toward impact, friction and ESD. Introduction of oxidizing anions like nitrates, cyanodinitromethanides, picrates or styphnates increases the sensitivity against impact, friction and ESD under most circumstances (impact: 2–40 J; friction: 160–360 N; ESD: 0.13–1.50 J). All water-free complexes with trinitrobenzene-derivatives as anions are more sensitive toward mechanical stimuli compared with their crystal water or aqua ligand containing analogs. The perchlorate complexes **14**–**26** are sensitive toward impact (1–10 J) and vary from sensitive to very sensitive against friction (54–216 N). The stability toward impact of the $[M^{II}(MTZ)_6](ClO_4)_2$ complexes (Figure S28) decreases in the order: Zn^{2+} (10 J) < Mn^{2+} (7 J) < Ni^{2+} (5 J) < Co^{2+} (3 J) < Cu^{2+} (2.5 J) < Fe^{2+} (1 J) and in the following order toward friction: Zn^{2+} (120 N) ≈ Mn^{2+} (120 N) < Ni^{2+} (60 N) ≈ Co^{2+} (60 N) ≈ Fe^{2+} (60 N) < Cu^{2+} (54 N). Similar trends have been observed in literature in correlation to energetic metal(II) diaminotetrazole perchlorate complexes.[45] Cocrystallization of the nitrogen-rich ligand (**21**–**26**) leads in most cases to a decrease in sensitivities toward mechanical stimuli in comparison to the related perchlorate complexes (Figure S29) while maintaining its highly energetic character and is therefore a great concept for the desensitization of energetic complexes (Figure 14).

Table 3. Sensitivities toward impact, friction and ESD of **1**, **3**–**10**, **12**–**27** and **29**–**37**.

compound	*IS* (J)[a]	*FS* (N)[b]	*ESD* (J)[c]	Grain size (µm)
1	> 40	> 360	1.50	< 100
3	> 40	> 360	1.50	100–500
4	> 40	> 360	1.30	500–1000
5	> 40	> 360	1.50	< 100
6	> 40	> 360	1.00	< 100
7	> 40	> 360	0.80	< 100
8	> 40	> 360	1.50	< 100
9	> 40	324	1.50	100–500
10	> 40	> 360	0.40	100–500
12	> 40	> 360	1.50	100–500
13	40	160	0.15	< 100
14	9	160	0.036	< 100
15	7	120	0.08	< 100
16	1	60	0.10	< 100
17	3	60	0.50	< 100
18	5	60	0.10	< 100
19	2.5	54	0.08	< 100
20	10	120	0.25	< 100
21	7	216	0.46	100–500
22	10	120	0.40	100–500
23	10	80	0.13	500–1000

24	6	192	0.20	< 100
25	7	72	0.20	500–1000
26	10	144	0.60	100–500
27	4	324	1.50	100–500
29	> 40	> 360	1.00	100–500
30	> 40	> 360	1.50	100–500
31	4	> 360	0.30	500–1000
32	15	> 360	0.25	100–500
33	15	288	0.20	100–500
34	25	> 360	0.23	100–500
35	25	> 360	0.15	< 100
36	2	160	1.50	100–500
37	4	240	0.80	500–1000

[a] Impact sensitivity according to the BAM drophammer (method 1 of 6); [b] friction sensitivity according to the BAM friction tester (method 1 of 6); [c] electrostatic discharge sensitivity (OZM ESD tester); Impact: insensitive > 40 J, less sensitive ≥ 35 J, sensitive ≥ 4 J, very sensitive ≤ 3 J; Friction: insensitive > 360 N, less sensitive = 360 N, sensitive < 360 N and > 80 N, very sensitive ≤ 80 N, extremely sensitive ≤ 10 N. According to the UN Recommendations on the Transport of Dangerous Goods.

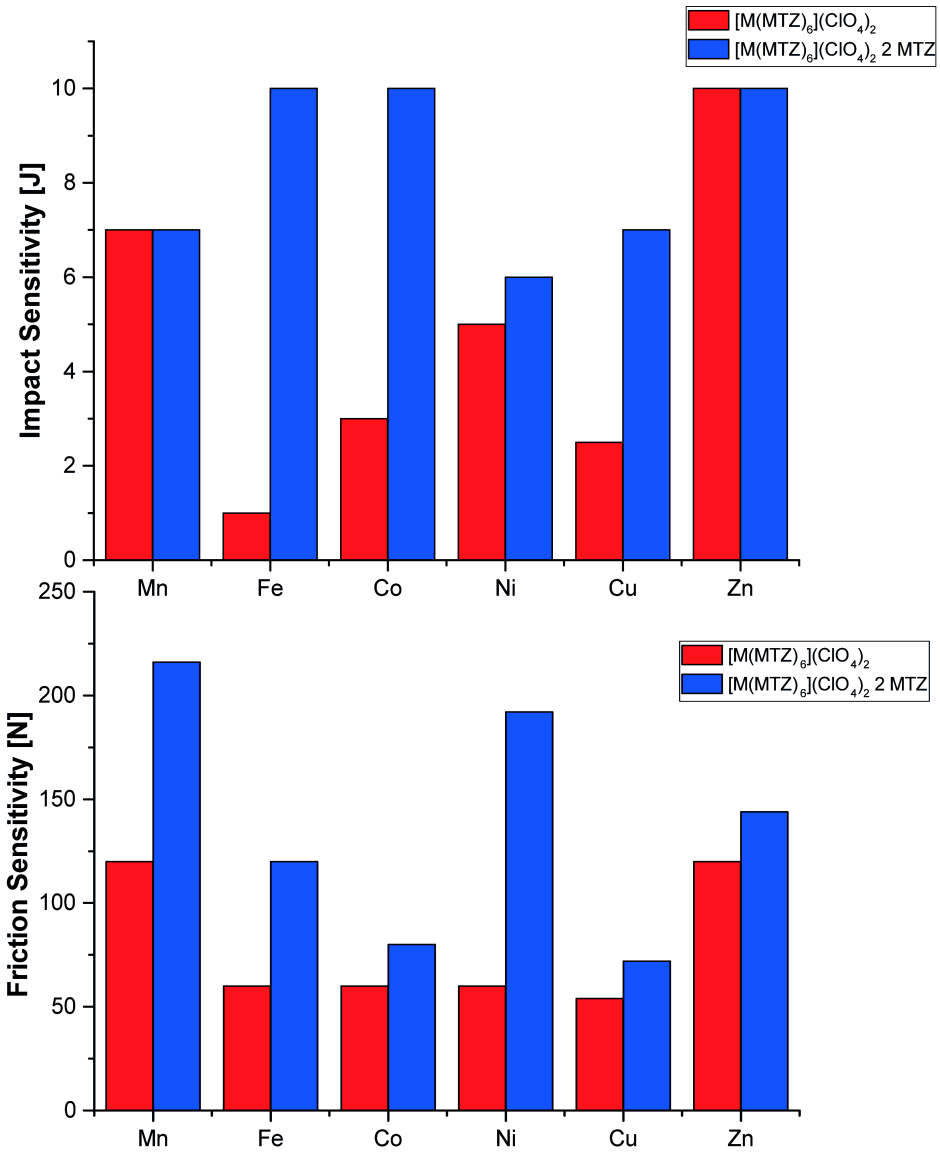


Figure 14. Comparison of the impact and friction sensitivities of both the metal perchlorates with and without cocrystallization of 1-methyl-5*H*-tetrazole (**1**).

Hot needle and hot plate tests of the investigated compounds **16**, **19** and **25** showed deflagrations (Figure 15 and Figure S30–33). The samples were fixed on an aluminum plate using adhesive tape. Detonation of the compound typically indicates a valuable primary explosive. The safe and practicable hot plate test shows only the behavior of the unconfined sample toward fast heating on a copper plate. It does not necessarily allow any conclusions on a compound`s capability as a primary explosive.

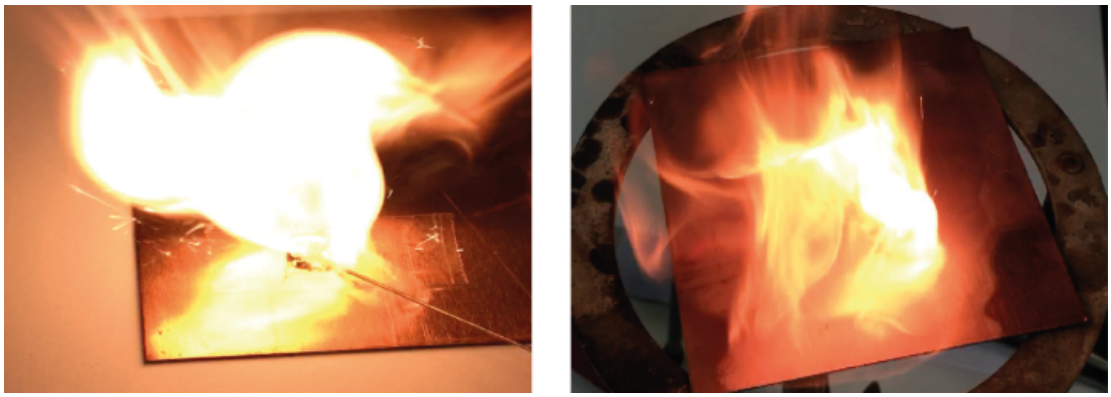


Figure 15. Moment of deflagration of compound **16** during the hot needle tests (left) and hot plate test (right).

10.2.4 Toxicity

The toxicity of the uncoordinated free ligand 1-methyl-5*H*-tetrazole (**1**) was determined together with the most promising perchlorate complexes **16**, **19** and **25** using the known luminescence bacteria inhibition test in aqueous media.[46] The luminescent marine bacterium Vibrio fischeri NRRL-B-11177, which is part of the commercially available bioassay system LUMIStox, is a representative species for other aquatic organisms and therefore a valuable indicating device when it comes to groundwater contamination. The half maximal effective concentration EC_{50} of these compounds was determined after an incubation time of 30 minutes. This toxicological parameter is defined as concentration of the investigated compound, at which the bioluminescence of the bacteria strain is halved after a certain exposure time (e.g 15 or 30 min) and then compared to the original bioluminescence of the sample before being treated. With EC_{50} (30 min) values of 5.45 g/L for the free tetrazole **1** and 1.66 g/L for the iron(II) perchlorate complex **16**, both compounds can be considered as non-toxic (toxicity level after 30 min incubation: very toxic < 0.10 g/L; toxic 0.10–1.00 g/L; non-toxic > 1.00 g/L).[47] As expected, the copper(II) perchlorate compounds showed half maximum effective concentrations of 0.13 g/L for **19** and 0.26 g/L for **25**. Therefore, both complexes have to be

classified as toxic, which is not surprising, due to the known toxicity of copper compounds toward microorganisms.[48]

10.2.5 Laser Initiation

Chavez *et al*. and our group showed that iron(II) and copper(II) perchlorate complexes of suitable ligands can be initiated in laser ignition experiments.[22,49] These compounds could be potential candidates for laser ignition systems in the future. About 15 mg of the carefully pestled complex to be investigated were filled into a transparent plastic cap, pressed with a pressure force of 1 kN and sealed by a UV-curing adhesive. The laser initiation experiments were carried out with a 45 W InGaAs laser diode operating in the single-pulsed mode. The diode was connected to an optical fiber with a core diameter of 400 µm and a cladding diameter of 480 µm. The optical fiber was coupled via a SMA type connecter directly to the laser and to a collimator. This collimator was linked to an optical lens, which was positioned in its focal distance (f = 29.9 mm) to the sample. The lens was protected from the explosive by a sapphire glass. Only complexes with sensitivities in the range of PETN (IS: ≥ 2.5 J, FS: ≥ 54 N) were tested in laser initiation experiments. These compounds show slightly increased sensitivities toward mechanical stimuli but are still safe to handle. The confined samples were irradiated at a wavelength of 915 nm, a pulse length of 15 ms, a varying current of 7–10 A and a voltage of 4 V, which combined results in an approximately energy output of 26–60 mJ. The investigated compounds (**14**–**20**, **22**, **24**, **25**, **27**, **31**, **36**, **37**) showed different responses to the laser irradiation depending on the used metal(II) and anion. The results of these tests are summarized in Table 4. No reaction was observed for the complexes **15**, **17**, **19** and **37** under the employed laser parameters. The other compounds could be initiated showing decompositions for **27**/**31**, deflagrations for **14**, **16**, **19**, **22**, **24**, **25** and **36** (Figure 16 and Figure S34–38) and detonation of compound **19** (Figure 17). The complexes exhibit different laser initiation thresholds at comparable sensitivities toward mechanical stimuli. The two cocrystallized MTZ molecules in **25** cause a higher initiation threshold in comparison to **19**, which is expressed in a higher required energy input. These results correlate with their observed sensitivities and the conclusion of a higher stability of the cocrystals. Consequently, copper(II) complex **19** represents a promising compound with manageable sensitivities, which can be initiated easily by laser at low initiation energies.

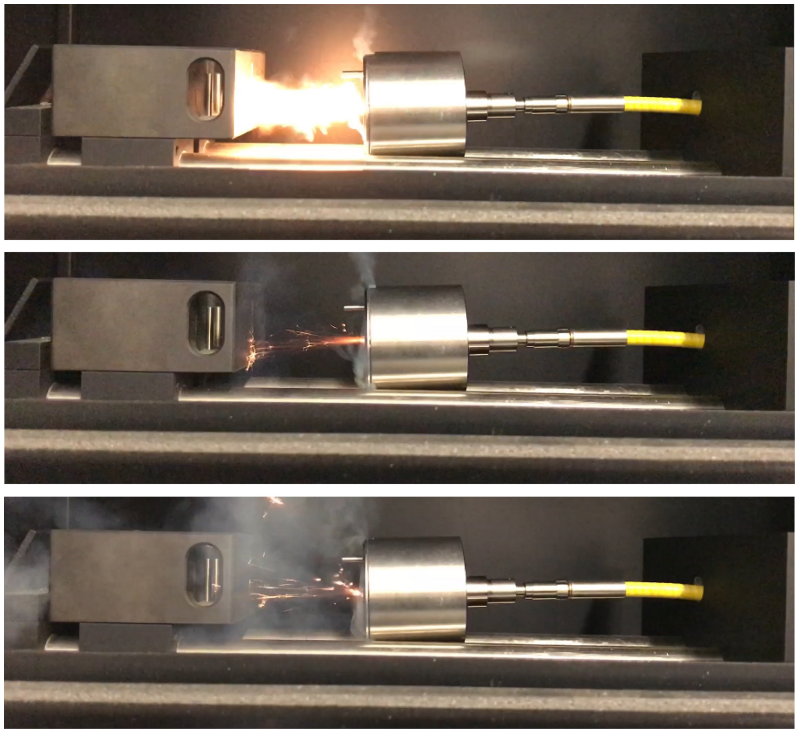


Figure 16. Moment of deflagration of compound **22** shown as sequence.

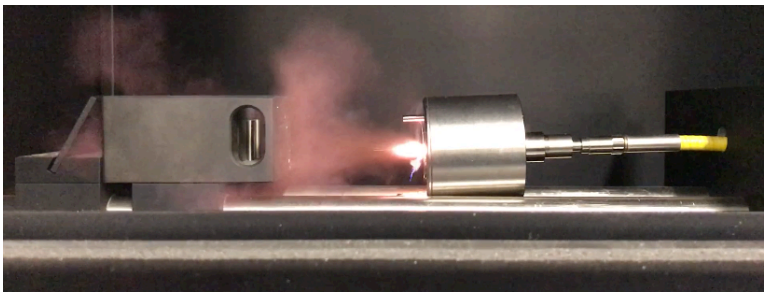


Figure 17. Moment of detonation of complex $[Cu(MTZ)_6](ClO_4)_2$ (**19**).

Table 4. Results of the laser ignition tests.

compound	7 A	8 A	9 A	10 A
14	–	–	deflag.	–
15	–	–	–	x
16	dec.	–	–	deflag.
17	–	–	–	x
18	–	–	–	deflag.
19	det.	–	–	det.
20	–	–	–	x
22	–	–	–	deflag.
24	–	–	–	deflag.
25	deflag.	deflag.	–	–
27	–	dec.	–	–
31	–	–	–	dec.
36	–	–	–	deflag.
37	–	–	–	x

(–: not tested, x: no ignition, dec.: decomposition, deflag.: deflagration, det.: detonation). Operating parameters: current I = 7–10 A; voltage U = 4 V; theoretical maximal output power P_{max} = 45 W; theoretical energy E_{max} = 26–60 mJ; wavelength λ = 915 nm; pulse length τ = 15 ms.

10.2.6 UV-Vis Spectroscopy

The solid state UV-Vis spectra for the complexes **14**–**27**, **31** and **36** were collected in the wavelength range of 350–1000 nm in order to get a better understanding of the laser ignition process. Observed optical properties are summarized in Table 5. The step in the absorption intensity at 800 nm in the spectra is caused by a detector change. The UV-Vis spectra exhibit only qualitative character. Selected complexes of different metal centers are exemplarily shown in Figure 18.

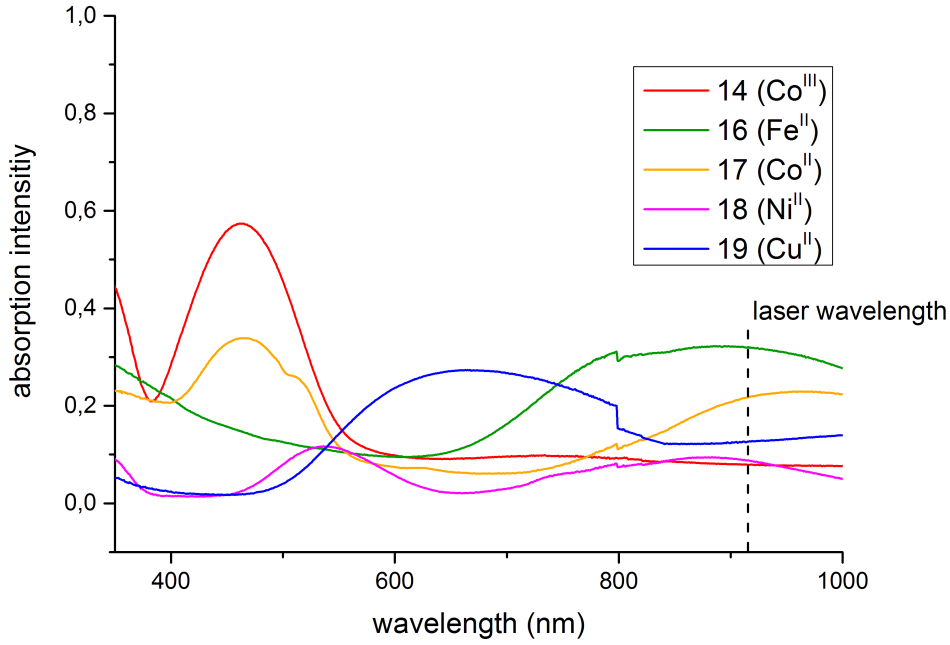


Figure 18. UV-Vis spectra in the solid state of selected complexes.

The coordination compounds had absorptions in the UV, visible and near-infrared region typical for the corresponding transition metals. These transitions can be assigned to the characteristic d-d-transitions and correlate with the complementary colors. As expected, the d^5 manganese(II) and d^{10} zinc(II) complexes showed no absorptions in the measured range and are illustrated together with the cocrystallized perchlorate compounds in the Supporting Information (Figure S39). The cocrystals diverged only minimally from their regular analogues. In addition, the copper(II) cyanodinitromethanide and trinitrobenzene derivative complexes **27**, **31** and **36** also have strong absorptions ranging from the UV to the visible region of the electromagnetic spectrum (Figure S40). These observations indicated the expected presence of additional electronic transitions in these compounds caused by the coordinating anions (n–π*: 358 (**27**); 380 (**31**); 404 (**36**) nm).

Table 5. Optical properties of **14**-**27**, **31** and **36**.

compound	M	color	$\lambda_{d\text{-}d}$[a]	$\lambda_{915}/\lambda_{d\text{-}d}$[b]
14	Co^{III} (*ls*)	orange	463	0.14
15	Mn^{II}	colorless	–	–
16	Fe^{II} (*hs*)	colorless	887	0.99
17	Co^{II}	orange	464, 960	0.64
18	Ni^{II}	purple	536, 883	0.75
19	Cu^{II}	blue	663	0.46
20	Zn^{II}	colorless	–	–
21	Mn^{II}	colorless	–	–
22	Fe^{II} (*hs*)	colorless	883	0.99
23	Co^{II}	orange	467, 961	0.59
24	Ni^{II}	purple	547, 904	0.84
25	Cu^{II}	blue	676	0.42
26	Zn^{II}	colorless	–	–
27	Cu^{II}	blue	358[c], 612	0.53
31	Cu^{II}	green	380[c], 630	0.74
36	Cu^{II}	green	404[c], 657	0.69

[a] absorption intensity maximum wavelength, which can be assigned to electron d-d excitations in the measured range of 350–1000 nm; [b] quotient of the absorption intensity at the laser wavelength and the intensity at the d-d absorption wavelength; [c] n–π* transitions.

The laser initiation mechanism is still not fully understood.[49] Many different reaction pathways (e.g. electronically or thermally) are imaginable. Simply regarding the absorption of the complexes at the laser wavelength of 915 nm as shown in Figure 18 and Table 5, one might derive a direct correlation to the performed laser ignition. In contrast to that, the examined Co(II) compound **17**, which clearly absorbs in the corresponding region, showed no reaction after exposure to laser irradiation. For MTZ complexes of iron(II) it is well known that the structure in the crystal as well as the counterion (e.g. ClO_4^-, BF_4^-, PF_6^- or $CF_3SO_3^-$) can have a profound effect on for example the spin crossover properties.[50] It is possible that not only the absorption properties but also subtle changes in the geometry or crystal packing influence the susceptibility of the complexes to laser ignition. The underlying initiation processes are likely to depend on multiple different parameters. Based on the presented results, a general tendency has been observed, that the examined compounds are more likely to deflagrate/detonate by applying laser irradiation if they exhibit high mechanical sensitivities. Due to the fact that the ligands´ influence on the laser initiation process, as well as the process itself has not been clarified yet, future investigation will be necessary to fully understand the laser initiation of energetic materials.

10.3 Conclusions

The nitrogen-rich heterocycle 1-methyl-5*H*-tetrazole (**1**, MTZ) was synthesized in a one-step synthesis by methylation of 1,5*H*-tetrazole. The resulting isomeric mixture was purified by distillation and yielded the desired product in a yield of 48%. In order to develop new laser-ignitable and environmentally benign primary explosives, diverse energetic coordination compounds were synthesized and characterized. Present energetic transition metal complexes are built up by the nitrogen-rich ligand 1-methyl-5-tetrazole, a transition metal (Mn, Fe, Co, Ni, Cu, Zn and Ag) and oxidizing anions such as perchlorate, nitrate, cyanodinitromethanide, picrate and styphnate. The synthetic route to these complexes is simple, low-cost and fulfills environmental requirements. 31 new coordination compounds, based on MTZ as the monodentate ligand, were prepared and comprehensively characterized. Thermal analysis by DTA showed thermal stabilities with exothermic decomposition temperatures higher or equal to 200 °C for most of the complexes (except **12** and **13**). Extraordinary endothermic events such as loss of MTZ and water during the DTA measurements were further investigated by thermal gravimetric analysis. Interesting results in terms of the decomposition pathways of selected compounds were achieved. In addition, X-ray crystal structures were determined for 28 complexes to get better insight into the interesting and challenging complex units showing (except for **13**) octahedral coordination spheres. To explore the structural diversity and to tailor the optical and energetic properties of these complexes, seven different metals and seven different ligands/counter-anions (Cl, NH_3, NO_3, ClO_4, CDNM, PA, HTNR) were used. Preparation of the metal perchlorate complexes **15**–**20** was strongly dependent on the stoichiometry of the ligand and yielded complex units without and with (**21**–**26)** two co-crystallized tetrazoles. Cocrystallization of the endothermic MTZ molecule leads in most cases to a decrease in sensitivities toward mechanical stimuli while maintaining its highly energetic character and is therefore an excellent concept for the desensitization of energetic coordination compounds. Environmentally benign iron and copper complexes **16**, **19** and **25** were also evaluated for use as primary explosives by hot needle tests, hot plate tests and toxicity assessments. Laser ignition experiments, which were carried out at a wavelength of 915 nm and a pulse length of 15 ms showed detonation of compound **16** (IS: 2.5 J, FS: 54 N, T_{exo}: 211 °C). The successful initiation makes **16** to a promising candidate for future laser initiation systems.

Supporting information available in the appendix in **Chapter 19.7** and under:

http://www.rsc.org/suppdata/c7/ta/c7ta07780g/c7ta07780g1.pdf

10.4 References

[1] https://echa.europa.eu/de/candidate-list-table Accessed August 2017.

[2] G. Belanger-Chabot, S. M. Kaplan, P. Deokar, N. Szimhardt, R. Haiges, K. O. Christe, *Chem. Eur. J.*, 2017, **23**, 13087–13099.

[3] Y. Tang, S. Dharavath, G. H. Imler, D. A. Parrish and J. M. Shreeve, *Chem. Eur. J.*, 2017, **23**, 9185–9191.

[4] J.-S. Qin, S.-J. Bao, P. Li, W. Xie, D.-Y. Du, L. Zhao, Y.-Q. Lan and Z.-M. Su, *Chem. Asian J.*, 2014, **9**, 749–753.

[5] A. Rudavskyi, R. W. A. Havenith, R. Broer, C. de Graaf and C. Sousa, *Dalton Trans.*, 2013, **42**, 14702–14709.

[6] S. Li, Y. Wang, C. Qi, X. Zhao, J. Zhang, S. Zhang and S. Pang, *Angew. Chem. Int. Ed.*, 2013, **52**, 14031–14035.

[7] T. Friščić and W. Jones, *Cryst. Growth Des.*, 2009, **3**, 1621–1637.

[8] J. Zhang and J. M. Shreeve, *CrystEngComm*, 2016, **18**, 6124–6133.

[9] J. Evers, I. Gospodinov, M. Joas, T. M. Klapötke and J. Stierstorfer, *Inorg. Chem.*, 2014, **53**, 11749–11756.

[10] A. F. Stassen, O. Roubeau, I. F. Gramage, J. Linarès, F. Varret, I. Mutikainen, U. Turpeinen, J. G. Haasnoot and J. Reedijk, *Polyhedron*, 2001, **20**, 1699–1707.

[11] T. Buchen, P. Poganiuch and P. Gütlich, *J. Chem. Soc. Dalton Trans.*, 1994, **15**, 2285–2288.

[12] O. Roubeau, M. Evangelisti and E. Natividad, *Chem. Commun.*, 2012, **48**, 7604–7606.

[13] O. S. Bushuyev, P. Brown, A. Maiti, R. H. Gee, G. R. Peterson, B. L. Weeks and L. J. Hope-Weeks, *J. Am. Chem. Soc.*, 2012, **134**, 1422–1425.

[14] T. M. Klapötke, *Chemistry of High-Energy Materials*. 2nd ed., Walter de Gruyter: Berlin, Boston, 2012.

[15] M. A. Ilyushin, I. V. Tselinsky and I. V. Shugalei, *Cent. Eur. J. Energ. Mater*., 2012, **9**, 293–327.

[16] B.-D. Wu, L. Yang, S.-W. Wang, T.-L. Zhang, J.-G. Zhang, Z.-N. Zhou and K.-B. Yu, *Z. Anorg. Allg. Chem.*, 2011, **637**, 450–455.

[17] Z. Shunguan, W. Youchen, Z. Wenyi and M. Jingyan, *Propellants, Explos., Pyrotech.*, 1997, **22**, 317–320.

[18] K. A. McDonald, S. Seth and A. J. Matzger, *Cryst. Growth Des.*, 2015, **15**, 5963–5972.

[19] T. W. Myers, K. E. Brown, D. E. Chavez, R. J. Scharff and J. M. Veauthier, *Eur. J. Inorg. Chem.*, 2016, **2016***,* 3178–3183.

[20] X. Fang and S. R. Ahmad, *Cent. Eur. J. Energ. Mater.*, 2016, **13***,* 103–115.

[21] M. Joas, T. M. Klapötke and N. Szimhardt, *Eur. J. Inorg. Chem.*, 2014, **2014***,* 493–498.

[22] T. W. Myers, J. A. Bjoorgard, K. E. Brown, D. E. Chavez, S. K. Hanson, R. J. Scharff, S. Tretiak and J. M. Veauthier, *J. Am. Chem. Soc.*, 2016*,* **138**, 4685–4692.

[23] S. C. Kunz and F. J. Salas, *Proceedings of the International Pyrotechnics Seminar*, 1988, 13th, 505–523.

[24] J. A. Merson, F. J. Salas and J. G. Harlan, *Proceedings of the International Pyrotechnics Seminar*, 1994, 19th, 191–206.

[25] Y.-h. Zhu, D.-l. Sheng, B. Yang, L.-K. Chen and F.-E. Ma, *Hanneng Cailiao*, 2009, **17**, 169–172.

[26] a.) E. Oliveri-Nandalà and B. Alagna, *Atti Reale Accad. Lincei.*, 1910, **19**, 228–231; b.) E. Oliveri-Nandalà and B. Alagna *Chem. Zentralbl.*, 1910, **1**, 1794–1795.

[27] P. E. M. Wijnands, J. S. Wood, J. Reedijk and W. J. A. Maaskant, *Inorg. Chem.*, 1996, **35**, 1214–1222.

[28] T. Buchen, D. Schollmeyer and P. Gütlich, *Inorg. Chem.*, 1996, **35**, 155–161.

[29] J. J. Sabatini, J. M. Raab, R. K. Hann, R. Damavarapu and T. M. Klapötke, *Chem. Asian J.*, 2012, **7**, 1657–1663.

[30] Q. Yang, S. Chen, G. Xie and S. Gao, *J. Hazard. Mater.*, 2011, **197**, 199–203.

[31] P. N. Gaponik, M. M. Degtyarik, A. S. Lyakhov, V. E. Matulis, O. A. Ivashkevih, M. Quesada and J. Reedijk, *Inorg. Chim. Acta*, 2005, **358**, 3949–3957.

[32] P. L. Franke, J. G. Haasnoot and A. P. Zuur, *Inorg. Chim. Acta*, 1982, **59**, 5–9.

[33] N. C. Baenzinger and R. J. Schultz, *Inorg. Chem.*, 1971, **10**, 661–667.

[34] L. S. Ivashkevich, A. S. Lyakhov, D. O. Ivashkevich, M. M. Degtyarik and P. N. Gponik, *Zh. Neorg. Khim.*, 2005, **50**, 82–86.

[35] A. Zhilin, M. Ilyushin, I. Tselinksi, A. Kozlov and N. Kuz´mina, *Russ. J. Appl. Chem.*, 2002, **75**, 1849–1851.

[36] Crystallographic data for the structures have been deposited with the Cambridge Crystallographic Data Centre. Copies of the data can be obtained free of charge on application to The Director, CCDC, 12 Union Road, Cambridge CB2 1EZ, UK (Fax: int.code_(1223)336-033; e-mail for inquiry: fileserv@ccdc.cam.ac.uk; e-mail for deposition: (deposit@ccdc.cam.ac.uk).

[37] L. Wiehl, *Acta Cryst. B.*, 1993, **49**, 289−303.

[38] M. H. Palmer and S. Parsons, *Acta Cryst. B.*, 1996, **52**, 2818−2822.

[39] M. Freis, T. M. Klapötke, J. Stierstorfer and N. Szimhardt, *Inorg. Chem.*, 2017, **56**, 7936−7947.

[40] Klewe, *Acta Chem. Scand. (1947–1973)*, 1972, **26**, 1921–1930.

[41] K. C. Patil, *J. Chem. Sci.*, 1986, **96**, 459–464.

[42] R. A. F. Sherriff and A. K. Galwey, *J. Chem. Soc. A*, 1967, 1705–1708.

[43] M. Joas, PhD thesis, Ludwig-Maximilians Universität München, 2014.

[44] K. Wang, D. Zeng, J.-G. Zhang, Y. Cui, T.-L. Zhang, Z.-M. Li and X. Jin, *Dalton Trans.*, 2015, **44**, 12497−12501.

[45] G. I. Sunahara, S. Dodard, M. Sarrazin, L. Paquet, G. Ampleman, S. Thiboutot, J. Hawari and A. Y. Renoux, *Ecotoxicol. Environ. Saf.*, 1998, **39**, 185−194.

[46] C. J. Cao, M. S. Johnson, M. M. Hurley and T. M. Klapötke, *JANNAF J. Propuls. Energet.*, 2012, **5**, 41–51.

[47] V. Ochoa-Herrera, G. Léon, Q. Banihani, J. A. Field and R. Sierra-Alvarez, *Sci. Total Environ.*, 2011, **380**, 412–413.

[48] M. Joas, T. M. Klapötke, J. Stierstorfer and N. Szimhardt, *Chem. Eur. J.*, 2013, **19**, 9995–10003.

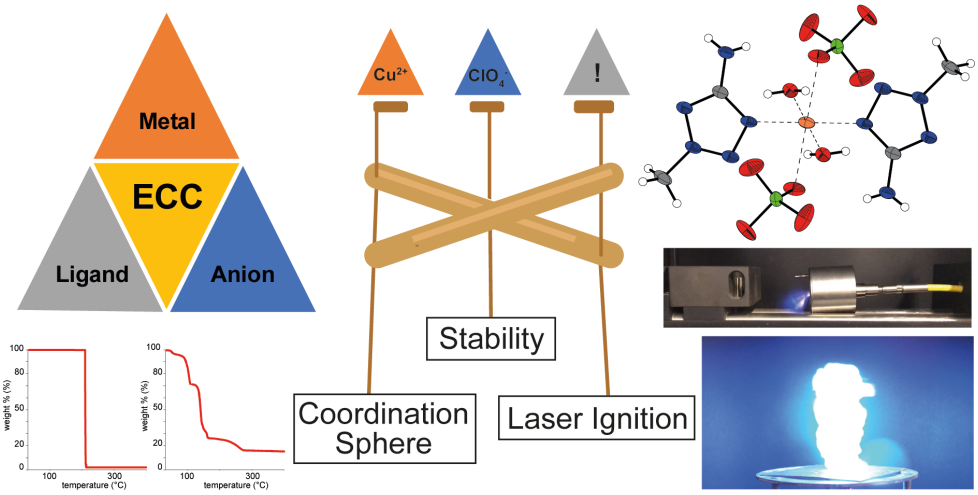
[49] E. D. Aluker, A. G. Krechetov, A. Y. Mitrofanov, D. R. Nurmukhametov and M. M. Kuklja, *J. Phys. Chem. C*, 2011, **115**, 6893–6901.

[50] M. Halcrow, Polyhedron, 2007, 26, 3523–3576.

11 2-Methyl-substituted Monotetrazoles in Copper(II) Perchlorate Complexes: Manipulating Coordination Chemistry and Derived Energetic Properties

Lukas Zeisel, Norbert Szimhardt, Maximilian H. H. Wurzenberger, Thomas M. Klapötke, and Jörg Stierstorfer

submitted to *Dalton Transactions*



Several new energetic coordination compounds (ECC) have been prepared using two different 2-methyl-substituted tetrazoles. By simply changing the reaction conditions, the coordination sphere of the metal center can be manipulated in order to obtain different complexes with varying energetic properties.

Abstract

A proposed correlation between coordination chemistry and deduced energetic properties (thermal behaviour, sensitivities towards mechanical and optical stimuli) of copper(II) complexes is investigated. Starting from a system comprising of $Cu(ClO_4)_2$ and either of the ligands 2-methyl-5-aminotetrazole (**1**, 2-MAT) or 2-methyl-5*H*-tetrazole (**2**, 2-MTZ), typically altered parameters like metal(II) centre, ligand, or counterion were predefined. Instead, solely slight changes in ligand concentration and solvent system were implemented in order to provide an insight into structure-property relationships of energetic coordination compounds (ECC) of this type. As a result, five highly energetic complexes $[Cu(H_2O)_2(2\text{-}MAT)_4](ClO_4)_2 \cdot H_2O$ (**3**), $[Cu(H_2O)_2(2\text{-}MAT)_4](ClO_4)_2$ (**4**), $[Cu(H_2O)_2(2\text{-}MAT)_4](ClO_4)_2 \cdot 2$ 2-MAT (**5**), $[Cu(ClO_4)_2(H_2O)_2(2\text{-}MAT)_2]$ (**6**), $[Cu(H_2O)_2(2\text{-}MTZ)_4](ClO_4)_2$ (**7**) were synthesized and, except for **5**, elaborately characterized. Besides structural elucidation via X-ray diffraction, NIR-spectroscopy, differential thermal analysis (DTA), standard sensitivity measurements (impact, friction, electrostatic discharge), UV-Vis-spectroscopy, and optical initiation experiments were conducted to deduce a precise relationship between coordination chemistry and consequential energetic characteristics of these complexes.

11.1 Introduction

Dominated by the oxidation states +I and +II, copper exhibits a diverse coordination chemistry. Especially the d^9 Cu^{II} cation is commonly applied in many areas of chemistry as metal center of coloring agents,[1] insecticides,[2,3] catalysts,[4] and metalloproteins.[5] In most of these cases, copper(II)'s coordination chemistry is influenced by oxygen- and nitrogen-donating ligands, typically forming square planar, tetrahedral and, predominantly, octahedral coordination environments.[3]

In recent years, the growing field of energetic coordination compounds (ECC) highly benefited from promising Cu^{II} complexes. Due to the urgent necessity of substituting commonly applied, toxic primary explosives like lead azide and lead styphnate, an approach using significantly less toxic transition metal complexes appeared to be highly encouraging.[6] In recent years, seminal reports from Shreeve,[7] Myers,[8] and Klapötke[9] set the stage for future applications of ECC. In targeting novel transition metal complexes with auspicious properties (convenient accessibility, thermal stability, safe initiation), a consistently implemented general approach

has emerged: starting from a desired transition metal cation with the corresponding counter-anion, energetic ligands, as well as the applied reaction conditions offer precise tailoring of the desired characteristics.[7–9] Whereas variation of parameters like ligand, metal centre, and anion tend to distinctly influence the coordination chemistry and the complexes' properties, additional fine tuning towards desired attributes might be achieved by accurately controlling the applied reaction conditions. While initial experiments in this direction already led to sought results, a comprehensive report is anticipated until today.[9b,10–12]

In regard of previously applied ligand systems, mostly nitrogen-rich, endothermic heterocycles were considered.[7–16] Among others, mono-substituted tetrazoles like the highly energetic 1,5-diaminotetrazole (1,5-DAT), 1-amino-5*H*-tetrazole (1-AT) and 2-amino-5*H*-tetrazole (2-AT) as well as 1-methyl-5*H*-tetrazole (1-MTZ) and 1-methyl-5-aminotetrazole (1-MAT) were investigated as ligands in ECC (Chart 1).[10,13,14] Hereby obtained transition metal complexes proved to be highly energetic, readily synthesized and partially exhibited auspicious properties as laser-ignitable primary explosives.[10, 13]

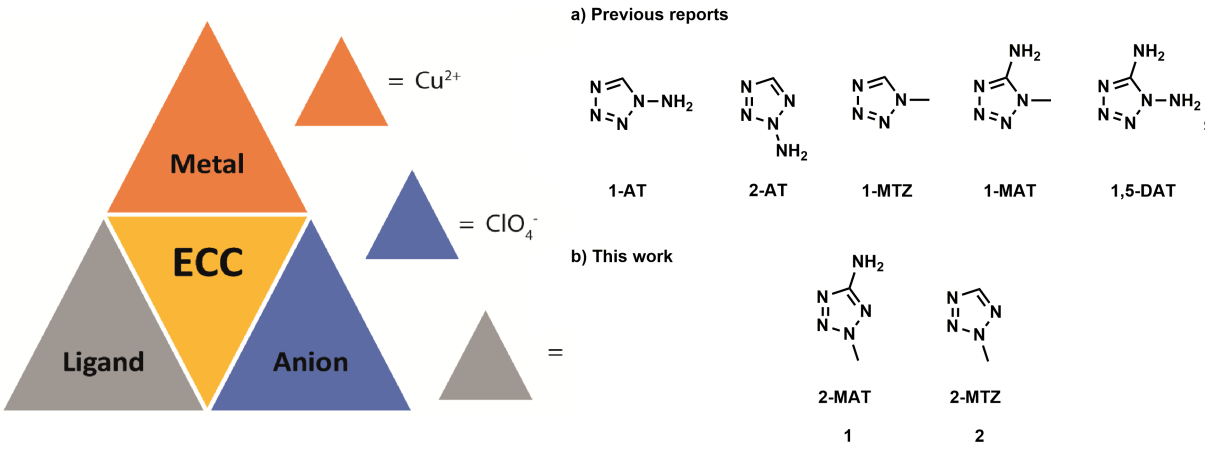


Chart 1. Precedents and current work using energetic monotetrazoles in ECC.

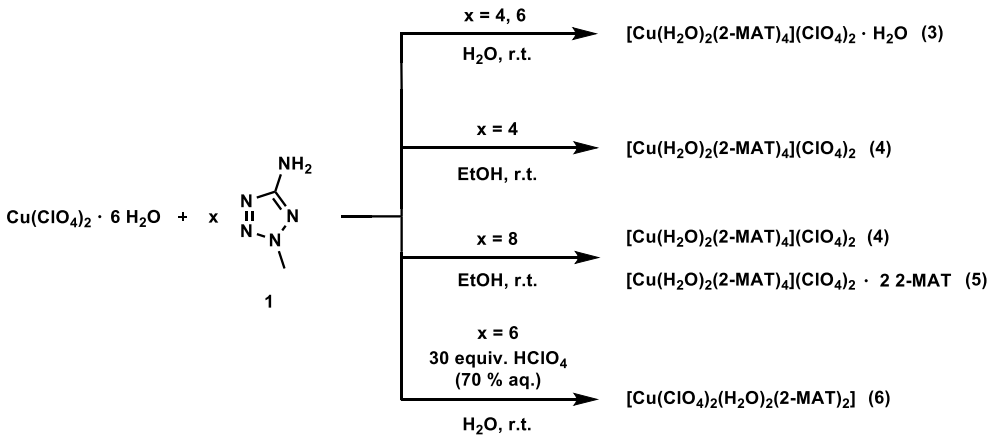
Based on these results, the present work aims for a deeper insight into the possibility of precisely manipulating an ECC's coordination chemistry and the resulting energetic properties (sensitivities, thermal properties, laser initiation) by solely modifying the reaction conditions (ligand concentration, solvent, additives) in hand. Predefinitions for the applied systems included copper(II) as metal species, perchlorate counter-anions and, as an extension to previously published reports, 2-methyl-5-aminotetrazole (**1**, 2-MAT, $\Delta_f H^0_{(g)} = 2802$ kJ kg^{-1})[17] and 2-methyl-5*H*-tetrazole (**2**, 2-MTZ, $\Delta_f H^0_{(g)}$ (2-MTZ) = 3347 kJ kg^{-1})[17] as endothermic ligands. Both nitrogen-rich heterocycles are expected to allow comparison to the respective 1-substituted tetrazoles and their energetic metal complexes. While recently published results

from Szimhardt *et al*. provide a comprehensive study of 1-MTZ and its transition metal complexes,[10] only few examples of 1-MAT ECC have been reported alongside a range of corresponding tetrazolium salts.[18–20] Moreover, and in relation to related, tremendously sensitive 2-aminotetrazole complexes,[13] 2-MAT and 2-MTZ incorporating ECC are proposed to combine efficient optical initiation with enhanced stability towards mechanical stimuli, thus allowing safe handling of these materials.

11.2 Results and Discussion

11.2.1 Synthesis

Initially, nitrogen-rich ligand **1** was synthesized via a convenient, single step reaction using commercially available 5-aminotetrazole as starting material (see Scheme S1). Due to the tautomerization of 1,5*H*-tetrazole, the dimethylsulfate-mediated methylation step provided the desired ligand alongside 1-methyl-5-aminotetrazole in a ratio of 3:4. With the targeted 2-MAT in hand, initial investigations concerning its coordination chemistry were accessed (Scheme 1).



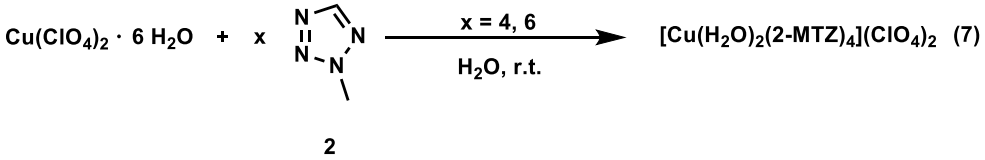
Scheme 1. Synthesis of complexes **3**–**6** using 2-methyl-5-aminotetrazole (**1**).

Performed reactions were carried out at ambient temperature by slowly adding pre-dissolved ligand to a solution of copper(II) perchlorate. By solely applying a minimal amount of solvent, the crystallization process at room temperature could be accelerated. Thereby received solids were filtered off, washed with cold ethanol and dried in air, not requiring further purification.

As a starting point, 6 and 4 equivalents of 2-MAT were applied to an aqueous solution of $Cu(ClO_4)_2$ aiming for a frequently observed hexacoordinate copper(II) center.[10,21] In contrast

to that and regardless of the applied ligand concentration, the present reaction provided $[Cu(H_2O)_2(2\text{-}MAT)_4](ClO_4)_2 \cdot H_2O$ (**3**) in 52 % yield after four days of crystallization. Proceeding from these preliminary results, the utilization of a solvent with decreased polarity was tested. Using ethanol as the reaction medium and 4 equiv. of ligand indeed led to the isolation of a new complex **4**. Nevertheless and despite successfully preventing the incorporation of cocrystallized water, $[Cu(H_2O)_2(2\text{-}MAT)_4](ClO_4)_2$ (**4**) simultaneously retained the actual coordination sphere with two coordinating aqua ligands. To further extend this condition screening, increased 2-MAT concentration (8 equivalents) was introduced while maintaining ethanol as the solvent. As a result, and immediately after combining ligand and copper(II) perchlorate, a light green precipitate occurred. After filtration, preliminary characterization of the residue by IR spectroscopy confirmed the formation of a previously unknown complex $[Cu(H_2O)_2(2\text{-}MAT)_4](ClO_4)_2 \cdot 2$ 2-MAT (**5**) alongside ECC **4**. Since conducted attempts of clean isolation or purification of **5** proved to be unsuccessful, further characterization was impeded. Interestingly, the earlier collected filtrate of the present reaction once again provided **4** after crystallization for six days. A final attempt of interfering with the previously observed coordination chemistry of this system was to apply concentrated perchloric acid. According to reported syntheses, this approach promised a water-free ECC with enhanced energetic characteristics by substituting aqua ligands with coordinating perchlorate counter-anions.[22] Unfortunately, charging the aqueous reaction mixture with 30 equivalents of $HClO_4$ led to complex **6**, which still exhibited coordinating aqua ligands (yield: 76 %). In contrast to previously obtained ECC, the coordination sphere of $[Cu(ClO_4)_2(H_2O)_2(2\text{-}MAT)_2]$ indeed comprises of two copper(II) associated perchlorato anions while solely exhibiting two equivalents of the nitrogen-rich ligand **1**. A possible and reoccurring explanation for a decrease of coordinating tetrazole ligand might be the protonation and simultaneous elimination of an N-coordination site.[9f,12] In comparison to that, the corresponding 1-methyl-5-aminotetrazole exhibited low solubility in water, thus leading to the reoccurring precipitation of the ligand.[19] Moreover, and whenever ligand crystallization could be prevented, collected X-ray data of isolated crystals repeatedly proved the simultaneous presence of multiple ECC species.[19]

Conclusively, 2-methyl-5*H*-tetrazole (2-MTZ) was investigated as a comparative example for additional 2-substituted monotetrazoles (Scheme 2). The ligand itself was accessed via a straightforward two-step reaction starting from basic building blocks (see Scheme S2). Once again, tautomerization led to a significant decrease in yield of 2-MTZ due to the formation of isomeric 1-methyl-5*H*-tetrazole (1-MTZ) (1-MTZ/2-MTZ = 2:1).



Scheme 2. Formation of the copper(II) perchlorate complex **7**.

When being applied to an aqueous solution of copper(II) perchlorate, 2-MTZ exhibits remarkable similarity to the previously investigated 2-MAT. In comparison to complexes **3** and **4**, $[Cu(H_2O)_2(2\text{-}MTZ)_4](ClO_4)_2$ (**7**), which was isolated from the mother liquor after one day (yield: 73 %), features almost equivalent coordination chemistry under identical reaction conditions. Moreover, and in contrast to the 2-MAT system, change of solvent (ethanol) or stoichiometry (x = 4, 6, 10) exclusively lead to the same product **7**. Whenever the metal(II) center was altered (Fe^{2+}, Zn^{2+}, Mn^{2+}) no crystallization of a potential ECC was achieved. Interestingly and in accordance with previous reports, 2-substituted tetrazoles as ligands appear to consistently promote the incorporation of aqua ligands.[18b,21] Reasons for this could be the steric hindrance of six tetrazoles coordinating to the transition metal or the thermodynamically and kinetically preferred formation of more inert complexes. However, further studies including thermodynamic calculations are needed for the future.

11.2.2 Crystal Structures

Since each of the obtained complexes was obtained as single crystals, structural characterization was conducted using low temperature X-ray diffraction. Measurement and refinement data are provided in the Supporting Information. Additionally, details of the obtained crystal structures were deposited in the CSD database and can be obtained free of charge with the CCDC no. 1850124 (**3**), 1850121 (**4**), 1850122 (**5**), 1850120 (**6**), 1850123 (**7**).[23] In terms of the observed coordination geometry, examined copper(II) centres provided Jahn-Teller distorted octahedra, which consistently exhibited N4-coordinating ligands. Considering calculated electrostatic potentials at the respective ligand's binding sites (Figure 1), the highest electron density of both, 2-MAT and 2-MTZ, occurs at the tetrazole's carbon-adjacent nitrogen N4, thus explaining the observed coordination behaviour observed by X-ray diffraction and additionally conducted IR spectroscopy (See SI, Figure S1).

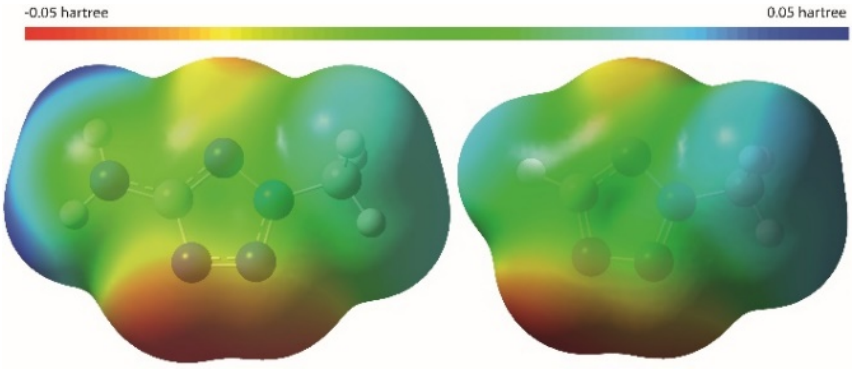


Figure 1. Calculated (B3LYP/6-31G(d,p)) electrostatic potentials (3D isosurface of electron density) of 2-MAT (**1**, left) and 2-MTZ (**2**, right).

Ahead of the comprehensive analysis of received crystal structures it should be stated that structural data of coordinating 2-MAT and 2-MTZ consistently resemble corresponding, literature-known X-ray data of the respective non-coordinating ligand or comparable ECC and are therefore not discussed any further.[24,25] The first of the obtained complexes, $[Cu(H_2O)_2(2\text{-}MAT)_4](ClO_4)_2 \cdot H_2O$ (**3**), crystallizes in the form of blue blocks in the monoclinic space group *C*2/*c* with 16 formula units per unit cell and a calculated density of 1.669 g cm^{-3} at 173 K. The Jahn-Teller distorted, octahedral copper(II) coordination sphere comprises of two axial aqua and four equatorial 2-MAT ligands (Figure 2) forming a slightly tilted O–Cu–O axis and a marginally distorted plane, respectively.

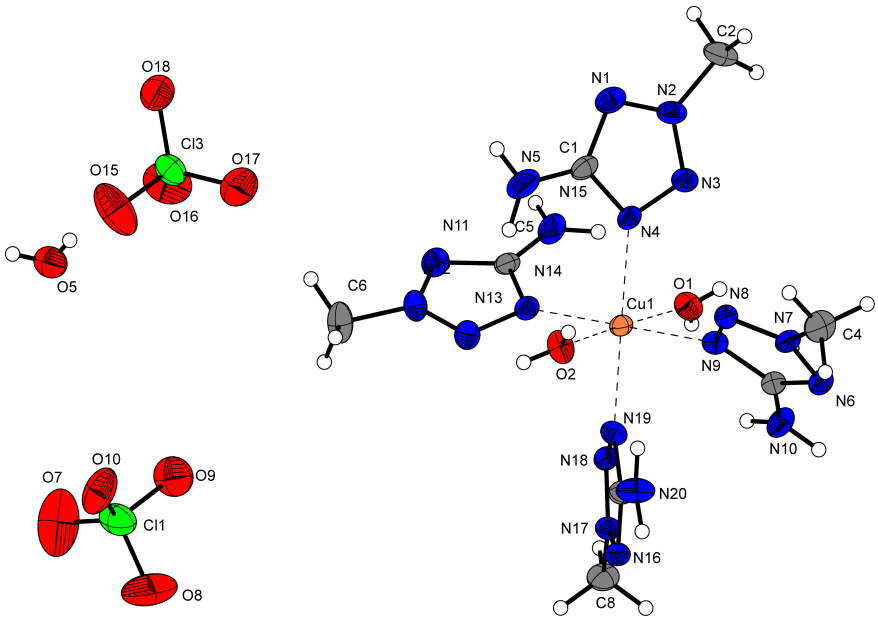


Figure 2. Molecular unit of complex **3**. Thermal ellipsoids of non-hydrogen atoms in all structures are set to the 50 % probability level. Selected bond lengths (Å): O1–Cu1 2.430(6), O2–Cu1 2.363(5), Cu1–N14 2.014(5), Cu1–N19 2.004(4), Cu1–N4 2.003(4), Cu1–N9 2.008(5); selected bond angles (°): O1–Cu1–O2 177.2(2), N4–Cu1–O1 86.95(19), N4–Cu1–O2 93.91(18), N4–Cu1–N9 91.07(19), N4–

Cu1–N14 88.89(19), N14–Cu1–O1 92.9(2), N9–Cu1–O1 87.2(2); symmetry codes: (i) −x, y, 1.5−z; (ii) −x, y, 0.5−z.

In addition to these observations in regard of the structure of a single complex unit, the three-dimensional topology of this compound reveals interesting stacking patterns (Figure 3).

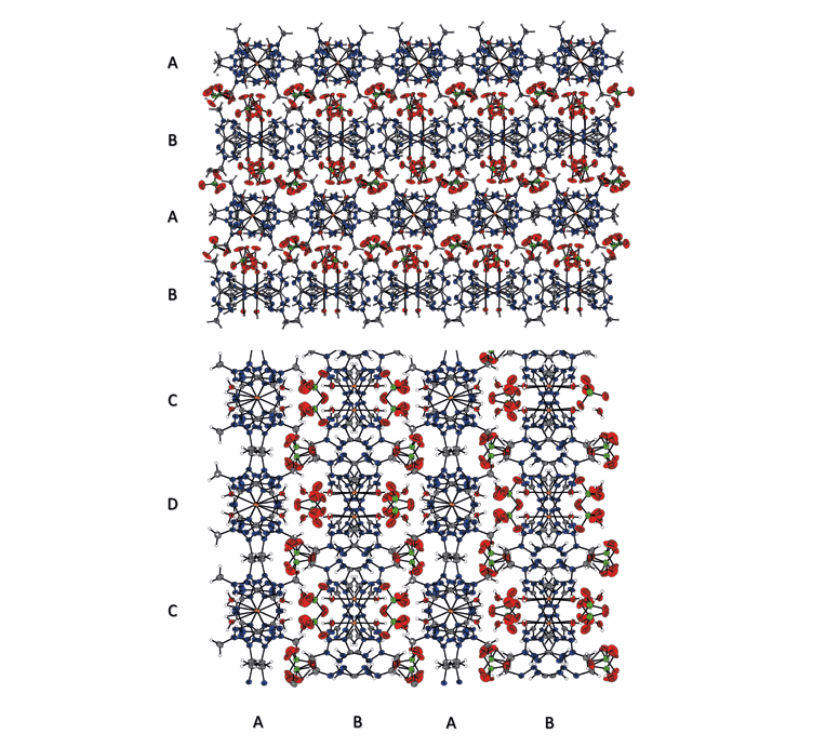


Figure 3. Structure of **3** with the direction of view along the crystallographic b- (top) and c-axis (bottom).

When viewing along the crystallographic *b*-axis, a chain pattern with altering components can be observed. In addition to this ABAB pattern, which ECC-layers are aligned along the crystallographic *c*-axis, equally oriented planes of perchlorate anions and cocrystallized water function as H-bond-mediating linkers between adjacent complex layers (Table 1). The aggregation of complexes to said layers, equally benefits from intermolecular hydrogen bonding. In addition to that, viewing along the *c*-axis reveals a similar, but even more complex picture. While exhibiting the same ABAB pattern in between distinguishable chains, B lines further reveal an intrinsic CDCD motif along *b*.

Table 1. Lengths and angles of selected hydrogen bonds in **3**.

D–H···A	d (D–H) [Å]	d (H···A) [Å]	d (D···A) [Å]	< D–H···A [°]
N5–H5···N16	0.88	2.27	3.03	144.0
O3–H31···O6	0.83	1.89	2.71	173.6
N15–H15B···O9	0.88	2.57	2.96	107.0
N10–H10A···O9	0.88	2.17	3.02	163.0

Crystals of **4** have been isolated in the form of blue blocks in the monoclinic space group $P2_1$ with two formula units per unit cell and a calculated density of 1.788 g cm^{-3} at 173 K. The molecular unit consists of four 2-MAT and two aqua ligands once again resulting in an octahedral coordination sphere (Figure 4). The corresponding perchlorate anions are non-coordinating. Regarding the appearance of the coordination polyhedron it becomes obvious that there is yet again a Jahn-Teller distortion to be observed along an axis that connects the copper(II) center with the two aqua ligands in axial positions. Considering these first observations it becomes clear that the structural parameters of **4** are almost identical to the previously discussed compound **3** with four 2-MAT ligands in the plane. The only significant differences such as the space group and the cell volume are caused by the absence of crystal water molecules. Another slight alteration can be observed regarding the bond angles between the coordinating ligands and copper(II), especially among the aqua and 2-MAT ligands.

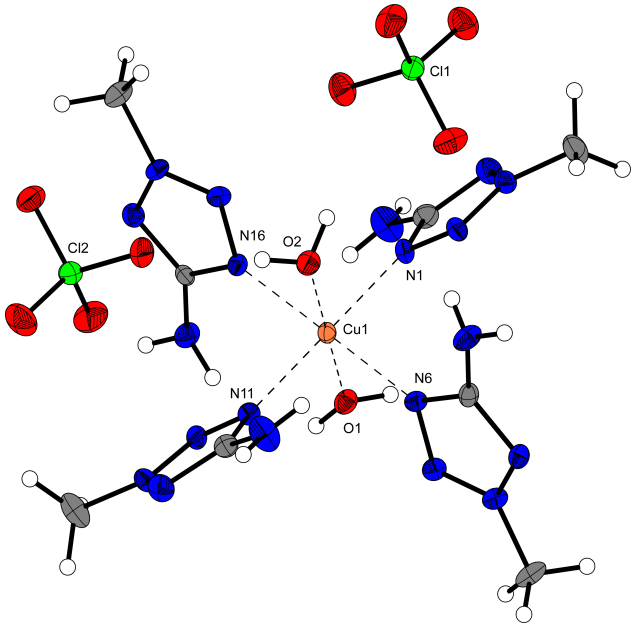


Figure 4. Molecular unit of $[Cu(H_2O)_2(2\text{-MAT})_4](ClO_4)_2$ (**4**). Selected bond lengths (Å): O1–Cu1 2.417(5), O2–Cu1 2.397(5), N1–Cu1 1.999(5), N6–Cu1 2.049(6), N11–Cu1 2.000(5), N16–Cu1 2.065(6); selected bond angles (°): O1–Cu1–O2 179.34(19), N1–Cu1–O1 87.6(2), N1–Cu1–O2 91.9(2), N6–Cu1–O1 88.2(2), N6–Cu1–O2 92.2(2), N16–Cu1–O1 90.85(19), N16–Cu1–O2 88.8(2).

In the case of **4**, the bond angles approach the 90° of an ideal octahedron. Crystallizing in the space group $P\bar{1}$, ECC **5** comprises of two formula units per unit cell and a calculated density of 1.699 g cm^{-3} at 173 K. The observed octahedral coordination sphere builds up the molecular unit including four 2-MAT and two aqua ligands. In addition, two equivalents of ligand **1** have been found as cocrystallized species (Figure 5). Due to the reoccurring Jahn-Teller effect, the bond lengths along the tilted distortion axis O1–Cu1–O2 are significantly longer than those of

the metal and the equatorial ligands. Since the equatorial 2-MAT-organized plane is not situated perpendicular on the O1–Cu1 and O2–Cu1 axes, a noticeable deviation from ideal flatness is observed.

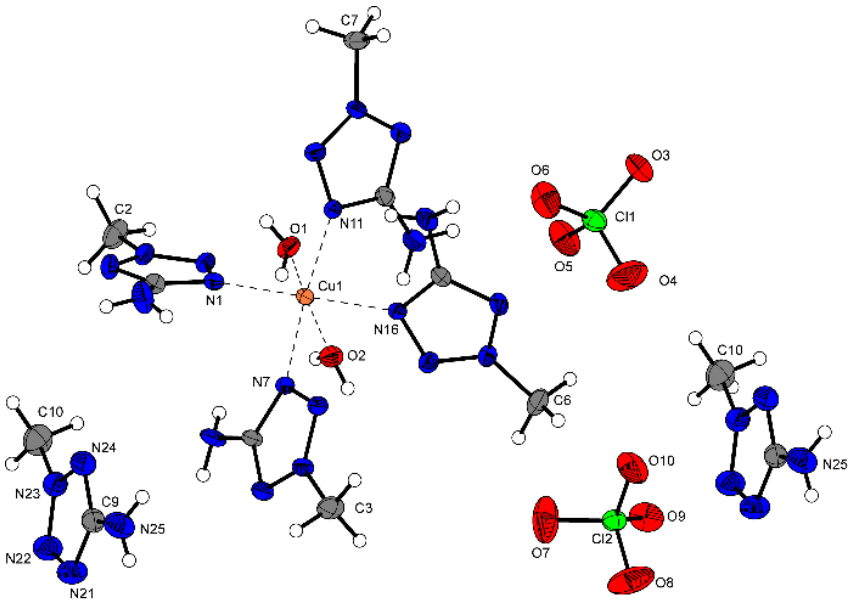


Figure 5. Molecular unit of $[Cu(H_2O)_2(2\text{-MAT})_4](ClO_4)_2 \cdot 2$ 2-MAT (**5**). Selected bond lengths (Å): O1–Cu1 2.385(2), O2–Cu1 2.501(2), N1–Cu1 2.006(2), N7–Cu1 2.004(2), N11–Cu1 2.020(2), N16–Cu1 2.000(2); selected bond angles (°): O1–Cu1–O2 173.44(7), N1–Cu1–O1 93.38(8), N1–Cu1–O2 92.11(8), N7–Cu1–O2 85.43(8), N16–Cu1–O2 85.14(8), N7–Cu1–N16 88.68(9), N11–Cu1–N16 86.82(9), N1–Cu1–N16 176.71(9), N7–Cu1–N11 175.13(9); symmetry codes: (i) 1−x, 1−y, 1−z, (ii) −x, 2−y, 1−z.

As the final representative of the 2-MAT derived complexes, **6** crystallizes in the form of blue rods in the monoclinic space group $P2_1/n$ with two formula units per unit cell and a remarkably high calculated density of 1.997 g cm^{-3} at 173 K. Two asymmetric unit cells built up the molecular unit. The latter consists of a copper(II) center, two aqua, two perchlorato, and two 2-MAT ligands forming a Jahn-Teller distorted, octahedral coordination sphere (Figure 6).

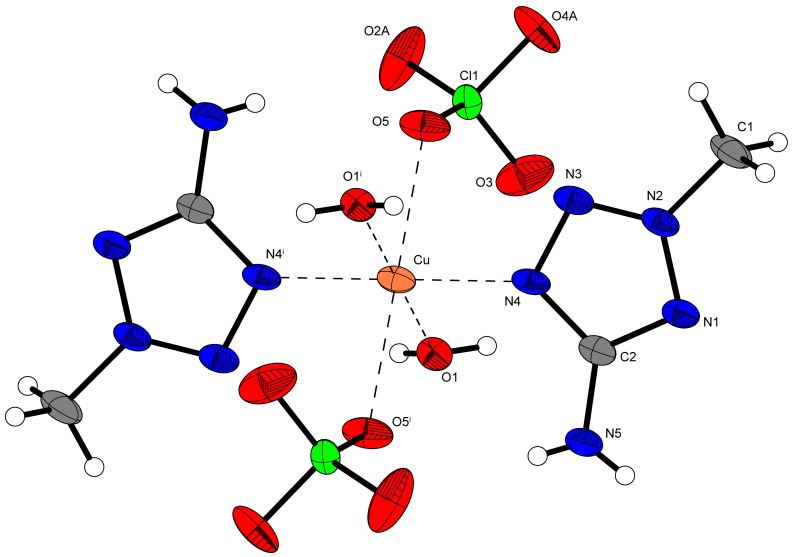


Figure 6. Molecular unit of $[Cu(ClO_4)_2(H_2O)_2(2\text{-MAT})_2]$ (**6**). Selected bond lengths (Å): Cu1–O5 2.443(3), Cu1–N4 1.998(3), Cu1–O1 1.960(3); selected bond angles (°): O1–Cu1–O5 96.32(10), O1–Cu1–O5^{i} 83.69(10), O1–Cu1–N4 90.59(12), O1–Cu1–N4^{i} 89.41(12), O5–Cu1–O5^{i} 180.00; symmetry codes: (i) 2−x, −y, −z.

The resulting polyhedron is built up by three straight axes which are caused by the fact that the two ligands of each kind coordinate *trans* to one another. The remaining four ligands are located in an ideal plane with bond lengths between the metal(II) center and the respective ligand being expectedly shorter than along the O5–Cu1–O5^{i} axis. Another significant deviation from an ideal octahedron can be observed regarding the bond angles between axial ligands and coordinating molecules in the equatorial plane. Lastly, the molecular structure of **7** was investigated. In analogy to complex **6**, $[Cu(H_2O)_2(2\text{-MTZ})_4](ClO_4)_2$ crystallizes in the monoclinic space group $P2_1/n$ (Z = 2), while exhibiting a significantly lower calculated density at 173 K (1.702 g cm^{-3}). As stated beforehand, the obtained crystal structure displays remarkable resemblance to the molecular structures of **3** and **4** (Figure 7). Nevertheless, copper(II) –aqua distances along the Jahn-Teller distorted O1–Cu–O1^{i} axis proved to be distinguishably shorter. Despite this deviation, measured torsion angles consistently exhibit values close to those of an ideal octahedron.

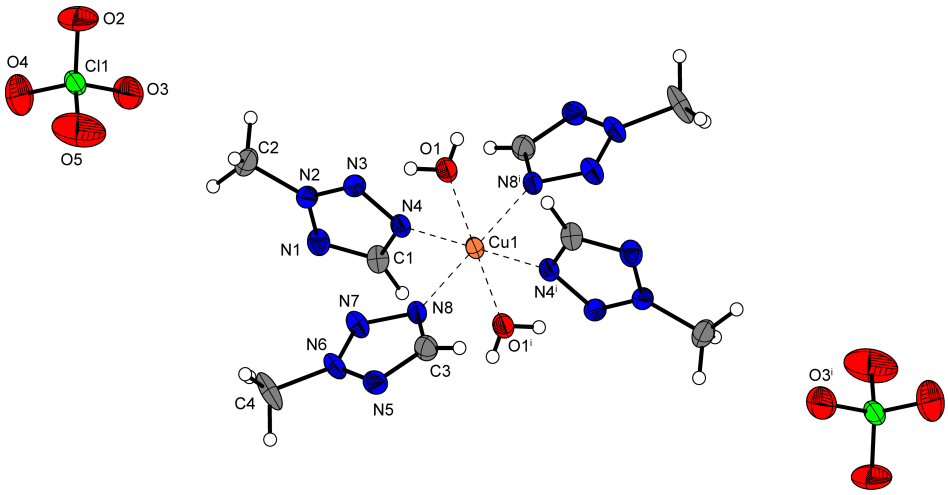


Figure 7. Molecular unit of $[Cu(H_2O)_2(2\text{-MTZ})_4](ClO_4)_2$ (**7**). Selected bond lengths (Å): Cu1–O1 2.300(3), Cu1–N4 2.023(2), Cu1–N8 2.029(2); selected bond angles (°): O1–Cu1–N4 93.15(11), O1–Cu1–N8 88.31(11), O1–Cu1–O1^i 180.00, N4–Cu1–N8 88.11(9), O1^i–Cu1–N8 91.69(11), N4–Cu1–N4^i 180.00; symmetry code: (i) 1−x, −y, 2−z.

11.2.3 Thermal Properties and Sensitivities

Ensuing the structural characterization of the received complexes, energetic properties in terms of thermal stability and sensitivities towards mechanical stimuli were investigated. Thereby conducted differential thermal analysis (DTA, heating rate: $\beta = 5$ °C min^{-1}, see Table 2, Figure S5) provided a distinct differentiation between uncoordinated ligands **1** and **2** and the obtained ECC. While the nitrogen-rich ligands 2-MAT (**1**) and 2-MTZ (**2**) both exhibit high thermal stability in the measured range of 25–400 °C, the corresponding copper(II) complexes each show exothermic decomposition temperatures from 171 °C (**3**) to 240 °C (**7**). Endothermic events observed for both ligands are assumed to be caused either by melting (T_{endo1} (**1**)) or evaporation of the compound (T_{endo2} (**1**), T_{endo1} (**2**), see corresponding TGA plots, Figure S6). Expectedly, the loss of cocrystallized water from **3** to **4** solely marginally influences the measured exothermic decomposition temperatures. In case of the structurally analogue complexes **3**, **4**, and **7**, endothermic events which are most likely caused by evaporation of cocrystallized or coordinated water were detected in an expectedly narrow range (125 °C (**3**), 110 °C (**4**), 115 °C (**7**)). To gain a better understanding of this partial ECC decomposition prior to the actual exothermic event, thermal gravimetric analysis was implemented for ECC **3**, **4** (see SI, Figure S6), and $[Cu(H_2O)_2(2\text{-MTZ})_4](ClO_4)_2$ (**7**) (Figure 8).

Table 2. Thermal stability measurements of **1**–**4**, **6**, and **7** by DTA.[a]

compound	T_{endo1}[b] [°C]	T_{endo2}[b] [°C]	T_{exo}[c] [°C]
1	104	252	–
2	152	–	–
3	125	–	176
4	110	–	171
6	–	–	192
7	115	208	240

[a] Onset temperatures at a heating rate of β = 5 °C min^{-1}. [b] Endothermic peak, which indicates melting, dehydration, or loss of coordinating or cocrystallized molecules. [c] Exothermic peak, indicating decomposition.

Whereas TGA plots of **3** and **4** (see SI, Figure S6) show an almost continuous loss of the compounds' mass between 100–250 °C and no sharp mass decrease at the decomposition temperature, the corresponding plot of **7** exhibits distinct disintegration events. Affirmatively, the observed mass loss starting below 100 °C (5.67 %) can be assigned to the loss of present aqua ligands and refers to the first endothermic event (115 °C) during the DTA measurement. Moreover, T_{endo2} (DTA: 208 °C) was confirmed by a matching 26.5 % mass loss during the TGA measurement, a fact that presumably is effected by ligand evaporation. The final step of decomposition is identified by an exothermic event at the remarkably high temperature of 240 °C. Lastly, complex **6**, which exhibited two copper(II)-perchlorato bonds proved to similarly disintegrate at high, but slightly lower temperatures without indicating an event of endothermic decomposition (Table 2, Figure 8). In order to explain this rather unusual observation, one might consult the complex' coordination chemistry: contrary to complexes **3**, **4**, **5**, and **7**, coordinating aqua ligands are in the plane and exhibit significantly shortened (≈ 0.4 Å) copper-aqua bond lengths which presumably lead to aggravated dissociation. Additionally, the sharp mass loss observed during TGA measurements further proves ECC **6** to remain at its distinct composition until being exposed to its decomposition temperature (Figure 8). Resulting from the observed thermal properties, the incorporation of cocrystallized water as well as the introduction of coordinating perchlorato anions cause a measureable increase in thermal stability.[10,22]

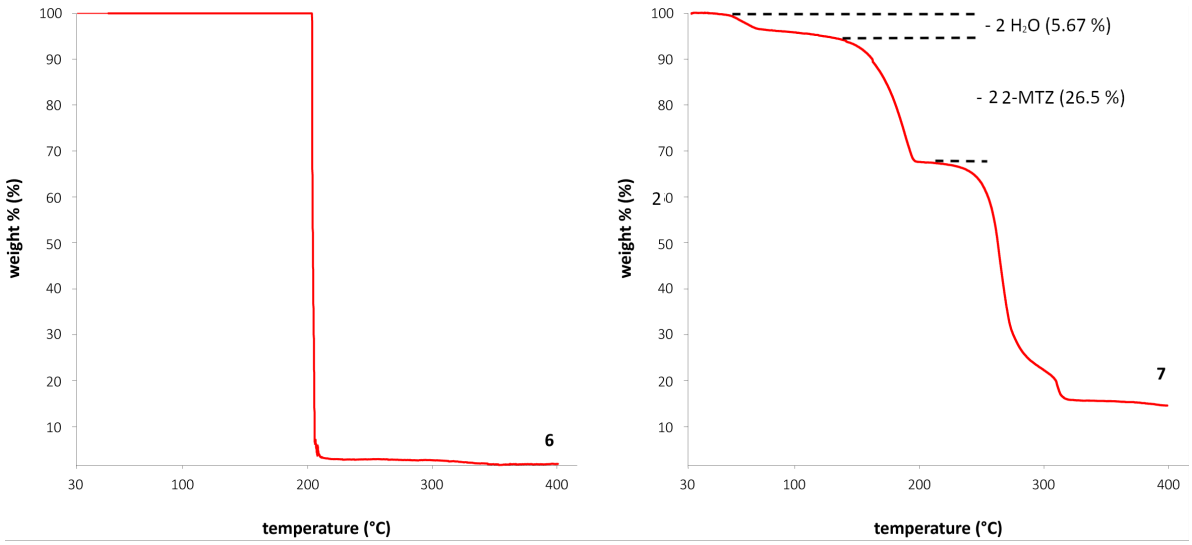


Figure 8. TGA measurements (5 °C min^{-1}) of **6** and **7**.

Regarding the investigated compounds' sensitivities towards mechanical stimuli, **1** and **2** both can be classified as insensitive according to UN standards (impact: > 40 J, friction: > 360 N). In contrast to that, introducing the highly oxidizing perchlorate anion and a coordination site like copper(II) once more approves the potential of the ECC approach due to the formation of distinctly more sensitive compounds (Table 3). Considering the series of 2-MAT based copper(II) complexes, one might recognize the tendency that with decreasing content of water, more specifically the loss of the cocrystallized species, the resulting complexes show increased sensitivities (**3** vs. **4** and **6**).[10] Unfortunately, proceeding from this initial proposition, ECC **4**, **6**, and **7** each exhibit sensitivities at the lower end of the measuring range. As a result, a quantitative evaluation of sought structure-property relationships most likely is indisposed by possibly varying fractal characteristics and particle sizes.[26] Moreover, the correlation between sensitivities and molecular structure are proposed to be dependent on multiple factors like oxygen balance (OB),[27] electronic band gap,[28] molecular electrostatic potentials,[29] and dissociation energies of critical bonds.[30] Nevertheless, complex **6**, which exhibits the lowest nitrogen ("fuel") content and the OB closest to 0 represents the overall most sensitive compound in terms of impact and friction and can be compared to the analogous chlorate complex.[31] ECC **4**, which, in comparison to structurally equivalent **7**, incorporates the less energetic ligand, displays a higher nitrogen content and exhibits the highest sensitivities towards impact and electrostatic discharge. Conducted hot plate and hot needle tests for each of the characterized ECC showed sharp deflagration events (see SI, Figures S9–S14).

Table 3. Sensitivities towards the external stimuli impact, friction, and ESD.

compound	*IS*[a] [J]	*FS*[b] [N]	*ESD*[c] [mJ]	Grain size [µm]
1	> 40	> 360	1500	100–500
2	> 40	> 360	–	100–500
3	5	30	260	500–1000
4	< 1	24	20	< 100
6	2	2.2	150	< 100
7	5	5	50	100–500

[a] Impact sensitivity according to the BAM drophammer (method 1 of 6). [b] Friction sensitivity according to the BAM friction tester (method 1 of 6). [c] Electrostatic discharge sensitivity (OZM ESD tester); impact: insensitive > 40 J, less sensitive ≥ 35 J, sensitive ≥ 4 J, very sensitive ≤ 3 J; friction: insensitive > 360 N, less sensitive = 360 N, sensitive < 360 N and > 80 N, very sensitive ≤ 80 N, extremely sensitive ≤ 10 N. According to the UN Recommendations on the Transport of Dangerous Goods.

11.2.4 Optical Initiation and UV-Vis Spectroscopy

In addition to the well-established initiation of energetic compounds via mechanical and thermal stimuli, recent developments in this field dealt with the neglected sensitivities of these species towards optical initiation.[10,21,32] Until today, a broad range (Fe, Co, Ni, Cu) of 3*d* transition metal complexes and energetic materials have been successfully initiated via laser irradiation while an unambiguous mechanistic proposal is still awaited. On one hand, common suggestions discuss a photochemical initiation mechanism through an excitation-relaxation process during which photonic energy is translated to the decomposition-initiating vibrational energy.[9c,32] Additionally, a reoccurring proposal deals with a photothermal mechanism, during which photonic energy is directly converted into lattice heat and vibrational energy, which according to the "hot-spot"-theory further leads to decomposition of the material.[10,32b] To investigate the optical sensitivities of **3**–**7** and a possible coherence with either of the proposed initiation mechanisms, laser initiation experiments were conducted along with UV-Vis spectroscopy (Table 4, Figure 9). The distinction between deflagration and detonation was made by means of acoustic output and high-speed recordings (Figure S7).

Table 4. Results of laser ignition tests[a] and UV-Vis spectroscopy.

compound	reaction	color	$\lambda_{d\text{-}d}$[b]	OD(λ_{915})/OD($\lambda_{d\text{-}d}$)[c]
3	deflag.	blue	613	0.39
4	dec.	blue	620	0.37
6	det.	blue	658	0.46
7	det.	blue	681	0.34

[a] dec.: decomposition, deflag.: deflagration, det.: detonation. Operating parameters: current $I = 7$ A; voltage $U = 4$ V; theoretical maximal output power $P_{max} = 45$ W; theoretical energy $E_{max} = 0.17$ mJ; wavelength $\lambda = 915$ nm; pulse length $\tau = 0.1$ ms; [b] absorption intensity maximum wavelength, which can be assigned to electron d-d excitations in the measured range of 350–1000 nm; [c] quotient of the absorption intensity at the laser wavelength and the intensity at the d-d absorption wavelength.

While each of the investigated ECC showed a reaction resulting from the applied conditions, solely perchlorato ligand incorporating complex **6**, as well as the 2-MTZ complex **7** detonated in the course of the experiment.

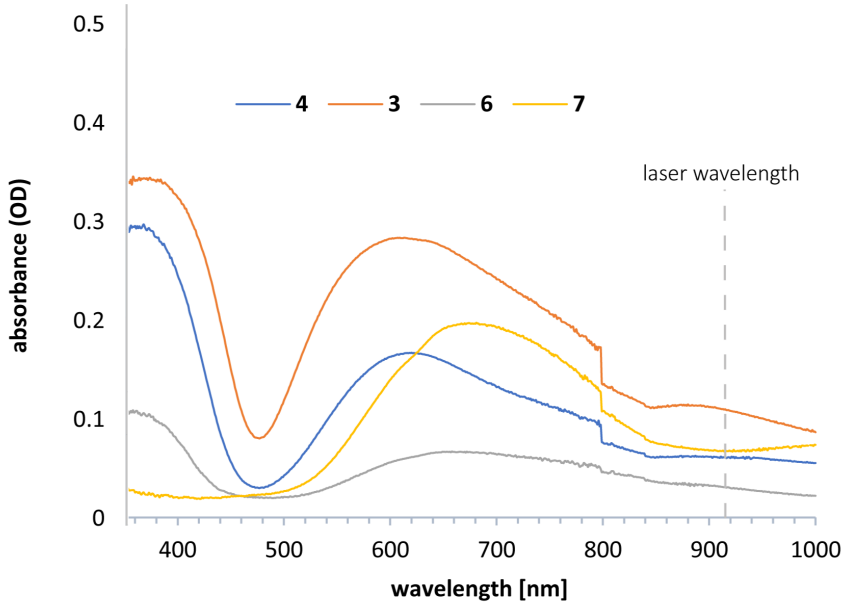


Figure 9. Solid state UV-Vis spectra of selected copper(II) complexes. The step in the absorption intensity at 800 nm is caused by a detector change. The UV-Vis spectra have only qualitative character.

While **3** exhibited a sharp deflagration upon laser irradiation, **4** solely decomposed without any sign of an exothermic reaction. Resulting from that, an unambiguous confirmation of either of the proposed initiation mechanisms (photochemical or thermal) remains anticipated. In contrast to literature, the comparably strong response of the least sensitive compound **3** towards optical stimuli suggests no distinct correlation between mechanical and optical sensitivites, further being approved by the observed difference between **4** and **7**.[10,12,21] Furthermore, an obvious coherence between thermal properties (see Table 2) and optical initiation is equally prohibited since **6** and **7**, which proved to be highly thermally stable, gave the most violent responses upon laser irradiation (see SI, Figure S7). Regarding the densities of the complexes and their outcome in the initiation tests, no general trend can be observed. Whereas compound **6** shows the highest density and a positive result in the experiments, complex **3** with the lowest one gives a stronger response to the irradiation than compound **4**. Conducted solid state UV/Vis measurements, which solely provide qualitative information, equally lack unequivocal trends (Figure 9). To begin with, the spectra of **3** and **4**, both reacting noticably differently during laser experiments, are almost identical in terms of observed d–d-transitions (613 and 620 nm) and curve shape. Moreover, the detected absorbance at the applied irradiation (915 nm) solely corresponds to a

fraction of the d–d-transition's maximum (see Table 4). Resulting from these conclusions, a desired correlation between coordination chemistry and optical sensitivity once again remained unfulfilled. Based on the previously noted, vague but highly relevant impact of fractal characteristics and the overall inconclusive current state of research in the field of laser-ignitable ECC, further investigations remain indispensable.

11.3 Conclusions

In summary, a series of energetic copper(II) perchlorate complexes was successfully synthesized and characterized by manipulating the present coordination chemistry through adjusting the parameters solvent, stoichiometry, acidity, and the applied 2-substituted tetrazole ligand. In regard of the 2-MAT complexes $[Cu(H_2O)_2(2\text{-MAT})_4](ClO_4)_2 \cdot H_2O$ (**3**), $[Cu(H_2O)_2(2\text{-MAT})_4](ClO_4)_2$ (**4**) and $[Cu(ClO_4)_2(H_2O)_2(2\text{-MAT})_2]$ (**6**), a decrease of the compound's water content as well as the incorporation of perchlorato ligands led to a rough increase of thermal stability and overall sensitivity. Inconsistencies especially in regard of measured sensitivities and laser ignitability might be addressed to fractal characteristics and particle sizes. Introducing a new nitrogen-rich ligand with increased energetic character (2-MTZ, **2**) results in novel patterns of the examined properties despite identical coordination chemistry (**7** vs **4**). In the present case, higher thermal stability was accompanied by an increase in optical and friction sensitivity and simultaneous decrease of ESD and impact sensitivities. Consequently, the present report provides leadoff insights into the correlation of an ECC's coordination chemistry and derived energetic properties, while future investigations might further develop observed patterns. Moreover, the obtained complexes, especially **6** and **7**, indeed meet targeted properties including exceptionally high thermal stability, decreased mechanical sensitivities in comparison to 2-aminotetrazole ECC and retained laser ignitability. Therefore, both conveniently synthesized ECC represent promising candidates for being applied in future ignition (optical or mechanical) systems.

Supporting information available in the appendix in **Chapter 19.8**.

11.4 References

[1] (a) E. Platania, N. L.W. Streeton, H. Kutzke, A. Karlsson, E. Uggerud and N. H. Andersen, *Vib. Spectrosc.*, 2018, **97**, 66–74. (b) S. Bette, R. K. Kremer, G. Eggert and R. E. Dinnebier, *Dalton Trans.*, 2018, **47**, 8209–8220.

[2] (a) F. Brunel, N. E. El Gueddari and B. M. Moerschbacher, *Carbohyd. Polym.*, 2013, **92**, 1348–1356. (b) S. Chandraleka and G. Chandramohan, *Int. J. ChemTech Res.*, 2014, **6**, 5450–5457.

[3] R. R. Conry, "Copper: Inorganic & Coordination Chemistry" in *Encyclopedia of Inorganic Chemistry*, John Wiley & Sons, Ltd., 1st edn., 2006.

[4] (a) H.-J. Zhang, A. W. Schuppe, S.-T. Pan, J.-X. Chen, B.-R.Wang, T. R. Newhouse and L. Yin, *J. Am. Chem. Soc.*, 2018, **140**, 5300−5310. (b) S. B. Thorpe, J. A. Calderone and W. L. Santos, *Org. Lett.*, 2012, **14**, 1918–1921. (c) P. C. Roest, N. W. M. Michel, and R. A. Batey, *J. Org. Chem.*, 2016, **81**, 6774–6778.

[5] (a) P. L. Holland and W. B. Tolman, *Coord. Chem. Rev.*, 1999, **190**–**192**, 855–869. (b) W. L. Nettles, H. Song, E. R. Farquhar, N. C. Fitzkee and J. P. Emerson, *Inorg. Chem.*, 2015, 54, **12**, 5671–5680. (c) C. A. Blasie and J. M. Berg, *J. Am. Chem. Soc.*, 2003, **125**, 6866–6867.

[6] T. M. Klapötke, Chemistry of High-Energy Materials, Walter de Gruyter, Berlin, Boston, 2nd edition, 2012.

[7] (a) G.-H. Tao, D. A. Parrish and J. M. Shreeve, *Inorg. Chem.*, 2012, **51**, 5305–5312. (b) R. P. Singh, R. D. Verma, D. T. Meshri, and J. M. Shreeve, *Angew. Chem. Int. Ed.*, 2006, **45**, 3584–3601. (c) Q. Zhang and J. M. Shreeve, *Angew. Chem. Int. Ed.*, 2014, **53**, 2540–2542.

[8] (a) T. W. Myers, D. E. Chavez, S. K. Hanson, R. J. Scharff, B. L. Scott, J. M. Veauthier and R. Wu, *Inorg. Chem.*, 2015, **54**, 8077–8086. (b) T. W. Myers, K. E. Brown, D. E. Chavez, R. J. Scharff and J. M. Veauthier, *Inorg. Chem.*, 2017, **56**, 2297−2303. (c) T. W. Myers, J. A. Bjorgaard, K. E. Brown, D. E. Chavez, S. K. Hanson, R. J. Scharff, S. Tretiak and J. M. Veauthier, *J. Am. Chem. Soc.*, 2016, **138**, 4685–4692.

[9] (a) M. Friedrich, J. C. Gálvez-Ruiz, T. M. Klapötke, P. Mayer, B. Weber and J. J. Weigand, *Inorg. Chem.*, 2005, **44**, 8044–8052. (b) G. Geisberger, T. M. Klapötke and

J. Stierstorfer, *Eur. J. Inorg. Chem.*, 2007, **2007**, 4743–4750. (c) M. Joas, T. M. Klapötke, J. Stierstorfer and N. Szimhardt, *Chem. Eur. J.*, 2013, **19**, 9995–10003. (d) M. Joas, T. M. Klapötke and N. Szimhardt, *Eur. J. Inorg. Chem.*, 2014, **2014**, 493–498. (e) M. Joas and T. M. Klapötke, *Z. Anorg. Allg. Chem.*, 2014, **640**, 1886–1891. (f) T. M. Klapötke, P. C. Schmid, J. Stierstorfer and N. Szimhardt, *Z. Anorg. Allg. Chem.*, 2016, **642**, 383–389.

[10] N. Szimhardt, M. H. H. Wurzenberger, A. Beringer, L. J. Daumann and J. Stierstorfer, *J. Mater. Chem. A*, 2017, **5**, 23753–23765.

[11] J. Evers, I. Gospodinov, M. Joas, T. M. Klapötke and J. Stierstorfer, *Inorg. Chem.*, 2014, **53**, 11749–11756.

[12] N. Szimhardt and J. Stierstorfer, *Chem. Eur. J.*, 2018, **24**, 2687–2698.

[13] N. Szimhardt, M. H. H. Wurzenberger, L. Zeisel, Michael S. Gruhne, M. Lommel, J. Stierstorfer, *J. Mater. Chem. A*, 2018, **6**, 16257–16272.

[14] (a) Y. Cui, T.-L. Zhang, J.-G. Zhang, L. Yang, X.-C. Hu, J. Zhang, *J. Mol. Struct.*, 2008, **889**, 177–185. (b) Y. Cui, J. Zhang, T. Zhang, L. Yang, J, Zhang, X. Hu, *J. Hazard. Mater.*, 2008, **160**, 45–50.

[15] A. V. Smirnov, M. A. Ilyushin and I. V. Tselinskii, *Russ. J. Appl. Chem.*, 2004, **77**, 794–796.

[16] Y. Xu, W. Liu, D. Li, H. Chen and M. Lu, *Dalton Trans.*, 2017, **46**, 11046–11052.

[17] Gas phase enthalpies of formation were calculated using the atomization method ($\Delta_f H^0_{(g,M)} = H_{(M)} - \Sigma H^0_{(A)} + \Sigma \Delta_f H^0_{(A)}$) using Gaussian09 computed CBS-4M electronic enthalpies.

[18] (a) A. Y. Zhilin, M. A. Ilyushin, I. V. Tselinskii, A. S. Kozlov, and N. E. Kuz'mina, *Russ. J. Appl. Chem.*, 2002, **75**, 1849–1851. (b) M. H. H. Wurzenberger, N. Szimhardt and J. Stierstorfer, *J. Am. Chem. Soc.*, 2018, **140**, 3206−3209.

[19] H. Radies, „Synthesis and Characterization of Energetic Transition Metal-Tetrazolate Complexes", *Diploma thesis*, 2006.

[20] (a) K. Karaghiosoff, T. M. Klapötke, P. Mayer, C. M. Sabaté, A. Penger, J. M. Welch, *Inorg. Chem.*, 2008, **47**, 1007-1019. (b) T. M. Klapötke, and J. Stierstorfer, *Eur. J. Inorg.*

Chem., 2008, **2008**, 4055–4062. (c) T. M. Klapötke, and C. M. Sabaté, *Eur. J. Inorg. Chem.*, 2008, **2008**, 5350–5366.

[21] N. Szimhardt, M. H. H. Wurzenberger, T. M. Klapötke, J. T. Lechner, H. Reichherzer, C. C. Unger, J. Stierstorfer, *J. Mater. Chem. A*, 2018, **6**, 6565−6577.

[22] M. Freis, T. M. Klapötke, J. Stierstorfer and N. Szimhardt, *Inorg. Chem.*, 2017, **56**, 7936−7947.

[23] Crystallographic data for the structures have been deposited. with the Cambridge Crystallographic Data Centre.

[24] J. H. Bryden, *Acta Cryst.*, 1956, **9**, 874–878.

[25] (a) P. N. Gaponik, M. M. Degtyarik, A. S. Lyakhov, V. E. Matulis, O. A. Ivashkevich, M. Quesada, J. Reedijk, *Inorg. Chim. Acta*, 2005, **358**, 3949–3957. (b) E. J. van den Huevel, P. L. Franke, G. C. Verschoor and A. P. Zuur, *Acta Cryst.*, 1983, **39**, 337–339.

[26] (a) X. Song, Y. Wang, C. An, X. Guo and F. Li, *J. Hazard. Mater.*, 2008, **159**, 222–229. (b) Y. Wang, X. Song, D. Song, W. Jiang, H. Liu, F. Li, *Propellants Explos. Pyrotech.* 2011, **36**, 505–512.

[27] Storm, C. B.; Stine, J. R.; Kramer, J. F., *Chemistry and Physics of Energetic Materials*, 1990, **309**, 605−639.

[28] W. Zhu and H. Xiao, *Struct. Chem.*, 2010, **21**, 657−665.

[29] P. Politzer and J. S. Murray, *J. Mol. Model.*, 2015, **21**, 25.

[30] D. Mathieu, *Ind. Eng. Chem. Res.*, 2017, **56**, 8191−8201.

[31] (a) M. T. Greenfield, S. D. McGrane, C. A. Bolme, J. A. Bjorgaard, T. R. Nelson, S. Tretiak and R. J. Scharff, *J. Phys. Chem. A*, 2015, **119**, 4846−4855. (b) A. E. Sifain, J. A. Bjorgaard, T. W. Myers, J. M. Veauthier, D. E. Chavez, O. V. Prezhdo, R. J. Scharff and S. Tretiak, *J. Phys. Chem. C*, 2016, **120**, 28762−28773. (c) E. D. Aluker, A. G. Krechetov, A. Y. Mitrofanov, D. R. Nurmukhametov and M. M. Kuklja, *J. Phys. Chem. C*, 2011, **115**, 6893–6901.

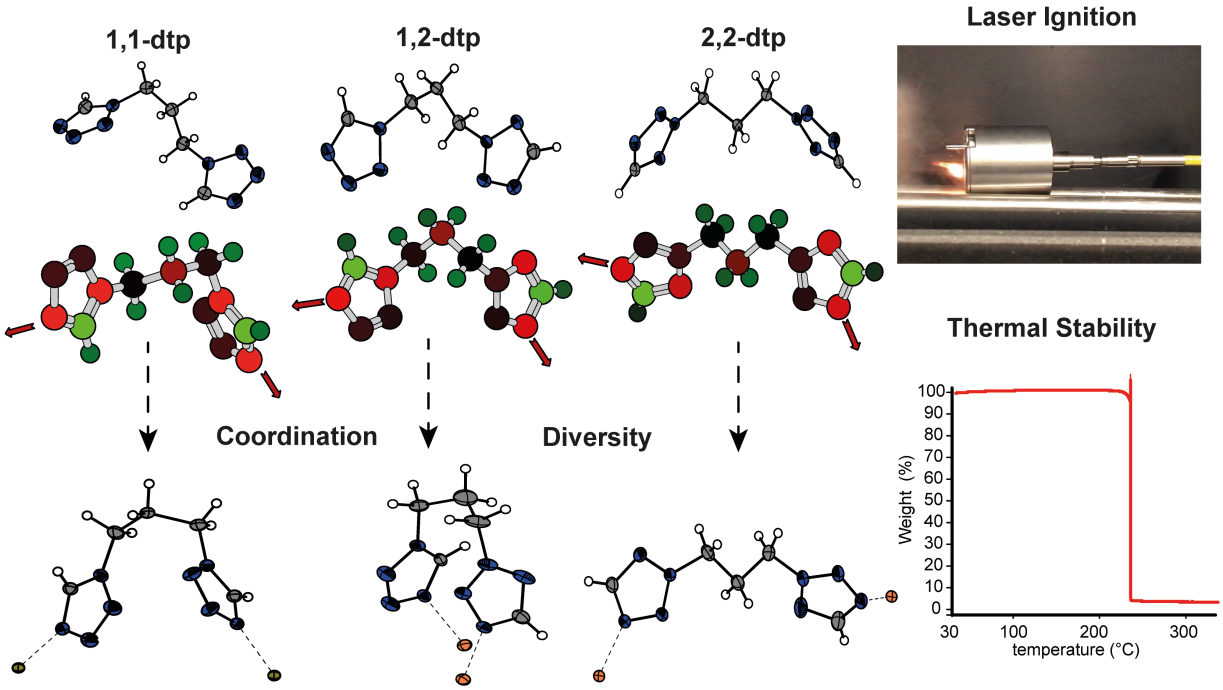
[32] (a) D. D. Dlott, M. D. Fayer, *J. Chern. Phys.*, 1990, **92**, 3798–3812. (b) E. D. Aluker, A. S. Zverev, A. G. Krechetov, A. Yu. Mitrofanov, A. O. Terentyeva, A. V. Tupitsyn, *Russ. J. Phys. Ch. B*, 2014, **8**, 687–691.

12 Highly Functional Energetic Complexes: Stability Tuning through Coordination Diversity of Isomeric Propyl-linked Ditetrazoles

Norbert Szimhardt, Maximilian H. H. Wurzenberger, Thomas M. Klapötke, Jasmin T. Lechner, Hannes Reichherzer, Cornelia C. Unger, and Jörg Stierstorfer

published in *Journal of Materials Chemistry A*, **2018,** *6,* 6565-6577

DOI: 10.1039/C8TA01412D



A series of highly functional new energetic coordination compounds (ECC) were prepared and their physicochemical properties tuned by the use of various metal(II) centers and three different ditetrazolylpropane isomers.

Abstract

Currently used primary explosives suffer from various drawbacks like insidious sensitivities toward mechanical stimuli and electrostatic discharge, but also from environmental concerns largely attributed to toxic lead compounds. These issues can directly be related to higher risk during processing and handling of these sensitive materials. In this research, 12 new lead-free energetic coordination compounds (ECC) based on three isomeric propyl-linked ditetrazoles as ligands with moderate sensitivities are described, which can be initiated reliable and safely by irradiation with near infrared light (NIR). Excellent thermal stabilities for all complexes up to an outstanding decomposition temperature of 297 °C for compound **7** could be achieved through the formation of stable polymeric networks. The optical and energetic properties of these complexes can easily be customized by variation of various building blocks like different transition metals (Mn^{2+}, Fe^{2+}, Ni^{2+}, Co^{2+}, Cu^{2+}, Zn^{2+}, and Ag^{+}), anions (perchlorate, styphnate, cyanodinitromethanide and dinitramide) and for the first time by the use of three different isomeric ditetrazole ligands. 1,3-di(tetrazol-1-yl)propane (1,1-dtp), 1-(tetrazol-1-yl)-3-(tetrazol-2-yl)propane (1,2-dtp) and 1,3-di(tetrazol-2-yl)propane (2,2-dtp) were prepared in a convenient and straightforward one-step alkylation reaction of 1,5*H*-tetrazole. The obtained compounds were extensively characterized by e.g. XRD, IR, EA, UV/Vis and DTA. In addition, the sensitivities toward external stimuli (impact, friction and electrostatic discharge) were determined according to *Bundesamt für Materialforschung und –prüfung (BAM)* standard methods. The iron(II) **5** and copper(II) perchlorate complexes **8**, **11** and **12** show promising characteristics and could be potential candidates for possible applications in the future.

12.1 Introduction

The first tetrazole compound mentioned in the literature, 1-phenyl-1*H*-tetrazole-5-carbonitrile, was accidently synthesized by the Swedish chemist J. A. Bladin in 1885 at the University of Uppsala.[1] Since then numerous compounds based on this five-membered heterocycle have been prepared and extensively characterized.[2–4] Particularly in the challenging field of coordination chemistry, tetrazole ligands have proven to be versatile components that form a large number of functional materials.[5,6] These compounds show promise in many different applications ranging from molecular magnetism in spin-crossover systems,[7,8] porous metal-organic frameworks (MOF) for potential gas storage,[9] and possible use as energetic materials such as secondary and primary explosives.[10,11]

The spin crossover (SCO) phenomenon, wherein the spin state of the compound alters in consequence of an external stimuli (specific temperature, pressure or light irradiation), has attracted considerable attention in recent years.[12] Especially iron(II) complexes, but also other transition metals with d^4 to d^7 electronic configuration coordinated by alkylated mono- and ditetrazoles (Chart 1a) in combination with various counter-anions like ClO_4^- and BF_4^-, showed this behavior. The phenomenon appears as a result of the interaction between the electron-electron repulsion and the dependence of the ligand-field strength on the metal to ligand distance.[13] The complexes showed two different lattice sites for the metal centers with a spin transition (*hs* to *ls*) depending on the applied temperature. Emission of electromagnetic waves with wavelengths in the green or red region can initiate metastable long-lived *hs* and *ls* states on both sides, which makes these compounds attractive for use as molecular switches or in liquid crystals.[14] In contrast to magnetic properties, very little is known of transition metal complexes in association with energetic materials (Chart 1b), although these compounds could indeed solve two basic problems of current primary explosives: high toxicity and high sensitivity. Toxic compounds like lead azide and lead styphnate are still the main components in most priming compositions today. Due to the potential risk to the human health and the environment, many scientists from around the world are searching for alternatives with partly different approaches.[15–18]

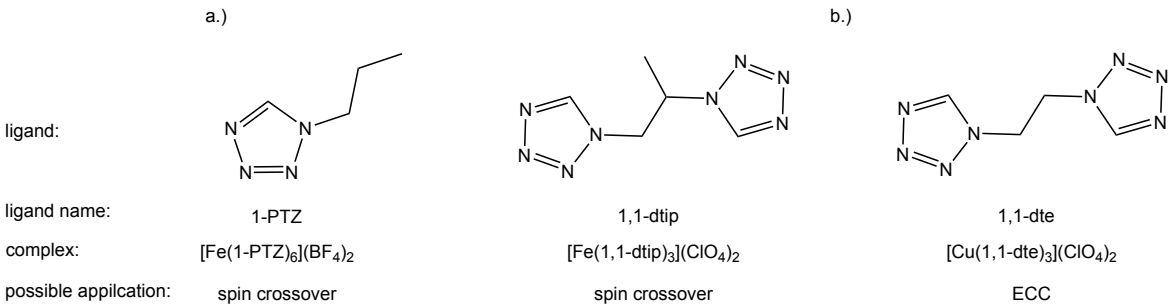


Chart 1. Overview of the selected mono- and ditetrazole ligands in combination with different metal salts proposed as: (a) spin crossover compounds or (b) ECC.[19–21]

Possible solutions comprise the use of non-toxic and sensitive: (a) neutral,[22,23] (b) ionic[24,25] or (c) coordination compounds (Chart 2).[26–28] Energetic coordination compounds (ECC) fulfill most of the desired requirements (low-cost, high yields, good compatibilities, low environmental impact, low toxicities etc.) and are therefore promising candidates for future applications in the field of high energy dense materials.[29–31]

Energetic complexes hold great potential in the area of optical initiation, which offers various benefits over conventional systems (electrical, mechanical, thermal).[32] The risk of accidental

initiation by unintended impulses (impact, friction, ESD) can be minimized through application of less sensitive explosives (Chart 2d) with the consequence of an easier processing and handling of these materials.[33] A further advantage of laser ignition is a shorter response time toward initiation pulses after irradiation by NIR, which allows safer and more reliable initiation of the materials.[34]

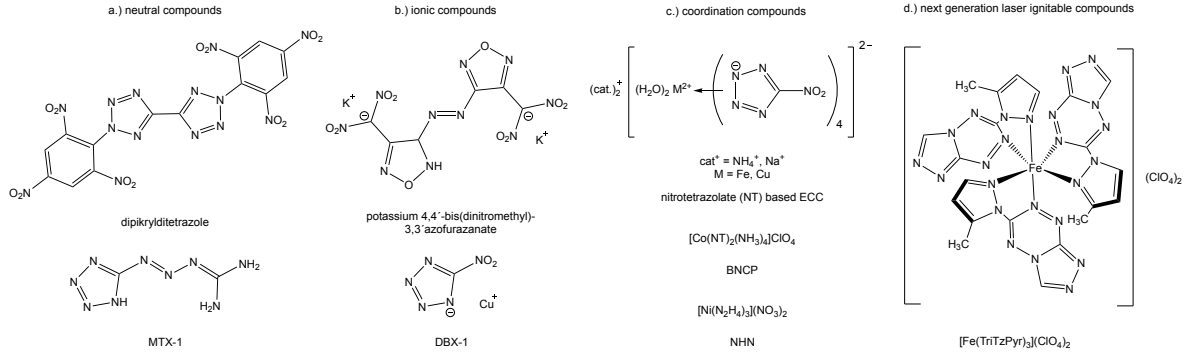


Chart 2. Different synthetic approaches in order to replace lead containing primary explosives through: (a) neutral,[22,23] (b) ionic,[24,25] (c) coordination compounds,[26–28] (d) new generation of laser ignitable explosives.[33]

Many recently developed primary explosives are struggling to meet the desired criteria regarding thermostability, which are particularly important for special applications in industry (e.g. mining and oil drilling).[35] Especially complex monomers without extended structures suffer from low thermal stabilities, which can most likely be attributed to a high vapor pressure of the ligands in combination with relatively weak coordination bonds.[6]

In order to overcome the lack in thermal stability, modifications and further developments were made and bidentate bridging tetrazole ligands implemented into the ECC to build up stable multidimensional (1D, 2D or 3D) polymeric networks (MOF, Figure 1). In the past, investigations of the physico-chemical properties of these tetrazole based energetic complexes as well as toxicological studies toward aquatic life have proven the great suitability of these ligands.[6,17] For this purpose, three different isomeric propyl linked ditetrazoles prepared in a convenient one step reaction were selected, which until now, have only been described in correlation with magnetic studies in spin transition experiments.[36,37] Desired physicochemical properties of the compounds were easily adjusted by variation of the metal, the anion and for the first time by application of different isomers with varying complexation patterns resulting in a great coordination diversity. In this contribution, reasonable efforts have been made to use these nitrogen-rich ligands as building blocks for the preparation of new energetic coordination polymers with desired characteristics, such as thermal stability and laser-ignitibility.

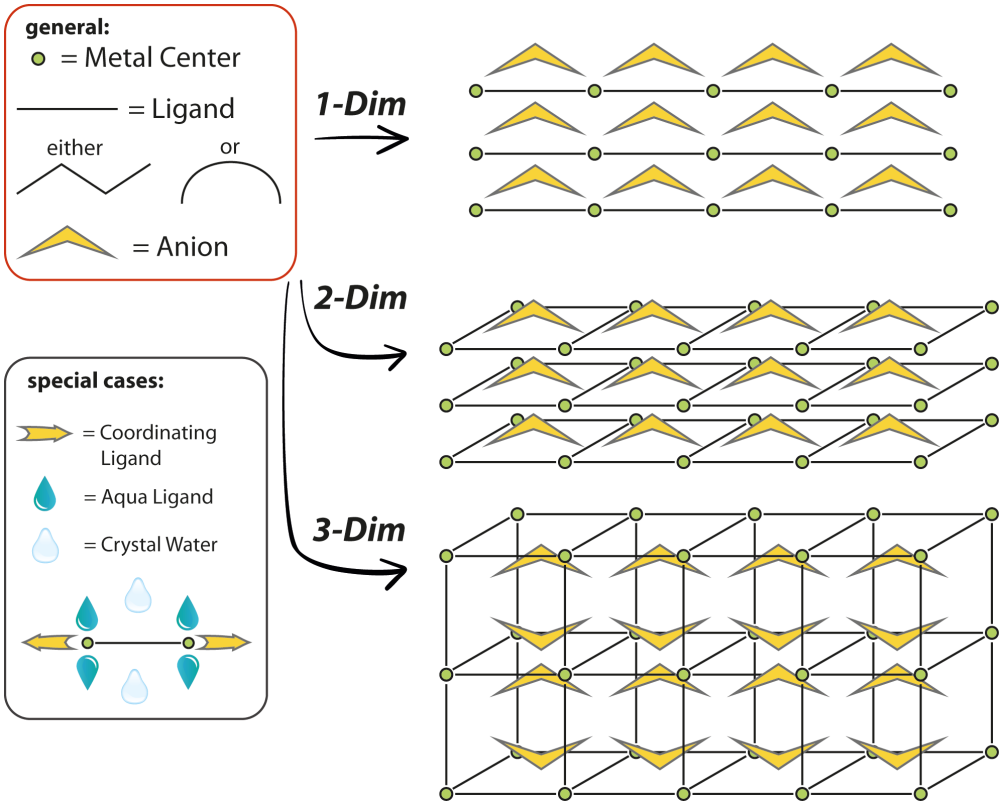


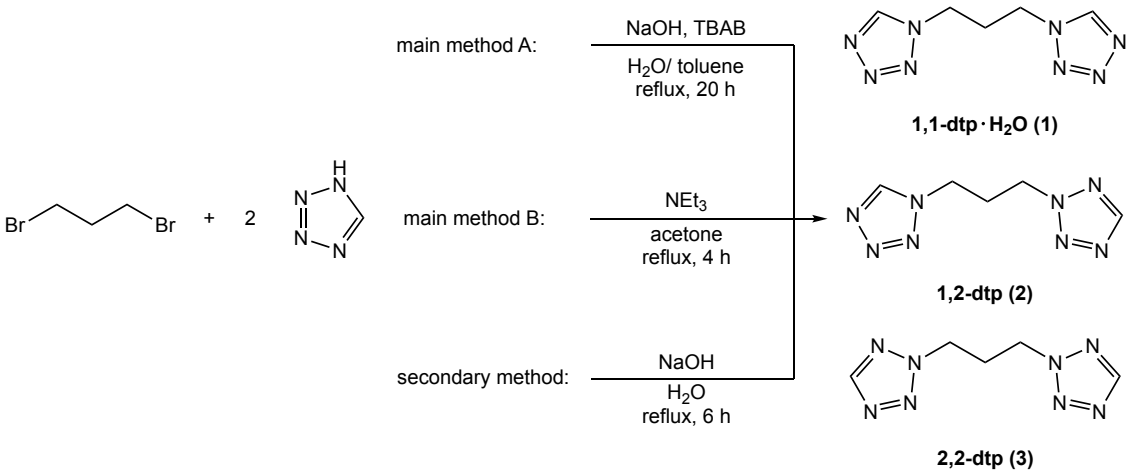
Figure 1. Concept of thermostability in energetic coordination compounds (ECC) achieved through the assembly of multidimensional (1D, 2D or 3D) polymeric networks (MOF) based on bidentate bridging ditetrazole ligands.

12.2 Results and Discussion

12.2.1 Synthesis

Various synthetic pathways toward tetrazole derivatives have been reported in the literature providing an easy access to this class of compounds.[38] One commonly used route starts from primary amine precursors and enables the preparation of *N*1-substituted tetrazoles free of other regioisomers.[39,40] Corresponding amines cyclize after treatment with sodium azide and triethyl orthoformate under acidic conditions in a [2+3] cycloaddition reaction. However, the synthesis of 1,3-di(tetrazol-1-yl)propane (1,1-dtp) via this conventional route fails and isolation of the desired compound is not possible. Therefore, two synthetic protocols have been developed, including the nucleophilic substitution reaction of 1,3-dibromopropane by sodium 5*H*-tetrazolate under various conditions.[36,37] However; this alkylation method affords an isomeric mixture containing not only 1,1-dtp but also the *N*2-substituted 1,3-di(tetrazol-2-yl)propane (**3**, 2,2-dtp) and the mixed *N*1,*N*2-substituted 1-(tetrazol-1-yl)-3-(tetrazol-2-yl)propane (**2**, 1,2-

dtp). Both heterocycles, which have already been described in the literature, cannot be synthesized directly as regioisomerically pure and suffer from the same issues as 1,1-dtp.[41–43] Therefore, an extensive investigation was carried out on the synthesis, purification and isolation of all three isomers from one reaction mixture by different preparative strategies (Scheme 1). After evaluation and comparison of these methods, information regarding the influence of a phase transfer catalyst, varying solvents, organic/inorganic bases and a differing work-up on the reaction products (yield and ratio) were obtained and are summarized in Table 1. All syntheses examined used 1,5*H*-tetrazole as the starting material, which was deprotonated to the corresponding tetrazolate salt by sodium hydroxide (main method A and secondary method) or by triethylamine (main method B) and further reacted with the alkylating agent 1,3-dibromopropane in a nucleophilic substitution reaction. In contrast to other described syntheses using solely acetone or water as solvents, method A included the use of a phase transfer catalyst (TBAB = tetrabutylammonium bromide) in combination with a water/toluene solvent mixture to facilitate the dispersion of the reactants. Heating of the reaction mixtures to reflux for a certain time period was accompanied with the formation of the associated bromide salts (sodium bromide or triethylammonium bromide), which were separated later during the work-up process. Separation of the crude material was accomplished through flash column chromatography on silica gel partly and through extraction and addition of different organic solvents (main method B and secondary method) based on the different polarities of the three isomers. Further details on the work-up procedures can be found in the experimental section.



Scheme 1. Preparation of the propyl-linked ditetrazole isomers **1**–**3** via different synthetic pathways.

The highest overall yield was observed for method A with a value of 71%, followed by 66% for method B and only 17% for the secondary method. A possible explanation for the low yield

of the secondary method could be an incomplete reaction of the starting materials due to the bad solubility of the reactants in water and losses during the work-up. Selectivity of alkylation is mainly dominated by the electronic structure of the substituents at the heterocycle and favors the formation of the mixed *N*1,*N*2-substituted ditetrazole **2**. Distinction of the obtained isomers can easily be made by infrared spectroscopy (Figure S1), ^{1}H and ^{13}C NMR spectroscopy. In addition, proton coupled ^{15}N NMR or two dimensional ^{1}H, ^{15}N NMR HMBC spectroscopy can be applied (Figure 2).

Various coordination compounds based on 1,2-di(tetrazol-5-yl)ethane (1,1-dte) as the ligand have shown promising results during laser initiation experiments in the past but were too sensitive for any application.[17] In order to increase the stability, ditetrazolylpropane ligands with higher carbon contents were used for the synthesis of new complexes in this contribution. The main focus was put on the analogous *N*1,*N*1-substituted ditetrazole (1,1-dtp), which has been proven to be an extraordinary ligand for the preparation of new energetic materials. Our synthetic concept includes the formation of neutral coordination compounds or complex cations with integrated oxidizing anions like perchlorates, trinitrorescorcinates (TNR), cyanodinitromethanides or dinitramides enabled through the incorporation of neutral non-acidic ligands. Copper(II) perchlorate containing energetic coordination compounds have shown to be very promising in laser initiation experiments and were synthesized in combination with three different propyl-linked ditetrazoles.[44]

Table 1. Overview of the different methods, associated yields and isomer ratios.

	Main method A	**Main method B**	**Secondary method**
Base	NaOH	NEt_3	NaOH
Solvent	water/toluene	acetone	water
Temp./ time	reflux/ 20 h	reflux/ 4 h	reflux/ 6 h
Phase transfer cat.	TBAB	—	—
Work-up	column chromatography	desorption/ column chromatography	extraction/ column chromatography
1,1-dtp • H_2O	12%	9%	8%
1,2-dtp	41%	33%	6%
2,2-dtp	18%	24%	3%
Overall yield	71%	66%	17%

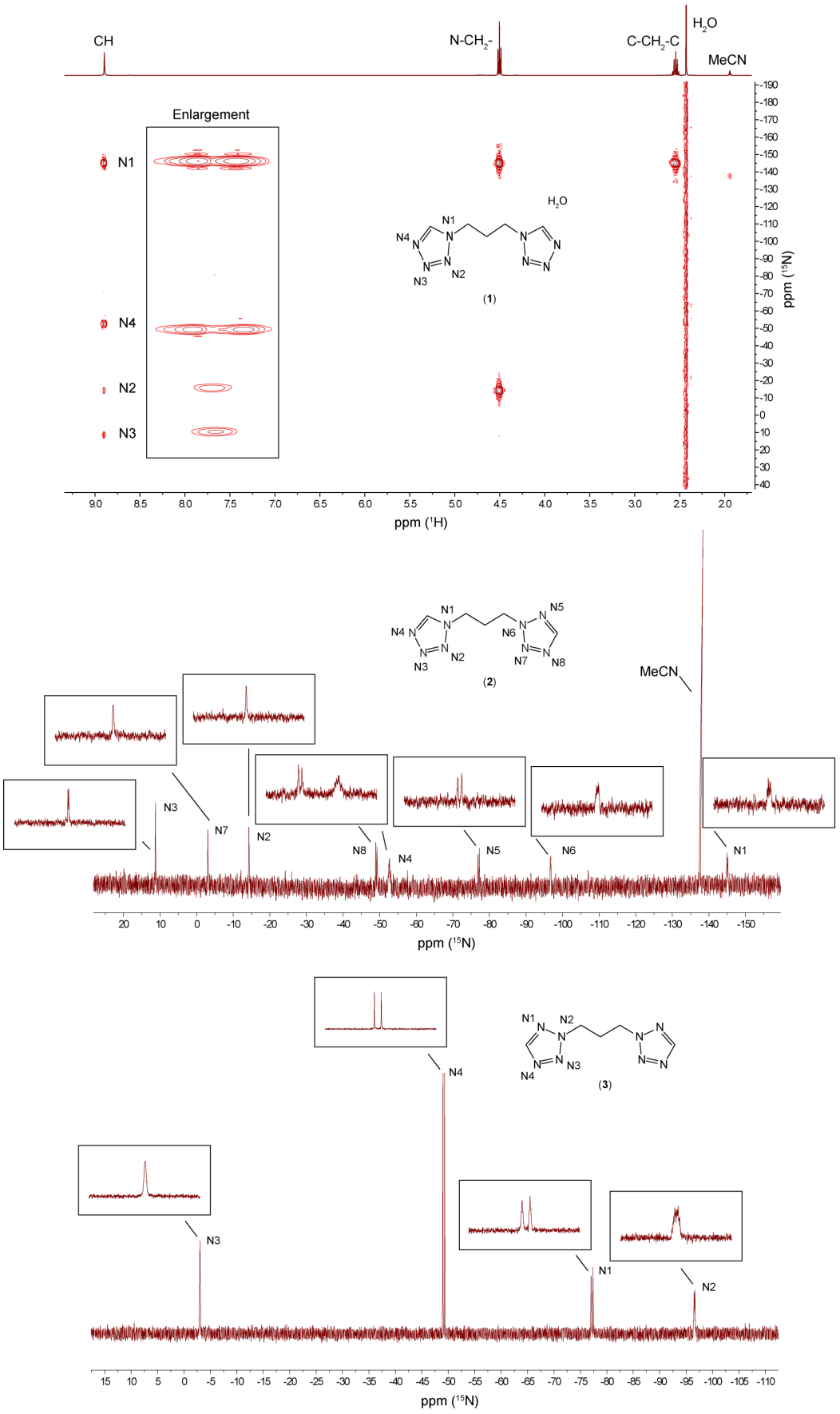
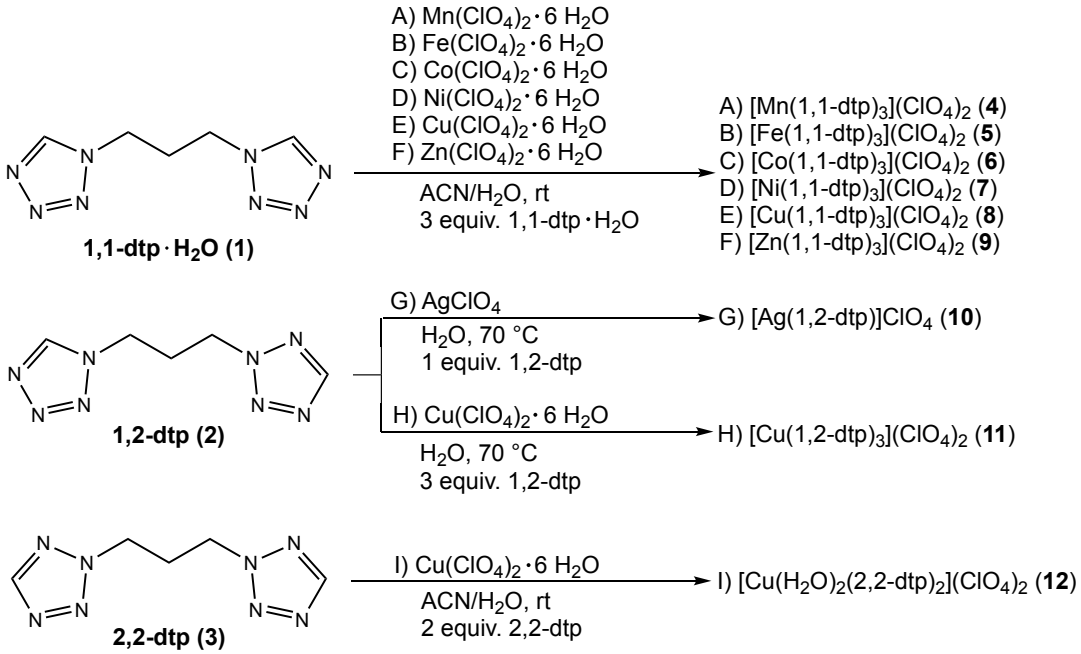


Figure 2. Two dimensional ^{1}H, ^{15}N HMBC NMR spectrum of **1** and proton coupled ^{15}N NMR spectra of **2** and **3**.

Synthesis of the coordination compounds **4**–**12** was achieved via combination of the associated metal(I,II) perchlorate salts and the respective ditetrazole ligands **1**–**3** in the corresponding stoichiometries at room temperature (Scheme 2). Exclusive use of water as solvent in the synthesis of **4**–**9** leads to the precipitation of compound **1** among the desired complexes due to the low solubility of **1** in water. In order to increase the solubility of the organic alkylated heterocycles, a mixture of water and acetonitrile was chosen as solvent and only small quantities were used to ensure fast crystallization of the desired complexes.

Coordination compounds **5** and **7** have already been described in relation to the SCO phenomenon and were prepared to close their physico-chemical gaps.[37] In addition, an intensive investigation and characterization of their energetic character has been conducted. All compounds (except **7**) were analyzed by single crystal diffraction. The nickel(II) perchlorate complex **7** precipitated, in contrast to the isotypic 1,1-dtp coordination compounds, as an amorphous powder and all recrystallization attempts failed to achieve single crystals. After comparision of the infrared spectra of **4**–**9** and elemental analysis, a complex composition of $[Ni(1,1\text{-dtp})_3](ClO_4)_2$ can be presumed for coordination compound **7**, analogous to the other perchlorate complexes (Figure S2).



Scheme 2. Synthesis of the metal(I,II) perchlorate complexes **4**–**12** based on different propyl-linked ditetrazole ligands.

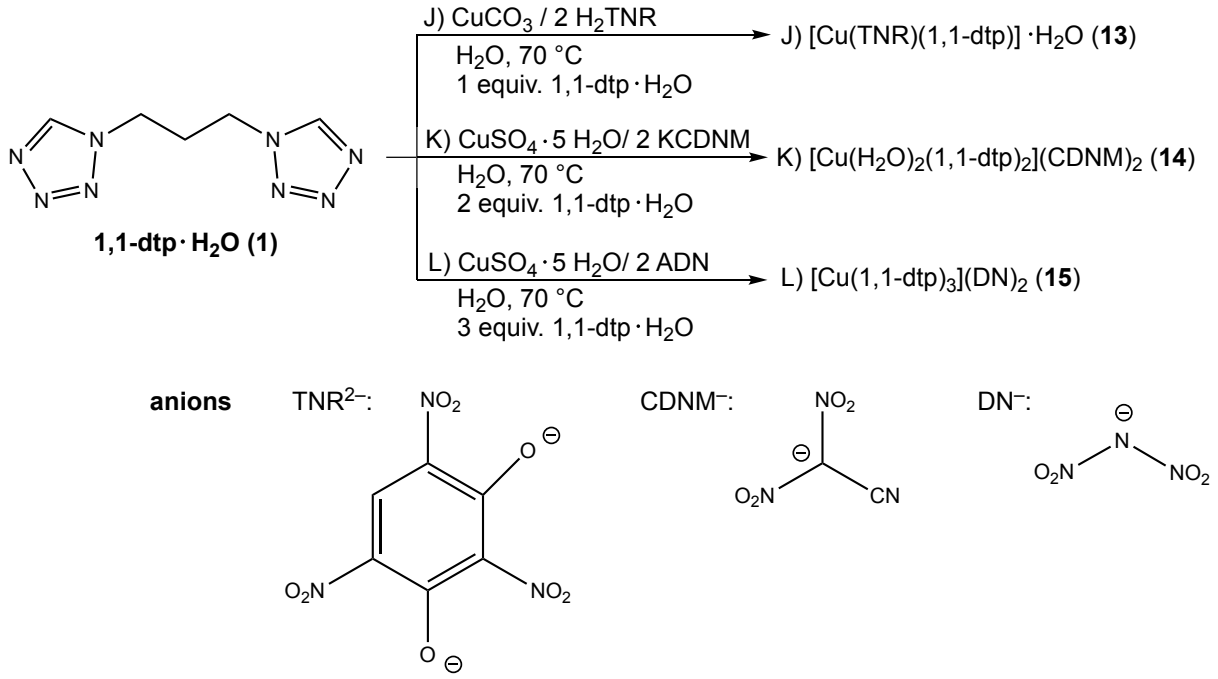
The nitrogen-rich compound 1-(tetrazol-1-yl)-3-(tetrazol-2-yl)propane (**2**), which has been succesfully inserted into the silver(I) and copper(II) perchlorate complexes (**10** and **11**), was

used for the first time as ligand in transition metal complexes. Each complex exhibits different absorptions in the infrared spectra showing a bidentate (**11**) or a tetradentate (**10**) complexation of the metal centers (Figure S3). The attempted preparation of silver(I) complexes with ligand **1** and **3** was unsuccesful.

The majority of the complexes could be achieved without crystal water or aqua ligand inclusion. This has a significant influence on the stability and performance of the compounds leading to more powerful molecules. Complex **12** crystallizes, in contrast to the reported copper(II) perchlorate coordination compound, as a diaqua species, which contains only two dtp ligands independent of the stochiometry applied (2 eqiv. vs. 3 equiv.).[42] A possible explanation could be the formation of a kinetic ($[Cu(2,2\text{-dtp})_3](ClO_4)_2$) complex first, which reacts slowly with the solvent molecules to the thermodynamic product ($[Cu(H_2O)_2(2,2\text{-dtp})_2](ClO_4)_2$). The copper(II) perchlorate complexes described here can easily be distinguished through IR spectroscopy due to the varying complexation manner of the three ditetrazole ligands (Figure S4). In particular, 2,2-dtp containing complexes have shown to crystallize primarily with solvent molecules, lowering the performance of the desired energetic material and making them unsuitable for any application.[42,43]

The commercially unavailable metal(II) salt precursors for the preparation of the coordination compounds **13**–**15** were synthesized in situ through metathesis or straightforward acid-base reaction between copper(II) carbonate and styphnic acid (H_2TNR) at 70 °C in water. The corresponding precursors were then reacted with the ditetrazole ligand **1** (Scheme 3) and the lower solubility of the complexes was used as the driving force. Coordination compound **13** precipitated unintentionalily as double deprotanated styphnate and crystal water containing complex immediately after addition of the ligand. Due to the low performance of the complex, no other trinitrobenzene containing anion (e.g. picrate) has been employed in the other complexes.

All described coordination compounds were left undisturbed for crystallization and were isolated by filtration after solid material appeared from the mother liquor in form of single crystals within hours or days (except nickel(II) complex **7**). The products were received in reasonable yields (35–89 %) after washing with ice-cold ethanol to remove unreacted materials when necessary and drying in air over night.



Scheme 3. Formation of the copper(II) coordination compounds **13**–**15** with varying anions (TNR^{2-} = trinitroresorcinate, $CDNM^-$ = cyanodinitromethanide, and DN^- = dinitramide; IR spectra illustrated in Figure S5).

12.2.2 Crystal Structures

The structure of all compounds including ligands and complexes (except **7**) was determined by low temperature X-ray diffraction. In contrast to the literature, ditetrazole **3** could be solidified through controlled freezing with liquid nitrogen and subsequent thawing to room temperature. The ligand stayed crystalline and single crystal blocks suitable for X-ray diffraction could be measured. Compound **7** emerged in form of an amorphous powder making single crystal experiments impossible. All central atoms, except the silver(I) metal ion in complex **10**, show an octahedral coordination sphere where the complexation to the metal ion takes place by the *N*4 and *N*8 nitrogen atoms of the ditetrazolylpropanes. Chelation of the ligand is prevented through the rigidity of the propyl chains, which disables the generation of complex monomers and leads to the formation of polymeric structures with varying dimensions by bridging between the metal centres. Poor quality single crystals of complex **13** were measured to get an indication of the most likely appearance of the structure. An appropriate finalization of the data set was not possible due to the strongly disordered moieties and the related weak diffractions. Nonetheless, elemental analysis in combination with infrared spectroscopy (Figure S5) validated its temporary observed structure. Details of the crystal structures of complexes **4**, **5**,

6, **9**, and **13** are given in the SI together with the measurement and refinement data of all compounds. The crystal structures were deposited in the CSD database[45] and can be obtained free of charge with the CCDC nos. 1816637 (**1**), 1816632 (**2**), 1816943 (**3**), 1816628 (**4**), 1816635 (**5**), 1816627 (**6**), 1816626 (**8**), 1816629 (**9**), 1816630 (**10**), 1816636 (**11**), 1816633 (**12**), 1816631 (**14**), 1816634 (**15**).

Compound **1** crystallizes as a monohydrate in the form of colorless blocks in the orthorhombic space group *Pbca* with eight formula units per unit cell and a calculated density of 1.439 g cm^{-3} at 173 K. One of the tetrazole rings stands in *gauche* (C1, N1–N4) orientation while the other stands in *anti* (C5, N5–N8) conformation to the propyl function (Figure 3), similar to the situation found in the anhydrous compound reported in literature.[36] The bond lengths of the propyl chain (C2–C3 1.5189(19) Å and C3–C4 1.5184(17) Å) are in the typical range of C–C single bonds and the distances in the tetrazole rings (N1–C1 1.3293(16) Å, N1–C2 1.4620(15) Å, N4–C1 1.3092(16) Å, N1–N2 1.3505(14) Å, N2–N3 1.2901(16) Å and N3–N4 1.3673(15) Å) are comparable to that of other 1-substituted tetrazoles.[46]

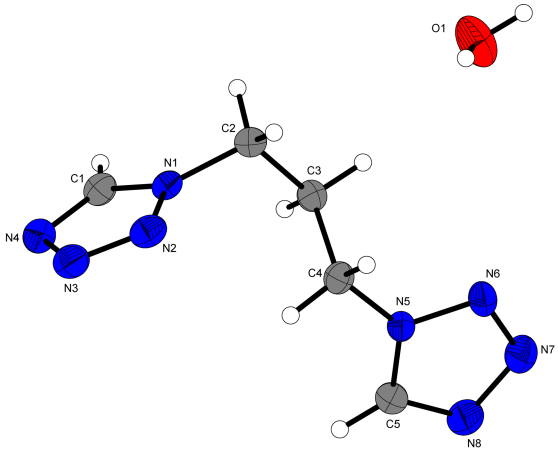


Figure 3. Molecular unit of 1,1-dtp · H_2O (**1**). Thermal ellipsoids of non-hydrogen atoms in all structures are set to the 50% probability level. Selected bond angles (°):C2–C3–C4 112.12(11), N1–C2–C3 111.38(11), and N5–C4–C3 110.96(10).

Nitrogen-rich ligand **2** crystallizes in the form of colorless blocks in the monoclinic space group $P2_1/n$ with four formula units per unit cell and a calculated density of 1.462 g cm^{-3} at 173 K. Ligand **2** shows, in contrast to compound **1**, a *gauche* conformation of both tetrazole rings to the propyl group with analogous bond lengths in the ring (C1, N1-N4) and the propyl bridge (Figure 4). In comparison to the other tetrazole moiety, only minor deviations can be observed in the bond lengths for the *N*2-substituted heterocycle (N5–C5 1.3249(15) Å, N6–C4

1.4655(14) Å, N8–C5 1.3376(15) Å, N5–N6 1.3265(13) Å, N6–N7 1.3177(12) Å and N7–N8 1.3239(13) Å).

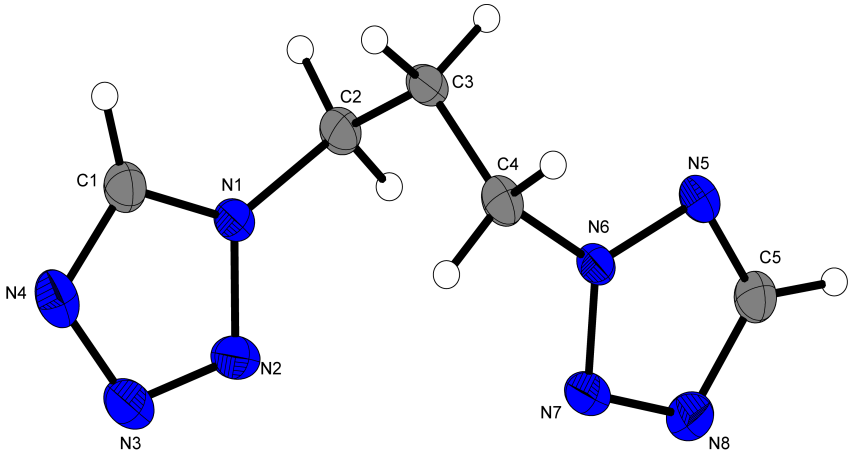


Figure 4. Molecular unit of 1,2-dtp (**2**). Selected bond lengths(Å): C2–C3 1.5204(17), C3–C4 1.5181(16), N1–C1 1.3308(14), N1–C2 1.4670(14), N4–C1 1.3070(16), N1–N2 1.3453(13), N2–N3 1.2932(14), N3–N4 1.3620(15); selected bond angles (°):C2–C3–C4 114.57(9), N1–C2–C3 112.19(9), and N6–C4–C3 111.93(9).

The *N*2,*N*2-substituted ditetrazole ligand **3** crystallizes in the form of colorless blocks in the monoclinic space group $P2_1/c$ with four formula units per unit cell and a calculated density of 1.474 g cm^{-3} at 143 K. The ligand shows unlike compound **1** and 1,2-dtp an *anti* conformation of both tetrazole heterocycles to the alkyl bridge but with similar bond lengths in the ring and chain (Figure 5).

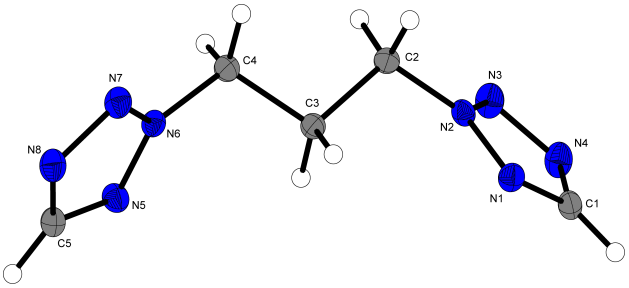


Figure 5. Molecular unit of 2,2-dtp (**3**). Selected bond lengths(Å): C2–C3 1.5209(15), C3–C4 1.5164(15), N1–C1 1.3260(16), N2–C2 1.4593(14), N6–C4 1.4590(15), N1–N2 1.3252(14), N2–N3 1.3200(14), N3–N4 1.3237(14); selected bond angles (°):C2–C3–C4 107.96(8), N2–C2–C3 112.05(8), and N6–C4–C3 112.19(8).

Coordination of the ditetrazole causes a reorientation of the ligands and is shown in Figure 6. The bond lengths of the coordinating ligands in the investigated complexes are in the same

range as the uncoordinated ditetrazole compounds **1**–**3** and are not discussed in detail in any of the following ECC.

The octahedrally coordinated metal(II) perchlorate complexes of heterocycle **1** (**4**–**6**, **8** and **9**) crystallize all isotypically in the trigonal space group *P*−3*c*1 with two formula units per unit cell showing almost the same metric with varying densities between 1.656 (**4**) and 1.754 g cm^{-3} (**5**) (Mn: 1.656 (173 K); Fe: 1.754 (123 K); Co: 1.712 (173 K); Cu: 1.721 (123 K) and Zn: 1.747 (123 K) g cm^{-3}). Interestingly the expected Jahn-Teller distortion, typical for d^9 electron configuration, cannot be observed in the structure of copper(II) complex **8** (Figure 7).

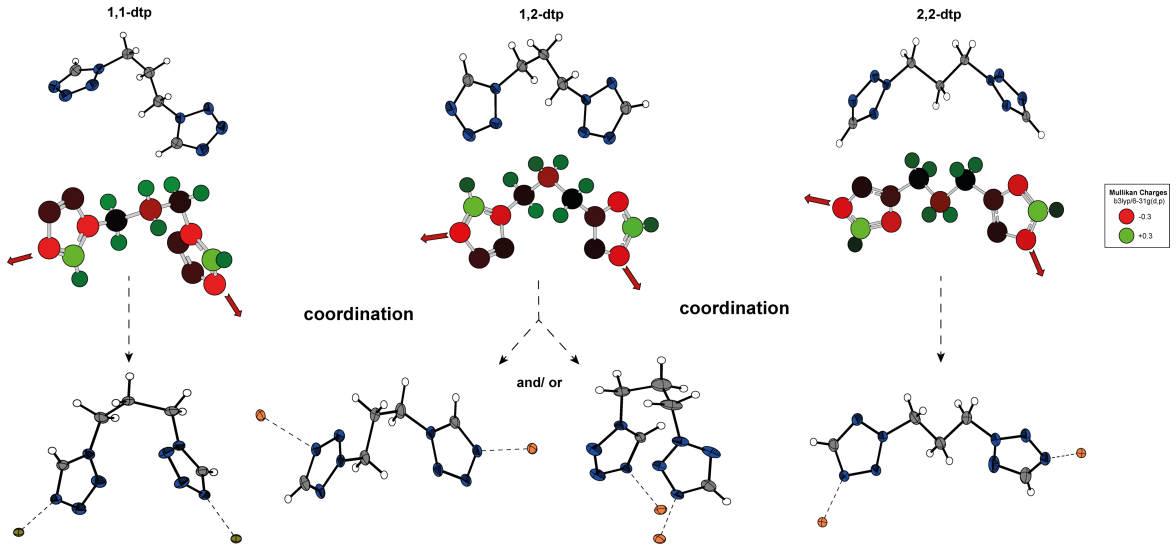


Figure 6. Reorientation of the ditetrazoles after complexation (except complex **10**) together with the calculated (B3LYP / 6-31G(d,p)) Mullikan charges of the uncoordinated dtp ligands.

Compared to the free ligand, both tetrazole rings are in *gauche* conformation to the propyl chain enabling the formation of polymeric chains made of transition metals(II), where the central atoms are connected by bridging ditetrazole units (Figure S6–9). In all perchlorate 1,1-dtp structures the central methylene units of the propylene bridges and also the perchlorate anions are heavily disordered and had to be refined as split positions.

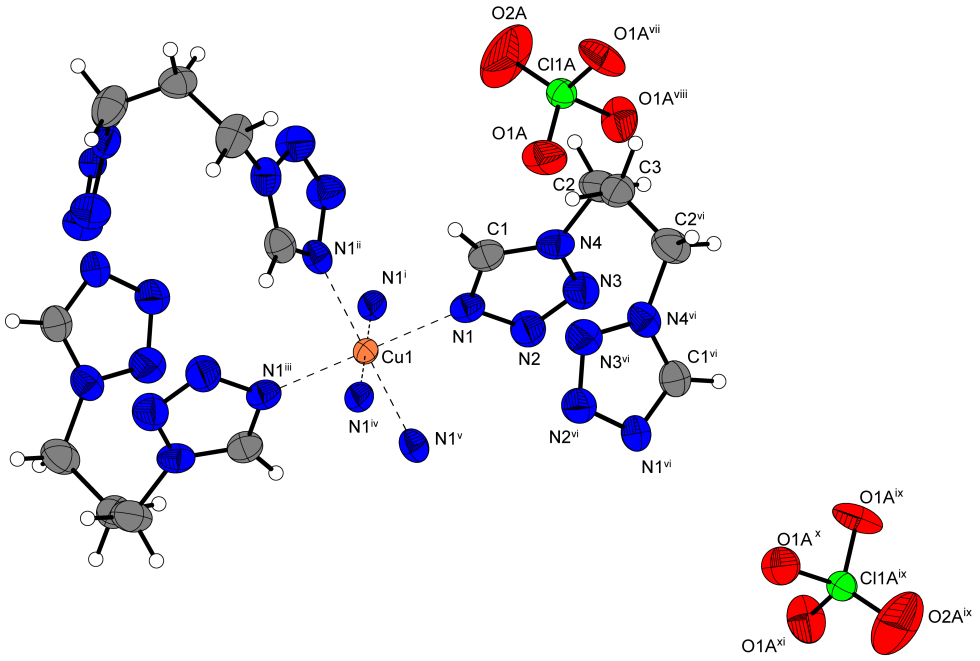


Figure 7. Copper(II) coordination environment of $[Cu(1,1\text{-dtp})_3](ClO_4)_2$ (**8**). Selected bond length (Å): Cu–N1 2.131(2); selected bond angles (°): N1–Cu1–N1^{i} 89.33(9), N1–Cu1–N1^{iii} 180.00, and N1–Cu1–N1^{iv} 90.68(9). Symmetry codes: (i) y, −x+y, 1−z; (ii) x−y, x, 1−z; (iii) –x, −y, 1−z; (iv) –y, x−y, z; (v) –x+y, −x, z; (vi) –x, −x+y, 1.5−z; (vii) –x+y, 1−x, z; (viii) 1−y, 1+x−y, z; (ix) 1+x−y, 1−y, 1.5−z; (x) y, x, 1.5−z; (xi) 1−x, −x+y, 1.5−z.

The d^{10} metal(I) perchlorate **10** is the only complex, that shows a tetrahedral coordination sphere. The compound crystallizes in the form of colorless blocks in the monoclinic space group $P2_1/c$ with four formula units per unit cell and a calculated density of 2.267 g cm^{-3} at 123 K, the highest density observed of all compounds. The silver(I) cation is bonded to only one neutral tetradentately (N1, N4, N7, N8) coordinating ditetrazole (Figure 8).

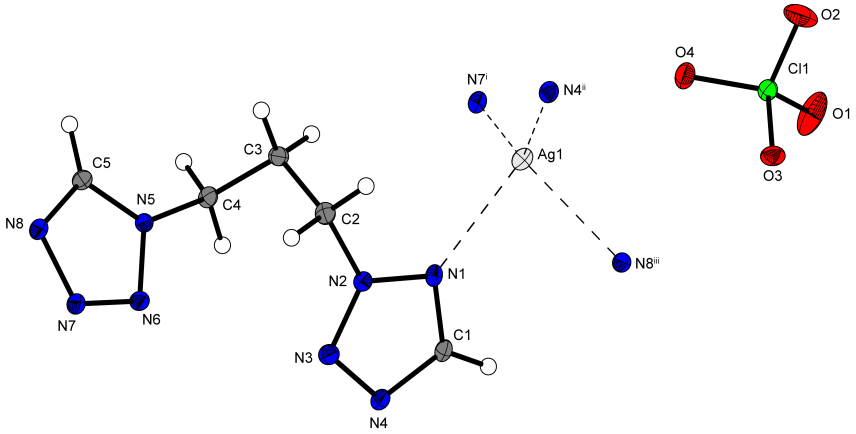


Figure 8. Silver(I) coordination environment of $[Ag(1,2\text{-dtp})]ClO_4$ (**10**). Selected bond lengths (Å): Ag1–N1 2.435(2), Ag1–N4^{ii} 2.264(2), Ag1–N7^{i} 2.265(2), Ag1–N8^{iii} 2.365(2); selected bond

angles (°): N1–Ag1–N7^{i} 105.96(6), N1–Ag1–N8^{iii} 83.91(6), N1–Ag1–N4^{ii} 109.10(6). Symmetry codes: (i) −x, 0.5+y, 0.5−z; (ii) x, 1.5−y, −0.5+z; (iii) −1+x, 1.5−y, −0.5+z.

The *N*1-substituted tetrazole bridges through its N3 and N4 donor atoms, whereas the 2-subsitituted ring binds with the N1 and N4 atoms. Compared to the free uncoordinated ligand, both rings maintain their *gauche* conformation to the propyl chain and each ditetrazolpropane bridges between four different silver(I) atoms (Figure 9 a) and b)) building up a three-dimensional polymeric network with incorporated non-coordinating perchlorate anions (Figure 9c) and d)).

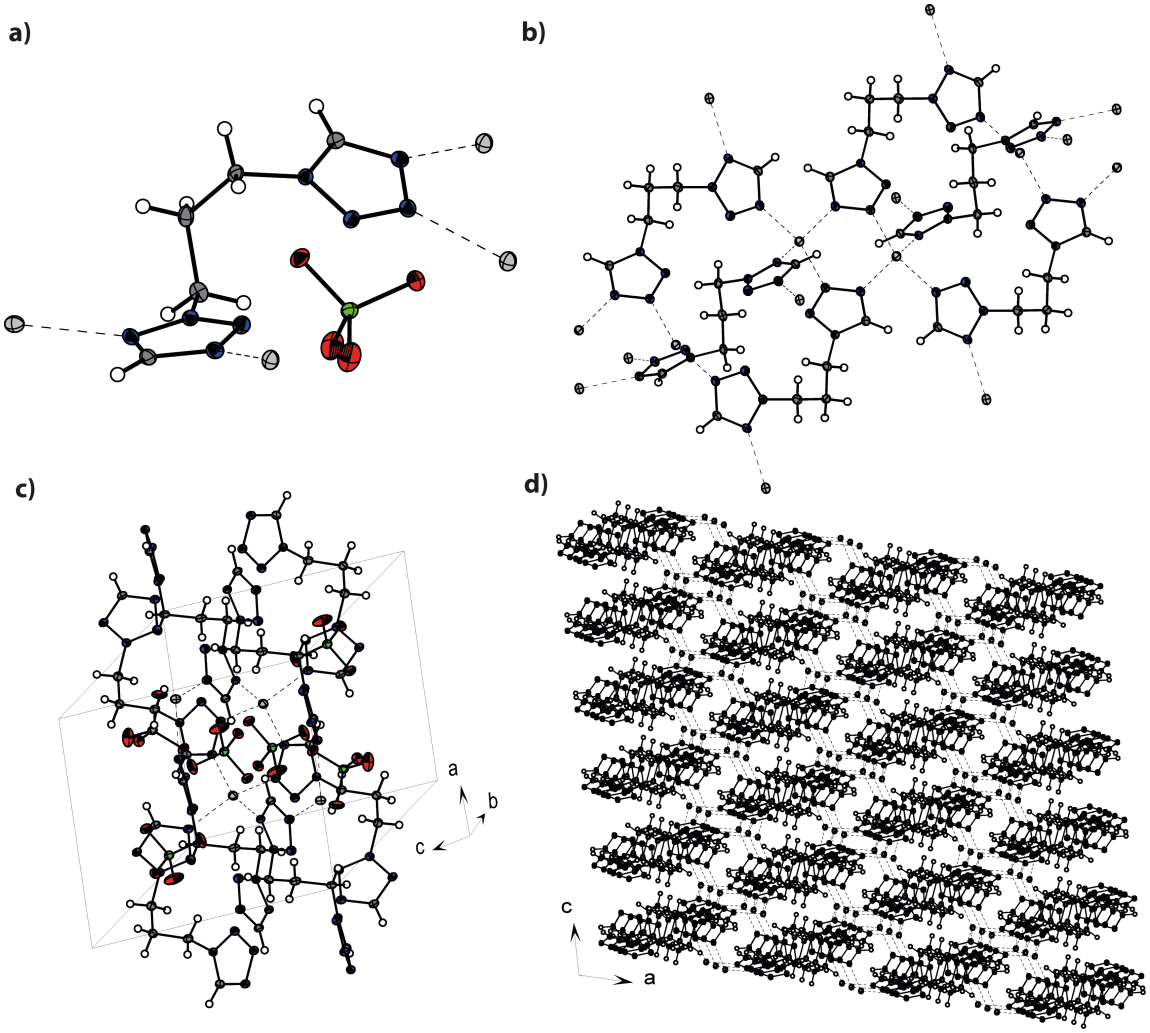


Figure 9. Coordination in [Ag(1,2-dtp)]ClO_4 (**10**): a) Formula unit with the linkage of the ligand between the metal(I) cations; b) bridging pattern of the tetradentately coordinating tetrazole **2** (omission of the perchlorate anions for better clarity); c) unit cell with 4 formula units; d) metal-organic framework (MOFs) depicted along the *b* axis (without perchlorate anions).

Complex **11** with 1.693 g cm^{-3} at 123 K shows the lowest density of all copper(II) complexes. It crystallizes in the form of blue rods in the triclinic space group *P*−1 with two formula units

per unit cell and shows every type of conformation (*gauche*/ *gauche*; *gauche*/ *anti*; and *anti*/ *anti*), in comparison to the free ligand **2**. The complex has an octahedral coordination sphere with six coordinating tetrazoles building up a three-dimensional polymeric network and shows, in contrast to **8**, the expected Jahn-Teller distortion along the axial direction (Figure 10). The inconsistent conformations of the ligand are accompanied by a loss of density.

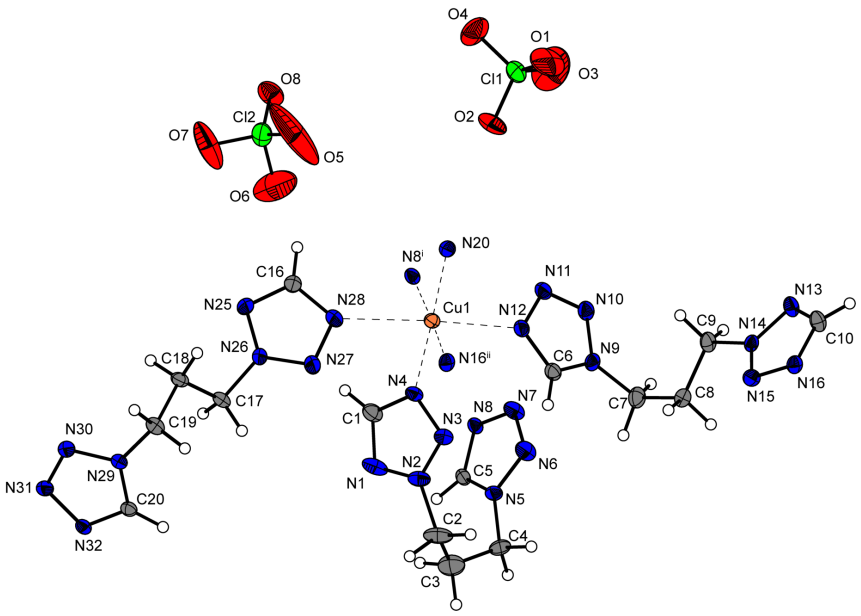


Figure 10. Coordination environment of $[Cu(1,2\text{-dtp})_3](ClO_4)_2$ (**11**). Selected bond lengths (Å): Cu1–N4 2.043(4), Cu1–N8 2.020(4), Cu1–N12 2.316(4), Cu1–N16 2.011(3), Cu1–N20 2.031(4), Cu1–N28 2.483(5); selected bond angles (°): N4–Cu1–N12 90.9(2), N4–Cu1–N8 94.1(2), N4–Cu1–N16 87.7(2). Symmetry codes: (i) 1−x, −y, 1−z; (ii) 2−x, −y, 1−z.

The diaqua complex **12** illustrated in Figure 11 crystallizes in the form of blue blocks in the monoclinic space group $P2_1/c$ with two formula units per unit cell and a calculated density of 1.765 g cm^{-3} at 233 K. Substitution of one ditetrazole through two aqua ligands leads to a slightly higher density in comparison to compound **8** (ρ = 1.721 g cm^{-3}) and **11** (ρ = 1.693 g cm^{-3}). Every tetrazole ring of the 2,2-dtp ligand is similar to the uncoordinated compound in *anti* conformation to the propyl chain linking the copper(II) metal center to four other metal ions. The oxygen atoms in axial positions prevent the formation of a 3D-polymeric structure leading to two dimensional layers with two non-coordinating perchlorate counter-anions.

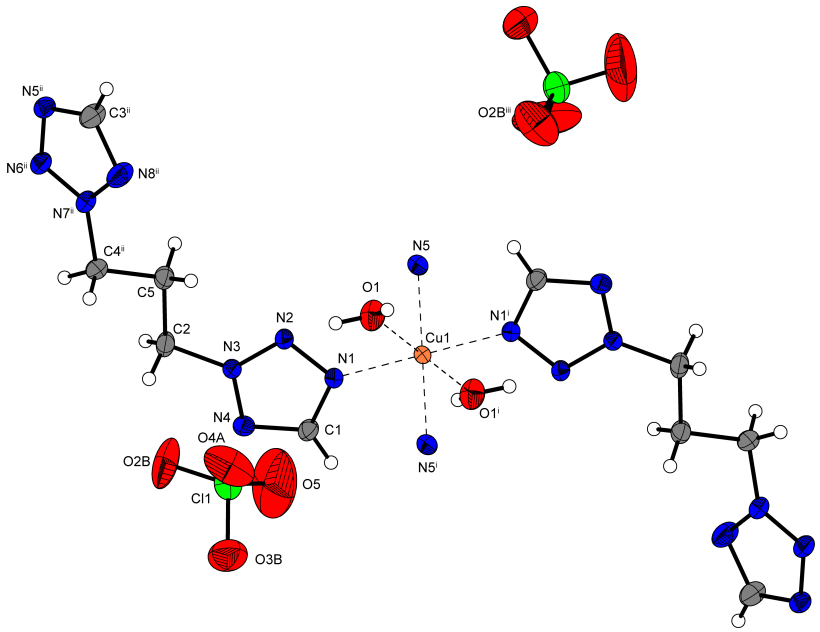


Figure 11. Copper(II) coordination environment of $[Cu(H_2O)_2(2,2\text{-dtp})_2](ClO_4)_2$ (**12**). Selected bond lengths (Å): Cu1–O1 2.294(2), Cu1–N1 2.0214(19), Cu1–N5 2.0317(19); selected bond angles (°): O1–Cu1–N1 90.00(8), O1–Cu1–N5 92.60(9), and N1–Cu1–N5 89.52(8). Symmetry codes: (i) 1−x, −y, 1−z; (ii) 2−x, 0.5+y, 1.5−z; (iii) 1−x, −0.5+y, 1.5−z.

The molecular unit of compound **14** consists of two non-coordinating cyanodinitromethanide counterions and one copper(II) cation, which is coordinated by two axial aqua ligands and four tetrazoles in a plane corresponding to two 1,1-dtps (Figure 12). Compared to the perchlorate complexes of 1,1-dtp, the ligands maintain the conformation with one tetrazole ring in *gauche* and one in *anti* position to the propyl chain preventing the bonding of two additional nitrogen atoms to the metal center. As already observed for compound **12**, the replacement of one ditetrazole trough two aqua ligands in **14** leads to a small increase in density (1.761 g cm^{-3}). The one-dimensional polymeric complex crystallizes in the form of blue blocks in the triclinic space group *P*−1 with two formula units per unit cell.

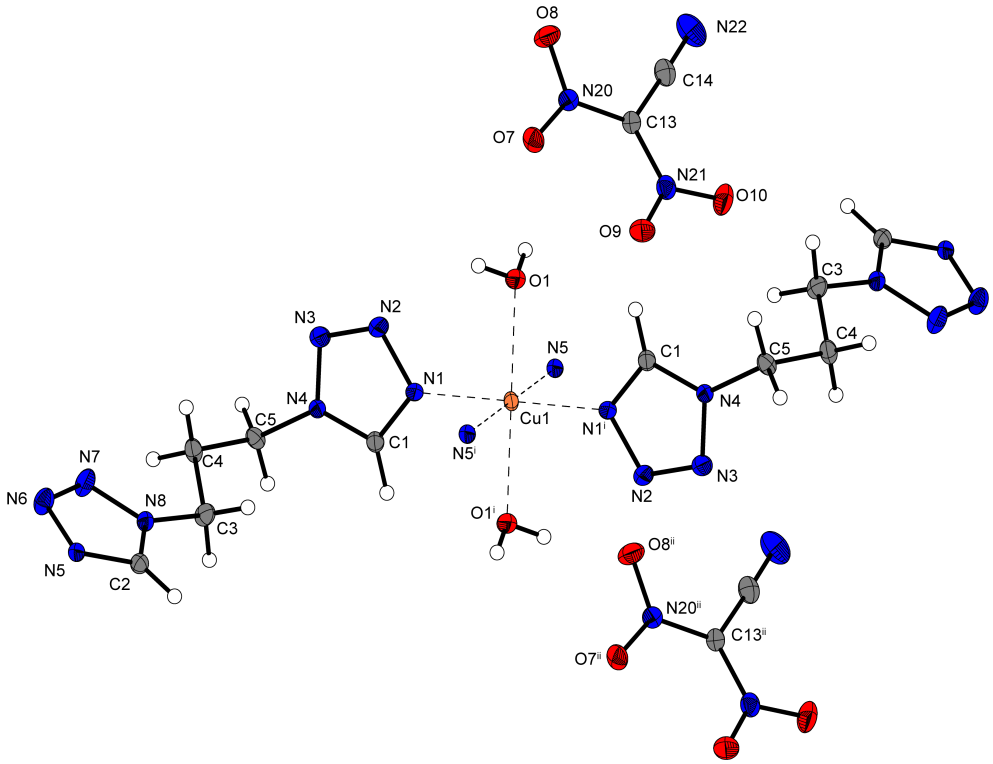


Figure 12. Copper(II) coordination environment of $[Cu(H_2O)_2(1,1\text{-dtp})_2](CDNM)_2$ (**14**). Selected bond lengths (Å): Cu1–O1 2.3298(15), Cu1–N1 2.0107(15), Cu1–N5 2.0241(15); selected bond angles (°): O1–Cu1–N1 94.98(6), O1–Cu1–N5 89.50(6), and N1–Cu1–N5 90.18(6). Symmetry codes: (i) 1−x, 1−y, 1−z; (ii) −1+x, y, z.

Similar to complex **8**, the octahedral coordination sphere of anhydrous compound **15** consists of six tetrazole rings with two non-coordinating dinitramide counterions in the molecular unit (Figure 13). All rings are in *anti* conformation to the propyl chain, which enables the linkage of one transition metal to six other copper(II) ions and leads to a tightly packed three-dimensional network with a density of 1.711 g cm^{-3}. The complex crystallizes in form of blue platelets in the monoclinic space group *C*2/*c* with 8 formula units per unit cell.

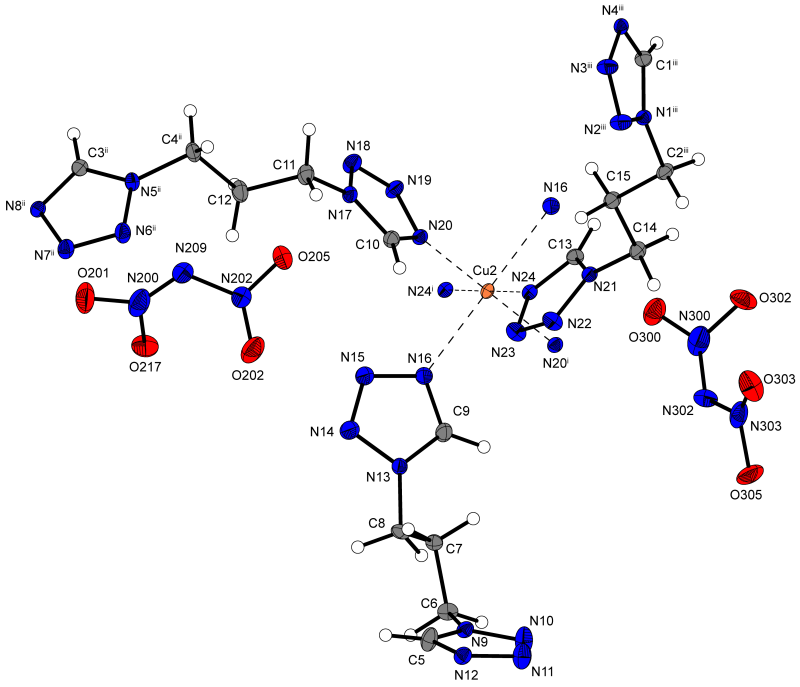


Figure 13. Coordination environment of the anhydrous copper(II) dinitramide complex **15**. Selected bond lengths (Å): Cu2–N16 2.3861(16), Cu2–N20 2.0437(14), and Cu2–N24 2.004(2); selected bond angles (°): N16–Cu2–N20 85.55(6), N16–Cu2–N24 90.87(7), and N20–Cu2–N24 88.81(7). Symmetry codes: (i) –x, 1−y, −1−z; (ii) x, y, −1+z; (iii) −0.5−x, 0.5−y, −1−z.

12.2.3 Sensitivities and Thermal Stabilities

Endothermic signals such as melting, dehydration or loss of aqua ligands, as well as other critical temperatures of all compounds were investigated by differential thermo analysis (DTA) with a heating rate of $\beta = 5$ °C min^{-1}. The determined onset temperatures are listed in Table 2. DTA plots and additional details of the coordination compounds **1**–**3**, **8** and **10**–**15** are displayed in Figures S11-13 in the Supporting Information. The ditetrazole ligands melt at 45 °C (2,2-dtp), 50 °C (1,2-dtp) and 126 °C (1,1-dtp). Higher melting points are observed the more *N*1 substitution is present at the heterocycle, which is in accordance with literature observed values.[47] All complexes (except **10** and **15**) show excellent exothermic decomposition temperatures with values greater than 210 °C. The thermal stabilities of the investigated compounds exceed in most cases the temperatures observed for the uncoordinated ligands. The silver(I) perchlorate **10** and copper(II) dinitramide **15** complexes show the lowest exothermic decomposition temperatures of all examined compounds with values of 186 °C (**10**) and 154 °C (**15**), respectively. The poor stability toward heat of dinitramide containing compounds is a well-known issue and has already been described in the literature.[48]

Table 2. Thermal stability measurements of **1**–**15** by DTA.

compound	$T_{endo.}$ (°C)[a]	$T_{exo.}$ (°C)[b]
1,1-dtp • H_2O (**1**)	68 (-H_2O), 126	205
1,2-dtp (**2**)	50	212
2,2-dtp (**3**)	45	246
$[Mn(1,1\text{-dtp})_3](ClO_4)_2$ (**4**)	—	243
$[Fe(1,1\text{-dtp})_3](ClO_4)_2$ (**5**)	—	234
$[Co(1,1\text{-dtp})_3](ClO_4)_2$ (**6**)	—	255
$[Ni(1,1\text{-dtp})_3](ClO_4)_2$ (**7**)	—	297
$[Cu(1,1\text{-dtp})_3](ClO_4)_2$ (**8**)	—	231
$[Zn(1,1\text{-dtp})_3](ClO_4)_2$ (**9**)	—	253
$[Ag(1,2\text{-dtp})]ClO_4$ (**10**)	—	185
$[Cu(1,2\text{-dtp})_3](ClO_4)_2$ (**11**)	—	222
$[Cu(H_2O)_2(2,2\text{-dtp})_2](ClO_4)_2$ (**12**)	132 (-H_2O)	257
$[Cu(TNR)(1,1\text{-dtp})]$ • H_2O (**13**)	88 (-H_2O)	248
$[Cu(H_2O)_2(1,1\text{-dtp})_2](CDNM)_2$ (**14**)	93 (-H_2O)	212
$[Cu(1,1\text{-dtp})_3](DN)_2$ (**15**)	—	153

Onset temperatures at a heating rate of 5 °C min^{-1}. [a] endothermic peak, which indicates melting, dehydration or loss of aqua ligands; [b] exothermic peak, which indicates decomposition.

The observation of endothermic signals, which indicate melting, dehydration or loss of aqua ligands for the compounds **1**–**3** and **12**–**14** match perfectly to the described structural composition. The outstanding thermal stabilities of most complexes can be explained by the formation of extended structures (MOFs) and the related strengthening of the scaffold within the coordination compounds. In contrast, complex monomers based on relatively volatile ligands suffer from a high vaporization tendency resulting in earlier decomposition after reaching the critical temperature.[6] Therefore, two selected complexes **6** and **8** were checked by thermal gravimetric analysis (TGA, Figure 14).

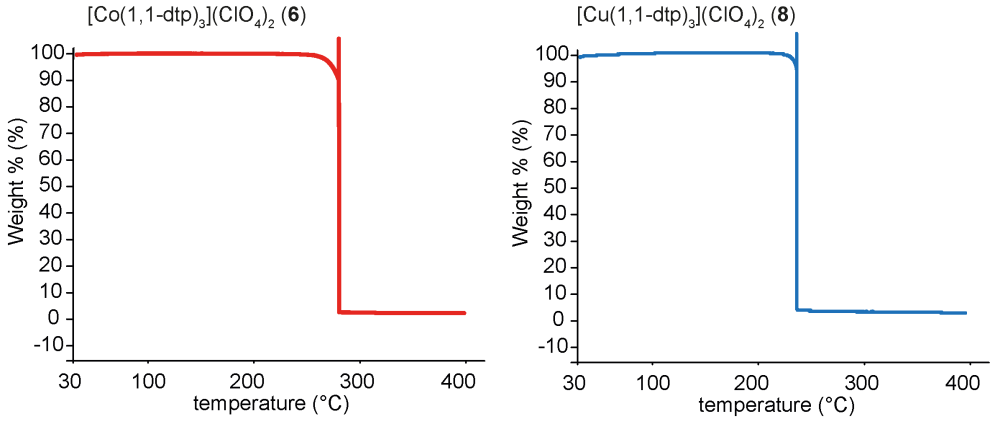


Figure 14. TGA measurements of the selected coordination compounds **6** and **8** at a heating rate of 5 °C min^{-1}.

The theory of a higher stability of coordination polymers could be confirmed. Both polymeric compounds showed no weight loss until decomposition during heating. The exothermic decomposition temperatures of the metal(II) 1,1-dtp perchlorate complexes **4**–**9**, depicted in

Figure 15, rise in the following order: Cu^{2+} (231 °C) < Fe^{2+} (234 °C) < Mn^{2+} (243 °C) < Zn^{2+} (253 °C) < Co^{2+} (255 °C) < Ni^{2+} (297 °C). A similar trend has been described in the literature for metal(II) perchlorate complexes bearing 1-methyl-5*H*-tetrazole as ligand.[6]

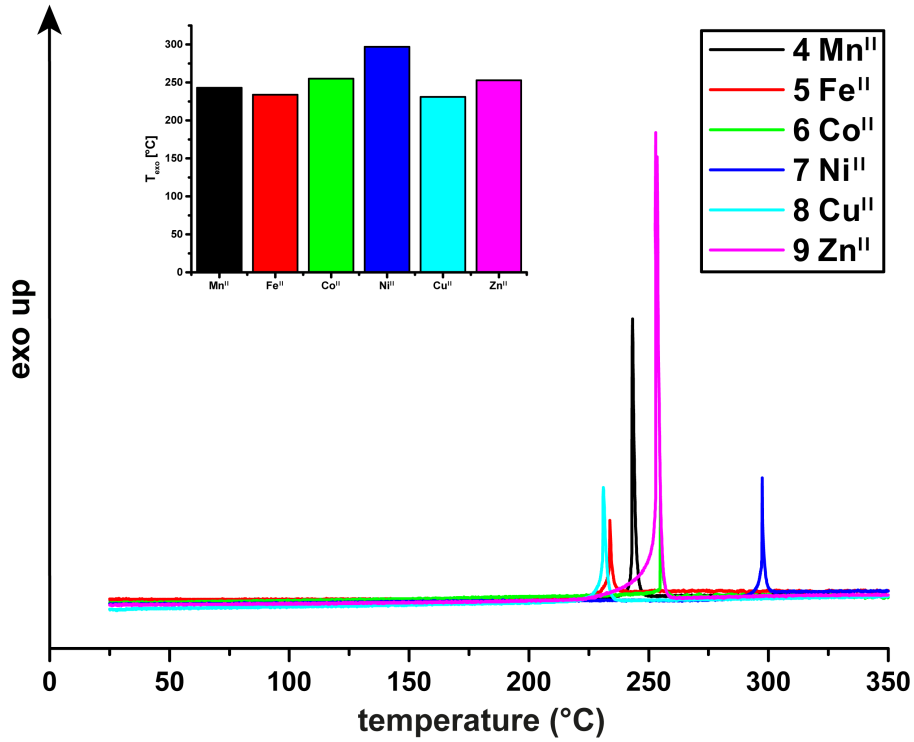


Figure 15. DTA plot (5 °C min^{-1}) comparison of the 1,1-dtp containing metal(II) perchlorate complexes **4**–**9**.

The nitrogen substitution pattern of the ditetrazoles has a strong influence on the exothermic decomposition temperature, which can be observed for the uncoordinated ligands **1**–**3** and their corresponding copper(II) perchlorate complexes (Figure S12). Comparing the 1,1-dtp complexes with copper(II) as metal, but varying anions showed again the relevance and dependency of different coordination environments for the thermal stabilities (Figure S13).

The sensitivities toward impact and friction were measured according to BAM standard methods together with the electrostatic discharge sensitivity for all compounds. Further, the compounds have been categorized in compliance with the "UN Recommendations on the Transport of Dangerous Goods" using the determined values. An outline of the sensitivities is given in Table 3. The uncoordinated ditetrazole ligands **1**–**3** can be described as "insensitive" with values greater than 40 J for impact, greater than 360 N for friction and ESD values between 0.15–1.50 J. All perchlorate complexes **4**–**12** (except **10** with a value of 8 J) can be considered as very sensitive against impact (1–3 J) and vary from sensitive to very sensitive toward friction (16–288 N).

Table 3. Sensitivities toward impact, friction and ESD of **1**–**15**.

compound	*IS* (J)[a]	*FS* (N)[b]	*ESD* (J)[c]
1	> 40	> 360	1.35
2	> 40	> 360	1.50
3	> 40	> 360	0.15
4	3	216	0.30
5	2	72	0.10
6	1	18	0.08
7	3	120	0.20
8	1	54	0.33
9	1	288	0.20
10	8	16	0.15
11	1.5	18	0.10
12	1.5	64	0.30
13	10	> 360	0.50
14	10	> 360	0.50
15	3	> 360	0.70

Determined at a grain size < 100 µm; [a] impact sensitivity according to the BAM drophammer (method 1 of 6); [b] friction sensitivity according to the BAM friction tester (method 1 of 6); [c] electrostatic discharge sensitivity (OZM ESD tester); Impact: insensitive > 40 J, less sensitive ≥ 35 J, sensitive ≥ 4 J, very sensitive ≤ 3 J; Friction: insensitive > 360 N, less sensitive = 360 N, sensitive < 360 N and > 80 N, very sensitive ≤ 80 N, extremely sensitive ≤ 10 N. According to the UN Recommendations on the Transport of Dangerous Goods.

Application of metal(II) salts with oxidizing anions like trinitrorescorinates, cyanodinitromethanides or dinitramides in combination with endothermic ligands usually caused intensified sensitivities toward various stimuli like impact, friction and ESD (impact: 3–10 J; friction: > 360 N; ESD: 0.50–0.70 J). Inclusion of crystal water molecules or aqua ligands on the other hand lowered the performance and lead to a lower sensitivity predominantly. The sensitivity toward impact of the $[M^{II}(1,1\text{-dtp})_3](ClO_4)_2$ coordination compounds (Figure 16) increases in the following order: Mn^{2+} (3 J) ≈ Ni^{2+} (3 J) < Fe^{2+} (2 J) < Zn^{2+} (1 J) ≈ Cu^{2+} (1 J) ≈ Co^{2+} (1 J) and in the following order against friction: Zn^{2+} (288 N) < Mn^{2+} (216 N) < Ni^{2+} (120 N) < Fe^{2+} (72 N) < Cu^{2+} (54 N) < Co^{2+} (18 N). Comparable results have been described in the literature in connection with 1,5-diaminotetrazole and 1-methyl-5*H*-tetrazole containing ECC.[6,49] In addition, fine-tuning of the complexes stability can be achieved through the appropriate choice of the implemented dtp ligands or oxygen-rich anions (Figure S14/15). The presented copper(II) perchlorate complexes show promising characteristics by having manageable sensitivities, which makes them highly suitable as laser ignitable substances in modern initiation devices.

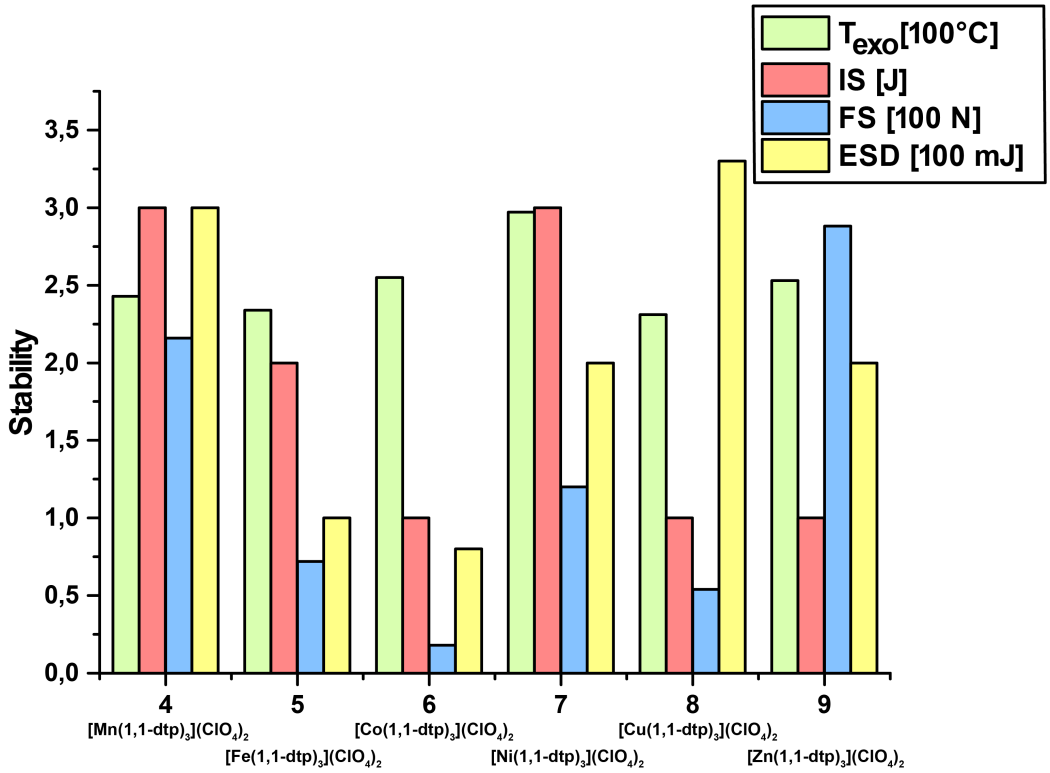


Figure 16. Comparison of the stabilities of the 1,1-dtp containing metal(II) perchlorate complexes **4**–**9**.



Figure 17. Moment of deflagration of compound **8** during the hot plate test shown as a sequence.

Initiation capability tests by hot plate and hot needle were performed for the most promising compounds **8**, **11** and **12**. All investigated complexes showed deflagrations in both tests and no

detonations indicating valuable compounds with moderate sensitivities and performances for laser ignition experiments (Figure 17 and Figure S16–18). More details on the procedures can be found in the experimental section.

12.2.4 Toxicity Assessment

In order to determine the toxicological impact of complexes with isomeric propyl-linked ditetrazoles, the uncoordinated free ligands (**1**, **2** and **3**), as well as their corresponding copper(II) complexes (**8**, **11** and **12**) were tested. The toxicity determinations were carried out with a LUMI-Stox 300 spectrometer obtained by HACH LANGE GmbH, as described by the provider. A ten-point dilution series was prepared according to DIN/EN/ISO 11348 (without G1 level) with a known weight of the compounds and a 2% NaCl stock solution.[50] The measurements were performed at a temperature of 15 °C starting with the determination of the bioluminescence of untreated reactivated *Vibrio fischeri* NRRL-B-11177 bacteria strains. The bioluminescence again is determined after 15 and 30 minutes' exposure time with a specific amount of component. At the concentration level where the bioluminescence is decreased by 50%, the EC_{50} (effective concentration) value is obtained. Compounds can be classified as non-toxic according to their EC_{50} values (non-toxic > 1.00 g/L; toxic 0.10–1.00 g/L; very toxic < 0.10 g/L).[51]

Table 4. Experimental EC_{50} values for the uncoordinated free ligands **1**–**3** in comparison to their respective copper(II) perchlorate complexes **8**, **11** and **12**.

compound	EC_{50} (15 min) [g/L]	EC_{50} (30 min) [g/L]
1,1-dtp • H_2O (1)	13.90	10.30
1,2-dtp (2)	0.81	0.79
2,2-dtp (3)	0.36	0.36
$[Cu(1,1\text{-dtp})_3](ClO_4)_2$ (8)	0.44	0.35
$[Cu(1,2\text{-dtp})_3](ClO_4)_2$ (11)	0.64	0.44
$[Cu(H_2O)_2(2,2\text{-dtp})_2](ClO_4)_2$ (12)	0.34	0.28

As shown in Table 4, the half-maximum effective concentrations of the propyl-linked ditetrazoles varies considerably. Compound **1** has an EC_{50} value of 10.30 g/L after 30 minutes and can be considered as non-toxic. It is interesting to note that in contrast to ligand **1**, the isomeric compounds **2** (0.84 g/L) and **3** (0.36 g/L) show increased toxicities by having only a slightly different substitution pattern. Similar values have been observed for all copper(II) complexes, which is not surprising due to the known toxicity toward microorganisms.[52] It also become apparent that the ditetrazole **3** and complexes containing this ligand are more toxic toward *Vibrio fischeri*. Copper(II) compound **12** is the most toxic complex, even though it

forms complexes with two aqua ligands and two ditetrazole ligands instead of three ditetrazole ligands (compounds **8** and **11**). Furthermore, the toxicity values of **8**, **11** and **12** are in a proportional range of other copper(II) perchlorate complexes, but slightly less toxic compared to already known 1-methyl-5*H*-tetrazole analogues.[6] This could lead to a general trend that 2-alkylated 5-*H*-tetrazoles are more toxic than their 1-alkyated analogues.

12.2.5 Laser Ignition Tests

Over the past few years, many new laser ignitable materials based on energetic coordination compounds have been explored and developed by several researchers all over the world.[33,53–55] Initiation by laser has various benefits in comparison to classical ignition methods like thermal initiation (bridge wire) or mechanical stimuli (e.g. stab initiation). Since high sensitivities against usual stimuli are no longer needed, almost insensitive highly energetic compounds can be used, which can reduce undesired initiations and allows safer processing. The "green" laser ignitable explosives presented in this study feature all desired characteristics like high performance, superior thermal stability, moderate sensitivities and no environmental impact. Approximately 15 mg of the carefully pestled complex to be investigated was filled into a transparent plastic cap (PC), pressed with a pressure force of 1 kN and sealed by a UV-curing adhesive. The laser initiation experiments were performed with a 45 W InGaAs laser diode operating in the single-pulsed mode. The diode is attached to an optical fiber with a core diameter of 400 µm and a cladding diameter of 480 µm. The optical fiber is connected via a SMA type connecter directly to the laser and to a collimator. This collimator is coupled to an optical lens, which was positioned in its focal distance (f = 29.9 mm) to the sample. The lens is shielded from the explosive by a sapphire glass. The confined samples were irradiated at a wavelength of 915 nm, a voltage of 4 V, a current of 8 A and varying pulse lengths (0.1 ms or 15 ms). The combined current and pulse length result in an energy output of about 0.20 mJ (0.1 ms/ 8 A) and 30 mJ (15 ms/ 8 A). Only selected complexes with promising characteristics and moderate sensitivities were tested showing different behaviors upon laser irradiation depending on the metal(II)/anion combination. An overview of the experimental results is given in Table 5.

Table 5. Results of the laser ignition tests.

compound	0.1 ms/ 8 A	1 ms/ 8 A	15 ms/ 8 A
5	det.	—	—
6	x	x	det.

7	—	—	dec.
8	det.	—	—
9	—	—	x
11	det.	—	—
12	det.	—	—
13	—	—	deflag.
14	—	—	dec.
15	—	—	deflag.

(–: not tested, x: no ignition, dec.: decomposition, deflag.: deflagration, det.: detonation). Operating parameters: current I = 8–9 A; voltage U = 4 V; theoretical maximal output power P_{max} = 45 W; theoretical energy E_{max} = 0.20–30 mJ; wavelength λ = 915 nm; pulse length τ = 0.1–15 ms.

The zinc(II) complex **9** was the only compound investigated, which showed no reaction after laser irradiation. All other complexes examined could be initiated showing decompositions for **7**/**14**, deflagrations for **13**/**15** and detonations for **5**, **6**, **8**, **11** and **12** (Figure 18 and Figure S19–22). Various laser initiation thresholds could be observed for the varying coordination compounds, which exhibit similar sensitivities toward mechanical stimuli, but showed different responses under the employed laser settings. The iron(II) and copper(II) perchlorate complexes **5**, **8**, **11** and **12** detonated at the lowest possible initiation energy available in the parameters of the laser device and could be promising candidates in future laser initiation systems based on their outstanding initiation capabilities and highly practicable sensitivities.

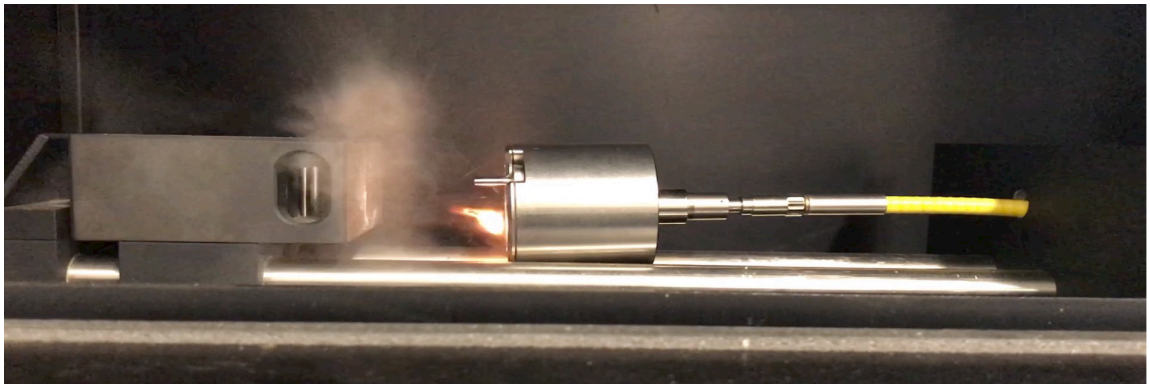


Figure 18. Moment of detonation of complex $[Fe(1,1\text{-dtp})_3](ClO_4)_2$ (**5**) in the laser initiation experiment.

12.2.6 UV-Vis Spectroscopy

The solid-state UV-Vis spectra of all coordination compounds **4**–**15** were recorded in the wavelength region of 350–1000 nm to acquire a better understanding and get a deeper insight into the laser initiation process (Figure 17 and Figure S23). Observed optical characteristics are collected and listed in Table 6. The investigated complexes showed characteristic transitions in the near-infrared, visible and UV region responsible for the complementary colours and typical

for the related transition metal. Observed absorptions can be primarily designated to the d-d transitions of the corresponding metals and are largely dependent on the inserted metal(II), anion and ligand (Figure 19).

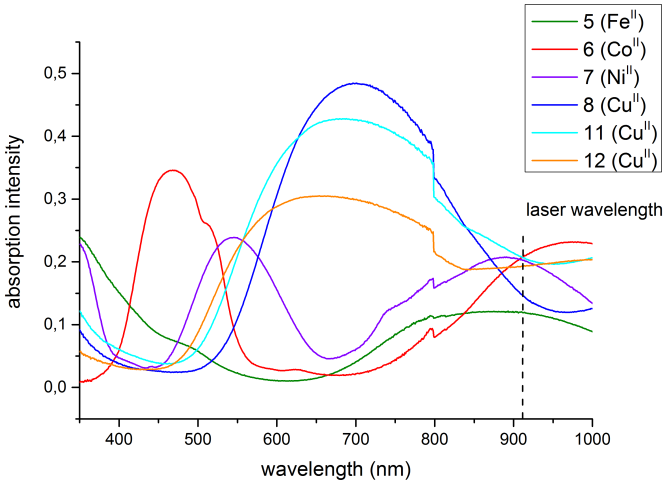


Figure 19. UV-Vis spectra in the solid state of selected complexes. The step in the absorption intensity at 800 nm in the spectra is caused by a detector change. The UV-Vis spectra have only qualitative character.

As assumed initially, no absorptions could be observed for the d^5 manganese(II) compound **4** and the two d^{10} complexes with zinc(II) **9** and silver(I) **10**. Additional strong n-π* transitions from the UV to the blue visible region (Figure S23) could be detected in the copper(II) complexes **13**–**15** caused by the nitro group containing anions (trinitroresorcinate, cyanodinitromethanide, dinitramide).

Many uncertainties of the fundamental basis of the laser initiation process (e.g. electronically, thermally or combined) have not been clarified yet and are still questionable.[34,56,57] Solely looking at the absorption of the coordination compounds at the laser wavelength of 915 nm one could conclude a possible direct interrelationship with the laser initiation capability once all complexes could be ignited. The initiation ability of energetic materials by laser does not only depend on the absorption at the relevant wavelength but also other factors like the electronic structure or the metal center surrounding. It can be assumed that reaction of the coordination compounds after irradiation by laser light may occur when energetic materials exhibit high sensitivities toward mechanical stimuli. Future studies are necessary to gain further insights into the laser initiation process, which should cover the effect of the compounds composition (metal, anion or ligand) and investigate the nature of the mechanism.

Table 6. Observed optical characteristics of **4**–**15**.

compound	M	color	$\lambda_{d\text{-}d}$ [a]	$\lambda_{915}/\lambda_{d\text{-}d}$ [b]
4	Mn^{II}	colorless	—	—
5	Fe^{II} (hs)	yellow	893	0.97
6	Co^{II}	orange	468, 982	0.61
7	Ni^{II}	purple	547, 891	0.84
8	Cu^{II}	blue	701	0.30
9	Zn^{II}	colorless	—	—
10	Ag^{I}	colorless	—	—
11	Cu^{II}	blue	688	0.48
12	Cu^{II}	blue	654	0.63
13	Cu^{II}	green	390 [c], 696	1.00
14	Cu^{II}	blue	389 [c], 624	0.51
15	Cu^{II}	blue	377 [c],630	0.41

[a] Absorption intensity maximum wavelength, which can be assigned to electron d-d excitations in the measured range of 350–1000 nm; [b] quotient of the absorption intensity at the laser wavelength and the intensity at the d-d absorption wavelength; [c] n-π* transitions.

12.3 Conclusions

Three isomeric ditetrazolylpropanes (1,3-di(tetrazol-1-yl)propane (1,1-dtp), 1-(tetrazol-1-yl)-3-(tetrazol-2-yl)propane (**2**, 1,2-dtp) and 1,3-di(tetrazol-2-yl)propane (**3**, 2,2-dtp), differing only in the nitrogen substitution pattern at the tetrazole, were prepared and purified in a straightforward one-step synthesis through alkylation of 1,5*H*-tetrazole. Different synthetic strategies were applied and the influence of various preparative parameters on the reaction product composition systematically investigated. Analysis and comparison of these procedures resulted in deep insights into the effect on the yield and ratio of the isomers from different solvent systems, various organic/inorganic bases, the influence of a phase transfer catalyst and a distinct work-up method. Obtained endothermic n-propyl linked ditetrazoles were exhaustively characterized by various methods including toxicity assessments, X-ray studies and heteronuclear ^{15}N NMR spectroscopy. Toxicity determinations toward aquatic life of the free uncoordinated ligands together with the promising related copper(II) perchlorate complexes showed that 1-alkylated species are less toxic than their 2-alkylated isomers. The concept of ECC is an excellent, fair and simple approach in order to find environmentally friendly primary explosives or materials applicable for laser ignition experiments with reasonable sensitives. Laser initiation experiments with 1,2-di(tetrazol-5-yl)ethane (1,1-dte) based transition metal(II) complexes have shown promising results in the past but were too sensitive for any application. As a logical consequence, ditetrazolylpropane ligands with higher carbon contents especially the *N*1,*N*1-substituted ditetrazole (1,1-dtp) were now implemented into the corresponding coordination compounds in order to increase the stability of the new

energetic materials. The present contribution covers the synthesis, characterization and comparison of 12 new eco-friendly energetic coordination compounds (ECC) based on three different isomeric propyl-linked ditetrazoles, which differ drastically in their coordination pattern. Complexation of the ligands leads to intramolecular reorientation of the ditetrazole molecules and enables the formation of polymeric chains. Optical as well as energetic properties of the highly functional complexes were accurately tuned by the careful selection of the varying metal(II) salts and also the appropriate choice of the isomers. Synthesized coordination compounds consist of a first-row transition metal(II) (Mn, Fe, Co, Ni, Cu, Zn), several different anions (ClO_4^-, TNR^{2-}, $CDNM^-$, DN^-) and one of the three isomeric ditetrazoles. Approaches utilizing Ag(I) as metal center failed with the exception of coordination compound **10** with 1,2-dtp as ligand. In order to form thermally stable materials, non-volatile bridging bidentate ditetrazole ligands were implemented into the complexes to establish highly stable multidimensional polymeric structures (MOFs). Through this strategy extraordinary exothermic decomposition temperatures could be achieved for all complexes up to a very impressive 297 °C for compound **7**, which were partly checked and confirmed by thermal gravimetric analysis (TGA). The powerful water-free nature of the majority of the energetic complexes was revealed through single crystal X-ray experiments of all compounds (except complex **7**), which allowed interesting correlations between the crystal structures and their stabilities toward mechanical stress (highest sensitivities for cobalt(II) perchlorate complex **6**). Laser initiation tests, which were performed at a wavelength of 915 nm showed detonations for the most promising iron(II) and copper(II) complexes **5**, **8**, **11**, **12** at the lowest configurable laser setup energy input (0.2 mJ). The successful initiations proved the suitability of these high performing and thermal stable candidates for future laser initiation systems, which can be easily synthesized from inexpensive chemicals in a simple, inexpensive and upscalable reaction.

Supporting information available in the appendix in **Chapter 19.9** and under:

http://www.rsc.org/suppdata/c8/ta/c8ta01412d/c8ta01412d1.pdf

12.4 References

[1] F. R. Benson, *Chem. Rev.,* 1947, **41**, 1–61.

[2] R. Haiges and K. O. Christe, *Inorg. Chem.,* 2013, **52**, 7249–7260.

[3] H. Xue, H. Gao, B. Twamley and J. n. M. Shreeve, *Chem. Mat.,* 2007, **19**, 1731–1739.

[4] T. M. Klapötke, J. Stierstorfer and A. U. Wallek, *Chem. Mat.,* 2008, **20**, 4519–4530.

[5] O. Sengupta and P. S. Mukherjee, *Inorg. Chem.,* 2010**, 49**, 8583–8590.

[6] N. Szimhardt, M. H. H. Wurzenberger, A. Beringer, L. J. Daumann and J. Stierstorfer, *J. Mater. Chem. A,* 2017, **5**, 23753–23765.

[7] C. M. Grunert, J. Schweifer, P. Weinberger, W. Linert, K. Mereiter, G. Hilscher, M. Müller, G. Wiesinger and P. J. van Koningsbruggen, *Inorg. Chem.,* 2004, **43**, 155–165.

[8] R. Bronisz, *Inorg. Chem.,* 2005, **44**, 4463–4465.

[9] P. Cui, Y.-G. Ma, H.-H. Li, B. Zhao, J.-R. Li, P. Cheng, P. B. Balbuena and H.-C. Zhou, *J. Am. Chem. Soc.,* 2012, **134**, 18892–18895.

[10] M. Joas, T. M. Klapötke and N. Szimhardt, *Eur. J. Inorg. Chem.,* 2014, **2014**, 493–498.

[11] M. H. V. Huynh, M. D. Coburn, T. J. Meyer and M. Wetzler, *Proc. Natl. Acad. Sci.,* 2006, **103**, 10322–10327.

[12] Z. Wu, J. F. Justo, C. R. S da Silva, S. de Gironcoli and R. M. Wentzcovitch, *Phys. Rev. B,* 2009, **80**, 014409.

[13] G. Aromí, L. A. Barrios, O. Roubeau and P. Gamez, *Coord. Chem. Rev.,* 2011, **255**, 485–546.

[14] O. Roubeau, M. Evangelisti and E. Natividad, *Chem. Commun.,* 2012, **48**, 7604–7606.

[15] T. M. Klapötke, *Chemistry of High-Energy Materials*. 2nd ed., Walter de Gruyter: Berlin, Boston, 2012.

[16] J.-G. Xu, C. Sun, M.-J. Zhang, B.-W. Liu, X.-Z. Li, J. Lu, S.-H. Wang, F.-K. Zheng and G.-C. Guo, *Chem. Mater.,* 2017, **29**, 9725–9733.

[17] T. Liu, X. Qi, K. Wang, J. Zhang, W. Zhang and Q. Zhang, *New J. Chem.,* 2017, **41**, 9070–9076.

[18] G.-H. Tao, D. A. Parrish and J. n. M. Shreeve, *Inorg. Chem.,* 2012, **51**, 5305–5312.

[19] L. Wiehl, *Acta Crystallogr. B.,* 1993, **B49**, 289–303.

[20] P. J. van Koningsbruggen, Y. Garcia, O. Kahn, L. Fournes, H. Kooijman, A. L. Spek, J. G. Haasnoot, J. Moscovici, K. Provost, A. Michalowicz, F. Renz and P. Guetlich, *Inorg. Chem.,* 2000, **39**, 1891–1900.

[21] M. Joas, PhD thesis, Ludwig-Maximilians Universität München, 2014.

[22] J. Koehler, Low-polluting pyrotechnic composition. AT410315B, 2003.

[23] J. W. Fronabarger, M. D. Williams, A. G. Stern and D. A. Parrish, *Eur. J. Energ. Mater.,* 2016, **13**, 33–52.

[24] Y. Tang, C. He, L. A. Mitchell, D. A. Parrish and J. n. M. Shreeve, *Angew. Chem., Int. Ed.,* 2016, **55**, 5565–5567.

[25] J. W. Fronabarger, M. D. Williams, W. B. Sanborn, J. G. Bragg, D. A. Parrish and M. Bichay, *Propellants, Explos., Pyrotech.,* 2011, **36**, 541–550.

[26] M. H. V. Huynh, M. A. Hiskey, T. J. Meyer and M. Wetzler, *Proc. Natl. Acad. Sci. U. S. A.,* 2006, **103**, 5409–5412.

[27] A. Y. Zhilin, M. A. Ilyushin, I. V. Tselinskii, A. S. Kozlov and I. S. Lisker, *Russ. J. Appl. Chem.,* 2003, **76**, 572–576.

[28] Z. Shunguan, W. Youchen, Z. Wenyi and M. Jingyan, *Propellants, Explos., Pyrotech.,* 1997, **22**, 317–320.

[29] Q. Zhang and J. n. M. Shreeve, *Angew. Chem., Int. Ed.,* 2014, **53**, 2540–2542.

[30] S. Zhang, Q. Yang, X. Liu, X. Qu, Q. Wei, G. Xie, S. Chen and S. Gao, *Coord. Chem. Rev.,* 2016, **307**, 292–312.

[31] S. Li, Y. Wang, C. Qi, X. Zhao, J. Zhang, S. Zhang and S. Pang, *Angew. Chem., Int. Ed.,* 2013, **52**, 14031–14035.

[32] M. Freis, T. M. Klapötke, J. Stierstorfer and N. Szimhardt, *Inorg. Chem.,* 2017**, 56**, 7936–7947.

[33] T. W. Myers, J. A. Bjorgaard, K. E. Brown, D. E. Chavez, S. K. Hanson, R. J. Scharff, S. Tretiak and J. M. Veauthier, *J. Am. Chem. Soc.,* 2016**, 138**, 4685–4692.

[34] S. R. Ahmad and M. Cartwright, Laser Ignition – Practical Considerations. In *Laser Ignition of Energetic Materials*, John Wiley & Sons, Ltd: 2014; 247–268.

[35] A. Cohen, Y. Yang, Q.-L. Yan, A. Shlomovich, N. Petrutik, L. Burstein, S.-P. Pang and M. Gozin, *Chem. Mat.,* 2016, **28**, 6118–6126.

[36] D. Müller, C. Knoll, B. Stöger, W. Artner, M. Reissner and P. Weinberger, *Eur. J. Inorg. Chem.,* 2013, **2013***,* 984–991.

[37] M. Weselski, M. Książek, J. Kusz, A. Białońska, D. Paliwoda, M. Hanfland, M. F. Rudolf, Z. Ciunik and R. Bronisz, *Eur. J. Inorg. Chem.,* 2017, **2017**, 1171–1179.

[38] S. J. Wittenberger, *Org. Prep. Proced. Int.,* 1994, **26**, 499–531.

[39] P. L. Franke, J. G. Haasnoot and A. P. Zuur, *Inorg. Chim. Acta,* 1982, **59**, 5–9.

[40] P. N. Gaponik, V. P. Karavai and Y. V. Grigoriev, *Khim. Geterotsikl. Soedin.,* 1985, **11**, 1521–1524.

[41] A. Białońska and R. Bronisz, *Tetrahedron,* 2008, **64**, 9771-9779.

[42] R. Bronisz, *Eur. J. Inorg. Chem.,* 2004, 3688–3695.

[43] R. Bronisz, *Inorg. Chem.* 2007, **46**, 6733–6739.

[44] J. Evers, I. Gospodinov, M. Joas, T. M. Klapötke and J. Stierstorfer, *Inorg. Chem.,* 2014, **53**, 11749–11756.

[45] Crystallographic data for the structures have been deposited with the Cambridge Crystallographic Data Centre. Copies of the data can be obtained free of charge on application to The Director, CCDC, 12 Union Road, Cambridge CB2 1EZ, UK (Fax: int.code_(1223)336-033; e-mail for inquiry: fileserv@ccdc.cam.ac.uk; e-mail for deposition: (deposit@ccdc.cam.ac.uk).

[46] M. H. Palmer and S. Parsons, *Acta Cryst.,* 1996, **C52**, 2818–2822.

[47] P. N. Gaponik, M. M. Degtyarik, A. S. Lyakhov, V. E. Matulis, O. A. Ivashkevich, M. Quesada and J. Reedijk, *Inorg. Chim. Acta,* 2005, **358**, 3949–3957.

[48] J. Zhang, Y. Du, K. Dong, H. Su, S. Zhang, S. Li and S. Pang, *Chem. Mat.,* 2016, **28**, 1472–1480.

[49] K. Wang, D. Zeng, J.-G. Zhang, Y. Cui, T.-L. Zhang, Z.-M. Li and X. Jin, *Dalton Trans.,* 2015, **44**, 12497–12501.

[50] Wasserbeschaffenheit - Bestimmung der Hemmwirkung von Wasserproben auf die Lichtemission von Vibrio Fischeri (Leuchtbakterientest), DIN EN ISO, 2009 11348–2.

[51] C. J. Cao, M. S. Johnson, M. M. Hurley and T. M. Klapötke, *JANNAF J. Propuls. Energet.* 2012, **5**, 41–51.

[52] V. Ochoa-Herrera, G. Leon, Q. Banihani, J. A. Field and R. Sierra-Alvarez, *Sci. Total Environ.,* 2011, **412–413**, 380–385.

[53] T. W. Myers, D. E. Chavez, S. K. Hanson, R. J. Scharff, B. L. Scott, J. M. Veauthier and R. Wu, *Inorg. Chem.,* 2015, **54**, 8077–8086.

[54] M. A. Ilyushin and I. V. Tselinskii, *Zhurnal Prikladnoi Khimii (Sankt-Peterburg, Russian Federation),* 2000, **73**, 1233–1240.

[55] N. Szimhardt and J. Stierstorfer, *Chem. Eur. J.,* 2018, **24**, 2687–2698.

[56] E. D. Aluker, A. G. Krechetov, A. Y. Mitrofanov, D. R. Nurmukhametov and M. M. Kuklja, *J. Phys. Chem. C,* 2011**, 115**, 6893–6901.

[57] T. W. Myers, K. E. Brown, D. E. Chavez, R. J. Scharff and J. M. Veauthier, *Inorg. Chem.,* 2017, **56**, 2297–2303

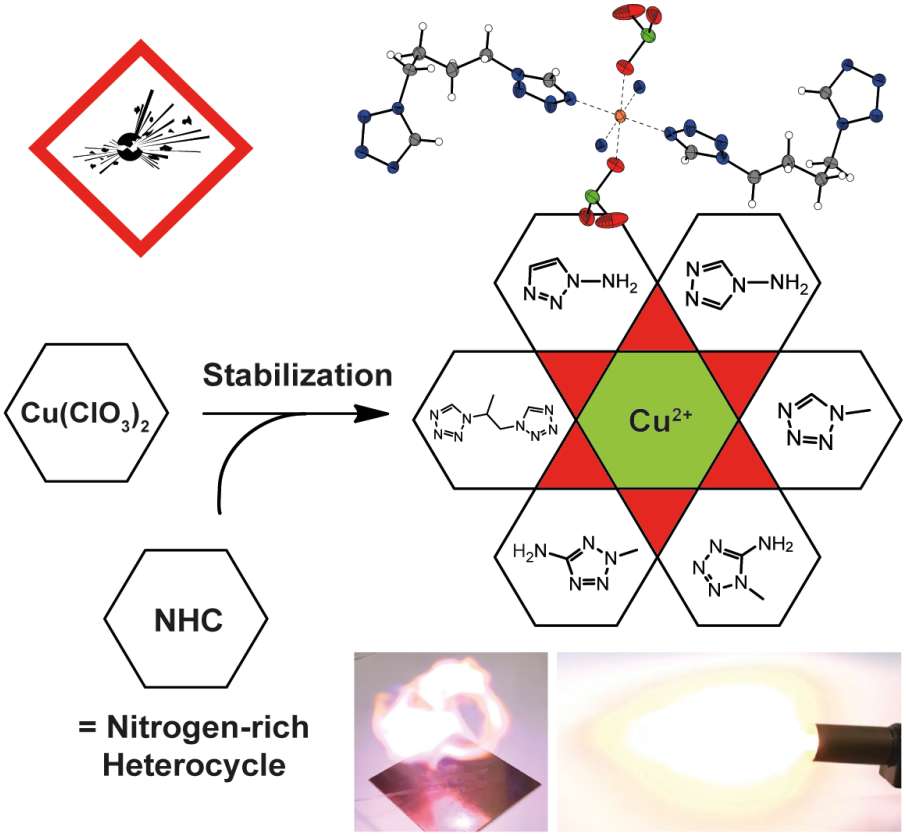
.

13 Copper(II) Chlorate Complexes – the Renaissance of a Forgotten and Misjudged Energetic Anion

Maximilian H. H. Wurzenberger, Norbert Szimhardt, Jörg Stierstorfer

published in *Journal of the American Chemical Society*, **2018,** *140,* 3206-3209

DOI: 10.1021/jacs.7b13230



CCC: Copper(II) Chlorate Complexes: Chlorate derivatives have been condemned for a long time due to the high risk of misuse. In the present work, modern copper(II) chlorate complexes are described with high potential as new energetic materials. They show great performance, adequate sensitivities and stabilities by having low aqueous toxicity.

Abstract

A convenient synthetic route toward new copper(II) chlorate complexes, for potential use in modern advanced ignition or initiation systems is described. Obtained compounds were not only accurately characterized (XRD, IR, UV-Vis, EA and DTA) but also investigated for their energetic character (sensitivities, initiation capability and laser ignition). A copper 4-aminotriazolyl chlorate complex showed excellent initiation of PETN, while being thermally stable and safe to handle. Solid-state UV-Vis measurements were performed to get a possible insight toward the laser initiation mechanism. In contrast to expectations the presented copper(II) chlorate energetic coordination compounds show manageable sensitivities which can be tamed or boosted by the appropriate choice of nitrogen-rich ligands.

13.1 Introduction

The use of chlorates is still omnipresent in everydays life. The main application is to be found in bleach (both $NaClO_3$ and $KClO_3$ are responsible for the production of ClO_2 in elemental chlorine-free bleaching processes), in oxygen candles (for aircrafts or submarines), in herbicides and even in form of medicine (e.g. $Al(ClO_3)_3$ in mouth washes against mild inflammation in the pharynx due to its astringent effect).[1] The deployment of approx. 65–80 w% potassium chlorate together with 20–35 w% red phosphorus in one of the most spectacular and sensitive formulations, called the *Armstrong's mixture* (Figure 1A), can cause disastrous accidents. The mixture tends to spontaneous ignition when mixed or grinded. It is used in matches, fireworks, toy cap guns and earlier in primers and guns. In the meanwhile, it has nearly been completely replaced due to corrosion issues. Also, the risk of misuse is high and led to many accidents through incorrect handling.[2] Especially mixtures containing chlorates with different reducing agents such as sugar, metal powders, saw dust, carbon black or graphite are extremely dangerous.[3] Chlorates possess a high oxidation potential (performance), are thermally stable ($T_{dec.}$ $NaClO_3$: 255 °C, $KClO_3$: 368 °C) and show low toxicities (LD_{50} ($NaClO_3$) 1200 mg kg^{-1}).[4] Investigations of the European Food Safety Authority showed that the potency of chlorate to the human body is 10 times lower compared with perchlorate and only chronic exposure over a long time period could cause inhibition of the thyroid iodine uptake.[5] The ongoing use of lead containing priming mixtures and the accompanied environmental accumulation holds a high ecological risk. Finally, lead styphnate and lead azide, the most commonly used substances in primer mixtures, were put on the

candidate list of authorization (substances of very high concern, Annex XIV) during the REACH (Registration, Evaluation, Authorization and Restriction of Chemicals)[6] regulations in 2011 due to their high toxicity. This could lead to prohibition or restriction of the compounds, which makes research into possible alternatives very important.[7]

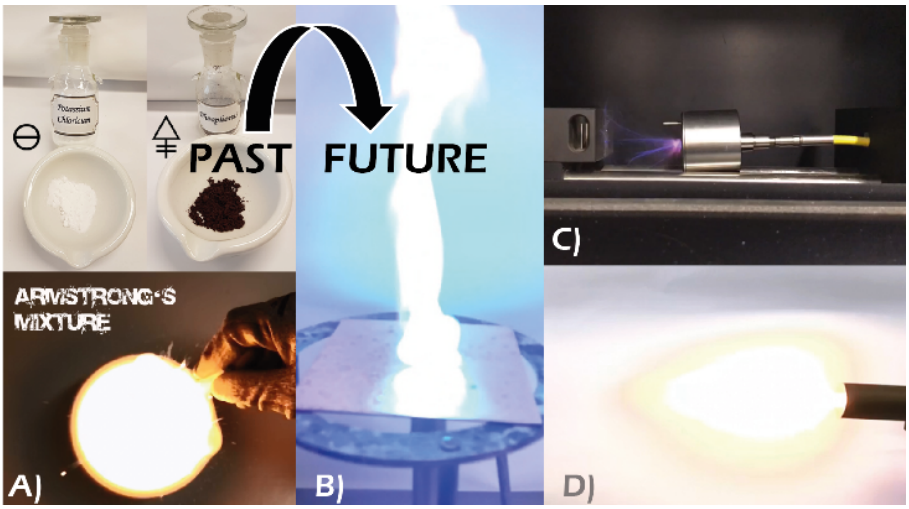
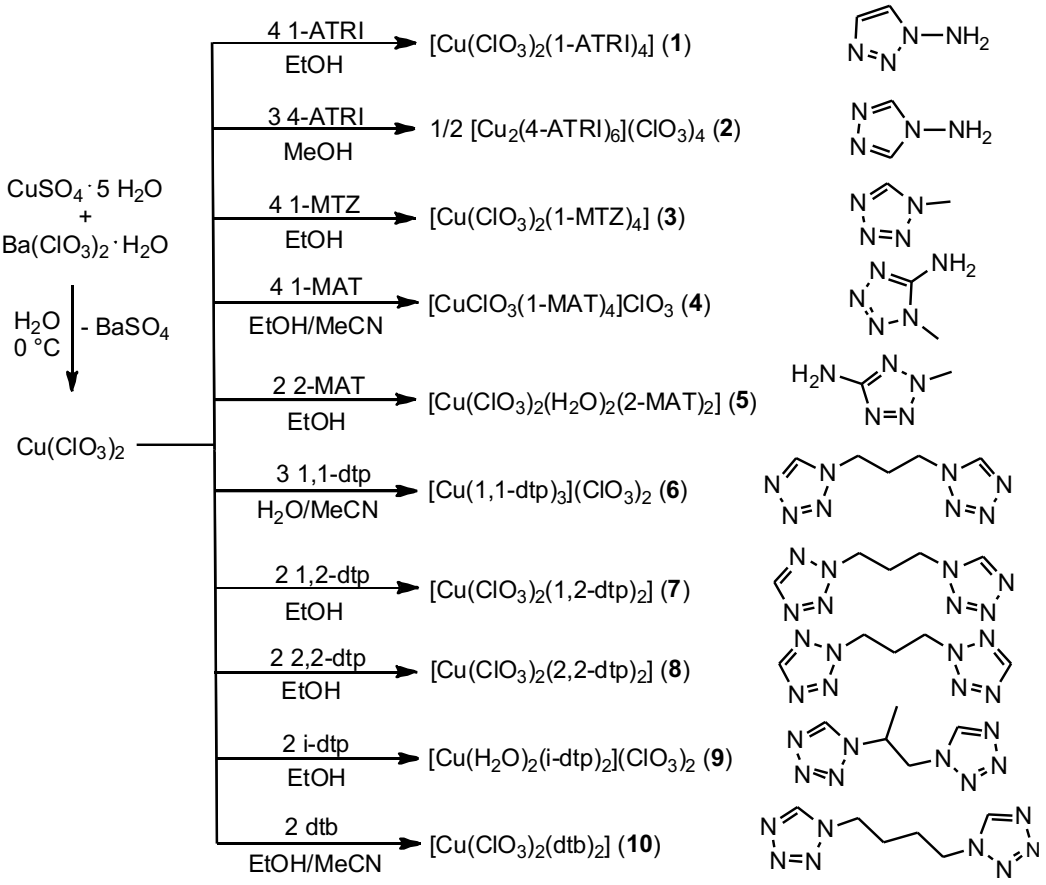


Figure 1. Old versus new: A) Armstrong's mixture containing potassium chlorate and red phosphorus; B) hot plate test showing blue light emission during the decomposition from copper(II) chlorates; C) laser ignition of a copper(II) chlorate complex **8**; D) smokeless muzzle flash of a new ignition mixture.

13.2 Synthesis

The described approach herein for the replacement of lead containing primary explosives in the use of energetic copper(II) chlorate complexes, which were stabilized and tuned with different endothermic nitrogen-rich ligands and can be handled in a safe way. Interestingly, up to date very few copper(II) complexes using chlorate as the counter-anion or ligand are described. These include ammonia, few primary amines, ethylenediamine and 4-amino-1,2,4-triazole (4-ATRI).[8] However, crystal structures and sensitivities have not been reported and energetic investigations are limited to their decomposition temperatures. This may be a consequence of the poor accessibility toward copper(II) chlorate, which is not commercially available, exists with variable water contents (4–6 H_2O) and is highly hygroscopic.[9]Although perchlorates are stronger oxidizers, the reduction of chlorates is favored, leading to an easier initiation.[10] The higher reactivity can also be explained by the missing shielding of the chlorine(+V) atom. The difficult but main goal in the synthesis of metal chlorate complexes is the stabilization of the desired products. For that reason, neutral tri- and tetrazole derivatives were utilized, which are

either commercially available or easy to synthesize.[11] The next challenge we had to face with was the difficult access to hardly available copper(II) chlorate, which has been solved by a simple metathesis reaction exploiting the precipitation of barium sulfate as driving force (Scheme 1). Due to the high hygroscopicity of copper(II) chlorate, freshly prepared alcoholic solutions (except **6**) of copper(II) chlorate were combined with respective stoichiometric amounts of the ligands dissolved in organic solvents (MeOH, EtOH, MeCN).



Scheme 1. Synthesis of the complexes **1**–**10** starting from copper(II) sulfate and barium chlorate. Overview of used nitrogen-rich ligands: 1-ATRI: 1-amino-1,2,3-triazole; 4-ATRI: 4-amino-1,2,4-triazole; 1-MTZ: 1-methyltetrazole; 1-MAT: 1-methyl-5-aminotetrazole; 2-MAT: 2-methyl-5-aminotetrazole; 1,1-dtp: 1,3-di(tetrazol-1-yl)propane; 1,2-dtp: 1-(tetrazol-1-yl)-3-(tetrazol-2-yl)propane; 2,2-dtp: 1,3-di(tetrazol-2-yl)propane; i-dtp: 1,1'-(propane-1,2-diyl)bis(tetrazole); dtb: 1,4-di(tetrazol-1-yl)butane.

13.3 Results and Discussion

13.3.1 Crystal Structures

All compounds were analyzed by low temperature single crystal X-ray diffraction. Figure 2 shows exemplary six different coordination modes of the complexes with no (**2**, **6** and **9**), one (**4**) and two (**5** and **8**) coordinating chlorato ions. The most favored mode in the present study is the octahedral coordination sphere with two coordinating chlorato ligands surrounding the copper(II) metal center. Also, an extraordinary square pyramidal coordination in compound **4** with both a coordinating chlorato ligand and a non-binding chlorate counter-anion could be observed.

Monodentate ligands such as 1-ATRI, 1-MTZ, 1-MAT and 2-MAT lead to the formation of closed octahedral coordination spheres in the complexes **1** and **3**–**5**. Whereas 4-ATRI and the propyl-linked ditetrazole isomers are bidentate and form 1D polymeric chains by coordinating between the same copper(II) cation in compounds **2** and **6**–**9**. A different situation can be found in complex **10** where each butyl ligand bridges two different center metals forming 2D polymeric networks. While complex **2** and **6** are the only presented compounds with copper(II) ions exclusively coordinated by six nitrogen donors, the coordination sphere of **5** shows the greatest variety with two aqua, chlorato and tetrazole ligands each. The molecular unit of **2** consists of two different crystallographic center atoms, both showing a Jahn-Teller distortion. Whereas Cu1 exhibit a rare compressed coordination sphere with shorter axial Cu–N-bonds compared to the equatorial ones, the stretched coordination environment of Cu2 is composed of longer axial and shorter equatorial Cu–N-bonds. In contrast, the copper(II) centers in complex **6** show no distortion at all, possessing six Cu-N-bond lengths of almost the same distance.

For the determination of the compounds' deflagration to detonation transition (DDT) capability the hot plate test, hot needle test and plate dent test (Figure 3) were performed. The most promising compounds in terms of performance and thermal stability are complex **2** and **8**. Their physicochemical properties are summarized in Table 1 and compared with that of lead azide. The sensitivities toward mechanical stimuli are comparable to those observed for $Pb(N_3)_2$, whereas the susceptibility against electrostatic discharge is lower, making them safer to handle. The compounds possess both good densities and thermal stabilities.

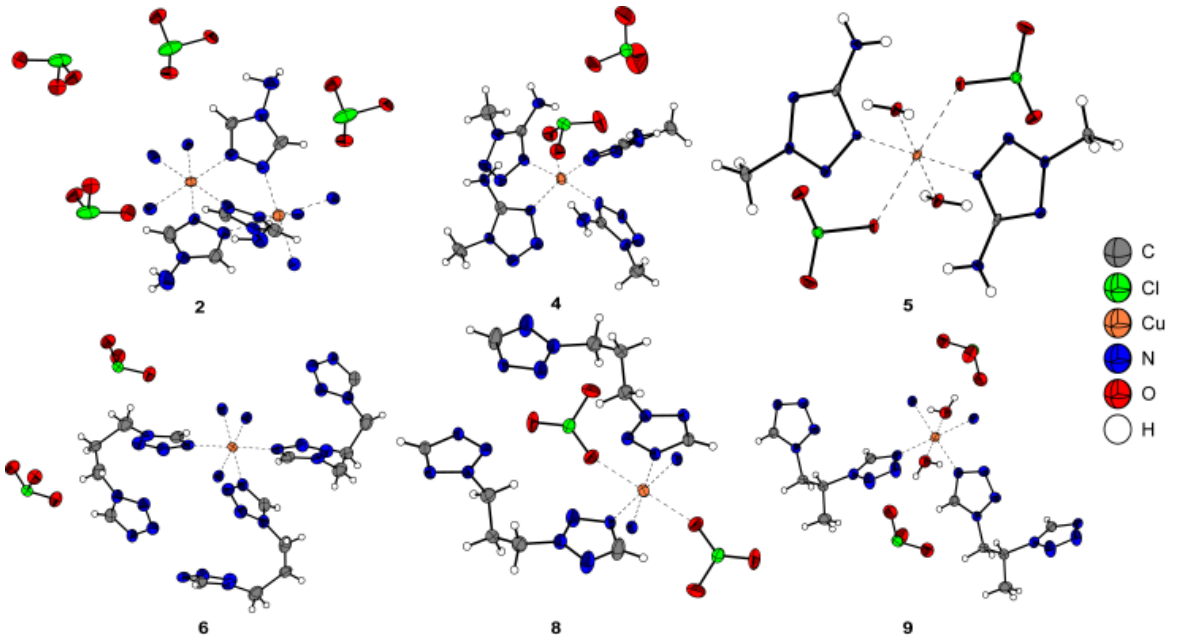


Figure 2. Different coordination modes of copper(II) chlorate complexes $[Cu_2(4\text{-ATRI})_6](ClO_3)_4$ **(2)**, $[CuClO_3(1\text{-MAT})_4]ClO_3$ **(4)**, $[Cu(ClO_3)_2(H_2O)_2(2\text{-MAT})_2]$ **(5)**, $[Cu(1,1\text{-dtp})_3](ClO_3)_2$ **(6)**, $[Cu(ClO_3)_2(2,2\text{-dtp})_2]$ **(8)** and $[Cu(H_2O)_2(i\text{-dtp})_2](ClO_3)_2$ **(9)** determined by low temperature X-ray diffraction. Ellipsoids are drawn at the 50% probability level.[12]

13.3.2 Sensitivities, Thermal Stability and UV-Vis Spectroscopy

Copper(II) chlorate complexes **2** and **8** were tested in copper shell initiation tests and showed positive DDTs toward the secondary explosive PETN (Figure 3 A) and B)). In laser ignition tests (Figure 1C) all complexes, except diaqua compound **9**, showed a detonation differing in the required energy input between 0.17–25.5 mJ. However, UV-Vis measurements showed that the complexes only exhibit moderate absorption in the laser wavelength area (Figure 3C).

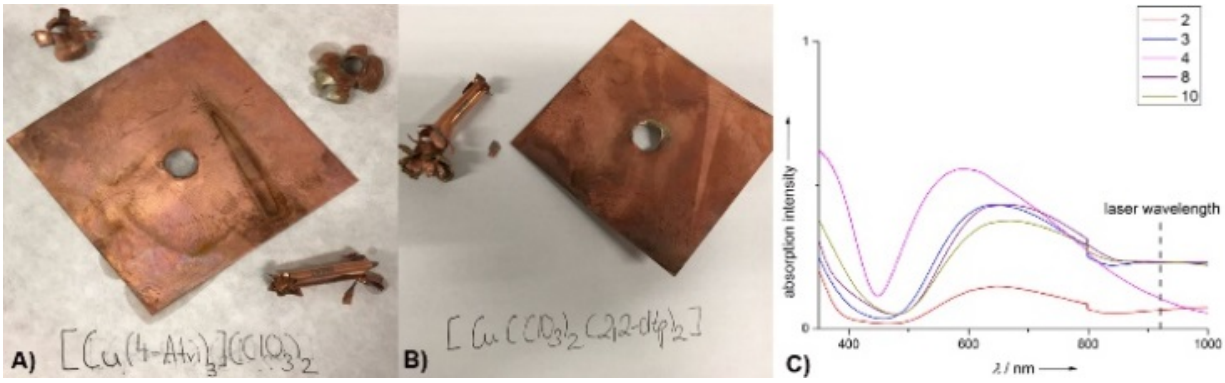


Figure 3. Positive PETN initiation test of compound **2** A) and 8 B); C): solid-state UV-Vis measurements which were correlated to the laser initiation experiments.

Complex **2** cannot be compared with its perchlorate analogue since no energetic properties were explored.[13] Comparing **8** to the corresponding perchlorate complex (4-ATRI as ligand), a higher decom- position temperature (250 °C), and a significantly lower density can be observed. It shows a higher friction sensitivity (8.8 N) and was positive in PETN initiation tests.[14]

Table 1. Physicochemical properties of compound **2** and **8** compared to lead azide[15].

	2	**8**	**$Pb(N_3)_2$**[15]
Formula	$C_{12}H_{24}Cl_4Cu_2N_{24}O_{12}$	$C_{10}H_{16}Cl_2CuN_{16}O_6$	PbN_6
FW [g mol^{-1}]	965.37	590.79	291.24
$\rho_{calc.}$ [g cm^{-3}] (T [K])	1.964 (143)	1.821 (173)	4.8
***IS* [J]**[a]	1	1	2.5–4
***FS* [N]**[b]	< 5	< 5	0.1–1
***ESD* [mJ]**[c]	15	50	6–12
T_{dec} [°C][d]	186	176	320–360

a) impact sensitivity according to the BAM drophammer (method 1 of 6). b) friction sensitivity according to the BAM friction tester (method 1 of 6). c) electrostatic discharge sensitivity (OZM ESD tester). d) temperature of decomposition indicated by exothermic event according to DTA (onset temperatures at a heating rate of 5 °C min^{-1}).

13.3.3 Toxicity

The toxicity measurements, using luminescent marine bacterium *Vibrio fischeri* NRRL-B-11177, for compound **3** and comparison with the corresponding copper(II) perchlorate complex – recently published by our group[16] – prove the lower toxicity toward aquatic life of chlorate compounds.

13.4 Conclusions

In conclusion, we demonstrated a straightforward and low-cost synthetic route toward modern energetic copper(II) chlorate complexes. Complexation of $Cu(ClO_3)_2$ assures stabilization on the one hand side and tuning of the energetic character on the other side by the simple selection of different nitrogen-rich ligands based on tri- and tetrazole derivatives. In the course of this work, ten new coordination compounds could successfully be achieved and comprehensively compared with each other. All ten ligands lead to a disappearance of the high hygroscopy of pure copper(II) chlorate. For the first time, X-ray crystal structures of all compounds were determined and the previously predicted structure of **2**[8c] successfully proven. Thermal stability measurements by DTA showed exothermic decomposition temperatures above 150 °C for most

of the compounds. Easy ignition by heat was proven by the hot needle and hot plate tests. In addition, the most promising primary explosives **2** and **8** showed excellent initiation capabilities toward the secondary PETN indicated by positive deflagration to detonation transitions. The use of alkyl-bridged ditetrazoles with longer chain lengths leads to an improvement of the mechanical sensitivities while maintaining its highly energetic character. This could be a promising concept for desensitization of energetic (copper(II) chlorate) complexes in the future. Toxicity measurements using *vibrio fischeri* of compound **3** showed a lower toxicity in comparison to the analogous perchlorate complex and confirmed the higher environmental friendliness of chlorate compounds. Detonations during the laser ignition experiments of almost every single compound demonstrated the great suitability of chlorate complexes in future laser initiation systems.

Supporting information available in the appendix in **Chapter 19.10** and under:

https://pubs.acs.org/doi/suppl/10.1021/jacs.7b13230/suppl_file/ja7b13230_si_001.pdf

13.5 References

[1] (a) Holleman, A. F.; Wiberg, E.; Wiberg, N. *Lehrbuch der Anorganischen Chemie*, de Gruyter: Berlin, 2007, pp. 469–470. (b) Bruchhausen, F. v. *Hagers Handbuch der pharmazeutischen Praxis*, Springer Verlag: Berlin, 1995, pp. 171. (c) Glasner, A.; Weidenfeld, L. *J. Am. Chem. Soc.* **1952**, *74*, 2464–2467.

[2] Kosanke, K. L.; Kosanke, B. J. *Selected Pyrotechnic Publications of K. L. and B. J. Kosanke, Part 4 (1995 Through 1997)*, Journal of Pyrotechnics: Whitewater, **1999**, pp. 42–43.

[3] Hofmann, K. A. In *Anorganische Chemie*; 21st ed., Hofmann, U.; Rüdorff, W., Eds.; Springer Verlag: Berlin; 2013, pp. 447.

[4] www.sigmaaldrich.com (accessed Nov 6, 2017).

[5] European Food Safety Authority (EFSA), *EFSA J.* **2015**, *13*, 4135–4238.

[6] https://echa.europa.eu/de/candidate-list-table (Accessed Nov 6, 2017).

[7] (a) Zhang, J.; Dharavath, S.; Shreeve, J. M.; Mitchell, L. A.; Parrish D. A. *J. Am. Chem. Soc.* **2016**, *138*, 7500–7503. (b) Myers, T. W.; Bjorgaard, J. A.; Brown, K. E.; Chavez, D. E.; Hanson, S. K.; Scharff, R. J.; Tretiak, S.; Veauthier, J. M. *J. Am. Chem. Soc.* **2016**, *138*, 4685–4692. (c) Landenberger, K. B.; Bolton, O.; Matzger, A. J. *J. Am. Chem. Soc.* **2015**, *137*, 5074–5079. (d) Ilyushin, M. A.; Tselinsky, I. V.; Shugalei, I. V. *Cent. Eur. J. Energ. Mater.* **2012**, *9*, 293–327. (e) Petrie, M. A.; Sheehy, J. A.; Boatz, J. A.; Rasul, G.; Prakash, G. K. S.; Olah, G. A..; Christe, K. O. *J. Am. Chem. Soc.* **1997**, *119* , 8802–8809. (f) Mi, Z.; Chen, S.; Jing, Z.; Yang, L.; Zhang, T. *Eur. J. Inorg. Chem.* **2016**, *2016*, 3978–3983. (f) Klapötke, T. M.; Petermayer, C.; Piercey, D. G.; Stierstorfer, J. *J. Am. Chem. Soc.*, **2012**, *134*, 20827–20836.

[8] (a) Amiel, J. *Compt. rend.* **1934**, *199*, 51–53. (b) Amiel, J. *Compt. rend*. **1934**, *199*, 201–203. (c) Sinditskii, V. P.; Vernidub, T. Y.; Fogel'zang, A. E.; Zueva, N. A. *Izv. Vyssh. Uchebn. Zaved., Khim. Khim. Tekhnol.* **1991**, *34*, 15–19.

[9] (a) Blackburn, A.C.; Gallucci, J. C.; Gerkin, R. E. *Acta Crystallogr. B* **1991**, *47*, 474–479. (b) Perry, D. L.; Phillips, S. L. In *Handbook of Inorganic Compounds*, 1st ed., Perry, D. L.; Phillips, S. L., Eds.; CRC Press: Boca Raton, 1995, pp. 139.

[10] Brown, G. M.; Gu, B. In *Perchlorate Environmental Occurrence, Interactions and Treatment*, 1st ed., Gu, B.; Coates, J. D., Eds.; Springer Verlag: New York, 2006, pp. 17–47.

[11] (a) https://www.abcr.de/startseite/ (accessed Oct 26, 2017). (b) van Koningsbruggen, P. J.; Garcia, Y.; Kahn, O.; X Fournès, O.; Kooijman, H.; Spek, A. L.; Haasnoot, J. G.; Moscovici, J.; Provost, K.; Michalowicz, A.; Renz, F.; Gütlich, P. *Inorg. Chem.* **2000**, *39*, 1891–1900. (c) van Koningsbruggen, P. J.; Garcia, Y.; Kooijman, H.; Spek, A. L.; Haasnoot, J. G.; Kahn, O.; Linares, J.; Codjovi, E.; Varret, F. *J. Chem. Soc., Dalton Trans.* **2001**, *4*, 466–471.

[12] Selected X-ray data: **2**: *C*2/*m*, a 13.5622(16) Å, b 15.5713(18) Å, c 7.7338(15) Å, β 91.559(12) °, V 1632.6(4) Å^3, Z 4, ρ 1.964 g cm^{-3}; **4**: $P2_1/n$, a 13.1028(10) Å, b 10.7288(8) Å, c 16.2265(14) Å, β 95.036(7) °, V 2272.3(3) Å^3, Z 4, ρ 1.832 g cm^{-3}; **5**: *P*–1, a 6.5617(3) Å, b 7.5260(4) Å, c 9.0097(4) Å, α 111.762(2) °, β 98.711(2) °, γ 104.197(2) °, V 385.81(3) Å^3, Z 1, ρ 2.000 g cm^{-3}; **6**: *P*–3*c*1, a 10.9642(2) Å, c 14.3772(4) Å, V 1496.78(8) Å^3, Z 2, ρ 1.711 g cm^{-3}; **8**: *C*2/*c*, a 14.6638(7) Å, b 8.9883(5) Å, c 16.3538(8) Å, β 90.324(5) °, V 2155.44(19) Å^3, Z 4, ρ 1.821 g cm^{-3}; **9**:

*C*2/*c*, a 15.0672(5) Å, b 9.0113(3) Å, c 17.5426(6) Å, β 97.696(3) °, V 2360.39(14) Å^3, Z 4, ρ 1.764 g cm^{-3}.

[13] Bronisz, R. *Eur. J. Inorg. Chem.* **2004**, *18*, 3688–3695.

[14] Cudziło, S.; Nita, M. *J. Hazard. Mater.* **2010**, *177*, 146–149.

[15] Meyer, R.; Köhler, J.; Homburg, A. In *Explosives*, Wiley-VCH: Weinheim, 2002, pp. 196–197.

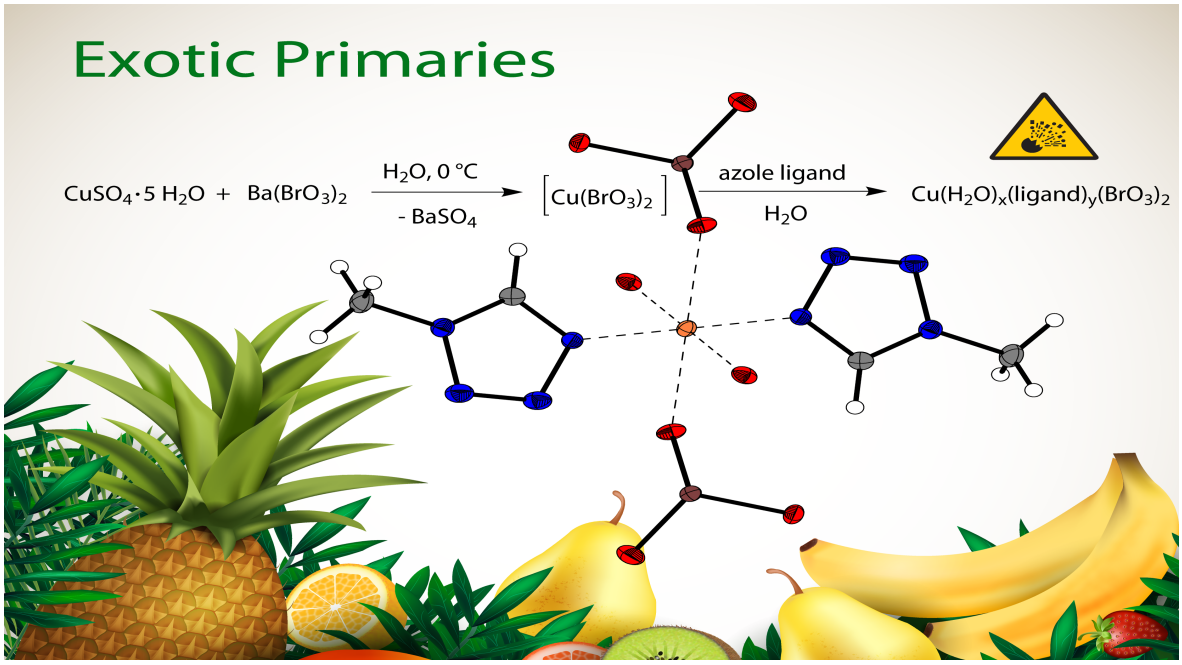
[16] Szimhardt, N.; Wurzenberger, M. H. H.; Behringer, A.; Daumann, L.; Stierstorfer, J. *J. Mater. Chem. A* **2017**, *5*, 23753–23765.

14 Nitrogen-Rich Copper(II) Bromate Complexes: an Exotic Class of Primary Explosives

Maximilian H. H. Wurzenberger, Norbert Szimhardt, Jörg Stierstorfer

published in *Inorganic Chemistry* **2018**, *57*, 7940-7949.

DOI: 10.1021/acs.inorgchem.8b01045



This study covers the synthesis, characterization, and application of six new copper(II)-based coordination compounds including different triazole and tetrazole ligands featuring bromate as an "exotic" oxygen-rich energetic building block. The obtained complexes exhibit great properties such as laser-ignitable lead and perchlorate free primary explosives, which interestingly show low toxicity toward aquatic life organisms.

Abstract

Because of the ongoing very challenging search for potential replacements of the currently used toxic lead-based primary explosives, new synthetic strategies have to be developed. In particular, the smart concept of energetic coordination compounds (ECC) has proven to hold great potential to solve this difficult and complex problem. The herein described approach combines the exotic and neglected class of copper(II) bromate ECC with different environmentally friendly nitrogen-rich heterocycles, which exhibit the energetic properties of powerful primary explosives. The concept is the simple adjustment of the energetic properties of the complexes through alteration of the corresponding azoles. Six new copper(II) bromate complexes with reasonable sensitivities are featured in this study, which were synthesized in a practical and straightforward fashion assured through easy access to copper(II) bromate obtained by metathesis reaction. Obtained compounds were comprehensively characterized through various analytical methods such as low-temperature X-ray diffraction, IR spectroscopy, and elemental analysis. Their sensitivities toward impact and friction were assessed through BAM standard techniques, together with their sensitivity against electrostatic discharge. Evaluation of the energetic properties of the newly synthesized compounds included the examination of the respective thermal stabilities by differential thermal analysis (DTA). Furthermore, the complexes were tested regarding their behavior toward laser irradiation. Additionally, to receive insight into a possible correlation between the laser-investigated compounds' optical absorption and their ability to ignite by exposure to laser irradiation, UV–vis–near-IR spectra were recorded.

14.1 Introduction

Energetic materials include a wide range of chemical compounds and can be classified into four main subgroups: primary explosives, secondary explosives, pyrotechnics, and propellants.[1] In contrast to the high-performing secondary explosives, primaries embody compounds showing a very fast deflagration-to-detonation transition (DDT) after being initiated by a nonexplosive simple initiation impulse.[1,2] The most commonly used primary explosives nowadays are lead styphnate (LS) and lead azide (LA), two compounds that possess highly toxic potential toward human and nature.[3,4] To avoid exposure of toxic chemicals during the utilization and manufacturing of lead-containing primaries, modern research in the field of primary explosives

focuses on the synthesis of new, green compounds while maintaining the desired properties of LS and LA (Chart 1).[5–10]

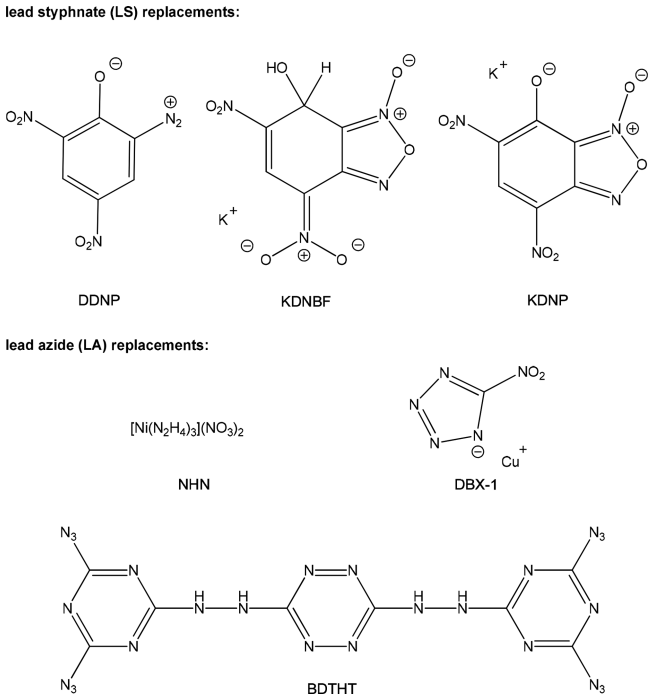


Chart 1. Molecular structures of possible LS and LA replacements: DDNP = diazoniumdinitrophenolate,[11] KDNBF = potassium dinitrobenzofuroxan,[12] KDNP = 5,7-dinitro-[2,1,3]-benzoxadiazol-4-olate 3-oxide,[13] NHN = nickel(II) hydrazine nitrate,[14] DBX-1 = copper(I) nitrotetrazolate[15] and BDTHT = 3,6-bis(2-(4,6-diazido-1,3,5-triazin-2-yl)hydrazinyl)-1,2,4,5-tetrazine [16].

From all energetic characteristics, the previously discussed sensitivities are of high importance as well as high decomposition temperature and chemical and physical stability during long-term storage.[2] Moreover, to enable the substitution of commonly used compounds, the required synthesis of a new primary explosive should include as few as possible reaction steps and ought to be compatible with conventional materials (detonators, secondaries, and blasting caps).[2]

One promising approach to obtaining green primary explosives includes the synthesis of energetic coordination compounds (ECC), a strategy that has gained increased attention in recent years.[7,17–20] Regarding the numerous parameters (metal center, ligand system, and counterion) that can be modified, the specific properties of a desired compound can be tailored incrementally toward the final target. In that manner, copper(II) bears great potential considering previous investigations,[19,21] and thus was examined extensively in combination with bromate as the anion in the course of this work. Besides the tedious search for possible

replacements of LS and LA, recently, the research on primary explosives focused on laser-ignitable compounds.[22] In contrast to the conventional methods of initiation through impact, friction, and electrostatic discharge, this new initiation method bears encouraging potential, because of the circumstance that examined compounds do not require high sensitivities toward the customary stimuli.[23] Consequently, laser-ignitable energetic materials with high performance, high thermal stability and an uncritical impact on the environment can be used as insensitive but powerful charges to allow much safer handling and to prevent undesired initiations.[22] On the basis of the idea of primary explosives in the form of coordination compounds, Zhilin *et al.* isolated several very promising complexes in the early 2000s (Chart 2a,b), including the well-known *cis*-bis(5-nitro-2*H*-tetrazolato-*N*2)cobalt(III) perchlorate and 5-hydrazino-1*H*-tetrazolemercury(II) perchlorate.[24–27] On the basis of these promising results, several research groups were starting to examine laser-sensitive ECCs for future applications in military and civil areas.[28–30]

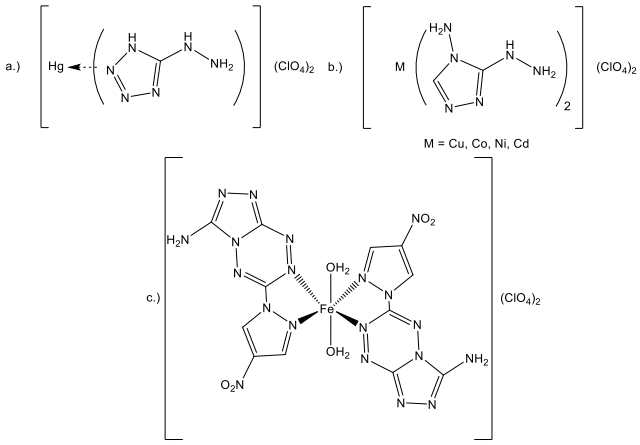


Chart 2. Different laser-ignitable coordination compounds*:* a.) 5-Hydrazino-1*H*-tetrazolemercury(II) perchlorate[26] b.) 3-hydrazino-4-amino-1,2,4-triazole based metal(II) perchlorates[27] or c.) $[(H_2NTriTz^{NO2}Pyr)_2Fe(H_2O)_2](ClO_4)_2$.[31]

Bromates, particularly in the form of alkali salts, can be found in many different industrial processes (food production, synthetic reagents, dyeing, cosmetics etc.) and are therefore an integral part of our daily life. While the use of alkali bromates ($NaBrO_3$ and $KBrO_3$) is rather common, the investigation of transition metal bromates is relatively poor, especially with copper(II). Their high thermal stabilities,[32] exceptional performances, and relatively low prices make alkali bromates promising candidates in explosive mixtures. The latter fact led to the development of manageable potassium bromate containing concrete cracking agents and airbag gas generating compositions, as well as the invention of detectors for bromate containing explosive mixtures.[33–35] Because of the strong oxidizing power of bromates and their high

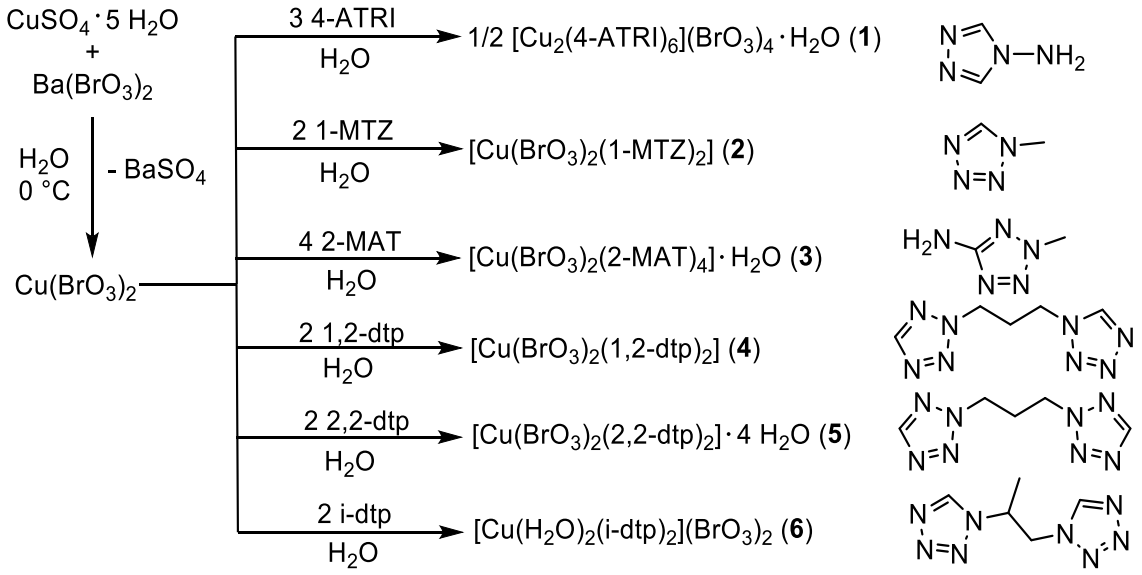
redox reactivity, mixtures with fuels or reducing agents have to be handled with great care. In particular, compositions with sulfur or organic compounds, such as dinitrotoluene or malonic acid, are highly unstable and tend to self-ignite within hours.[36]

Only very few copper(II) complexes (including complexes with ammonia, primary amines, 4-amino-1,2,4-triazole (4-ATRI)) using bromate as the counteranion are known in the literature so far.[37,38] However, none of them were investigated for its crystal structure or has been described in relation to energetic materials. One of the very few, literature reported examples, uses the compound as source for in situ generated CuBr and as an alternative oxidizer (BrO_3^- vs. ClO_4^-) in blue light emitting pyrotechnics.[39] The current contribution covers, as further development of our recently published copper(II) chlorate complexes, analogous bromate containing compounds with sensitivities in the range of primary explosives.[40] Obtained exceptional copper(II) bromate coordination compounds could be initiated by laser irradiation and their energetic character precisely tailored through the application of different nitrogen donating azole-based ligands.

14.2 Results and Discussion

14.2.1 Synthesis

Copper(II) bromate, is poorly accessible, not commercially available and exists with variable water contents (2–6 H_2O).[41,42] Therefore, the driving force of barium sulfate precipitation was utilized to synthesize copper(II) bromate stoichiometrically in situ as intermediate for further reaction with the ligands (Scheme 1) through metathesis of copper(II) sulfate and barium bromate. All ligands used are commercially available or were synthesized according to literature. Because of the very good solubility of the used nitrogen-rich azoles and copper(II) bromate, a minimum amount of water was chosen as reaction medium for the synthesis of ECC **1**–**6**. As a result, the compounds often contain crystal water or aqua ligands. All attempts to change the reaction media to organic solvents led to decomposition of bromate to bromide because of its high redox activity (redox potential of E^0 = 1.45 V (to BrO^-); pH = 0), which is even slightly higher than the one of perchlorate or chlorate (E^0 = 1.43 V (to ClO^-)).[43]



Scheme 1. Synthesis of the complexes **1**–**6** starting from copper(II) sulfate and barium bromate. Overview of used nitrogen-rich ligands: 4-ATRI: 4-amino-1,2,4-triazole; 1-MTZ: 1-methyltetrazole; 2-MAT: 2-methyl-5-aminotetrazole; 1,2-dtp: 1-(tetrazol-1-yl)-3-(tetrazol-2-yl)propane; 2,2-dtp: 1,3-di(tetrazol-2-yl)propane; i-dtp: 1,1'-(propane-1,2-diyl)bis(tetrazole).

Most of the compounds were received in decent yields (57–85 %) directly from the mother liquor in the form of single crystals suitable for X-ray diffraction. Only compound **1** was isolated as a light blue powder and crystal growth was achieved through layering and very slow formation at the phase boundary.

All coordination compounds were filtered off, washed with small amounts of cold water and dried in air. The complexes can easily be distinguished by IR spectroscopy (Figures S1 and S2) because of the different coordination modes of the anions, the water molecules or through the absence of crystal water.

14.2.2 Crystal Structures

All complexes were characterized by low-temperature single crystal X-ray diffraction. The crystal structures were uploaded to the CSD database[44] and can be obtained free of charge with the CCDC nos. 1836542 (**1**), 1836543 (**2**), 1836539 (**3**), 1836540 (**4**), 1836537 (**5**), 1836541 (**6**), 1836544 (**7**), 1836538 (**8**). The bond lengths and angles of the coordinating ligands in the analyzed complexes are in the typical range of the tetrazole and triazole ligands and nearly the same as in the noncoordinating ligands.[45–47] The ligands are therefore not part of the discussion in any of the following coordination compounds. All copper(II) bromate complexes show an

octahedral coordination with a Jahn-Teller distortion along the axial coordination sphere. In general copper(II) bromate complexes tend to crystallize with water as solvent molecules (**1**, **3** and **5**) or in form of aqua ligands (**6** and **7**). Only the bridging bromato anions in compound **2** and **4** prevented the inclusion of aqua molecules.

The monohydrated complex **1** is the only presented with copper(II) ions exclusively coordinated by nitrogen atoms. It crystallizes in the form of blue blocks in the monoclinic space group *C*2/*c* with four formula units per unit cell and a calculated density of 2.299 g cm^{-3} at 143 K. The molecular unit contains two different copper(II) cations (Figure 1), and each is octahedrally coordinated by six triazole ligands. Both central atoms show a Jahn-Teller distortion, whereas the axial Cu–N-bonds of Cu1 are shorter compared with those of Cu2. Three ligands are bridging between the same two copper(II) atoms and form polymeric chains.

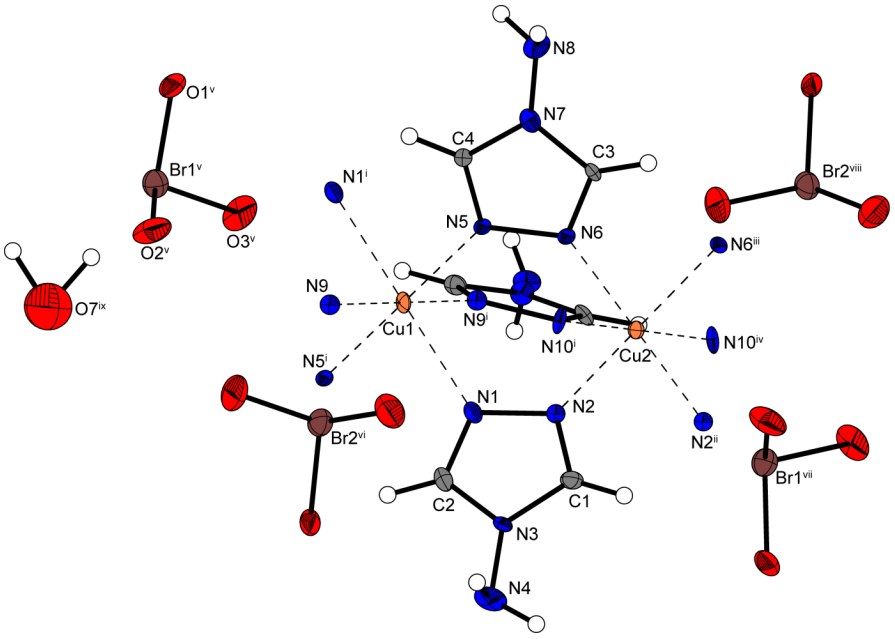


Figure 1. Copper(II) coordination environment of **1**. Thermal ellipsoids of non-hydrogen atoms in all structures are set to the 50 % probability level. Selected bond lengths (Å): Cu1–N1 2.298(6), Cu1–N5 2.052(6), Cu1–N9 2.022(7), Cu2–N2 2.019(6), Cu2–N6 2.036(6), Cu2–N10^{i} 2.408(7); Selected bond angles (°): N1–Cu1–N5 88.6(2), N1–Cu1–N9 88.8(2), N5–Cu1–N9 89.7(2), N2–Cu2–N6 91.4(2), N2–Cu2–N10^{i} 89.7(2), N6–Cu2–N10^{i} 88.0(2). Symmetry codes: (i) −x, −y, 1−z; (ii) −x, y, 1.5−z; (iii) −x, y, 1.5−z; (iv) x, −y, 0.5+z; (v) −1.5+x, 0.5+y, z; (vi) 0.5−x, −0.5−y, 1−z; (vii) 0.5+x, −0.5−y, 0.5+z; (viii) 0.5−x, 0.5+y, 1.5−z; (ix) −1+x, y, z.

[Cu(BrO$_3$)$_2$(1-MTZ)$_2$] (**2**) shows the highest density (2.491 g cm^{-3} at 143 K) of all bromate complexes and crystallizes in the form of blue plates in the monoclinic space group *P*2$_1$/*c* with two formula units per unit cell. The bromate anions in **2** are now coordinating to the transition

metal(II) center in comparison to compound **1** (Figure 2). Each of the bromato ligands is bridging between two different metal(II) atoms building up polymeric 2D-layers.

The monodentate ligand 2-MAT leads to the formation of a closed octahedral coordination sphere in complex **3**. It crystallizes in the form of green blocks in the monoclinic space group $P2_1/c$ with four formula units per unit cell and exhibits the lowest density (1.983 g cm^{-3} at 143 K) of all compounds. The molecular unit consists of one copper(II) cation (Figure 3), coordinated by two bromato and four tetrazole ligands together with an additional crystal water molecule. In contrast to compound **2** the bromatos are only coordinating to one copper(II) central atom and therefore, the formation of polymeric structures does not occur. The water-free compound **4** crystallizes in the form of blue blocks in the monoclinic space group $P2_1/c$ with two formula units per unit cell and a calculated density of 2.142 g cm^{-3} at 130 K. The molecular unit is built up by one copper(II) cation (Figure 4), two coordinating ligands in equatorial positions and two bridging bromato anions. The ditetrazole ligands are only connected with the 1-substituted tetrazole ring, while the 2-substituted ring is not coordinating at all. Similar to complex **2**, every bromato is bridging between two different copper(II) atoms building up polymeric 2D-layers.

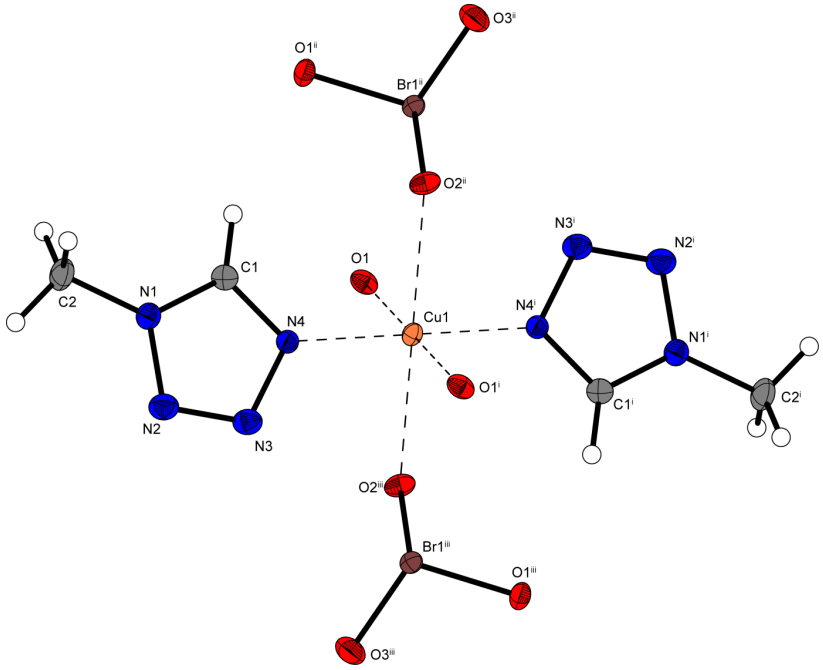


Figure 2. Copper(II) coordination environment of $[Cu(BrO_3)_2(1\text{-}MTZ)_2]$ (**2**). Selected bond lengths (Å): Cu1–O1 2.009(2), Cu1–O2^{ii} 2.346(2), Cu1–N4 1.987(3); Selected bond angles (°): O1–Cu1–N4 90.71(10), O1–Cu1–O2^{ii} 87.89(8), O2^{ii}–Cu1–N4 89.80(9). Symmetry codes: (i) −x, 2−y, −z; (ii) −x, 0.5+y, 0.5−z; (iii) x, 1.5−y, −1.5+z.

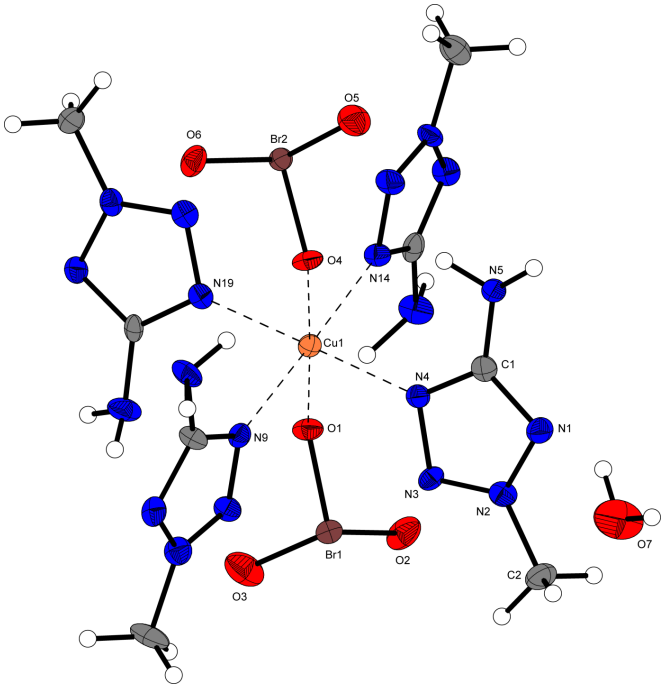


Figure 3. Molecular unit of $[Cu(BrO_3)_2(2\text{-MAT})_4] \cdot H_2O$ (**3**). Selected bond lengths (Å): Cu1–O1 2.367(4), Cu1–O4 2.381(4), Cu1–N4 2.018(5), Cu1–N9 2.057(5), Cu1–N14 2.043(5), Cu1–N19 2.033(5); Selected bond angles (°): O1–Cu1–N9 88.57(17), O4–Cu1–N9 90.95(17), N4–Cu1–N9 91.08(19), N4–Cu1–N14 89.84(19).

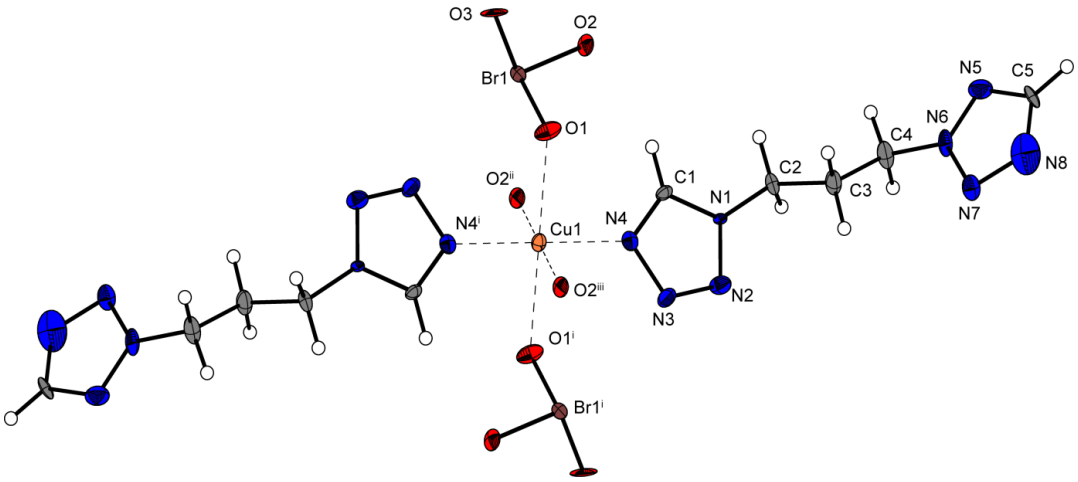


Figure 4. Copper(II) coordination environment of $[Cu(BrO_3)_2(1,2\text{-dtp})_2]$ (**4**). Selected bond lengths (Å): Cu1–O1 2.352(11), Cu1–$O2^{ii}$ 2.033(12), Cu1–N4 1.976(12); Selected bond angles (°): O1–Cu1–N4 90.9(5), O1–Cu1–$O2^{ii}$ 96.2(4), $O2^{ii}$–Cu1–N4 90.4(5). Symmetry codes: (i) 2−x, −y, −z; (ii) x, −0.5−y, −0.5+z; (iii) 2−x, 0.5+y, 0.5−z.

$[Cu(BrO_3)_2(2,2\text{-dtp})_2] \cdot 4\ H_2O$ (**5**) crystallizes in the form of blue blocks in the triclinic space group *P*−1 with one formula unit per unit cell and a calculated density of 2.002 g cm^{-3} at 143 K. The molecular unit is composed of a copper(II) cation (Figure 5) with two coordinating bromato ligands in the axial positions, two 2,2-dtp ligands in a plane and four noncoordinating crystal

water molecules. In contrast to compounds **2** and **3**, the bromates are not bridging, but two neutral ligands are linking between two central metals building up polymeric chains.

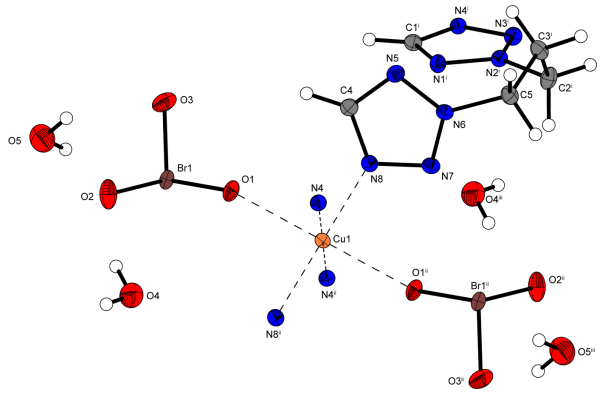


Figure 5. Copper(II) coordination environment of $[Cu(BrO_3)_2(2,2\text{-dtp})_2] \cdot 4\ H_2O$ (**5**). Selected bond lengths (Å): Cu1–O1 2.3200(13), Cu1–N4 2.0042(15), Cu1–N8 2.0335(15); Selected bond angles (°):O1–Cu1–N4 93.85(5), O1–Cu1–N8 86.72(5), N4–Cu1–N8 91.38(6). Symmetry codes: (i) 3−x, −y, 2−z; (ii) 2−x, −y, 2−z; (iii) 1−x, 1−y, 2−z.

The diaqua coordination compound **6** crystallizes in the form of blue blocks in the monoclinic space group *C*2/*c* with four formula units per unit cell and a calculated density of 1.989 g cm^{-3} at 143 K. In contrast to the other aqua complexes, the water molecules act as ligands whereas the bromate counterions are not coordinating. The molecular unit contains one central metal(II) (Figure 6) with two aqua ligands in axial positions, two equatorial ditetrazole molecules, and two noncoordinating counterions. Analogously to complex **5**, the ligands are bridging between the copper(II) ions, building up polymeric chains.

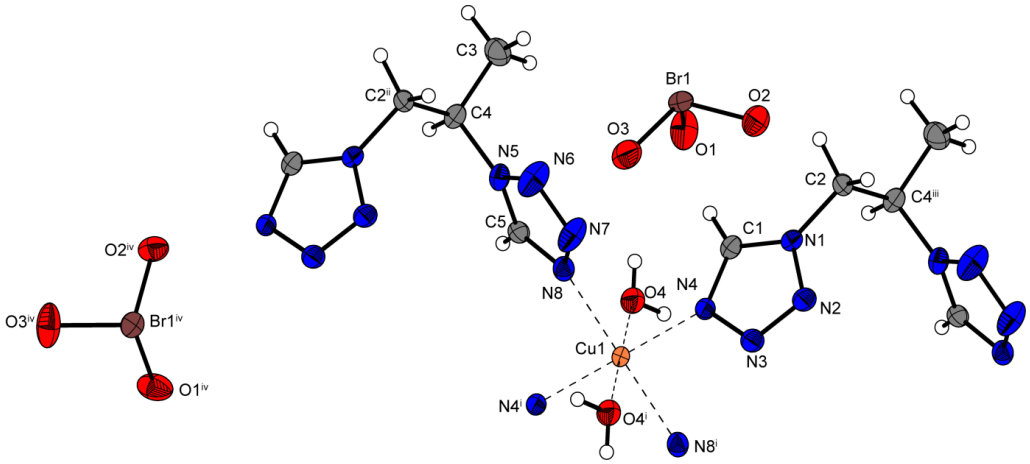
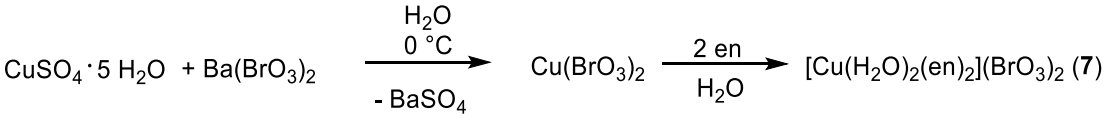


Figure 6. Copper(II) coordination environment of $[Cu(H_2O)_2(i\text{-dtp})_2](BrO_3)_2$ (**6**). Selected bond lengths (Å): Cu1–O4 2.258(2), Cu1–N4 2.030(2), Cu1–N8 2.078(2); Selected bond angles (°):O4–Cu1–N4 91.46(9), O4–Cu1–N8 85.56(9), N4–Cu1–N8 89.45(9). Symmetry codes: (i) 2−x, 2−y, 1−z; (ii) 0.5+x, −0.5+y, z; (iii) −0.5+x, 0.5+y, z; (iv) 0.5+x, 0.5−y, −0.5+z.

Amiel described the synthesis of one of the first ever copper(II) bromate complexes with ethylenediamine (en) as the ligand in 1935 (Scheme 2). He suggested a monoclinic space group for the obtained violet compound with a formula of $(BrO_3)_2Cu(en)_2(H_2O)$.[37] This compound was reinvestigated by single crystal X-Ray diffraction.



Scheme 2. Synthesis of the reinvestigated complex **7.**

The reinvestigation of this compound (Figure 7) verifies indeed a monoclinic space group ($P2_1/c$) for compound **7**. Two chelating en molecules in the equatorial position and two aqua ligands in the axial position are building up closed octahedral coordination spheres around the copper(II) center with noncoordinating bromate counteranions in the molecular unit. The diaqua coordination compound crystallizes in the form of purple blocks with six formula units per unit cell and a calculated density of 2.201 g cm^{-3} at 143 K.

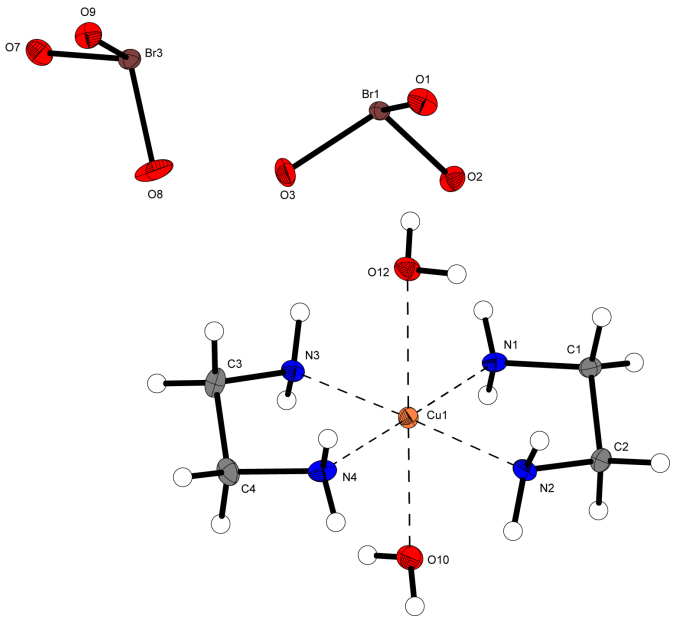


Figure 7. Molecular unit of $[Cu(H_2O)_2(en)_2](BrO_3)_2$ (**7**). Selected bond lengths (Å): Cu1–N1 2.000(4), Cu1–N2 2.027(3), Cu1–N3 2.014(4), Cu1–N4 1.995(4), Cu1–O10 2.555(4), Cu1–O12 2.551(3); Selected bond angles (°): N1–Cu1–N2 84.82(16), N1–Cu1–N3 94.90(16), N1–Cu1–N4 179.17(17), N1–Cu2–O10 83.98(15), N1–Cu2–O12 92.00(15).

The ligands highly influence the coordination mode of the bromate counterions. This affinity can also be observed in the various hydrates of copper(II) bromate. In $[Cu(BrO_3)_2(H_2O)_2]$ the coordination sphere around the metal(II) center is built up of four bridging bromato and two

aqua ligands.[41] Blackburn et al. published the crystal structure of $[Cu(H_2O)_6](BrO_3)_2$ with noncoordinating anions, and the up-to-now unknown structure of $[Cu(BrO_3)_2(H_2O)_4]$ (**8**), measured in the course of this work, shows coordination but no linking of the bromato ligands.[42] The tetraaqua form of copper(II) bromate (**8**) crystallizes in the form of blue blocks in the orthorhombic space group Pbca with four formula units per unit cell and a calculated density of 2.975 g cm^{-3} at 143 K. Similar to complexes **3** and **5,** the coordination sphere around the copper(II) atom contains nonbridging bromato ligands in axial positions and four extra equatorial aqua ligands (Figure 8).

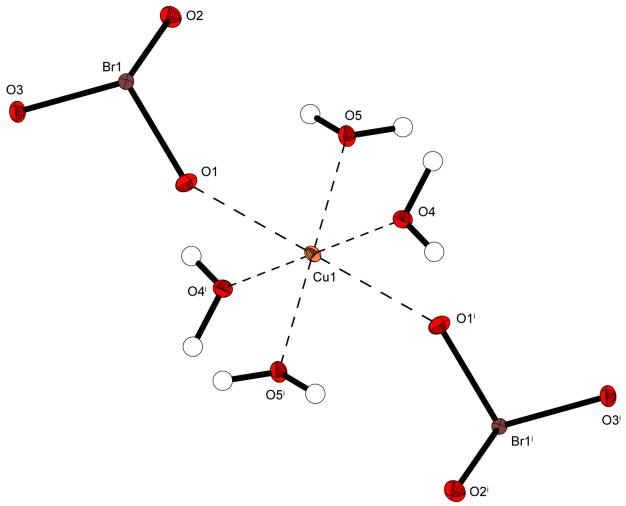


Figure 8. Molecular unit of $[Cu(BrO_3)_2(H_2O)_4]$ (**8**). Selected bond lengths (Å): Cu1–O1 2.399(2), Cu1–O4 1.9572(19), Cu1–O5 1.9520(19); Selected bond angles (°): O1–Cu1–O4 88.94(7), O1–Cu1–O5 95.11(7), O4–Cu1–O5 89.07(8). Symmetry code: (i) 1−x, −y, 1−z.

14.2.3 Sensitivities and Thermal Stability

For the investigation of endothermic events, like dehydration or melting, and for the determination of the thermal stabilities, differential thermal analysis (DTA) measurements with a heating rate of β = 5 °C min^{-1} were performed. The sensitivities of the complexes toward electric discharge as well as against impact and friction have been determined according to BAM standards, and all compounds were classified in accordance with the U.N. recommendations on the transport of dangerous goods.[48] An overview of the physicochemical properties of all compounds is given in Table 1. The sensitivities toward mechanical stress are comparable to those for LS and LA, whereas the susceptibility against electrostatic discharge sensitivity (ESD) is lower, making them more secure.[49]

Table 1. Physicochemical properties of compound **1**–**6** as well as LS and LA.[50]

compound	*IS* [J][a]	*FS* [N][b]	*ESD* [mJ][c]	T_{endo} [°C][d]	T_{exo} [°C][e]	Grain Size [µm]
1	2	< 5	25	-	137	< 100
2	1	< 5	60	-	169	100–500
3	2	< 5	90	-	92	100–500
4	< 1	10	150	-	146	100–500
5	8	108	260	103	150	100–500
6	1	40	150	129	146	100–500
LS	2.5–5	1.5	0.02–1.0	115	275–280	-
LA	2.5–4	0.1–1	6–12	-	320–360	-

[a]Impact sensitivity according to the BAM drophammer (method 1 of 6). [b]Friction sensitivity according to the BAM friction tester (method 1 of 6). [c]Electrostatic discharge sensitivity (OZM ESD tester). [d]Endothermic peak, indicating dehydration or loss of aqua ligands according to DTA (onset temperatures at a heating rate of 5 °C min^{-1}). [e]Exothermic peak, indicating decomposition according to DTA (onset temperatures at a heating rate of 5 °C min^{-1}).

The only endothermic occasions occurred during heating of coordination compounds **5** and **6** (Figure 9C) with the loss of their crystal water (**5**) or aqua (**6**) ligands at 103 and 129 °C, respectively. The loss of crystal water molecules after heating in compounds **1** and **3** leads to instability of the whole molecule and results therefore in exothermic decomposition. One possible explanation of the higher thermal stability of compounds **5** and **6** could be the formation of water-free species that decompose at a later stage. All ECCs have an exothermic decomposition temperature above 130 °C, except complex **3**, which possesses a very low thermal stability of 92 °C due to the loss of crystal water. The highest temperature stability (169 °C) shows the water-free 2D-polymer $[Cu(BrO_3)_2(1\text{-}MTZ)_2]$. The general trend becoming apparent is that bridging bromatos lead to crystallization of anhydrous complexes with higher thermal stabilities. Determination of the compounds' DDT capability by hot-plate and hot-needle testing (Figure 9A and 9B) was performed. Hot-needle tests were conducted by fixation of the sample underneath adhesive tape on a copper plate followed by penetration with a red-heated needle. A compound's detonation typically indicates a valuable primary explosive, whereas the safe and practicable hot-plate test shows the performance of the unconfined sample toward fast heating on a copper plate. It does not necessarily allow any conclusions on a compound's capability as a primary explosive. All compounds, except complex **1**, showed deflagration in both tests. While the water-free compound **2** shows relatively high-temperature stability and only weak DDT, it is the other way around with compound **1**, possessing a great DDT but a low decomposition temperature.

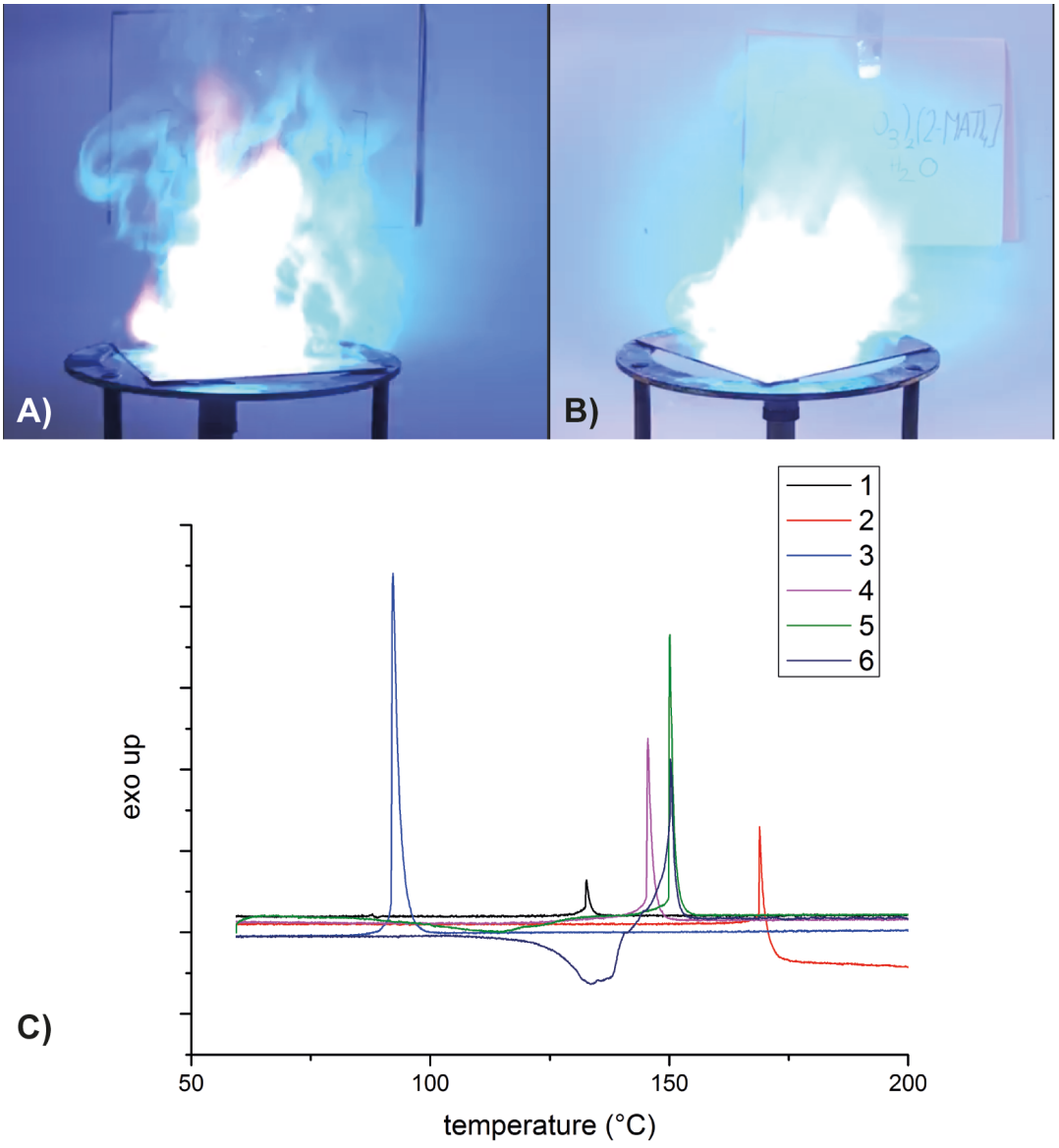


Figure 9. Hot-plate test of compounds **2** (A) and **3** (B); (C): DTA plots (5 °C min^{-1}) of complexes **1**–**6** shown in the range of 50–200 °C.

14.2.4 Laser Ignition Tests und UV-Vis Measurements

The laser ignition tests were performed with a single-pulsed 45 W InGaAs laser diode in the single-pulsed mode. The diode was coupled directly to an optical fiber with a core diameter of 400 µm and a cladding diameter of 480 µm. The optical fiber was linked via a SMA-type connecter directly to the laser and to a collimator. The collimator, in turn, was connected to an optical lens, which was stationed in its focal distance (f = 29.9 mm) to the sample. The lens was shielded from the explosive with sapphire glass. Transparent polycarbonate percussion caps

were filled with approximately 25 mg of the compound, pressed with a pressure force of 1 kN and sealed by a UV-curing adhesive. The confined samples were irradiated at a wavelength of 915 nm, a varying current of 7–8 A, a voltage of 4 V and a varying pulse length of 0.10–15 ms, which combined the results in an approximate energy output of 0.17–30 mJ. The results of the laser experiments, which are classified in decomposition, deflagration or detonation according to the generated sound, are summarized in Table 2.

Table 2. Results of the laser ignition tests of compounds **1**–**6.**

	1	**2**	**3**	**4**	**5**	**6**
E_{max} [mJ]	0.17	30.0	0.20	0.17	5.10	2.55
outcome[a]	det.	det.	det.	det.	dec.	det.

[a]det. = detonation; dec. = decomposition. Operating parameters: current I = 7–8 A; voltage U = 4 V; theoretical maximal output power P_{max} = 45 W; wavelength λ = 915 nm; pulse length τ = 0.10–15 ms.

All complexes except tetraaqua compound **5**, showed a detonation (Figure 10 A, B) differing in the required energy input between 0.17 and 2.55 mJ. Compared to LA[51] (3–30 mJ cm^{-2}) and LS[52] (1.3 J cm^{-2}), the ignition of the most of the ECCs is possible with lower energy input, although the results are difficult to compare because of their different setups. These results correlate with the observed sensitivities and make copper(II) bromate complexes promising compounds for laser ignition with low initiation energies.

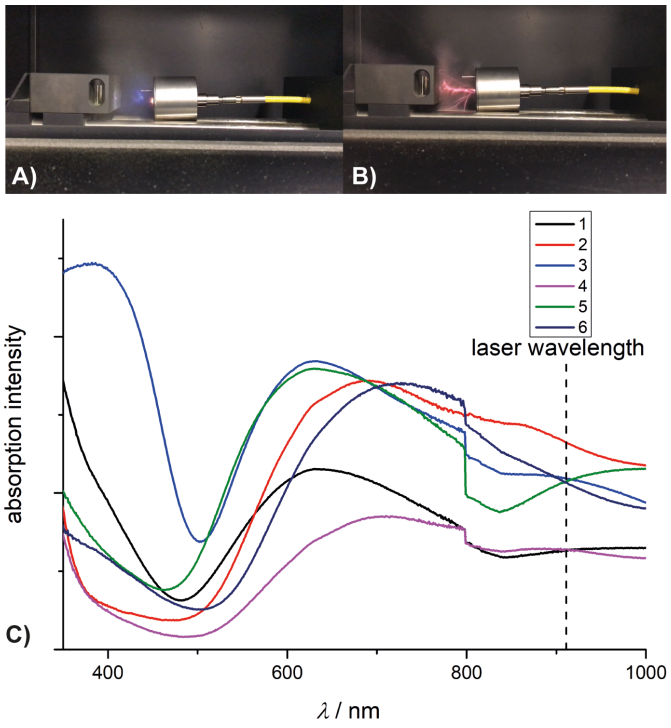


Figure 10. Positive laser initiation tests of compounds **2** (A) and **6** (B); (C): Solid-state UV-Vis measurements that were correlated with the laser initiation experiments.

In order to gain insight toward the laser-initiation mechanism, solid-state UV-Vis measurments were performed in the range of 350–1000 nm for all complexes (Figure 10 C). The step in the absorption intensity at 800 nm in the spectra is caused by a detector change. The UV-Vis spectra exhibit only qualitative character.

Because of the characteristic d-d-transitions, the spectra show absorptions in the UV, visible and near-IR regions typical for copper(II) compounds. The mechanism for laser initiation is still not fully understood and many pathways such as electronic or thermal are imaginable.[52] Because of the different coordination spheres, no conclusions can be drawn about the influence of the metal-ligand bond energy toward the color of the compounds. Compound **3** the only green copper(II) bromate complex shows absorption maxima close to 400 and 600 nm. All other copper(II) bromate complexes show absorption maxima close to 350 and 600 nm with only minor deviations among each other. All complexes show only minor absorptions at the laser wavelength of 915 nm. The excitation at 915 nm could be a conceivable explanation for the initiation. The process of laser ignition probably depends on multiple parameters and more investigations are necessary for a better understanding of the laser-initiation mechanism in the future.

14.2.5 Toxicity Determination and Mass Spectrometry (MS) of Decomposition Gases

The commercially available bioassay system LUMIStox test (luminescent marine bacterium *Vibrio fischeri* NRRL-B-11177), which measured the toxicity in aqueous media is a valuable indicating device when it comes to groundwater contamination. The half maximal effective concentration EC_{50} of these compounds was determined after an incubation time of 30 min (the toxicity level after 30 min of incubation: very toxic, < 0.10 g/L^{-1}; toxic 0.10–1.00 g/L^{-1}; nontoxic > 1.00 g/L^{-1}).[53] With an EC_{50} (30 min) value of 0.21 g/L^{-1} for compound **2**, it has to be considered as toxic, which is not surprising, because of the known toxicity of copper(II) compounds toward microorganisms.[54] Compared to the corresponding copper(II) chlorate and perchlorate complex – recently published by our group[55,40] – with EC_{50} values of 0.19 g/L^{-1} and 0.13 g/L^{-1}, respectively, the lower toxicity toward aquatic life of bromate compounds is proven.

For analysis of the gaseous decomposition products, a sample of approximately 40 mg of compound **2** was heated to 200 °C in a nitrogen gas flow and the formed gases were detected with a Cirrus3^{TM}-XD quadrupole mass spectrometer (Figure 11). The spectra show the

formation of oxygen (32), CO_2 (44) and small amounts of water (18). No formation of toxic Br_2 or HBr was observed.

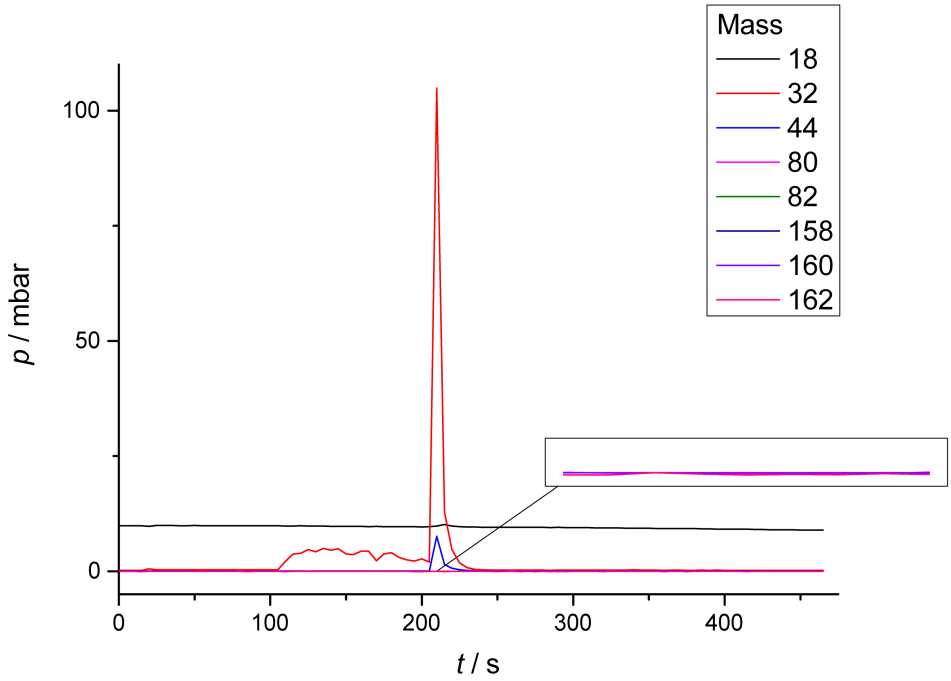


Figure 11. Results of the MS gas analysis of the decomposition products of compound **2**.

14.3 Conclusions

We demonstrated the next step in the development toward environmentally benign perchlorate-free ECCs with our exclusive concept of using bromate anions as "exotic" oxidizing species. The six newly synthesized and investigated copper(II) bromate compounds with azole ligands represent a considerable contribution to the coordination chemistry in general and in particular to ECC, because of the enormous lack of literature regarding this topic. The displayed synthesis of the complexes is a straightforward and low-cost synthetic route toward modern lead-free primary explosives with promising performance characteristics. The simple complexation of $Cu(BrO_3)_2$ with different nitrogen-rich ligands based on tri- and tetrazole derivatives assures the formation of energetic compounds with high densities. The trend of inclusion of water into many of the structures can hardly be explained by the average oxophilicity of copper(II); however, it can be prevented by the formation of 2D-polymeric layers caused by bridging bromato ligands. X-ray studies of all compounds gave insight into the fascinating coordination variety of copper(II) bromate complexes highly depending on the ligands used. The

compositions of complexes **1**–**6** were confirmed by elemental analysis and are in accordance with the crystal structures observed. In addition, the X-ray structure of the up to now unknown tetrahydrate of copper(II) bromate **8** could successfully be determined and the previously predicted structures of **1**[38] and **7**[37] proven wrong. Most of the compounds showed exothermic decomposition temperatures above 135 °C in thermal stability measurements by DTA. In comparison to the analogous perchlorate and chlorate complexes, ECC **2** showed a lower environmental hazardousness toward aquatic life in toxicity assessments using *V. fischeri*, which proves the higher environmental friendliness of bromate compounds. Within preliminary analysis of decomposition gases, no HBr and Br_2 formation was observed in the MS spectra. Detonations during laser-ignition experiments of nearly every single compound revealed the great capability of copper(II) bromate complexes in future laser-initiation systems.

14.4 Experimental Section

All chemicals and solvents were employed as received (Sigma-Aldrich, Fluka, Acros, and ABCR). ^{1}H and ^{13}C NMR spectra were recorded with neat solids as samples at ambient temperature using a JEOL Eclipse 270, JEOL EX 400 or JEOL Eclipse 400 instrument. The chemical shifts quoted in parts per million in the text refer to typical standards such as tetramethylsilane (^{1}H and^{13}C). Dehydration, melting and decomposition temperatures of the described compounds were measured through differential thermal analysis (DTA) with an OZM Research DTA 552-Ex instrument. The samples were measured in a range of 25–400 °C at a heating rate of 5 °C min^{-1}. Infrared spectra were measured with pure samples on a Perkin-Elmer BXII FT-IR system with a Smith DuraSampler IR II diamond ATR. Determination of the carbon, hydrogen, nitrogen and sulfur contents was carried out by combustion analysis using an Elementar Vario El (nitrogen values determined are often lower than the calculated ones due to their explosive behavior). UV-Vis spectra were recorded in the solid state using a Varian Cary 500 spectrometer in the wavelength range of 350–1000 nm. Impact sensitivity tests were carried out according to STANAG 4489[56] modified instruction[57] using a BAM (Bundesanstalt für Materialforschung) drophammer.[58] Friction sensitivity tests were carried out according to STANAG 4487[59] modified instruction[60] using the BAM friction tester. The classification of the tested compounds results from the "U.N. Recommendations on the Transport of Dangerous Goods".[48] Additionally all compounds were tested for their sensitivity toward electrical discharge using the Electric Spark Tester ESD 2010 EN.S7[61] Liquid-dried

luminescent bacteria of the strain *V. fischeri* NRRL-B-11177 provided by the HACH LANGE GmbH were used for the luminescent bacteria inhibition test to determine their toxicity toward aquatic organisms according to a modified procedure.[62] All the obtained coordination compounds were washed with cold water, dried overnight in air and used for analytics without further purification.

CAUTION! *All investigated compounds are potentially explosive energetic materials, which show partly increased sensitivities toward various stimuli (e.g. elevated temperatures, impact, friction or electrostatic discharge). Therefore, proper security precautions (safety glass, face shield, earthed equipment and shoes, leather coat, Kevlar gloves, Kevlar sleeves and ear plugs) have to be applied while synthesizing and handling the described compounds. Especially compound **1** must be handled with great care!*

General Procedure for the Preparation of Complexes **1**–**7**:

Copper(II) sulfate pentahydrate (62.4 mg, 0.25 mmol) and barium bromate (98.3 mg, 0.25 mmol), each dissolved in 5 mL of water, were combined and stirred mechanically for 10 min and the precipitated barium sulfate was filtered off. The aqueous filtrate was dried under reduced pressure and the obtained copper(II) bromate dissolved in 2 mL of water. Stoichiometric amounts of the ligand dissolved in 1 mL of water were added under stirring. The reaction mixtures were left to crystallize, and the solids were filtered off, washed with cold water (2 mL) and dried in air. Only one single crystal of compound **7** was picked for X-Ray determination experiments and the complex was not further analyzed. The up to now unknown structure of $[Cu(BrO_3)_2(H_2O)_4]$ (**8**) was picked out of a complex solution, which was left for crystallization as a single crystal, and a pure product for further investigation was not obtained.

$[Cu_2(4\text{-ATRI})_6](BrO_3)_4 \cdot H_2O$ (**1**)

Compound **1** was isolated as a light blue precipitate. Yield: 116 mg (0.20 mmol, 80 %). Single crystal growth was achieved by overlaying an aqueous solution (8 mL) of copper(II) bromate with an ethanolic solution (8 mL) of 4-ATRI, separated by a mixture (4 mL) of water/ethanol (50/50). After 7 days blue rods suitable for X-ray determination were obtained.

DTA (5 °C min^{-1}) onset: 137 °C (exothermic); IR (ATR, cm^{-1}): $\tilde{\nu}$ = 3545 (vw), 3250 (m), 3208 (w), 3153 (m), 3126 (m), 3089 (m), 3063 (m), 3018 (w), 2965 (w), 1644 (w), 1631 (w), 1553 (w), 1539 (w), 1491 (vw), 1424 (vw), 1396 (w), 1373 (w), 1321 (vw), 1222 (m), 1207 (w), 1095 (m), 1085 (m), 1050 (m), 1007 (w), 992 (w), 979 (w), 913 (w), 890 (w), 818 (s), 808 (s), 783(vs), 761 (vs), 693(w), 679 (w), 622 (vs); EA ($C_{12}H_{26}Br_4Cu_2N_{24}O_{13}$, 1161.29): calcd: C 12.41, H 2.26, N 28.95 %; found: C 12.78, H 2.28, N 28.64 %; BAM drophammer: 2 J; friction tester: < 5 N; ESD: 25 mJ (at grain size < 100 µm).

$[Cu(BrO_3)_2(1\text{-MTZ})_2]$ (**2**)

Blue platelike crystals of complex **2** were obtained within 5 days and were suitable for X-ray determination. Yield: 89.4 mg (0.18 mmol, 73 %).

DTA (5 °C min^{-1}) onset: 169 °C (exothermic); IR (ATR, cm^{-1}): $\tilde{\nu}$ = 3143 (m), 3034 (w), 1762 (vw), 1522 (m), 1472 (w), 1304 (w), 1202 (m), 1178 (vw), 1109 (m), 1066 (w), 1036 (w), 1003 (w), 883 (m), 862 (vs), 788 (s), 726 (s), 708 (s), 686 (vs), 652 (s); EA ($C_4H_8Br_2CuN_8O_6$, 487.51): calcd: C 9.85, H 1.65, N 22.99 %; found: C 10.11, H 1.81, N 23.13 %; BAM drophammer: 1 J; friction tester: < 5 N; ESD: 60 mJ (at grain size 100–500 µm).

$[Cu(BrO_3)_2(2\text{-MAT})_4] \cdot H_2O$ (**3**)

Green blocks suitable for X-ray determination of the monohydrated complex **3** crystallized within 3 days. Yield: 106 mg (0.14 mmol, 58 %).

DTA (5 °C min^{-1}) onset: 92 °C (exothermic); IR (ATR, cm^{-1}): $\tilde{\nu}$ = 3359 (m), 3317 (m), 3306 (m), 3223 (m), 3174 (w), 3020 (w), 2962 (w), 1629 (m), 1606 (m), 1557 (s), 1439 (m), 1422 (m), 1383 (w), 1345 (w), 1333 (w), 1195 (m), 1132 (w), 1103 (w), 1075 (w), 1023 (w), 803 (vs), 760 (vs), 749 (vs), 680 (m), 670 (w), 631 (m), 571 (w); EA ($C_8H_{22}Br_2CuN_{20}O_7$, 733.75): calcd: C 13.10, H 3.02, N 38.18 %; found: C 13.13, H 2.95, N 38.37 %; BAM drophammer: 2 J; friction tester: < 5 N; ESD: 90.0 mJ (at grain size 100–500 µm).

$[Cu(BrO_3)_2(1,2\text{-dtp})_2]$ (**4**)

Blue blocklike crystals of the water-free compound **4** were isolated within 7 days and were suitable for X-ray determination. Yield: 96.9 mg (0.14 mmol, 57 %).

DTA (5 °C min^{-1}) onset: 146 °C (exothermic); IR (ATR, cm^{-1}): $\tilde{\nu}$ = 3144 (m), 1764 (w), 1741 (m), 1571 (w), 1516 (m), 1466 (m), 1457 (m), 1446 (m), 1396 (w), 1381 (m), 1366 (m), 1301 (w), 1287 (m), 1198 (m), 1180 (m), 1141 (m), 1134 (m), 1108 (w), 1059 (w), 1031 (m), 1015 (m), 1008 (m), 886 (m), 860 (s), 786 (s), 751 (m), 727 (s), 713 (s), 700 (vs), 677 (m), 654 (s); EA ($C_{10}H_{16}Br_2CuN_{16}O_6$, 679.70): calcd: C 17.67, H 2.37, N 32.97 %; found: C 17.20, H 2.47, N 32.51 %; BAM drophammer: < 1 J; friction tester: 10 N; ESD: 150 mJ (at grain size 100–500 µm).

$[Cu(BrO_3)_2(2,2\text{-dtp})_2] \cdot 4\ H_2O$ (**5**)

The four crystal water containing complex **5** crystallized within 7 days in the form of blue blocks suitable for X-ray determination. Yield: 113 mg (0.15 mmol, 60 %).

DTA (5 °C min^{-1}) onset: 103 °C (loss of water), 150 °C (exothermic); IR (ATR, cm^{-1}): $\tilde{\nu}$ = 3524 (w), 3441 (w), 3367 (w), 3151 (w), 3125 (w), 3014 (w), 2985 (vw), 2970 (vw), 2945 (vw), 1741 (vw), 1737 (vw), 1652 (vw), 1623 (w), 1608 (w), 1573 (vw), 1512 (w), 1488 (w), 1474 (w), 1464 (w), 1447 (w), 1438 (w), 1382 (w), 1373 (w), 1359 (w), 1322 (w), 1306 (w), 1285 (w), 1254 (vw), 1209 (w), 1199 (w), 1187 (w), 1172 (m), 1153 (m), 1137 (m), 1101 (m), 1086 (m), 1076 (w), 1059 (w), 1031 (m), 1021 (m), 1012 (w), 982 (w), 936 (w), 890 (vw), 861(w); EA ($C_{10}H_{24}Br_2CuN_{16}O_{10}$, 751.76): calcd: C 15.98, H 3.22, N 29.81 %; found: C 16.46, H 3.36, N 31.06 %; BAM drophammer: 8 J; friction tester: 108 N; ESD: 260 mJ (at grain size 100–500 µm).

$[Cu(H_2O)_2(i\text{-dtp})_2](BrO_3)_2$ (**6**)

Product **6** was received within 8 days in the form of blue blocks suitable for X-ray determination. Yield: 152 mg (0.21 mmol, 85 %).

DTA (5 °C min^{-1}) onset: 129 °C (loss of water followed by dec.); IR (ATR, cm^{-1}): $\tilde{\nu}$ = 3357 (w), 3267 (w), 3151 (w), 3116 (w), 3016 (w), 2986 (w), 2945 (vw), 2776 (vw), 2661 (vw), 1741

(vw), 1652 (w), 1571 (vw), 1512 (w), 1489 (w), 1437 (m), 1391 (w), 1376 (w), 1360 (w), 1321 (vw), 1304 (w), 1287 (w), 1211 (w), 1187 (m), 1173 (m), 1160 (w), 1127 (w), 1100 (m), 1086 (m), 1039 (m), 1031 (w), 1011 (m), 990 (w), 916 (w), 891 (w), 840 (s), 782 (vs), 753 (s), 719 (w), 675 (m), 665 (m), 632 (m), 532 (vw); EA ($C_{10}H_{20}Br_2CuN_{16}O_8$, 715.73): calcd: C 16.78, H 2.82, N 31.31 %; found: C 16.91, H 2.92, N 31.81 %; BAM drophammer: 1 J; friction tester: 40 N; ESD: 150 mJ (at grain size 100–500 μm).

Supporting information available in the appendix in **Chapter 19.11** and under:

https://pubs.acs.org/doi/suppl/10.1021/acs.inorgchem.8b01045/suppl_file/ic8b01045_si_001.pdf

14.5 References

[1] Klapötke T. M. *Chemistry of High-Energy Materials*, 3rd ed., Walter De Gruyter, Berlin/Boston, 2015.

[2] Brinck, T. *Green Energetic Materials*, 1st ed., John Wiley & Sons, Chichester, 2014.

[3] Fairhall, L. T.; Jenrette, W. V.; Jones, S. W.; Prittchard, E. A. The toxicity of lead azide. *Public Health Rep.* **1943**, *58*, 607–617.

[4] Gidlow, D. A. Lead toxicity. *Occup. Med.* **2015**, *65*, 348–356.

[5] Haiges, R.; Christe, K. O. Energetic High-Nitrogen Compounds: 5-(Trinitromethyl)-2*H*-tetrazole and -tetrazolates, Preparation, Characterization, and Conversion into 5-(Dinitromethyl)tetrazoles. *Inorg. Chem.* **2013**, *52*, 7249–7260.

[6] Huynh, M. H. V.; Coburn, M. D.; Meyer, T. J.; Wetzler, M. Green primary explosives: 5-Nitrotetrazolato-*N*2-ferrate hierarchies. *Proc. Natl. Acad. Sci.* **2006**, *103*, 10322–10327.

[7] Xu, J.-G.; Sun, C.; Zhang, M.-J.; Liu, B.-W.; Li, X.-Z.; Lu, J.; Wang, S.-H.; Zheng, F.-K.; Guo, G.-C. Coordination Polymerization of Metal Azides and Powerful Nitrogen-Rich Ligand toward Primary Explosives with Excellent Energetic Performances. *Chem. Mater.* **2017**, *29*, 9725–9733.

[8] Liu, T.; Qi, X.; Wang, K.; Zhang, J.; Zhang, W.; Zhang, Q. Green primary energetic materials based on N-(3-nitro-1-(trinitromethyl)-1*H*-1,2,4-triazol-5-yl)nitramide. *New J. Chem.* **2017**, *41*, 9070–9076.

[9] Tang, Y.; He, C.; Mitchell, L. A.; Parrish, D. A.; Shreeve, J. n. M. Potassium 4,4'-Bis(dinitromethyl)-3,3'-azofurazanate: A Highly Energetic 3D Metal-Organic Framework as a Promising Primary Explosive. *Angew. Chem., Int. Ed.* **2016**, *55*, 5565–5567.

[10] He, P.; Wu, L.; Wu, J.; Wang, Q.; Li, Z.; Gozin, M.; Zhang, J. Green Energetic Nitrogen-Rich Salts of 1,1′-Dinitramino-5,5′-bistetrazolate. *Chem. Eur. J.* **2017,** *23*, 11159–11168.

[11] Clark, L. V. Diazodinitrophenol, a Detonating Explosive. *Ind. Eng. Chem. Res.* **1933**, *25*, 663–669.

[12] Spear, R. J.; Norris, W. P. Structure and properties of the potassium hydroxide-dinitrobenzofuroxan adduct (KDNBF) and related explosive salts. *Propellants, Explos., Pyrotech.* **1983,** *8*, 85–88.

[13] Fronabarger, J. W.; Williams, M. D.; Sanborn, W. B.; Parrish, D. A.; Bichay, M. KDNP – A Lead Free Replacement for Lead Styphnate. *Propellants, Explos., Pyrotech* **2011,** *36*, 459–470.

[14] Shunguan, Z.; Youchen, W.; Wenyi, Z.; Jingyan, M. Evaluation of a New Primary Explosive: Nickel Hydrazine Nitrate (NHN) complex. *Propellants, Explos., Pyrotech.* **1997**, *22*, 317–320.

[15] Fronabarger, J. W.; Williams, M. D.; Sanborn, W. B.; Bragg, J. G.; Parrish, D. A.; Bichay, M. DBX-1 - A Lead Free Replacement for Lead Azide. *Propellants, Explos., Pyrotech.* **2011**, *36*, 541–550.

[16] Chen, D.; Yang, H.; Yi, Z.; Xiong, H.; Zhang, L.; Zhu, S.; Cheng, G. $C_8N_{26}H_4$: An Environmentally Friendly Primary Explosive with High Heat of Formation. *Angew. Chem. Int. Ed.* **2018**, *57*, 2081–2084.

[17] Ilyushin, M. A.; Aleksandrova, M. A.; Bachurina, I. V.; Smirnov, A. V.; Tselinskii, I. V. Synthesis and properties of an energetic complex pentaamminecobalt (III)

perchlorate, with 4-amino-1,2,4-triazole as ligand. *Russ. J. Appl. Chem.* **2010**, *83*, 92–96.

[18] Chen, S.; Guo, W.; Bi, Y.; Zhang T. Synthesis and Properties of $[Cd(HTRTR)_2(H_2O)_4](HTNR)_2$ as an Energetic Complex. *Z. Anorg. Allg. Chem.* **2016**, *642*, 761–765.

[19] Talawar, M. B.; Agrawal, A. P.; Asthana, S. N. Energetic coordination compounds: Synthesis, characterization and thermolysis studies on bis-(5-nitro-2H-tetrazolato-N2)tetraammine cobalt (III) perchlorate (BNCP) and its new transition metal (Ni/Cu/Zn) perchlorate analogues. *J. Hazard. Mater.* **2005**, *120*, 25–35.

[20] Szimhardt, N; Wurzenberger, M. H. H.; Klapötke, T. M.; Lechner, J. T.; Reichherzer, H.; Unger, C.; Stierstorfer, J. Highly functional energetic complexes: stability tuning through coordination diversity of isomeric propyl-linked ditetrazoles. *J. Mater. Chem. A* **2018**, *6*, 6565–6577.

[21] Evers, J.; Gospodinov, I.; Joas, M.; Klapötke, T. M.; Stierstorfer, J. Cocrystallization of Photosensitive Energetic Copper(II) Perchlorate Complexes with the Nitrogen-rich Ligand 1,2-Di(1*H*-tetrazol-5-yl)ethane. *Inorg. Chem.* **2014**, *53*, 11749–11756.

[22] Ahmad, S. R.; Cartwright, M. Laser Ignition – Practical Considerations. In *Laser Ignition of Energetic Materials*, John Wiley & Sons, Ltd: 2014; 247–268.

[23] Schirra, R.; Zöllner, H. A fast low-energy optical detonator. In *Proceedings of the 42nd International Pyrotechnics Seminar*, Grand Junction, CO, July 10–15, 2016, IPSUSA. 2016; pp 422–428.

[24] Zhilin, A. Y.; Ilyushin, M. A.; Tselinskii, I. V.; Brykov A. S. Synthesis of a high-energy-capacity compound, cis-tetraamminebis(5-nitro-2*H*-tetrazolato-N2)cobalt(III) perchlorate. *Russ. J. Appl. Chem.* **2001**, *74*, 99–102.

[25] Zhilin, A. Y.; Ilyushin, M. A.; Tselinskii, I. V.; Kozlov, A. S.; Lisker, I. S. High-energy-capacity cobalt(III) tetrazolates. *Russ. J. Appl. Chem.* **2003**, *76*, 572.

[26] Ilyushin, M. A.; Tselinsky, I. V.; Ugryumov, I. A.; Zhilin, A. Y.; Kozlov, A. S. Coordination complexes as inorganic primary explosives. *New Trends in Research of Energetic Materials, Proceedings of the Seminar, 6th, Pardubice, Czech Republic, Apr. 22–24, 2003* **2003**, 146–152.

[27] Ugryumov, I. A.; Ilyushin, M. A.; Tselinskii, I. V.; Kozlov, A. S. Synthesis and properties of photosensitive complex perchlorates of d metals with 3(5)-hydrazino-4-amino-1,2,4-triazole as ligand. *Russ. J. Appl. Chem.* **2003**, *76*, 439–441.

[28] Myers, T. W.; Brown, K. E.; Chavez, D. E.; Scharff, R. J.; Veauthier, J. M. Correlating the Structural, Electronic, and Explosive Sensitivity Properties of CuII Tetrazine Complexes. *Eur. J. Inorg. Chem.* **2016**, *2016*, 3178–3183.

[29] Myers, T. W.; Bjorgaard, J. A.; Brown, K. E.; Chavez, D. E.; Hanson, S. K.; Scharff, R. J.; Tretiak, S. Veauthier, J. M. Energetic Chromophores: Low-Energy Laser Initiation in Explosive Fe(II) Tetrazine Complexes. *J. Am. Chem. Soc.* **2016**, *138*, 4685–4692.

[30] Joas, M. *PhD thesis*, Ludwig-Maximilians Universität München, 2014.

[31] Myers, T. W.; Brown, K. E.; Chavez, D. E.; Scharff, R. J.; Veauthier, J. M. Laser Initiation of Fe(II) Complexes of 4-Nitro-pyrazolyl Substituted Tetrazine Ligands. *Inorg. Chem.* **2017**, *56*, 2297–2303.

[32] Yoffe D.; Frim R.; Ukeles S. D.; Dagani M. J.; Barda H. J.; Benya T. J.; Sanders D. C. Bromin Compounds. in Ullmann‘s Encyclopedia of Industrial Chemistry, 7th ed. (Ed.: Elvers B.) Wiley-VCH Verlag, Weinheim 2013, pp. 27–28.

[33] Yoshinaga S.; Matsumoto M.; Nagaishi T. Reaction among potassium bromate, aluminium and dinitrotoluene. *Kogyo Kayaku* **1979**, *40*, 101–108.

[34] Yoshida T. Air bag gas generating composition. US5898126 A, **1999**.

[35] Menzel R. E. Method for detecting trace explosives using photoluminescence. US 7910376 B2, **2011**.

[36] Urben P. G. *Bretherick’s Handbook of Reactive Chemical Hazards*, 8nd ed., Elsevier, Amsterdam, 2017, pp. 69–70.

[37] Amiel J. Complex cupric perchlorates and bromates with primary amines. *Compt. rend.* **1935**, *200*, 672–674.

[38] Sinditskii V. P.; Vernidub T. Y.; Fogel'zang A. E.; Zueva N. A. Coordination compounds of 4-amino-1,2,4-triazole with metal chlorates, bromates and nitrates. *Izv. Vyssh. Uchebn. Zaved., Khim. Khim. Tekhnol.* **1991**, *34*, 15–19.

[39] Juknelevicius D.; Karvinen E.; Klapötke T. M.; Kubilius R.; Ramanavicius A.; Rusan M. Copper(I) Bromide: An Alternative Emitter for Blue-Colored Flame Pyrotechnics. *Chem. Eur. J.* **2015**, *21*, 15354–15359.

[40] Wurzenberger M. H. H.; Szimhardt N.; Stierstorfer J. Copper(II) Chlorate Complexes – the Renaissance of a Forgotten and Misjudged Energetic Anion. *J. Am. Chem. Soc.* **2018**, *140*, 3206–3209.

[41] Markin, V. N.; Rozhdestvenskaya, I. V.; Fedosova, O. I. Crystal structure of copper bromate dihydrate ($Cu(BrO_3)_2\ 2H_2O$). *Vestn. Leningr. Univ., Ser. 4: Fiz., Khim.* **1985**, *1*, 104–107.

[42] Blackburn, A. C.; Gallucci, J. C.; Gerkin, R. E. Structure of hexaaquacopper(II) bromate. *Acta Crystallogr., Sect. C: Cryst. Struct. Commun.* **1991**, *47*, 2019–2023.

[43] Holleman, A. F.; Wiberg, E; Wiberg, N. *Lehrbuch der Anorganischen Chemie*; de Gruyter: Berlin, 2007; pp 464–474.

[44] Crystallographic data for the structures have been deposited with the Cambridge Crystallographic Data Centre. Copies of the data can be obtained free of charge on application to The Director, CCDC, 12 Union Road, Cambridge CB2 1EZ, UK (Fax: int.code_(1223)336-033; e-mail for inquiry: fileserv@ccdc.cam.ac.uk; e-mail for deposition: (deposit@ccdc.cam.ac.uk).

[45] Wiehl, L. Structures of hexakis(1-propyltetrazole)iron(II) bis(tetrafluoroborate), $[Fe(CHN_4C_3H_7)_6](BF_4)_2$, hexakis(1-methyltetrazole)iron(II) bis(tetrafluoroborate), $[Fe(CHN_4CH_3)_6](BF_4)_2$, and the analogous perchlorates. Their relation to spin crossover behavior and comparison of Debye-Waller factors from structure determination and Moessbauer spectroscopy. *Acta Cryst. B.* **1993**, *49*, 289–303.

[46] van Koningsbruggen, P. J.; Garcia, Y.; Kahn, O.; Fournès, L.; Kooijman, H.; Spek, A. L.; Haasnoot, J. G.; Moscovici, J.; Provost, K.; Michalowicz, A.; Renz, F.; Gütlich, P. Synthesis, Crystal Structure, EXAFS, and Magnetic Properties of Catena [μ-Tris(1,2-bis(tetrazol-1-yl)propane-*N*1,*N*1')iron(II)] Bis(perchlorate). First Crystal Structure of an Iron(II) Spin-Crossover Chain Compound. *Inorg. Chem.* **2000**, *39*, 1891–1900.

[47] Romanenko, G. V.; Savelieva, Z. A.; Podberezskaya, N. V.; Larionov, S. V. Structure of the Cu(II) chloride complex with 4-amino-1,2,4-triazole $Cu(C_2H_4N_4)Cl_2$. *J. Struct. Chem.* **1997**, *38*, 171–176.

[48] Impact: insensitive > 40 J, less sensitive ≥ 35 J, sensitive ≥ 4 J, very sensitive ≤ 3 J; Friction: insensitive > 360 N, less sensitive = 360 N, sensitive < 360 N and > 80 N, very sensitive ≤ 80 N, extremely sensitive ≤ 10 N. According to the UN Recommendations on the Transport of Dangerous Goods, (+) indicates not safe for transport.

[49] Meyer, R.; Köhler, J.; Homburg, A. in *Explosives*, *5th ed.*, Wiley-VCH Verlag, Weinheim, 2002, pp. 196–197.

[50] Hagan, J. T.; Chaudhri, M. M. Low energy laser initiation of single crystals of *β*-lead azide. *J. Mater. Sci.* **1981**, *16*, 2457–2466

[51] de Yon, L.; Nguyen, T.; Waschl, J. *Laser ignition of explosives, pyrotechnics and propellants.* Defence Science and Technology Organization: 1995.

[52] Aluker, E. D.; Krechetov, A. G.; Mitrofanov, A. Y.; Nurmukhametov, D. R.; Kuklja, M. M. Laser Initiation of Energetic Materials: Selective Photoinitiation Regime in Pentaerythritol Tetranitrate. *J. Phys. Chem. C*, **2011**, *115*, 6893–6901.

[53] Cao, C. J.; Johnson, M. S.; Hurley, M. M.; Klapötke, T. M. *In Vitro* Approach to Rapid Toxicity Assessment of Novel High-Nitrogen Energetics. *JANNAF J. Propuls. Energet.*, **2012**, *5*, 41–51.

[54] Ochoa-Herrera, V.; Léon, G.; Banihani, Q.; Field, J. A.; Sierra-Alvarez, R. Toxicity of copper(II) ions to microorganisms in biological wastewater treatment systems. *Sci. Total Environ.*, **2011**, *380*, 412–413.

[55] Szimhardt, N.; Wurzenberger, M. H. H.; Behringer, A.; Daumann, L.; Stierstorfer, J. Coordination chemistry with 1-methyl-5*H*-tetrazole: cocrystallization, laser-ignition, lead-free primary explosives - one ligand, three goals. *J. Mater. Chem. A* **2017**, *5*, 23753–23765.

[56] NATO standardization agreement (STANAG) on explosives, impact sensitivity tests, no. 4489, 1st ed., Sept. 17, 1999.

[57] WIWEB-Standardarbeitsanweisung 4-5.1.02, Ermittlung der Explosionsgefährlichkeit, hier der Schlagempfindlichkeit mit dem Fallhammer, Nov. 8, 2002.

[58] http://www.bam.de, Accessed April 2018.

[59] NATO standardization agreement (STANAG) on explosive, friction sensitivity tests, no. 4487, 1st ed., Aug. 22, 2002.

[60] WIWEB-Standardarbeitsanweisung 4-5.1.03, Ermittlung der Explosionsgefährlichkeit oder der Reibeempfindlichkeit mit dem Reibeapparat, Nov. 8, 2002.

[61] http://www.ozm.cz, Accessed April 2018.

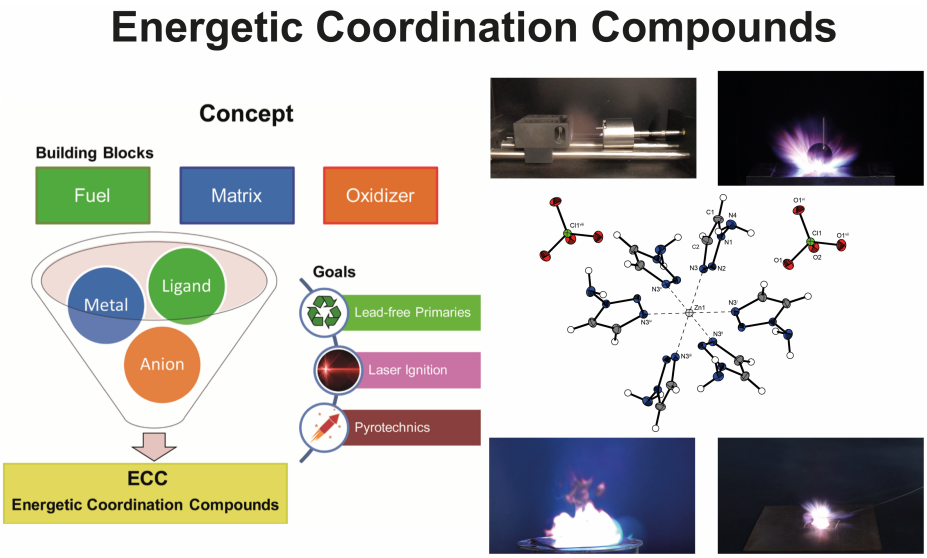
[62] R. Scharf, PhD thesis, Ludwig-Maximilians Universität München, 2016.

15 1-Amino-triazole Transition Metal Complexes as Laser Ignitable and Lead-free Primary Explosives

Norbert Szimhardt, Maximilian H. H. Wurzenberger, Lukas Zeisel, Michael S. Gruhne, Marcus Lommel, Thomas M. Klapötke and Jörg Stierstorfer

published in *Chemistry An European Journal, **2018***.

DOI: 10.1002/chem.201803372



The nitrogen-rich aminotriazole ligands 1-amino-1,2,3-triazole (1-ATRI) and 1-amino-1,2,4-triazole (1-A-1,2,4-TRI) were successfully implemented as suitable building blocks in 14 new energetic transition metal complexes. By varying the metals and anions, a variety of different functional materials could be synthesized, some of which have great potential as laser-ignitable and classical primary explosives.

Abstract

This unique complex study describes two isomeric aminotriazoles as auspicious, nitrogen-rich ligands for energetic coordination compounds (ECC) in order to replace commonly used, highly poisonous and environmentally harmful lead-based primary explosives. The triazoles have been obtained via easily scalable and convenient synthesis routes solely requiring commercially available starting materials. 1-Amino-1,2,3-triazole (**1**, 1-ATRI) and for the first time 1-amino-1,2,4-triazole (**2**, 1A-1,2,4-TRI) could be implemented as ligands to form highly energetic transition metal(II) complexes. The desired characteristics could be altered successively using various non-poisonous metal(II) centers (Cu^{2+}, Mn^{2+}, Fe^{2+}, and Zn^{2+}) and anions (Cl^-, NO_3^-, ClO_3^-, ClO_4^-, picrate, styphnate, 2,4,6-trinitro-3-hydroxyphenolate or 2,4,6-trinitro-3,5-dihydroxyphenolate). The synthesized 14 coordination compounds were characterized comprehensively using XRD, IR, EA, UV/Vis, DTA, TGA and sensitivities toward electrostatic discharge. Ball drop impact, ESD and mechanical stimuli (impact and friction) were determined according to BAM-standard methods. In addition, to laser ignition experiments selected ECC were evaluated in classical secondary explosive initiation tests (nitropenta filled detonators) showing their enormous potential and making them very attractive for future applications.

15.1 Introduction

The demanding field of energetic materials can be roughly divided into four main areas: (i) primary explosives, (ii) secondary explosives, (iii) propellants, and (iv) pyrotechnics.[1] The majority of these currently used explosives or at least their degradation products exhibit enormous toxicity for human life and the environment, making research into green alternatives indispensable.[2-4] Especially in the field of primary explosives, there is an urgent need for development, as the extremely toxic lead compounds lead azide and lead styphnate are still in use.[5-7] Both compounds, which have been added to the REACH candidate list in the meantime, are the main components in various ignition systems such as primers or detonators which are of great importance in ammunition, warheads but also in other even civilian areas such as mine construction.[8]

A very promising strategy to face the issues mentioned above is the synthesis of energetic transition metal complexes based on endothermic azole ligands.[9-12] The most significant

advantage of this concept is the possible alteration of three different components (i) metal, (ii) anion, and (iii) ligand, which allows an exact adjustment of the optical and energetic properties (Figure 1). In recent years, a large number of different combinations have been reported in the literature.[13,14] Another benefit of this approach, in addition to its ease of manufacture, includes the possibility to proceed from toxic heavy metals like lead or mercury to more environmentally friendly alternatives such as copper, iron, manganese, or zinc, which exhibit significantly lower toxicity.[15] Especially the selection of these transition metals is a good compromise between price, availability, and environmental compatibility.

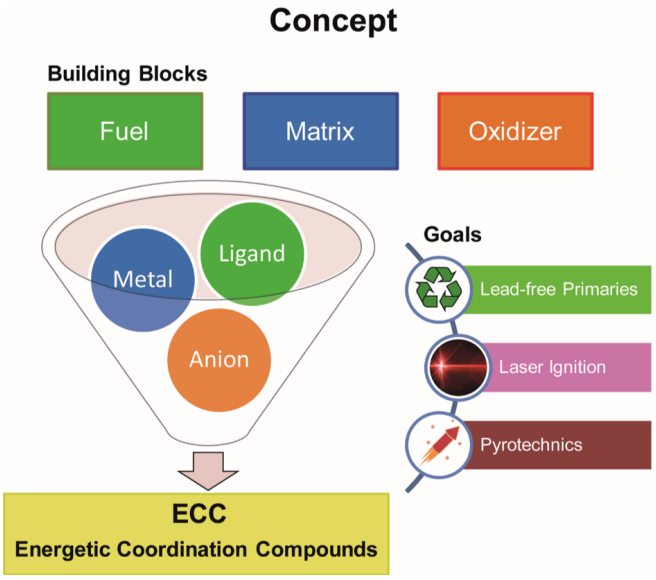


Figure 1. Concept of energetic coordination compounds (ECC) based on the three building blocks.

Compounds or mixtures can be ignited by various methods or ignition sources such as mechanical stimuli, light, electricity, or heat, depending on the application. Especially initiation by laser irradiation, which has several advantages over classical initiation methods, has made considerable progress recently.[16-21] Compared to conventional initiation methods, the number of unwanted ignitions could be reduced by using less mechanically sensitive compounds which instead react preferably on optical excitation. ECC based on azole ligands such as tetrazoles or triazoles have so far shown promising results both in the field of laser-ignitable energetic materials and lead-free primary explosives.[22] Triazole complexes in particular, whose energetic character can be adapted by isomerism (1,2,3-triazoles vs. 1,2,4-triazoles) or functionalization (nitrogen or carbon substitution), are discussed in a large number of different potential fields of application like MOF´s for gas storage or optical devices.[23] Of exceptional interest are ligands with an incorporated hydrazine function to increase the energy content

respectively the endothermic character. The literature contains a multitude of interesting 4-aminotriazole coordination compounds, but until now no complexes have been synthesized with the 1-isomer nor the more energetic 1-amino-1,2,3-triazole analog (Figure 2).[24,25] Both ligands exhibit a relatively high nitrogen content (66.63 %) and have been known for almost half a century.[26,27]

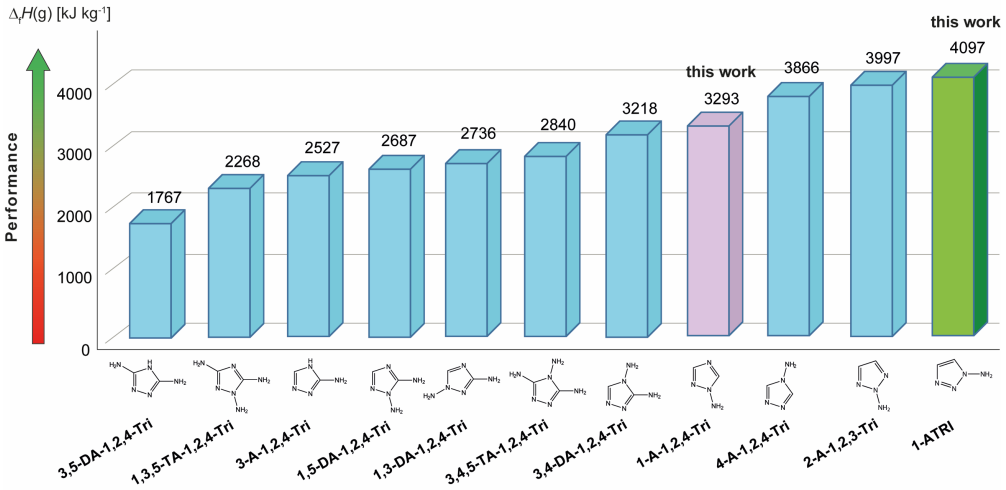


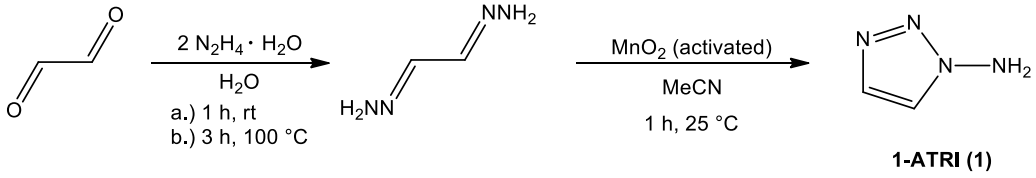
Figure 2. Comparison of the per unit mass calculated gas phase enthalpies of formation for several different triazoles. Enthalpies of formation were calculated using the atomization method ($\Delta_f H^0_{(g,\,M)} = H_{(M)} - \Sigma H^0_{(A)} + \Sigma \Delta_f H^0_{(A)}$) using Gaussian09 computed CBS-4M electronic enthalpies.

The majority of the known triazole complexes do not have the necessary power to be considered as potential primary explosives or laser-ignitable compounds. To further increase the energy content of the complexes, 1-amino-1,2,4-triazole (1-A-1,2,4-TRI) and 1-amino-1,2,3-triazole (1-ATRI) were used as ligands. Especially 1-ATRI, which contains four nitrogen atoms in a row shows a highly endothermic character (Figure 2) and can be synthesized by straightforward amination or oxidation reaction. The ligand shows an excellent complexation behavior, and the resulting ECC confirmed their tremendous potential during the laser ignition and nitropenta initiation tests.

15.2 Results and Discussion

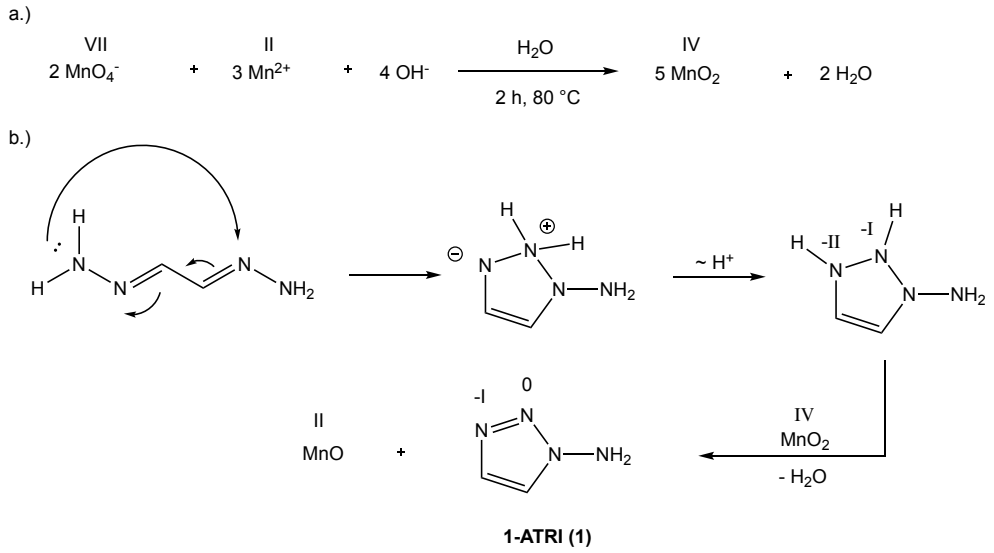
15.2.1 Synthesis

1-Amino-1,2,3-triazole (**1**) can be synthesized by different methods. On the one hand by amination of 1,2,3-triazole which unfortunately leads to a mixture of isomers and on the other hand by a 2-step synthesis which leads directly to the desired product isomerically pure (Scheme 1). Freshly precipitated manganese dioxide has the ability to promote intramolecular cyclization of organic molecules through oxidation.[28,29] To obtain the mild oxidizing agent MnO_2 in its activated form, Mn^{II} salts react in a redox reaction with MnO_4^- in an alkaline milieu (Scheme 2a). The preparation of the bishydrazone key intermediate is realized by condensation of hydrazine hydrate and glyoxal.[30] This reaction is performed twice, once at each carbonyl function of the dialdehyde. It may occur that only one carbonyl group of glyoxal reacts, decreasing the yield of the reaction by simultaneous contamination. Possible impurities of the reaction product were prevented by recrystallization from ethanol.



Scheme 1. Isomerically pure two-step synthesis of 1-ATRI (**1**) starting from the commercially available starting materials hydrazine hydrate and glyoxal.

The following reaction of an intramolecular cyclization of the intermediate can be formulated as concerted electron shifts between the atoms of this molecule and is realized in acetonitrile at room temperature (Scheme 1, 2b).[31] One possible mechanism of this patent procedure could take place in the following way: The lone pair from one primary amine attacks the nitrogen of the farther away imine group nucleophilic, whereupon the two electrons that form the nitrogen-carbon double bond relocate to provide a carbon-carbon double bond. Finally, the remaining carbon-nitrogen double bond is terminated, with the two electrons shifting to the adjacent nitrogen atom. The resulting unstable five-membered ring, in particular the N2- and N3-atoms are oxidized by the mild oxidizing agent $Mn^{IV}O_2$ forming stable 1-ATRI (**1**), $Mn^{II}O$ and water (Scheme 2b).

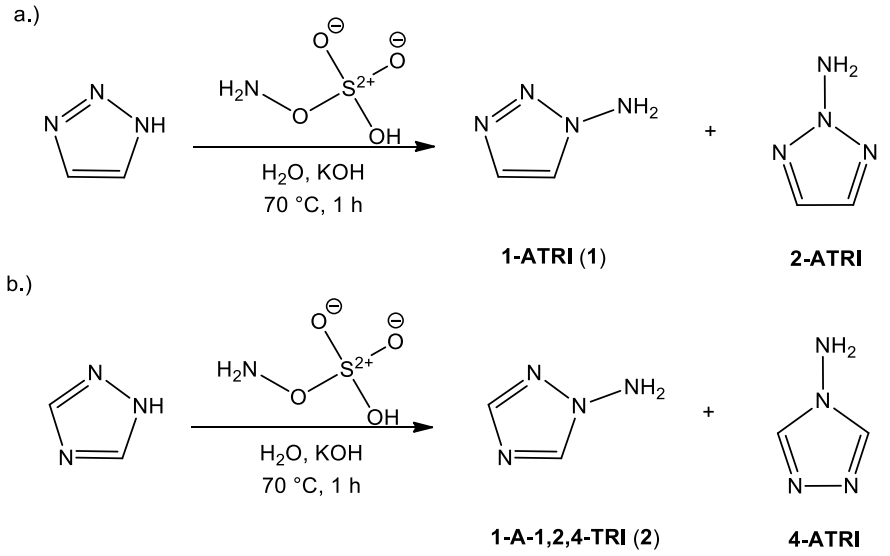


Scheme 2. a.) Synthesis of activated manganese dioxide; b.) Proposed mechanism for the formation of 1-ATRI.

The ability of activated MnO_2 to perform the discussed oxidation turned out to be highly dependent on the time frame between its precipitation and its application during this reaction. Already four days after the preparation, this mild oxidation agent was unable to promote the cyclization of 1-ATRI in reasonable yields. Moreover, the excess of the oxidizing MnO_2 partially leads to further oxidation of two equivalents of **1** to the associated azo compound. Due to major contamination of the reaction product and its high viscosity, a proper crystallization of compound **1** at low temperatures turned out to be rather challenging. The crystallized solids were constantly enclosed by the remaining viscous oil, which could not be separated through filtration. Since 1-A-1,2,3-TRI (**1**) turned out to be low-melting, Sublimation of the obtained reaction product at 80 °C proved to be the most convenient way to purify the synthesized compound. The triazole could be isolated in form of colorless crystals. To increase the reaction's yield (33 %), the variation of the reaction conditions regarding the molar ratio MnO_2/glyoxal bishydrazone, the reaction time and the temperature seems to be one important aspect. Whilst increasing temperature results in decreasing yields, a longer reaction time and higher molar ratios MnO_2/glyoxal bishydrazone lead to evermore of the desired product.[30]

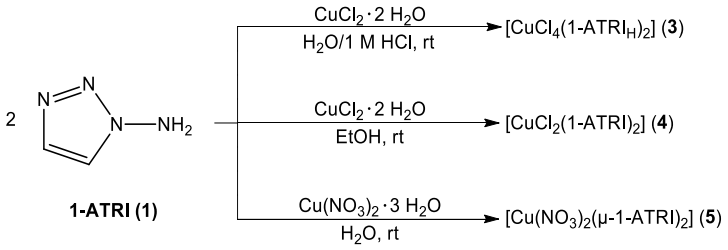
The second reaction pathway can be performed analogously for the preparation of 1-ATRI (**1**) and 1-A-1,2,4-TRI (**2**). During the reaction, the potassium triazolate generated in situ is treated with the common amination reagent hydroxylamine-*O*-sulfonic acid (HOSA) in water at a temperature of 70 °C in analogy to a standard literature procedure (Scheme 3).[32,33] The obtained isomeric mixture was then purified by column chromatography (EtOAc/EtOH 9:1) on

silica gel yielding 1-ATRI (19 %) and by vacuum sublimation (80 °C, 1.5 x 10^{-2} mbar) resulting in the isolation of 1-A-1,2,4-TRI with a yield of 31 %. Possible explanations for the relatively low yield are the formation of the isomeric mixture, the weak nucleophilic character of the starting material, the sensitivity of the amination reagent toward hydrolysis, and the sensibility to pH value fluctuations.



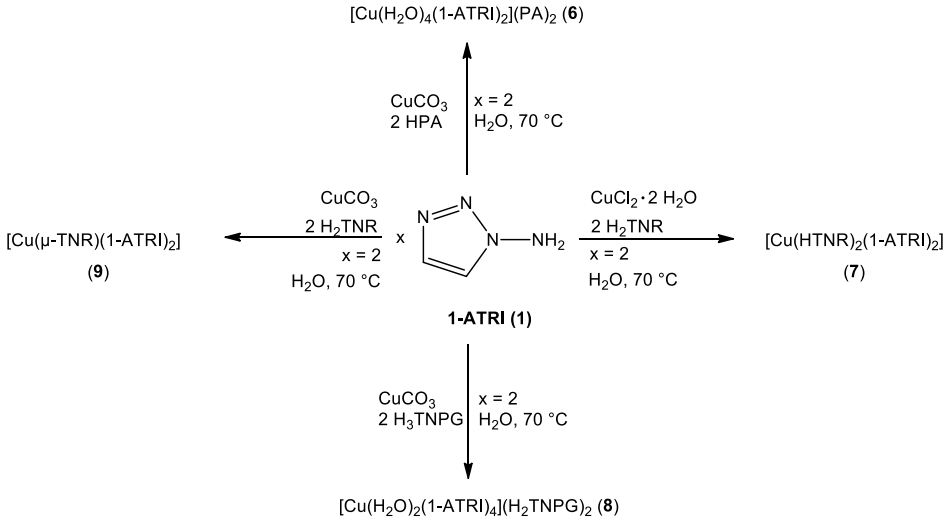
Scheme 3. Synthesis of a.) 1-ATRI (**1**) and b.) 1-A-1,2,4-TRI (**2**) through amination reaction of the corresponding triazoles.

Since a large number of complexes based on 4-aminotriazole have already been reported in the literature, this work aimed to increase the energy content of these coordination compounds further by utilizing 1-ATRI (**1**) as the ligand (Figure 2). Our concept to synthesize promising primary explosives includes the preparation of cationic or neutral complex units to assure the inclusion of anionic oxidizing agents (e.g. nitrate or perchlorate). This could be realized through blocking of the acidic triazole sites by the amino units as the functional groups. The synthesis of the complexes **3**–**5** and **10**–**14** (easy to differentiate by IR, Figure S1/S3) was carried out by mixing aqueous or ethanolic solutions of metal(II) salts and the ligand **1** in the respective stoichiometry at room temperature (Scheme 4/6). Immediately after the addition of all reactants during the synthesis of the copper(II) chloride complex, a green solid precipitated from the solution, most likely compound **4**, which was dissolved again through the addition of hydrochloric acid. Addition of the acid resulted in the isolation of the rare tetrachlorido triazolium species **3**.



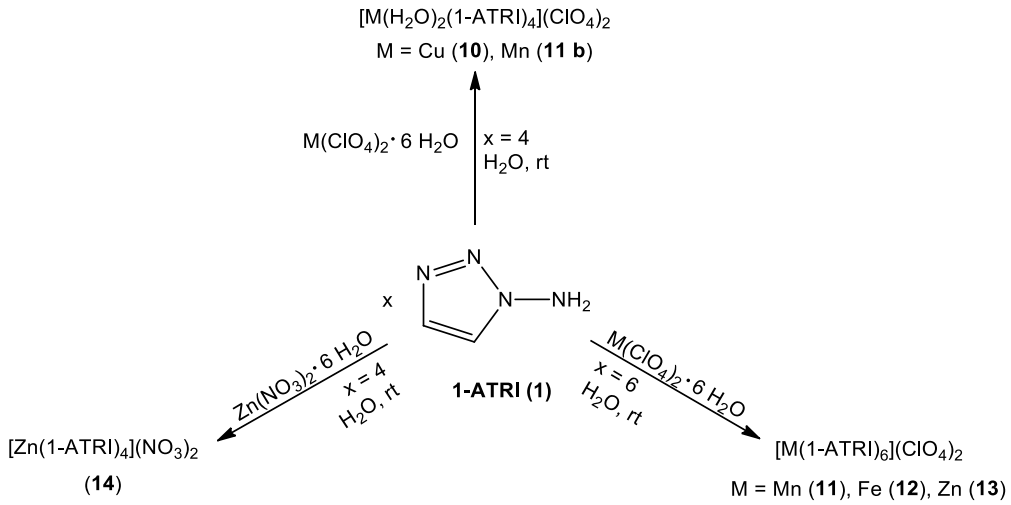
Scheme 4. Synthesis of the 1-ATRI based copper(II) complexes **3**–**5**.

The commercially unavailable metal(II) salt starting materials for the synthesis of the complexes **6**–**9** were prepared by simple acid-base or metathesis reactions in water and subsequently further reacted with the nitrogen-rich ligand **1** (Scheme 5). The reaction of styphnic acid with **1** and a copper(II) source (copper(II) chloride vs. copper(II) carbonate) is highly pH dependent and resulted either in the isolation of a complex with a single (**7**) or double deprotonated anion (**9**) (distinguishable by IR, Figure S2). Particular attention should be paid to compound **8**, which, to the best of our knowledge, is the first of its type since no copper(II) complexes with trinitrophloroglucinol based anions have been reported in the literature so far.



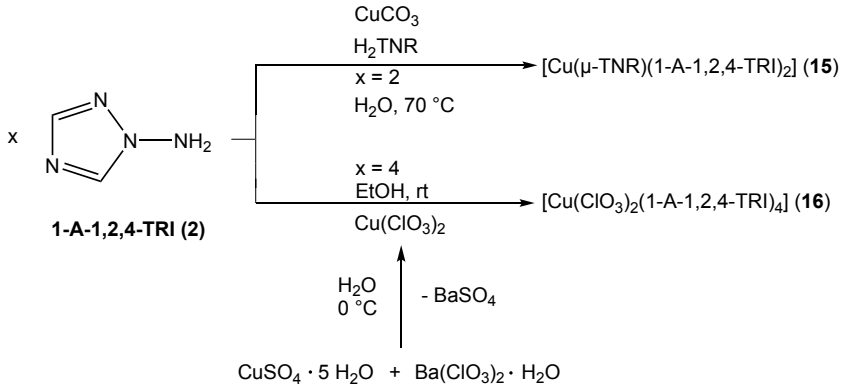
Scheme 5. Formation of the copper(II) 1-ATRI picrate (PA), 2,4,6-trinitro-3-hydroxyphenolate (HTNR), 2,4,6-trinitro-3,5-dihydroxyphenolate (H_2TNPG), styphnate (TNR) transition metal(II) complexes **6**–**9**.

The manganese(II) perchlorate complexes were highly sensitive to the stoichiometry applied and yielded either a four **11b** or six **11** folded 1-ATRI coordinated species. The synthesis of the copper(II) perchlorate **10** and zinc(II) nitrate **14** complexes, on the other hand, showed only fourfold coordinated complex compounds even when six equivalents are added (Scheme 6).



Scheme 6. Synthesis of complexes **10**–**14** with different metal(II) centers and anions.

For better comparison and classification of the complexes, the isomer 1-A-1,2,4-TRI (**2**) has also been investigated as a ligand. Therefore, selected complexes with copper(II) styphnate **15** and chlorate **16** have been prepared analogously to their related 1-ATRI homologs (Scheme 7).[22] Nevertheless, the attempted synthesis of a copper(II) perchlorate complex yielded, unfortunately, no unitary crystalline product.



Scheme 7. Preparation of the energetic coordination compound **15**/**16** based on 1-amino-1,2,4-triazole.

Although water was selected as the solvent to assure slow crystallization, the majority of the complexes crystallized (except **4**) in satisfying yields (23–91 %) without aqua ligands (except **6**, **8**, **10**) or inclusion of crystal water resulting in higher performance of the complexes. Therefore, only the water free complex **11** and not the diaqua species **11b** has been characterized. Using ethanol instead of water leads in most cases, due to the low solubility of the coordination compound, to precipitation of the desired products.

15.2.2 Crystal Structures

The crystal structure of 1-ATRI (**1**) is already described in the literature, whereas the one of 1A-1,2,4-TRI (**2**) is still unknown.[31] Therefore, single crystal X-ray diffraction studies of ligand **2** and all complexes, except compound **4**, were performed. Details on the crystal structures of compounds **6**, **11**, **11b**, **13**, **14**, and **15** are given in the SI together with the measurement and refinement data. The crystal structures were deposited to the CSD database[34] and can be obtained free of charge with the CCDC nos. 1847945 (**2**), 1847943 (**3**), 1847948 (**5**), 1847946 (**6**), 1847952 (**7**), 1847944 (**8**), 1847951 (**9**), 1847947 (**10**), 1847949 (**11**), 1847939 (**11b**), 1847941 (**12**), 1847950 (**13**), 1847942 (**14**), 1847940 (**15**), and 1848019 (**16**). Both ligands are coordinating with their heterocyclic nitrogen atoms to the central metals in all complexes. Additionally, the amino group of ligand **1** is coordinating in compound **5**. All central metals show an octahedral coordination sphere except for complex **14**, which is tetrahedrally coordinated.

Ligand **2** crystallizes in the form of colorless blocks in the monoclinic space group *P*2/*c* with eight formula units per unit cell and a calculated density of 1.420 g cm^{-3} at 150 K. All non-hydrogen atoms of 1-A-1,2,4-TRI lie within a plane which is confirmed by the torsion angles (C2–N2–N3–C1 0.5(2)°, N1–N2–C2–N4 178.0(2)° and C2–N4–C1–N3 0.2(3)°). The ligand shows comparable bond lengths as well as angles to those of 1-ATRI (Figure 3).[31]

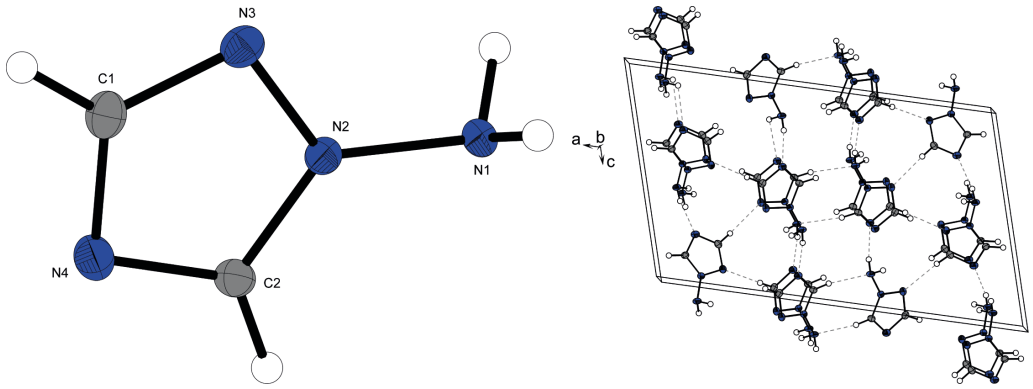


Figure 3. Molecular unit of 1A-1,2,4-TRI (**2**). Selected bond lengths (Å): N1–N2 1.400(3), N2–N3 1.365(3), N2–C2 1.322(3), N3–C1 1.317(3), N4–C1 1.356(3), N4–C2 1.328(3); selected bond angles (°): N1–N2–N3 123.17(18), N1–N2–C2 126.3(2), N3–N2–C2 110.47(19), N2–N3–C1 101.61(19), C1–N4–C2 102.43(19).

1-Amino-1,2,3-triazole (**1**) has been protonated during the synthesis of compound **3** under the applied acidic conditions. The resulting tetrachlorido copper(II) complex crystallizes in the

form of green blocks in the triclinic space group *P*−1 with one formula unit per unit cell and a calculated density of 2.038 g cm^{-3} at 173 K. Two asymmetric unit cells build up the molecular unit which consists of four chlorido ligands and two equivalents of 1-amino-1,2,3-triazolium forming an octahedral coordination sphere around the copper(II) center (Figure 4). As expected, the present d^9-copper(II) shows a strong Jahn-Teller distortion along the N2–Cu1–N2^i axis with the nitrogen-copper(II) bond lengths being impressively long. The remaining four coordination positions are occupied by four chlorido ligands forming a vertical plane that is not perpendicular to the mentioned N2–Cu1–N2^i axis.

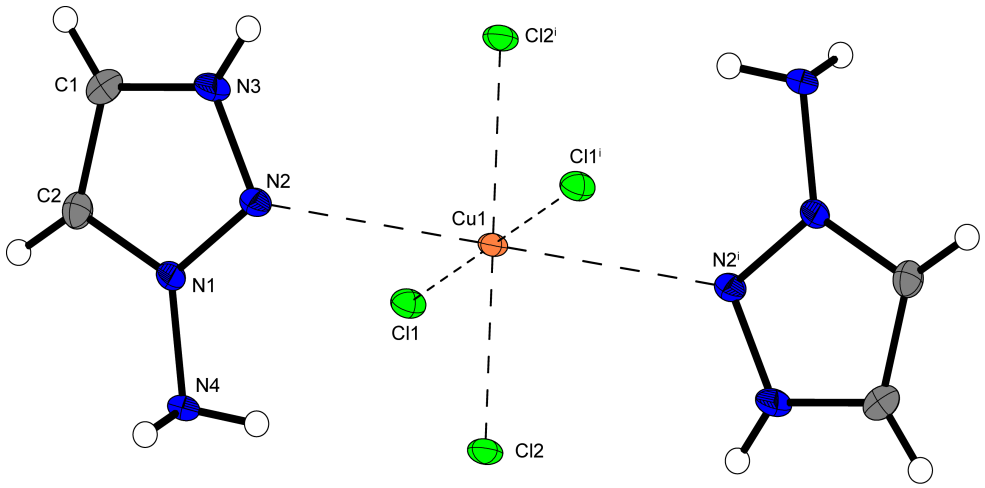


Figure 4. Molecular unit of [$CuCl_4$(1-$ATRI_H$)$_2$] (**3**). Selected bond lengths (Å): Cu1–N2 2.799(2),Cu1–Cl1 2.2835(7),Cu1–Cl2 2.2818(7); selected bond angles (°): Cl1–Cu1–N2 84.49(5), Cl2–Cu1–N2 91.62(5), Cl1–Cu1–Cl2 89.68(2). Symmetry code: (i) −x, 2−y, −z.

The nitrato complex **5** is the only compound with bridging 1-ATRI ligands. The nitrogen-rich molecules coordinate with the amino group as well as one heterocyclic nitrogen atom, leading to the formation of 2D-polymeric layers. The compound crystallizes in the form of blue stabs in the monoclinic space group *P*2$_1$/*n* with two formula units per unit cell and a calculated density of 2.165 g cm^{-3} at 173 K. This coordination compound consists of a copper(II) center with an octahedral coordination sphere including two Jahn-Teller distorted axial nitrato ligands along the O1–Cu1–O1^i axis (Figure 5). The four equatorial positions of the coordination polyhedron are occupied by ligand **1**, forming an ideal plane. While the bond angles between the equatorial ligands are almost 90° in each case, the axis built up by the nitrato anions runs obliquely through the N1^{iii}–N4–N1^{ii}– N4^i plane. A detailed description of the polymeric structure (Figure S5) and the hydrogen bonds (Table S5) is given in the SI.

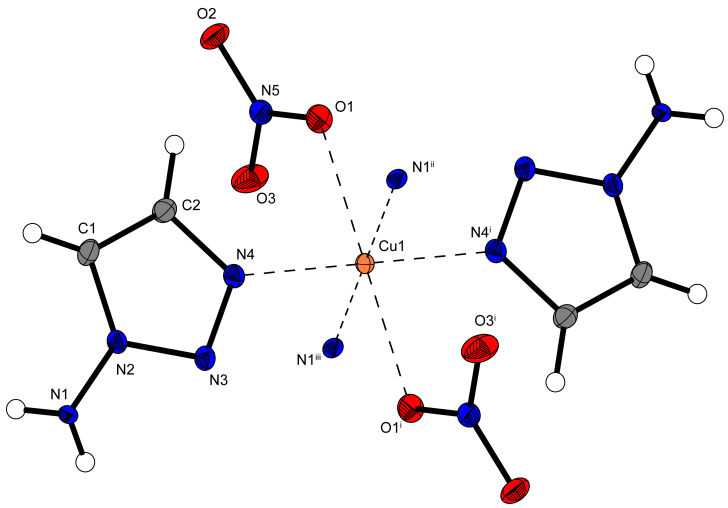
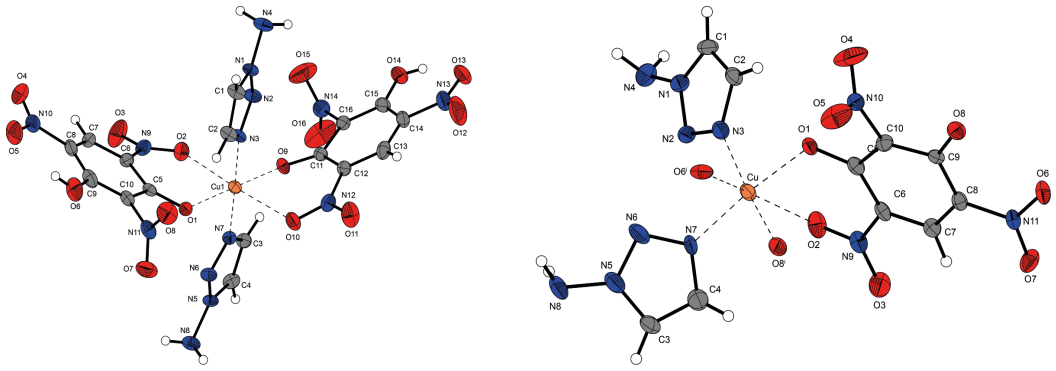


Figure 5. Coordination environment of $[Cu(NO_3)_2(\mu\text{-}1\text{-}ATRI)_2]$ (**5**). Selected bond lengths (Å): Cu1–O1 2.3738(16), Cu1–N4 1.9946(17), Cu1–N1^{ii} 2.092(3); selected bond angles (°): N1^{ii}–Cu1–N4 90.03(8), O1^{iii}–Cu1–N4 92.43(6), O1–Cu1–N1^{v} 93.58(7), O1–Cu1–N1^{ii} 86.42(7), O1–Cu1–N4 87.57(6). Symmetry codes: (i) −x, −y, −z; (ii) 1.5+x, 0.5−y, 1.5+z; (iii) −0.5−x, 0.5+y, −0.5−z; (iv) −0.5−x, −0.5+y, −0.5−z.

Depending on the starting material two different complexes of copper(II), ligand **1**, and single- or double-deprotonated trinitroresorcinate as counter-anion can be synthesized (Figure 6). 2,4,6-Trinitro-3-hydroxyphenolate causes the formation of closed octahedral coordination spheres (**7**), whereas the bridging styphnate as counter-anion builds up 1D-polymeric chains (**9**). Both compounds differ only slightly in their densities (1.842 g cm^{-3} (**7**) and 1.876 g cm^{-3} (**9**) at 173 K) and crystallize in similar space groups $P2_1$ and $P2_1/c$. Both complexes possess an octahedral coordination sphere with two equivalents of ligand **1** and deprotonated hydroxy groups in equatorial positions. The Jahn-Teller distortion along the axial coordination sites is formed by the oxygen atoms of two nitro groups. Given the fixed structures of the counter-anions, it becomes clear why the coordination polyhedrons of the investigated complexes are significantly distorted. The complexation of copper(II) styphnate with ligand **2** is analogous to compound **9**, and the crystal structure of the resulting complex **15** can be found in Figure S10.



7 9

Figure 6. Molecular unit of compound **7** (left) and copper(II) coordination environment of **9** (right). Selected bond lengths (Å): **7**: Cu1–O1 1.947(3), Cu1–O2 2.329(3), Cu1–N7 1.977(3); **9**: Cu1–O2 2.440(4), Cu1–O1 1.951(3), Cu1–N3 1.981(4), Cu1–N7 1.981(4); selected bond angles (°): **7**: O1–Cu1–O2 82.11(12), O9–Cu1–O10 78.55(12), O1–Cu1–N7 90.65(15), O2–Cu1–N7 87.00(13), O9–Cu1–N3 92.60(15), O10–Cu1–N3 88.29(13), O10–Cu1–N7 92.71(13), O1–Cu1–O9 178.54(13); **9**: O2–Cu1–O6^{ii} 161.56(13), O8^{ii}–Cu1–N3 173.16(17), O1–Cu1–O2 75.67(14), O6^{ii}–Cu1–O8^{ii} 79.21(14), O1–Cu1–N386.90(16), O2–Cu1–N7 99.20(15), O2–Cu1–O8^{ii} 84.09(14), O8^{ii}–Cu1–N7 88.37(17). Symmetry codes: **9**: (i) −x, 0.5+y, 0.5−z; (ii) −x, −0.5+y, 0.5−z.

Copper(II) complex **8** crystallizes in the form of green blocks in the triclinic space group *P*−1 with one formula unit per unit cell and a calculated density of 1.840 g cm^{-3} at 173 K. Compared to compounds **7** and **9** the counter-anion, 2,4,6-trinitro-3,5-dihydroxyphenolate, is not participating in the coordination sphere, which consists of four equatorial 1-ATRIs and two axial aqua ligands (Figure 7). Once again, the complex monomers show a Jahn-Teller distortion along the O1–Cu–O1^{i} axis.

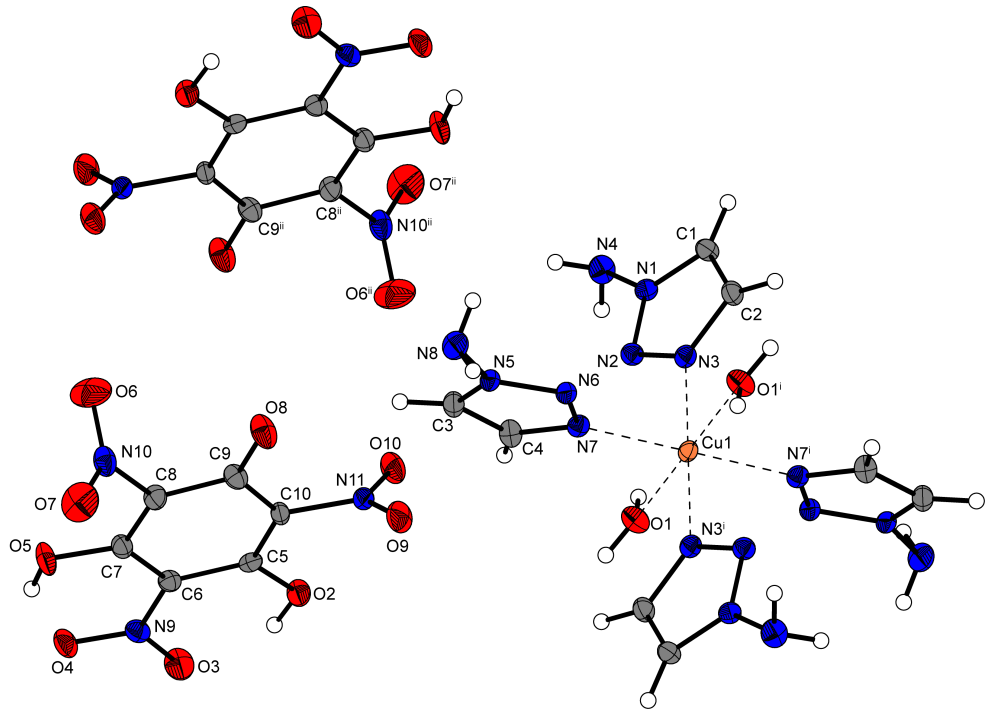
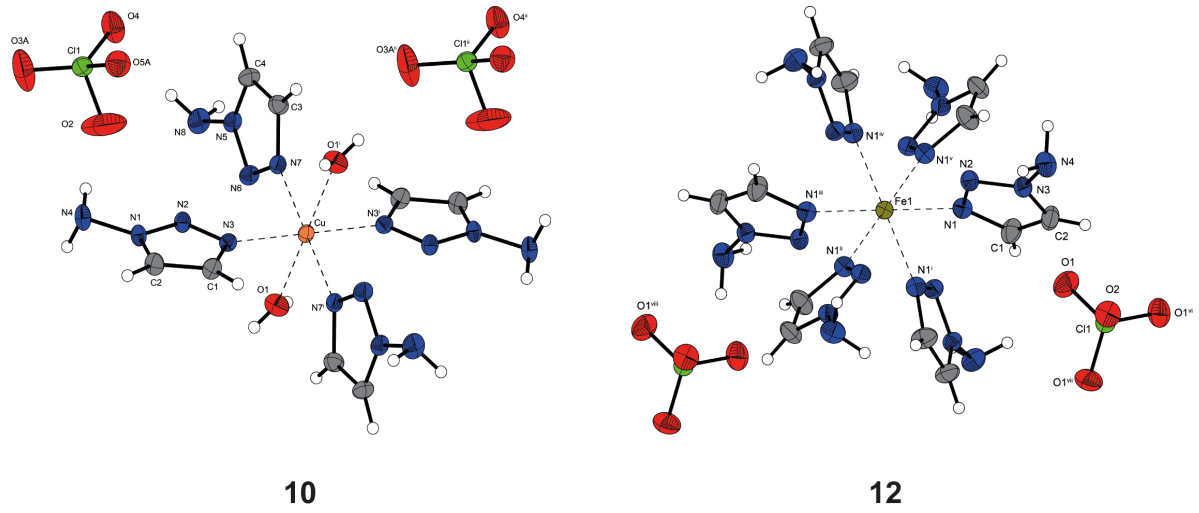


Figure 7. Molecular unit of compound **8**. Selected bond lengths (Å): **8**: Cu1–O1 2.3287(16), Cu1–N3 2.0051(17), Cu1–N7 2.0407(16); selected bond angles (°): O1–Cu1–N3 87.43(6), O1–Cu1–N7 88.49(6) N3–Cu1–N7 88.80(7). Symmetry codes: (i) 2−x, −y, −z; (ii) 2−x, 1−y, 1−z.

The perchlorate complexes of ligand **1** are forming two different species with transition metal(II) cations. They crystallize either as water-free hexakis- or as tetrakis(1-amino-1,2,3-triazole) compounds with two aqua ligands (Figure 8). Within both forms, the complexes are isotypic and exhibit similar cell dimensions. The dihydrates **10** and **11b** crystallize in the triclinic space group *P*−1 with one formula unit per unit cell and differ only slightly in their densities (Cu: 1.810 g cm^{-3} (173 K); Mn: 1.721 g cm^{-3} (173 K)). The octahedral coordination spheres consist of four equivalents of **1** and two axial water molecules. Also, the d^9-copper(II) in compound **10** shows a Jahn-Teller distortion along the O1–Cu1–O1^i axis, which causes significantly higher copper(II)-oxygen coordination distances in comparison with those of the respective copper(II)- and manganese(II)-nitrogen atoms. The equatorial positions of the coordination polyhedrons are forming an ideal plane. The water-free complexes **11**–**13** crystallize in the trigonal space group *R*−3 with three formula units per unit cell and similar densities (Mn: 1.673 g cm^{-3} (143 K); Fe: 1.697 g cm^{-3} (123 K); Zn: 1.740 g cm^{-3} (133 K)). The molecular units consist of six-fold coordinated central(II) metals and non-coordinating perchlorate counter-anions, whereas the octahedral coordination sphere is only slightly distorted.



10 **12**

Figure 8. Molecular units of compounds **10** (left) and **12** (right). Selected bond lengths (Å): **10**: Cu–O1 2.357(3), Cu–N3 2.020(2), Cu–N7 2.032(2); **12**: Fe1–N1 2.2011(17); selected bond angles (°): **10**: O1–Cu–N3 87.01(10), O1–Cu–N7 92.13(9), N3–Cu–N7 90.69(9), O1–Cu–N3^{i} 92.99(10); **12**: N1–Fe1–N^{ii} 92.86(8), N1–Fe1–N^{v} 87.14(17). Symmetry codes: **10**: (i) 2−x, −y, −z; **12**: (i) 0.67+x−y, 0.33+x, 0.33−z; (ii) 1−y, 1+x−y, z; (iii) 0.67−x, 1.33−y, 0.33−z; (iv) −x+y,1−x, z; (v) −0.33+y, 0.33−x+y,0.33−z; (vi) −y, −y, z; (vii) −x+y, −x, z; (viii) 1+x, +y, z.

The zinc(II) compound $[Zn(1\text{-}ATRI)_4](NO_3)_2$ (**14**) is the only tetrahedral complex (Figure 9). It crystallizes in the form of colorless blocks in the tetragonal space group $I4_1/a$ with four formula units per unit cell and a calculated density of 1.768 g cm^{-3} at 173 K. The complex is built up by four triazole ligands with N-Zn-N bond angles slightly differing from the perfect tetrahedral angle of 109.47° and non-coordinating counter-anions.

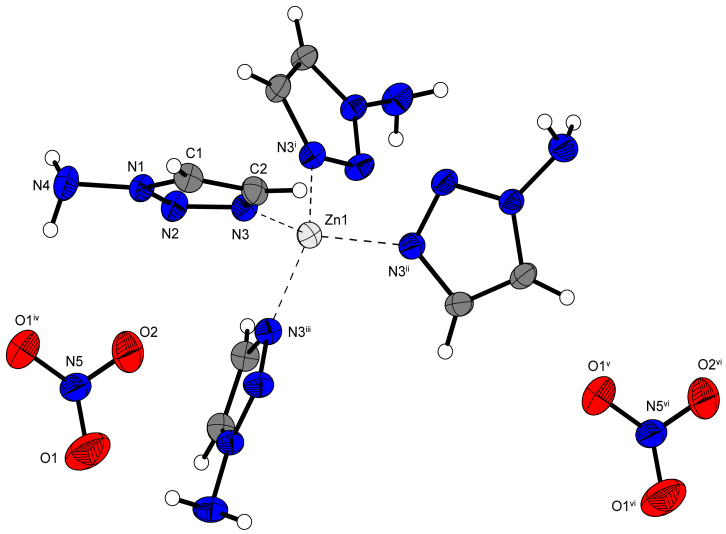


Figure 9. Molecular unit of the zinc(II) nitrate complex **14**. Selected bond length (Å): Zn1–N3 1.9879(17); selected bond angles (°): N3–Zn1–N3^{i} 112.25(7), N3–Zn1–N3^{ii} 104.06(7). Symmetry

codes: (i) 0.25–y, 0.25+x, 0.25–z; (ii) –0.25+y, 0.25–x, 0.25–z; (iii) –x, 0.5–y, z; (iv) –x, 0.5–y, z; (v) 0.5–x, –y, –0.5+z; (vi) 0.5+x, –0.5+y, –0.5+z.

In comparison to the perchlorate compounds **10**–**13** discussed so far, the chlorate counter-anions are coordinating to the copper(II) center in compound **16**. It crystallizes in the triclinic space group *P*−1 with one formula unit per unit cell and a calculated density of 1.888 g cm^{-3} at 143 K. The molecular unit of the complex, illustrated in Figure 10, is built up by two axial chlorato and four equatorial triazole ligands. The compound shows again a typical Jahn-Teller distortion along the O1–Cu1–O1^{i} axis.

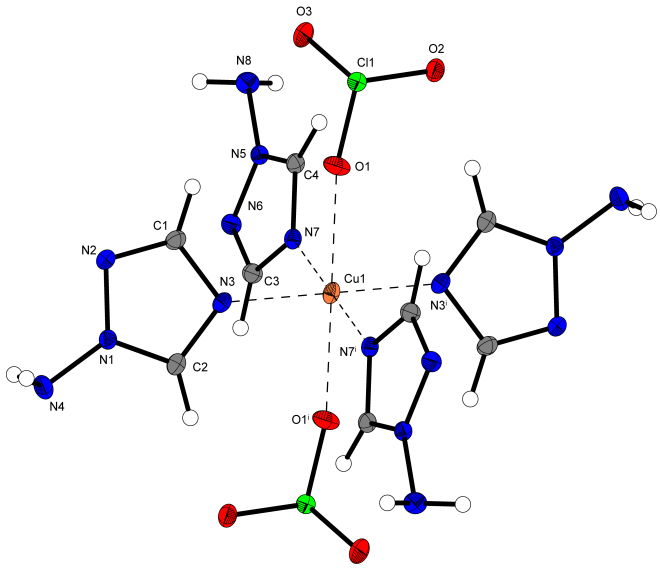


Figure 10. Complex unit of compound **16**. Selected bond lengths (Å): Cu1–O1 2.497(2), Cu1–N3 2.000(2), Cu1–N7 1.998(2); selected bond angles (°): O1–Cu1–N3 87.05(8), O1–Cu1–N7 91.58(8), N3–Cu1–N7 88.94(9). Symmetry code: (i) 2−x, −y, −z.

15.2.3 Scanning Electron Microscopy (SEM) and Energy Dispersive X-ray Spectroscopy (EDX)

For the determination of the compounds' morphology and chemical composition, scanning electron microscopy experiments in combination with energy-dispersive X-ray spectroscopy was performed. The results of the measurements, exemplarily conducted for compounds **10** and **12**, are shown in Figure 11 and 12. Also, the grain sizes and crystal habits were examined by microscope imaging (Figure S11–15), since both can strongly influence the compounds' sensitivity data.

Figure 11 confirms the plate-like crystal habitus of complex **10**. The plates can form up to 300 µm-sized blocks. No other elements, which are not included in the complex composition, can be observed in the EDX spectrum, which indicate the compound's purity.

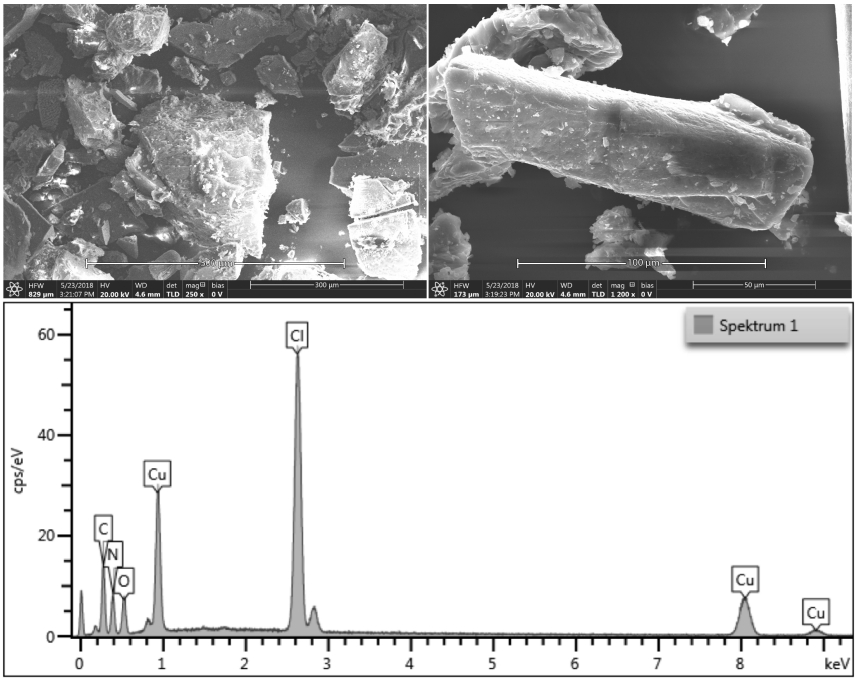


Figure 11. SEM images (250 x magnitude (left, scale 500 µm) and 1200 x magnitude (right, 100 µm)) and EDX spectrum of compound **10**.

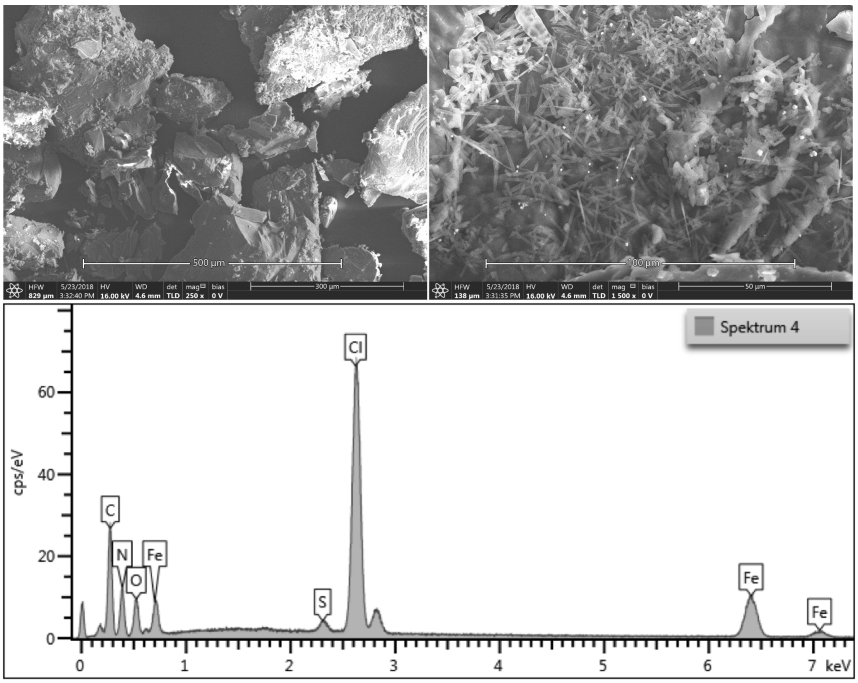


Figure 12. SEM images (250 x magnitude (left, scale 500 µm) and 1500 x magnitude (right, scale 100 µm)) and EDX spectrum of compound **12**.

The iron(II) perchlorate compound **12** forms up to 300 µm-sized blocks beside small needle-like crystals. Compared to complex **10**, higher contents of non-oxygen atoms can be observed which is consistent with the chemical compositions of the two coordination compounds. Besides insignificant trace amounts of sulfur, the EDX spectrum did not show any other atoms present in the complex.

15.2.4 Sensitivities and Thermal Stability

All compounds were investigated by differential thermal analysis (DTA) at a heating rate of $\beta = 5$ °C min^{-1}. The observed decomposition temperatures as well as endothermic events (melting, dehydration, or loss of coordinating 1-ATRI ligands) are listed in Table 1.

Table 1. Thermal stability measurements of 4-ATRI and **1**–**16** by DTA.

	$T_{endo1.}$ (°C)[a]	$T_{endo2.}$ (°C)[a]	$T_{exo.}$ (°C)[b]
1-ATRI (**1**)	39	267	267
1-A-1,2,4-TRI (**2**)	39	222	222
4-ATRI	80	—	261
$[CuCl_4(1\text{-}ATRI_H)_2]$ (**3**)	148	—	148
$[CuCl_2(1\text{-}ATRI)_2]$ (**4**)	165	—	165
$[Cu(NO_3)_2(\mu\text{-}1\text{-}ATRI)_2]$ (**5**)	—	—	167
$[Cu(H_2O)_4(1\text{-}ATRI)_2](PA)_2$ (**6**)	66	—	188
$[Cu(HTNR)_2(1\text{-}ATRI)_2]$ (**7**)	—	—	177
$[Cu(H_2O)_2(1\text{-}ATRI)_4](H_2TNPG)_2$ (**8**)	123	—	153
$[Cu(\mu\text{-}TNR)(1\text{-}ATRI)_2]$ (**9**)	—	—	194
$[Cu(H_2O)_2(1\text{-}ATRI)_4](ClO_4)_2$ (**10**)	—	—	167
$[Mn(1\text{-}ATRI)_6](ClO_4)_2$ (**11**)	161	—	194
$[Fe(1\text{-}ATRI)_6](ClO_4)_2$ (**12**)	—	—	166
$[Zn(1\text{-}ATRI)_6](ClO_4)_2$ (**13**)	91	—	188
$[Zn(1\text{-}ATRI)_4](NO_3)_2$ (**14**)	134	—	188
$[Cu(\mu\text{-}TNR)(1\text{-}A\text{-}1,2,4\text{-}TRI)_2]$ (**15**)	—	—	237
$[Cu(ClO_3)_2(1\text{-}A\text{-}1,2,4\text{-}TRI)_4]$ (**16**)	—	—	132

Onset temperatures at a heating rate of 5 ° C min^{-1}. [a] endothermic peak, which indicates melting, vaporization, dehydration or loss of coordinating 1-ATRI molecules; [b] exothermic peak, which indicates decomposition.

DTA plots of the compounds **1**–**9** and **14**–**16**, as well as additional information regarding the thermal stabilities, can be found in the Figures S17–19 in the Supporting Information. For a closer examination of the endothermic events, thermal gravimetric analysis (TGA) of both ligands as well as complexes **11**, **13**, and **14**, were performed (Figure 13 and S16). Compounds **1** and **2** both possess melting points at 39 °C and the TGA measurements reveal constant evaporation of the ligands till their exothermic decomposition temperatures at 267 and 222 °C, respectively. Compared to 4-amino-1,2,4-triazole (4-ATRI), the two ligands show lower melting points, but 1-ATRI is slightly more thermally stable. Both zinc(II) complexes show endothermic events in the DTA. The nitrate compound **14** shows the evaporation of two ligands

during the TGA experiment (Figure 13) before it decomposes, whereas the perchlorate complex **13** shows no loss of mass, proving its thermal stability and indicating a melting point at 134 °C (Figure S16). In similarity to **14**, compound **11** equally exhibits the loss of one ligand before its thermal decomposition. The endothermic events of the aqua complexes **6** and **8** indicate the formation of stable water-free compounds during heating, whereas in diaqua complex **10**, the water molecules are necessary for the crystal structure's stability.

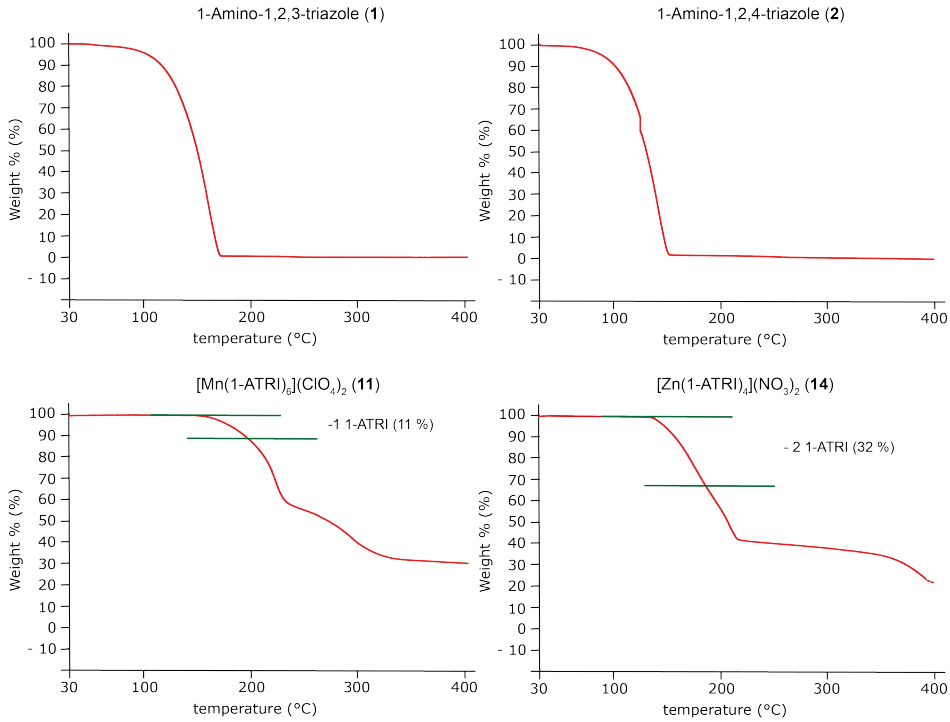


Figure 13. TGA measurements of the free ligands **1** and **2** as well as the selected complexes **11** and **14** at a heating rate of 5 °C min^{-1}.

Except **15**, all of the investigated compounds show exothermic decomposition events lower than the uncoordinated ligands. But still, most of the compounds (except **3**, **8**, and **16**) show excellent exothermic thermal decomposition temperatures between 165 (**4**) and 237 °C (**15**). The very good thermal stabilities of **9** and **15** can be explained by the formation of polymeric structures, whereas the exceptional low thermal stability of chlorate complex **16** is consistent with our former observations for the copper(II) chlorate complex with 1-ATRI as ligand ($[Cu(ClO_3)_2(1\text{-ATRI})_4]$).[22]

The perchlorate based metal(II) complexes **10**–**13** possess relatively high thermal stabilities (Figure 14), which increase in the following order Fe^{II} ($T_{exo.}$ = 166 °C) ≈ Cu^{II} ($T_{exo.}$ = 167 °C) < Zn^{II} ($T_{exo.}$ = 188 °C) < Mn^{II} ($T_{exo.}$ = 194 °C). Analogical complexes with 1-methyl-5*H*-

tetrazole or trend, which could be a useful indicator for the design of future energetic complexes with high-temperature stability.[35] Compared to the copper(II) perchlorate complex of 4-ATRI with a decomposition temperature of 250 °C,[36] it becomes clear that the formation of closed octahedral coordination spheres with the absence of polymeric structures leads to a significant decrease in temperature stability. Interestingly, the nitrate complexes **5** and **14**, which show usually lower thermal stabilities exhibit the same decomposition temperatures as the analogous perchlorate ones.[36]

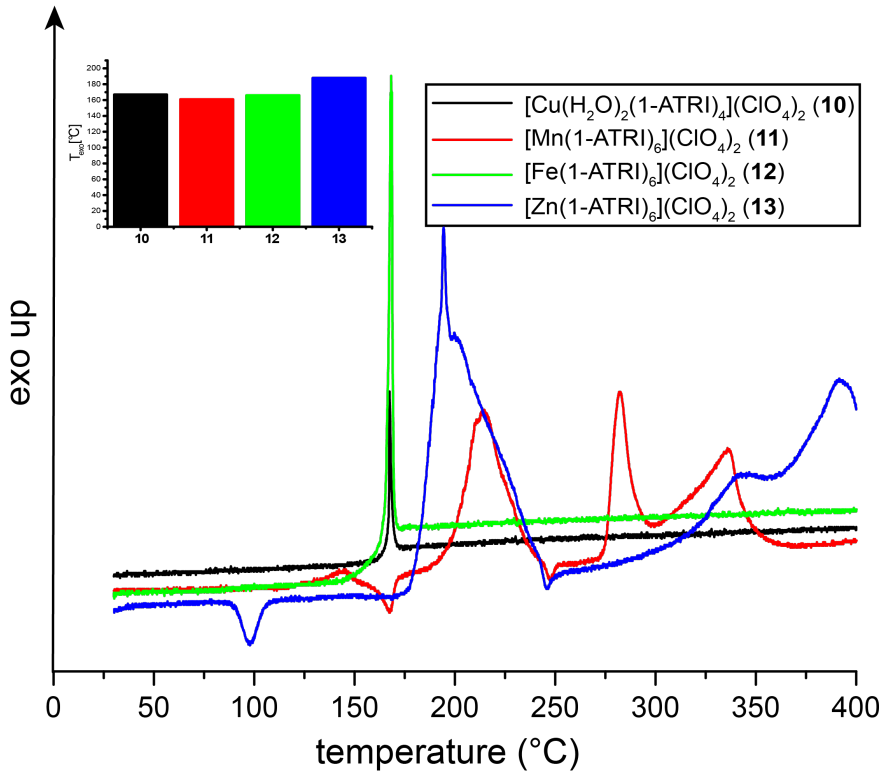


Figure 14. DTA plot (5 °C min^{-1}) comparison of the perchlorate compounds **10**–**13**.

The sensitivities toward impact and friction were explored according to BAM standard methods (1 of 6). Additionally, the electrostatic discharge sensitivities were determined and received data categorized in accordance with the "UN Recommendations on the Transport of Dangerous Goods". An overview of the sensitivities can be found in Table 3.

Table 3. Sensitivities toward impact, friction and ESD of **1**–**16**.

compound	*IS* (J)[a]	*FS* (N)[b]	*ESD* (J)[c]
1	35	> 360	1.50
2	> 40	> 360	1.50
3	35	216	1.40
4	> 40	> 360	0.70
5	< 1	30	0.10
6	> 40	> 360	1.22

7	1.5	80	0.04
8	2	160	0.30
9	3	60	0.05
10	1	0.45	0.10
11	3	10	0.06
12	1.5	2	0.04
13	3	6.75	0.07
14	6	45	0.70
15	30	240	0.09
16	< 1	23	0.01

Determined at a grain size of 100–500 µm except **4**, **6**, **7**, **10**, and **16** (**4**, **16**: > 100 µm; **6**, **7**, **10**: 500–1000 µm). [a] Impact sensitivity according to the BAM drophammer (method 1 of 6); [b] friction sensitivity according to the BAM friction tester (method 1 of 6); [c] electrostatic discharge sensitivity (OZM ESD tester); Impact: insensitive > 40 J, less sensitive ≥ 35 J, sensitive ≥ 4 J, very sensitive ≤ 3 J; Friction: insensitive > 360 N, less sensitive = 360 N, sensitive < 360 N and > 80 N, very sensitive ≤ 80 N, extremely sensitive ≤ 10 N. As per the UN Recommendations on the Transport of Dangerous Goods.

The free ligand **2** as well as dichlorido compound **4** and picrate complex **6** can be considered as "insensitive" toward impact and friction, whereas ligand **1** is "less sensitive" toward impact. Compared to complex **4**, tetrachlorido compound **3** is slightly less stable. The perchlorate compounds are "extremely sensitive" to both impact and friction, while the copper(II) nitrato and chlorate complexes show the lowest stability toward impact, they are only "very sensitive" toward friction. The implementation of less oxidizing anions such as styphnate or 2,4,6-trinitro-3,5-dihydroxyphenolate leads to stabilization of the complexes toward applied friction and impact stimuli (Figure S21). Comparing complexes with (nitrate) and without (chloride) oxidizing-anions reveals the destabilization while enhancing the performance of the nitrate complexes (Figure S20). The stability of the perchlorate complexes toward friction and impact rises in the following order $Cu^{2+} < Fe^{2+} < Zn^{2+} \leq Mn^{2+}$ (Figure 15).

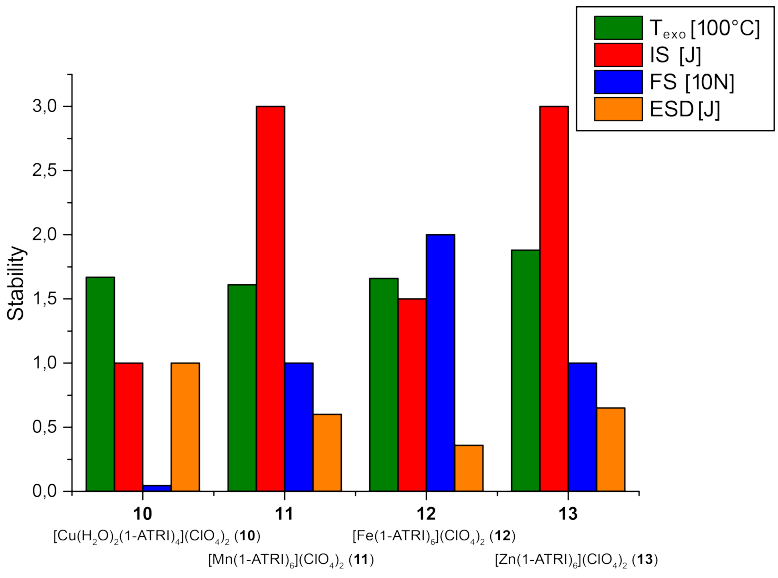


Figure 15. Stabilities of the perchlorate coordination compounds **10**–**13**.

The most promising compounds **6**, **10**–**13**, and **16** were tested in ball drop impact experiments (Figure 16) to gain a better insight into the behaviour against external stimuli. The measured sensitivities (Figure 17) of the perchlorate complexes toward ball drop impact, summarized in Table 4, are consistent with the values observed for drophammer impact and friction (although unfortunately) no explanation can be given for the high stability of **11**.

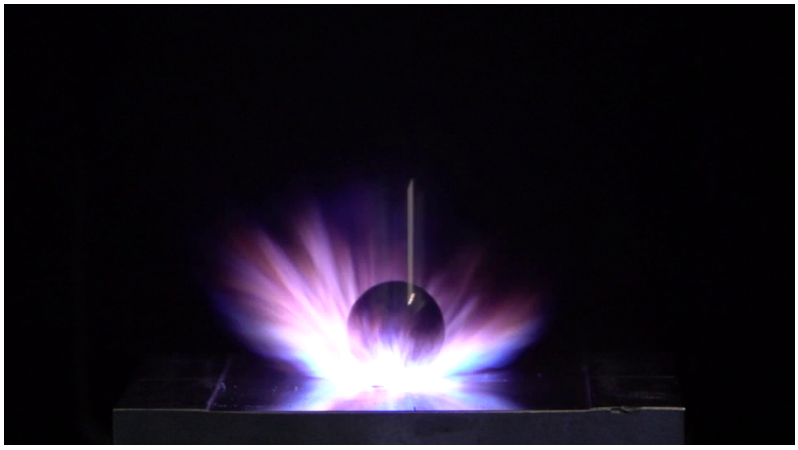


Figure 16. Moment of detonation of complex **10**.

Table 4. Ball drop impact sensitivities for **6**, **10**–**13**, and **16**.[a]

	6	**10**	**11**	**12**	**13**	**16**
***BDIS* (mJ)**	66	< 4	> 100	29	53	8

[a] ball drop impact sensitivity determined with the OZM ball drop tester applying the 1 of 6 method in accordance with the MIL-STD 1751A (method 1016). For the testing a 30 mg sample size, a drop weight of a 0.500-inch diameter steel ball (m = 8.35 g) and a steel ball guidance track, which rose 32-inches vertically from a steel base were used.

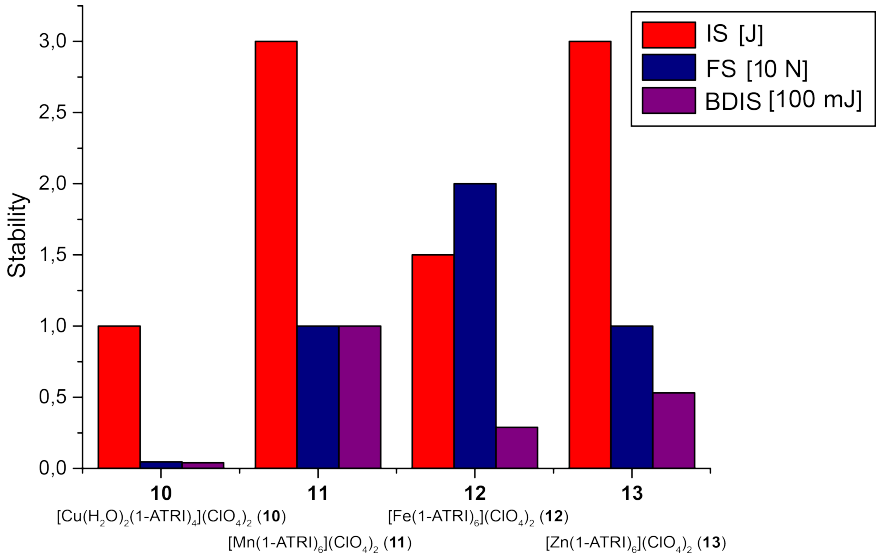


Figure 17. Comparison of the impact (drophammer) and friction sensitivities with the ball drop impact sensitivities of the metal(II) perchlorate complexes **10**–**13**.

To get an initial indication of the suitability of the most promising complexes (**5**, **10**–**14**, and **16**) as primary explosives and their behaviour toward rapid heating, hot plate and hot needle tests were carried out (Figure 18, 19 and Figure S22–32). An overview of the experimental results is compiled in Table 5. All investigated compounds showed sharp deflagrations during the tests except for the powerful compound **10**, which detonated during the hot needle test and deformed the used needle (Figure 18).

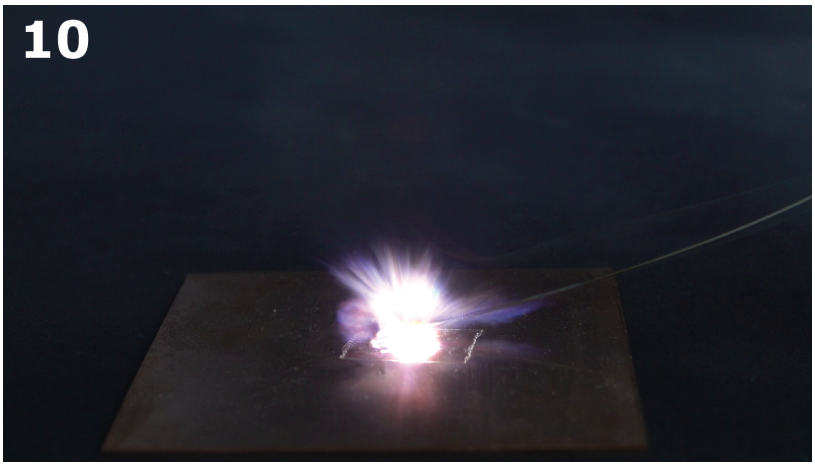


Figure 18. Moment of detonation of copper(II) complex **10** during the hot needle (HN) test (right: deformed needle).



Figure 19. Deflagration of coordination compound **10** during the hot plate (HP) test shown in sequence.

Table 5. Summary of the hot plate and hot needle test results for **5**, **10**–**14**, and **16**.[a]

compound	HP	HN	compound	HP	HN
5	def.	def.	**13**	def.	def.
10	def.	det.	**14**	def.	def.
11	def.	def.	**16**	def.	def.
12	def.	def.			

[a] def.: deflagration; det.: detonation.

After performing the hot plate and hot needle tests, the initiation capability of the complexes toward nitropenta (PETN) as the main charge in copper shells was investigated. Further

information on the test setup can be found in the General Methods of the Supporting Information.

A positive test indicated by a hole in the copper witness plate and fragmentation of the shell caused by a deflagration-to-detonation transition (DDT) of the secondary explosive PETN was only observed for the very promising complexes **10** and **13** (Figure 20).

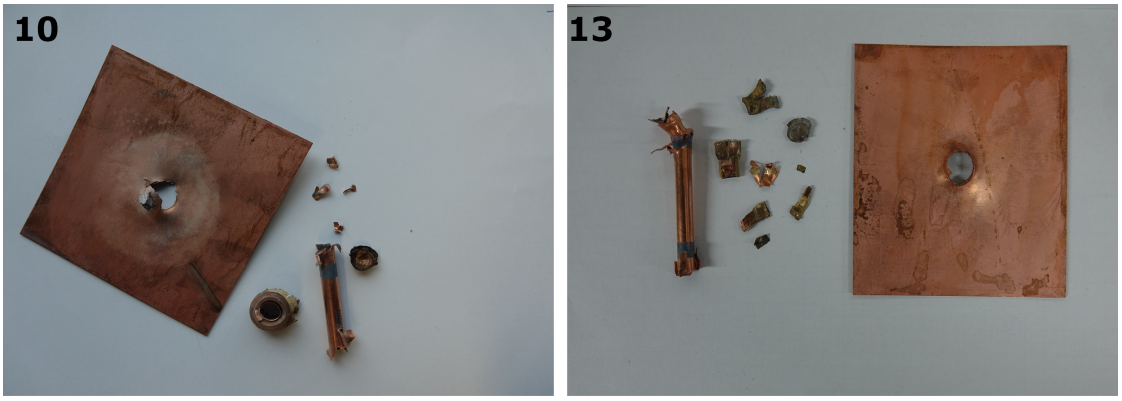


Figure 20. Positive nitropenta (PETN) initiation tests for the metal(II) perchlorate complexes **10** and **13**.

A negative test, represented by an undamaged copper plate and shell, was obtained for the other tested compounds (**5**, **11**, **12**, **14**, and **16**).

15.2.5 Toxicity

The toxicity toward aquatic organisms of the nitrogen-rich triazole **1** was determined using the known luminescence marine bacterium *Vibrio fischeri* NRRL-B-1177 strain in order to predict the possible toxicological impact of the appropriate coordination compounds.[37] With a value of 3.11 g L^{-1} for the half maximal effective concentration EC_{50} after 30 min, the compound can practically be considered as non-toxic (toxicity level after 30 min incubation: very toxic < 0.10 g L^{-1}; toxic 0.10–1.00 g L^{-1}; non-toxic > 1.00 g L^{-1}).[38]

15.2.6 Laser Initiation

Energetic materials can be ignited by a variety of different initiation methods (mechanical, heat, electrical, etc.). In particular, the initiation by optical means such as laser has drawn more and more attention in recent years.[13,20] Most of the ignition mechanisms currently in use are still

carried out by traditional techniques due to their great simplicity. Nevertheless, more and more applications based on optical initiation are coming onto the market, as this method has some advantages over conventional methods.[18,39] Since a photothermal and not a photochemical mechanism can be assumed, only selected colored compounds were tested. The behavior toward laser irradiation correlates to a large extent with the observed sensitivities and is entirely different depending on the metal, ligand and anion combination which allows precise tailoring of the compounds to the requirements in future systems. Decompositions could be observed for the complexes **6**–**9**, deflagrations for **5**, **15**, and **16** and detonations for the metal(II) perchlorate compounds **10** and **12** (Figure 21 and S33). The complexes could all be ignited with the low energies applied, which underlines the great suitability of these compounds. A detailed overview of the results is given in Table 6. Further details on sample preparation and experimental setup can be found in the Supporting Information.

Table 6. Laser ignition tests.

compound	reaction	compound	reaction
5	def.	**10**	det.
6	dec.	**12**	det.
7	dec.	**15**	def.
8	dec.	**16**	def.
9	dec.		

(dec.: decomposition, def.: deflagration, det.: detonation). Operating parameters: current I = 7 A; voltage U = 4 V; theoretical maximal output power P_{max} = 45 W; theoretical energy E_{max} = 0.17 mJ; wavelength λ = 915 nm; pulse length τ = 0.1 ms.

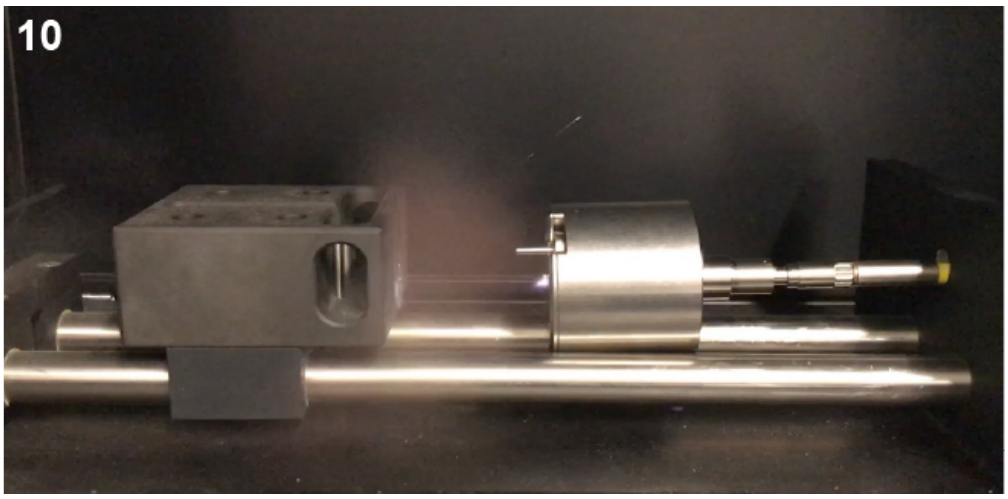


Figure 21. Moment of detonation of coordination compound **10**.

15.2.7 UV-Vis Spectroscopy

Solid-state UV-Vis spectra of the laser-ignitable compounds were recorded in the range of 350–1000 nm to investigate a possible correlation between absorption and laser ignitability (Figure 22). The measured optical properties of the compounds are summarized in Table 7. The investigated compounds have characteristic absorptions in the NIR, visible and UV range resulting from the typical d-d transitions, which are strongly dependent on the coordination sphere and the respective inserted metal, anion and ligand.

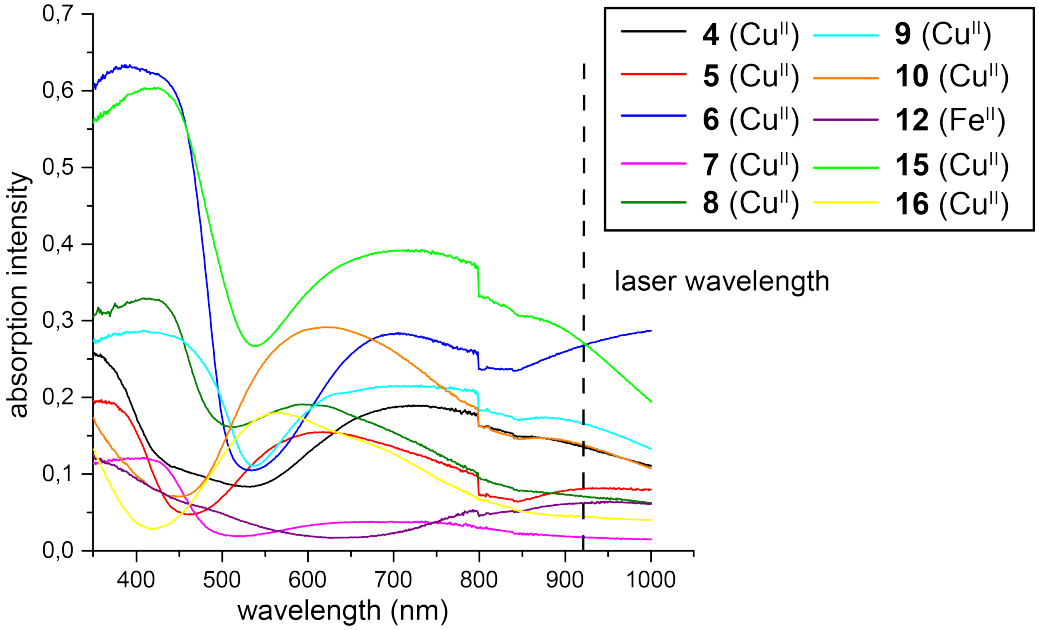


Figure 22. UV-Vis spectra in the solid state of selected complexes.

Table 7. Optical properties of **4**–**10**, **12**, **15** and **36**.

compound	M	color	$\lambda_{d\text{-}d}$[a]	$\lambda_{915}/\lambda_{d\text{-}d}$[b]
4	Cu^{II}	green	737	0.72
5	Cu^{II}	blue	617	0.52
6	Cu^{II}	green	393[c], 708	0.94
7	Cu^{II}	green	408[c], 737	0.47
8	Cu^{II}	green	408[c], 595	0.38
9	Cu^{II}	green	408[c], 711	0.78
10	Cu^{II}	blue	618	0.48
12	Fe^{II}	colorless	950	0.97
15	Cu^{II}	green	410[c], 732	0.70
16	Cu^{II}	violet	565	0.25

[a] absorption intensity maximum wavelength, which can be assigned to electron d-d excitations in the measured range of 350–1000 nm; [b] quotient of the absorption intensity at the laser wavelength and the intensity at the d-d absorption wavelength; [c] n–π^* transitions.

The exact mechanism remains still unclear.[40] However, it is assumed that compounds with increased absorption in the laser wavelength range generate photothermally induced hot spots

and are therefore rather laser-ignitable. Nevertheless, further mechanistic studies are needed to fully understand the mechanism. Additional strong absorption bands n–π^* in the UV up to the visible blue range could be observed for the copper(II) complexes **6**–**9** and **15** which can most likely be derived from the trinitrobenzene anions.

15.3 Conclusions

The two *N*1-substituted aminotriazoles 1-amino-1,2,3-triazole (**1**, 1-ATRI) and 1-amino-1,2,4-triazole (**2**, 1-A-1,2,4-TRI) could be prepared by a simple one-step synthesis starting from the respective triazoles (1,2,3- or 1,2,4-triazole) and the conventional amination reagent hydroxylamine-*O*-sulfonic acid (HOSA). The resulting isomeric mixtures were then purified by simple column chromatography or vacuum sublimation and yielded the desired products in satisfying yields. Due to the enormous potential of 1-ATRI as a ligand and its high energetic coordination compounds, an upscalable, cheap and isomerically pure two-step synthesis was elaborated. The ligands 1-ATRI and 1-A-1,2,4-TRI were extensively characterized by multinuclear NMR spectroscopy and partly by X-ray diffraction and toxicity determinations. The toxicological investigation of 1-ATRI showed the non-toxic character toward aquatic organisms. After a multitude of 4-ATRI complexes are known in the literature, the overall goal of this work was to further increase the energy content by implementing more endothermic ligands and thus produce useful new lead-free primary explosives. The present work deals with the synthesis, characterization and evaluation of 14 new complexes composed of two isomeric aminotriazoles, four metals (Mn, Fe, Cu and Zn) and seven different anions. The complexes with a very interesting variety of coordination spheres can be synthesized by an upscalable and cost-effective route. The concept of energetic coordination compounds (ECC) which allows fine tuning by varying individual components has once again revealed its great potential in addressing the problems of lead-free primary explosives and laser ignition. X-ray studies in combination with SEM and microscope images of the most promising complexes provided fascinating insights and allowed correlations between the structure and the observed sensitivities. The majority of the synthesized complexes could be laser-ignited and showed different reactions which could be well associated with the measured sensitivities. Positive initiation capability tests ($[Cu(H_2O)_2(1\text{-}ATRI)_4](ClO_4)_2$ and $[Zn(1\text{-}ATRI)_6](ClO_4)_2$) with PETN

loaded copper tube detonators underlined the enormous potential of single complexes as lead-free primary explosive alternatives.

Supporting information available in the appendix in **Chapter 19.12**.

15.4 References

[1] T. M. Klapötke, *Chemistry of High-Energy Materials*, 3nd ed., Walter de Gruyter, Berlin/Boston, **2015**.

[2] E. C. Johnson, J. J. Sabatini, D. E. Chavez, R. C. Sausa, E. F. C. Byrd, L. A. Wingard, P. E. Guzman, *Org. Process Res. Dev.* **2018**, *22*, 736–740.

[3] Y. Tang, C. He, G. H. Imler, D. A. Parrish, J. n. M. Shreeve, *J. Mater. Chem. A* **2018**, *6*, 5136–5142.

[4] G. Belanger-Chabot, S. M. Kaplan, P. Deokar, N. Szimhardt, R. Haiges, K. O. Christe, *Chem. - Eur. J.* **2017**, *23*, 13087–13099.

[5] D. Chen, H. Yang, Z. Yi, H. Xiong, L. Zhang, S. Zhu, G. Cheng, *Angew. Chem. Int. Ed.* **2018**, *57*, 2081–2084.

[6] J. W. Fronabarger, M. D. Williams, W. B. Sanborn, J. G. Bragg, D. A. Parrish, M. Bichay, *Propellants, Explos., Pyrotech.* **2011**, *36*, 541–550.

[7] D. Fischer, T. M. Klapötke, J. Stierstorfer, N. Szimhardt, *Chem. Eur. J.* **2016**, *22*, 4966–4970.

[8] https://echa.europa.eu/de/regulations/reach/understanding-reach, Accessed June 2018.

[9] Q. Zhang, J. n. M. Shreeve, *Angew. Chem., Int. Ed.* **2014**, *53*, 2540–2542.

[10] K. A. McDonald, S. Seth, A. J. Matzger, *Cryst. Growth Des.* **2015**, *15*, 5963–5972.

[11] J.-G. Xu, C. Sun, M.-J. Zhang, B.-W. Liu, X.-Z. Li, J. Lu, S.-H. Wang, F.-K. Zheng, G.-C. Guo, *Chem. Mater.* **2017**, *29*, 9725–9733.

[12] M. Joas, T. M. Klapötke, J. Stierstorfer, N. Szimhardt, *Chem. Eur. J.* **2013**, *19*, 9995–10003.

[13] T. W. Myers, J. A. Bjorgaard, K. E. Brown, D. E. Chavez, S. K. Hanson, R. J. Scharff, S. Tretiak, J. M. Veauthier, *J. Am. Chem. Soc.* **2016**, *138*, 4685–4692.

[14] W. Shan, W. Qianyou, F. Xiao, W. Bo, Y. Li, *Advanced Materials* **2017**, *29*, 1701898.

[15] N. Szimhardt, J. Stierstorfer; *Chem. Eur. J.* **2018**, *24*, 2687–2698.

[16] A. Y. Zhilin, M. A. Ilyushin, I. V. Tselinskii, A. S. Kozlov, I. S. Lisker, *Russ. J. Appl. Chem.* **2003**, *76*, 572–576.

[17] Y.-h. Zhu, D.-l. Sheng, B. Yang, L.-k. Chen, F.-e. Ma, *Hanneng Cailiao* **2009**, *17*, 169–172.

[18] R. Schirra, H. Zöllner, *Proceedings of the 42nd International Pyrotechnics Seminar*, Grand Junction, CO, July 10–15, 2016 **2016**, 422–428.

[19] M. H. V. Huynh, M. D. Coburn, T. J. Meyer, M. Wetzler, *Proceedings of the National Academy of Sciences* **2006**, *103*, 10322–10327.

[20] M. A. Ilyushin, I. V. Tselinsky, I. V. Shugalei, *Cent. Eur. J. Energ. Mater.* **2012**, *9*, 293–327.

[21] T. W. Myers, K. E. Brown, D. E. Chavez, R. J. Scharff, J. M. Veauthier, *Eur. J. Inorg. Chem.* **2016**, *2016*, 3178–3183.

[22] M. H. H. Wurzenberger, N. Szimhardt, J. Stierstorfer, *J. Am. Chem. Soc.* **2018**, *140*, 3206–3209.

[23] O. Kahn, C. J. Martinez, *Science* **1998**, *279*, 44–48.

[24] M. A. Ilyushin, M. A. Aleksandrova, I. V. Bachurina, A. V. Smirnov, I. V. Tselinskii, *Russ. J. Appl. Chem.* **2010**, *83*, 92–96.

[25] S. Cudzilo, M. Nita, *J. Hazard. Mater.* **2010**, *177*, 146–149.

[26] S. Hauptmann, H. Wilde, K. Moser, *Tetrahedron Lett.* **1967**, 3295–3297.

[27] J. De Mendoza, M. L. Castellanos, J. P. Fayet, M. C. Vertut, J. Elguero, *J. Chem. Res., Synop.* **1980**, 50–51.

[28] F. Grande, A. Brizzi, A. Garofalo, F. Aiello, *Tetrahedron* **2013**, *69*, 9951.

[29] F. Aiello, A. Garofalo, F. Grande, *Tetrahedron* **2010**, *66*, 274.

[30] K. Shigeno, T. Ono, M. Tanaka, S. Yamada, T. Asao, *EP0727418B1* **1999**.

[31] G. Kaplan, G. Drake, K. Tollison, L. Hall, T. Hawkins, *J. Heterocyclic Chem.* **2005**, *42*, 19–27.

[32] H-X. Hu, H-X Niu, Y. Wang, Y-C. Li, S-P. Pang, *Mater. Res. Innovations* **2014**, *18*, 1127–1131.

[33] G. Laus, W. Kloetzer, *Synthesis* **1989**, 269–272.

[34] Crystallographic data for the structures have been deposited with the Cambridge Crystallographic Data Centre. Copies of the data can be obtained free of charge on application to The Director, CCDC, 12 Union Road, Cambridge CB2 1EZ, UK (Fax: int.code_(1223)336-033; e-mail for inquiry: fileserv@ccdc.cam.ac.uk; e-mail for deposition: (deposit@ccdc.cam.ac.uk).

[35] N. Szimhardt, M. H. H. Wurzenberger, A. Beringer, L. J. Daumann, J. Stierstorfer, *J. Mater. Chem. A* **2017**, *5*, 23753–23765.

[36] S. Cudziło, M. J. Nita, *Hazard. Mater.* **2010**, *177*, 146–149.

[37] G. I. Sunahara, S. Dodard, M. Sarrazin, L. Paquet, G. Ampleman, S. Thiboutot, J. Hawari, A. Y. Renoux, *Ecotoxicol. Environ. Saf.*, **1998**, *39*, 185−194.

[38] C. J. Cao, M. S. Johnson, M. M. Hurley, T. M. Klapötke, *JANNAF J. Propuls. Energet.*, **2012**, *5*, 41–51.

[39] H. Lebreton, D. Cazajous, S. Larue, *Proceedings of the International Pyrotechnics Seminar* **2015**, 41st, 1–6.

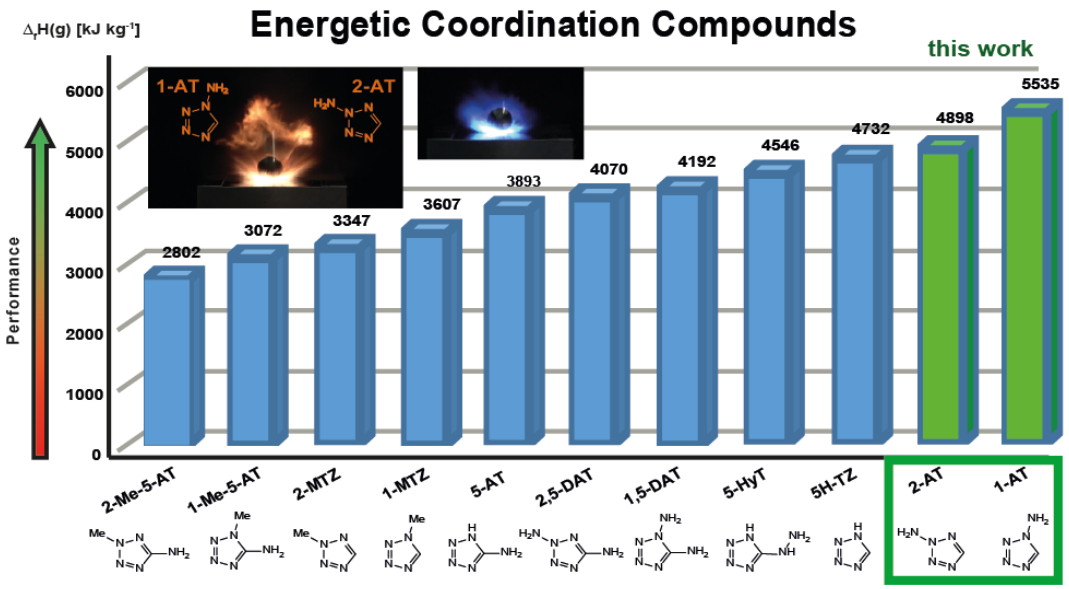
[40] E. D. Aluker, A. G. Krechetov, A. Y. Mitrofanov, D. R. Nurmukhametov, M. M. Kuklja, *J. Phys. Chem. C*, **2011**, *115*, 6893−6901.

16 Maximization of the Energy Capability Level in Transition Metal Complexes through Application of 1-Amino- and 2-Amino-5*H*-tetrazole Ligands

Norbert Szimhardt, Maximilian H. H. Wurzenberger, Lukas Zeisel, Michael S. Gruhne, Marcus Lommel, and Jörg Stierstorfer

published in *Journal of Materials Chemistry A* **2018**, *6,* 16257–16272

DOI: 10.1039/C8TA06326E



This comprehensive study features the synthesis, characterization and evaluation of new energetic coordination compounds (ECC) based on two of the most powerful neutral tetrazoles, which have great potential as lead-free primary explosives.

Abstract

Toxic lead compounds (especially lead azide and lead styphnate), reliable but highly harmful compounds, still dominate the field of primary explosives used in most ignition and initiation systems to this day. Therefore, an extensive investigation into energetic materials with similar performance and minimized toxicity led to the very promising strategy of developing energetic coordination compounds (ECC). For the first time in literature, two isomeric amino-5*H*-tetrazoles with sensitivities already in the range of primaries, which could be obtained via practicable, easily scalable synthesis, proved to be very promising new energetic ECC ligands. By variation of the respective isomer (1-AT, 2-AT), metal(II) center (Mn^{II}, Fe^{II}, Cu^{II}, Zn^{II}) and the corresponding counter-anion (Cl^-, NO_3^-, ClO_3^-, ClO_4^-, styphnate, trinitrophloroglucinate) desired properties could be tailored gradually, yielding 20 new, highly energetic and easily accessible transition metal(II) complexes. In addition to comprehensive characterization by XRD, IR, EA, solid-state UV/Vis, DTA and TGA, BAM standard sensitivity measurements as well as ESD and ball drop impact sensitivities were determined. Classical initiation tests (nitropenta filled detonator) validated the present approach to be extraordinarily promising for potential use in advanced initiation systems. Beyond successfully achieving set goals in terms of sensitivity and toxicity, investigated complexes match or even outperform lead-based primaries' high performance and, more importantly, do not necessarily depend on initiation by mechanical stimuli. Laser irradiation of the received primary explosives with near-infrared light (NIR) yielded initiation reliably and safely, further extending their potential for future applications.

16.1 Introduction

In recent years, the demand for "green" chemicals, with respect to the invention, design and application of chemical products and processes, has grown continuously with the objective of reducing or eliminating the use and generation of hazardous substances.[1] The wide and fast expanding field of "green" chemicals comprises biodegradable plastics, bio-based polymers and environmentally friendly explosives from different portfolios of sustainable, eco-sufficient materials feasible of outclassing products based on petroleum feedstock or toxic heavy metals such as lead, mercury, barium and others.[2] Interaction between the chemical industry and academic research plays a key part in this social and economic evolution and the eventual success of green and sustainable materials. A guideline relevant to applied research in this area

is the candidate list of substances of very high concern for authorization (Annex XIV) from the REACH (Registration, Evaluation, Authorization and Restriction of Chemicals) regulations.[3]

The REACH regulations were established in June 2007 as a European Union-wide project to reduce the amount of harmful or at least suspected-to-be-harmful chemicals to which European citizens were exposed to in their everyday life. In fact, REACH is not restricted to industrial processes, and also covers the chemicals used in everyday products such as paint, cleaning products or personal hygiene articels.[4] ECHA (European Chemicals Agency) uses this decree to hold the chemical industry responsible for collecting information about their manufactured chemicals, while also assessing their hazards and potential risk to the environment. Based on the simple "one substance, one registration" principle manufacturers and importers register their chemicals in conjunction with each other for later evaluation to clarify if these registered chemicals bear any risk to the environment or health.[5] The subsequent authorization process ensures that substances of very high concern (SVHCs) are gradually replaced with other less dangerous and less harmful alternatives – if possible and readily available. As soon as the committee or the commission reaches an agreement that the addition of a SVHC to the candidate list is reasonable, the substance is added to the database.[6]

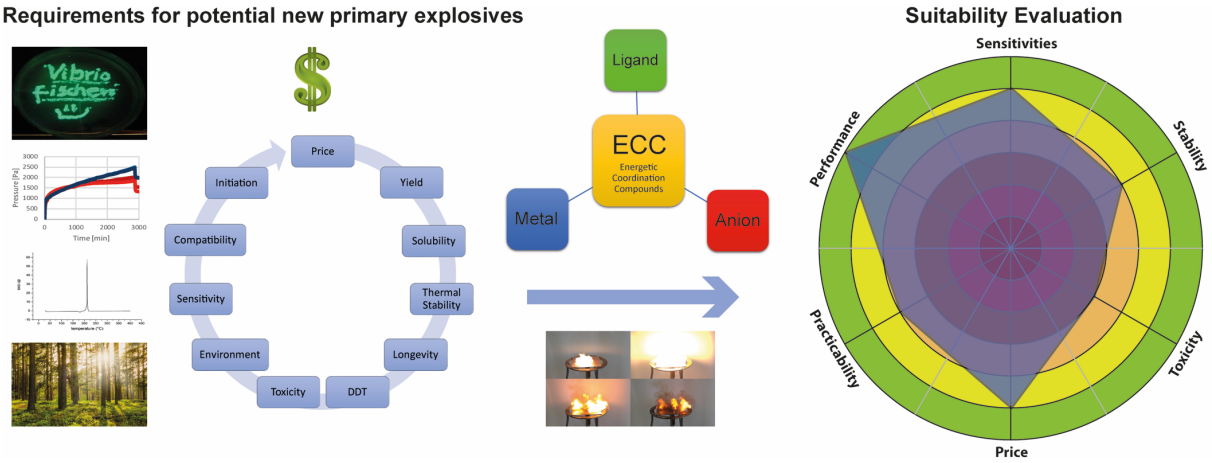


Figure 1. List of requirements to be met for new potential primary explosives, which are compiled in our suitability evaluation diagram.

One of the many candidates mentioned on this list are lead azide and lead styphnate, which are widely used as primary explosives. A total of 31 lead containing compounds appear on the REACH list, with all of them being suspected to be toxic for reproduction and some also to be carcinogenic (e.g. lead chromate since 2009).[7] As lead azide and lead styphnate are mainly used in small arm ammunition for military and commercial applications (mining, deconstruction works, etc.), there is a strong drive for substitution of these currently used-

primary explosives. Scientists in many countries from all over the world are therefore looking for possible alternatives and replacements.[8–14] Thought must be given to many different factors (fast deflagration-to-detonation transition (DDT), compatibility, energetic properties etc.) during the design, the synthesis and evaluation of potential new primary explosives. The most important characteristics for suitable candidates include the sensitivities, the chemical and physical stability, low toxicity, low price, high performance and practicabilities according to industrial needs (Figure 1). The concept of energetic coordination compounds (ECC), containing nitrogen rich ligands with low or non-toxic metals (e.g. Mn, Fe, Cu, Zn), stands out from other competing strategies and fulfills all of the desired criteria.[15–17] One of the biggest advantages of this promising approach is that the simple adjustment of one of the three building blocks (metal, ligand, anion) allows exact tailoring of the complexes in regard to the physico-chemical properties. Another important benefit of energetic coordination compounds, making them highly promising and suitable candidates for potential future applications, is their ignitability by optical methods like laser irradiation.[18,19] This approach offers various advantages in comparison to conventional initiation methods like short function times or the high isolation toward other stimuli.[20]

In particular endothermic tetrazoles have proven themselves in the past as very promising ligands in energetic complexes.[21–23] Their energetic character can easily be modified by various methods such as alteration of the functional groups (alkyl chains, nitro groups, nitramine units, hydrazinyl derivatives, attached tetrazoles etc.) or their substitution pattern (*N*1-substituted vs. *N*2-substituted vs. *C*5-substituted).[15,24] Many coordination compounds are well-known with different tetrazole ligands but surprisingly no complexes have been prepared up to date with two of the most energetic and powerful neutral ligands, 1-amino-5*H*-tetrazole (**1**, 1-AT) and 2-amino-5*H*-tetrazole (**2**, 2-AT, Figure 2).[25–31] These two isomers, which proved to be non-toxic toward aquatic organisms (see 2.5) and have an incorporated hydrazine function ($N_{Tetrazole}$–NH_2) exhibit an outstandingly high nitrogen content of 82.33% and were described almost 50 years ago for the first time in 1966 and 1969 respectively.[32,33] Several recently published energetic coordination compounds based on 1-methyl-5*H*-tetrazole as the ligand show a deficit in energetic performance.[15] Substitution of the methyl group by an amino group tremendously increases the energy content of the molecule due to the additional N–N single bond (Figure 2). The highly endothermic character and the resulting driving force of nitrogen gas formation, makes these tetrazoles exceptional great ligands, which show potential in combination with oxygen-rich anions as primary explosives.

The obtained compounds easily outperform commonly used-primaries like lead azide or lead styphnate through the maximization of the energy content in the resulting transition metal complexes.

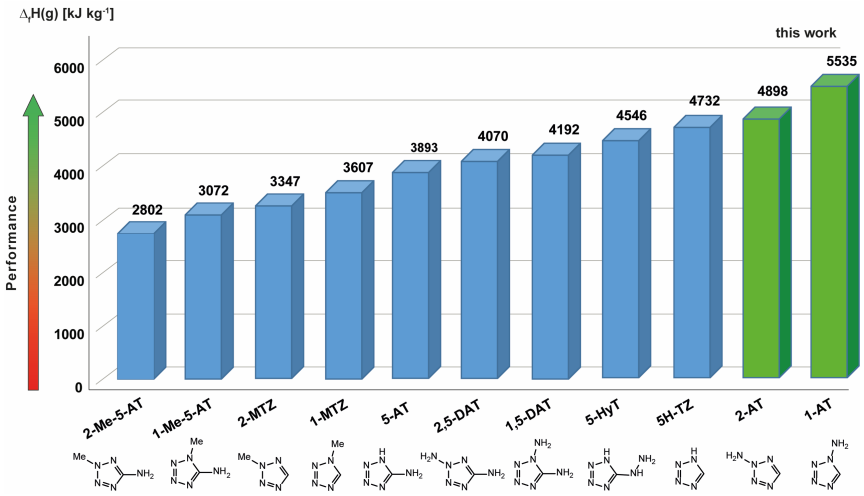


Figure 2. Comparision of the per unit mass calculated enthalpies of formation for various monotetrazoles shows the highest values for 1- and 2-amino-5*H*-tetrazole. Gas phase enthalpies of formation were calculated using the atomization method ($\Delta_f H^0_{(g,\,M)} = H_{(M)} - \Sigma H^0_{(A)} + \Sigma \Delta_f H^0_{(A)}$) using Gaussian09 computed CBS-4M electronic enthalpies.

In this comprehensive study, considerable efforts have been made to implement the highly endothermic ligands 1-amino-5*H*-tetrazole (**1**) and 2-amino-5*H*-tetrazole (**2**) into a large number of promising coordination compounds, which show great potential for possible future applications (optical and classical initiation systems).

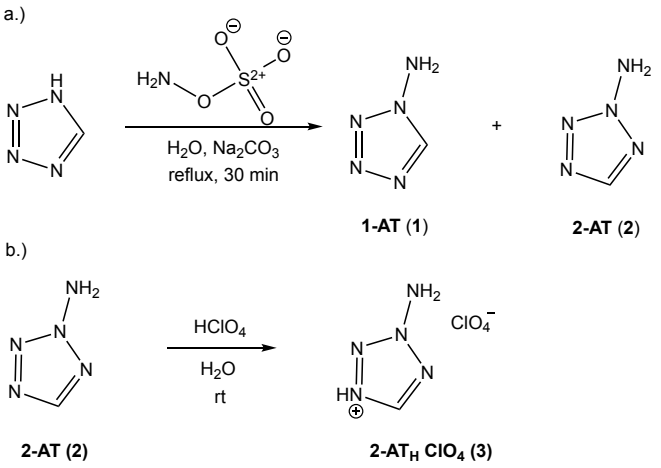
16.2 Results and Discussion

16.2.1 Synthesis

CAUTION! All investigated compounds are potentially explosive energetic materials (the majority of the compounds lie in the range of primary explosives), which show partly increased sensitivities toward various stimuli (e.g. elevated temperatures, impact, friction or electrostatic discharge). Therefore, proper security precautions (safety glasses, face shield, earthed equipment and shoes, leather jacket, Kevlar gloves, Kevlar sleeves and ear plugs) have to be worn while synthesizing and handling the described compounds. Especially the very sensitive compounds **4**–**7** and **18**–**23** must be handled with great care! An excess of ligand **2** has to be

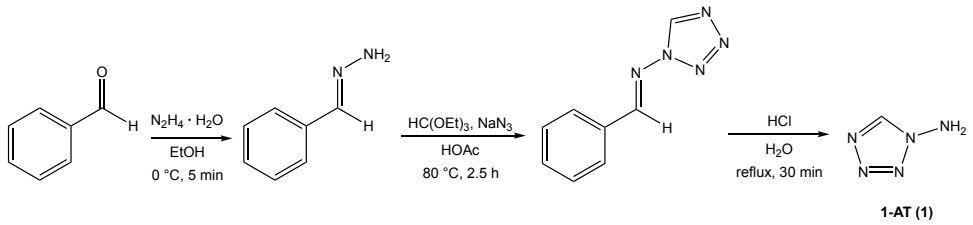
applied during the synthesis of complex **18** in order to prevent the formation of unisolable side species (most likely a diperchlorato or hexacoordinated tetrazole complex), which tends to spontaneous violent decomposition during crystallization.

In principle, the preparation of 1-amino-5*H*-tetrazole (**1**) can be achieved via two different synthetic protocols. One way is the amination of 1,5*H*-tetrazole, reported in 1969 for the first time, which leads to an isomeric mixture of compound **1** and 2-amino-5*H*-tetrazole (**2**) as a side product.[33] As of today, unfortunately no direct synthetic path has been developed for this isomer, which in comparison to compound **1**, is surprisingly more sensitive. The amination reaction of the in situ generated sodium tetrazolate proceeds via a nucleophilic substitution mechanism and has been performed with the well-known amination reagent hydroxylamine-*O*-sulfonic acid (HOSA) in water under reflux and a constantly readjusted pH value of 7–8 according to a modified literature procedure (Scheme 1).[33,34] Instead of the very dangerous separation by distillation of the isomeric mixture obtained, a much safer and more efficient purification by flash column chromatography (EtOAc/DCM 5:1) on silica gel was developed. The two isomers could be isolated in yields of 27% for compound **1** and 19% for the nitrogen-rich ligand **2**. The relatively low yields can most likely be attributed to the electron-poor character of the aromatic heterocycle and its related low nucleophilicity. Treatment of the two amino-5*H*-tetrazoles **1** and **2** with aqueous diluted acids (HNO_3 and $HClO_4$) resulted in ionic liquids and were therefore not been investigated in more detail. The only exception was the protonated 2-amino-5*H*-tetrazolium perchlorate salt (**3**), which crystallized within 5 days and has been comprehensively characterized (Scheme 1).



Scheme 1. a.) Synthesis of 1-amino-5*H*-tetrazole (**1**) and 2-amino-5*H*-tetrazole (**2**) by amination of 1,5*H*-tetrazole by hydroxylamine-*O*-sulfonic acid (HOSA). b.) Synthesis of 2-amino-5*H*-tetrazolium perchlorate (**3**).

1-Amino-5*H*-tetrazole (**1**) can be prepared (overall yield: 32 %), in contrast to compound **2**, directly and isomerically pure via a simple and upscalable three-step synthesis (Scheme 2). In the first step, one amino group of the hydrazine molecule is protected as benzhydrazone by treatment with benzaldehyde in a condensation reaction. Particular attention should be given to the low reaction temperature, the sequence of starting materials added and the reaction time to prevent formation of a further reaction to the bisbenzhydrazone. The next step entails the ring closure of the remaining free amino group of benzhydrazone in a [3+1+1] cyclization with triethyl orthoformate and sodium azide carried out at 80 °C for 2.5 h under acidic conditions. The resulting tetrazole immediately precipitates in the form of a yellow-orange solid right after pouring into water. The benzyl protection group is cleaved almost quantitatively in the last reaction step under acidic conditions with hydrochloric acid and the resulting benzaldehyde was removed using the rotary evaporator at elevated temperatures under vacuum. This reaction step has been greatly improved and simplified in comparison to literature-reported procedures where water steam distillation and distillation under vacuum are applied to remove the emerging benzaldehyde.[32,35]



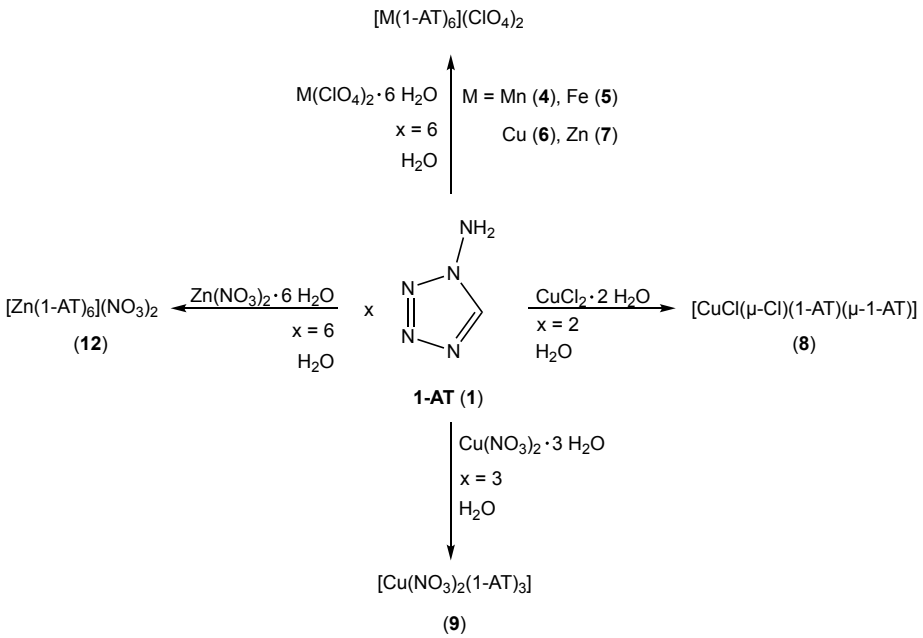
Scheme 2. Selective and isomerically pure preparation of 1-amino-5*H*-tetrazole (**1**) in a three-step reaction starting from benzaldehyde and hydrazine monohydrate.

Both isomers can easily be differed by infrared spectroscopy (Figure S1) or proton and carbon NMR spectroscopy. Furthermore, two dimensional ^{1}H, ^{15}N NMR HMBC or proton coupled ^{15}N NMR spectroscopy can be performed (Figure 3).

A large number of complexes based on various monotetrazoles like 1,5-diaminotetrazole or 1-methyl-5*H*-tetrazole have been described in literature but have insufficient power for any possible application as a primary explosive.[16,30] Owing to this lack of power and to maximize the energetic performance, new transition metal complexes were synthesized with even more powerful endothermic ligands. Our synthetic strategy comprises the preparation of cationic or neutral complex units to increase the energetic character of the coordination compounds and to ensure the integration of oxidizing anions, facilitated through the application of neutral basic nitrogen-rich ligands. In addition, the influence on the coordination sphere and the physico-

chemical properties were investigated by alteration of the tetrazole isomers while maintaining the metal(II) and anion building blocks.

The synthesis of the divalent transition metal(II) complexes **4**–**9** and **12** was accomplished through combination of aqueous solutions of the relevant metal(II) salts and the ligand **1** in the corresponding stoichiometries at room temperature (Scheme 3).



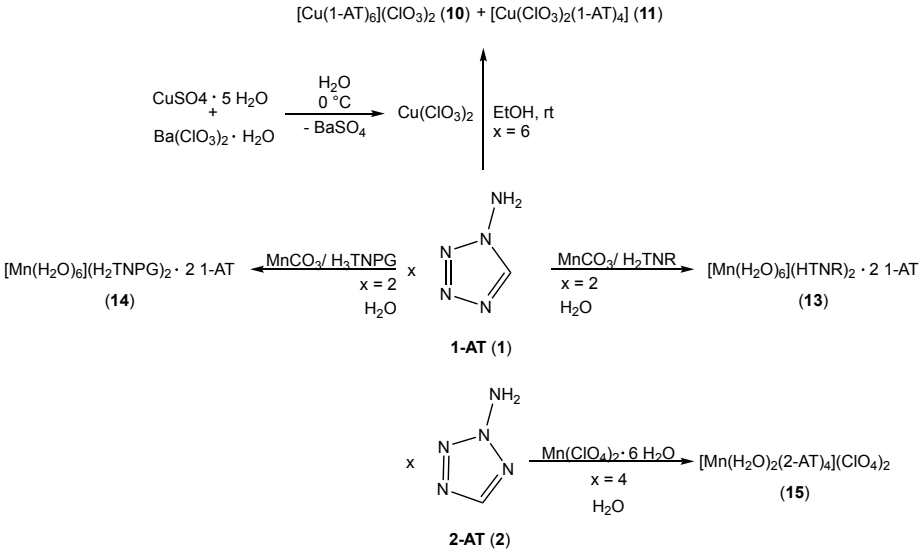
Scheme 3. Synthesis of the transition metal(II) complexes **4**–**9** and **12** based on 1-amino-5*H*-tetrazole (**1**) as ligand.

Water has been selected as the green solvent for all reaction mixtures to ensure slow crystallization of the desired complexes and because of the good solubilities of the ligands and the transition metal(II) salt starting materials in this solvent system. All coordination compounds crystallized with decent yields (32–79%) without inclusion of aqua ligands or crystal water molecules resulting in a higher performance of the complexes. The exclusive use of ethanol as solvent instead of water leads to precipitation of the complexes in most cases in the form of amorphous powders.

Analogous to our recently published work, an ethanolic solution of copper(II) chlorate was reacted with 1-amino-5*H*-tetrazole (**1**) in order to synthesize the corresponding copper(II) chlorate coordination compound (Scheme 4).[36] After a few days and evaporation of the solvent, two different crystalline species appeared from the reaction mixture, which could be picked and handled while still wet. X-ray diffraction analysis revealed a complex species with

six coordinating 1-AT ligands (**10**, Figure S9) and a species with four 1-AT ligands and two coordinating chlorato anions (**11**, Figure S10).

All attempts to dry the compounds for further characterization failed due to the extreme sensitivity and resulted in violent detonations. Unfortunately, only a few single crystals suitable for X-ray diffraction of the manganese(II) complexes **13**–**15** (Scheme 4) could be isolated in between amorphous bulk material with indefinite composition and unreacted starting materials. Therefore, only their X-ray crystal structures, which are shown in the SI can be presented. All attempted syntheses to achieve a pure elemental analysis of the complexes were unsuccessful.



Scheme 4. Formation of complexes **10**, **11** and **13**–**15** with varying metal(II) centers, anions and ligands.

The 2-amino-5*H*-tetrazole (**2**) based coordination compounds **16**–**23** (Scheme 5) were synthesized in analogy to their 1-substituted isomers (easily distinguishable by IR, Figure S3) through a straightforward reaction of the corresponding metal(II) salts in the necessary stoichiometries in water or ethanol at room temperature. An excess of ligand **2** had to be applied during the synthesis of complex **18** in order to prevent the formation of an unisolable side species (most likely a diperchlorato or hexacoordinated tetrazole complex), which tended to spontaneous violent decomposition during crystallization. It should also be noted, that the use of six equivalents of **2** instead of five during the synthesis of the complexes **19**–**20** leads to the same monoaqua species and has no influence on the composition of the resulting coordination compounds. The preparation of the metal(II) perchlorate complexes **18**–**23** yields for each metal(II) salt two different species depending largely on the applied stoichiometry and solvent system. In addition to the aqua ligand containing coordination compounds **18**-**20**, complex units with two additional cocrystallized aminotetrazoles **21**-**23** can be isolated when an excess of ligand is used. Both species can easily be detected and distinguished from each other by IR spectroscopy (Figure S4/5).

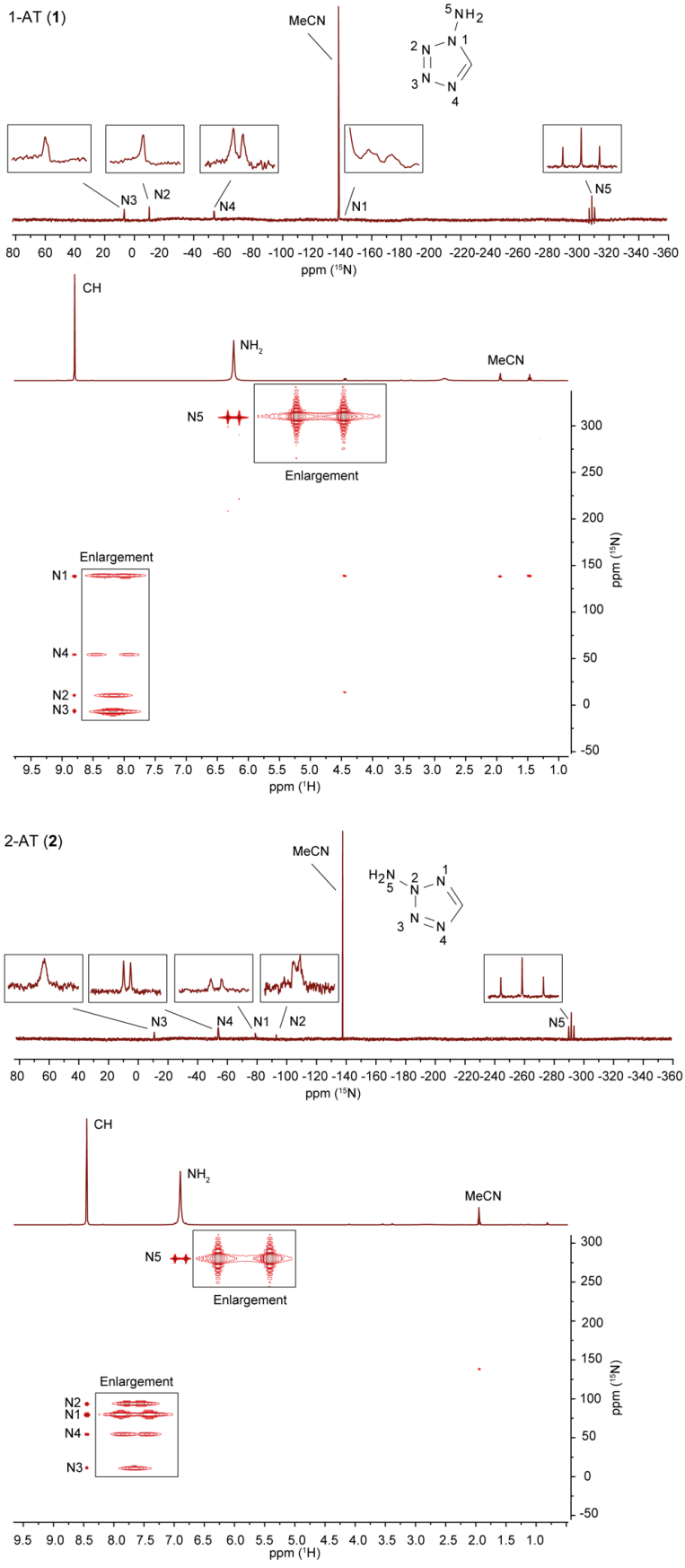
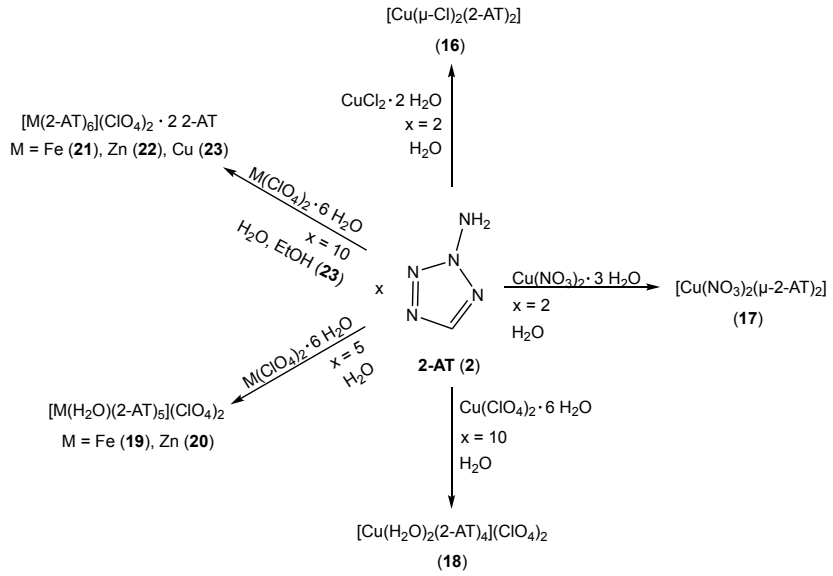


Figure 3. Proton coupled ^{15}N NMR spectra and two dimensional ^{1}H, ^{15}N-HMBC NMR spectra of **1** and **2**.

In the case of the copper(II) perchlorate complexes **18**/**23**, the solvent system plays an important role in the formation of the relevant complexes. Water leads to the diaqua species **18**, whereas ethanol as solvent results in the formation of the cocrystallized compound **23**.



Scheme 5. Synthesis of selected energetic coordination compounds **16**–**23** based on 2-amino-5*H*-tetrazole (**2**) as ligand.

All coordination compounds were directly obtained from the mother liquor and crystallized in satisfactory yields with exception of the cocrystallized species. The crystalline materials, all suitable for X-ray diffraction, were filtered off, washed with a small amount of ice-cold ethanol when necessary in order to remove unreacted starting materials and were then dried in air overnight.

16.2.2 Crystal Structures

The nitrogen-rich ligand **1**, the perchlorate salt **3** and all complexes were characterized by low temperature single crystal X-ray diffraction. In contrast to ligand **2**, 1-amino-5*H*-tetrazole (**1**) could be solidified through controlled freezing with liquid nitrogen. Its low melting point of 5 °C[35] allowed the picking of a single crystal at 0 °C for X-ray determination. The measurements of compound **4** and **11** showed considerable structural disorders within the tetrazole rings as well as in the perchlorate (**4**) and chlorate (**11**) anions. Nevertheless, they allow the identification of the complexes' composition. Elemental analysis and infrared spectra comparison (Figure S2) verified the analogous structure of **4** as in the other isotypic hexakis(1-amino-5*H*-tetrazole) metal(II) perchlorate complexes **5**–**7**. The high degree of disorder

observed for the copper(II) chlorate complex **11** unfortunately allowed only an isotropic illustration (Figure S10) of the molecular structure. All complexes, except compound **9**, show an octahedral coordination sphere of the metal(II) center. Complexation of the ligands **1** and **2** always takes place through the N4 nitrogen atom of the tetrazole ring, except for compounds **8** and **19** which show bidentate aminotetrazole ligands. The crystal datasets were uploaded to the CSD database[37] and can be obtained free of charge with the CCDC no. 1834855 (**1**), 1834849 (**3**), 1834847 (**5**), 1834859 (**6**), 1834851 (**7**), 1834845 (**8**), 1834844 (**9**), 1834853 (**10**), 1834852 (**12**), 1834858 (**13**), 1834857 (**14**), 1834854 (**15**), 1834842 (**16**), 1834843 (**17**), 1834841 (**18**), 1834856 (**19**), 1834846 (**20**), 1834848 (**21**), 1834850 (**22**), 1838980 (**23**).

Compound **1** crystallizes in the form of colorless rods in the orthorhombic space group $P2_12_12_1$ with four formula units per unit cell and a calculated density of 1.515 g cm^{-3} at 143 K. All non-hydrogen atoms lie within a plane with torsion angles close to 0° (C1–N1–N2–N3 0.31(15)°, N5–N2–C1–N1 1.59(1)° and N2–N1–C1–N4 0.12(16)°) and show bond lengths as well as angles comparable to those of other 1-substituted tetrazole compounds (Figure 4).[38]

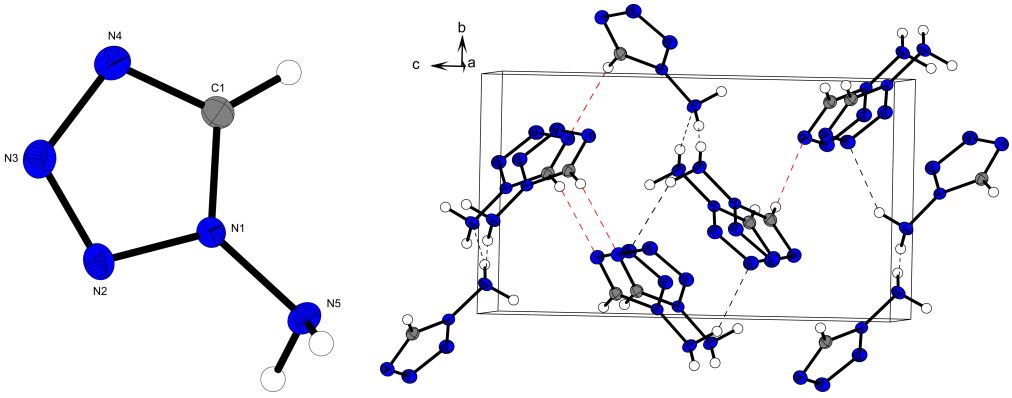


Figure 4. Molecular unit (left) and unit cell (right) of 1-AT (**1**). Thermal ellipsoids of non-hydrogen atoms in all structures are set to the 50 % probability level. Selected bond lengths (Å): N1–C1 1.3256(18), N1–N5 1.4000(17), N1–N2 1.3441(15), N2–N3 1.2986(19), N3–N4 1.370(2), N4–C1 1.3128(19); selected bond angles (°): N2–N1–N5 123.21(11), N2–N1–C1 109.17(11), N5–N1–C1 127.54(12), N1–N2–N3 105.71(11), N2–N3–N4 110.82(12), N3–N4–C1 105.18(12).

The perchlorate salt **3**, crystallizes in the form of colorless blocks in the monoclinic space group $P2_1/n$ with four formula units per unit cell and a calculated density of 1.963 g cm^{-3} at 173 K. The distances between the ring atoms lie within the range of partial double bonds and the torsion angle C1–N1–N2–N3 is very close to 0° (C1–N1–N2–N3 −0.5(2)°). Moreover, every bond length besides the N1–N2 distance is slightly shorter in the non-coordinating tetrazole ring of **3**. In addition to these results, the aromaticity of the heterocycle is proved by the bond angles

amongst the ring atoms. The bond distance between the amine's and the adjacent ring nitrogen is close to those of the tetrazole's π-system. In regard to the N2's sp^2-hybridization as part of an aromatic heterocycle, the bond angles between N5, N1 and the neighboring ring atoms are close to be the ideal 120°. The interesting conclusion, that the whole aminotetrazolium cation appears as one plane molecule when including the amino group at N5, can be made based on the torsion angle N5–N2–N3–N4 which almost amounts to 180° (N5–N2–N3–N4 = 175.03(15)°). Due to the previously mentioned sp^2-hybridization of the atoms of this aromatic heterocycle, the hydrogen atoms at N4 and C1 are part of the molecule's plane. On the other hand, the hydrogen atoms of the sp^3-hybridized N5 are both orientated toward in the same direction. The perchlorate counter-ion of the tetrazolium cation is only marginally distorted exhibiting typical Cl–O bond distances and bond angles based on their tetrahedral molecular structure (Figure 5). In summary, the resulting structural parameters almost exclusively match data quoted in literature of similar tetrazolium perchlorate salts.[39]

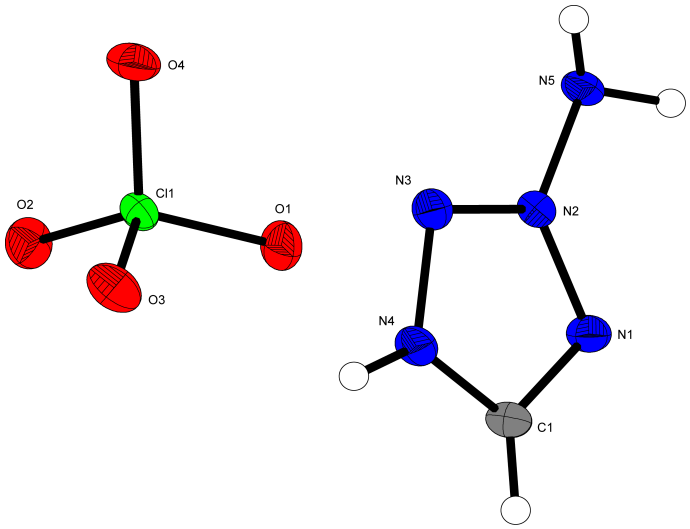


Figure 5. Molecular unit of 2-AT_H ClO_4 (**3**). Selected bond lengths (Å): Cl1–O1 1.4369(14), N1–C1 1.318(2), N1–N2 1.333(2), N2–N3 1.289(2), N2–N5 1.369(2), N3–N4 1.331(2), N4–C1 1.322(2); selected bond angles (°): O1–Cl1–O3 109.82(8), O2–Cl1–O4 108.65(8), N2–N1–C1 101.68(14), N1–N2–N3 116.77(15), N1–N2–N5 121.17(15), N2–N3–N4 101.33(15), N3–N4–C1 110.89(15), N1–C1–N4 109.33(15).

The bond lengths and angles of the coordinating ligands in the complexes analyzed are in the same range as in the non-coordinating ligand **1** and are therefore not part of the discussion in any of the following coordination compounds.

The metal(II) perchlorate compounds of 1-AT (**4**–**7**) all crystallize isotypically in the trigonal space group *P*−3 with densities between 1.736 (**4**) and 1.918 g cm^{-3} (**6**) (Mn: 1.736 g cm^{-3}

(143 K); Fe: 1.766 g cm^{-3} (173 K); Cu: 1.918 g cm^{-3} (173 K); Zn: 1.783 g cm^{-3} (173 K)). All complexes consist of two distinguishable metal centers with one exhibiting an ideal coordination polyhedron and the other being slightly distorted. Six nitrogen-rich ligands are bound to each metal(II) center and the perchlorate counter-anions are non-coordinating (Figures 6 and S6–8).

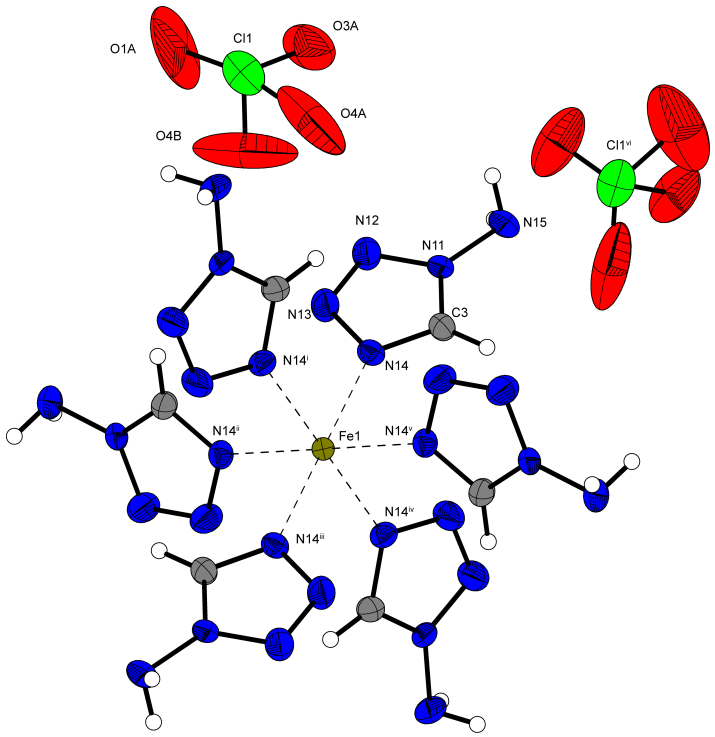


Figure 6. Molecular unit of complex $[Fe(1\text{-}AT)_6](ClO_4)_2$ (**5**). Selected bond length (Å): Fe1–N14 2.185(3); selected bond angles (°): N14–Fe1–N14^{vii} 88.88(11), N14–Fe1–N14^{iii} 91.12(12). Symmetry codes: (i) 1−y, x−y, z; (ii) 1−x+y, 1−x, z; (iii) −x, −y, −z; (iv) x−y, x, −z; (v) −x+y, −x, z; (vi) −y, x−y, z; (vii) y, −x+y, −z.

In each case, the three dimensional stability is guaranteed by several hydrogen bonds represented in Table S6, exemplarily illustrated for complex $[Fe(1\text{-}AT)_6](ClO_4)_2$ (**5**). The unit cell of **5** is depicted in Figure 7 illustrating the two-dimensional packing in view along the crystallographic *c*-axis. The comparison of the investigated perchlorate complexes with 1-amino-5*H*-tetrazole as the coordinating ligand shows no major differences besides the Jahn-Teller distorted Cu2 center in **6** (Figure S7) and the previously mentioned densities. Notwithstanding, one might recognize the slight differences regarding the bond coordination distances between the ligands and the respective metal(II) center. While all complexes show disordered perchlorate anions, the manganese(II) compound **4** additionally possesses strong disorders in the heterocyclic ligands (Figure S6).

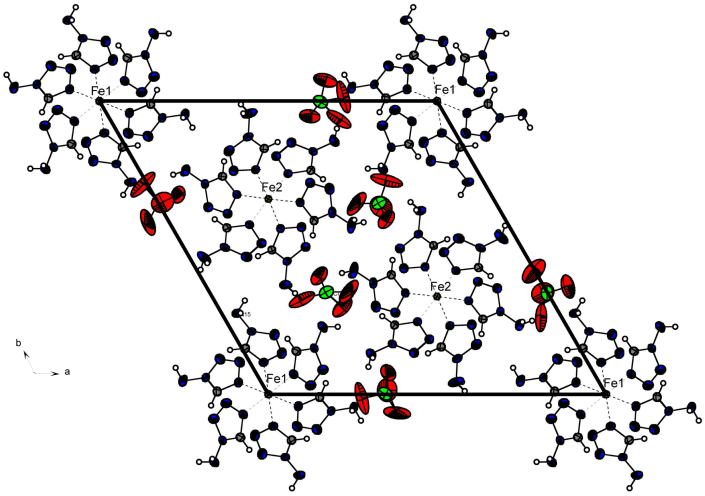


Figure 7. Unit cell of $[Fe(1\text{-}AT)_6](ClO_4)_2$ (**5**) in the direction of view along the *c*-axis.

The copper(II) chloride coordination compounds of 1-AT and 2-AT both crystallize in the form of green blocks in similar monoclinic space groups $P2_1/n$ (**8**) and $P2_1/c$ (**16**) with four and two formula units per unit cell respectively. The calculated densities at 173 K vary only slightly (2.146 g cm^{-3} (**8**) and 2.177 g cm^{-3} (**16**) respectively). The two complexes show completely different coordination spheres, which are highly dependent on the inserted ligand. 2-Amino-5*H*-tetrazole acts as a monodentate ligand in complex **16** with bridging chlorido ligands, which are responsible for the assembly of 1D polymeric chains. The 1-AT ligand instead shows a bidentate behavior in compound **8** leading to the formation of 2D polymeric layers. The copper(II) center of **8** is octahedrally coordinated and bridged to polymeric planes over two chlorido and two 1-amino-5*H*-tetrazole ligands (Figure 8). The equatorial positions are occupied by one bridging and one terminal equivalent of each, the chlorido and the 1-amino-5*H*-tetrazole ligand, generating a plane. The coordination octahedron exhibits a Jahn-Teller distortion along the Cl2^{ii}–Cu1–N5 axis with N5 being part of the second bridging equivalent of **8**. Moreover, the structure of the complex is close to an ideal octahedron with the maximum deviation of the bond angles between two *cis*-ligands from 90° being 5.76° and of two *trans*-ligands from 180° being 4.41°. In contrast, the molecular unit of **16** consists of four bridging chlorido and two terminal 2-amino-5*H*-tetrazole ligands forming an octahedral coordination sphere (Figure 8). Once again, the d^9-copper center shows a significant Jahn-Teller distortion along the Cl1–Cu–Cl1^{iv} axis. The equatorial coordination sites are occupied by two bridging chlorido ligands and the remaining two equivalents of 2-AT building up an almost ideal plane. Considering the findings that the bond angles between ligands in *cis* positions are close to the ideal 90° and angles amongst molecules coordinating *trans* to each other are exclusively 180°,

the coordination polyhedron shows multiple signs of being an ideal octahedron, despite the previously discovered distortions in regard to the bond lengths.

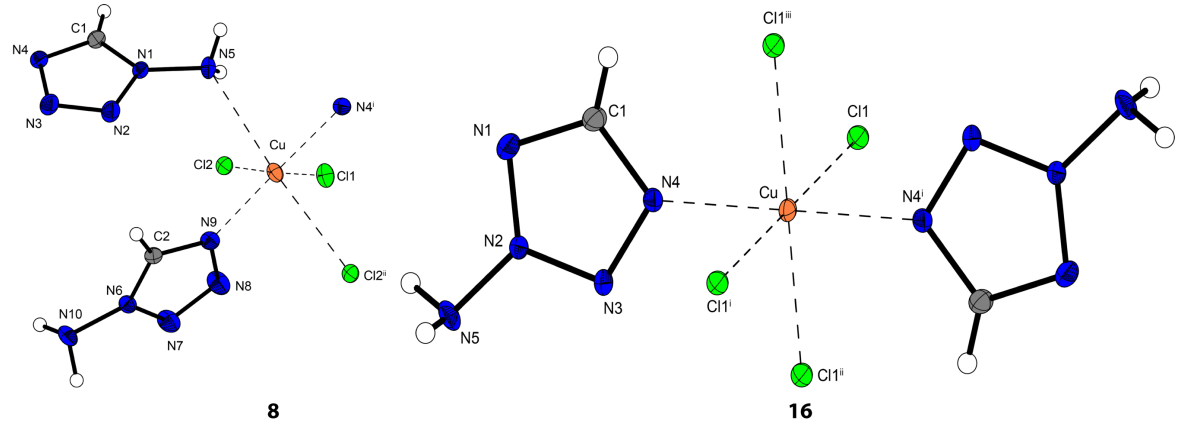


Figure 8. Copper(II) coordination environments of [CuCl(μ-Cl)(1-AT)(μ-1-AT)] (**8**) (left) and [Cu(μ-Cl)$_2$(2-AT)$_2$] (**16**) (right). Selected bond lengths (Å) of **8**: Cu1–Cl1 2.2854(6), Cu1–Cl2 2.3122(6), Cu1–N9 2.0113(19), Cu1–N5 2.725(2); selected bond angles (°) of **8**: Cl1–Cu1–Cl2 177.96(2), Cl2–Cu1–N5 93.90(5), N5–Cu1–Cl1 84.55(5), N9–Cu1–Cl1 90.78(5), Cl2–Cu1–N9 90.64(5), . Symmetry codes of **8**: (i) 0.5+x, 1.5−y, 0.5+z; (ii) 1.5+x, 1.5−y, 1.5+z. Selected bond lengths (Å) of **16**: Cu–Cl1 2.8124(6), Cu–N4 2.0422(19); selected bond angles (°) of **16**: Cl1–Cu–N4 90.25(5), Cl1–Cu–Cl1^{ii} 91.30(2), Cl1^{iv}–Cu–N4 89.76(5), Cl1^{ii}–Cu–N4 88.84(6). Symmetry codes of **16**: (i) 2−x, 2−y, −z; (ii) x, 1+y, z; (iii) 2−x, 1−y, −z; (iv) x, −1+y, z.

Analogous to the chlorido complexes, the copper(II) nitrate coordination compounds **9** and **17** show a completely different metal(II) coordination environment. In contrast to **8** and **16**, 1-AT now behaves monodentately, a fact leading to the formation of closed coordination spheres, whereas the bidentate behavior of 2-AT causes the building-up of 2D polymeric layers. The very interesting copper(II) nitrate complex **9** crystallizes in the form of blue rods in the monoclinic space group *Cc* with four formula units per unit cell and a calculated density of 1.968 g cm^{-3} at 173 K. Despite the usually observed octahedral copper(II) coordination sphere with significant Jahn-Teller distortion, compound **9** consists of a sevenfold coordinated metal(II) center leading to the coordination polyhedron of an unusual pentagonal-like bipyramid (Figure 9). The equatorial positions are occupied by two chelating nitrate anions and one equivalent of **1** forming a distinctly deformed plane. The ideal properties of a pentagonal bipyramid prescribe the bond angles between the equatorial ligands to be 72° – a requirement, which is definitely not fulfilled for the investigated complex due to the nitrate anion's fixed structure. In addition, the axis through the two-remaining amino-5*H*-tetrazole ligands in axial positions is crooked, differing considerably from the ideal 180°. Another deviation from the perfect pentagonal bipyramid can be observed regarding the bond angles between axial and

equatorial ligands partially varying by up to 10° from the expected 90°. The nitrate complex **17** crystallizes in the form of blue plates in the monoclinic space group $P2_1/n$ with two formula units per unit cell and a calculated density of 2.169 g cm^{-3} at 173 K. This coordination compound consists of an octahedrally coordinated copper(II) center including a straight, Jahn-Teller distorted N5^{ii}–Cu1–N5^{iv} axis between the axial 2-AT ligands (Figure 9). The equatorial positions of **17** are occupied by the remaining two equivalents of **2** and the coordinating nitrate anions building up an almost ideal plane. Every bond angle of *cis* coordinating axial or equatorial ligands in **17** slightly differs from the ideal 90°.

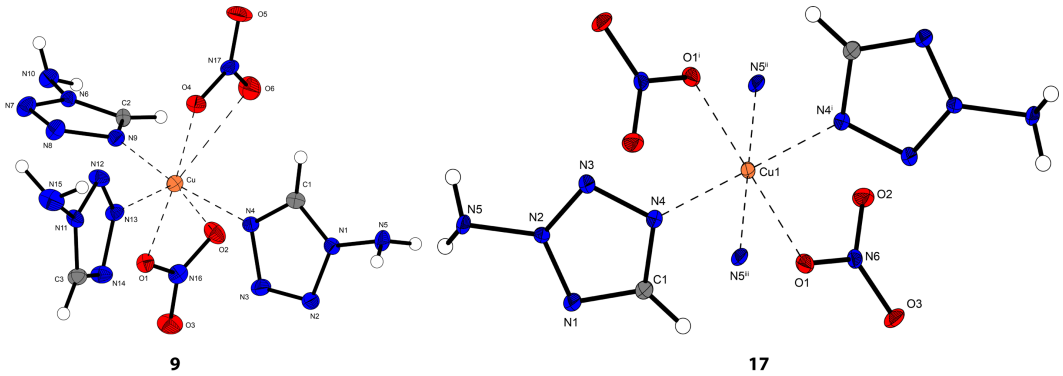


Figure 9. Molecular unit of $[Cu(NO_3)_2(1\text{-AT})_3]$ (**9**) (left) and the copper(II) coordination environment of $[Cu(NO_3)_2(\mu\text{-}2\text{-AT})_2]$ (**17**) (right). Selected bond lengths (Å) of (**9**): Cu–O1 1.987(3), Cu–O2 2.637(3), Cu–O4 1.990(3), Cu–O6 2.742(4), Cu–N13 2.287(4), Cu–N4 2.003(4), Cu–N9 1.999(4); selected bond angles (°) of (**9**): N4–Cu–N9 162.97(13), O1–Cu–O2 54.03(11), O1–Cu–N13 84.56(13), O2–Cu–O6 80.11(10), O4–Cu–O6 51.81(11), O4–Cu–N13 89.95(13), O1–Cu–N4 92.57(15), O1–Cu–N9 88.03(14), O2–Cu–N4 82.95(12), O2–Cu–N9 83.65(12), O4–Cu–N4 90.25(14), O4–Cu–N9 90.85(14), O6–Cu–N4 87.65(14), O6–Cu–N9 79.72(13). Selected bond lengths (Å) of (**17**): Cu1–N5^{ii} 2.4208(16), Cu1–O1 2.0339(12), Cu1–N4 1.9831(16); selected bond angles (°) of (**17**): O1–Cu1–N4 87.42(6), O1–Cu1–N5^{ii} 81.45(5), O1–Cu1–N5^{iv} 98.55(5). Symmetry codes of (**17**): (i) −x, −y, −z; (ii) 0.5+x, 0.5−y, 0.5+z; (iii) 0.5−x, 0.5+y, 0.5−z; (iv) 0.5−x, −0.5+y, 0.5−z.

The spatial order of the investigated copper(II) nitrate complex (**17**) reveals some very interesting observations: Each of the coordinating 2-amino-5*H*-tetrazole ligands possesses bridging characteristics and thus causes cross-linking of adjacent copper(II) centers.

The extremely sensitive copper(II) perchlorate complex **18** is the only compound which crystallizes in the tetragonal space group $P4_2/n$ with two formula units per unit cell and a calculated density of 1.947 g cm^{-3} at 173 K. Once again, the Jahn-Teller distortion along the O1–Cu–O1^{iii} axis induces significant deviations between the coordination distances of axial and equatorial ligands (Figure 10). The four equatorial 2-AT ligands form a crooked plane, a

fact that causes the bond angles between axial and equatorial ligands to slightly differ from the ideal 90°. On the other hand, the angles between *cis* amino-5*H*-tetrazole ligands in the plane almost perfectly conform to 90°. The angles amongst two equatorial ligands coordinating *trans* to each other are also influenced by the obliqueness of the N1–N1^{iii}–N1^{ii}–N1^{i} plane (N1–Cu–N1^{ii} 177.77(12)°). The analogous manganese(II) complex **15** crystallizes in the form of colorless blocks in the triclinic space group *P*−1 with two formula units per unit cell and a calculated density of 1.897 g cm^{-3} at 173 K. Compared to compound **18** the Mn–N bonds are slightly longer than the Cu–N ones with simultaneous shorter Mn–O bonds (Figure S14).

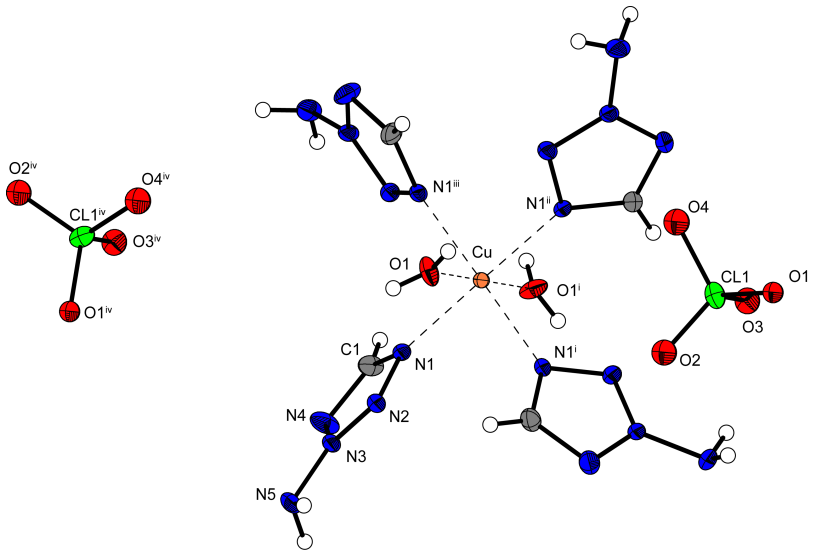


Figure 10. Molecular unit of [Cu(H$_2$O)$_2$(2-AT)$_4$](ClO$_4$)$_2$ (**18**). Selected bond lengths (Å): Cu–O1 2.311(4), Cu–N1 2.025(2); selected bond angles (°): N1–Cu–N1ii 177.77(12), O1–Cu–N1 91.11(9), N1–Cu–N1^{iii} 90.02(8). Symmetry codes: (i) y, 0.5−x, 0.5−z; (ii) 0.5−x, 0.5−y, z; (iii) 0.5−y, x, 0.5−z; (iv) 1−y, −0.5+x, −0.5+z.

The isotypic complexes **19** and **20**, two coordination isomers containing an iron(II) (**19**) or alternatively a zinc(II) (**20**) metal center both crystallize in the form of colorless blocks in the triclinic space group *P*−1 with two formula units per unit cell and calculated densities of 1.855 g cm^{-3} (**19**) and 1.884 g cm^{-3} (**20**) at 173 K. The coordination polyhedrons built up by five equivalents of **2** are completed by one aqua ligand forming an octahedral coordination sphere around the respective metal center (Figure 11 and S17). In both complexes, the M^{2+}–N distances are significantly longer than the particular M^{2+}–O coordination distances between the metal(II) center and the aqua ligands. Regarding the bond angles of the metal(II) centers, it becomes clear that there is no major distortion to be observed. Nevertheless, none of the bond angles of either of these perchlorate compounds conform the ideal values of 90° for *cis*

coordinating ligands and 180° for molecules coordinating *trans* to each other. On an additional note, the perchlorate counter-anions containing Cl2 are significantly distorted.

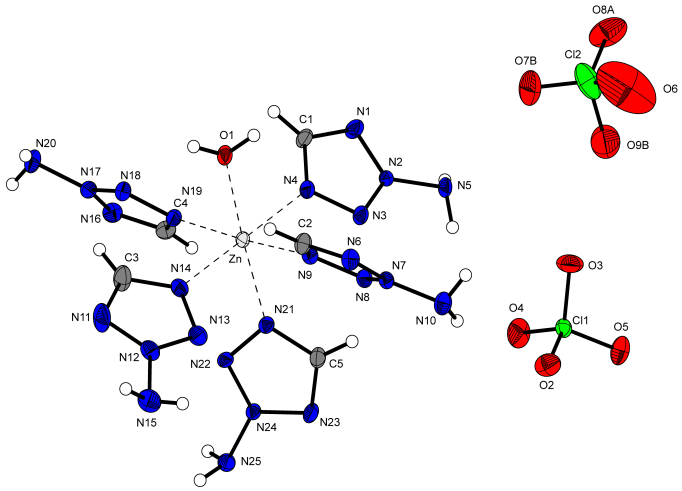


Figure 11. Molecular unit of $[Zn(H_2O)(2\text{-AT})_5](ClO_4)_2$ (**20**). Selected bond lengths (Å): Zn–O1 2.083(3), Zn–N4 2.146(3), Zn–N9 2.197(3), Zn–N14 2.147(3), Zn–N19 2.166(3), Zn–N21 2.160(3); selected bond angles (°): O1–Zn–N21 176.80(11), N4–Zn–N14 177.92(11), O1–Zn–N4 87.56(12), O1–Zn–N9 86.13(11), O1–Zn–N14 91.08(12), O1–Zn–N19 89.52(11), N4–Zn–N9 90.45(11), N4–Zn–N19 90.29(11), N4–Zn–N21 89.63(11), N9–Zn–N14 87.89(11).

The investigated complexes **21**–**23**, all including cocrystallized 2-amino-5*H*-tetrazole, crystallize in the triclinic space group *P*−1 with two formula units per unit cell and calculated densities between 1.784 g cm^{-3} (**21**) and 1.815 g cm^{-3} (**23**) (Fe: 1.784 g cm^{-3} (173 K); Cu: 1.815 g cm^{-3} (143 K); Zn: 1.812 g cm^{-3} (173 K)). In comparison to the very similar coordination compounds **19** and **20**, once again, no major differences regarding the structural parameters, besides the substitution of the aqua ligand by one additional equivalent of **2**, could be observed. The cocrystallized 2-AT molecules show no considerable deviations from the previously examined coordinating **2** referring to the bond lengths and bond distances. The octahedral coordination spheres of the d^{10} and d^6 metal centers zinc(II) and iron(II) show no Jahn-Teller distortion but differ slightly from the ideal octahedron (Figure 12 and S18). Nevertheless, the d^9 copper(II) center possesses a typical Jahn-Teller distortion along the axial Cu–N bonds (Figure S19). The coordination distances between the metal(II) center and the coordinating ligand are roughly within the same range as for the compounds **19** and **20** but appear to be somewhat longer than in the previous cases. All perchlorate counter-anions show no significant distortion.

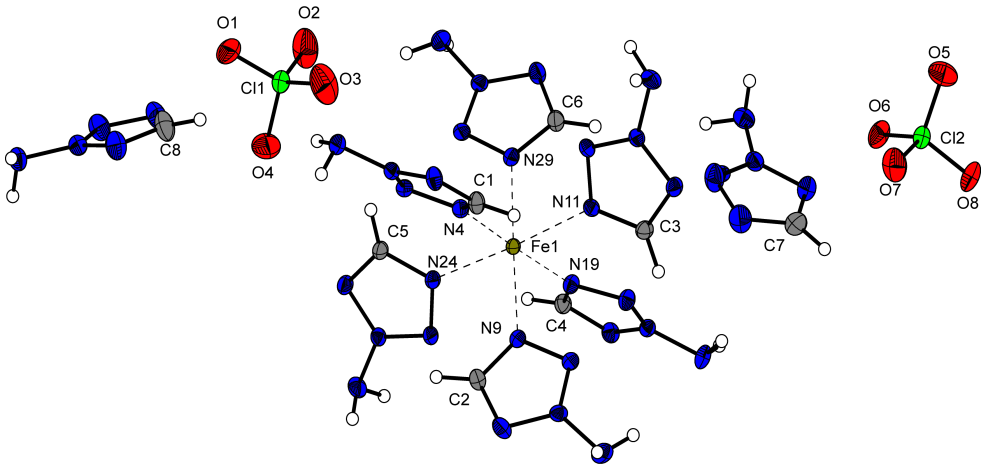


Figure 12. Molecular unit of $[Fe(2\text{-}AT)_6](ClO_4)_2 \cdot 2$ 2-AT (**21**). Selected bond lengths (Å): Fe1–N4 2.2191(16), Fe1–N9 2.1618(16), Fe1–N11 2.2135(16), Fe1–N19 2.1868(16), Fe1–N24 2.2157(16), Fe1–N29 2.1629(16); selected bond angles (°): N4–Fe1–N19 175.41(6), N4–Fe1–N9 89.38(6), N4–Fe1–N11 86.35(6), N4–Fe1–N24 91.91(6), N24–Fe1–N29 90.62(6).

16.2.3 Powder Diffraction

Due to the possible formation of different species or polymorphs, X-ray powder diffraction measurements were carried out in addition to elemental analysis to ensure the purity of the bulk material. Figure 13 shows the powder diffraction patterns for the compounds **5**, **6**, **9** and **17**. The results prove the purity of the nitrogen-rich coordination compounds. Small deviations between the measured and the calculated data sets can be observed in all diffractograms and are caused by the temperature differences be between the single crystal and powder diffraction experiments. The larger differences in the intensities for the iron(II) and copper(II) complexes **5** and **6** can be attributed to the heavy disorders in the perchlorate moieties (Figure 13A) and B)).

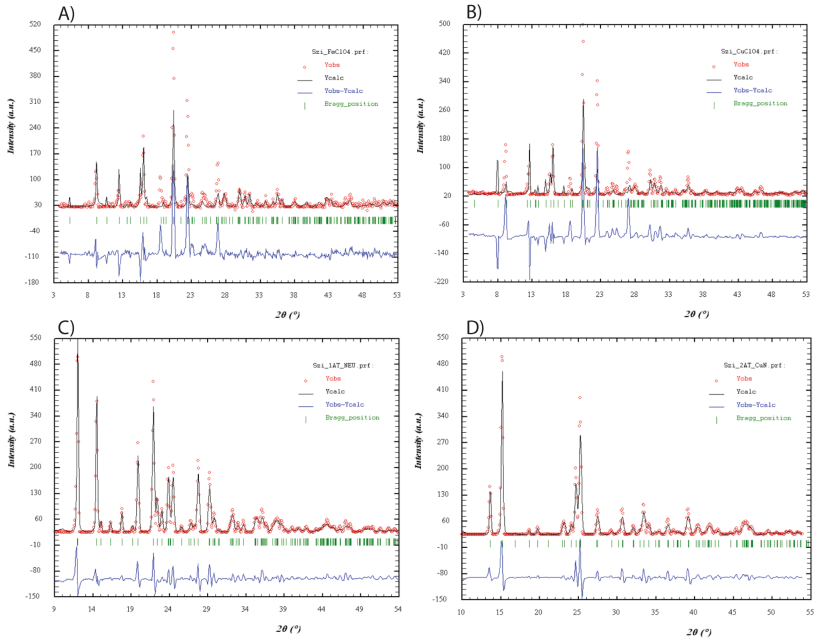


Figure 13. Powder diffraction experiments (comparision of the measured and calculated data) for the complexes **5** (A), **6** (B), **9** (C) and **17** (D).

16.2.4 Scanning Electron Microscopy (SEM) and Energy Dispersive X-ray Spectroscopy (EDX)

Since sensitivity data are strongly dependent on the grain size and crystal habitus (microscope images S20–25), scanning electron microscopy and energy dispersive X-ray spectroscopy were performed to explore the compounds' morphology but also the chemical composition. The results of the measurements for compounds **5**, **6**, **9** and **17** are shown in Figures 14–17. The iron(II) perchlorate complex **5** forms up to 200 µm-sized blocks beside plate-like crystals. Aside from insignificant trace amounts of silicon, the EDX spectrum did not show any other atoms present in the complex. Complex **6**, illustrated in Figure 15 reveals the consistency of the block-like crystals except for small spikes. Compared to compound **5**, no other elements, which are not included in the complex composition, can be observed in the EDX spectrum. The SEM image of complex **15** exposes an amorphous constitution in comparison to its microscope images. The phase-purity is confirmed by the EDX spectrum. Compound **17** shows a plate-like morphology and compared to nitrate complex **9** a lower content of carbon and nitrogen, which is consistent with the chemical compositions of the two coordination compounds.

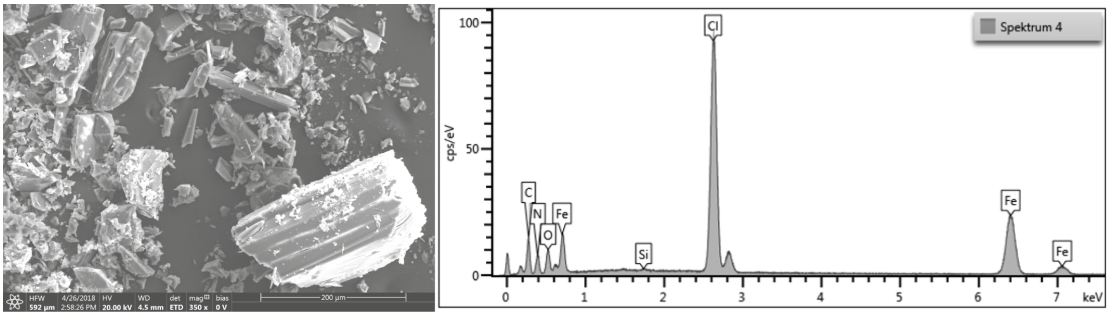


Figure 14. SEM image (350 x magnitude) and EDX spectrum of compound **5**.

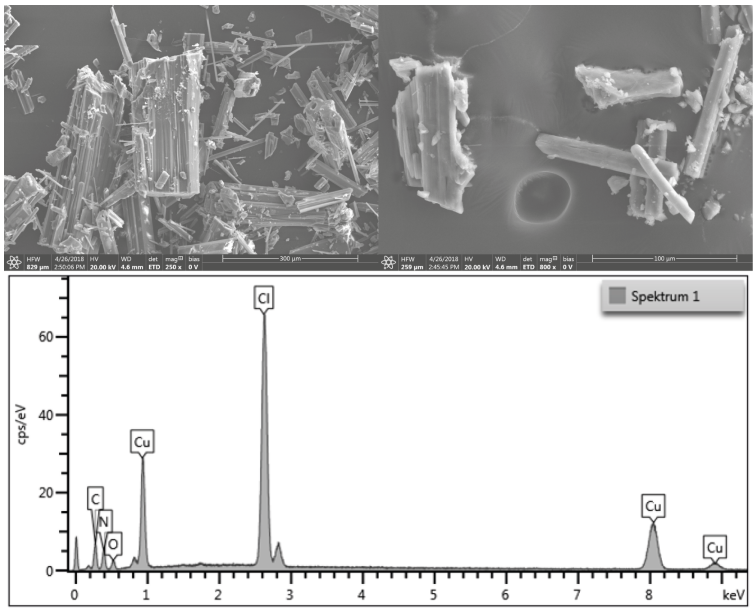


Figure 15. SEM images (250 x magnitude (left) and 800 x magnitude (right)) and EDX spectrum of compound **6**.

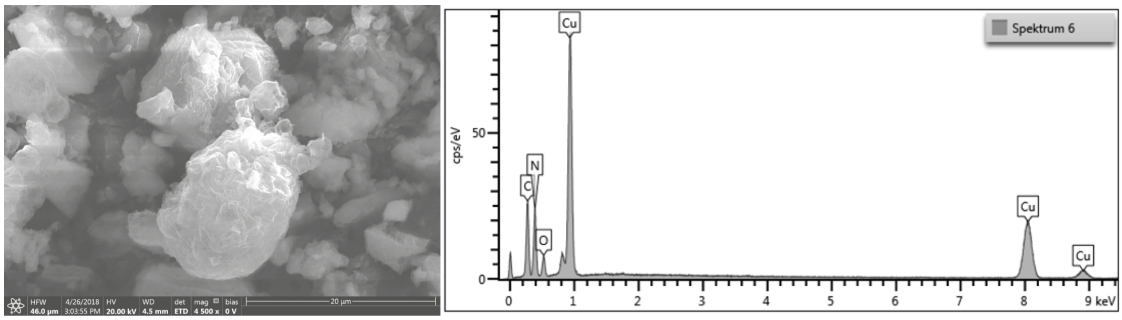


Figure 16. SEM image (4500 x magnitude) and EDX spectrum of compound **9**.

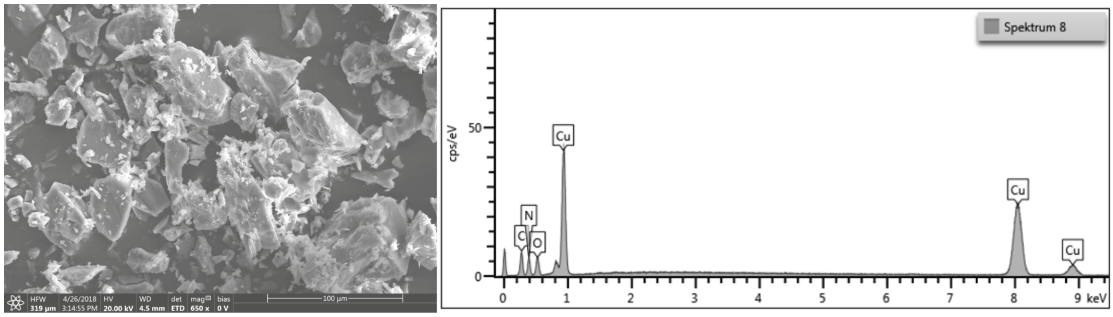


Figure 17. SEM image (650 x magnitude) and EDX spectrum of compound **17**.

16.2.5 Sensitivities and Thermal Stability

The behavior of all compounds toward heating in a certain range was investigated by differential thermal analysis (DTA) at a heating rate of $\beta = 5$ °C min^{-1}. The observed endothermic events (melting, dehydration or loss of coordinating/cocrystallized AT ligands) as well as other critical temperatures are listed in Table 1. DTA plots of the compounds **1**–**3**, **8**, **9**, **12**, **16**–**23**, and additional information regarding the thermal stabilities can be found in the Figures S27–30 in the Supporting Information. In accordance with our previous findings and literature reports, higher vaporization temperatures $T_{vap.}$,[34] (and melting temperatures) in combination with lower exothermic decomposition temperatures can be observed for 1-AT and 2-AT, and the more *N*1 substitution pattern is existent at the tetrazole.[40,43] Both tetrazoles are liquids under ambient conditions and start to vaporize slowly at certain temperatures until both compounds reach their respective exothermic decomposition stages and deflagrate, as the TGA plot of both ligands clearly illustrates (Figure S26). The thermal stabilities of most of the investigated compounds lie in the satisfying range of 175–180 °C (except **3**). Nevertheless, the lowest decomposition temperatures can be observed for the 2-amino-5*H*-tetrazolium perchlorate salt (**3**, $T_{exo.}$ = 122 °C) and for the copper(II) nitrato complexes **9** ($T_{exo.}$ = 161 °C) and **17** ($T_{exo.}$ = 157 °C). Notably the poor thermal stabilities for the nitrato coordination compounds **9** and **17** are not surprising and a known issue in the literature.[15]

Table 1. Thermal stability measurements of **1**–**9**, **12**, and **16**–**23** by DTA.[a]

compound	$T_{endo.}$[b] (°C)	$T_{exo.}$[c] (°C)
1-AT (**1**)	—	182
2-AT (**2**)	—	197
2-AT_H ClO_4 (**3**)	122	122
$[Mn(1\text{-}AT)_6](ClO_4)_2$ (**4**)	—	195
$[Fe(1\text{-}AT)_6](ClO4)_2$ (**5**)	—	187
$[Cu(1\text{-}AT)_6](ClO_4)_2$ (**6**)	—	174
$[Zn(1\text{-}AT)_6](ClO_4)_2$ (**7**)	—	189
[CuCl(μ-Cl)(1-AT)(μ-1-AT)] (**8**)	—	175
$[Cu(NO_3)_2(1\text{-}AT)_3]$ (**9**)	—	161
$[Zn(1\text{-}AT)_6](NO_3)_2$ (**12**)	115	180
$[Cu(\mu\text{-}Cl)_2(2\text{-}AT)_2]$ (**16**)	—	171
$[Cu(NO_3)_2(\mu\text{-}2\text{-}AT)_2]$ (**17**)	—	157
$[Cu(H_2O)_2(2\text{-}AT)_4](ClO_4)_2$ (**18**)	110	173
$[Fe(H_2O)(2\text{-}AT)_5](ClO4)_2$ (**19**)	—	159
$[Zn(H_2O)(2\text{-}AT)_5](ClO_4)_2$ (**20**)	132	200
$[Fe(2\text{-}AT)_6](ClO_4)_2 \cdot$ 2-AT (**21**)	106	169
$[Zn(2\text{-}AT)_6](ClO_4)_2 \cdot$ 2-AT (**22**)	96	192
$[Cu(2\text{-}AT)_6](ClO_4)_2 \cdot$ 2-AT (**23**)	108	157

[a] Onset temperatures at a heating rate of 5 °C min^{-1}. [b] Endothermic peak, which indicates melting, dehydration, or loss of coordinating/cocrystallized AT ligands. [c] Exothermic peak, which indicates decomposition.

Relatively high thermal stabilities have been determined for the water-free 1-AT based metal(II) perchlorate complexes (Figure 18), which increase in the following order Cu^{II} ($T_{exo.}$ = 174 °C) < Fe^{II} ($T_{exo.}$ = 187 °C) < Zn^{II} ($T_{exo.}$ = 189 °C) < Mn^{II} ($T_{exo.}$ = 195 °C). Analogical complexes with 1-methyl-5*H*-tetrazole instead of 1-amino-5*H*-tetrazole (methyl vs. amino group) showed, interestingly exactly the same tendency, which could possibly be a useful indicator during the planning and design of future high-temperature stable energetic complexes.[15] Dehydration (complex **18** and **20**) or loss of co-crystallized 2-amino-5*H*-tetrazoles during heating of **21**–**23** indicated by endothermic signals strongly agree with the identified X-ray crystal structures. Drying of the iron(II) monoaqua complex **19** is not possible and leads to an unstable intermediate, which detonates immediately without significant endothermic signal. An exceptional endothermic peak could be detected during the DTA measurement of the zinc(II) nitrate coordination compound **12** and was therefore investigated into more detail by thermal gravimetric analysis together with complex **4** as reference sample (Figure 19). While no change in weight after heating has been detected for the manganese(II) complex **4** until it decomposes, a gradual loss of coordinating 1-AT molecules beginning at 110 °C up to its decomposition point for coordination complex **12** can be observed. It can be assumed that this endothermic loss leads to the formation of an intermediate species, which later decomposes exothermically.[41]

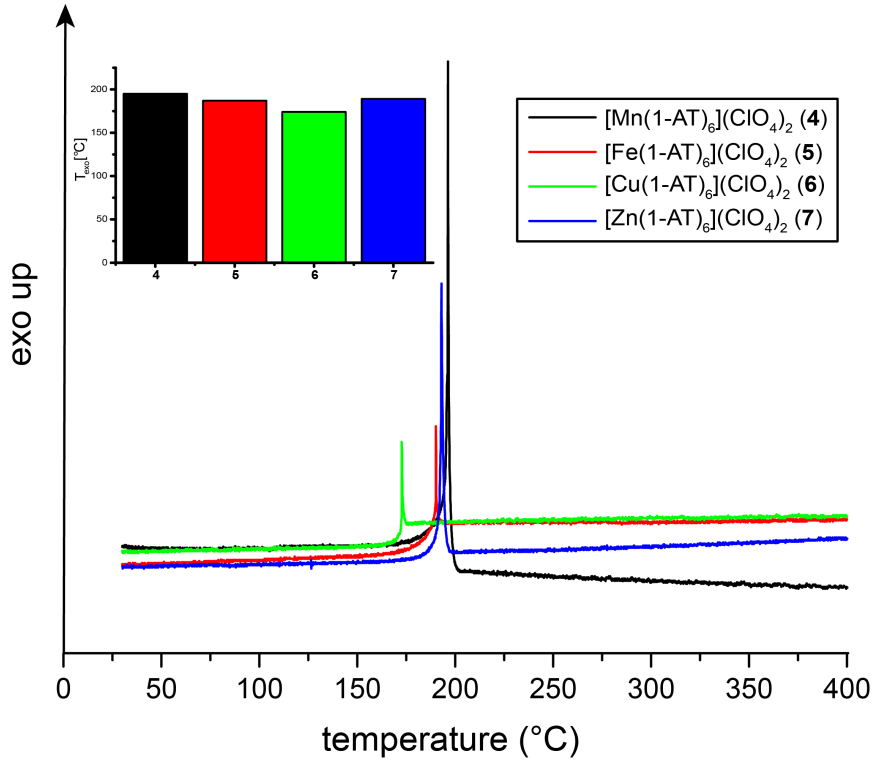


Figure 18. Comparision of the thermal stabilities (β = 5 °C min^{-1}) of the 1-AT containing metal(II) perchlorate complexes **4**–**7**.

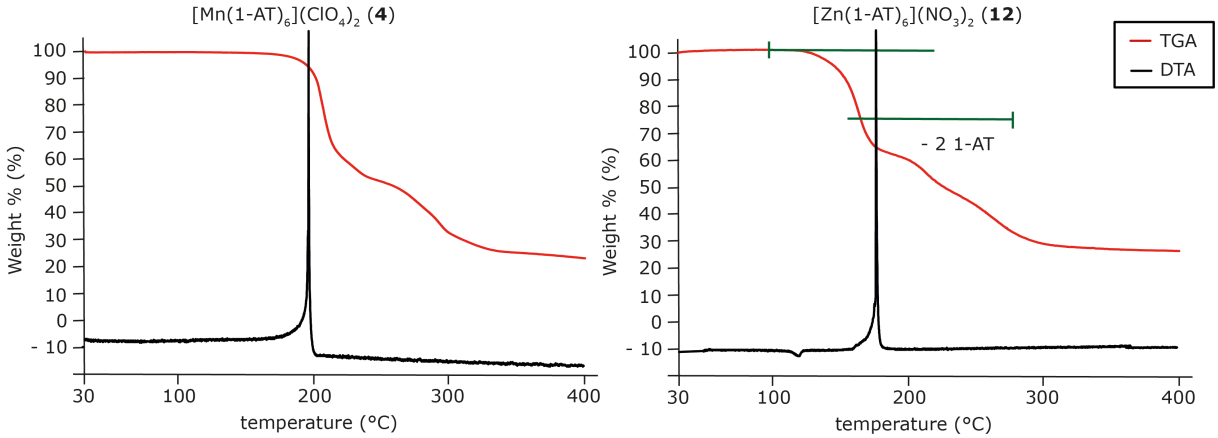


Figure 19. TGA measurements (β = 5 °C min^{-1}) of selected compounds **4** and **12**.

By comparison of complexes with the same transition metal(II) but with varying AT isomers or anions (except **9** and **17**), no general trend regarding their exothermic decomposition temperatures can be drawn.

The sensitivities toward impact and friction were assessed according to BAM standard methods (1 of 6) together with the electrostatic discharge sensitivity for all compounds. In addition, the compounds have been categorized in accordance with the "UN Recommendations on the Transport of Dangerous Goods" using the determined sensitivities. An overview of the

sensitivities is given in Table 2. The ligands as well as all complexes have to be considered as very sensitive to all applied stimuli (impact, friction and ESD) and should therefore be categorized as primary explosives. The majority of the synthesized coordination compounds can even be described as "extremely sensitive" with values smaller than 10 N against friction. Implementation of non-oxidizing chlorido anions into the complexes lowered the performance on the one hand but on the other hand led to a desensitization of the coordination compounds.

Table 2. Sensitivities toward impact, friction, and ESD of **1**–**9**, **12** and **16**–**23** compared to lead styphnate and lead azide.[a] [42]

compound	*IS*[b] (J)	*FS*[c] (N)	*ESD*[d] (mJ)
1[e]	< 1	64	—
2[e]	< 1	36	—
3	< 1	0.2	10
4	< 1	0.5	11[f]
5	< 1	< 0.1	12
6	< 1	< 0.1	5
7	< 1	0.5	12
8	3	60	50
9	3	2.25	10
12	< 1	6	620[f]
16	< 2	40	10
17	< 1	2	10
18	1	0.4	10
19	1.5	0.15	10
20	1.5	0.5	10
21	< 1	0.1	25
22	2	0.2	30
23	1	< 0.2	1.2[f]
lead styphnate[g]	2.5–5	1.5	0.02–1.0
lead azide[g]	2.5–4	0.1–1	6–12

[a] Determined at a grain size of < 100 µm were **3**, **6**, **8**, **9**, **16**, **17**, and **20**. The sensitivities of the remaining complexes were determined at grain sizes between 100 and 500 µm. [b] Impact sensitivity according to the BAM drophammer test (method 1 of 6). [c] Friction sensitivity according to the BAM friction tester (method 1 of 6). [d] Electrostatic discharge sensitivity (OZM ESD tester). Impact: insensitive > 40 J, less sensitive ≥ 35 J, sensitive ≥ 4 J, very sensitive ≤ 3 J; Friction: insensitive > 360 N, less sensitive = 360 N, sensitive < 360 N and > 80 N, very sensitive ≤ 80 N, extremely sensitive ≤ 10 N. As per the UN Recommendations on the Transport of Dangerous Goods. [e] From reference.[34] [f] measured on our new OZM Electric Spark XSpark10 device. [g] From reference.[42]

The sensitivity against ball drop impact is a very realistic and safety-relevant parameter for compounds with a potential industrial application. Therefore, and in order to get a better understanding of their stability, the sensitivity toward ball drop impact has been determined for the very promising water-free $[M^{II}(1\text{-AT})_6](ClO_4)_2$ coordination compounds **4**–**7** and the copper(II) nitrato complex **9** (Figure 20). An overview of the experimental results is given in Table 3.

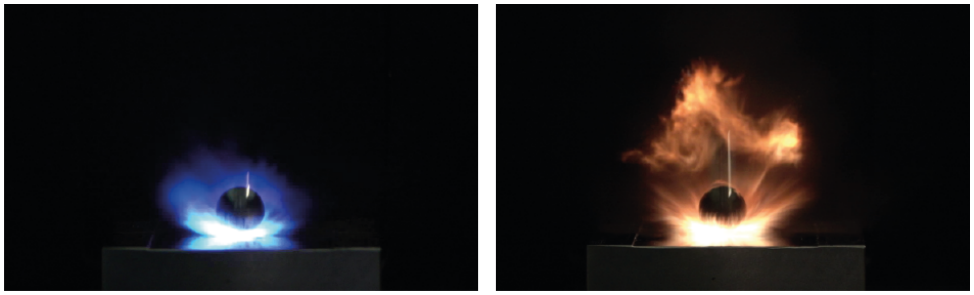


Figure 20. Moment of detonation of compounds **6** and **9** during the ball drop impact test.

Table 3. Ball drop impact sensitivities for **4–7** and **9**.[a]

	4	**5**	**6**	**7**	**9**
***IS* (mJ)**	14	25	< 4	16	6

[a] ball drop impact sensitivity determined with the 1 of 6 method in accordance with the MIL-STD 1751A (method 1016). For the testing a 30 mg sample size, a drop weight of a 0.500-inch diameter steel ball (m = 8.35 g) and a steel ball guidance track, which rose 32-inches vertically from a steel base were used.

The sensitivity (Figure 21) of the 1-AT perchlorate complexes against ball drop impact rises in the following order Fe^{2+} (25 mJ) < Zn^{2+} (16 mJ) < Mn^{2+} (14 mJ) < Cu^{2+} (< 4 mJ) and in the following order toward friction Zn^{2+} (0.5 N) ~ Mn^{2+} (0.5 N) < Fe^{2+} (< 0.1 N) ~ Cu^{2+} (< 0.1 N).

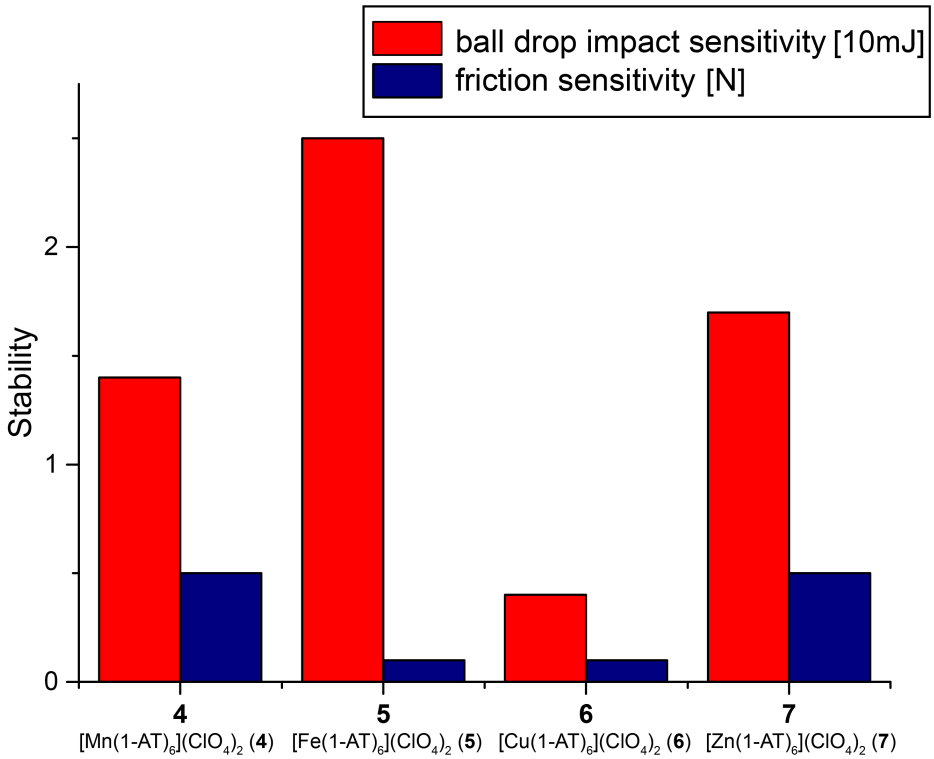


Figure 21. Comparision of the ball drop impact and friction sensitivities of the metal(II) 1-AT perchlorates **4**–**7**.

The implementation of oxidizing anions like nitrates or perchlorates into the nitrogen-rich coordination compounds, in comparison to halides, generally leads to increased sensitivities toward mechanical stimuli (Figure 22). The same trend can be observed when **2** is applied as a ligand instead of **1**. Therefore, exact tailoring of the desired optical and energetic properties can be easily accomplished by variation of the corresponding coordination environment, facilitating the synthesis of a wide range of different materials (Figure S 31/32).

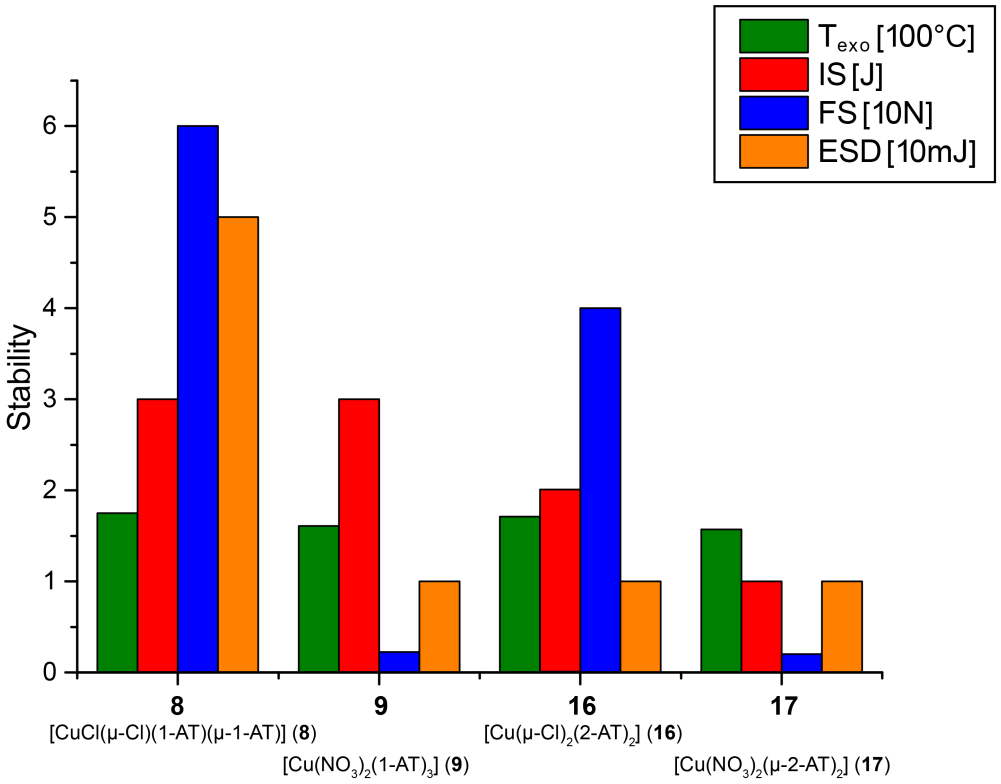


Figure 22. Stabilities of the copper(II) chlorido and nitrato complexes **8**/**9** and **16**/**17** based on the isomeric amino-5*H*-tetrazoles.

16.2.6 Primary Explosive Suitability Evaluation

Hot plate and hot needle tests of the most promising compounds were carried out in order to evaluate their applicability as suitable primary explosives (Figure 23/24 and S33–48) and to observe their behavior toward fast heating with and without confinement. An outline of the experimental results is given in Table 4. All compounds showed strong detonations during the tests, which was indicated by the heavy deformations of the used copper plate and needles which were used in the analysis (except **9**, **12**, and **17**, which deflagrated only sharply).

Table 4. Overview of the hot plate and hot needle test results for **3–7, 9, 12,** and **17–23**.[a]

compound	HP	HN	compound	HP	HN
3	det.	det.	**17**	def.	def.
4	det.	def.	**18**	det.	det.
5	det.	det.	**19**	det.	det.
6	det.	det.	**20**	det.	det.
7	def.	det.	**21**	det.	def.
9	def.	def.	**22**	det.	det.
12	def.	def.	**23**	det.	det.

[a] def.: deflagration; det.: detonation.

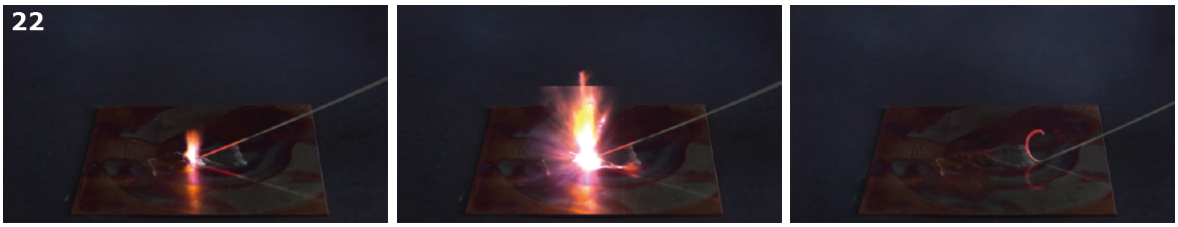


Figure 23. Moment of detonation of compound **22** during the hot needle (HN) initiation shown in sequence.

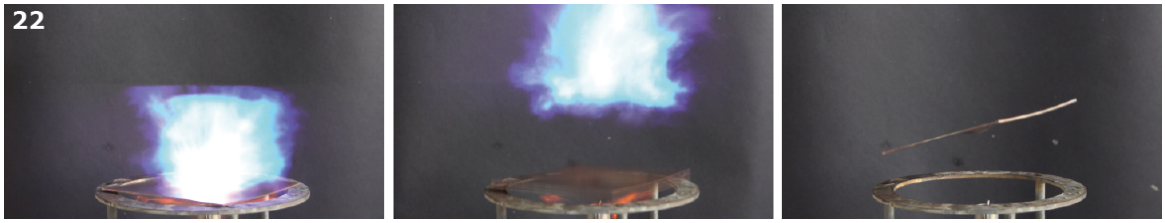


Figure 24. Moment of detonation of complex **22** during the hot plate (HP) test shown in sequence.

On the basis of the positive results of the hot needle and hot plate tests, which gave a first indication of its suitability as a primary explosive, the initiation capability for most of the promising compounds toward pentaerythritol tetranitrate (PETN) as the main charge in copper shells was explored (Figure 25). Additional details on the test procedures can be found in the Experimental Section of the SI.

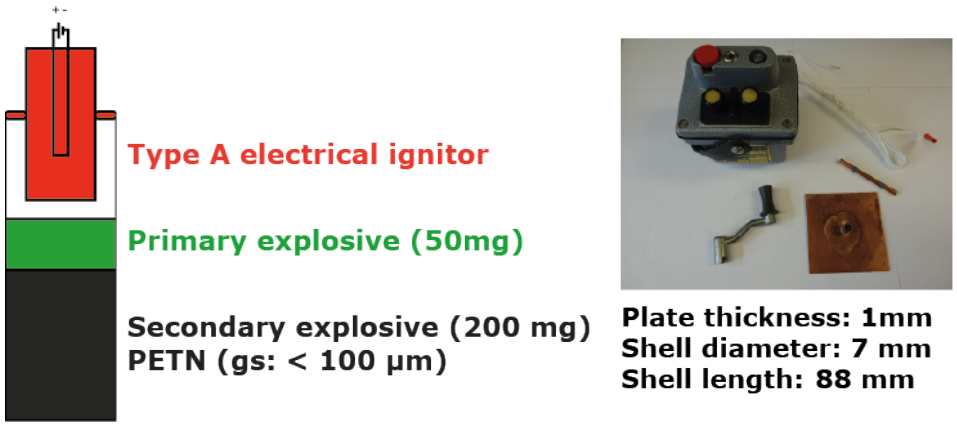


Figure 25. PETN initiation capability test setup.

Positive initiation tests caused by a DDT of PETN indicated by a hole in the witness plate and fragmentation of the copper shell (Figure 26 and Figure S49–52) were observed for **3**, **5**, **6**, **9**, **17**–**19**, and **21**–**23**. Energetic coordination compounds bearing nitrates as anions are usually unable to initiate common secondary explosives, due to their lack of performance. Thus, it is even more astounding that both copper(II) nitrate complexes **9** and **17**, which show great promise for the future, were able to initiate PETN. Negative test results, indicated by intact copper shells and plates were surprisingly obtained for the perchlorate complexes **4**, **7** and **20**. An overview of the test results can be found in Table 5.

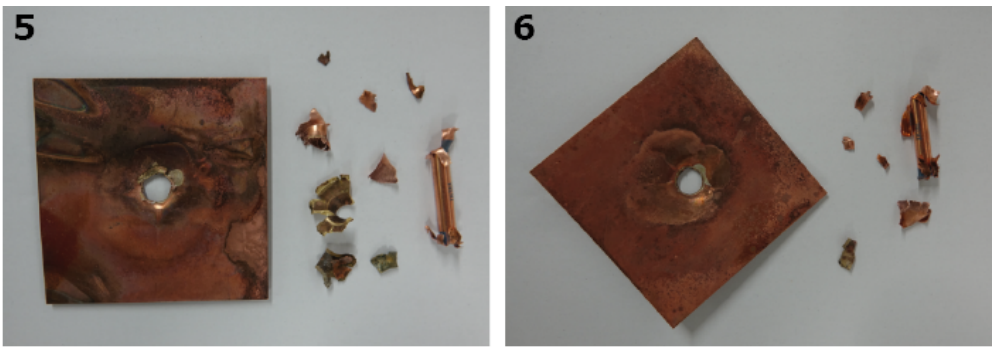


Figure 26. Positive PETN initiation tests for the coordination compounds **5** and **6**.

Table 5. Results of PETN initiation tests of **3–7**, **9** and **17–23**.[a]

compound	initiation	compound	initiation
3	pos.	**18**	pos.
4	neg.	**19**	pos.
5	pos.	**20**	neg.
6	pos.	**21**	pos.
7	neg.	**22**	pos.
9	pos.	**23**	pos.
17	pos.		

[a] pos.: positive; neg.: negative.

16.2.7 Toxicity

In order to evaluate the toxicity of the synthesized complexes, the toxicological impact on aquatic organisms of the two uncoordinated nitrogen-rich ligands **1** and **2** was measured using the commonly known luminescence marine bacterium *Vibrio Fischeri* NRRL-B-11177 strain.[43] Both tetrazoles can be classified as non-toxic (toxicity level after 30 min exposure: very toxic < 0.10 g/L; toxic 0.10–1.00 g/L; non-toxic > 1.00 g/L) with half the maximal effective concentration values EC_{50} of 4.58 g/L for **1** and 3.87 g/L for **2** determined after an incubation time of 30 minutes. The values obtained lie within the range of 1-methyl-5*H*-

tetrazole, the methylated analogue of 1,5*H*-tetrazole,[15] and confirm the recently observed trend of higher toxicities for 2-subsituted tetrazoles in comparison to their 1-subsituted isomers.[44]

16.2.8 Laser Initiation

The optical initiation of energetic materials has received considerable attention in the last decades and a lot of research has been done from many scientists all over the world.[18, 44–46] Laser initiation has several advantages over classical ignition methods (thermal or mechanical) and could therefore be of great interest for industrial applications (e.g. laser ignitable ammunition or optical detonators).[20] All here investigated compounds suffer from their increased sensitivities toward mechanical stimuli making them highly suitable for application as lead-free primaries but unfortunately not for any use in laser ignition systems. Therefore, the focus of this contribution was placed on more academic questions like the laser ignitibility of the complexes at different energy thresholds. Only selected colored coordination compounds showed a response to laser irradiation differing in the required energy input depending on the isomer/metal(II)/anion combination. A summary of the performed experiments is given in Table 6.

Table 6. Laser initiation test results.

compound	0.15 mJ	0.17 mJ	26 mJ
5	det.	—	det.
6	det.	—	det.
9	det.	det.	—
16	—	—	x
17	x	det.	—
18	x	det.	—
19	det.	—	—
21	det.	—	—
23	x	det.	—

(–: not tested, x: no ignition, dec.: decomposition, deflag.: deflagration, det.: detonation). Operating parameters: current I = 6–7 A; voltage U = 4 V; theoretical maximal output power P_{max} = 45 W; theoretical energy E_{max} = 0.15–26 mJ; wavelength λ = 915 nm; pulse length τ = 0.1–15 ms.

More details on the experimental setup can be found in the Supporting Information. All complexes investigated except the copper(II) chloride complex **16** detonated heavily under the employed settings resulting in deformations of the sample holder and destruction of the optical lens and sapphire glass due to the extreme powerful nature of the complexes (Figure 27, Figure S53–57). The complexes exhibited similar initiation thresholds and could be ignited at the lowest applicable initiation energy settable in the parameters of the laser. Even the very

sensitive copper(II) nitrate complexes **9** and **17** were successfully be initiated and are therefore one of the rare examples of laser-ignitable nitrate complexes in literature.[47,48]

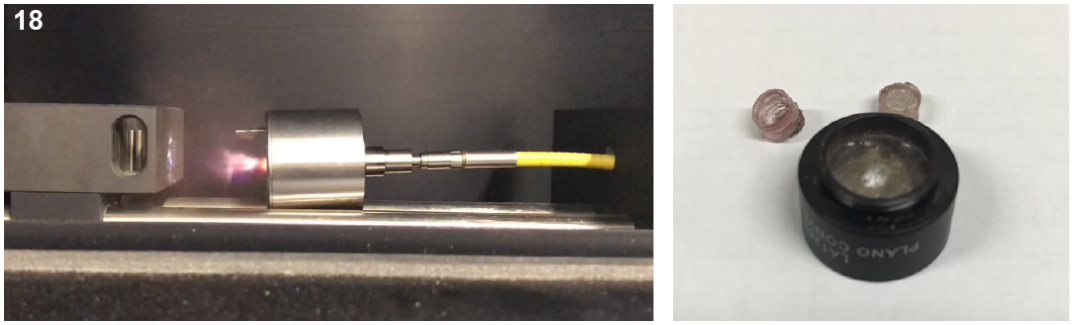


Figure 27. Moment of detonation of complex **18** (left) and destroyed lens and sample holder (right) caused by the tremendous shockwave.

16.2.9 UV-Vis Spectroscopy

The UV-Vis spectra in the solid state, illustrated in Figure 28 and S58, were measured for selected laser-ignitable complexes in the range of 350–1000 nm with regard to any possible correlation between the laser ignitability and the absorption of the compounds at the corresponding wavelength. The investigated optical properties of the complexes are compiled and summarized in Table 7. The examined energetic coordination compounds showed typical absorptions in the NIR, visible and ultra-violet region resulting from the corresponding d-d transitions, which are highly dependent on the implemented 3d metal(II), anion and isomeric ligand. The exact mechanism of the underlying laser initiation process (e.g. thermal, electronical) is still questionable and has not been understood completely.[49,50]

Table 7. Measured optical properties of complexes **5, 6, 8, 9, 16, 17–19, 21** and **23**.

compound	M	color	$\lambda_{d\text{-}d}{}^{a}$	$\lambda_{915}/\lambda_{d\text{-}d}{}^{b}$
5	Fe^{II} (hs)	yellowish	871	0.97
6	Cu^{II}	blue	677	0.27
8	Cu^{II}	green	768	0.92
9	Cu^{II}	blue	686	0.68
16	Cu^{II}	green	796	0.63
17	Cu^{II}	blue	689	0.50
18	Cu^{II}	blue	647	0.37
19	Fe^{II} (hs)	yellowish	868	0.95
21	Fe^{II} (hs)	yellowish	795	0.93
23	Cu^{II}	blue	655	0.35

[a] Absorption intensity maximum wavelength, which can be assigned to electron d-d transitions in the measured range of 350–1000 nm; [b] quotient of the absorption intensity at the laser wavelength and the intensity at the d-d absorption wavelength.

All investigated complexes show a moderate absorption in the laser wavelength region of 915 nm, which could be a possible explanation for the laser ignitibility of the coordination compounds since none of the colorless complexes (Mn^{II} or Zn^{II}) could be initiated. The laser ignitibility is not only linked to its absorption behavior but also to several other parameters like the coordination sphere of the corresponding transition metal(II) or its electronic configuration. One plausible explanation of the laser ignitibility of the complexes and imaginable initiation pathway could be the formation of several hot spots in the material caused by photothermal excitations after irradiation. It should be emphasized that contrary to literature assumings, complexes bearing the nitrate anion could be ignited.[47] Additional studies in the future should be carried out to obtain further information regarding the initiation process, which should cover the influence of the complexes´ structure and the type of the mechanism.

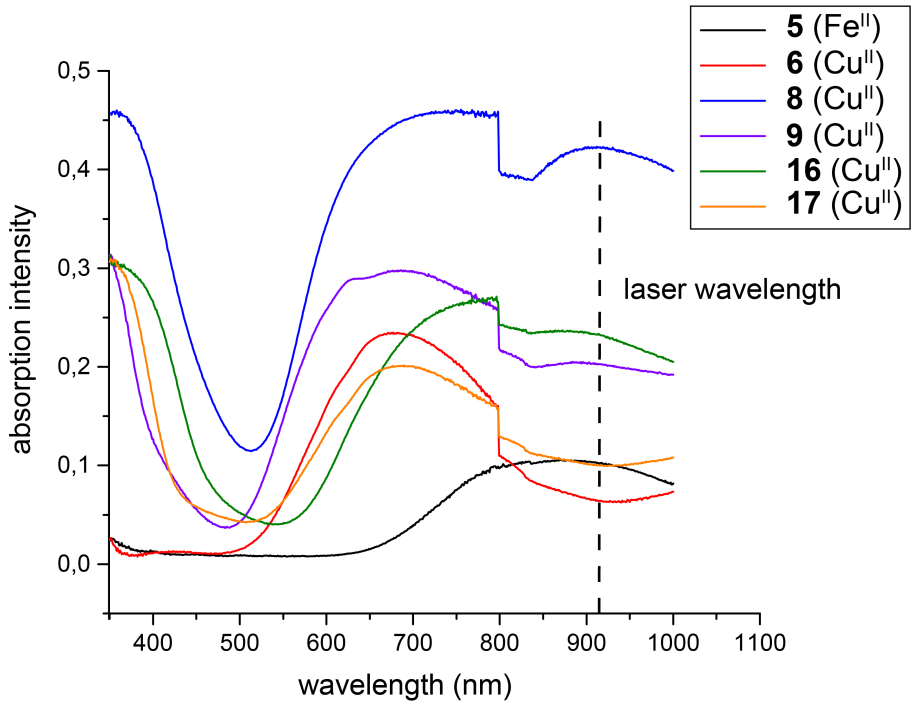


Figure 28. Solid state UV-Vis spectra of selected copper(II) and iron(II) complexes. The step in the absorption intensity at 800 nm is caused by a detector change. The UV-Vis spectra have only qualitative character.

16.3 Conclusions

Two isomeric amino-5*H*-tetrazoles (1-amino-5*H*-tetrazole (**1**, 1-AT) and 2-amino-5*H*-tetrazole (**2**, 2-AT)) with sensitivities already in the range of primary explosives were synthesized in a

simple one step reaction starting from 1,5*H*-tetrazole and the commercially available amination reagent hydroxylamine-*O*-sulfonic acid (HOSA). The obtained isomeric mixture was purified by column chromatography, preventing the highly risky distillation mentioned in the literature and yielded the products in satisfying yields. Due to the great potential of 1-AT as ligand in powerful energetic transition metal(II) complexes, a selective, upscalable and isomerically pure route toward this highly endothermic compound has been developed. The received nitrogen-rich aminoazoles were comprehensively characterized by diverse analytical methods enclosing heteronuclear ^{15}N NMR spectroscopy, X-ray studies and toxicity determinations. The toxicity assessments toward aquatic organisms revealed the non-toxicity of both heterocycles. Transition metal(II) complexes based on 1-methyl-5*H*-tetrazole as ligand have shown great promise in the past but had not enough power to be appropriate candidates as lead-free primary explosives. As obvious and logical consequence, *N*-aminoazoles with a higher nitrogen content exhibiting the powerful outer N–N single bond have been incorporated into the equivalent complexes resulting in a tremendous performance increase releasing several of the most energetic coordination compounds synthesized so far. The present study features the preparation, analysis and evaluation of 20 new lead, nickel and cobalt-free energetic complexes, which are built-up by two isomeric aminotetrazoles, four different metals and six varying anions. The synthesized complexes, which show a great coordination sphere diversity depending on the inserted components, can be prepared by an easily upscalable and low-cost synthetic route. The strategy of energetic coordination compounds (ECC), which enables the fine-tuning of the optical and energetic properties through easy change of the building blocks (metal, anion and ligand) has proved once again its suitability in the difficult and challenging research area of lead-free primary explosives. The synthesis of the metal(II) perchlorate coordination compounds based on 2-amino-5*H*-tetrazole were highly dependent on the reaction conditions like stoichiometry or solvent system and yielded either aqua complexes or co-crystallized species. Single X-ray studies in combination with powder diffraction and electron microscopy of the auspicious and mostly water-free complexes gave interesting insights and allowed correlations between the observed structure and their sensitivity against mechanical stimuli. After comparing all compounds, the following trends can be formulated: i.) iron(II) and copper(II) complexes are more sensitive than manganese(II) and zinc(II) coordination compounds; ii.) the more oxidizing the anion, the more sensitive the compound; iii.) complexes with 1-AT are more sensitive than those with 2-AT, which can be attributed to the anhydrous nature of those. Laser initiation experiments executed with NIR light at a wavelength of 915 nm showed fast deflagration-to-detonation transitions at extremely low energy thresholds for most

of the coordination compounds and destroyed large parts of the laser setup due to the destructive power of the complexes. The initiation capability toward pentaerythritol tetranitrate (PETN) filled copper shell detonators was tested for several pre-selected complexes (hot plate and hot needle experiments) and demonstrated the enormous potential of the synthesized complexes as lead-free primary explosive replacements. Besides the lead-free, but not completely environmentally friendly perchlorate compounds, the nitrato complexes show excellent properties and can therefore be considered as promising primary explosive candidates.

Supporting information available in the appendix in **Chapter 19.13** and under:

www.rsc.org/suppdata/c8/ta/c8ta06326e/c8ta06326e1.pdf

16.4 References

[1] T. D. Ngo, M. Nofar, M. T. Ton-That, M. Sepehr, W. Hu and J. Denault, presented in part at the 68th Annu. Tech. Conf. - Soc. Plast. Eng., Orlando, May, 2010.

[2] A. K. Mohanty, M. Misra and L. T. Drzal, *J. Polym. Environ.*, 2002, **10**, 19.

[3] SVHC identification, https://echa.europa.eu/substances-of-very-high-concern-identification-explained (accessed March, 2018).

[4] Understanding REACH, https://echa.europa.eu/regulations/reach/understanding-reach, (accessed March, 2018).

[5] REACH Evaluation, https://echa.europa.eu/regulations/reach/evaluation, (accessed March, 2018).

[6] SVHC identification, https://echa.europa.eu/substances-of-very-high-concern-identification-explained, (accessed March, 2018).

[7] SVHC List, https://echa.europa.eu/candidate-list-table, (accessed March, 2018).

[8] J. W. Fronabarger, M. D. Williams, W. B. Sanborn, J. G. Bragg, D. A. Parrish and M. Bichay, *Propellants, Explos., Pyrotech.*, 2011, **36**, 541.

[9] Y. Tang, C. He, L. A. Mitchell, D. A. Parrish and J. n. M. Shreeve, *Angew. Chem., Int. Ed.*, 2016, **55**, 5565.

[10] R. Haiges and K. O. Christe, *Inorg. Chem.*, 2013, **52**, 7249.

[11] D. Chen, H. Yang, Z. Yi, H. Xiong, L. Zhang, S. Zhu and G. Cheng, *Angew. Chem., Int. Ed.*, 2018, **57**, 2081.

[12] J.-G. Xu, C. Sun, M.-J. Zhang, B.-W. Liu, X.-Z. Li, J. Lu, S.-H. Wang, F.-K. Zheng and G.-C. Guo, *Chem. Mater.*, 2017, **29**, 9725.

[13] M. H. V. Huynh, M. A. Hiskey, D. E. Chavez, D. L. Naud and R. D. Gilardi, *J. Am. Chem. Soc.*, 2005, **127**, 12537.

[14] M. H. V. Huynh, M. D. Coburn, T. J. Meyer and M. Wetzler, *Proc. Natl. Acad. Sci.*, 2006, **103**, 10322.

[15] N. Szimhardt, M. H. H. Wurzenberger, A. Beringer, L. J. Daumann and J. Stierstorfer, *J. Mater. Chem. A*, 2017, **5**, 23753.

[16] Q. Zhang and J. n. M. Shreeve, *Angew. Chem., Int. Ed.*, 2014, **53**, 2540.

[17] K. A. McDonald, S. Seth and A. J. Matzger, *Cryst. Growth Des.*, 2015, **15**, 5963.

[18] T. W. Myers, J. A. Bjorgaard, K. E. Brown, D. E. Chavez, S. K. Hanson, R. J. Scharff, S. Tretiak and J. M. Veauthier, *J. Am. Chem. Soc.*, 2016, **138**, 4685.

[19] I. A. Ugryumov, M. A. Ilyushin, I. V. Tselinskii and A. S. Kozlov, *Russ. J. Appl. Chem.*, 2003, **76**, 439.

[20] R. Schirra and H. Zöllner, presented in part at the 42nd International Pyrotechnics Seminar, Colorado, July, 2016.

[21] A. Y. Zhilin, M. A. Ilyushin, I. V. Tselinskii, A. S. Kozlov and N. E. Kuz'mina, *Russ. J. Appl. Chem.*, 2002, **75**, 1849.

[22] K. Karaghiosoff, T. M. Klapötke and C. M. Sabaté, *Chem. Eur. J.*, 2009, **15**, 1164.

[23] M. A. Ilyushin, I. V. Bachurina, A. V. Smirnov, I. V. Tselinsky and I. V. Shugalei, *Cent. Eur. J. Energ. Mater.*, 2009, **7**, 33.

[24] P. N. Gaponik, M. M. Degtyarik, A. S. Lyakhov, V. E. Matulis, O. A. Ivashkevich, M. Quesada and J. Reedijk, *J. Inorg. Chim. Acta*, 2005, **358**, 3949.

[25] A. Hahma, and E. Karvinen, Diehl BGT Defence GmbH & Co. KG, EU Pat., 2450329A2, 2012.

[26] A. Y. Zhilin, M. A. Ilyushin, I. V. Tselinskii, A. S. Kozlov and I. S. Lisker, *Russ. J. Appl. Chem.*, 2003, **76**, 572.

[27] A. V. Smirnov, M. A. Ilyushin and I. V. Tselinskii, *Russ. J. Appl. Chem.*, 2004, **77**, 794.

[28] J. G. Zhang, J. Y. Li, Y. Zang, Y. J. Shu, T. L. Zhang, L. Yang and P. P. Power, *Z. Anorg. Allg. Chem.*, 2010, **636**, 1147.

[29] M. H. V. Huynh, Los Alamos National Security LLC, WIPO Pat., 2008143724A2, 2008.

[30] M. H. V. Huynh, Los Alamos National Security LLC, US Pat., 20080200688A1, 2008.

[31] K. Wang, D. Zeng, J.-G. Zhang, Y. Cui, T.-L. Zhang, Z.-M. Li and X. Jin, *Dalton Trans.*, 2015, **44**, 12497.

[32] I. Hagedorn and H. D. Winkelmann, *Chem. Ber.*, 1966, **99**, 850.

[33] R. Raap, *Can. J. Chem.*, 1969, **47**, 3677.

[34] T. M. Klapötke, D. G. Piercey and J. Stierstorfer, *Dalton Trans.*, 2012, **41**, 9451.

[35] P. N. Gaponik and V. P. Karavai, *Khim. Geterotsikl. Soedin.*, 1983, **6**, 841.

[36] M. H. H. Wurzenberger, N. Szimhardt and J. Stierstorfer, *J. Am. Chem. Soc.*, 2018, **140**, 3206.

[37] Crystallographic data for the structures have been deposited with the Cambridge Crystallographic Data Centre. Copies of the data can be obtained free of charge on application to The Director, CCDC, 12 Union Road, Cambridge CB2 1EZ, UK (Fax: int.code_(1223)336-033; e-mail for inquiry: fileserv@ccdc.cam.ac.uk; e-mail for deposition: (depos-it@ccdc.cam.ac.uk).

[38] M. H. Palmer and S. Parsons, *Acta Crystallogr.*, 1996, **52**, 2818-2822.

[39] T. M. Klapötke, C. M. Sabate and J. Stierstorfer, *Z. Anorg. Allg. Chem.*, 2016, **634**, 1867.

[40] P. N. Gaponik, M. M. Degtyarik, A. S. Lyakhov, V. E. Matulis, O. A. Ivashkevich, M. Quesada and J. Reedijk, *Inorg. Chim. Acta*, 2005, **358**, 3949.

[41] N. Szimhardt and J. Stierstorfer, *Chem. Eur. J.*, 2017, **24**, 2687.

[42] R. Meyer, J. Köhler and A. Homburg, *Explosives*, Wiley-VCH, Weinheim, 5th edn, 2002.

[43] G. I. Sunahara, S. Dodard, M. Sarrazin, L. Paquet, G. Ampleman, S. Thiboutot, J. Hawari and A. Y. Renoux, *Ecotoxicol. Environ. Saf.*, 1998, **39**, 185.

[44] N. Szimhardt, M. H. H. Wurzenberger, T. M. Klapötke, J. T. Lechner, H. Reichherzer, C. C. Unger and J. Stierstorfer, *J. Mater. Chem. A*, 2018, **6**, 6565.

[45] T. W. Myers, K. E. Brown, D. E. Chavez, R. J. Scharff and J. M. Veauthier, *Inorg. Chem.*, 2017, **56**, 2297.

[46] M. A. Ilyushin and I. V. Tselinskii, *Zh. Prikl. Khim.*, 2000, **73**, 1233.

[47] T. W. Myers, K. E. Brown, D. E. Chavez, R. J. Scharff and J. M. Veauthier, *Eur. J. Inorg. Chem.*, 2016, **2016**, 3178.

[48] T. W. Myers, D. E. Chavez, S. K. Hanson, R. J. Scharff, B. L. Scott, J. M. Veauthier and R. Wu, *Inorg. Chem.*, 2015, **54**, 8077.

[49] S. R. Ahmad and M. Cartwright, *Laser Ignition of Energetic Materials*, John Wiley & Sons, Hoboken, 2014.

[50] E. D. Aluker, A. G. Krechetov, A. Y. Mitrofanov, D. R. Nurmukhametov and M. M. Kuklja, *J. Phys. Chem. C*, 2011, **115**, 6893.

17 Use of a Copper(II) Azide Complex as a Primary Explosive

Thomas M. Klapötke, Jörg Stierstorfer, Norbert Szimhardt and Maximilian H. H. Wurzenberger

EP 18150491.1 and EP 18151497.7

Abstract

The invention concerns the use of a copper(II) azide complex as a primary explosive, wherein the copper(II) azide complex is of general formula $Cu_a(N_3)_{2a}(L)_x$, wherein L is a ligand, a = 1 to 6 and x = 1 to 6.

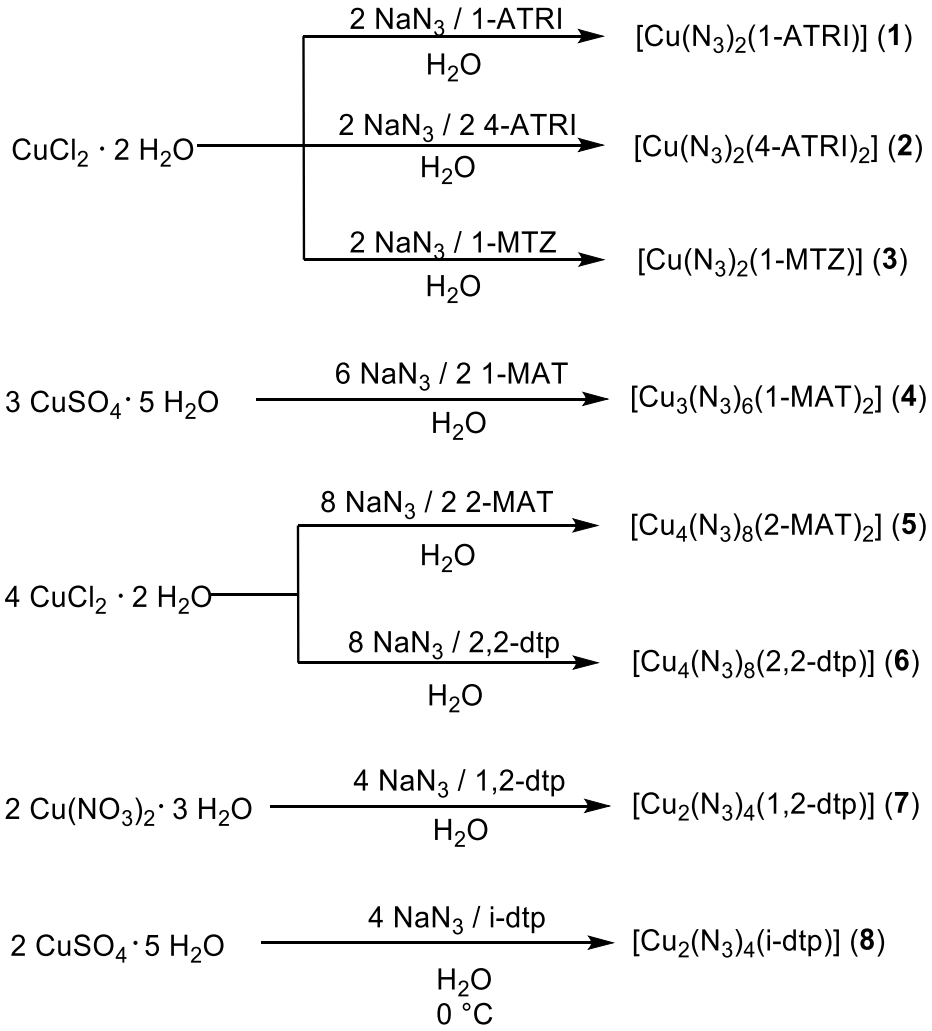


Figure 1. Shows schematically syntheses of a copper(II) azide complex comprising the following ligands: 1-ATRI: 1-amino-1,2,3-triazole; 4-ATRI: 4-amino-1,2,4-triazole; 1-MTZ: 1-methyltetrazole; 1-MAT: 1-methyl-5-aminotetrazole; 2-MAT: 2-methyl-5-aminotetrazole; 1,2-dtp: 1-(tetrazol-1-yl)-3-(tetrazol-2-yl)propane; 2,2-dtp: 1,3-di(tetrazol-2-yl)propane; i-dtp: 1,1'-(propane-1,2-diyl)bis(tetrazole).

17.1 Introduction

The invention concerns the use of copper(II) azide complex as a primary explosive, a new copper(II) azide complex, a method for synthesizing a copper(II) azide complex and a ligand for the formation of a copper(II) azide complex.

From Puszynski, M. M., *et al.*, J. J. Inorg. Chem. 2016, 1(1): 003 tetraazido(1,2-di(1*H*-tetrazol-1-yl)ethane)dicopper(II) is known. The intent of the authors was to replace lead styphnate in the M42 primer, while maintaining other compounds in the formulation. Experiments in which the copper salt was used in primer cups showed that the primer cups suffered a firing pin perforation and punched-out on majority of the fired primers. Though the authors stated that further investigation into the failure of the primer integrity is required to provide a full understanding, they concluded that the copper salt may be suited as lead azide replacement candidate. However, no solution for the observed problem of primer cup punch-out was provided.

Wu, Bi-Dong, *et al.*, Z. Anorg. Allg. Chem. 2014, 640, (7), 1467 to 1473 discloses synthesis of six multi-ligand coordination compounds of the general formula $[M_3(AMTz)_4(N_3)_6]$, wherein M is Cu, Co, Ni, Zn, Mn, and Cd and wherein AMTz is 4-amino-3,5-dimethyl-1,2,4-triazole. It has been observed by sensitivity measuring that the compounds were insensitive.

The most applied primary explosive in percussion caps still is lead styphnate. Lead styphnate is reliable, cheap, easy to manufacture and shows perfect initiation behavior. However, the compound was put on the candidate list of authorization (substances of very high concern, Annex XIV) for the REACH (Registration, Evaluation, Authorization and Restriction of Chemicals) regulations in 2011 due to its toxicity and its significant contamination of the environment.

"Green" alternatives for lead containing primer mixtures were introduced onto the market in the past, using diazodinitrophenol (DDNP) as primary explosive and tetrazene as sensitizer. A mixture by the former Dynamit Nobel company with these ingredients is called SINTOX®. However, DDNP and tetrazene, suffer from various disadvantages. DDNP for example can cause allergic reactions and pollutes the groundwater. Tetrazene has a poor thermal stability and low initiation efficiency.

The problem to be solved by the present invention is to provide a substance that can be used as a primary detonator or igniter, the use of such a substance, a method for synthesizing such a

substance and a ligand for the formation of such a substance. The substance shall be able to replace lead styphnate and/or lead azide in a primary detonator or igniter.

The problem is solved by the features of claims 1, 11, 12 and 15 of the present invention. Embodiments of the invention are subject-matter of claim 2 to 10, 13 and 14.

According to the invention a use of a copper(II) azide complex as a primary explosive is provided, wherein the copper(II) azide complex is of general formula $Cu_a(N_3)_{2a}(L)_x$, wherein L is a ligand, a = 1 to 6, in particular 1 to 5, in particular 1 to 4, and x = 1 to 6,

- wherein L consists of an azole or comprises at least one azole moiety, wherein in case of presence of more than one azole moiety the azole moieties are directly linked, linked via a single carbon, single nitrogen or single oxygen atom or linked via a carbon atoms comprising linker which linker comprises at least 3 carbon atoms or at least one aromatic structure

or

- wherein L comprises more than one azole moiety, wherein the azole moieties are linked via a linker which linker comprises or consists of at least 3 nitrogen atoms or comprises at least 2 carbon atoms and one oxygen atom

or

- wherein L comprises more than one azole moiety, wherein the azole moieties are linked via a linker which linker comprises 2 carbon atoms or comprises or consists of 2 nitrogen atoms, wherein at least one of the azole moieties is substituted

or

- wherein L is 1,2-di(tetrazol-1-yl)ethane (1,1-dte), 1,2-di(tetrazol-2-yl)ethane (2,2-dte) or 1-(tetrazol-1-yl)-2-(tetrazol-2-yl)ethane (1,2-dte), a = 2 and the copper(II) azide complex is contained in a mixture consisting of 5% by weight to 25% by weight, in particular 10% by weight to 25% by weight, in particular 14% by weight to 20% by weight, in particular 15% by weight to 18% by weight, of the copper(II) azide complex and for the rest of Al or another reducing agent, $Ba(NO_3)_2$ or another oxidizing agent, Sb_2S_3 or a further reducing agent, pentaerythritol tetranitrate (PETN) or another energetic compound and a binding agent, wherein tetrazene is not present in the mixture

or

- wherein L is 1,2-di(tetrazol-1-yl)ethane (1,1-dte), 1,2-di(tetrazol-2-yl)ethane (2,2-dte) or 1-(tetrazol-1-yl)-2-(tetrazol-2-yl)ethane (1,2-dte), a = 2 and the copper(II) azide complex is contained in a mixture consisting of 90% by weight to 99% by weight, in particular 93% by weight to 98% by weight, in particular 95% by weight to 98% by weight, in particular 95% by weight to 97% by weight, of the copper(II) azide complex and for the rest of a binding agent.

The single carbon atom or single nitrogen atom linking the azole moieties is understood as atom which binding sites not occupied by azole moieties are occupied by hydrogen atoms. A substituted azole or azole moiety is understood as an azole or an azole moiety in which a hydrogen atom bound to a carbon or nitrogen atom is substituted by another atom or an atom group. The inventors found in particular that an unwanted high sensitivity and/or maximum pressure occurring during reaction of the primary explosive can be prevented when at least one acidic proton, i. e. a hydrogen atom bound to nitrogen or oxygen, is substituted by another atom or an atom group and in particular when all of the acidic protons are substituted by other atoms or atom groups.

The azole may be pyrrol, imidazole, pyrazole, 1,2,3-triazole, 1,2,4-triazole or pentazole and the azole moiety may be any moiety of pyrrol, imidazole, pyrazole, 1,2,3-triazole, 1,2,4-triazole, tetrazole or pentazole.

Al or the other reducing agent, such as Mg, B, Zr, Ti, Si, Ce and/or another metal and/or an alloy thereof and/or a metal hydride, usually functions as fuel.

The primary explosive may be a primary detonator compound or igniter compound in a primary detonator device or an igniter device. A use as primary explosive can replace lead styphnate in percussion or in igniting mixtures for a propelling charge e. g. in small arm ammunition (e. g. for rifles, pistols etc.) or big bore ammunition (e. g. for mortars etc.) as well as in gas generators, airbags and chemical oxygen generators. A use as main component in a priming composition can replace lead azide in such a composition, e. g., in a stab detonator or in a bridgewire detonator.

By the use according to the invention it is possible to provide a primary explosive for igniter and detonator devices which is free of lead and of the known primary explosives such as diazodinitrophenol (DDNP) or diazodinitrophenolate, potassium-5,7-dinitro-[2,1,3]-benzoxadiazole-4-olate-3-oxide, potassium dinitrobenzofuroxanate, tetrazene and copper(I) 5-

nitrotetrazolate (DBX-1). DDNP and diazodinitrophenolate are light sensitive and not compatible with many desired further substances.

The binding agent can be any binding agent known in the art, e. g. paraffin, dextrin, nitrocellulose, a polyacetate or a polyvinyl comprising compound such as polyvinylacetate. The inventors have recognized that the problems known from Puszynski, M. M., *et al.* can be solved either by the specific design of the ligand indicated in the first, second, third or fifth alternative of claim 1 or by the specific mixture given in the fourth alternative of claim 1. An important feature of the specific mixture is the absence of tetrazene present in the mixture known from Puszynski, M. M., *et al.*.

In an embodiment the azole, the azole moiety, the azole moieties or at least one of the azole moieties is/are substituted by a substituent at least at one position. The substituent may be an alkyl, in particular an alkyl comprising 1 to 4 carbon atoms or an amino, azido or hydrazino group.

In an embodiment the ligand comprises at least two azole moieties, in particular two azole moieties or three azole moieties.

The linker may comprise 3 carbon atoms or at least one aromatic structure.

The ligand L may be selected from a group consisting of 1,4-di(tetrazol-1-yl)butane (1,1-dtb), 1,1'-(propane-1,2-diyl)bis(tetrazole) (1,1,-idtp), 4,4'-bi(1,2,4-triazole) (BTz), 1-methyltetrazole (1-MTZ), 2-methyl-5-aminotetrazole (2-MAT), 4-amino-1,2,4-triazole (4-ATRI), 1-methyl-5-aminotetrazole (1-MAT), 1,3-di(tetrazol-2-yl)propane (2,2-dtp), 1-(tetrazol-1-yl)-3-(tetrazol-2-yl)propane (1,2-dtp), 1,3-di(tetrazol-1-yl)propane (1,1-dtp), 1-ethyltetrazole (1-ETZ), 1-amino-1,2,3-triazole (1-ATRI), 1-amino-1,2,4-triazole (1A-1,2,4-TRI), 3,5-dimethyl-1,2,4-triazol-4-amine (admtrz), 3,5-di(pyridin-4-yl)-1,2,4-triazol-4-amine (4-abpt), 4-(1,2,4-triazol-4-yl)pyridine (2-ptrz), 5-(1-methylpyridin-1-ium-4-yl)-tetrazol-5-ide (mptz), 1,4-bis((1,2,4-triazol-1-yl)methyl)benzene (btix), 1*H*-tetrazole (TZ), 1-(1-(tetrazol-2-yl)propan-2-yl)-tetrazole (1,2-idtp), 2,2'-(propane-1,2-diyl)bis(tetrazole) (2,2-idtp), 1-(tetrazol-1-yl)-4-(tetrazol-2-yl)butane (1,2-dtb), 1,4-di(tetrazol-2-yl)butane (2,2-dtb), 1-isopropyltetrazole (1-iPTZ), 1-propyltetrazole (1-PTZ), 1-aminotetrazole (1-AT), 2-aminotetrazole (2-AT), 2-methyltetrazole (2-MTZ), 1,5-diaminotetrazole (1,5-DAT), 2,5-diaminotetrazole (2,5-DAT), (tetrazol-1-yl)methanol (HMTZ), 1,1'-(2-methylpropane-1,2-diyl)bis(tetrazole) (1,1-idtb), 1-(2-methyl-1-(tetrazol-2-yl)propan-2-yl)-tetrazole (1,2-idtb), 2,2'-(2-methylpropane-1,2-diyl)bis(tetrazole) (2,2-idtb), 3,4-diamino-1,2,4-triazole (DATRI), 3,4,5-triamino-1,2,4-

triazole (TATRI), 4-methyl-1,2,4-triazole (MeTRI), 2-amino-1,2,3-triazole (2-ATRI), 1-(1,2,4-triazol-4-yl)-1,2,3-triazole (1,4-BTz), 1,4'-bi(1,2,4-triazole) (iBTz), 2-(1,2,4-triazol-4-yl)-1,2,3-triazole (2,4-BTz), 1-(4-methyl-1,2,4-triazol-3-yl)-tetrazole (MeTRITZ), 4-methyl-5-(tetrazol-1-yl)-1,2,4-triazol-3-amine (AMeTRITZ), para-phenylenbitetrazole (p-PBT), meta-phenylenbitetrazole (m-PBT), ortho-phenylenbitetrazole (o-PBT), tris(2-(tetrazol-1-yl)ethyl)amine (TETA), di(1*H*-tetrazol-1-yl)methane (1,1-dtm), 1-((2*H*-tetrazol-2-yl)methyl)-1H-tetrazole (1,2-dtm), di(2*H*-tetrazol-2-yl)methane (2,2-dtm), 1-(2-azidomethyl)-1*H*-tetrazole (AMT), 1-(2-azidoethyl)-1*H*-tetrazole (AET), 1-(3-azidopropyl)-1H-tetrazole (APT), 1-(4-azidobutyl)-1H-tetrazole (ABT), 1,2-(di-5-methylhydrazinotetrazol-1-yl)ethane (1,1-dmhte) and 3-hydrazino-4-amino-1,2,4-triazole (3-HATri).

In an embodiment L is neither 1,1-dte nor 2,2-dte nor 1,2-dte and the copper(II) azide complex is used as a primary explosive in a detonation mixture in an amount exceeding 75% by weight to an amount of 99% by weight, wherein the detonation mixture further comprises a stabilizing agent and/or a binding agent. Alternatively, the copper(II) azide complex may be used as a primary explosive in an igniting mixture in an amount of 5% by weight to 75% by weight, in particular 5% by weight to 50% by weight, wherein the igniting mixture further comprises an oxidizing agent and a reducing agent and optionally a further energetic compound and/or a friction agent and/or a stabilizing agent and/or a binding agent and/or a sensibilizing agent. The oxidizing agent may comprise or consist of KNO_3, NH_4NO_3, $Sr(NO_3)_2$, $Ba(NO_3)_2$ and/or another nitrate, ZnO_2, BaO_2 and/or another peroxide, $CaSO_4$ and/or another sulfate, Fe_2O_3, Fe_3O_4, CeO_2, WO_3, SnO_2, SiO_2, MnO_2, $KMnO_4$, CuO, Bi_2O_3, KO_2 and/or another oxide, $KClO_3$ and/or another chlorate and/or $KClO_4$, NH_4ClO_4 and/or another perchlorate. The reducing agent may comprise or consist of Al, Mg, B, Zr, Ti, Si, Ce and/or another metal and/or an alloy thereof, a metal hydride and/or S_8, Sb_2S_3 and/or another sulfur containing compound. The further energetic compound is designated as further energetic compound because the copper(II) azide complex is considered as first energetic compound in the igniting mixture. The further energetic compound may comprise or consist of pentaerythritol tetranitrate (PETN), hexogen, octogen and/or nitrocellulose. The friction agent can comprise or consist of glass powder, Sb_2S_3, $CaSi_2$ and/or boron nitride. The stabilizing agent can comprise or consist of dextrin and/or graphite. The binding agent may comprise or consist of paraffin, dextrin, nitrocellulose, a polyacetate and/or a polyvinyl comprising compound and the sensibilizing agent can comprise or consist of tetrazene.

In the case wherein L is 1,1-dte, 2,2-dte or 1,2-dte the other reducing agents, the other oxidizing agent, the further reducing agent and the other energetic compound may be selected from the above mentioned reducing agents other than Al and Sb_2S_3, from the above mentioned oxidizing agents other than $Ba(NO_3)_2$, and from the above mentioned further energetic compound other than PETN.

In an specific embodiment the oxidizing agent is KNO_3, the reducing agent is boron and the further energetic compound is PETN. Alternatively, the oxidizing agent is $Ba(NO_3)_2$, the reducing agent comprises Al and Sb_2S_3 and the further energetic compound is PETN. Both specific compositions may be with or without tetrazene.

In the case wherein L is 1,1-dte, 2,2-dte or 1,2-dte Al or the other reducing agent may be present in an amount of 6% by weight to 8% by weight, $Ba(NO_3)_2$ or the other oxidizing agent may be present in an amount of 27% by weight to 37% by weight, Sb_2S_3 or the further reducing agent may be present in an amount of 13% by weight to 17% by weight, pentaerythritol tetranitrate (PETN) or the other energetic compound may be present in an amount of 4% by weight to 6% by weight and the binding agent may be present in an amount of 0.1% by weight to 1% by weight in the mixture. A molar ratio of Al : $Ba(NO_3)_2$: Sb_2S_3 : PETN in the mixture may be 2600 : 1200 : 400 : 158 or about 2600 : 1200 : 400 : 158.

The invention further concerns a copper(II) azide complex, wherein the copper(II) azide complex is $Cu(N_3)_2$(4-amino-1,2,4-triazole)$_2$ or $Cu_3(N_3)_6$(4-amino-1,2,4-triazole)$_2$*H_2O or is of general formula $Cu_a(N_3)_{2a}(L)_x$, wherein L is a ligand, a = 1 to 6, in particular 1 to 5, in particular 1 to 4, and x = 1 to 6, wherein L is selected from a group consisting of 1,1'-(propane-1,2-diyl)bis(tetrazole) (1,1,-idtp), 4,4'-bi(1,2,4-triazole) (BTz), 1-methyltetrazole (1-MTZ), 2-methyl-5-aminotetrazole (2-MAT), 1-methyl-5-aminotetrazole (1-MAT), 1,3-di(tetrazol-2-yl)propane (2,2-dtp), 1-(tetrazol-1-yl)-3-(tetrazol-2-yl)propane (1,2-dtp), 1,3-di(tetrazol-1-yl)propane (1,1-dtp), 1-ethyltetrazole (1-ETZ), 1-amino-1,2,3-triazole (1-ATRI), 1-amino-1,2,4-triazole (1A-1,2,4-TRI), 1-(1-(tetrazol-2-yl)propan-2-yl)-tetrazole (1,2-idtp), 2,2'-(propane-1,2-diyl)bis(tetrazole) (2,2-idtp), 1-(tetrazol-1-yl)-4-(tetrazol-2-yl)butane (1,2-dtb), 1,4-di(tetrazol-2-yl)butane (2,2-dtb), 1-isopropyltetrazole (1-iPTZ), 1-propyltetrazole (1-PTZ), 1-aminotetrazole (1-AT), 2-aminotetrazole (2-AT), 2-methyltetrazole (2-MTZ), 1,5-diaminotetrazole (1,5-DAT), 2,5-diaminotetrazole (2,5-DAT), (tetrazol-1-yl)methanol (HMTZ), 1,1'-(2-methylpropane-1,2-diyl)bis(tetrazole) (1,1-idtb), 1-(2-methyl-1-(tetrazol-2-yl)propan-2-yl)-tetrazole (1,2-idtb), 2,2'-(2-methylpropane-1,2-diyl)bis(tetrazole) (2,2-idtb), 3,4-diamino-1,2,4-triazole (DATRI), 3,4,5-triamino-1,2,4-triazole (TATRI), 4-methyl-1,2,4-

triazole (MeTRI), 2-amino-1,2,3-triazole (2-ATRI), 1-(1,2,4-triazol-4-yl)-1,2,3-triazole (1,4-BTz), 1,4'-bi(1,2,4-triazole) (iBTz), 2-(1,2,4-triazol-4-yl)-1,2,3-triazole (2,4-BTz), 1-(4-methyl-1,2,4-triazol-3-yl)-tetrazole (MeTRITZ), 4-methyl-5-(tetrazol-1-yl)-1,2,4-triazol-3-amine (AMeTRITZ), para-phenylenbitetrazole (p-PBT), meta-phenylenbitetrazole (m-PBT), ortho-phenylenbitetrazole(o-PBT), tris(2-(tetrazol-1-yl)ethyl)amine (TETA), di(1*H*-tetrazol-1-yl)methane (1,1-dtm), 1-((2*H*-tetrazol-2-yl)methyl)-1H-tetrazole (1,2-dtm), di(2*H*-tetrazol-2-yl)methane (2,2-dtm), 1-(2-azidomethyl)-1*H*-tetrazole (AMT), 1-(2-azidoethyl)-1*H*-tetrazole (AET), 1-(3-azidopropyl)-1H-tetrazole (APT), 1-(4-azidobutyl)-1*H*-tetrazole (ABT), 1,2-(di-5-methylhydrazinotetrazol-1-yl)ethane (1,1-dmhte) and 3-hydrazino-4-amino-1,2,4-triazole (3-HATri).

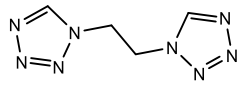
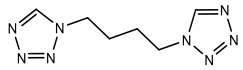
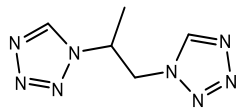
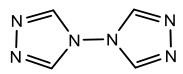
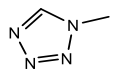
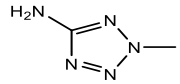
The invention further concerns a method for synthesizing a copper(II) azide complex, wherein the copper(II) azide complex is of general formula $Cu_a(N_3)_{2a}(L)_x$, wherein L is a ligand, a = 1 to 6, in particular 1 to 5, in particular 1 to 4, and x = 1 to 6, wherein a copper(II) salt and the ligand are dissolved in water, an alcohol, in particular methanol, ethanol or a propanol, or acetonitrile thus forming a first solution, an azide is dissolved in water, an alcohol, in particular methanol, ethanol or a propanol, or acetonitrile thus forming a second solution, wherein the first solution is agitated and the second solution is added to the first solution resulting in the precipitation of the copper(II) azide complex.

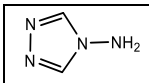
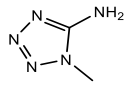
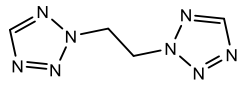
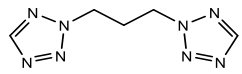
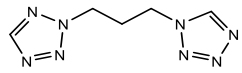
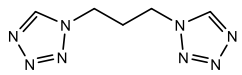
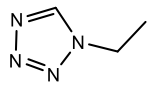
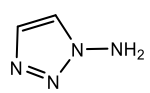
The copper(II) salt may be a chloride, a sulfate, a nitrate, an acetate, a perchlorate or a carbonate and/or the azide may be sodium azide, lithium azide, potassium azide or hydrazoic acid.

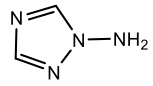
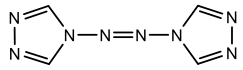
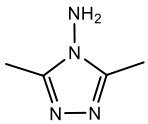
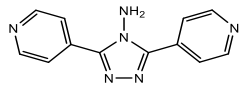
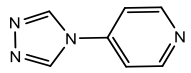
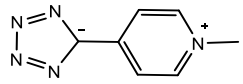
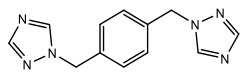
In an embodiment of the method the copper(II) azide complex is separated from the mixed first and second solutions. The separation may be performed by filtration and washing. Subsequently the separated copper(II) azide complex may be dried.

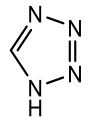
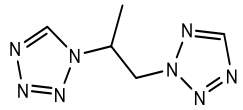
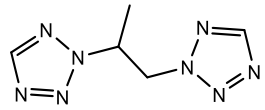
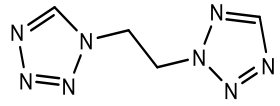
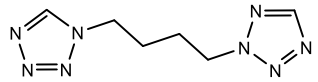
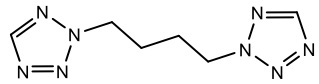
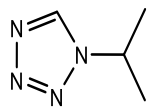
The invention further concerns a ligand for the formation of a copper(II) azide complex of general formula $Cu_a(N_3)_{2a}(L)_x$, wherein L is the ligand, a = 1 to 6, in particular 1 to 5, in particular 1 to 4, and x = 1 to 6, wherein the ligand is 1-(1-(tetrazol-2-yl)propan-2-yl)-tetrazole (1,2-idtp), 2,2'-(propane-1,2-diyl)bis(tetrazole) (2,2-idtp), 1-(2-methyl-1-(tetrazol-2-yl)propan-2-yl)-tetrazole (1,2-idtb), 2,2'-(2-methylpropane-1,2-diyl)bis(tetrazole) (2,2-idtb), 1-(1,2,4-triazol-4-yl)-1,2,3-triazole (1,4-BTz), 1-(4-methyl-1,2,4-triazol-3-yl)-tetrazole (MeTRITZ), 4-methyl-5-(tetrazol-1-yl)-1,2,4-triazol-3-amine (AMeTRITZ), di(1*H*-tetrazol-1-yl)methane (1,1-dtm), 1-((2*H*-tetrazol-2-yl)methyl)-1H-tetrazole (1,2-dtm), di(2*H*-tetrazol-2-yl)methane (2,2-dtm), 1-(3-azidopropyl)-1H-tetrazole (APT) or 1-(4-azidobutyl)-1*H*-tetrazole (ABT).

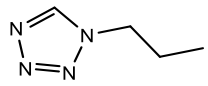
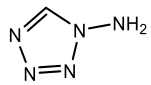
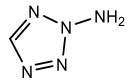
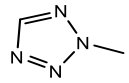
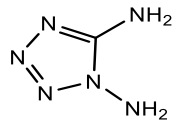
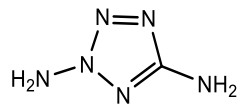
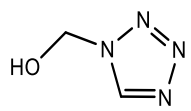
The following table shows possible ligands, complexes and molecular formula of specific ligands and corresponding copper(II) azide complexes according to the invention or that can be used according to the invention:

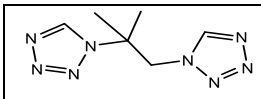
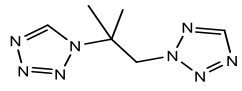
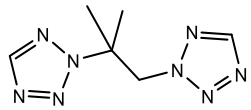
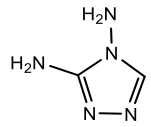
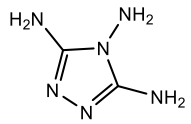
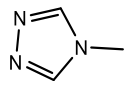
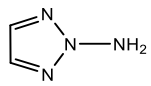
Ligand	**Complex**	**Molecular Formula**
1,1-dte  1,2-di(tetrazol-1-yl)ethane ($C_4H_6N_8$)	$[Cu_2(N_3)_4(1,1\text{-dte})]$	$C_4H_6Cu_2N_{20}$
1,1-dtb  1,4-di(tetrazol-1-yl)butane ($C_6H_{10}N_8$)	$[Cu_2(N_3)_4(1,1\text{-dtb})]$	$C_6H_{10}Cu_2N_{20}$
1,1,-idtp  1,1'-(propane-1,2-diyl)bis(tetrazole) ($C_5H_8N_8$)	$[Cu_2(N_3)_4(1,1\text{-idtp})]$	$C_5H_8Cu_2N_{20}$
BTz  4,4'-bi(1,2,4-triazole) ($C_4H_4N_6$)	1. $[Cu_2(N_3)_4(BTz)]$ 2. $([Cu(N_3)_2(BTz)])$	$C_4H_4Cu_2N_{18}$ $C_4H_4CuN_{12}$
1-MTZ  1-methyltetrazole ($C_2H_4N_4$)	$[Cu(N_3)_2(1\text{-MTZ})]$	$C_2H_4CuN_{10}$
2-MAT  2-methyl-5-aminotetrazole ($C_2H_5N_5$)	$[Cu_2(N_3)_4(2\text{-MAT})]$	$C_2H_5Cu_2N_{17}$
4-ATRI	$[Cu(N_3)_2(4\text{-ATRI})_2)]$	$C_4H_8CuN_{14}$

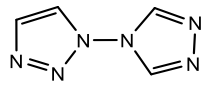
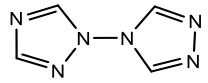
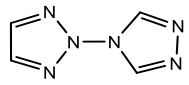
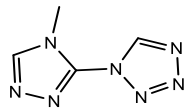
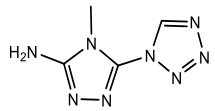
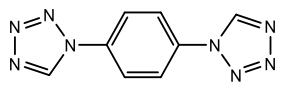
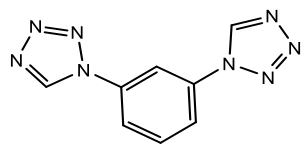
 4-amino-1,2,4-triazole ($C_2H_4N_4$)		
1-MAT  1-methyl-5-aminotetrazole ($C_2H_5N_5$)	1. $[Cu_3(N_3)_6(1\text{-MAT})_2]$ 2. $([Cu_3(N_3)_6(1\text{-MAT})_4] \cdot H_2O)$	$C_4H_{10}Cu_3N_{28}$ $C_8H_{22}Cu_3N_{38}O$
2,2-dte  1,2-di(tetrazol-2-yl)ethane ($C_4H_6N_8$)	$[Cu_4(N_3)_8(2,2\text{-dte})]$	$C_4H_6Cu_4N_{32}$
2,2-dtp  1,3-di(tetrazol-2-yl)propane ($C_5H_8N_8$)	$[Cu_4(N_3)_8(2,2\text{-dtp})]$	$C_5H_8Cu_4N_{32}$
1,2-dtp  1-(tetrazol-1-yl)-3-(tetrazol-2-yl)propane ($C_5H_8N_8$)	$[Cu_2(N_3)_4(1,2\text{-dtp})]$	$C_5H_8Cu_2N_{20}$
1,1-dtp  1,3-di(tetrazol-1-yl)propane ($C_5H_8N_8$)	$[Cu_2(N_3)_4(1,1\text{-dtp})]$	$C_5H_8Cu_2N_{20}$
1-ETZ  1-ethyltetrazole ($C_3H_6N_4$)	$[Cu(N_3)_2(1\text{-ETZ})]$	$C_3H_6CuN_{10}$
1-ATRI  1-amino-1,2,3-triazole ($C_2H_4N_4$)	$[Cu(N_3)_2(1\text{-ATRI})]$	$C_2H_4CuN_{10}$

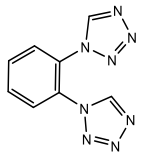
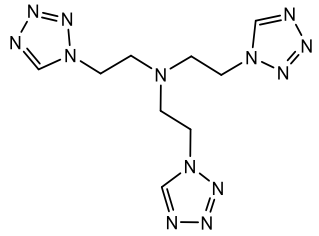
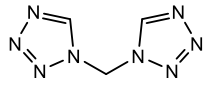
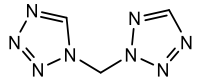
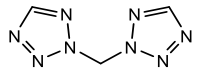
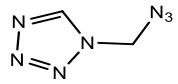
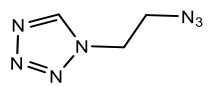
1A-1,2,4-TRI  1-amino-1,2,4-triazole ($C_2H_4N_4$)	$[Cu_2(N_3)_4(1A\text{-}1,2,4\text{-}TRI)]$	$C_2H_4Cu_2N_{16}$
ABTz  1,2-di(1,2,4-triazol-4-yl)diazene ($C_4H_4N_8$)	$[Cu(N_3)_2(atrz)_3]$	$C_{12}H_{12}CuN_{30}$
admtrz  3,5-dimethyl-1,2,4-triazol-4-amine ($C_4H_8N_4$)	1. $[Cu_3(N_3)_6(admtrz)_4]$ 2. $([Cu_2(N_3)_4(admtrz)_2])$	1. $C_{16}H_{32}Cu_3N_{34}$ 2. $C_8H_{16}Cu_2N_{20}$
4-abpt  3,5-di(pyridin-4-yl)-1,2,4-triazol-4-amine ($C_{12}H_{10}N_6$)	$[Cu(N_3)_2(4\text{-}abpt)] \cdot 2\ H_2O$	$C_{12}H_{14}CuN_{12}O_2$
2-ptrz  4-(1,2,4-triazol-4-yl)pyridine ($C_7H_6N_4$)	$[Cu_3(N_3)_6(2\text{-}ptrz)_2]$	$C_{14}H_{12}Cu_3N_{26}$
mptz  5-(1-methylpyridin-1-ium-4-yl)-tetrazol-5-ide ($C_7H_7N_5$)	$[Cu(N_3)_2(mptz)]$	$C_7H_7CuN_{11}$
btix  1,4-bis((1,2,4-triazol-1-yl)methyl)benzene ($C_{12}H_{12}N_6$)	$[Cu(N_3)_2(btix)_2]$	$C_{24}H_{24}CuN_{18}$
TZ	$[Cu(N_3)(TZ)]$	CH_2CuN_7

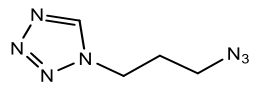
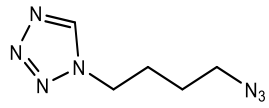
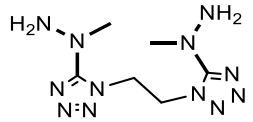
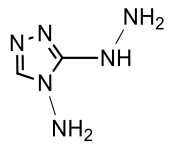
 1H-tetrazole (CH_2N_4)		
1,2-idtp  1-(1-(tetrazol-2-yl)propan-2-yl)-tetrazole ($C_5H_8N_8$)	$[Cu_2(N_3)_4(1,2\text{-idtp})]$	$C_5H_8Cu_2N_{20}$
2,2-idtp  2,2'-(propane-1,2-diyl)bis(tetrazole) ($C_5H_8N_8$)	$[Cu_4(N_3)_8(2,2\text{-idtp})]$	$C_5H_8Cu_4N_{32}$
1,2-dte  1-(tetrazol-1-yl)-2-(tetrazol-2-yl)ethane ($C_4H_6N_8$)	$[Cu_2(N_3)_4(1,2\text{-dte})]$	$C_4H_6Cu_2N_{20}$
1,2-dtb  1-(tetrazol-1-yl)-4-(tetrazol-2-yl)butane ($C_6H_{10}N_8$)	$[Cu_2(N_3)_4(1,2\text{-dtb})]$	$C_6H_{10}Cu_2N_{20}$
2,2-dtb  1,4-di(tetrazol-2-yl)butane ($C_6H_{10}N_8$)	$[Cu_4(N_3)_8(2,2\text{-dtb})]$	$C_6H_{10}Cu_4N_{32}$
1-iPTZ  1-isopropyltetrazole ($C_4H_8N_4$)	$[Cu(N_3)_2(1\text{-iPTZ})]$	$C_4H_8CuN_{10}$
1-PTZ	$[Cu(N_3)_2(1\text{-PTZ})]$	$C_4H_8CuN_{10}$

 1-propyltetrazole ($C_4H_8N_4$)		
1-AT  1-aminotetrazole (CH_3N_5)	$[Cu(N_3)_2(1\text{-AT})]$	CH_3CuN_{11}
2-AT  2-aminotetrazole (CH_3N_5)	$[Cu_2(N_3)_4(2\text{-AT})]$	$CH_3Cu_2N_{17}$
2-MTZ  2-methyltetrazole ($C_2H_4N_4$)	$[Cu_2(N_3)_4(2\text{-MTZ})]$	$C_2H_4Cu_2N_{16}$
1,5-DAT  1,5-diaminotetrazole (CH_4N_6)	$[Cu_2(N_3)_4(1,5\text{-DAT})]$	$CH_4Cu_2N_{18}$
2,5-DAT  2,5-diaminotetrazole (CH_4N_6)	$[Cu_2(N_3)_4(2,5\text{-DAT})]$	$CH_4Cu_2N_{18}$
HMTZ  (tetrazol-1-yl)methanol ($C_2H_4N_4O$)	$[Cu(N_3)_2(HMTZ)]$	$C_2H_4CuN_{10}O$
1,1-idtb	$[Cu_2(N_3)_4(1,1\text{-idtb})]$	$C_6H_{10}Cu_2N_{20}$

 1,1'-(2-methylpropane-1,2-diyl)bis(tetrazole) ($C_6H_{10}N_8$)		
1,2-idtb  1-(2-methyl-1-(tetrazol-2-yl)propan-2-yl)-tetrazole ($C_6H_{10}N_8$)	$[Cu_2(N_3)_4(1,2\text{-idtb})]$	$C_6H_{10}Cu_2N_{20}$
2,2-idtb  2,2'-(2-methylpropane-1,2-diyl)bis(tetrazole) ($C_6H_{10}N_8$)	$[Cu_4(N_3)_8(2,2\text{-idtb})]$	$C_6H_{10}Cu_4N_{32}$
DATRI  3,4-diamino-1,2,4-triazole ($C_2H_5N_5$)	$[Cu_2(N_3)_4(DATRI)]$	$C_2H_5Cu_2N_{17}$
TATRI  3,4,5-triamino-1,2,4-triazole ($C_2H_6N_6$)	$[Cu_2(N_3)_4(TATRI)]$	$C_2H_6Cu_2N_{18}$
MeTRI  4-methyl-1,2,4-triazole ($C_3H_5N_3$)	$[Cu_2(N_3)_4(MeTRI)]$	$C_3H_5Cu_2N_{15}$
2-ATRI  2-amino-1,2,3-triazole ($C_2H_4N_4$)	$[Cu(N_3)_2(2\text{-ATRI})]$	$C_2H_4CuN_{10}$

1,4-BTz  1-(1,2,4-triazol-4-yl)-1,2,3-triazole ($C_4H_4N_6$)	$[Cu_2(N_3)_4(1,4\text{-BTz})]$	$C_4H_4Cu_2N_{18}$
iBTz  1,4'-bi(1,2,4-triazole) ($C_4H_4N_6$)	$[Cu_2(N_3)_4(iBTz)]$	$C_4H_4Cu_2N_{18}$
2,4-BTz  2-(1,2,4-triazol-4-yl)-1,2,3-triazole ($C_4H_4N_6$)	$[Cu_2(N_3)_4(2,4\text{-BTz})]$	$C_4H_4Cu_2N_{18}$
MeTRITZ  1-(4-methyl-1,2,4-triazol-3-yl)-tetrazole ($C_4H_5N_7$)	$[Cu_2(N_3)_4(MeTRITZ)]$	$C_4H_5Cu_2N_{19}$
AMeTRITZ  4-methyl-5-(tetrazol-1-yl)-1,2,4-triazol-3-amine ($C_4H_6N_8$)	$[Cu_2(N_3)_4(AMeTRITZ)]$	$C_4H_6Cu_2N_{20}$
p-PBT  para-phenylenbitetrazole ($C_8H_6N_8$)	$[Cu_2(N_3)_4(p\text{-PBT})]$	$C_8H_6Cu_2N_{20}$
m-PBT  meta-phenylenbitetrazole ($C_8H_6N_8$)	$[Cu_2(N_3)_4(m\text{-PBT})]$	$C_8H_6Cu_2N_{20}$

o-PBT  ortho-phenylenbitetrazole ($C_8H_6N_8$)	$[Cu_2(N_3)_4(o\text{-}PBT)]$	$C_8H_6Cu_2N_{20}$
TETA  tris(2-(tetrazol-1-yl)ethyl)amine ($C_9H_15N_{13}$)	$[Cu_3(N_3)_6(TETA)]$	$C_9H_{15}Cu_3N_{31}$
1,1-dtm  di(1H-tetrazol-1-yl)methane ($C_3H_4N_8$)	$[Cu_2(N_3)_4(1,1\text{-}dtm)]$	$C_3H_4Cu_2N_{20}$
1,2-dtm  1-((2H-tetrazol-2-yl)methyl)-1H-tetrazole ($C_3H_4N_8$)	$[Cu_2(N_3)_4(1,2\text{-}dtm)]$	$C_3H_4Cu_2N_{20}$
2,2-dtm  di(2H-tetrazol-2-yl)methane ($C_3H_4N_8$)	$[Cu_2(N_3)_4(2,2\text{-}idtm)]$	$C_3H_4Cu_2N_{20}$
AMT  1-(2-azidomethyl)-1*H*-tetrazole ($C_2H_3N_7$)	$[Cu_2(N_3)_4(AMT)]$	$C_3H_5Cu_2N_{19}$
AET 	$[Cu_2(N_3)_4(AET)]$	$C_2H_3Cu_2N_{19}$

1-(2-azidoethyl)-1*H*-tetrazole ($C_3H_5N_7$)		
APT  1-(3-azidopropyl)-1*H*-tetrazole ($C_4H_7N_7$)	$[Cu_2(N_3)_4(APT)]$	$C_4H_7Cu_2N_{19}$
ABT  1-(4-azidobutyl)-1*H*-tetrazole ($C_5H_9N_7$)	$[Cu_2(N_3)_4(ABT)]$	$C_5H_9Cu_2N_{19}$
1,1-dmhte  1,2-(di-5-methylhydrazinotetrazol-1-yl)ethane ($C_6H_{14}N_{12}$)	$[Cu_2(N_3)_4(1,1\text{-dmhte})]$	$C_6H_{14}Cu_2N_{28}$
3-HATri  3-hydrazino-4-amino-1,2,4-triazole ($C_2H_6N_6$)	$[Cu(N_3)_2(3\text{-HATRI})]$	$C_2H_6CuN_{12}$

17.2 Synthesis

Some of the ligands are commercially available, e. g. from the following sources:

1-ATRI: https://www.abcr.de/shop/de/1H-1-2-3-Triazol-1-amine-707315.html/

4-ATRI: http://www.tcichemicals.com/eshop/de/de/commodity/A1137/

1-MTZ: https://www.abcr.de/shop/de/1-Methyl-1H-tetrazole-97-410116.html/

1-MAT: https://www.abcr.de/shop/de/1-Methyl-1H-tetrazol-5-amine-98.html/

2-MAT: https://www.abcr.de/shop/de/5-Amino-2-methyl-2H-tetrazole-98-499286.html/

All chemicals and solvents were employed as received (Sigma-Aldrich, Fluka, Acros, ABCR). ^{1}H and ^{13}C NMR spectra were recorded with neat solids as samples at ambient temperature using a JEOL Eclipse 270, JEOL EX 400 or a JEOL Eclipse 400 instrument. The chemical shifts quoted in ppm in the text refer to typical standards such as tetramethylsilane (^{1}H, ^{13}C). Dehydration, melting and decomposition temperatures of the described compounds were measured through differential thermal analysis (DTA) with an OZM Research DTA 552-Ex instrument. The samples were measured in a range of 25–400 °C at a heating rate of 5 °C min^{-1}. Infrared spectra were measured with pure samples on a Perkin-Elmer BXII FT-IR system with a Smith DuraSampler IR II diamond ATR. Determination of the carbon, hydrogen, nitrogen and sulfur contents was carried out by combustion analysis using an Elementar Vario El (nitrogen values determined are often lower than the calculated ones due to their explosive behavior). UV-Vis spectra were recorded in the solid state using a Varian Cary 500 spectrometer in the wavelength range of 350–1000 nm. Impact sensitivity tests were carried out according to STANAG 4489[1] modified instruction[2] using a BAM (Bundesanstalt für Materialforschung) drophammer.[3] Friction sensitivity tests were carried out according to STANAG 4487[4] modified instruction[5] using the BAM friction tester. The classification of the tested compounds results from the "UN Recommendations on the Transport of Dangerous Goods".[6] Additionally all compounds were tested upon the sensitivity toward electrical discharge using the Electric Spark Tester ESD 2010 EN.[7] All the obtained coordination compounds were washed with water, dried overnight in air and used for analytics without further purification.

General procedure for the preparation of complexes 1 to 8:

The numbering of complexes **1** to **8** is according to Fig. 1. Stoichiometric amounts for the theoretical synthesis of 0.25 mmol of the coordination compounds were used. Copper(II) chloride dihydrate (**1**–**3**, **5**), copper(II) sulfate pentahydrate (**4**, **8**) or copper(II) nitrate trihydrate (**7**) and the ligand were stirred mechanically in 7 mL water, the corresponding quantity of sodium azide, dissolved in 1 mL water, was added dropwise within 1 min and the suspension was stirred for 15 min. The precipitated complex compounds were filtered off, washed with water (3 x 2 mL) and dried in air.

Single crystals growth of **1**, **3**, **4** and **6**–**8** were achieved by overlaying an aqueous solution (8 mL) of sodium azide and the ligand with an ethanolic solution (8 mL) of copper(II) chloride dihydrate, separated by a mixture (4 mL) of water/ethanol (50/50). After 7 to 14 days crystals suitable for X-ray determination were obtained.

[Cu(N$_3$)$_2$(1-ATRI)] (1)

Complex compound **1** was obtained as dark brown precipitate. Yield: 46.8 mg (0.20 mmol, 81 %).

DTA (5 °C min^{-1}) onset: 123 °C (dec.); IR (ATR, cm^{-1}): $\tilde{\nu}$= 3326 (w), 3267 (w), 3164 (vw), 3148 (vw), 2102 (vs), 2069 (vs), 1621 (w), 1509 (vw), 1483 (vw), 1469 (vw), 1336 (w), 1286 (w), 1264 (m), 1239 (vw), 1174 (vw), 1138 (m), 1079 (w), 1045 (vw), 983 (m), 967 (w), 864 (vw), 785 (m), 776 (m), 701 (w), 674 (w), 650 (w), 629 (vw), 600 (w), 591 (w); EA ($C_2H_4CuN_{10}$, 231.67): calcd: C 10.37, H 1.74, N 60.46 %; found: C 10.40, H 1.81, N 56.77 %; BAM drophammer: 3 J; friction tester: < 5 N; ESD: 5 mJ (at grain size < 100 µm).

[Cu(N$_3$)$_2$(4-ATRI)$_2$] (2)

From the reaction mixture, product **2** could be isolated as a green powder. Yield: 60.5 mg (0.19 mmol, 77 %). Slow evaporation of the mother liquor gave green needle-like crystals within 10 days suitable for X-ray determination.

DTA (5 °C min^{-1}) onset: 161 °C (dec.); IR (ATR, cm^{-1}): $\tilde{\nu}$= 3321 (w), 3223 (w), 3123 (w), 3090 (w), 3036 (w), 2975 (w), 2058 (s), 1803 (w), 1711 (w), 1621 (w), 1530 (w), 1463 (w), 1386 (w), 1349 (w), 1319 (w), 1289 (w), 1220 (m), 1192 (w), 1102 (vw), 1066 (m), 1030 (w), 962 (s), 906 (m), 860 (m), 681 (w), 670 (vw), 647 (w), 619 (vs), 607 (m); EA ($C_4H_8CuN_{14}$, 315.75): calcd: C 15.22, H 2.55, N 62.10 %; found: C 15.46, H 2.60, N 59.57 %; BAM drophammer: 10 J; friction tester: > 360 N; ESD: 300 mJ (at grain size < 100 µm).

[Cu(N$_3$)$_2$(1-MTZ)] (3)

The copper(II) azide complex **3** was received as a brown solid. Yield: 47.2 mg (0.20 mmol, 81 %).

DTA (5 °C min^{-1}) onset: 157 °C (dec.); IR (ATR, cm^{-1}): $\tilde{\nu}$= 3120 (w), 2075 (s), 2045 (vs), 1814 (w), 1570 (vw), 1522 (w), 1476 (w), 1424 (w), 1344 (w), 1297 (w), 1284 (m), 1177 (m), 1107 (m), 1066 (w), 1022 (w), 1000 (m), 912 (w), 716 (vw), 682 (m), 656 (m), 604 (w); EA

($C_2H_4CuN_{10}$, 231.67): calcd: C 10.37, H 1.74, N 60.46 %; found: C 10.59, H 1.95, N 58.05 %; BAM drophammer: 1 J; friction tester: < 5 N; ESD: 20 mJ (at grain size < 100 µm).

$[Cu_4(N_3)_8(2\text{-MAT})_2]$ (5)

Complex **5** was obtained as a brown precipitate. Yield: 164 mg (0.21 mmol, 83 %). Suitable crystals in the form of red rods for X-ray diffraction were picked directly out of the reaction mixture.

DTA (5 °C min^{-1}) onset: 161 °C (dec.); IR (ATR, cm^{-1}): $\tilde{\nu}$ = 3415 (m), 3338 (m), 3291 (w), 3245 (w), 3182 (w), 2102 (vs), 2053 (s), 2036 (s), 1634 (s), 1554 (m), 1439 (w), 1425 (m), 1416 (w), 1376 (w), 1352 (w), 1326 (w), 1294 (m), 1266 (m), 1193 (m), 1128 (w), 1105 (w), 1070 (w), 1022 (w), 901 (w), 812 (m), 751 (w), 694 (w), 675 (w), 648 (m); EA ($C_4H_{10}Cu_4N_{36}$, 788.55) calc.: C 6.09, H 1.28, N 60.39 %; found: C 6.67, H 1.58, N 57.57 %; BAM drophammer: < 1 J; friction tester: < 5 N; ESD: 13 mJ (at grain size < 100 µm).

$[Cu_4(N_3)_8(2,2\text{-dtp})]$ (6)

Compound **6** was received as a brown solid. Yield: 151 mg (0.20 mmol, 78 %).

DTA (5 °C min^{-1}) onset: 195 °C (dec.); IR (ATR, cm^{-1}): $\tilde{\nu}$= 3143 (w), 2121 (vs), 2096 (vs), 2056 (s), 2044 (m), 2005 (w), 1573 (w), 1465 (w), 1444 (w), 1386 (w), 1349 (w), 1304 (w), 1278 (m), 1201 (w), 1167 (w), 1158 (vw), 1141 (w), 1083 (vw), 1053 (w), 1017 (w), 962 (w), 910 (w), 848 (w), 758 (vw), 694 (m), 680 (w), 650 (w), 589 (w), 577 (w); EA ($C_3H_{10}Cu_4N_{32}$, 770.53): calcd: C 7.79, H 1.05, N 58.17 %; found: -; BAM drophammer: 1 J; friction tester: < 5 N; ESD: 5 mJ (at grain size < 100 µm).

$[Cu_2(N_3)_4(1,2\text{-dtp})]$ (7)

Product **7** precipitated as a brown powder out of the mother liquor. Yield: 103 mg (0.22 mmol, 86 %).

DTA (5 °C min^{-1}) onset: 146 °C (dec.); IR (ATR, cm^{-1}): $\tilde{\nu}$= 3151 (w), 3126 (vw), 2088 (s), 2046 (vs), 1572 (vw), 1500 (w), 1466 (vw), 1451 (w), 1439 (w), 1379 (w), 1356 (w), 1339 (w),

1292 (m), 1205 (w), 1183 (w), 1167 (w), 1147 (w), 1103 (w), 1083 (vw), 1054 (vw), 1039 (vw), 1025 (w), 1003 (vw), 983 (m), 908 (w), 899 (w), 872 (vw), 829 (w), 700 (m), 685 (w), 662 (m), 642 (w), 601 (w), 586 (w); EA ($C_5H_8Cu_2N_{20}$, 475.35): calcd: C 12.63, H 1.70, N 58.93 %; found: C 13.14, H 1.85, N 57.93 %; BAM drophammer: 3 J; friction tester: < 5 N; ESD: 18 mJ (at grain size < 100 µm).

$[Cu_2(N_3)_4$(i-dtp)] (8)

Azide complex **8** was isolated as a brown precipitate. Yield: 84.8 mg (0.18 mmol, 71 %).

DTA (5 °C min^{-1}) onset: 165 °C (dec.); IR (ATR, cm^{-1}): $\tilde{\nu}$= 3362 (vw), 3318 (vw), 3100 (w), 3012 (vw), 2976 (vw), 2089 (s), 2072 (s), 2041 (vs), 1825 (vw), 1498 (w), 1464 (w), 1444 (w), 1397 (w), 1372 (vw), 1345 (w), 1281 (m), 1202 (w), 1182 (m), 1124 (w), 1107 (w), 1091 (m), 1054 (vw), 1041 (w), 1005 (m), 911 (w), 792 (vw), 715 (vw), 681 (m), 666 (m), 602 (w), 589 (w); EA ($C_5H_8Cu_2N_{20}$, 475.35): calcd: C 12.63, H 1.70, N 58.93 %; found: C 13.14, H 1.80, N 57.90 %; BAM drophammer: 2 J; friction tester: < 5 N; ESD: 5 mJ (at grain size < 100 µm).

General procedure applicable for the synthesis of N1-substituted tetrazoles exemplarily described for 1,4-di(tetrazol-1-yl)butane (1,1-dtb):

The ligand 1,1-dtb has been synthesized with slight modifications according to the literature procedure of Kamiya and Saito:[8] 1,4-diamino-butane (1.76 g, 0.02 mol) and sodium azide (1.76 g, 0.02 mol) have been suspended in triethyl orthoformate (30 g, 0.20 mol) and afterwards treated with glacial acetic acid (40 mL) under stirring. After heating the reaction mixture overnight at 75 °C, the solvent has been removed and the remaining residue was washed with cold water. After filtration of the water, the solid was recrystallized from methanol yielding plate shaped colorless crystals.

A general procedure applicable for the synthesis of tetrazoles is also known from P. N. Gaponik, V. P. Karavai, Y. V. Grigor'ev, Khim. Geterotsikl. Soedin. 1985, 11, 1521-1524.

17.3 References

[1] NATO standardization agreement (STANAG) on explosives, impact sensitivity tests, no. 4489, 1st ed., Sept. 17, **1999**.

[2] WIWEB-Standardarbeitsanweisung 4-5.1.02, Ermittlung der Explosionsgefährlichkeit, hier der Schlagempfindlichkeit mit dem Fallhammer, Nov. 8, **2002**.

[3] http://www.bam.de; Accessed September 2017.

[4] NATO standardization agreement (STANAG) on explosive, friction sensitivity tests, no. 4487, 1st ed., Aug. 22, **2002**.

[5] WIWEB-Standardarbeitsanweisung 4-5.1.03, Ermittlung der Explosionsgefährlichkeit oder der Reibeempfindlichkeit mit dem Reibeapparat, Nov. 8, **2002**.

[6] Impact: insensitive > 40 J, less sensitive ≥ 35 J, sensitive ≥ 4 J, very sensitive ≤ 3 J; Friction: insensitive > 360 N, less sensitive = 360 N, sensitive < 360 N and > 80 N, very sensitive ≤ 80 N, extremely sensitive ≤ 10 N. According to the UN Recommendations on the Transport of Dangerous Goods, (+) indicates not safe for transport.

[7] http://www.ozm.cz; Accessed September 2017.

[8] T. Kamiya and Y. Saito, Ger. Offen., 2147023, 1973.

17.4 Claims

1. Use of a copper(II) azide complex as a primary explosive, wherein the copper(II) azide complex is of general formula $Cu_a(N_3)_{2a}(L)_x$, wherein L is a ligand, a = 1 to 6 and x = 1 to 6,

- wherein L consists of an azole or comprises at least one azole moiety, wherein in case of presence of more than one azole moiety the azole moieties are directly linked, linked via a single carbon, single nitrogen or single oxygen atom or linked via a carbon atoms comprising linker which linker comprises at least 3 carbon atoms or at least one aromatic structure

or

- wherein L comprises more than one azole moiety, wherein the azole moieties are linked via a linker which linker comprises or consists of at least 3 nitrogen atoms or comprises at least 2 carbon atoms and one oxygen atom

or

- wherein L comprises more than one azole moiety, wherein the azole moieties are linked via a linker which linker comprises 2 carbon atoms or comprises or consists of 2 nitrogen atoms, wherein at least one of the azole moieties is substituted

or

- wherein L is 1,2-di(tetrazol-1-yl)ethane (1,1-dte), 1,2-di(tetrazol-2-yl)ethane (2,2-dte) or 1-(tetrazol-1-yl)-2-(tetrazol-2-yl)ethane (1,2-dte), a = 2 and the copper(II) azide complex is contained in a mixture consisting of 5% by weight to 25% by weight of the copper(II) azide complex and for the rest of Al or another reducing agent, $Ba(NO_3)_2$ or another oxidizing agent, Sb_2S_3 or a further reducing agent, pentaerythritol tetranitrate (PETN) or another energetic compound and a binding agent, wherein tetrazene is not present in the mixture

or

- wherein L is 1,2-di(tetrazol-1-yl)ethane (1,1-dte), 1,2-di(tetrazol-2-yl)ethane (2,2-dte) or 1-(tetrazol-1-yl)-2-(tetrazol-2-yl)ethane (1,2-dte), a = 2 and the copper(II) azide complex is contained in a mixture consisting of 90% by weight to 99% by weight of the copper(II) azide complex and for the rest of a binding agent.

2. Use according to claim 1, wherein the azole, the azole moiety, the azole moieties or at least one of the azole moieties is/are substituted by a substituent at least at one position.

3. Use according to claim 2, wherein the substituent is an alkyl particular an alkyl comprising 1 to 4 carbon atoms or an amino, azido or hydrazino group.

4. Use according to any of the preceding claims, wherein the ligand comprises at least two azole moieties, in particular two azole moieties or three azole moieties.

5. Use according to any of the preceding claims, wherein the linker comprises 3 carbon atoms or at least one aromatic structure.

6. Use according to any of the preceding claims, wherein L is selected from a group consisting of 1,4-di(tetrazol-1-yl)butane (1,1-dtb), 1,1'-(propane-1,2-diyl)bis(tetrazole) (1,1,-idtp), 4,4'-bi(1,2,4-triazole) (BTz), 1-methyltetrazole (1-MTZ), 2-methyl-5-aminotetrazole (2-MAT), 4-amino-1,2,4-triazole (4-ATRI), 1-methyl-5-aminotetrazole (1-MAT), 1,3-di(tetrazol-2-yl)propane (2,2-dtp), 1-(tetrazol-1-yl)-3-(tetrazol-2-yl)propane (1,2-dtp), 1,3-di(tetrazol-1-yl)propane (1,1-dtp), 1-ethyltetrazole (1-ETZ), 1-amino-1,2,3-triazole (1-ATRI), 1-amino-1,2,4-triazole (1A-1,2,4-TRI), 3,5-dimethyl-1,2,4-triazol-4-amine (admtrz), 3,5-di(pyridin-4-yl)-1,2,4-triazol-4-amine (4-abpt), 4-(1,2,4-triazol-4-yl)pyridine (2-ptrz), 5-(1-methylpyridin-1-ium-4-yl)-tetrazol-5-ide (mptz), 1,4-bis((1,2,4-triazol-1-yl)methyl)benzene (btix), 1*H*-tetrazol (TZ), 1-(1-(tetrazol-2-yl)propan-2-yl)-tetrazole (1,2-idtp), 2,2'-(propane-1,2-diyl)bis(tetrazole) (2,2-idtp), 1-(tetrazol-1-yl)-4-(tetrazol-2-yl)butane (1,2-dtb), 1,4-di(tetrazol-2-yl)butane (2,2-dtb), 1-isopropyltetrazole (1-iPTZ), 1-propyltetrazole (1-PTZ), 1-aminotetrazole (1-AT), 2-aminotetrazole (2-AT), 2-methyltetrazole (2-MTZ), 1,5-diaminotetrazole (1,5-DAT), 2,5-diaminotetrazole (2,5-DAT), (tetrazol-1-yl)methanol (HMTZ), 1,1'-(2-methylpropane-1,2-diyl)bis(tetrazole) (1,1-idtb), 1-(2-methyl-1-(tetrazol-2-yl)propan-2-yl)-tetrazole (1,2-idtb), 2,2'-(2-methylpropane-1,2-diyl)bis(tetrazole) (2,2-idtb), 3,4-diamino-1,2,4-triazole (DATRI), 3,4,5-triamino-1,2,4-triazole (TATRI), 4-methyl-1,2,4-triazole (MeTRI), 2-amino-1,2,3-triazole (2-ATRI), 1-(1,2,4-triazol-4-yl)-1,2,3-triazole (1,4-BTz), 1,4'-bi(1,2,4-triazole) (iBTz), 2-(1,2,4-triazol-4-yl)-1,2,3-triazole (2,4-BTz), 1-(4-methyl-1,2,4-triazol-3-yl)-tetrazole (MeTRITZ), 4-methyl-5-(tetrazol-1-yl)-1,2,4-triazol-3-amine (AMeTRITZ), para-phenylenbitetrazole (p-PBT), meta-phenylenbitetrazole (m-PBT), ortho-phenylenbitetrazole (o-PBT), tris(2-(tetrazol-1-yl)ethyl)amine (TETA), di(1*H*-tetrazol-1-yl)methane (1,1-dtm), 1-((2*H*-tetrazol-2-yl)methyl)-1H-tetrazole (1,2-dtm), di(2*H*-tetrazol-2-yl)methane (2,2-dtm), 1-(2-azidomethyl)-1*H*-tetrazole (AMT), 1-(2-azidoethyl)-1*H*-tetrazole (AET), 1-(3-azidopropyl)-1*H*-tetrazole (APT), 1-(4-azidobutyl)-1*H*-tetrazole (ABT), 1,2-(di-5-methylhydrazinotetrazol-1-yl)ethane (1,1-dmhte) and 3-hydrazino-4-amino-1,2,4-triazole (3-HATri).

7. Use according to any of the preceding claims, wherein L is neither 1,1-dte nor 2,2-dte nor 1,2-dte and the copper(II) azide complex is used as a primary explosive in a detonation mixture in an amount exceeding 75% by weight to an amount of 99% by weight, wherein the detonation mixture further comprises a stabilizing agent and/or a binding agent or wherein the copper(II) azide complex is used as a primary explosive in an igniting mixture in an amount of 5% by weight to 75% by weight, wherein the igniting mixture further comprises an oxidizing agent and a reducing agent and optionally a further energetic compound and/or a friction agent and/or a stabilizing agent and/or a binding agent and/or a sensibilizing agent.

8. Use according to claim 7, wherein the oxidizing agent comprises or consists of KNO_3, NH_4NO_3, $Sr(NO_3)_2$, $Ba(NO_3)_2$ and/or another nitrate, ZnO_2, BaO_2 and/or another peroxide, $CaSO_4$ and/or another sulfate, Fe_2O_3, Fe_3O_4, CeO_2, WO_3, SnO_2, SiO_2, MnO_2, $KMnO_4$, CuO, Bi_2O_3, KO_2 and/or another oxide, $KClO_3$ and/or another chlorate and/or $KClO_4$, NH_4ClO_4 and/or another perchlorate, the reducing agent comprises or consists of Al, Mg, B, Zr, Ti, Si, Ce and/or another metal and/or an alloy thereof, a metal hydride and/or S_8, Sb_2S_3 and/or another sulfur containing compound, the further energetic compound comprises or consists of pentaerythritol tetranitrate (PETN), hexogen, octogen and/or nitrocellulose, the friction agent comprises or consists of glass powder, Sb_2S_3, $CaSi_2$ and/or boron nitride, the stabilizing agent comprises or consists of graphite, the binding agent comprises or consists of paraffin, dextrin, nitrocellulose, a polyacetate and/or a polyvinyl comprising compound and the sensibilizing agent comprises or consists of tetrazene.

9. Use according to claim 7 or 8, wherein the oxidizing agent is KNO_3, the reducing agent is boron and the further energetic compound is pentaerythritol tetranitrate (PETN) or wherein the oxidizing agent is $Ba(NO_3)_2$, the reducing agent comprises Al and Sb_2S_3, the further energetic compound is pentaerythritol tetranitrate (PETN).

10. Use according to claim 1, wherein Al or the other reducing agent is present in an amount of 6% by weight to 8% by weight, $Ba(NO_3)_2$ or the other oxidizing agent is present in an amount of 27% by weight to 37% by weight, Sb_2S_3 or the further reducing agent is present in an amount of 13% by weight to 17% by weight, pentaerythritol tetranitrate (PETN) or the other energetic compound is present in an

amount of 4% by weight to 6% by weight and the binding agent is present in an amount of 0.1% by weight to 1% by weight in the mixture.

11. Copper(II) azide complex, wherein the copper(II) azide complex is $Cu(N_3)_2$(4-amino-1,2,4-triazole)$_2$ or $Cu_3(N_3)_6$(4-amino-1,2,4-triazole)$_2$*H_2O or is of general formula $Cu_a(N_3)_{2a}(L)_x$, wherein L is a ligand, a = 1 to 6 and x = 1 to 6, wherein L is selected from a group consisting of 1,1'-(propane-1,2-diyl)bis(tetrazole) (1,1,-idtp), 4,4'-bi(1,2,4-triazole) (BTz), 1-methyltetrazole (1-MTZ), 2-methyl-5-aminotetrazole (2-MAT), 1-methyl-5-aminotetrazole (1-MAT), 1,3-di(tetrazol-2-yl)propane (2,2-dtp), 1-(tetrazol-1-yl)-3-(tetrazol-2-yl)propane (1,2-dtp), 1,3-di(tetrazol-1-yl)propane (1,1-dtp), 1-ethyltetrazole (1-ETZ), 1-amino-1,2,3-triazole (1-ATRI), 1-amino-1,2,4-triazole (1A-1,2,4-TRI), 1-(1-(tetrazol-2-yl)propan-2-yl)-tetrazole (1,2-idtp), 2,2'-(propane-1,2-diyl)bis(tetrazole) (2,2-idtp), 1-(tetrazol-1-yl)-4-(tetrazol-2-yl)butane (1,2-dtb), 1,4-di(tetrazol-2-yl)butane (2,2-dtb), 1-isopropyltetrazole (1-iPTZ), 1-propyltetrazole (1-PTZ), 1-aminotetrazole (1-AT), 2-aminotetrazole (2-AT), 2-methyltetrazole (2-MTZ), 1,5-diaminotetrazole (1,5-DAT), 2,5-diaminotetrazole (2,5-DAT), (tetrazol-1-yl)methanol (HMTZ), 1,1'-(2-methylpropane-1,2-diyl)bis(tetrazole) (1,1-idtb), 1-(2-methyl-1-(tetrazol-2-yl)propan-2-yl)-tetrazole (1,2-idtb), 2,2'-(2-methylpropane-1,2-diyl)bis(tetrazole) (2,2-idtb), 3,4-diamino-1,2,4-triazole (DATRI), 3,4,5-triamino-1,2,4-triazole (TATRI), 4-methyl-1,2,4-triazole (MeTRI), 2-amino-1,2,3-triazole (2-ATRI), 1-(1,2,4-triazol-4-yl)-1,2,3-triazole (1,4-BTz), 1,4'-bi(1,2,4-triazole) (iBTz), 2-(1,2,4-triazol-4-yl)-1,2,3-triazole (2,4-BTz), 1-(4-methyl-1,2,4-triazol-3-yl)-tetrazole (MeTRITZ), 4-methyl-5-(tetrazol-1-yl)-1,2,4-triazol-3-amine (AMeTRITZ), para-phenylenbitetrazole (p-PBT), meta-phenylenbitetrazole (m-PBT), ortho-phenylenbitetrazole(o-PBT), tris(2-(tetrazol-1-yl)ethyl)amine (TETA), di(1*H*-tetrazol-1-yl)methane (1,1-dtm), 1-((2*H*-tetrazol-2-yl)methyl)-1*H*-tetrazole (1,2-dtm), di(2*H*-tetrazol-2-yl)methane (2,2-dtm), 1-(2-azidomethyl)-1*H*-tetrazole (AMT), 1-(2-azidoethyl)-1*H*-tetrazole (AET), 1-(3-azidopropyl)-1*H*-tetrazole (APT), 1-(4-azidobutyl)-1*H*-tetrazole (ABT), 1,2-(di-5-methylhydrazinotetrazol-1-yl)ethane (1,1-dmhte) and 3-hydrazino-4-amino-1,2,4-triazole (3-HATri).

12. Method for synthesizing a copper(II) azide complex, wherein the copper(II) azide complex is of general formula $Cu_a(N_3)_{2a}(L)_x$, wherein L is a ligand, a = 1 to 6 and x = 1 to 6, wherein a copper(II) salt and the ligand are dissolved in water, an alcohol

or acetonitrile thus forming a first solution, an azide is dissolved in water, an alcohol or acetonitrile thus forming a second solution, wherein the first solution is agitated and the second solution is added to the first solution resulting in the precipitation of the copper(II) azide complex.

13. Method according to claim 12, wherein the copper(II) salt is a chloride, a sulfate, a nitrate, an acetate, a perchlorate or a carbonate and/or the azide is sodium azide, lithium azide, potassium azide or hydrazoic acid.

14. Method according to claim 12 or 13, wherein the copper(II) azide complex is separated from the mixed first and second solutions, in particular by filtration and washing, and subsequently dried.

15. Ligand for the formation of a copper(II) azide complex of general formula $Cu_a(N_3)_{2a}(L)_x$, wherein L is the ligand, a = 1 to 6 and x = 1 to 6, wherein the ligand is 1-(1-(tetrazol-2-yl)propan-2-yl)-tetrazole (1,2-idtp), 2,2'-(propane-1,2-diyl)bis(tetrazole) (2,2-idtp), 1-(2-methyl-1-(tetrazol-2-yl)propan-2-yl)-tetrazole (1,2-idtb), 2,2'-(2-methylpropane-1,2-diyl)bis(tetrazole) (2,2-idtb), 1-(1,2,4-triazol-4-yl)-1,2,3-triazole (1,4-BTz), 1-(4-methyl-1,2,4-triazol-3-yl)-tetrazole (MeTRITZ), 4-methyl-5-(tetrazol-1-yl)-1,2,4-triazol-3-amine (AMeTRITZ), di(1*H*-tetrazol-1-yl)methane (1,1-dtm), 1-((2*H*-tetrazol-2-yl)methyl)-1*H*-tetrazole (1,2-dtm), di(2*H*-tetrazol-2-yl)methane (2,2-dtm), 1-(3-azidomethyl)-1*H*-tetrazole (AMT), 1-(3-azidopropyl)-1*H*-tetrazole (APT) or 1-(4-azidobutyl)-1*H*-tetrazole (ABT).

Supporting information available in the appendix in **Chapter 19.14**.

18 Summary and Conclusion

Chapters 3–16 were published or submitted as 14 articles in the following peer-reviewed scientific journals:

- *Zeitschrift für Allgemeine und Anorganische Chemie (2x)*,
- *Propellants, Explosives, Pyrotechnics*,
- *Dalton Transactions (2x)*,
- *Inorganic Chemistry (2x)*,
- *Chemistry A European Journal (4x)*,
- *Journal of Materials Chemistry A (3x)*,
- *Journal of the American Chemical Society*.

Chapter 17, however, corresponds to the international patent application "EP18150491.1 and EP 18151497.7: Use of a copper(II) azide complex as a primary explosive" from 12th January 2018 on the class of copper(II) azide complexes as green primary explosives. The articles and patent application have been slightly modified in order to provide a better fit into the unified structure of this work.

The objectives of this work were the synthesis and characterization of new laser-ignitable energetic materials as well as environmentally-friendly primary explosives. In particular, research into the concept of energetic coordination compounds (ECC) and the strategy of nitrogen-rich nitraminotetrazolate salts has shown very promising results in these areas in the past and were therefore used for solving a number of intricate challenges.[1–7] The synthesized compounds were extensively characterized by using the following analytical methods:

- differential thermal analysis,
- differential scanning calorimetry,
- thermal gravimetric analysis,
- elemental analysis,
- infrared spectroscopy,
- Raman spectroscopy,
- mass spectrometry,
- multinuclear NMR spectroscopy,
- UV-Vis-NIR spectroscopy,
- scanning electron microscopy,

- energy-dispersive X-ray spectroscopy,
- inductively coupled plasma atomic emission spectroscopy,
- vacuum stability tester,
- X-ray diffraction,
- and powder X-ray diffraction.

In addition, the sensitivities of the synthesized compounds toward impact, friction, electrostatic discharge and ball drop impact were determined by the

- BAM drophammer,
- BAM friction tester,
- electrostatic discharge tester,
- OZM ball drop impact tester.

The most promising compounds were then either laser-ignited or tested for their suitability as primary explosives by applying the

- hot plate test,
- hot needle test,
- secondary explosive initiation capability,
- priming mixture suitability test.

The ECC consists of three elementary building blocks; the ligand, the metal, and the anion (Figure 1). In total, 22 different nitrogen-rich ligands, 7 different transition metals and 17 different anions were used in this work and inserted into the ECC in various combinations. By replacing the individual components, both the energetic and optical properties could be precisely adapted to meet the desired requirements. With the exception of the water-containing compounds (aqua ligands or crystal water), the general complex sum formula can be given as $[metal(nitrogen\text{-}rich\ ligand)_x](anion)_y$ and in the case of coordinating anions as $[metal(anion)_y(nitrogen\text{-}rich\ ligand)_x]$. With the exception of silver (4d, oxidation state +I), the transition metals came predominantly from the 3d series (Mn, Fe, Co, Ni, Cu, Zn) and were present in the oxidation state +II. However, some transition metal complexes were oxidized to the next higher oxidation stage by the use of oxidizing acids as solvents (Co^{II}/Co^{III} and Fe^{II}/Fe^{III}).

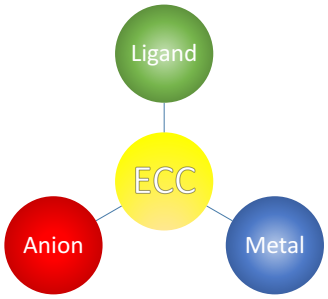


Figure 1. Concept of energetic coordination compounds (ECC).

The ligands came primarily from the azole family (chiefly triazoles and tetrazoles) however there were a few exceptions, namely the ammonia molecule and the methylhydrazine ligand MSC (Chart 1).

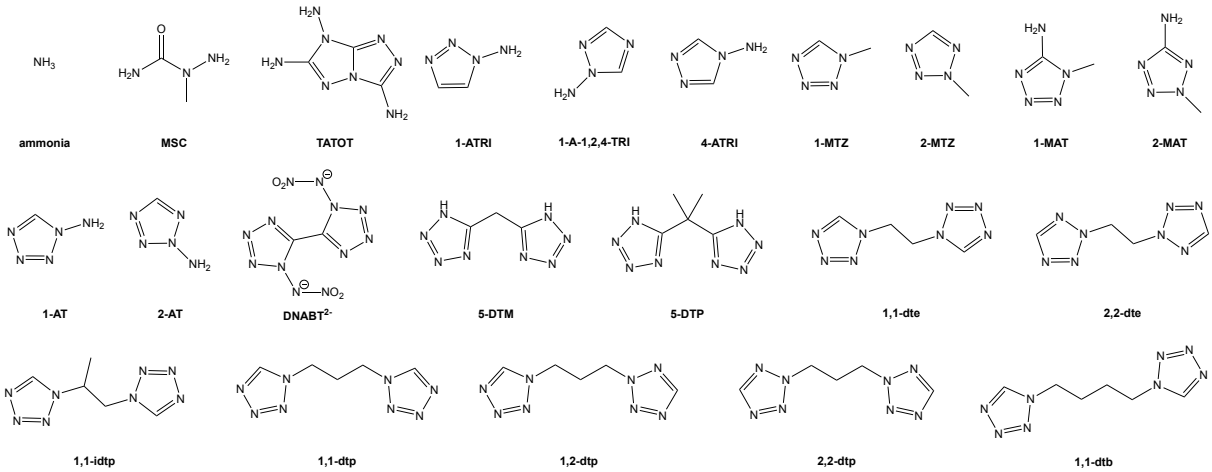


Chart 1. Overview of the nitrogen-rich ligands used in this thesis.

The inorganic and organic anions used were either non-oxidizing, oxidizing or endothermic and with a single or double negative charge (Chart 2).

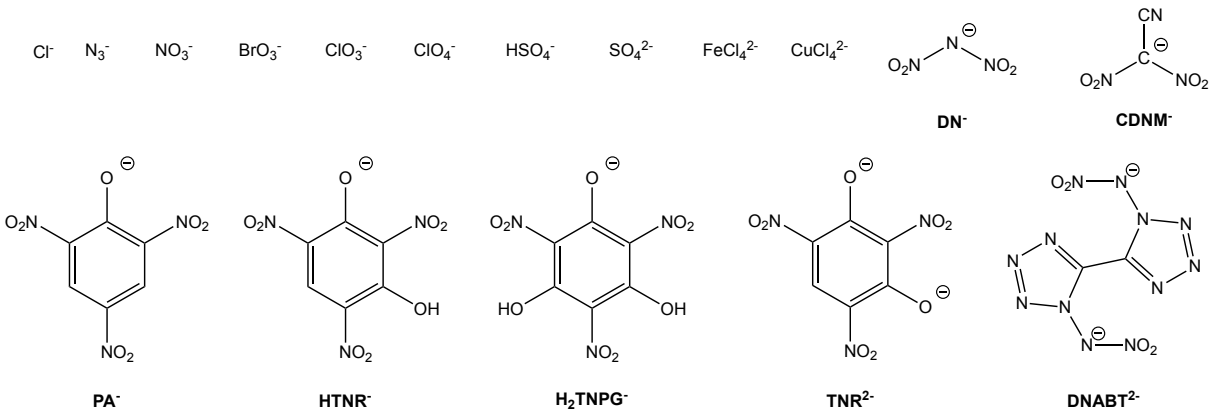


Chart 2. Overview of the anions applied in this work.

The thermal stability and sensitivity of the compounds toward various stimuli are strongly dependent on the coordination sphere of the complex. Important factors besides the choice of metals, ligands, and anions can be, for example, the water content and the formation of bridging or polymeric structures. The effects the coordination sphere can have on the stability can be seen very clearly in the examples in Chapter 11, in which different complexes based on 2-MAT were synthesized as ligands and copper(II) perchlorate as metal(II) salt. The thermal stability of complexes with volatile ligands (water, some triazoles, and tetrazoles) is generally low. Complexes with bridging ligands (e.g. ditetrazoles) that form multidimensional complex polymers, on the other hand, generally show much higher stabilities. Nevertheless, trends can be observed when comparing the complexes and the variation of individual building blocks.

The thermal stability, exemplarily shown for the metal(II) perchlorate complexes of 1-methyl-5*H*-tetrazole (Figure 2), usually increases in the order: $Cu^{II} \approx Fe^{II} < Zn^{II} \approx Mn^{II} < Co^{II} < Ni^{II}$. The highest sensitivities can usually be observed for complexes with the metals Ag^{I}, Co^{II}, Ni^{II}, Cu^{II}, and Fe^{II}. Complexes with half full and completely occupied d-shells like Mn^{II} and Zn^{II} are typically less sensitive.

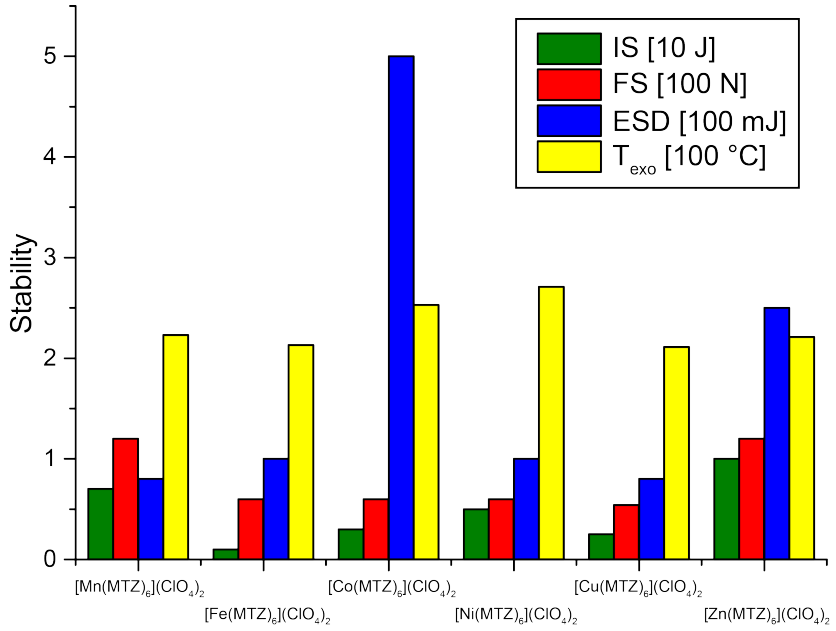


Figure 2. Comparison of the stabilities of 1-MTZ containing metal(II) perchlorate complexes.

The next building block that can have a massive influence on the stability and sensitivity of the complexes is the selection of the anion. Decisive factors here are the endothermic character, the oxidizing power and the reactivity of the molecules. Figure 3 shows different copper(II) 1-ATRI complexes with varying anions. Remarkably low thermal stability can be observed in complexes with nitrates, dinitramides, bromates, chlorates, and sometimes azides. In contrast,

complexes with nitroaromatic anions generally exhibit higher thermal stability. In turn, differences can be observed depending on whether they coordinate, act only as a counterion or are even tetradentaley bridging (e.g. dianionic styphnate anion, Chart 2). The most sensitive complexes are based on azides, chlorates, bromates and perchlorates, followed by nitrates, dinitramides, cyanodinitromethanides and nitroaromatics (picrate, styphnate, etc.). The least sensitive are sulfate compounds and without endothermic or oxidizing anions (Cl^-, $CuCl_4^{2-}$, $FeCl_4^{2-}$).

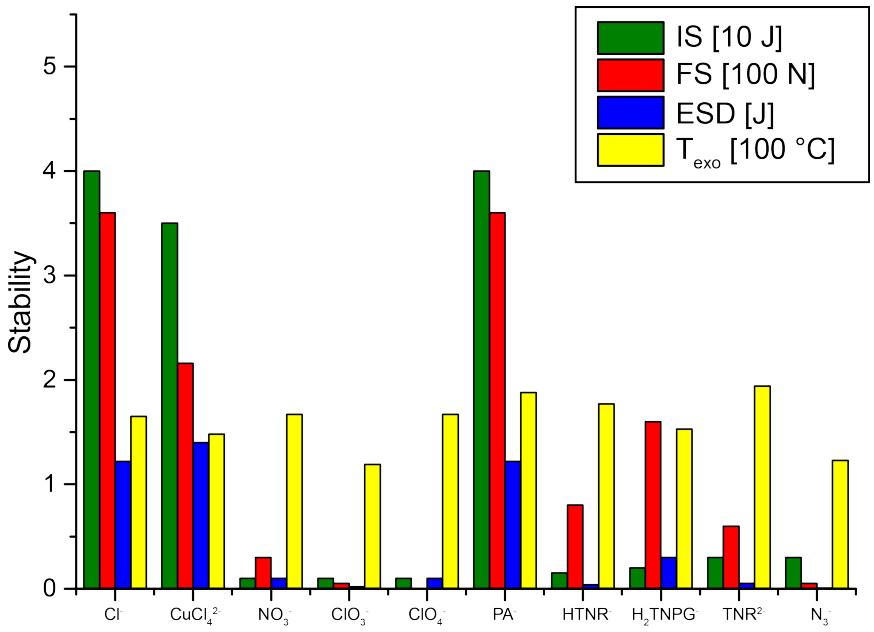


Figure 3. Comparison of the stability and the influence of varying anions on different complexes based on copper(II) as the metal and 1-ATRI as the ligand. Cl^- = $[CuCl_2(1\text{-}ATRI)_2]$; $CuCl_4^{2-}$ = $[CuCl_4(1\text{-}ATRI_H)_2]$; NO_3^- = $[Cu(NO_3)_2(\mu\text{-}1\text{-}ATRI)_2]$; ClO_3^- = $[Cu(ClO_3)_2(1\text{-}ATRI)_4]$; ClO_4^- = $[Cu(H_2O)_2(1\text{-}ATRI)_4](ClO_4)_2$; PA^- = $[Cu(H_2O)_4(1\text{-}ATRI)_2](PA)_2$; $HTNR^-$ = $[Cu(HTNR)_2(1\text{-}ATRI)_2]$; H_2TNPG^- = $[Cu(H_2O)_2(1\text{-}ATRI)_4](H_2TNPG)_2$; TNR^{2-} = $[Cu(\mu\text{-}TNR)(1\text{-}ATRI)_2]$; N_3^- = $[Cu(N_3)_2(1\text{-}ATRI)]$.

The third crucial parameter for the stability of the energetic coordination compounds is the ligand. Critical influencing factors here are the nitrogen content, the substitution pattern and the type of functionalization by, for example, side chains, potential isomeric ligands, ligand acidities and the formation of cocrystallized species. A column diagram of different copper(II) perchlorate complexes based on a large number of different nitrogen-rich ligands is shown in Figure 4. Increased sensitivities can be observed in the case of:

- high nitrogen or low carbon content (e.g. alkylation vs. amination)
- *N*-amination ($N_{Tetrazole}$-NH_2 vs. $C_{Tetrazole}$-NH_2)
- high acidities of the ligand (e.g. $N_{Tetrazole}$-H vs. $C_{Tetrazole}$-H)

- no ligand cocrystallization
- *N*2 isomers ($N_{Tetrazole}2$ vs. $N_{Tetrazole}1$).

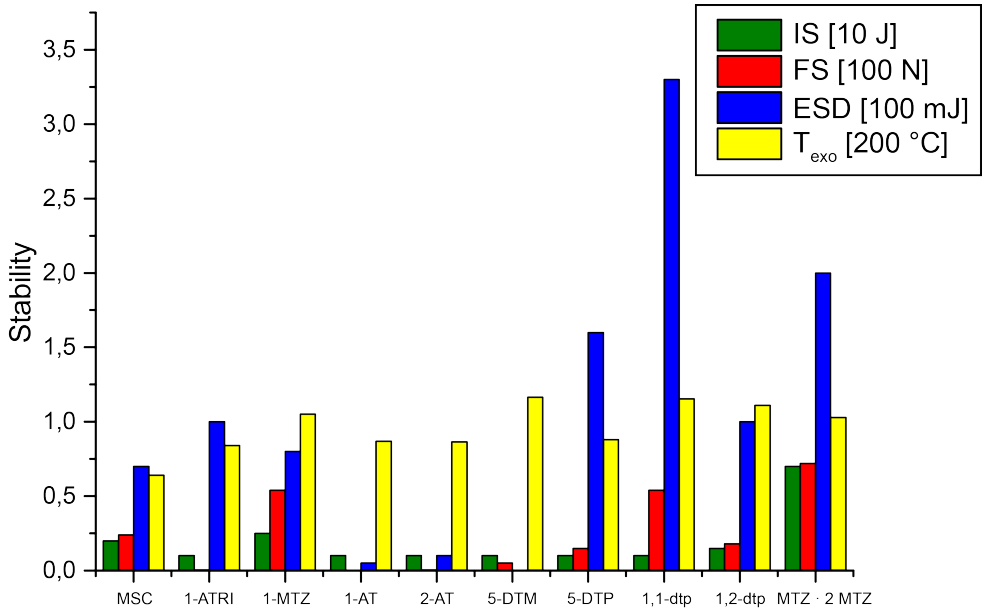


Figure 4. Stabilities of different copper(II) perchlorate complexes with varying ligands. MSC = $[Cu(ClO_4)_2(MSC)_2]$; 1-ATRI = $[Cu(H_2O)_2(1\text{-ATRI})_4](ClO_4)_2$; 1-MTZ = $[Cu(1\text{-MTZ})_6](ClO_4)_2$; 1-AT = $[Cu(1\text{-AT})_6](ClO_4)_2$; 2-AT = $[Cu(H_2O)_2(2\text{-AT})_4](ClO_4)_2$; 5-DTM = $[Cu(ClO_4)_2(5\text{-DTM})_2]$; 5-DTP = $[Cu(H_2O)(5\text{-DTP})_2](ClO_4)_2 \cdot H_2O$; 1,1-dtp = $[Cu(1,1\text{-dtp})_3](ClO_4)2$; 1,2-dtp = $[Cu(1,2\text{-dtp})_3](ClO_4)$; $[Cu(1\text{-MTZ})_6](ClO_4)_2 \cdot 2$ 1-MTZ.

The second strategy to address the problematic lead content in primary explosives in this work was the use of energetic nitraminotetrazolate salts (Figure 5). In addition to nitrogen-rich cations, 4 different nitraminotetrazolate anions and 11 different cations from the group of alkali or earth alkali metals but also nitrogen-rich cations were used.

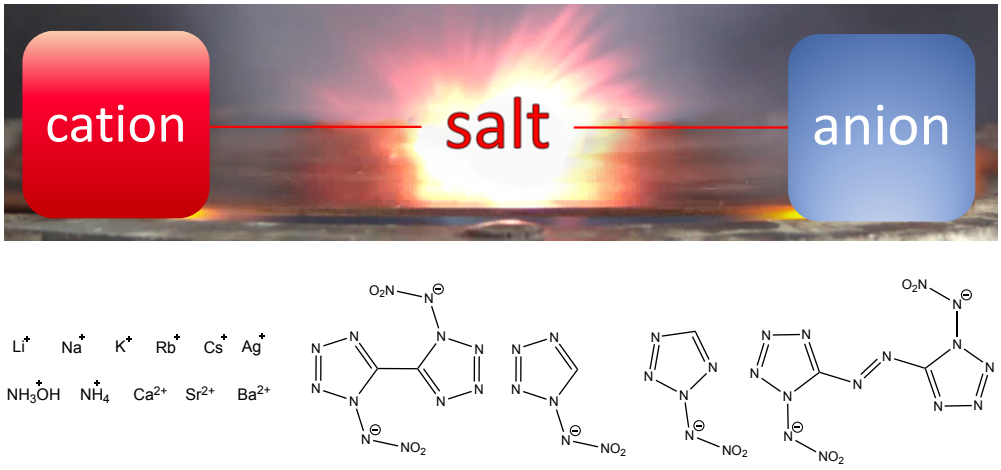


Figure 5. Strategy of energetic salts based on nitrogen-rich nitraminotetrazolates.

In total, 218 compounds were synthesized and the crystal structure of 165 of these compounds was determined. Of the total of 218 compounds, 195 were investigated in more detail, and characterized in a more comprehensive manner. Based on their observed sensitivities, 90 compounds can be classified as primary explosives (Figure 6). The best compounds from selected chapters are summarized together with their physicochemical properties in Figure 7. Promising compounds, which showed extraordinary characteristics, and which combine both excellent performance and manageable sensitivities were examined in additional experiments, namely the hot plate and hot needle tests for their suitability in potential applications. The compounds were investigated in laser initiation experiments, in blasting caps and as part of priming mixtures in primer caps. The laser ignition tests were performed with a single pulsed diode laser at different pulse lengths (0.1–15 ms), a constant voltage (4 V) and varying currents (5–10 A) at a wavelength of 915 nm. In summary, it can be stated that ECC are very well suited as laser-ignitable materials. 77 of these complexes could be positively ignited in the course of this work in laser ignition experiments (Figure 8). Depending on the building blocks of the complexes and the corresponding coordination sphere, different initiation energies could be observed. The complexes with the lowest thresholds consisted of copper(II) or iron(II) as the metal(II) center. The more sensitive the compounds were to mechanical stimuli, the greater the probability of a positive ignition. For most of the laser-ignitable compounds, the absorptions were measured by UV-Vis-NIR spectroscopy to gather further information on a potential mechanism. Unfortunately, this did not allow us to draw any major conclusions regarding the mechanism, as each complex system behaves differently. It is nevertheless assumed that the initiation pathway is of a photothermal nature.

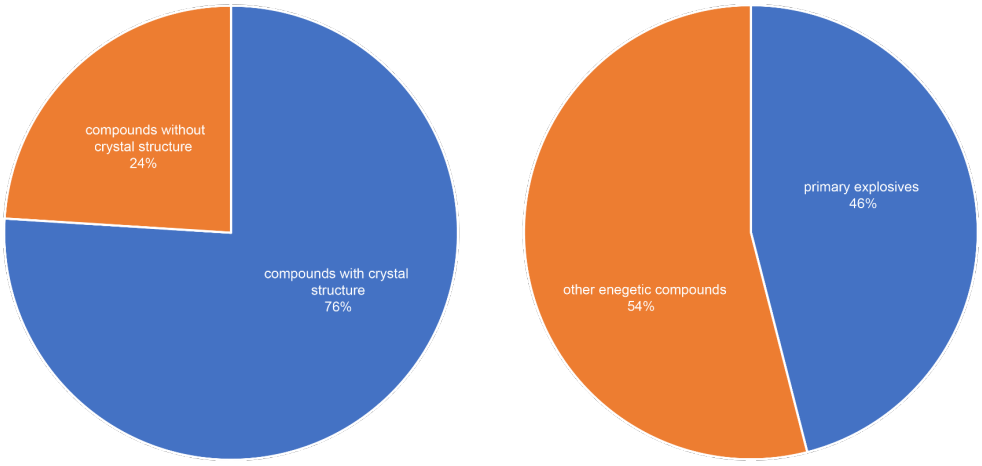


Figure 6. Pie charts of crystal structure distribution and percentage of primary explosives in this thesis.

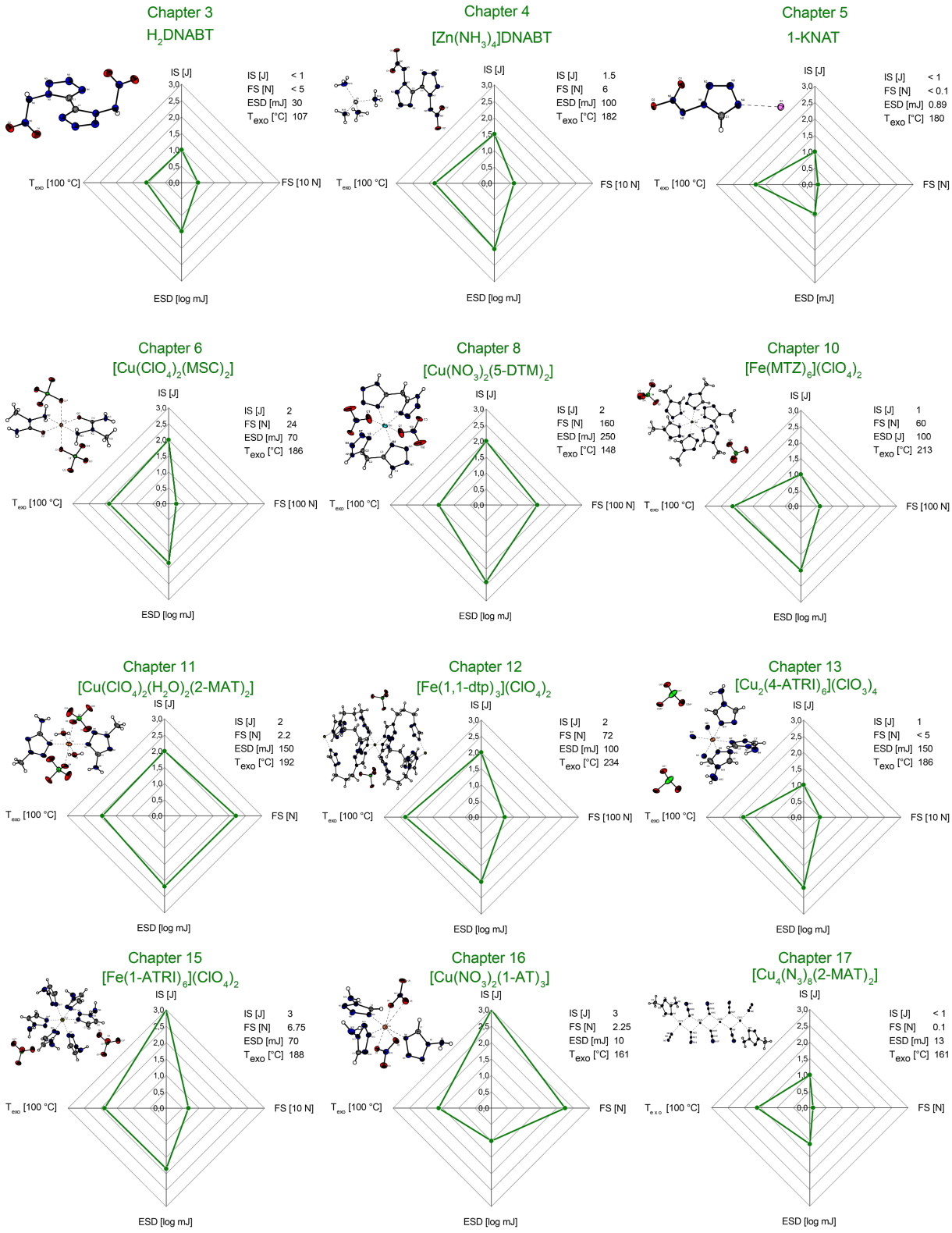


Figure 7. Overview of the best compounds from selected chapters and their physicochemical properties.

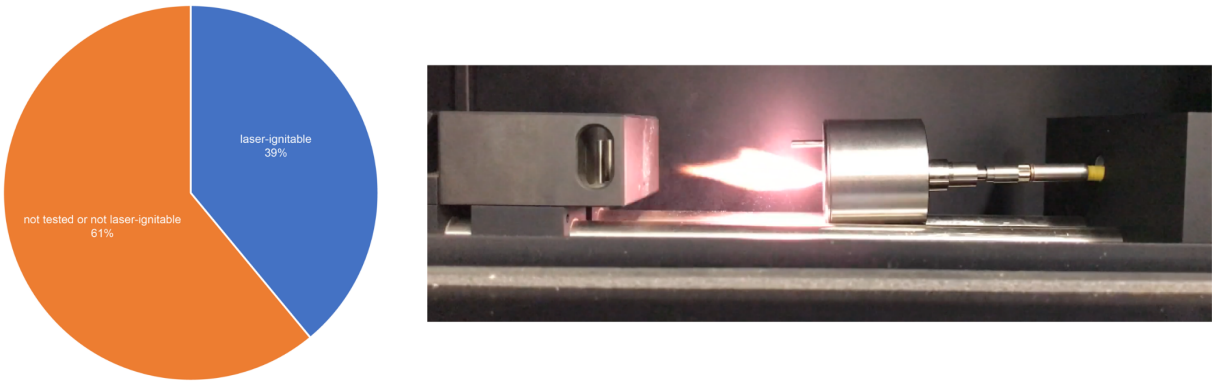


Figure 8. Pie chart distribution of the laser-ignitable compounds.

In addition to laser ignitability, various compounds were tested for their suitability as lead-free primary explosives. Great progress was made, and excellent results have been achieved. In particular, the class of copper(II) azide complexes has unique potential in this context and as a result a patent has been filed (Chapter 17). Selected compounds can, therefore, be considered as lead styphnate (LS) or lead azide (LA) substitutes (Figure 9). The compounds fulfill most of the desired requirements and show satisfying thermal stabilities, manageable sensitivities, excellent initiation properties, fast DDTs, low solubility in water and are cheap and easy to synthesize. The compounds show enormous potential both in priming mixtures in primer caps for the ignition of propellant powders and as initiating explosives of secondaries in blasting caps (Figure 10).

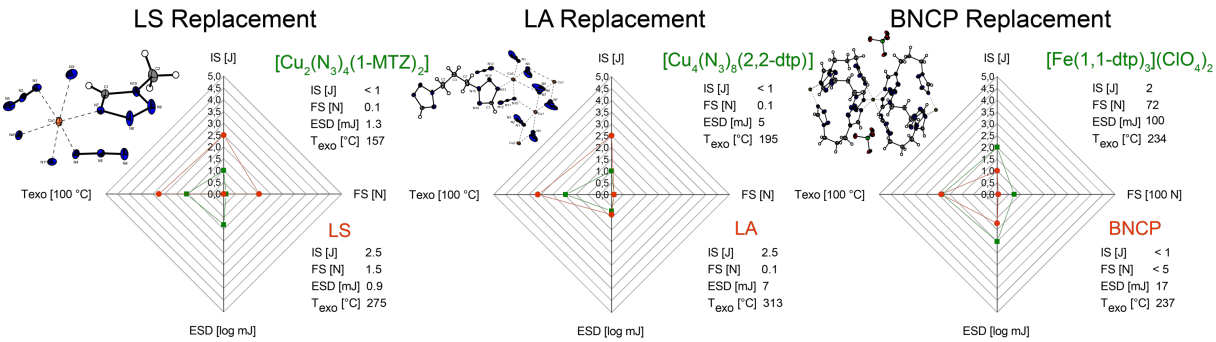


Figure 9. Comparison of LS, LA, and BNCP with their possible substitutes.

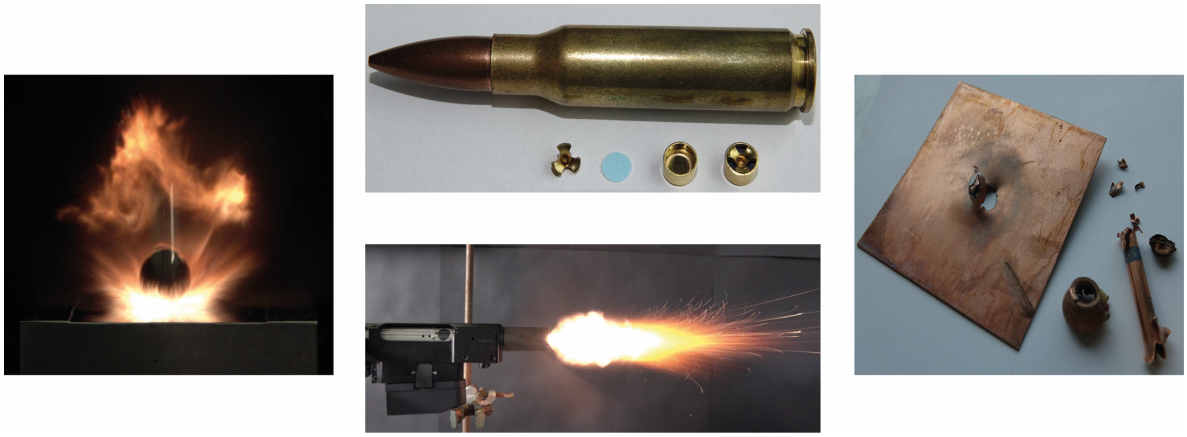


Figure 10. Tests of primary explosives in ball drop impact experiments, as well as primer and blasting caps.

The compound, which comes closest to the booster explosive requirements and, after further research, could in fact meet these requirements, is $[Fe(1,1\text{-dtp})_3](ClO_4)_2$. This complex has good sensitivity values (Figure 9), which could be further improved by adjustment of the formulation and the particle size. Use of this compound could bring about a significant increase in safety and initial positive results in laser ignition tests have already been observed. Nevertheless, further tests will be needed to clarify whether the compound has the potential to reliably ignite a secondary explosive.

In summary and based on the results shown here, the concept of ECC holds enormous potential for the future due to the many potential combinations and the resulting promising compounds for potential applications.

18.1 References

[1] D. Fischer, T. M. Klapötke, J. Stierstorfer, *Angew. Chem., Int. Ed.* **2014**, *53*, 8172–8175.

[2] M. Joas, dissertation, Ludwig-Maximilians Universität München, **2014**.

[3] T. W. Myers, J. A. Bjorgaard, K. E. Brown, D. E. Chavez, S. K. Hanson, R. J. Scharff, S. Tretiak, J. M. Veauthier, *J. Am. Chem. Soc.*, **2016**, *138*, 4685–4692.

[4] A. Y. Zhilin, M. A. Ilyushin, I. V. Tselinksii, A. S. Kozlov, I. S. Lisker, *Russ. J. Appl. Chem.* **2003**, *76*, 572–576.

[5] I. A. Ugryumov, M. A. Ilyushin, I. V. Tselinksii, A. S. Kozlov, *Russ. J. Appl. Chem.* **2003**, *76*, 439–441.

[6] M. A. Ilyushin, I. V. Tselinsii, I. A. Ugryumov, A. Y. Zhilin, A. S. Kozlov, *6th New Trends in Research of Energetic Materials Seminar*, Pardubice, Czech Republic, April 22–24, **2003**, 146–152.

[7] M. Joas, T. M. Klapötke, J. Stierstorfer, N. Szimhardt, *Chem. Eur. J.* **2013**, *19*, 9995–10003.

19 Appendix

19.1 Supplementary Information: 1,1'-Nitramino-5,5'-bitetrazoles

19.1.1 X-Ray-Diffraction

For all compounds except for **5**, an Oxford Xcalibur3 diffractometer with a CCD area detector was employed for data collection using Mo-*K*α radiation (λ = 0.71073 Å). By using the CRYSALISPRO software[S1] the data collection and reduction were performed. Single crystals of **5** were measured on a Bruker TXS (rotating anode) in a D8 VENTURE systeme. The structures were solved by direct methods (SIR-92,[S3] or SHELXS-97[S4]) and refined by full-matrix least-squares on *F*2 (SHELXL[S4]) and finally checked using the PLATON software[S5] integrated in the WinGX software suite. The non-hydrogen atoms were refined anisotropically and the hydrogen atoms were located and freely refined. The absorptions were corrected by a SCALE3 ABSPACK multiscan method.[S6] All DIAMOND2 plots are shown with thermal ellipsoids at the 50% probability level and hydrogen atoms are shown as small spheres of arbitrary radius.

Table S1. Crystallographic data and refinement parameters of compound **1**, **4** and **5–7**.

	1	**4**	**5**	**6**	**7**
Formula	$C_2H_2N_{12}O_4$	$C_2N_{14}O_4K_2$	$C_2H_8N_{14}O_4$	$C_2H_8N_{14}O_6$	$C_2H_8N_{16}O_4$
FW [g mol^{-1}]	258.16	362.36	292.22	324.22	320.24
Crystal system	Monoclinic	Triclinic	Monoclinic	Triclinic	Triclinic
Space Group	$P2_1/n$ (No. 14)	P–1 (No. 2)	$P2_1/c$ (No. 14)	P–1 (No. 2)	P–1 (No. 2)
Color / Habit	Colorless block	Colorless block	Colorless block	Colorless block	Colorless block
Size [mm]	0.08 x 0.12 x 0.18	0.10 x 0.14 x 0.24	0.09 x 0.14 x 0.18	0.08 x 0.16 x 0.36	0.10 x 0.11 x 0.35
a [Å]	7.9670(8)	7.0812(6)	8.2195(4)	5.1764(5)	7.3504(6)
b [Å]	6.0063(3)	8.7424(8)	11.1016(6)	6.6488(10)	8.7924(6)
c [Å]	9.5768(7)	9.5547(8)	5.9124(3)	8.4762(13)	9.6302(8)
α [°]	90	72.066(8)	90	96.933(13)	106.459(7)
β [°]	108.020(9)	86.402(7)	103.269(2)	90.164(10)	93.462(7)
γ [°]	90	89.851(7)	90	97.887(11)	90.906(6)
V [Å^3]	435.79(6)	561.56(9)	525.10(5)	286.80(7)	595.43(8)
Z	2	2	2	1	2
$\rho_{calc.}$ [g cm^{-3}]	1.967	2.143	1.848	1.877	1.786
μ [mm^{-1}]	0.179	0.900	0.165	0.173	0.158
F(000)	260	360	300	166	328
$\lambda_{MoK\alpha}$[Å]	0.71073	0.71073	0.71073	0.71073	0.71073
T [K]	173	100	100	173	173
ϑ min-max [°]	4.3, 26.5	4.4, 26.0	3.1, 27.0	4.2, 26.3	4.4, 26.0
Dataset h; k; l	-9:10; -7:7; -12:12	-8:8; -10:7; -11:11	-10:9; -14:14; -7:7	-6:6; -8:7; -10:10	-8:9; -10:10; -11:11
Reflect. coll.	3342	4202	12184	1831	4489
Independ. refl.	893	2203	1147	1157	2322
R_{int}	0.031	0.030	0.026	0.028	0.018
Reflection obs.	729	1809	1042	868	1954
No. parameters	893	199	107	116	231
R_1 (obs)	0.0320	0.0322	0.0267	0.0421	0.0324
wR_2 (all data)	0.0789	0.0707	0.0697	0.0970	0.0861
S	1.05	1.03	1.09	1.03	1.04
Resd. Dens.[e Å^{-3}]	-0.18, 0.21	-0.28, 0.39	-0.27, 0.38	-0.28, 0.28	-0.27, 0.25
Device type	Oxford XCalibur3 CCD	Oxford XCalibur3 CCD	Bruker TXS	Oxford XCalibur3 CCD	Oxford XCalibur3 CCD
Solution	SIR-92	SIR-92	SHELXS-97	SIR-92	SIR-92
Refinement	SHELXL-97	SHELXL-97	SHELXL-97	SHELXL-97	SHELXL-97
Absorpt. corr.	multi-scan	multi-scan	multi-scan	multi-scan	multi-scan
CCDC	1430341	1430338	1430342	1430339	1430340

19.1.2 Computations

All calculations were carried out using the Gaussian G09W (revision A.02) program package. The enthalpies (H), listed in Table S3, were calculated using the complete basis set (CBS) method of Petersson and coworkers in order to obtain very accurate energies. The CBS models use the known asymptotic convergence of pair natural orbital expressions to extrapolate from calculations using a finite basis set to the estimated complete basis set limit. CBS-4 begins with a HF/3-21G(d) geometry optimization; the zero-point energy is computed at the same level. It then uses a large basis set SCF calculation as a base energy, and a MP2/6-31+G calculation with a CBS extrapolation to correct the energy through second order. A MP4(SDQ)/6-31+(d,p) calculation is used to approximate higher order contributions. In this study we applied the modified CBS-4M method (M referring to the use of Minimal Population localization) which is a re-parametrized version of the original CBS-4 method and also includes some additional empirical corrections.[S7] The enthalpies of the gas-phase species M were computed according to the atomization energy method (eq.1).

$$\Delta_f H^\circ_{(g,\,M,\,298)} = H_{(Molecule,\,298)} - \sum H^\circ_{(Atoms,\,298)} + \sum \Delta_f H^\circ_{(Atoms,\,298)} \quad (1)$$

Table S3. CBS-4M results and calculated gas-phase enthalpies.

	M	$-H^{298}$ / a.u.	$\Delta_f H^\circ$(g,M) / kcal mol^{-1}
1	$CH_2N_8O_4$	1033.68003	239.4
DNABT^{2-}	$CN_8O_4^{2-}$	1032.612357	176.6
DNAAzT^{2-}	$CN_8O_4^{2-}$	1141.92746	232.9
K$^+$	K^+	599.035967	116.5
NH$_4^+$	NH_4^+	56.796608	151.9
NH$_4$O$^+$	NH_4O^+	131.863249	164.1

Table S4. CBS-4M values and literature values for atomic $\Delta H_f^{\circ 298}$ / kcal mol^{-1}.

	$-H^{298}$ / a.u.	NIST [S8] / $\Delta H^\circ_f{}^{298}$
H	0.500991	52.1
C	37.786156	171.3
N	54.522462	113.0
O	74.991202	59.6
K	599.187712	21.3

The gas phase heat of formation of **1** and **3** is converted to the solid state value by subtracting its sublimation enthalpy calculated with Trouton's rule ($\Delta H_{sub} = 188 \cdot T_m = 72.0$ kJ mol^{-1}) In the case of the ionic compounds, the lattice energy (U_L) and lattice enthalpy (ΔH_L) were calculated from the corresponding X-ray molecular volumes according to the equations provided by Jenkins and Glasser. With the calculated lattice enthalpy (Table S5) the gas-phase enthalpy of formation (Table S3) was converted into the solid state (standard conditions) enthalpy of

formation (Table S6). These molar standard enthalpies of formation (ΔH_m) were used to calculate the molar solid state energies of formation (ΔU_m) according to equation 2.

$$\Delta U_m = \Delta H_m - \Delta n\, RT \quad \textbf{(2)}$$

(Δn being the change of moles of gaseous components)

Table S5. Calculated gas phase heat of formation, molecular volumes, lattice energies and lattice enthalpies of **1** as well as **3**–**7**.

	$\Delta_f H°$(g,M) / kJ mol^{-1}	V_M / nm^3	U_L / kJ mol^{-1}	ΔH_L / kJ mol^{-1}
1	1002.3			
3	1714.0	0.2632	1321.1	1324.9
4	1950.4	0.2891	1335.8	1324.9
5	2010.3	0.2703	1355.1	1362.6
6	2113.0	0.2922	1315.8	1323.3
7	2246.7	0.3033	1297.4	1304.8

Table S6. Solid state energies of formation ($\Delta_f U°$) of **1** as well as **3**–**7**.

	$\Delta_f H°$(s) / kcal mol^{-1}	$\Delta_f H°$(s) / kJ mol^{-1}	Δn	$\Delta_f U°$(s) / kJ mol^{-1}	M / g mol^{-1}	$\Delta_f U°$(s) / kJ kg^{-1}
1	222.6	932.1	9	954.4	258.12	3697.1
3	81.6	341.5	8	361.3	334.30	1081.3
4	149.4	625.5	9	647.9	362.31	1788.8
5	154.7	647.7	13	679.9	292.18	2327.0
6	188.5	789.8	14	824.5	324.18	2543.3
7	224.9	941.9	14	976.6	320.19	3050.0

Notes: Δn being the change of moles of gaseous components when formed.

19.1.3 ^{15}N NMR Spectrum of 1,1'-Dinitramino-5,5'-bitetrazole (1)

A ^{15}N spectrum of **1** was measured in DMSO-*d6* which is depicted in the following Figure S1. The resonanced were assigned accordingto our experience and a MP2 GIAO NMR calculation using the Gaussian09 software.[S11]

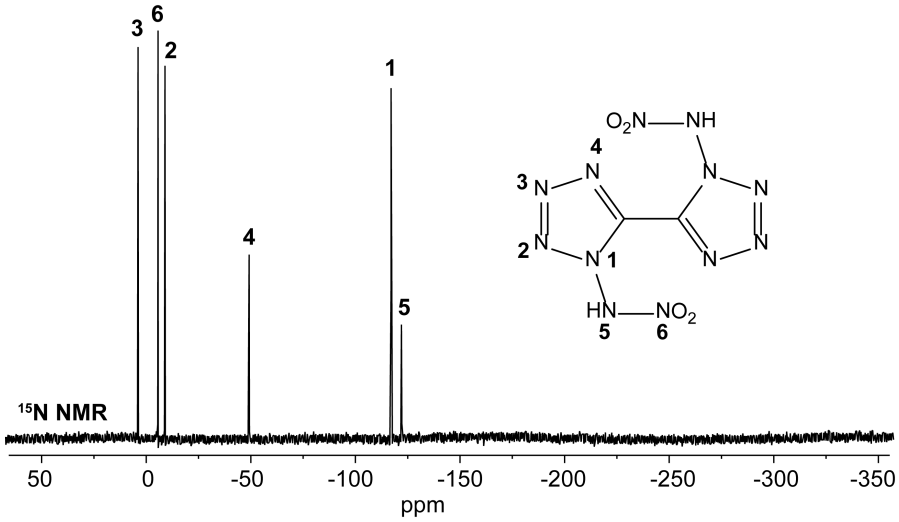


Figure S1. ^{15}N NMR spectra of **1**.

19.1.4 Experimental Part

General Procedures

Raman spectra were recorded with a Bruker MultiRAM FT-Raman instrument fitted with a liquid-nitrogen-cooled germanium detector and a Nd:YAG laser (λ = 1064 nm), infrared spectra were measured with a Perkin–Elmer Spectrum BX-FTIR spectrometer equipped with a Smiths DuraSamplIR II ATR device. All spectra were recorded at ambient temperature; the samples were neat solids. NMR spectra were recorded with a JEOL Eclipse 400 ECX instrument, all samples were measured at 25 °C. Mass spectrometric data were obtained with a JEOL MStation JMS 700 spectrometer (DEI^+ / $FAB^{+/-}$). C/H/N analysis was carried out by the department's internal micro analytical laboratory on a *Elementar Vario el* by pyrolysis of the sample and subsequent analysis of the formed gases. Differential Scanning Calorimetry (DSC) was performed on a *LINSEIS DSC PT10* with about 1 mg substance in a perforated aluminum vessel and a heating rate of 5 K min^{-1} and a nitrogen steam of 5 L h^{-1}. Melting points were determined in the same way. The sensitivities of the compounds were determined according to the BAM (German: Bundesanstalt für Materialforschung und Prüfung) standard for friction and impact.[S9] The impact sensitivities were tested according to STANAG 4489 modified instruction using a BAM drophammer. The friction sensitivities were tested according to STANAG 4487 modified instructions using a BAM friction tester. The tested compounds were classified from the results by the "UN Recommendations on the Transport of Dangerous Goods". Additionally, all compounds were tested for sensitivity towards electrical discharge using an Electric Spark Tester ESD 2010 EN. Energetic properties have been calculated with the EXPLO5 6.02 computer[S10] code using the to RT converted X-ray density and calculated

solid state heats of formation. These were computed by the atomization method as described in recently published papers. Electronic enthalpies were calculated with the Gaussian09 software[S11] suite using the CBS-4M method.

19.1.5 References

[S1] *CrysAlisPro*, Oxford Diffraction Ltd., version 171.33.41, **2009**.

[S2] *SIR-92*, *A program for crystal structure solution*: A. Altomare, G. Cascarano, C. Giacovazzo, A. Guagliardi, *J. Appl. Crystallogr.* **1993**, *26*, 343.

[S3] a) A. Altomare, G. Cascarano, C. Giacovazzo, A. Guagliardi, A. G. G. Moliterni, M. C. Burla, G. Polidori, M. Camalli, R. Spagna, *SIR97*, **1997**; b) A. Altomare, M. C. Burla, M. Camalli, G. L. Cascarano, C. Giacovazzo, A. Guagliardi, A. G. G. Moliterni, G. Polidori, R. Spagna, *J. Appl. Crystallogr.* **1999**, *32*, 115–119.

[S4] a) G. M. Sheldrick, *SHELX-97*, University of Göttingen, Göttingen, Germany, **1997**; b) G. M. Sheldrick, *Acta Crystallogr., Sect. A* **2008**, *64*, 112–122.

[S5] A. L. Spek, *PLATON*, *A Multipurpose Crystallographic Tool*, Utrecht University, The Netherlands, **1999**.

[S6] *SCALE3 ABSPACK – An Oxford Diffraction program* (1.0.4, gui: 1.0.3), Oxford Diffraction Ltd., **2005**.

[S7] a) J. W. Ochterski, G. A. Petersson, J. A. Montgomery, *J. Chem. Phys*. **1996**, *104*, 2598–2619; b) J. A. Montgomery, M. J. Frisch, J. W. Ochterski, G. A. Petersson, *J. Chem. Phys.* 2**000**, *12*, 6532–6542.

[S8] P. J. Lindstrom, W. G. Mallard (Editors), NIST Standard Reference Database Number 69, http://webbook.nist.gov/chemistry/ (Juni **2011**).

[S9] a) Reichel & Partner GmbH, http://www.reichel-partner.de; b) Test methods according to the UN Recommendations on the Transport of Dangerous Goods, *Manual of Test and Criteria*, fourth revised edition, United Nations Publication, New York and Geneva, **2003**, ISBN 92–1-139087–7, Sales No. E.03.VIII.2; 13.4.2 Test 3 a (ii) BAM Fallhammer.

[S10] M. Sućeska, EXPLO5 V6.02 program, *Brodarski Institute,* Zagreb, Croatia, **2014**.

[S11] Gaussian 09, M. J. Frisch, G. W. Trucks, H. B. Schlegel, G. E. Scuseria, M. A. Robb, J. R. Cheeseman, G. Scalmani, V. Barone, B. Mennucci, G. A. Petersson, H. Nakatsuji, M. Caricato, X. Li, H. P. Hratchian, A. F. Izmaylov, J. Bloino, G. Zheng, J. L. Sonnenberg, M. Hada, M. Ehara, K. Toyota, R. Fukuda, J. Hasegawa, M. Ishida, T. Nakajima, Y. Honda, O. Kitao, H. Nakai, T. Vreven, J. A. Montgomery, Jr., J. E. Peralta, F. Ogliaro, M. Bearpark, J. J. Heyd, E. Brothers, K. N. Kudin, V. N. Staroverov, R. Kobayashi, J. Normand, K. Raghavachari, A. Rendell, J. C. Burant, S. S. Iyengar, J. Tomasi, M. Cossi, N. Rega, J. M. Millam, M. Klene, J. E. Knox, J. B. Cross, V. Bakken, C. Adamo, J. Jaramillo, R. Gomperts, R. E. Stratmann, O. Yazyev, A. J. Austin, R. Cammi, C. Pomelli, J. W. Ochterski, R. L. Martin, K. Morokuma, V. G. Zakrzewski, G. A. Voth, P. Salvador, J. J. Dannenberg, S. Dapprich, A. D. Daniels, Ö. Farkas, J. B. Foresman, J. V. Ortiz, J. Cioslowski, and D. J. Fox, Gaussian, Inc., Wallingford CT, 2009.

19.2 Supplementary Information: Metal Salts and Complexes of 1,1'-Dinitramino-5,5'-bitetrazole

19.2.1 X-Ray Diffraction

For all compounds (except for **4**, **15** and **16**), an Oxford Xcalibur3 diffractometer with a CCD area detector was employed for data collection using Mo-*K*α radiation (λ = 0.71073 Å). By using the CRYSALISPRO software[S2] the data collection and reduction were performed. The structures were solved by direct methods (SIR-92,[S3] SIR-97[S4] or SHELXS-97[S5]) and refined by full-matrix least-squares on *F*2 (SHELXL[S5]) and finally checked using the PLATON software[S6] integrated in the WinGX software suite. The non-hydrogen atoms were refined anisotropically and the hydrogen atoms were located and freely refined. The absorptions were corrected by a SCALE3 ABSPACK multiscan method.[S7] All DIAMOND2 plots are shown with thermal ellipsoids at the 50% probability level and hydrogen atoms are shown as small spheres of arbitrary radii. The crystal structures of compounds **4**, **15** and **16** were determined at 100 K on a Bruker D8 Venture TXS diffractometer equipped with a multilayer monochromator, a Photon 2 detector, and a rotating-anode generator (MoKα radiation). The SADABS program embedded in the Bruker APEX3 software has been used for multi-scan absorption corrections in all structures.[S8]

Table S1. Crystallographic data and refinement parameters of compound **2**, **6**, **7a** and **7b**.

	2	**6**	**7a**	**7b**
Formula	$C_6H_8N_{10}O_4$	$CH_2LiN_4O_4$	$C_2H_4N_{12}Na_2O_6$	$C_2H_4N_{12}Na_2O_6$
FW [g mol^{-1}]	284.22	306.06	338.08	338.08
Crystal system	Triclinic	Monoclinic	Monoclinic	Orthorhombic
Space Group	*P*−1 (No. 2)	$P2_1/c$ (No. 14)	$P2_1/c$ (No. 14)	*Pbca* (No. 61)
Color / Habit	Colorless block	Colorless block	Colorless block	Colorless block
Size [mm]	0.01 x 0.03 x 0.10	0.15 x 0.34 x 0.39	0.08 x 0.15 x 0.28	0.29 x 0.45 x 0.56
a [Å]	4.1866(7)	8.2760(9)	8.8347(5)	6.2136(3)
b [Å]	7.2348(10)	10.8140(8)	9.4711(5)	10.9858(6)
c [Å]	10.3368(13)	6.0650(4)	7.2402(4)	16.9609(8)
α [°]	81.092(5)	90	90	90
β [°]	83.309(6)	106.073(10)	105.804(5)	90
γ [°]	75.044(6)	90	90	90
V [Å^3]	297.88(8)	521.58(8)	582.92(6)	1157.77(10)
Z	1	2	2	4
$\rho_{calc.}$ [g cm^{-3}]	1.584	1.949	1.927	1.940
μ [mm^{-1}]	0.134	0.176	0.236	0.238
F(000)	146	308	340	680
$\lambda_{MoK\alpha}$[Å]	0.71073	0.71073	0.71073	0.71073
T [K]	173	173	173	123
ϑ min-max [°]	3.3, 26.0	4.2, 26.7	4.3, 26.0	4.4, 26.0
Dataset h; k; l	−5:4; −8:8; −12:12	−5:10; −13:13; −7:7	−10:10; −11:11; −6:8	−7:6; −13:13; −20:20
Reflect. coll.	3156	3905	2933	8554
Independ. refl.	1159	1105	1136	1132
R_{int}	0.039	0.032	0.027	0.022
Reflection obs.	880	893	956	1059
No. parameters	96	108	108	108
R_1 (obs)	0.0481	0.0334	0.0305	0.0277
wR_2 (all data)	0.1184	0.0805	0.0812	0.0791
S	1.08	1.08	1.11	1.09
Resd. Dens.[e Å^{-3}]	−0.22, 0.22	−0.28, 0.26	−0.26, 0.26	−0.21, 0.37
Device type	Bruker D8 Venture rotating anode	Oxford XCalibur3 CCD	Oxford XCalibur3 CCD	Oxford XCalibur3 CCD
Solution	SIR-92	SIR-92	SIR-92	SHELXS-97
Refinement	SHELXL-97	SHELXL-97	SHELXL-97	SHELXL-97
Absorpt. corr.	multi-scan	multi-scan	multi-scan	multi-scan
CCDC	1502966	1500005	1500002	1500003

Table S2. Crystallographic data and refinement parameters of compound **8**–**11**.

	8	**9**	**10**	**11**
Formula	$C_2N_{12}O_4Rb_2$	$C_2N_{12}O_4Cs_2$	$C_2Ag_2N_{12}O_4$	$C_2H_{18}N_{18}O_4Ni$
FW [g mol^{-1}]	427.08	521.96	471.88	417.05
Crystal system	Triclinic	Monoclinic	Monoclinic	Monoclinic
Space Group	*P*−*1* (No. 2)	$P2_1/c$ (No. 14)	*P*2/*c* (No. 13)	$P2_1/c$ (No. 14)
Color / Habit	Colorless needle	Colorless needle	Colorless plate	Purple cylinder
Size [mm]	0.03 x 0.05 x 0.44	0.04 x 0.09 x 0.37	0.02 x 0.10 x 0.12	0.09 x 0.13 x 0.26
a [Å]	5.3034(5)	5.5885(2)	6.7520(4)	13.5062(12)
b [Å]	7.0632(6)	12.4847(4)	5.0649(4)	11.5426(8)
c [Å]	8.5675(7)	8.7893(3)	14.1529(9)	10.4455(7)
α [°]	66.821(8)	90	90	90
β [°]	86.667(7)	92.250(3)	92.180(6)	95.176(7)
γ [°]	70.964(8)	90	90	90
V [Å^3]	277.98(5)	612.76(4)	483.65(6)	1621.8(2)
Z	1	2	2	4
$\rho_{ccalc.}$ [g cm^{-3}]	2.551	2.829	3.240	1.708
μ [mm^{-1}]	8.845	5.989	4.097	1.255
F(000)	202	476	444	864
$\lambda_{MoK\alpha}$[Å]	0.71073	0.71073	0.71073	0.71073
T [K]	173	173	173	173
ϑ min-max [°]	4.3, 26.0	4.6, 26.0	4.3, 26.0	4.1, 25.0
Dataset h; k; l	−6:6; −8:8; −10:10	−6:6; −15:15; −10:10	−7:8; −5:6; −17:17	−10:16; −13:13; −12: 12
Reflect. coll.	3969	8446	2377	7466
Independ. refl.	1096	1195	955	2837
R_{int}	0.041	0.034	0.029	0.063
Reflection obs.	1000	1061	761	1838
No. parameters	91	91	93	232
R_1 (obs)	0.0242	0.0172	0.0333	0.0503
wR_2 (all data)	0.0509	0.0386	0.0779	0.0992
S	1.04	1.08	1.05	0.97
Resd. Dens.[e Å^{-3}]	−0.47, 0.49	−0.37, 0.77	−1.43, 0.85	−0.53, 0.81
Device type	Oxford XCalibur3 CCD	Oxford XCalibur3 CCD	Oxford XCalibur3 CCD	Bruker D8 Venture rotating anode
Solution	SIR-92	SIR-92	SHELXS-97	SHELXS-97
Refinement	SHELXL-97	SHELXL-97	SHELXL-97	SHELXL-97
Absorpt. corr.	multi-scan	multi-scan	multi-scan	multi-scan
CCDC	1500001	1500004	1524647	1524646

Table S3. Crystallographic data and refinement parameters of compound **12**, **13**, **15** and **16**.

	12	**13**	**15**	**16**
Formula	$C_2H_{14}CuN_{16}O_5$	$C_2H_{12}N_{16}O_4Zn$	$C_2H_8N_{12}O_8Ba$	$C_2H_{12}N_{12}O_{10}Ba$
FW [g mol^{-1}]	405.83	389.65	415.82	501.58
Crystal system	Monoclinic	Monoclinic	Monoclinic	Monoclinic
Space Group	*C*2/*c* (No. 15)	*P*2$_1$/*n* (No. 14)	*P*2$_1$/*c* (No. 14)	*P*2$_1$/*n* (No. 14)
Color / Habit	Blue block	Colorless block	Colorless block	Colorless block
Size [mm]	0.05 x 0.11 x 0.23	0.10 x 0.13 x 0.20	0.03 x 0.07 x 0.10	0.03 x 0.06 x 0.09
a [Å]	11.4131(5)	10.2414(3)	10.7948(3)	8.9593(3)
b [Å]	7.4648(3)	10.6483(3)	15.0619(4)	9.5952(3)
c [Å]	17.2079(8)	13.1297(4)	9.3539(2)	17.9981(6)
α [°]	90	90	90	90
β [°]	98.739(5)	94.149(3)	110.333(1)	92.798(1)
γ [°]	90	90	90	90
V [Å^3]	1449.03(11)	1428.09(7)	1426.09(6)	1545.39(9)
Z	4	4	4	4
$\rho_{ccalc.}$ [g cm^{-3}]	1.860	1.812	1.937	2.156
μ [mm^{-1}]	1.570	1.774	3.849	2.651
F(000)	828	792	824	976
$\lambda_{MoK\alpha}$[Å]	0.71073	0.71073	0.71073	0.71073
T [K]	123	173	100	173
ϑ min-max [°]	4.2, 26.0	4.1, 26.0	2.8, 27.5	2.3, 26.0
Dataset h; k; l	−13:14; −9:9; −21:21	−12:12; −13:8; −16:14	−14:14; −19:19; −12:12	−11:11; −11:11; −22:22
Reflect. coll.	5250	10947	23112	49826
Independ. refl.	1422	2785	3271	3024
R_{int}	0.040	0.030	0.029	0.030
Reflection obs.	1205	2310	2910	2875
No. parameters	117	256	240	246
R_1 (obs)	0.0300	0.0257	0.0202	0.0162
wR_2 (all data)	0.0695	0.0675	0.0501	0.0868
S	1.08	1.03	1.07	1.43
Resd. Dens.[e Å^{-3}]	−0.31, 0.27	−0.37, 0.58	−0.29, 0.86	−1.12, 0.80
Device type	Oxford XCalibur3 CCD	Oxford XCalibur3 CCD	Oxford XCalibur3 CCD	Oxford XCalibur3 CCD
Solution	SHELXS-97	SHELXS-97	SHELXS-97	SHELXS-97
Refinement	SHELXL-97	SHELXL-97	SHELXL-97	SHELXL-97
Absorpt. corr.	multi-scan	multi-scan	multi-scan	multi-scan
CCDC	1502968	1510459	1510459	1510459

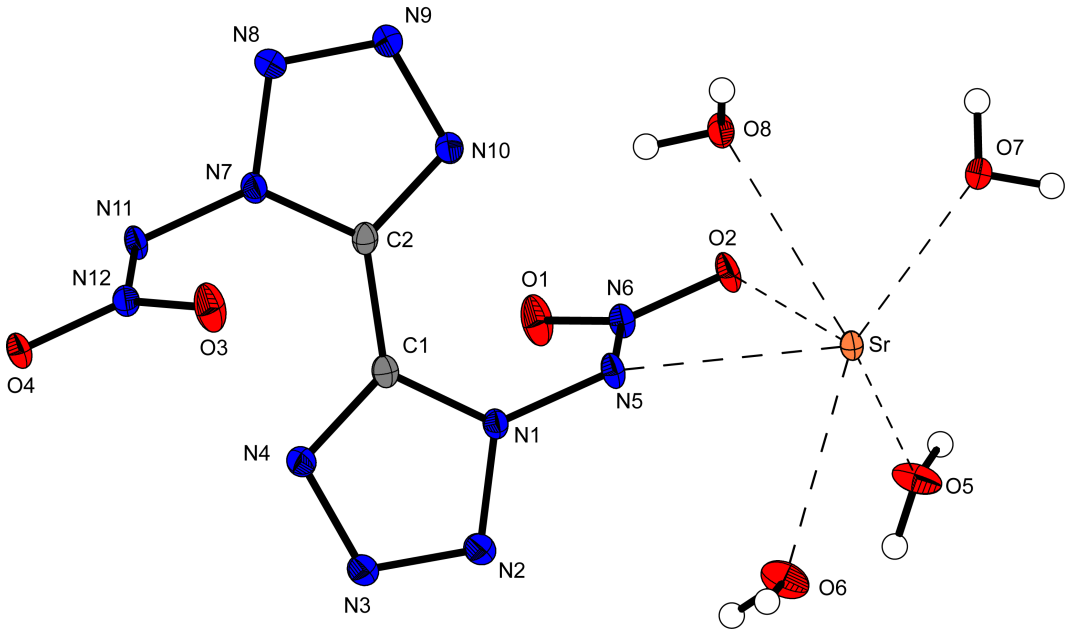


Figure S1. Molecular structure of **15** showing the atom-labelling scheme. Thermal ellipsoids represent the 50% probability level.

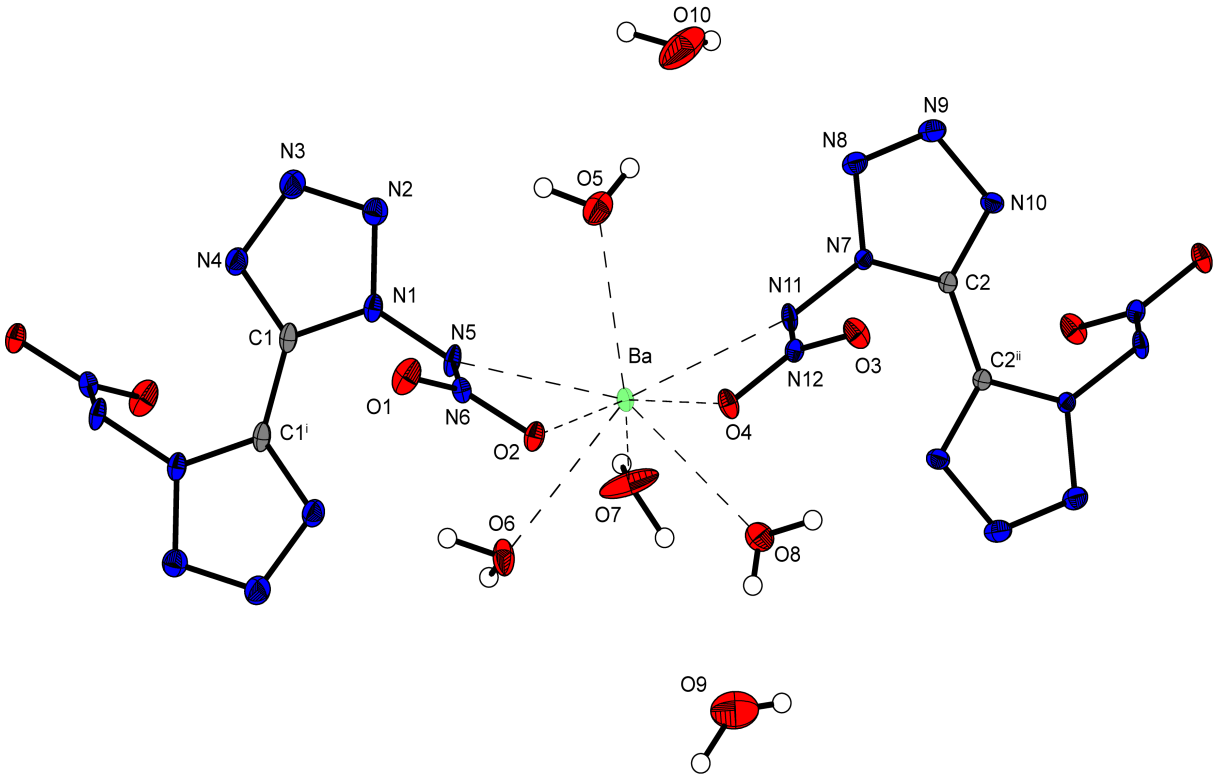


Figure S2. Extended molecular structure of **16** showing the atom-labelling scheme. Thermal ellipsoids represent the 50% probability level. Symmetry codes: (i) −x, −y, 2−z; (ii) 1−x, −y, 1−z.

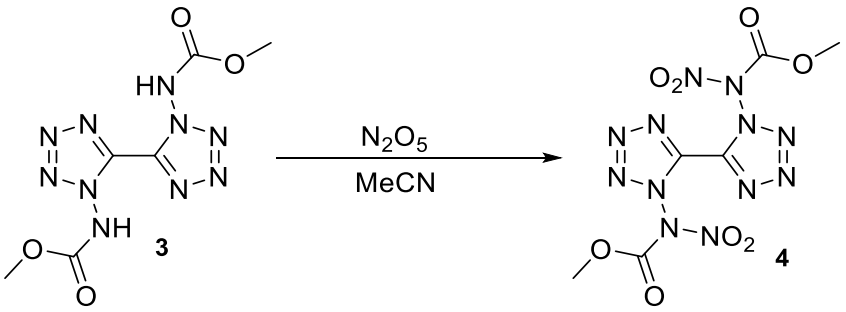
19.2.2 Experimental Part

General Procedures

Differential Scanning Calorimetry (DSC) was performed on a LINSEIS DSC PT10 with about 1 mg substance in a perforated aluminum vessel with a heating rate of 5 $K \cdot min^{-1}$ and a nitrogen flow of 5 $dm^3 \cdot h^{-1}$. Differential Thermal Analysis (DTA) measurements were carried out in glass tubes on an OZM DTA 552-Ex device with a heating rate of 5 $K \cdot min^{-1}$. Thermal gravimetric analysis (TGA) measurements were performed on a Perkin Elmer TGA4000 with a heating rate of 5 K min^{-1} in Al_2O_3 crucibles. The NMR spectra were recorded with a 400 MHz instrument (^1H 399.8 MHz, ^{13}C 100.5 MHz, ^{14}N 28.9 MHz, and ^{15}N 40.6 MHz). Chemical shifts are given in parts per million relative to tetramethylsilane (^1H, ^{13}C) and nitromethane (^{14}N, ^{15}N). Infrared spectra were measured with a Perkin-Elmer Spectrum BX-FTIR spectrometer equipped with a Smiths DuraSamplIR II ATR device. Transmittance values are qualitatively described as "very strong" (vs), "strong" (s), "medium" (m), and "weak" (w). Raman spectra were recorded using a Bruker MultiRAM FT-Raman instrument fitted with a liquid-nitrogen cooled germanium detector and a Nd:YAG laser (λ = 1064 nm). The intensities are quoted as percentages of the most intense peak and are given in parentheses. Low-resolution mass spectra were recorded with a JEOL MStation JMS 700 (DEI^+ / $FAB^{+/-}$). Elemental analysis was carried out using a Vario Micro from the Elementar Company.

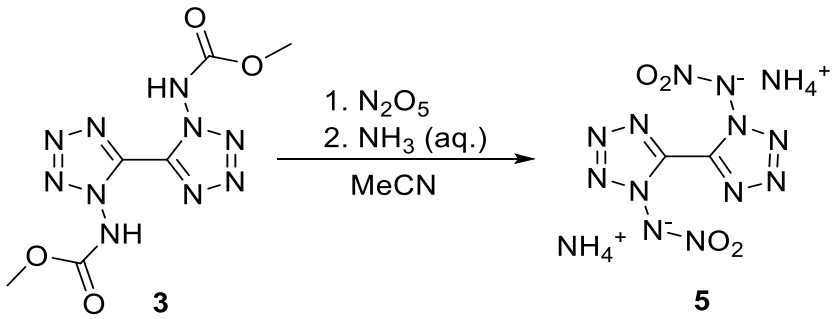
The impact sensitivity tests were carried out according to STANAG 4489[S9] modified instruction[S10] using a Bundesanstalt für Materialforschung (BAM) drophammer.[S11] The friction sensitivity tests were carried out according to STANAG 4487[S12] modified instruction[S13] using the BAM friction tester. The classification of the tested compounds results from the "UN Recommendations on the Transport of Dangerous Goods".[S14] All compounds were tested upon the sensitivity toward electrical discharge using the Electric Spark Tester ESD 2010 EN.[S15]

***1N,1N'*-Dimethylnitrocarbamate-*5,5'*-bitetrazole (4)**



0.45 g (4.17 mmol) N_2O_5 was dissolved in 50 mL MeCN at −5 °C and 0.3 g **3**[S1] (1.05 mmol) was added portion wise. The mixture was stirred for 2.5 h at −5 °C and finally quenched by adding the mixture to 50 g of ice-water. The precipitate was filtered off giving **4** (355 mg, 0.95 mmol, 90 %). **DTA** (5 °C min^{-1}): 102 °C (dec.); **IR** (atr, cm^{-1}) $\tilde{\nu}$ = 3223 (w), 2969 (w), 1794 (m), 1658 (m), 1438 (w), 1408 (w), 1322 (m), 1220 (s), 1180 (m), 1103 (w), 1041 (w), 990 (w), 936 (w), 864 (w), 818 (m), 769 (s), 732 (m), 666 (m), 590 (w); **^{1}H NMR** (dmso-*d_6*, 25 °C, ppm): δ: 3.85 (s, 6H, CH_3); **^{13}C{^{1}H} NMR** (dmso-*d_6*, 25 °C, ppm) δ: 48.7 (CH_3), 124.3 (C_Q), 141.0 (C=O); **^{14}N NMR** (dmso-*d_6*, 25 °C, ppm): δ = −66; **MS** *m/z* (FAB^+): 375.4 ($C_6H_7N_{12}O_8^+$); **EA** ($C_6H_6N_{12}O_8$, 374.19): calc.: C 19.26, H 1.62; N 44.92; found: C 20.31, H 1.90, N 44.73 %; **BAM drophammer**: 1 J, **friction tester**: < 5 N, **ESD**: 3 mJ.

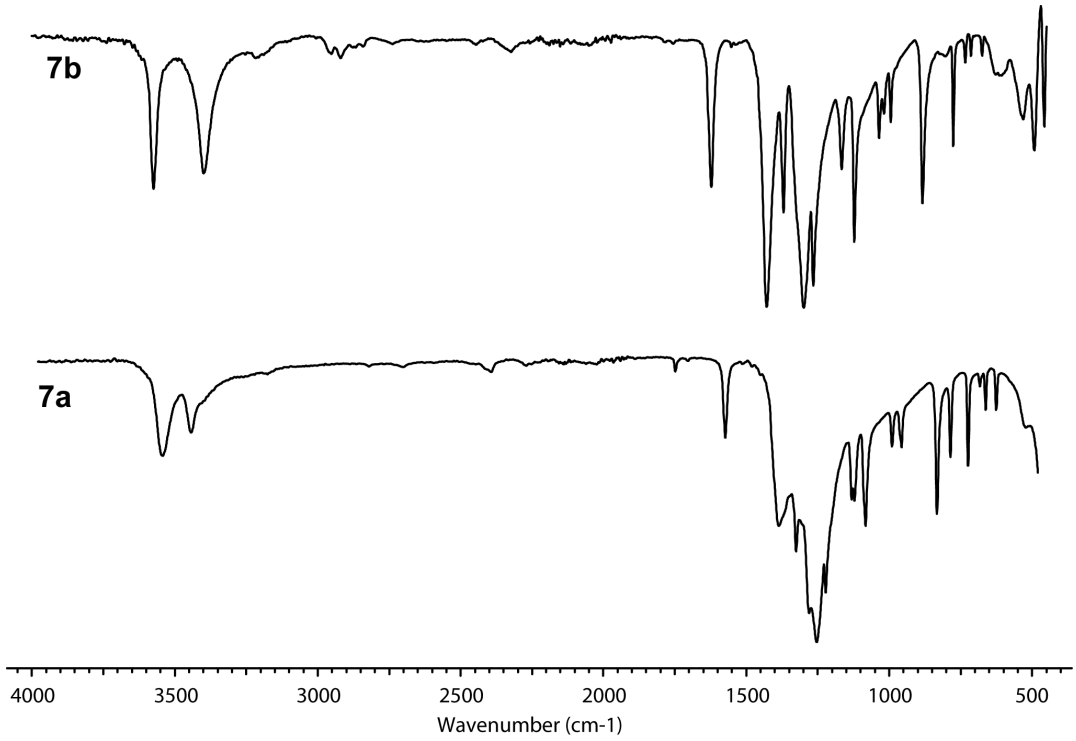
Diammonium 1,1'-dinitramino-5,5'-bitetrazolate (5)



1.00 g (3.52 mmol) of **3**[S1] was suspended in 50 mL dry acetonitrile and cooled to −10 °C. 1.5 g of dinitrogen pentoxide (13.9 mmol) was added all at once and the reaction mixture was stirred for 2 h at the initial temperature. An excess of concentrated ammonia solution (3 mL) was added to the obtained solution and the suspension was stirred for 20 minutes. The pH-value was checked to be above 9 and the colorless precipitate was collected by suction filtration and washed with ice-cold water (1 mL) and ethanol to give **5** (0.89 g, 3.06 mmol, 87 %). **IR** (atr, cm^{-1}) $\tilde{\nu}$ = 3177 (w), 3050 (w), 1395 (s), 1368 (s), 1280 (s), 1259 (s), 1179 (w), 1126 (m), 1036

(w), 1009 (w), 995 (w), 875 (s), 778 (m), 772 (w); **^{1}H NMR** (dmso-d_6, 25 C, ppm): δ: 7.07 (s, 8H, NH_4^+); **^{13}C{^{1}H} NMR** (dmso-d_6, 25 °C, ppm) δ: 140.4 (C_Q); **^{14}N NMR** (dmso-d_6, 25 °C, ppm): δ = −359.

19.2.3 IR Spectroscopy of 7a and 7b



19.2.4 References

[S1] D. Fischer, T. M. Klapötke, J. Stierstorfer, *Angew. Chem. Int. Ed.* **2014**, *53*, 8172−8175.

[S2] *CrysAlisPro*, Oxford Diffraction Ltd., version 171.33.41, **2009**.

[S3] *SIR-92*, *A program for crystal structure solution*: A. Altomare, G. Cascarano, C. Giacovazzo, A. Guagliardi, *J. Appl. Crystallogr.* **1993**, *26*, 343.

[S4] a) A. Altomare, G. Cascarano, C. Giacovazzo, A. Guagliardi, A. G. G. Moliterni, M. C. Burla, G. Polidori, M. Camalli and R. Spagna, *SIR97*, 1997; b) A. Altomare, M. C. Burla, M. Camalli, G. L. Cascarano, C. Giacovazzo, A. Guagliardi, A. G. G. Moliterni, G. Polidori and R. Spagna, *J. Appl. Crystallogr.* 1999, **32**, 115.

[S5] a) G. M. Sheldrick, *SHELX-97*, University of Göttingen, Göttingen, Germany, **1997**; b) G. M. Sheldrick, *Acta Crystallogr., Sect. A* 2008, **64**, 112.

[S6] A. L. Spek, *PLATON*, *A Multipurpose Crystallographic Tool*, Utrecht University, The Netherlands, **1999**.

[S7] *SCALE3 ABSPACK – An Oxford Diffraction program* (1.0.4, gui: 1.0.3), Oxford Diffraction Ltd., **2005**.

[S8] *APEX3*. Bruker AXS Inc., Madison, Wisconsin, USA.

[S9] NATO standardization agreement (STANAG) on explosives, *impact sensitivity tests*, no. 4489, 1st ed., Sept. 17, 1999.

[S10] WIWEB-Standardarbeitsanweisung 4-5.1.02, Ermittlung der Explosionsgefährlichkeit, hier der Schlagempfindlichkeit mit dem Fallhammer, Nov. 8, 2002.

[S11] http://www.bam.de

[S12] NATO standardization agreement (STANAG) on explosive, *friction sensitivity tests*, no. 4487, 1st ed., Aug. 22, 2002.

[S13] WIWEB-Standardarbeitsanweisung 4-5.1.03, Ermittlung der Explosionsgefährlichkeit oder der Reibeempfindlichkeit mit dem Reibeapparat, Nov. 8, 2002.

[S14] Impact: insensitive > 40 J, less sensitive ≥ 35 J, sensitive ≥ 4 J, very sensitive ≤ 3 J; Friction: insensitive > 360 N, less sensitive = 360 N, sensitive < 360 N and > 80 N, very sensitive ≤ 80 N, extremely sensitive ≤ 10 N, According to: *Recommendations on the Transport of Dangerous Goods, Manual of Tests and Criteria*, 4th edition, United Nations, New York-Geneva, 1999.

[S15] http://www.ozm.cz

19.3 Supplementary Information: Potassium *N*-Nitramino-5*H*-tetrazolates — Powerful Green Primary Explosives with High Initiation Capabilities

19.3.1 Experimental Procedure and General Methods

All chemicals and solvents were employed as received (Sigma-Aldrich, Fluka, Acros, ABCR). The chemical composition and morphology of selected samples were investigated with a Scanning electron microscope (SEM) NanoLab G3 (Helios). The samples were carbon-coated (BAL-TEC MED 020, Bal Tec AG) to prevent electrostatic charging and to increase the conductivity. Energy dispersive X-ray spectroscopy (EDX) was carried out with an acceleration voltage of 20 kV using an X-Max 80 SDD detector (Oxford Instruments). ^{1}H, ^{13}C, ^{14}N and ^{15}N spectra were recorded at ambient temperature using a JEOL Bruker 400, Eclipse 270, JEOL EX 400 or a JEOL Eclipse 400 instrument. The chemical shifts quoted in ppm in the text refer to typical standards such as tetramethylsilane (^{1}H, ^{13}C) and nitromethane (^{14}N, ^{15}N) in d_6-DMSO or $CDCl_3$ as the solvent. Endothermic and exothermic events of the described compounds, which indicate melting, evaporation, or decomposition, are given as the extrapolated onset temperatures. The samples were measured in a range of 25–400 °C at a heating rate of 5 °C min^{-1} through differential thermal analysis (DTA) with an OZM Research DTA 552-Ex instrument. Infrared spectra were measured with pure samples on a Perkin-Elmer BXII FT-IR system with a Smith DuraSampler IR II diamond ATR. Determination of the carbon, hydrogen, and nitrogen contents was carried out by combustion analysis using an Elementar Vario El (nitrogen values determined are often lower than those calculated due to their explosive behavior). Impact sensitivity tests were carried out according to STANAG 4489[S1] with a modified instruction[S2] using a BAM (Bundesanstalt für Materialforschung) drophammer.[S3,4] Ball drop impact sensitivities were determined for selected compounds on an OZM ball drop machine (BIT-132) following MIL-STD-1751A (method 1016) by dropping a free-falling steel ball onto the explosive compound.[S5] A sample of approximately 30 mg was placed on a steel block and spread into a 0.33 mm layer of substance. The steel ball guide was set to the desired height and the loaded impact block positioned underneath. By releasing the ball shield, a 1.27 cm steel ball, weighing 8.35 g, was allowed to fall onto the sample. Any visual observation of decomposition was regarded as a positive result. If no reaction occurred, the remaining substance was disposed, and the impact block loaded with a freshly prepared sample.[S6] The impact energy was calculated as the product of the weight of the steel ball and its fall height. The limiting impact energy was determined in conformity with the recommended UN method

for testing impact and friction sensitivities (1-in-6 approach), according to ST/SG/AC.10/11/Rev.6 (s. 13.4.2.3.3).[S7] An initial drop height was chosen, at which an explosion of the sample could be ensured. The impact energy level (ball guide height) was now stepwise decreased until no more reaction was observed. At this point, testing was continued up to a total of six trials at that certain energy level. If an explosion occurred, the procedure was repeated by decreasing the drop height. As soon as six trials at a fixed energy level emerge as negative, the next higher energy level, where at least one out of at least six trials resulted in an explosion, is determined as the limiting impact energy. The E_{50} impact energy represents the 50 % initiation probability level and was determined by the application of probit analysis as described by Šelešovský and Pachman.[S8] The probabilities of ignition were calculated at 6 levels of drop height, with 10 trials at each level and transformed into probit values. The probit values versus the logarithmic form of impact energies results in linear dependence, which enables a linear regression fit. The regression line was transformed back into the original coordinates (initiation probability vs. impact energy), expressing the whole sensitivity curve. The desired impact energies (E_{50}, all-fire, no-fire) were therefore obtained, as well as the corresponding 95 % confidence intervals according to the linear regression. Friction sensitivity tests were carried out according to STANAG 4487[S9] with a modified instruction[S10] using the BAM friction tester. The classification of the tested compounds results from the "UN Recommendations on the Transport of Dangerous Goods".[S11] Additionally all compounds were tested to determine the sensitivity toward electrical discharge using the OZM Electric Spark Tester ESD 2010 EN or OZM Electric Spark XSpark10 device.[S3] Hot plate and hot needle tests were performed in order to classify the initiation capability of selected complexes. The samples were fixed on a copper plate underneath adhesive tape and initiated by a red hot needle. Strong deflagration or detonation of the compound usually indicates a valuable primary explosive. The safe and straightforward hot plate test only shows the behavior of the unconfined sample toward fast heating on a copper plate. It does not necessarily allow any conclusions on a compound´s capability as a suitable primary explosive. Initiation capability tests of the newly investigated salts toward pentaerythritol tetranitrate (PETN) or hexogen (RDX) were carried out in a copper shell with a diameter of 7 mm and length of 88 mm filled with 200 mg of sieved secondary explosive (grain size < 100 µm). First, the secondary explosive was pressed with a weight of 8 kg, then the primary explosive to be investigated was subsequently filled on top of the main charge and pressed with the same pressure force. The shell was sealed by an insulator, placed in a retaining ring, which was soldered to a copper witness plate with a thickness of

1 mm and finally initiated by a type A electric igniter. A positive test is indicated by a hole in the copper plate and fragmentation of the shell caused by a deflagration-to-detonation transition (DDT) of the secondary explosive. Liquid-dried luminescent bacteria of the strain *Vibrio fischeri* NRRL-B-11177 provided by the HACH LANGE GmbH were used for the luminescent bacteria inhibition test to determine their toxicity toward aquatic organisms according to a modified procedure.[S12]

Procedure for the preparation of 1-amino-5*H*-tetrazole and 2-amino-5*H*-tetrazole:

Selective 1-amino-5*H*-tetrazole synthesis:

Hydrazine monohydrate (46.2 mL, 940 mmol) was dissolved in 200 ml ethanol and the mixture cooled to 0 °C with an ice bath. Under vigorous stirring benzaldehyde (24 mL, 236 mmol) was added dropwise over a time period of 5 min. After complete addition, the resulting mixture was further stirred for 1 min at this temperature before quenching with water (300 mL). The milky white aqueous phase was extracted with dichloromethane (3 x 300 mL) and the combined organic phases dried over $MgSO_4$. The solvent was removed under reduced pressure yielding benzhydrazone in form of a yellow, odorous oil (20.8 g, 193 mmol, 82 %). ^{1}H NMR ($CHCl_3$-*d*, 25 °C, ppm) δ: 7.71 (s, 1H, NC-*H*), 7.54–7.49 (m, 2H, C_{aromat}-*H*), 7.36–7.23 (m, 3H, C_{aromat}-*H*), 5.48 (s, 2H, -N*H*$_2$). Benzhydrazone (20.8 g, 193 mmol) was dissolved in triethyl orthoformate (60 mL, 364 mmol) and subsequently further reacted with sodium azide (16.0 g, 246 mmol). While stirring, glacial acetic acid (100 mL) was added dropwise and the resulting reaction mixture heated to 80 °C for 2.5 h. During the reaction, a color change from yellow to orange and finally red could be observed. After complete reaction, the warm mixture was poured into water (200 mL) and stirred overnight. The yellow precipitate formed was filtrated, washed with a small amount of water and dried overnight in air yielding 1-benzylideneaminotetrazole (13.2 g, 76.2 mmol, 40 %). ^{1}H NMR ($CHCl_3$-*d*, 25 °C, ppm) δ: 9.37 (s, 1H, N_4C-*H*), 8.87 (s, 1H, NC-*H*), 7.96–7.84 (m, 2H, C_{aromat}-*H*), 7.67–7.47 (m, 3H, C_{aromat}-*H*). Under vigorous stirring, concentrated hydrochloric acid (150 mL) was added to 1-benzylideneaminotetrazole (13.2 g, 76.2 mmol) and water (200 mL). The suspension obtained was refluxed for 30 min resulting in a clear yellow solution. The cleaved benzaldehyde was removed together with the solvent in vacuo at 80 °C and the residues checked by TLC upon reaction completion. The received yellow-white residue was neutralized with a saturated

solution of $NaHCO_3$ and extracted with EtOAc (3 x 400 mL). The combined organic phases were dried over $MgSO_4$ and the solvent removed under reduced pressure, yielding 1-amino-5*H*-tetrazole (6.40 g, 75.2 mmol, 99 %) in form of a yellow liquid.

Amination of 1,5*H*-tetrazole:

The performed synthesis of the two isomers was carried out analogous to a modified literature procedure.[S13] 1,5*H*-Tetrazole (14.0 g, 200 mmol) was dissolved in water (150 mL) and treated with Na_2CO_3 (23.2 g, 219 mmol). The resulting solution was heated to 75 °C, followed by the dropwise addition of hydroxylamine-*O*-sulfonic acid (27.2 g, 240 mmol) in water (120 mL). In the meantime, the pH value of the solution was maintained between 7 and 8 by periodic addition of a saturated solution of $NaHCO_3$. The reaction mixture was refluxed for 30 minutes followed by the evaporation of approximately half of the solvent under reduced pressure. After continuously extracting the remaining solution with ethyl acetate for two days, the evaporation of the extract gave a viscous oil containing both isomers. The isomers were separated by column chromatography (SiO_2, ethyl acetate/ dichloromethane 5:1, R_f = 0.71, 0.47) yielding highly pure 2-amino-5*H*-tetrazole (3.17 g, 37.2 mmol, 19 %) and 1-amino-5*H*-tetrazole (4.54 g, 53.4 mmol, 27 %) as colorless liquids.

1-Amino-5*H*-tetrazole

DTA (5 °C min^{-1}): 182 °C (exothermic); IR (ATR, cm^{-1}): $\tilde{\nu}$ = 3326 (m), 3197 (m), 3144 (m), 1626 (m), 1491 (w), 1430 (w), 1342 (w), 1273 (w), 1185 (s), 1098 (vs), 962 (s), 871 (s), 723 (m), 695 (m), 643 (vs); ^{1}H NMR (DMSO-d_6, 25 °C, ppm) δ: 9.24 (s, 1H, -C*H*), 7.10 (s, 2H, -NH_2); ^{13}C NMR (DMSO-d_6, 25 °C, ppm) δ: 143.4 (-*C*N_4); ^{15}N NMR (MeCN-d_3, 25 °C, ppm) δ: 6.8 (N3), −10.0 (N2), −53.8 (N4, d, $^2J_{N\text{-}H}$ = 11.2 Hz), −138.0 (N1, d, $^2J_{N\text{-}H}$ = 8.4 Hz), −308.4 (N5, t, $J_{N\text{-}H}$ = 73.1 Hz); EA: (CH_3N_5, 85.07) calcd: C 14.12, H 3.55, N 82.33 %; found: C 14.60, H 3.63, N 82.16 %.

2-Amino-5*H*-tetrazole

DTA (5 °C min^{-1}): 197 °C (exothermic); IR (ATR, cm^{-1}): $\tilde{\nu}$ = 3314 (m), 3144 (m), 3128 (m), 3083 (w), 3012 (w), 2978 (w), 1685 (w), 1613 (m), 1488 (m),1451 (m), 1434 (m), 1388 (w), 1374 (w), 1361 (w), 1285 (s), 1259 (w), 1218 (m), 1174 (s), 1141 (s), 1111 (s), 1103 (s), 1064 (m), 1024 (s), 992 (s), 975 (s), 928 (s), 876 (s), 803 (w), 797 (w), 745 (m), 722 (m), 704 (s), 680 (m), 666 (vs), 644 (m); ^{1}H NMR (DMSO-d_6, 25 °C, ppm) δ: 8.72 (s, 1H, -C*H*), 8.03 (s, 2H, -NH_2); ^{13}C NMR (DMSO-d_6, 25 °C, ppm) δ: 151.8 (-CN$_4$); ^{15}N NMR (MeCN-d_3, 25 °C, ppm) δ: −11.2 (N3), −53.9 (N4, d, $^{2}J_{N\text{-}H}$ = 12.2 Hz), −78.9 (N1, d, $^{2}J_{N\text{-}H}$ = 14.5 Hz), −92.6 (N2, d, $^{2}J_{N\text{-}H}$ = 7.9 Hz), −289.6 (N5, t, $J_{N\text{-}H}$ = 72.5 Hz); EA: (CH_3N_5, 85.07) calcd: C 14.12, H 3.55, N 82.33 %; found: C 14.45, H 3.58, N 82.26 %.

19.3.2 IR Spectroscopy

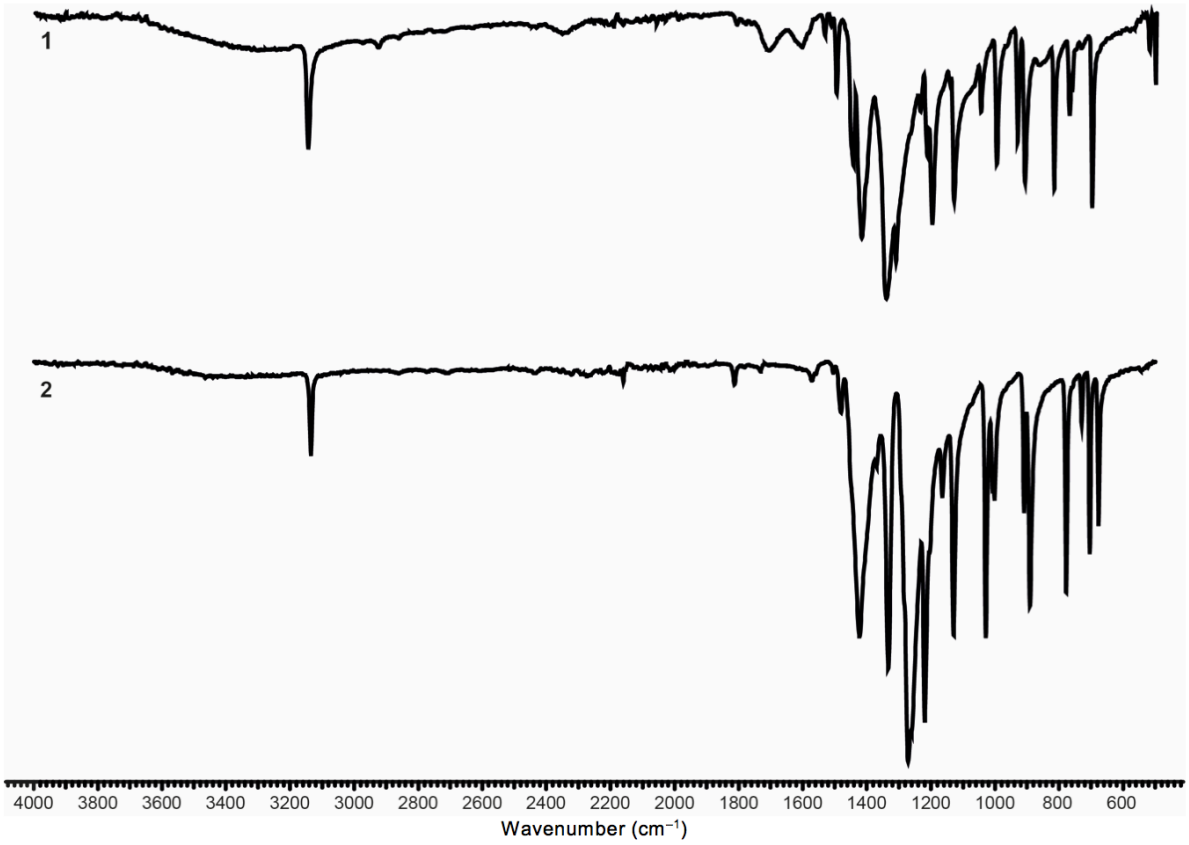


Figure S1. IR spectra of the potassium salts **1** and **2**.

19.3.3 X-Ray Diffraction

For all crystalline compounds, an Oxford Xcalibur3 diffractometer with a CCD area detector or Bruker D8 Venture TXS diffractometer equipped with a multilayer monochromator, a Photon 2 detector and a rotating-anode generator were employed for data collection using Mo-*K*α radiation (λ = 0.7107 Å). On the Oxford device, data collection and reduction were carried out using the Crysalispro software.[S14] On the Bruker diffractometer, the data were collected with the Bruker Instrument Service v3.0.21, the data reduction was performed using the SAINT V8.18C software (Bruker AXS Inc., 2011). The structures were solved by direct methods (SIR-92[S15], SIR-97[S16] or SHELXS-97[S17]) and refined by full-matrix least-squares on *F*2 (ShelxL[S17]) and finally checked using the platon software[S18] integrated in the WinGX[S19] software suite. The non-hydrogen atoms were refined anisotropically and the hydrogen atoms were located and freely refined. The absorptions were corrected by a Scale3 Abspack or Sadabs Bruker Apex3 multiscan method.[S20,21] All Diamond2 plots are shown with thermal ellipsoids at the 50 % probability level and hydrogen atoms are shown as small spheres of arbitrary radius.

Table S1. Crystallographic data of **1** and **2**.

	1	**2**
Formula	$CHKN_6O_2$	$CHKN_6O_2$
FW [g mol^{-1}]	167.98	167.98
Crystal system	monoclinic	orthorhombic
Space Group	$P2_1/c$	$Pbca$
Color/ Habit	colorless block	colorless rod
Size [mm]	0.22 x 0.29 x 0.60	0.15 x 0.30 x 0.30
a [Å]	9.0148(5)	12.1337(5)
b [Å]	8.1009(4)	6.7398(3)
c [Å]	8.7490(6)	13.7784(5)
α [°]	90	90
β [°]	117.605(8)	90
γ [°]	90	90
V [Å^3]	566.19(7)	1126.78(8)
Z	4	8
ρ_{calc} [g cm^{-3}]	1.973 (143 K)	1.983 (143 K)
μ [mm^{-1}]	0.879	0.884
F(000)	336	672
$\lambda_{MoK\alpha}$[Å]	0.71073	0.71073
T[K]	143 K	143 K
ϴ Min–Max [°]	4.7, 27.0	4.5, 26.0
Dataset	–11: 11; –10: 10; –11: 5	–14: 14; –8: 8; –16: 16
Reflections collected	4453	7959
Independent reflections	1232	1104
R_{int}	0.022	0.029
Observed reflections	1126	971
Parameters	95	95
R_1(obs)	0.0222	0.0196
w$R2$ (all data)	0.0576	0.0509
GooF	1.08	1.10
Resd. Dens. [eÅ^{-3}]	–0.28, 0.28	–0.24, 0.19
Absorption correction	multi-scan	multi-scan
CCDC	1849956	1849957

a) $R_1 = \Sigma||F_0|- |F_c||/ \Sigma|F_0|$; b) $wR_2 = [\Sigma[w(F_0 2\text{-}F_C^2)^2]/\Sigma[w(F_0)^2]]^{1/2}$; $w = [\sigma c^2(F_0^2)+(xP)^2+yP]^{-1}$ and $P=(F_0^2+2F_C^2)/3$; c) GooF = $\{\Sigma[w(F_O^2\text{-}F_C^2)^2]/(n\text{-}p)\}^{1/2}$ (n = number of reflections; p = total number of parameters).

19.3.4 Initiation Capability Tests



Figure S2. Positive initiation capability tests of compound **1** toward PETN using different amounts (5 mg, 10 mg, 20 mg, 50 mg).



Figure S3. Positive initiation capability tests of compound **1** toward RDX using different amounts (5 mg, 10 mg, 20 mg).



Figure S4. Positive initiation tests toward PETN (top) and RDX (bottom) using different amounts (5 mg, 10 mg) of compound **2**.

19.3.5 Hot Needle Tests

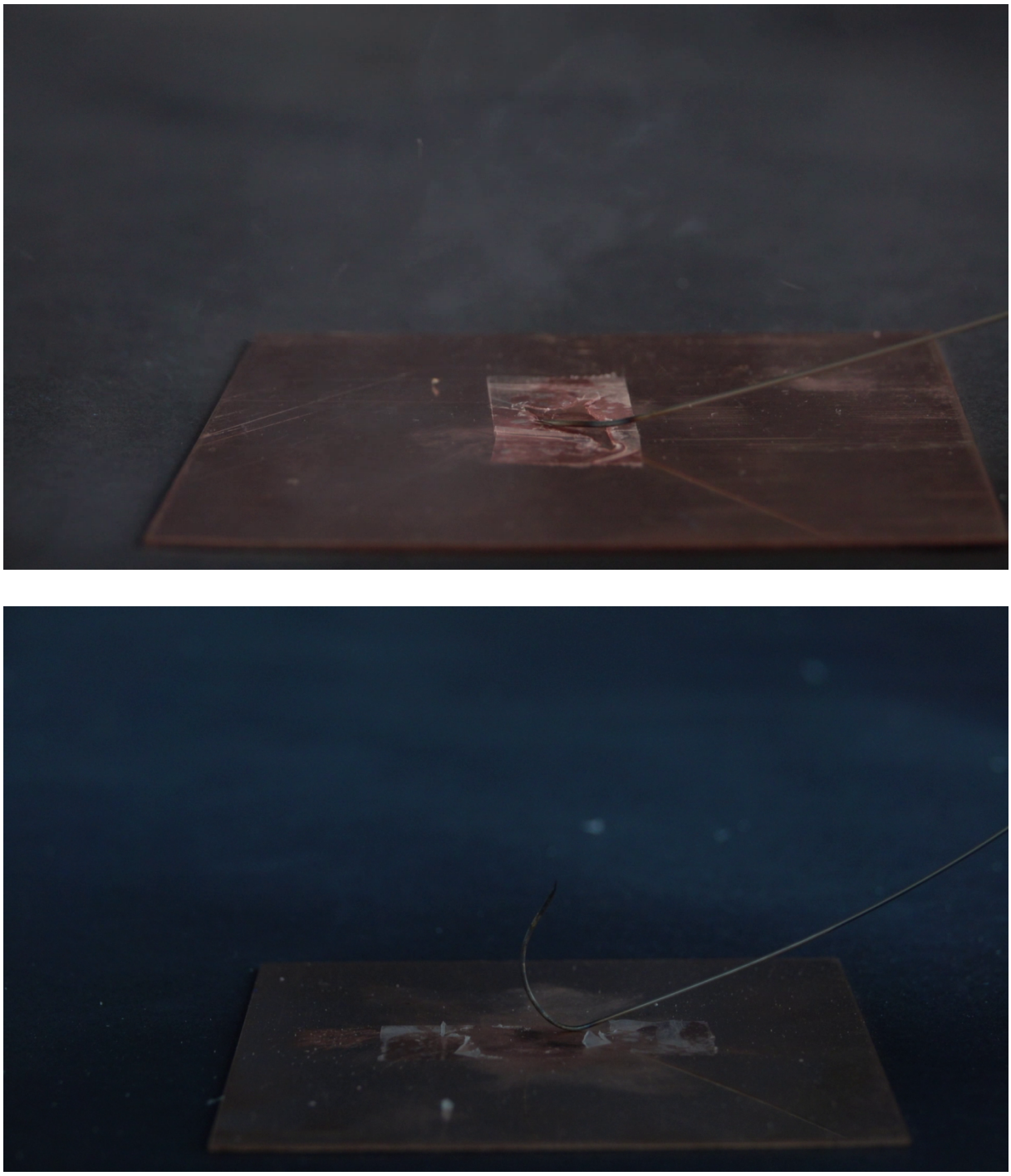


Figure S5 Deformed needles after the performed hot needle tests of **1** (top) and **2** (bottom).

19.3.6 Heat of Formation Calculations

All quantum chemical calculations were carried out using the Gaussian G09 program package.[S22] The enthalpies (H) and free energies (G) were calculated using the complete basis set (CBS) method of Petersson and coworkers in order to obtain very accurate energies. The CBS models are using the known asymptotic convergence of pair natural orbital expressions to extrapolate from calculations using a finite basis set to the estimated CBS limit. CBS-4 starts with an HF/3-21G(d) geometry optimization; the zero-point energy is computed at the same level. It then uses a large basis set SCF calculation as a base energy, and an MP2/6-31+G calculation with a CBS extrapolation to correct the energy through second order. A MP4(SDQ)/6-31+(d,p) calculation is used to approximate higher order contributions. In this study, we applied the modified CBS-4M.

Heats of formation of the synthesized potassium salts **1** and **2** were calculated using the atomization method (equation S1) using room temperature CBS-4M enthalpies, which are summarized in Table S2.[S23,S24]

$$\Delta_f H^\circ_{(g,\,M,\,298)} = H_{(Molecule,\,298)} - \sum H^\circ_{(Atoms,\,298)} + \sum \Delta_f H^\circ_{(Atoms,\,298)} \quad (S1)$$

Table S2. CBS-4M enthalpies for atoms C, H, N and O and their literature values for atomic $\Delta H_f^{\circ 298}$ / kJ mol^{-1}.

	$-H^{298}$ / a.u.	NIST[S11]
H	0.500991	218.2
C	37.786156	717.2
N	54.522462	473.1
O	74.991202	249.5

For ionic compounds, the lattice energy (U_L) and lattice enthalpy (ΔH_L) are calculated from the corresponding X-ray molecular volumes (converted to RT) according to the equations provided by *Jenkins* and *Glasser*.[S25] With the calculated lattice enthalpy the gas-phase enthalpy of formation was converted into the solid state (standard conditions) enthalpy of formation. The calculation results are summarized in Table S3.

Table S3. Heat of formation calculation of **1** and **2**.

M	$-H^{298}$[a] /a.u.	$\Delta_f H°$(g,M) /kJ mol^{-1}[b]	V_M /nm^3[c]	ΔU_L, ΔH_L;[d] /kJ mol^{-1}	$\Delta_f H°$(s)[e] /kJ mol^{-1}	Δn[f]	$\Delta_f U$(s)[g] /kJ kg^{-1}
1 anion	516.929042	267.2					
2 anion	516.934638	252.5					
K+	599.035967	487.4					
1		725.1	0.1448	630.4, 631.6	93.4	4.5	621.8
2		710.4	0.1441	631.2, 632.5	77.9	4.5	529.4

[a] CBS-4M electronic enthalpy; [b] gas phase enthalpy of formation; [c] molecular volumes taken from X-ray structures and corrected to room temperature; [d] lattice energy and enthalpy (calculated using Jenkins and Glasser equations); [e] standard solid state enthalpy of formation; [f] Δn being the change of moles of gaseous components when formed; [g] solid state energy of formation.

19.3.7 References

[S1] NATO standardization agreement (STANAG) on explosives, impact sensitivity tests, no. 4489, 1st ed., Sept. 17, 1999.

[S2] WIWEB-Standardarbeitsanweisung 4-5.1.02, Ermittlung der Explosionsgefährlichkeit, hier der Schlagempfindlichkeit mit dem Fallhammer, Nov. 8, 2002.

[S3] http://www.ozm.cz, Accessed June 2018.

[S4] http://www.bam.de, Accessed June 2018.

[S5] Military Standard 1751A (MIL-STD-1751A): safety and performance tests for qualification of explosives (high explosives, propellants and pyrotechnics), method 1016, Dec. 11, 2001.

[S6] OZM Research: Ball Drop Impact Test BIT-132, Instruction Manual, Rev. No. 1/17, 2017.

[S7] UN Model Regulation: Recommendations on the Transport of Dangerous Goods – Manual of Tests and Criteria, section 13.4.2.3.3, 2015.

[S8] J. Šelešovský, J. Pachman, Probit Analysis – a Promising Tool for Evaluation of Explosive´s Sensitivity, *Cent. Eur. J. Energ. Mater.* **2010**, *7*, 269–278.

[S9] NATO standardization agreement (STANAG) on explosive, friction sensitivity tests, no. 4487, 1st ed., Aug. 22, 2002.

[S10] WIWEB-Standardarbeitsanweisung 4-5.1.03, Ermittlung der Explosionsgefährlichkeit oder der Reibeempfindlichkeit mit dem Reibeapparat, Nov. 8, 2002.

[S11] Impact: insensitive > 40 J, less sensitive ≥ 35 J, sensitive ≥ 4 J, very sensitive ≤ 3 J; Friction: insensitive > 360 N, less sensitive = 360 N, sensitive < 360 N and > 80 N, very sensitive ≤ 80 N, extremely sensitive ≤ 10 N. According to the UN Recommendations on the Transport of Dangerous Goods, (+) indicates not safe for transport.

[S12] R. Scharf, Synthesis and characterization of new polynitro compounds and aquatic toxicity determination of energetic materials, PhD thesis, Ludwig Maximilian University Munich, 2016.

[S13] T. M. Klapötke, D. G. Piercey, J. Stierstorfer, Amination of energetic anions: high-performing energetic materials, *Dalton Trans.* **2012**, *41*, 9451–9459.

[S14] CrysAlisPRO (Version 171.33.41), Oxford Diffraction Ltd., 2009.

[S15] A. Altomare, G. Cascarano, C. Giacovazzo, A. Guagliardi, A Completion and refinement of crystal structures with SIR92, *J. Appl. Crystallogr.*, **1992**, *26*, 343–350.

[S16] a) A. Altomare, G. Cascarano, C. Giacovazzo, A. Guagliardi, A. G. G. Moliterni, M. C. Burla, G. Polidori, M. Camalli, R. Spagna, SIR97, **1997**; b) A. Altomare, M. C. Burla, M. Camalli, G. L. Cascarano, C. Giacovazzo, A. Guagliardi, A. G. G. Moliterni, G. Polidori, R. Spagna, A new tool for crystal structure determination and refinement, *J. Appl. Crystallogr.*, **1999**, *32*, 115–119.

[S17] a) G. M. Sheldrick, SHELXL-97, Program for the Refinement of Crystal Structures, University of Göttingen, Germany, **1997**; b) G. M. Sheldrick, A short history of SHELX, *Acta Crystallogr. Sect. A*, **2008**, *64*, 112–122.

[S18] A. L. Spek, PLATON, A Multipurpose Crystallographic Tool, Utrecht University, The Netherlands, **1999**.

[S19] L. J. Farrugia, *WinGX and ORTEP for Windows: an update*, *J. Appl. Cryst.*, **2012**, *45*, 849–854.

[S20] Empirical absorption correction using spherical harmonics, implemented in SCALE3 ABSPACK scaling algorithm (CrysAlisPro Oxford Diffraction Ltd., Version 171.33.41, **2009**).

[S21] *APEX3*. Bruker AXS Inc., Madison, Wisconsin, USA.

[S22] M. J. Frisch, G. W. Trucks, H. B. Schlegel, G. E. Scuseria, M. A. Robb, J. R. Cheeseman, G. Scalmani, V. Barone, B. Mennucci, G. A. Petersson, H. Nakatsuji, M. Caricato, X. Li, H.P. Hratchian, A. F. Izmaylov, J. Bloino, G. Zheng, J. L. Sonnenberg, M. Hada, M. Ehara, K. Toyota, R. Fukuda, J. Hasegawa, M. Ishida, T. Nakajima, Y. Honda, O. Kitao, H. Nakai, T. Vreven, J. A. Montgomery, Jr., J. E. Peralta, F. Ogliaro, M. Bearpark, J. J. Heyd, E. Brothers, K. N. Kudin, V. N. Staroverov, R. Kobayashi, J. Normand, K. Raghavachari, A. Rendell, J. C. Burant, S. S. Iyengar, J. Tomasi, M. Cossi, N. Rega, J. M. Millam, M. Klene, J. E. Knox, J. B. Cross, V. Bakken, C. Adamo, J. Jaramillo, R. Gomperts, R. E. Stratmann, O. Yazyev, A. J. Austin, R. Cammi, C. Pomelli, J. W. Ochterski, R. L. Martin, K. Morokuma, V. G. Zakrzewski, G. A. Voth, P. Salvador, J. J. Dannenberg, S. Dapprich, A. D. Daniels, O. Farkas, J.B. Foresman, J. V. Ortiz, J. Cioslowski, D. J. Fox, Gaussian 09 A.02, Gaussian, Inc., Wallingford, CT, USA, **2009**.

[S23] a) J. W. Ochterski, G. A. Petersson, and J. A. Montgomery Jr., A complete basis set model chemistry. V. Extensions to six or more heavy atmos, *J. Chem. Phys.* **1996**, *104*, 2598–2619; b) J. A. Montgomery Jr., M. J. Frisch, J. W. Ochterski G. A. Petersson, A complete basis set model chemistry. VI. Use of density functional geometries and frequencies, *J. Chem. Phys.* **2000**, *112*, 6532–6542.

[S24] a) L. A. Curtiss, K. Raghavachari, P. C. Redfern, J. A. Pople, Assessment of Gaussian-2 and density functional theories for the computation of enthalpies of formation, *J. Chem. Phys.* **1997**, *106*, 1063–1079; b) E. F. C. Byrd, B. M. Rice, Improved Prediction of Heats of Formation of Energetic Materials Using Quantum Mechanical Calculations, *J. Phys. Chem*. A **2006**, *110*, 1005–1013; c) B. M. Rice, S. V. Pai, J. Hare, Predicting heats of formation of energetic materials using quantum mechanical calculations, *Comb. Flame* **1999**, *118*, 445–458.

[S25] a) H. D. B. Jenkins, H. K. Roobottom, J. Passmore, L. Glasser, Relationships among Ionic Lattice Energies, Molecular (Formula Unit) Volumes, and Thermochemical Radii, *Inorg. Chem.* **1999,** *38,* 3609–3620; b) H. D. B. Jenkins, D. Tudela, L. Glasser, Lattice Potential Energy Estimation for Complex Ionic Salts from Density Measurements, *Inorg. Chem.* **2002**, *41*, 2364–2367.

19.4 Supplementary Information: Methylsemicarbazide as a Ligand in Late 3d Transition Metal Complexes

19.4.1 Compound Overview

Metal Salt	Ligand	co-Anion	Solvent	Conditions	Product	No.
$CuSO_4 \cdot 5\ H_2O$	2 MSC		H_2O	RT	$[Cu(H_2O)_2(MSC)_2]SO_4$	(**4**)
$CuCl_2 \cdot 2\ H_2O$	2 MSC		H_2O, 15% HCl	RT	$[CuCl_2(MSC)_2]$	(**5**)
$Cu(NO_3)_2 \cdot 3\ H_2O$	2 MSC		H_2O, EtOH	RT	$[Cu(NO_3)_2(MSC)_2]$	(**6**)
$Cu(ClO_4)_2 \cdot 6\ H_2O$	2 MSC		H_2O, 70% $HClO_4$	RT	$[Cu(ClO_4)_2(MSC)_2]$	(**7**)
$CuSO_4 \cdot 5\ H_2O$	1 MSC	2 NaN_3	H_2O	60 °C, 5 min	$[Cu(N_3)_2(MSC)_2]$	(**8**)
$ZnCl_2$	2 MSC		H_2O	RT	$[ZnCl_2(MSC)_2]$	(**9**)
$Zn(NO_3)_2 \cdot 6\ H_2O$	2 MSC		H_2O, EtOH	RT	$[Zn(NO_3)_2(MSC)_2]$	(**10**)
$Zn(ClO_4)_2 \cdot 6\ H_2O$	2 MSC		H_2O	RT	$[Zn(H_2O)_2(MSC)_2](ClO_4)_2$	(**11**)
$Zn(ClO_4)_2 \cdot 6\ H_2O$	3 MSC		H_2O	RT	$[Zn(MSC)_3](ClO_4)_2 \cdot H_2O$	(**12**)
$MnCl_2 \cdot 2\ H_2O$	2 MSC		H_2O	RT	$[MnCl_2(MSC)_2]$	(**13**)
$Mn(NO_3)_2 \cdot 4\ H_2O$	2 MSC		H_2O	RT	$[Mn(NO_3)_2(MSC)_2]$	(**14**)
$Mn(ClO_4)_2 \cdot 6\ H_2O$	2 MSC		H_2O	RT	$[Mn(H_2O)_2(MSC)_2](ClO_4)_2$	(**15**)
$CoCl_2 \cdot 6\ H_2O$	2 MSC		H_2O, conc. HCl	RT	$[CoCl_2(MSC)_2]$	(**16**)
$CoCl_2 \cdot 6\ H_2O$	2 MSC		H_2O, 2M HCl	RT	$[Co(H_2O)_2(MSC)_2]Cl_2$	(**17**)
$Ni(ClO_4)_2 \cdot 6\ H_2O$	3 MSC		H_2O	50 °C, 5 min	$[Ni(MSC)_3](ClO_4)_2$	(**18**)
$CuCO_3$	2 MSC	2 HPA	H_2O	70 °C, 5 min	$[Cu(PA)_2(MSC)_2]$	(**19**)
$ZnCO_3 \cdot 3\ Zn(OH)_2$	12 MSC	2 HPA	H_2O	70 °C, 5 min	$[Zn(MSC)_3](PA)_2$	(**20**)
$MnCO_3$	2 MSC	2 HPA	H_2O	70 °C, 5 min	$[Mn(PA)_2(MSC)_2]$	(**21**)
$CoCO_3 \cdot H_2O$	2 MSC	2 H_2TNR	H_2O	70 °C, 5 min	$[Co(PA)_2(MSC)_2]$	(**22**)
$NiCO_3 \cdot 2\ Ni(OH)_2 \cdot 4\ H_2O$	9 MSC	2 H_2TNR	H_2O	70 °C, 5 min	$[Ni(MSC)_3](PA)_2$	(**23**)
$CuCO_3$	2 MSC	2 H_2TNR	H_2O	70 °C, 5 min	$[Cu(H_2O)_2(MSC)_2](HTNR)_2$	(**24**)
$ZnCO_3 \cdot 3\ Zn(OH)_2$	8 MSC	2 H_2TNR	H_2O	70 °C, 5 min	$[Zn(H_2O)_2(MSC)_2](HTNR)_2$	(**25**)
$MnCO_3$	2 MSC	2 H_2TNR	H_2O	70 °C, 5 min	$[Mn(HTNR)_2(MSC)_2]$	(**26**)
$CoCO_3 \cdot H_2O$	2 MSC	2 H_2TNR	H_2O	70 °C, 5 min	$[Co(H_2O)_2(MSC)_2](HTNR)_2$	(**27**)
$NiCO_3 \cdot 2\ Ni(OH)_2 \cdot 4\ H_2O$	6 MSC	2 H_2TNR	H_2O	70 °C, 5 min	$[Ni(H_2O)_2(MSC)_2](HTNR)_2$	(**28**)

19.4.2 X-ray Diffraction

For thee structure elucidation of all compounds, an Oxford Xcalibur3 diffractometer with a CCD area detector using Mo-*K*α radiation (λ = 0.71073 Å) was employed. The data collection and reduction was carried out using the CRYSALISPRO software.[S1] The structures were solved by direct methods (SIR-92,[S2] SIR-97[S3] or SHELXS-97[S4]) and refined by full-matrix least-squares on *F*2 (SHELXL[S4]) and finally checked using the PLATON software[S5] integrated in the WinGX[S6] software suite. The non-hydrogen atoms were refined anisotropically and the hydrogen atoms were located and freely refined. The absorptions were corrected by a SCALE3

ABSPACK multiscan method.[S7] All DIAMOND2 plots are shown with thermal ellipsoids at the 50% probability level and hydrogen atoms are shown as small spheres of arbitrary radius.

Table S1. Crystallographic data of **1**–**5**.

	1	**2**	**3**	**4**	**5**
Formula	$C_2H_7N_3O$	$C_2H_8N_3O_4Cl$	$C_8H_{10}N_6O_8$	$C_4H_{18}CuN_6O_4S$	$C_4H_{14}Cl_2CuN_6O_2$
FW [g mol^{-1}]	89.11	189.56	318.22	373.84	312.66
Crystal system	Monoclinic	Monoclinic	Triclinic	Monoclinic	Monoclinic
Space Group	$P2_1/n$	$P2_1/c$	$P\bar{1}$	$P2_1/c$	$P2_1/c$
Color / Habit	Colorless block	Colorless block	Yellow rod	Blue rod	Green block
Size [mm]	0.15 × 0.20 × 0.30	0.13 x 0.27 x 0.39	0.05 x 0.10 x 0.10	0.10 x 0.15 x 0.20	0.05 x 0.20 x 0.20
a [Å]	5.5130(5)	14.9390(4)	3.8100(6)	9.304(1)	7.0830(6)
b [Å]	8.5490(6)	9.8650(2)	11.5580(16)	11.468(1)	12.8340(9)
c [Å]	10.0830(9)	19.7160(5)	13.8140(16)	13.2880(14)	6.8450(6)
α [°]	90	90	95.975(10)	90	90
β [°]	104.808(10)	90.867(2)	90.550(11)	109.455(12)	114.767(10)
γ [°]	90	90	93.324(12)	90	90
V [Å^3]	459.44(7)	2905.28(12)	603.92(15)	1336.9(3)	565.00(9)
Z	4	16	2	4	2
$\rho_{calc.}$ [g cm^{-3}]	1.288	1.734	1.750	1.857	1.838
μ [mm^{-1}]	0.103	0.511	0.158	1.839	2.398
F(000)	192	1568	328	722	318
$\lambda_{MoK\alpha}$ [Å]	0.71069	0.71069	0.71069	0.71073	0.71069
T [K]	173	123	143	123	173
θ Min–Max [°]	4.2, 26.0	4.1, 26.0	4.4, 26.0	4.6, 26.0	4.5, 26.0
Dataset	−6:6; −10:10; −11:12	−18:7; −12:11; −24:22	−4:4; −14:14; −17:7	−11:11; −7:14; −16:16	−8:8; −15:15; −8:8
Reflections collected	2902	22476	4583	6761	3461
Independent refl.	903	5683	2372	2622	1105
R_{int}	0.024	0.031	0.059	0.051	0.040
Observed reflections	724	4953	1352	1764	933
Parameters	83	481	220	226	87
R_1 (obs)[a]	0.0383	0.0462	0.0678	0.0417	0.0308
wR_2 (all data)[b]	0.0988	0.1131	0.1962	0.0985	0.0749
GooF[c]	1.06	1.10	0.99	1.00	1.01
Resd. Dens. [e Å^{-3}]	−0.16, 0.15	−0.73, 0.98	−0.33, 0.38	−0.44, 0.90	−0.35, 0.47
Absorption correction	multi-scan	multi-scan	multi-scan	multi-scan	multi-scan
CCDC	1534424	1534443	1574510	1534432	1534425

a) $R_1 = \Sigma||F_0|- |F_c||/ \Sigma|F_0|$; b) $wR_2 = [\Sigma[w(F_0^2-F_c^2)^2]/\Sigma[w(F_0)^2]]^{1/2}$; $w = [\sigma c^2(F_0^2)+(xP)^2+yP]^{-1}$ and $P=(F_0^2+2F_c^2)/3$; c) GooF = $\{\Sigma[w(F_o^2-F_c^2)^2]/(n-p)\}^{1/2}$ (n = number of reflections; p = total number of parameters).

Table S2. Crystallographic data of **6**–**10**.

	6	**7**	**8**	**9**	**10**
Formula	$C_4H_{14}CuN_8O_8$	$C_4H_{14}Cl_2CuN_6O_{10}$	$C_2H_7CuN_9O$	$C_4H_{14}Cl_2N_6O_2Zn$	$C_4H_6N_8O_8Zn$
FW [g mol^{-1}]	365.77	440.65	236.71	314.48	367.60
Crystal system	Triclinic	Monoclinic	Monoclinic	Monoclinic	Monoclinic
Space Group	$P\bar{1}$	$P2_1/c$	$P2_1/n$	$P2_1$	$P2_1$
Color / Habit	Blue block	Blue block	Green needle	Colorless block	Colorless block
Size [mm]	0.36 x 0.50 x 0.73	0.06 x 0.12 x 0.17	0.06 x 0.07 x 0.51	0.12 x 0.15 x 0.20	0.08 x 0.21 x 0.30
a [Å]	7.0820(5)	7.2581(3)	7.7191(4)	6.5001(7)	7.2774(4)
b [Å]	7.4600(7)	13.4295(6)	5.9972(2)	12.8540(13)	13.1386(7)
c [Å]	7.5970(7)	7.3479(3)	17.2431(7)	7.4157(7)	7.6317(4)
α [°]	64.761(9)	90	90	90	90
β [°]	77.757(7)	96.175(4)	102.249(5)	110.420(12)	115.923(7)
γ [°]	63.311(8)	90	90	90	90
V [Å^3]	324.26(6)	712.06(5)	780.06(6)	580.66(11)	656.28(7)
Z	1	2	4	2	2
$\rho_{calc.}$ [g cm^{-3}]	1.873	2.055	2.016	1.799	1.860
μ [mm^{-1}]	1.743	1.975	2.777	2.567	1.930
F(000)	187	446	476	320	376
$\lambda_{MoK\alpha}$ [Å]	0.71069	0.71073	0.71073	0.71069	0.71073
T [K]	173	123	123	123	123
θ Min–Max [°]	4.4, 26.0	4.1, 26.0	4.2, 26.0	4.3, 32.4	4.3, 26.0
Dataset	−8:8; −8:9; −9:9	−8:8; −16:16; −8:9	−5:9; −7:7; −21:10	−9:9; −18:16; −7:11	−8:8; −16:16; −9:9
Reflections collected	2292	5254	3878	6036	9335
Independent refl.	1269	1390	1531	3201	2564
R_{int}	0.017	0.032	0.036	0.044	0.033
Observed reflections	1247	1234	1280	3015	2394
Parameters	98	123	127	133	192
R_1 (obs)[a]	0.0247	0.0253	0.0293	0.1210	0.0581
wR_2 (all data)[b]	0.0671	0.0647	0.0726	0.3360	0.1573
GooF[c]	1.07	1.09	1.06	1.15	1.08
Resd. Dens. [e Å^{-3}]	−0.33, 0.35	−0.34, 0.32	−0.30, 0.74	−2.49, 6.01	−0.46, 2.43
Absorption correction	multi-scan	multi-scan	multi-scan	multi-scan	multi-scan
CCDC	1534426	1534428	1534427	1580445	1534421

a) $R_1 = \Sigma||F_0|- |F_c||/ \Sigma|F_0|$; b) $wR_2 = [\Sigma[w(F_0^2-F_c^2)^2]/\Sigma[w(F_0)^2]]^{1/2}$; $w = [\sigma c^2(F_0^2)+(xP)^2+yP]^{-1}$ and $P=(F_0^2+2F_c^2)/3$; c) GooF = $\{\Sigma[w(F_o^2-F_c^2)^2]/(n-p)\}^{1/2}$ (n = number of reflections; p = total number of parameters).

Table S3. Crystallographic data of **13**, **14**, **16**, **17** and **19**.

	13	**14**	**16**	**17**	**19**
Formula	$C_4H_{14}Cl_2MnN_6O_2$	$C_4H_{14}MnN_8O_8$	$C_4H_{14}Cl_2CoN_6O_2$	$C_4H_{18}Cl_2CoN_6O_4$	$C_{16}H_{18}CuN_{12}O_{16}$
FW [g mol^{-1}]	304.05	357.17	308.04	344.07	697.96
Crystal system	Monoclinic	Triclinic	Monoclinic	Monoclinic	Triclinic
Space Group	$P2_1/n$	$P\bar{1}$	$P2_1/c$	$P2_1/n$	$P\bar{1}$
Color / Habit	Colorless block	Colorless block	Blue block	Orange block	Green block
Size [mm]	0.14 x 0.19 x 0.35	0.10 x 0.10 x 0.15	0.13 x 0.19 x 0.19	0.18 x 0.18 x 0.13	0.11 x 0.15 x 0.24
a [Å]	7.4586(5)	6.0133(5)	7.3901(4)	11.2526(4)	7.1993(4)
b [Å]	24.4389(11)	7.6877(10)	12.9662(5)	10.4036(3)	7.4864(5)
c [Å]	6.5846(4)	7.7664(7)	6.3552(3)	11.8634(4)	12.1409(8)
α [°]	90	92.222(9)	90	90	100.318(6)
β [°]	107.552(6)	101.938(8)	110.240(6)	108.514(4)	93.197(5)
γ [°]	90	104.538(10)	90	90	106.037(5)
V [Å^3]	1144.36(12)	338.45(6)	571.36(5)	1316.94(8)	614.88(7)
Z	4	1	2	4	1
$\rho_{calc.}$ [g cm^{-3}]	1.765	1.752	1.791	1.735	1.885
μ [mm^{-1}]	1.613	1.032	1.961	1.722	0.997
F(000)	620	183	314	708	355
$\lambda_{MoK\alpha}$ [Å]	0.71073	0.71073	0.71073	0.71073	0.71073
T [K]	173	173	123	123	123
θ Min–Max [°]	4.2, 32.3	4.4, 26.0	4.3, 26.0	4.2, 26.0	4.3, 27.0
Dataset	−9:9; −30:26; −8:5	−7:7; −9:8; −9:9	−8:9; −11:15; −7:7	−13:12; −9:12; −14:14	−9:9; −9:9; −15:15
Reflections collected	4635	2494	2891	9873	9615
Independent refl.	2232	1328	1113	2578	2687
R_{int}	0.027	0.027	0.025	0.028	0.046
Observed reflections	1847	1172	985	2189	2279
Parameters	170	114	86	207	241
R_1 (obs)[a]	0.0295	0.0335	0.0279	0.0355	0.0355
wR_2 (all data)[b]	0.0664	0.0738	0.0755	0.0710	0.0862
GooF[c]	1.01	1.08	1.07	1.026	1.04
Resd. Dens. [e Å^{-3}]	−0.29, 0.34	−0.27, 0.30	−0.47, 0.45	−0.37, 0.40	−0.42, 0.38
Absorption correction	multi-scan	multi-scan	multi-scan	multi-scan	multi-scan
CCDC	1534435	1534440	1534429	1534441	1534429

a) $R_1 = \Sigma||F_0|- |F_c||/ \Sigma|F_0|$; b) $wR_2 = [\Sigma[w(F_0^2-F_c^2)^2]/\Sigma[w(F_0)^2]]^{1/2}$; $w = [\sigma c^2(F_0^2)+(xP)^2+yP]^{-1}$ and $P=(F_0^2+2F_c^2)/3$; c) GooF = $\{\Sigma[w(F_o^2-F_c^2)^2]/(n-p)\}^{1/2}$ (n = number of reflections; p = total number of parameters).

Table S4. Crystallographic data of **21**, **22** and **24**–**26**.

	21	**22**	**24**	**25**	**26**
Formula	$C_{16}H_{18}MnN_{12}O_{16}$	$C_{16}H_{18}CoN_{12}O_{16}$	$C_{16}H_{22}CuN_{12}O_{20}$	$C_{16}H_{22}N_{12}O_{20}Zn$	$C_{16}H_{18}MnN_{12}O_{18}$
FW [g mol^{-1}]	689.36	693.35	766.00	767.82	721.36
Crystal system	Triclinic	Triclinic	Triclinic	Triclinic	Triclinic
Space Group	*P*−1	*P*−1	*P*−1	*P*−1	*P*−1
Color / Habit	Yellow block	Orange block	Green needle	Yellow block	Orange block
Size [mm]	0.10 x 0.20 x 0.30	0.30 x 0.40 x 0.60	0.04 x 0.05 x 0.10	0.14 x 0.37 x 0.47	0.15 x 0.18 x 0.26
a [Å]	7.433(2)	7.3600(5)	7.1270(4)	7.2150(5)	7.4180(5)
b [Å]	7.446(2)	7.4180(6)	9.1490(4)	9.1380(5)	7.4770(5)
c [Å]	12.0324(15)	11.9640(12)	11.1420(6)	11.0940(8)	12.1030(8)
α [°]	99.826(18)	99.672(8)	105.174(2)	105.044(5)	92.578(5)
β [°]	91.183(16)	92.327(7)	92.536(2)	92.229(6)	99.475(5)
γ [°]	106.53(2)	105.770(6)	103.833(2)	103.377(6)	106.120(6)
V [Å^3]	627.4(3)	617.10(9)	676.41(6)	683.38(8)	633.17(8)
Z	1	1	1	1	1
$\rho_{calc.}$ [g cm^{-3}]	1.825	1.866	1.880	1.866	1.892
μ [mm^{-1}]	0.633	0.804	0.926	1.016	0.637
F(000)	351	353	391	392	367
$\lambda_{MoK\alpha}$ [Å]	0.71073	0.71069	0.71073	0.71069	0.71069
T [K]	143	143	173	123	123
θ Min–Max [°]	4.6, 26.0	4.6, 26.0	1.9, 25.4	4.2, 26.1	4.2, 26.2
Dataset	−6:9; −9:9; −14:14	−9:7; −9:9; −14:12	−8:8; −11:11; −13: 3	−8:8; −11:11; −8:13	−9:9; −9:9; -14:15
Reflections collected	4813	3855	11498	5189	4864
Independent refl.	2445	2404	2500	2696	2535
R_{int}	0.075	0.020	0.051	0.022	0.031
Observed reflections	1736	2164	2166	2696	2038
Parameters	222	222	252	252	235
R_1 (obs)[a]	0.0763	0.0323	0.0339	0.0284	0.0387
wR_2 (all data)[b]	0.2159	0.0794	0.1110	0.0721	0.0984
GooF[c]	1.03	1.04	1.19	1.07	1.04
Resd. Dens. [e Å^{-3}]	−1.03, 1.24	−0.36, 0.29	−0.41, 0.44	−0.39, 0.36	−0.31, 0.86
Absorption correction	multi-scan	multi-scan	multi-scan	multi-scan	multi-scan
CCDC	1574511	1574509	1534442	1534434	1534437

a) $R_1 = \Sigma||F_0|- |F_c||/ \Sigma|F_0|$; b) $wR_2 = [\Sigma[w(F_0^2-F_c^2)^2]/\Sigma[w(F_0)^2]]^{1/2}$; $w = [\sigma c^2(F_0^2)+(xP)^2+yP]^{-1}$ and $P=(F_0^2+2F_c^2)/3$; c) GooF = $\{\Sigma[w(F_o^2-F_c^2)^2]/(n-p)\}^{1/2}$ (n = number of reflections; p = total number of parameters).

Table S5. Crystallographic data of **27** and **28**.

	27	**28**
Formula	$C_{16}H_{22}CoN_{12}O_{20}$	$C_{16}H_{22}NiN_{12}O_{20}$
FW [g mol^{-1}]	761.39	761.16
Crystal system	Triclinic	Triclinic
Space Group	*P*−1	*P*−1
Color / Habit	Yellow block	Green block
Size [mm]	0.09 x 0.17 x 0.31	0.12 x 0.21 x 0.26
a [Å]	7.2043(5)	7.2679(6)
b [Å]	9.1400(6)	9.1444(8)
c [Å]	11.0759(7)	11.0210(9)
α [°]	105.013(6)	104.661(7)
β [°]	92.022(5)	91.879(7)
γ [°]	103.042(5)	103.604(7)
V [Å^3]	682.84(8)	685.41(11)
Z	1	1
$\rho_{calc.}$ [g cm^{-3}]	1.852	1.844
μ [mm^{-1}]	0.746	0.825
F(000)	389	390
$\lambda_{MoK\alpha}$ [Å]	0.71073	0.71073
T [K]	123	173
θ Min–Max [°]	4.2, 26.0	4.2, 26.0
Dataset	−8:8; −11:6; −12:13	−8:4; −10:11; −13:13
Reflections collected	3543	5112
Independent refl.	2656	2673
R_{int}	0.027	0.037
Observed reflections	2656	2673
Parameters	252	252
R_1 (obs)[a]	0.0449	0.0409
wR_2 (all data)[b]	0.1083	0.0834
GooF[c]	1.01	1.01
Resd. Dens. [e Å^{-3}]	−0.55, 0.52	−0.35, 0.34
Absorption correction	multi-scan	multi-scan
CCDC	1534430	1534423

a) $R_1 = \Sigma||F_0|- |F_c||/ \Sigma|F_0|$; b) $wR_2 = [\Sigma[w(F_0^2-F_c^2)^2]/\Sigma[w(F_0)^2]]^{1/2}$; $w = [\sigma c^2(F_0^2)+(xP)^2+yP]^{-1}$ and $P=(F_0^2+2F_c^2)/3$; c) GooF = $\{\Sigma[w(F_o^2-F_c^2)^2]/(n-p)\}^{1/2}$ (n = number of reflections; p = total number of parameters).

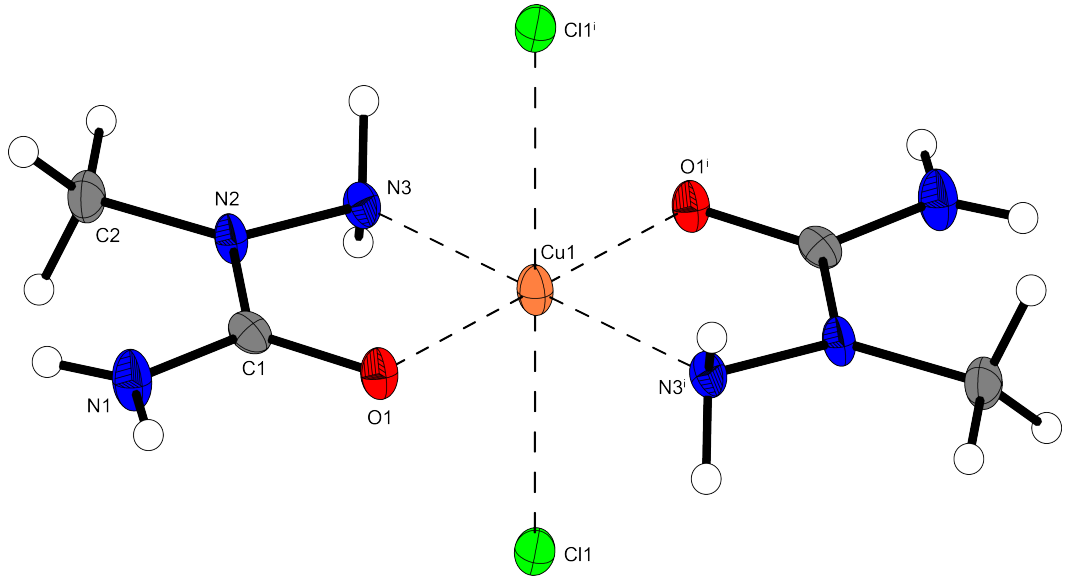


Figure S1. Molecular unit of $[CuCl_2(MSC)_2]$ (**5**). Selected bond lengths (Å): Cu1–Cl1 2.8492(7), Cu1–O1 1.930(2), Cu1–N3 2.011(3); selected bond angles (°): O1–Cu1–O1 92.95(6), Cl1–Cu1–N3 88.54(7), Cl1–Cu1–O1^{i} 87.05(6), Cl1–Cu1–N3^{i} 91.46(7), O1–Cu1–N3 82.50(9), O1–Cu1–N3^{i} 97.50(9). Symmetry code: (i) 1−x, −y, 2−z.

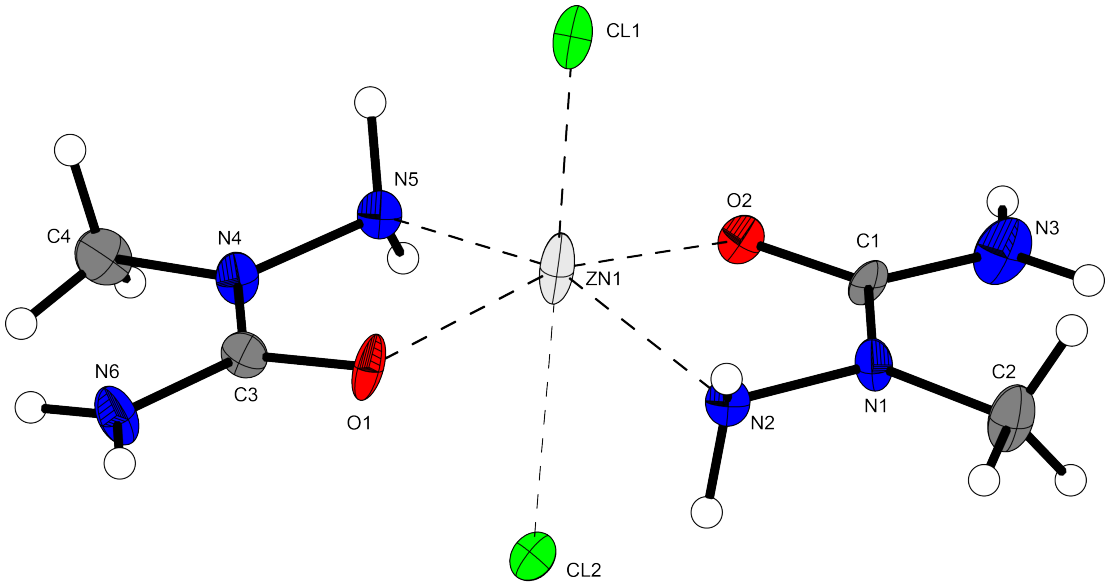


Figure S2. Molecular moiety of **9**. Selected bond lengths (Å): Zn1–Cl1 2.371(2), Zn1–O1 2.062(11), Zn1–O2 2.029(12), Zn1–N2 2.115(16), Zn1–N5 2.089(15), Zn1–Cl2 3.051(5); selected bond angles (°): Cl1–Zn1–O1 98.0(4), Cl1–Zn1–O2 100.7(4), Cl1–Zn1–N2 99.1(4), Cl1–Zn1–N5 102.1(5), O1–Zn1–O2 161.3(6), O1–Zn1–N2 96.5(4), O1–Zn1–N5 79.0(5), O2–Zn1–N2 78.7(5), O2–Zn1–N5 98.9(5), N2–Zn1–N5 158.8(6), Cl1–Zn1–Cl2 177.3(2).

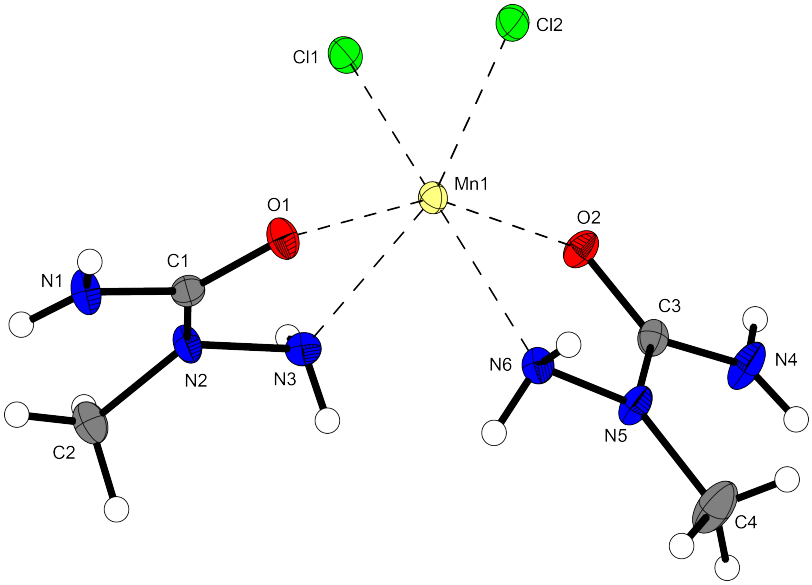


Figure S3. Complex unit of $[MnCl_2(MSC)_2]$ (**13**). Selected bond lengths (Å): Mn1–Cl1 2.6138(7), Mn1–Cl2 2.4007(7), Mn1–O1 2.1512(17), Mn1–O2 2.1233(17), Mn1–N3 2.354(2), Mn1–N6 2.339(2); selected bond angles (°): Cl1–Mn1–Cl2 94.14(2), Cl1–Mn1–O1 106.63(5), Cl1–Mn1–O2 89.50(4), Cl1–Mn1–N3 82.33(6), Cl1–Mn1–N6 158.58(6), Cl2–Mn1–O1 96.08(5), Cl2–Mn1–O2 103.64(4), Cl2–Mn1–N3 163.99(6), Cl2–Mn1–N6 100.43(6), O1–Mn1–O2 153.58(7), O1–Mn1–N3 70.27(7), O1–Mn1–N6 87.48(8), O2–Mn1–N3 91.98(8), O2–Mn1–N6 71.92(8), N3–Mn1–N6 87.62(8).

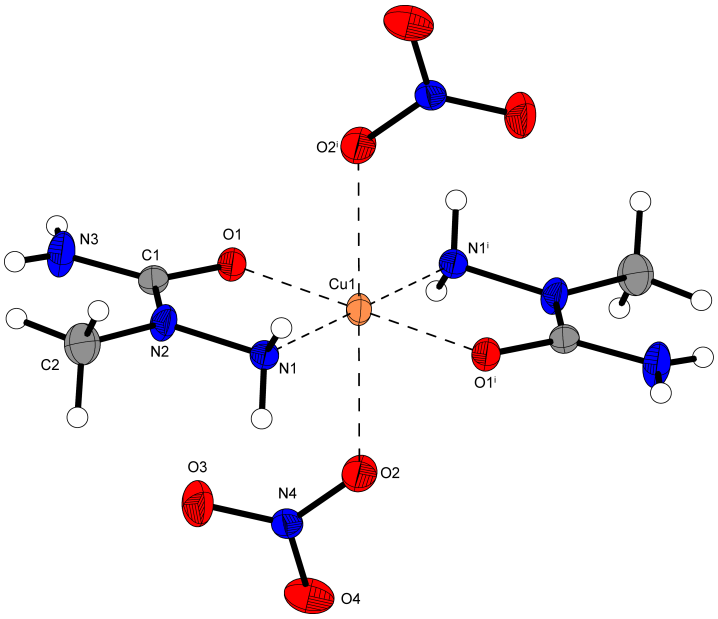


Figure S4. Complex unit of $[Cu(NO_3)_2(MSC)_2]$ (**6**). Selected bond lengths (Å): Cu1–O1 1.9389(13), Cu1–O2 2.4375(15), Cu1–N1 1.9812(17); selected bond angles (°): O1–Cu1–O2 94.70(6), O1–Cu1–N1 82.83(6), O1–Cu1–$O2^i$ 85.30(6), O1–Cu1–$N1^i$ 97.17(6), O2–Cu1–N1 93.39(8), O2–Cu1–$N1^i$ 86.61(8). Symmetry code: (i) −x, 2−y, −z.

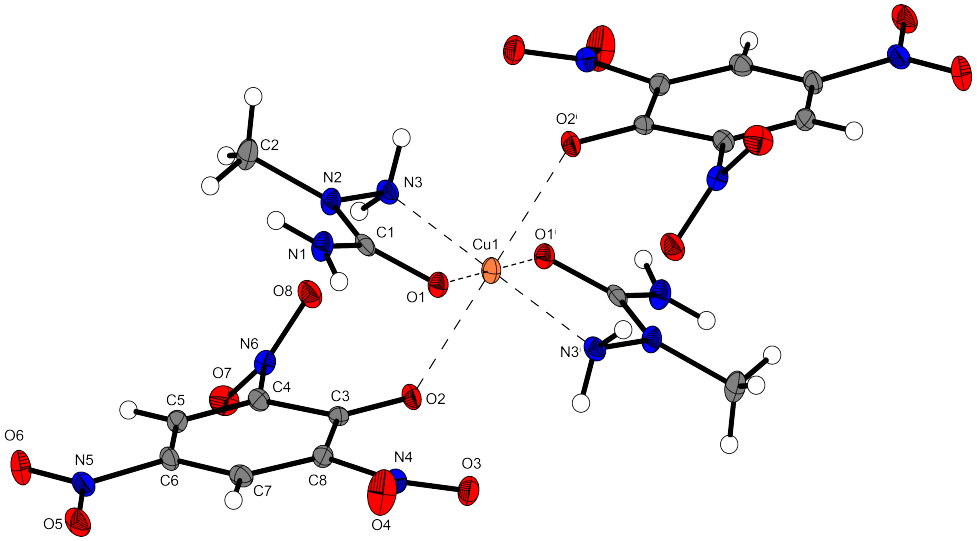


Figure S5. Complex unit of $[Cu(PA)_2(MSC)_2]$ (**19**). Selected bond lengths (Å): Cu1–O1 1.9542(15), Cu1–O2 2.3714(15), Cu1–N3 1.994(2); selected bond angles (°): O1–Cu1–O2 90.28(6), O1–Cu1–N3 82.27(8), O1–Cu1–$O2^i$ 89.72(6), O1–Cu1–$N3^i$ 97.73(8), O2–Cu1–N3 89.29(7), O2–Cu1–$N1^i$ 90.71(7). Symmetry code: (i) 2–x, 1–x, 1–z.

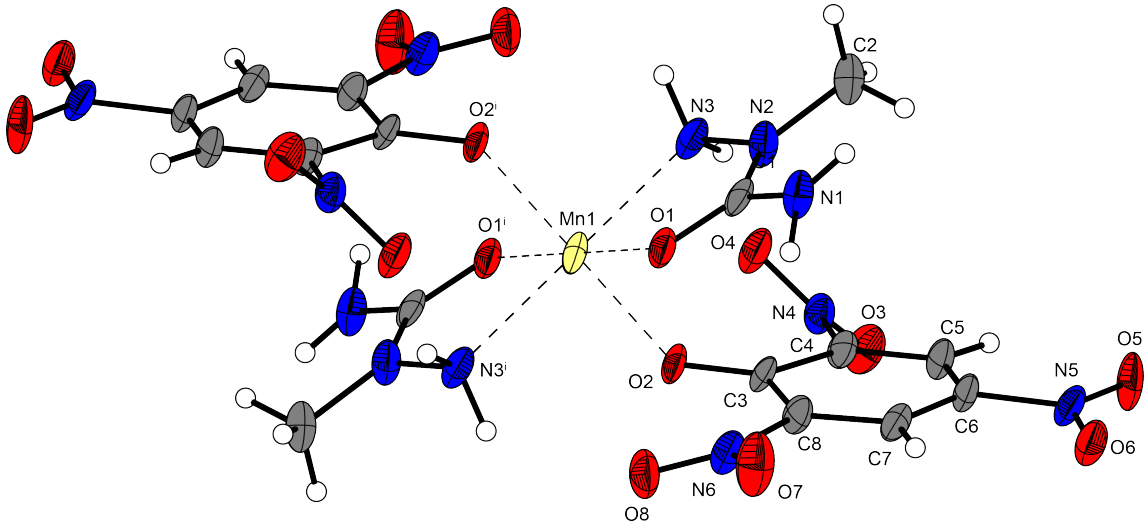


Figure S6. Molecular unit of $[Mn(PA)_2(MSC)_2]$ (**21**). Selected bond lengths (Å): Mn1–O1 2.158(3), Mn1–O2 2.179(3), Mn1–N3 2.259 (4); selected bond angles (°): O1–Mn1–O2 88.97(2), O1–Mn1–N3 72.84(12), O1–Mn1–$O2^i$ 91.03(12), O1–Mn1–$N3^i$ 107.16(12), O2–Mn1–N3 89.23(12), O2–Mn1–$N3^i$ 90.78(12). Symmetry code: (i) −x, 2−x, −z.

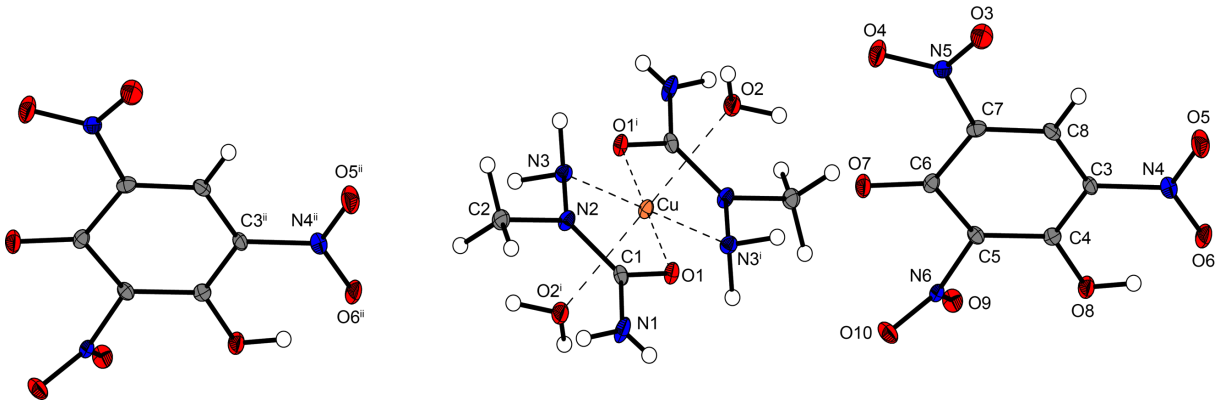


Figure S7. Complex unit of $[Cu(H_2O)_2(MSC)_2](HTNR)_2$ (**24**). Selected bond lengths (Å): Cu1–N3 2.013(3), Cu1–O1 1.931(2), Cu1–O2 2.418(2); selected bond angles (°): O1–Cu1–O2^i 86.29(6), O1–Cu1–N3^i 97.18(10), O2–Cu1–N3 97.11(11), O2–Cu1–N3^i 82.89(11), O1^i–Cu1–O2^i 93.71(9), O1^i–Cu1–N3^i 82.82(6). Symmetry code: (i) 1−x, 1−y, 1−z.

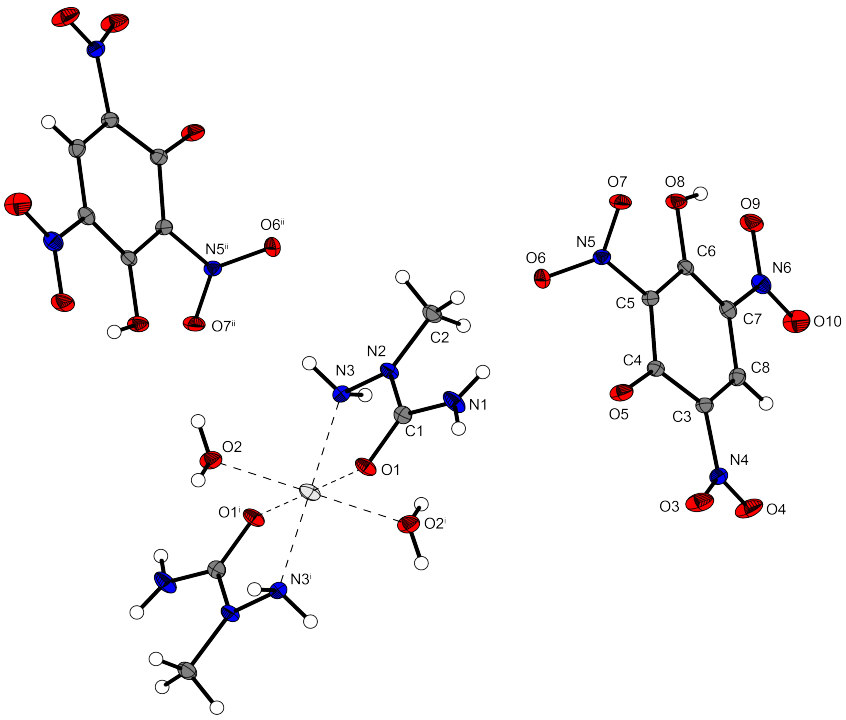


Figure S8. Molecular unit of $[Zn(H_2O)_2(MSC)_2](HTNR)_2$ (**25**). Selected bond lengths (Å): Zn1–N3 2.1066(18), Zn1–O1 2.0036(13), Zn1–O2 2.2426(15); selected bond angles (°): O1–Zn1–O2^i 88.33(6), O1–Zn1–N3^i 100.36(6), O2–Zn1–N3 95.72(6), O2–Zn1–N3^i 84.28(6), O1^i–Zn1–O2^i 91.68(6), O1^i–Zn1–N3^i 79.64(6). Symmetry code: (i) −x, −y, 1−z.

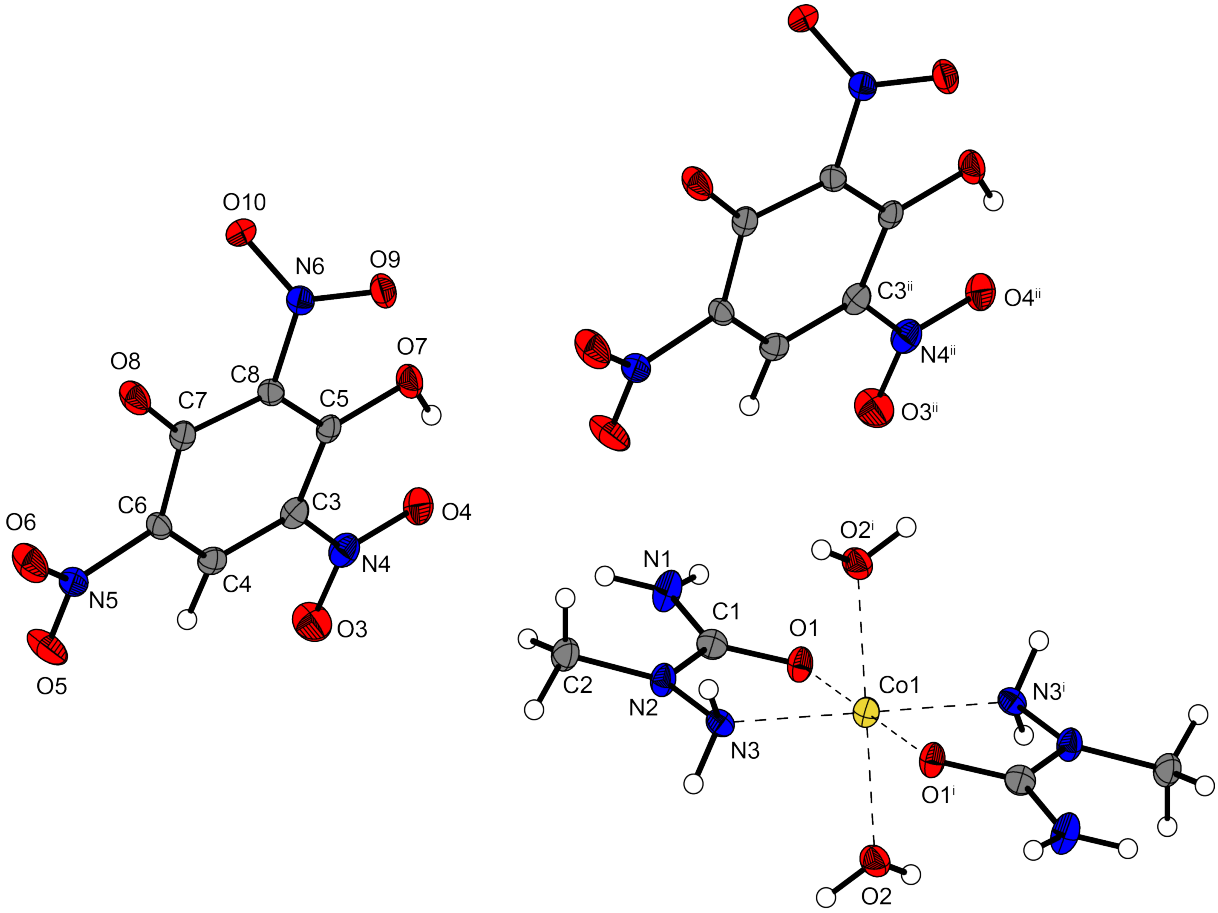


Figure S9. Molecular unit of $[Co(H_2O)_2(MSC)_2](HTNR)_2$ (**27**). Selected bond lengths (Å): Co1–N3 2.125(3), Co1–O1 2.001(2), Co1–O2 2.173(2); selected bond angles (°): O1–Co1–$O2^i$ 89.23(10), O1–Co1–$N3^i$ 100.96(10), O2–Co1–N3 95.50(11), O2–Co1–$N3^i$ 84.51(11), $O1^i$–Co1–$O2^i$ 90.77(10), $O1^i$–Co1–$N3^i$ 79.04(10), $O2^i$–Co1–$N3^i$ 95.50(11). Symmetry code: (i) 1−x, 2−y, −z.

19.4.3 IR Spectroscopy of 11, 12, 15, 18, 20 and 23

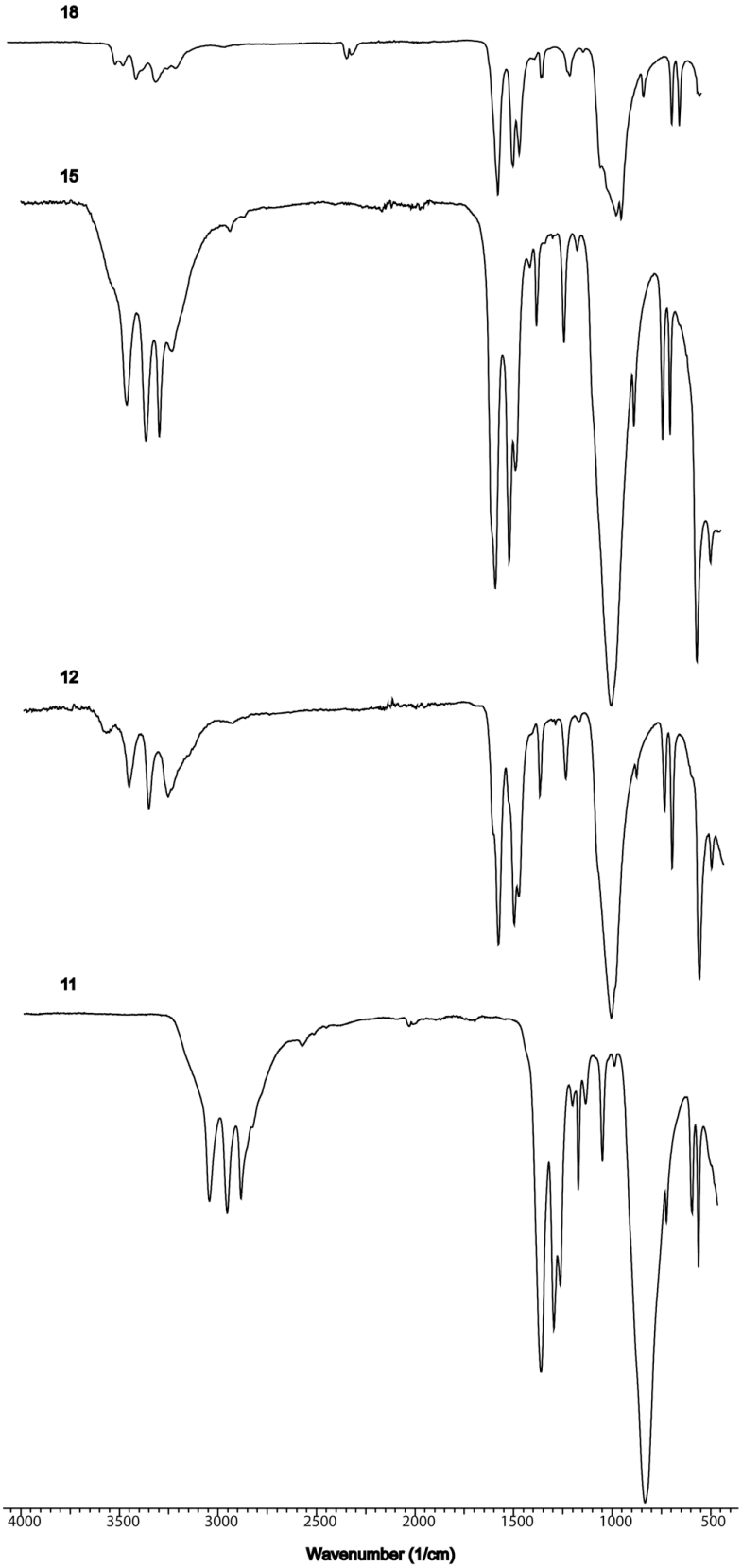


Figure S10. Infrared spectra of **11**, **12**, **15** and **18**.

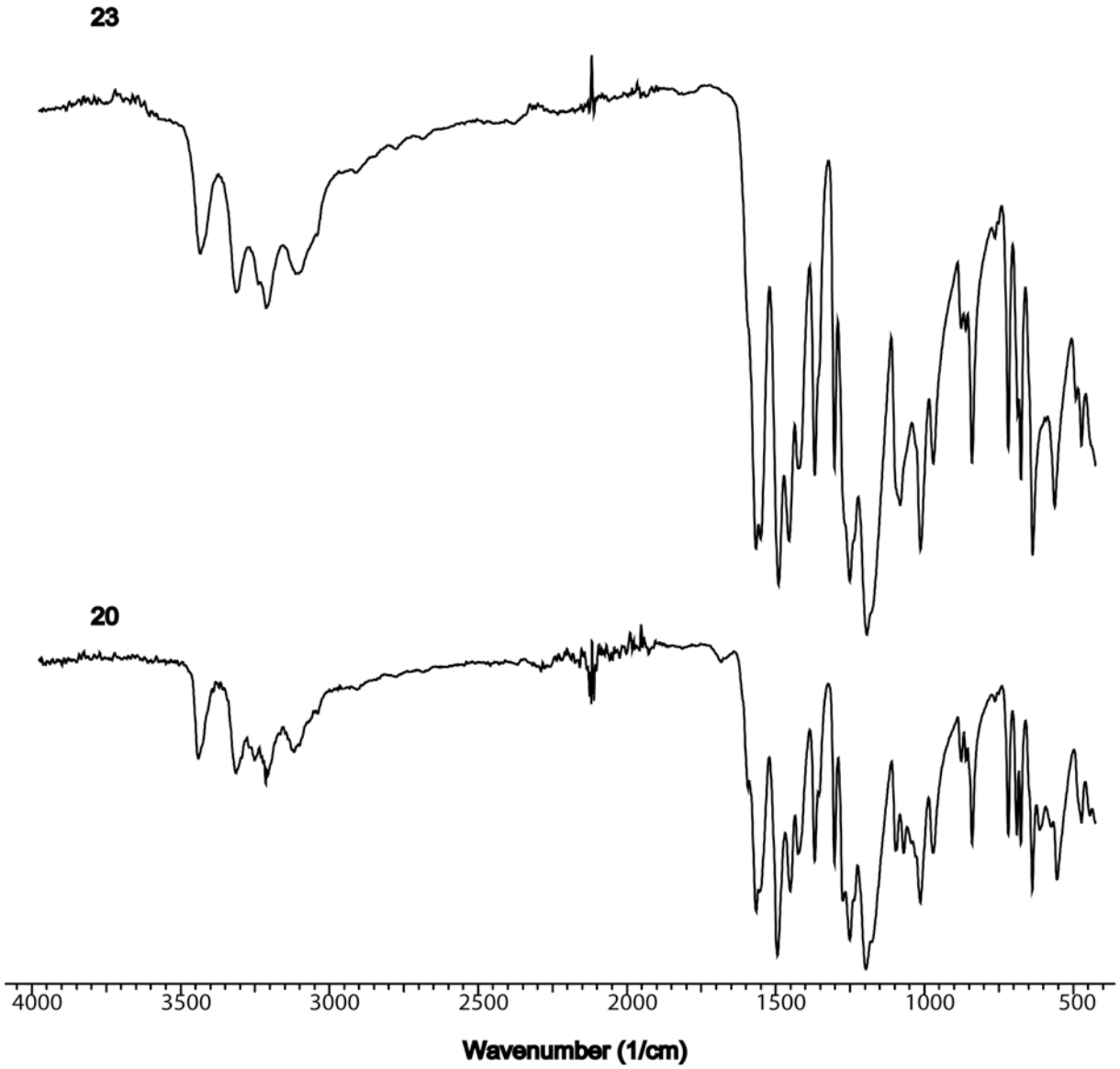


Figure S11. Infrared spectra of **20** and **23**.

19.4.4 DTA Plots of 6–8, 11, 12, 15 and 18

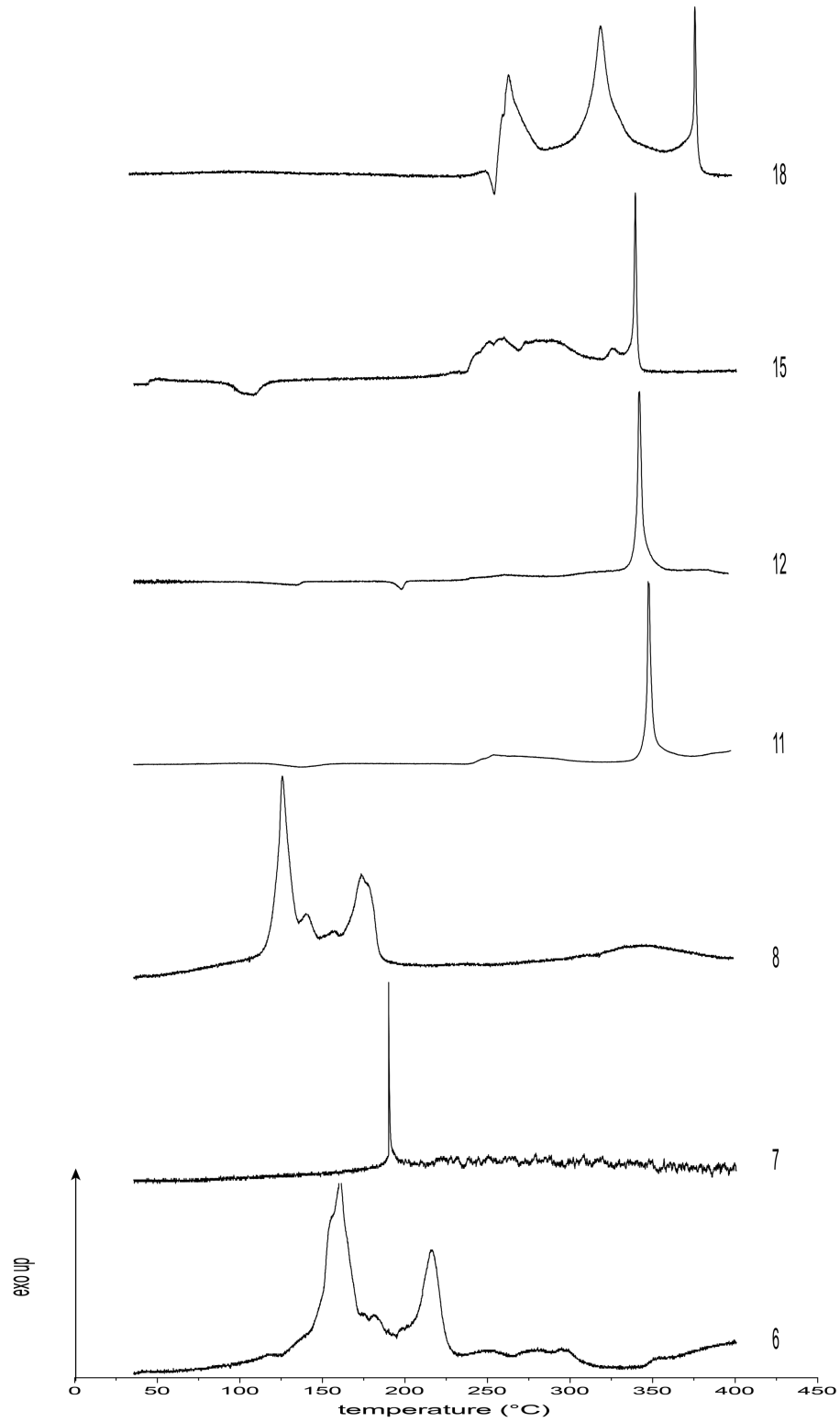


Figure S12. DTA plots of **6**–**8**, **11**, **12**, **15** and **18**.

19.4.5 UV-Vis Spectra of 4–8

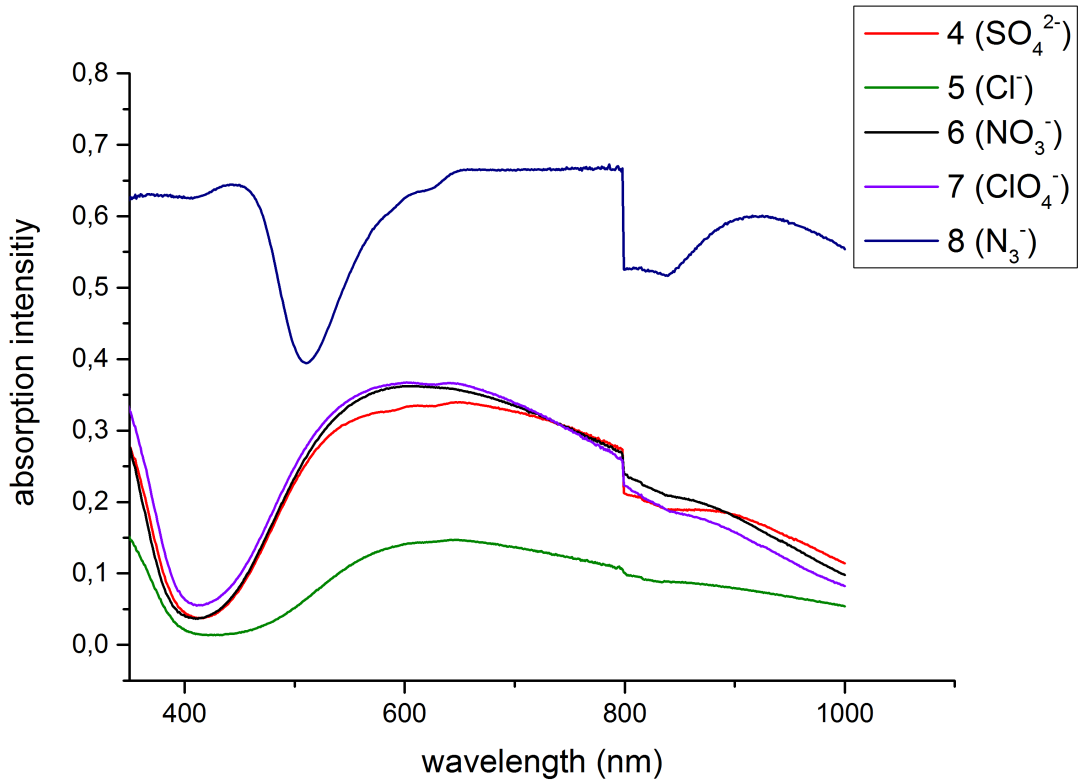


Figure S13. Comparison of the absorption spectra in the solid state for selected copper(II) MSC complexes with different coordination anions. The step in the absorption spectra at 800 nm result from a lamp change.

19.4.6 Experimental Part and General Methods

All chemicals and solvents were employed as received (Sigma-Aldrich, Fluka, Acros, ABCR). ^{1}H and ^{13}C NMR spectra were recorded at ambient temperature on a Bruker 400, JEOL Eclipse 270, JEOL EX 400 or a JEOL Eclipse 400 instrument. The chemical shifts quoted in ppm in the text refer to typical standards such as tetramethylsilane (^{1}H, ^{13}C). Endothermic and exothermic events of the described compounds, which indicate melting, evaporation, loss of ligand/water or decomposition, are given as the extrapolated onset temperatures. The samples were measured in a range of 25–400 °C at a heating rate of 5 °C min^{-1} through differential thermal analysis (DTA) with an OZM Research DTA 552-Ex instrument, through differential scanning calorimetry (DSC) with a LINSEIS DSC PT10 or by thermal gravimetric analysis (TGA) with a PerkinElmer TGA4000. Infrared spectra were measured with pure samples on a Perkin-Elmer

BXII FT-IR system with a Smith DuraSampler IR II diamond ATR. Determination of the carbon, hydrogen and nitrogen contents were carried out by combustion analysis using an Elementar Vario El (nitrogen values determined are often lower than the calculated ones due to their explosive behavior). UV-Vis spectra were recorded in the solid state using a Varian Cary 500 spectrometer in the wavelength range of 350–1000 nm. Impact sensitivity tests were carried out according to STANAG 4489[S8] with a modified instruction[S9] using a BAM (Bundesanstalt für Materialforschung) drophammer.[S10] Friction sensitivity tests were carried out according to STANAG 4487[S11] with a modified instruction[S12] using the BAM friction tester. The classification of the tested compounds results from the "UN Recommendations on the Transport of Dangerous Goods".[S13] Additionally all compounds were tested upon the sensitivity toward electrical discharge using the OZM Electric Spark Tester ESD 2010 EN.[S14] Liquid-dried luminescent bacteria of the strain Vibrio fischeri NRRL-B-11177 provided by the HACH LANGE GmbH were used for the luminescent bacteria inhibition test to determine their toxicity toward aquatic organisms according to a modified procedure.[S15] The obtained coordination compounds were washed with small quantities of cold ethanol when stated to remove unreacted starting materials, dried overnight in air and used for analytics without further purification.

CAUTION! *All investigated compounds are potentially explosive energetic materials, which show partly increased sensitivities (especially compound* ***7****) toward various stimuli (e.g. elevated temperatures, impact, friction or electrostatic discharge). Therefore, proper security precautions (safety glass, face shield, earthed equipment and shoes, leather coat, Kevlar gloves, Kevlar sleeves and ear plugs) have to be applied while synthesizing and handling the described compounds.*

Methylsemicarbazide (1)

Methylsemicarbazide (**1**) was synthesized according to a modified literature procedure[S16]: a methylhydrazine (7.90 mL, 0.15 mol) solution in dry THF (45 mL) under nitrogen atmosphere was cooled down to 0 °C and stirred for 15 min. Trimethylsilylisocyanate (13.5 mL, 0.10 mol) was added dropwise and the resulting dispersion stirred for one hour at 0 °C. The reaction mixture was treated with methanol (40 mL), heated for 5 h at 40 °C and cooled down to room temperature. After removal of the solvents under reduced pressure, drying under high vacuum, the product could be isolated in the form of colorless crystals. Yield: 8.50 g (95.4 mmol, 95 %).

DTA (5 °C min^{-1}): 60 °C (endothermic), 111 °C (endothermic); IR (ATR, cm^{-1}): $\tilde{\nu}$ = 3457 (m), 3308 (m), 3211 (m), 2954 (w), 2922 (w), 2869 (w), 1660 (m), 1626 (s), 1557 (s), 1481 (m), 1444 (m), 1399 (m), 1399 (s), 1272 (m), 1211 (w), 1068 (m), 1045 (m), 945 (m), 784 (m), 762 (s), 703 (m); ^{1}H NMR (DMSO-*d*$_6$, 25 °C, ppm) δ: 5.94 (s, 2H, -*H*$_2$NCO), 4.47 (s, 2H, -N*H*$_2$), 2.92 (s, 3H, -C*H*$_3$); ^{13}C NMR (DMSO-*d*$_6$, 25 °C, ppm) δ: 160.6 (-*C*O), 37.8 (-*C*H$_3$); EA: ($C_2H_7N_3O$ 89.10) calcd: C 26.96, H 7.92, N 47.16 %; found: C 27.12, H 7.92, N 46.33 %; BAM drophammer: > 40 J; friction tester: > 360 N; ESD: 1.50 J (at grain size < 100 μm).

MSC$_H$ PA (3)

An aqueous solution of MSC (89.1 mg, 1.00 mmol) was added to an aqueous suspension of picric acid (229 mg, 1.00 mmol) and heated to 70 °C under stirring until both reactants dissolved. After one hour, the product started to crystallize in the form of yellow rods suitable for X-ray determination. The product was filtered off and dried in air. Yield: 126 mg (0.40 mmol, 40 %).

DTA (5 °C min^{-1}): 166 °C (exothermic); IR (ATR, cm^{-1}): $\tilde{\nu}$ = 3481 (m), 3384 (m), 3087 (m), 2936 (m), 2885 (m), 2771 (m), 2727 (m), 2604 (m), 2514 (w), 1683 (m), 1631 (m), 1596 (s), 1567 (s), 1525 (s), 1470 (s), 1464 (s), 1412 (s), 1362 (m), 1339 (vs), 1270 (vs), 1163 (s), 1087 (s), 1072 (s), 1014 (s), 943 (m), 936 (s), 925 (s), 912 (s), 838 (m), 822 (m), 810 (m), 788 (s), 770 (m), 758 (m), 741 (s), 713 (s), 666 (m), 602 (m), 552 (m), 518 (s); ^{1}H NMR (DMSO-*d*$_6$, 25 °C, ppm) δ: 8.59 (s, 2H, C$_{aromat.}$-*H*), 6.94 (s, 2H, -*H*$_2$NCO), 3.44 (br, s, 3H, -N*H*$_3$), 3.06 (s, 3H, -C*H*$_3$); ^{13}C NMR (DMSO-*d*$_6$, 25 °C, ppm) δ: 160.9 (-*C*O), 158.9 (*C*$_{aromat.}$), 141.9 (*C*$_{aromat.}$), 125.3 (*C*$_{aromat.}$), 124.4 (*C*$_{aromat.}$), 36.9 (-*C*H$_3$); EA: ($C_8H_{10}N_6O_8$ 318.20) calcd: C 30.20, H 3.17, N 26.41 %; found: C 30.00, H 3.23, N 26.38 %; BAM drophammer: > 40 J; friction tester: 160 N; ESD: 0.65 J (at grain size < 100 μm).

General procedure for the preparation of the copper(II) MSC complexes (4–7):

MSC (**4**/**7**: 180 mg, 2.00 mmol, **5**: 44.5 mg, 0.50 mmol, **6**: 89.0 mg, 1.00 mmol) was dissolved in distilled water or ethanol (**6**) at room temperature. The corresponding copper(II) salt solution (**4**: copper(II) sulfate pentahydrate (250 mg, 1.00 mmol); **5**: copper(II) chloride dihydrate

(42.6 mg, 0.25 mmol); **6**: copper(II) nitrate trihydrate (121 mg, 0.50 mmol); **7**: copper(II) perchlorate hexahydrate (371 mg, 1.00 mmol)) in water or diluted hydrochloric acid (**5**, 15 %, 1 mL) was added and the reaction mixture stirred mechanically for 1 min at room temperature. Two drops of concentrated perchloric acid (70 %) as co-solvent were added in the synthesis of complex **7** in order to grow single crystals and to ensure slow evaporation. The colored solutions were left to crystallize, the solids formed were filtered off, washed with cold ethanol (2 mL) and dried in air.

$[Cu(H_2O)_2(MSC)_2]SO_4$ (4)

Compound **4** was obtained after 1 hour in the form of blue needles suitable for X-ray determination. Yield: 268 mg (0.72 mmol, 72 %).

DTA (5 °C min^{-1}): 144 °C (endothermic), 156 °C (exothermic); IR (ATR, cm^{-1}): $\tilde{\nu}$ = 3330 (w), 3139 (m), 3036 (w), 1650 (m), 1547 (m), 1417 (vw), 1294 (w), 1178 (w), 1062 (vs), 804 (m), 727 (m), 613 (s), 591 (s), 490 (s); UV-Vis spectrum: λ_{max} = 646 nm; EA ($C_4H_{18}CuN_6O_8S$, 373.83): calcd: C 12.85, H 4.85, N 22.48, S 8.58 %; found: C 12.52, H 4.96, N 22.23 S 8.11 %; BAM drophammer: > 40 J; friction tester: > 360 N; ESD: 1.50 J (at grain size < 100 µm).

$[CuCl_2(MSC)_2]$ (5)

Blue single crystals suitable for X-ray determination of copper(II) complex **5** could be isolated within one day. Yield: 63.7 mg (0.20 mmol, 82 %).

DTA (5 °C min^{-1}): 146 °C (endothermic), 166 °C (exothermic); IR (ATR, cm^{-1}): $\tilde{\nu}$ = 3402 (m), 3318 (m), 3235 (m), 3170 (m), 3105 (s), 2362 (vw), 1681 (m), 1619 (vs), 1527 (vs), 1448 (s), 1400 (vs), 1301 (m), 1275 (m), 1126 (s), 1083 (s), 1034 (s), 1020 (s), 800 (m), 746 (s), 639 (s); UV-Vis spectrum: λ_{max} = 642 nm; EA ($C_4H_{14}Cl_2CuN_6O_2$, 312.64): calcd: C 15.37, H 4.51, N 26.88 %; found: C 15.26, H 4.81, N 26.88 %; BAM drophammer: > 40 J; friction tester: > 360 N; ESD: 1.50 J (at grain size < 100 µm).

$[Cu(NO_3)_2(MSC)_2]$ (6)

Product **5** was obtained after 8 days in the form of blue blocks suitable for X-ray determination. Yield: 132 mg (0.36 mmol, 70 %).

DTA (5 °C min^{-1}): 147 °C (exothermic); IR (ATR, cm^{-1}): $\tilde{\nu}$ = 3424 (vw), 3338 (w), 3196 (w), 3114 (w), 2359 (vw), 2337 (vw), 1640 (s), 1556 (s), 1538 (s), 1344 (vs), 1311 (vs), 1286 (vs), 1150 (s), 1089 (m), 1040 (s), 819 (m), 798 (m), 754 (m), 652 (m); UV-Vis spectrum: λ_{max} = 603 nm; EA ($C_4H_{14}CuN_8O_8$, 365.75): calcd: C 13.14, H 3.86, N 30.64 %; found: C 13.23, H 3.91, N 30.34 %; BAM drophammer: > 40 J; friction tester: 324 N; ESD: 1.50 J (at grain size < 100 µm).

$[Cu(ClO_4)_2(MSC)_2]$ (7)

The very sensitive perchlorate complex **7** crystallized within one day in the form of dark blue blocks, which were suitable for X-ray determination. Yield: 277 mg (0.63 mmol, 63 %).

DTA (5 °C min^{-1}): 186 °C (exothermic); IR (ATR, cm^{-1}): $\tilde{\nu}$ = 3474 (vw), 3364 (vw), 3248 (w), 3153 (w), 1664 (m), 1629 (m), 1554 (m) 1424 (w), 1294 (vw), 1163 (w), 1044 (vs), 931 (w), 810 (w), 749 (m), 698 (w), 659 (w) 618 (s), 556 (w), 436 (w); UV-Vis spectrum: λ_{max} = 602 nm; EA ($C_4H_{14}Cl_2CuN_6O_{10}$, 440.64): calcd: C 10.90, H 3.20, N 19.07 %; found: C 11.02, H 3.21, N 18.98 %; BAM drophammer: 2 J; friction tester: 24 N; ESD: 70.0 mJ (at grain size < 100 µm).

$[Cu(N_3)_2(MSC)]$ (8)

Copper(II) sulfate pentahydrate (124.8 mg, 0.50 mmol) and methylsemicarbazide (**1**, 44.5 mg, 0.50 mmol) were dissolved in distilled water, heated to 60 °C for 5 min and treated dropwise with an aqueous solution of sodium azide (65.0 mg, 1.00 mmol). After 1 min the product appeared slowly in the form of green crystals suitable for X-ray determination. The azide complex was filtered off and dried in air overnight. Yield: 80.0 mg (0.34 mmol, 68 %).

DTA (5 °C min^{-1}): 121 °C (exothermic); IR (ATR, cm^{-1}): $\tilde{\nu}$ = 3422 (vw), 3334 (vw), 3030 (vw), 2946 (vw), 2086 (w), 2025 (vs), 1744 (vw), 1623 (s), 1528 (s), 1418 (m), 1334 (w), 1285

(m), 1217 (w), 1163 (m) 1072 (w), 1031 (m), 788 (w), 749 (m), 639 (s), 607 (m) 577 (s), 461 (vs); UV-Vis spectrum: λ_{max} = 786 nm; EA ($C_2H_7CuN_9O$, 236.69): calcd: C 10.15, H 2.98, N 53.26 %; found: C 10.00, H 2.96, N 51.84 %; BAM drophammer: 10 J; friction tester: > 360 N; ESD: 1.50 J (at grain size < 100 µm).

General procedure for the preparation of zinc(II) MSC complexes (9–12):

The urea derivative ligand MSC (**9**: 178 mg, 2 mmol; **10**: 89.0 mg, 1.00 mmol; **11**: 44.5 mg, 0.50 mmol); **12**: 93.5 mg, 1.05 mmol) was dissolved in a minimum amount of water (**9**, **11**, **12**) or ethanol (**10**) and added to an aqueous solution of the corresponding zinc(II) salt (**9**: zinc(II) chloride (136 mg, 1.00 mmol); **10**: zinc(II) nitrate hexahydrate (149 mg, 0.50 mmol); **11**/ **12**: zinc(II) perchlorate hexahydrate (**11**: 93.1 mg, 0.25 mmol; **12**: 130 mg, 0.35 mmol). The reaction mixtures were stirred mechanically for 1 min at room temperature and left to crystallize until a solid material appeared. The products were filtered off, washed with cold ethanol (2 mL) and dried in air.

$[ZnCl_2(MSC)_2]$ (9)

Colorless blocks of compound **9** suitable for X-ray determination could be isolated after one week. Yield: 170 mg (0.54 mmol, 54 %).

DTA (5 °C min^{-1}): 171 °C (endothermic) 186 °C (exothermic); IR (ATR, cm^{-1}): $\tilde{\nu}$ = 3328 (m), 3201 (m), 3080 (m), 2972 (m), 2172 (m), 1666 (s), 1629 (vs), 1567 (s), 1533 (s), 1423 (m), 1290 (s), 1228 (m), 1146 (s), 1095 (s), 1041 (m), 801 (m), 763 (s), 635 (s), 527 (vs); EA ($C_4H_{14}Cl_2N_6O_2Zn$, 314.48) calcd: C 15.28, H 4.49, N 26.72 %; found: C 15.31, H 4.32, N 26.55 %; BAM drophammer: > 40 J; friction tester: > 360 N; ESD: 1.50 J (at grain size < 100 µm).

$[Zn(NO_3)_2(MSC)_2]$ (10)

The zinc(II) nitrate complex **9** was obtained in the form of colorless crystals suitable for X-ray determination within four days. Yield: 84 mg (0.21 mmol, 83 %).

DTA (5 °C min^{-1}): 183 °C (endothermic), 208 °C (exothermic); IR (ATR, cm^{-1}): $\tilde{\nu}$ = 3399 (m), 3258 (s), 3223 (m), 3196 (m), 2337 (vw), 1750 (vw), 1671 (s), 1636 (vs), 1568 (s), 1537 (s), 1424 (s), 1305 (vs), 1277 (vs), 1138 (vs), 1081 (vs), 1036 (vs), 820 (m), 801(s), 760 (s), 724 (m), 712 (m), 680 (m); EA ($C_4H_{14}N_8O_8Zn$, 366.02): calcd: C 13.07, H 3.84, N 30.48 %; found: C 13.16, H 3.80, N 30.18 %; BAM drophammer: > 40 J; friction tester: > 360 N; ESD: 1.50 J (at grain size < 100 µm).

$[Zn(H_2O)_2(MSC)_2](ClO_4)_2$ (11)

Within two weeks, colorless needles of **11** suitable for X-ray determination were obtained from the mother liquor. Yield: 51.0 mg (0.11 mmol, 43 %).

DTA (5 °C min^{-1}): 114 °C (endothermic), 231 °C (exothermic), 328 °C (exothermic); IR (ATR, cm^{-1}): $\tilde{\nu}$ = 3370 (vw), 3295 (w), 1628 (m), 1557 (w), 1522 (w), 1454 (vw), 1422 (vw), 1381 (vw), 1288 (vw), 1051 (vs), 932 (w), 790 (vw), 755 (w); EA ($C_4H_{18}Cl_2N_6O_{12}Zn$, 478.50): calcd: C 10.04, H 3.79, N 17.56 %; found: C 10.61, H 3.82, N 18.03 %; BAM drophammer: > 40 J; friction tester: 160 N; ESD: 300 mJ (at grain size < 100 µm).

$[Zn(MSC)_3](ClO_4)_2 \bullet H_2O$ (12)

Coordination compound **12** was obtained within six days in the form of colorless needles suitable for X-ray determination. Yield: 51 mg (0.11 mmol, 43 %).

DTA (5 °C min^{-1}): 123 °C (endothermic), 187 °C (endothermic), 333 °C (exothermic); IR (ATR, cm^{-1}): $\tilde{\nu}$ = 3587 (w), 3473 (w), 3375 (m), 3279 (m), 1626 (s), 1547 (s), 1524 (s), 1419 (m), 1289 (w), 1061 (vs), 794 (m), 757 (m), 620 (s), 559 (m); EA ($C_6H_{23}Cl_2N_9O_{12}Zn$, 549.58): C 13.11, H 4.22, N 22.94 %; found: C 13.24, H 4.13, N 22.87 %; BAM drophammer: 25 J; friction tester: > 360 N; ESD: 600 mJ (at grain size < 100 µm).

General procedure for the preparation of manganese(II) MSC coordination compounds (13–15):

An aqueous solution of MSC (**13**, **14**: 44.5 mg, 0.50 mmol; **15**: 71.3 mg, 0.80 mmol) was added to the corresponding manganese(II) salt (**13**: manganese(II) chloride dihydrate (40.5 mg, 0.25 mmol); **14**: manganese(II) nitrate tetrahydrate (62.8 mg, 0.25 mmol); **15**: manganese(II) perchlorate hexahydrate (90.5 mg, 0.40 mmol)) in water. The reaction mixtures were stirred mechanically for 1 min at room temperature and left to crystallize. After crystallization, the products were filtered off, washed with ethanol (2 mL) and dried in air.

$[MnCl_2(MSC)_2]$ (13)

Complex **13** emerged in the form of pale rose blocks suitable for X-ray determination. Due to the high solubility of the compound in ethanol, only very small quantities very used for the purification step. Yield: 21.0 mg (0.07 mmol, 28 %).

DTA (5 °C min^{-1}): 107 °C (endothermic), 189 °C (endothermic), 209 °C (exothermic); IR (ATR, cm^{-1}): $\tilde{\nu}$ = 3370 (m), 3322 (m), 3268 (m), 3236 (s), 3134 (m), 1660 (s), 1652 (s), 1622 (s), 1615 (s), 1556 (s), 1551 (s), 1517 (s), 1418 (m), 1273 (m), 1129 (m), 1081 (s), 1028 (m), 1007 (m), 793 (m), 772 (m), 763 (m), 616 (s), 594 (m), 562 (s), 522 (vs); EA: ($C_4H_{14}Cl_2MnN_6O_2$, 304.04): calcd: C 15.80, H 4.64, N 27.64 %; found: C 15.57, H 4.74, N 27.45 %.

$[Mn(NO_3)_2(MSC)_2]$ (14)

Colorless blocks of **14**, which were suitable for X-ray analysis started to crystallize within four days. Yield: 86.4 mg (0.24 mmol, 97 %).

DTA (5 °C min^{-1}): 169 °C (endothermic), 208 °C (exothermic); IR (ATR, cm^{-1}): $\tilde{\nu}$ = 3408 (m), 3354 (m), 3271 (m), 3220 (m), 2978 (w), 1657 (s), 1636 (s), 1565 (s), 1537 (s), 1430 (s), 1418 (s), 1306 (vs), 1279 (vs), 1214 (m), 1129 (s), 1086 (s), 1035 (s), 820 (m), 798 (m), 762 (s), 724 (m), 711 (m), 686 (m), 626 (s), 596 (s), 566 (s); EA: ($C_4H_{14}MnN_8O_8$, 357.14): calcd: C 13.45,

H 3.95, N 31.38 %; found: C 13.41, H 4.06, N 31.38 %; BAM drophammer: 40 J; friction tester: > 360 N; ESD: 1.25 J (at grain size < 100 µm).

$[Mn(H_2O)_2(MSC)_2](ClO_4)_2$ (15)

After five days, **15** was isolated in the form of colorless crystals suitable for X-ray determination. Yield: 135 mg (0.29 mmol, 72 %).

DTA (5 °C min^{-1}): 96 °C (endothermic), 234 °C (exothermic), 333 °C (exothermic); IR (ATR, cm^{-1}): $\tilde{\nu}$ = 3471 (m), 3375 (m), 3308 (m), 3246 (w), 1627 (s), 1558 (s), 1455 (w), 1422 (w), 1284 (w), 1048 (vs), 934 (m), 790 (m), 753 (m), 619 (vs), 551 (s), 507 (s); EA ($C_4H_{18}Cl_2MnN_6O_{12}$, 468.06): calcd: C 10.26, H 3.88, N 17.06 %; found: C 10.25, H 3.82, N 17.72 %; BAM drophammer: 10 J; friction tester: 216 N; ESD: 1.00 J (at grain size < 100 µm).

$[Co(H_2O)_2(MSC)_2]Cl_2$ (17)

Methylsemicarbazide (**1**, 178 mg, 2.00 mmol) was dissolved in water, two drops of diluted aqueous 2M hydrochloric acid as co-solvent were added and the reaction mixture subsequently reacted with cobalt(II) chloride hexahydrate (238 mg, 1.00 mmol). The reddish solution was stirred mechanically for 1 min and left undisturbed for crystallization. Orange blocks of **17**, which were suitable for X-ray analysis started to crystallize within three weeks. The product was filtered off and dried in air overnight. Yield: 208 mg (0.61 mmol, 61 %).

DTA (5 °C min^{-1}): 99 °C (endothermic), 259 °C (endothermic), 266 °C (exothermic); IR (ATR, cm^{-1}): $\tilde{\nu}$ = 3453 (vw), 3278 (m), 3202 (m), 2360 (vw), 2339 (vw), 1632 (vs), 1561 (vs), 1527 (s), 1412 (m), 1218 (w), 1153 (s), 1084 (s), 1036 (w), 793 (m), 751 (w), 719 (m), 667 (m); EA: ($C_4H_{18}Cl_2CoN_6O_4$, 344.06): calc.: C 13.96, H 5.27, N 24.43 %; found: C 14.01, H 5.19, N 24.38 %; BAM drophammer: > 40 J; friction tester: > 360 N; ESD: 0.35 J (at grain size < 100 µm).

$[Ni(MSC)_3](ClO_4)_2$ (18)

Three equivalents of MSC (53.5 mg, 0.60 mmol) and one equivalent of nickel(II) perchlorate hexahydrate (73.1 mg, 0.20 mmol) were separately dissolved in water, combined and then heated to 50 °C for 5 min under stirring. The product appeared in form of a blue crystalline solid suitable for X-ray diffraction after one week. The complex was filtered off and dried in air. Yield: 71.0 mg (0.14 mmol, 68 %).

DTA (5 °C min^{-1}): 252 °C (endothermic), 258 °C (exothermic); IR (ATR, cm^{-1}): $\tilde{\nu}$ = 3441 (vw), 3379 (w), 3284 (w), 2361 (vw), 2339 (vw), 1631 (vs), 1558 (s), 1527 (s), 1422 (vw), 1284 (vw), 1059 (vs), 1035 (vs), 928 (w), 790 (m), 754 (m), 658 (w); UV-Vis spectrum: λ_{max} = 581, 952 nm; EA: ($C_6H_{21}Cl_2N_9NiO_{11}$, 524.88): calc.: C 13.73, H 4.03, N 24.02 %; found: C 13.76, H 3.94, N 23.72 %; BAM drophammer: 10 J; friction tester: < 60 N; ESD: 0.10 J (at grain size < 100 µm).

General procedure for the preparation of metal(II) (Cu^{II}, Zn^{II}, Mn^{II}, Co^{II}, Ni^{II}) MSC picrate (PA) complexes (19–23):

Picric acid (115 mg, 0.50 mmol) and the corresponding metal(II) carbonate (**19**: copper(II) carbonate (30.9 mg, 0.25 mmol); **20**: $ZnCO_3 \cdot 3\ Zn(OH)_2$ (34.3 mg, 0.25 mmol); **21**: manganese(II) carbonate (28.7 mg, 0.25 mmol); **22**: cobalt(II) carbonate hydrate (34.2 mg, 0.25 mmol); **23**: $NiCO_3 \cdot 2\ Ni(OH)_2$ (31.4 mg, 0.25 mmol)) were mechanically stirred at 70 °C in H_2O until a clear solution was obtained. MSC (**19**, **21**, **22**: 44.6 mg, 0.50 mmol; **20**, **23**: 66.8 mg, 0.75 mmol) dissolved in water was added and the reaction mixture further stirred for 5 min. The reaction mixtures were left undisturbed until a solid material appeared. The products were filtered off and dried in air.

$[Cu(PA)_2(MSC)_2]$ (19)

Within 1 hour, compound **19** was obtained in the form of green blocks suitable for X-ray determination. The complex was filtered off, washed with a small amount of ethanol and dried in air. Yield: 67.0 mg (0.10 mmol, 38 %).

DTA (5 °C min^{-1}): 179 °C (exothermic); IR (ATR, cm^{-1}): $\tilde{\nu}$ = 3405 (vw), 3330 (vw), 3289 (w), 3241 (w), 3193 (vw), 3077 (vw), 1631 (m), 1603 (m), 1556 (s), 1528 (s), 1508 (s), 1486 (m), 1426 (w), 1361 (m), 1323 (s), 1265 (vs), 1163 (s), 1081 (s), 1030 (s), 937 (m), 914 (vs), 836 (w), 793 (s), 740 (s), 702 (vs), 691 (s), 643 (s), 575(s), 541 (vs), 520 (vs); EA: ($C_{16}H_{18}CuN_{12}O_{16}$, 697.94) calcd: C 27.53, H 2.60, N 24.08 %; found: C 27.49, H 2.89, N 24.21 %; BAM drophammer: 30 J; friction tester: > 360 N; ESD: 0.30 J (at grain size < 100 µm).

[Zn(MSC)$_3$](PA)$_2$ (20)

Compound **20** precipitated as amorphous yellow powder within 1 hour. Yield: 81.9 mg (0.10 mmol, 42 %).

DTA (5 °C min^{-1}): 190 °C (exothermic); IR (ATR, cm^{-1}): $\tilde{\nu}$ = 3473 (m), 3348 (m), 3249 (m), 3156 (m), 2172 (m), 1624 (s), 1610 (s), 1553 (vs), 1511 (s), 1485 (s), 1430 (s), 1364 (s), 1337 (s), 1314 (vs), 1260 (vs), 1161 (s), 1135 (s), 1110 (s), 1095 (s), 1080 (s), 1038 (s), 944 (m), 929 (m), 908 (s), 788 (s), 760 (s), 747 (s), 709 (s), 685 (m), 646 (m), 627 (s), 545 (m), 518 (m); EA: ($C_{18}H_{25}N_{15}O_{17}Zn$, 788.87) calcd: C 27.41, H 3.19, N 26.63 %; found: C 27.41 H 3.05, N 26.20 %; BAM drophammer: 10 J; friction tester: 360 N; ESD: 1.00 J (at grain size < 100 µm).

[Mn(PA)$_2$(MSC)$_2$] (21)

After two days, the manganese(II) picrate compound **21** was received in the form of yellow blocks suitable for X-ray determination. Yield: 91.3 mg (0.13 mmol, 53 %).

DTA (5 °C min^{-1}): 190 °C (exothermic); IR (ATR, cm^{-1}): $\tilde{\nu}$ = 3458 (w), 3363 (m), 3326 (m), 3246 (w), 3082 (w), 1652 (m), 1631 (m), 1605 (s), 1566 (s), 1534 (s), 1512 (vs), 1492 (s), 1482 (s), 1424 (m), 1355 (s), 1325 (vs), 1270 (vs), 1166 (s), 1081 (s), 1003 (s), 942 (m), 934 (m), 914 (s), 838 (m), 825 (w), 788 (s), 748 (m), 740 (s), 704 (vs), 617 (s), 549 (s), 541 (vs), 531 (s); EA: ($C_{16}H_{18}MnN_{12}O_{16}$, 689.33) calcd: C 27.88, H 2.63, N 24.38 %; found: C 27.71, H 2.69, N 24.25 %; BAM drophammer: 9 J; friction tester: 288 N; ESD: 0.55 J (at grain size < 100 µm).

$[Co(PA)_2(MSC)_2]$ (22)

The cobalt(II) picrate complex **22** crystallized within 1 hour in the form of orange blocks suitable for X-ray determination. Yield: 120 mg (0.17 mmol, 69 %).

DTA (5 °C min^{-1}): 211 °C (exothermic); IR (ATR, cm^{-1}): $\tilde{\nu}$ = 3454 (m), 3359 (m), 3324 (m), 3246 (w), 3080 (w), 1649 (m), 1624 (m), 1605 (s), 1562 (s), 1533 (s), 1514 (vs), 1493 (s), 1479 (s), 1423 (m), 1355 (s), 1327 (vs), 1271 (vs), 1167 (s), 1081 (s), 1013 (s), 943 (m), 933 (m), 915 (vs), 838 (m), 825 (w), 791 (s), 750 (m), 739 (s), 713 (s), 703 (vs), 629 (s), 616 (s), 582 (s), 560 (s), 542 (s), 530 (s); EA: ($C_{16}H_{18}CoN_{12}O_{16}$, 693.32) calcd: C 27.72, H 2.62, N 24.24 %; found: C 27.79, H 2.68, N 24.31 %; BAM drophammer: 5 J; friction tester: 288 N; ESD: 0.30 J (at grain size < 100 μm).

$[Ni(MSC)_3](PA)_2$ (23)

Nickel(II) complex **23** was obtained as a green precipitate within 1 hour. Yield: 109 mg (0.14 mmol, 56 %).

DTA (5 °C min^{-1}): 217 °C (exothermic); IR (ATR, cm^{-1}): $\tilde{\nu}$ = 3466 (m), 3347 (m), 3247 (m), 3149 (m), 1624 (s), 1609 (s), 1550 (vs), 1515 (s), 1484 (s), 1430 (s), 1364 (s), 1314 (vs), 1257 (vs), 1147 (s), 1079 (s), 1037 (s), 944 (m), 929 (m), 908 (s), 788 (s), 757 (s), 746 (s), 708 (s), 665 (s), 635 (s), 564 (m), 546 (s); 3473 (m), 3348 (m), 3249 (m), 3156 (m), 2172 (m), 1624 (s), 1610 (s), 1553 (vs), 1511 (s), 1485 (s), 1430 (s), 1364 (s), 1337 (s), 1314 (vs), 1260 (vs), 1161 (s), 1135 (s), 1110 (s), 1095 (s), 1080 (s), 1038 (s), 944 (m), 929 (m), 908 (s), 788 (s), 760 (s), 747 (s), 709 (s), 685 (m), 646 (m), 627 (s), 545 (m), 518 (m)EA: ($C_{18}H_{25}N_{15}NiO_{17}$, 782.18) calcd: C 27.64, H 3.22, N 26.86 %; found: C 26.99, H 3.20, N 25.62 %; BAM drophammer: 10 J; friction tester: > 360 N; ESD: 0.75 J (at grain size < 100 μm).

General procedure for the preparation of metal(II) (Cu^{II}, Zn^{II}, Mn^{II}, Co^{II}, Ni^{II}) MSC styphnate (HTNR) complexes (24–28):

Styphnic acid (245 mg, 1.00 mmol) and the corresponding metal(II) carbonate (**24**: copper(II) carbonate (61.8 mg, 0.50 mmol); **25**: $ZnCO_3 \cdot 3\ Zn(OH)_2$ (68.6 mg, 0.50 mmol); **26**:

manganese(II) carbonate (57.4 mg, 0.50 mmol); **27**: cobalt(II) carbonate hydrate (68.4 mg, 0.50 mmol); **28**: $NiCO_3 \cdot 2\ Ni(OH)_2$ (62.8 mg, 0.50 mmol)) were stirred in water at 70 °C until all the starting materials dissolved. An aqueous solution of MSC (89.1 mg, 1.00 mmol) was added, the mixture stirred for 5 min and subsequently left for crystallization. The products were filtered off, washed with a small amount of cold ethanol (2 mL) and dried in air.

$[Cu(H_2O)_2(MSC)_2](HTNR)_2$ (24)

Complex **24** crystallized in the form of green needles suitable for X-ray determination within 2 hours. Yield: 106 mg (0.14 mmol, 55 %).

DTA (5 °C min^{-1}): 119 °C (endothermic), 179 °C (exothermic); IR (ATR, cm^{-1}): $\tilde{\nu}$ = 3626 (w), 3465 (w), 3431 (vw), 3250 (m), 3086 (w), 1666 (vw), 1620 (m), 1578 (m), 1538 (vs), 1490 (s), 1444 (m), 1410 (w), 1379 (m), 1339 (m), 1276 (vs), 1236 (s), 1180 (s), 1154 (s), 1080 (s), 1037 (m), 932 (m), 809 (w), 785 (m), 750 (s), 712 (m), 693 (s), 634 (m), 584 (s), 546 (m), 453 (vs); EA: ($C_{16}H_{22}CuN_{12}O_{20}$, 765.96) calcd: C 25.09, H 2.90, N 21.94 %; found: C 24.85, H 3.15, N 21.63 %; BAM drophammer: > 40 J; friction tester: > 360 N; ESD: 0.40 J (at grain size < 100 µm).

$[Zn(H_2O)_2(MSC)_2](HTNR)_2$ (25)

Within one week, the zinc(II) styphnate complex **25** was isolated in the form of yellow blocks suitable for X-ray determination. Yield: 222 mg (0.29 mmol, 58 %).

DTA (5 °C min^{-1}): 134 °C (endothermic), 195 °C (exothermic); IR (ATR, cm^{-1}): $\tilde{\nu}$ = 3617 (w), 3482 (w), 3279 (w), 3127 (w), 2360 (w), 2339 (vw), 1672 (m), 1645 (s), 1619 (s), 1568 (s), 1530 (vs), 1492 (s), 1444 (m), 1410 (w), 1377 (m), 1337 (s), 1291 (vs), 1240 (m), 1185 (vs), 1137 (s), 1082 (vs), 1033 (m), 931 (m), 826 (w), 782 (s), 758 (vs), 712 (s), 694 (vs); EA: ($C_{16}H_{22}N_{12}O_{20}Zn$, 767.80) calcd: C 25.03, H 2.89, N 21.89 %; found: C 24.94, H 2.87, N 21.72 %; BAM drophammer: > 40 J; friction tester: > 360 N; ESD: 1.00 J (at grain size < 100 µm).

[Mn(HTNR)$_2$(MSC)$_2$] (26)

The water-free compound **26** was obtained within 3 days in the form of orange blocks suitable for X-ray determination. Yield: 97.0 mg (0.13 mmol, 54 %).

DTA (5 °C min^{-1}): 184 °C (exothermic); IR (ATR, cm^{-1}): $\tilde{\nu}$ = 3405 (vw), 3330 (vw), 3289 (w), 3241 (w), 3193 (vw), 3077 (vw), 1631 (m), 1603 (m), 1556 (s), 1528 (s), 1508 (s), 1486 (m), 1426 (w), 1361 (m), 1323 (s), 1265 (vs), 1163 (s), 1081 (s), 1030 (s), 937 (m), 914 (vs), 836 (w), 793 (s), 740 (s), 702 (vs), 691 (s), 643 (s), 575(s), 541 (vs), 520 (vs); EA: ($C_{16}H_{18}MnN_{12}O_{18}$, 721.33) calcd: C 26.64, H 2.52, N 23.30 %; found: C 23.42, H 2.72, N 23.30 %; BAM drophammer: 25 J; friction tester: 324 N; ESD: 0.60 J (at grain size < 100 µm).

[Co(H$_2$O)$_2$(MSC)$_2$](HTNR)$_2$ (27)

Within one week, complex **27** emerged in the form of yellow blocks suitable for X-ray determination. Yield: 278 mg (0.78 mmol, 78 %).

DTA (5 °C min^{-1}): 155 °C (endothermic), 205 °C (exothermic); IR (ATR, cm^{-1}): $\tilde{\nu}$ = 3614 (vw), 3477 (vw), 3284 (w), 3143 (vw), 3079 (vw), 1669 (vw), 1643 (w), 1620 (s), 1583 (m), 1560 (m), 1529 (s), 1492 (s), 1441 (m), 1375 (m), 1333 (s), 1282 (vs), 1182 (vs), 1136 (s), 1077 (vs), 1028 (m), 932 (m), 823 (w), 803 (w), 778 (m), 757 (vs), 694 (vs), 639 (vs), 574 (s), 518 (s); EA: ($C_{16}H_{22}CoN_{12}O_{20}$, 761.35) calcd: C 25.24, H 2.91, N 22.08 %; found: C 25.01, H 3.11, N 22.05 %; BAM drophammer: > 40 J; friction tester: > 360 N; ESD: 1.50 J (at grain size < 100 µm).

[Ni(H$_2$O)$_2$(MSC)$_2$](HTNR)$_2$ (28)

X-ray suitable green blocks of **28** started to crystallize within 2 days. Yield: 238 mg (0.31 mmol, 63 %).

DTA (5 °C min^{-1}) onset: 172 °C (endothermic), 193 °C (exothermic); IR (ATR, cm^{-1}): $\tilde{\nu}$ = 3616 (w), 3481 (w), 3276 (w), 3128 (w), 2361 (w), 1671 (w), 1646 (m), 1619 (s), 1567 (s), 1532 (vs), 1492 (s), 1443 (m), 1410 (w), 1376 (m), 1335 (s), 1290 (vs), 1184 (vs), 1149 (s), 1081 (vs), 1032 (m), 932 (m), 825 (m), 802 (m), 778 (m), 757 (vs), 693 (vs); EA:

($C_{16}H_{22}N_{12}NiO_{20}$, 761.11) calcd: C 25.25, H 2.91, N 22.08 %; found: C 25.04, H 2.97, N 21.81 %; BAM drophammer: > 40 J; friction tester: > 360 N; ESD: 1.50 J (at grain size < 100 µm).

19.4.7 References

[S1] *CrysAlisPro*, Oxford Diffraction Ltd., version 171.33.41, **2009**.

[S2] A. Altomare, G. Cascarano, C. Giacovazzo, A. Guagliardi, *J. Appl. Crystallogr.*, **1992**, *26*, 343–350.

[S3] a) A. Altomare, G. Cascarano, C. Giacovazzo, A. Guagliardi, A. G. G. Moliterni, M. C. Burla, G. Polidori, M. Camalli, R. Spagna, *SIR97*, **1997**; b) A. Altomare, M. C. Burla, M. Camalli, G. L. Cascarano, C. Giacovazzo, A. Guagliardi, A. G. G. Moliterni, G. Polidori, R. Spagna, *J. Appl. Crystallogr.*, **1999**, *32*, 115–119.

[S4] a) G. M. Sheldrick, *SHELXL-97*, *Program for the Refinement of Crystal Structures*, University of Göttingen, Germany, **1997**; b) G. M. Sheldrick, *Acta Crystallogr. Sect. A*, **2008**, *64*, 112–122.

[S5] A. L. Spek, *PLATON*, *A Multipurpose Crystallographic Tool*, Utrecht University, The Netherlands, **1999**.

[S6] L. J. Farrugia, *J. Appl. Cryst.*, **2012**, *45*, 849–854.

[S7] Empirical absorption correction using spherical harmonics, implemented in SCALE3 ABSPACK scaling algorithm (CrysAlisPro Oxford Diffraction Ltd., Version 171.33.41, **2009**).

[S8] NATO standardization agreement (STANAG) on explosives, impact sensitivity tests, no. 4489, 1st ed., Sept. 17, **1999**.

[S9] WIWEB-Standardarbeitsanweisung 4-5.1.02, Ermittlung der Explosionsgefährlichkeit, hier der Schlagempfindlichkeit mit dem Fallhammer, Nov. 8, **2002**.

[S10] http://www.bam.de, Accessed October 2017.

[S11] NATO standardization agreement (STANAG) on explosive, friction sensitivity tests, no. 4487, 1st ed., Aug. 22, **2002**.

[S12] WIWEB-Standardarbeitsanweisung 4-5.1.03, Ermittlung der Explosionsgefährlichkeit oder der Reibeempfindlichkeit mit dem Reibeapparat, Nov. 8, **2002**.

[S13] Impact: insensitive > 40 J, less sensitive ≥ 35 J, sensitive ≥ 4 J, very sensitive ≤ 3 J; Friction: insensitive > 360 N, less sensitive = 360 N, sensitive < 360 N and > 80 N, very sensitive ≤ 80 N, extremely sensitive ≤ 10 N. According to the UN Recommendations on the Transport of Dangerous Goods, (+) indicates not safe for transport.

[S14] http://www.ozm.cz, Accessed October 2017.

[S15] R. Scharf, PhD thesis, Ludwig-Maximilians Universität München, **2016**.

[S16] A. Shibayama, R. Kajiki, M. Kobayashi, T. Mitsunari, A. Nagamatsu, Kumiai Chemical Industry Co., Ltd., Japan; Ihara Chemical Industry Co., Ltd., **2012**, 226.

19.5 Supplementary Information: Di(1*H*-tetrazol-5-yl)methane as Neutral Ligand in Energetic Transition Metal Complexes

19.5.1 X-ray Diffraction

For all compounds, an Oxford Xcalibur3 diffractometer with a CCD area detector was employed for data collection using Mo-*K*α radiation (λ = 0.71073 Å). The data collection and reduction were carried out using the CRYSALISPRO software[S1]. The structures were solved by direct methods (SIR-92[S2], SIR-97[S3] or SHELXS-97[S4]) and refined by full-matrix least-squares on *F*2 (SHELXL[S4]) and finally checked using the PLATON software[S5] integrated in the WinGX software suite. The non-hydrogen atoms were refined anisotropically and the hydrogen atoms were located and freely refined. The absorptions were corrected by a SCALE3 ABSPACK multiscan method[S6]. All DIAMOND2 plots are shown with thermal ellipsoids at the 50% probability level and hydrogen atoms are shown as small spheres of arbitrary radius.

Table S1. Crystallographic data of **2**–**6**.

	2	**3**	**4**	**5**	**6**
Formula	$C_6H_{12}Cl_2CuN_{16}O_2$	$C_6H_{12}Cl_2CoN_{16}O_2$	$C_6H_{12}Cl_2N_{16}NiO_2$	$C_3H_8Cl_2MnN_8O_2$	$C_6H_{12}CoN_{18}O_8$
FW [g mol^{-1}]	474.76	470.15	469.91	314.01	523.27
Crystal system	Monoclinic	Monoclinic	Monoclinic	Orthorhombic	Orthorhombic
Space Group	*C*2/*c*	$P2_1/c$	$P2_1/c$	*Pbca*	*Pnma*
Color / Habit	Blue rhomb	Clear gold prism	Blue needle	Light-yellow block	Orange needle
Size [mm]	0.06 × 0.19 × 0.44	0.08 x 0.30 x 0.32	0.13 x 0.13 x 0.40	0.22 x 0.35 x 0.39	0.01 x 0.03 x 0.18
a [Å]	20.4779(9)	6.7322(4)	6.7210(3)	8.2635(2)	6.4845(2)
b [Å]	6.9223(3)	12.2567(7)	12.2590(5)	15.2891(3)	24.6593(7)
c [Å]	14.6440(6)	10.0547(6)	10.0690(4)	17.0726(5)	11.3352(4)
α [°]	90	90	90	90	90
β [°]	125.206(4)	101.435(6)	101.604(4)	90	90
γ [°]	90	90	90	90	90
V [Å^3]	1696.14(13)	813.19(8)	812.66(6)	2156.98(9)	1812.54(10)
Z	4	2	2	8	4
$\rho_{calc.}$ [g cm^{-3}]	1.859	1.920	1.920	1.934	1.918
μ [mm^{-1}]	1.649	1.432	1.570	1.720	1.037
F(000)	956	474	476	1256	1060
$\lambda_{MoK\alpha}$ [Å]	0.71073	0.71073	0.71073	0.71073	0.71073
T [K]	173	173	298	173	173
θ Min–Max [°]	4.2, 26.0	4.1, 26.0	4.1, 26.0	4.3, 26.0	4.4, 26.0
Dataset	-25:20; -7:8; -17:8	-8:5; -15:12; -12: 12	-8:8; -15:10; -12:11	-10:10; -17:18; -21:20	-7:7; -30:22; -13:13
Reflections collected	3225	3238	6019	15672	12622
Independent refl.	1667	1598	1595	2112	1801
Rint	0.023	0.026	0.026	0.033	0.044
Observed reflections	1488	1405	1422	1871	1472
Parameters	148	148	177	161	173
R_1 (obs)[a]	0.0283	0.0276	0.0241	0.0278	0.0326
wR_2 (all data)[b]	0.0692	0.0721	0.0661	0.0857	0.0849
GooF[c]	1.07	1.05	1.03	1.12	1.04
Resd. Dens. [e Å^{-3}]	-0.64, 0.38	-0.32, 0.37	-0.31, 0.32	-0.70, 0.40	-0.36, 0.85
Absorption correction	multi-scan	multi-scan	multi-scan	multi-scan	multi-scan
CCDC	1528237	1528239	1528244	1528241	1528233

a) $R_1 = \Sigma||F_0|- |F_c||/ \Sigma|F_0|$; b) $wR_2 = [\Sigma[w(F_0^2-F_c^2)^2]/\Sigma[w(F_0)^2]]^{1/2}$; $w = [\sigma c^2(F_0^2)+(xP)^2+yP]^{-1}$ and $P=(F_0^2+2F_c^2)/3$; c) GooF = $\{\Sigma[w(F_o^2-F_c^2)^2]/(n-p)\}^{1/2}$ (n = number of reflections; p = total number of parameters).

Table S2. Crystallographic data of **8**–**12**.

	8	**9**	**10**	**11**	**12**
Formula	$C_6H_{12}ZnN_{18}O_8$	$C_{12}H_{26}Cu_3N_{32}O_{14}S_2$	$C_6H_{12}CuN_{18}O_{14}$	$C_6H_{12}CuN_{18}O_8$	$C_6H_{12}CuN_{18}O_8$
FW [g mol^{-1}]	529.71	1097.39	399.88	527.88	527.88
Crystal system	Orthorhombic	Triclinic	Monoclinic	Monoclinic	Triclinic
Space Group	*Pnma*	*P*-1	$P2_1/c$	$P2_1/c$	*P*-1
Color / Habit	Colorless plate	Blue plate	Blue plate	Blue block	Blue rod
Size [mm]	0.06 x 0.21 x 0.39	0.02 x 0.17 x 0.19	0.02 x 0.17 x 0.21	0.06 x 0.21 x 0.34	0.08 x 0.14 x 0.19
a [Å]	6.5101(4)	6.787(5)	9.865(5)	11.7457(2)	6.6619(4)
b [Å]	24.7154(11)	10.723(5)	9.841(5)	6.4235(1)	7.6212(4)
c [Å]	11.3454(5)	12.201(5)	8.302(5)	12.4612(3)	9.5399(6)
α [°]	90	97.539(5)	90	90	74.513(5)
β [°]	90	102.719(5)	109.868(5)	100.181(2)	75.073(5)
γ [°]	90	91.092(5)	90	90	79.769(4)
V [Å^3]	1825.47(16)	857.6(8)	758.0(7)	925.38(3)	447.93(5)
Z	4	1	2	2	1
$\rho_{calc.}$ [g cm^{-3}]	1.928	2.125	1.752	1.895	1.957
μ [mm^{-1}]	1.435	2.080	1.480	1.269	1.310
F(000)	1072	553	406	534	267
$\lambda_{MoK\alpha}$ [Å]	0.71073	0.71073	0.71073	0.71073	0.71073
T [K]	173	173	173	173	173
θ Min–Max [°]	4.4, 26.0	4.4, 26.0	4.1, 26.0	4.1, 26.5	4.3, 26.4
Dataset	-7:8; -26:30; -13:13	-8:8; -13:13; -15:15	-12:11; -12:11; -8:10	-14:14; -8:8; -15:15	-8:8; -9:9; -11:11
Reflections collected	14158	5708	5593	13223	6720
Independent refl.	1817	3358	1480	1902	1822
Rint	0.051	0.054	0.034	0.028	0.023
Observed reflections	1558	2277	1289	1761	1756
Parameters	169	313	131	175	175
R_1 (obs)[a]	0.0299	0.0734	0.0301	0.0219	0.0325
wR_2 (all data)[b]	0.0797	0.2056	0.0864	0.0576	0.0808
GooF[c]	1.05	1.05	1.07	1.11	1.08
Resd. Dens. [e Å^{-3}]	-0.41, 0.91	-2.17, 1.32	-0.25, 0.80	-0.25, 0.33	-0.68, 0.50
Absorption correction	multi-scan	multi-scan	multi-scan	multi-scan	multi-scan
CCDC	1528246	1528236	1528238	1528240	1528245

a) $R_1 = \Sigma||F_0|- |F_c||/ \Sigma|F_0|$; b) $wR_2 = [\Sigma[w(F_0^2-F_c^2)^2]/\Sigma[w(F_0)^2]]^{1/2}$; $w = [\sigma c^2(F_0^2)+(xP)^2+yP]^{-1}$ and $P=(F_0^2+2F_c^2)/3$; c) GooF = $\{\Sigma[w(F_o^2-F_c^2)^2]/(n-p)\}^{1/2}$ (n = number of reflections; p = total number of parameters).

Table S3. Crystallographic data of **14**–**18**.

	14	**15**	**16**	**17**	**18**
Formula	$C_6H_{12}Cl_2CuN_{16}O_{10}$	$C_6H_8Cl_2CuN_{16}O_8$	$C_3H_5N_9O_3$	$C_3H_8N_{10}O_8Zn$	$C_3H_4N_8O_2$
FW [g mol^{-1}]	602.76	566.72	215.16	377.56	184.14
Crystal system	Orthorhombic	Triclinic	Monoclinic	Monoclinic	Orthorhombic
Space Group	*Pbca*	$P2_1/n$	$P2_1/c$	$P2_1/n$	*Pbca*
Color / Habit	Blue rod	Blue block	Colorless plate	Colorless block	Colorless block
Size [mm]	0.11 x 0.14 x 0.25	0.18 x 0.23 x 0.54	0.04 x 0.11 x 0.43	0.07 x 0.15 x 0.18	0.07 x 0.10 x 0.12
a [Å]	10.1690(2)	9.2384(3)	4.8873(5)	8.1622(3)	7.0187(5)
b [Å]	8.4071(1)	16.2943(6)	16.8667(12)	13.1906(4)	9.6459(6)
c [Å]	22.9825(4)	11.7962(5)	9.6156(10)	10.8315(4)	19.9397(14)
α [°]	90	90	90	90	90
β [°]	90	94.901(3)	101.005(13)	99.312(4)	90
γ [°]	90	90	90	90	90
V [Å^3]	1964.82(6)	1769.23(12)	778.06(13)	1150.80(7)	1349.95(16)
Z	4	4	4	4	8
$\rho_{calc.}$ [g cm^{-3}]	2.038	2.128	1.837	2.179	1.812
μ [mm^{-1}]	1.476	1.634	0.160	2.209	0.153
F(000)	1212	1132	440	760	752
$\lambda_{MoK\alpha}$ [Å]	0.71073	0.71073	0.71073	0.71073	0.71073
T [K]	173	173	173	173	173
θ Min–Max [°]	4.1, 26.0	4.1, 26.0	4.2, 26.2	4.1, 27.0	4.3, 26.5
Dataset	-12:12; -10:8; -28:28	-11:11; -19:20; -14:11	-6:6; -20:20; -11:11	-9:10 ; -16:16; -10:13	-8:8; -12:11; -21:25
Reflections collected	13815	14393	5296	9398	9878
Independent refl.	1927	3469	1558	2503	1379
Rint	0.025	0.032	0.041	0.032	0.057
Observed reflections	1791	2956	1155	2235	1140
Parameters	184	330	156	231	134
R_1 (obs)[a]	0.0232	0.0282	0.0403	0.0327	0.0546
wR_2 (all data)[b]	0.0629	0.0743	0.0986	0.0815	0.1491
GooF[c]	1.08	1.04	1.03	1.11	1.14
Resd. Dens. [e Å^{-3}]	-0.43, 0.31	-0.47, 0.41	-0.30, 0.24	-0.43, 0.63	-0.29, 0.45
Absorption correction	multi-scan	multi-scan	multi-scan	multi-scan	multi-scan
CCDC	1528245	1528235	1528234	1528243	1532131

a) $R_1 = \Sigma||F_0|- |F_c||/ \Sigma|F_0|$; b) $wR_2 = [\Sigma[w(F_0^2-F_c^2)^2]/\Sigma[w(F_0)^2]]^{1/2}$; $w = [\sigma c^2(F_0^2)+(xP)^2+yP]^{-1}$ and $P=(F_0^2+2F_c^2)/3$; c) GooF = $\{\Sigma[w(F_o^2-F_c^2)^2]/(n-p)\}^{1/2}$ (n = number of reflections; p = total number of parameters).

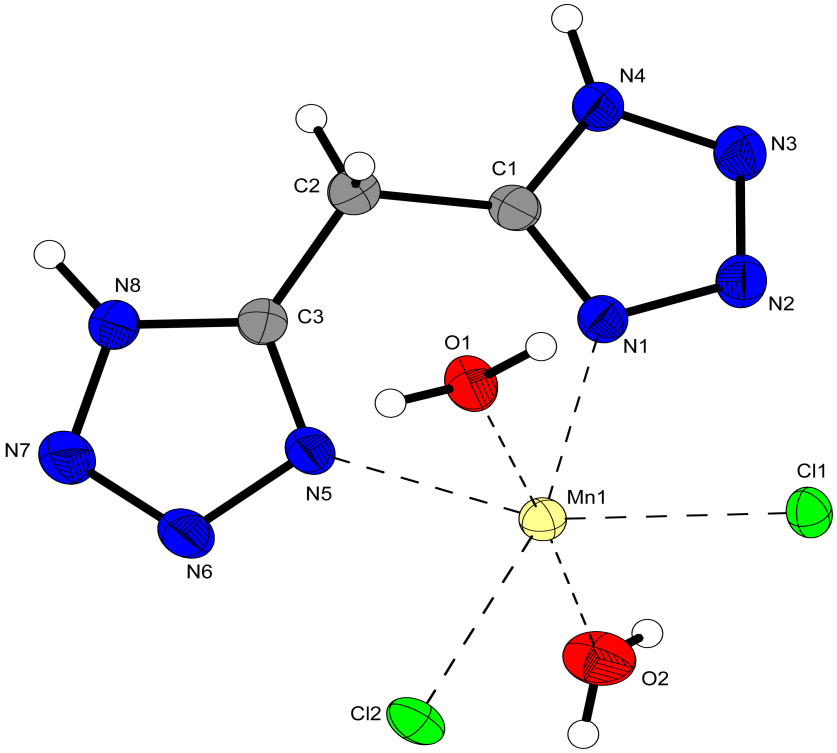


Figure S1. Molecular structure of **5** showing the atom-labeling scheme. Thermal ellipsoids represent the 50 % probability level.

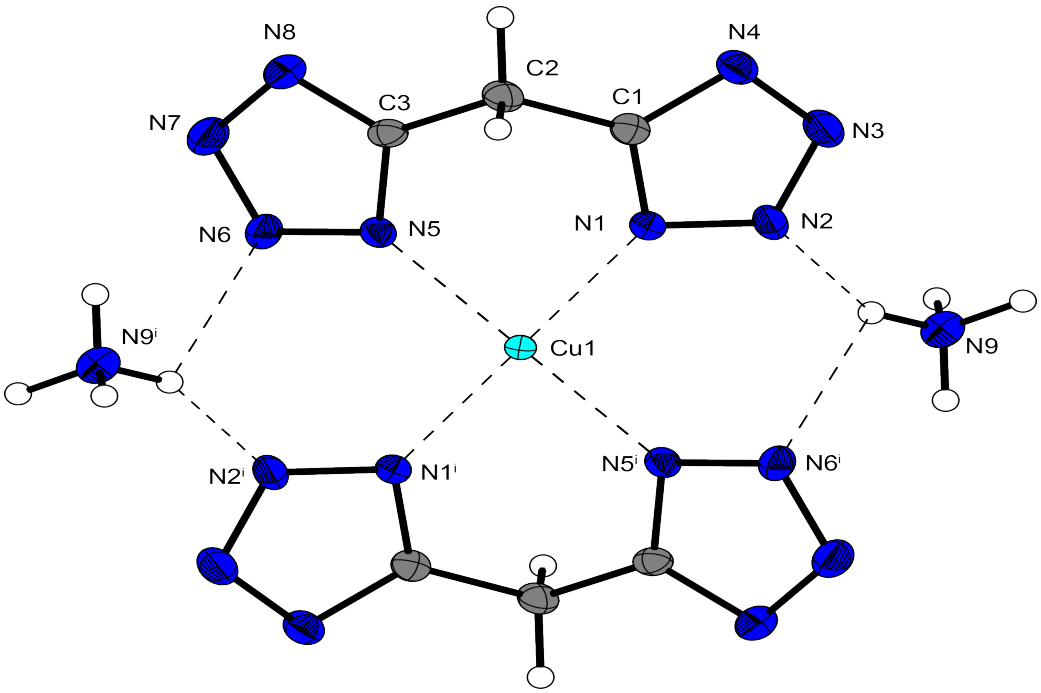


Figure S2. Molecular structure of **10** showing the atom-labeling scheme. Thermal ellipsoids represent the 50 % probability level. Symmetry code: (i) −x, 1−y, 1−z.

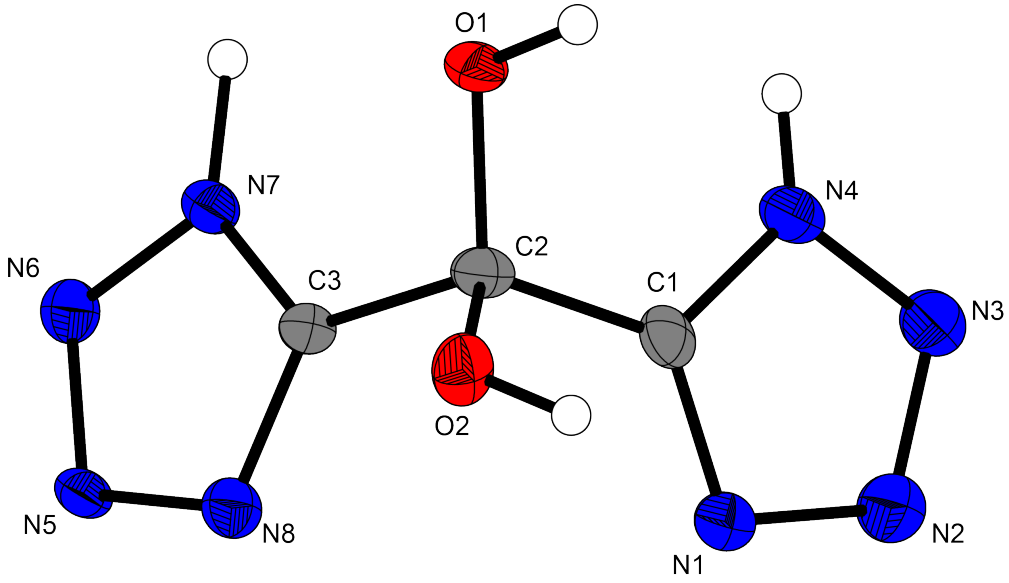


Figure S3. Molecular structure of **18** showing the atom-labeling scheme. Thermal ellipsoids represent the 50% probability level.

19.5.2 IR Spectroscopy of 11, 12 and 14, 15

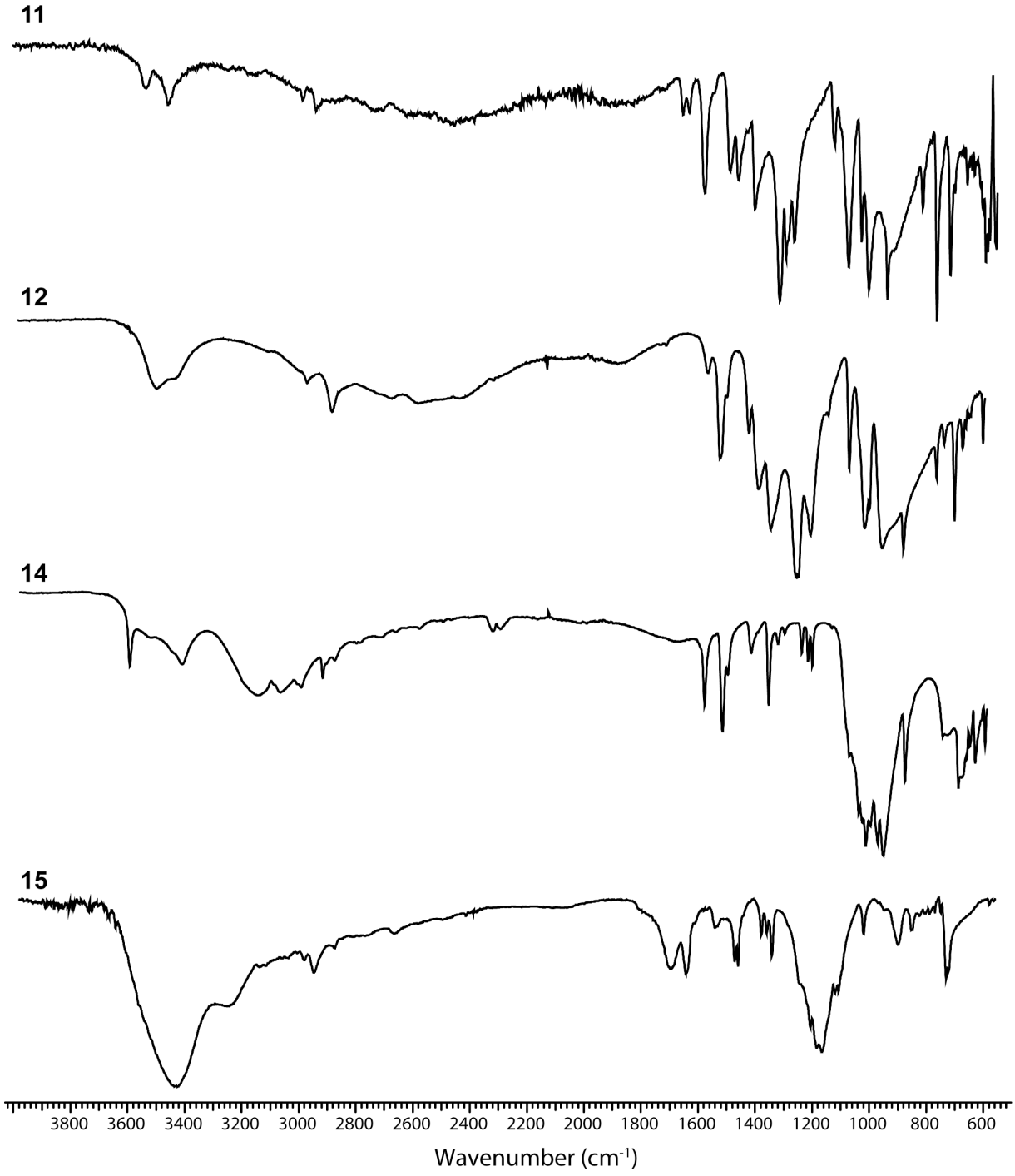


Figure S4. Infrared spectra of **11**, **12** and **14**, **15**.

19.5.3 DTA Plots of 6–8, 11–13 and 15

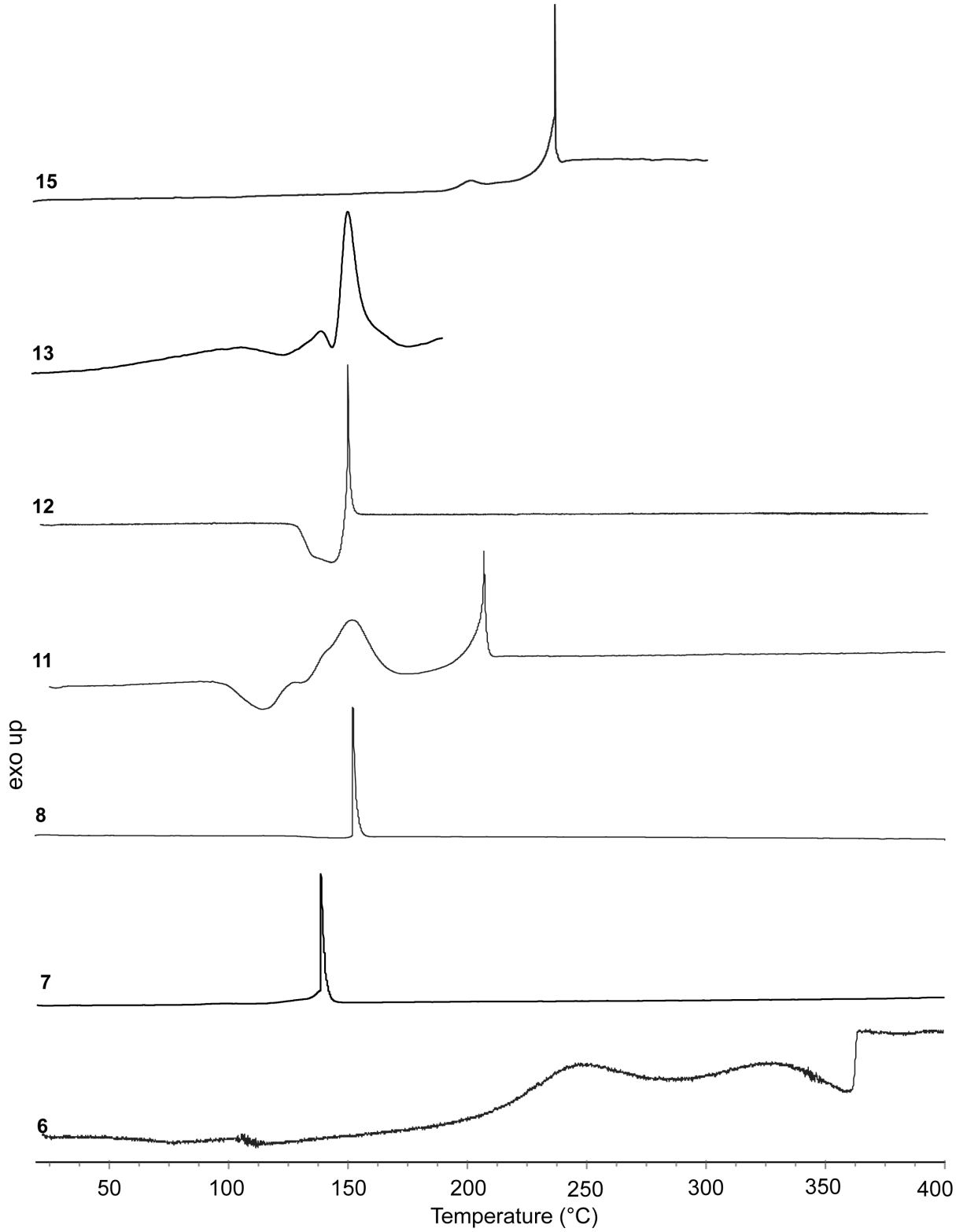


Figure S5. DTA plots of **6**–**8** and **11**–**13** and **15**.

19.5.4 TGA Plot of Compound 12

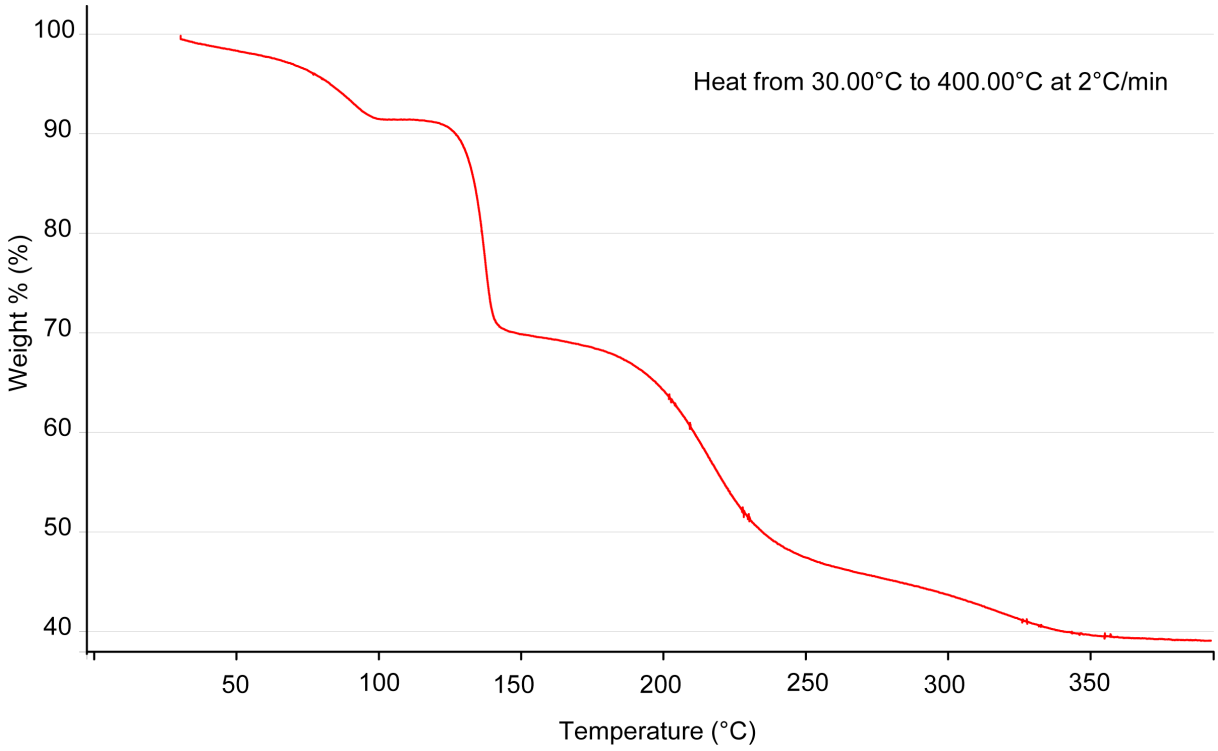


Figure S6. TGA plot of compound **12**.

19.5.5 Hot Plate and Hot Needle Tests



Figure S7. Detonation of compound **15** during the hot plate test.



Figure S8. Hot plate test of $[Cu(NO_3)_2(5\text{-DTM})_2] \cdot 2\ H_2O$ (**12**).

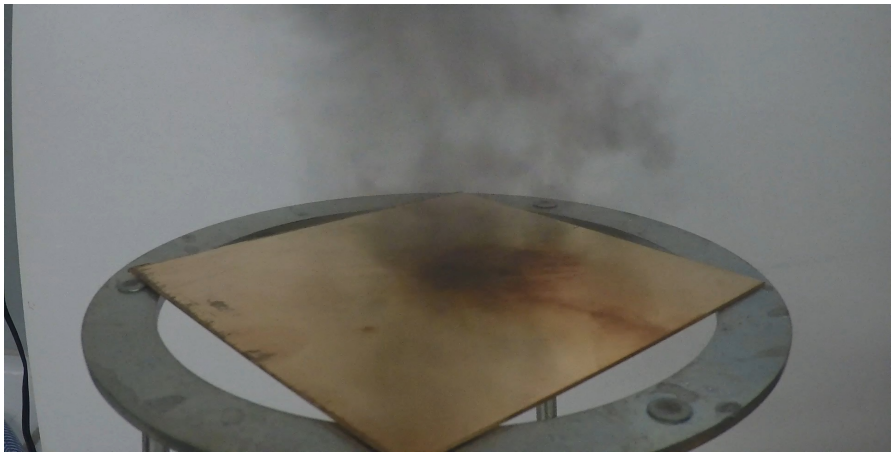


Figure S9. Deflagration of compound **13** during the hot plate tests.

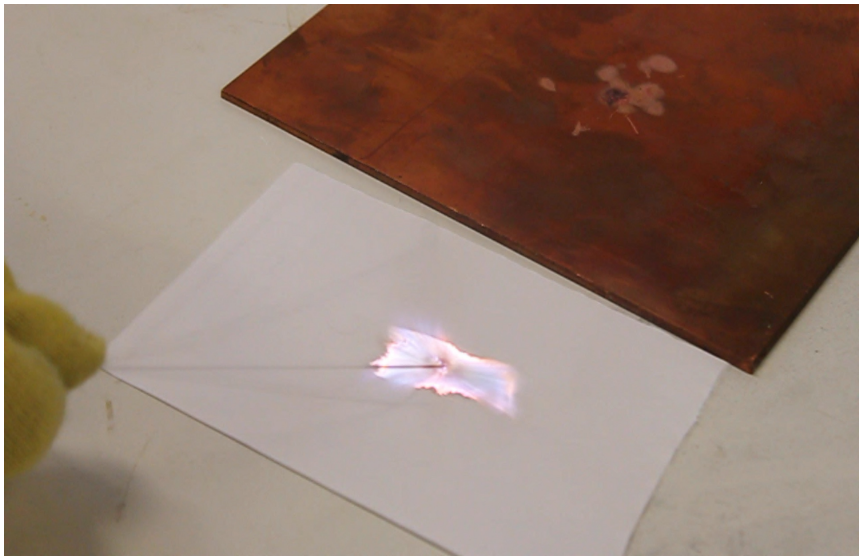


Figure S10. Moment of ignition during the hot needle test of $[Cu(ClO_4)_2(5\text{-DTM})_2]$ (**15**).

19.5.6 References

[S1] *CrysAlisPro*, Oxford Diffraction Ltd., version 171.33.41, **2009**.

[S2] Altomare, A.; Cascarano, G.; Giacovazzo, C.; Guagliardi, A. *J. Appl. Crystallogr.* **1992**, *26*, 343–350.

[S3] a) Altomare, A.; Cascarano, G.; Giacovazzo, C.; Guagliardi, A.; Moliterni, A. G. G.; Burla, M. C.; Polidori, G.; Camalli, M.; Spagna, R. *SIR97*, **1997**; b) Altomare, A.; Burla, M. C.; Camalli, M.; Cascarano, G. L.; Giacovazzo, C.; Guagliardi, A.; Moliterni, A. G. G.; Polidori, G.; Spagna, R. *J. Appl. Crystallogr.* **1999**, *32*, 115–119.

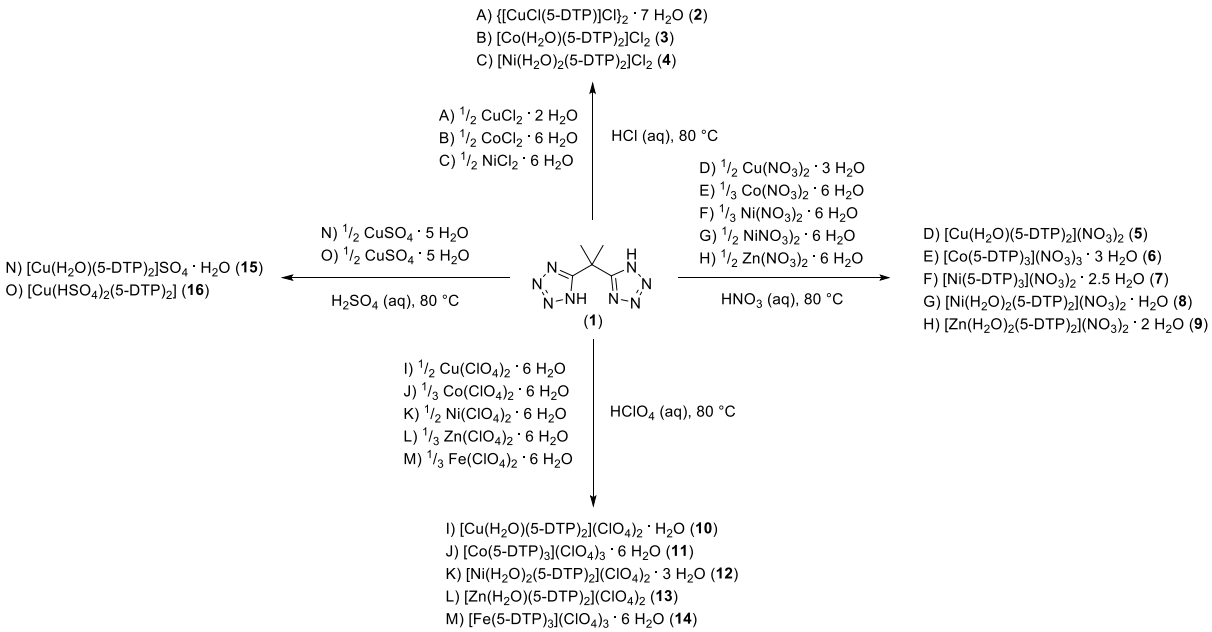
[S4] a) Sheldrick, G. M. *SHELXL-97*, *Program for the Refinement of Crystal Structures*, University of Göttingen, Germany, **1997**; b) Sheldrick, G. M. *Acta Crystallogr. Sect. A* **2008**, *64*, 112–122.

[S5] Spek, A. L. *PLATON*, *A Multipurpose Crystallographic Tool*, Utrecht University, The Netherlands, **1999**.

[S6] Empirical absorption correction using spherical harmonics, implemented in SCALE3 ABSPACK scaling algorithm (CrysAlisPro Oxford Diffraction Ltd., Version 171.33.41, 2009).

19.6 Supplementary Information: 2,2-Bis(5-tetrazolyl)propane as Ligand in Energetic 3d Transition Metal Complexes

19.6.1 Compounds Overview



19.6.2 IR Spectroscopy of 1–15

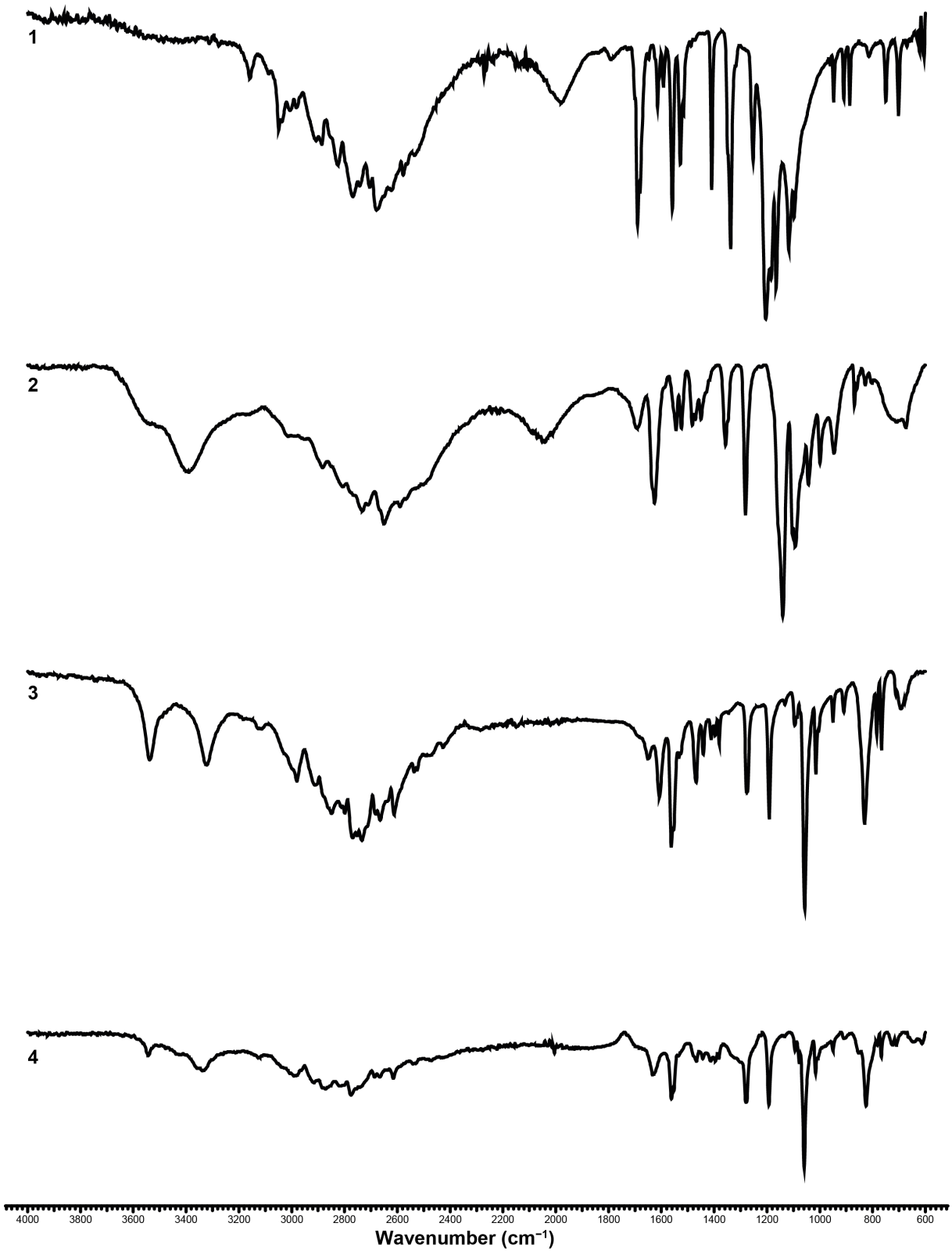


Figure S1. Infrared spectra of compounds **1**–**4**.

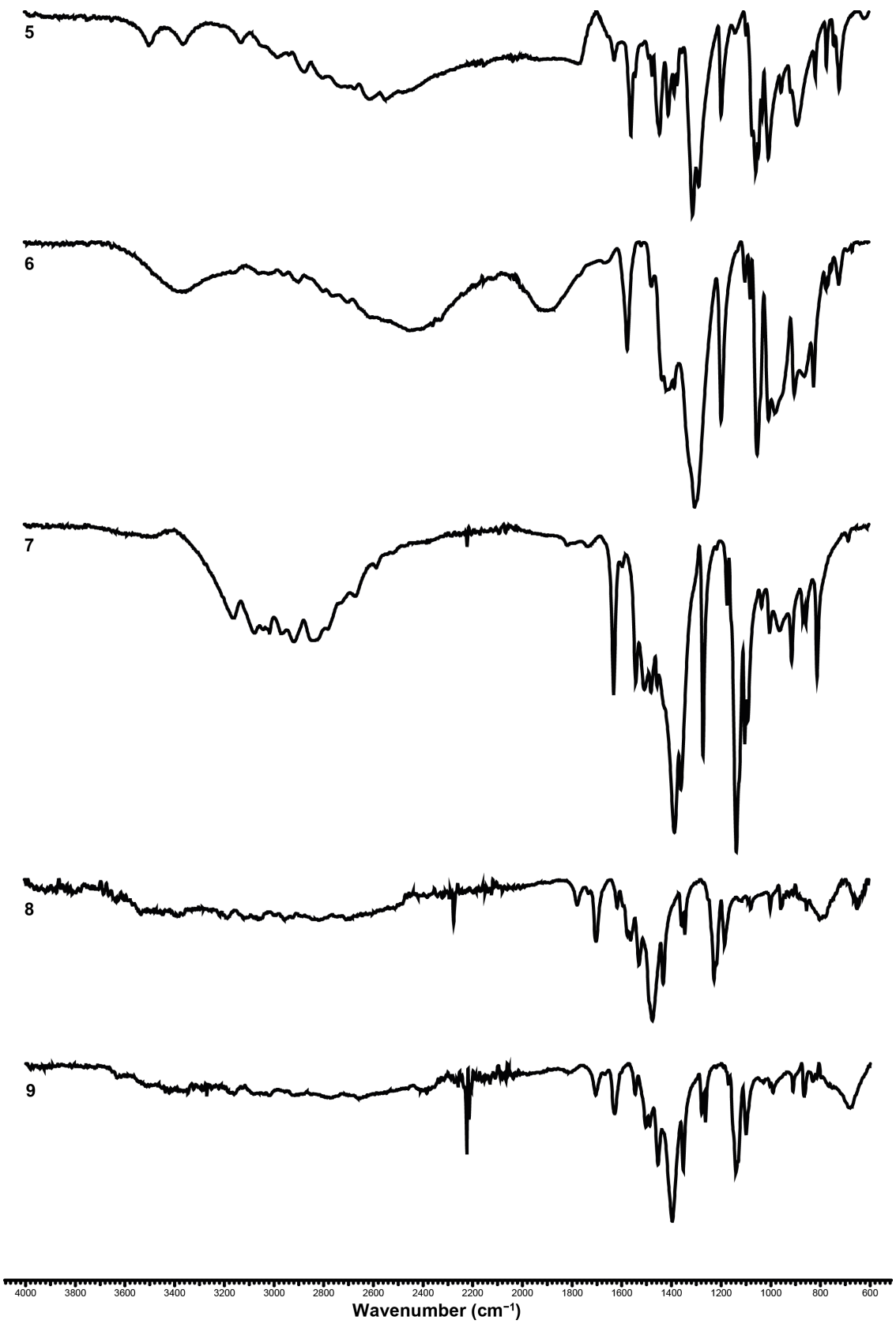


Figure S2. Infrared spectra of the nitrate complexes **5**–**9.**

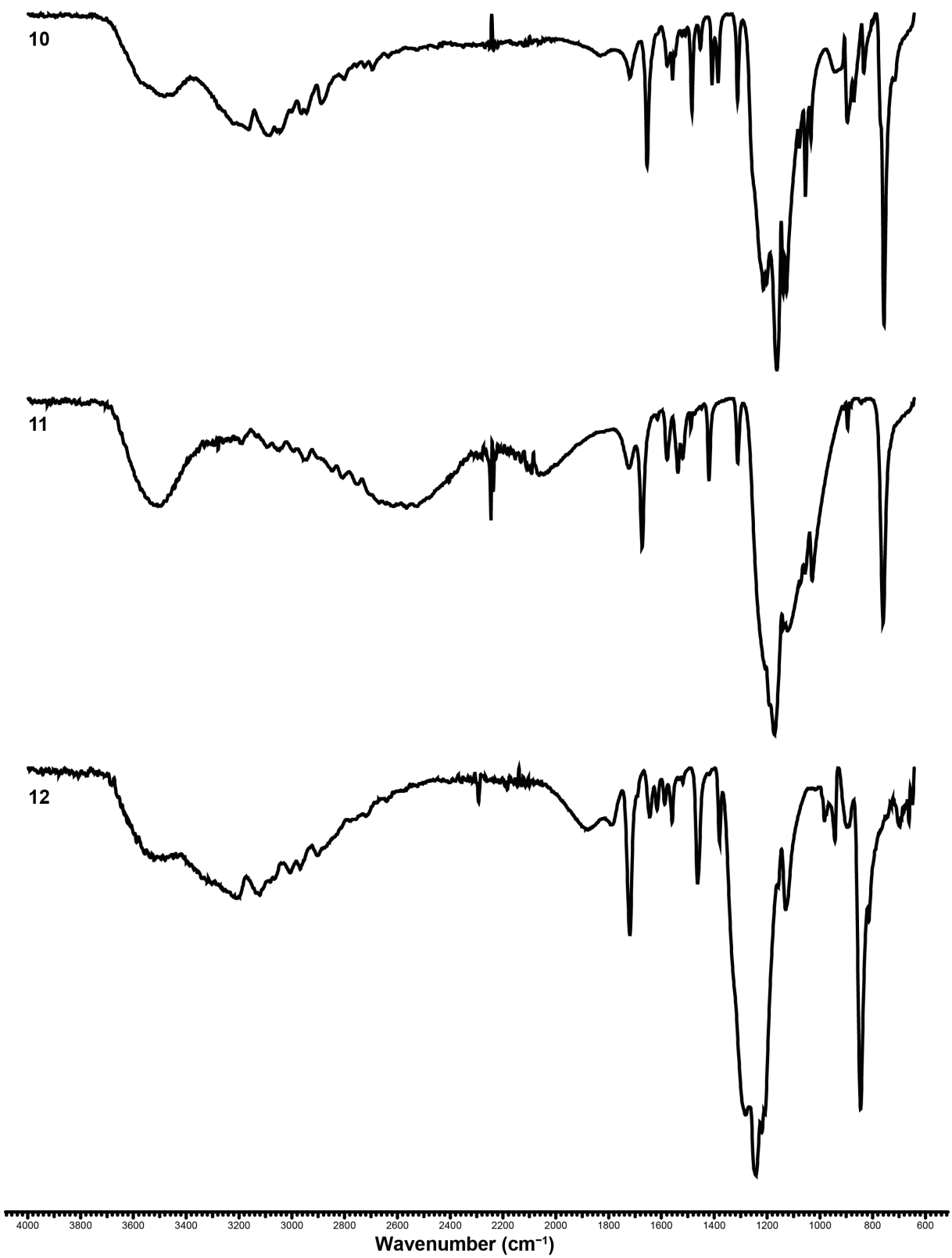


Figure S3. Infrared spectra of coordination compounds **10**–**12.**

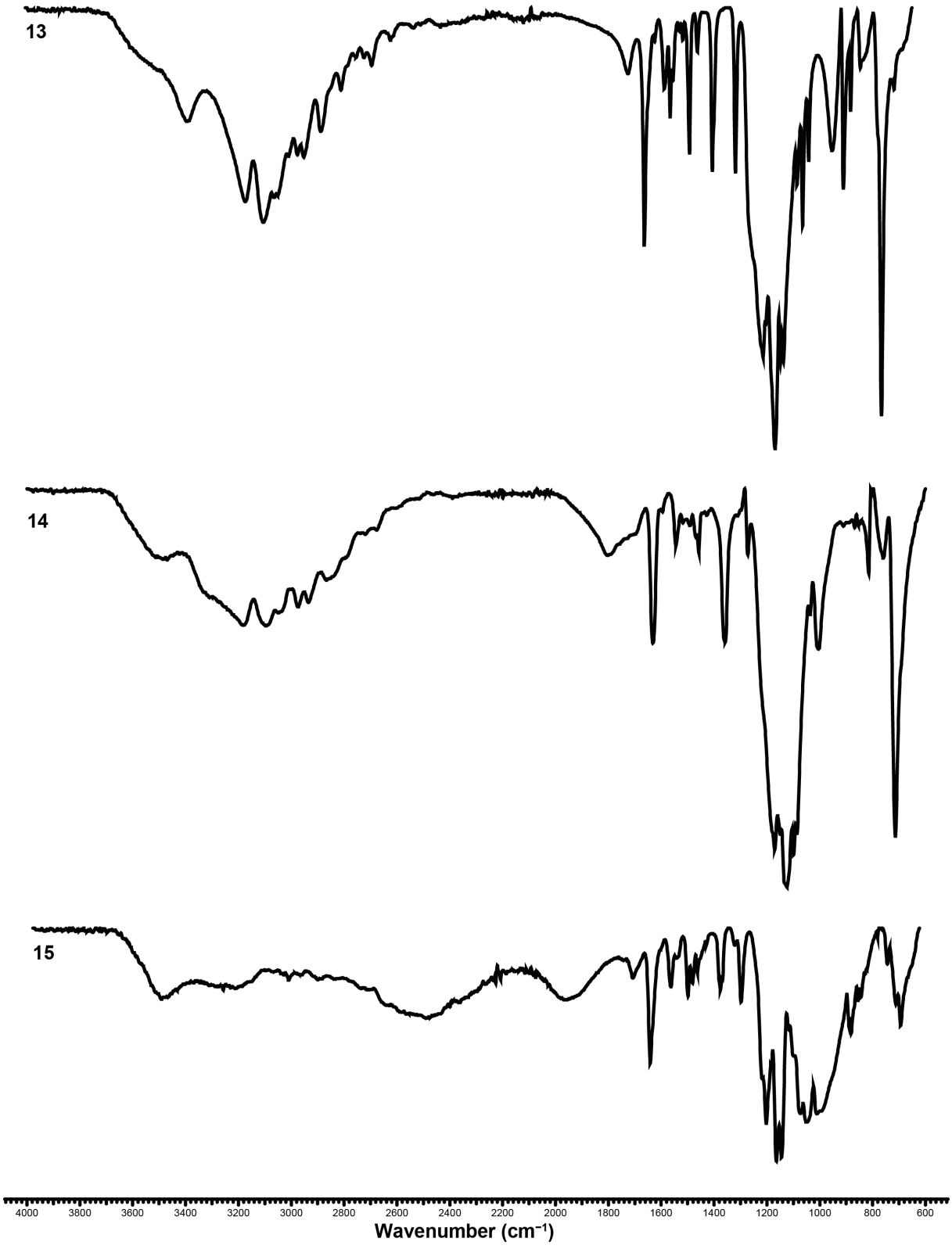


Figure S4. Infrared spectra of complexes **13**–**15**.

19.6.3 X-ray Diffraction

For all crystalline compounds, an Oxford Xcalibur3 diffractometer with a CCD area detector or Bruker D8 Venture TXS diffractometer equipped with a multilayer monochromator, a Photon 2 detector and a rotating-anode generator were employed for data collection using Mo-*K*α radiation (λ = 0.7107 Å). On the Oxford device, data collection and reduction were carried out using the Crysalispro software.[S1] On the Bruker diffractometer, the data were collected with the Bruker Instrument Service v3.0.21, the data reduction was performed using the SAINT V8.18C software (Bruker AXS Inc., 2011). The structures were solved by direct methods (Sir-92[S2], Sir-97[S3] or Shelxs-97[S4]) and refined by full-matrix least-squares on $F2$ (ShelxL[S4]) and finally checked using the platon software[S5] integrated in the WinGX[S6] software suite. The non-hydrogen atoms were refined anisotropically and the hydrogen atoms were located and freely refined. The absorptions were corrected by a Scale3 Abspack or Sadabs Bruker Apex3 multiscan method.[S7,8] All Diamond2 plots are shown with thermal ellipsoids at the 50% probability level and hydrogen atoms are shown as small spheres of arbitrary radius.

Table S1. Crystallographic data of **1**–**4**.

	1	**2**	**3**	**4**
Formula	$C_5H_8N_8$	$C_{20}H_{46}Cl_4Cu_2N_{32}O_7$	$C_{10}H_{20}Cl_2CoN_{16}O_2$	$C_{10}H_{20}Cl_2N_{16}NiO_2$
FW [g mol^{-1}]	180.19	1115.77	526.21	525.97
Crystal system	Orthorhombic	Monoclinic	Monoclinic	Monoclinic
Space Group	*Fdd*2	$P2_1/n$	$P2/c$	$P2/n$
Color / Habit	Colorless rod	Blue block	Orange rod	Green block
Size [mm]	0.11 x 0.23 x 0.38	0.12 x 0.18 x 0.24	0.07 x 0.23 x 0.26	0.10 x 0.12 x 0.18
a [Å]	13.3645(5)	13.2110(3)	7.5800(3)	15.0152(5)
b [Å]	18.6360(7)	19.3065(5)	7.7840(3)	7.5233(2)
c [Å]	6.6904(3)	18.6882(5)	17.9870(8)	19.0646(6)
α [°]	90	90	90	90
β [°]	90	103.104(3)	101.038(4)	105.398(3)
γ [°]	90	90	90	90
V [Å^3]	1666.32(12)	4642.5(2)	1041.65(8)	2076.31(11)
Z	8	4	2	4
$\rho_{calc.}$ [g cm^{-3}]	1.437	1.596	1.678	1.683
μ [mm^{-1}]	0.105	1.222	1.127	1.239
F(000)	752	2288	538	1080
$\lambda_{MoK\alpha}$ [Å]	0.71073	0.71073	0.71073	0.71073
T [K]	173	173	173	173
θ Min–Max [°]	4.4, 26.0	4.2, 26.0	4.1, 26.0	4.1, 26.0
Dataset	−16: 16; −22: 22; −8: 8	−15: 16; −23: 23; −23: 21	−9: 8; −9: 9; −20: 22	−18: 18; −9: 9; −22: 23
Reflections collected	5810	35728	6658	16476
Independent refl.	448	9089	2048	4075
*R*int	0.028	0.061	0.041	0.051
Observed reflections	438	6640	1710	3248
Parameters	76	495	181	361
R_1 (obs)[a]	0.0206	0.0600	0.0356	0.0386
wR_2 (all data)[b]	0.0524	0.1599	0.0924	0.0893
GooF[c]	1.10	1.07	1.08	1.10
Resd. Dens. [e Å^{-3}]	−0.11, 0.13	−1.04, 1.89	−0.26, 0.68	−0.31, 0.41
Absorption correction	multi-scan	multi-scan	multi-scan	multi-scan
CCDC	1850236	1850244	1850246	1850239

a) $R_1 = \Sigma||F_0|- |F_c||/ \Sigma|F_0|$; b) $wR_2 = [\Sigma[w(F_0^2-F_c^2)^2]/\Sigma[w(F_0)^2]]^{1/2}$; $w = [\sigma c^2(F_0^2)+(xP)^2+yP]^{-1}$ and $P=(F_0^2+2F_c^2)/3$; c) GooF = $\{\Sigma[w(F_o^2-F_c^2)^2]/(n-p)\}^{1/2}$ (n = number of reflections; p = total number of parameters).

Table S2. Crystallographic data of **5**–**10**.

	5	**8**	**9**	**10**
Formula	$C_{10}H_{18}Cu\,N_{18}O_7$	$C_{10}H_{22}N_{18}\,NiO_9$	$C_{10}H_{22}N_{18}O_9\,Zn$	$C_{10}H_{20}Cl_2\,CuN_{16}O_8$
FW [g mol^{-1}]	565.92	565.92	565.92	658.82
Crystal system	Monoclinic	Monoclinic	Triclinic	Monoclinic
Space Group	$P2_1/c$	$P2/c$	$P\bar{1}$	$C2/c$
Color / Habit	Blue plate	Green block	Clear colorless block	Clear blue needle
Size [mm]	0.07 x 0.11 x 0.46	0.13 x 0.23 x 0.29	0.10 x 0.15 x 0.25	0.12 x 0.18 x 0.26
a [Å]	20.6320(7)	21.9643(6)	7.7379(7)	28.345(4)
b [Å]	6.6110(2)	7.3465(2)	7.9723(7)	7.6373(8)
c [Å]	15.3330(5)	14.5064(4)	10.1040(9)	24.492(3)
α [°]	90	90	81.001(8)	90
β [°]	96.284(3)	99.794(3)	84.345(8)	116.70(2)
γ [°]	90	90	75.478(8)	90
V [Å^3]	2078.83(12)	2306.65(11)	594.82(10)	4736.7(13)
Z	4	4	1	8
$\rho_{calc.}$ [g cm^{-3}]	1.808	1.719	1.736	1.848
μ [mm^{-1}]	1.133	0.927	1.121	1.233
F(000)	1156	1232	320	2680
$\lambda_{MoK\alpha}$ [Å]	0.71073	0.71073	0.71073	0.71073
T [K]	173	173	173	173
θ Min–Max [°]	4.1, 26.0	4.2, 26.0	4.1, 26.0	4.2, 26.0
Dataset	−25: 24; −8: 7; −18: 18	−27: 27; −9: 9; −17: 17	−9: 9; −9: 9; −12: 12	−34: 29; −9: 9; −14: 30
Reflections collected	15184	17864	4414	12314
Independent refl.	4067	4504	2334	4639
Rint	0.039	0.047	0.036	0.169
Observed reflections	3372	3584	1952	2135
Parameters	349	432	204	364
R_1 (obs)[a]	0.0311	0.0357	0.0353	0.0789
wR_2 (all data)[b]	0.0748	0.0874	0.0777	0.1579
GooF[c]	1.07	1.04	1.05	0.95
Resd. Dens. [e Å^{-3}]	−0.37, 0.45	−0.31, 0.60	−0.35, 0.34	−0.95, 0.71
Absorption correction	multi-scan	multi-scan	multi-scan	multi-scan
CCDC	1850243	1850238	1850237	1850245

a) $R_1 = \Sigma||F_0|- |F_c||/ \Sigma|F_0|$; b) $wR_2 = [\Sigma[w(F_0^2-F_c^2)^2]/\Sigma[w(F_0)^2]]^{1/2}$; $w = [\sigma c^2(F_0^2)+(xP)^2+yP]^{-1}$ and $P=(F_0^2+2F_c^2)/3$; c) GooF = $\{\Sigma[w(F_o^2-F_c^2)^2]/(n-p)\}^{1/2}$ (n = number of reflections; p = total number of parameters).

Table S3. Crystallographic data of **13**–**16**.

	13	**15**	**16**
Formula	$C_{10}H_{18}Cl_2N_{16}O_9Zn$	$C_{10}H_{20}Cu\ N_{16}O_6S$	$C_{10}H_{18}CuN_{16}O_8S_2$
FW [g mol^{-1}]	642.67	556.02	618.06
Crystal system	Monoclinic	Monoclinuic	Triclinic
Space Group	*I*2	$P2_1/c$	*P*−1
Color / Habit	Colorless block	Blue rod	Blue Plate
Size [mm]	0.10 x 0.12 x 0.25	0.10 x 0.10 x 0.60	0.05 x 0.30 x 0.30
a [Å]	12.6220(9)	11.4802(9)	7.5180(7)
b [Å]	7.8436(3)	25.3787(14)	7.8240(7)
c [Å]	13.1981(13)	7.4442(5)	9.7440(13)
α [°]	90	90	90.925(9)
β [°]	115.336(10)	106-477(7)	95.793(9)
γ [°]	90	90	103.992(7)
V [Å^3]	1180.96(18)	2079.8(3)	552.82(10)
Z	2	4	1
$\rho_{calc.}$ [g cm^{-3}]	1.807	1.776	1.857
μ [mm^{-1}]	1.346	1.221	1.256
F(000)	652	1140	315
$\lambda_{MoK\alpha}$ [Å]	0.71073	0.71073	0.71069
T [K]	173	133	123
θ Min–Max [°]	4.1, 26.0	4.1 26.0	4.2, 26.0
Dataset	−15: 15; −9: 7; −15: 16	−11: 14; −31: 31; −9: 9	−9: 9; −8: 9; −12: 12
Reflections collected	4557	16764	4087
Independent refl.	2094	4074	2157
*R*int	0.027	0.048	0.030
Observed reflections	2016	3362	1805
Parameters	188	343	205
R_1 (obs)[a]	0.0244	0.0373	0.0336
wR_2 (all data)[b]	0.0582	0.0927	0.0795
GooF[c]	1.04	1.18	1.04
Resd. Dens. [e Å^{-3}]	−0.22, 0.28	−0.50, 0.65	−0.45, 0.40
Absorption correction	multi-scan	multi-scan	multi-scan
CCDC	1850242	1850241	1850240

a) $R_1 = \Sigma||F_0|- |F_c||/ \Sigma|F_0|$; b) $wR_2 = [\Sigma[w(F_0^2-F_c^2)^2]/\Sigma[w(F_0)^2]]^{1/2}$; $w = [\sigma c^2(F_0^2)+(xP)^2+yP]^{-1}$ and $P=(F_0^2+2F_c^2)/3$; c) GooF = $\{\Sigma[w(F_o^2-F_c^2)^2]/(n-p)\}^{1/2}$ (n = number of reflections; p = total number of parameters).

The octahedral coordination sphere of complex **6** is built up by three molecules of 5-DTP, each coordinating twice. Due to heavy disorder, the structure could not be refined anisotropically.

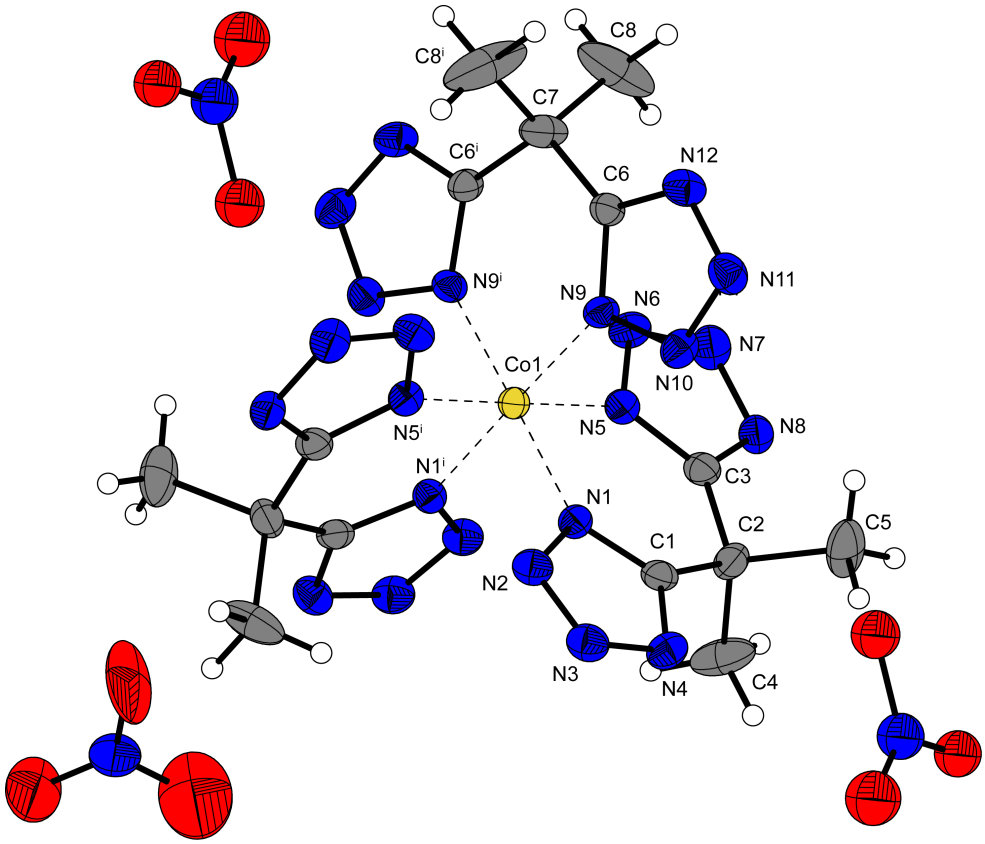


Figure S5. Section of the isotropic illustration of $[Co(5\text{-DTP})_3](NO_3)_2 \bullet H_2O$ (**6**).

Compound **11** crystallizes in the trigonal space group *P*–3 with six formula units per unit cell and a calculated density of 1.687 g cm^{-3} at 173 K. The cobalt(III) center is octahedrally coordinated by three 5-DTP molecules. Due to heavy disorder, the structure could not be refined anisotropically.

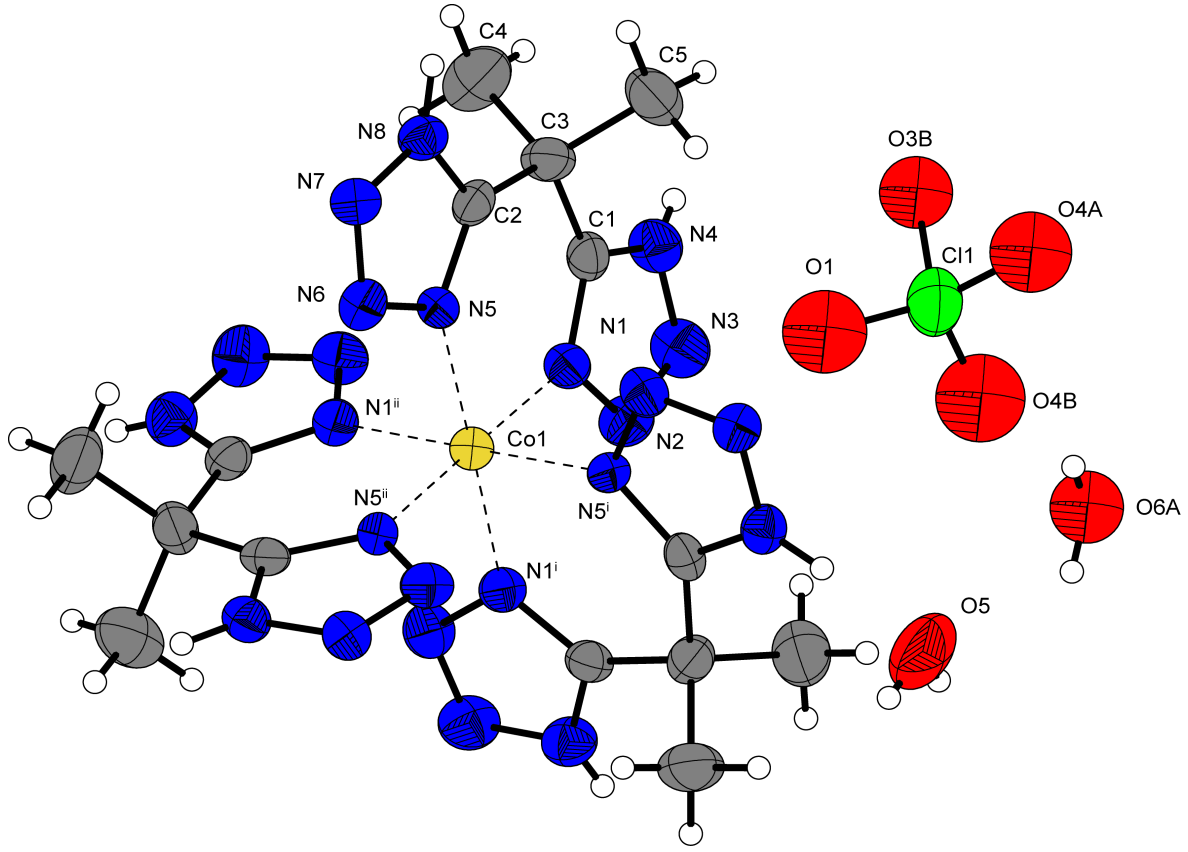


Figure S6. Isotropic illustration of the coordination environment of $[Co(5\text{-DTP})_3](ClO_4)_3 \bullet H_2O$ (**11**). Selected bond length (Å): Co1–N1 1.920(7), Co1–N5 1.904(3), Cl1–O1 1.366(10), Cl1–O3B 1.42(2); selected bond angles (°): N1–Co1–$N5^{i}$ 86.55(19), $N5^{i}$–Co1–$N5^{ii}$ 93.49(13), $N5^{ii}$–Co1–$N1^{ii}$ 87.8(2), $N1^{ii}$–Co1–N1 91.1(3), N1–Co1-$N5^{ii}$ 187.6(2), $N5^{i}$–Co1–$N1^{ii}$ 178.6(3), N5–Co1–$N1^{i}$ 178.6(2), O1–Co1–O4B 105.1(10), O3B–Co1–O4A (89.6(17). Symmetry codes: (i) −y, x −y, z; (ii) −x+y, −x, z.

$[Cu(HSO_4)_2(5\text{-DTP})_2]$ (**16**) crystallizes in the triclinic space group *P*−1 in form of blue plates. The calculated density of 1.857 g mL^{-3} at 123 K varies only slightly from the copper(II) sulfate complex **15** (1.776 g mL^{-3}, 133 K). The hydrogen sulfate complex consists of a closed octahedral coordination sphere with two molecules of 5-DTP and two coordinating hydrogen sulfato ligands, in contrast to **15** which shows no coordinating anions. Whereas both complexes are coordinated bidentately by two molecules of 5-DTP, the sulfate derivative possesses an additional aqua ligand and one molecule of crystal water, leading to a square pyramidal coordination polyhedron. A Jahn-Teller distortion is observed for the complex along the axial positions.

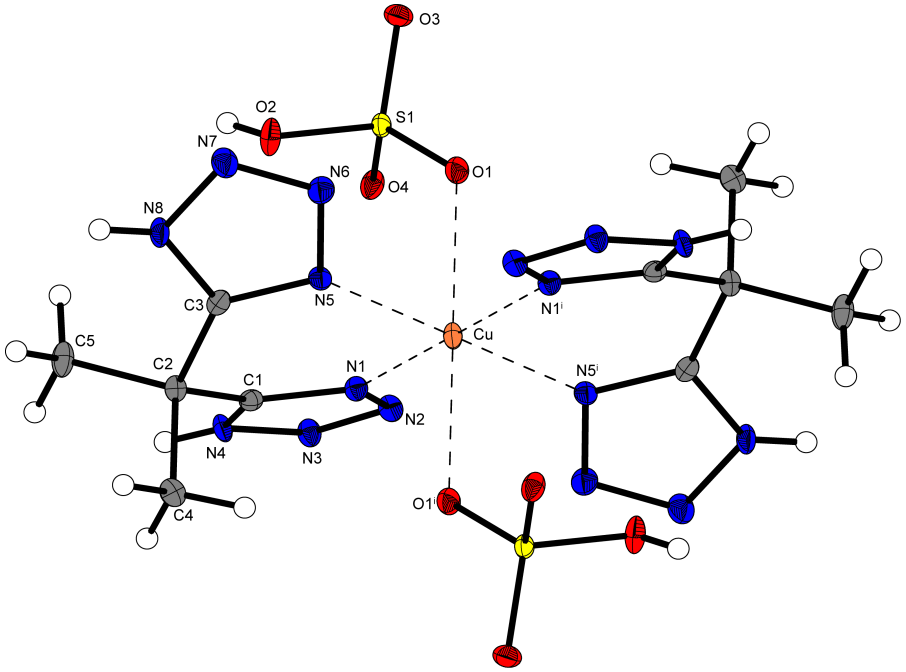


Figure S7. Molecular unit of $[Cu(HSO_4)_2(5\text{-DTP})_2]$ (**16**). Selected bond length (Å): Cu1–N1 2.003(2), Cu1–N5 1.989(2), Cu1–O1 2.4720(19), S1–O1 1.439(2), S1–O4 1.471(2), S1–O2 1.560(2); selected bond angles (°): N1–Cu1–N5 85.51(9), N5–Cu1–$N1^{i}$ 94.47(9), $N1^{i}$–Cu1–$N5^{i}$ 85.54(9), $N5^{i}$–Cu1–N1 94.47(9), $N5^{i}$–Cu1–$O1^{i}$ 84.89(8), $N1^{a}$–Cu1–O1 93.86(7), O1–Cu1–$O1^{i}$ 180.00, N1–Cu1–$N1^{i}$ 180.00, N5–Cu1–$N5^{i}$ 180.00. Symmetry code: (i) −x, −y, −z.

19.6.4 DTA Plots of 1–15

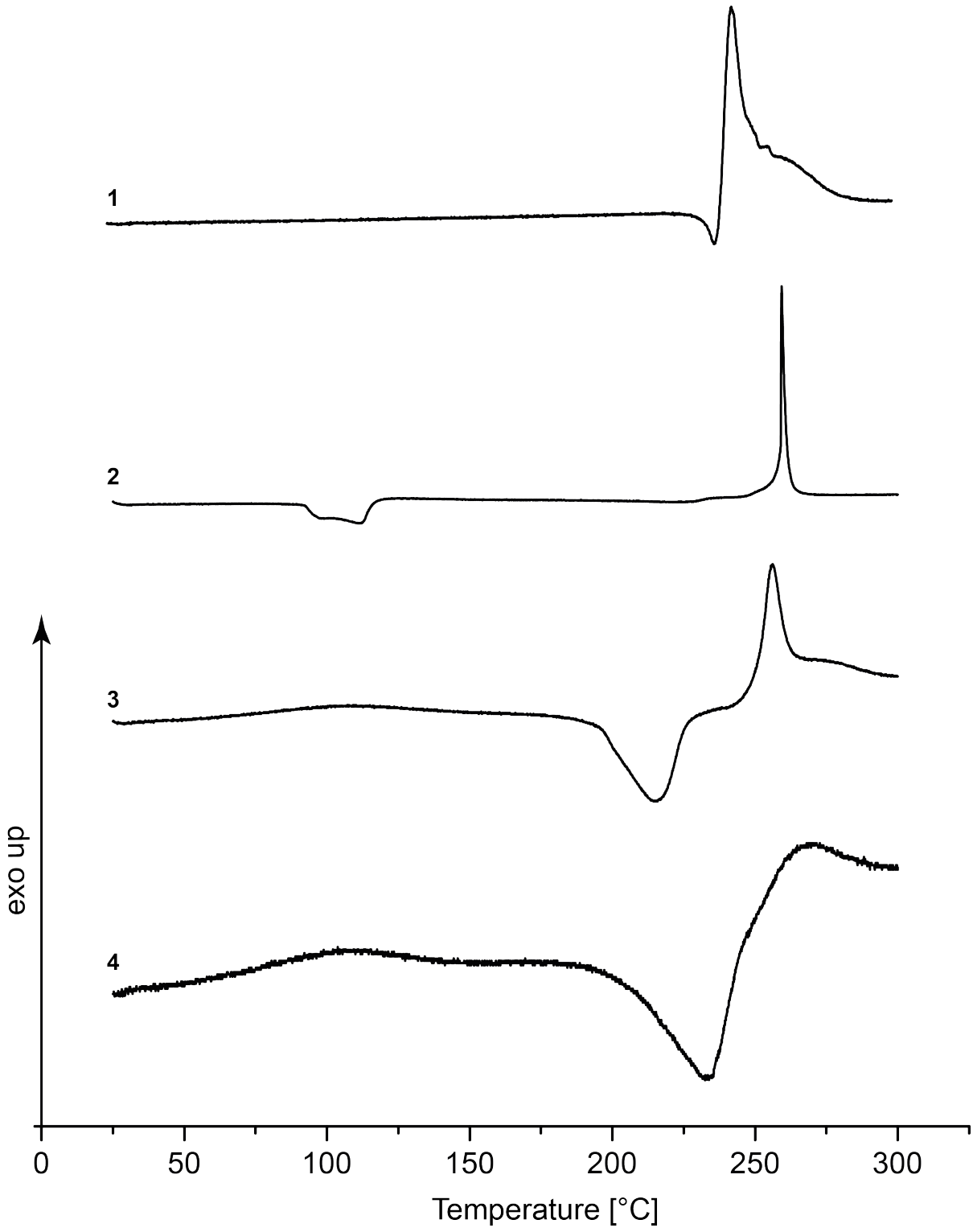


Figure S8. DTA plots (5 °C min^{-1}) of ligand (**1**) and chloride complexes **2**–**4** in the range of 25–300 °C.

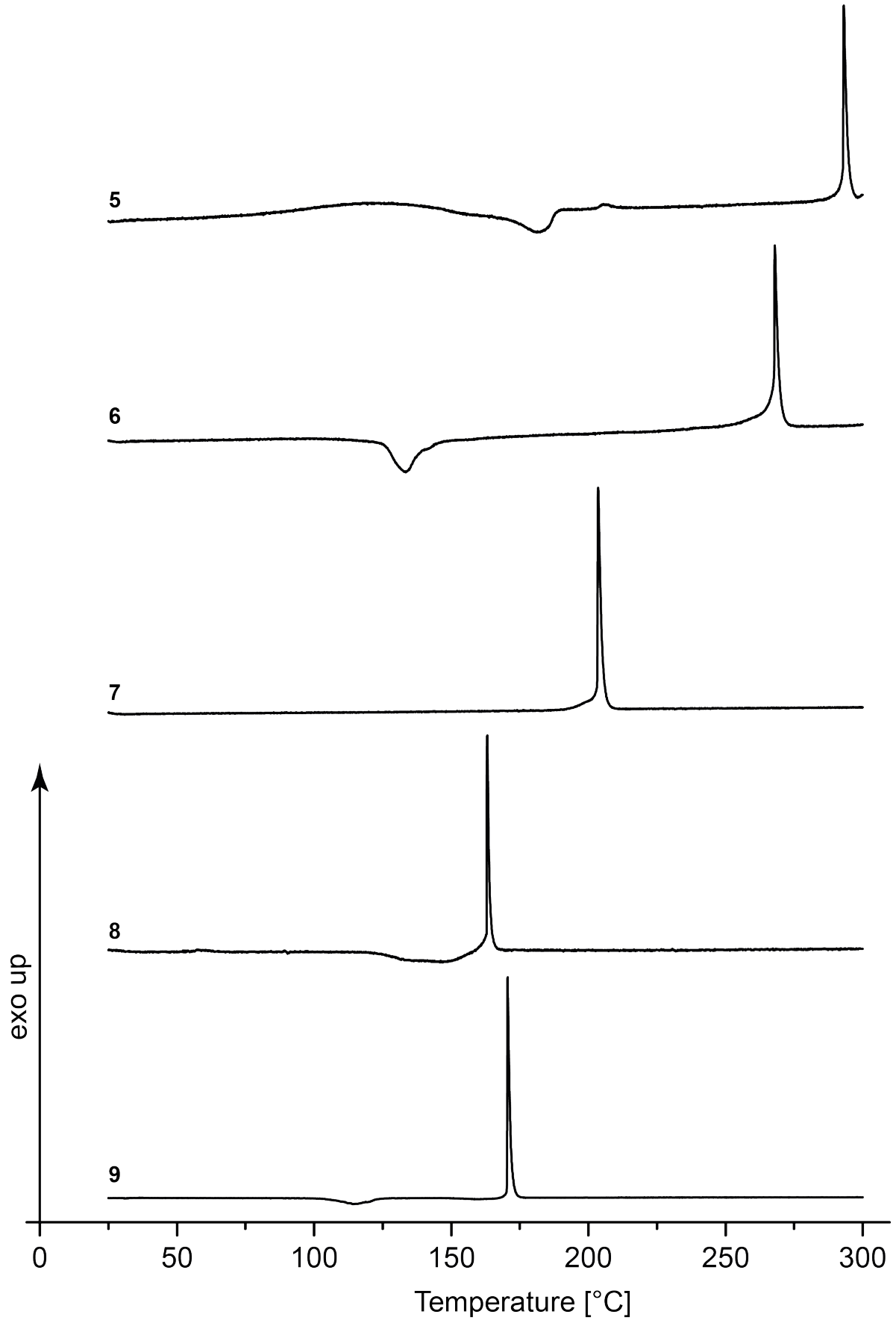


Figure S9. DTA plots (5 °C min^{-1}) of the nitrate complexes **5**–**9** in the range of 25–300 °C.

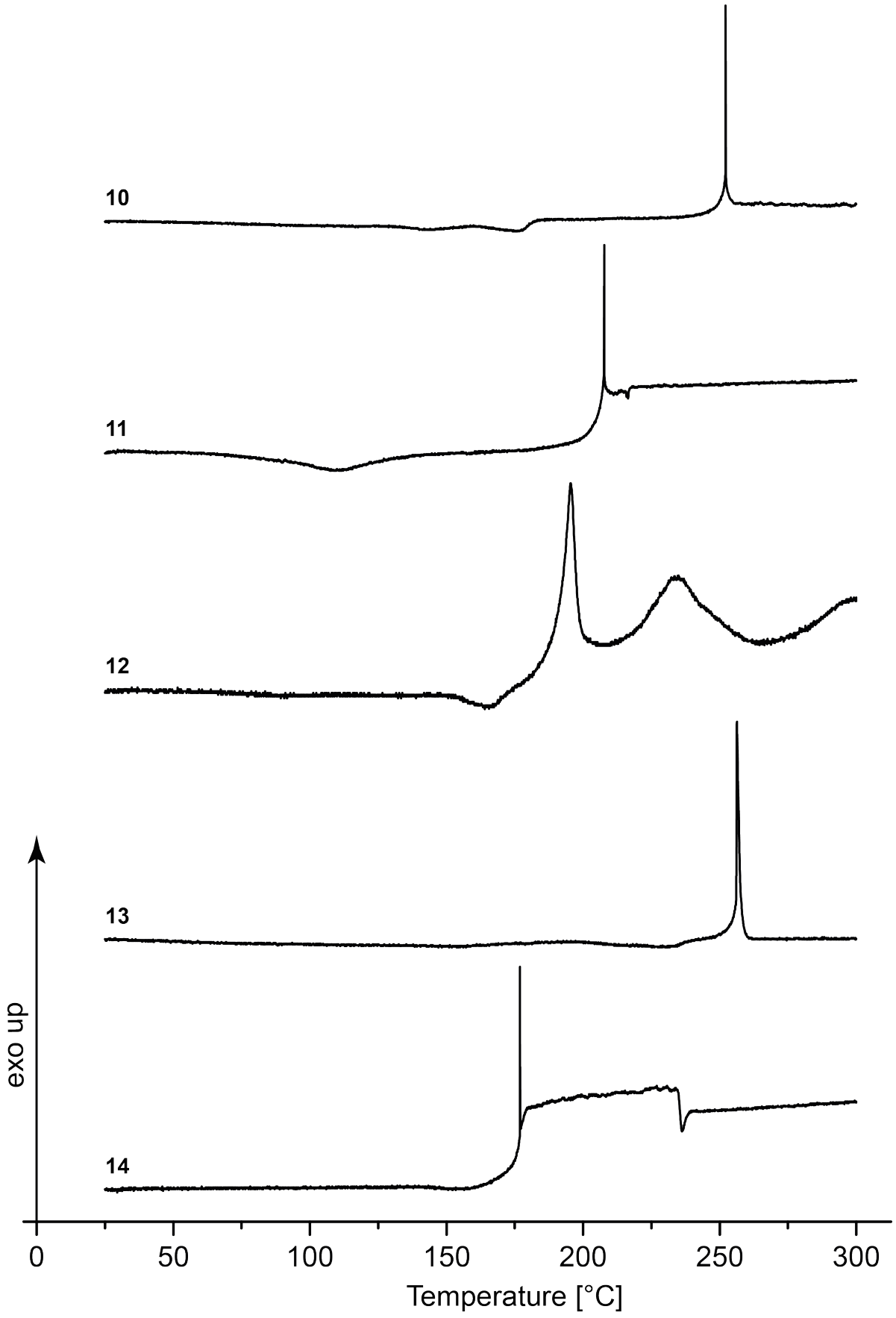


Figure S10. DTA plots (5 °C min^{-1}) of the perchlorate complexes **10**–**14** in the range of 25–300 °C.

19.6.5 Hot Plate and Hot Needle Tests

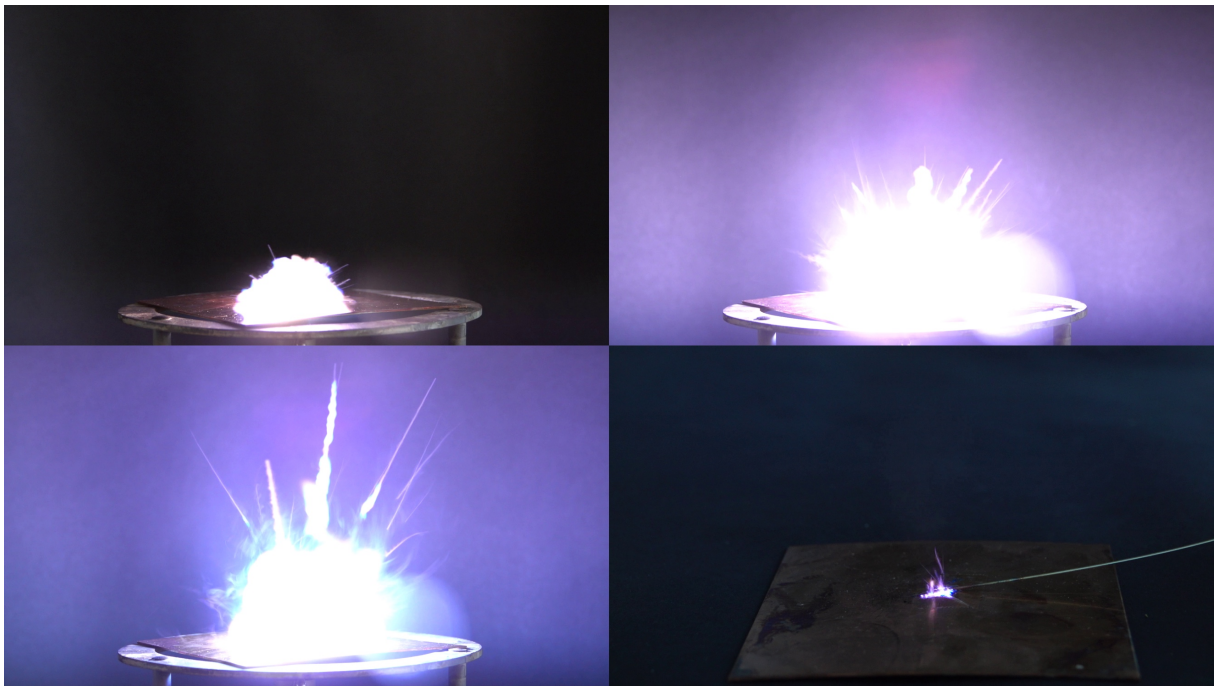


Figure S11. Deflagrations of **10** during the hot needle and hot plate tests, shown as a sequence.

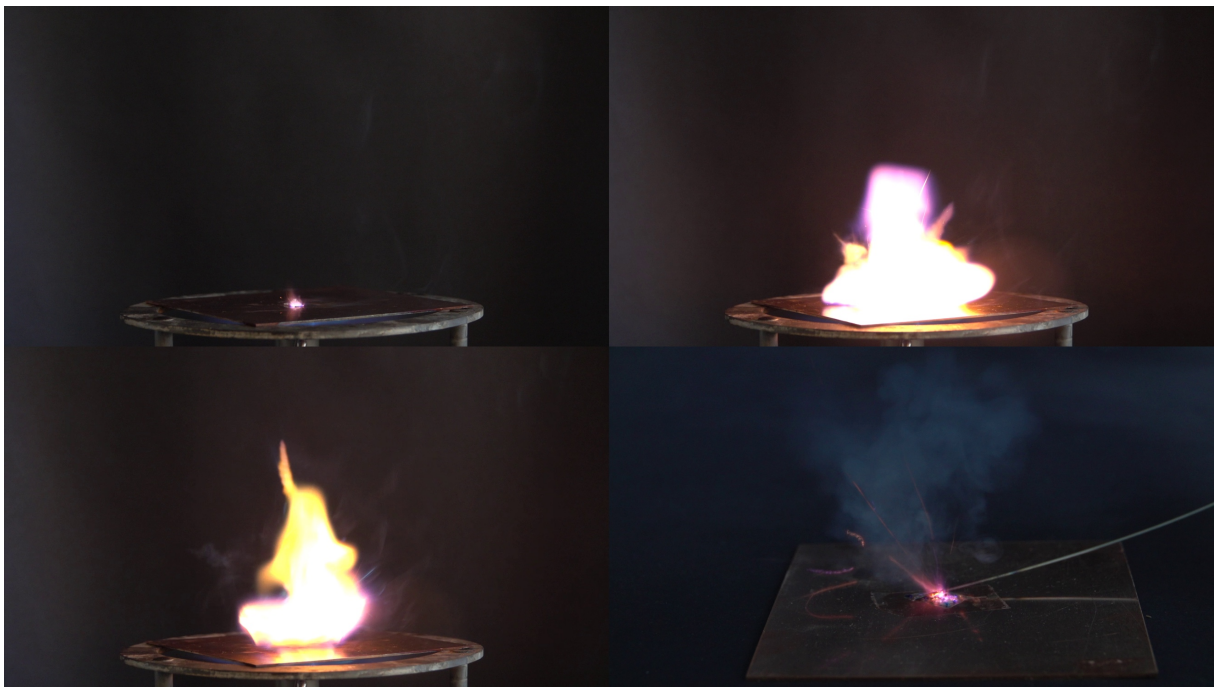


Figure S12. Hot plate test shown as a sequence and hot needle test of complex compound **13**.

19.6.6 UV-Vis Spectra of 10, 13 and 14

In order to correlate the absorption behavior of the complexes in the UV-Vis-NIR region with the laser ignitibility, diluted solutions of perchloric acid (15 %, 10 mM) of **10**, **13**, and **14** were investigated by UV-VIS-NIR spectroscopy (Figure S13). If a correlation between laser ignitability and absorption would be observed, laser ignitable explosive complexes could more easily be designed in the future.

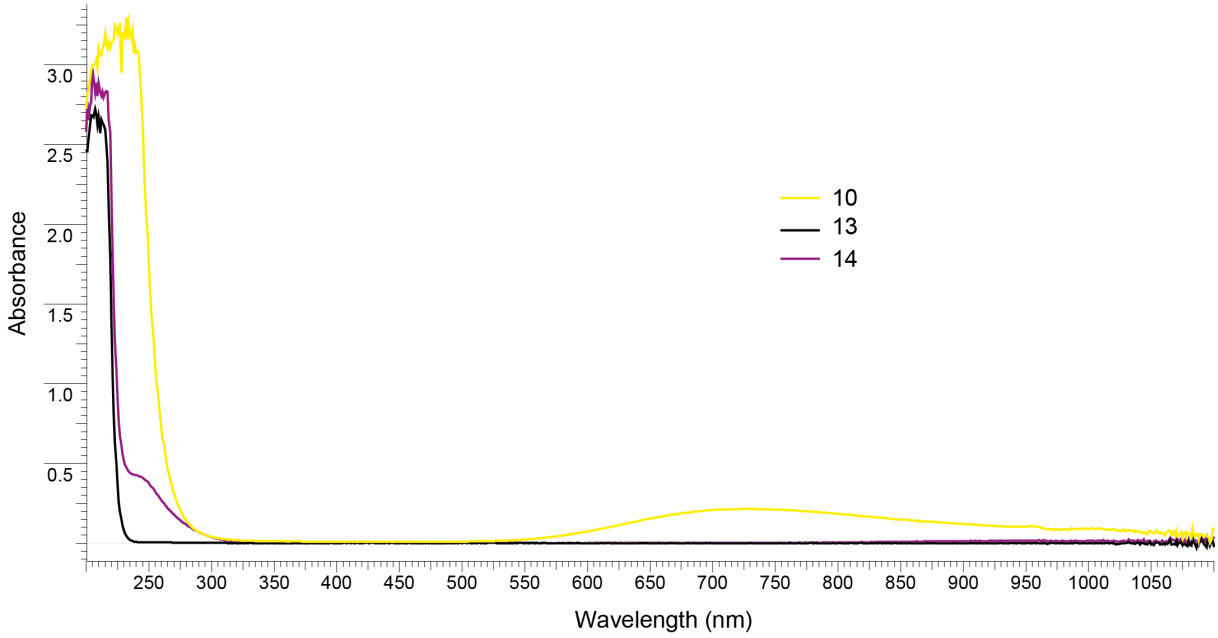


Figure S13. UV-VIS-NIR spectra of **10**, **13** and **14** in 10 mM solutions.

All measured compounds showed absorptions in the UV-region, caused by charge-transfer transitions between the metal(II) and the ligand. As expected, characteristic d-d transitions of copper are observable as broad signal in the range of 520–1100 nm for the copper(II) complex **10**. The maximum lies between the visible and near infrared region of the electromagnetic spectrum at a wavelength of 728 nm. The compounds **10** and **14** were ignitable by laser irradiation at a wavelength of 915 nm, but only **10** absorbs light at 915 nm. Furthermore, no other similarities between these compounds, which could be a reason for ignitibility by laser irradiation, are observable in the UV-Vis-NIR spectra, so light absorption is not a cause for laser ignitibility. The same conclusions were published in recent years.

19.6.7 Experimental Part and General Methods

All chemicals and solvents were employed as received (Sigma-Aldrich, Fluka, Acros, ABCR). ^{1}H and ^{13}C spectra were recorded at ambient temperature using a JEOL Bruker 400, Eclipse 270, JEOL EX 400 or a JEOL Eclipse 400 instrument. The chemical shifts quoted in ppm in the text refer to typical standards such as tetramethylsilane (^{1}H, ^{13}C) in d_6-DMSO as the solvent. Endothermic and exothermic events of the described compounds, which indicate melting, evaporation or decomposition, are given as the extrapolated onset temperatures. The samples were measured in a range of 25–400 °C at a heating rate of 5 °C min^{-1} through differential thermal analysis (DTA) with an OZM Research DTA 552-Ex instrument. Infrared spectra were measured with pure samples on a Perkin-Elmer BXII FT-IR system with a Smith DuraSampler IR II diamond ATR. Determination of the carbon, hydrogen and nitrogen contents were carried out by combustion analysis using an Elementar Vario El (nitrogen values determined are often lower than the calculated ones' due to their explosive behavior). UV-Vis spectra were recorded using an Agilent Cary 60 UV-Vis spectrometer with Peltier Element or a Cary300 Dual Beam UV Vis spectrometer with Peltier element in the wavelength range of 200–1100 nm. Impact sensitivity tests were carried out according to STANAG 4489[S9] with a modified instruction[S10] using a BAM (Bundesanstalt für Materialforschung) drop hammer.[S11,12] Friction sensitivity tests were carried out according to STANAG 4487[S13] with a modified instruction[S14] using the BAM friction tester. The classification of the tested compounds results from the "UN Recommendations on the Transport of Dangerous Goods".[S15] Additionally all compounds were tested upon the sensitivity toward electrical discharge using the OZM Electric Spark Tester ESD 2010 EN or OZM Electric Spark XSpark10 device.[S11] Hot plate and hot needle tests were performed in order to classify the initiation capability of selected complexes. The samples were fixed on a copper plate underneath adhesive tape and initiated by a red hot needle. Strong deflagration or detonation of the compound usually indicates a valuable primary explosive. The safe and straightforward hot plate test shows only the behavior of the unconfined sample toward fast heating on a copper plate. It does not necessarily allow any conclusions on a compound´s capability as a suitable primary explosive. The laser initiation experiments were performed with a 45 W InGaAs laser diode operating in the single-pulsed mode. The diode is attached to an optical fiber with a core diameter of 400 µm and a cladding diameter of 480 µm. The optical fiber is connected via a SMA type connecter directly to the laser and to a collimator. This collimator is coupled to an optical lens, which was positioned in its focal distance (f = 29.9 mm) to the sample. The lens is shielded from the explosive by a sapphire glass.

Approximately 15 mg of the carefully pestled compound to be investigated was filled into a transparent plastic cap (PC), pressed with a pressure force of 1 kN and sealed by a UV-curing adhesive. The confined samples were irradiated at a wavelength of 915 nm, a voltage of 4 V, a current of 7 A and pulse lengths of 0.1 ms. The combined currents and pulse lengths result in an energy output of about 0.17 mJ.

The obtained coordination compounds were washed with cold ethanol when stated, dried overnight in air and used for analytics without further purification.

CAUTION! *All investigated compounds are potentially explosive energetic materials (the majority of the compounds lie in the range of primary explosives), which show partly increased sensitivities toward various stimuli (e.g. elevated temperatures, impact, friction or electrostatic discharge). Therefore, proper security precautions (safety glass, face shield, earthed equipment and shoes, leather coat, Kevlar gloves, Kevlar sleeves and ear plugs) have to be applied while synthesizing and handling the described compounds. Due to their sensitivity toward mechanical stimuli, especially compounds **11**, **13** and **14** have to be handled with enhanced care.*

2,2-Bis(5-tetrazolyl)propane (1):

2,2-Bis(5-tetrazolyl)propane (**1**, 5-DTP) was synthesized according to a procedure published by Z. P. Demko and K. B. Sharpless:[S16] to a solution of dimethylmalononitrile (2.59 g, 26.0 mmol) in water (65 mL) and isopropanol (7 mL), sodium azide (3.78 g, 58.0 mmol) and zinc(II) bromide (11.9 g, 53.0 mmol) were added. The reaction mixture was stirred at 110 °C for 24 h. After cooling down to room temperature, the resulting suspension was dissolved in 2 m hydrochloric acid (60 mL). The solution was extracted with ethyl acetate (3 x 300 mL), the combined organic layers dried over magnesium sulfate and the solution was concentrated. The crude product was recrystallized from water and dried under high vacuum for 3 h. The product was obtained in the form of colorless crystals suitable for X-ray determination. Yield: 2.60 g (14.0 mmol, 55 %).

DTA (5 °C min^{-1}): 235 °C (endothermic, followed by exothermic signal); IR (ATR, cm^{-1}): $\tilde{\nu}$ = 3109 (w), 2993 (m), 2820 (m), 2756 (m), 2696 (s), 2602 (s), 2541 (m), 2494 (m), 2447 (m), 1861 (m), 1564 (w), 1554 (s), 1545 (m), 1474 (m), 1451 (w), 1415 (s), 1383 (m), 1370 (m), 1257 (m), 1181 (s), 1091 (m), 1040 (vs), 1019 (s), 999 (vs), 948 (s), 927 (s), 768 (w), 727 (w),

703 (m), 559 (w), 508 (m); ^{1}H NMR (DMSO-d_6, 25 °C, ppm) δ: 1.88 (s, 6H, C(CH_3)$_2$); ^{13}C NMR (DMSO-d_6, 25 °C, ppm) δ: 161.2 (CN$_4$), 33.5 (C(CH$_3$)$_2$), 27.0 (C(CH$_3$)$_2$); EA ($C_5H_8N_8$, 180.18) calcd.: C 33.33, H 4.48, N 62.19 %; found: C 33.37, H 4.37, N 61.93 %; BAM drop hammer: 30 J; friction tester: > 360 N; ESD: 1.50 J (at grain size 100–500 µm).

General procedure for the preparation of metal(II) (5-DTP) chloride complexes (2–4):

5-DTP (**2**: 180 mg, 1.00 mmol; **3**, **4**: 145 mg, 0.80 mmol) was dissolved in diluted hydrochloric acid (15 %, 3 mL) under stirring at 80 °C. A solution of the corresponding metal(II) chloride (**2**: copper(II) chloride dihydrate (85.2 mg, 0.50 mmol); **3**: cobalt(II) chloride hexahydrate (95.2 mg, 0.40 mmol); **4**: nickel(II) chloride hexahydrate (95.1 mg, 0.40 mmol)) in diluted hydrochloric acid (15 %, 1.0 mL) was added. The colored reaction mixtures were stirred for 1 min and were left to crystallize at room temperature.

{[CuCl(5-DTP)$_2$]Cl}$_2$ • 7 H$_2$O (2)

Complex **2** was obtained within two weeks in the form of blue crystals suitable for X-ray determination. Yield: 110 mg (0.15 mmol, 58 %).

DTA (5 °C min^{-1}): 92 °C (endothermic), 259 °C (exothermic); IR (ATR, cm^{-1}): $\tilde{\nu}$= 3372 (m), 2850 (m), 2695 (m), 2611 (s), 2548 (m), 1984 (m), 1624 (m), 1556 (m), 1472 (m), 1451 (m), 1409 (m), 1397 (w), 1375 (w), 1279 (m), 1202 (s), 1056 (vs), 1019 (s), 1007 (s), 956 (s), 911 (m), 856 (m), 777 (m), 767 (m), 734 (m), 575 (s); EA ($C_{20}H_{46}Cl_4Cu_2N_{32}O_7$, 1115.70) calcd.: C 21.53, H 4.16, N 40.17 %; found: C 22.09, H 4.16, N 40.75 %. BAM drophammer: > 40 J; friction tester: > 360 N; ESD: 1.50 J (at grain size 100–500 µm).

[Co(H$_2$O)$_2$(5-DTP)$_2$]Cl$_2$ (3)

Coordination compound **3** was obtained within two days in the form of small orange crystals suitable for X-ray determination. Yield: 77.5 mg (0.15 mmol, 37 %).

DTA (5 °C min^{-1}): 194 °C (endothermic), 253 °C (exothermic); IR (ATR, cm^{-1}): $\tilde{\nu}$ = 3538 (m), 3321 (m), 2980 (m), 2849 (m), 2812 (m), 2799 (m), 2769 (s), 2752 (s), 2734 (s), 2683 (m), 2665 (s), 2612 (s), 2536 (m), 2525 (m), 2426 (m), 1651 (m), 1607 (m), 1562 (s), 1554 (s), 1534 (m), 1526 (m), 1468 (m), 1441 (m), 1411 (w), 1397 (w), 1381 (m), 1277 (m), 1274 (m), 1191 (s), 1057 (vs), 1015 (m), 831 (s), 784 (w), 766 (m); EA ($C_{10}H_{20}Cl_2CoN_{16}O_2$, 526.21) calcd.: C 22.83, H 3.83, N 42.39 %; found: C 23.02, H 3.77, N 42.39 %. BAM drophammer: > 40 J; friction tester: > 360 N; ESD: 1.50 J (at grain size 500–1000 µm).

$[Ni(H_2O)_2(5\text{-DTP})_2]Cl_2$ (4)

Compound **4** was obtained within three days in the form of purple single crystals, which were suitable for X-ray determination. Yield: 138 mg (0.26 mmol, 66 %).

DTA (5 °C min^{-1}): 207 °C (endothermic, followed by exothermic signal); IR (ATR, cm^{-1}): $\tilde{\nu}$ = 3339 (w), 3008 (w), 2992 (w), 2915 (m), 2872 (m), 2820 (m), 2776 (m), 2686 (m), 2667 (m), 2636 (w), 2615 (m), 1633 (m), 1562 (m), 1553 (m), 1395 (w), 1280 (m), 1193 (m), 1077 (m), 1059 (vs), 1016 (m), 1007 (m), 950 (w), 825 (s), 782 (m), 767 (m), 724 (m), 710 (m), 672 (m), 609 (s); EA ($C_{10}H_{20}Cl_2N_{16}NiO_2$, 525.97) calcd.: C 22.84, H 3.83, N 42.61 %; found: C 22.89, H 3.81, N 42.43 %. BAM drophammer: > 40 J; friction tester: > 360 N; ESD: 1.50 J (at grain size 500–1000 µm).

General procedure for the preparation of metal(II/III) (5-DTP) nitrate complexes (5–9):

To a boiling solution of 5-DTP (**5**: 145 mg, 0.80 mmol; **6**: 162 mg, 0.90 mmol; **7**, **9**: 108 mg, 0.60 mmol; **8**: 135 mg, 0.75 mmol) in diluted nitric acid (15 %, 3 mL) a solution of the corresponding metal(II) nitrate (**5**: copper(II) nitrate trihydrate (96.6 mg, 0.40 mmol); **6**: cobalt(II) nitrate hexahydrate (87.3 mg, 0.30 mmol); **7**: zinc(II) nitrate hexahydrate (89.2 mg, 0.30 mmol); **8**: nickel(II) nitrate hexahydrate (72.7 mg, 0.25 mmol); **9**: nickel(II) nitrate hexahydrate (87.2 mg, 0.30 mmol)) in diluted nitric acid (15 %, 1 mL) was added under stirring. After 1 min the reaction mixtures were cooled down to room temperature and subsequently left to crystallize.

$[Cu(H_2O)(5\text{-}DTP)_2](NO_3)_2$ (5)

Product **5** was obtained within one day in the form of blue crystals suitable for X-ray determination. Yield: 132 mg (0.23 mmol, 58 %).

DTA (5 °C min^{-1}): 172 °C (endothermic), 293 °C (exothermic); IR (ATR, cm^{-1}): $\tilde{\nu}$= 3499 (w), 3361 (w), 3126 (w), 2982 (w), 2872 (w), 2800 (m), 2611 (m), 2548 (m), 1626 (w), 1558 (s), 1542 (m), 1473 (m), 1443 (m), 1408 (m), 1384 (m), 1310 (vs), 1285 (s), 1195 (m), 1095 (w), 1071 (s), 1055 (s), 1044 (s), 1030 (m), 1005 (s), 954 (m), 916 (m), 889 (m), 816 (m), 771 (w), 742 (w), 720 (m); EA ($C_{10}H_{18}CuN_{18}O_7$, 565.92) calcd.: C 21.22, H 3.21, N 44.55 %; found: C 21.41, H 3.16, N 44.39 %. BAM drophammer: 8 J; friction tester: 360 N; ESD: 1.50 J (at grain size 100–500 µm).

$[Co(5\text{-}DTP)_3](NO_3)_3 \bullet 3\ H_2O$ (6)

Complex **6** was obtained within two days in the form of X-ray suitable small orange single crystals. Yield: 132 mg (0.16 mmol, 52 %).

DTA (5 °C min^{-1}): 125 °C (endothermic), 267 °C (exothermic); IR (ATR, cm^{-1}): $\tilde{\nu}$= 3365 (w), 2896 (w), 2757 (w), 2699 (w), 2449 (m), 2355 (m), 1893 (w), 1573 (m), 1476 (w), 1433 (m), 1416 (m), 1384 (m), 1302 (vs), 1195 (s), 1099 (w), 1078 (w), 1050 (s), 1004 (s), 901 (m), 860 (m), 823 (m), 774 (w), 765 (w), 721 (w); EA ($C_{15}H_{30}CoN_{27}O_{12}$, 839.52) calcd.: C 21.46, H 3.60, N 45.05 %; found: C 21.66, H 3.56, N 45.02 %. BAM drophammer: 10 J; friction tester: > 360 N; ESD: 1.50 J (at grain size 100–500 µm).

$[Ni(5\text{-}DTP)_3](NO_3)_2 \bullet 2{,}5\ H_2O$ (7)

Compound **7** was obtained within two weeks in the form of purple crystals suitable for X-ray determination. Yield: 113 mg (0.15 mmol, 59 %).

DTA (5 °C min^{-1}): 203 °C (exothermic); IR (ATR, cm^{-1}): $\tilde{\nu}$= 3131 (w), 3046 (m), 2984 (m), 2934 (m), 2882 (m), 2797 (m), 2628 (w), 1558 (m), 1466 (m), 1431 (m), 1403 (m), 1378 (m), 1306 (vs), 1279 (s), 1187 (s), 1088 (w), 1049 (vs), 1014 (s), 1002 (s), 945 (w), 911 (m), 871 (m), 820 (m), 773 (m), 762 (m), 715 (m); EA ($C_{30}H_{58}N_{52}Ni_2O_{17}$, 1536.54) calcd.: C 23.45, H

3.80, N 47.40 %; found: C 23.55, H 3.50, N 47.79 %. BAM drophammer: 5 J; friction tester: 324 N; ESD: 1.50 J (at grain size 500–1000 µm).

$[Ni(H_2O)_2(5\text{-DTP})_2](NO_3)_2 \bullet H_2O$ (8)

Complex **8** was obtained within four weeks in the form of purple crystals suitable for X-ray determination. Yield: 102 mg (0.16 mmol, 54 %).

DTA (5 °C min^{-1}): 126 °C (endothermic), 163 °C (exothermic); IR (ATR, cm^{-1}): $\tilde{\nu}$= 3503 (w), 3140 (w), 2627 (w), 2170 (m), 1644 (w), 1563 (m), 1473 (w), 1429 (m), 1416 (m), 1380 (s), 1323 (vs), 1277 (s), 1199 (m), 1185 (m), 1060 (s), 1049 (s), 1015 (m), 820 (m), 775 (m), 611 (m), 452 (m); EA ($C_{10}H_{22}N_{18}NiO_9$, 565.92) calcd.: C 20.12, H 3.71, N 42.23 %; found: C 20.17, H 3.61, N 41.82 %. BAM drophammer: 10 J; friction tester: 360 N; ESD: 0.15 J (at grain size 100–500 µm).

$[Zn(H_2O)_2(5\text{-DTP})_2](NO_3)_2 \bullet 2\ H_2O$ (9)

Complex **9** was obtained within two weeks in the form of colorless hexagonal crystals suitable for X-ray determination. Yield: 80.0 mg (0.13 mmol, 43 %).

DTA (5 °C min^{-1}): 107 °C (endothermic), 170 °C (exothermic); IR (ATR, cm^{-1}): $\tilde{\nu}$= 2736 (w), 2615 (w), 2172 (m), 2163 (m), 1638 (w), 1560 (m), 1474 (w), 1430 (m), 1414 (m), 1380 (s), 1321 (vs), 1275 (s), 1199 (m), 1183 (m), 1057 (s), 1047 (s), 1015 (m), 820 (m), 775 (m), 738 (m), 583 (m); EA ($C_{10}H_{22}N_{18}O_9Zn$, 565.92) calcd.: C 19.89, H 3.67, N 41.76 %; found: C 20.13, H 3.63, N 41.87 %. BAM drophammer: 40 J; friction tester: > 360 N; ESD: 200 mJ (at grain size 100–500 µm).

General procedure for the preparation of metal(II/III) (5-DTP) perchlorate complexes (10–14):

A solution of the corresponding metal(II) perchlorate (**10**: copper(II) perchlorate hexahydrate (111 mg, 0.30 mmol); **11**: cobalt(II) perchlorate hexahydrate (91.5 mg, 0.25 mmol); **12**:

nickel(II) perchlorate hexahydrate (91.4 mg, 0.25 mmol) **13**: zinc(II) perchlorate hexahydrate (112 mg, 0.30 mmol); **14**: iron(II) perchlorate hexahydrate (90.7 mg, 0.25 mmol)) in diluted perchloric acid (15 %, 1 mL) was mixed with a boiling solution of 5-DTP (**1**, (**10**, **12**: 108 mg, 0.60 mmol; **11**, **13**, **14**: 135 mg, 0.75 mmol)) in diluted perchloric acid (15 %, 3 mL). The mixtures were stirred for 1 min at 80 °C and the solutions were left to crystallize after cooling down to room temperature.

$[Cu(H_2O)(5\text{-}DTP)_2](ClO_4)_2 \cdot H_2O$ (10)

Compound **10** was obtained within three weeks in the form of blue crystals suitable for X-ray determination. Yield: 161 mg (0.25 mmol, 82 %).

DTA (5 °C min^{-1}): 138 °C (endothermic), 168 °C (endothermic), 251 °C (exothermic); IR (ATR, cm^{-1}): $\tilde{\nu}$ = 3462 (w), 3130 (w), 3048 (w), 2921 (w), 2843 (w), 1623 (w), 1555 (m), 1476 (w), 1455 (w), 1378 (w), 1299 (w), 1275 (w), 1198 (w), 1096 (s), 1083 (s), 1043 (vs), 1018 (s), 1005 (s), 953 (m), 930 (m), 908 (m), 804 (m), 764 (m), 739 (m), 699 (m), 664 (w), 619 (vs), 575 (m), 508 (m); UV-Vis spectrum: λ_{max} = 232 nm, 729 nm; EA ($C_{10}H_{20}Cl_2CuN_{16}O_8$, 658.82) calcd.: C 18.23, H 3.06, N 34.02 %; found: C 17.53, H 2.98, N 32.33 %. BAM drop hammer: 3 J; friction tester: 10 N; ESD: 65 mJ (at grain size 500–1000 µm).

$[Co(5\text{-}DTP)_3](ClO_4)_3 \cdot 6\ H_2O$ (11)

Coordination compound **11** was obtained within two weeks in the form of small orange crystals suitable for X-ray determination. Yield: 172 mg (0.17 mmol, 68 %).

DTA (5 °C min^{-1}): 88 °C (endothermic), 206 °C (exothermic); IR (ATR, cm^{-1}): $\tilde{\nu}$ = 3487 (m), 2506 (m), 2172 (m), 2163 (m), 1627 (w), 1575 (m), 1476 (w), 1433 (w), 1415 (w), 1311 (w), 1197 (w), 1088 (s), 1071 (vs), 1052 (vs), 1014 (s), 1000 (s), 948 (s), 931 (s), 903 (s), 776 (m), 763 (m), 750 (m), 623 (s), 504 (s); EA ($C_{15}H_{36}Cl_3CoN_{24}O_{18}$, 1005.89) calcd.: C 17.91, H 3.61, N 33.42 %; found: C 17.36, H 3.67, N 32.06 %. BAM drop hammer: 12.5 J; friction tester: 72 N; ESD: 500 mJ (at grain size 500–1000 µm).

$[Ni(H_2O)_2(5\text{-DTP})_2](ClO_4)_2 \bullet 3\ H_2O$ (12)

Complex **12** was obtained within three weeks in the form of purple single crystals, which were suitable for X-ray determination. Yield: 95.8 mg (0.14 mmol, 54 %).

DTA (5 °C min^{-1}): 159 °C (endothermic), 190 °C (exothermic); IR (ATR, cm^{-1}): $\tilde{\nu}$= 3158 (m), 3059 (m), 2935 (w), 2894 (w), 2822 (w), 1725 (w), 1630 (w), 1555 (m), 1474 (w), 1445 (w), 1414 (w), 1384 (w), 1280 (m), 1191 (m), 1083 (s), 1043 (vs), 1019 (vs), 1006 (s), 922 (m), 764 (m), 722 (m), 665 (m), 618 (vs), 585 (s); EA ($C_{10}H_{26}Cl_2N_{16}NiO_{13}$, 708.01) calcd.: C 16.95, H 3.76, N 31.65 %; found: C 17.20, H 3.58, N 31.68 %. BAM drop hammer: 20 J; friction tester: 216 N; ESD: 750 mJ (at grain size 500-1000 µm).

$[Zn(H_2O)(5\text{-DTP})_2](ClO_4)_2$ (13)

Product **13** was obtained within three weeks in the form of colorless hexagonal crystals suitable for X-ray determination. Yield: 98.4 mg (0.15 mmol, 51 %).

DTA (5 °C min^{-1}): 256 °C (exothermic); IR (ATR, cm^{-1}): $\tilde{\nu}$= 3364 (w), 3132 (m), 3061 (m), 2901 (m), 2834 (w), 2754 (w), 1621 (w), 1557 (m), 1478 (w), 1455 (w), 1444 (w), 1378 (m), 1288 (m), 1197 (m), 1088 (s), 1077 (s), 1040 (vs), 1019 (s), 1007 (s), 954 (m), 932 (s), 908 (m), 814 (m), 771 (m), 742 (m), 704 (m), 620 (vs), 571 (m); UV-Vis spectrum: λ_{max} = 207 nm; EA ($C_{10}H_{18}Cl_2N_{16}O_9Zn$, 642.64) calcd.: C 18.69, H 2.82, N 34.87 %; found: C 17.92, H 2.76, N 33.67 %. BAM drop hammer: 2 J; friction tester: 20 N; ESD: 200 mJ (at grain size < 100 µm).

$[Fe(5\text{-DTP})_3](ClO_4)_3 \bullet 6\ H_2O$ (14)

Product **14** was obtained within three weeks in the form of dark purple cubic crystals suitable for X-ray determination. Yield: 98.2 mg (0.10 mmol, 39 %).

DTA (5 °C min^{-1}): 145 °C (endothermic), 176 °C (exothermic); IR (ATR, cm^{-1}): $\tilde{\nu}$= 3158 (m), 3068 (m), 2945 (m), 2904 (w), 1562 (m), 1472 (w), 1383 (w), 1280 (m), 1192 (m), 1087 (vs), 1065 (s), 1040 (vs), 1014 (vs), 1001 (vs), 949 (m), 915 (s), 721 (m), 663 (m), 617 (vs); UV-Vis spectrum: λ_{max} = 205 nm, 237 nm; EA ($C_{15}H_{36}Cl_3FeN_{24}O_{18}$, 1002.80) calcd.: C 17.97, H 3.62,

N 33.52 %; found: C 17.79, H 3.50, N 32.90 %. BAM drop hammer: < 1 J; friction tester: 15 N; ESD: 100 mJ (at grain size 100–500 µm).

$[Cu(H_2O)(5\text{-DTP})_2]SO_4 \bullet H_2O$ (15)

A boiling solution of 5-DTP (**1**, 144 mg, 0.80 mmol) in diluted sulfuric acid (15 %, 3 mL) was added to a solution of copper(II) sulfate pentahydrate (99.9 mg, 0.40 mmol) in diluted sulfuric acid (15 %, 1 mL). After stirring for 1 min, the reaction mixture was left to crystallize. Diluted sulfuric acid (15 %, 10 mL) has been added to recrystallize the resulting precipitate, which appeared after one hour and the solution was left to crystallize again. Compound **15** was obtained within two weeks in the form of blue needles suitable for X-ray determination. Yield: 80.0 mg (0.14 mmol, 36 %).

DTA (5 °C min^{-1}): 162 °C (endothermic), 188 °C (endothermic), 225 °C (exothermic); IR (ATR, cm^{-1}): $\tilde{\nu}$ = 2442 (m), 1890 (m), 1632 (w), 1563 (m), 1482 (m), 1414 (m), 1396 (m), 1286 (m), 1278 (m), 1205 (m), 1105 (s), 1085 (s), 1065 (vs), 1045 (vs), 943 (vs), 904 (vs), 778 (s), 770 (s), 626 (s), 593 (s), 574 (vs); EA ($C_{10}H_{20}CuN_{16}O_6S$, 555.98) calcd.: C 21.60, H 3.63, N 40.31 %; found: C 21.26, H 3.38, N 38.36 %. BAM drop hammer: > 40 J; friction tester: > 360 N; ESD: 0.75 J (at grain size 100–500 µm).

19.6.8 References

[S1] *CrysAlisPro*, Oxford Diffraction Ltd., version 171.33.41, **2009**.

[S2] Altomare, A.; Cascarano, G.; Giacovazzo, C.; Guagliardi, A. *J. Appl. Crystallogr.* **1992**, *26*, 343.

[S3] a) Altomare, A.; Cascarano, G.; Giacovazzo, C.; Guagliardi, A.; Moliterni, A. G. G.; Burla, M. C.; Polidori, G.; Camalli, M.; Spagna, R. *SIR97*, **1997**; b) Altomare, A.; Burla, M. C.; Camalli, M.; Cascarano, G. L.; Giacovazzo, C.; Guagliardi, A.; Moliterni, A. G. G.; Polidori, G.; Spagna, R. *J. Appl. Crystallogr.* **1999**, *32*, 115.

[S4] a) Sheldrick, G. M. *SHELXL-97*, University of Göttingen, Germany, **1997**; b) Sheldrick, G. M. *Acta Crystallogr. Sect. A* **2008**, *64*, 112.

[S5] Spek, A. L. *PLATON*, Utrecht University, The Netherlands, **1999**.

[S6] Farrugia, L. J. *J. Appl. Cryst.* **2012**, *45*, 849.

[S7] Empirical absorption correction using spherical harmonics, implemented in SCALE3 ABSPACK scaling algorithm (CrysAlisPro Oxford Diffraction Ltd., Version 171.33.41, 2009).

[S8] *APEX3*. Bruker AXS Inc., Madison, Wisconsin, USA.

[S9] NATO standardization agreement (STANAG) on explosives, impact sensitivity tests, no. 4489, 1st ed., Sept. 17, 1999.

[S10] WIWEB-Standardarbeitsanweisung 4-5.1.02, Ermittlung der Explosionsgefährlichkeit, hier der Schlagempfindlichkeit mit dem Fallhammer, Nov. 8, 2002.

[S11] http://www.ozm.cz, Accessed April 2018.

[S12] http://www.bam.de, Accessed April 2018.

[S13] NATO standardization agreement (STANAG) on explosive, friction sensitivity tests, no. 4487, 1st ed., Aug. 22, 2002.

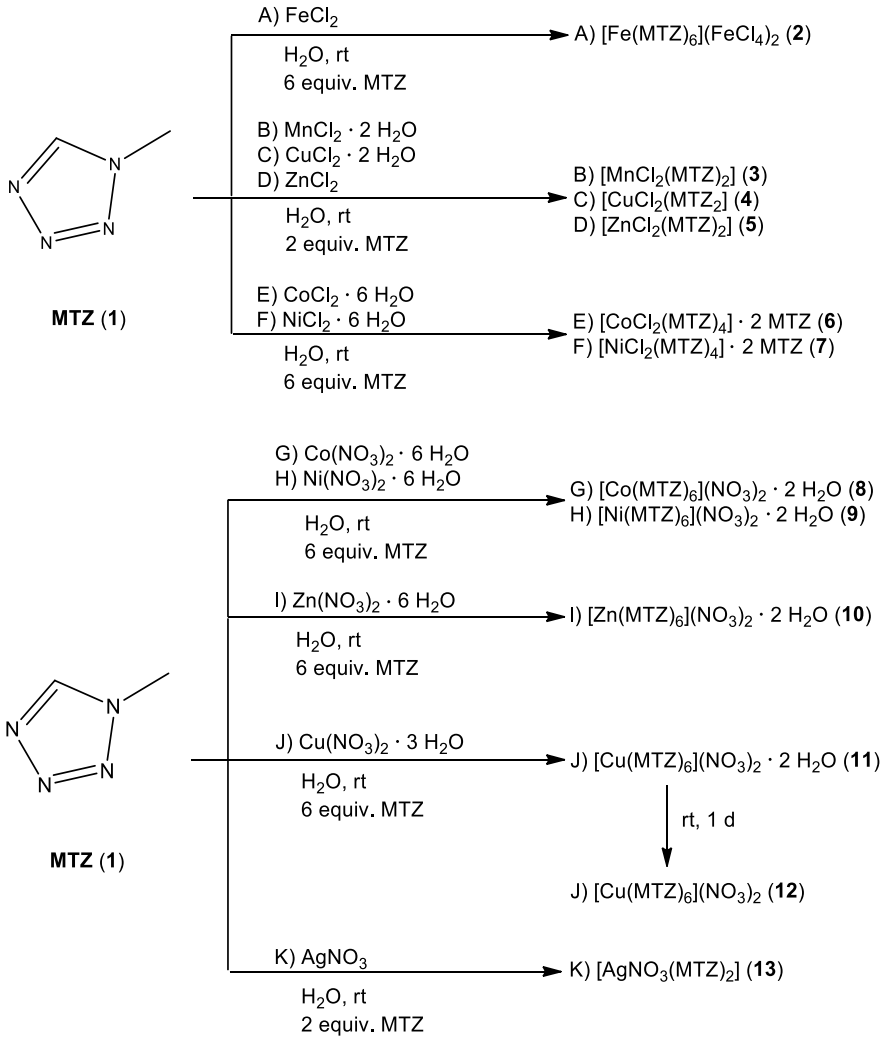
[S14] WIWEB-Standardarbeitsanweisung 4-5.1.03, Ermittlung der Explosionsgefährlichkeit oder der Reibeempfindlichkeit mit dem Reibeapparat, Nov. 8, 2002.

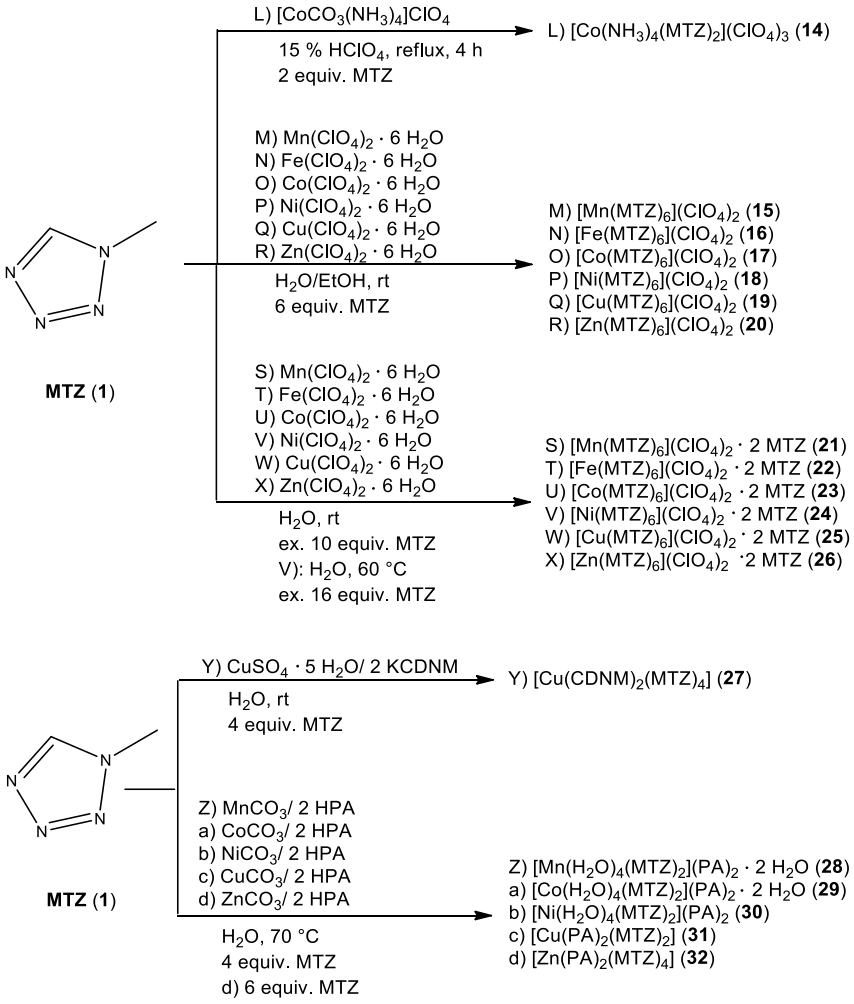
[S15] Impact: insensitive > 40 J, less sensitive ≥ 35 J, sensitive ≥ 4 J, very sensitive ≤ 3 J; Friction: insensitive > 360 N, less sensitive = 360 N, sensitive < 360 N and > 80 N, very sensitive ≤ 80 N, extremely sensitive ≤ 10 N. According to the UN Recommendations on the Transport of Dangerous Goods, (+) indicates not safe for transport.

[S16] Z. P. Demko, K. B. Sharpless, *J. Org. Chem.* **2001**, *66*, 7945–7950.

19.7 Supplementary Information: Coordination Chemistry with 1-Methyl-5*H*-tetrazole: Cocrystallization, Laser-ignition, Lead-free Primary Explosives – One Ligand, three Goals

19.7.1 Compounds Overview





19.7.2 X-ray Diffraction

For all compounds, an Oxford Xcalibur3 diffractometer with a CCD area detector was employed for data collection using Mo-*K*α radiation (λ = 0.71073 Å). The data collection and reduction were carried out using the Crysalispro software[S1]. The structures were solved by direct methods (Sir-92[S2], Sir-97[S3] or Shelxs-97[S4]) and refined by full-matrix least-squares on *F*2 (ShelxL[S4]) and finally checked using the platon software[S5] integrated in the WinGX software suite. The non-hydrogen atoms were refined anisotropically and the hydrogen atoms were located and freely refined. The absorptions were corrected by a Scale3 Abspack multiscan method.[S6] All Diamond2 plots are shown with thermal ellipsoids at the 50% probability level and hydrogen atoms are shown as small spheres of arbitrary radius.

Table S1. Crystallographic data of **2**, **3**, **6**, **10** and **11**.

	2	**3**	**6**	**10**	**11**
Formula	$C_{12}H_{24}Cl_8Fe_2N_{24}$	$C_4H_8Cl_2MnN_8$	$C_{12}H_{24}Cl_2CoN_{24}$	$C_{12}H_{28}N_{26}O_8Zn$	$C_{12}H_{28}CuN_{26}O_8$
FW [g mol^{-1}]	955.63	294.02	634.38	729.41	728.14
Crystal system	Trigonal	Monoclinic	Monoclinic	Triclinic	Triclinic
Space Group	*P*–3	$P2_1/c$	$P2_1/c$	*P*–1	*P*–1
Color / Habit	Yellow block	Colorless block	Yellow block	Colorless block	Blue block
Size [mm]	0.39 x 0.48 x 0.57	0.10 x 0.15 x 0.20	0.10 x 0.19 x 0.26	0.10 x 0.15 x 0.16	0.16 x 0.30 x 0.35
a [Å]	12.5500(4)	11.4607(4)	11.9613(6)	6.9267(5)	6.8722(2)
b [Å]	12.5500(4)	6.7022(4)	6.7360(2)	13.2751(5)	13.2085(4)
c [Å]	6.6590(3)	7.0108(5)	16.8524(8)	16.9711(11)	16.9461(5)
α [°]	90	90	90	92.342(4)	88.192(3)
β [°]	90	102.511(8)	106.389(5)	90.442(5)	88.492(3)
γ [°]	120	90	90	104.792(5)	75.344(3)
V [Å^3]	908.30(8)	525.73(7)	1302.65(10)	1507.29(16)	1487.43(8)
Z	1	2	2	2	2
$\rho_{calc.}$ [g cm^{-3}]	1.747	1.857	1.617	1.608	1.626
μ [mm^{-1}]	1.818	1.744	0.920	0.900	0.821
F(000)	478	294	650	752	750
$\lambda_{MoK\alpha}$ [Å]	0.71069	0.71073	0.71073	0.71073	0.71073
T [K]	123	123	123	123	123
θ Min–Max [°]	4.5, 26.0	4.3, 26.0	4.6, 25.0	4.4, 26.0	4.5, 26.0
Dataset	−15: 15; −15: 15; −8: 8	−14: 13; −8: 8; −8: 8	−14: 14; −8: 8; −20: 20	−8:8; −16:16; −20:16	−8: 8; −16: 16; −20: 20
Reflections collected	6610	3702	16601	12378	21999
Independent refl.	1196	1028	2262	5911	5834
Rint	0.022	0.035	0.052	0.038	0.027
Observed reflections	1107	951	2054	4537	5065
Parameters	77	75	185	473	473
R_1 (obs)[a]	0.0212	0.0848	0.0822	0.0409	0.0286
wR_2 (all data)[b]	0.0574	0.2323	0.2310	0.0923	0.0774
GooF[c]	1.07	1.12	1.14	1.05	1.04
Resd. Dens. [e Å^{-3}]	−0.31, 0.31	−0.70, 4.04	−0.85, 3.08	−0.48, 0.63	−0.32, 0.34
Absorption correction	multi-scan	multi-scan	multi-scan	multi-scan	multi-scan
CCDC	1566368	1566362	1566371	1566381	1566384

a) $R_1 = \Sigma||F_0|- |F_c||/ \Sigma|F_0|$; b) $wR_2 = [\Sigma[w(F_0^2-F_c^2)^2]/\Sigma[w(F_0)^2]]^{1/2}$; $w = [\sigma c^2(F_0^2)+(xP)^2+yP]^{-1}$ and $P=(F_0^2+2F_c^2)/3$; c) GooF = $\{\Sigma[w(F_o^2-F_c^2)^2]/(n-p)\}^{1/2}$ (n = number of reflections; p = total number of parameters).

Table S2. Crystallographic data of **13, 15** and **17–19**.

	13	**15**	**17**	**18**	**19**
Formula	$C_4H_8AgN_9O_3$	$C_{12}H_{24}N_{24}O_8Cl_2Mn$	$C_{12}H_{24}N_{24}O_8Cl_2Co$	$C_{12}H_{24}N_{24}O_8Cl_2Ni$	$C_{12}H_{24}N_{24}O_8Cl_2Cu$
FW [g mol^{-1}]	338.04	758.39	762.38	762.16	767.00
Crystal system	Monoclinic	Monoclinic	Trigonal	Trigonal	Triclinic
Space Group	$P2_1/n$	$P2_1/n$	$R\bar{3}$	$R\bar{3}$	$P\bar{1}$
Color / Habit	Colorless block	Colorless block	Orange plate	Lilac plate	Blue rod
Size [mm]	0.30 x 0.30 x 0.60	0.10 x 0.21 x 0.40	0.09 x 0.10 x 0.48	0.07 x 0.07 x 0.11	0.15 x 0.18 x 0.20
a [Å]	5.4897(3)	18.0701(11)	19.5455(3)	19.4382(11)	10.4126(6)
b [Å]	29.2446(12)	10.2773(4)	19.5455(3)	19.4382(11)	17.9765(9)
c [Å]	6.8299(4)	18.7841(9)	21.3390(5)	21.3656(10)	18.3433(9)
α [°]	90	90	90	90	64.772(5)
β [°]	104.214(5)	114.147(7)	90	90	87.906(4)
γ [°]	90	90	120	120	85.765(5)
V [Å^3]	1062.93(10)	3183.2(2)	7059.9(3)	6991.3(10)	3097.5(3)
Z	4	4	9	9	4
$\rho_{calc.}$ [g cm^{-3}]	2.113	1.582	1.614	1.629	1.645
μ [mm^{-1}]	1.914	0.661	0.797	0.877	0.958
F(000)	664	1548	3501	3510	1564
$\lambda_{MoK\alpha}$ [Å]	0.71073	0.71073	0.71073	0.71073	0.71069
T [K]	123	123	123	123	123
θ Min–Max [°]	4.2, 26.5	4.1, 26.0	4.2, 26.0	4.2, 26.0	4.2, 32.3
Dataset	−6: 6; −36: 36;−8: 8	−20: 22; −12: 12; −23: 17	−24: 24; −24: 24; −26: 26	−19: 23; −23: 18; −25: 26	−15: 15; −24: 26; −25: 26
Reflections collected	8289	26034	35040	21514	35144
Independent refl.	2194	6239	3069	3052	19936
Rint	0.028	0.042	0.049	0.123	0.020
Observed reflections	2129	4638	2547	1972	14850
Parameters	164	551	261	216	865
R_1 (obs)[a]	0.0382	0.0433	0.0334	0.0460	0.0421
wR_2 (all data)[b]	0.0654	0.1221	0.0878	0.0996	0.1182
GooF[c]	1.49	1.05	1.05	1.00	1.03
Resd. Dens. [e Å^{-3}]	−0.75, 0.68	−0.38, 0.61	−0.51, 0.89	−0.39, 0.51	−0.77, 0.79
Absorption correction	multi-scan	multi-scan	multi-scan	multi-scan	multi-scan
CCDC	1566379	1566370	1566366	1566363	1566364

a) $R_1 = \Sigma||F_0|- |F_c||/ \Sigma|F_0|$; b) $wR_2 = [\Sigma[w(F_0^2-F_c^2)^2]/\Sigma[w(F_0)^2]]^{1/2}$; $w = [\sigma c^2(F_0^2)+(xP)^2+yP]^{-1}$ and $P=(F_0^2+2F_c^2)/3$; c) GooF = $\{\Sigma[w(F_o^2-F_c^2)^2]/(n-p)\}^{1/2}$ (n = number of reflections; p = total number of parameters).

Table S3. Crystallographic data of **20**–**24**.

	20	**21**	**22**	**23**	**24**
Formula	$C_{12}H_{24}N_{24}O_8Cl_2Zn$	$C_{16}H_{32}Cl_2MnN_{32}O_8$	$C_{16}H_{32}Cl_2FeN_{32}O_8$	$C_{16}H_{32}Cl_2CoN_{32}O_8$	$C_{16}H_{32}Cl_2NiN_{32}O_8$
FW [g mol^{-1}]	768.82	926.49	927.39	930.56	930.34
Crystal system	Monoclinic	Triclinic	Triclinic	Triclinic	Triclinic
Space Group	$P2_1/n$	$P\bar{1}$	$P\bar{1}$	$P\bar{1}$	$P\bar{1}$
Color / Habit	Colorless block	Colorless block	Yellow block	Yellow block	Purple plate
Size [mm]	0.03 x 0.15 x 0.35	0.17 x 0.25 x 0.32	0.19 x 0.26 x 0.54	0.14 x 0.21 x 0.46	0.08 x 0.14 x 0.23
a [Å]	17.9700(18)	6.9801(4)	7.0337(4)	7.0040(3)	7.0227(6)
b [Å]	10.2320(7)	11.4163(6)	11.3122(10)	11.2557(4)	11.1679(11)
c [Å]	18.5730(17)	13.4480(8)	13.4921(9)	13.4811(5)	13.4907(13)
α [°]	90	111.348(5)	111.433(7)	111.269(4)	111.317(9)
β [°]	113.811(11)	100.966(5)	101.254(5)	101.299(4)	101.502(8)
γ [°]	90	94.176(4)	94.220(6)	94.311(3)	94.379(7)
V [Å^3]	3124.3(5)	967.98(10)	967.64(13)	958.68(7)	952.95(17)
Z	4	1	1	1	1
$\rho_{calc.}$ [g cm^{-3}]	1.635	1.590	1.592	1.612	1.621
μ [mm^{-1}]	1.037	0.565	0.614	0.674	0.736
F(000)	1568	475	476	477	478
$\lambda_{MoK\alpha}$ [Å]	0.71069	0.71073	0.71073	0.71073	0.71073
T [K]	123	123	173	143	143
θ Min–Max [°]	4.1, 26.0	4.2, 31.7	4.5, 26.0	4.5, 26.0	4.5, 26.0
Dataset	−22: 21; −12: 12; −16: 22	−8: 8; −14: 13; −16: 14	−8: 8; −13: 13; −16: 16	−8: 8; −12: 13; −16: 16	−8: 8; −13: 13; −14: 16
Reflections collected	15544	7471	7361	7437	7547
Independent refl.	6113	3788	3791	3758	3741
Rint	0.074	0.023	0.021	0.023	0.052
Observed reflections	4638	3273	3162	3287	2667
Parameters	479	332	288	285	272
R_1 (obs)[a]	0.0650	0.0345	0.0428	0.0349	0.0562
wR_2 (all data)[b]	0.1895	0.0902	0.1190	0.0920	0.1467
GooF[c]	1.00	1.04	1.05	1.04	1.04
Resd. Dens. [e Å^{-3}]	−0.47, 1.11	−0.37, 0.50	−0.45, 0.63	−0.40, 0.58	−0.71, 0.91
Absorption correction	multi-scan	multi-scan	multi-scan	multi-scan	multi-scan
CCDC	1566361	1566359	1566380	1566382	1566385

a) $R_1 = \Sigma||F_0|- |F_c||/ \Sigma|F_0|$; b) $wR_2 = [\Sigma[w(F_0^2-F_c^2)^2]/\Sigma[w(F_0)^2]]^{1/2}$; $w = [\sigma c^2(F_0^2)+(xP)^2+yP]^{-1}$ and $P=(F_0^2+2F_c^2)/3$; c) GooF = $\{\Sigma[w(F_o^2-F_c^2)^2]/(n-p)\}^{1/2}$ (n = number of reflections; p = total number of parameters).

Table S4. Crystallographic data of **25**–**29**.

	25	**26**	**27**	**28**	**29**
Formula	$C_{16}H_{32}Cl_2CuN_{32}O_8$	$C_{16}H_{32}Cl_2N_{32}O_8Zn$	$C_{12}H_{16}CuN_{22}O_8$	$C_{16}H_{24}MnN_{14}O_{20}$	$C_{16}H_{24}CoN_{14}O_{20}$
FW [g mol^{-1}]	935.17	936.93	659.95	787.43	791.42
Crystal system	Triclinic	Triclinic	Triclinic	Monoclinic	Monoclinic
Space Group	*P*−1	*P*−1	*P*−1	$P2_1/c$	$P2_1/c$
Color / Habit	Blue block	Colorless block	Blue block	Light-yellow block	Yellow block
Size [mm]	0.29 x 0.43 x 0.64	0.17 x 0.21 x 0.33	0.17 x 0.44 x 0.64	0.06 x 0.15 x 0.22	0.10 x 0.14 x 0.15
a [Å]	6.9979(2)	6.9713(3)	8.5663(6)	15.564(1)	15.5380(5)
b [Å]	11.2379(4)	11.2765(4)	8.9435(8)	5.2200(2)	5.2291(1)
c [Å]	13.4606(5)	13.4545(5)	9.9252(9)	18.552(1)	18.5676(6)
α [°]	111.450(3)	111.256(3)	69.408(9)	90	90
β [°]	101.356(3)	101.267(3)	69.665(7)	102.645(6)	102.713(3)
γ [°]	93.102(3)	94.278(3)	65.094(8)	90	90
V [Å^3]	956.69(6)	954.42(7)	627.56(10)	1470.68(14)	1471.83(7)
Z	1	1	1	2	2
$\rho_{calc.}$ [g cm^{-3}]	1.623	1.630	1.746	1.778	1.786
μ [mm^{-1}]	0.797	0.870	0.959	0.563	0.698
F(000)	479	480	335	806	810
$\lambda_{MoK\alpha}$ [Å]	0.71073	0.71073	0.71073	0.71069	0.71073
T [K]	143	173	123	123	173
θ Min–Max [°]	4.5, 26.0	4.5, 26.0	4.3, 26.0	4.1, 26.0	4.2, 26.0
Dataset	−8: 8; −13: 13; −16: 16	−8: 8; −13: 13; −16: 16	−10: 10; −11: 10; −12: 12	−18: 19; −6: 6; −21: 22	−19: 17; −6: 6; −22: 22
Reflections collected	6934	13753	4809	9834	10884
Independent refl.	3748	3737	2459	2887	2893
Rint	0.018	0.025	0.023	0.046	0.029
Observed reflections	3361	3428	2250	2191	2482
Parameters	272	332	206	269	269
R_1 (obs)[a]	0.0370	0.0325	0.0289	0.0406	0.0292
wR_2 (all data)[b]	0.1023	0.0860	0.0710	0.0984	0.0718
GooF[c]	1.06	1.05	1.07	1.02	1.05
Resd. Dens. [e Å^{-3}]	−0.47, 0.76	−0.51, 0.73	−0.36, 0.30	−0.34, 0.52	−0.24, 0.34
Absorption correction	multi-scan	multi-scan	multi-scan	multi-scan	multi-scan
CCDC	1566386	1566360	1566378	1566377	1566376

a) $R_1 = \Sigma||F_0|- |F_c||/ \Sigma|F_0|$; b) $wR_2 = [\Sigma[w(F_0^2-F_c^2)^2]/\Sigma[w(F_0)^2]]^{1/2}$; $w = [\sigma c^2(F_0^2)+(xP)^2+yP]^{-1}$ and $P=(F_0^2+2F_c^2)/3$; c) GooF = $\{\Sigma[w(F_o^2-F_c^2)^2]/(n-p)\}^{1/2}$ (n = number of reflections; p = total number of parameters).

Table S5. Crystallographic data of **30**–**34**.

	30	**31**	**32**	**33**	**34**
Formula	$C_{20}H_{24}NiN_{22}O_{16}$	$C_{16}H_{12}CuN_{14}O_{14}$	$C_{20}H_{20}N_{22}O_{14}Zn$	$C_{20}H_{20}MnN_{22}O_{16}$	$C_{16}H_{24}CoN_{14}O_{22}$
FW [g mol^{-1}]	887.32	687.95	857.95	879.52	823.42
Crystal system	Monoclinic	Monoclinic	Monoclinic	Monoclinic	Monoclinic
Space Group	$P2_1/c$	$P2_1/c$	$P2_1/n$	$P2_1/n$	$P2_1/c$
Color / Habit	Yellow-green block	Green needle	Yellow rod	Yellow block	Yellow block
Size [mm]	0.18 x 0.24 x 0.27	0.06 x 0.06 x 0.20	0.05 x 0.11 x 0.32	0.16 x 0.26 x 0.45	0.14 x 0.32 x 0.41
a [Å]	13.5772(4)	10.9660(6)	11.2981(6)	11.2818(4)	15.3750(9)
b [Å]	16.6129(6)	5.7912(4)	8.9988(5)	9.0093(3)	5.8840(2)
c [Å]	7.5443(3)	19.6839(10)	16.2583(13)	16.5990(8)	18.4840(8)
α [°]	90	90	90	90	90
β [°]	99.707(3)	91.344(5)	91.512(6)	91.382(6)	114.220(6)
γ [°]	90	90	90	90	90
V [Å^3]	1677.30(10)	1249.71(13)	1652.40(18)	1686.65(12)	1524.99(14)
Z	2	2	2	2	2
$\rho_{calc.}$ [g cm^{-3}]	1.757	1.828	1.724	1.732	1.793
μ [mm^{-1}]	0.688	0.976	0.846	0.500	0.682
F(000)	908	694	872	894	842
$\lambda_{MoK\alpha}$ [Å]	0.71073	0.71073	0.71073	0.71073	0.71069
T [K]	123	123	173	123	123
θ Min–Max [°]	4.2, 26.0	4.1, 26.0	4.3, 26.0	4.1, 26.0	4.2, 26.0
Dataset	−16: 16; −20: 20; −9: 8	−13: 13; −7: 7; −23: 24	−13: 12; −11: 11; −18: 20	−13: 13; −11: 8; −20: 19	−18: 16; −6: 7; −19: 22
Reflections collected	10946	8943	12751	12905	11195
Independent refl.	3283	2447	3228	3292	2978
Rint	0.035	0.060	0.050	0.035	0.023
Observed reflections	2791	1937	2420	2692	2582
Parameters	294	218	261	271	278
R_1 (obs)[a]	0.0316	0.0470	0.0374	0.0575	0.0275
wR_2 (all data)[b]	0.0801	0.1358	0.0933	0.1646	0.0708
GooF[c]	1.04	1.04	1.03	1.03	1.08
Resd. Dens. [e Å^{-3}]	−0.24, 0.31	−1.01, 0.95	−0.28, 0.36	−0.65, 2.48	−0.35, 0.30
Absorption correction	multi-scan	multi-scan	multi-scan	multi-scan	multi-scan
CCDC	1566372	1566375	1566383	1566373	1566367

a) $R_1 = \Sigma||F_0|- |F_c||/ \Sigma|F_0|$; b) $wR_2 = [\Sigma[w(F_0^2-F_c^2)^2]/\Sigma[w(F_0)^2]]^{1/2}$; $w = [\sigma c^2(F_0^2)+(xP)^2+yP]^{-1}$ and $P=(F_0^2+2F_c^2)/3$; c) GooF = $\{\Sigma[w(F_o^2-F_c^2)^2]/(n-p)\}^{1/2}$ (n = number of reflections; p = total number of parameters).

Table S6. Crystallographic data of **35**–**37**.

	35	**36**	**37**
Formula	$C_{16}H_{24}NiN_{14}O_{22}$	$C_{16}H_{12}CuN_{14}O_{16}$	$C_{16}H_{12}ZnN_{14}O_{16}$
FW [g mol^{-1}]	823.20	719.90	721.77
Crystal system	Monoclinic	Monoclinic	Triclinic
Space Group	$P2_1/c$	$P2_1/c$	$P\bar{1}$
Color / Habit	Green block	Blue plate	Colorless block
Size [mm]	0.38 x 0.47 x 0.58	0.10 x 0.22 x 0.25	0.26 x 0.30 x 0.42
a [Å]	15.2670(4)	6.0790(3)	9.6200(3)
b [Å]	5.8850(1)	20.0450(7)	11.4310(4)
c [Å]	18.4360(5)	10.8420(4)	12.0220(3)
α [°]	90	90	81.920(2)
β [°]	113.712(3)	93.129(4)	82.467(2)
γ [°]	90	90	74.196(3)
V [Å^3]	1516.57(7)	1319.17(9)	1253.42(7)
Z	2	2	2
$\rho_{calc.}$ [g cm^{-3}]	1.803	1.812	1.913
μ [mm^{-1}]	0.759	0.935	1.092
F(000)	844	726	728
$\lambda_{MoK\alpha}$ [Å]	0.71069	0.71069	0.71069
T [K]	123	123	123
θ Min–Max [°]	42, 26.0	4.3, 26.0	4.3, 26.0
Dataset	−16: 16; −20: 20; −9: 8	−7: 7; −17: 24; −13: 13	−11: 11; −14: 14; −14: 14
Reflections collected	10946	10304	18110
Independent refl.	3283	2581	4898
Rint	0.018	0.035	0.022
Observed reflections	2791	2164	4608
Parameters	294	227	434
R_1 (obs)[a]	0.0316	0.0337	0.0232
wR_2 (all data)[b]	0.0801	0.0841	0.0607
GooF[c]	1.04	1.05	1.05
Resd. Dens. [e Å^{-3}]	−0.24, 0.31	−0.32, 0.35	−0.34, 0.35
Absorption correction	multi-scan	multi-scan	multi-scan
CCDC	1566374	1566365	1566369

a) $R_1 = \Sigma||F_0|- |F_c||/ \Sigma|F_0|$; b) $wR_2 = [\Sigma[w(F_0^2-F_c^2)^2]/\Sigma[w(F_0)^2]]^{1/2}$; $w = [\sigma c^2(F_0^2)+(xP)^2+yP]^{-1}$ and $P=(F_0^2+2F_c^2)/3$; c) GooF = $\{\Sigma[w(F_o^2-F_c^2)^2]/(n-p)\}^{1/2}$ (n = number of reflections; p = total number of parameters).

The manganese(II) chloride complex **3** (Figure S1) crystallizes isotypically to its copper(II) analog **4**[S7] in the form of colorless blocks in the monoclinic space group $P2_1/c$ with two formula units per unit cell and a calculated density of 1.857 g cm^{-3} at 123 K. The metal(II) center has an octahedral coordination sphere containing four bridging chloride anions in a plane and two MTZ molecules in axial positions (Mn1–N1 = 2.233(6) Å, Mn1–Cl1 = 2.566(2) Å, Mn1–Cl1^{ii} = 2.566(2) Å). The coordination octahedron angles deviate only slightly from the ideal 90 ° (< (Cl1—Mn1—N1) = 90.90(2)°, (< (Cl1—Mn1—Cl1^{ii}) = 86.35(4)°, (< (Cl1—Mn1—N1^{i}) = 89.10(2)°), which results in a small distortion. The distances between the manganese(II) and chloride atoms lie in the range of coordinative bonds reported in the literature.[S8]

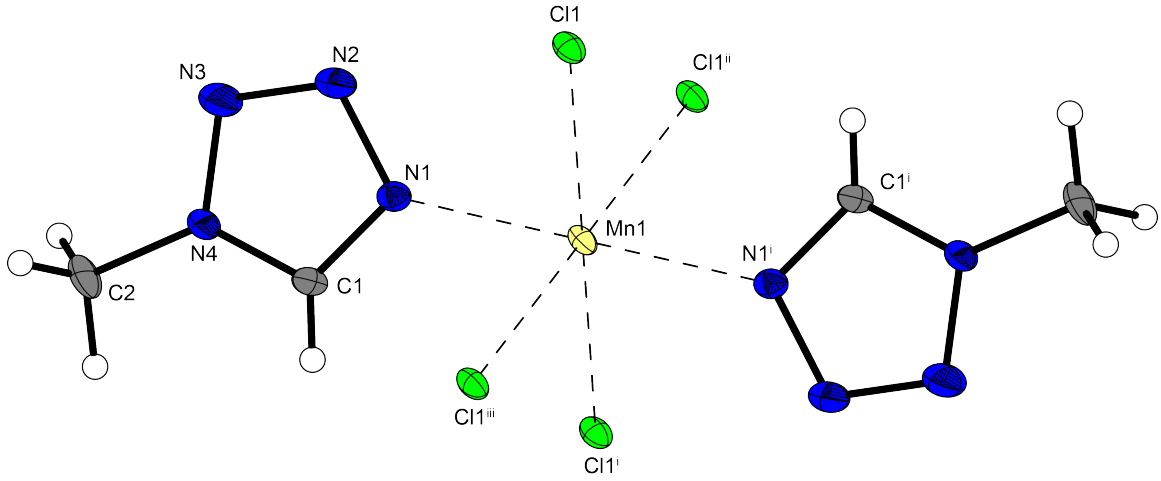


Figure S1. Molecular unit of [$MnCl_2(MTZ)_2$] (**3**). Selected bond lengths (Å): Mn1–Cl1 2.566(2), Mn1–Cl1^{ii} 2.588(2), Mn1–N1 2.233(6); selected bond angles (°): Cl1–Mn1–N1 90.90(2), Cl1–Mn1–N1^{i} 89.10(2), Cl1–Mn1–Cl1^{ii} 86.35(4), Cl1–Mn1–Cl1^{iii} 93.65(4). Symmetry codes: (i) −x, 1−y, −z; (ii) x, 1.5−y, 0.5+z; (iii) −x, 0.5 +y, −0.5−z.

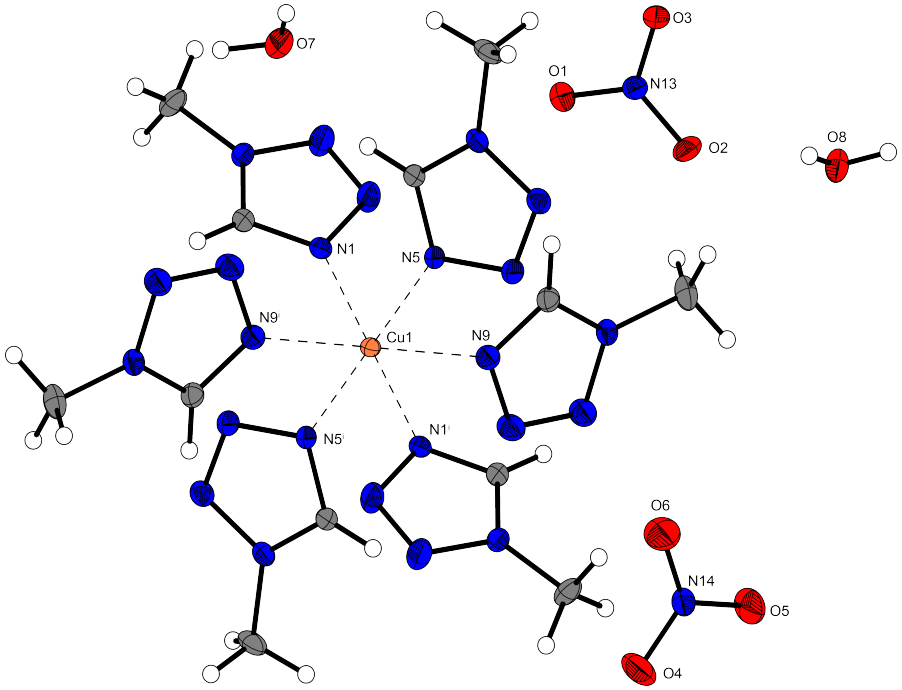


Figure S2. Molecular moiety of **11**. Selected bond lengths (Å): Cu1–N1 2.038(2), Cu1–N5 2.017(2), Cu1–N9 2.400(2); selected bond angles (°): N1–Cu1–N5 88.97(6), N1–Cu1–N9 90.77(5), N5–Cu1–N9 88.55(5). Symmetry code: (i) 1−x, 1−y, −z.

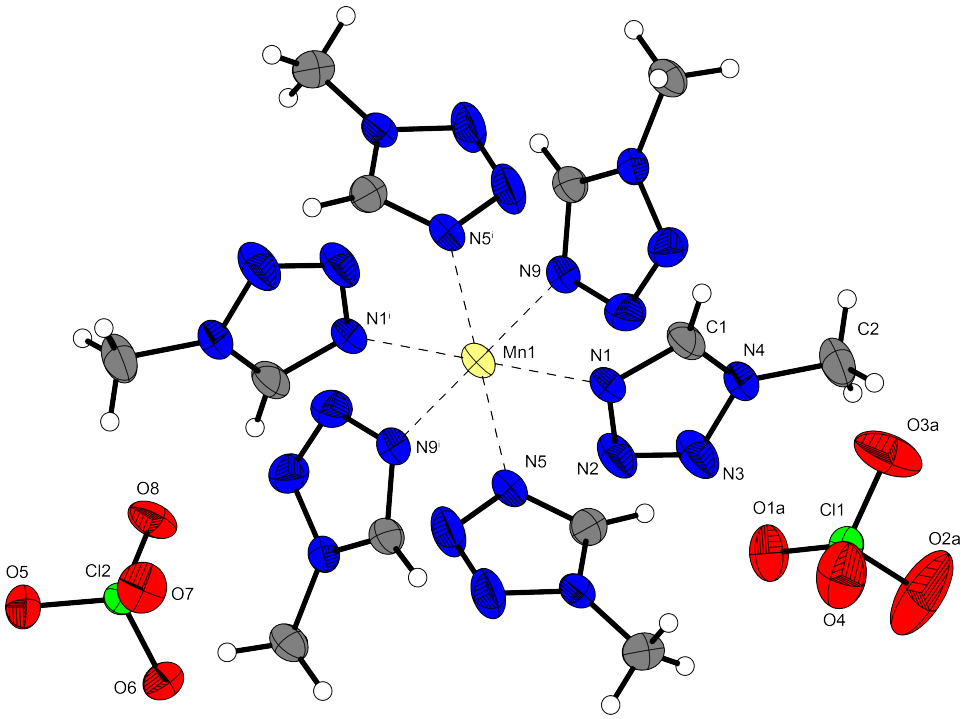


Figure S3. Complex unit of $[Mn(MTZ)_6](ClO_4)_2$ (**15**). Selected bond lengths (Å): Mn1–N1 2.254(2), Mn1–N5 2.251(2), Mn1–N9 2.260(2); selected bond angles (°): N1–Mn1–N5 88.85(2), N1–Mn1–N9 87.40(2), N5–Mn1–N9 90.02(2). Symmetry code: (i) 1−x, 1−y, 1−z.

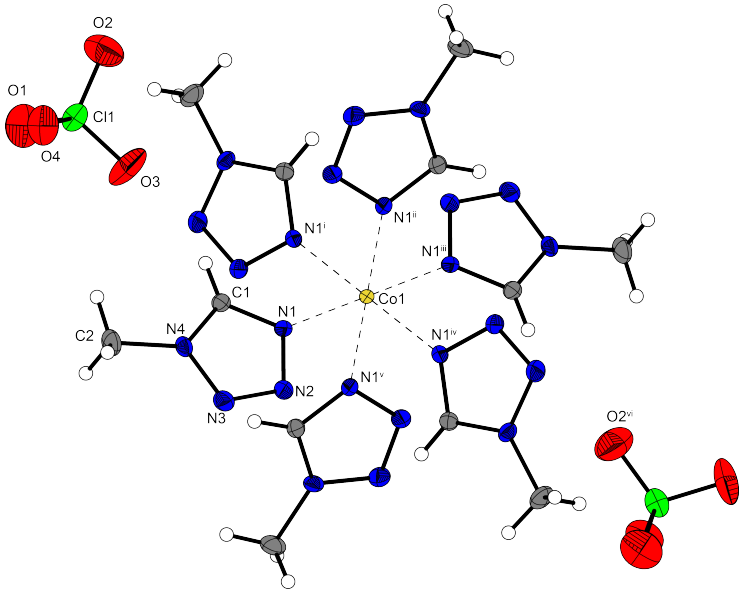


Figure S4. Complex unit of $[Co(MTZ)_6](ClO_4)_2$ (**17**). Selected bond lengths (Å): Co1–N1 2.135(2), Cl1–O1 1.463(2); selected bond angles (°): N1–Co1–N1^{i} 87.53(2), N1–Co1–N1^{ii} 92.46(2), O1–Cl1–O2 109.37(2). Symmetry codes: (i) −x+y, −x, z; (ii) −y, x−y, z; (iii) −x, −y, −z; (iv) y, −x+y, −z; (v) x−y, x, −z.

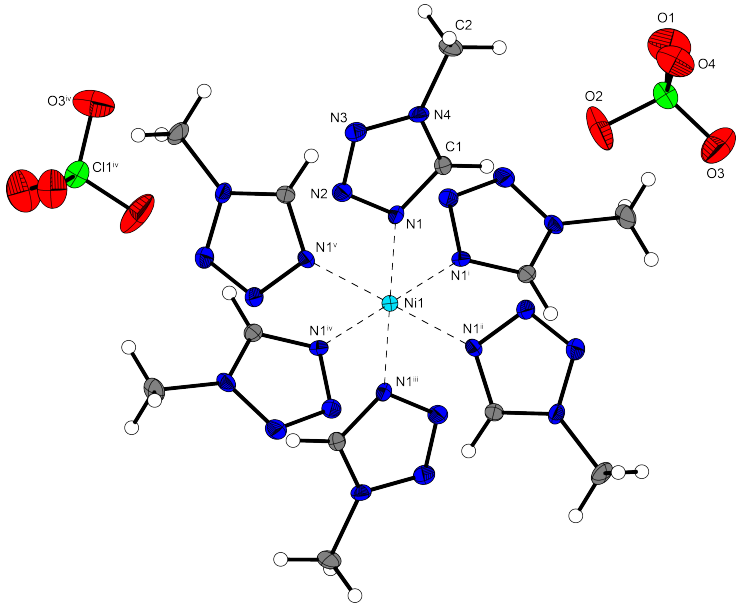


Figure S5. Complex unit of $[Ni(MTZ)_6](ClO_4)_2$ (**18**). Selected bond lengths (Å): Ni1–N1 2.088(2), Cl1–O1 1.426(2); selected bond angles (°): N1–Ni1–N1^{i} 88.27(2), N1–Ni1–N1^{ii} 91.65(2), N1–Ni1–N1^{iii} 179.33(2), N1–Ni1–N1^{iv} 91.69(2), N1–Ni1–N1^{v} 88.31(2). Symmetry codes: (i) 1–y, 1+x, z; (ii) −x+y, 1−y, z; (iii) −x+y, −x, z; (iv) −y, x−y, z; (v) 0.66667+x−y, 0.33333+x, 0.33333 −z.

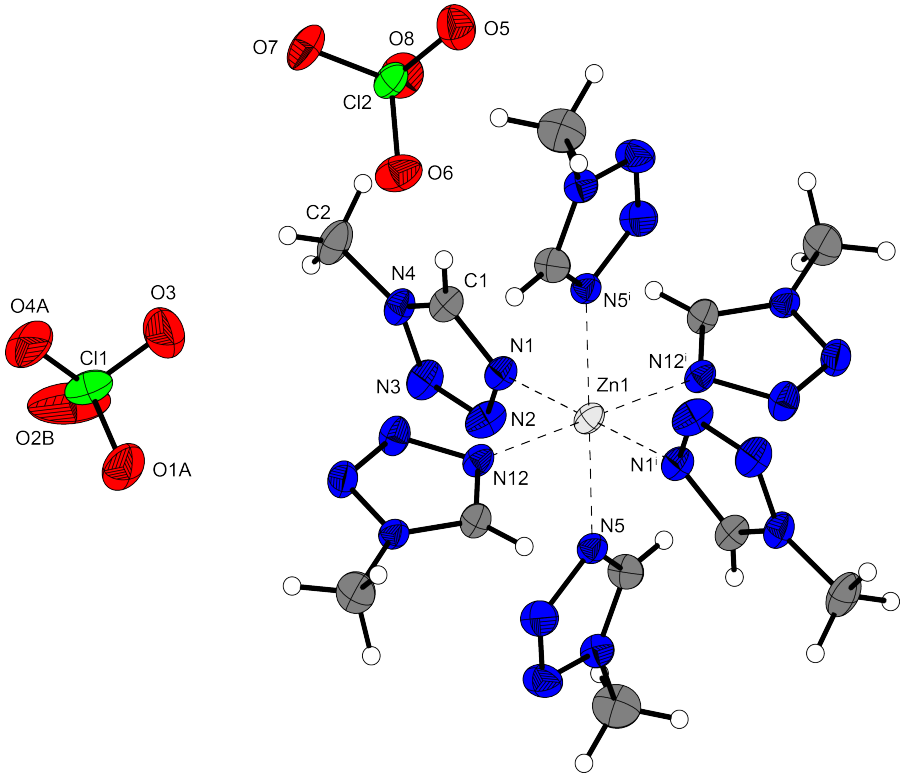


Figure S6. Complex unit of $[Zn(MTZ)_6](ClO_4)_2$ (**20**). Selected bond lengths (Å): Zn1–N1 2.155(2), Zn1–N5 2.130(2), Zn1–N12 2.212 (2); selected bond angles (°): N1–Zn1–N5 90.83(2), N1–Zn1–N12 90.80(2), N5–Zn1–N12 89.28(2). Symmetry codes: (i) 1−x+y, −x, z; (ii) −x, 1−y, 1−z.

Due to the already mentioned low sterical hindrance of MTZ, octahedral coordination is possible. In the case of a metal with d^{10} configuration, the ligand field stabilization energies (LFSE) are zero.

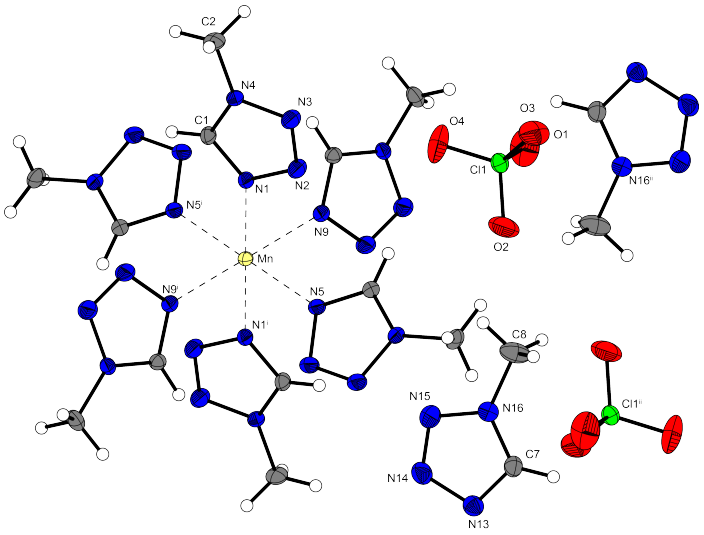


Figure S7. Complex unit of $[Mn(MTZ)_6](ClO_4)_2 \bullet 2$ MTZ (**21**). Selected bond lengths (Å): Mn1–N9 2.244(66), Mn1–N1 2.247(17), Mn1–N5 2.261(17), Cl1–O1 1.415(2); selected bond angles (°): $N9^{i}$–

Mn1–N1^{i} 88.55(6), N9–Mn1–N1^{i} 91.46(6), N9^{i}–Mn1–N5^{i} 87.90(6), N9–Mn1–N5^{i} 92.10(6), N1^{i}–Mn1–N5^{i} 90.72(6), N1–Mn1–N5^{i} 89.29(6). Symmetry codes: (i) −x, −y, −z; (ii) 1−x, 1−y, 1−z.

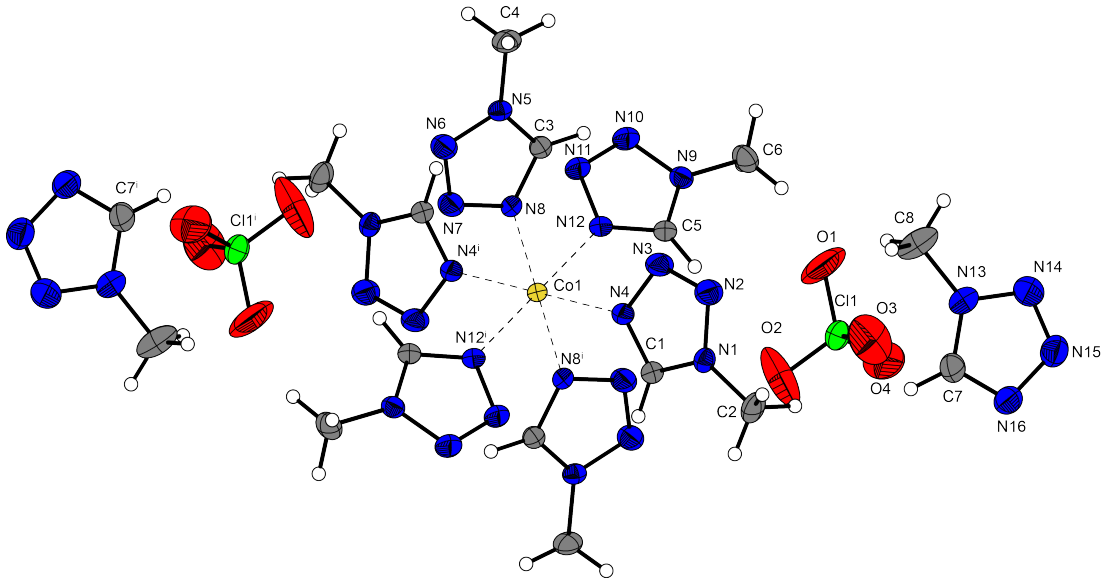


Figure S8. Molecular unit of $[Co(MTZ)_6](ClO_4)_2$ • 2 MTZ (**23**). Selected bond lengths (Å): Co1–N4 2.1386(16), Co1–N8 2.1402(17), Co1–N12 2.1579(17), Cl1–O2 1.404(3); selected bond angles (°): N4–Co1–N8 91.17(6), N4–Co1–N12 88.01(6), N8–Co1–N12 88.97(6), N4–Co1–N8^{i} 88.83(6), N4–Co1–N12^{i} 91.99(6), N8–Co1–N12^{i} 91.03(6). Symmetry code: (i) 1−x, 1−y, 1−z.

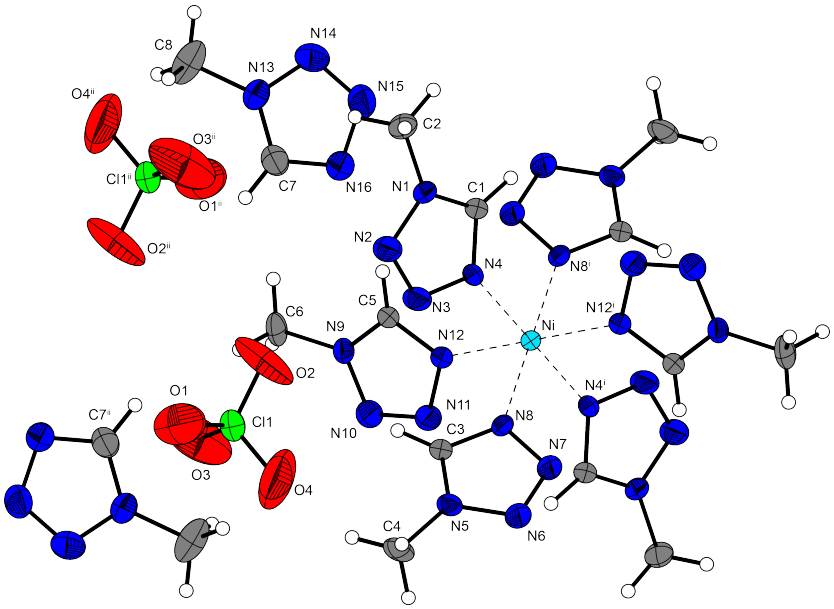


Figure S9. Molecular unit of $[Ni(MTZ)_6](ClO_4)_2$ • 2 MTZ (**24**). Selected bond lengths (Å): Ni–N4 2.105(4), Ni–N8 2.105(4), Ni–N12 2.096(4), Cl1–O2 1.400(6); selected bond angles (°): N4–Ni–N8 90.43(14), N4–Ni–N12 89.34(14), N4–Ni–N8^{i} 89.57(14), N4–Ni–N12^{i} 90.66(14), N8–Ni–N12 88.56(14), N8–Ni–N12^{i} 91.44(14). Symmetry codes: (i) 1−x, 1−y, 1−z; (ii) –x, 1−y, −z.

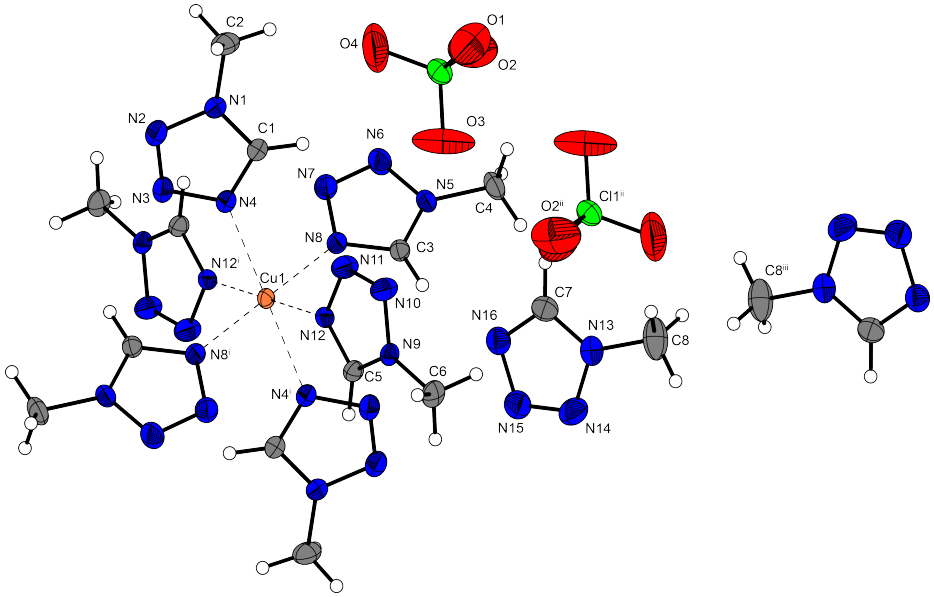


Figure S10. Molecular unit of $[Cu(MTZ)_6](ClO_4)_2$ • 2 MTZ (**25**). Selected bond lengths (Å): Cu1–N4 2.379(2), Cu1–N8 2.0306(19), Cu1–N12 2.039(2), Cl1–O2 1.406(3); selected bond angles (°): N4–Cu1–N8 88.76(7), N4–Cu1–N12 91.15(8), N4–Ni–N8^{i} 91.24(7), N4–Cu1–N12^{i} 88.85(8), N8–Cu1–N12 89.15(8), N8–Cu1–N12^{i} 90.85(8). Symmetry codes: (i) 2−x, −y, 2−z; (ii) 1−x, 1−y, 1−z.

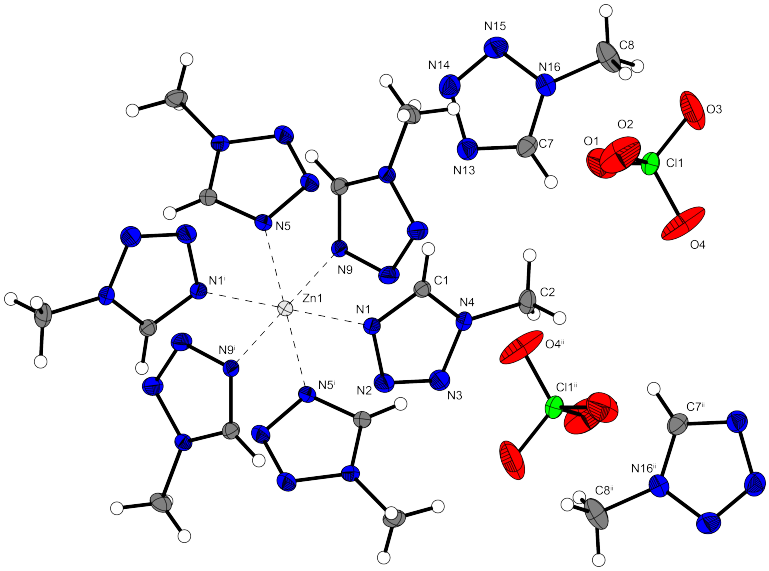


Figure S11. Molecular unit of $[Zn(MTZ)_6](ClO_4)_2$ • 2 MTZ (**26**). Selected bond lengths (Å): Zn1–N1 2.156(15), Zn1–N9 2.157(17), Zn1–N5 2.182(17), Cl1–O2 1.408(2); selected bond angles (°): N1–Zn1–N9^{i} 91.04(6), N1^{i}–Zn1–N9^{i} 88.96(6), N1–Zn1–N5 91.81(6), N1^{i}–Zn1–N5 88.19(6), N9^{i}–Zn1–N5 90.67(6). Symmetry codes: (i) 1−x, 1−y, −z; (ii) 1−x, 1−y, 1−z.

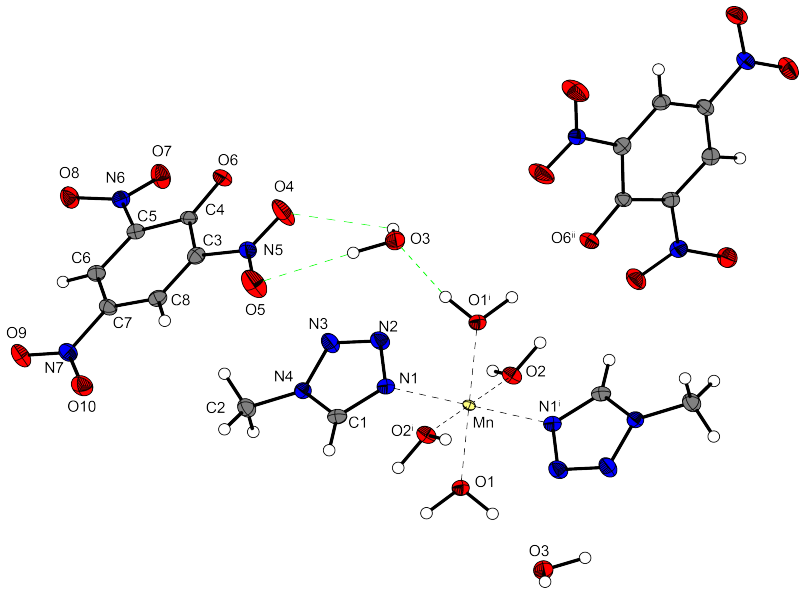


Figure S12. Molecular unit of complex $[Mn(H_2O)_4(MTZ)_2](PA)_2 \bullet 2\ H_2O$ (**28**). Selected bond lengths (Å): Mn1–O1 2.1122(19), Mn1–O2 2.100(2), Mn1–N1 2.132(2); selected bond angles (°): O1–Mn1–O2 91.36(8), O1–Mn1–N1 87.11(8), O1–Mn1–O2^{i} 88.65(8), O1–Mn1–N1^{i} 92.89(8), O2–Mn1–N1 91.09(8), O2–Mn1–N1^{i} 88.91(8). Symmetry code: (i) −x, 1−y, −z.

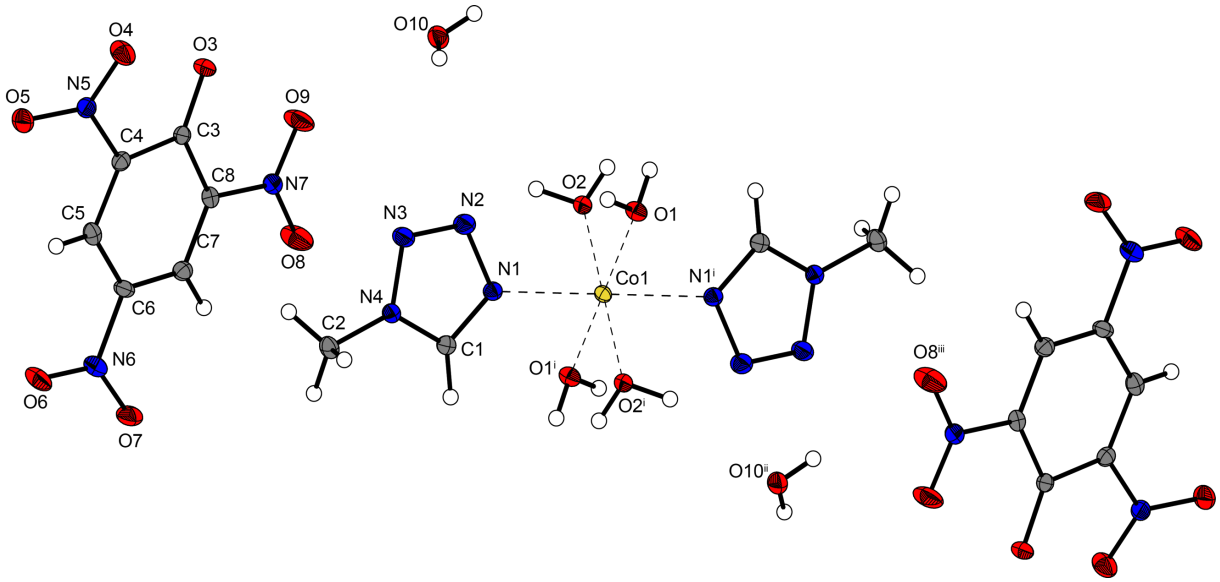


Figure S13. Molecular unit of the coordination compound $[Co(H_2O)_4(MTZ)_2](PA)_2 \bullet 2\ H_2O$ (**29**). Selected bond lengths (Å): Co1–O1 2.096(2), Co1–O2 2.109(2), Co1–N1 2.133(2); selected bond angles (°): O1–Co1–O2 88.85(5), O1–Co1–N1 90.94(6), O2–Co1–N1 92.91(6). Symmetry codes: (i) 1−x, −y, 1−z; (ii) x, −0.5−y, 0.5 +z; (iii) 1−x, 1−y, 1−z.

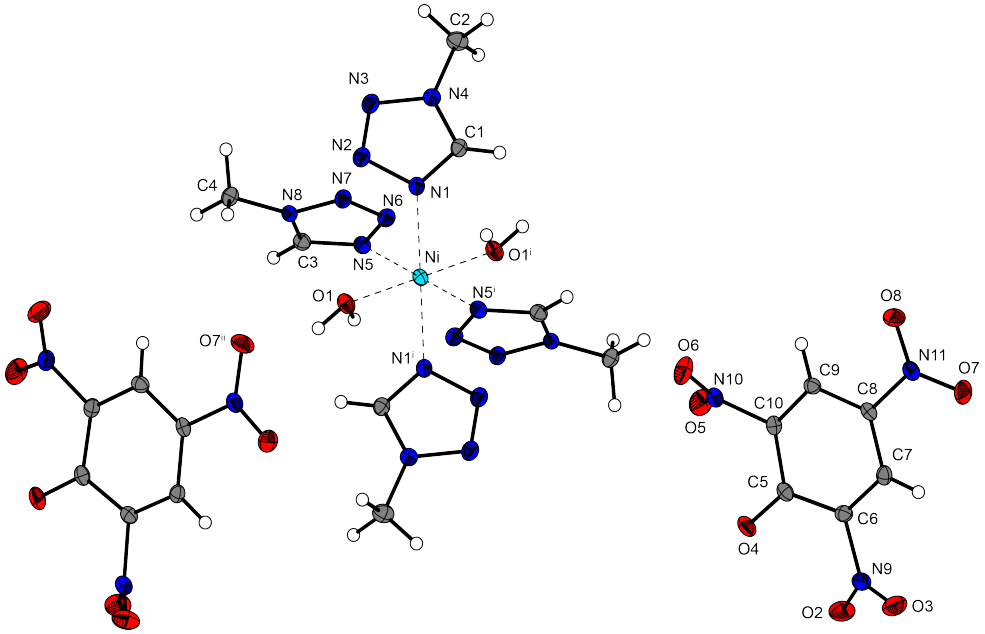


Figure S14. Molecular unit of complex $[Ni(H_2O)_2(MTZ)_4](PA)_2$ (**30**). Selected bond lengths (Å): Ni1–O1 2.068(2), Ni1–N1 2.087(2), Ni1–N5 2.071(2); selected bond angles (°): N1–Ni1–N5 89.75(6), O1–Ni1–N1 92.06(6), O1–Ni1–N5 88.91(6). Symmetry codes: (i) −x, 1−y, −z; (ii) −1+x, 0.5−y, −0.5+z.

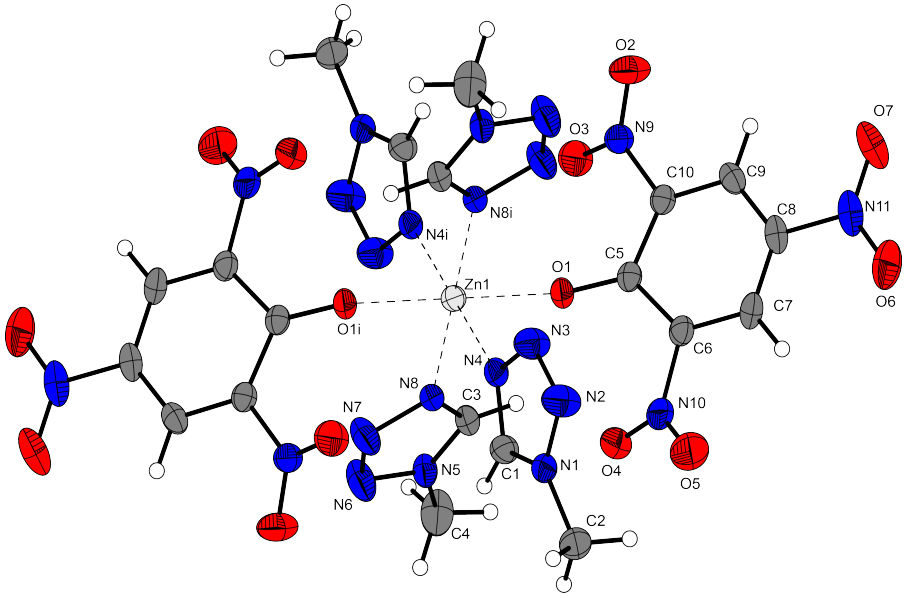


Figure S15. Molecular unit of $[Zn(PA)_2(MTZ)_4]$ (**32**). Selected bond lengths (Å): Zn1–O1 2.1654(17), Zn1–N4 2.123(2), Zn1–N8 2.1288(19); selected bond angles (°): O1–Zn1–N4 91.21(7), O1–Zn1–N8 86.42(7), N4–Zn1–N8 91.33(8). Symmetry code: (i) 1−x, 1−y, −z.

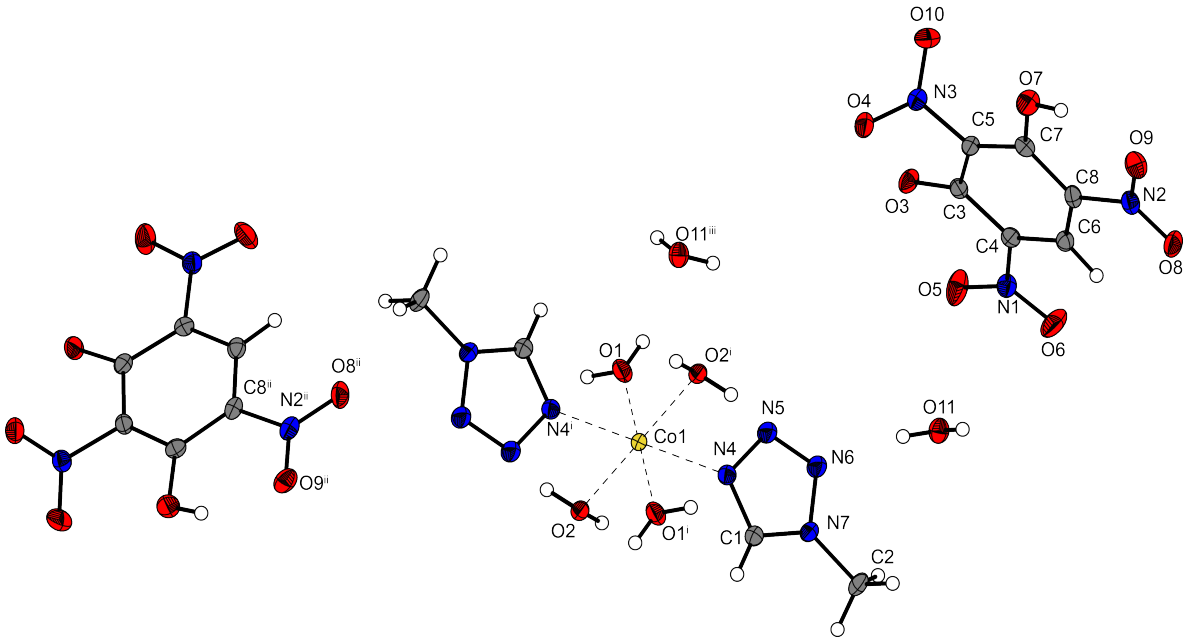


Figure S16. Molecular unit of $[Co(H_2O)_4(MTZ)_2](HTNR)_2 \bullet 2\ H_2O$ (**34**). Selected bond lengths (Å): Co1–O1 2.0474(14), Co1–O2 2.1203(14), Co1–N4 2.1303(15); selected bond angles (°): O1–Co1–O2 88.12(5), O1–Co1–N4 92.11(6), O2–Co1–N4 93.47(5). Symmetry codes: (i) 1−x, 1.5−y, 0.5+z; (ii) −x, 1−y, 1−z.

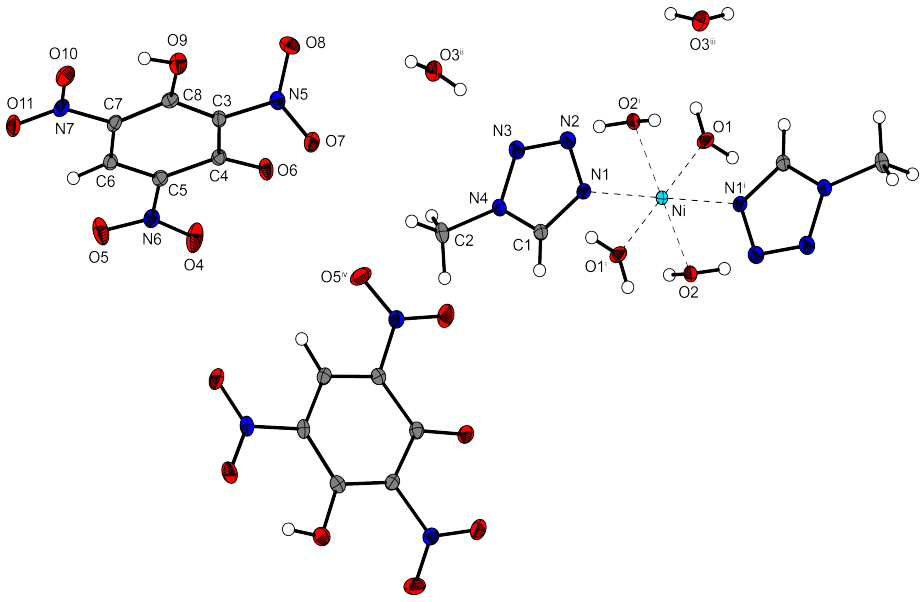


Figure S17. Molecular unit of $[Ni(H_2O)_4(MTZ)_2](HTNR)_2 \bullet 2\ H_2O$ (**35**). Selected bond lengths (Å): Ni1–O1 2.037(2), Ni1–O2 2.081(2), Ni1–N1 2.069(2); selected bond angles (°): O1–Ni1–O2 89.19(5), O1–Ni1–N1 92.31(5), O2–Ni1–N1 92.19(5). Symmetry codes: (i) 1−x, −y, −z; (ii) x, −1+y, z; (iii) 1−x, −1.5+y, 0.5−z; (iv) x, 1.5−y, −0.5+z.

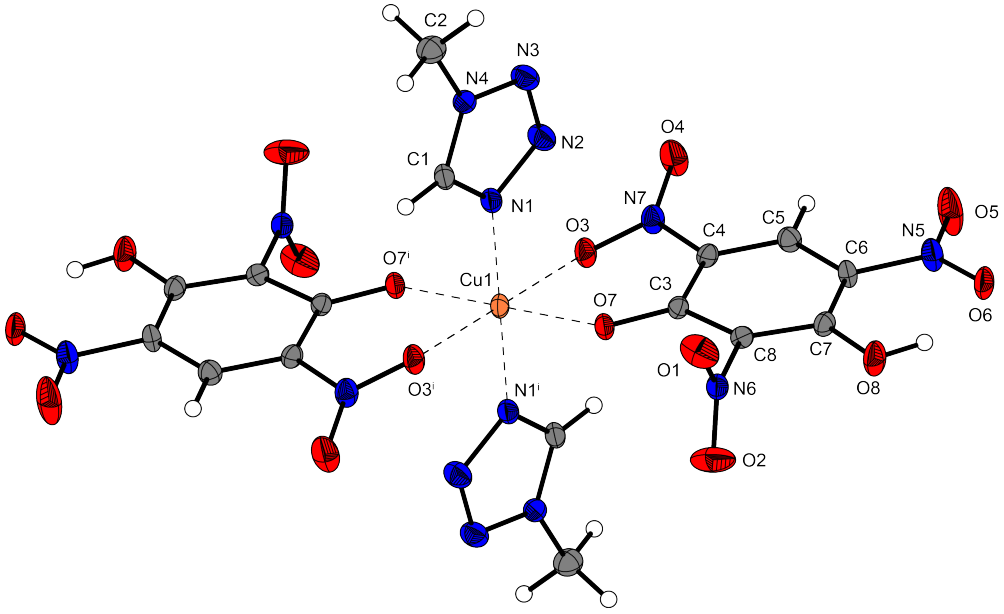


Figure S18. Molecular unit of $[Cu(HTNR)_2(MTZ)_2]$ (**36**). Selected bond lengths (Å): Cu1–N1 1.987(2), Cu1–O3 2.321(2), Cu1–O7 1.962(2); selected bond angles (°): N1–Cu1–O3 92.32(5), N1–Cu1–O7 89.86(5), O3–Cu1–O7 81.55(5). Symmetry code: (i) −x, −y, −z.

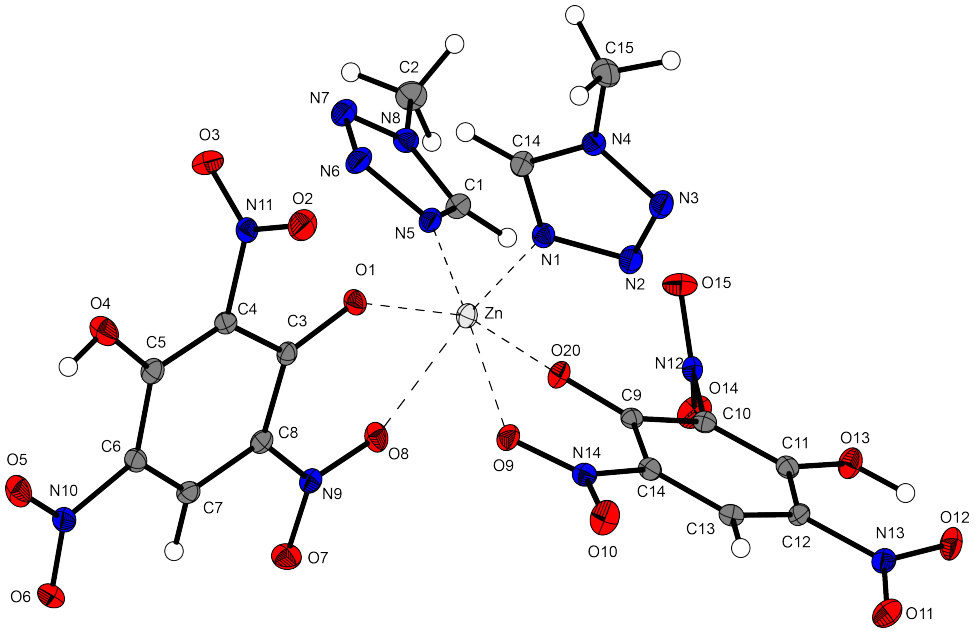


Figure S19. Molecular unit of $[Zn(HTNR)_2(MTZ)_2]$ (**37**). Selected bond lengths (Å): Zn1–O1 1.956(2), Zn1–O8 2.348(2), Zn1–O9 2.248(2), Zn1–O20 1.985(2), Zn1–N1 2.075(2), Zn1–N5 2.052(2); selected bond angles (°): N1–Zn1–N5 102.48(5), O1–Zn1–O8 78.14(4), O1–Zn1–O9 89.78(4), O1–Zn1–N1 93.44(5), O1–Zn1–N5 95.15(5), O9–Zn1–O20 80.06(4).

19.7.3 IR Spectroscopy of 3, 6–9, 12, 17 and 23

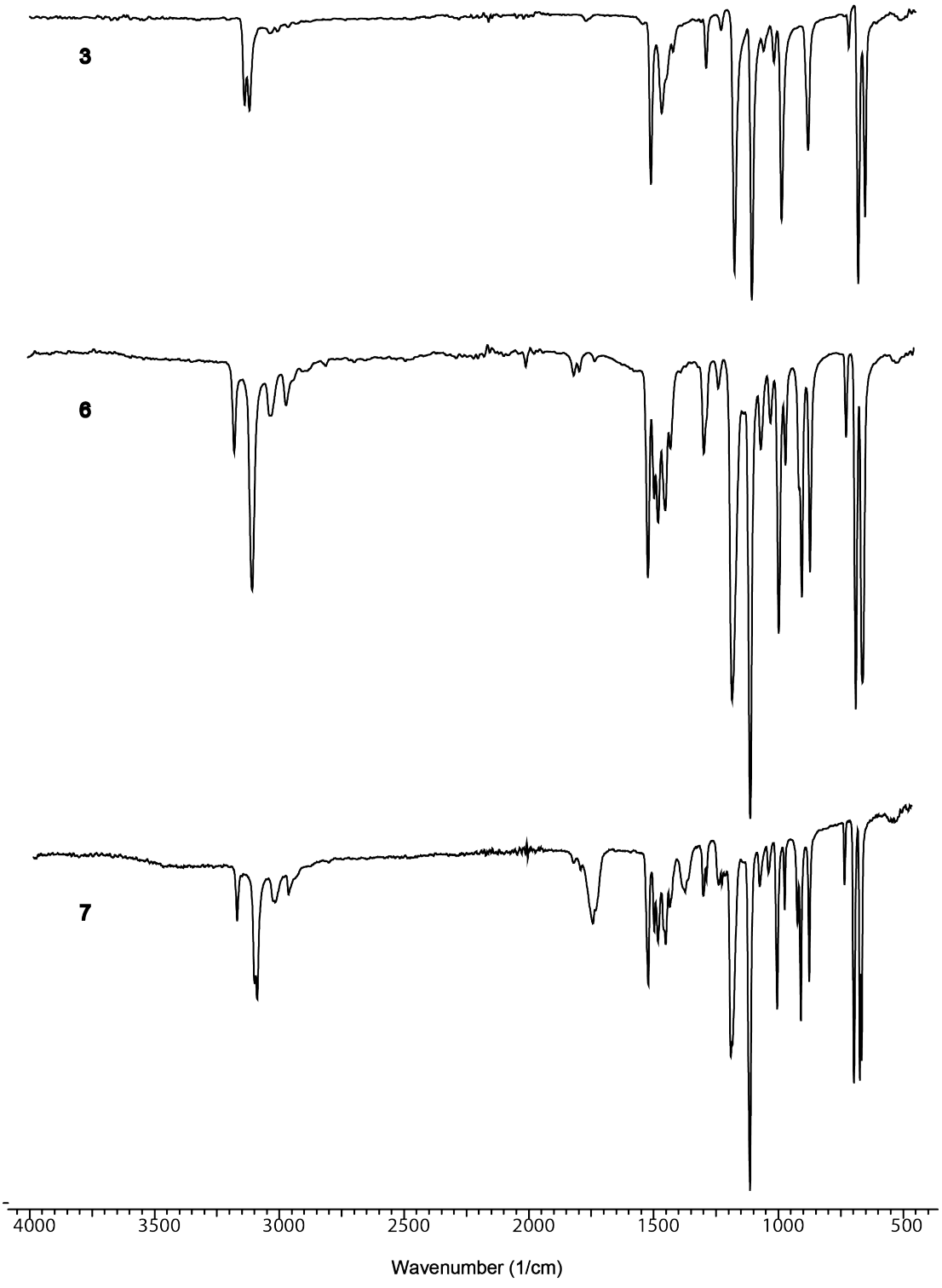


Figure S20. Infrared spectra of **3**, **6** and **7**.

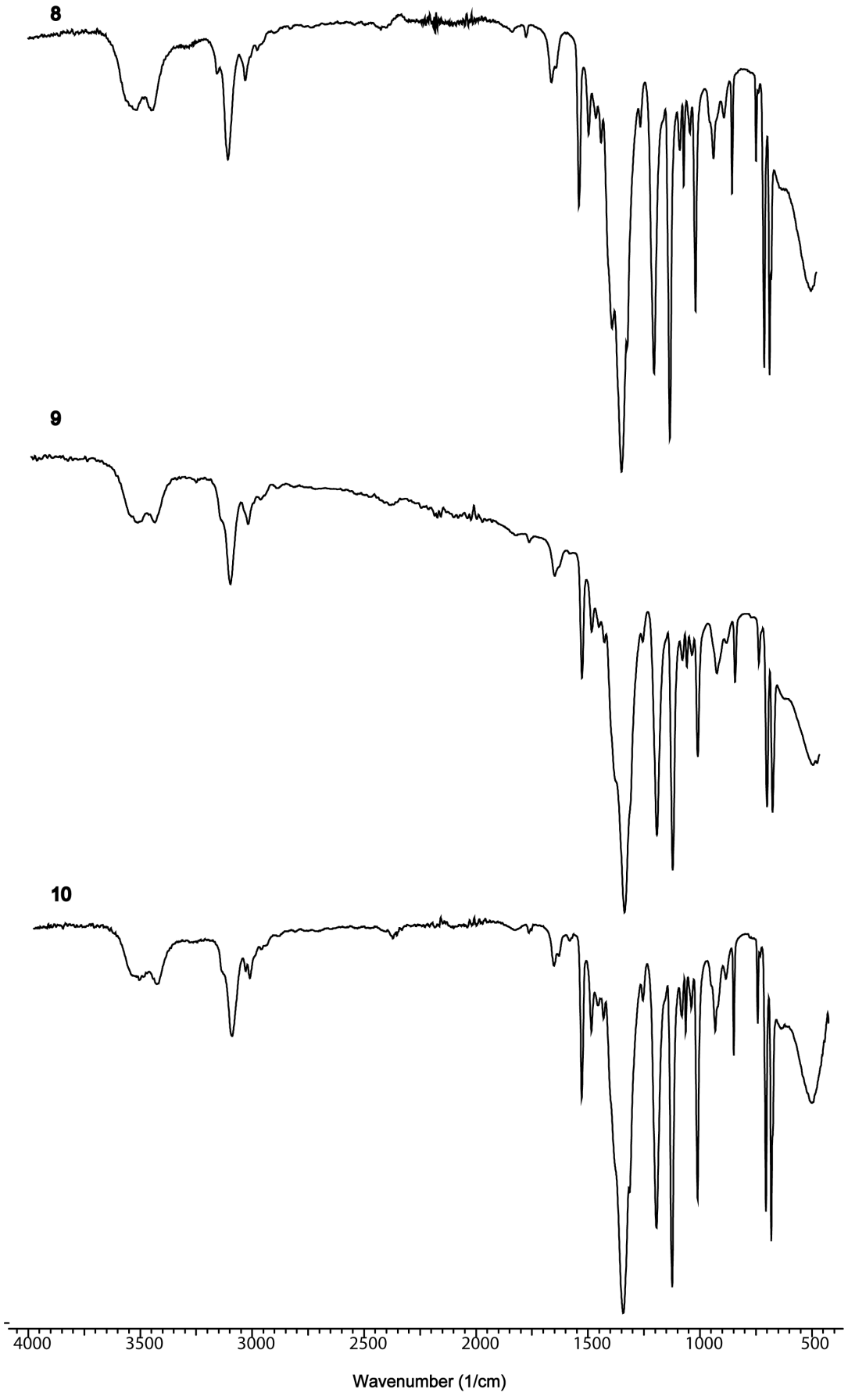


Figure S21. Infrared spectra of **8**, **9** and **10**.

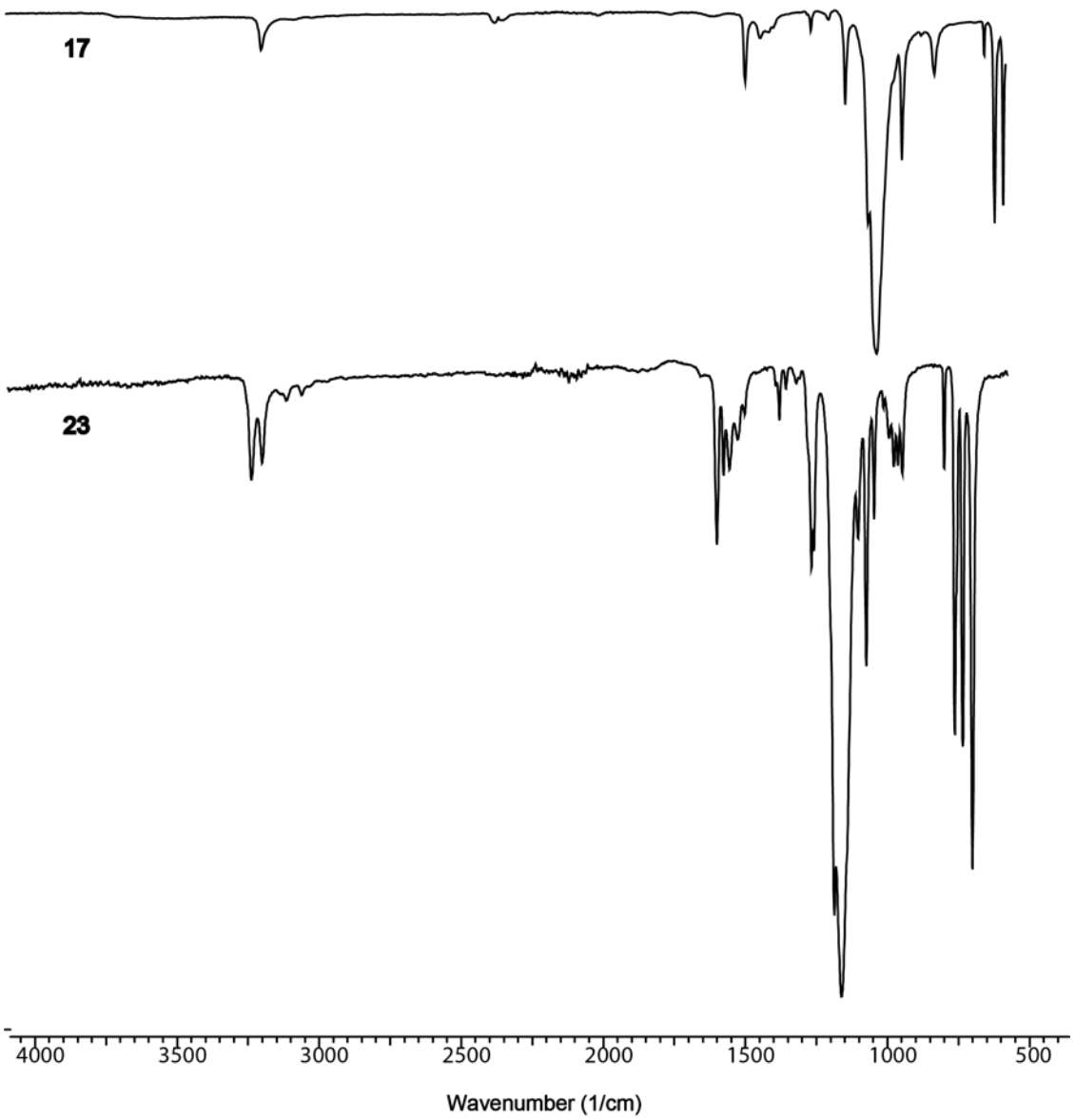


Figure S22. Infrared spectra of **17** and **23**.

19.7.4 DTA plots of 1–10, 12–14, 27 and 29–37

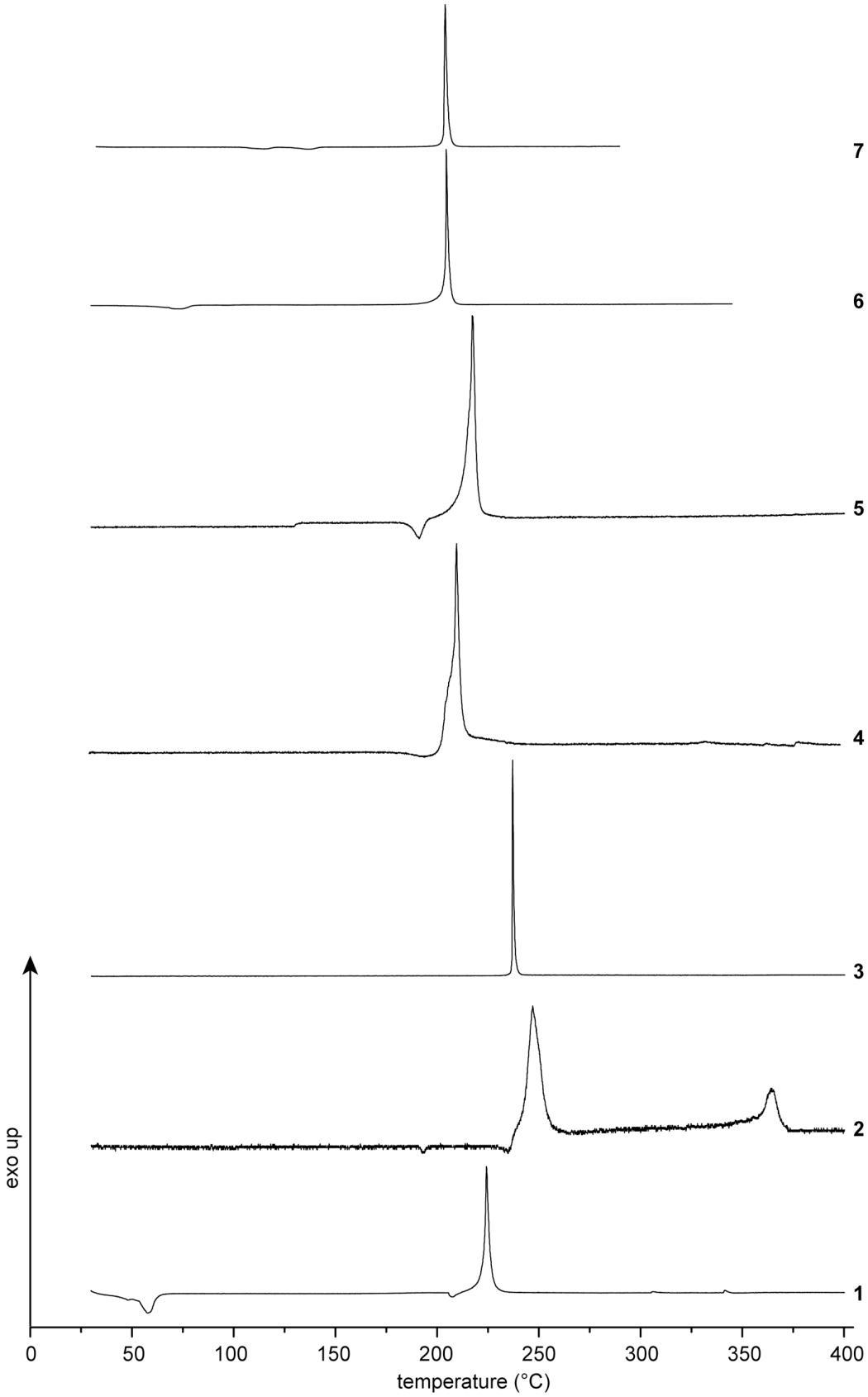


Figure S23. DTA plots of **1**–**7**.

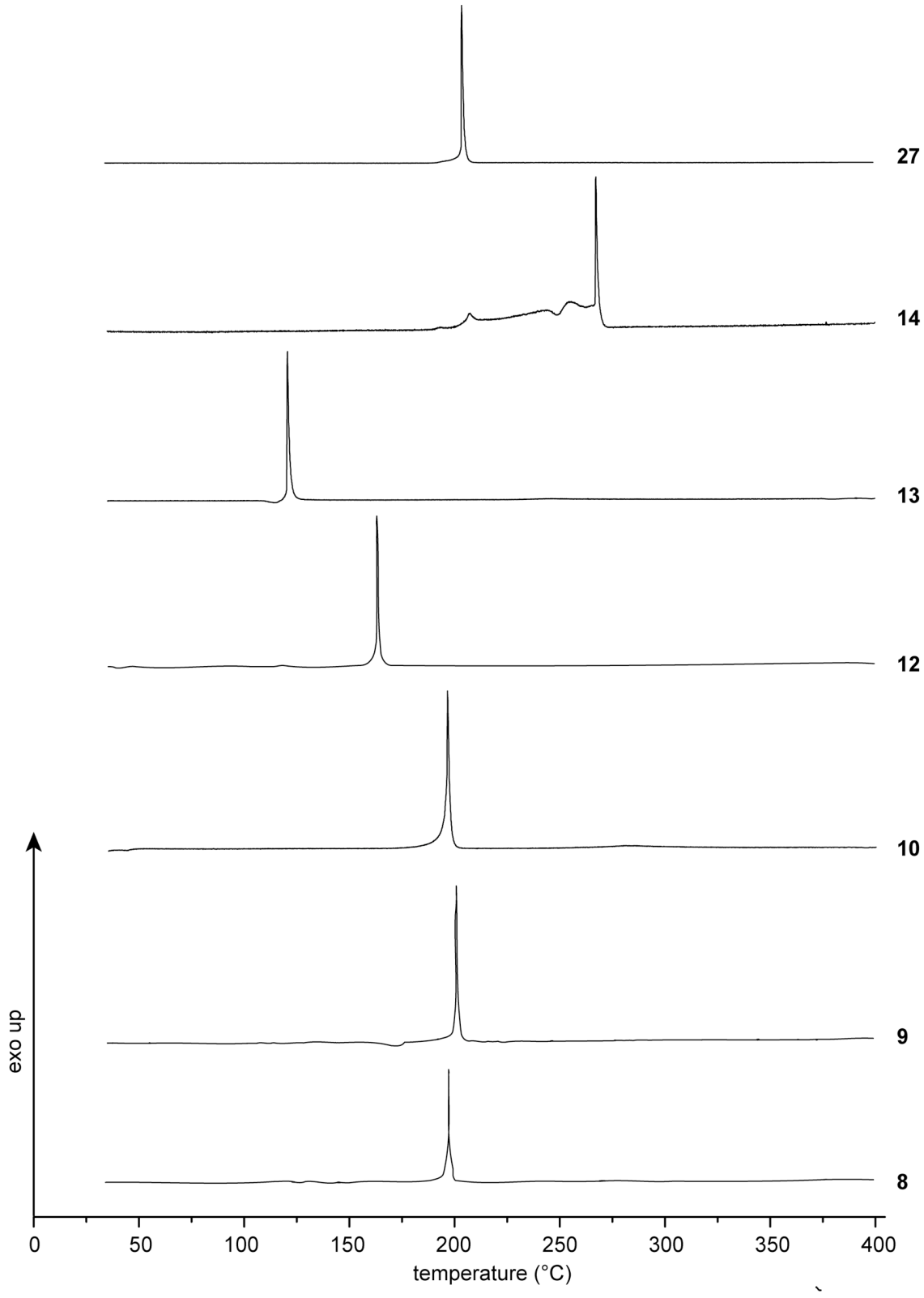


Figure S24. DTA plots of **8**–**10**, **12**–**14** and **27**.

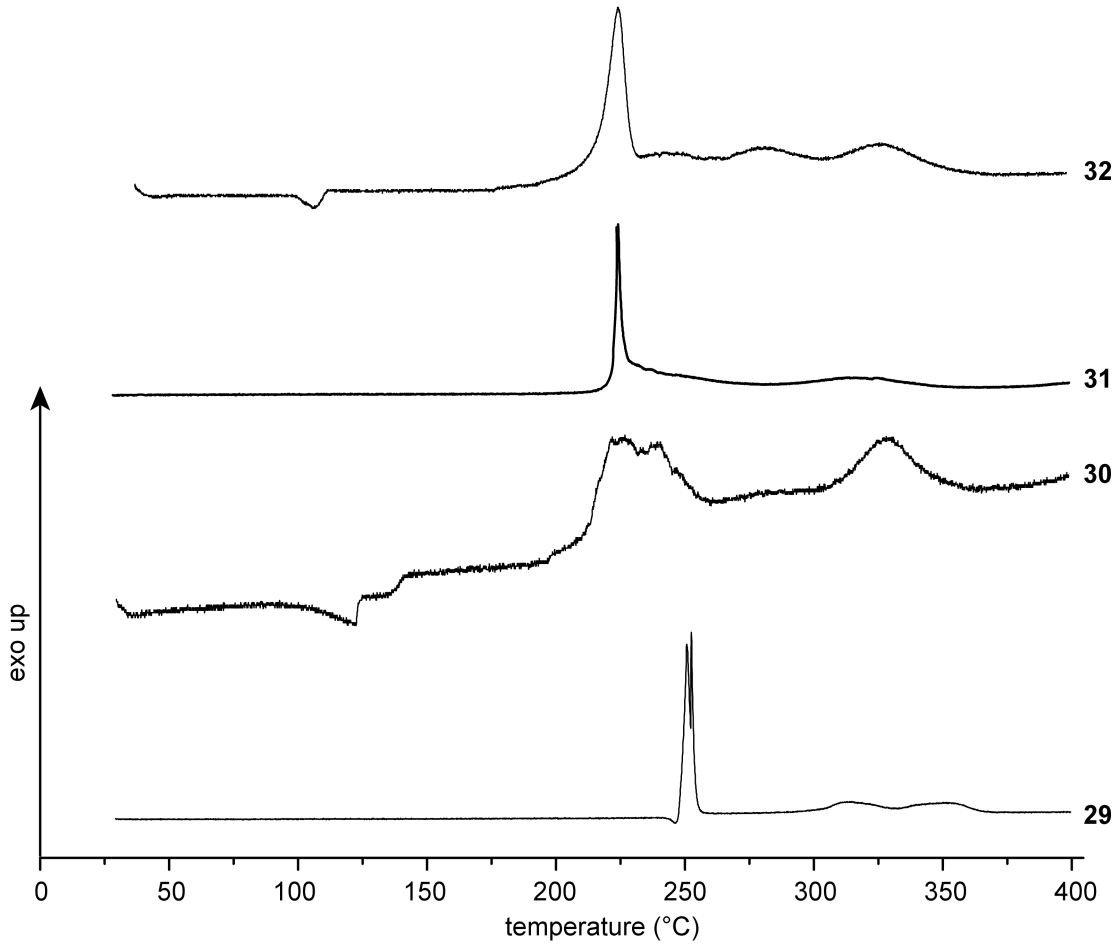


Figure S25. DTA plots of **29**–**32**.

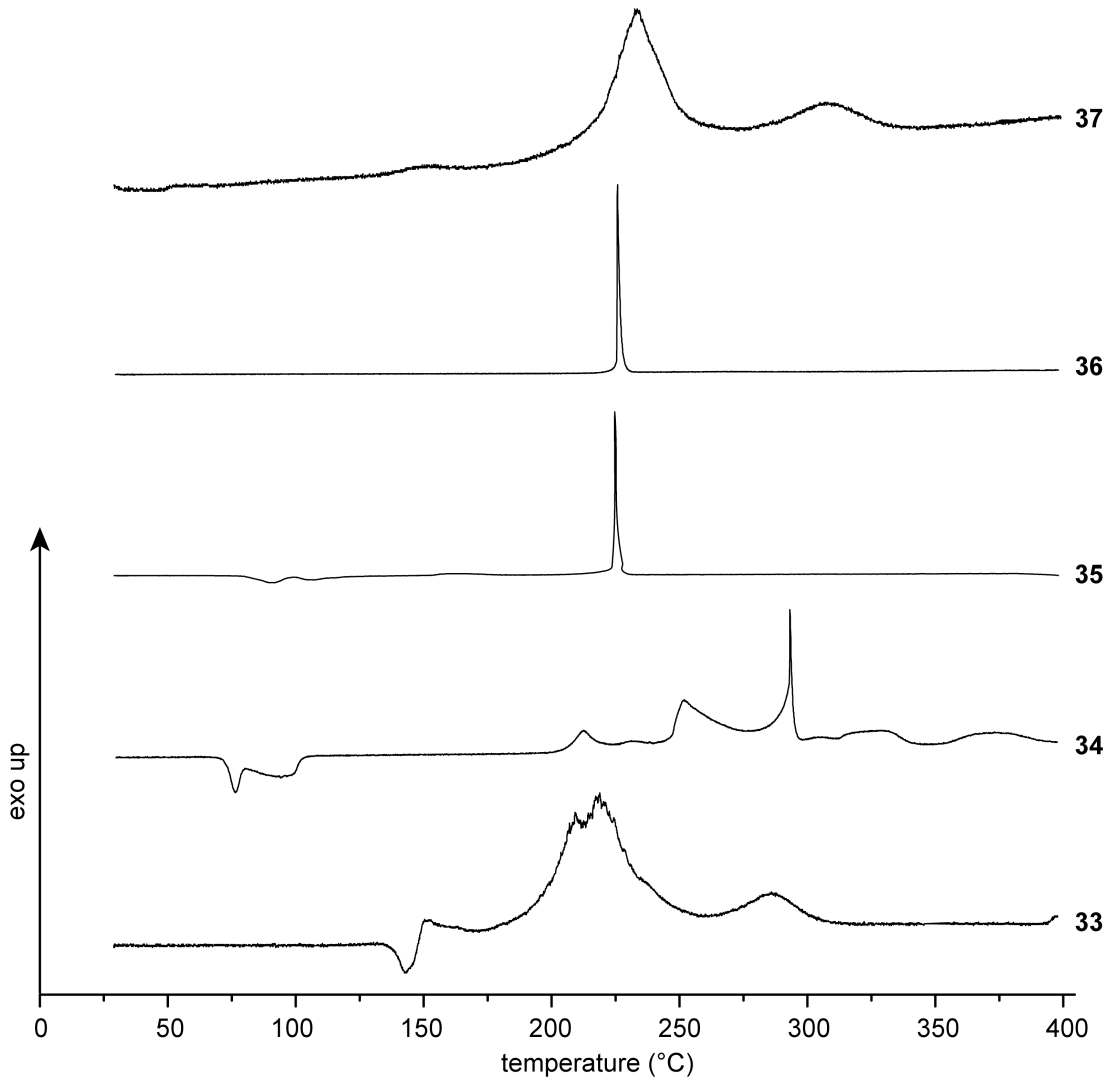


Figure S26. DTA plots of **33**–**37**.

19.7.5 Thermal Gravimetric Analysis of 4, 9, 17 and 24

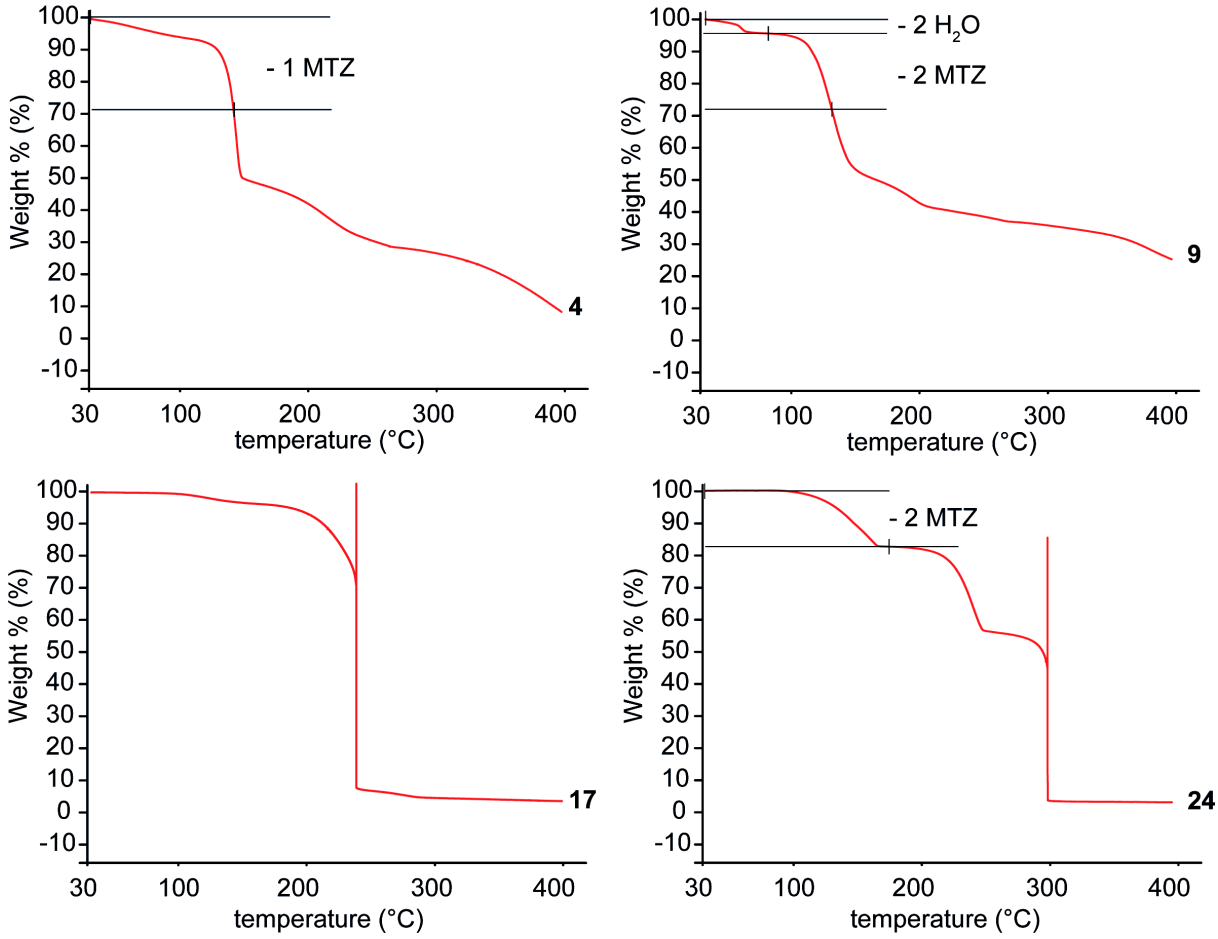


Figure S27. TGA plots of **4**, **9**, **17** and **24**.

19.7.6 Column Diagrams of the Complexes 15–26

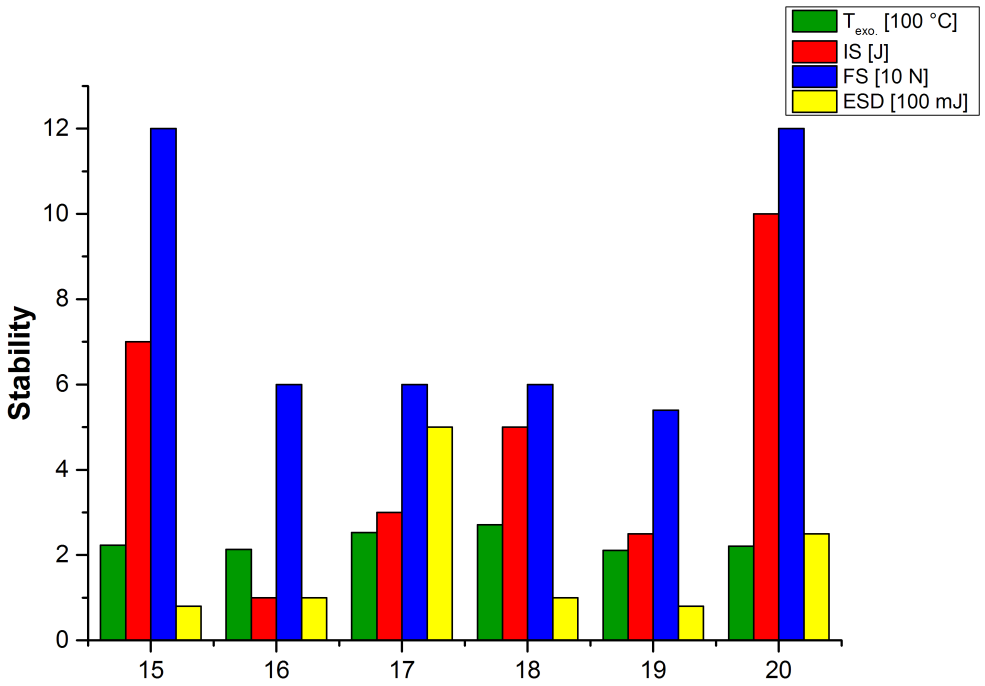


Figure S28. Stabilities of the metal(II) perchlorate complexes **15–20**.

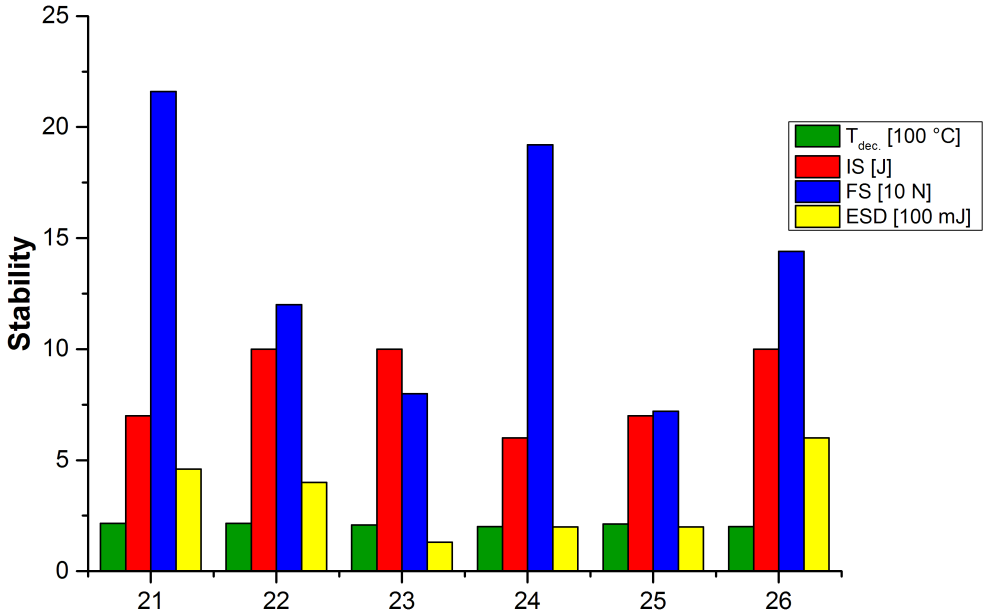


Figure S29. Stabilities of the cocrystallized metal(II) perchlorate complexes **21–26**.

19.7.7 Hot Plate and Hot Needle Tests



Figure S30. Deflagration of compound **19** during the hot plate test.

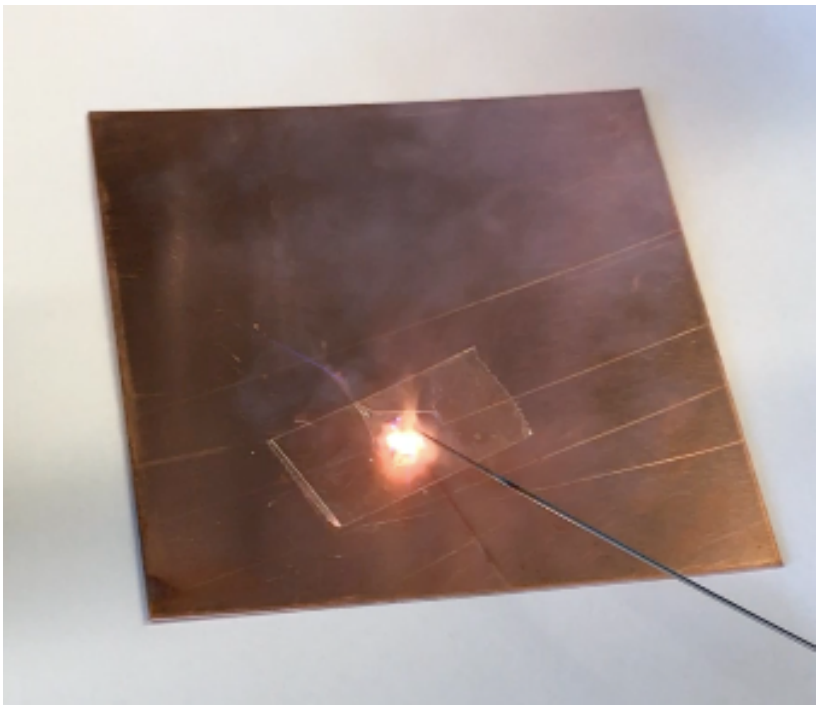


Figure S31. Moment of ignition during the hot needle test of $[Cu(MTZ)_6](ClO_4)_2$ (**19**).

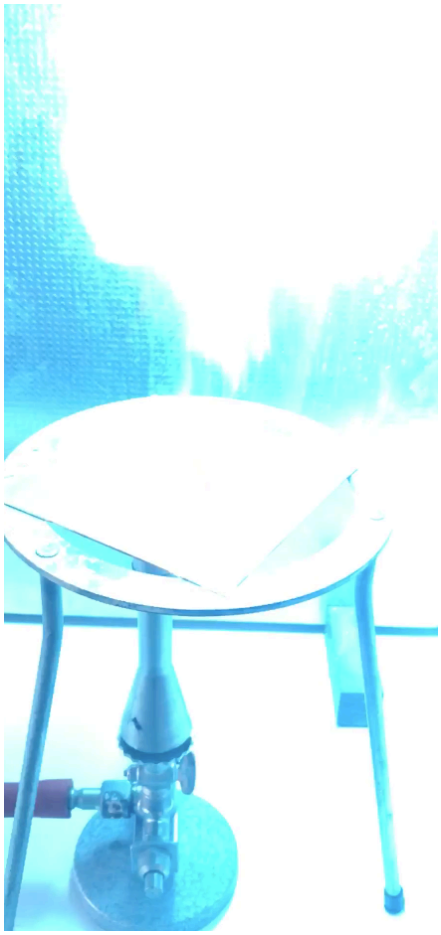


Figure S32. Deflagration of compound **25** during the hot plate test.

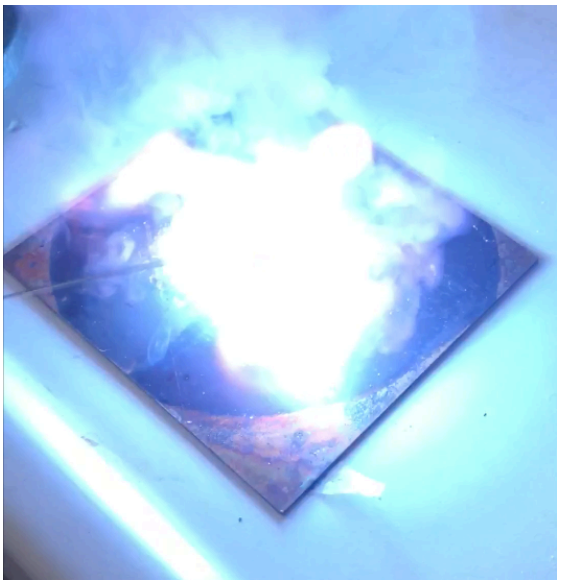


Figure S33. Hot needle test of $[Cu(MTZ)_6](ClO_4)_2 \cdot 2\ MTZ$ (**25**).

19.7.8 Laser Ignition Tests

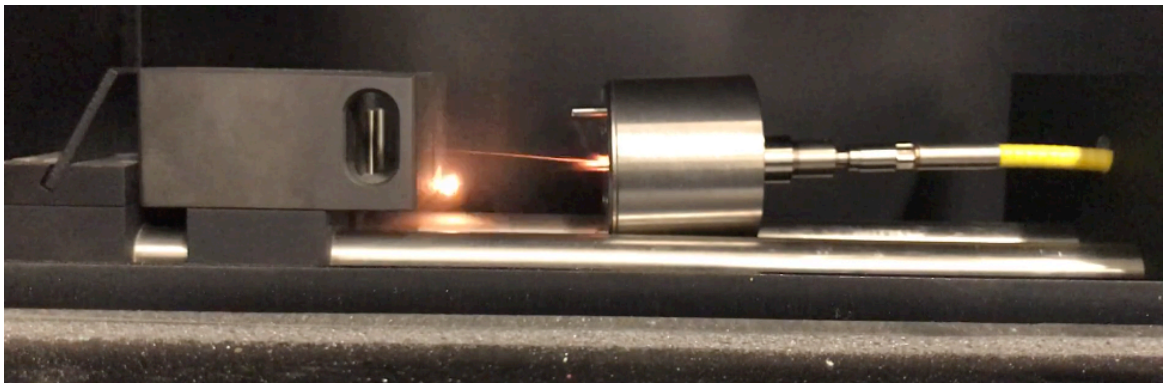


Figure S34. Moment of deflagration of $[Co(NH_3)_4(MTZ)_2](ClO_4)_3$ (**14**) during the laser initiation tests.

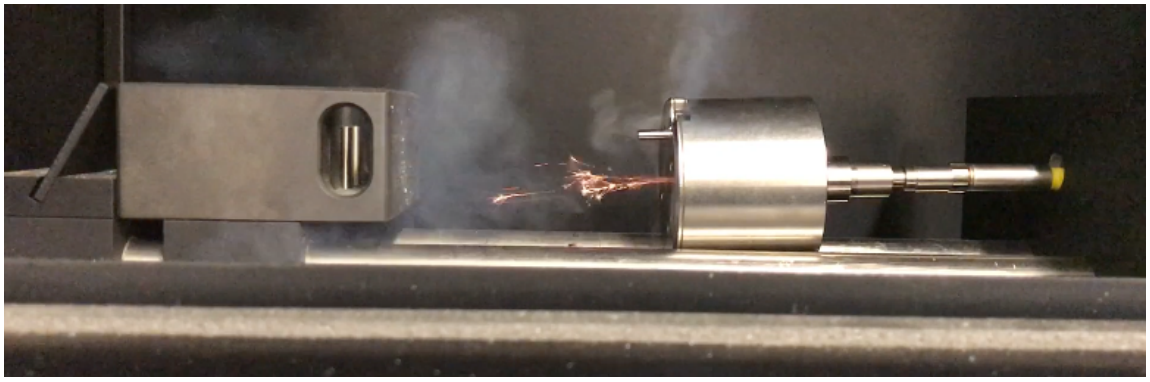


Figure S35. Deflagration of compound **16** during the laser ignition experiments.

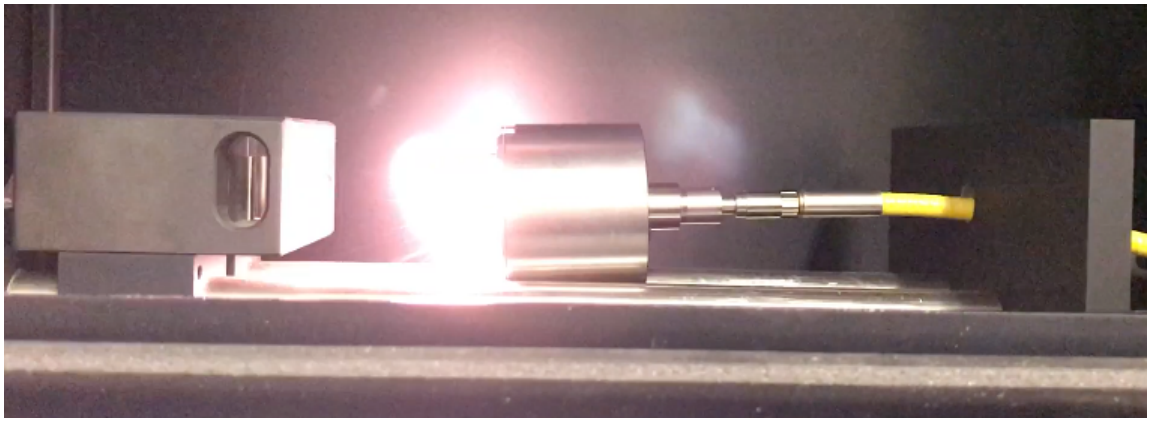


Figure S36. Reaction of compound **18** to laser irradiation.

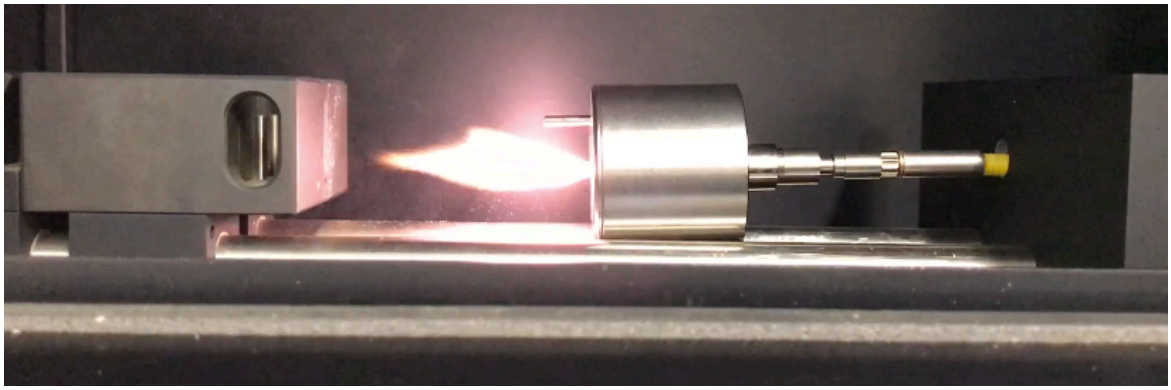


Figure S37. Deflagration of compound **24** during the laser ignition experiments.

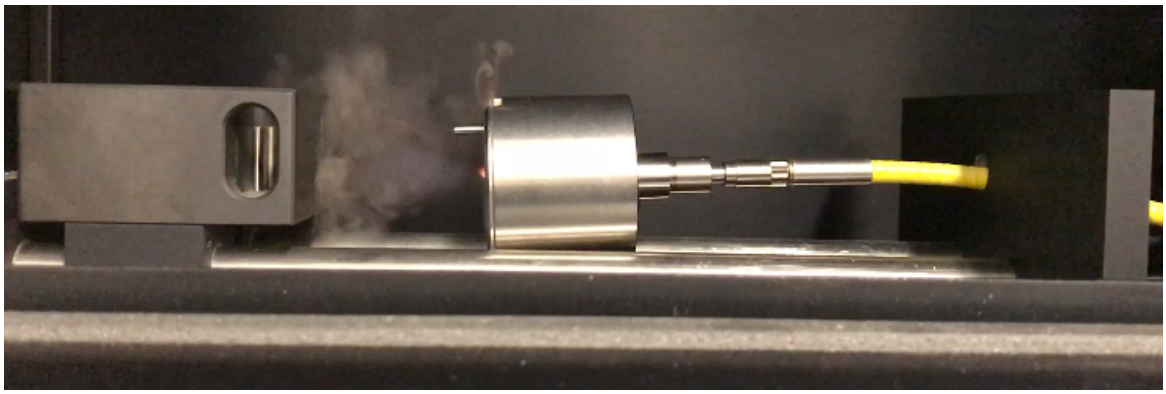


Figure S38. Moment of deflagration of compound **36**.

19.7.9 UV-Vis Spectra of 15, 20–27, 31 and 36

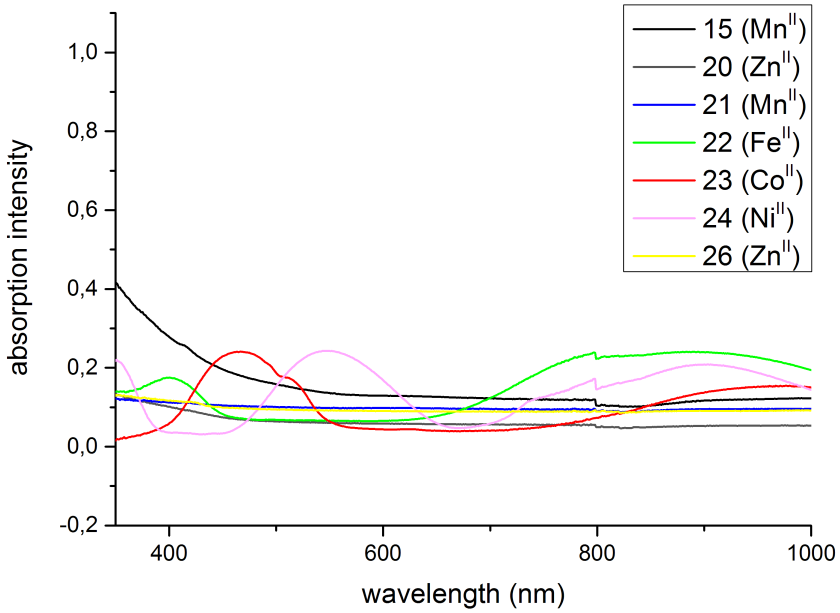


Figure S39. UV-Vis spectra in the solid state of compounds **15**, **20–24** and **26**.

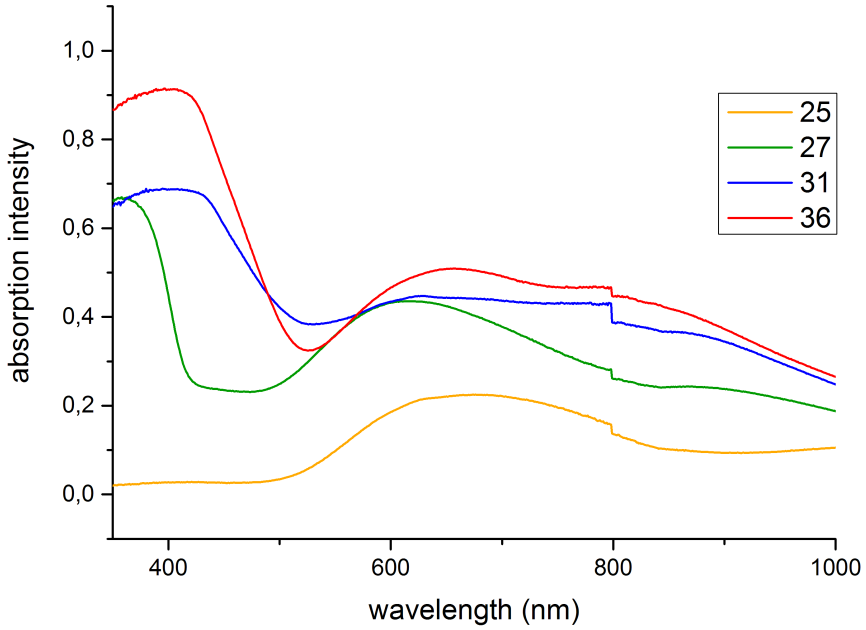


Figure S40. UV-Vis spectra in the solid state of the copper(II) complexes **25**, **27**, **31** and **36**.

19.7.10 Experimental Part

All chemicals and solvents were employed as received (Sigma-Aldrich, Fluka, Acros, ABCR). ^{1}H and ^{13}C NMR spectra were recorded with at ambient temperature using a JEOL Eclipse 270, JEOL EX 400 or a JEOL Eclipse 400 instrument. The chemical shifts quoted in ppm in the text refer to typical standards such as tetramethylsilane (^{1}H, ^{13}C). Endothermic and exothermic events of the described compounds, which indicate melting, evaporation or decomposition, are given as the extrapolated onset temperatures. The samples were measured in a range of 25–400 °C at a heating rate of 5 °C min^{-1} through differential thermal analysis (DTA) with an OZM Research DTA 552-Ex instrument, through differential scanning calorimetry (DSC) with a LINSEIS DSC PT10 or by thermal gravimetric analysis (TGA) with a PerkinElmer TGA4000. Infrared spectra were measured with pure samples on a Perkin-Elmer BXII FT-IR system with a Smith DuraSampler IR II diamond ATR. Determination of the carbon, hydrogen and nitrogen contents were carried out by combustion analysis using an Elementar Vario El (nitrogen values determined are often lower than the calculated ones due to their explosive behavior). UV-Vis spectra were recorded in the solid state using a Varian Cary 500 spectrometer in the wavelength range of 350–1000 nm. Impact sensitivity tests were carried out according to STANAG 4489[S9] with a modified instruction[S10] using a BAM (Bundesanstalt für Materialforschung) drophammer.[S11] Friction sensitivity tests were carried out according to STANAG 4487[S12] with a modified instruction[S13] using the BAM friction tester. The classification of the tested compounds results from the "UN Recommendations on the Transport of Dangerous Goods".[S14] Additionally all compounds were tested upon the sensitivity toward electrical discharge using the OZM Electric Spark Tester ESD 2010 EN.[S15] Liquid-dried luminescent bacteria of the strain Vibrio fischeri NRRL-B-11177 provided by the HACH LANGE GmbH were used for the luminescent bacteria inhibition test to determine their toxicity toward aquatic organisms according to a modified procedure.[S16]

The obtained coordination compounds were washed with cold ethanol when stated, dried overnight in air and used for analytics without further purification.

CAUTION! *All investigated compounds are potentially explosive energetic materials, which show partly increased sensitivities toward various stimuli (e.g. elevated temperatures, impact, friction or electrostatic discharge). Therefore, proper security precautions (safety glass, face*

shield, earthed equipment and shoes, leather coat, Kevlar gloves, Kevlar sleeves and ear plugs) have to be applied while synthesizing and handling the described compounds.

1-Methyl-5*H*-tetrazole (1)

The synthesis of 1-methyl-5*H*-tetrazole was performed according to a modified literature procedure:[S17] To a stirring suspension of 1*H*-tetrazole (8.00 g, 114 mmol) and potassium carbonate (15.9 g, 115 mmol) in acetone (30 mL), methyl iodide (8 mL, 129 mmol) was added dropwise over a time period of 10 min. The resulting reaction mixture was stirred for 16 h at 40 °C under reflux, cooled to room temperature, filtered and washed with acetone (60 mL). The organic layers were combined and the solvent was removed under reduced pressure. The resulting isomeric mixture was purified using vacuum distillation to afford 2-methyl-5*H*-tetrazole (40 °C, 12 mbar; 2.22 g, 26.6 mmol, 23 %) as a colorless clear liquid and compound **1** (90 °C, 0.01 mbar) in form of colorless crystals. Yield: 4.59 g (54.6 mmol, 48 %).

DTA (5 °C min^{-1}): 39 °C (endothermic), 206 °C (exothermic); IR (ATR, cm^{-1}): $\tilde{\nu}$ = 3111 (m), 3032 (vw), 2962 (vw), 1843 (vw), 1491 (m), 1477 (m), 1471 (m), 1445 (w), 1422 (w), 1413 (w), 1384 (vw), 1276 (w), 1220 (w), 1172 (s), 1107 (vs), 1053 (w), 1043 (w), 1019 (w), 965 (s), 924 (m), 876 (w), 722 (w), 678 (vs), 664 (s), 657 (s); ^{1}H NMR (DMSO-d_6, 25 °C, ppm) δ: 9.31 (s, 1H, -C*H*), 4.10 (s, 3H, -CH_3); ^{13}C NMR (DMSO-d_6, 25 °C, ppm) δ: 144.5 (-*C*N$_4$), 34.1 (-*C*H$_3$); EA: ($C_2H_4N_4$ 84.08) calcd: C 28.57, H 4.80, N 66.63 %; found: C 28.47, H 4.89, N 65.51 %; BAM drophammer: > 40 J; friction tester: > 360 N; ESD: 1.50 J (at grain size < 100 μm).

[Fe(MTZ)$_6$](FeCl$_4$)$_2$ (2)

An aqueous solution of MTZ (151 mg, 1.80 mmol) was added to an aqueous solution of anhydrous iron(II) chloride (38.0 mg, 0.30 mmol). The reaction mixture was stirred for 1 min and left to crystallize. After one week, a powder was isolated, which was recrystallized from ethanol. Yellow crystals of **2**, which were suitable for X-ray, started to crystallize within 4 days. The crystals were filtered off and dried in air. Yield: 48.0 mg (0.05 mmol, 17 %).

DTA (5 °C min^{-1}): 236 °C (exothermic); IR (ATR, cm^{-1}): $\tilde{\nu}$ = 3142 (m), 2167 (w), 1761 (w), 1570 (w), 1519 (m), 1426 (w), 1300 (w), 1183 (s), 1158 (w), 1109 (vs), 1068 (w), 995 (s), 883 (m), 720 (w), 683 (s), 656 (s); EA ($C_{12}H_{24}Cl_8Fe_2N_{24}$, 955.63) calc.: C 15.08, H 2.53, N 35.18 %; found: C 15.64, H 2.68, N 35.24 %.

General procedure for the preparation of metal(II) (Mn^{II}, Cu^{II}, Zn^{II}) MTZ chloride complexes (3–5):

1-Methyl-5*H*-tetrazole (**1**, 85.0 mg, 1.00 mmol) was dissolved in distilled water (0.5 mL) at room temperature. The corresponding aqueous metal(II) chloride solution (**3**: manganese(II) chloride dihydrate (81.0 mg, 0.50 mmol); **4**: copper(II) chloride dihydrate (85.0 mg, 0.50 mmol); **5**: zinc(II) chloride (68.0 mg, 0.50 mmol)) was added and the reaction mixture stirred mechanically for 1 min at room temperature. The colored solutions were left to crystallize, the solids were filtered off, washed with cold ethanol (2 mL) and dried in air.

$[MnCl_2(MTZ)_2]$ (3)

Compound **3** was obtained within 6 days in the form of colorless blocks suitable for X-ray determination. Yield: 121 mg (0.41 mmol, 82 %).

DTA (5 °C min^{-1}): 234 °C (exothermic); IR (ATR, cm^{-1}): $\tilde{\nu}$ = 3139 (m), 3120 (m), 3039 (vw), 3007 (vw), 2965 (vw), 1771 (vw), 1511 (s), 1467 (m), 1422 (w), 1290 (w), 1230 (vw), 1176 (vs), 1106 (vs), 1059 (w), 1018 (w), 987 (s), 881 (m), 718 (w), 680 (vs), 653 (s); EA ($C_4H_8Cl_2MnN_8$, 294.00): calcd: C 16.34, H 2.74, N 38.11 %; found: C 16.61, H 2.74, N 38.24 %; BAM drophammer: > 40 J; friction tester: > 360 N; ESD: 1.50 J (at grain size 100–500 μm).

$[CuCl_2(MTZ)_2]$ (4)

Complex **4** was isolated in the form of turquoise crystals. Yield: 69.0 mg (0.23 mmol, 46 %).

DTA (5 °C min^{-1}): 185 °C (endothermic), 199 °C (exothermic); IR (ATR, cm^{-1}): $\tilde{\nu}$ = 3137 (m), 3036 (w), 2961 (w), 1757 (vw), 1513 (s), 1467 (m), 1446 (m), 1421 (w), 1292 (w), 1236 (w), 1175 (s), 1098 (vs), 1062 (w), 1022 (m), 996 (s), 880 (s), 716 (w), 681 (vs), 653 (s); EA: ($C_4H_8Cl_2CuN_8$, 302.61) calcd: C 15.88, H 2.66, N 37.03 %; found: C 16.28, H 2.79, N 37.12 %; BAM drophammer: > 40 J; friction tester: > 360 N; ESD: 1.30 J (at grain size 500–1000 µm).

$[ZnCl_2(MTZ)_2]$ (5)

Product **5** was obtained within 8 days in the form of a colorless solid. Yield: 111 mg (0.37 mmol, 73 %).

DTA (5 °C min^{-1}): 184 °C (endothermic), 204 °C (exothermic); IR (ATR, cm^{-1}): $\tilde{\nu}$ = 3139 (s), 1519 (s), 1309 (m), 1302 (m), 1181 (vs), 1110 (s), 1101 (vs), 1064 (m), 1028 (m), 1012 (m), 1002 (m), 994 (s), 890 (s), 883 (s), 718 (m), 679 (vs), 651 (s); EA: ($C_4H_8Cl_2N_8Zn$, 304.45) calcd: C 15.78, H 2.65, N 36.81 %; found: C 15.80, H 2.60, N 36.34 %; BAM drophammer: > 40 J; friction tester: > 360 N; ESD: 1.50 J (at grain size < 100 µm).

General procedure for the preparation of metal(II) (Co^{II}, Ni^{II}) MTZ chloride complexes (6/7):

An aqueous solution of MTZ (252 mg, 3.00 mmol) was added to the corresponding aqueous metal(II) chloride solution (**6**: cobalt(II) chloride hexahydrate (119 mg, 0.50 mmol); **7**: nickel(II) chloride hexahydrate (119 mg, 0.50 mmol)) and stirred mechanically for 1 min at room temperature. The reaction mixtures were left to crystallize, the resulting solids were filtered off, washed with cold ethanol (2 mL) and dried in air.

$[CoCl_2(MTZ)_4]$ • 2 MTZ (6)

The cocrystal compound **6** was obtained within 6 days in the form of yellow blocks suitable for X-ray determination. Yield: 72.0 mg (0.11 mmol, 23 %).

DTA (5 °C min^{-1}): 66 °C (endothermic), 206 °C (exothermic); IR (ATR, cm^{-1}): $\tilde{\nu}$ = 3173 (w), 3101 (m), 3030 (w), 2965 (w), 2005 (vw), 1812 (vw), 1790 (vw), 1728 (vw), 1515 (m), 1490 (m), 1474 (m), 1446 (m), 1425 (w), 1291 (w), 1233 (vw), 1178 (s), 1105 (vs), 1063 (w), 1024 (w), 991 (s), 964 (w), 909 (m), 898 (m), 865 (m), 721 (w), 682 (s), 655 (s); EA ($C_{12}H_{24}Cl_2CoN_{24}$, 634.33): calcd: C 22.72, H 3.81, N 53.00 %; found: C 23.65, H 4.01, N 53.70 %; BAM drophammer: > 40 J; friction tester: > 360 N; ESD: 1.00 J (at grain size < 100 µm).

[NiCl$_2$(MTZ)$_4$] • 2 MTZ (7)

Nickel(II) complex **7** was obtained as a blue solid within 13 days. Yield: 223 mg (0.35 mmol, 70 %).

DTA (5 °C min^{-1}): 106 °C (endothermic), 199 °C (dec.); IR (ATR, cm^{-1}): $\tilde{\nu}$ = 3177 (w), 3107 (m), 3096 (m), 3023 (w), 2969 (w), 1817 (w), 1789 (w), 1739 (w), 1515 (m), 1491 (w), 1476 (m), 1444 (m), 1428 (w), 1366 (w), 1292 (w), 1280 (w), 1217 (w), 1181 (s), 1175 (s), 1104 (vs), 1065 (w), 1029 (w), 994 (m), 964 (w), 912 (w), 898 (m), 864 (m), 722 (w), 684 (s), 660 (s), 652 (s); EA: ($C_{12}H_{24}Cl_2N_{24}Ni$, 634.09) calcd: C 22.73, H 3.82, N 53.02 %; found: C 22.25, H 3.99, N 50.75 %; BAM drophammer: > 40 J; friction tester: > 360 N; ESD: 0.80 J (at grain size < 100 µm).

General procedure for the preparation of metal(II) (Co^{II}, Ni^{II}, Zn^{II}, Cu^{II}) MTZ nitrate complexes (8–11):

The nitrogen-rich ligand MTZ (**8**, **9**, **11**: 126 mg, 1.50 mmol; **10**: 151 mg, 1.80 mmol) was dissolved in a minimum amount of water and added to an aqueous solution of the corresponding metal(II) nitrate (**8**: cobalt(II) nitrate hexahydrate (73.0 mg, 0.25 mmol); **9**: nickel(II) nitrate hexahydrate (73.0 mg, 0.25 mmol); **10**: zinc(II) nitrate hexahydrate (89.2 mg, 0.30 mmol); **11**: copper(II) nitrate trihydrate (60.0 mg, 0.25 mmol)) and stirred mechanically for 1 min at room temperature. The reaction mixtures were left to crystallize until a solid material appeared. The products were filtered off, washed with cold ethanol (2 mL) and dried in air.

$[Co(MTZ)_6](NO_3)_2 \cdot 2\ H_2O$ (8)

After three days compound **8** was isolated in the form of orange crystals suitable for X-ray determination. Yield: 124 mg (0.19 mmol, 72 %).

DTA (5 °C min^{-1}): 73 °C (endothermic), 195 °C (exothermic); IR (ATR, cm^{-1}): $\tilde{\nu}$ = 3513 (w), 3446 (w), 3150 (w), 3100 (m), 3022 (w), 2968 (vw), 1758 (vw), 1643 (w), 1622 (vw), 1519 (m), 1475 (w), 1442 (w), 1419 (w), 1370 (s), 1327 (vs), 1301 (s), 1242 (w), 1180 (s), 1109 (vs), 1064 (w), 1047 (m), 1019 (w), 993 (s), 912 (w), 866 (w), 829 (m), 720 (w), 684 (s), 660 (s), 652 (m), 616 (vw), 483 (w); EA: ($C_{12}H_{28}CoN_{26}O_8$, 723.46) calcd: C 19.92, H 3.90, N 50.34 %; found: C 20.34, H 4.01, N 50.18 %; BAM drophammer: > 40 J; friction tester: > 360 N; ESD: 1.50 J (at grain size < 100 μm).

$[Ni(MTZ)_6](NO_3)_2 \cdot 2\ H_2O$ (9)

The nickel(II) nitrate complex **9** was obtained in the form of purple crystals suitable for X-ray determination within 4 days. Yield: 142 mg (0.21 mmol, 83 %).

DTA (5 °C min^{-1}): 86 °C (endothermic), 166 °C (endothermic), 194 °C (exothermic); IR (ATR, cm^{-1}): $\tilde{\nu}$ = 3521 (w), 3446 (w), 3103 (w), 3023 (w), 2967 (vw), 1757 (vw), 1642 (vw), 1519 (m), 1475 (w), 1442 (w), 1418 (w), 1327 (vs), 1245 (w), 1181 (s), 1110 (s), 1066 (w), 1046 (w), 1023 (w), 997 (m), 911 (w), 869 (w), 829 (w), 721 (w), 685 (m), 660 (m), 486 (w); EA: ($C_{12}H_{28}N_{26}NiO_8$, 723.22) calcd: C 19.93, H 3.90, N 50.36 %; found: C 20.51, H 3.87, N 50.47 %; BAM drophammer: > 40 J; friction tester: 324 N; ESD: 1.50 J (at grain size 100–500 μm).

$[Zn(MTZ)_6](NO_3)_2 \cdot 2\ H_2O$ (10)

From the reaction mixture, complex **10** could be isolated in the form of colorless crystals suitable for X-ray determination after one week. Yield: 124 mg (0.17 mmol, 57 %).

DTA (5 °C min^{-1}): 196 °C (exothermic); TGA (5 °C min^{-1}): 50–75 °C (loss of crystal water); IR (ATR, cm^{-1}): $\tilde{\nu}$ = 3522 (w), 3442 (w), 3102 (w), 3021 (w), 1644 (w), 1518 (m), 1474 (w), 1419 (w), 1330 (vs), 1301 (s), 1241 (w), 1179 (s), 1108 (vs), 1065 (w), 1047 (w), 1021 (w),

993 (s), 913 (w), 829 (m), 721 (w), 684 (s), 659 (s), 616 (w), 473 (m), 418 (m); EA ($C_{12}H_{28}N_{26}O_8Zn$, 729.41) calcd: C 19.75, H 3.87, N 49.89 %; found: C 20.01, H 3.58, N 50.00 %; BAM drophammer: > 40 J; friction tester: > 360 N; ESD: 400 mJ (at grain size 100–500 µm).

$[Cu(MTZ)_6](NO_3)_2 \cdot 2\ H_2O$ (11)

Within 8 days, compound **11** was obtained with two crystal water molecules in the form of blue blocks suitable for X-ray determination. After drying in air overnight the compound lost the crystal water molecules and was analyzed in its anhydrous form **12**.

$[Cu(MTZ)_6](NO_3)_2$ (12)

The water-free copper(II) nitrate complex was isolated as a blue solid. Yield: 137 mg (0.20 mmol, 79 %).

DTA (5 °C min^{-1}): 160 °C (exothermic); IR (ATR, cm^{-1}): $\tilde{\nu}$ = 3132 (w), 3035 (w), 2970 (vw), 2378 (w), 1745 (w), 1523 (m), 1507 (w), 1471 (w), 1414 (w), 1340 (vs), 1288 (m), 1234 (w), 1217 (w), 1172 (s), 1106 (vs), 1072 (w), 1027 (m), 1005 (m), 980 (m), 907 (m), 898 (m), 830 (m), 722 (w), 682 (s), 658 (s); (EA: $C_{12}H_{24}CuN_{26}O_6$, 692.05) calcd: C 20.83, H 3.50, N 52.62 %; found: C 20.99, H 3.76, N 52.68 %; BAM drophammer: > 40 J; friction tester: > 360 N; ESD: 1.50 J (at grain size 100–500 µm).

$[AgNO_3(MTZ)_2]$ (13)

Silver(I) nitrate (84.9 mg, 0.50 mmol) and MTZ (84.1 mg, 1.00 mmol) were mixed, dissolved in water and mechanically stirred for 1 minute at room temperature. From this solution, complex **13** could be obtained in the form of colorless blocks suitable for X-ray determination after one week. The crystals were filtered off and dried in air. Yield: 93.8 mg (0.28 mmol, 55 %).

DTA (5 °C min^{-1}): 119 °C (dec.); IR (ATR, cm^{-1}): $\tilde{\nu}$ = 3254 (w), 3118 (m), 1571 (w), 1504 (m), 1470 (m), 1449 (w), 1326 (vs), 1283 (s), 1235 (m), 1175 (m), 1108 (s), 1057 (w), 1039 (w), 986 (m), 899 (m), 820 (m), 717 (w), 679 (m), 657 (s); EA ($C_4H_8AgN_9O_3$, 338.04) calcd: C 14.21, H 2.39, N 37.29 %; found: C 14.49, H 2.44, N 37.09 %; BAM drophammer: 40 J; friction tester: 160 N; ESD: 0.15 J (at grain size < 100 µm).

$[Co(NH_3)_4(MTZ)_2](ClO_4)_3$ (14)

MTZ (294 mg, 3.50 mmol) was dissolved in perchloric acid (15 %, 2 mL), added to a hot solution of carbonatotetraaminecobalt(III) perchlorate (501 mg, 1.80 mmol) in diluted perchloric acid (15 %, 15 mL) and stirred under reflux for 4 hours. After cooling down to room temperature, the solution was left to crystallize. The resulting powder was filtered off and recrystallized from hot water yielding an orange amorphous powder. Yield: 187 mg (0.32 mmol, 18 %).

DTA (5 °C min^{-1}): 201 °C (exothermic); IR (ATR, cm^{-1}): $\tilde{\nu}$ = 3308 (m), 3231 (m), 1624 (w), 1391 (w), 1342 (m), 1196 (w), 1041 (vs), 930 (m), 830 (s), 688 (m), 659 (m), 618 (vs); UV-Vis spectrum: λ_{max} = 463 nm; EA ($C_4H_{20}N_{12}O_{12}Cl_3Co$, 593.57) calcd: C 8.09, H 3.40, N 29.32 %; found: C 8.36, H 3.34, N 28.24 %; BAM drophammer: 9 J; friction tester: 160 N; ESD: 36 mJ (at grain size < 100 µm).

General procedure for the preparation of metal(II) (Mn^{II}, Fe^{II}, Co^{II}, Ni^{II}, Cu^{II}, Zn^{II}) MTZ perchlorate complexes (15–20):

A solution of 1-methyl-5*H*-tetrazole (**1**, 380 mg, 4.50 mmol) in ethanol (2 mL) was heated to 50 °C and added to the corresponding metal(II) perchlorate salt (**15**: manganese(II) perchlorate hexahydrate (274 mg, 0.75 mmol); **16**: iron(II) perchlorate hexahydrate (272 mg, 0.75 mmol); **17**: cobalt(II) perchlorate hexahydrate (274 mg, 0.75 mmol); **18**: nickel(II) perchlorate hexahydrate (278 mg, 0.75 mmol); **19**: copper(II) perchlorate hexahydrate (278 mg, 0.75 mmol); **20**: zinc(II) perchlorate hexahydrate (279 mg, 0.75 mmol)) dissolved in water (1 mL). The colored reaction mixtures were stirred mechanically for 1 min at room temperature

and left to crystallize. After crystallization, the products were filtered off, washed with ethanol (2 mL) and dried in air.

$[Mn(MTZ)_6](ClO_4)_2$ (15)

Within one week, colorless blocks suitable for X-ray determination were obtained from the mother liquor. Yield: 442 mg (0.58 mmol, 77 %).

DTA (5 °C min^{-1}): 223 °C (exothermic); IR (ATR, cm^{-1}): $\tilde{\nu}$ = 3142 (m), 2970 (vw), 1514 (m), 1494 (w), 1472 (w), 1445 (w), 1296 (w), 1236 (vw), 1184 (m), 1105 (vs), 1080 (vs), 988 (s), 965 (m), 896 (m), 884 (w), 866 (w), 720 (w), 682 (s), 654 (s); UV-Vis spectrum: λ_{max} = none; EA: ($C_{12}H_{24}N_{24}O_8Cl_2Mn$, 758.32): calcd: C 19.01, H 3.19, N 44.33 %; found: C 19.83, H 3.29, N 44.46 %; BAM drophammer: 7 J; friction tester: 120 N; ESD: 0.08 mJ (at grain size < 100 µm).

$[Fe(MTZ)_6](ClO_4)_2$ (16)

Pale yellow block like crystals of compound **16** were received within five days. Yield: 550 mg (0.72 mmol, 97 %).

DTA (5 °C min^{-1}): 213 °C (exothermic); IR (ATR, cm^{-1}): $\tilde{\nu}$ = 3144 (m), 2970 (vw), 1516 (m), 1493 (w), 1472 (w), 1445 (w), 1298 (w), 1238 (vw), 1184 (m), 1106 (vs), 1082 (vs), 990 (s), 966 (m), 896 (m), 720 (w), 682 (s), 654 (s); UV-Vis spectrum: λ_{max} = 887 nm; EA: ($C_{12}H_{24}N_{24}O_8Cl_2Fe$, 759.23): calcd: C 18.98, H 3.19, N 44.28 %; found: C 19.58, H 3.27, N 44.54 %; BAM drophammer: 1 J; friction tester: 60 N; ESD: 0.10 J (at grain size < 100 µm).

$[Co(MTZ)_6](ClO_4)_2$ (17)

Complex **17** was obtained in the form of orange plates from the mother liquor suitable for X-ray determination within three days. Yield: 562 mg (0.74 mmol, 98 %).

DTA (5 °C min^{-1}): 253 °C (exothermic); IR (ATR, cm^{-1}): $\tilde{\nu}$ = 3144 (w), 1522 (m), 1472 (w), 1443 (w), 1302 (w), 1242 (vw), 1186 (m), 1080 (vs), 996 (s), 932 (w), 888 (m), 720 (w), 686

(s), 658 (s); UV-Vis spectrum: λ_{max} = 464, 960 nm; EA: ($C_{12}H_{24}N_{24}O_8Cl_2Co$, 762.31): calcd: C 18.91, H 3.17, N 44.10 %; found: C 18.51, H 3.14, N 43.33 %; BAM drophammer: 3 J; friction tester: 60 N; ESD: 0.50 J (at grain size < 100 µm).

$[Ni(MTZ)_6](ClO_4)_2$ (18)

After addition of the metal(II) salt solution a fine lilac precipitate was formed. Within two days small lilac platelet like crystals suitable for X-Ray determination were obtained from the mother liquor. Yield: 529 mg (0.69 mmol, 92 %).

DTA (5 °C min^{-1}): 271 °C (exothermic); IR (ATR, cm^{-1}): $\tilde{\nu}$ = 3146 (w), 1524 (m), 1470 (w), 1442 (vw), 1302 (vw), 1246 (vw), 1188 (m), 1080 (vs), 1000 (m), 888 (m), 721 (w), 686 (s), 658 (s); UV-Vis spectrum: λ_{max} = 536, 883 nm; EA: ($C_{12}H_{24}N_{24}O_8Cl_2Ni$, 762.07): calcd: C 18.91, H 3.17, N 44.11 %; found: C 18.93, H 3.22, N 43.42 %; BAM drophammer: 5 J; friction tester: 60 N; ESD: 0.10 J (at grain size < 100 µm).

$[Cu(MTZ)_6](ClO_4)_2$ (19)

Blue rods of **19**, which were suitable for X-ray analysis started to crystallize within one day. Yield: 529 mg (0.69 mmol, 92 %).

DTA (5 °C min^{-1}): 178 °C (endothermic), 211 °C (exothermic); IR (ATR, cm^{-1}): $\tilde{\nu}$ = 3142 (w), 1526 (w), 1470 (w), 1306 (vw), 1274 (vw), 1188 (m), 1080 (vs), 1004 (m), 974 (m), 888 (m), 720 (w), 686 (s), 656 (s); UV-Vis spectrum: λ_{max} = 663 nm; EA: ($C_{12}H_{24}N_{24}O_8Cl_2Cu$, 766.93): calc.: C 18.79, H 3.15, N 43.83 %; found: C 18.57, H 3.24, N 43.71 %; BAM drophammer: 2.5 J; friction tester: 54 N; ESD: 0.08 mJ (at grain size < 100 µm).

$[Zn(MTZ)_6](ClO_4)_2$ (20)

Within two days, X-ray suitable single crystals were obtained in the form of colorless plates. Yield: 543 mg (0.71 mmol, 95 %).

DTA (5 °C min^{-1}): 196 °C (endothermic), 221 °C (exothermic); IR (ATR, cm^{-1}): $\tilde{\nu}$ = 3144 (w), 1516 (m), 1493 (w), 1470 (w), 1446 (w), 1298 (w), 1240 (vw), 1186 (m), 1108 (s), 1084 (vs), 988 (m), 966 (w), 896 (m), 720 (w), 682 (s), 656 (s); UV-Vis spectrum: λ_{max} = none; EA: ($C_{12}H_{24}N_{24}O_8Cl_2Zn$, 768.76): calc.: C 18.75, H 3.15, N 43.73 %; found: C 19.23, H 3.40, N 44.00 %; BAM drophammer: 10 J; friction tester: 120 N; ESD: 0.25 J (at grain size < 100 µm).

General procedure for the preparation of metal(II) (Mn^{II}, Fe^{II}, Co^{II}, Ni^{II}, Cu^{II}, Zn^{II}) MTZ perchlorate complexes with cocrystallized MTZ´s (21–26):

The corresponding metal(II) perchlorate salt (**21**: manganese(II) perchlorate hexahydrate (72.4 mg, 0.20 mmol); **22**: iron(II) perchlorate hexahydrate (72.6 mg, 0.20 mmol); **23**: cobalt(II) perchlorate hexahydrate (366 mg, 1.00 mmol); **24**: nickel(II) perchlorate hexahydrate (366 mg, 1.00 mmol); **25**: copper(II) perchlorate hexahydrate (371 mg, 1.00 mmol); **26**: zinc(II) perchlorate hexahydrate (74.5 mg, 0.20 mmol)) was dissolved in the least necessary amount of water. While stirring mechanically, an aqueous solution of the ligand (**21**, **22**, **26**: 168 mg, 2.00 mmol; **23**, **25**: 841 mg, 10 mmol; **24**: 1.68 g, 16 mmol) was added slowly. The colored reaction mixtures were left for crystallization until a crystalline material appeared. The cocrystallized compounds were filtered off, washed with cold ethanol (2 mL) and dried in air.

$[Mn(MTZ)_6](ClO_4)_2$ • 2 MTZ (21)

Product **21** was obtained within one week in the form of colorless crystals suitable for X-ray determination. Yield: 120 mg (0.13 mmol, 65 %).

DTA (5 °C min^{-1}): 105 °C (endothermic), 216 °C (exothermic); IR (ATR, cm^{-1}): $\tilde{\nu}$ = 3143 (w), 3107 (w), 1572 (w), 1515 (m), 1494 (w), 1472 (w), 1445 (w), 1297 (w), 1197 (w), 1184 (m), 1176 (w), 1106 (s), 1082 (vs), 1021 (w), 989 (m), 966 (w), 897 (w), 884 (w), 867 (w), 721 (w), 684 (m), 656 (m), 622 (s); UV-Vis spectrum: λ_{max} = none; EA ($C_{16}H_{32}Cl_2MnN_{32}O_8$, 926.49) calcd: C 20.74, H 3.48, N 48.38 %; found: C 20.96, H 3.44, N 48.53 %; BAM drophammer: 7 J; friction tester: 216 N; ESD: 0.46 J (at grain size 100–500 µm).

$[Fe(MTZ)_6](ClO_4)_2 \bullet 2$ MTZ (22)

After one week, **21** was isolated in the form of colorless crystals suitable for X-ray determination. Yield: 107 mg (0.12 mmol, 58 %).

DTA (5 °C min^{-1}): 111 °C (endothermic), 215 °C (exothermic); IR (ATR, cm^{-1}): $\tilde{\nu}$ = 3144 (w), 3107 (w), 2168 (m), 1515 (m), 1493 (w), 1472 (w), 1298 (w), 1184 (m), 1176 (m), 1105 (s), 1079 (vs), 1021 (m), 991 (m), 966 (w), 897 (w), 883 (w), 867 (w), 721 (w), 684 (m), 655 (s), 622 (s); UV-Vis spectrum: λ_{max} = 883 nm; EA ($C_{16}H_{32}Cl_2FeN_{32}O_8$, 927.39) calcd: C 20.72, H 3.48, N 48.33 %; found: C 20.99, H 3.58, N 48.03 %; BAM drophammer: 10 J; friction tester: 120 N; ESD: 400 mJ (at grain size 100–500 µm).

$[Co(MTZ)_6](ClO_4)_2 \bullet 2$ MTZ (23)

The cobalt(II) complex **23** was obtained in the form of X-ray suitable yellow blocks within 2 weeks. Yield: 383 mg (0.41 mmol, 41 %).

DTA (5 °C min^{-1}): 107 °C (endothermic), 210 °C (exothermic); IR (ATR, cm^{-1}): $\tilde{\nu}$ = 3147 (w), 3109 (w), 1517 (w), 1494 (w), 1473 (w), 1419 (vw), 1298 (vw), 1186 (m), 1177 (w), 1106 (s), 1080 (vs), 1023 (w), 994 (m), 967 (w), 934 (vw), 914 (w), 897 (w), 883 (w), 868 (w), 721 (w), 684 (m), 656 (s), 622. (s); UV-Vis spectrum: λ_{max} = 467, 961 nm; EA ($C_{16}H_{32}Cl_2CoN_{32}O_8$, 930.48) calcd: C 20.65, H 3.47, N 48.17 %; found: C 20.84, H 3.50, N 47.92 %; BAM drophammer: 10 J; friction tester: 80 N; ESD: 130 mJ (at grain size 500–1000 µm).

$[Ni(MTZ)_6](ClO_4)_2 \bullet 2$ MTZ (24)

Coordination compound **24** was obtained within one day in the form of X-ray suitable purple plates after reduction of the solvent at 60 °C to the minimum amount where everything stayed in solution. Yield: 695 mg (0.75 mmol, 75 %).

DTA (5 °C min^{-1}): 93 °C (endothermic), 207 °C (exothermic); IR (ATR, cm^{-1}): $\tilde{\nu}$ = 3148 (w), 3111 (w), 1518 (w), 1493 (w), 1473 (w), 1187 (w), 1178 (w), 1107 (s), 1083 (vs), 1027 (w), 1080 (vs), 1023 (w), 997 (m), 967 (w), 915 (w), 896 (w), 881 (w), 869 (w), 722 (w), 685 (m), 656 (m), 623 (s); UV-Vis spectrum: λ_{max} = 547, 904 nm; EA ($C_{16}H_{32}Cl_2NiN_{32}O_8$, 930.24) calcd:

C 20.66, H 3.47, N 48.18 %; found: C 20.93, H 3.37, N 47.89 %; BAM drophammer: 6 J; friction tester: 192 N; ESD: 200 mJ (at grain size < 100 µm).

$[Cu(MTZ)_6](ClO_4)_2 \bullet 2$ MTZ (25)

After two weeks, **25** was obtained in the form of blue blocks suitable for X-ray diffraction. Yield: 417 mg (0.45 mmol, 45 %).

DTA (5 °C min^{-1}): 78 °C (endothermic), 206 °C (exothermic); IR (ATR, cm^{-1}): $\tilde{\nu}$ = 3150 (w), 3107 (w), 1520 (w), 1508 (w), 1494 (w), 1473 (w), 1420 (vw), 1184 (m), 1178 (m), 1105 (s), 1080 (vs), 1025 (m), 1001 (m), 983 (w), 966 (w), 933 (w), 912 (w), 894 (w), 882 (w), 871 (w), 721 (w), 684 (s), 656 (s), 622 (s); UV-Vis spectrum: λ_{max} = 676 nm; EA ($C_{16}H_{32}Cl_2CuN_{32}O_8$, 935.10) calcd: C 20.55, H 3.45, N 47.93 %; found: C 20.51, H 3.44, N 47.07 %; BAM drophammer: 7 J; friction tester: 72 N; ESD: 200 mJ (at grain size 500–1000 µm).

$[Zn(MTZ)_6](ClO_4)_2 \bullet 2$ MTZ (26)

The zinc complex **26** was obtained within one week in the form of colorless single crystals, which were suitable for X-ray diffraction. Yield: 170 mg (0.18 mmol, 91 %).

DTA (5 °C min^{-1}): 108 °C (endothermic), 212 °C (exothermic); IR (ATR, cm^{-1}): $\tilde{\nu}$ = 3146 (w), 3109 (w), 1516 (m), 1494 (w), 1473 (w), 1420 (w), 1298 (w), 1186 (m), 1177 (m), 1106 (s), 1079 (vs), 1026 (m), 993 (m), 967 (m), 934 (w), 914 (w), 897 (w), 884 (w), 868 (w), 721 (w), 684 (s), 656 (s), 622 (s); UV-Vis spectrum: λ_{max} = none; EA ($C_{16}H_{32}Cl_2N_{32}O_8Zn$, 936.93) calcd: C 20.51, H 3.44, N 47.84 %; found: C 20.80, H 3.41, N 47.84 %; BAM drophammer: 10 J; friction tester: 144 N; ESD: 0.60 J (at grain size 100–500 µm).

$[Cu(CDNM)_2(MTZ)_4]$ (27)

To an aqueous solution of potassium cyanodinitromethanide (84.6 mg, 0.50 mmol) and copper(II) sulfate pentahydrate (61.4 mg, 0.25 mmol), a solution of MTZ (84.1 mg, 1.00 mmol) in water was added under stirring. The reaction mixture was left for crystallization. X-ray

suitable blue single crystals of **27** were obtained after one day. Yield: 113 mg (0.17 mmol, 69 %).

DTA (5 °C min^{-1}): 201 °C (dec.); IR (ATR, cm^{-1}): $\tilde{\nu}$ = 3184 (w), 3134 (m), 2221 (s), 1508 (s), 1469 (s), 1423 (s), 1365 (w), 1344 (w), 1312 (w), 1249 (vs), 1189 (vs), 1151 (s), 1103 (s), 1061 (s), 1021 (m), 996 (s), 880 (s), 850 (s), 766 (m), 741 (s), 718 (m), 681 (s), 652 (vs), 573 (m), 506 (m); UV-Vis spectrum: λ_{max} = 358, 676 nm; EA ($C_{12}H_{16}CuN_{22}O_8$, 659.95) calcd: C 21.84, H 2.44, N 46.69 %; found: C 21.85, H 2.42, N 46.41 %; BAM drophammer: 4 J; friction tester: 324 N; ESD: 1.50 J (at grain size 100–500 µm).

General procedure for the preparation of metal(II) (Mn^{II}, Co^{II}, Ni^{II}, Cu^{II}, Zn^{II}) MTZ picrate (PA) complexes (29–32):

Picric acid (**29**–**31**: 115 mg, 0.50 mmol; **32**: 343 mg, 1.50 mmol) and the corresponding metal(II) carbonate (**29**: cobalt(II) carbonate (30.0 mg, 0.25 mmol); **30**: nickel(II) carbonate (30.0 mg, 0.25 mmol); **31**: copper(II) carbonate (31.0 mg, 0.25 mmol); **32**: zinc(II) carbonate (94.0 mg, 0.75 mmol)) were mechanically stirred in H_2O (5 mL) at 70 °C. After the complete dissolution of the reactants, the ligand MTZ (**29**–**31**: 84.0 mg, 1.00 mmol; **32**: 377 mg, 4.50 mmol), dissolved in water (0.50 mmol), was added to the yellow solution, which was afterwards further stirred mechanically for 5 min. The reaction mixtures were left to crystallize at room temperature, the crystals were filtered off, washed with cold ethanol (2 mL) and dried in air.

$[Co(H_2O)_4(MTZ)_2](PA)_2 \bullet 2\ H_2O$ (29)

Within 9 days, compound **29** was obtained in the form of yellow blocks suitable for X-ray determination. Yield: 118 mg (0.15 mmol, 60 %).

DTA (5 °C min^{-1}): 248 °C (exothermic); DSC (5 °C min^{-1}): 61 °C (endothermic), 79 °C (endothermic), 246 °C (exothermic); IR (ATR, cm^{-1}): $\tilde{\nu}$ = 3603 (w), 3387 (m), 3158 (m), 3136 (m), 3079 (m), 1651 (w), 1608 (s), 1568 (s), 1549 (s), 1516 (m), 1426 (m), 1365 (m), 1332 (vs), 1258 (vs), 1240 (s), 1189 (m), 1158 (m), 1108 (s), 1082 (m), 1060 (m), 994 (m), 943 (m), 909 (m), 891 (w), 833 (w), 789 (m), 746 (m), 710 (s), 686 (m), 656 (m), 545 (m), 525 (w); EA:

($C_{16}H_{24}CoN_{14}O_{20}$, 791.38) calcd: C 24.28, H 3.06, N 24.78 %; found: C 24.30, H 3.13, N 24.69 %; BAM drophammer: > 40 J; friction tester: > 360 N; ESD: 1.00 J (at grain size 100–500 µm).

$[Ni(H_2O)_2(MTZ)_4](PA)_2$ (30)

After 16 days, compound **30** was obtained in the form of yellow-green blocks suitable for X-ray determination. Yield: 154 mg (0.17 mmol, 69 %).

DTA (5 °C min^{-1}): 106 °C (endothermic), 211 °C (exothermic); IR (ATR, cm^{-1}): $\tilde{\nu}$ = 3518 (w), 3137 (m), 3122 (m), 3065 (m), 1630 (m), 1609 (s), 1563 (s), 1540 (s), 1516 (s), 1487 (s), 1473 (s), 1434 (m), 1363 (s), 1319 (vs), 1273 (vs), 1194 (m), 1167 (s), 1109 (s), 1081 (m), 1064 (m), 1026 (w), 999 (m), 943 (w), 913 (m), 883 (m), 840 (w), 821 (vw), 790 (w), 746 (m), 721 (m), 710 (s), 685 (vs), 653 (s), 541 (m), 525 (w); EA: ($C_{20}H_{24}N_{22}NiO_{16}$, 887.24) calcd: C 27.07, H 2.73, N 34.73 %; found: C 27.09, H 2.69, N 34.63 %; BAM drophammer: > 40 J; friction tester: > 360 N; ESD: 1.50 J (at grain size 100–500 µm).

$[Cu(PA)_2(MTZ)_2]$ (31)

Compound **31** crystallized within 10 min in the form of green needles suitable for X-ray determination. Yield: 148 mg (0.22 mmol, 86 %).

DTA (5 °C min^{-1}): 226 °C (exothermic); IR (ATR, cm^{-1}): $\tilde{\nu}$ = 3170 (w), 3085 (w), 1646 (vw), 1612 (m), 1578 (s), 1541 (s), 1511 (vs), 1480 (s), 1422 (m), 1378 (m), 1351 (s), 1332 (s), 1302 (m), 1267 (vs), 1182 (m), 1169 (s), 1103 (s), 1083 (m), 1021 (m), 1001 (m), 942 (m), 934 (m), 926 (m), 916 (m), 870 (w), 852 (m), 826 (w), 782 (m), 744 (m), 731 (w), 719 (s), 702 (s), 682 (s), 652 (m), 562 (w), 542 (m), 519 (w); UV-Vis spectrum: λ_{max} = 380, 630 nm; EA: ($C_{16}H_{12}CuN_{14}O_{14}$, 687.90) calcd: C 27.94, H 1.76, N 28.51 %; found: C 27.85, H 1.79, N 28.37 %; BAM drophammer: 4 J; friction tester: > 360 N; ESD: 0.30 J (at grain size 500–1000 µm).

[Zn(PA)$_2$(MTZ)$_4$] (32)

After two weeks, the zinc(II) picrate compound **32** was received in the form of yellow rods suitable for X-ray determination. Yield: 529 mg (0.62 mmol, 82 %).

DTA (5 °C min^{-1}): 92 °C (endothermic), 212 °C (exothermic); IR (ATR, cm^{-1}): $\tilde{\nu}$ = 3171 (w), 3158 (w), 1629 (m), 1607 (s), 1569 (s), 1543 (s), 1516 (m), 1484 (s), 1425 (m), 1361 (s), 1340 (s), 1319 (vs), 1300 (s), 1271 (vs), 1242 (s), 1181 (s), 1161 (s), 1110 (s), 1101 (vs), 1081 (s), 1059 (m), 1027 (m), 993 (s), 942 (m), 934 (m), 912 (s), 888 (m), 878 (m), 836 (w), 822 (w), 788 (m), 746 (m), 725 (m), 720 (m), 712 (s), 684 (s), 652 (vs), 608 (w), 539 (m), 509 (w); EA: ($C_{20}H_{20}ZnN_{22}O_{14}$, 857.90) calcd: C 28.00, H 2.35, N 35.92 %; found: C 27.93, H 2.52, N 35.75 %; BAM drophammer: 15 J; friction tester: > 360 N; ESD: 0.25 J (at grain size 100–500 µm).

General procedure for the preparation of metal(II) (Mn^{II}, Co^{II}, Ni^{II}, Cu^{II}, Zn^{II}) MTZ styphnate (HTNR) complexes (33–37):

Styphnic acid (**33**, **34**: 490 mg, 2.00 mmol; **35**–**37**: 123 mg, 0.50 mmol) and the corresponding metal(II) carbonate (**33**: manganese(II) carbonate (115 mg, 1.00 mmol); **34**: cobalt(II) carbonate (119 mg, 1.00 mmol); **35**: nickel(II) carbonate (30.0 mg, 0.25 mmol); **36**: copper(II) carbonate (31.0 mg, 0.25 mmol); **37**: zinc(II) carbonate (31.0 mg, 0.25 mmol)) were dissolved and stirred in water (5 mL) at 70 °C until a clear solution was obtained. An aqueous solution of MTZ (**33**: 336 mg, 4.00 mmol, **34**: 168 mg, 2.00 mmol; **35**–**37**: 84.0 mg, 1.00 mmol) was added, which was afterwards further stirred mechanically for 5 min. The reaction mixtures were left to crystallize at room temperature until a solid appeared. The products were filtered off, washed with a small amount of cold ethanol (2 mL) and dried in air.

[Mn(HTNR)$_2$(MTZ)$_4$] (33)

The styphnate complex **33** was obtained in the form of yellow blocks suitable for X-ray determination within 2 weeks. Due to the high solubility of the compound in ethanol, no purification step was performed. Yield: 726 mg (0.82 mmol, 82 %).

DTA (5 °C min^{-1}): 141 °C (endothermic), 202 °C (exothermic); IR (ATR, cm^{-1}): $\tilde{\nu}$ = 3163 (w), 3144 (w), 1626 (s), 1562 (s), 1533 (s), 1523 (s), 1513 (s), 1489 (m), 1447 (m), 1373 (s), 1338 (s), 1299 (vs), 1247 (m), 1185 (s), 1173 (vs), 1109 (m), 1101 (s), 1084 (vs), 1061 (m), 1018 (w), 986 (s), 925 (m), 882 (m), 822 (w), 783 (m), 760 (m), 729 (s), 720 (s), 704 (m), 688 (s), 678 (s), 653 (s), 564 (w), 549 (w), 528 (w), 518 (w); EA: ($C_{20}H_{20}MnN_{22}O_{16}$, 879.46) calcd: C 27.31, H 2.29, N 35.04 %; found: C 27.10, H 2.28, N 34.19 %; BAM drophammer: 15 J; friction tester: 288 N; ESD: 0.20 J (at grain size 100–500 μm).

[Co(H$_2$O)$_4$(MTZ)$_2$](HTNR)$_2$ • 2 H$_2$O (34)

Within 5 days, complex **34** emerged in the form of yellow blocks suitable for X-ray determination. Yield: 639 mg (0.78 mmol, 78 %).

DTA (5 °C min^{-1}): 70 °C (endothermic), 80 °C (endothermic), 200 °C (exothermic); IR (ATR, cm^{-1}): $\tilde{\nu}$ = 3551 (w), 3137 (m), 3071 (m), 1627 (m), 1567 (s), 1532 (s), 1514 (s), 1495 (m), 1483 (m), 1454 (m), 1371 (m), 1364 (m), 1337 (s), 1303 (vs), 1291 (vs), 1249 (s), 1187 (s), 1170 (s), 1115 (s), 1088 (vs), 1040 (m), 1000 (m), 947 (m), 927 (m), 899 (m), 825 (m), 786 (s), 760 (s), 733 (s), 709 (s), 695 (vs), 678 (s), 658 (vs), 623 (s), 610 (s), 591 (s), 516 (s); EA: ($C_{16}H_{24}CoN_{14}O_{22}$, 823.38) calcd: C 23.34, H 2.94, N 23.82 %; found: C 23.26, H 2.92, N 24.02 %; BAM drophammer: 25 J; friction tester: > 360 N; ESD: 0.23 J (at grain size 100–500 μm).

[Ni(H$_2$O)$_4$(MTZ)$_2$](HTNR)$_2$ • 2 H$_2$O (35)

X-ray suitable green blocks of **35** started to crystallize within 15 days. Yield: 178 mg (0.22 mmol, 86 %).

DTA (5 °C min^{-1}) onset: 86 °C (endothermic), 105 °C (endothermic), 227 °C (exothermic); IR (ATR, cm^{-1}): $\tilde{\nu}$ = 3554 (w), 3133 (m), 3108 (m), 3071 (m), 1629 (s), 1566 (s), 1561 (s), 1534 (s), 1514 (s), 1492 (m), 1483 (m), 1453 (m), 1372 (m), 1334 (s), 1304 (vs), 1292 (vs), 1249 (m), 1188 (s), 1170 (s), 1115 (m), 1088 (vs), 1043 (w), 1004 (w), 947 (w), 928 (m), 902 (w), 825 (w), 787 (m), 762 (m), 733 (m), 715 (s), 695 (s), 679 (s), 660 (s), 629 (m), 606 (m); EA: ($C_{16}H_{24}N_{14}NiO_{22}$, 823.14) calcd: C 23.35, H 2.94, N 23.82 %; found: C 23.37, H 3.06, N

24.07 %; BAM drophammer: 25 J; friction tester: > 360 N; ESD: 0.15 J (at grain size < 100 µm).

[Cu(HTNR)$_2$(MTZ)$_2$] (36)

Compound **36** was obtained within 10 min in the form of blue plates suitable for X-ray determination. Yield: 151 mg (0.21 mmol, 84 %).

DTA (5 °C min^{-1}): 231 °C (dec.); IR (ATR, cm^{-1}): $\tilde{\nu}$ = 3161 (w), 3070 (w), 1628 (m), 1564 (s), 1525 (vs), 1483 (s), 1455 (s), 1377 (m), 1356 (m), 1313 (s), 1283 (s), 1175 (s), 1110 (m), 1089 (s), 1033 (m), 1009 (m), 929 (m), 877 (w), 775 (w), 760 (m), 736 (m), 697 (s), 678 (s), 651 (s), 537 (w); UV-Vis spectrum: λ_{max} = 404, 657 nm; EA: ($C_{16}H_{12}CuN_{14}O_{16}$, 719.90) calcd: C 26.69, H 1.68, N 27.24 %; found: C 26.52, H 1.91, N 27.72 %; BAM drophammer: 2 J; friction tester: 160 N; ESD: 1.50 J (at grain size 100–500 µm).

[Zn(HTNR)$_2$(MTZ)$_2$] (37)

Within one week, the zinc(II) styphnate complex **37** was isolated in the form of yellow blocks suitable for X-ray determination. Yield: 120 mg (0.17 mmol, 67 %).

DTA (5 °C min^{-1}): 214 °C (dec.); IR (ATR, cm^{-1}): $\tilde{\nu}$ = 3143 (m), 2961 (vw), 1632 (s), 1580 (s), 1567 (s), 1533 (vs), 1514 (vs), 1471 (m), 1456 (s), 1367 (s), 1332 (s), 1316 (s), 1270 (vs), 1175 (vs), 1101 (s), 1082 (vs), 1013 (m), 1002 (m), 994 (m), 931 (m), 916 (m), 895 (m), 882 (m), 786 (m), 778 (m), 763 (m), 734 (m), 716 (s), 700 (vs), 689 (vs), 678 (vs), 651 (vs), 546 (w); EA: ($C_{16}H_{12}ZnN_{14}O_{16}$, 721.74) calcd: C 26.63, H 1.68, N 27.17 %; found: C 26.56, H 1.86, N 27.57 %; BAM drophammer: 4 J; friction tester: 240 N; ESD: 0.80 J (at grain size 500–1000 µm).

19.7.11 References

[S1] *CrysAlisPro*, Oxford Diffraction Ltd., version 171.33.41, 2009.

[S2] A. Altomare, G. Cascarano, C. Giacovazzo, A. Guagliardi, *J. Appl. Crystallogr.* 1992, **26**, 343–350.

[S3] a) A. Altomare, G. Cascarano, C. Giacovazzo, A. Guagliardi, A. G. G. Moliterni, M. C. Burla, G. Polidori, M. Camalli, R. Spagna, *SIR97*, 1997; b) A. Altomare, M. C. Burla, M. Camalli, G. L. Cascarano, C. Giacovazzo, A. Guagliardi, A. G. G. Moliterni, G. Polidori, R. Spagna, *J. Appl. Crystallogr.* 1999, **32**, 115–119.

[S4] a) G. M. Sheldrick, *SHELXL-97*, *Program for the Refinement of Crystal Structures*, University of Göttingen, Germany, 1997; b) G. M. Sheldrick, *Acta Crystallogr. Sect. A* 2008, **64**, 112–122.

[S5] A. L. Spek, *PLATON*, *A Multipurpose Crystallographic Tool*, Utrecht University, The Netherlands, 1999.

[S6] Empirical absorption correction using spherical harmonics, implemented in SCALE3 ABSPACK scaling algorithm (CrysAlisPro Oxford Diffraction Ltd., Version 171.33.41, 2009).

[S7] L. S. Ivashkevich, A. S. Lyakhov, D. O. Ivashkevich, M. M. Degtyarik, P. N. Gaponik, *Zh. Neorg. Khim.*, 2005, **50**, 82–86.

[S8] A. Song, I. Hwang, K. Ha, *Z. Kristallogr. – New Cryst. Struct.*, 2007, **222**, 43–44.

[S9] NATO standardization agreement (STANAG) on explosives, impact sensitivity tests, no. 4489, 1st ed., Sept. 17, 1999.

[S10] WIWEB-Standardarbeitsanweisung 4-5.1.02, Ermittlung der Explosionsgefährlichkeit, hier der Schlagempfindlichkeit mit dem Fallhammer, Nov. 8, 2002.

[S11] http://www.bam.de, Accessed August 2017.

[S12] NATO standardization agreement (STANAG) on explosive, friction sensitivity tests, no. 4487, 1st ed., Aug. 22, 2002.

[S13] WIWEB-Standardarbeitsanweisung 4-5.1.03, Ermittlung der Explosionsgefährlichkeit oder der Reibeempfindlichkeit mit dem Reibeapparat, Nov. 8, 2002.

[S14] Impact: insensitive > 40 J, less sensitive ≥ 35 J, sensitive ≥ 4 J, very sensitive ≤ 3 J; Friction: insensitive > 360 N, less sensitive = 360 N, sensitive < 360 N and > 80 N, very

sensitive ≤ 80 N, extremely sensitive ≤ 10 N. According to the UN Recommendations on the Transport of Dangerous Goods, (+) indicates not safe for transport.

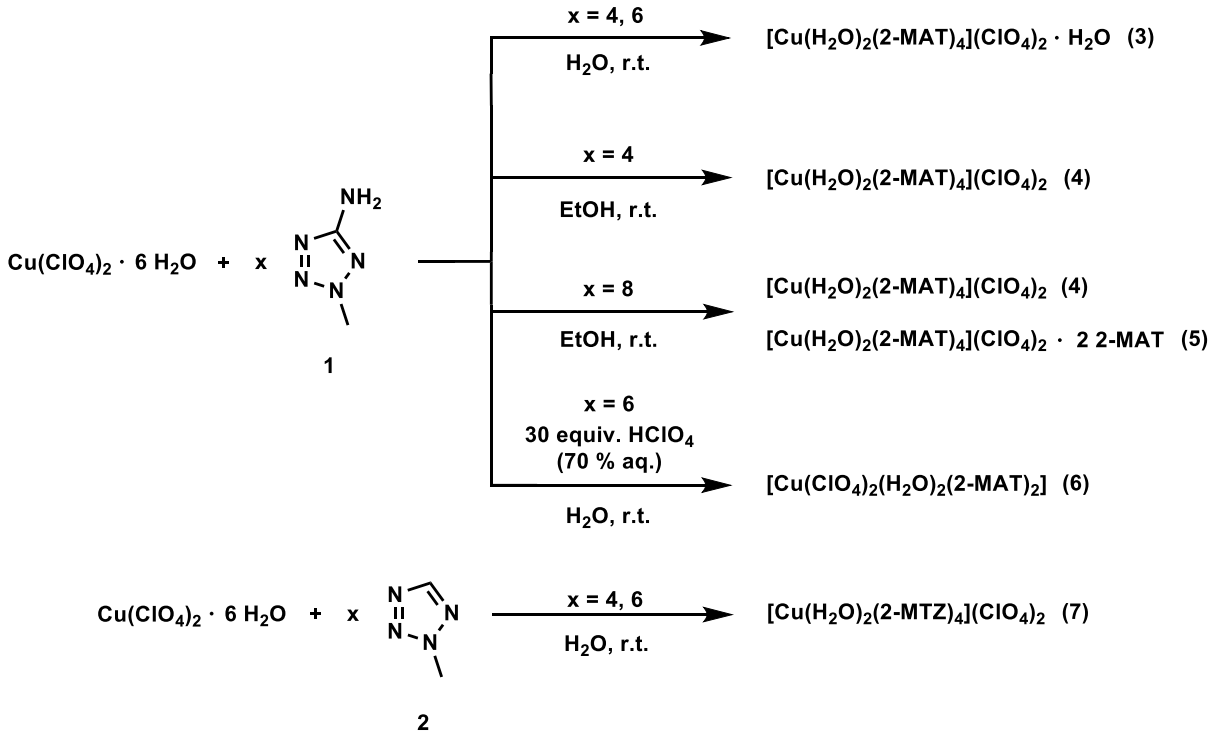
[S15] http://www.ozm.cz, Accessed August 2017.

[S16] R. Scharf, PhD thesis, Ludwig-Maximilians Universität München, 2016.

[S17] P. N. Gaponik, M. M. Degtyarik, A. S. Lyakhov, V. E. Matulis, O. A. Ivashkevih, M. Quesada, J. Reedijk, *Inorg. Chim. Acta*, 2005, **358**, 3949–3957.

19.8 Supplementary Information: 2-Methyl-substituted Monotetrazoles in Copper(II) Perchlorate Complexes: Manipulating Coordination Chemistry and Derived Energetic Properties

19.8.1 Overview of Synthesized Compounds



19.8.2 Experimental and General Methods

All chemicals and solvents were employed as received (Sigma-Aldrich, Fluka, Acros, ABCR). ^{1}H and ^{13}C spectra were recorded at ambient temperature using a JEOL Bruker 400, Eclipse 270, JEOL EX 400 or a JEOL Eclipse 400 instrument. The chemical shifts quoted in ppm in the text refer to typical standards such as tetramethylsilane (^{1}H, ^{13}C) in d_6-DMSO as the solvent. Endothermic and exothermic events of the described compounds, which indicate melting, evaporation or decomposition, are given as the extrapolated onset temperatures. The samples were measured in a range of 25–400 °C at a heating rate of 5 °C min^{-1} through differential thermal analysis (DTA) with an OZM Research DTA 552-Ex instrument, by differential scanning calorimetry (DSC) with a LINSEIS DSC PT10 and partly by thermal gravimetric analysis (TGA) with a PerkinElmer TGA4000. Differential thermal analysis measurements

were carried out in open glass tubes with approximately 3–4 mg substance, TGA measurements with 1–2 mg substance in total in Al_2O_3 crucibles, whereas the differential scanning calorimetric measurements were performed with about 1 mg substance in a perforated aluminium vessel and a nitrogen flow of 5 $dm^3\ h^{-1}$. Both devices were calibrated with the literature known melting point of Indium. The balance of the TGA device was calibrated with a 55.97 mg ball and the temperature calibrated with the Perkin Elmer calibration kit including three different metals or alloys (alumel, nickel, perkalloy, iron). Infrared spectra were measured with pure samples on a Perkin-Elmer BXII FT-IR system with a Smith DuraSampler IR II diamond ATR. Determination of the carbon, hydrogen and nitrogen contents was carried out by combustion analysis using an Elementar Vario El (nitrogen values determined are often lower than those calculated due to their explosive behaviour). UV-Vis spectra were recorded in the solid state using a Varian Cary 500 spectrometer in the wavelength range of 350–1000 nm. Impact sensitivity tests were carried out according to STANAG 4489[S1] with a modified instruction[S2] using a BAM (Bundesanstalt für Materialforschung) drophammer.[S3, S4] Friction sensitivity tests were carried out according to STANAG 4487[S5] with a modified instruction[S6] using the BAM friction tester. The classification of the tested compounds results from the "UN Recommendations on the Transport of Dangerous Goods".[S7] Additionally, all compounds were tested to determine the sensitivity toward electrical discharge using the OZM Electric Spark Tester ESD 2010 EN or OZM Electric Spark XSpark10 device.[S3] Hot plate and hot needle tests were performed in order to classify the initiation capability of selected complexes. The samples were fixed on a copper plate underneath adhesive tape and initiated by a red hot needle. Strong deflagration or detonation of the compound usually indicates a valuable primary explosive. The safe and straightforward hot plate test only shows the behaviour of the unconfined sample toward fast heating on a copper plate. It does not necessarily allow any conclusions on a compound´s capability as a suitable primary explosive. The laser initiation experiments were performed with a 45 W InGaAs laser diode operating in the single-pulsed mode. The diode is attached to an optical fibre with a core diameter of 400 μm and a cladding diameter of 480 μm. The optical fibre is connected via a SMA type connecter directly to the laser and to a collimator. This collimator is coupled to an optical lens, which was positioned in its focal distance (f = 29.9 mm) to the sample. The lens is shielded from the explosive by a sapphire glass. Approximately 15 mg of the carefully pestled complex to be investigated was filled into a transparent plastic cap (PC), pressed with a pressure force of 1 kN and sealed by a UV-curing adhesive. The confined samples were irradiated at a wavelength of 915 nm, a

voltage of 4 V, a current of 7 A, and pulse length of 0.1 ms. The combined current and pulse length result in an energy output of about 0.17 mJ. The obtained coordination compounds were washed with cold ethanol when stated, dried overnight in air and used for analytics without further purification.

Caution! *All investigated compounds are potentially explosive energetic materials, which show partly increased sensitivities towards various stimuli (e.g. elevated temperatures, impact, friction, or electrostatic discharge). Therefore, proper security precautions (safety glass, face shield, earthed equipment and shoes, leather coat, Kevlar gloves, Kevlar sleeves and ear plugs) have to be applied while synthesizing and handling the described compounds. Especially the very sensitive compound* ***6*** *must be handled with great care! Whenever handling concentrated perchloric acid, avoid combining it with organic solvents due to the explosive potential of the resulting mixtures.*

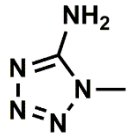
Dimethyl sulfate is carcinogenic, mutagenic, highly poisonous, corrosive, environmentally hazardous. In addition to the standard safety instructions, it is recommended to wear gloves with this toxic chemical at all times.

Methylation of 5-aminotetrazole

The synthesis of the methylated species **1** and **2** was performed to a slightly modified literature procedure from Ismael *et al.*.[S8] At first, 5-aminotetrazole (11.9 g, 140 mmol, 1.0 equiv.) was suspended in water (30 mL) and an aqueous solution of sodium hydroxide (20 wt. %, 100 mL) was added to the suspension until complete dissolution of the starting material. The subsequent, dropwise addition of dimethylsulfate (26.9 mL, 148 mmol, 1.1 equiv.) was accompanied by sequentially maintaining the reaction alkaline (20 wt % NaOH, phenolphthalein as indicator). After complete addition of dimethylsulfate, the obtained mixture was refluxed for 1 hour and cooled to 3 °C. After two days, the product could be filtrated and recrystallized from water yielding colourless crystals of 1-methyl-5-aminotetrazole (**1**, 5.69 g, 57.4 mmol, 41 %). The collected filtrate was repeatedly extracted with diethylether, the combined organic phases were dried, and the solvent was evaporated *in vacuo*. The hereby obtained colourless residue was recrystallized from water yielding 2-methyl-5-aminotetrazole (**2**) as colourless crystals (4.02 g,

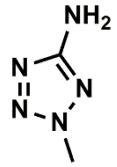
47.8 mmol, 34 %). Conducted characterization for **1** and **2** was consistent with data provided by Cristiano and coworkers.[S8]

1-Methyl-5-aminotetrazole



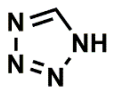
^{1}H NMR (DMSO-d_6, 25 °C, ppm): δ = 3.70 (s, 3H, -CH_3), 6.64 (s, 2H, -NH_2); **^{13}C NMR** (DMSO-d_6, 25 °C, ppm): δ = 32.0 -CH_3), 156.3 (CN$_4$); **DSC** (5 °C min^{-1}) onset: 225 °C (endothermic); **IR** (ATR, cm^{-1}): $\tilde{\upsilon}$ = 3314 (s), 3148 (vs), 2951 (w), 1667 (vs), 1594 (vs), 1486 (s), 1462 (m), 1320 (s), 1279 (m), 1236 (m), 1162 (w), 1120 (m), 1087 (s), 1045 (s), 969 (m), 863 (w), 789 (m), 742 (m), 672 (vs), 632 (s), 624 (s); **EA**: ($C_2H_5N_5$, 99.10) calc.: C 24.24, H 5.09, N 70.67 %; found: C 24.11, H 4.96, N 66.22 %; **BAM drophammer**: > 40 J; **friction tester**: > 360 N; **ESD**: 1.50 J (at grain size 500–1000 µm).

2-Methyl-5-aminotetrazole (1)



^{1}H NMR (DMSO-d_6, 25 °C, ppm): δ = 4.08 (s, 3H, -CH_3), 5.96 (s, 2H, -NH_2); **^{13}C NMR** (DMSO-d_6, 25 °C, ppm): δ = 167.6 (CN$_4$); **DTA** (5 °C min^{-1}) onset: 104 °C (endothermic), 252 °C (endothermic); **TGA** (5 °C min^{-1}): 110–200 °C (melting and evaporation of 2-MAT), 210–400 °C (further evaporation of 2-MAT) **IR** (ATR, cm^{-1}): $\tilde{\upsilon}$ = 3374 (s, N-H), 3304 (s, N-H), 3216 (m, N-H), 3086 (w, C-H), 1628 (s), 1549 (vs, C=N), 1446 (m), 1420 (m), 1409 (s), 1377 (m), 1340 (w), 1314 (m), 1203 (s), 1150 (w), 1122 (w), 1084 (w), 1054 (m), 1015 (m), 959 (w), 901 (w), 808 (m), 756 (s), 740 (w), 712 (w), 689 (w), 678 (w), 647 (vs), 606 (s); **EA**: ($C_2H_5N_5$, 99.10) calc.: C 24.24, H 5.09, N 70.67 %; found: C 24.40, H 4.99, N 70.75 %; **BAM drophammer**: > 40 J; **friction tester**: > 360 N; **ESD**: 1.50 J (at grain size 100–500 µm).

1,5*H*-Tetrazole



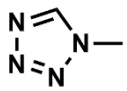
According to a modified procedure from Thomann *et al.*,[S9] sodium azide (39.0 g, 600 mmol, 1.0 equiv.) and ammonium chloride (31.8 g, 600 mmol, 1.0 equiv.) were suspended in triethyl orthoformate (266 g, 1.80 mol, 3.0 equiv.). In the following, glacial acetic acid (144 g, 2.40 mol, 4.0 equiv.) was added drop wise and the resulting mixture was refluxed for ten hours at 80 °C. Afterwards, the suspension was evaporated to dryness, acetone (600 mL) was added and the obtained mixture was heated and filtrated while hot. The filtrate was evaporated to dryness again and the residue was recrystallized from ethyl acetate yielding 1,5*H*-tetrazole as light orange crystals (13.3 g, 190 mmol, 32 %). The filtrate was evaporated to dryness and recrystallized again from ethyl acetate giving another batch of 1,5*H*-tetrazole (8.20 g, 117 mmol, 20 %). Analytical data are consistent with previously reported results.[SI9]

^{1}H NMR (DMSO-d_6, 25 °C, ppm): δ = 9.38 (s, 1H, -C*H*); **^{13}C NMR** (DMSO-d_6, 25 °C, ppm): δ = 143.6 (*C*N_4). **DSC** (5 °C min^{-1}) onset: 104 °C (endothermic); **IR** (ATR, cm^{-1}): $\tilde{\upsilon}$ = 3374 (s), 3304 (s), 3216 (m), 3086 (w), 1628 (s), 1549 (vs), 1446 (m), 1420 (m), 1409 (s), 1377 (m), 1340 (w), 1314 (m), 1203 (s), 1150 (w), 1122 (w), 1084 (w), 1054 (m), 1015 (m), 959 (w), 901 (w), 808 (m), 756 (s), 740 (w), 712 (w), 689 (w), 678 (w), 647 (vs), 606 (s).

Methylation of 1,5*H*-tetrazole

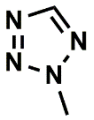
According to a literature procedure from Gaponik *et al.*,[S10] a stirring suspension of 1,5*H*-tetrazole (8.00 g, 114 mmol, 1.0 equiv.) and K_2CO_3 (15.9 g, 115 mmol, 1.0 equiv.) in acetone (30 mL) was charged with methyl iodide (8.0 mL, 129 mmol, 1.1 equiv.) in a dropwise manner. After keeping the resulting reaction mixture under reflux for 16 h, cooling to room temperature was followed by filtration and several washings of the obtained residue with acetone. Concentration of the filtrate and subsequent vacuum distillation of the resulting crude product gave 2-methyl-5*H*-tetrazole (**1**, 40 °C, 12 mbar, 2.22 g, 26.6 mmol, 23 %) as a colourless liquid and 1-methyl-5*H*-tetrazole (90 °C, 0.01 mbar, 4.59 g, 54.6 mmol, 48 %) as colourless crystals.

1-Methyl-5*H*-tetrazole



^{1}H NMR (DMSO-d_6, 25 °C, ppm) δ: 9.31 (s, 1H, -C*H*), 4.10 (s, 3H, -CH_3); **^{13}C NMR** (DMSO-d_6, 25 °C, ppm) δ: 144.5 (-*C*N_4), 34.1 (-*C*H_3); **DTA** (5 °C min^{-1}): 39 °C (endothermic), 206 °C (exothermic); **IR** (ATR, cm^{-1}): $\tilde{\upsilon}$ = 3111 (m), 3032 (vw), 2962 (vw), 1843 (vw), 1491 (m), 1477 (m), 1471 (m), 1445 (w), 1422 (w), 1413 (w), 1384 (vw), 1276 (w), 1220 (w), 1172 (s), 1107 (vs), 1053 (w), 1043 (w), 1019 (w), 965 (s), 924 (m), 876 (w), 722 (w), 678 (vs), 664 (s), 657 (s); **EA**: ($C_2H_4N_4$, 84.08) calc.: C 28.57, H 4.80, N 66.63 %; found: C 28.47, H 4.89, N 65.51 %; **BAM drophammer**: > 40 J; **friction tester**: > 360 N; **ESD**: 1.50 J (at grain size < 100 μm).

2-Methyl-5*H*-tetrazole (2)



^{1}H NMR (DMSO-d_6, 25 °C, ppm) δ: 8.92 (s, 1H, -C*H*), 4.38 (s, 3H, -CH_3); **^{13}C NMR** (DMSO-d_6, 25 °C, ppm) δ: 153.2 (-CN_4), 39.3 (-CH_3); **DTA** (5 °C min^{-1}): 152 °C (endothermic); **TGA** (5 °C min^{-1}): 30–100 °C (evaporation of 2-MTZ due to high vapor pressure), 152 °C (boiling point of 2-MTZ); **IR** (ATR, cm^{-1}): $\tilde{\upsilon}$ = 3142 (vw, C-H), 2964 (vw, C-H), 2215 (vw), 1767 (vw), 1717 (vw), 1630 (vw), 1443 (m, C=N), 1411(w), 1362(m), 1278(s), 1178(m), 1137(m), 1039(s), 1017(m), 885(m), 708(s), 699(vs), 681(vs), 665(w), 484(w), 476(w), 466(w), 434(w), 434(w), 427(w), 419(w); **EA**: ($C_2H_4N_4$, 84.08) calc.: C 28.57, H 4.80, N 66.63 %; found: C 28.49, H 4.65, N 66.17 %; **BAM drophammer**: > 40 J; **friction tester**: > 360 N; **ESD**: 1.50 J (at grain size 100–500 μm).

[Cu(H$_2$O)$_2$(2-MAT)$_4$](ClO$_4$)$_2$ · H$_2$O (3)

To a mechanically stirred aqueous solution (1 mL) of Cu(ClO$_4$)$_2$ · 6 H$_2$O (92.6 mg, 0.25 mmol, 1.0 equiv.), 2-methyl-5-aminotetrazole (**1**, 99.1 mg, 1.00 mmol, 4.0 equiv.) dissolved in water (2 mL) was added dropwise. In the course of crystallization and purification, and within four

days, **3** could be isolated in the form of blue blocks suitable for X-ray diffraction (90.4 mg, 0.13 mmol, 52 %).

DTA (5 °C min^{-1}) onset: 125 °C (endothermic), 176 °C (exothermic); **IR** (ATR, cm^{-1}): $\tilde{\upsilon}$ = 3447 (m, O-H/N-H), 3340 (m, O-H/N-H), 1632 (s, C=N), 1552 (m), 1442 (m), 1420 (w), 1385 (w), 1349 (w), 1331 (w), 1193 (w), 1064 (vs, Cl-O), 936 (w), 811 (m), 750 (m), 674 (w), 649 (m), 623 (s); **EA**: ($C_8H_{26}Cl_2CuN_{20}O_{11}$, 712.87) calc.: C 13.48, H 3.68, N 39.30 %; found: C 13.43, H 3.58, N 39.32 %; **BAM drophammer**: 5 J; **friction tester**: 30 N; **ESD**: 0.26 J (at grain size 500–1000 µm).

$[Cu(H_2O)_2(2\text{-}MAT)_4](ClO_4)_2$ (4) & $[Cu(H_2O)_2(2\text{-}MAT)_4](ClO_4)_2 \cdot 2$ 2-MAT (5)

The ligand 2-methyl-5-aminotetrazole (**1**, 198 mg, 2.00 mmol, 8.0 equiv.) was dissolved in ethanol (2 mL) and slowly added to an ethanolic solution (1 mL) of the used copper(II) species $Cu(ClO_4)_2 \cdot 6\ H_2O$ (92.6 mg, 0.25 mmol, 1.0 equiv.). The resulting reaction mixture soon began to mist leading to a turquoise precipitate which was filtered immediately. After six days, compound **4** crystallized from the filtrate in the form of blue blocks suitable for X-ray diffraction (82.8 mg, 0.12 mmol, 48 %). The residue of the previous filtration contained a mixture of **4** and the light green compound **5**. The structure of the latter has been determined through X-ray diffraction. To avoid the precipitation of **5**, the perchlorate complex **4** can also be isolated through an analogous synthesis using only four equivalents of 2-MAT.

$[Cu(H_2O)_2(2\text{-}MAT)_4](ClO_4)_2$ (4)

DTA (5 °C min^{-1}) onset: 110 °C (endothermic), 171 °C (exothermic); **IR** (ATR, cm^{-1}): $\tilde{\upsilon}$ = 3487 (m, O-H/N-H), 3426 (m, O-H/N-H), 3385 (m, O-H/N-H), 3347 (m, O-H/N-H), 3244 (w, O-H/N-H), 1634 (s, C=N), 1555 (s), 1439 (m), 1386 (w), 1351 (w), 1335 (w), 1210 (w), 1191 (w), 1143 (m), 1117 (s), 1101 (s), 1033 (s, Cl-O), 925 (m), 815 (m), 769 (m), 756 (m), 747 (m), 724 (m), 674 (m), 666 (m), 643 (s), 623 (vs); **EA**: ($C_8H_{26}Cl_2CuN_{20}O_{11}$, 694.86) calc.: C 13.83, H 3.48, N 40.32 %; found: C 14.10, H 3.48, N 40.08 %; **BAM drophammer**: < 1 J; **friction tester**: 24 N; **ESD**: 20 mJ (at grain size < 100 µm).

$[Cu(ClO_4)_2(H_2O)_2(2\text{-MAT})_2]$ (6)

A solution of 2-methyl-5-aminotetrazole (**1**, 99.1 mg, 1.00 mmol, 4.0 equiv.) in water (2 mL) was slowly added to an aqueous solution (1 mL) of $Cu(ClO_4)_2 \cdot 6\ H_2O$ (92.6 mg, 0.25 mmol, 1.0 equiv.). Before stirring mechanically for 10 min, $HClO_4$ (70 % wt., 0.5 mL, 8.3 mmol, 30 equiv.) was added. The copper(II) perchlorate complex **6** with coordinating perchlorate anions was obtained after four days in the form of blue rods suitable for X-ray diffraction (93.7 mg, 0.19 mmol, 76 %).

DTA (5 °C min^{-1}) onset: 192 °C (exothermic); **TGA** (5 °C min^{-1}): 195 °C (dec.); **IR** (ATR, cm^{-1}): $\tilde{\upsilon}$ = 3450 (m, O-H/N-H), 3361 (m, O-H/N-H), 1634 (s, C=N), 937 (m), 811 (m), 748 (m), 691 (m), 673 (m), 648 (m), 621 (vs); **EA**: ($C_4H_{14}Cl_2CuN_{10}O_{10}$, 496.66) calc.: C 9.67, H 2.84, N 28.20 %; found: C 9.78, H 2.96, N 27.50 %; **BAM drophammer**: 2 J; **friction tester**: 2.2 N; **ESD**: 0.15 J (at grain size < 100 µm).

$[Cu(H_2O)_2(2\text{-MTZ})_4](ClO_4)_2$ (7)

2-Methyltetrazole (**2**, 84.1 mg, 1.25 mmol, 4.0 equiv.) was added to a stirred aqueous solution (1 mL) of copper(II) perchlorate hexahydrate (92.6 mg, 0.25 mmol, 1.0 equiv.). Resulting from subsequent crystallization at room temperature, $[Cu(H_2O)_2(2\text{-MTZ})_4](ClO_4)_2$ (**7**, 114.3 mg, 0.18 mmol, 73 %) was obtained within a day as blue blocks, suitable for X-ray determination.

DTA (5 °C min^{-1}): 115 °C (endothermic), 208 °C (endothermic), 240 °C (exothermic); **TGA** (5 °C min^{-1}): 75–110 °C (loss of coordinating aqua ligands), 140–208 °C (partial loss of 2-MTZ ligands), 240 °C (dec.); **IR** (ATR, cm^{-1}): $\tilde{\upsilon}$ = 3522 (m, O-H/N-H), 3475 (m, O-H/N-H), 3160 (w, C-H), 3147 (w, C-H), 1634 (w, C=N), 1473 (vw), 1447 (w), 1428 (w), 1369 (w), 1314 (w), 1297 (m), 1196 (w), 1155 (m), 1070 (vs, Cl-O), 1020 (s), 935 (w), 898 (m), 704 (s), 684 (s), 623 (s); **EA**: ($C_8H_{20}Cl_2CuN_{16}O_{10}$, 634.80): calc.: C 15.14, H 3.18, N 35.30 %; found: C 15.39, H 3.05, N 34.97 %; **BAM drophammer**: 5 J; **friction tester**: 5 N; **ESD**: 50 mJ (at grain size 100–500 µm).

19.8.3 IR Spectroscopy of 1–7

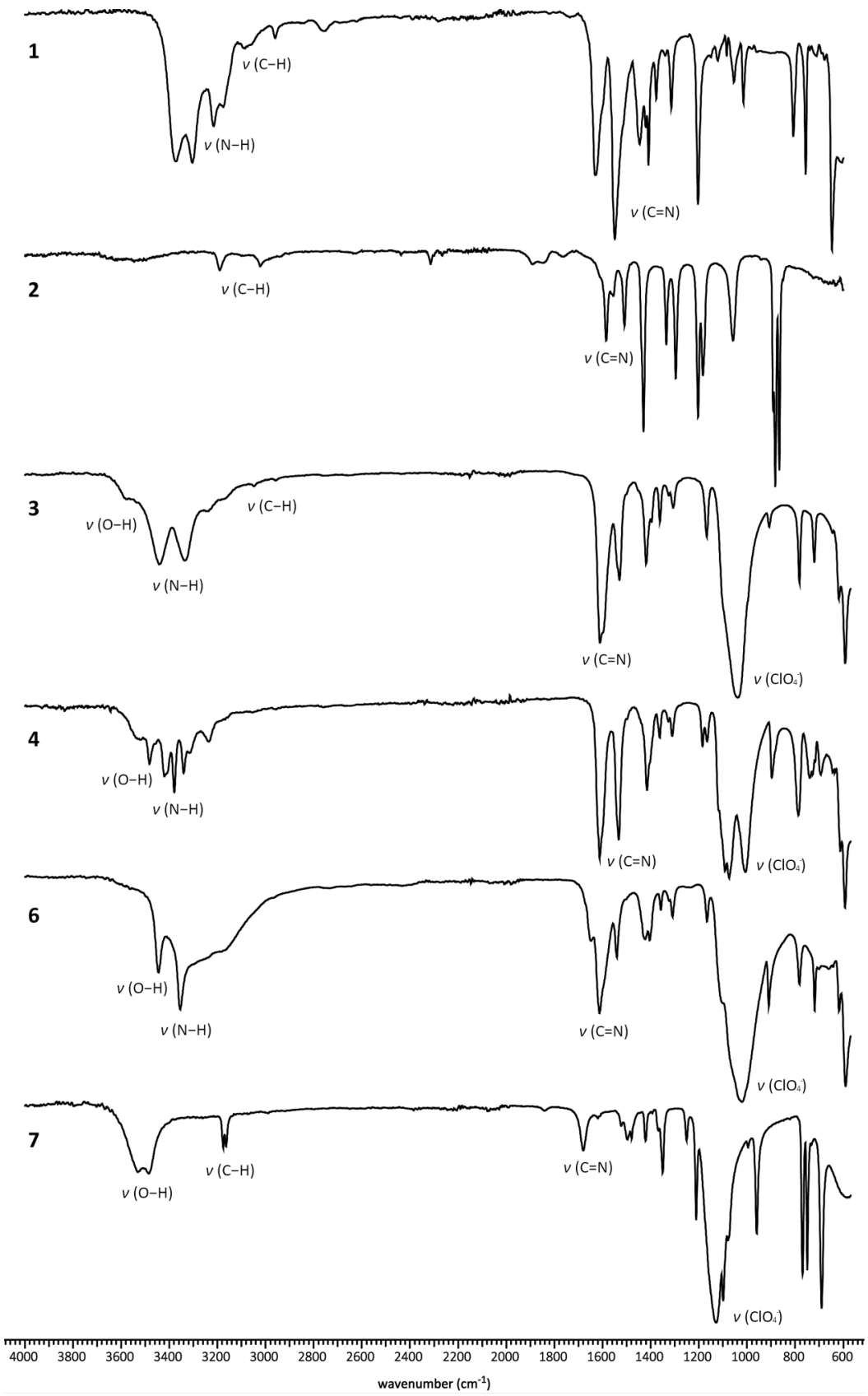


Figure S1. IR spectra of the ligand **1** and **2** as well as the ECC **3**, **4**, **6**, and **7**.

19.8.4 X-ray Diffraction

For all crystalline compounds, an Oxford Xcalibur3 diffractometer with a CCD area detector or Bruker D8 Venture TXS diffractometer equipped with a multilayer monochromator, a Photon 2 detector and a rotating-anode generator were employed for data collection using Mo-*K*α radiation (λ = 0.7107 Å). On the Oxford device, data collection and reduction were carried out using the Crysalispro software.[S11] On the Bruker diffractometer, the data were collected with the Bruker Instrument Service v3.0.21, the data reduction was performed using the SAINT V8.18C software (Bruker AXS Inc., 2011). The structures were solved by direct methods (Sir-92[S12], Sir-97[S13], or Shelxs-97[S14]) and refined by full-matrix least-squares on *F*2 (ShelxL[S14]) and finally checked using the platon software[S15] integrated in the WinGX[S16] software suite. The non-hydrogen atoms were refined anisotropically and the hydrogen atoms were located and freely refined. The absorptions were corrected by a Scale3 Abspack or Sadabs Bruker Apex3 multiscan method.[S17, S18] All Diamond2 plots are shown with thermal ellipsoids at the 50 % probability level and hydrogen atoms are shown as small spheres of arbitrary radius.

$[Cu(H_2O)_2(2\text{-}MTZ)_4](ClO_4)_2$ (7)

By examining received data along the crystallographic *c*-axis, the three-dimensional topology of **7**, which is built up by a layer structure comprising of $[Cu(H_2O)_2(2\text{-}MTZ)_4](ClO_4)_2$ units with altering alignment along *b* becomes clear (Figure 8). In between the observed complex-formed pattern, perchlorate counter-anions once again act as the layers' "cohesive" due to the provision of several hydrogen bond acceptors for aqua and tetrazole ligands.

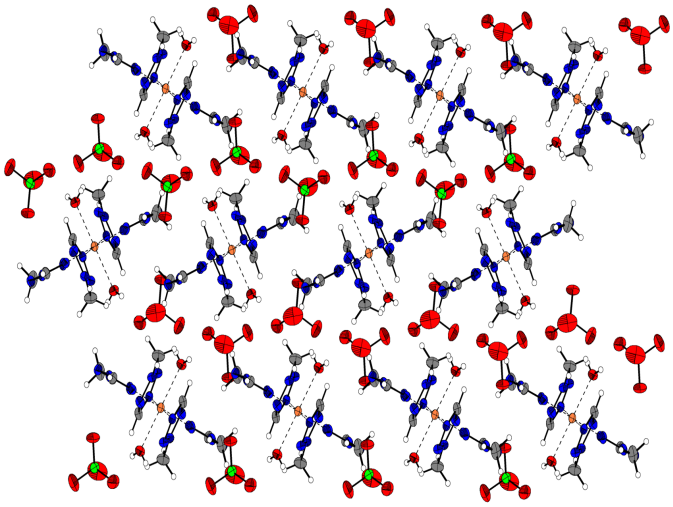


Figure S2. Structure of **7** with the direction of view along the crystallographic *c*-axis.

Table S1. Crystallographic data of **3**–**5**.

	3	**4**	**5**
Formula	$C_8H_{26}Cl_2CuN_{20}O_{11}$	$C_8H_{24}Cl_2CuN_{20}O_{10}$	$C_{10}H_{29}Cl_2CuN_{25}O_{10}$
FW [g mol^{-1}]	712.93	694.91	794.02
Crystal system	Monoclinic	Monoclinic	Triclinic
Space Group	*C*2/*c*	$P2_1$	*P*–1
Color / Habit	Blue blocks	Blue blocks	Blue blocks
Size [mm]	0.15 x 0.15 x 0.20	0.16 x 0.35 x 0.59	0.11 x 0.28 x 0.42
a [Å]	37.8504(12)	7.8894(7)	10.6159(6)
b [Å]	18.5558(5)	19.9150(15)	10.7796(5)
c [Å]	18.0159(5)	8.3691(6)	13.8295(7)
α [°]	90	90	89.498(4)
β [°]	116.272(3)	101.004(8)	80.568(4)
γ [°]	90	90	83.990(4)
V [Å^3]	11346.3(6)	1290.76(18)	1552.55(14)
Z	16	2	2
$\rho_{calc.}$ [g cm^{-3}]	1.669	1.788	1.699
μ [mm^{-1}]	1.043	1.140	0.964
F(000)	5840	710	814
$\lambda_{MoK\alpha}$ [Å]	0.71073	0.71073	0.71073
T [K]	173	173	173
θ Min–Max [°]	4.1, 26.0	4.4, 28.0	4.2, 26.0
Dataset	−46:46; −22:22; −22:22	−10:10; −18:26; −11:11	–13:13; –13:12; –14:17
Reflections collected	46903	11360	11962
Independent refl.	11093	4524	6072
*R*int	0.082	0.041	0.032
Observed reflections	7133	3937	4695
Parameters	832	423	494
R_1 (obs)[a]	0.0643	0.0511	0.0386
wR_2 (all data)[b]	0.1697	0.1278	0.0976
GooF[c]	1.05	1.05	1.03
Resd. Dens. [e Å^{-3}]	−0.51, 1.24	–0.37, 3.24	–0.29, 0.46
Absorption correction	multi-scan	multi-scan	multi-scan
CCDC	1850124	1850121	1850122

a) $R_1 = \Sigma||F_0|- |F_c||/ \Sigma|F_0|$; b) $wR_2 = [\Sigma[w(F_0^2-F_c^2)^2]/\Sigma[w(F_0)^2]]^{1/2}$; $w = [\sigma c^2(F_0^2)+(xP)^2+yP]^{-1}$ and $P=(F_0^2+2F_c^2)/3$; c) GooF = $\{\Sigma[w(F_o^2-F_c^2)^2]/(n-p)\}^{1/2}$ (n = number of reflections; p = total number of parameters).

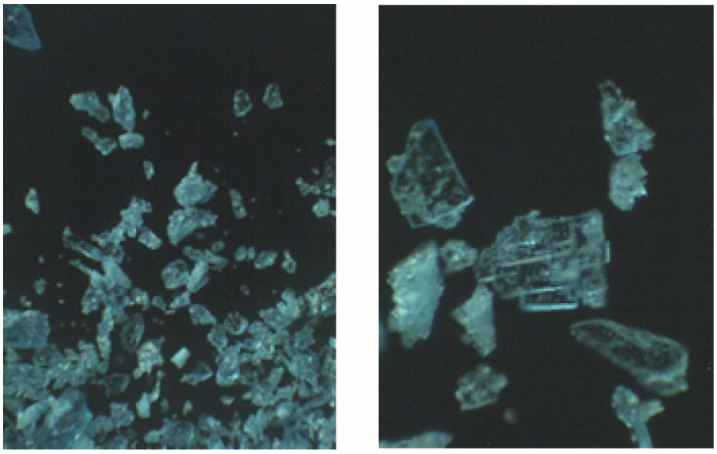


Figure S3. Microscope image of **3** (left; fourfold magnitude) and **4** (right; tenfold magnitude).

Table S2. Crystallographic data of **6** and **7**.

	6	**7**
Formula	$C_4H_{14}Cl_2CuN_{10}O_{10}$	$C_8H_{20}Cl_2CuN_{16}O_{10}$
FW [g mol^{-1}]	496.69	634.80
Crystal system	Monoclinic	Monoclinic
Space Group	$P2_1/n$	$P2_1$
Color / Habit	Blue rods	Blue blocks
Size [mm]	0.10 x 0.14 x 0.22	0.08 x 0.21 x 0.31
a [Å]	7.0476(3)	7.9548(3)
b [Å]	7.4569(3)	14.4157(6)
c [Å]	15.8059(6)	10.8494(4)
α [°]	90	90
β [°]	96.021(4)	95.303(3)
γ [°]	90	90
V [Å^3]	826.07(6)	1238.82(8)
Z	2	2
$\rho_{calc.}$ [g cm^{-3}]	1.997	1.702
μ [mm^{-1}]	1.722	1.175
F(000)	502	646
$\lambda_{MoK\alpha}$ [Å]	0.71069	0.71073
T [K]	173	173
θ Min–Max [°]	4.3, 26.0	4.4, 26.0
Dataset	−8:8; −9:9; −18:19	–9: 9 ; –14:17 ; –12:13
Reflections collected	6210	9189
Independent refl.	1617	2417
Rint	0.023	0.040
Observed reflections	1480	1935
Parameters	160	187
R_1 (obs)[a]	0.0369	0.0412
wR_2 (all data)[b]	0.1030	0.1093
GooF[c]	1.07	1.05
Resd. Dens. [e Å^{-3}]	–0.54, 0.78	–0.50, 0.79
Absorption correction	multi-scan	multi-scan
CCDC	1850120	1850123

a) $R_1 = \Sigma||F_0|- |F_c||/ \Sigma|F_0|$; b) $wR_2 = [\Sigma[w(F_0^2-F_c^2)^2]/\Sigma[w(F_0)^2]]^{1/2}$; $w = [\sigma c^2(F_0^2)+(xP)^2+yP]^{-1}$ and $P=(F_0^2+2F_c^2)/3$; c) GooF = $\{\Sigma[w(F_o^2-F_c^2)^2]/(n-p)\}^{1/2}$ (n = number of reflections; p = total number of parameters).

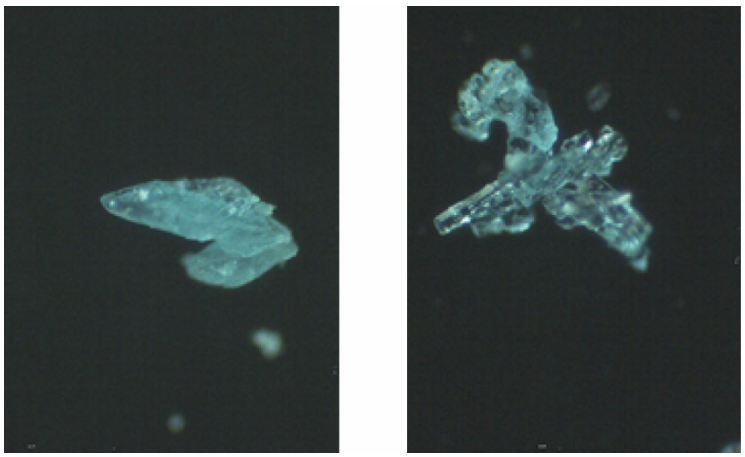


Figure S4 Microscope image of **6** (left; fourfold magnitude) and **7** (right; tenfold magnitude).

19.8.5 DTA Plots of 1–7

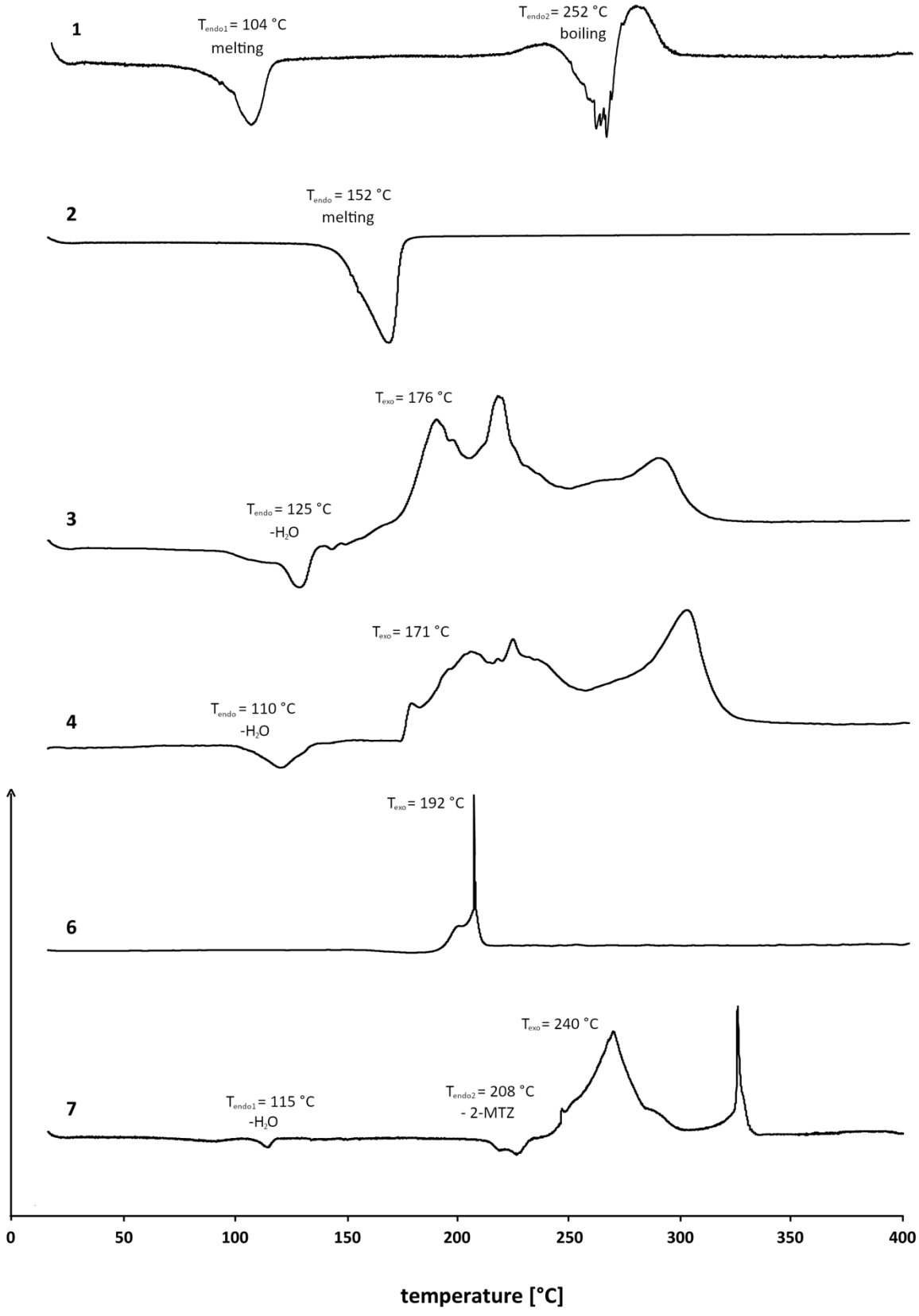


Figure S5. DTA plots of **1–4**, **6**, and **7**.

19.8.6 TGA Plots of 1–4

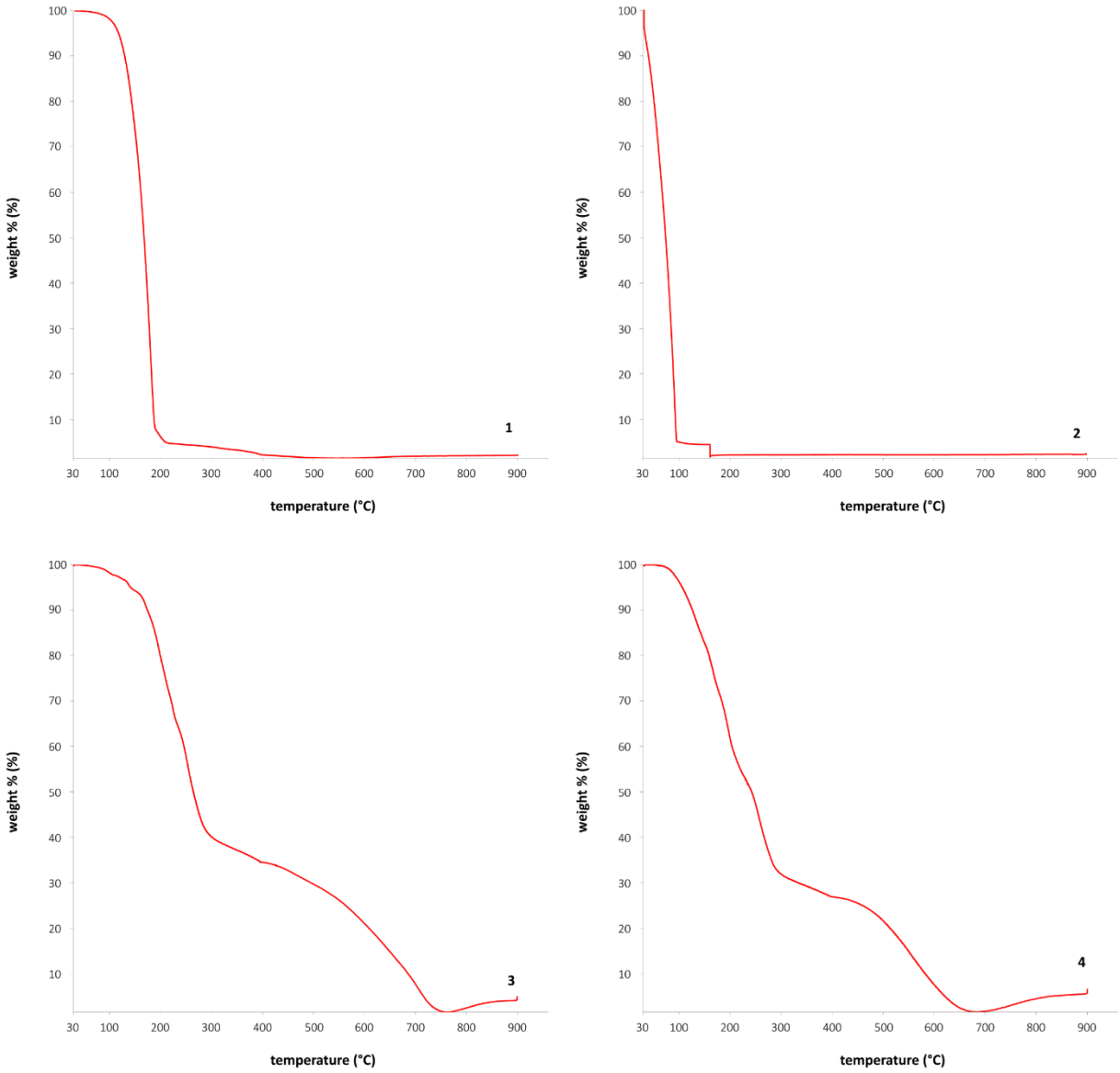


Figure S6. TGA plots (5 °C min^{-1}) of the ligands **1** and **2** as well as the copper(II) perchlorate complexes **3** and **4**.

19.8.8 Hot Plate, Hot Needle and Optical Initiation Tests

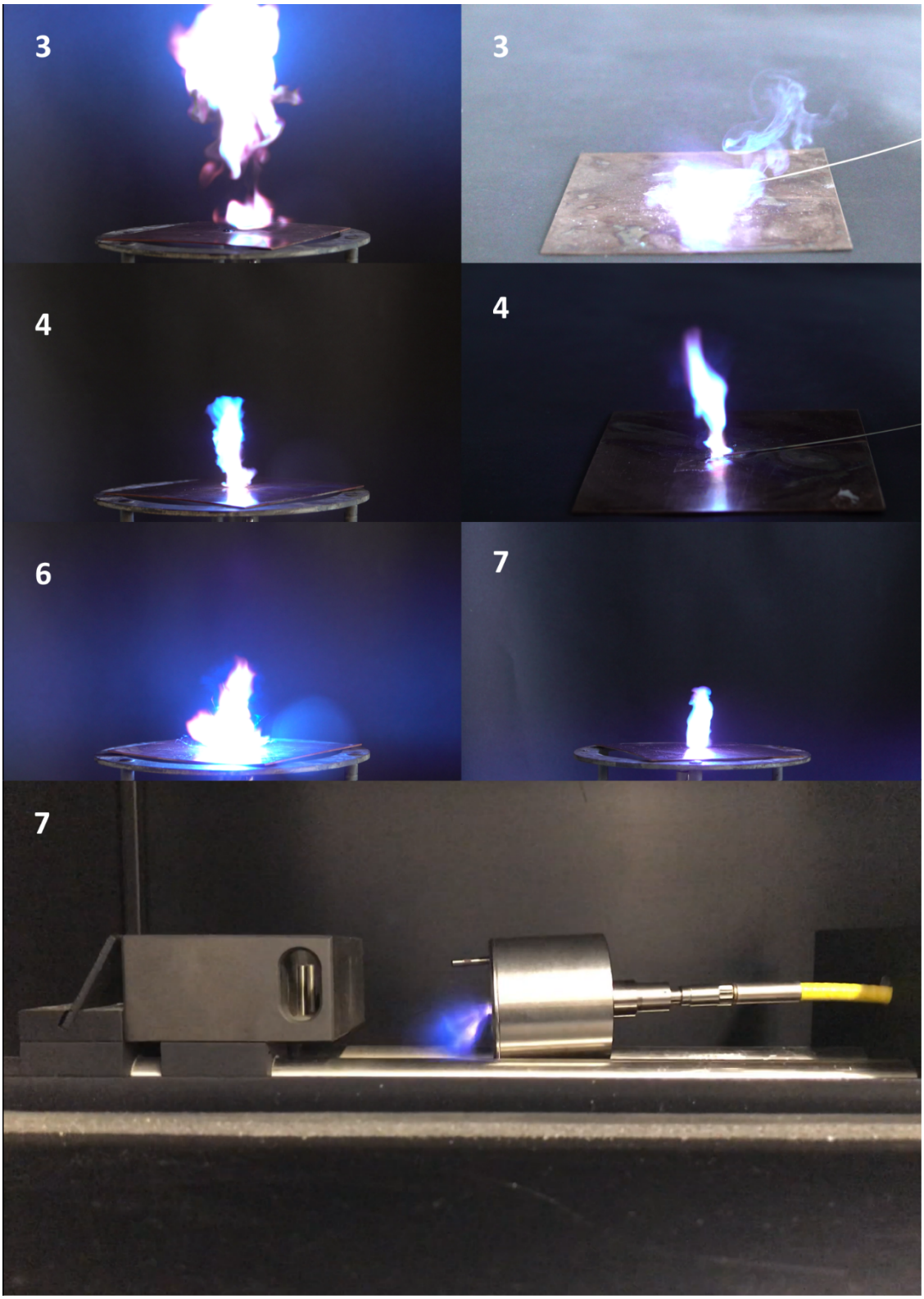


Figure S7. Hot plate tests of **3**, **4**, **6** and **7**, hot needle tests of **3** and **4**, as well as optical initiation of **7**.

19.8.9 References

[S1] NATO standardization agreement (STANAG) on explosives, impact sensitivity tests, no. 4489, 1st ed., Sept. 17, **1999**.

[S2] WIWEB-Standardarbeitsanweisung 4-5.1.02, Ermittlung der Explosionsgefährlichkeit, hier der Schlagempfindlichkeit mit dem Fallhammer, Nov. 8, **2002**.

[S3] http://www.ozm.cz, Accessed May 2018.

[S4] http://www.bam.de, Accessed May 2018.

[S5] NATO standardization agreement (STANAG) on explosive, friction sensitivity tests, no. 4487, 1st ed., Aug. 22, **2002**.

[S6] WIWEB-Standardarbeitsanweisung 4-5.1.03, Ermittlung der Explosionsgefährlichkeit oder der Reibeempfindlichkeit mit dem Reibeapparat, Nov. 8, **2002**.

[S7] Impact: insensitive > 40 J, less sensitive ≥ 35 J, sensitive ≥ 4 J, very sensitive ≤ 3 J; Friction: insensitive > 360 N, less sensitive = 360 N, sensitive < 360 N and > 80 N, very sensitive ≤ 80 N, extremely sensitive ≤ 10 N. According to the UN Recommendations on the Transport of Dangerous Goods, (+) indicates not safe for transport.

[S8] A. Ismael, J. A. Paixão, R. Fausto and M. L. S. Cristiano, *J. Mol. Struct.*, 2012, **1023**, 129.

[S9] A. Thomann, J. Eberhard, G. Allegretta, M. Empting, R. W. Hartmann, *Synlett*, 2015, **26**, 2606–2610.

[S10] P. N. Gaponik, M. M. Degtyarik, A. S. Lyakhov, V. E. Matulis, O. A. Ivashkevih, M. Quesada and J. Reedijk, *Inorg. Chim. Acta*, 2005, **358**, 3949–3957.

[S11] *CrysAlisPro*, Oxford Diffraction Ltd., version 171.33.41, **2009**.

[S12] A. Altomare, G. Cascarano, C. Giacovazzo, A. Guagliardi, *J. Appl. Crystallogr.*, 1992, **26**, 343–350.

[S13] a) A. Altomare, G. Cascarano, C. Giacovazzo, A. Guagliardi, A. G. G. Moliterni, M. C. Burla, G. Polidori, M. Camalli, R. Spagna, *SIR97*, **1997**; b) A. Altomare, M. C. Burla,

M. Camalli, G. L. Cascarano, C. Giacovazzo, A. Guagliardi, A. G. G. Moliterni, G. Polidori, R. Spagna, *J. Appl. Crystallogr.*, 1999, **32**, 115–119.

[S14] a) G. M. Sheldrick, *SHELXL-97*, *Program for the Refinement of Crystal Structures*, University of Göttingen, Germany, **1997**; b) G. M. Sheldrick, *Acta Crystallogr. Sect. A*, 2008, **64**, 112–122.

[S15] A. L. Spek, *PLATON*, *A Multipurpose Crystallographic Tool*, Utrecht University, The Netherlands, **1999**.

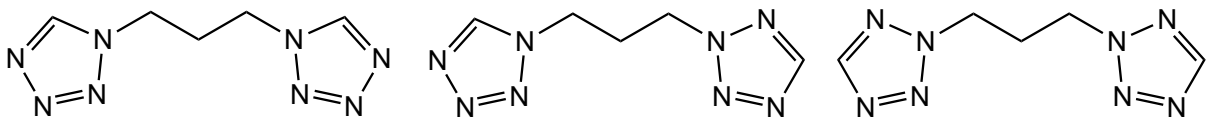
[S16] L. J. Farrugia, *J. Appl. Cryst.*, 2012, **45**, 849–854.

[S17] Empirical absorption correction using spherical harmonics, implemented in SCALE3 ABSPACK scaling algorithm (CrysAlisPro Oxford Diffraction Ltd., Version 171.33.41, **2009**).

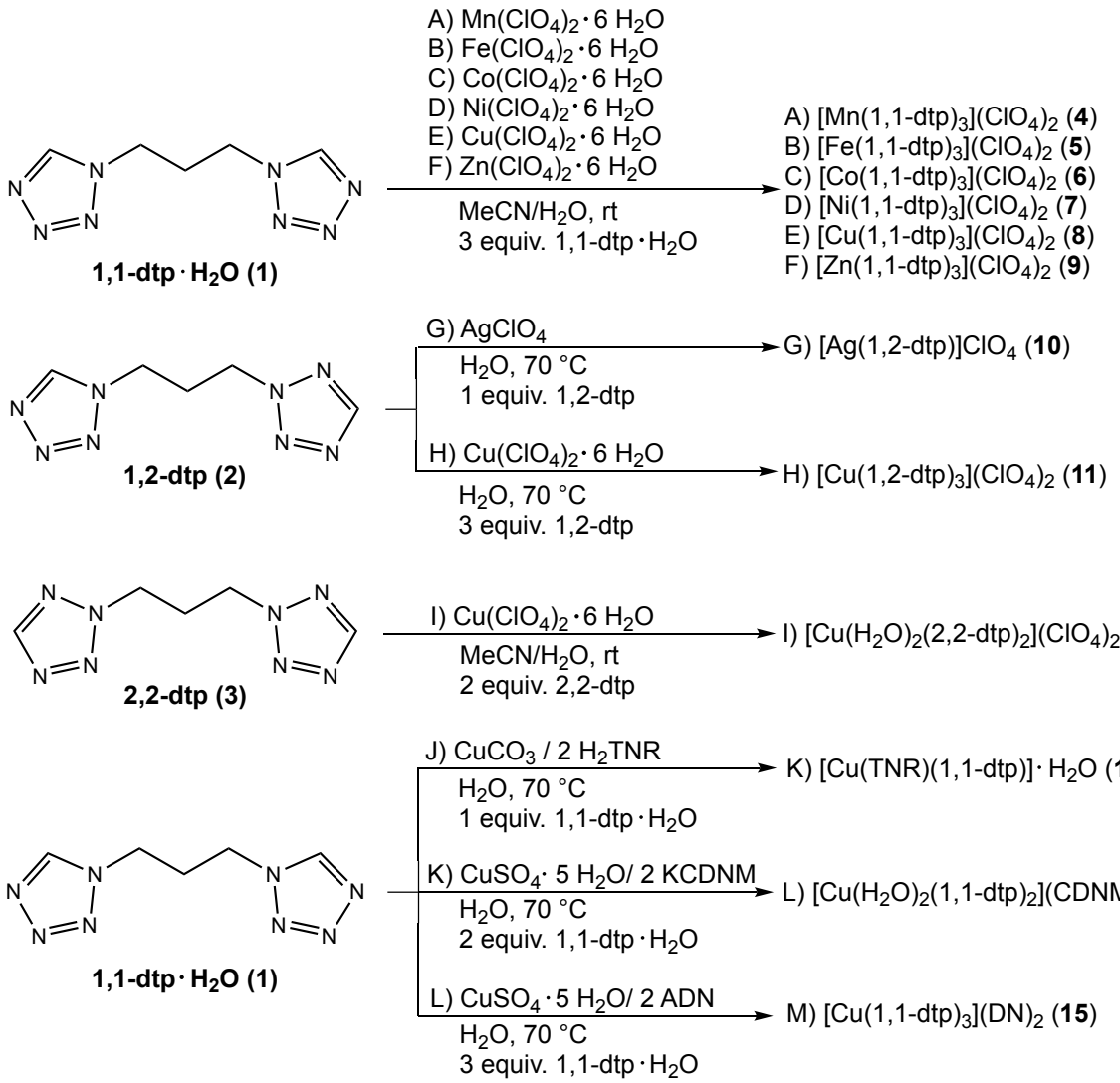
[S18] *APEX3*. Bruker AXS Inc., Madison, Wisconsin, USA.

19.9 Supplementary Information: Highly Functional Energetic Complexes: Stability Tuning through Coordination Diversity of Isomeric Propyl-linked Ditetrazoles

19.9.1 Compounds overview



1,1-dtp ·H_2O (1) **1,2-dtp (2)** **2,2-dtp (3)**



19.9.2 IR Spectroscopy of 1–15

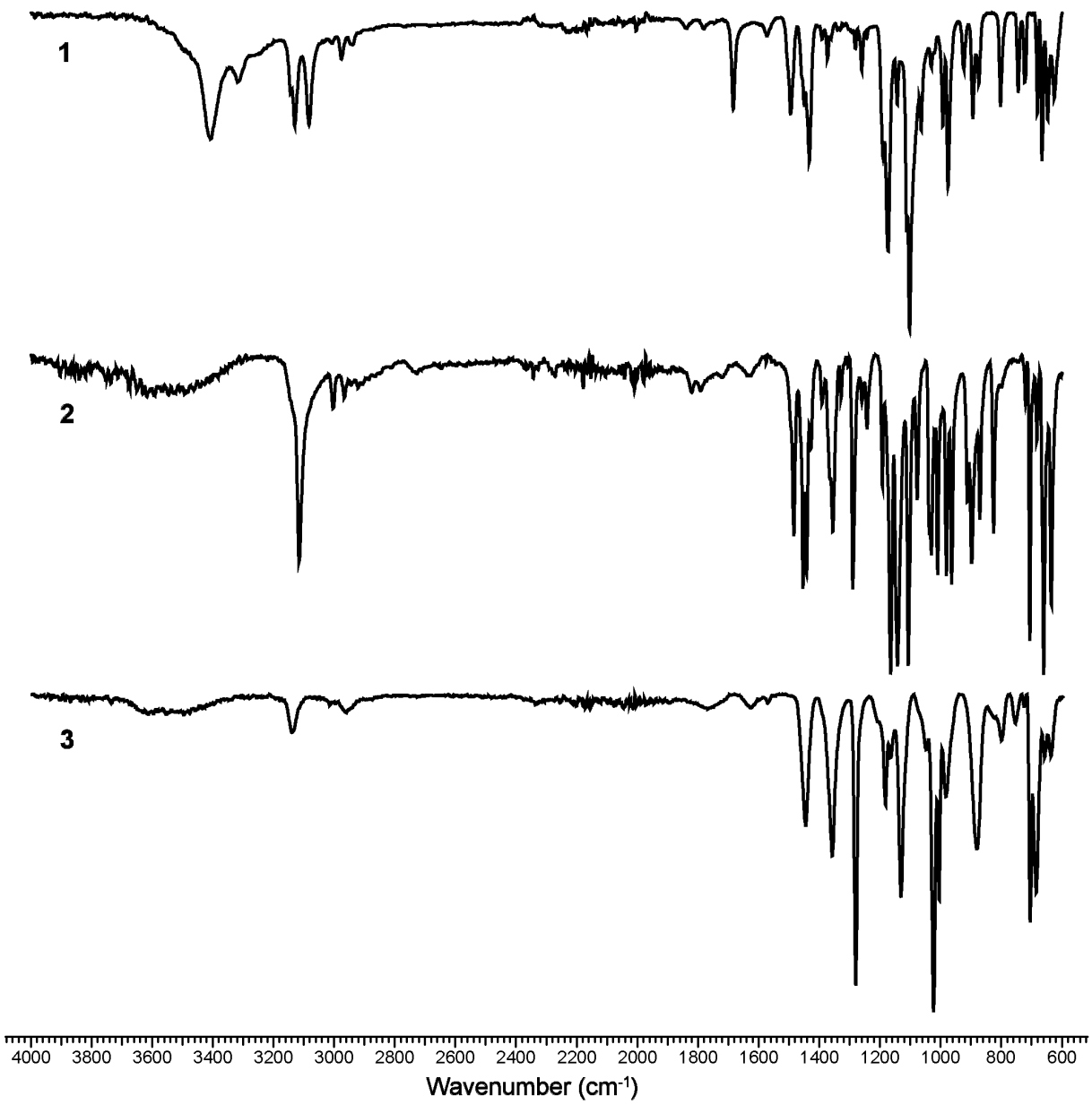


Figure S1. Infrared spectra of **1**–**3**.

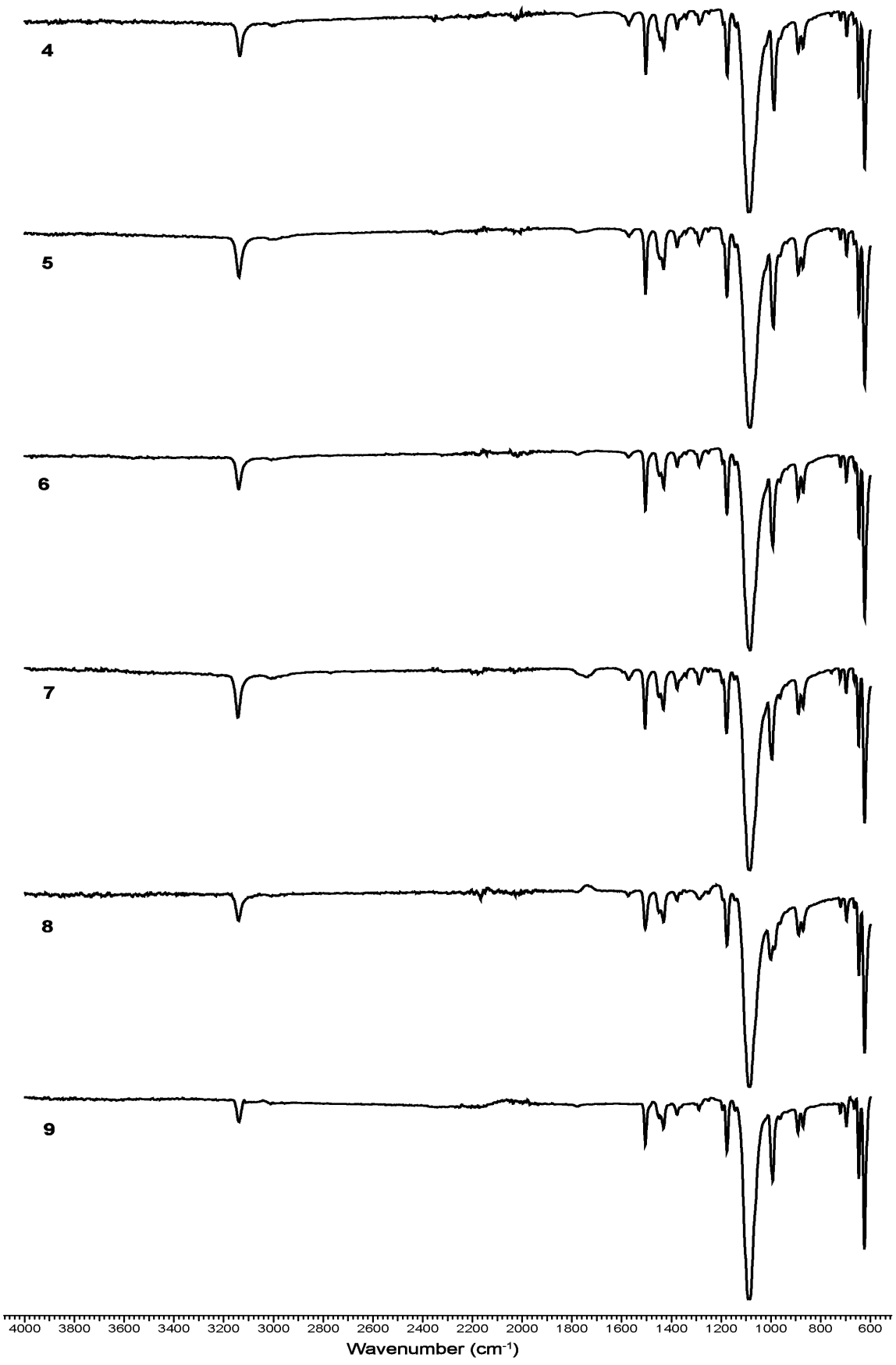


Figure S2. Infrared spectra of **4**–**9**.

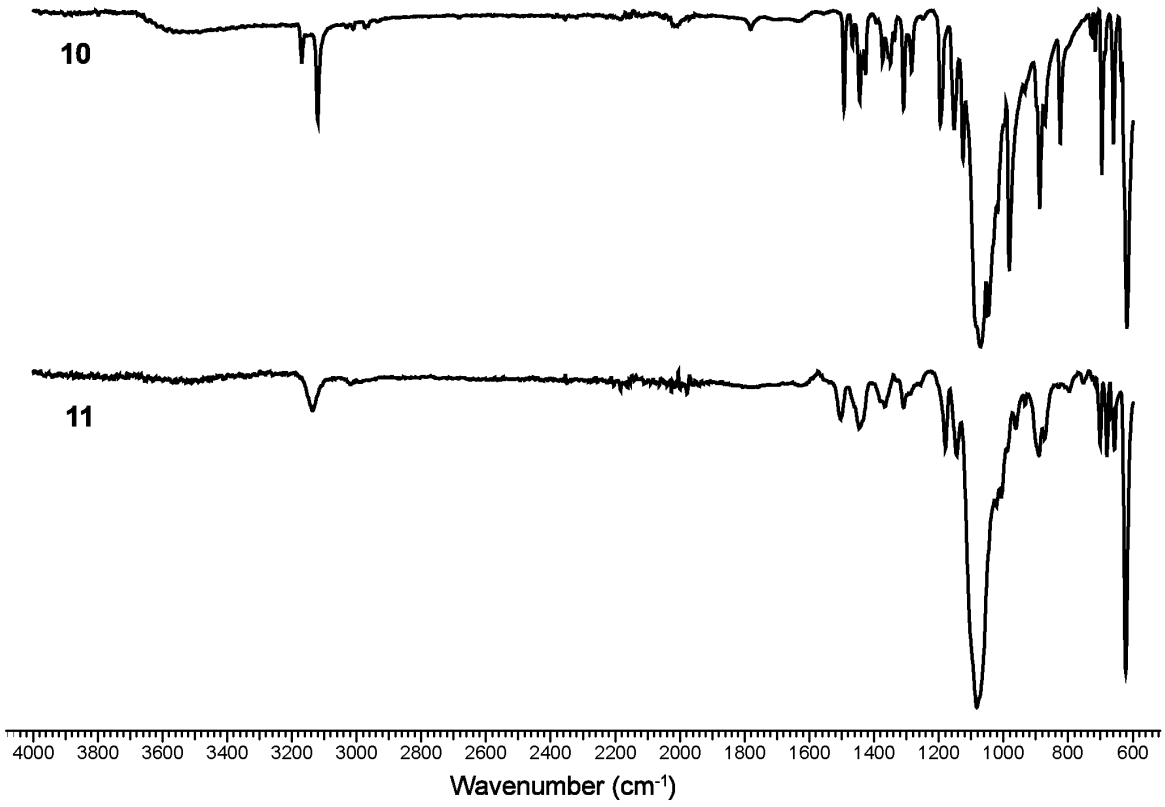


Figure S3. Infrared spectra of **10** and **11**.

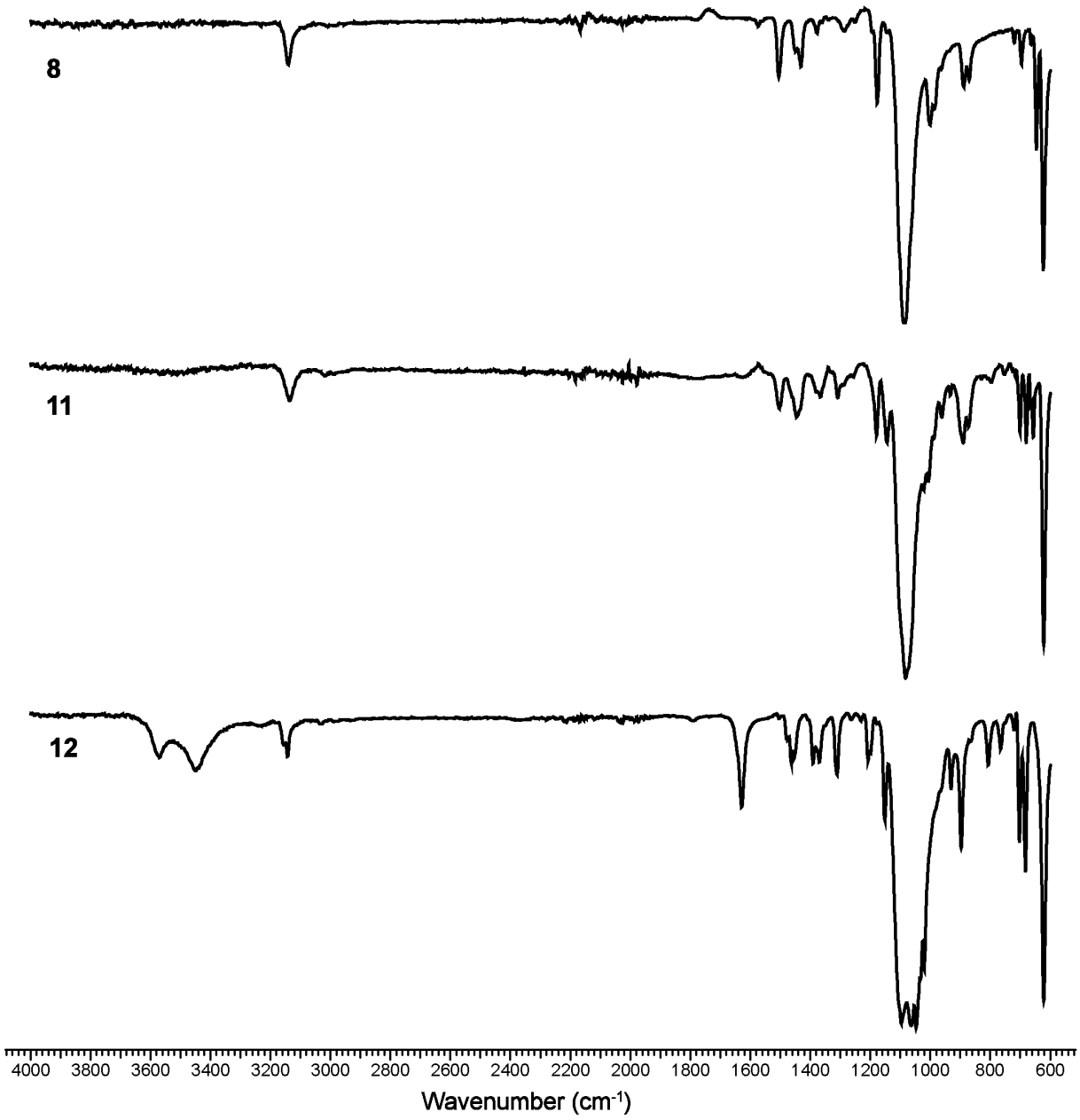


Figure S4. Infrared spectra of **8** and **11**/**12**.

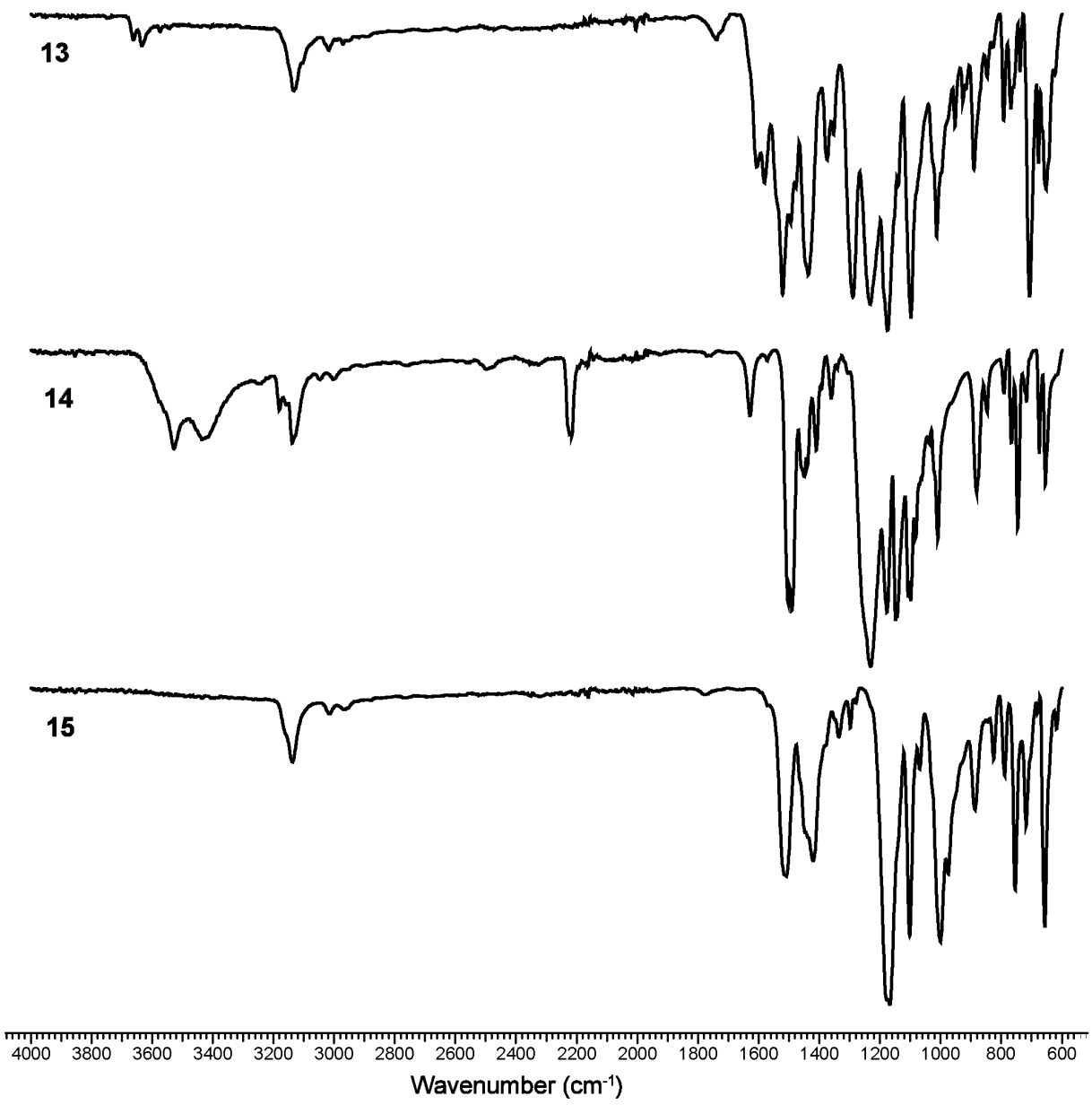


Figure S5. Infrared spectra of **13**–**15**.

19.9.3 X-ray Diffraction

For all crystalline compounds, an Oxford Xcalibur3 diffractometer with a CCD area detector or Bruker D8 Venture TXS diffractometer equipped with a multilayer monochromator, a Photon 2 detector and a rotating-anode generator were employed for data collection using Mo-*K*α radiation (λ = 0.7107 Å). On the Oxford device, data collection and reduction were carried out using the Crysalispro software[S1]. On the Bruker diffractometer, the data were collected with the Bruker Instrument Service v3.0.21, the data reduction was performed using the SAINT V8.18C software (Bruker AXS Inc., 2011). The structures were solved by direct methods (Sir-92[S2], Sir-97[S3] or Shelxs-97[S4]) and refined by full-matrix least-squares on *F*2 (ShelxL[S4]) and finally checked using the platon software[S5] integrated in the WinGX[S6] software suite. The non-hydrogen atoms were refined anisotropically and the hydrogen atoms were located and freely refined. The absorptions were corrected by a Scale3 Abspack or Sadabs Bruker Apex3 multiscan method[S7,8]. All Diamond2 plots are shown with thermal ellipsoids at the 50% probability level and hydrogen atoms are shown as small spheres of arbitrary radius.

Table S1. Crystallographic data of **1**–**5**.

	1	**2**	**3**	**4**	**5**
Formula	$C_5H_{10}N_8O$	$C_5H_8N_8$	$C_5H_8N_8$	$C_{15}H_{24}Cl_2MnN_{24}O_8$	$C_{15}H_{24}Cl_2FeN_{24}O_8$
FW [g mol^{-1}]	198.19	180.18	180.18	794.36	795.26
Crystal system	Orthorhombic	Monoclinic	Monoclinic	Trigonal	Trigonal
Space Group	*Pbca*	$P2_1/n$	$P2_1/c$	$P\bar{3}c1$	$P\bar{3}c1$
Color / Habit	Colorless block	Colorless block	Colorless block	Colorless block	Yellow block
Size [mm]	0.38 x 0.54 x 0.59	0.31 x 0.41 x 0.42	0.11 x 0.33 x 0.47	0.23 x 0.37 x 0.66	0.11 x 0.14 x 0.21
a [Å]	10.2283(10)	10.6063(6)	11.6710(6)	11.1661(2)	10.9450(4)
b [Å]	10.9670(12)	6.5631(4)	4.7586(2)	11.1661(2)	10.9450(4)
c [Å]	16.3177(15)	11.7632(7)	15.1639(7)	14.7523(4)	14.5170(5)
α [°]	90	90	90	90	90
β [°]	90	90.685(5)	105.362(5)	90	90
γ [°]	90	90	90	120	120
V [Å^3]	1830.4(3)	818.78(8)	812.08(7)	1592.92(8)	1506.05(14)
Z	8	4	4	2	2
$\rho_{calc.}$ [g cm^{-3}]	1.439	1.462	1.474	1.656	1.754
μ [mm^{-1}]	0.111	0.107	0.108	0.665	0.765
F(000)	832	376	376	810	812
$\lambda_{MoK\alpha}$ [Å]	0.71073	0.71073	0.71073	0.71073	0.71069
T [K]	173	173	143	173	123
θ Min–Max [°]	4.4, 26.0	4.7, 26.0	4.5, 26.0	4.2, 26.0	4.3, 26.3
Dataset	−10: 12; −13: 13; −20: 19	−13: 12; −7: 8; −14: 14	−13: 14; −5: 5; −17: 18	−13: 13; −13: 13; −18: 18	−13: 13; −13: 13; −18: 17
Reflections collected	13404	6419	5707	11705	11272
Independent refl.	1792	1598	1588	1036	1032
*R*int	0.034	0.020	0.022	0.022	0.039
Observed reflections	1485	1387	1370	925	873
Parameters	167	150	118	98	101
R_1 (obs)[a]	0.0301	0.0310	0.0319	0.0292	0.0304
wR_2 (all data)[b]	0.0772	0.083	0.0805	0.0825	0.080
GooF[c]	1.04	1.05	1.04	1.08	1.07
Resd. Dens. [e Å^{-3}]	−0.19, 0.19	−0.28, 0.17	−0.22, 0.15	−0.34, 0.40	−0.39, 0.56
Absorption correction	multi-scan	multi-scan	multi-scan	multi-scan	multi-scan
CCDC	1816637	1816632	1816632	1816628	1816635

a) $R_1 = \Sigma||F_0|- |F_c||/ \Sigma|F_0|$; b) $wR_2 = [\Sigma[w(F_0^2-F_c^2)^2]/\Sigma[w(F_0)^2]]^{1/2}$; $w = [\sigma c^2(F_0^2)+(xP)^2+yP]^{-1}$ and $P=(F_0^2+2F_c^2)/3$; c) GooF = $\{\Sigma[w(F_o^2-F_c^2)^2]/(n-p)\}^{1/2}$ (n = number of reflections; p = total number of parameters).

Table S2. Crystallographic data of **6** and **8**–**11**.

	6	**8**	**9**	**10**	**11**
Formula	$C_{12}H_{28}CoN_{26}O_8$	$C_{15}H_{24}Cl_2CuN_{24}O_8$	$C_{15}H_{24}Cl_2N_{24}O_8Zn$	$C_5H_8AgClN_8O_4$	$C_{15}H_{24}Cl_2CuN_{24}O_8$
FW [g mol^{-1}]	798.41	802.96	804.80	387.49	802.96
Crystal system	Triclinic	Trigonal	Trigonal	Monoclinic	Triclinic
Space Group	*P*−3*c*1	*P*−3*c*1	*P*−3*c*1	$P2_1/c$	*P*−1
Color / Habit	Orange block	Blue block	Colorless block	Colorless block	Blue rod
Size [mm]	0.06 x 0.07 x 0.10	0.18 x 0.27 x 0.28	0.23 x 0.37 x 0.50	0.10 x 0.20 x 0.46	0.16 x 0.19 x 0.24
a [Å]	11.085(5)	11.061(5)	11.0824(3)	9.8070(2)	13.2260(6)
b [Å]	11.085 (5)	11.061(5)	11.0824(3)	10.7250(2)	13.7860(8)
c [Å]	14.554(5)	14.622(5)	14.7279(8)	11.1830(3)	20.2220(8)
α [°]	90	90	90	90	99.253(4)
β [°]	90	90	90	105.128(2)	102.001(4)
γ [°]	120	120	120	90	114.596(5)
V [Å^3]	1548.8(17)	1549.3(17)	1566.53(14)	1135.47(5)	3150.0(3)
Z	2	2	2	4	2
$\rho_{calc.}$ [g cm^{-3}]	1.712	1.721	1.706	2.267	1.693
μ [mm^{-1}]	0.811	0.962	1.038	2.039	0.947
F(000)	814	818	820	760	1636
$\lambda_{MoK\alpha}$ [Å]	0.71069	0.71069	0.71073	0.71069	0.71069
T [K]	173	123	173	123	123
θ Min–Max [°]	3.5, 26.0	4.6, 26.2	4.2, 32.4	4.2, 26.0	4.2, 26.0
Dataset	−13: 13; −13:13; −17: 16	−11: 13; −13: 13; −18: 15	−16: 15; −15: 16; −21: 21	−12: 12; −12: 13; −13: 13	−16: 16; −11:17; −24: 24
Reflections collected	13757	11267	15991	8392	22717
Independent refl.	1023	1037	1815	2218	12300
*R*int	0.045	0.041	0.057	0.020	0.041
Observed reflections	918	828	1210	2071	9173
Parameters	99	103	97	204	925
R_1 (obs)[a]	0.0309	0.0329	0.0397	0.0170	0.0651
wR_2 (all data)[b]	0.0823	0.0927	0.1050	0.0413	0.1860
GooF[c]	1.09	1.10	1.02	1.04	1.03
Resd. Dens. [e Å^{-3}]	−0.38, 0.54	−0.24, 0.51	−0.37, 0.54	−0.39, 0.45	−0.94 / 2.98
Absorption correction	multi-scan	multi-scan	multi-scan	multi-scan	multi-scan
CCDC	1816627	1816626	1816629	1816630	1816636

a) $R_1 = \Sigma||F_0|- |F_c||/ \Sigma|F_0|$; b) $wR_2 = [\Sigma[w(F_0^2-F_c^2)^2]/\Sigma[w(F_0)^2]]^{1/2}$; $w = [\sigma c^2(F_0^2)+(xP)^2+yP]^{-1}$ and $P=(F_0^2+2F_c^2)/3$; c) GooF = $\{\Sigma[w(F_o^2-F_c^2)^2]/(n-p)\}^{1/2}$ (n = number of reflections; p = total number of parameters).

Table S3. Crystallographic data of **12**, **14** and **15**.

	12	**14**	**15**
Formula	$C_{10}H_{20}Cl_2CuN_{16}O_{10}$	$C_{14}H_{20}CuN_{22}O_{10}$	$C_{15}H_{24}CuN_{30}O_8$
FW [g mol^{-1}]	658.86	720.06	816.11
Crystal system	Monoclinic	Triclinic	Monoclinic
Space Group	$P2_1/c$	$P\bar{1}$	$C2/c$
Color / Habit	Blue block	Blue block	Blue platelet
Size [mm]	0.10 x 0.25 x 0.30	0.28 x 0.40 x 0.60	0.02 x 0.04 x 0.10
a [Å]	8.4824(4)	9.4670(5)	27.0187(10)
b [Å]	14.4398(5)	10.3140(5)	18.5080(6)
c [Å]	10.7195(5)	14.0761(7)	15.4569(5)
α [°]	90	90.390(4)	90
β [°]	109.217	92.808(4)	124.910(1)
γ [°]	90	98.412(4)	90
V [Å^3]	1239.81(10)	1357.87(12)	6338.5(4)
Z	2	2	8
$\rho_{calc.}$ [g cm^{-3}]	1.765	1.761	1.711
μ [mm^{-1}]	1.178	0.900	0.784
F(000)	670	734	3336
$\lambda_{MoK\alpha}$ [Å]	0.71073	0.71073	0.71073
T [K]	233	123	103
θ Min–Max [°]	4.2, 26.2	4.6, 26.0	2.5, 26.0
Dataset	−10: 10; −17: 17; −13: 13	−11: 11; −12: 12; −17: 17	−33: 33; −22: 22; −19: 17
Reflections collected	18445	11012	46253
Independent refl.	2490	5316	6221
Rint	0.033	0.023	0.043
Observed reflections	2224	4356	5166
Parameters	246	449	562
R_1 (obs)[a]	0.0395	0.0293	0.0283
wR_2 (all data)[b]	0.1110	0.0735	0.0774
GooF[c]	1.06	1.03	1.05
Resd. Dens. [e Å^{-3}]	−0.67, 0.83	−0.38, 0.45	−0.55, 0.35
Absorption correction	multi-scan	multi-scan	multi-scan
CCDC	1816633	1816631	1816634

a) $R_1 = \Sigma||F_0|- |F_c||/ \Sigma|F_0|$; b) $wR_2 = [\Sigma[w(F_0^2-F_c^2)^2]/\Sigma[w(F_0)^2]]^{1/2}$; $w = [\sigma c^2(F_0^2)+(xP)^2+yP]^{-1}$ and $P=(F_0^2+2F_c^2)/3$; c) GooF = $\{\Sigma[w(F_o^2-F_c^2)^2]/(n-p)\}^{1/2}$ (n = number of reflections; p = total number of parameters).

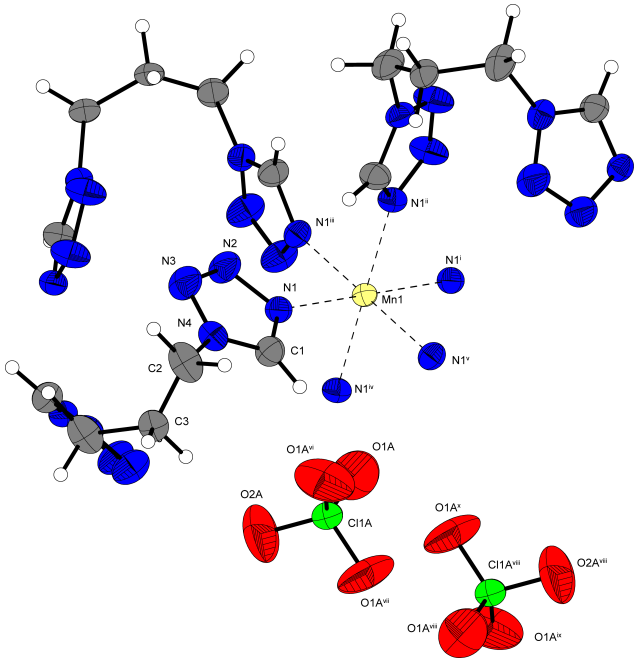


Figure S6. Manganese(II) coordination environment of $[Mn(1,1\text{-dtp})_3](ClO_4)_2$ (**4**). Selected bond length (Å): Mn1–N1 2.2533(13); selected bond angles (°): N1–Mn1–N1^{i} 180.00, N1–Mn1–N1^{iii} 91.25(5), and N1–Mn1–N1^{v} 88.76(5). Symmetry codes: (i) –x, –y, –z; (ii) x–y, x, –z; (iii) –y, x–y, z; (iv) –x+y, –x, z; (v) y, –x+y, –z; (vi) 1–x+y, 1–x, z; (vii) 1–y, x–y, z; (viii) 1–x, –y, –z; (ix) x–y, –1+x, –z; (x) y, –x+y, –z.

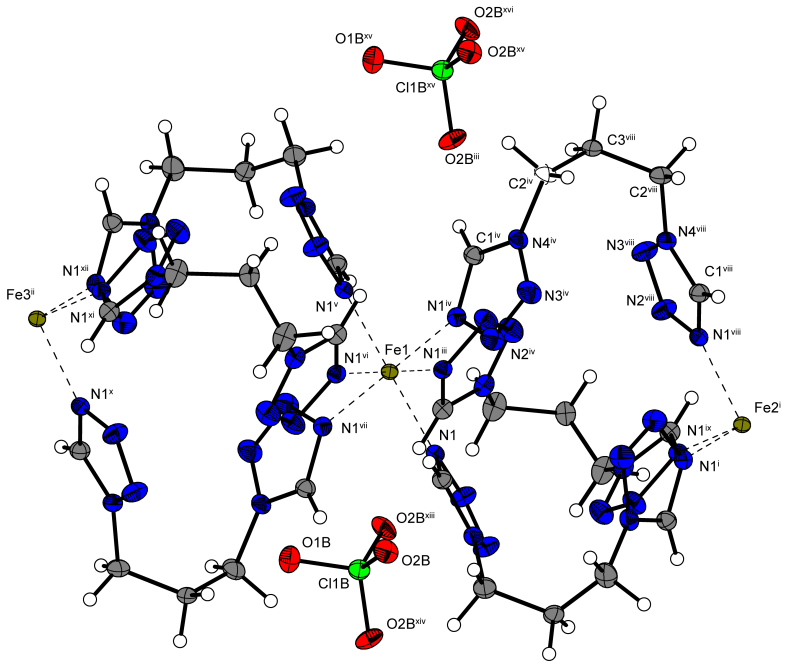


Figure S7. Complex unit of $[Fe(1,1\text{-dtp})_3](ClO_4)_2$ (**5**). Selected bond length (Å): Fe1–N1 1.9950(17); selected bond angles (°): N1–Fe1–N1^{iii} 90.55(7), N1–Fe1–N1^{v} 180.00, and N1–Fe1–N1^{iv} 89.45(7). Symmetry codes: (i) x–y, –y, 0.5–z; (ii) x–y, –y, 0.5–z; (iii) –y, x–y, z; (iv) –x+y, –x, z; (v)

–x, −y, −z; (vi) y, −x+y, −z; (vii) x−y, x, −z; (viii) –x, −x+y, 0.5−z; (ix) y, x, 0.5−z; (x) x, x−y, −0.5+z; (xi) –y, −x, −0.5+z; (xii) –x+y, y, −0.5+z; (xiii) –x+y, 1−x, z; (xiv) 1−y, 1+x−y, z; (xv) −1+x, −1+y, z; (xvi) −1−x+y, −x, z.

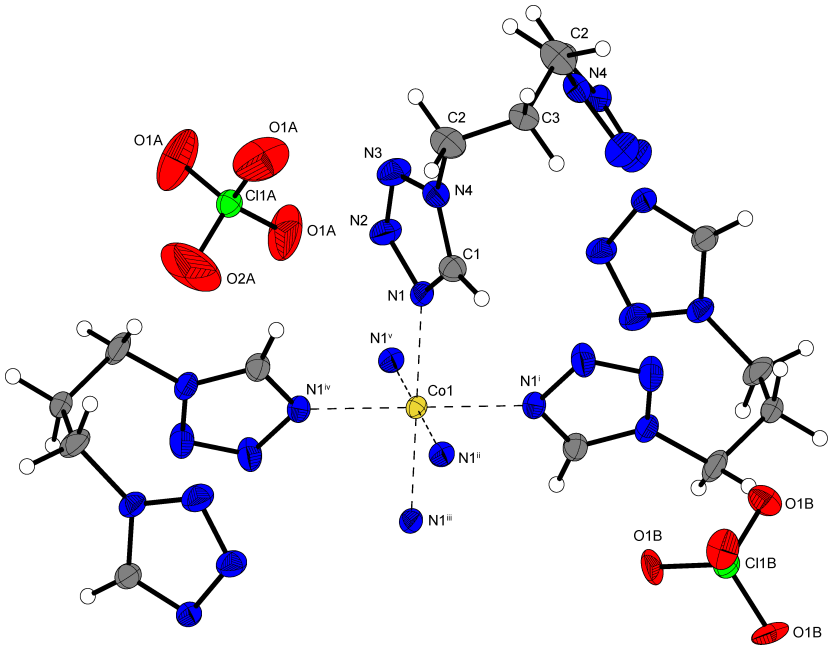


Figure S8. Cobalt(II) coordination environment of $[Co(1,1\text{-dtp})_3](ClO_4)_2$ (**6**). Selected bond length (Å): Co1–N1 2.1399(17). selected bond angles (°): N1–Co1–N1^{i} 91.19(6), N1–Co1–N1^{iii} 180.00, and N1–Zn1–N1^{ii} 88.81(7). Symmetry codes: (i) −y, x−y, z; (ii) x−y, x, 1−z; (iii) –x, −y, 1−z; (iv) y, −x+y, 1−z; (v) –x+y, −x, z.

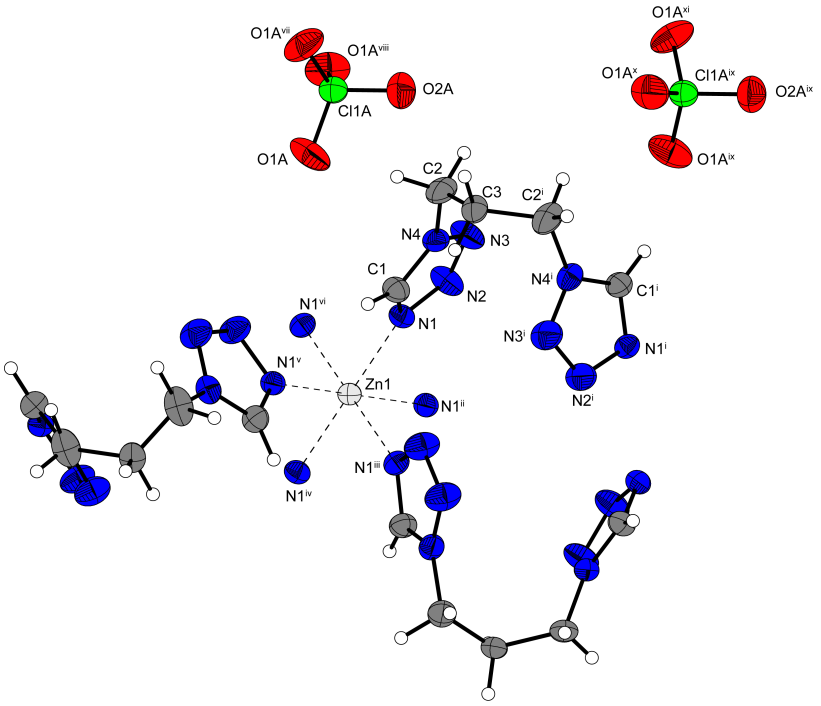


Figure S9. Zinc(II) coordination environment of $[Zn(1,1\text{-dtp})_3](ClO_4)_2$ (**9**). Selected bond length (Å): Zn1–N1 2.1647(15). selected bond angles (°): N1–Zn1–N1^{ii} 90.80(7), N1–Zn1–N1^{iv} 180.00, and N1–Zn1–N1^{vi} 89.20(7). Symmetry codes: (i) −x, −x+y, 0.5−z; (ii) –x+y, −x, z; (iii) –y, x−y, z; (iv) –x, −y, −z; (v) x−y, x, −z; (vi) y, −x+y, −z; (vii) –x+y, 1−x, z; (viii) 1–y, 1+x−y, z; (ix) –x+y, y, 0.5+z; (x) x, 1+x−y, 0.5+z; (xi) 1–y, 1−x, 0.5+z.

Complex **13** (Figure S10) shows an octahedral coordination sphere with a molecular unit containing one bidentate ditetrazole ligand and a tetradentate styphnate dianion (via the nitro- and deprotonated hydroxy groups). Bridging between the copper(II) metal centers through all ligands leads to the formation of polymeric chains.

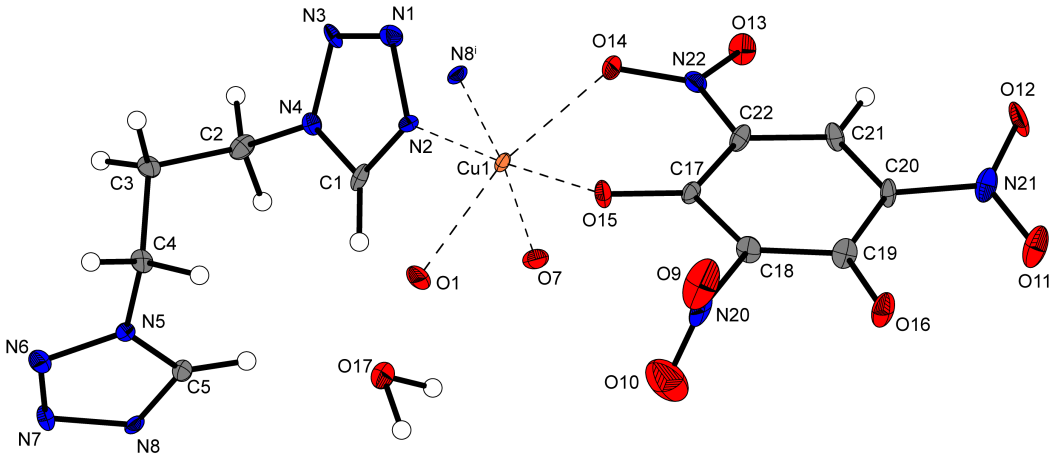


Figure S10. Copper(II) coordination environment of $[Cu(TNR)(1,1\text{-dtp})] \cdot H_2O$ (**13**).

19.9.4 DTA Plots of 1–3, 10 and 13–15

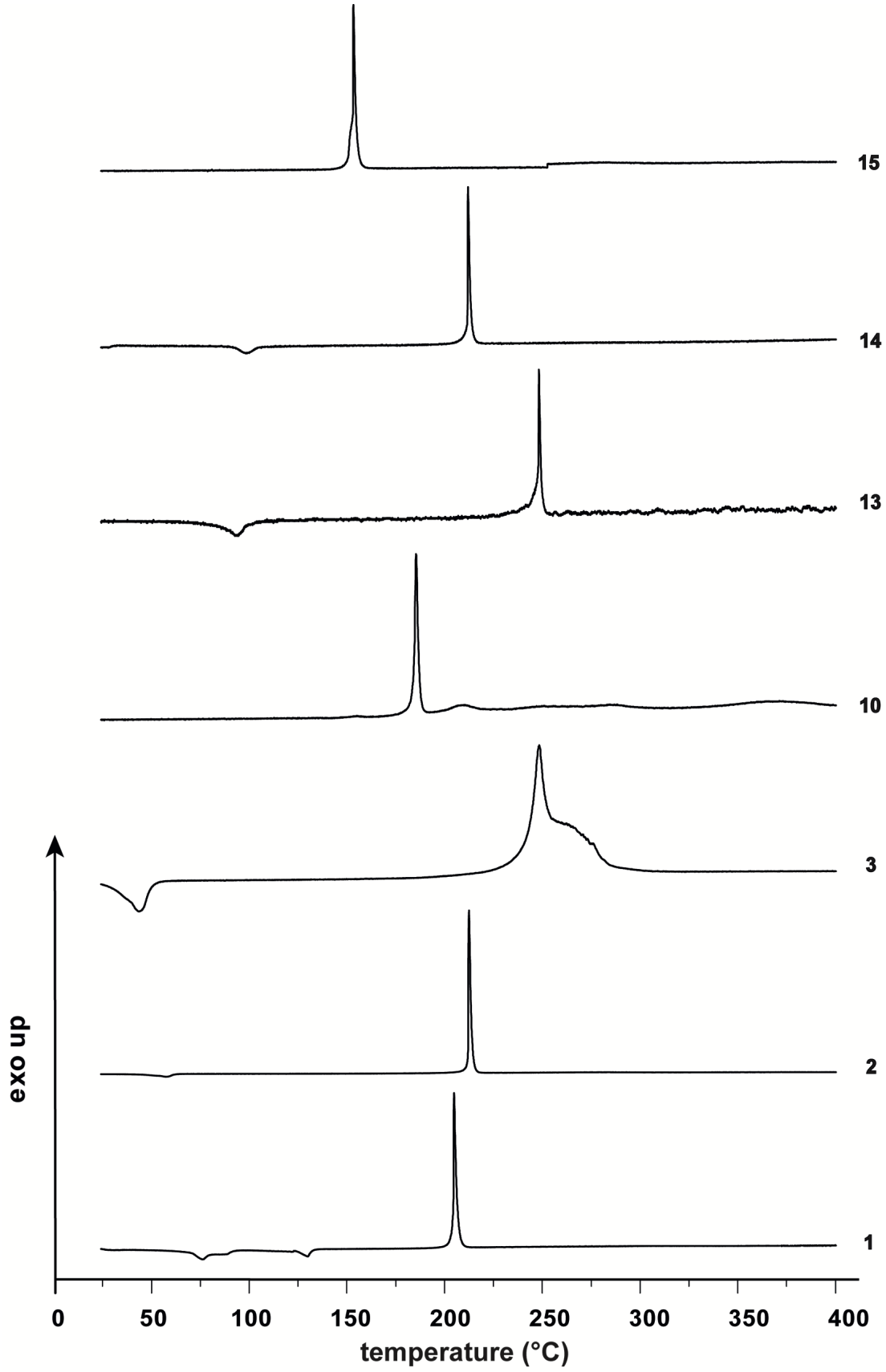


Figure S11. DTA plots of **1**–**3**, **10** and **13**–**15**.

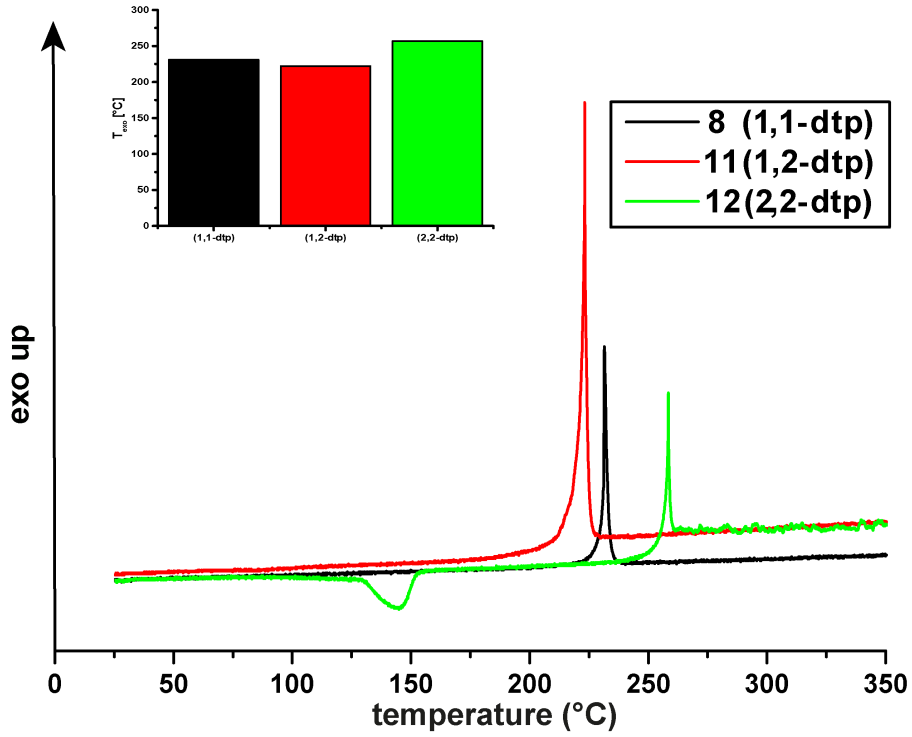


Figure S12. DTA plot (5 °C min^{-1}) comparison of the different dtp isomer containing copper(II) perchlorate complexes **8**, **11** and **12**.

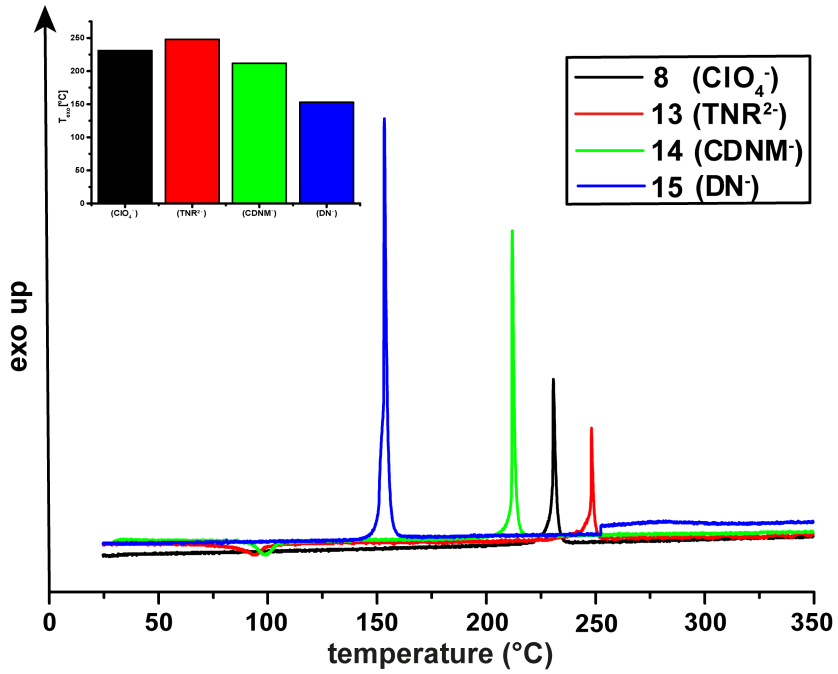


Figure S13. DTA plot (5 °C min^{-1}) comparison of the different 1,1-dtp based copper(II) complexes **8** and **13**–**15** with varying anions.

19.9.5 Column Diagrams of the Complexes of 8 and 11–15

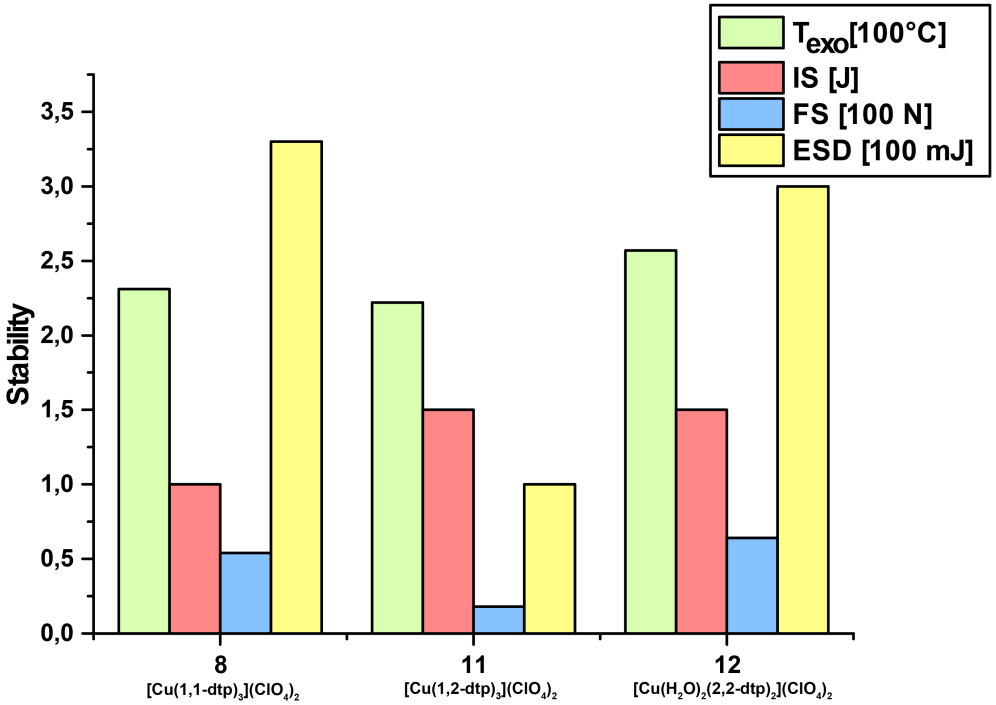


Figure S14. Stabilities of the copper(II) perchlorate complexes **8**, **11** and **12**.

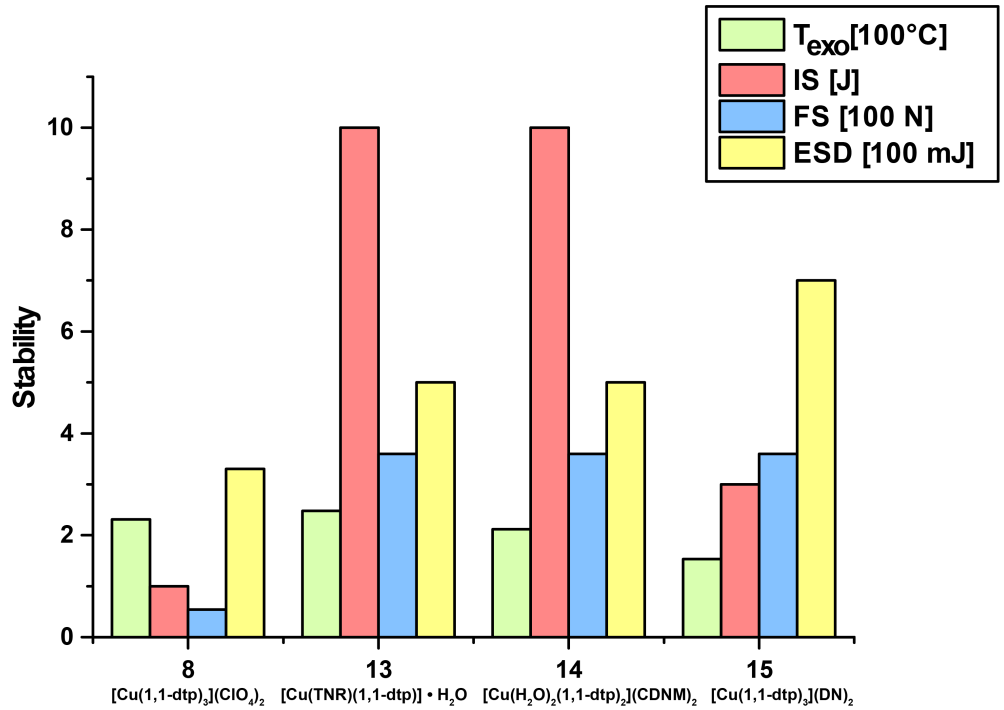


Figure S15. Stabilities of the copper(II) 1,1-dtp containing complexes **8** and **13**–**15**.

19.9.6 Hot Plate and Hot Needle Tests

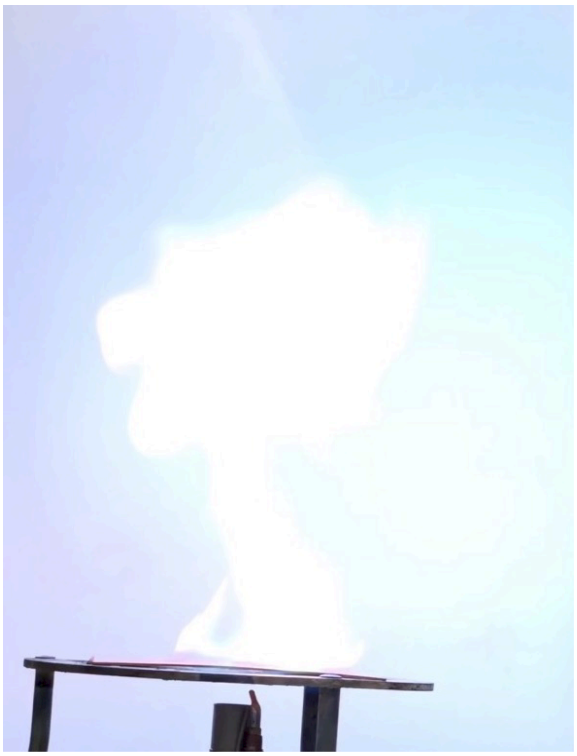


Figure S16. Moment of deflagration of complex **11** during the hot plate test.



Figure S17. Moment of deflagration during the hot plate test for compound **12** shown as sequence.

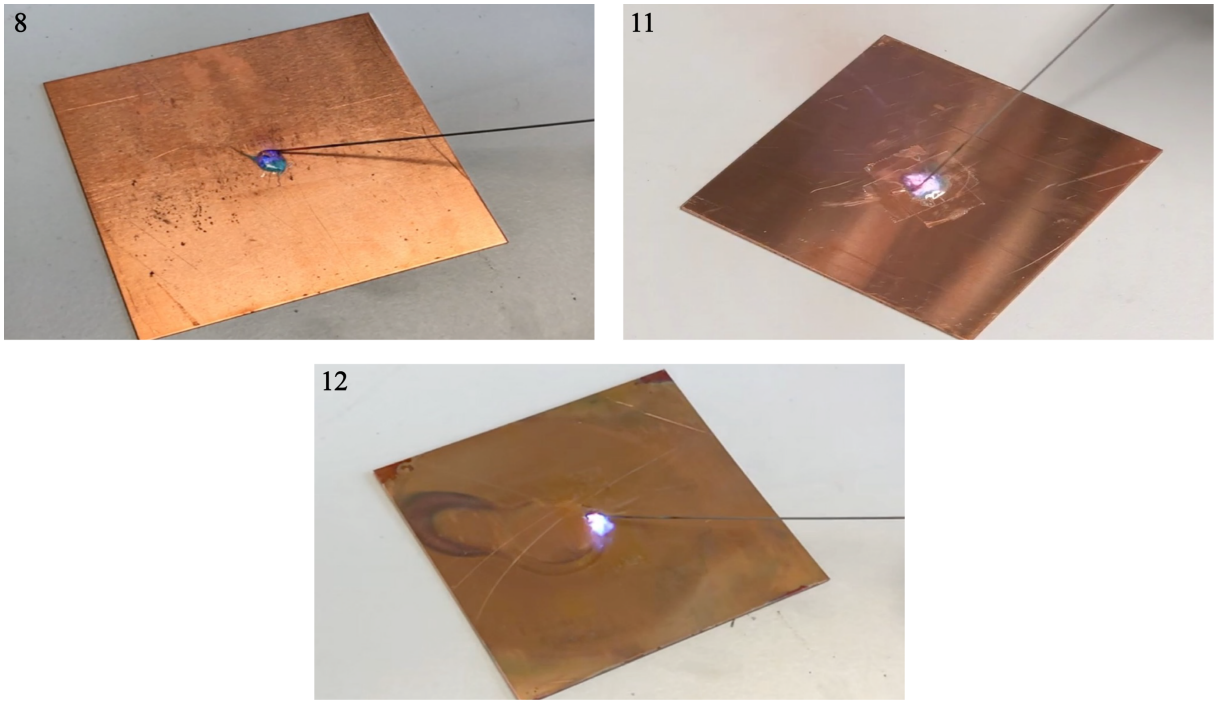


Figure S18. Deflagrations of **8**, **11** and **12** during the hot plate ignition tests.

19.9.7 Laser Ignition Tests

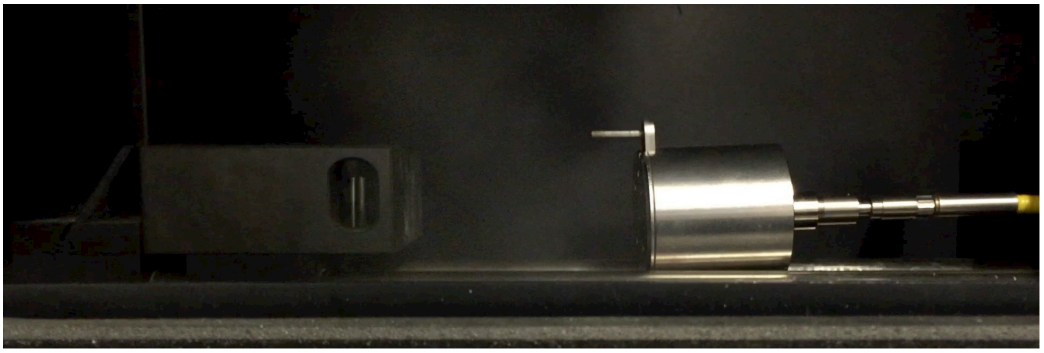


Figure S19. Detonation of **11** during the laser initiation test.

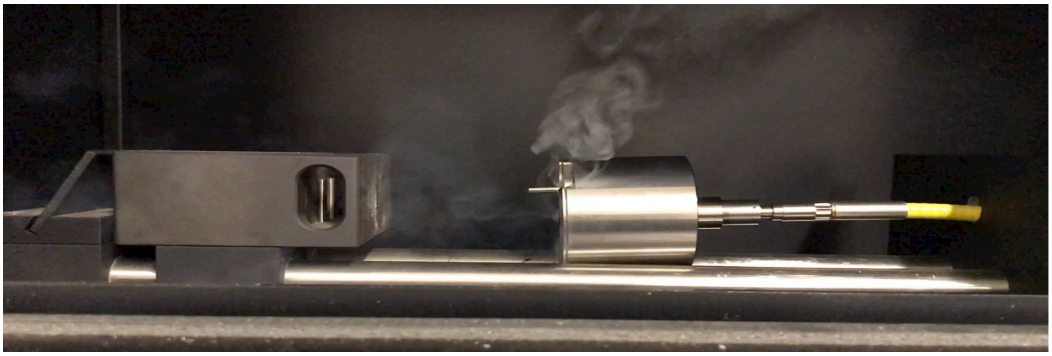


Figure S20. Decomposition of **13** as reaction to laser irradiation.

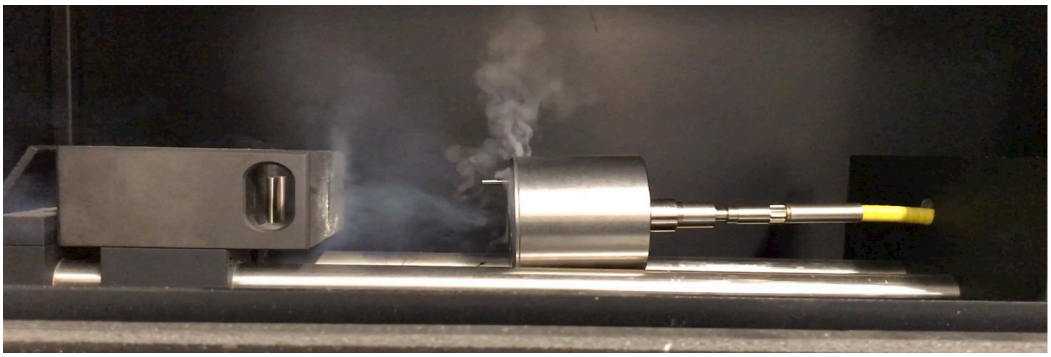


Figure S21. Moment of deflagration of complex **14**.

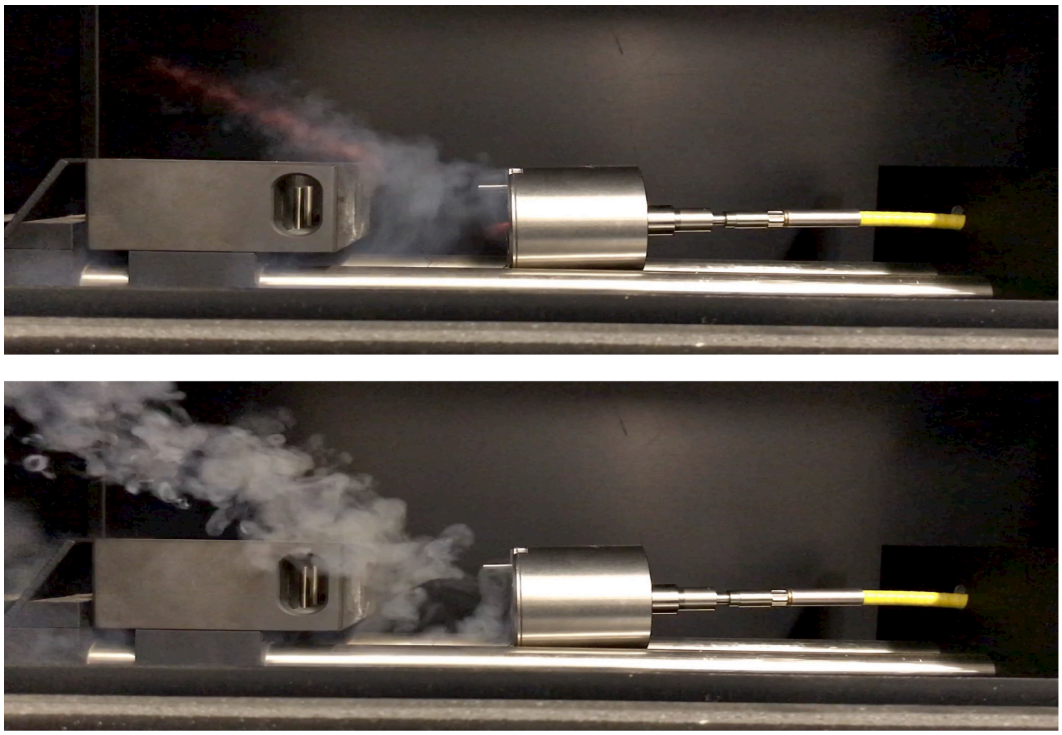


Figure S22. Deflagration reaction of complex **15** shown as sequence during laser initiation experiments.

19.9.8 UV-Vis Spectra of 4, 9, 10 and 13–15

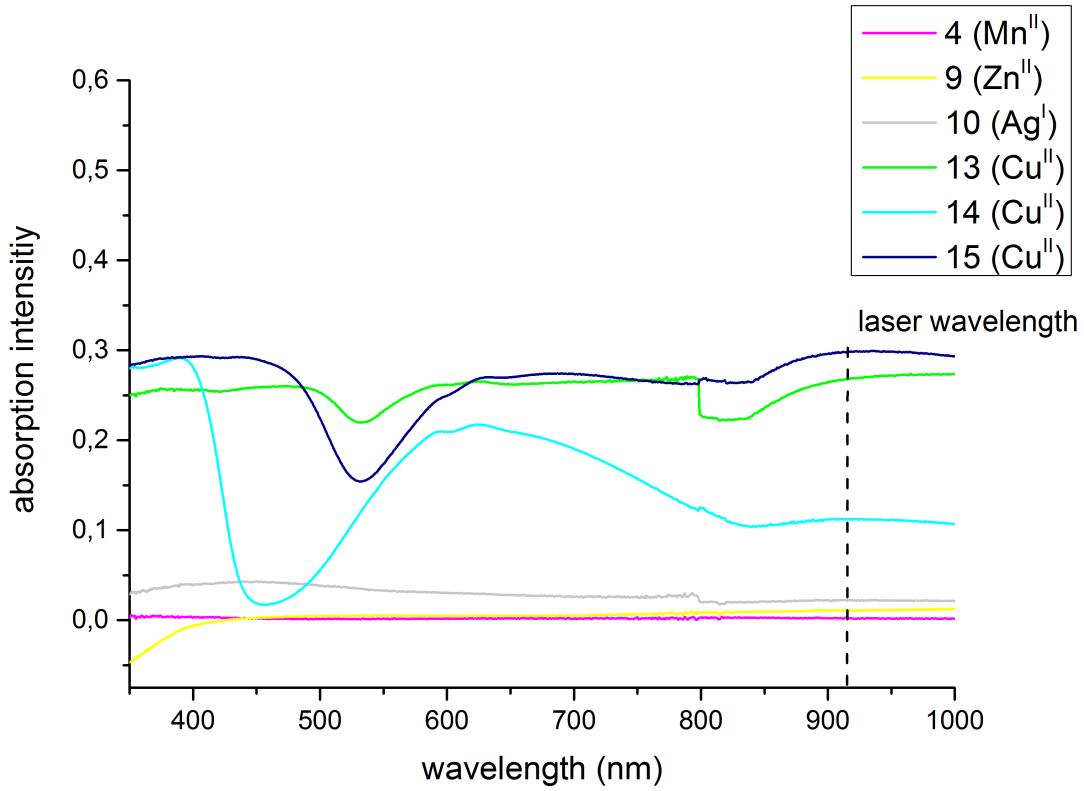


Figure S23. UV-Vis spectra in the solid state of coordination compounds **4**, **9**, **10** and **13**–**15**.

19.9.9 Experimental Part and General Methods

All chemicals and solvents were employed as received (Sigma-Aldrich, Fluka, Acros, ABCR). ^{1}H, ^{13}C and ^{15}N NMR spectra were recorded at ambient temperature using a JEOL Bruker 400, Eclipse 270, JEOL EX 400 or a JEOL Eclipse 400 instrument. The chemical shifts quoted in ppm in the text refer to typical standards such as tetramethylsilane (^{1}H, ^{13}C) and nitromethane (^{15}N) in d_6-DMSO or d_3-MeCN as the solvents. The ^{1}H,^{15}N-HMBC NMR spectrum was measured with a data matrix of 1024 x 256, an applied zero filling of 2048 x 4096, 32 scans per round, a relaxation delay of 1 second, an acquisition time of 0.3 second at a concentration of 140 mg/mL and an overall measurement time of approx. 3 h. Endothermic and exothermic events of the described compounds, which indicate melting, evaporation or decomposition, are given as the extrapolated onset temperatures. The samples were measured in a range of 25–400 °C at a heating rate of 5 °C min^{-1} through differential thermal analysis (DTA) with an OZM Research DTA 552-Ex instrument and partly by thermal gravimetric analysis (TGA) with a

PerkinElmer TGA4000. Infrared spectra were measured with pure samples on a Perkin-Elmer BXII FT-IR system with a Smith DuraSampler IR II diamond ATR. Determination of the carbon, hydrogen and nitrogen contents were carried out by combustion analysis using an Elementar Vario El (nitrogen values determined are often lower than the calculated ones' due to their explosive behavior). UV-Vis spectra were recorded in the solid state using a Varian Cary 500 spectrometer in the wavelength range of 350–1000 nm. The step in the absorption intensity at 800 nm is caused by a detector change. Impact sensitivity tests were carried out according to STANAG 4489[S9] with a modified instruction[S10] using a BAM (Bundesanstalt für Materialforschung) drophammer.[S11] Friction sensitivity tests were carried out according to STANAG 4487[S12] with a modified instruction[S13] using the BAM friction tester. The classification of the tested compounds results from the "UN Recommendations on the Transport of Dangerous Goods".[S14] Additionally all compounds were tested upon the sensitivity toward electrical discharge using the OZM Electric Spark Tester ESD 2010 EN or OZM Electric Spark XSpark10 device.[S15] Hot plate and hot needle tests were performed in order to classify the initiation capability of selected complexes. The samples were fixed on a copper plate underneath adhesive tape and initiated by a red-hot needle. Strong deflagration or detonation of the compound usually indicates a valuable primary explosive. The safe and straightforward hot plate test shows only the behavior of the unconfined sample toward fast heating on a copper plate. It does not necessarily allow any conclusions on a compound´s capability as a suitable primary explosive. Liquid-dried luminescent bacteria of the strain Vibrio fischeri NRRL-B-11177 provided by the HACH LANGE GmbH were used for the luminescent bacteria inhibition test to determine their toxicity toward aquatic organisms according to a modified procedure.[S16]

The obtained coordination compounds were washed with cold ethanol when stated, dried overnight in air and used for analytics without further purification.

CAUTION! *All investigated compounds are potentially explosive energetic materials, which show partly increased sensitivities (especially compounds **5**, **6**, **8**, **9** and **10**–**13**) toward various stimuli (e.g. elevated temperatures, impact, friction or electrostatic discharge). Therefore, proper security precautions (safety glass, face shield, earthed equipment and shoes, leather coat, Kevlar gloves, Kevlar sleeves and ear plugs) have to be applied while synthesizing and handling the described compounds.*

Procedure for the preparation of the propyl-linked ditetrazoles (1–3):

Main Method A:

The synthesis of the desired ditetrazoles was carried out analogously to a modified literature procedure:[S17] 1,3-dibromopropane (14.0 g, 69.3 mmol, 7.07 mL), sodium hydroxide (5.54 g, 139 mmol), 1,5*H*-tetrazole (9.72 g, 139 mmol) and tetrabutyl ammoniumbromide (2.23 g, 6.93 mmol) as phase transfer catalyst were dissolved in a mix of toluene and water (30 mL each). The resulting reaction mixture was stirred for 20 h at 120 °C under reflux, cooled to room temperature and concentrated through evaporation of the solvent under reduced pressure. The crude mixture was purified by column chromatography on silica using ethyl acetate/methanol mixtures (gradient: 0–10 % methanol) to yield 2.29 g (12.7 mmol, 18 %) 2,2-dtp (**3**) (0 % methanol, R_f 0.8) as a yellow oil, 5.13 g (28.5 mmol, 41 %) of 1,2-dtp (**2**) (0 % methanol, R_f 0.3) in form of colorless blocks and 1.46 g (8.10 mmol, 12 %) of 1,1-dtp (10 % methanol, R_f 0.3) as a colorless solid. After recrystallization of 1,3-di(tetrazol-1-yl)propane from water, filtration and drying overnight, compound **1** could be isolated in the form of colorless crystals.

Main Method B:

Alternative preparation of the ditetrazoles was achieved through addition of 1,3-dibromopropane (7.27 g, 36.0 mmol) in acetone (40 mL) to a mixture of 1,5*H*-tetrazole (6.00 g, 85.6 mmol) and triethylamine (8.66 g, 85.6 mmol) in acetone (40 mL). The reaction mixture was refluxed for four hours at 60 °C until a clear solution was obtained, which turned cloudy afterwards. After cooling down to room temperature and filtration of the triethylammonium bromide precipitate, the solvent was removed under reduced pressure. Treatment of the resulting oil with dioxane (100 mL) led to isolation of residual $HNEt_3Br$, which was filtered off. The obtained filtrate was treated with ethanol (100 mL) resulting in the precipitation of 1,1-dtp. The ditetrazole **1** was received in a yield of 586 mg (3.25 mmol, 9 %) after filtration and recrystallization from water. The two remaining isomers could be purified by column chromatography on silica gel using ethyl acetate, yielding 1.57 g (8.71 mmol, 24 %) of **3** (R_f 0.8) and 2.13 g (11.8 mmol, 33 %) of **2** (R_f 0.4).

Secondary Method:

Synthesis of the propyl-linked ditetrazoles with sodium hydroxide as base in water without phase transfer catalyst was performed according to a modified literature procedure described by Bronisz *et al*.[S18]. 1,3-Dibromopropane (5.05 g, 25.0 mmol) was added dropwise over a time period of 30 min to a suspension of 1,5*H*-tetrazole (4.20 g, 59.9 mmol) and sodium hydroxide (2.40 g, 60.0 mmol) in water (20 mL). This mixture was stirred under reflux for 6 h at 110 °C, cooled to room temperature and extracted with chloroform (8 x 20 mL) and dichloromethane (2 x 20 mL). The aqueous phase was concentrated under reduced pressure and the residue extracted with boiling acetonitrile (200 mL). The solid material obtained after evaporation was washed with ethanol and recrystallized from water affording 279 mg (1.41 mmol, 6 %) of ditetrazole **1**. The combined organic phases (CH_3Cl and CH_2Cl_2) were dried over magnesium sulfate and the solvent removed. The oily residue was washed with ethanol yielding a second crop of **1** (120 mg, 0.60 mmol, 2 %), which was filtrated and dried in air overnight. The remaining two isomers were separated by column chromatography on silica gel with ethyl acetate as mobile phase yielding 134 mg (0.74 mmol, 3 %) of **3** (R_f 0.8) and 277 mg (1.54 mmol, 6 %) of **2** (R_f 0.4).

1,3-Di(tetrazol-1-yl)propane • H_2O (1)

DTA (5 °C min^{-1}): 68 °C (endothermic), 126 °C (endothermic), 205 °C (exothermic); IR (ATR, cm^{-1}): $\tilde{\nu}$ = 3494 (w), 3481 (w), 3406 (m), 3317 (w), 3143 (w), 3130 (m), 3082 (m), 3007 (w), 2976 (w), 2938 (w), 1684 (m), 1495 (m), 1450 (m), 1433 (m), 1391 (w), 1373 (w), 1362 (w), 1281 (w), 1260 (w), 1244 (w), 1190 (m), 1173 (s), 1143 (m), 1112 (s), 1102 (vs), 1064 (m), 1031 (w), 993 (m), 976 (m), 924 (w), 894 (m), 874 (w), 803 (m), 744 (m), 722 (m), 681 (m), 666 (s), 647 (s), 625 (s);^{1}H NMR (DMSO-d_6, 25 °C, ppm) δ: 9.40 (s, 2H, -C*H*), 4.55 (t, 4H, -CH_2), 3.30 (s, 2H, H_2O), 2.50 (m, 2H, -CH_2); ^{13}C NMR (DMSO-d_6, 25 °C, ppm) δ: 144.1 (-*C*N_4), 44.8 (-*C*H_2), 29.0 (-*C*H_2); ^{1}H, ^{15}N HMBC NMR (MeCN-d_3, 25 °C, ppm) δ: 11.3 (N3), −14.3 (N2), −52.6 (N4, $^2J_{N\text{-}H}$ = 12 Hz), −145.1 (N1, $^2J_{N\text{-}H}$ = 8 Hz); EA: ($C_5H_{10}N_8O$, 198.19) calcd: C 30.30, H 5.09, N 56.84 %; found: C 30.80, H 4.92, N 56.78 %; BAM drophammer: > 40 J; friction tester: > 360 N; ESD: 1.35 J (at grain size < 100 µm).

1-(Tetrazol-1-yl)-3-(tetrazol-2-yl)propane (2)

DTA (5 °C min^{-1}): 50 °C (endothermic), 212 °C (exothermic); IR (ATR, cm^{-1}): $\tilde{\nu}$ = 3115 (s), 3003 (w), 2966 (w), 1821 (w), 1792 (w), 1484 (m), 1454 (s), 1442 (s), 1428 (w), 1391 (w), 1364 (m), 1356 (m), 1328 (w), 1290 (s), 1260 (w), 1243 (w), 1192 (m), 1165 (vs), 1142 (vs), 1107 (vs), 1077 (m), 1038 (m), 1031 (s), 1019 (w), 1010 (s), 981 (s), 964 (s), 912 (m), 898 (s), 871 (m), 826 (m), 720 (w), 706 (s), 683 (w), 660 (vs), 635 (s); ^{1}H NMR (DMSO-d_6, 25 °C, ppm) δ: 9.38 (s, 1H, -C*H*), 8.96 (s, 1H, -C*H*), 4.80 (t, 2H, -CH_2), 4.56 (t, 2H, -CH_2), 2.57 (pseudo quintet, 2H, -CH_2); ^{13}C NMR (DMSO-d_6, 25 °C, ppm) δ: 153.3 (-*C*N_4), 144.0 (-*C*N_4), 49.7 (-*C*H_2), 44.8 (-*C*H_2), 28.3 (-*C*H_2); ^{15}N NMR (MeCN-d_3, 25 °C, ppm) δ: 11.3 (N3, d, $^{3}J_{N\text{-}H}$ = 3.1 Hz), −3.3 (N7), −14.3 (N2), −49.0 (N8, d, $^{2}J_{N\text{-}H}$ = 13.4 Hz), −52.6 (N4), −77.3 (N5, d, $^{2}J_{N\text{-}H}$ = 14.5 Hz), −96.7 (N6, m), −145.1 (N1, m); EA: ($C_5H_8N_8$, 180.18) calcd: C 33.33, H 4.48, N 62.19 %; found: C 33.31, H 4.48, N 62.05 %; BAM drophammer: > 40 J; friction tester: > 360 N; ESD: 1.50 J (at grain size < 100 μm).

1,3-Di(tetrazol-2-yl)propane (3)

Ditetrazole **3** could be solidified through controlled freezing with liquid nitrogen and subsequent thawing to room temperature where the compound has been obtained in the form of colorless single crystal blocks suitable for X-ray diffraction.

DTA (5 °C min^{-1}): 45 °C (endothermic), 246 °C (exothermic); IR (ATR, cm^{-1}): $\tilde{\nu}$ = 3142 (w), 2964 (vw), 1628 (vw), 1574 (vw), 1448 (m), 1361 (m), 1283 (vs), 1185 (m), 1168 (w), 1134 (s), 1051 (w), 1026 (vs), 1008 (s), 986 (m), 883 (m), 826 (vw), 802 (w), 757 (vw), 728 (vw), 708 (s), 688 (s), 660 (w), 639 (w); ^{1}H NMR (DMSO-d_6, 25 °C, ppm) δ: 8.96 (s, 2H, -C*H*), 4.82 (t, 4H, -CH_2), 2.63 (q, 2H, -CH_2); ^{13}C NMR (DMSO-d_6, 25 °C, ppm) δ: 153.3 (-*C*N_4), 49.6 (-*C*H_2), 28.1 (-*C*H_2), ^{15}N NMR (MeCN-d_3, 25 °C, ppm) δ: −3.0 (N3), −49.0 (N4, d, $^{2}J_{N\text{-}H}$ = 12.5 Hz), −77.0 (N1, dt, $^{2}J_{N\text{-}H}$ = 14.5 Hz,$^{3}J_{N\text{-}H}$ = 1.6 Hz), −96.0 (N2, m); EA: ($C_5H_8N_8$, 180.18) calcd: C 33.33, H 4.48, N 62.19 %; found: C 33.38, H 4.47, N 62.00 %; BAM drophammer: > 40 J; friction tester: > 360 N; ESD: 0.15 J (at grain size < 100 μm).

General procedure for the preparation of metal(II) (Mn^{II}, Fe^{II}, Co^{II}, Ni^{II}, Cu^{II}, Zn^{II}) 1,1-dtp perchlorate complexes (4–9):

A solution of 1,3-di(tetrazol-1-yl)propane monohydrate (**1**, 178 mg, 0.90 mmol) in acetonitrile (2 mL) was added to the corresponding metal(II) perchlorate salt (**4**: manganese(II) perchlorate hexahydrate (109 mg, 0.30 mmol); **5**: iron(II) perchlorate hexahydrate (110 mg, 0.30 mmol); **6**: cobalt(II) perchlorate hexahydrate (110 mg, 0.30 mmol); **7**: nickel(II) perchlorate hexahydrate (110 mg, 0.30 mmol); **8**: copper(II) perchlorate hexahydrate (111 mg, 0.30 mmol); **9**: zinc(II) perchlorate hexahydrate (111 mg, 0.30 mmol)) dissolved in water (1 mL). The colored reaction mixtures were mechanically stirred for one minute at room temperature and left for crystallization. After precipitation of a solid material, the compounds were filtered off, washed and dried in air.

$[Mn(1,1\text{-dtp})_3](ClO_4)_2$ (4)

Within two hours, the manganese(II) complex **4** was obtained in the form of colorless blocks suitable for X-ray determination from the mother liquor. Yield: 183 mg (0.23 mmol, 77 %).

DTA (5 °C min^{-1}): 243 °C (exothermic); IR (ATR, cm^{-1}): $\tilde{\nu}$ = 3136 (w), 1503 (m), 1445 (w), 1430 (w), 1377 (vw), 1176 (m), 1091 (vs), 1085 (vs), 987 (m), 890 (w), 871 (w), 695 (w), 647 (m), 623 (s); UV-Vis spectrum: λ_{max} = none; EA: ($C_{15}H_{24}Cl_2MnN_{24}O_8$, 794.36): calcd: C 22.68, H 3.05, N 42.32 %; found: C 22.90, H 3.15, N 42.04 %; BAM drophammer: 3 J; friction tester: 216 N; ESD: 0.30 J (at grain size < 100 μm).

$[Fe(1,1\text{-dtp})_3](ClO_4)_2$ (5)

After one hour compound **5** was received in form of X-ray suitable yellow blocks. Yield: 191 mg (0.24 mmol, 80 %).

DTA (5 °C min^{-1}): 234 °C (exothermic); IR (ATR, cm^{-1}): $\tilde{\nu}$= 3139 (w), 1505 (m), 1447 (w), 1431 (w), 1377 (w), 1290 (vw), 1177 (m), 1144 (w), 1084 (vs), 990 (m), 936 (vw), 890 (w), 871 (w), 696 (w), 666 (vw), 647 (m), 623 (s); UV-Vis spectrum: λ_{max} = 893 nm; EA:

($C_{15}H_{24}Cl_2FeN_{24}O_8$, 795.26): calcd: C 22.65, H 3.04, N 42.27 %; found: C 22.92, H 3.06, N 42.15 %; BAM drophammer: 2 J; friction tester: 72 N; ESD: 0.10 J (at grain size < 100 µm).

$[Co(1,1\text{-dtp})_3](ClO_4)_2$ (6)

Overnight, cobalt(II) complex **6** was obtained in the form of orange crystals suitable for X-ray determination. Yield: 125 mg (0.16 mmol, 53 %).

DTA (5 °C min^{-1}): 255 °C (exothermic); IR (ATR, cm^{-1}): $\tilde{\nu}$ = 3140 (w), 1505 (m), 1448 (w), 1431 (w), 1377 (vw), 1290 (vw), 1177 (m), 1144 (vw), 1084 (vs), 993 (m), 964 (w), 890 (w), 870 (w), 720 (vw), 697 (w), 665 (vw), 646 (m), 623 (s); UV-Vis spectrum: λ_{max} = 468, 982 nm; EA: ($C_{15}H_{24}Cl_2CoN_{24}O_8$, 798.35): calcd: C 22.57, H 3.03, N 42.11 %; found: C 22.83, H 3.17, N 42.11 %; BAM drophammer: 1 J; friction tester: 18 N; ESD: 0.08 J (at grain size < 100 µm).

$[Ni(1,1\text{-dtp})_3](ClO_4)_2$ (7)

After addition of the nickel(II) salt a cloudy lilac solution was formed. Within one hour complex **7** was isolated in the form of a purple amorphous solid. Yield: 200 mg (0.25 mmol, 84 %).

DTA (5 °C min^{-1}): 297 °C (exothermic); IR (ATR, cm^{-1}): $\tilde{\nu}$ = 3143 (w), 1506 (m), 1450 (w), 1432 (w), 1378 (w), 1179 (m), 1085 (vs), 996 (m), 964 (w), 889 (w), 871 (w), 697 (w), 647 (m), 623 (s); UV-Vis spectrum: λ_{max} = 547, 891 nm; EA: ($C_{15}H_{24}Cl_2N_{24}NiO_8$, 798.11): calcd: C 22.57, H 3.03, N 42.12 %; found: C 22.67, H 3.05, N 42.01 %; BAM drophammer: 3 J; friction tester: 120 N; ESD: 0.20 J (at grain size < 100 µm).

$[Cu(1,1\text{-dtp})_3](ClO_4)_2$ (8)

Overnight, blue single crystal blocks of copper(II) complex **8** suitable for X-ray determination were received. Yield: 96.4 mg (0.12 mmol, 40 %).

DTA (5 °C min^{-1}): 231 °C (exothermic); IR (ATR, cm^{-1}): $\tilde{\nu}$ = 3141 (w), 1506 (w), 1449 (w), 1431 (w), 1177 (m), 1085 (vs), 1001 (m), 986 (m), 964 (w), 889 (w), 871 (w), 696 (w), 646 (m), 623 (s); UV-Vis spectrum: λ_{max} = 701 nm; EA: ($C_{15}H_{24}Cl_2CuN_{24}O_8$, 802.96): calcd:

C 22.44, H 3.01, N 41.87 %; found: C 22.51, H 3.03, N 41.71 %; BAM drophammer: 1 J; friction tester: 54 N; ESD: 0.33 J (at grain size < 100 µm).

[Zn(1,1-dtp)$_3$](ClO$_4$)$_2$ (9)

Coordination compound **9** was received within two hours in the form of colorless blocks suitable for X-ray determination. Yield: 193 mg (0.24 mmol, 80 %).

DTA (5 °C min^{-1}): 253 °C (exothermic); IR (ATR, cm^{-1}): $\tilde{\nu}$ = 3139 (w), 1505 (w), 1448 (w), 1431 (w), 1177 (w), 1091 (vs), 1085 (vs), 993 (m), 963 (w), 892 (w), 871 (w), 696 (w), 647 (m), 624 (s); UV-Vis spectrum: λ_{max} = none; EA: ($C_{15}H_{24}Cl_2N_{24}O_8Zn$, 804.80): calcd: C 22.39, H 3.01, N 41.77 %; found: C 22.50, H 2.99 , N 41.75 %; BAM drophammer: 1 J; friction tester: 288 N; ESD: 0.20 J (at grain size < 100 µm).

[Ag(1,2-dtp)]ClO$_4$ (10)

An aqueous solution (10 mL) of 1-(tetrazol-1-yl)-3-(tetrazol-2-yl)propane (**2**, 27.1 mg, 0.25 mmol) was heated to 70 °C and treated with silver(I) perchlorate (52.0 mg, 0.25 mmol), dissolved in water (10 mL). The reaction mixture was mechanically stirred for one minute and afterwards left to crystallize at room temperature. Silver(I) complex **10** crystallized within one day in the form of colorless blocks suitable for X-ray determination. The crystals were filtered off, washed with cold ethanol (2 mL) and dried in air. Yield: 55.0 mg (0.14 mmol, 57 %).

DTA (5 °C min^{-1}): 185 °C (exothermic); IR (ATR, cm^{-1}): $\tilde{\nu}$ = 3169 (w), 3120 (m), 3030 (vw), 3010 (vw), 2974 (vw), 2965 (vw), 1782 (vw), 1493 (w), 1467 (w), 1444 (w), 1435 (w), 1426 (w), 1373 (w), 1356 (w), 1349 (w), 1337 (vw), 1309 (w), 1284 (w), 1195 (m), 1153 (m), 1125 (m), 1071 (vs), 1047 (vs), 1018 (m), 998 (m), 982 (s), 934 (w), 888 (m), 871 (m), 824 (m), 729 (vw), 716 (w), 696 (m), 686 (w), 660 (m), 636 (w), 618 (vs); UV-Vis spectrum: λ_{max} = none; EA: ($C_5H_8AgClN_8O_4$, 387.49): calcd: C 15.50, H 2.08, N 28.92 %; found: C 15.73, H 2.45 , N 28.25 %; BAM drophammer: 8 J; friction tester: 16 N; ESD: 0.15 J (at grain size < 100 µm).

$[Cu(1,2\text{-dtp})_3](ClO_4)_2$ (11)

The ditetrazole ligand 1,2-dtp (135 mg, 0.75 mmol) was dissolved in distilled water (4 mL), heated to 70 °C and added to an aqueous solution (1 mL) of copper(II) perchlorate hexahydrate (93.0 mg, 0.25 mmol). After mechanically stirring for one minute at room temperature, the reaction mixture was left for crystallization. X-ray suitable single crystals of complex **11** were obtained after 5 days. The blue rods were filtered off, washed with cold ethanol (2 mL) and dried in air. Yield: 179 mg (0.22 mmol, 89 %).

DTA (5 °C min^{-1}): 222 °C (exothermic); IR (ATR, cm^{-1}): $\tilde{\nu}$ = 3136 (w), 1504 (w), 1445 (w), 1366 (w), 1309 (w), 1179 (w), 1145 (w), 1082 (vs), 1022 (m), 1006 (m), 988 (w), 962 (w), 933 (w), 890 (w), 872 (w), 701 (w), 680 (w), 665 (w), 657 (w), 622 (s); UV-Vis spectrum: λ_{max} = 688 nm; EA: ($C_{15}H_{24}Cl_2CuN_{24}O_8$, 802.96): calcd: C 22.44, H 3.01, N 41.87 %; found: C 22.28, H 2.98 , N 41.80 %; BAM drophammer: 1.5 J; friction tester: 18 N; ESD: 0.10 J (at grain size < 100 μm).

$[Cu(H_2O)_2(2,2\text{-dtp})_2](ClO_4)_2$ (12)

1,3-Di(tetrazol-2-yl)propane (**3**, 184 mg, 1.00 mmol) in acetonitrile (2 mL) was reacted with copper(II) perchlorate hexahydrate (185 mg, 0.50 mmol) dissolved in water (1 mL). The colored reaction mixture was stirred mechanically for one minute at room temperature and left for crystallization. After filtration of the product, the compound was washed with ethanol (2 mL) and dried in air. The diaqua complex **12** was received in form of blue block suitable for X-ray diffraction within one hour. Yield: 213 mg (0.32 mmol, 64 %).

DTA (5 °C min^{-1}): 132 °C (endothermic), 257 °C (exothermic); IR (ATR, cm^{-1}): $\tilde{\nu}$ =3569 (w), 3450 (w), 3347 (vw), 3156 (w), 3143 (w), 1629 (w), 1475 (vw), 1464 (w), 1454 (w), 1391 (w), 1370 (w), 1311 (w), 1207 (w), 1199 (w), 1152 (m), 1097 (vs), 1064 (vs), 1047 (vs), 1033 (s), 1020 (s), 931 (w), 897 (m), 807 (w), 765 (w), 720 (w), 703 (m), 683 (m), 622 (vs); UV-Vis spectrum: λ_{max} = 654 nm; EA: ($C_{10}H_{20}Cl_2CuN_{16}O_{10}$, 658.82): calcd: C 18.23, H 3.06, N 34.02 %; found: C 18.31, H 3.07 , N 34.02 %; BAM drophammer: 1.5 J friction tester: 64 N; ESD: 0.30 J (at grain size < 100 μm).

[Cu(TNR)(1,1-dtp)] · H_2O (13)

Styphnic acid (147 mg, 0.60 mmol) and copper(II) carbonate (37.0 mg, 0.30 mmol) were stirred in water (5 mL) at 70 °C until a clear solution was obtained. An aqueous solution of 1,3-di(tetrazol-1-yl)propane monohydrate (**1,** 59.5 mg, 0.30 mmol) was added, which was afterwards further stirred mechanically for five minutes. The reaction mixture was left for crystallization at room temperature until a solid appeared. The resulting product was filtered off, washed with a small amount of cold ethanol (2 mL) and dried in air. The copper(II) complex **13** was obtained in the form of green crystals suitable for X-ray determination after a few minutes. Yield: 119 mg (0.24 mmol, 80 %).

DTA (5 °C min^{-1}): 88 °C (endothermic), 248 °C (exothermic); IR (ATR, cm^{-1}): $\tilde{\nu}$ = 3662 (w), 3634 (w), 3574 (w), 3134 (w), 3018 (w), 2971 (w), 1606 (m), 1581 (m), 1521 (s), 1495 (s), 1478 (m), 1436 (s), 1374 (m), 1353 (m), 1289 (s), 1232 (vs), 1175 (vs), 1140 (s), 1098 (vs), 1013 (s), 953 (m), 926 (m), 916 (m), 890 (m), 847 (m), 827 (w), 792 (m), 768 (m), 759 (m), 738 (m), 706 (vs), 677 (s), 652 (s), 623 (m); UV-Vis spectrum: λ_{max} = 390, 696 nm; EA: ($C_{11}H_{11}CuN_{11}O_9$, 504.83): calcd: C 26.17, H 2.20, N 30.52 %; found: C 26.56, H 2.32, N 30.17 %; BAM drophammer: 10 J; friction tester: > 360 N; ESD: 0.50 J (at grain size < 100 μm).

[$Cu(H_2O)_2$(1,1-dtp)$_2$](CDNM)$_2$ (14)

Potassium cyanodinitromethanide (102 mg, 0.60 mmol) and copper(II) sulfate pentahydrate (75.0 mg, 0.30 mmol) were dissolved in water (3 mL), heated to 70 °C and stirred for three minutes. The nitrogen-rich ditetrazole **1** (119 mg, 0.60 mmol) dissolved in water (2 mL) was added, the whole reaction mixture further mechanically stirred for three more minutes and finally left for crystallization. From the mother liquor, blue single crystals suitable for X-ray determination of **14** could be obtained within two hours. Yield: 76.0 mg (0.11 mmol, 35 %).

DTA (5 °C min^{-1}): 93 °C (endothermic), 212 °C (exothermic); IR (ATR, cm^{-1}): $\tilde{\nu}$ = 3528 (m), 3435 (w), 3242 (w), 3180 (w), 3138 (m), 3048 (w), 3003 (w), 2223 (w), 2216 (w), 1629 (w), 1504 (s), 1491 (s), 1450 (m), 1438 (m), 1410 (m), 1393 (w), 1360 (w), 1341 (w), 1231 (vs), 1177 (s), 1149 (s), 1144 (s), 1107 (s), 1099 (s), 1082 (s), 1070 (m), 1062 (m), 1038 (m), 1009 (s), 882 (m), 847 (m), 791 (w), 766 (m), 746 (s), 717 (m), 675 (m), 654 (s), 611 (m); UV-Vis

spectrum: λ_{max} = 389, 624 nm; EA: ($C_{14}H_{20}CuN_{22}O_{10}$, 720.03): calcd: C 23.35, H 2.80, N 42.80 %; found: C 23.49, H 2.75, N 42.81 %; BAM drophammer: 10 J; friction tester: > 360 N; ESD: 0.50 J (at grain size < 100 μm).

[Cu(1,1-dtp)$_3$](DN)$_2$ (15)

Ammonium dinitramide (80.0 mg, 0.60 mmol) and copper(II) sulfate pentahydrate (75.0 mg, 0.30 mmol) were mechanically mixed at 70 °C in water (3 mL). To this blue solution, ligand **1** (178 mg, 0.90 mmol) dissolved in water (2 mL) was added and the whole reaction mixture stirred for three minutes. After two hours, dinitramide complex **15** could be isolated in the form of blue platelets suitable for X-ray determination. Yield: 202 mg (0.25 mmol, 83 %).

DTA (5 °C min^{-1}): 153 °C (exothermic); IR (ATR, cm^{-1}): $\tilde{\nu}$ = 3137 (w), 3015 (vw), 2968 (vw), 1509 (m), 1438 (m), 1420 (m), 1336 (w), 1298 (w), 1178 (vs), 1167 (vs), 1102 (s), 1069 (m), 1001 (s), 975 (s), 887 (m), 825 (m), 789 (m), 754 (s), 718 (m), 679 (w), 657 (s), 618 (w); UV-Vis spectrum: λ_{max} = 377, 630 nm; EA: ($C_{15}H_{24}CuN_{30}O_8$, 816.12): calcd: C 22.08, H 2.96, N 51.49 %; found: C 22.19, H 2.88, N 51.32 %; BAM drophammer: 3 J; friction tester: > 360 N; ESD: 0.70 J (at grain size < 100 μm).

19.9.10 References

[S1] *CrysAlisPro*, Oxford Diffraction Ltd., version 171.33.41, 2009.

[S2] A. Altomare, G. Cascarano, C. Giacovazzo, A. Guagliardi, *J. Appl. Crystallogr.* 1992, **26**, 343–350.

[S3] a) A. Altomare, G. Cascarano, C. Giacovazzo, A. Guagliardi, A. G. G. Moliterni, M. C. Burla, G. Polidori, M. Camalli, R. Spagna, *SIR97*, 1997; b) A. Altomare, M. C. Burla, M. Camalli, G. L. Cascarano, C. Giacovazzo, A. Guagliardi, A. G. G. Moliterni, G. Polidori, R. Spagna, *J. Appl. Crystallogr.* 1999, **32**, 115–119.

[S4] a) G. M. Sheldrick, *SHELXL-97*, *Program for the Refinement of Crystal Structures*, University of Göttingen, Germany, 1997; b) G. M. Sheldrick, *Acta Crystallogr. Sect. A* 2008, **64**, 112–122.

[S5] A. L. Spek, *PLATON*, *A Multipurpose Crystallographic Tool*, Utrecht University, The Netherlands, 1999.

[S6] L. J. Farrugia, *J. Appl. Cryst.*, 2012, **45**, 849.

[S7] Empirical absorption correction using spherical harmonics, implemented in SCALE3 ABSPACK scaling algorithm (CrysAlisPro Oxford Diffraction Ltd., Version 171.33.41, 2009).

[S8] *APEX3*. Bruker AXS Inc., Madison, Wisconsin, USA.

[S9] NATO standardization agreement (STANAG) on explosives, impact sensitivity tests, no. 4489, 1st ed., Sept. 17, 1999.

[S10] WIWEB-Standardarbeitsanweisung 4-5.1.02, Ermittlung der Explosionsgefährlichkeit, hier der Schlagempfindlichkeit mit dem Fallhammer, Nov. 8, 2002.

[S11] http://www.bam.de, Accessed December 2017.

[S12] NATO standardization agreement (STANAG) on explosive, friction sensitivity tests, no. 4487, 1st ed., Aug. 22, 2002.

[S13] WIWEB-Standardarbeitsanweisung 4-5.1.03, Ermittlung der Explosionsgefährlichkeit oder der Reibeempfindlichkeit mit dem Reibeapparat, Nov. 8, 2002.

[S14] Impact: insensitive > 40 J, less sensitive ≥ 35 J, sensitive ≥ 4 J, very sensitive ≤ 3 J; Friction: insensitive > 360 N, less sensitive = 360 N, sensitive < 360 N and > 80 N, very sensitive ≤ 80 N, extremely sensitive ≤ 10 N. According to the UN Recommendations on the Transport of Dangerous Goods, (+) indicates not safe for transport.

[S15] http://www.ozm.cz, Accessed December 2017.

[S16] R. Scharf, PhD thesis, Ludwig-Maximilians Universität München, 2016.

[S17] D. Müller, C. Knoll, B. Stöger, W. Artner, M. Reissner and P. Weinberger, *Eur. J. Inorg. Chem.,* 2013, **2013***,* 984–991.

[S18] M. Weselski, M. Książek, J. Kusz, A. Białońska, D. Paliwoda, M. Hanfland, M. F. Rudolf, Z. Ciunik and R. Bronisz, *Eur. J. Inorg. Chem.,* 2017, **2017**, 1171–1179.

19.10 Supplementary Information: Copper(II) Chlorate Complexes – the Renaissance of a Forgotten and Misjudged Energetic Anion

19.10.1 Experimental Procedure and General Methods

All chemicals and solvents were employed as received (Sigma-Aldrich, Fluka, Acros, ABCR). ^{1}H and ^{13}C NMR spectra were recorded with neat solids as samples at ambient temperature using a JEOL Eclipse 270, JEOL EX 400 or a JEOL Eclipse 400 instrument. The chemical shifts quoted in ppm in the text refer to typical standards such as tetramethylsilane (^{1}H, ^{13}C). Critical temperatures such as dehydration, melting and decomposition points of the described compounds were measured through differential thermal analysis (DTA) with an OZM Research DTA 552-Ex instrument. In addition, thermogravimetric measurements on a Perkin Elmer TG4000 were carried out for selected compounds. The samples were measured in a range of 25–400 °C at a heating rate of 5 °C min^{-1}. Infrared spectra were measured with pure samples on a Perkin-Elmer BXII FT-IR system with a Smith DuraSampler IR II diamond ATR. Determination of the carbon, hydrogen and nitrogen contents was carried out by combustion analysis using an Elementar Vario El (nitrogen values determined are often lower than the calculated ones due to their explosive behavior). UV-Vis spectra were recorded in the solid state using a Varian Cary 500 spectrometer in the wavelength range of 350–1000 nm. Impact sensitivity tests were carried out according to STANAG 4489[S1] modified instruction[S2] using a BAM (Bundesanstalt für Materialforschung) drophammer.[S3] Friction sensitivity tests were carried out according to STANAG 4487[S4] modified instruction[S5] using the BAM friction tester. The classification of the tested compounds results from the "UN Recommendations on the Transport of Dangerous Goods".[S6] Additionally all compounds were tested upon the sensitivity toward electrical discharge using the Electric Spark Tester ESD 2010 EN.[S7] Liquid-dried luminescent bacteria of the strain *Vibrio fischeri* NRRL-B-11177 provided by the HACH LANGE GmbH were used for the luminescent bacteria inhibition test to determine their toxicity toward aquatic organisms according to a modified procedure. All the obtained coordination compounds were washed with cold ethanol,[S8] dried over night in air and used for analytics without further purification.

CAUTION! *All investigated compounds and mixtures of copper(II) chlorate and organic solvents are potentially explosive, which show partly increased sensitivities toward various*

*stimuli (e.g. elevated temperatures, impact, friction or electrostatic discharge). Therefore, proper security precautions (safety glass, face shield, earthed equipment and shoes, leather coat, Kevlar gloves, Kevlar sleeves and ear plugs) have to be applied while synthesizing and handling the described compounds. Especially compounds **2** and **8** must be handled with great care!*

General procedure for the preparation of complexes 1–10:

Copper(II) sulfate pentahydrate (62.4 mg, 0.25 mmol) and barium chlorate monohydrate (80.6 mg, 0.25 mmol), each dissolved in 3 mL water were combined and stirred mechanically for 10 min. The precipitated barium sulfate was filtered off and the aqueous filtrate concentrated under reduced pressure. Obtained copper(II) chlorate was dissolved in 2 mL ethanol (**1**, **3**–**5**, **7**–**10**), methanol (**2**) or water (**6**) and stoichiometric amounts of the ligand dissolved in 1 mL ethanol (**1**, **3**, **5**, **7**–**9**) or acetonitrile (**4**, **6**, **10**) were added under stirring. The solids were filtered off, washed with cold ethanol (2 mL) and dried in air.

$[Cu(ClO_3)_2(1\text{-}ATRI)_4]$ (1)

The copper(II) chlorate complex **1** was obtained as a blue powder. Yield: 128 mg (0.23 mmol, 90 %). Evaporation of the ethanolic residue overnight gave single crystals in the form of blue blocks suitable for X-ray determination.

DTA (5 °C min^{-1}) onset: 119 °C (dec.); IR (ATR, cm^{-1}): $\tilde{\nu}$= 3346 (w), 3320 (m), 3257 (w), 3190 (w), 3172 (w), 3144 (w), 3121 (w), 1608 (w), 1505 (w), 1476 (w), 1339 (vw), 1239 (vw), 1220 (w), 1202 (w), 1138 (m), 1094 (m), 1047 (vw), 978 (s), 947 (vs), 925 (vs), 879 (m), 805 (s), 782 (s), 706 (w), 700 (w), 687 (w), 659 (vw), 637 (w), 608 (m); EA ($C_8H_{16}Cl_2CuN_{16}O_6$, 566.77): calcd: C 16.95, H 2.85, N 39.54 %; found: C 17.17, H 2.84, N 39.33 %; BAM drophammer: 1 J; friction tester: < 5 N; ESD: 20 mJ (at grain size < 100 µm).

$[Cu_2(4\text{-ATRI})_6](ClO_3)_4$ (2)

The water-free chlorate complex **2** was isolated as a blue precipitate. Yield: 112 mg (23 mmol, 93 %). Single crystal growth was achieved by overlaying an aqueous solution (8 mL) of copper(II) chlorate with an ethanolic solution (8 mL) of 4-ATRI, separated by a mixture (4 mL) of water/ethanol (50:50). After 5 days blue rods suitable for X-ray determination were obtained.

DTA (5 °C min^{-1}) onset: 186 °C (dec.); IR (ATR, cm^{-1}): $\tilde{\nu}$= 3279 (w), 3217 (w), 3175 (w), 3103 (w), 3078 (w), 1638 (w), 1554 (w), 1536 (w), 1401 (w), 1379 (w), 1327 (vw), 1225 (w), 1217 (w), 1096 (m), 1085 (m), 1051 (m), 974 (vs), 941 (vs), 918 (s), 903 (s), 883 (vs), 694 (w), 680 (w), 624 (s), 606 (m); EA ($C_6H_{12}Cl_2CuN_{12}O_6$, 965.37): calcd: C 14.93, H 2.51, N 34.82 %; found: C 15.26, H 2.51, N 34.47 %; BAM drophammer: 1 J; friction tester: < 5 N; ESD: 15 mJ (at grain size < 100 µm).

$[Cu(ClO_3)_2(1\text{-MTZ})_4]$ (3)

Complex **3** was isolated within 15 min in the form of blue blocks suitable for X-ray determination. Yield: 94.5 mg (0.17 mmol, 67 %).

DTA (5 °C min^{-1}) onset: 159 °C (dec.); IR (ATR, cm^{-1}): $\tilde{\nu}$= 3175 (w), 3152 (w), 3036 (vw), 2963 (vw), 1518 (m), 1498 (w), 1471 (w), 1437 (w), 1431 (w), 1302 (w), 1188 (m), 1113 (m), 1101 (s), 1028 (w), 988 (s), 952 (vs), 899 (vs), 883 (s), 871 (s), 719 (w), 682 (m), 652 (vs), 609 (m); EA ($C_8H_{16}Cl_2CuN_{16}O_6$, 566.77): calcd: C 16.95, H 2.85, N 39.54 %; found: C 17.13, H 2.84, N 39.30 %; BAM drophammer: 3 J; friction tester: 7 N; ESD: 100 mJ (at grain size 100–500 µm).

$[Cu(ClO_3)(1\text{-MAT})_4]ClO_3$ (4)

The square pyramidal complex **4** crystallized within 5 days in the form of blue blocks suitable for X-ray determination. Yield: 94.1 mg (0.15 mmol, 60 %).

DTA (5 °C min^{-1}) onset: 157 °C (dec.); IR (ATR, cm^{-1}): $\tilde{\nu}$= 3420 (w), 3321 (w), 3207 (w), 1644 (s), 1593 (m), 1505 (m), 1454 (w), 1427 (vw), 1378 (w), 1355 (w), 1233 (vw), 1138 (vw), 1074 (w), 1056 (w), 1042 (w), 984 (m), 952 (vs), 921 (vs), 780 (m), 736 (w), 689 (m), 680 (w),

608 (w); EA ($C_8H_{20}Cl_2CuN_{20}O_6$, 626.83): calcd: C 15.33, H 3.22, N 44.69 %; found: C 15.58, H 3.23, N 43.73 %; BAM drophammer: 2 J; friction tester: 16 N; ESD: 110 mJ (at grain size < 100 µm).

$[Cu(ClO_3)_2(H_2O)_2(2\text{-MAT})_2]$ (5)

Single crystals of compound **5** in the form of colorless blocks were obtained by slow evaporation overnight. Yield: 113 mg (0.24 mmol, 98 %).

DTA (5 °C min^{-1}) onset: 125 °C (dec.); IR (ATR, cm^{-1}): $\tilde{\nu}$= 3417 (m), 3321 (m), 3245 (m), 3173 (m), 3052 (w), 1641 (s), 1565 (w), 1445 (m), 1422 (w), 1388 (w), 1349 (vw), 1334 (w), 1195 (w), 1138 (vw), 1108 (vw), 1013 (s), 909 (vs), 813 (m), 748 (m), 678 (vw), 649 (m), 609 (m), 533 (w), 525 (w); EA ($C_4H_{14}Cl_2CuN_{10}O_8$, 464.67): calcd: C 10.34, H 3.04, N 30.14 %; found: C 10.52, H 2.91, N 29.93 %; BAM drophammer: 2 J; friction tester: < 5 N; ESD: 50 mJ (at grain size 100–500 µm).

$[Cu(1,1\text{-dtp})_3](ClO_3)_2$ (6)

Compound **6** crystallized within one day in the form of blue blocks. Yield: 143 mg (0.19 mmol, 74 %).

DTA (5 °C min^{-1}) onset: 168 °C (dec.); IR (ATR, cm^{-1}): $\tilde{\nu}$= 3107 (m), 2999 (vw), 2977 (vw), 1573 (vw), 1505 (m), 1451 (w), 1431 (m), 1376 (w), 1341 (vw), 1289 (vw), 1250 (vw), 1174 (s), 1146 (w), 1097 (s), 1068 (w), 969 (vs), 937 (s), 910 (m), 877 (m), 721 (vw), 697 (w), 667 (w), 648 (m), 619 (m), 604 (m); EA ($C_{15}H_{24}Cl_2CuN_{24}O_6$, 770.97): calcd: C 23.37, H 3.14, N 43.60 %; found: C 23.10, H 3.03, N 42.52 %; BAM drophammer: 2 J; friction tester: 18 N; ESD: 100 mJ (at grain size < 100 µm).

$[Cu(ClO_3)_2(1,2\text{-dtp})_2]$ (7)

The water-free coordination compound **7** precipitated as a blue powder. Yield: 90.2 mg (0.15 mmol, 61 %). Blue crystals suitable for X-ray determination were obtained from methanol as solvent.

DTA (5 °C min^{-1}) onset: 162 °C (dec.); IR (ATR, cm^{-1}): $\tilde{\nu}$= 3159 (w), 3126 (w), 1517 (w), 1460 (m), 1446 (w), 1366 (w), 1356 (w), 1304 (w), 1247 (w), 1198 (w), 1188 (m), 1163 (w), 1147 (m), 1108 (m), 1088 (w), 1059 (vw), 1044 (vw), 1030 (w), 992 (s), 962 (vs), 920 (s), 904 (m), 888 (s), 828 (m), 724 (w), 701 (m), 683 (m), 659 (m), 639 (w), 601 (m), 506 (vw); EA ($C_{10}H_{16}Cl_2CuN_{16}O_6$, 590.79): calcd: C 20.33, H 2.73, N 37.93 %; found: C 20.42, H 2.69, N 37.63 %; BAM drophammer: 1 J; friction tester: 9 N; ESD: 100 mJ (at grain size 100–500 µm).

$[Cu(ClO_3)_2(2,2\text{-dtp})_2]$ (8)

Compound **8** precipitated as a blue powder. Yield: 82.9 mg (0.14 mmol, 56 %). Single crystals were obtained within 9 days by slow evaporation of an aqueous solution in the form of blue plates.

DTA (5 °C min^{-1}) onset: 176 °C (dec.); IR (ATR, cm^{-1}): $\tilde{\nu}$= 3130 (w), 3044 (vw), 2997 (vw), 1469 (w), 1450 (w), 1427 (vw), 1373 (w), 1346 (w), 1309 (w), 1301 (w), 1195 (w), 1157 (w), 1144 (m), 1137 (m), 1065 (vw), 1049 (w), 994 (s), 962 (vs), 930 (m), 889 (vs), 839 (m), 799 (w), 763 (w), 728 (vw), 702 (m), 691 (m), 659 (vw), 632 (m), 606 (m); EA ($C_{10}H_{16}Cl_2CuN_{16}O_6$, 590.79): calcd: C 20.33, H 2.73, N 37.93 %; found: C 20.61, H 2.74, N 37.68 %; BAM drophammer: 1 J; friction tester: < 5 N; ESD: 50 mJ (at grain size 100–500 µm).

$[Cu(H_2O)_2(i\text{-dtp})_2](ClO_3)_2$ (9)

The diaqua complex **9** was isolated as a light blue solid. Yield: 84.7 mg (0.14 mmol, 54 %). Slow evaporation of an aqueous solution resulted in single crystals in the form of blue blocks suitable for X-ray determination.

DTA (5 °C min^{-1}) onset: 140 °C (broad endothermic signal, which can be attributed to the loss of aqua ligands), 156 °C (dec.); IR (ATR, cm^{-1}): $\tilde{\nu}$= 3399 (w), 3148 (w), 3121 (w), 1644 (w),

1514 (w), 1491 (w), 1437 (m), 1393 (w), 1378 (vw), 1361 (vw), 1306 (w), 1286 (w), 1212 (vw), 1186 (m), 1175 (m), 1161 (w), 1130 (w), 1110 (w), 1097 (m), 1087 (m), 1040 (w), 1004 (s), 921 (vs), 894 (s), 754 (m), 719 (w), 675 (m), 667 (m), 633 (m), 603 (s); EA ($C_{10}H_{20}Cl_2CuN_{16}O_8$, 626.82): calcd: C 19.16, H 3.22, N 35.75 %; found: C 19.25, H 3.17, N 35.62 %; BAM drophammer: 1 J; friction tester: 32 N; ESD: 65 mJ (at grain size 100–500 µm).

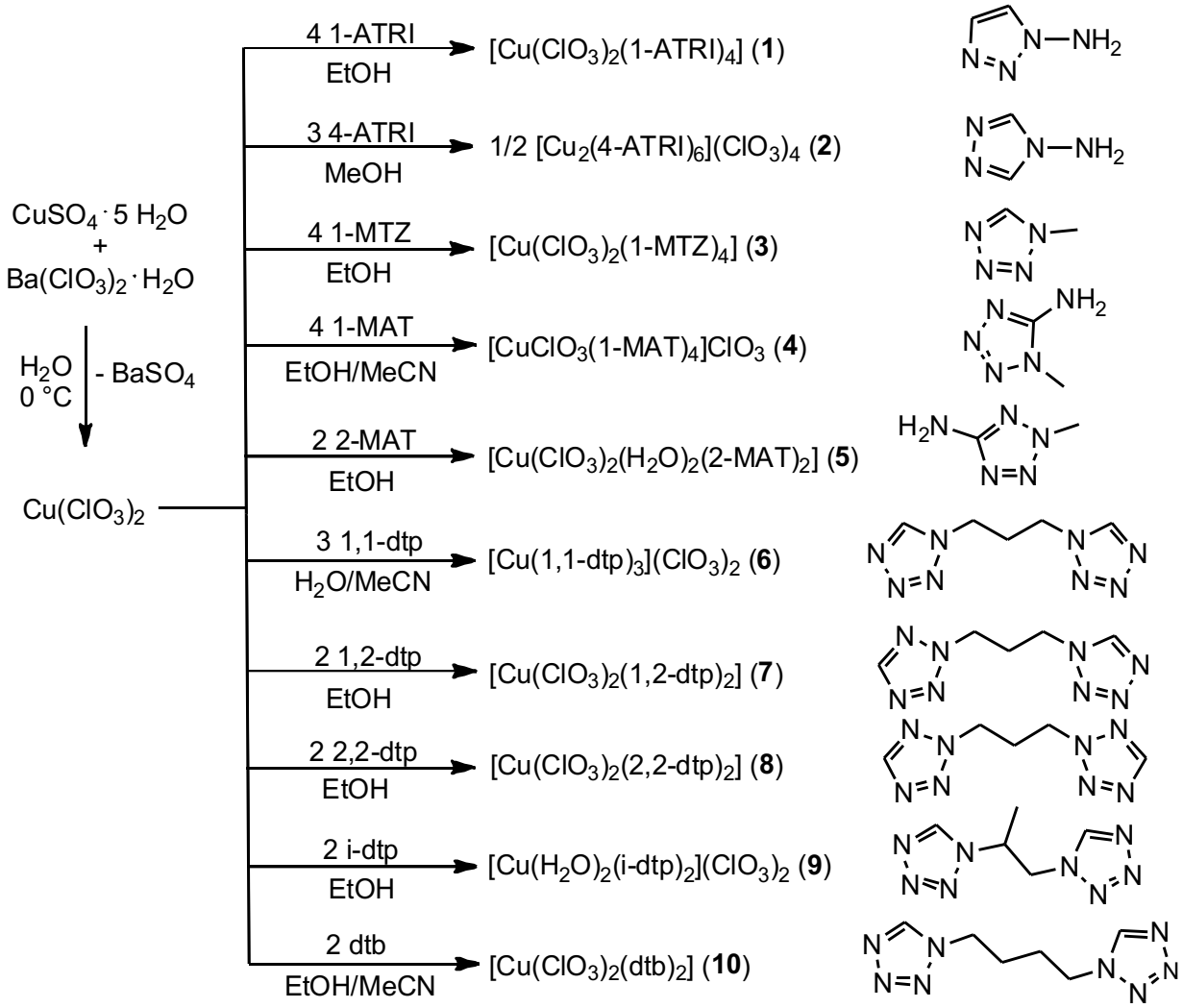
$[Cu(ClO_3)_2(dtb)_2]$ (10)

Product **10** was obtained as a blue solid. Yield: 115 mg (0.19 mmol, 74 %). Evaporation of aqueous solutions gave small amounts of single crystals suitable for X-ray determination.

DTA (5 °C min^{-1}) onset: 157 °C (dec.); IR (ATR, cm^{-1}): $\tilde{\nu}$= 3156 (vw), 3107 (w), 1511 (w), 1503 (w), 1468 (w), 1452 (w), 1442 (w), 1434 (w), 1392 (w), 1355 (vw), 1187 (m), 1169 (w), 1149 (w), 1106 (m), 1095 (m), 1055 (vw), 1013 (s), 950 (s), 898 (s), 877 (vs), 841 (m), 733 (m), 715 (w), 679 (m), 659 (m), 645 (m), 604 (s); EA ($C_{12}H_{20}Cl_2CuN_{16}O_6$, 618.85): calcd: C 23.29, H 3.26, N 36.21 %; found: C 23.31, H 3.21, N 35.01 %; BAM drophammer: 3 J; friction tester: 32 N; ESD: 100 mJ (at grain size < 100 µm).

19.10.2 Synthesis

The copper(II) complexes **3**–**6** (Scheme S1) were obtained as single crystals suitable for X-ray diffraction within minutes or days directly from the mother liquor in reasonable to very good yields (60–98 %). Compound **1**, **2** and **7**–**10** precipitated within 5 min as light to dark blue solids in satisfying to very good yields (54–93 %). It was possible to isolate small amounts of single crystals suitable for X-ray experiments out of the ethanolic (**1**), methanolic (**7**) or aqueous (**8**–**10**) reaction mixtures. Crystal growth of **2** was achieved by layering to ensure slow formation at the phase boundary. All products were filtered off, washed with cold ethanol to remove unreacted starting materials and dried in air.



Scheme S1. Synthesis of the complexes 1–10 starting from copper(II) sulfate and barium chlorate; Overview of used nitrogen-rich ligands: 1-ATRI: 1-amino-1,2,3-triazole; 4-ATRI: 4-amino-1,2,4-triazole; 1-MTZ: 1-methyltetrazole; 1-MAT: 1-methyl-5-aminotetrazole; 2-MAT: 2-methyl-5-aminotetrazole; 1,1-dtp: 1,3-di(tetrazol-1-yl)propane; 1,2-dtp: 1-(tetrazol-1-yl)-3-(tetrazol-2-yl)propane; 2,2-dtp: 1,3-di(tetrazol-2-yl)propane; i-dtp: 1,1'-(propane-1,2-diyl)bis(tetrazole); dtb: 1,4-di(tetrazol-1-yl)butane.

19.10.3 Crystal structures

All complexes were characterized by low temperature single crystal X-ray diffraction. The crystal structures were uploaded to the CSD database[S9] and can be obtained free of charge with the CCDC nos. 1574490 (**1**), 1574486 (**2**), 1574482 (**3**), 1574487 (**4**), 1574489 (**5**), 1574485 (**6**), 1574481 (**7**), 1574484 (**8**), 1574483 (**9**), 1574488 (**10**). The bond lengths and angles of the coordinating ligands in the analyzed complexes are in the typical range of tetrazole

and triazole ligands and nearly the same as in the non-coordinating ligands.[S10] The ligands are therefore not part of the discussion in any of the following coordination compounds. All copper(II) chlorate complexes, except compound **4**, show an octahedral coordination with a Jahn-Teller distortion along the axial coordination sphere.

$[Cu(ClO_3)_2(1\text{-ATRI})_4]$ (**1**) crystallizes in the form of blue blocks in the triclinic space group *P*−1 with one formula unit per unit cell and a calculated density of 1.916 g cm^{-3} at 100 K. The octahedral coordination sphere around the copper(II) cation (Figure S1) is built up of two chlorato ligands in axial positions and four aminotriazole molecules in a plane.

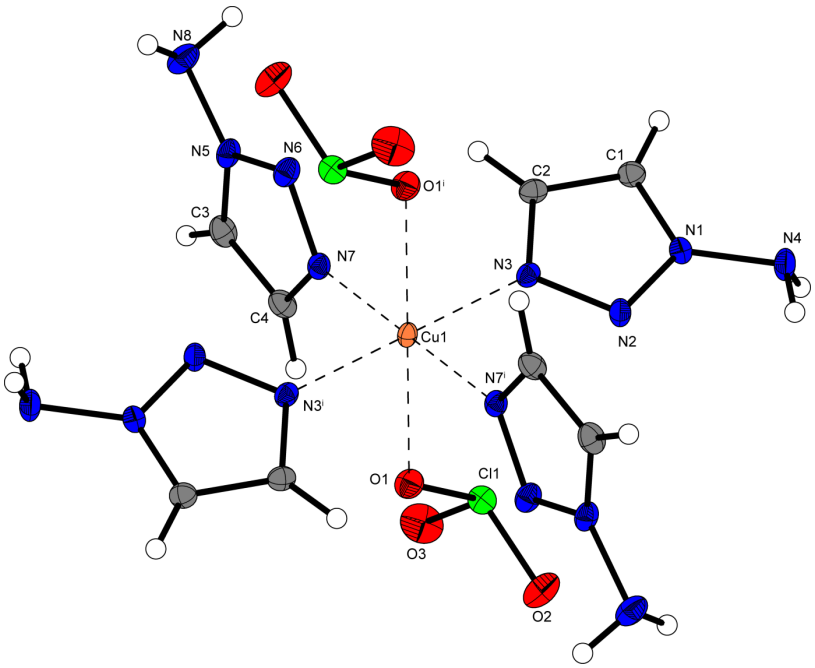


Figure S1. Molecular unit of $[Cu(ClO_3)_2(1\text{-ATRI})_4]$ (**1**). Selected bond lengths (Å): Cu1–O1 2.3698(17), Cu1–N3 2.027(2), Cu1–N7 2.026(2); selected bond angles (°): O1–Cu1–N3 93.77(7), O1–Cu1–N7 90.47(7), N3–Cu1–N7 88.76(8). Symmetry code: (i) 1−x, −y, 2−z.

The water-free compound **2** crystallizes in the form of blue rods in the monoclinic space group *C*2/*m* with four formula units per unit cell and a calculated density of 1.964 g cm^{-3} at 143 K. The molecular unit contains two different copper(II) ions (Figure S2), each is octahedrally coordinated by six donor atoms. Complex **2** and **6** are the only presented compounds with copper(II) ions exclusively coordinated by nitrogen atoms. Both center atoms show a Jahn-Teller distortion, whereas Cu1 shows a rare compressed coordination sphere with shorter axial Cu–N bonds compared to the equatorial ones. The stretched coordination environment of Cu2 is composed of longer axial and shorter equatorial Cu–N-bonds. Two copper(II) atoms are

bridged by three bidental ligands building up polymeric chains. In comparison to compound **1**, the chlorates are not participating in coordination and act only as counter-anions.

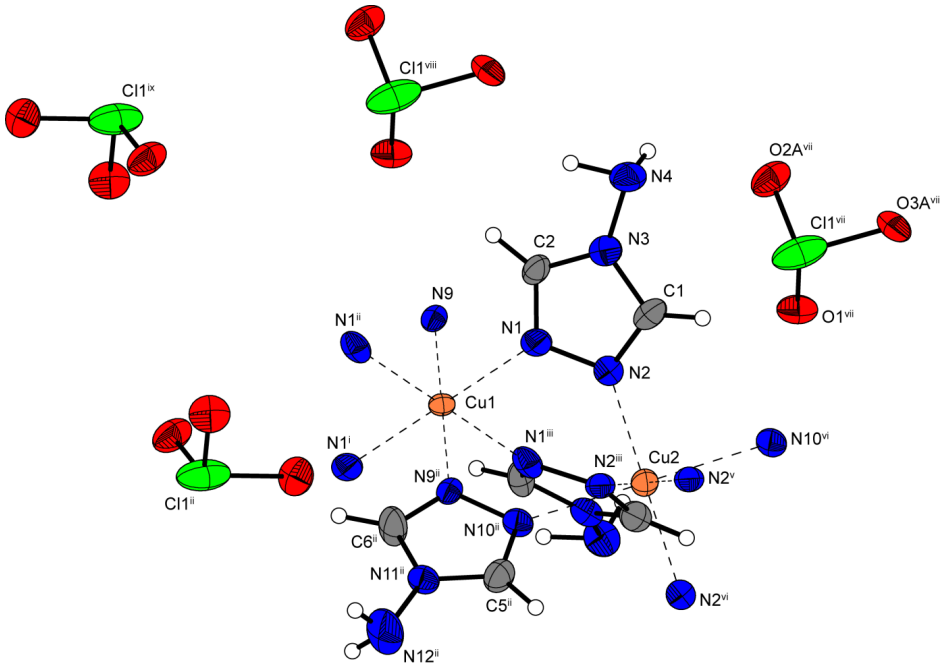


Figure S2. Copper(II) coordination environment of $[Cu_2(4\text{-ATRI})_6](ClO_3)_4$ (**2**). Selected bond lengths (Å): Cu1–N1 2.172(6), Cu1–N9 2.035(7), Cu2–N2 2.039(5), Cu2–N10^{ii} 2.411(7); selected bond angles (°): N1–Cu1–N9 89.34(17), N1–Cu1–N1^{ii} 91.5(2), N1^{ii}–Cu1–N9 90.66(17), N2–Cu2–N2^{iii} 91.01(19), N2–Cu2–N10^{ii} 87.66(17). Symmetry codes: (i) 1−x, 1−y, −z; (ii) 1−x, y, −z; (iii) x, 1−y, z; (iv) 1−x, 1−y, 1−z; (v) 1−x, y, 1−z; (vi) x, y, 1+z; (vii) 0.5−x, 0.5−y, 1−z; (viii) 0.5−x, 0.5−y; −z; (ix) 0.5+x, 0.5−y, −1+z.

$[Cu(ClO_3)_2(1\text{-MTZ})_4]$ (**3**), the structural isomer of **1**, crystallizes in the form of blue blocks in the monoclinic space group $P2_1/n$ with two formula units per unit cell and a calculated density of 1.807 g cm^{-3} at 173 K. Similar to compound **1**, the molecular unit is composed of one central metal (Figure S3) with two coordinating chlorato ligands in axial positions and four ligand molecules in a plane with comparable bond lengths to complex **1**.

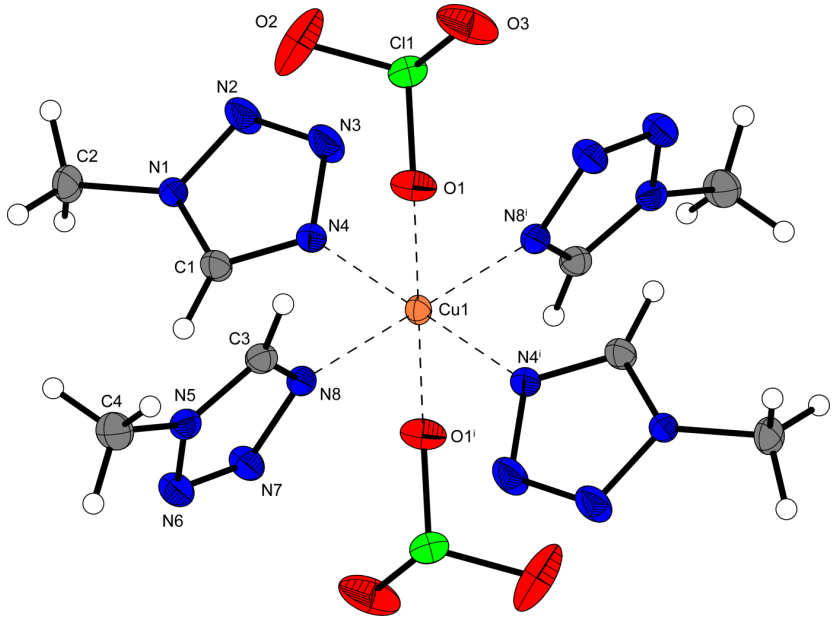


Figure S3. Molecular unit of $[Cu(ClO_3)_2(1\text{-MTZ})_4]$ (**3**). Selected bond lengths (Å): Cu1–O1 2.3458(14), Cu1–N4 2.0206(15), Cu1–N8 2.0254(15); selected bond angles (°): O1–Cu1–N4 94.78(6), O1–Cu1–N8 85.91(5), N4–Cu1–N8 89.02(6). Symmetry code: (i) 1−x, 1−y, −z.

In comparison to complex **1**, coordination compound **4** with a calculated density of 1.832 g cm^{-3} at 173 K, crystallizes in the same monoclinic space group $P2_1/n$ but with an extraordinary square pyramidal coordination sphere and four formula units per unit cell. The molecular unit is made up of one metal cation (Figure S4), one axial coordinated chlorato ligand, four coordinating ligands in a plane and one non-coordinating counter-anion. Compared to all other presented coordination compounds, the lower number of ligands around the copper(II) ion leads to shorter Cu–N-bonds.

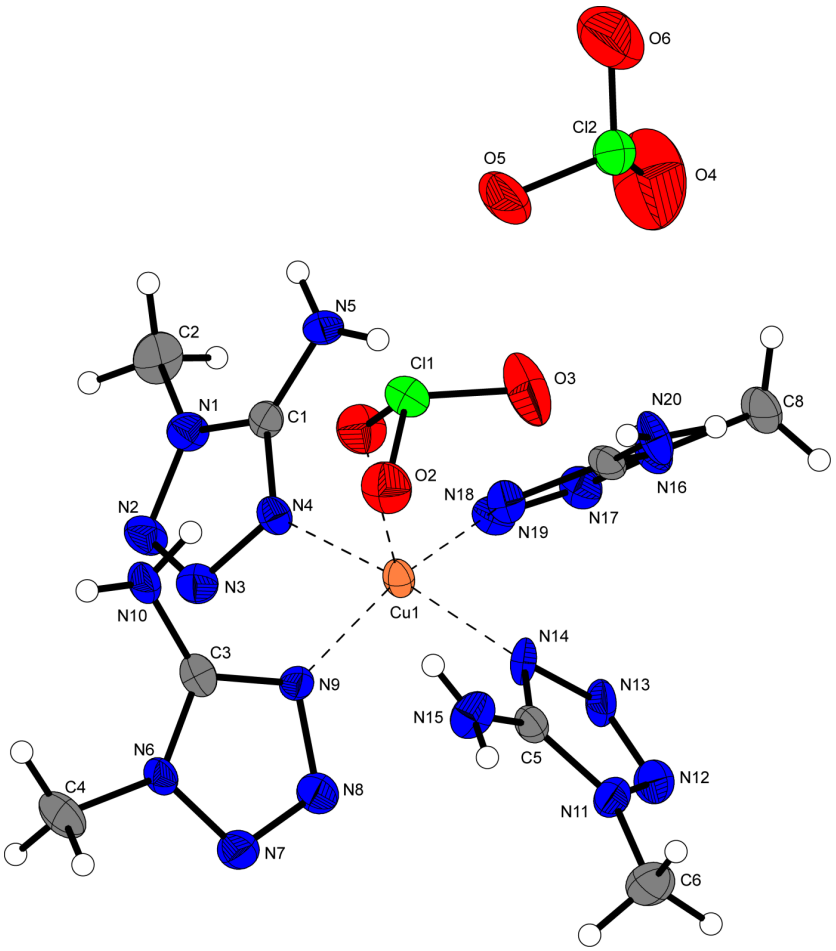


Figure S4. Molecular unit of $[CuClO_3(1\text{-}MAT)_4]ClO_3$ (**4**). Selected bond lengths (Å): Cu1–O1 2.369(7), Cu1–N4 2.020(7), Cu1–N9 1.963(6), Cu1–N14 2.003(7), Cu1–N19 1.982(7); selected bond angles (°): O1–Cu1–N9 96.9(2), O1–Cu1–N14 106.3(2), O1–Cu1–N19 97.2(2), N4–Cu1–N9 90.2(3), N9–Cu1–N19 165.9(3).

The diaqua complex **5** crystallizes in the form of colorless blocks in the triclinic space group *P*−1 with one formula unit per unit cell and possesses the highest density (2.000 g cm^{-3} at 100 K) of all compounds. The use of 2-MAT, a constitutional isomer of 1-MAT, is favoring an octahedral coordination sphere around the copper(II) cation (Figure S5) with two chlorato, two aqua and two tetrazole ligands.

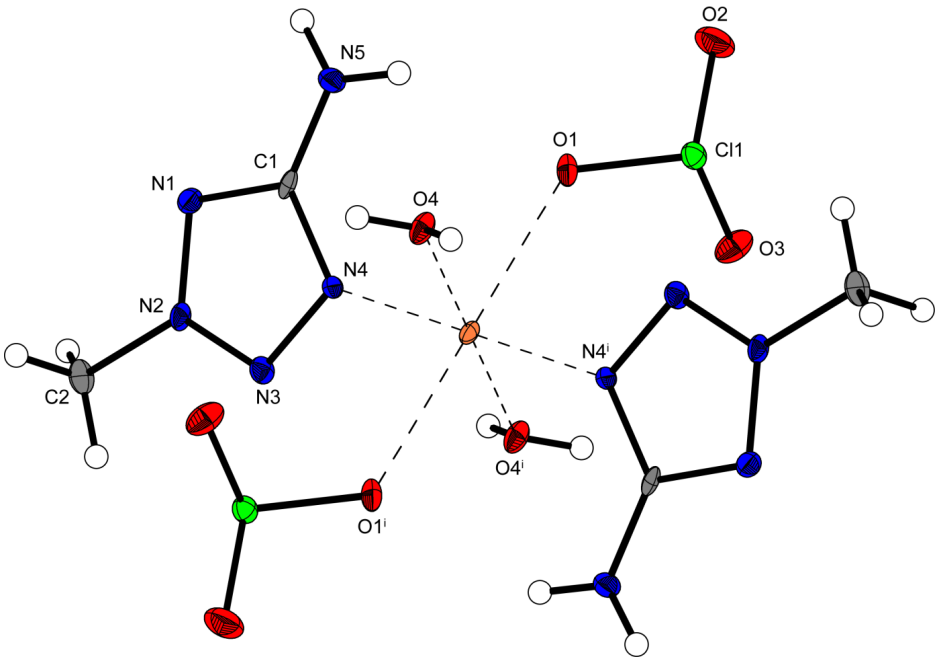


Figure S5. Molecular unit of $[Cu(ClO_3)_2(H_2O)_2(2\text{-MAT})_2]$ (**5**). Selected bond lengths (Å): Cu1–O1 2.422(3), Cu1–O4 1.983(3), Cu1–N4 1.995(3); selected bond angles (°): O1–Cu1–O4 88.56(10), O1–Cu1–N4 86.89(9), O4–Cu1–N4 91.09(12). Symmetry code: (i) −x, −y, 2−z.

The copper(II) chlorate complex **6** shows the lowest density (1.711 g cm^{-3} at 123 K) of all compounds and is the only trigonal crystal structure. It crystallizes in the form of blue blocks in the space group *P*−3*c*1 with two formula units per unit cell. The molecular unit contains one copper(II) cation (Figure S6) with three coordinating ditetrazole ligands and two non-coordinating chlorate anions. Two copper(II) cations are linked by three bidental ligands, building up linear polymeric chains.

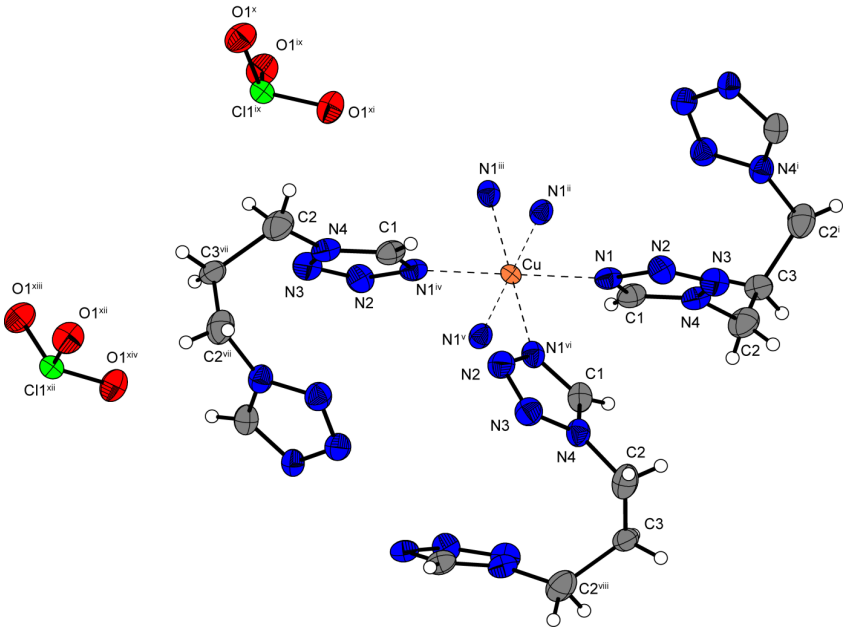


Figure S6. Copper(II) coordination environment of $[Cu(1,1\text{-dtp})_3](ClO_3)_2$ (**6**). Selected bond lengths (Å): Cu–N1 2.1280(17); selected bond angles (°): N1–Cu1–N1^{ii} 91.17(7), N1–Cu1–N1^{iii} 91.18(8), N1–Cu1–N1^{v} 88.82(8). Symmetry codes: (i) −x, −x+y, 0.5−z; (ii) −x+y, −x, z; (iii) −y, x−y, z; (iv) −x, −y, −z; (v) x−y, x, −z; (vi) y, −x+y, −z; (vii) x, x−y, −0.5+z; (viii) −x+y, y, 0.5+z; (ix) −1+x, −1+y, −1+z; (x) −y, −1+x−y, −1+z; (xi) −x+y, −x, −1+z; (xii) −x+y, −1+y, −1.5+z; (xiii) −1+x, −1+x−y, −1.5+z; (xiv) −y, −x, −1.5+z.

$[Cu(ClO_3)_2(1,2\text{-dtp})_2]$ (**7**) crystallizes in the form of blue blocks in the triclinic space group *P*−1 with one formula unit per unit cell and a calculated density of 1.863 g cm^{-3} at 173 K. Compared to complex **6**, the central metal (Figure S7) is linked to one ditetrazole ligand less due to the two coordinating chlorato ligands in axial positions. Two equatorial ligands each are bridging between two cations, building up linear chains.

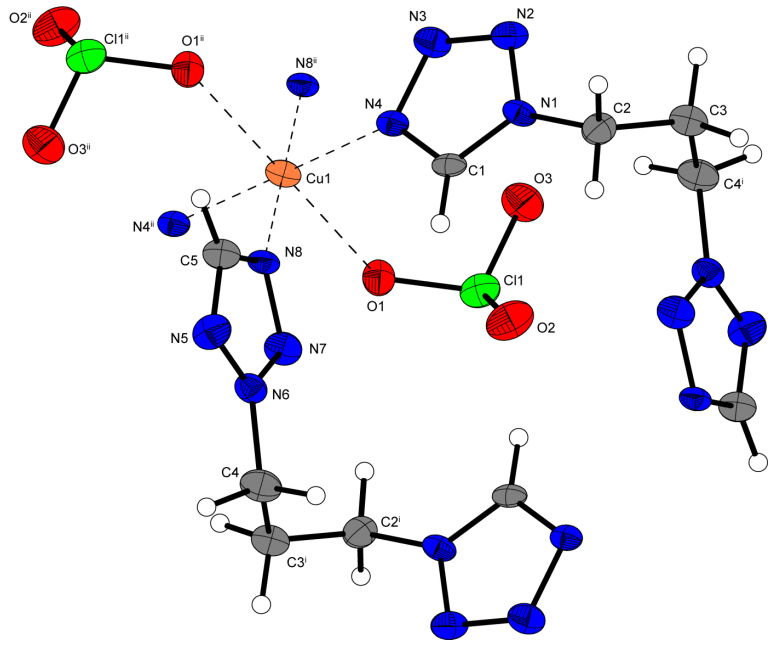


Figure S7. Copper(II) coordination environment of $[Cu(ClO_3)_2(1,2\text{-dtp})_2]$ (**7**). Selected bond lengths (Å): Cu1–O1 2.410(3), Cu1–N4 2.004(4), Cu1–N8 2.020(4); selected bond angles (°): O1–Cu1–N4 91.31(14), O1–Cu1–N8 92.09(14), N4–Cu1–N8 89.88(16). Symmetry codes: (i) 1−x, 1−y, 1−z; (ii) 1−x, −y, 1−z.

Complex compound **8** crystallizes in the form of blue plates in the monoclinic space group *C*2/*c* with four formula units per unit cell and a calculated density of 1.821 g cm^{-3} at 173 K. The coordination sphere around the copper(II) central metal (Figure S8) is identical to compound **7** with two coordinating chlorato ions in axial positions and two neutral ditetrazole molecules in a plane, bridging between copper(II) atoms and building up polymeric chains.

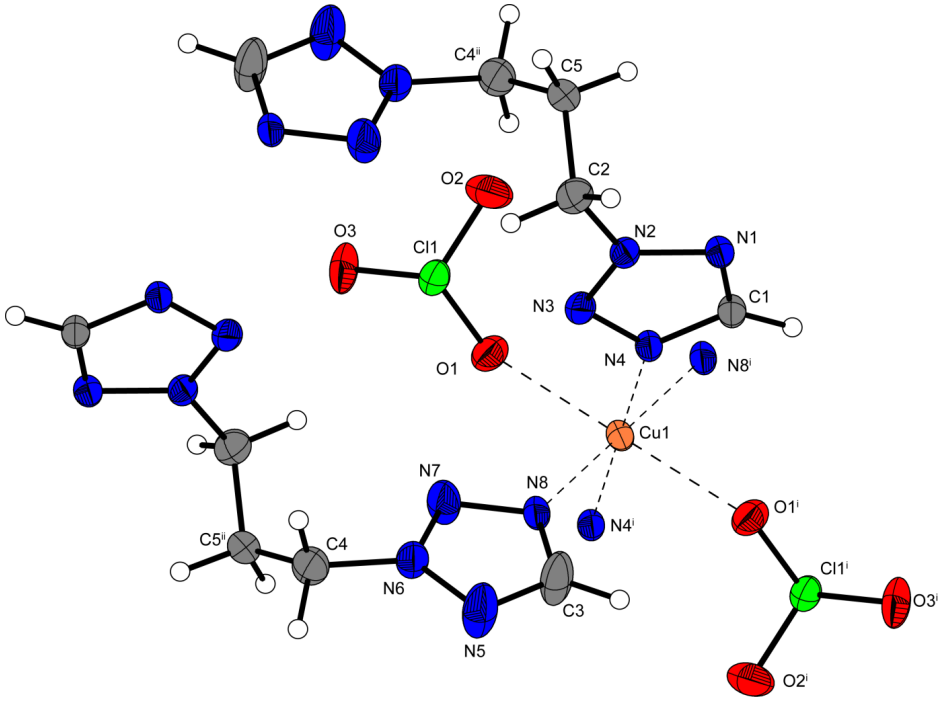


Figure S8. Copper(II) coordination environment of $[Cu(ClO_3)_2(2,2\text{-dtp})_2]$ (**8**). Selected bond lengths (Å): Cu1–O1 2.312(3), Cu1–N4 2.011(3), Cu1–N8 2.046(3); selected bond angles (°): O1–Cu1–N4 95.27(10), O1–Cu1–N8 92.25(10), N4–Cu1–N8 90.12(11). Symmetry codes: (i) 1−x, −y, 1−z; (ii) 0.5−x, 0.5−y, 1−z.

Like complex **8**, coordination compound **9**, with a calculated density of 1.764 g cm^{-3} at 173 K, crystallizes in the monoclinic space group *C*2/*c* with four formula units per unit cell. However, the chlorate counterions are not involved in the formation of the octahedron. The central metal (Figure S9) is again coordinated by two equatorial ditetrazole molecules and by two axial complexing aqua ligands instead of the chlorates. Like complex **6** and **7**, the nitrogen-rich ligands are bridging between the copper(II) ions, building up polymeric chains.

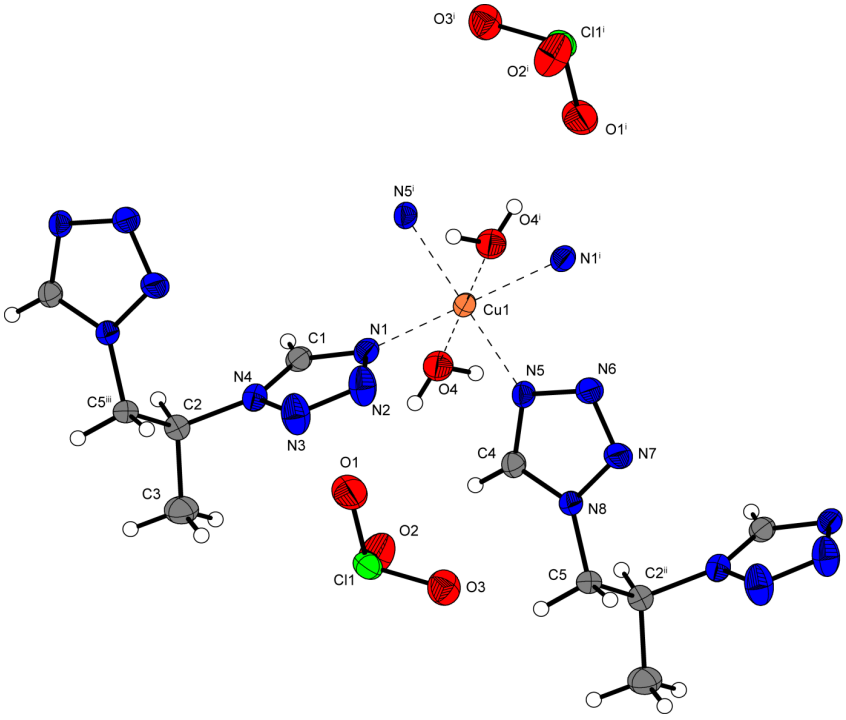


Figure S9. Copper(II) coordination environment of $[Cu(H_2O)_2(i\text{-}dtp)_2](ClO_3)_2$ (**9**). Selected bond lengths (Å): Cu1–O4 2.2951(18), Cu1–N1 2.0498(18), Cu1–N5 2.0307(17); selected bond angles (°): O4–Cu1–N1 86.35(7), O4–Cu1–N5 90.43(7), N1–Cu1–N5 89.54(7). Symmetry codes: (i) 1−x, −y, −z; (ii) −0.5+x, −0.5+y, z; (iii) 0.5+x, 0.5+y, z.

The copper(II) chlorate complex **10** crystallizes in the form of blue blocks in the monoclinic space group $P2_1/n$ with two formula units per unit cell and a calculated density of 1.840 g cm^{-3} at 143 K. The molecular unit consists of one copper(II) cation (Figure S10), two coordinating chloratos and two bridging ditetrazole ligands. In contrast to compounds **7**–**9** each ligand is linking two different copper(II) atoms, which leads to the formation of a 2D-network.

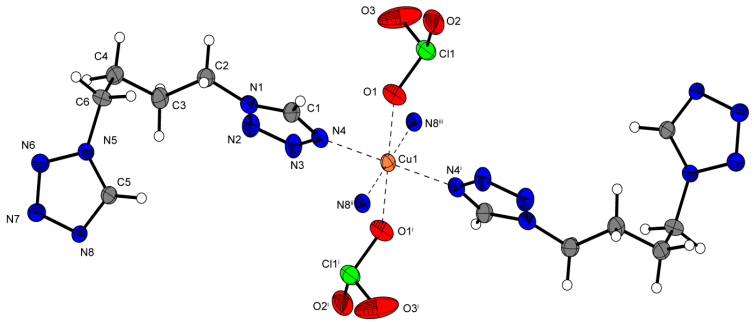


Figure S10. Copper(II) coordination environment of $[Cu(ClO_3)_2(dtb)_2]$ (**10**). Selected bond lengths (Å): Cu1–O1 2.360(3), Cu1–N4 2.017(3), Cu1–N8 2.050(2); selected bond angles (°): O1–Cu1–N4 86.63(10), O1–Cu1–N8 96.25(9), N4–Cu1–N8 91.93(10). Symmetry code: (i) 1−x, −1−y, 1−z.

19.10.4 Sensitivities and Thermal Stability

For the investigation of endothermic events, like dehydration or melting and for the determination of the thermal stabilities, DTA measurements with a heating rate of β = 5 °C min^{-1} were performed. The sensitivities of the complexes toward impact, friction and electric discharge have been determined according to BAM standards and all compounds were classified in accordance to the UN recommendations on the transport of dangerous goods. An overview of the physicochemical properties of all compounds is given in Tables S1 and S2.

Table S5. Physicochemical properties of compound **1**–**5**.

	1	**2**	**3**	**4**	**5**
Formula	$C_8H_{16}Cl_2CuN_{16}O_6$	$C_{12}H_{24}Cl_4Cu_2N_{24}O_{12}$	$C_8H_{16}Cl_2CuN_{16}O_6$	$C_8H_{20}Cl_2CuN_{20}O_6$	$C_4H_{14}Cl_2CuN_{10}O_8$
FW [g mol^{-1}]	566.77	965.37	566.77	626.83	464.67
$\rho_{calc.}$ [g cm^{-3}] @(K)	1.916 (100)	1.964 (143)	1.807 (173)	1.832 (173)	2.000 (100)
***IS* [J][a)]**	1	1	3	2	2
***FS* [N][b)]**	< 5	< 5	7	16	< 5
***ESD* [mJ][c)]**	20	15	100	110	50
$T_{dec.}$ [°C][d)]	119	186	159	157	125
Grain size [µm]	< 100	< 100	100–500	< 100	100–500

a) impact sensitivity according to the BAM drophammer (method 1 of 6); b) friction sensitivity according to the BAM friction tester (method 1 of 6); c) electrostatic discharge sensitivity (OZM ESD tester); d) temperature of decomposition indicated by exothermic event according to DTA (onset temperatures at a heating rate of 5 °C min^{-1}).

Table S6. Physicochemical properties of compound **6**–**10**.

	6	**7**	**8**	**9**	**10**
Formula	$C_{15}H_{24}Cl_2CuN_{24}O_6$	$C_{10}H_{16}Cl_2CuN_{16}O_6$	$C_{10}H_{16}Cl_2CuN_{16}O_6$	$C_{10}H_{20}Cl_2CuN_{16}O_8$	$C_{12}H_{20}Cl_2CuN_{16}O_6$
FW [g mol^{-1}]	770.97	590.79	590.79	626.82	618.85
$\rho_{calc.}$ [g cm^{-3}] @(K)	1.711 (123)	1.863 (173)	1.821 (173)	1.764 (173)	1.840 (143)
***IS* [J][a)]**	2	1	1	1	3
***FS* [N][b)]**	18	9	< 5	32	32
***ESD* [mJ][c)]**	100	100	50	65	100
$T_{dec.}$ [°C][d)]	168	162	176	156	157
Grain size [µm]	< 100	100–500	100–500	100–500	< 100

a) impact sensitivity according to the BAM drophammer (method 1 of 6); b) friction sensitivity according to the BAM friction tester (method 1 of 6); c) electrostatic discharge sensitivity (OZM ESD tester); d) temperature of decomposition indicated by exothermic event according to DTA (onset temperatures at a heating rate of 5 °C min^{-1}).

Only one endothermic occasion has been observed for coordination compound **9** (Figure S12) which loses its aqua ligands at 140 °C. The other diaqua complex (**5**) (Figure S11) however, exhibits only an exothermic event at 125 °C. One possible explanation for the thermal stability of compound **9** could be the formation of a stable water-free species which decomposes at a later stage, whereas compound **5** directly decomposes after the loss of the water molecules. All other energetic coordination compounds show a higher exothermic decomposition temperature between 157 °C (**4**, **10**) and 186 °C (**2**), except complex **1**, which possesses a very low thermal stability of 119 °C. Even though no general trend for the thermal stability, regarding the

coordination mode of the chlorates, the bridging or non-bridging ligands and the chain length of the ditetrazole ligands, can be observed, it stands out that $[Cu_2(4\text{-ATRI})_6](ClO_3)_4$ (**2**) with alternating stretched and compressed Jahn-Teller distortions shows the highest decomposition temperature. This makes it, together with complex **8** (T_{dec} = 176 °C), the most promising candidates of all the presented compounds.

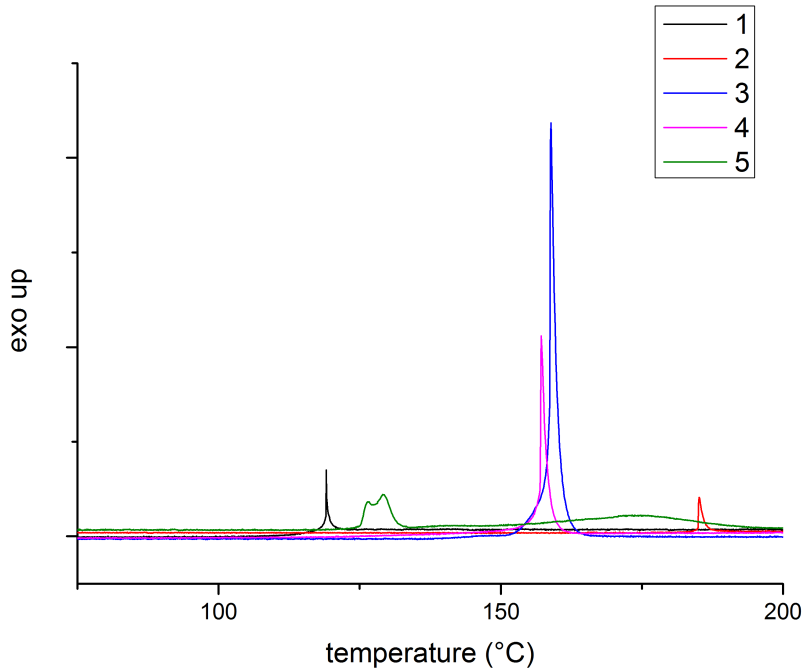


Figure S11. DTA plots (5 °C min^{-1}) of chlorate complexes **1**–**5** shown in the range of 75–200 °C.

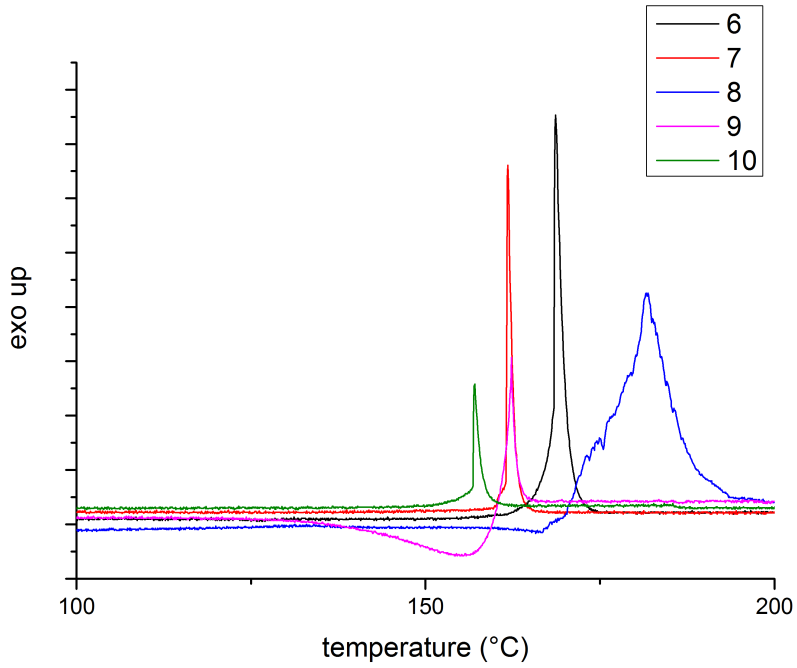


Figure S12. DTA plots (5 °C min^{-1}) of the ditetrazole complexes **6**–**10** shown in the range of 100–200 °C.

The parameters given in Tables S1 and S2 show that all complexes are, in accordance to the UN recommendations on the transport of dangerous goods, very sensitive toward impact and friction. [S21] Even though the chlorate complexes show relatively high impact sensitivities from 1–3 J, the compounds can be still handled in a safe way. In the row of ditetrazole ligands it can be seen that dtb complex **10** shows decreased sensitivities (3 J, 32 N) compared to the propyl linked compounds. Additionally, coordination compounds with non-coordinated chlorates **6**, **9** show a slightly higher stability (2 J, 16 N/ 1 J, 32 N) than complexes with coordinating chlorato ligands **7**, **8** (1 J, 9 N/ 1 J, < 5 N). Surprisingly the two aqua ligands in compound **5** are not leading to a higher stability (1 J, < 5 N) of the explosive compound compared with the anhydrous complexes.

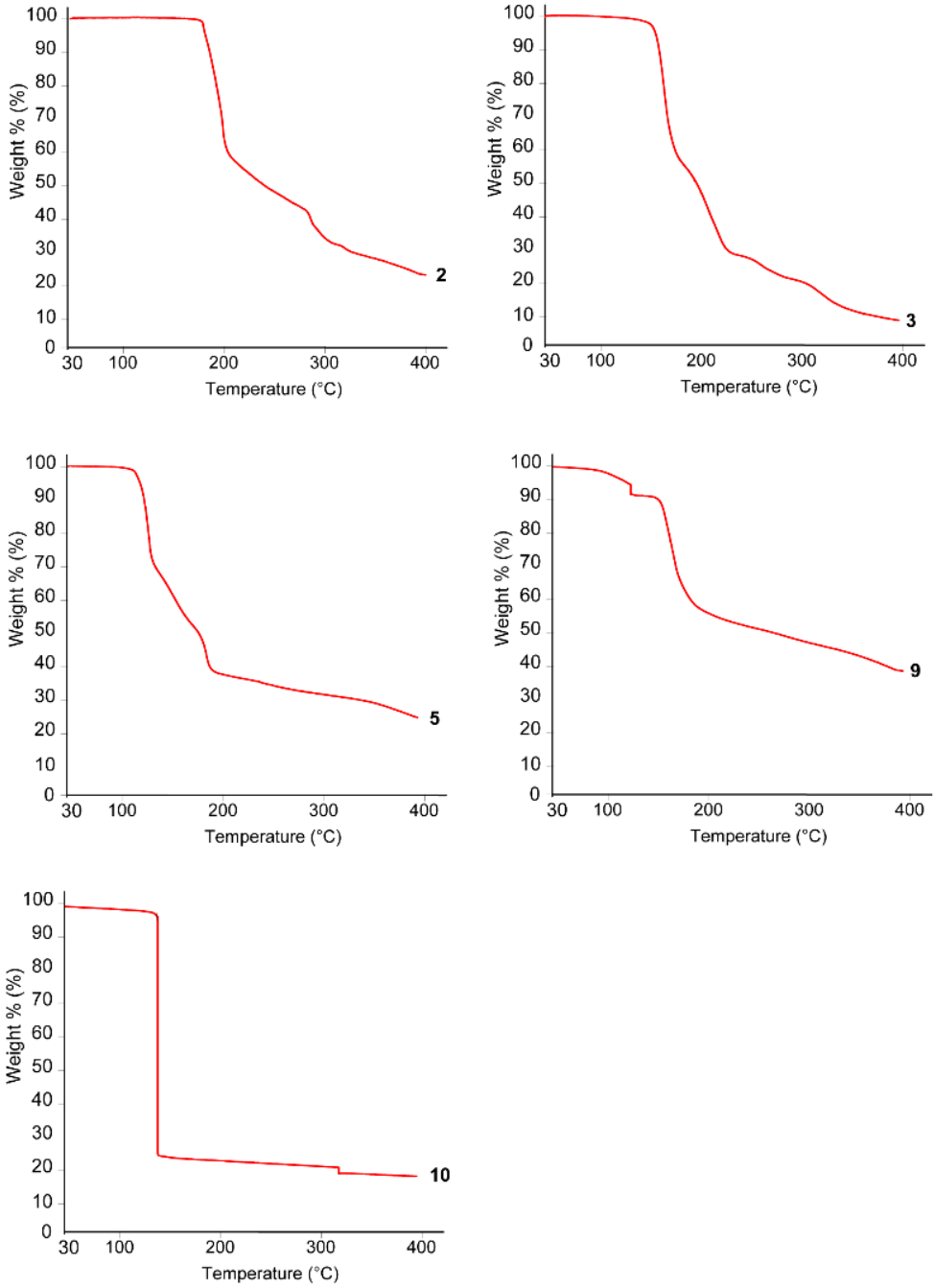


Figure S13. TG plots of selected compounds.

19.10.5 Laser Ignition Tests

The laser ignition tests were performed with a single-pulsed 45 W InGaAs laser diode in the single-pulsed mode. The diode was coupled directly to an optical fiber with a core diameter of 400 µm and a cladding diameter of 480 µm. The optical fiber was linked via a SMA type connecter directly to the laser and to a collimator. The collimator, in turn, was connected to an

optical lens, which was stationed in its focal distance (f = 29.9 mm) to the sample. The lens was shielded from the explosive with sapphire glass. Transparent polycarbonate firing caps were filled with approx. 25 mg of the compound, pressed with a pressure force of 1 kN and sealed by a UV-curing adhesive. The confined samples were irradiated at a wavelength of 915 nm, a varying current of 7–8 A, a voltage of 4 V and a varying pulse length of 0.10–15 ms, which combined results in an approximately energy output of 0.17–25.5 mJ. The results of the laser experiments are summarized in Table S3. All complexes, except diaqua compound **9**, showed a detonation (Figure S14) differing in the required energy input. These results make copper(II) chlorate complexes promising compounds for laser ignition with low initiation energies.

Table S3. Results of the laser ignition tests.

	1	**2**	**3**	**4**	**5**	**6**	**7**	**8**	**9**	**10**
E_{max} [mJ]	0.20	1.70	25.5	0.43	0.20	0.20	0.43	0.85	1.70	0.85
outcome[a]	det.	det.	det.	det.	det.	det.	det.	det.	def.	det.

[a] (det. = detonation; def. = deflagration). Operating parameters: current I = 7 A; voltage U = 4 V; theoretical maximal output power P_{max} = 45 W; wavelength λ = 915 nm; pulse length τ = 0.10-15 ms.

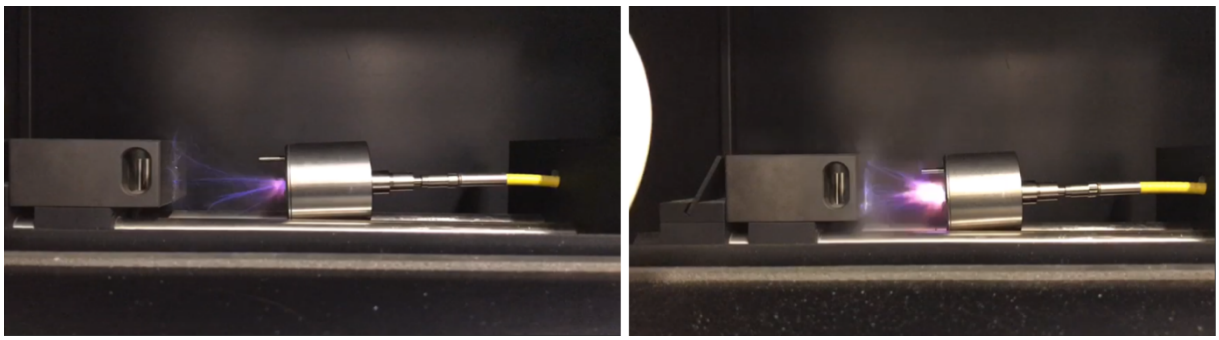


Figure S14. Moment of detonation of compounds **6** (left) and **10** (right).

19.10.6 UV-Vis Spectroscopy

In order to get an insight toward a possible laser initiation mechanism, solid-state UV-Vis spectra were measured in the range of 350–1000 nm for all complexes. Compounds are shown in Figure S15 and S16. The step in the absorption intensity at 800 nm in the spectra is caused by a detector change. The UV-Vis spectra exhibit only qualitative character.

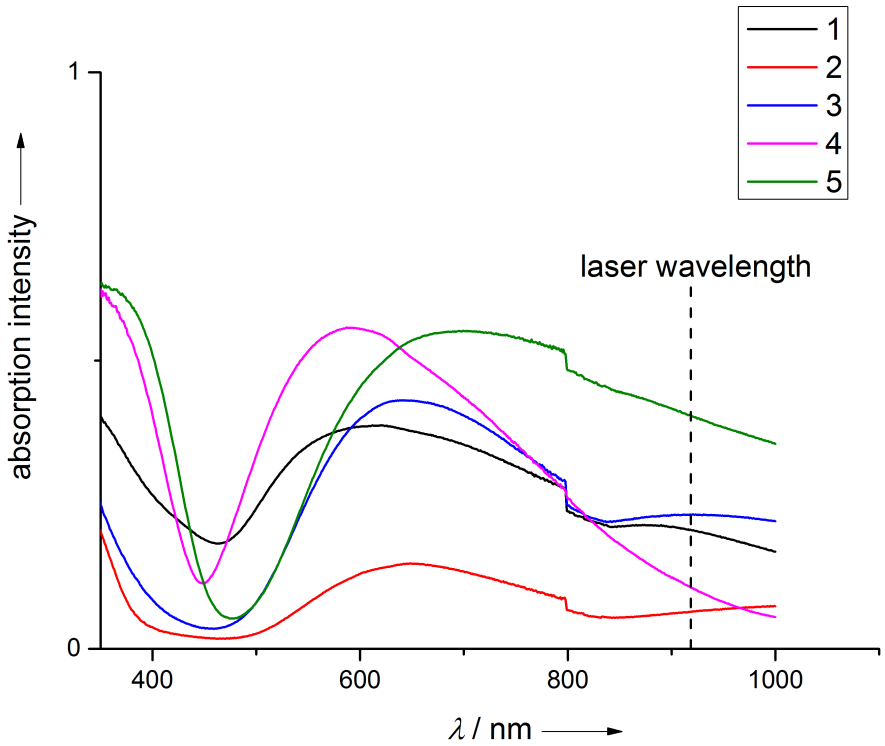


Figure S15. UV-Vis spectra in the solid-state of compounds **1**–**5**.

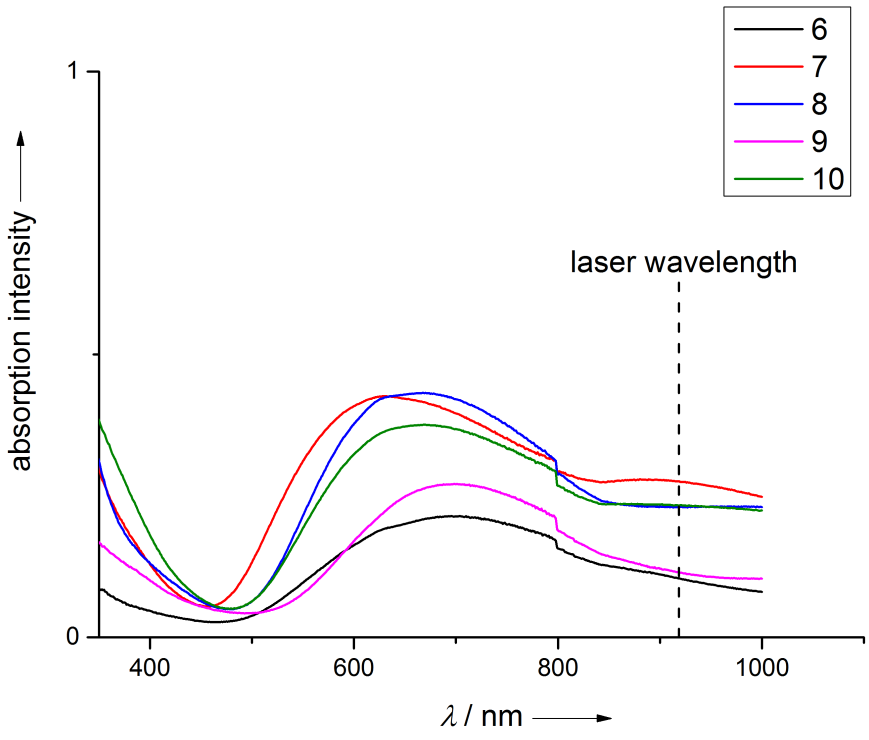


Figure S16. UV-Vis spectra in the solid-state of selected compounds **6**–**10**.

Due to the characteristic d-d-transitions, the spectra show absorptions in the UV, visible and near-infrared region typical for blue copper(II) compounds with only minor deviations among

each other. The mechanism for laser initiation is still not understood and many pathways such as electronically or thermally are imaginable.[S11] All copper(II) chlorate complexes show absorption maxima close to 350 and 600 nm, whereas only minor absorptions occur at the laser wavelength of 915 nm. The excitation at 915 nm could be a conceivable explanation for the initiation. It is quite sure that the process of laser ignition depends on multiple parameters and more investigations are necessary for a better understanding of the laser initiation mechanism in the future.

19.10.7 Initiation capability tests

For the determination of the compounds' deflagration to detonation transition (DDT) capability hot plate and hot needle test were performed (Figure S17). The most promising complexes were tested in copper shell initiation tests with PETN as secondary explosive. Hot needle tests were performed by fixation of the sample underneath adhesive tape on a copper plate followed by penetration with a red heated needle.

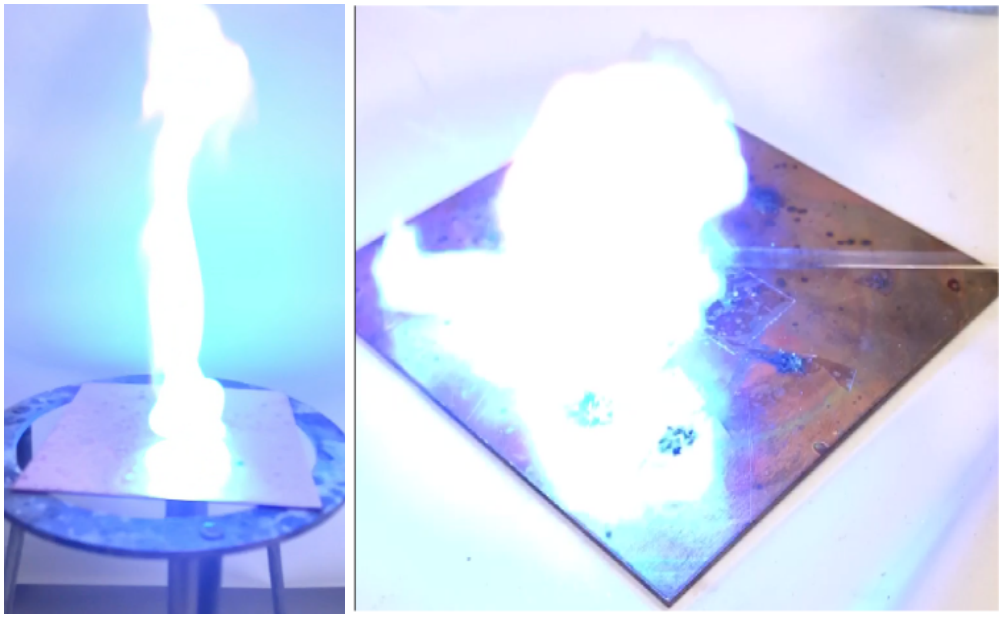


Figure S17. left: moment of deflagration of compound **3** during the hot plate test; right: moment of detonation of compound **2** during the hot needle test.

A compound's detonation typically indicates a valuable primary explosive, whereas the safe and practicable hot plate test shows only the performance of the unconfined sample toward fast heating on a copper plate. It does not necessarily allow any conclusions on a compound`s

capability as a primary explosive. For the copper shell initiation tests, 200 mg of sieved PETN (grain size 100–500 µm) were filled into a shell (diameter of 7 mm, length of 88 mm) and pressed with a weight of 8 kg. On top 50 mg of the primary explosive were pressed with the same pressure force. The shell was placed in a retaining ring on a copper plate with a thickness of 1 mm and ignited with a type A electrical igniter (Figure S18).



Figure S18. left: schematic diagram of the initiation test; right: copper shell and plate test setup.

A positive DDT from the primary explosive toward the secondary PETN is indicated by a hole in the copper plate. Figure S19 illustrates the remnants of the copper plate and shell from the positive initiation tests with the most promising compounds **2** and **8**.

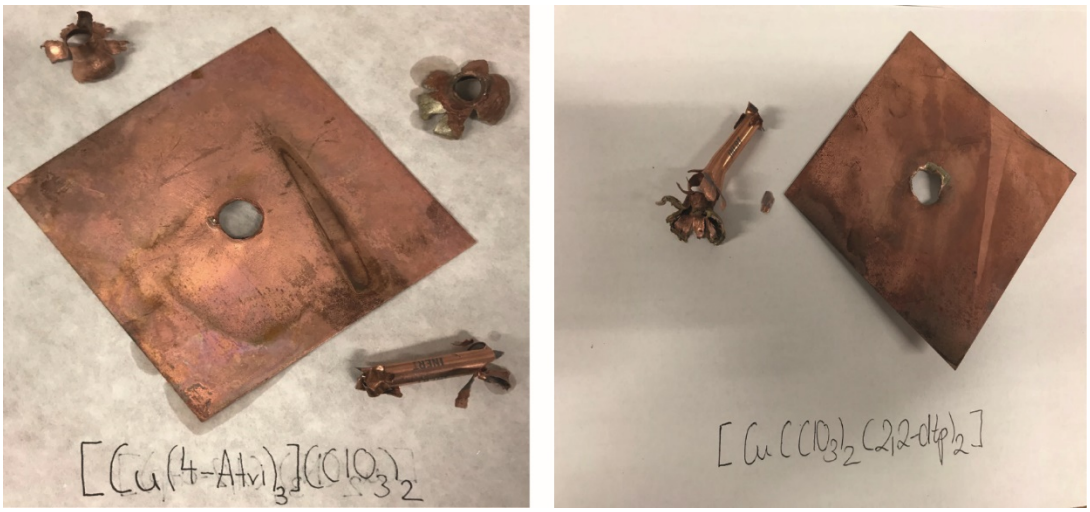


Figure S19. Positive initiation test of compound **2** (left) and **8** (right).

The only other tested compound **3** showed no positive DDT from the primary explosive toward PETN.

19.10.8 Toxicity

The toxicity measurements using the commercially available bioassay system LUMIStox test (luminescent marine bacterium *Vibrio fischeri* NRRL-B-11177) in aqueous media is a valuable indicating device when it comes to groundwater contamination. The half maximal effective concentration EC_{50} of these compounds was determined after an incubation time of 30 min (toxicity level after 30 min incubation: very toxic < 0.10 g/L; toxic 0.10–1.00 g/L; non-toxic > 1.00 g/L).[S12] With a EC_{50} (30 min) value of 0.19 g/L for compound **3** it has to be considered as toxic, which is not surprising, due to the known toxicity of copper(II) compounds toward microorganisms.[S13] Compared to the corresponding copper(II) perchlorate complex with a EC_{50} value of 0.13 g/L – recently published by our group[S14] – the lower toxicity toward aquatic life of chlorate compounds is proven.

19.10.9 X-ray Diffraction

For all crystalline compounds, an Oxford Xcalibur3 diffractometer with a CCD area detector or Bruker D8 Venture TXS diffractometer equipped with a multilayer monochromator, a Photon 2 detector and a rotating-anode generator were employed for data collection using Mo-*K*α radiation (λ = 0.7107 Å). The data collection and reduction were carried out using the Crysalispro software[S15]. The structures were solved by direct methods (Sir-92[S16], Sir-97[S17] or SHELXS-97[S18]) and refined by full-matrix least-squares on *F*2 (SHELXS[S18]) and finally checked using the platon software[S19] integrated in the WinGX software suite. The non-hydrogen atoms were refined anisotropically and the hydrogen atoms were located and freely refined. The absorptions were corrected by a Scale3 Abspack multiscan method.[S20] All Diamond2 plots are shown with thermal ellipsoids at the 50% probability level and hydrogen atoms are shown as small spheres of arbitrary radius.

Table S4. Crystallographic data of **1**–**5.**

	1	**2**	**3**	**4**	**5**
Formula	$C_8H_{16}Cl_2CuN_{16}O_6$	$C_{12}H_{24}Cl_4Cu_2N_{24}O_{12}$	$C_8H_{16}Cl_2CuN_{16}O_6$	$C_8H_{20}Cl_2CuN_{20}O_6$	$C_4H_{14}Cl_2CuN_{10}O_8$
FW [g mol^{-1}]	566.77	965.37	566.77	626.83	464.67
Crystal system	Triclinic	Monoclinic	Monoclinic	Monoclinic	Triclinic
Space Group	*P*−1	*C*2/*m*	$P2_1/n$	$P2_1/n$	*P*−1
Color / Habit	Blue block	Blue rod	Blue block	Blue block	Colorless block
Size [mm]	0.03 x 0.05 x 0.07	0.10 x 0.10 x 0.15	0.16 x 0.18 x 0.21	0.09 x 0.10 x 0.19	0.03 x 0.03 x 0.04
a [Å]	7.2932(2)	13.5622(16)	7.6403(3)	13.1028(10)	6.5617(3)
b [Å]	10.9456(3)	15.5713(18)	10.0072(4)	10.7288(8)	7.5260(4)
c [Å]	12.4170(3)	7.7338(15)	13.6230(5)	16.2265(14)	9.0097(4)
α [°]	93.041(1)	90	90	90	111.762(2)
β [°]	96.845(1)	91.559(12)	90.400(5)	95.036(7)	98.711(2)
γ [°]	91.156(1)	90	90	90	104.197(2)
V [Å^3]	982.43(4)	1632.6(4)	1041.56(7)	2272.3(3)	385.81(3)
Z	2	4	2	4	1
$\rho_{calc.}$ [g cm^{-3}]	1.916	1.964	1.807	1.832	2.000
μ [mm^{-1}]	1.455	1.725	1.372	1.272	1.826
F(000)	574	972	574	1276	235
$\lambda_{MoK\alpha}$ [Å]	0.71073	0.71073	0.71073	0.71073	0.71073
T [K]	100	143	173	173	100
θ Min–Max [°]	2.4, 26.0	4.2, 27.0	4.3, 26.0	4.2, 26.0	3.0, 26.0
Dataset	−8:8; −13:13; −15:15	−17:17; −19:19; −9:9	−9:8; −12:12; −16:16	−16:16; −7:13; −18:20	−8:7; −9:8; 0:11
Reflections collected	17068	6915	7926	17379	1500
Independent refl.	3838	1844	2038	4436	1500
Rint	0.033	0.109	0.021	0.071	0.0402
Observed reflections	3421	1166	1852	3224	1392
Parameters	333	158	153	370	144
R_1 (obs)[a]	0.0243	0.0716	0.0244	0.0853	0.0295
wR_2 (all data)[b]	0.0940	0.1861	0.0628	0.2549	0.0635
GooF[c]	1.26	1.03	1.10	1.13	1.12
Resd. Dens. [e Å^{-3}]	−0.59, 0.45	−0.57, 2.21	−0.34, 0.26	−0.81, 2.22	−0.33, 0.41
Absorption correction	multi-scan	multi-scan	multi-scan	multi-scan	multi-scan
CCDC	1574490	1574486	1574482	1574487	1574489

a) $R_1 = \Sigma||F_0|-|F_c||/\Sigma|F_0|$; b) $wR_2 = [\Sigma[w(F_0^2-F_c^2)^2]/\Sigma[w(F_0)^2]]^{1/2}$; $w = [\sigma c^2(F_0^2)+(xP)^2+yP]^{-1}$ and $P=(F_0^2+2F_c^2)/3$; c) GooF = $\{\Sigma[w(F_o^2-F_c^2)^2]/(n-p)\}^{1/2}$ (n = number of reflections; p = total number of parameters).

Table S5. Crystallographic data of **6**–**10.**

	6	**7**	**8**	**9**	**10**
Formula	$C_{15}H_{24}Cl_2CuN_{24}O_6$	$C_{10}H_{16}Cl_2CuN_{16}O_6$	$C_{10}H_{16}Cl_2CuN_{16}O_6$	$C_{10}H_{20}Cl_2CuN_{16}O_8$	$C_{12}H_{20}Cl_2CuN_{12}O_6$
FW [g mol^{-1}]	770.97	590.79	590.79	626.82	618.85
Crystal system	Trigonal	Triclinic	Monoclinic	Monoclinic	Monoclinic
Space Group	*P*−3*c*1	*P*−1	*C*2/*c*	*C*2/*c*	$P2_1/n$
Color / Habit	Blue block	Blue block	Blue plate	Blue block	Blue block
Size [mm]	0.10 x 0.22 x 0.29	0.04 x 0.09 x 0.13	0.08 x 0.16 x 0.34	0.17 x 0.23 x 0.36	0.08 x 0.17 x 0.31
a [Å]	10.9642(2)	6.7837(8)	14.6638(7)	15.0672(5)	10.7286(6)
b [Å]	10.9642(2)	8.182(1)	8.9883(5)	9.0113(3)	6.8178(4)
c [Å]	14.3772(4)	10.1959(12)	16.3538(8)	17.5426(6)	15.5263(12)
α [°]	90	108.068(11)	90	90	90
β [°]	90	101.188(10)	90.324(5)	97.696(3)	100.469(6)
γ [°]	120	90.137(10)	90	90	90
V [Å^3]	1496.78(8)	526.60(12)	2155.44(19)	2360.39(14)	1116.77(13)
Z	2	1	4	4	2
$\rho_{calc.}$ [g cm^{-3}]	1.711	1.863	1.821	1.764	1.840
μ [mm^{-1}]	0.987	1.361	1.331	1.226	1.289
F(000)	786	299	1196	1276	630
$\lambda_{MoK\alpha}$ [Å]	0.71073	0.71073	0.71073	0.71073	0.71073
T [K]	123	173	173	173	143
θ Min–Max [°]	4.3, 26.0	4.2, 25.2	4.5, 26.0	4.3, 26.0	4.1, 26.0
Dataset	−13:13; −13:9; −17:17	−7:7; −9:6; −10:10	−18:18; −11:11; −20:20	−18:18; −11:11; −21:21	−13:13; −8:8; −19:19
Reflections collected	10648	2222	8158	9395	8061
Independent refl.	989	1471	2109	2306	2186
Rint	0.032	0.039	0.058	0.034	0.046
Observed reflections	825	987	1607	2094	1756
Parameters	98	160	160	198	169
R_1 (obs)[a]	0.0289	0.0439	0.0437	0.0310	0.0433
wR_2 (all data)[b]	0.0818	0.0658	0.1043	0.0834	0.1155
GooF[c]	1.06	0.89	1.06	1.08	1.09
Resd. Dens. [e Å^{-3}]	−0.24, 0.34	−0.49, 0.38	−0.34, 0.75	−0.45, 0.61	−0.44, 0.90
Absorption correction	multi-scan	multi-scan	multi-scan	multi-scan	multi-scan
CCDC	1574485	1574481	1574484	1574483	1574488

a) $R_1 = \Sigma||F_0|-|F_c||/\Sigma|F_0|$; b) $wR_2 = [\Sigma[w(F_0^2-F_c^2)^2]/\Sigma[w(F_0)^2]]^{1/2}$; $w = [\sigma c^2(F_0^2)+(xP)^2+yP]^{-1}$ and $P=(F_0^2+2F_c^2)/3$; c) GooF = $\{\Sigma[w(F_o^2-F_c^2)^2]/(n-p)\}^{1/2}$ (n = number of reflections; p = total number of parameters).

19.10.10 IR Spectroscopy

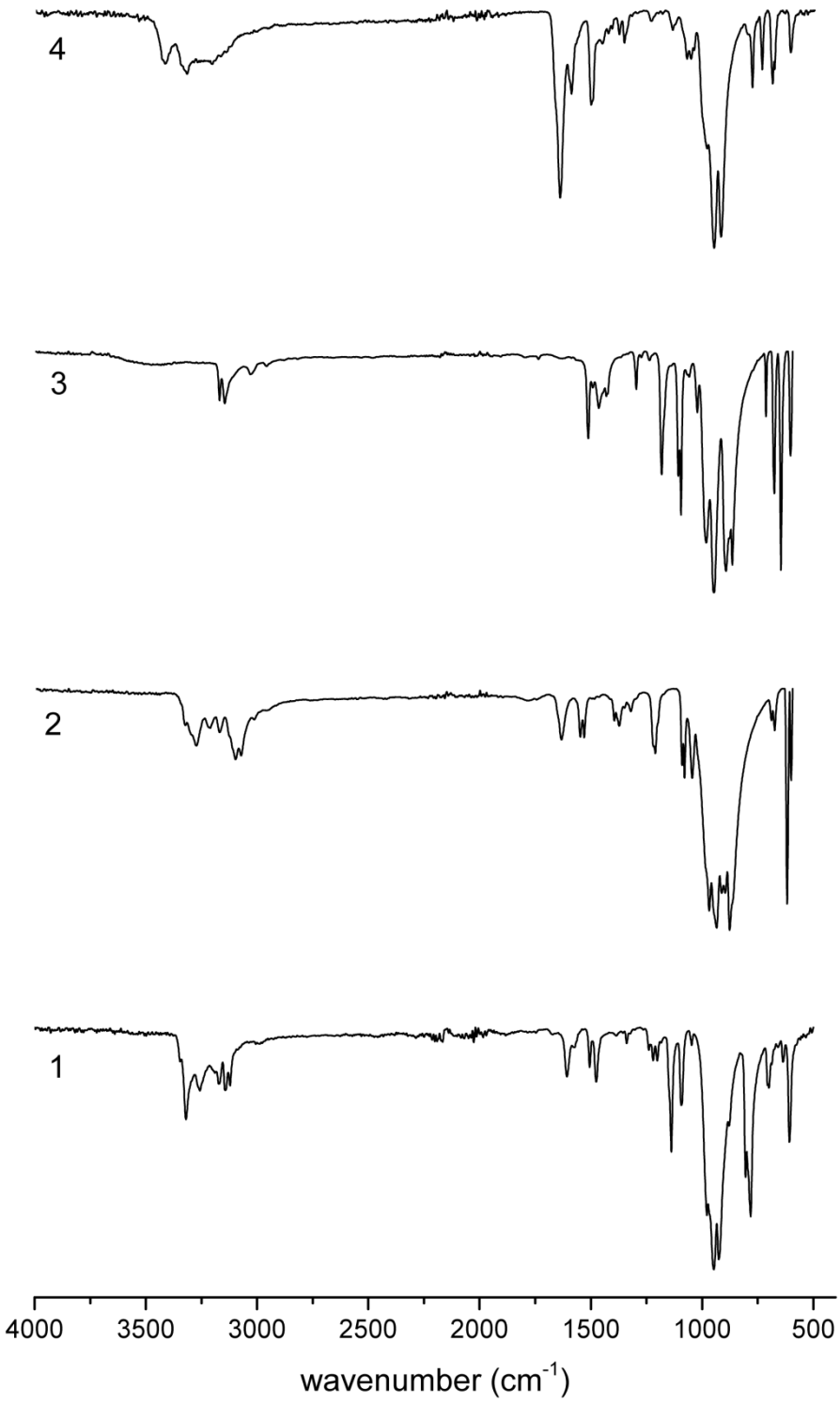


Figure S20. Infrared spectra of compounds **1**–**4**.

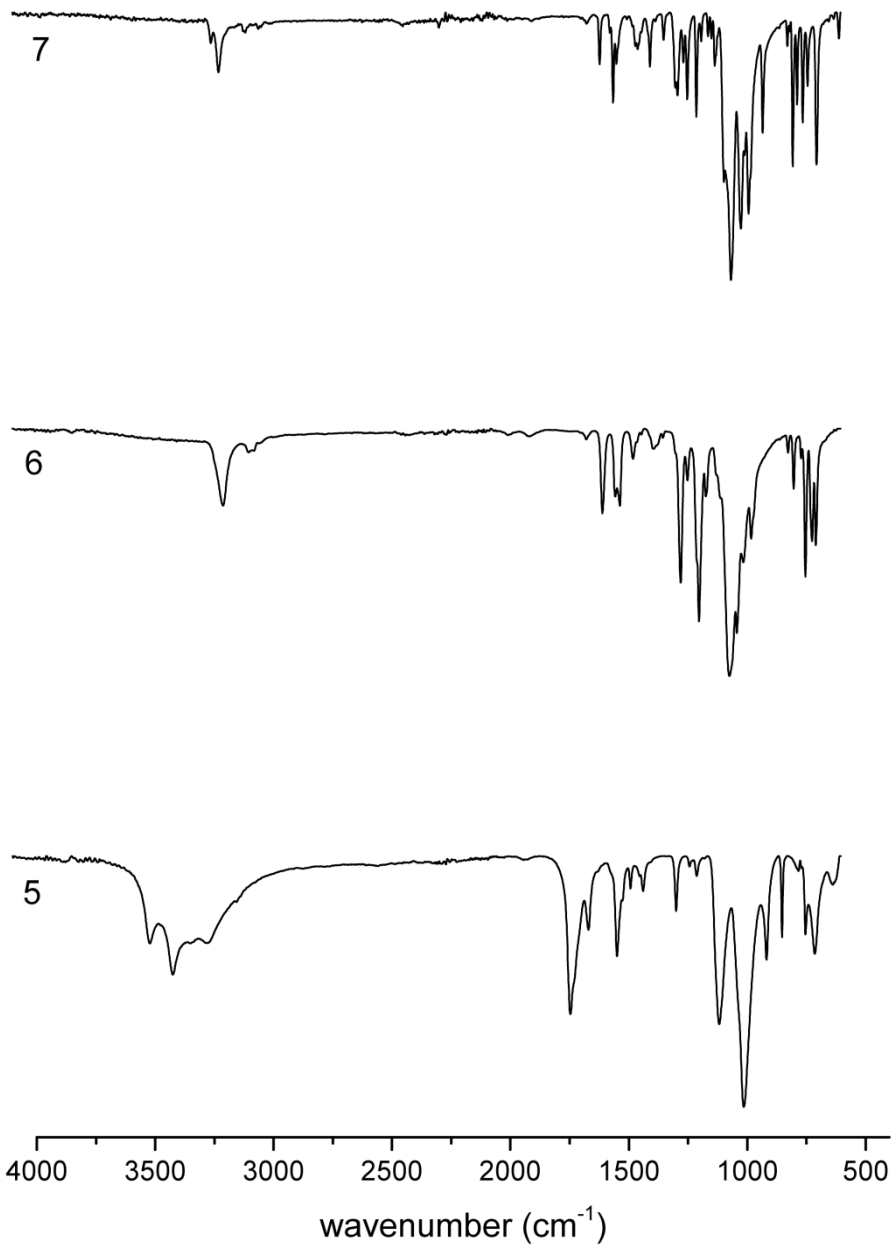


Figure S21. Infrared spectra of compounds **5**–**7**.

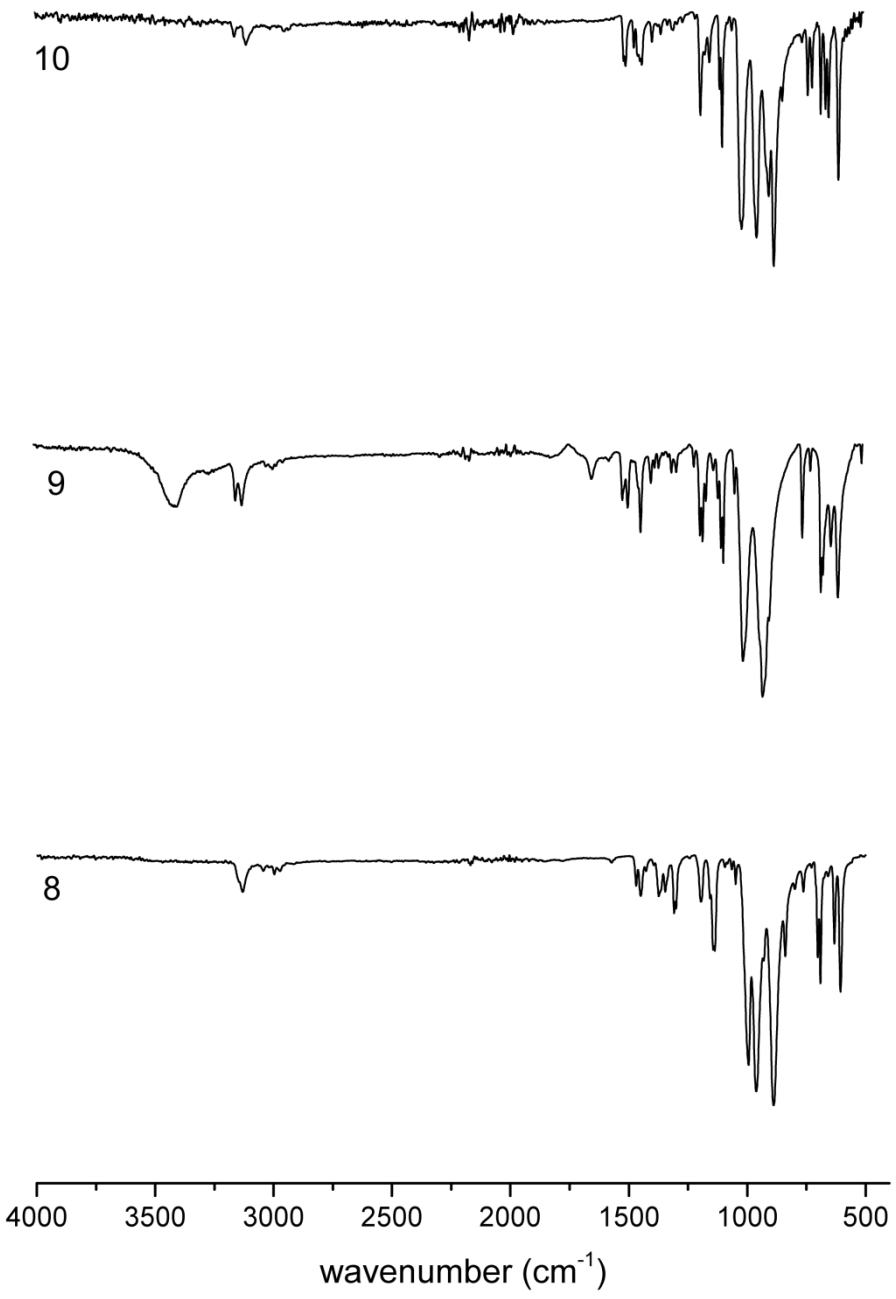


Figure S22. Infrared spectra of compounds **8–10**.

19.10.11 References

[S1] NATO standardization agreement (STANAG) on explosives, impact sensitivity tests, no. 4489, 1st ed., Sept. 17, **1999**.

[S2] WIWEB-Standardarbeitsanweisung 4-5.1.02, Ermittlung der Explosionsgefährlichkeit, hier der Schlagempfindlichkeit mit dem Fallhammer, Nov. 8, **2002**.

[S3] http://www.bam.de Accessed December 2017.

[S4] NATO standardization agreement (STANAG) on explosive, friction sensitivity tests, no. 4487, 1st ed., Aug. 22, **2002**.

[S5] WIWEB-Standardarbeitsanweisung 4-5.1.03, Ermittlung der Explosionsgefährlichkeit oder der Reibeempfindlichkeit mit dem Reibeapparat, Nov. 8, **2002**.

[S6] Impact: insensitive > 40 J, less sensitive ≥ 35 J, sensitive ≥ 4 J, very sensitive ≤ 3 J; Friction: insensitive > 360 N, less sensitive = 360 N, sensitive < 360 N and > 80 N, very sensitive ≤ 80 N, extremely sensitive ≤ 10 N. According to the UN Recommendations on the Transport of Dangerous Goods, (+) indicates not safe for transport.

[S7] http://www.ozm.cz Accessed December 2017.

[S8] R. Scharf, PhD thesis, Ludwig-Maximilians Universität München, **2016**.

[S9] Crystallographic data for the structures have been deposited with the Cambridge Crystallographic Data Centre. Copies of the data can be obtained free of charge on application to The Director, CCDC, 12 Union Road, Cambridge CB2 1EZ, UK (Fax: int.code_(1223)336-033; e-mail for inquiry: fileserv@ccdc.cam.ac.uk; e-mail for deposition: (deposit@ccdc.cam.ac.uk).

[S10] a.) L. Wiehl, *Acta Cryst. B.*, **1993**, *49*, 289–303; b.) D. Mueller, C. Knoll, B. Stoeger, W. Artner, M. Reissner, P. Weinberger, *Eur. J. Inorg. Chem.* **2013**, *2013*, 984–991; c.) P. J. van Koningsbruggen, Y. Garcia, O. Kahn, L. Fournès, H. Kooijman, A. L. Spek, J. G. Haasnoot, J. Moscovici, K. Provost, A. Michalowicz, F. Renz, P. Gütlich, *Inorg. Chem.* **2000**, *39*, 1891–1900.

[S11] E. D. Aluker, A. G. Krechetov, A. Y. Mitrofanov, D. R. Nurmukhametov, M. M. Kuklja, J.Phys. Chem. C, **2011**, *115*, 6893–6901.

[S12] C. J. Cao, M. S. Johnson, M. M. Hurley, T. M. Klapötke, *JANNAF J. Propuls. Energet.*, **2012**, *5*, 41–51.

[S13] V. Ochoa-Herrera, G. Léon, Q. Banihani, J. A. Field, R. Sierra-Alvarez, *Sci. Total Environ.*, **2011**, *380*, 412–413.

[S14] N. Szimhardt, M. H. H. Wurzenberger, A. Behringer, L. Daumann, J. Stierstorfer, Article ASAP.

[S15] *CrysAlisPro*, Oxford Diffraction Ltd., version 171.33.41, **2009**.

[S16] A. Altomare, G. Cascarano, C. Giacovazzo, A. Guagliardi, *J. Appl. Crystallogr.* **1992**, *26*, 343–350.

[S17] a) A. Altomare, G. Cascarano, C. Giacovazzo, A. Guagliardi, A. G. G. Moliterni, M. C. Burla, G. Polidori, M. Camalli, R. Spagna, *SIR97*, **1997**; b) A. Altomare, M. C. Burla, M. Camalli, G. L. Cascarano, C. Giacovazzo, A. Guagliardi, A. G. G. Moliterni, G. Polidori, R. Spagna, *J. Appl. Crystallogr.* **1999**, *32*, 115–119.

[S18] a) G. M. Sheldrick, *SHELXL-97*, *Program for the Refinement of Crystal Structures*, University of Göttingen, Germany, 1997; b) Sheldrick, G. M. *Acta Crystallogr. Sect. A* **2008**, *64*, 112–122.

[S19] A. L. Spek, *PLATON*, *A Multipurpose Crystallographic Tool*, Utrecht University, The Netherlands, **1999**.

[S20] Empirical absorption correction using spherical harmonics, implemented in SCALE3 ABSPACK scaling algorithm (CrysAlisPro Oxford Diffraction Ltd., Version 171.33.41, **2009**).

19.11 Supplementary Information: Nitrogen-Rich Copper(II) Bromate Complexes: an Exotic Class of Primary Explosives

19.11.1 X-ray Diffraction

For all crystalline compounds, an Oxford Xcalibur3 diffractometer with a CCD area detector or Bruker D8 Venture TXS diffractometer equipped with a multilayer monochromator, a Photon 2 detector and a rotating-anode generator were employed for data collection using Mo-*K*α radiation (λ = 0.7107 Å). The data collection and reduction were carried out using the CRYSALISPRO software.[S1] The structures were solved by direct methods (SIR-92[S2], SIR-97[S3,S4] or SHELXS-97[S5,S6]) and refined by full-matrix least-squares on *F*2 (SHELXL[S5]) and finally checked using the PLATON software[S7] integrated in the WinGX software suite. The non-hydrogen atoms were refined anisotropically and the hydrogen atoms were located and freely refined. The absorptions were corrected by a SCALE3 ABSPACK multiscan method.[S8] All DIAMOND2 plots are shown with thermal ellipsoids at the 50% probability level and hydrogen atoms are shown as small spheres of arbitrary radius.

Table S1. Crystallographic data of **1**–**4**.

	1	**2**	**3**	**4**
Formula	$C_{12}H_{26}Br_4Cu_2N_{24}O_{13}$	$C_4H_8Br_2CuN_8O_6$	$C_8H_{22}Br_2CuN_{20}O_7$	$C_{10}H_{16}Br_2CuN_{16}O_6$
FW [g mol^{-1}]	1161.21	487.53	733.81	679.75
Crystal system	Monoclinic	Monoclinic	Monoclinic	Monoclinic
Space Group	*C*2/*c*	$P2_1/c$	$P2_1/c$	$P2_1/c$
Color / Habit	Blue block	Blue plate	Green block	Blue block
Size [mm]	0.06 x 0.12 x 0.17	0.07 x 0.39 x 0.45	0.04 x 0.10 x 0.25	0.10 x 0.10 x 0.20
a [Å]	13.7831(16)	10.5446(5)	7.7919(6)	16.5302(7)
b [Å]	15.7896(17)	6.8317(3)	16.8822(11)	6.5743(3)
c [Å]	15.4202(13)	9.2634(5)	18.8716(14)	9.7369(5)
α [°]	90	90	90	90
β [°]	91.373(10)	103.055(5)	98.031(7)	95.125(4)
γ [°]	90	90	90	90
V [Å^3]	3354.9(6)	650.06(6)	2458.1(3)	1053.92(9)
Z	4	2	4	2
$\rho_{calc.}$ [g cm^{-3}]	2.299	2.491	1.983	2.142
μ [mm^{-1}]	6.129	7.871	4.215	4.899
F(000)	2272	470	1460	670
$\lambda_{MoK\alpha}$ [Å]	0.71073	0.71073	0.71073	0.71073
T [K]	143	143	143	130
θ Min–Max [°]	4.1, 24.0	4.5, 26.0	4.2, 26.0	4.2, 26.0
Dataset	−15:15; −18:17; −11:17	−11:12; −8:7; −11:11	−9: 8; −20:18; −22:23	−20:20; −8:8; −12:11
Reflections collected	10238	4552	20093	7371
Independent refl.	2594	1272	4813	2040
R_{int}	0.090	0.034	0.101	0.043
Observed reflections	1773	1204	3188	1906
Parameters	232	98	341	142
R_1 (obs)[a]	0.0532	0.0269	0.0492	0.1039
wR_2 (all data)[b]	0.1122	0.0733	0.1142	0.2634
GooF[c]	1.04	1.11	1.03	1.24
Resd. Dens. [e Å^{-3}]	−0.75, 0.79	−0.67, 0.75	−0.78, 1.06	−2.78, 3.72
Absorption correction	multi-scan	multi-scan	multi-scan	multi-scan
CCDC	1836542	1836543	1836539	1836540

a) $R_1 = \Sigma||F_0|- |F_c||/ \Sigma|F_0|$; b) $wR_2 = [\Sigma[w(F_0^2-F_c^2)^2]/\Sigma[w(F_0)^2]]^{1/2}$; $w = [\sigma c^2(F_0^2)+(xP)^2+yP]^{-1}$ and $P=(F_0^2+2F_c^2)/3$; c) GooF = $\{\Sigma[w(F_o^2-F_c^2)^2]/(n-p)\}^{1/2}$ (n = number of reflections; p = total number of parameters).

Table S2. Crystallographic data of **5**–**8**.

	5	**6**	**7**	**8**
Formula	$C_{10}H_{24}Br_2CuN_{16}O_{10}$	$C_{10}H_{20}Br_2CuN_{16}O_8$	$C_4H_{20}Br_2CuN_4O_8$	$H_8Br_2CuO_{10}$
FW [g mol^{-1}]	751.81	715.78	475.60	391.42
Crystal system	Triclinic	Monoclinic	Monoclinic	Orthorhombic
Space Group	*P*−1	*C*2/*c*	$P2_1/c$	*Pbca*
Color / Habit	Blue block	Blue block	Purple block	Blue block
Size [mm]	0.16 x 0.34 x 0.36	0.10 x 0.15 x 0.25	0.08 x 0.15 x 0.40	0.10 x 0.23 x 0.36
a [Å]	7.8692(3)	15.1113(5)	7.2970(3)	9.6361(5)
b [Å]	8.0515(2)	8.9694(3)	15.3327(5)	7.2172(4)
c [Å]	10.2521(3)	17.7869(7)	19.2554(7)	12.5678(6)
α [°]	76.605(2)	90	90	90
β [°]	80.773(3)	97.542(3)	92.154(3)	90
γ [°]	87.471(2)	90	90	90
V [Å^3]	623.70(3)	2389.97(15)	2152.82(14)	874.04(8)
Z	1	4	6	4
$\rho_{calc.}$ [g cm^{-3}]	2.002	1.989	2.201	2.975
μ [mm^{-1}]	4.160	4.332	7.128	11.675
F(000)	375	1420	1410	748
$\lambda_{MoK\alpha}$ [Å]	0.71073	0.71073	0.71073	0.71073
T [K]	143	143	143	143
θ Min–Max [°]	4.1, 26.0	4.2, 26.0	4.1, 26.0	4.2, 26.0
Dataset	−8:9; −9:9; −12:12	−18:18; −10:11; −21:21	−9:8; −18:18; −23:22	−10:11; −8:8; −13:15
Reflections collected	4757	9165	16689	5975
Independent refl.	2432	2336	4198	856
Rint	0.015	0.033	0.054	0.039
Observed reflections	2288	2046	3401	731
Parameters	194	178	323	62
R_1 (obs)[a]	0.0188	0.0279	0.0315	0.0218
wR_2 (all data)[b]	0.0485	0.0648	0.0688	0.0584
GooF[c]	1.07	1.09	1.06	1.13
Resd. Dens. [e Å^{-3}]	−0.41, 0.57	−0.38, 0.70	−0.64, 0.76	−0.59, 0.60
Absorption correction	multi-scan	multi-scan	multi-scan	multi-scan
CCDC	1836537	1836541	1836544	1836538

a) $R_1 = \Sigma||F_0|-|F_c||/\Sigma|F_0|$; b) $wR_2 = [\Sigma[w(F_0^2-F_c^2)^2]/\Sigma[w(F_0)^2]]^{1/2}$; $w = [\sigma c^2(F_0^2)+(xP)^2+yP]^{-1}$ and $P=(F_0^2+2F_c^2)/3$; c) GooF = $\{\Sigma[w(F_o^2-F_c^2)^2]/(n-p)\}^{1/2}$ (n = number of reflections; p = total number of parameters).

19.11.2 IR Spectroscopy of 1–6

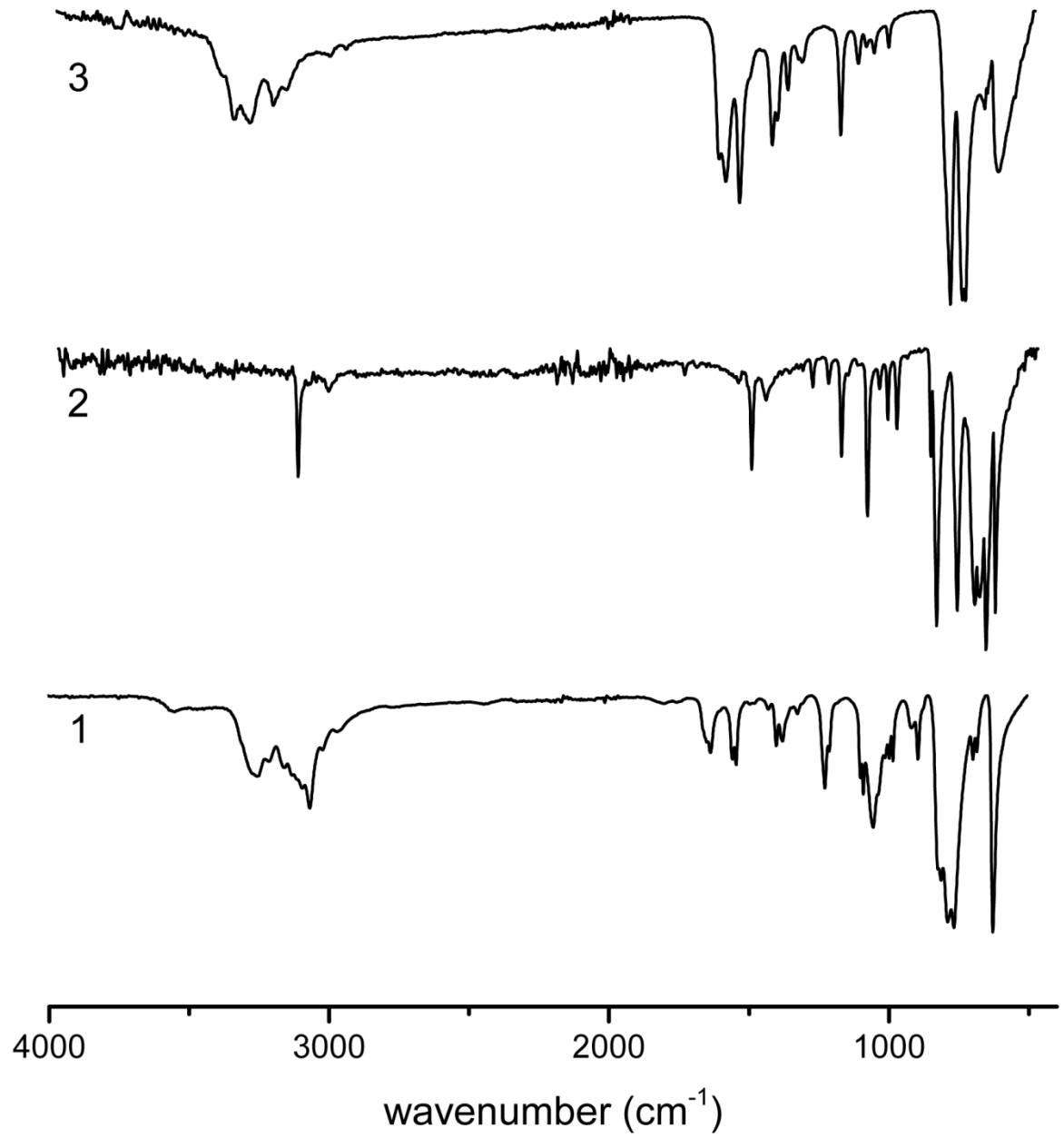


Figure S1. Infrared spectra of coordination compounds **1**–**3**.

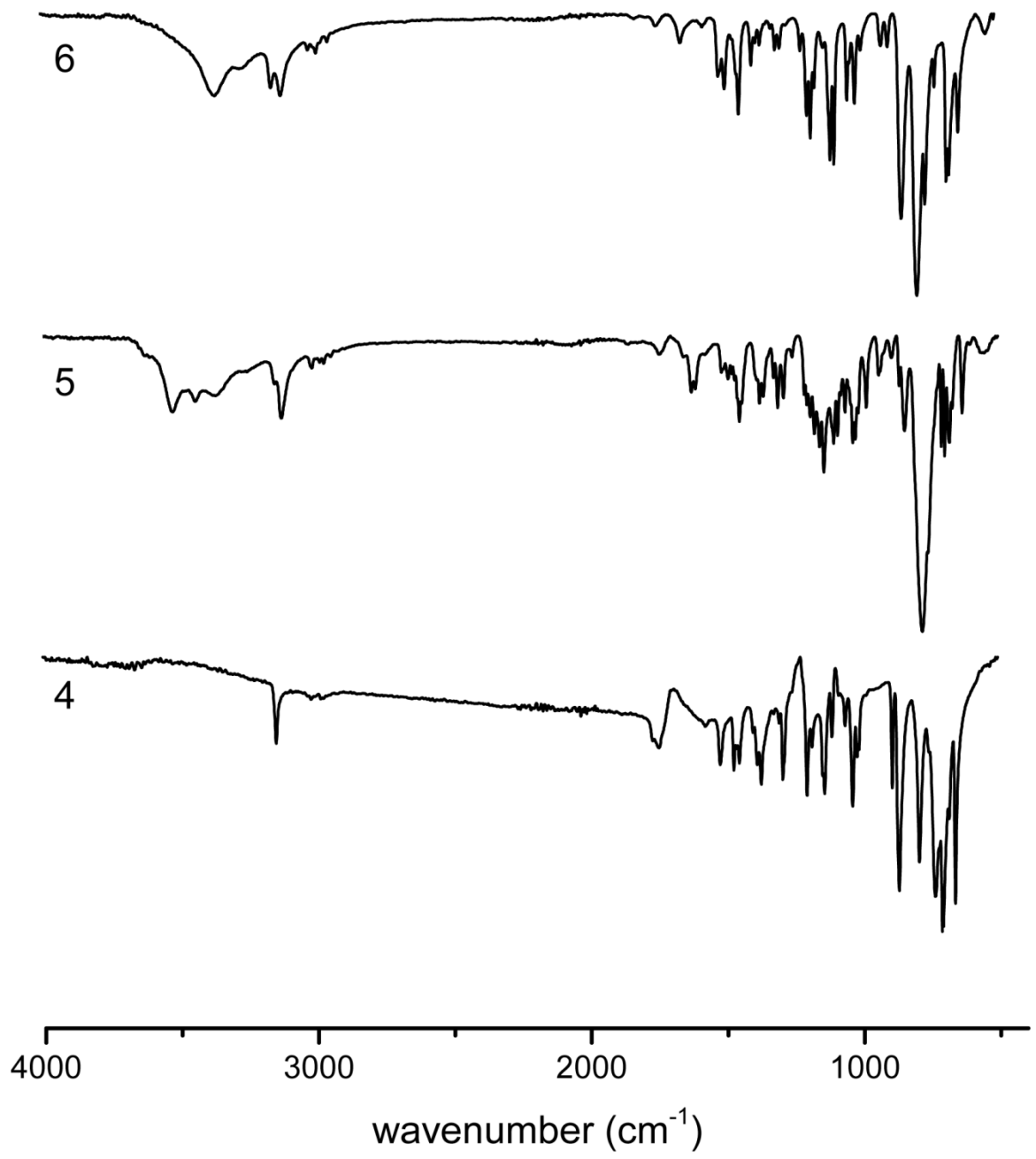


Figure S2. Infrared spectra of complexes **4**–**6.**

19.11.3 References

[S1] *CrysAlisPro*, Oxford Diffraction Ltd., version 171.33.41, **2009**.

[S2] Altomare, A.; Cascarano, G.; Giacovazzo, C.; Guagliardi, A. Completion and refinement of crystal structures with SIR92. *J. Appl. Crystallogr.* **1993**, *26*, 343–350.

[S3] Altomare, A.; Cascarano, G.; Giacovazzo, C.; Guagliardi, A.; Moliterni, A. G. G.; Burla, M. C.; Polidori, G.; Camalli, M.; Spagna, R. *SIR97*, **1997**.

[S4] Altomare, A.; Burla, M. C.; Camalli, M.; Cascarano, G. L.; Giacovazzo, C.; Guagliardi, A.; Moliterni, A. G. G.; Polidori, G.; Spagna, R. SIR97: a new tool for crystal structure determination and refinement. *J. Appl. Crystallogr.* **1999**, *32*, 115–119.

[S5] Sheldrick, G. M. *SHELXL-97*, *Program for the Refinement of Crystal Structures*, University of Göttingen, Germany, **1997**.

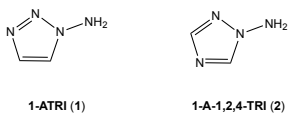
[S6] Sheldrick, G. M. A short history of SHELX. *Acta Crystallogr. Sect. A* **2008**, *64*, 112–122.

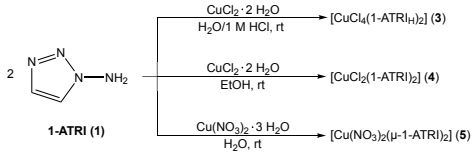
[S7] Spek, A. L. *PLATON*, *A Multipurpose Crystallographic Tool*, Utrecht University, The Netherlands, **1999**.

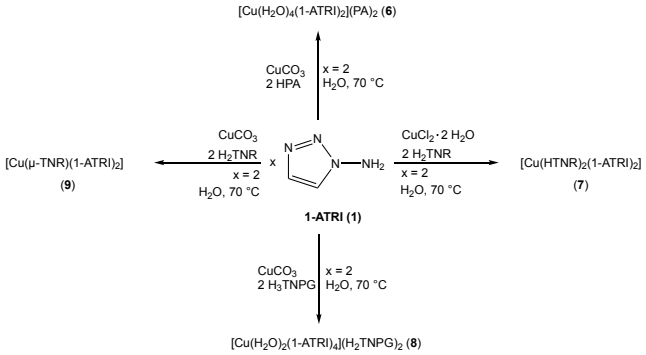
[S8] Empirical absorption correction using spherical harmonics, implemented in SCALE3 ABSPACK scaling algorithm (CrysAlisPro Oxford Diffraction Ltd., Version 171.33.41, **2009**).

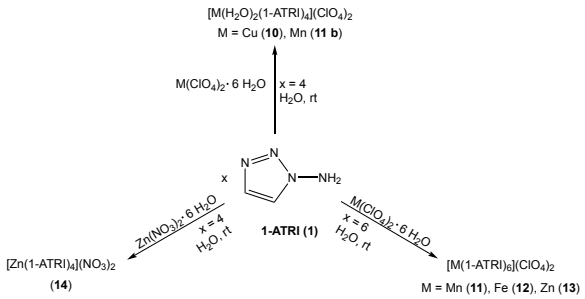
19.12 Supplementary Information: 1-Amino-triazole Transition Metal Complexes as Laser Ignitable and Lead-free Primary Explosives

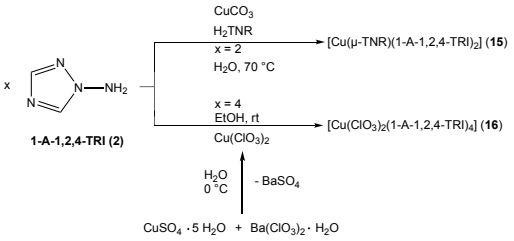
19.12.1 Compounds Overview











19.12.2 IR Spectroscopy of 1–16

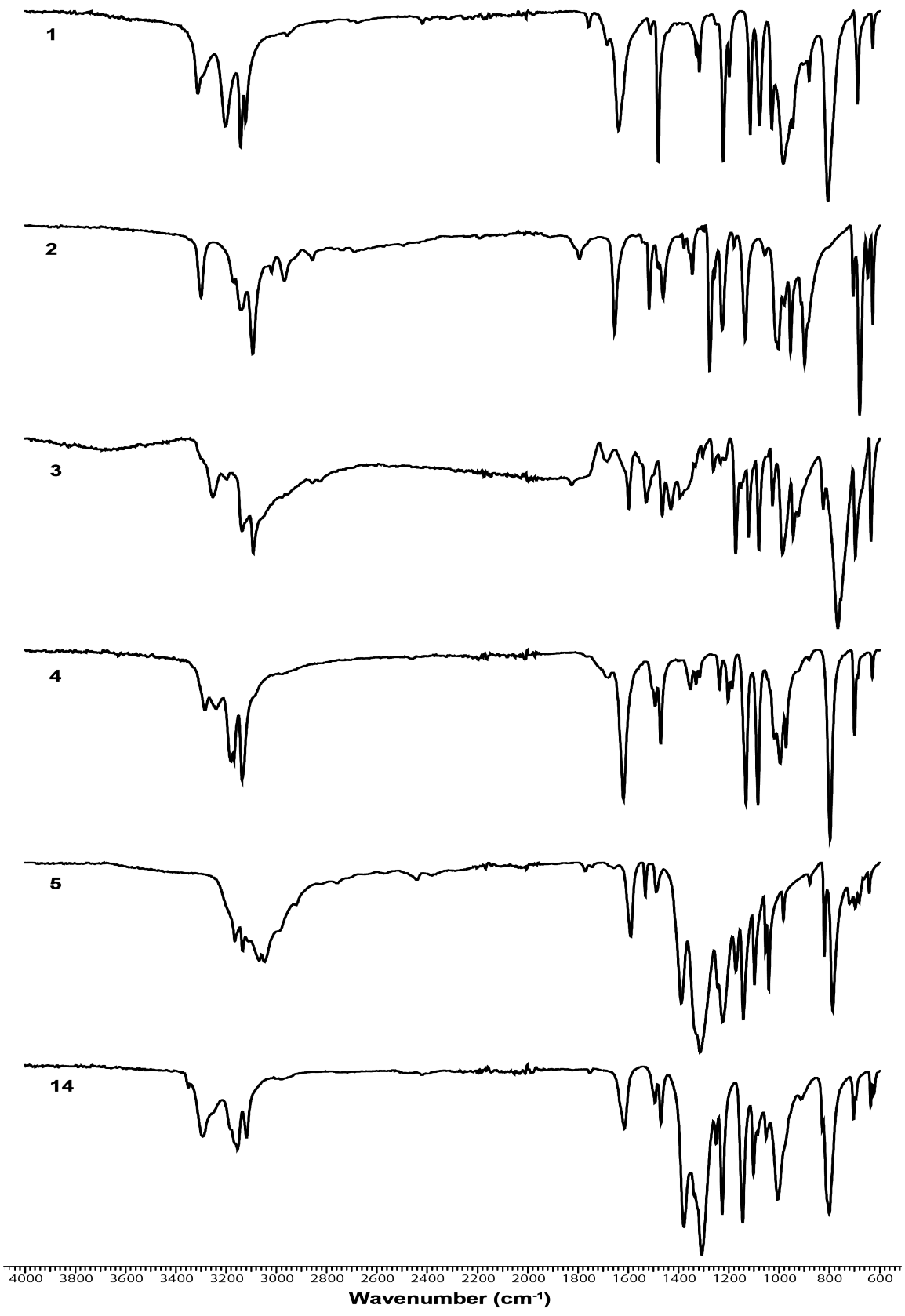


Figure S1. Infrared spectra of the compounds **1**–**5** and **14**.

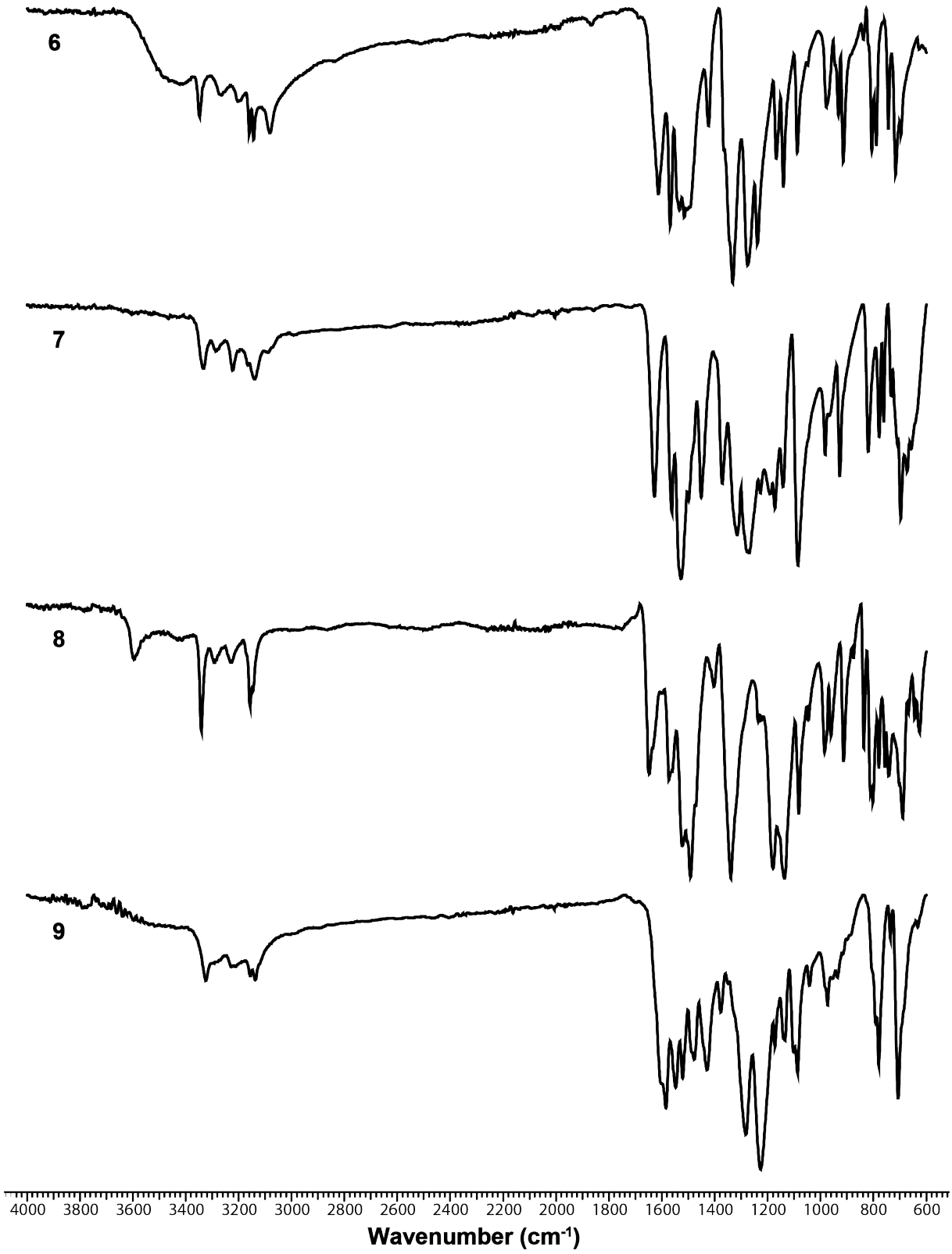


Figure S2. IR spectra of **6**–**9**.

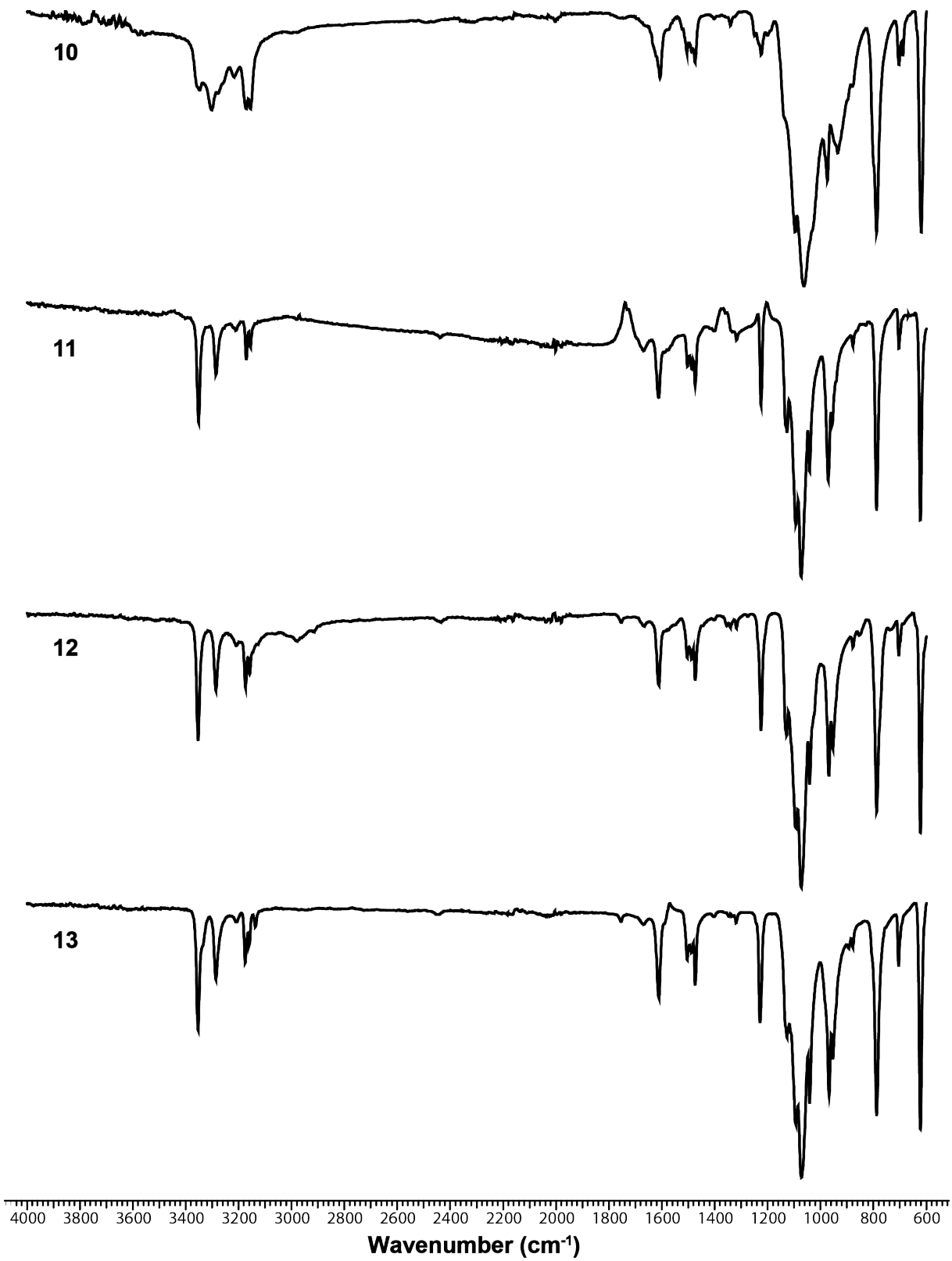


Figure S3. Infrared spectra of **10**–**13**.

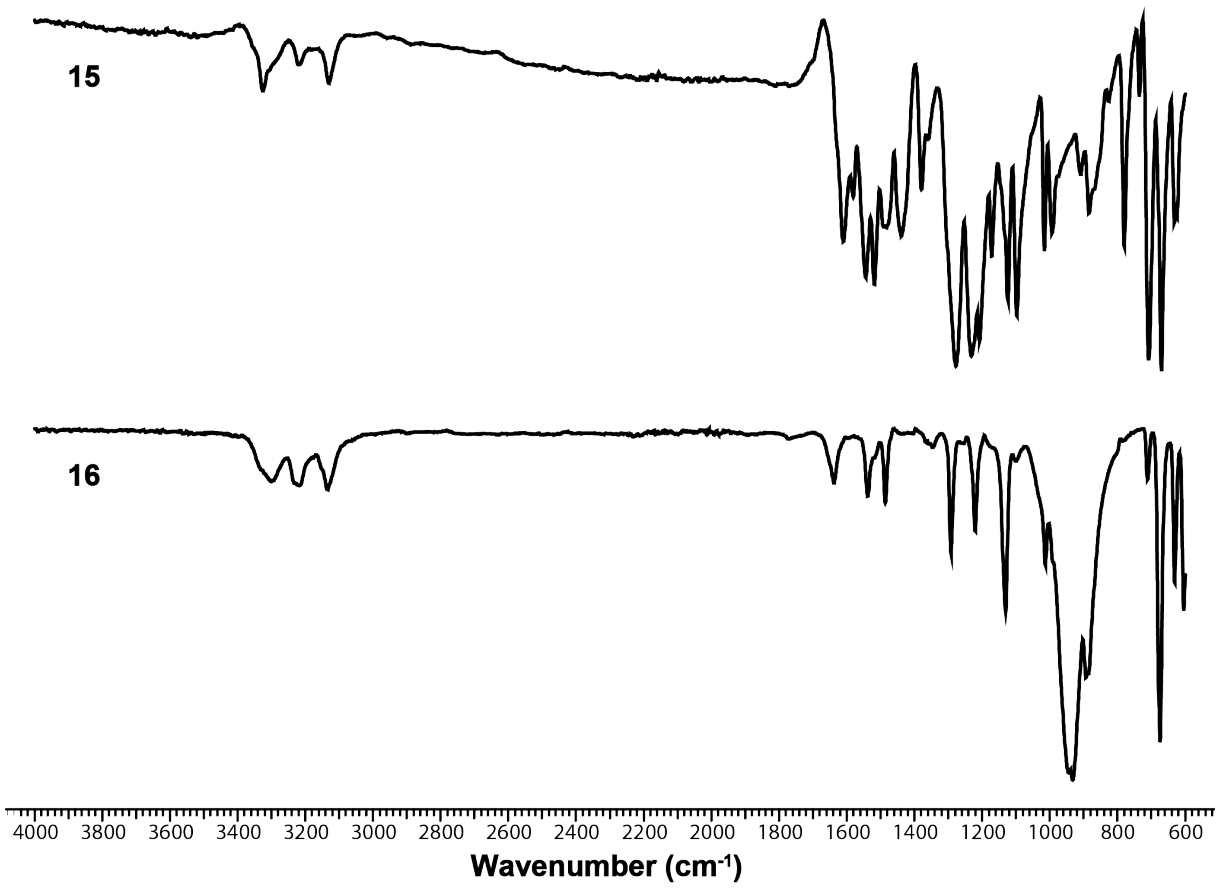


Figure S4. Infrared spectra of the complexes **15** and **16**.

19.12.3 X-ray Diffraction

For all crystalline compounds, an Oxford Xcalibur3 diffractometer with a CCD area detector or Bruker D8 Venture TXS diffractometer equipped with a multilayer monochromator, a Photon 2 detector and a rotating-anode generator were employed for data collection using Mo-*K*α radiation (λ = 0.7107 Å). On the Oxford device, data collection and reduction were carried out using the Crysalispro software.[S1] On the Bruker diffractometer, the data were collected with the Bruker Instrument Service v3.0.21, the data reduction was performed using the SAINT V8.18C software (Bruker AXS Inc., 2011). The structures were solved by direct methods (Sir-92[S2], Sir-97[S3] or Shelxs-97[S4]) and refined by full-matrix least-squares on *F*2 (ShelxL[S4]) and finally checked using the platon software[S5] integrated in the WinGX[S6] software suite. The non-hydrogen atoms were refined anisotropically and the hydrogen atoms were located and freely refined. The absorptions were corrected by a Scale3 Abspack or Sadabs Bruker Apex3 multiscan method.[S7,8] All Diamond2 plots are shown with thermal ellipsoids at the 50% probability level and hydrogen atoms are shown as small spheres of arbitrary radius.

Table S1. Crystallographic data of **2**, **3**, **5**, and **6**.

	2	**3**	**5**	**6**
Formula	$C_2H_4N_4$	$C_4H_{10}Cl_4CuN_8$	$C_4H_8CuN_{10}O_6$	$C_{16}H_{20}CuN_{14}O_{18}$
FW [g mol^{-1}]	84.09	375.55	355.74	760.00
Crystal system	Monoclinic	Triclinic	Monoclinic	Monoclinic
Space Group	*P*2/*c*	*P*−1	$P2_1/n$	*C*2/*c*
Color / Habit	Colorless block	Green block	Blue stab	Green rod
Size [mm]	0.05 x 0.06 x 0.10	0.10 x 0.16 x 0.61	0.20 x 0.20 x 0.40	0.13 x 0.28 x 0.40
a [Å]	18.8277(15)	6.1923(8)	7.8200(5)	6.9599(5)
b [Å]	3.8795(3)	6.8044(10)	8.3270(3)	27.8692(18)
c [Å]	11.2297(9)	7.9469(9)	9.1550(5)	14.3477(9)
α [°]	90	97.816(10)	90	90
β [°]	106.447(3)	105.242(11)	113.759(7)	96.407(6)
γ [°]	90	104.155(12)	90	90
V [Å^3]	786.68(11)	305.99(8)	545.62(6)	2765.6(3)
Z	8	1	2	4
$\rho_{calc.}$ [g cm^{-3}]	1.420	2.038	2.165	1.825
μ [mm^{-1}]	0.106	2.647	2.061	0.902
F(000)	352	187	358	1548
$\lambda_{MoK\alpha}$ [Å]	0.71073	0.71073	0.71073	0.71069
T [K]	150	173	173	143
θ Min–Max [°]	3.3, 27.1	4.6, 26.0	4.4, 26.5	4.4, 29.0
Dataset	−23:24; −4:4; −14:14	−7:7; −8:5; −9:9	−9:9; −10:10; −9:11	−9:9; −38:36; −19:19
Reflections collected	7944	2210	4124	14010
Independent refl.	1710	1201	1128	3676
*R*int	0.032	0.020	0.027	0.099
Observed reflections	1590	1090	996	3002
Parameters	126	99	113	245
R_1 (obs)[a]	0.0527	0.0266	0.0257	0.0960, ,
wR_2 (all data)[b]	0.1538	0.0660	0.0660	0.2247
GooF[c]	1.09	1.07	1.07	1.15
Resd. Dens. [e Å^{-3}]	−0.27, 0.22	−0.60, 0.29	−0.27, 0.40	−1.03, 2.37
Absorption correction	multi-scan	multi-scan	multi-scan	multi-scan
CCDC	1847945	1847943	1847948	1847946

a) $R_1 = \Sigma||F_0|- |F_c||/ \Sigma|F_0|$; b) $wR_2 = [\Sigma[w(F_0^2-F_c^2)^2]/\Sigma[w(F_0)^2]]^{1/2}$; $w = [\sigma c^2(F_0^2)+(xP)^2+yP]^{-1}$ and $P=(F_0^2+2F_c^2)/3$; c) GooF = $\{\Sigma[w(F_o^2-F_c^2)^2]/(n-p)\}^{1/2}$ (n = number of reflections; p = total number of parameters).

Table S2. Crystallographic data of **7**–**10**.

	7	**8**	**9**	**10**
Formula	$C_{16}H_{12}CuN_{14}O_{16}$	$C_{20}H_{24}CuN_{22}O_{20}$	$C_{10}H_9CuN_{11}O_8$	$C_8H_{20}Cl_2CuN_{16}O_{10}$
FW [g mol^{-1}]	719.94	956.15	474.82	634.84
Crystal system	Monoclinic	Triclinic	Monoclinic	Triclinic
Space Group	$P2_1$	$P\bar{1}$	$P2_1/c$	$P\bar{1}$
Color / Habit	Green block	Dark green block	Green block	Blue plate
Size [mm]	0.15 x 0.25 x 0.30	0.23 x 0.39 x 0.71	0.10 x 0.20 x 0.40	0.14 x 0.18 x 0.25
a [Å]	7.2057(2)	8.4997(6)	7.3258(8)	7.8930(6)
b [Å]	20.6026(6)	9.0556(8)	10.2754(9)	7.9740(5)
c [Å]	8.8536(3)	11.8091(10)	22.442(2)	10.1424(8)
α [°]	90	80.909(7)	90	74.124(6)
β [°]	99.029(3)	83.743(7)	95.551(9)	82.881(7)
γ [°]	90	74.479(7)	90	71.720(6)
V [Å^3]	1298.09(7)	862.67(13)	1681.4(3)	582.51(8)
Z	2	1	4	1
$\rho_{calc.}$ [g cm^{-3}]	1.842	1.840	1.876	1.810
μ [mm^{-1}]	0.950	0.754	1.374	1.250
F(000)	726	487	956	323
$\lambda_{MoK\alpha}$ [Å]	0.71073	0.71073	0.71073	0.71073
T [K]	173	173	173	173
θ Min–Max [°]	4.1, 27.0	4.3, 26.0	4.2, 26.0	4.2, 26.0
Dataset	−8:9; −26:26; −11:11	−10:10; −11:11; −13:14	−9:9; −12:12; −27:20	−9:8; −9:9; −12:7
Reflections collected	10834	6428	12502	4342
Independent refl.	5061	3366	3284	2278
Rint	0.033	0.026	0.086	0.021
Observed reflections	4504	3028	2207	2016
Parameters	472	312	307	219
R_1 (obs)[a]	0.0344	0.0313	0.0584	0.0366
wR_2 (all data)[b]	0.0722	0.0794	0.1531	0.0928
GooF[c]	1.02	1.05	1.06	1.05
Resd. Dens. [e Å^{-3}]	−0.27, 0.35	−0.44, 0.31	−0.52, 0.94	−0.54, 1.14
Absorption correction	multi-scan	multi-scan	multi-scan	multi-scan
CCDC	1847952	1847944	1847951	1847947

a) $R_1 = \Sigma||F_0|- |F_c||/ \Sigma|F_0|$; b) $wR_2 = [\Sigma[w(F_0^2-F_c^2)^2]/\Sigma[w(F_0)^2]]^{1/2}$; $w = [\sigma c^2(F_0^2)+(xP)^2+yP]^{-1}$ and $P=(F_0^2+2F_c^2)/3$; c) GooF = $\{\Sigma[w(F_o^2-F_c^2)^2]/(n-p)\}^{1/2}$ (n = number of reflections; p = total number of parameters).

Table S3. Crystallographic data of **11**–**13**.

	11	**11b**	**12**	**13**
Formula	$C_{12}H_{24}Cl_2MnN_{24}O_8$	$C_8H_{20}Cl_2MnN_{16}O_{10}$	$C_{12}H_{24}Cl_2FeN_{24}O_8$	$C_{12}H_{24}Cl_2N_{24}O_8Zn$
FW [g mol^{-1}]	758.39	626.24	759.30	768.82
Crystal system	Trigonal	Triclinic	Trigonal	Trigonal
Space Group	*R*–3	*P*–1	*R*–3	*R*–3
Color / Habit	Colorless rod	Colorless block	Colorless block	Colorless block
Size [mm]	0.17 x 0.36 x 0.44	0.12 x 0.25 x 0.51	0.15 x 0.20 x 0.20	0.17 x 0.39 x 0.62
a [Å]	10.3011(3)	7.8356(7)	10.2549(3)	10.1876(2)
b [Å]	10.3011(3)	7.9377(7)	10.2549(3)	10.1876(2)
c [Å]	24.5701(11)	10.4440(9)	24.4806(14)	24.4867(8)
α [°]	90	83.746(7)	90	90
β [°]	90	74.820(7)	90	90
γ [°]	120	74.756(7)	120	120
V [Å^3]	2257.90(19)	604.30(10)	2229.5(2)	2200.92(13)
Z	3	1	3	3
$\rho_{calc.}$ [g cm^{-3}]	1.673	1.721	1.697	1.740
μ [mm^{-1}]	0.699	0.847	0.771	1.104
F(000)	1161	319	1164	1176
$\lambda_{MoK\alpha}$ [Å]	0.71073	0.71073	0.71073	0.71073
T [K]	143	173	123	133
θ Min–Max [°]	4.6, 25.9	4.3, 26.0	4.7, 26.0	4.7, 26.0
Dataset	−12:11; −12:12; −30:27	−9:9; −9:9; −12:9	−12:12; −12:10; −29:30	−12:12; −12:10; −30:27
Reflections collected	6414	4441	6935	7058
Independent refl.	983	2363	979	969
*R*int	0.023	0.021	0.036	0.022
Observed reflections	907	2004	851	908
Parameters	80	228	88	72
R_1 (obs)[a]	0.0255	0.0361	0.0294	0.0263
wR_2 (all data)[b]	0.0660	0.0914	0.0720	0.0685
GooF[c]	1.06	1.06	1.10	1.14
Resd. Dens. [e Å^{-3}]	−0.40, 0.64	−0.44, 0.74	−0.35, 1.39	−0.41, 1.74
Absorption correction	multi-scan	multi-scan	multi-scan	multi-scan
CCDC	1847949	1847939	1847941	1847950

a) $R_1 = \Sigma||F_0|- |F_c||/ \Sigma|F_0|$; b) $wR_2 = [\Sigma[w(F_0^2-F_c^2)^2]/\Sigma[w(F_0)^2]]^{1/2}$; $w = [\sigma c^2(F_0^2)+(xP)^2+yP]^{-1}$ and $P=(F_0^2+2F_c^2)/3$; c) GooF = $\{\Sigma[w(F_o^2-F_c^2)^2]/(n-p)\}^{1/2}$ (n = number of reflections; p = total number of parameters).

Table S4. Crystallographic data of **14**–**16**.

	14	**15**	**16**
Formula	$C_8H_{16}ZnN_{18}O_6$	$C_{10}H_9CuN_{11}O_8$	$C_8H_{16}Cl_2CuN_{16}O_6$
FW [g mol^{-1}]	525.76	474.82	566.81
Crystal system	Tetragonal	Orthorhombic	Triclinic
Space Group	$I4_1/a$	$P2_12_12_1$	P–1
Color / Habit	Colorless block	Green block	Violet plate
Size [mm]	0.13 x 0.16 x 0.22	0.16 x 0.19 x 0.25	0.03 x 0.15 x 0.35
a [Å]	10.7293(2)	8.3524(12)	6.8340(6)
b [Å]	10.7293(2)	8.5731(8)	8.2492(8)
c [Å]	17.1567(6)	23.3337(16)	10.4151(9)
α [°]	90	90	67.974(8)
β [°]	90	90	89.924(7)
γ [°]	90	90	68.131(9)
V [Å^3]	1975.04(10)	1670.8(3)	498.55(9)
Z	4	4	1
$\rho_{calc.}$ [g cm^{-3}]	1.768	1.888	1.888
μ [mm^{-1}]	1.318	1.383	1.433
F(000)	1072	956	287
$\lambda_{MoK\alpha}$ [Å]	0.71073	0.71073	0.71073
T [K]	173	173	143
θ Min–Max [°]	4.4, 26.0	4.2, 26.0	4.2, 26.0
Dataset	−13: 11; −13: 12; −21: 17	−10: 10; −10: 9; −28: 28	−8: 8; −8: 10; −8: 12
Reflections collected	7438	12347	3523
Independent refl.	967	3281	1955
Rint	0.030	0.059	0.027
Observed reflections	898	2603	1692
Parameters	97	307	167
R_1 (obs)[a]	0.0284	0.0497	0.0313, ,
wR_2 (all data)[b]	0.0711	0.1238	0.0762
GooF[c]	1.06	1.03	1.07
Resd. Dens. [e Å^{-3}]	−0.38, 0.57	−0.51, 0.81	−0.36, 0.43
Absorption correction	multi-scan	multi-scan	multi-scan
CCDC	1847942	1847940	1848019

a) $R_1 = \Sigma||F_0|- |F_c||/ \Sigma|F_0|$; b) $wR_2 = [\Sigma[w(F_0^2-F_c^2)^2]/\Sigma[w(F_0)^2]]^{1/2}$; $w = [\sigma c^2(F_0^2)+(xP)^2+yP]^{-1}$ and $P=(F_0^2+2F_c^2)/3$; c) GooF = $\{\Sigma[w(F_o^2-F_c^2)^2]/(n-p)\}^{1/2}$ (n = number of reflections; p = total number of parameters).

An interesting observation for the one-dimensional structure of **5** can be made by viewing along the crystallographic *b*-axis: The investigated compound obviously consists of multiple layers built up by the four bridging aminotriazole ligands (Figure S5). This layer structure's formation is caused by the fact that adjacent aminotriazole ligands do not connect the same two copper(II) centers, but occupy torsion angles of about 90° (< N2^{iii}–N1^{iii}–Cu1–N4 = 90.63°, < N2^{ii}–N1^{ii}–Cu1–N4 = 89.37°). The one-dimensional stability of complex **5** is ensured through several hydrogen bonds between the terminal nitrato ligands and the hydrocarbon backbone of **1** and the triazoles' amino groups, respectively (Table S5).

Table S5. Selected hydrogen bonds of **5**.

D–H···A	***d*** **(D–H) (Å)**	***d*** **(H···A) (Å)**	***d*** **(D···A) (Å)**	**< D–H···A (°)**
N1–H11···O2	0.78(3)	2.17(3)	2.911(3)	160(3)
N1–H12···O2	0.75(3)	2.20(3)	2.905(3)	157(3)
C1–H1···O3	0.87(3)	2.51(3)	3.322(3)	157(3)

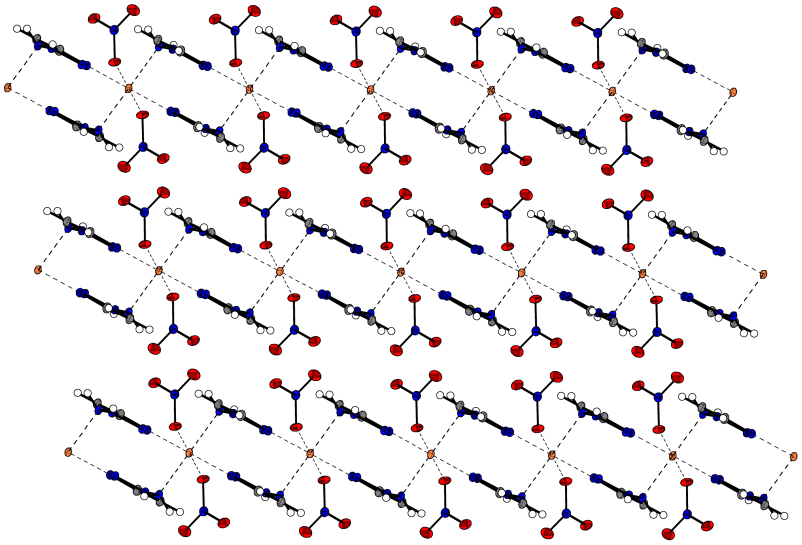


Figure S5. Projection of the structure of **5** with the direction of view along the crystallographic *b*-axis.

Copper(II) picrate compound **6** crystallizes in the form of green rods in the monoclinic space group *C*2/*c* with four formula units per unit cell and a calculated density of 1.825 g cm^{-3} at 143 K. The octahedral copper(II) coordination sphere consists of four aqua ligands, two axial and two equatorial ones, as well as two equatorial 1-ATRI ligands. Similar to compound **8** the counter-anions are not coordinating to the metal(II) center (Figure S6). The octahedron is moderately distorted together with two nitro groups of the picrate counter-anions.

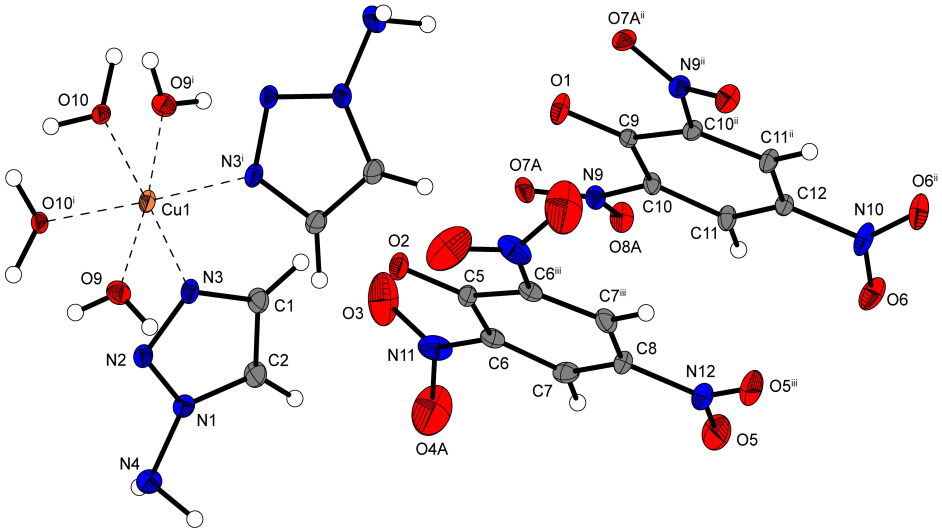


Figure S6. Molecular unit of $[Cu(H_2O)_4(1\text{-ATRI})_2](PA)_2$ (**6**). Selected bond lengths (Å): Cu1–N3 1.995(4), Cu1–O9 2.349(4), Cu1–O10 2.005(3); selected bond angles (°): O9–Cu1–O10 85.97(14), O9–

Cu1–N3 91.99(17), O10–Cu1–N3 177.61(17). Symmetry codes: (i) 1−x, y, 0.5−z; (ii) 2−x, y, 1.5−z; (iii) 1−x, y, 1.5−z.

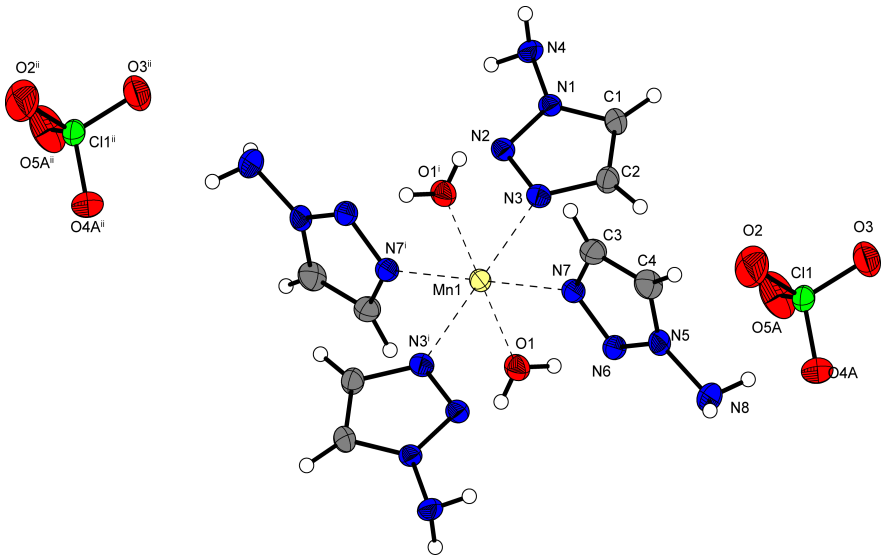


Figure S7. Molecular unit of $[Mn(H_2O)_2(1\text{-ATRI})_4](ClO_4)_2$ (**11b**). Selected bond lengths (Å): Mn1–O1 2.184(2), Mn1–N3 2.232(2), Mn1–N7 2.259(2); selected bond angles (°): O1–Mn1–N3 93.94(9), O1–Mn1–Cu7 92.22(8), N3–Mn1–N7 88.45(8). Symmetry codes: (i) −x, 1−y, −z; (ii) −1+x, y, −1+z.

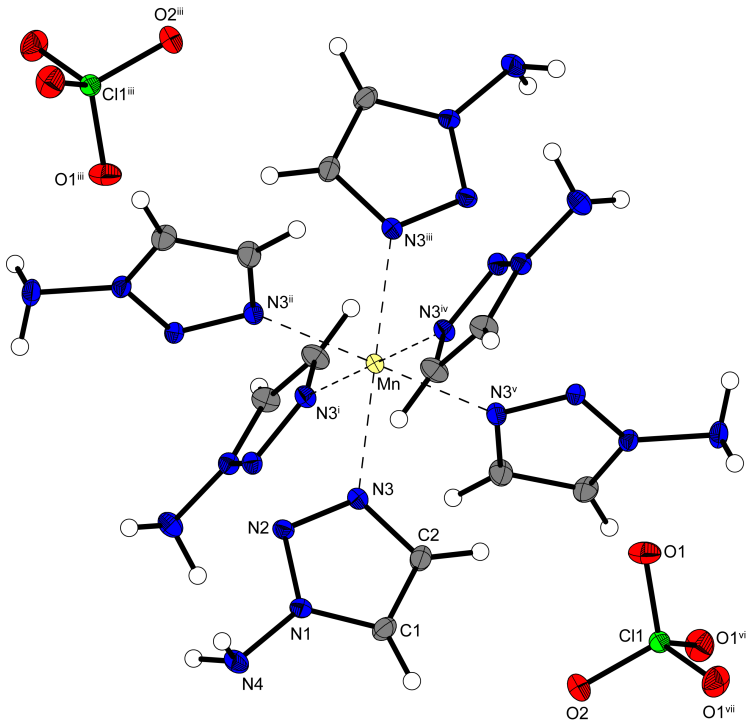


Figure S8. Molecular unit of $[Mn(1\text{-ATRI})_6](ClO_4)_2$ (**11**). Selected bond length (Å): Mn1–N3 2.2652(13); selected bond angles (°): N3–Mn1–N3^{i} 93.16(6), N3–Mn1–N3^{iv} 86.84(6). Symmetry codes:

(i) 1−y, 1+x−y, z; (ii) −x+y, 1−x, z; (iii) 0.67−x, 1.33−y, 0.33−z; (iv) −0.33+y, 0.33−x+y, 0.33−z; (v) 0.67+x−y, 0.33+x, 0.33−z; (vi) −x+y, −x, z; (vii) −y, x−y, z.

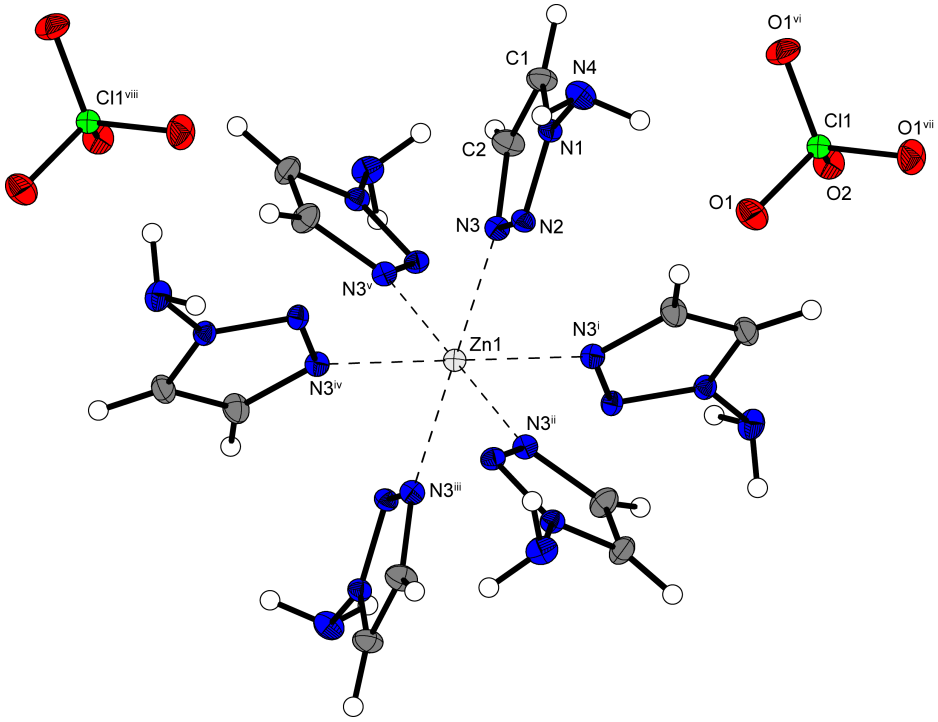


Figure S9. Molecular unit of $[Zn(1\text{-ATRI})_6](ClO_4)_2$ (**13**). Selected bond length (Å): Zn1–N3 2.1782(16); selected bond angles (°): N3–Zn1–N^{iv} 92.57(8), N3–Zn1–N^{i} 87.44(8). Symmetry codes: (i) y, −x+y, −z; (ii) −x+y, x, z; (iii) −x, −y, −z; (iv) −y, x−y, z; (v) x−y, x, z; (vi) 1−x+y, 1−x, z; (vii) 1−y, −y, z; (viii) −1+x, y, z.

Complex **15** crystallizes in the form of green blocks in the orthorhombic space group $P2_1$ with four formula units per cell and a calculated density of 1.888 gcm^{-3} at 173 K. The octahedral coordination sphere is built up in an analogous way to complex **9** (Figure S10).

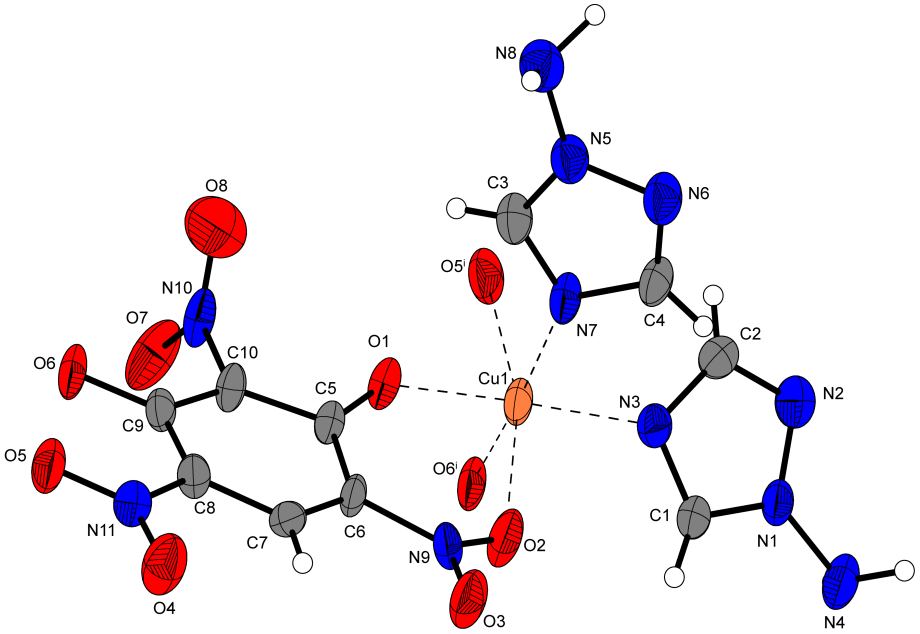


Figure S10. Copper(II) coordination environment of $[Cu(TNR)(1\text{-}A\text{-}1,2,4\text{-}TRI)_2]$ (**15**). Selected bond length (Å): Cu1–O1 1.925(5), Cu1–O2 2.381(7), Cu1–N3 1.998(7), Cu1–N7 1.986(7); selected bond angles (°): O1–Cu1–O2 79.8(2), O1–Cu1–N3 176.6(3), O1–Cu1–N7 91.6(3), O2–Cu1–N2 100.4(2), O2–Cu1–N7 94.9(3). Symmetry code: (i) 1−x, 0.5+y, 0.5−z.

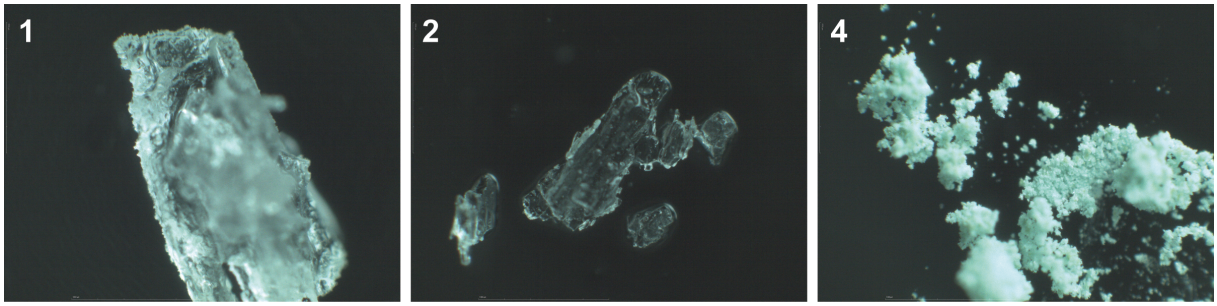


Figure S11. Microscope images of **1**, **2**, and **4** (fourfold magnitude).

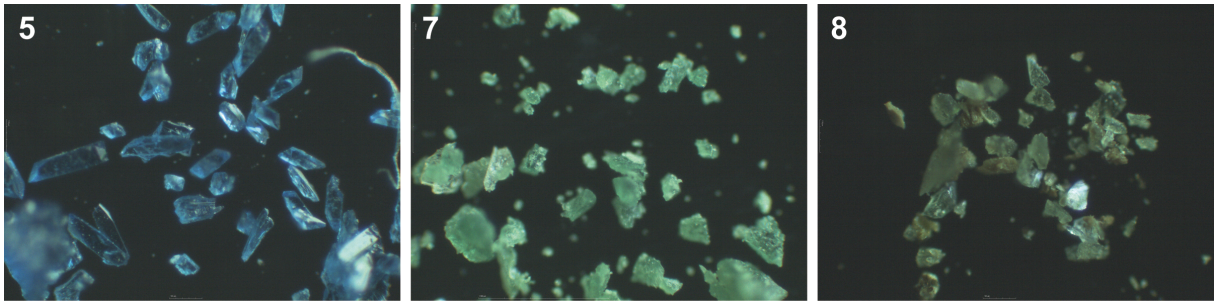


Figure S12. Microscope images of **5**, **7**, and **8** (tenfold magnitude).

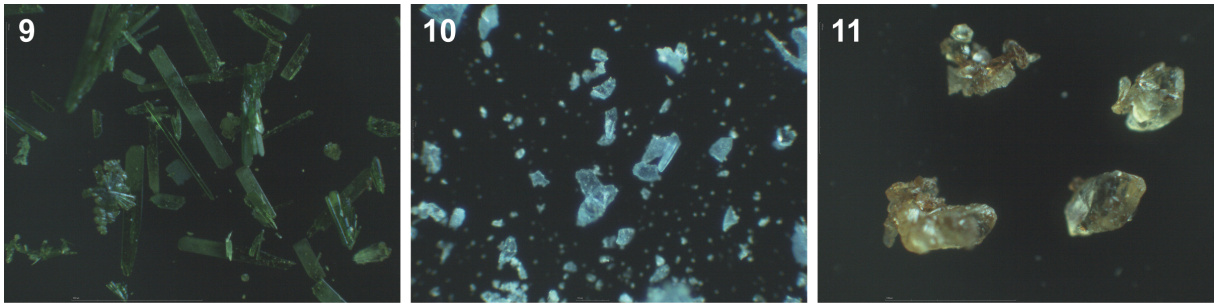


Figure S13. Microscope images of **9**–**11** (**9** and **11**: fourfold magnitude; **10**: tenfold magnitude)

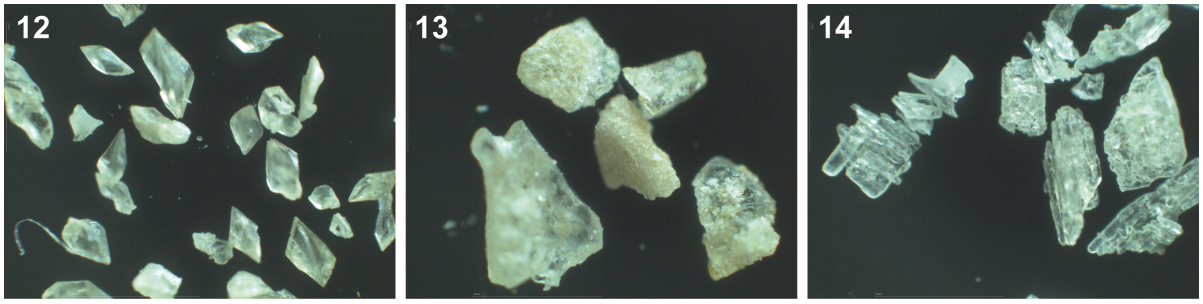


Figure S14. Microscope images of **12**–**14** (fourfold magnitude).

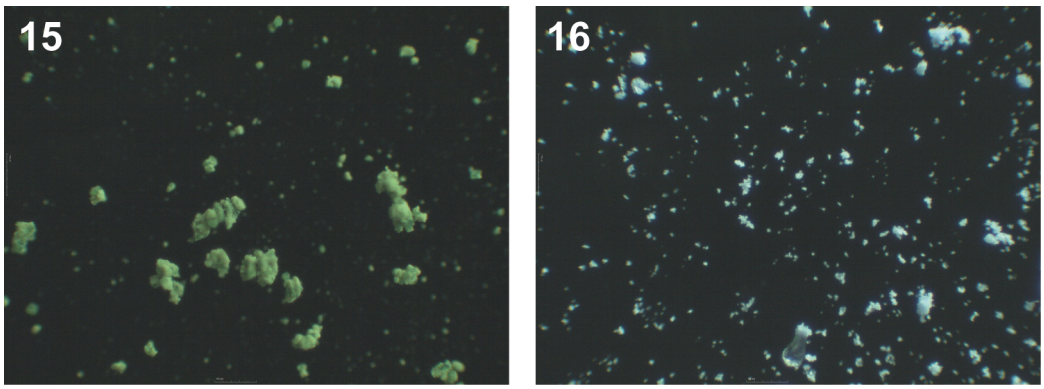


Figure S15. Microscope images of **15** and **16** (**15**, **16**: tenfold magnitude).

19.12.4 TGA Plot of the Zinc(II) Perchlorate Complex 13

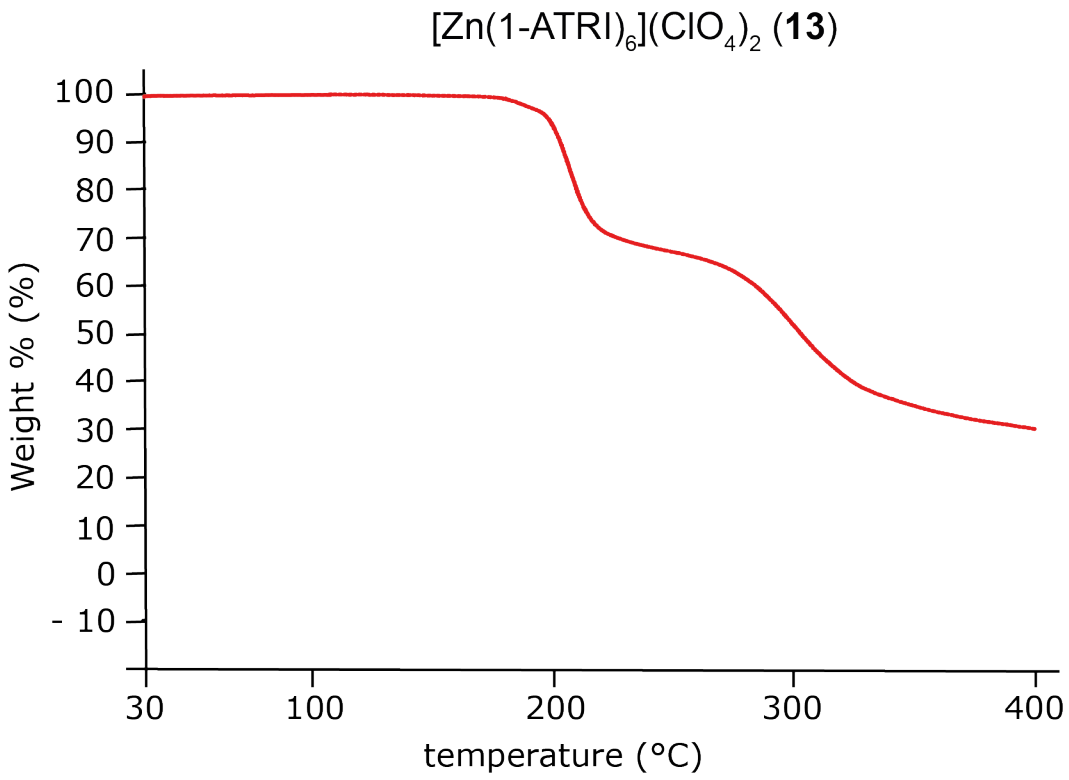


Figure S16. TGA plot of the zinc(II) perchlorate complex **13**.

19.12.5 DTA Plots of 1–9 and 14–16

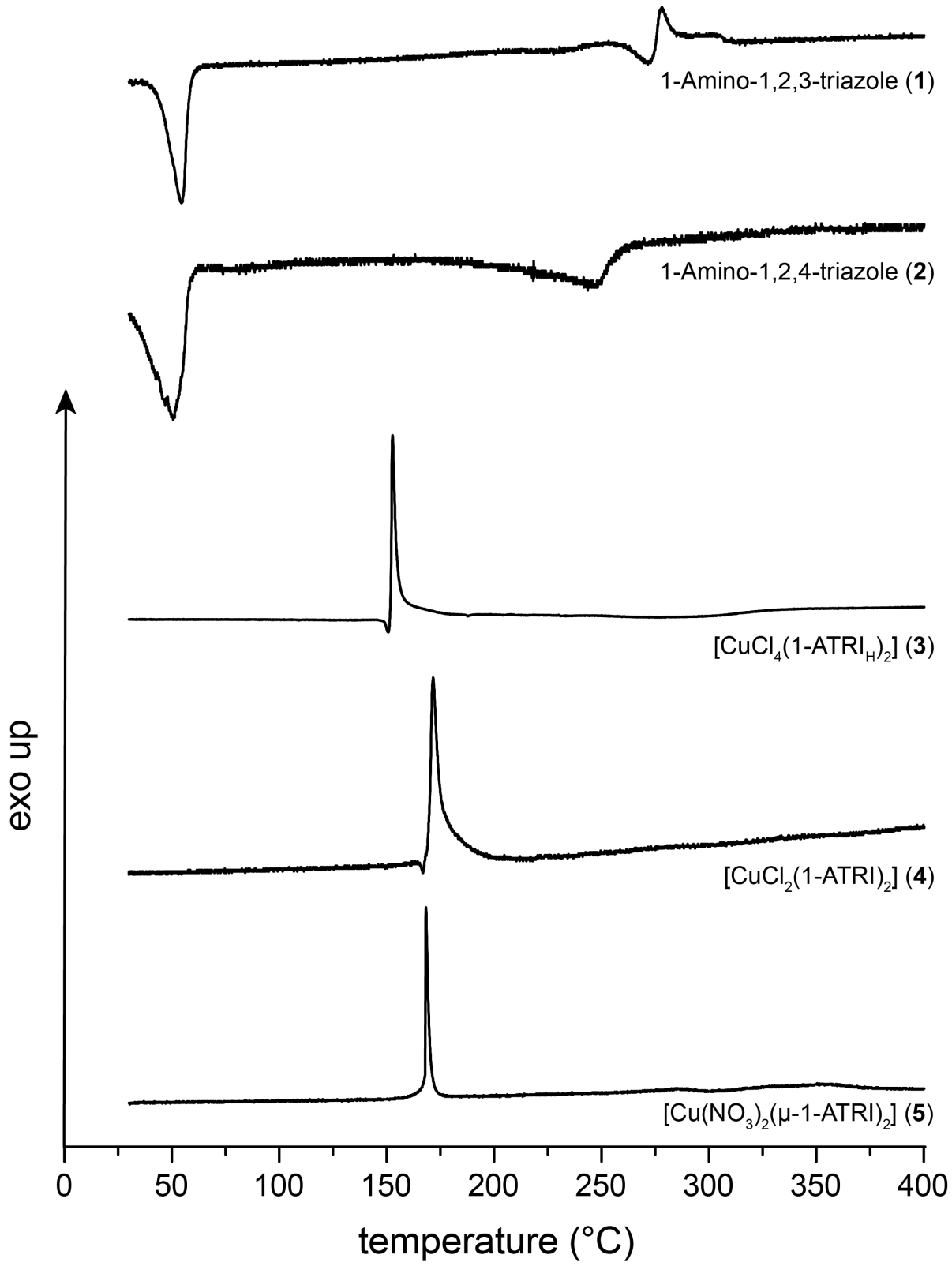


Figure S17. DTA plots of **1**–**5**.

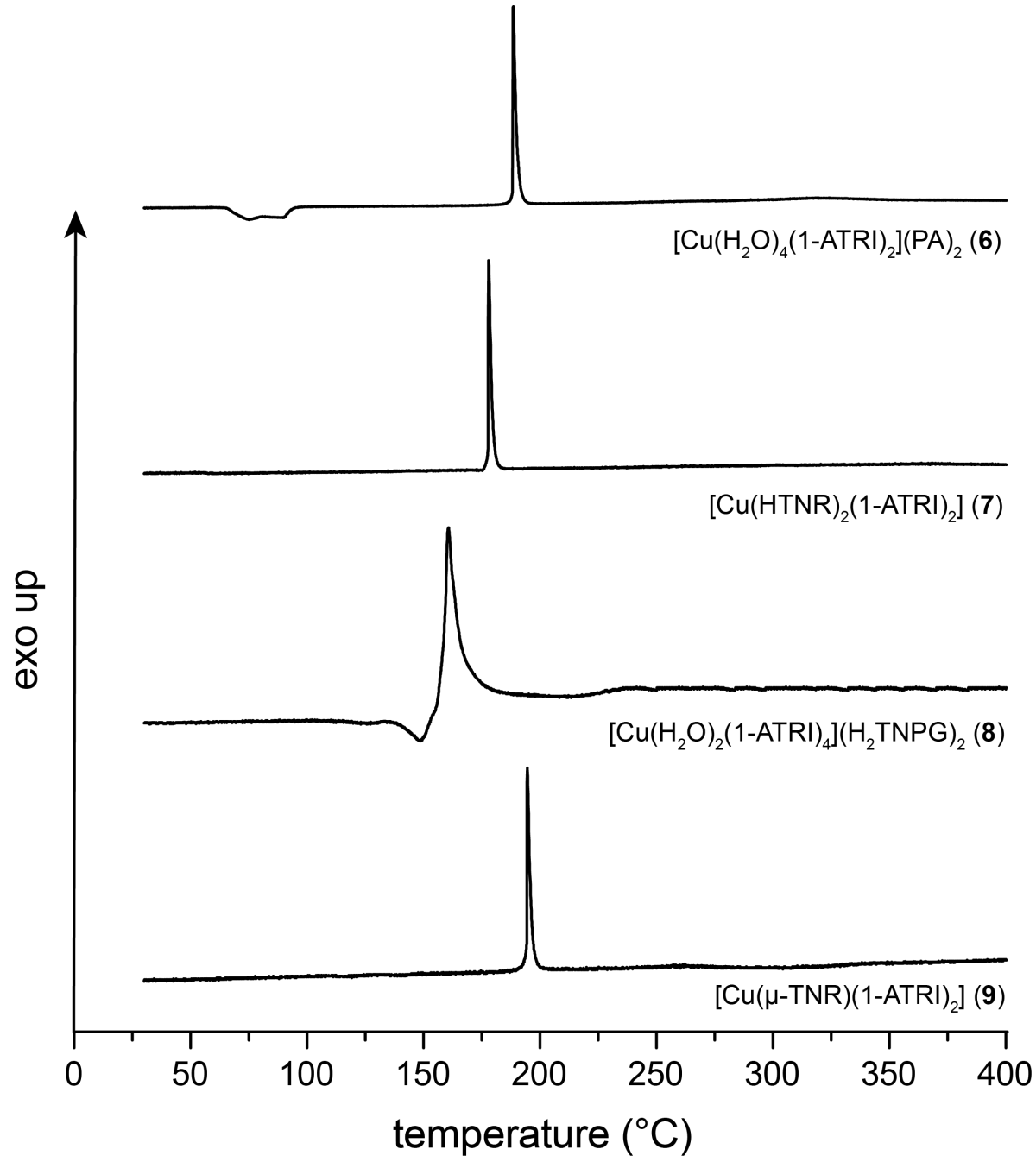


Figure S18. Different thermal analysis (DTA) plots of **6**–**9**.

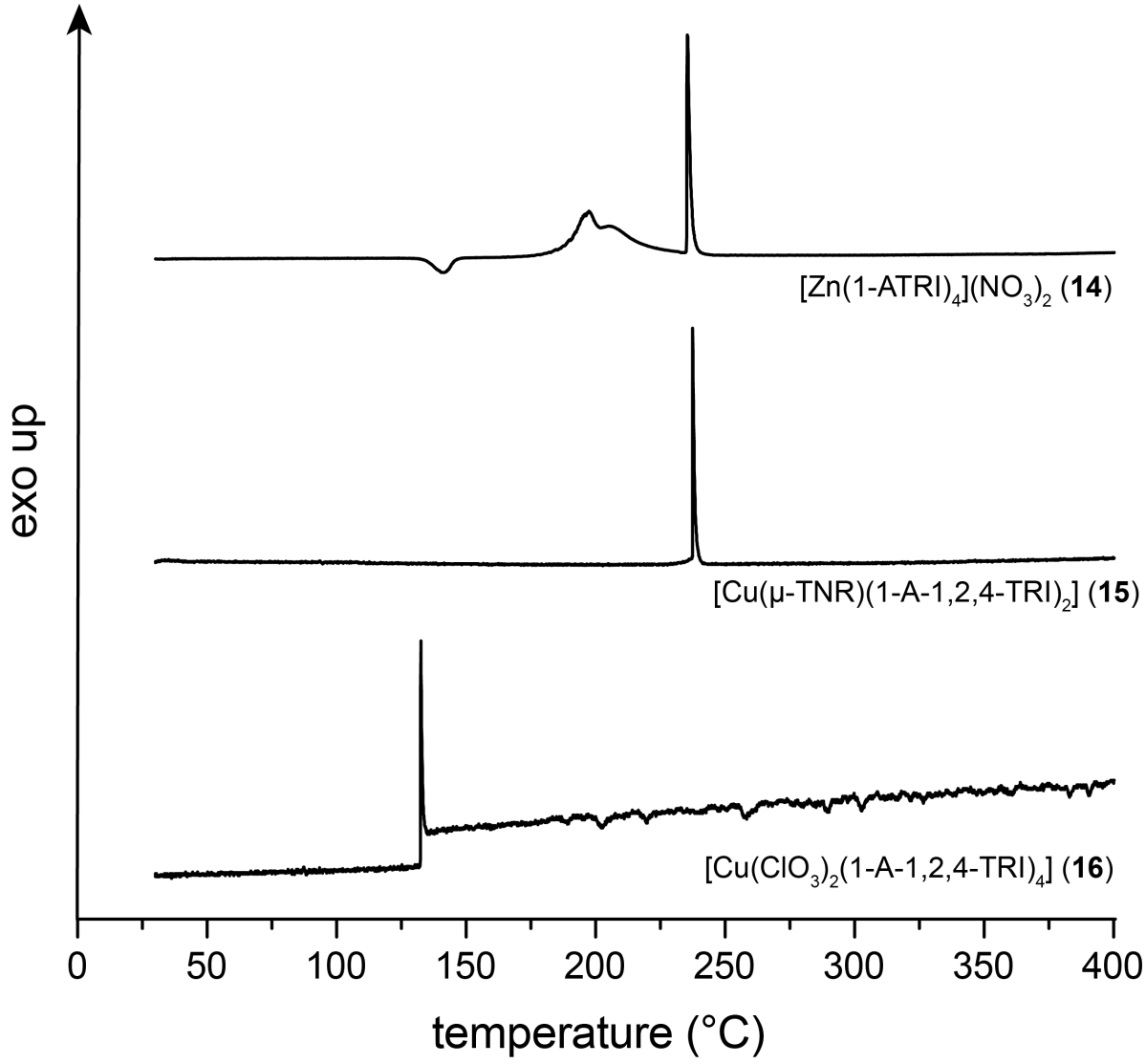


Figure S19. DTA plots of **14**–**16**.

19.12.6 Column Diagrams of the Complexes 3–9

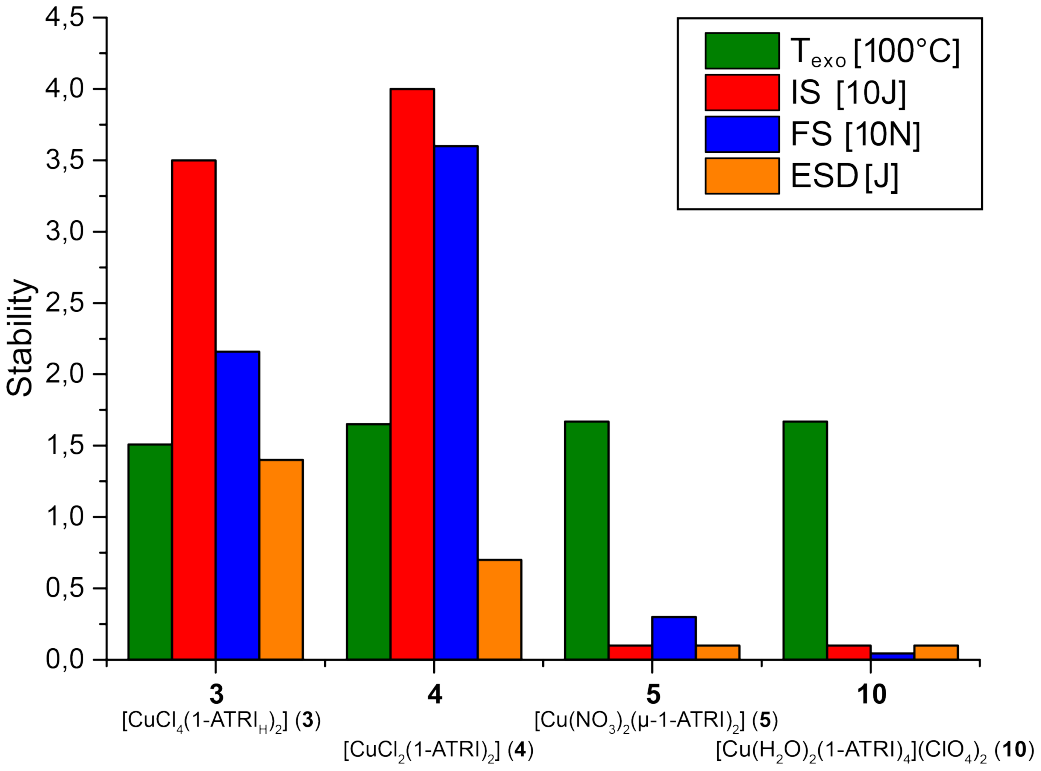


Figure S20. Stability comparison of the copper(II) complexes **3**, **4**, **5** and **10**.

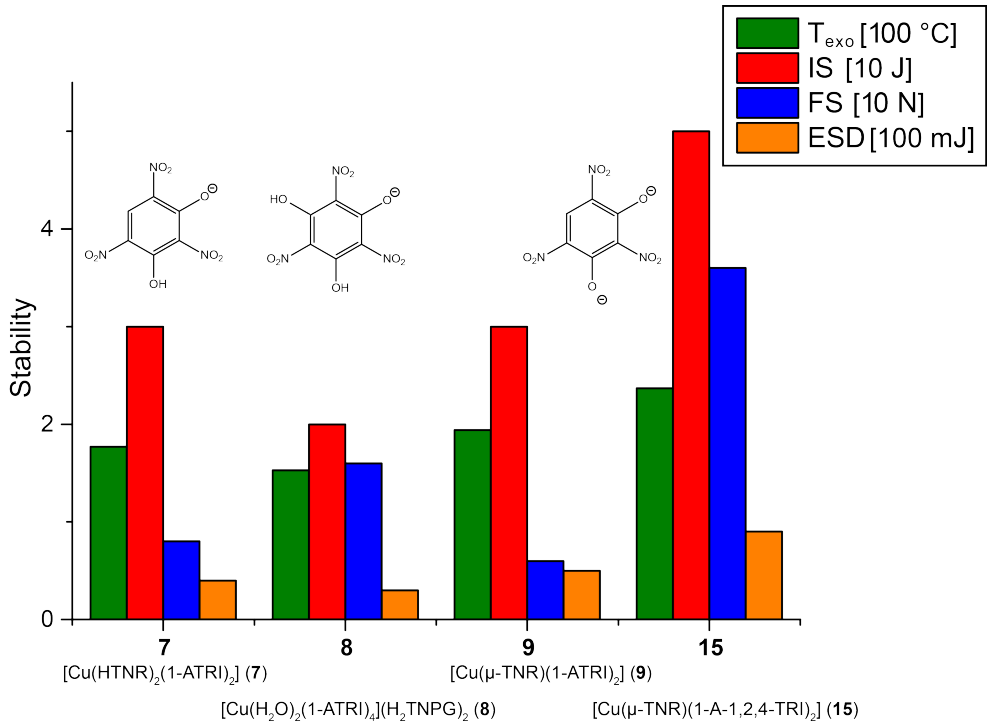


Figure S21. Stabilities of selected copper(II) 1-aminotriazole coordination compounds **7**–**9** and **15**.

19.12.7 Hot Plate and Hot Needle Tests

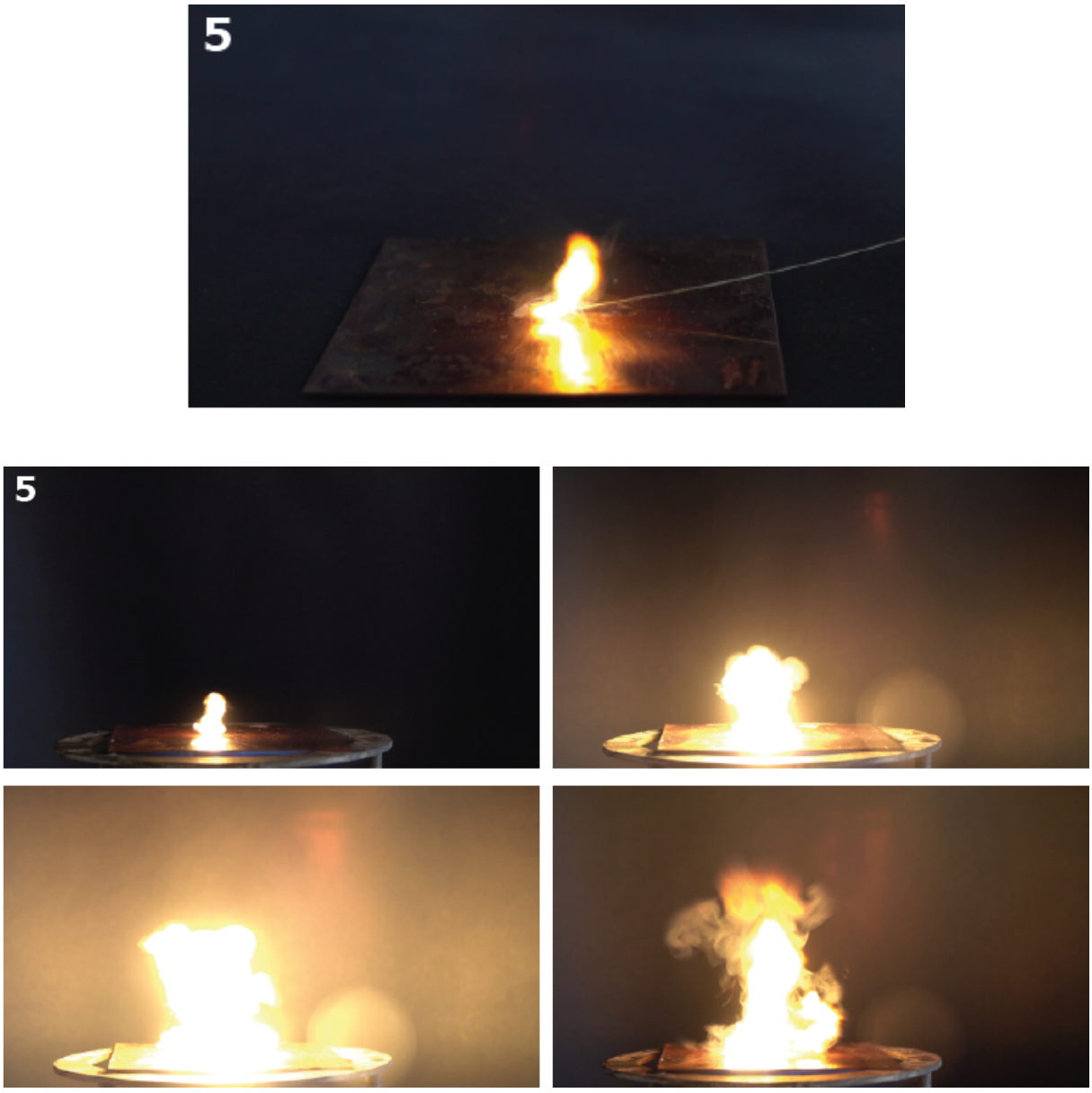


Figure S22. Hot needle and hot plate (shown as a sequence) tests of the copper(II) nitrate complex **5**.



Figure S23. Hot needle test of the manganese(II) complex **11** shown as a sequence.

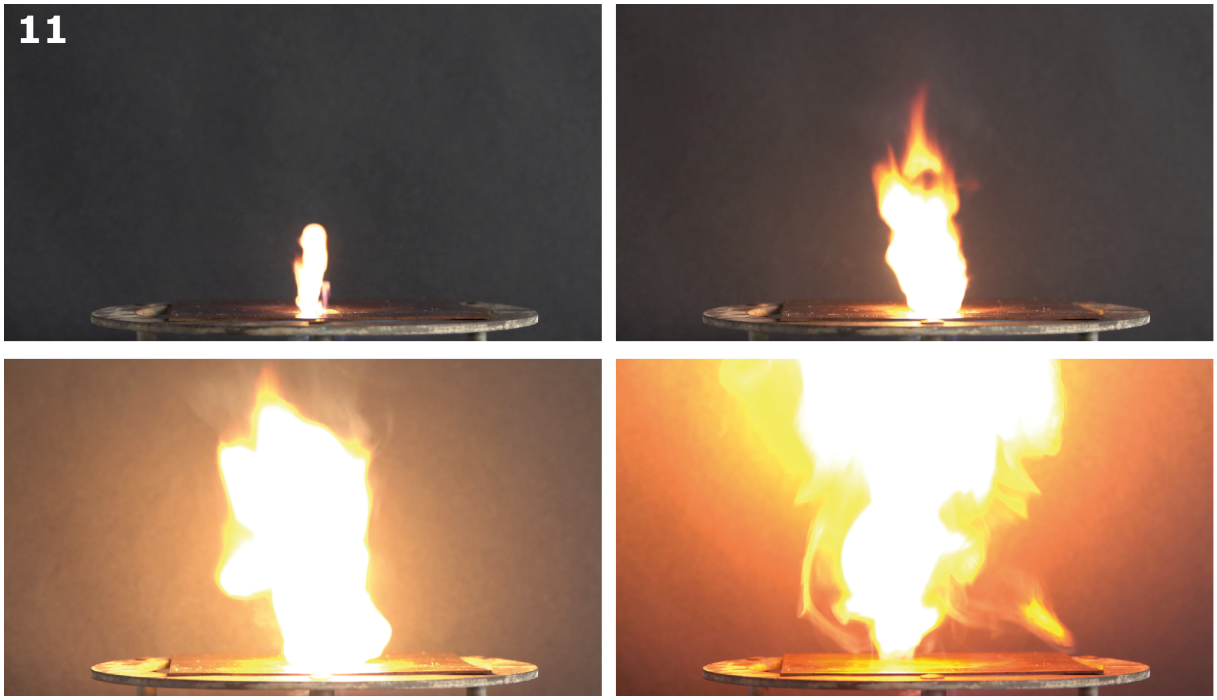


Figure S24. Moment of deflagration of the manganese(II) perchlorate **11** shown as a sequence during the hot plate test.

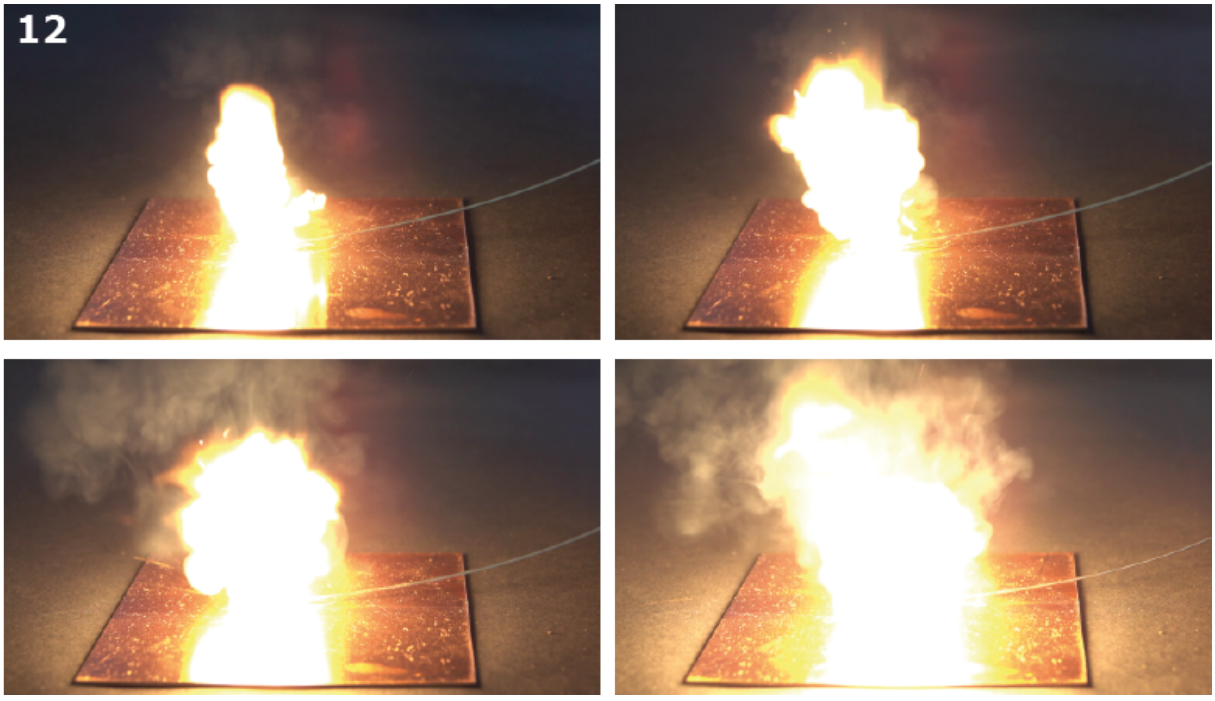


Figure S25. Hot needle test of iron(II) complex **12** shown as a sequence.

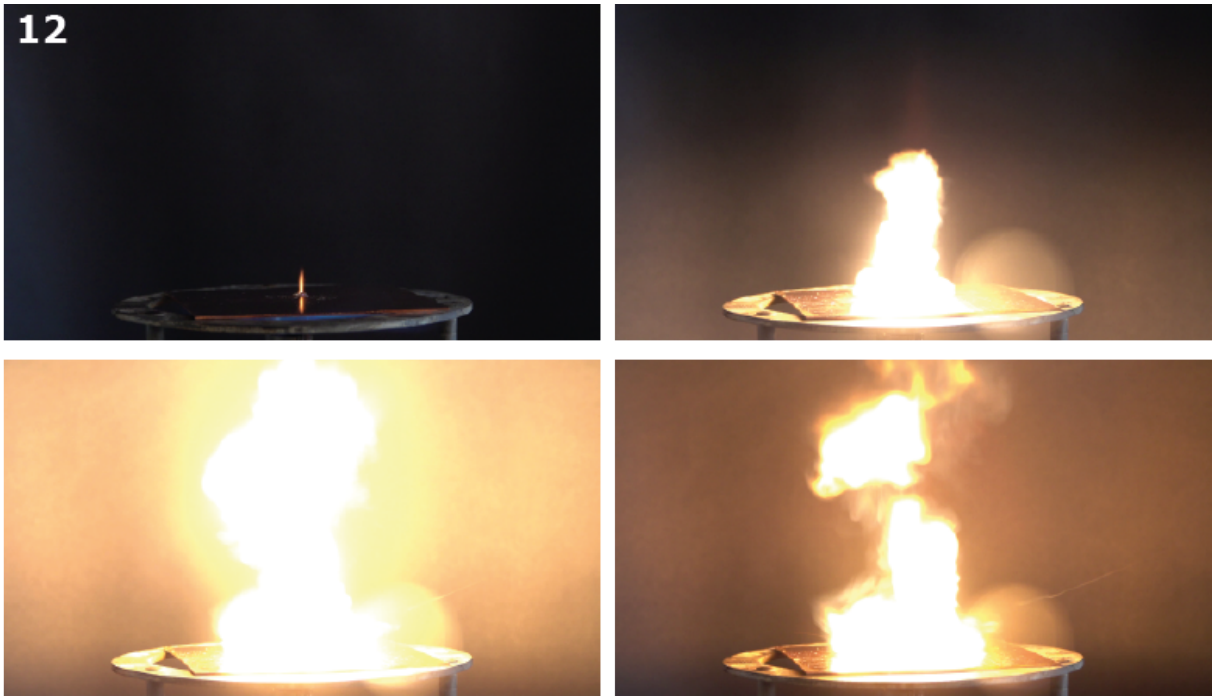


Figure S26. Hot plate test of the iron(II) perchlorate **12** shown as a sequence.



Figure S27. Initiation of zinc (II) complex **13** shown as a sequence during the hot needle test.

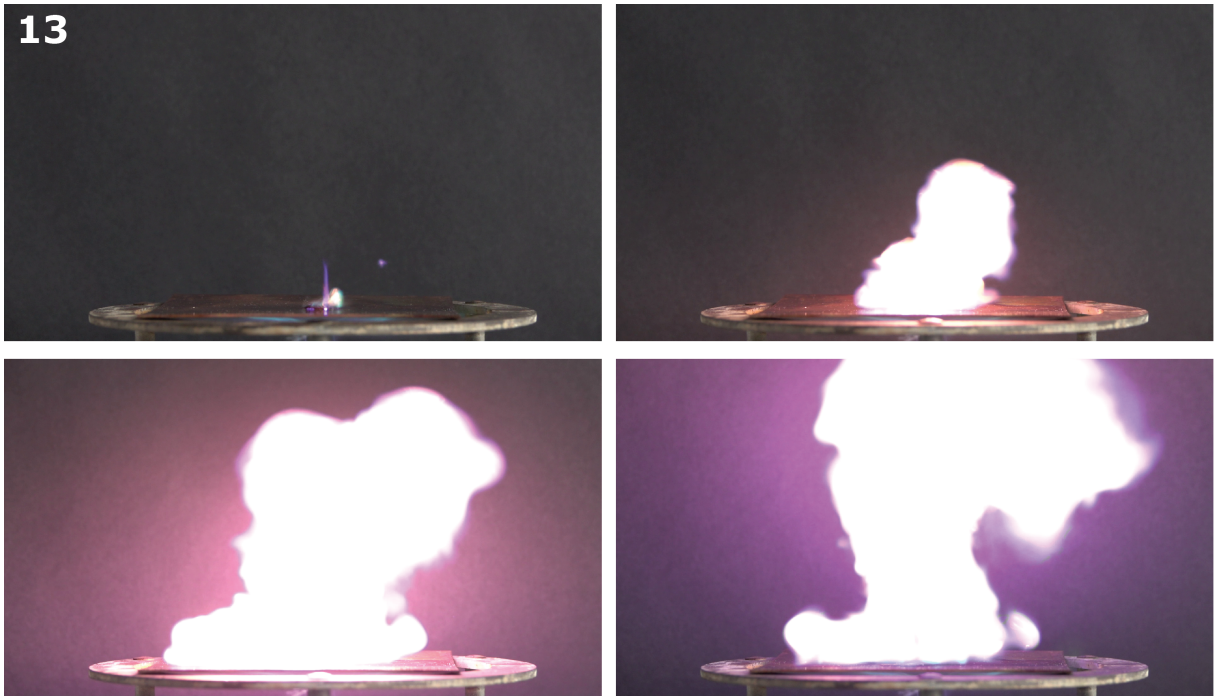


Figure S28. Hot plate test of complex **13** shown as a sequence.

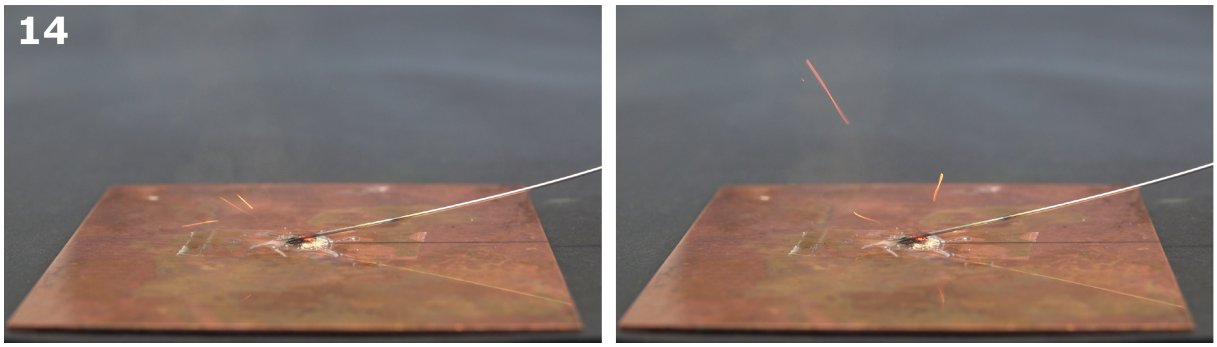


Figure S29. Moment of initiation of zinc(II) nitrate complex **14** shown as a sequence.

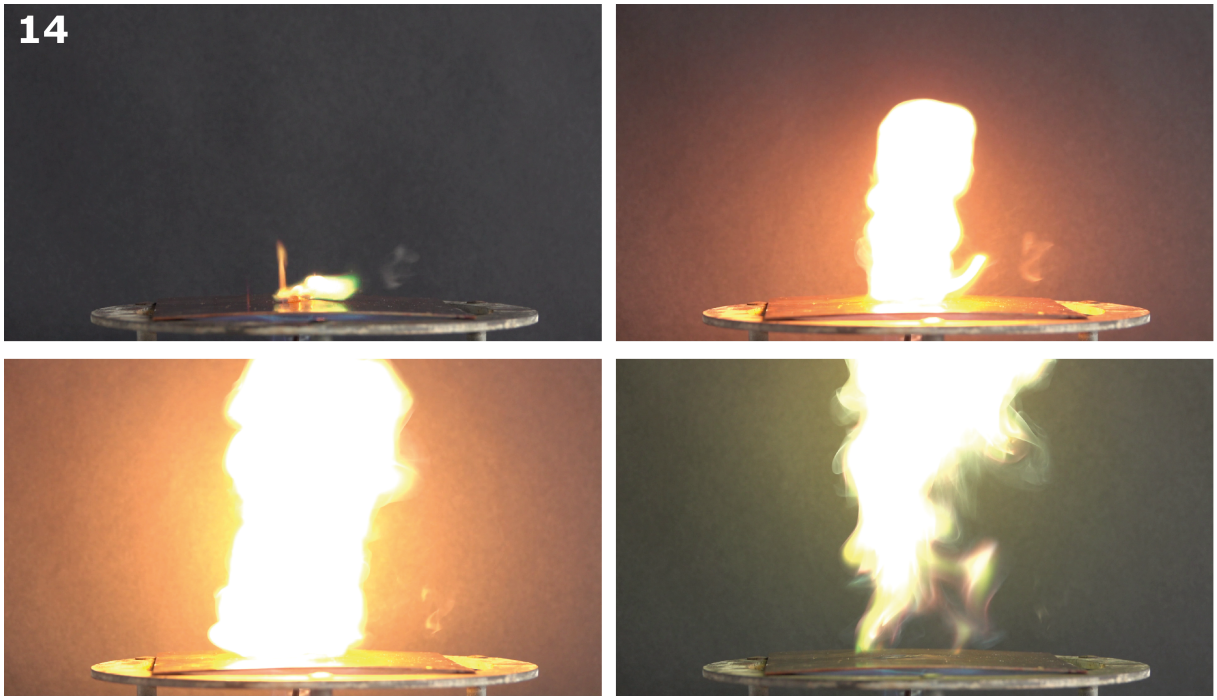


Figure S30. Behavior of complex **14** during the hot plate test shown as a sequence.

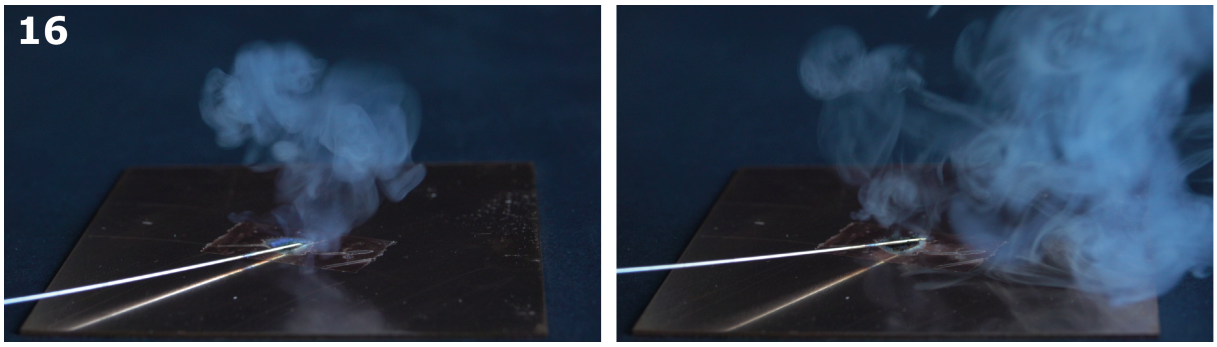


Figure S31. Moment of initiation during the hot needle test of complex **16** shown as a sequence.

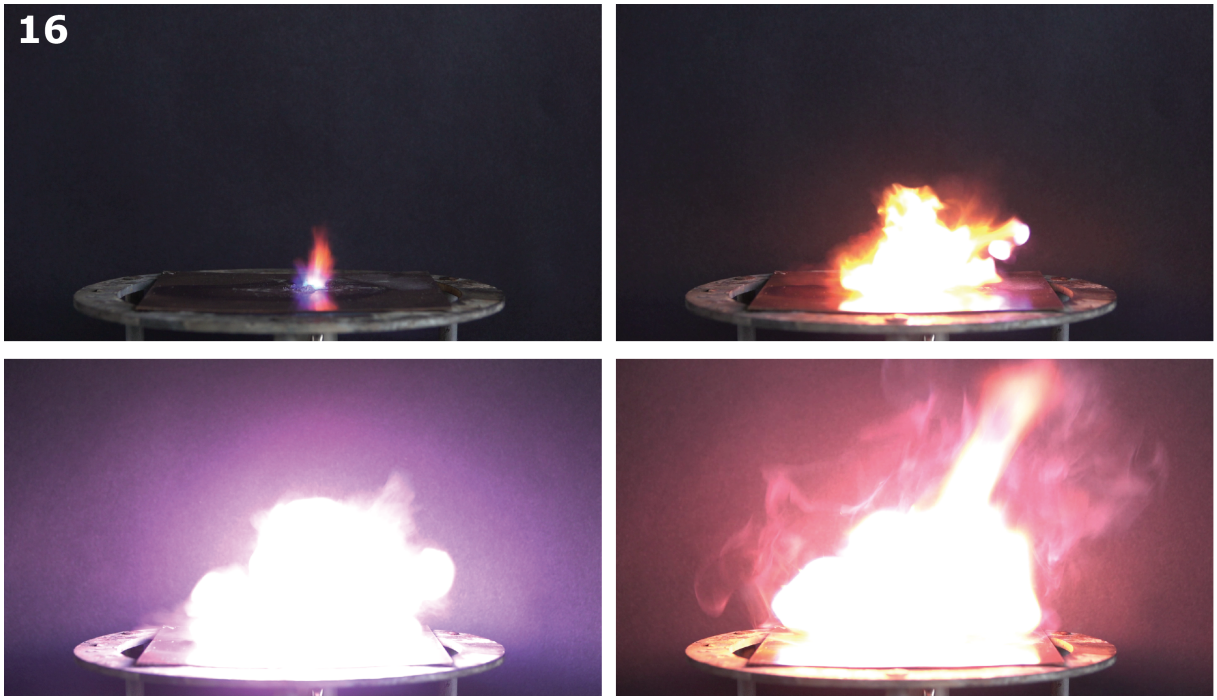


Figure S32. Moment of deflagration of the coordination compound **16** shown as sequence during the hot plate test.

19.12.8 Laser Ignition Test of Complex 16

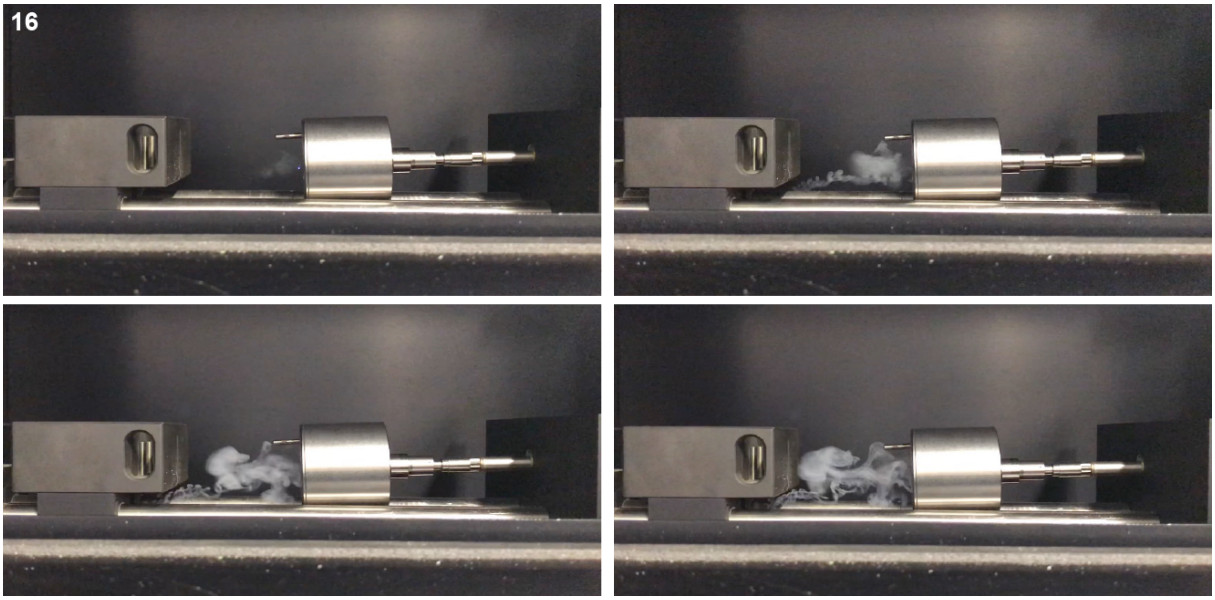


Figure S33. Deflagration of the copper(II) chlorate complex **16** during the laser initiation test shown as a sequence.

19.12.9 Experimental Part and General Methods

All chemicals and solvents were employed as received (Sigma-Aldrich, Fluka, Acros, ABCR). Copper(II) chlorate as starting material for the synthesis of complex **16** was prepared according to a literature reported synthetic protocol.[S9] The chemical composition and morphology of selected samples were investigated with a scanning electron microscope (SEM) NanoLab G3 (Helios). The samples were carbon-coated (BAL-TEC MED 020, Bal Tec AG) to prevent electrostatic charging and to increase the conductivity. Energy dispersive X-ray spectroscopy (EDX) was carried out with an acceleration voltage of 20 kV using an X-Max 80 SDD detector (Oxford Instruments). ^{1}H and ^{13}C spectra were recorded at ambient temperature using a JEOL Bruker 400, Eclipse 270, JEOL EX 400 or a JEOL Eclipse 400 instrument. The chemical shifts quoted in ppm in the text refer to typical standards such as tetramethylsilane (^{1}H, ^{13}C) in d_6-DMSO as the solvent. Endothermic and exothermic events of the described compounds, which indicate melting, evaporation or decomposition, are given as the extrapolated onset temperatures. The samples were measured in a range of 25–400 °C at a heating rate of 5 °C min^{-1} through differential thermal analysis (DTA) with an OZM Research DTA 552-Ex instrument and partly by thermal gravimetric analysis (TGA) with a PerkinElmer TGA4000. Infrared spectra were measured with pure samples on a Perkin-Elmer BXII FT-IR system with a Smith DuraSampler IR II diamond ATR. Determination of the carbon, hydrogen and nitrogen contents was carried out by combustion analysis using an Elementar Vario El (nitrogen values determined are often lower than those calculated due to their explosive behavior). UV-Vis spectra were recorded in the solid state using a Varian Cary 500 spectrometer in the wavelength range of 350–1000 nm. The step in the absorption intensity at 800 nm is caused by a detector change and spectra have only qualitative character. Impact sensitivity tests were carried out according to STANAG 4489[S10] with a modified instruction[S11] using a BAM (Bundesanstalt für Materialforschung) drophammer.[S12,13] Ball drop impact sensitivities were determined for selected compounds on an OZM ball drop machine (BIT-132) following MIL-STD-1751A (method 1016) by dropping a free-falling steel ball onto the explosive compound.[S14] A sample of approximately 30 mg was placed on a steel block and spread into a 0.33 mm layer of substance. The steel ball guide was set to the desired height and the loaded impact block positioned underneath. By releasing the ball shield, a 0.50 inch steel ball, weighing 8.35 g, was allowed to fall onto the sample. Any visual observation of decomposition was regarded as a positive result. If no reaction occurred, the remaining substance was disposed, and the impact block loaded with a freshly prepared sample. The limiting impact energy was determined in

conformity with the recommended UN method for testing impact and friction sensitivities (1-in-6 approach), according to ST/SG/AC.10/11/Rev.6 (s. 13.4.2.3.3).[S15] The impact energy was calculated as the product of the weight of the steel ball and its fall height. An initial drop height was chosen, at which an explosion of the sample could be ensured. The impact energy level (ball guide height) was now stepwise decreased until no reaction was observed. At this point, testing was continued up to a total of six trials at that certain energy level. If an explosion occurred, the procedure was repeated by decreasing the drop height. As soon as six trials at a fixed energy level emerged as negative, the next higher energy level, where at least one out of at least six trials resulted in an explosion, is determined as the limiting impact energy. Friction sensitivity tests were carried out according to STANAG 4487[S16] with a modified instruction[S17] using the BAM friction tester. The classification of the tested compounds results from the "UN Recommendations on the Transport of Dangerous Goods".[S18] Additionally all compounds were tested to determine the sensitivity toward electrical discharge using the OZM Electric Spark Tester ESD 2010 EN or OZM Electric Spark XSpark10 device.[S12] Hot plate and hot needle tests were performed in order to classify the initiation capability of selected complexes. The samples were fixed on a copper plate underneath adhesive tape and initiated by a red hot needle. Strong deflagration or detonation of the compound usually indicates a valuable primary explosive. The safe and straightforward hot plate test only shows the behavior of the unconfined sample toward fast heating on a copper plate. It does not necessarily allow any conclusions on a compound´s capability as a suitable primary explosive. Initiation capability tests of the newly investigated complexes toward pentaerythritol tetranitrate (PETN) were carried out in a copper shell with a diameter of 7 mm and length of 88 mm filled with 200 mg of sieved secondary explosive (grain size < 100 µm). First, the secondary explosive was pressed with a weight of 8 kg, then the primary explosive to be investigated was subsequently filled on top of the main charge and pressed with the same pressure force. The shell was sealed by an insulator, placed in a retaining ring, which was soldered to a copper witness plate with a thickness of 1 mm and finally initiated by a type A electric igniter. A positive test is indicated by a hole in the copper plate and fragmentation of the shell caused by a deflagration-to-detonation transition (DDT) of PETN. Liquid-dried luminescent bacteria of the strain *Vibrio fischeri* NRRL-B-11177 provided by the HACH LANGE GmbH were used for the luminescent bacteria inhibition test to determine their toxicity toward aquatic organisms according to a modified procedure.[S19] The laser initiation experiments were performed with a 45 W InGaAs laser diode operating in the single-pulsed mode. The diode is attached to an

optical fiber with a core diameter of 400 µm and a cladding diameter of 480 µm. The optical fiber is connected via a SMA type connecter directly to the laser and to a collimator. This collimator is coupled to an optical lens, which was positioned in its focal distance (f = 29.9 mm) to the sample. The lens is shielded from the explosive by a sapphire glass. Approximately 15 mg of the carefully pestled complex to be investigated was filled into a transparent plastic cap (PC), pressed with a pressure force of 1 kN and sealed by a UV-curing adhesive. The confined samples were irradiated at a wavelength of 915 nm, a voltage of 4 V, a current of 7 A and pulse lengths of 0.1 ms. The combined currents and pulse lengths result in an energy output of about 0.17 mJ.

The obtained coordination compounds were washed with cold ethanol when stated, dried overnight in air and used for analytics without further purification.

CAUTION! *All investigated compounds are potentially explosive energetic materials (the majority of the compounds lie in the range of primary explosives), which show partly increased sensitivities toward various stimuli (e.g. elevated temperatures, impact, friction or electrostatic discharge). Therefore, proper security precautions (safety glasses, face shield, earthed equipment and shoes, leather jacket, Kevlar gloves, Kevlar sleeves and ear plugs) have to be worn while synthesizing and handling the described compounds. Especially the very sensitive compounds **5**, **10**–**13** and **16** must be handled with great care!*

Selective 1-amino-1,2,3-triazole (1) synthesis:

1-Amino-1,2,3-triazole (**1**) was prepared in a two-step reaction according to a patent and a modified literature procedure.[S20,21] Hydrazine monohydrate (24.1 g, 482 mmol) in water (25 mL) was slowly added to an aqueous solution of glyoxal (40 %, 14.0 g, 241 mmol) and the resulting reaction mixture stirred at room temperature for 1 hour followed by heating to 100 °C for 3 h. The solvent was removed, the residue extracted with ethyl acetate (3 x 50 mL) and the combined phases dried over $MgSO_4$. After removal of the solvent in *vacuo*, the remaining solid was dissolved in a small amount of ethanol and left for crystallization at room temperature. After three days glyoxal bishydrazone could be obtained in the form of yellow crystals (12.0 g, 139 mmol, 58 %).

^{1}H NMR (DMSO-d_6, 25 °C, ppm) δ: 7.37 (s, 2H, -C*H*), 6.62 (s, 4H, -NH_2); ^{13}C NMR (DMSO-d_6, 25 °C, ppm) δ: 139.8 (-*C*HNNH$_2$).

Activated manganese dioxide was prepared according to the method described in literature:[S22] To a hot stirred solution of $KMnO_4$ (96.0 g, 0.61 mol) in water (600 mL) a solution of manganese sulfate tetrahydrate (110 g, 0.49 mol) in water (150 mL) and NaOH (40 % wt., 117 mL) were added simultaneously during one hour. After a few minutes, a dark brown solid began to precipitate. The obtained suspension was stirred for another hour to increase the yield of freshly precipitated MnO_2. Afterwards, the brown solid was collected and washed with water, until the washings lost their purple color caused by remaining $KMnO_4$. The obtained activated MnO_2 was dried in the drying oven at 100 °C.

Glyoxal bishydrazone (21.5 g, 249 mmol) was dispersed in acetonitrile (320 mL) at room temperature. Activated manganese dioxide[S22] (32.0 g, 0.367 mol) was added portion wise to the heavily stirred solution within 10 min. After 40 min, additional MnO_2 (11.0 g, 126 mmol) was added to the dark brown suspension and stirred for an additional 20 min. The resulting slurry was filtered through diatomaceous earth, the filtrate concentrated under reduced pressure and the residual viscous oil left for crystallization at 5 °C. After crystallization, the resulting solid was filtered off and sublimed at 80 °C yielding 1-amino-1,2,3-triazole (**1**) in the form of colorless crystals. Yield: 6.85 g (81.5 mmol, 33 %).

Amination of 1*H*-1,2,3-triazole:

The amination of 1*H*-1,2,3-triazole was performed in analogy to a modified literature synthetic protocol.[S23] 1*H*-1,2,3-Triazole (6.00 g, 86.7 mmol) was dissolved in water (600 mL) and treated with potassium hydroxide (23.2 g, 414 mmol). The obtained solution was heated to 70 °C, hydroxylamine-*O*-sulfonic acid (27.6 g, 244 mmol) was added portion wise and the resulting reaction mixture stirred for 1 h. The solution was neutralized with sodium bicarbonate followed by the evaporation of approximately two thirds of the solvent under reduced pressure. The residue was extracted with ethyl acetate (3 x 150 mL) and dried over magnesium sulfate. After filtration, the solvent was removed, and the crude isomeric mixture separated by column chromatography (SiO_2, ethyl acetate/ ethanol 9:1, R_f = 0.62, 0.32) yielding 2-amino-1,2,3-triazole (0.97 g, 11.5 mmol, 13 %) as liquid and 1-amino-1,2,3-triazole (**1**, 1.42 g, 16.8 mmol, 19 %) in the form of colorless crystals.

1-Amino-1,2,3-triazole (1)

DTA (5 °C min^{-1}): 39 °C(endothermic), 267 °C (endothermic, followed by exothermic signal); IR (ATR, cm^{-1}): $\tilde{\nu}$ = 3312 (m), 3203 (m), 3142 (s), 3122 (m), 2957 (w), 1757 (vw), 1684 (w), 1638 (s), 1513 (w), 1481 (s), 1382 (w), 1329 (w), 1317 (m), 1254 (w), 1223 (s), 1198 (m), 1115 (s), 1078 (s), 1029 (s), 983 (s), 945 (s), 881 (m), 806 (vs), 688 (m), 628 (m); ^{1}H NMR (DMSO-d_6, 25 °C, ppm) δ: 7.89 (d, 1H, C5-*H*), 7.64 (d, 1H, C4-*H*), 6.99 (s, 2H, -NH_2); ^{13}C NMR (DMSO-d_6, 25 °C, ppm) δ: 132.8 (*C*4-H), 124.4 (*C*5-H); EA: ($C_2H_4N_4$, 84.08) calcd: C 28.57, H 4.80, N 66.63 %; found: C 29.59, H 4.59, N 65.73 %; BAM drophammer: 35 J; friction tester: > 360 N; ESD: 1.50 J (at grain size 100–500 μm).

Amination of 1*H*-1,2,4-triazole:

The performed synthesis of ligand **2** was carried out according to a modified literature procedure.[S24] 1*H*-1,2,4-Triazole (6.70 g, 97.0 mmol) was dissolved in solution of potassium hydroxide (15.2 g, 271 mmol) in water (300 mL) and the resulting reaction mixture treated portion wise with hydroxylamine-*O*-sulfonic acid (27.6 g, 244 mmol) at a temperature of 70 °C. The pH-value was constantly checked and maintained between 8 and 9 through periodic addition of a saturated sodium bicarbonate solution. The reaction mixture was refluxed for 1 h, neutralized with $NaHCO_3$ and the solvent removed under reduced pressure. The residual solid was extracted with ethyl acetate (3 x 150 mL) and the combined organic phases dried over magnesium sulfate. $MgSO_4$ was filtered off and the filtrate concentrated leaving an isomeric mixture of 1-amino-1,2,4-triazole (**1**) and 4-amino-1,2,4-triazole. The isomers were purified by vacuum sublimation (80 °C, 1.5 x 10^{-2} mbar) resulting in the isolation of highly pure 1-amino-1,2,4-triazole (**2**, 2.50 g, 29.7 mmol, 31 %) in the form of colorless crystals suitable for X-ray diffraction.

1-Amino-1,2,4-triazole (2)

DTA (5 °C min^{-1}): 39 °C (endothermic), 222 °C (endothermic, followed by exothermic signal); IR (ATR, cm^{-1}): $\tilde{\nu}$ = 3299 (m), 3171 (m), 3141 (m), 3094 (s), 3020 (w), 2968 (m), 2856 (w), 2743 (w), 2689 (w), 2575 (w), 2496 (w), 1794 (w), 1654 (m), 1517 (m), 1481 (w), 1462 (m),

1379 (w), 1345 (w), 1277 (s), 1258 (w), 1226 (m), 1179 (w), 1135 (s), 1056 (w), 1011 (s), 1003 (s), 980 (m), 955 (s), 912 (m), 899 (s), 705 (m), 680 (vs), 648 (m), 628 (m); ^{1}H NMR (DMSO-d_6, 25 °C, ppm) δ: 8.29 (s, 1H, C-*H*), 7.81 (s, 1H, C-*H*), 6.53 (s, 2H, -N*H*$_2$); ^{13}C NMR (DMSO-d_6, 25 °C, ppm) δ: 148.9 (*C*-H), 142.3 (*C*-H); EA: ($C_2H_4N_4$, 84.08) calcd: C 28.57, H 4.80, N 66.63 %; found: C 28.27, H 5.18, N 60.87 %; BAM drophammer: > 40 J; friction tester: > 360 N; ESD: 1.50 J (at grain size 100–500 μm).

General procedure for the preparation of copper(II) chloride (3/4) and nitrate (5) based 1-ATRI complexes:

Aqueous or ethanolic (**4**) solutions of 1-amino-1,2,3-triazole (**1**, 42.0 mg, 0.50 mmol) were added dropwise to the corresponding copper(II) salt (**3**/**4**: copper(II) chloride dihydrate (42.6 mg, 0.25 mmol); **5**: copper(II) nitrate trihydrate (60.4 mg, 0.25 mmol)) dissolved in a minimum amount of water or ethanol (**4**). The resulting reaction mixtures were stirred mechanically for 1 min at room temperature and left to crystallize until a solid material appeared. The products obtained were filtered off, washed and dried in air.

[$CuCl_4$(1-$ATRI_H$)$_2$] (3)

A green precipitate, which emerged right after the addition of the ligand, has been dissolved by treatment of the reaction mixture with 1 M hydrochloric acid (2 mL). Within two weeks, X-ray suitable crystals were obtained in the form of green blocks. Yield: 68.0 mg (0.18 mmol, 71 %).

DTA (5 °C min^{-1}): 148 °C (endothermic, followed by exothermic signal); IR (ATR, cm^{-1}): $\tilde{\nu}$ = 3253 (m), 3198 (w), 3136 (m), 3092 (m), 2857 (w), 1825 (w), 1686 (w), 1598 (m), 1529 (m), 1465 (m), 1431 (m), 1394 (w), 1385 (w), 1334 (w), 1261 (w), 1234 (w), 1173 (m), 1152 (w), 1122 (m), 1080 (m), 1026 (m), 986 (s), 944 (m), 923 (m), 824 (m), 766 (vs), 697 (s), 635 (s); EA: ($C_4H_{10}Cl_4CuN_8$, 375.53): calcd: C 12.79, H 2.68, N 29.84 %; found: C 12.97, H 2.63, N 29.61 %; BAM drophammer: 35 J; friction tester: 216 N; ESD: 1.40 J (at grain size 100–500 μm).

$[CuCl_2(1\text{-}ATRI)_2]$ (4)

The copper(II) chloride complex **4** precipitated immediately after addition of the ligand in the form an amorphous green powder. Yield: 59.0 mg (0.19 mmol, 78 %).

DTA (5 °C min^{-1}): 165 °C (endothermic, followed by exothermic signal); IR (ATR, cm^{-1}): $\tilde{\nu}$ = 3284 (m), 3240 (m), 3181 (m), 3169 (m), 3137 (s), 2977 (w), 1682 (w), 1620 (s), 1493 (m), 1471 (m), 1353 (w), 1330 (w), 1316 (w), 1237 (w), 1203 (m), 1188 (w), 1132 (s), 1084 (s), 1045 (w), 1036 (w), 1018 (m), 996 (s), 972 (m), 882 (w), 797 (vs), 700 (m), 688 (w), 629 (w); UV-Vis spectrum: λ_{max} = 737 nm; EA: ($C_4H_8Cl_2CuN_8$, 302.61): calcd: C 15.80, H 2.66, N 37.03 %; found: C 16.18, H 2.78, N 36.48 %; BAM drophammer: > 40 J; friction tester: > 360 N; ESD: 0.70 J (at grain size < 100 µm).

$[Cu(NO_3)_2(\mu\text{-}1\text{-}ATRI)_2]$ (5)

After four days, blue rods suitable for X-ray diffraction were received for coordination compound **5**. Yield: 33.3 mg (0.09 mmol, 37 %).

DTA (5 °C min^{-1}): 167 °C (exothermic); IR (ATR, cm^{-1}): $\tilde{\nu}$ = 3165 (m), 3134 (m), 3068 (m), 3048 (m), 2758 (w), 2570 (vw), 2443 (vw), 2380 (vw), 2286 (vw), 1771 (vw), 1590 (m), 1532 (w), 1489 (w), 1389 (s), 1314 (vs), 1244 (s), 1224 (s), 1172 (m), 1143 (s), 1098 (s), 1054 (m), 1041 (s), 983 (m), 877 (w), 820 (m), 787 (s), 720 (m), 712 (m), 697 (m), 682 (m), 664 (w), 642 (m); UV-Vis spectrum: λ_{max} = 617 nm; EA: ($C_4H_8CuN_{10}O_6$, 355.72): calcd: C 13.51, H 2.27, N 39.28 %; found: C 13.33, H 2.54, N 39.24 %; ball drop impact tester: 66 mJ; BAM drophammer: < 1 J; friction tester: 30 N; ESD: 100 mJ (at grain size 100–500 µm).

General procedure for the preparation of the copper(II) 1-ATRI picrate (PA), 2,4,6-trinitro-3-hydroxyphenolate (HTNR), 2,4,6-trinitro-3,5-dihydroxyphenolate (H_2TNPG), styphnate (TNR) complexes (6–9):

Copper(II) carbonate (**6**: 61.8 mg, 0.50 mmol; **8**, **9**: 30.9 mg, 0.25 mmol) or copper(II) chloride (**7**: 42.6 mg, 0.25 mmol) and the corresponding trinitrobenzene derivative based acid (**6**: picric acid (229 mg, 1.00 mmol); **7**, **9**: styphnic acid (123 mg, 0.50 mmol); **8**: trinitrophloroglucinol

monohydrate (140 mg, 0.50 mmol)) were mechanically stirred in H_2O (5 mL) at 70 °C. After a clear solution was obtained, the reaction mixture was treated under stirring with 1-amino-1,2,3-triazole (**7**, **9**: 42.0 mg, 0.50 mmol; **6**, **8**: 84.1 mg, 1.00 mmol) and finally left for crystallization until a solid material appeared. After crystallization, the complexes were filtered off, washed with cold ethanol and dried in air.

$[Cu(H_2O)_4(1\text{-ATRI})_2](PA)_2$ (6)

The copper(II) picrate complex **6** could be obtained within one day in the form of green blocks suitable for X-ray determination. Yield: 167 mg (0.21 mmol, 43 %).

DTA (5 °C min^{-1}): 66 °C (endothermic), 188 °C (exothermic); IR (ATR, cm^{-1}): $\tilde{\nu}$ = 3348 (m), 3264 (m), 3200 (m), 3159 (m), 3143 (m), 3082 (m), 1613 (s), 1568 (s), 1533 (s), 1515 (s), 1502 (s), 1423 (m), 1365 (m), 1332 (vs), 1275 (vs), 1238 (s), 1167 (s), 1140 (s), 1088 (s), 1048 (m), 978 (m), 945 (m), 932 (m), 914 (m), 838 (s), 806 (m), 789 (s), 743 (s), 716 (s), 695 (s), 627 (s); UV-Vis spectrum: λ_{max} = 393, 708 nm; EA: ($C_{16}H_{20}CuN_{14}O_{18}$, 759.96): calcd: C 25.29, H 2.65, N 25.80 %; found: C 25.30, H 2.61, N 25.62 %; BAM drophammer: > 40 J; friction tester: > 360 N; ESD: 1.22 J (at grain size 500–1000 μm).

$[Cu(HTNR)_2(1\text{-ATRI})_2]$ (7)

Green blocks suitable for X-ray diffraction of the copper(II) complex compound **7** were obtained in less than one day. Yield: 102 mg (0.14 mmol, 56 %).

DTA (5 °C min^{-1}): 177 °C (exothermic); IR (ATR, cm^{-1}): $\tilde{\nu}$ = 3333 (w), 3285 (w), 3222 (w), 3165 (w), 3140 (m), 1628 (s), 1562 (s), 1528 (vs), 1499 (s), 1451 (s), 1371 (s), 1315 (s), 1278 (vs), 1269 (vs), 1227 (s), 1189 (s), 1172 (s), 1142 (s), 1085 (vs), 982 (s), 927 (s), 820 (s), 778 (s), 761 (s), 733 (m), 710 (s), 697 (vs), 672 (s), 656 (s); UV-Vis spectrum: λ_{max} = 408, 737 nm; EA: ($C_{16}H_{12}CuN_{14}O_{16}$, 719.90): calcd: C 26.69, H 1.68, N 27.24 %; found: C 26.73, H 1.77, N 26.97 %; BAM drophammer: 1.5 J; friction tester: 80 N; ESD: 40 mJ (at grain size 500–1000 μm).

$[Cu(H_2O)_2(1\text{-ATRI})_4](H_2TNPG)_2$ (8)

Within 10 days, complex **8** emerged in the form of dark green blocks suitable for X-ray determination. Yield: 200 mg (0.21 mmol, 84 %).

DTA (5 °C min^{-1}) onset: 123 °C (endothermic), 153 °C (exothermic); IR (ATR, cm^{-1}): $\tilde{\nu}$ = 3594 (w), 3341 (m), 3291 (w), 3228 (w), 3157 (m), 3145 (m), 1647 (s), 1573 (s), 1523 (s), 1491 (vs), 1472 (s), 1403 (m), 1339 (vs), 1235 (m), 1224 (m), 1179 (vs), 1137 (vs), 1082 (s), 1046 (m), 984 (m), 960 (m), 913 (m), 875 (w), 836 (m), 811 (s), 802 (s), 779 (m), 757 (m), 742 (s), 689 (s), 668 (m), 644 (m), 626 (m); UV-Vis spectrum: λ_{max} = 408, 595 nm; EA: ($C_{20}H_{24}CuN_{22}O_{20}$, 956.09): calcd: C 25.13, H 2.53, N 32.23 %; found: C 25.12, H 2.54, N 32.03 %; BAM drophammer: 2 J; friction tester: 160 N; ESD: 300 mJ (at grain size 100–500 μm).

$[Cu(\mu\text{-TNR})(1\text{-ATRI})_2]$ (9)

The copper(II) styphnate complex **9** was received within one day in form of green blocks suitable for X-ray diffraction. Yield: 108 mg (0.23 mmol, 91 %).

DTA (5 °C min^{-1}) onset: 194 °C (exothermic); IR (ATR, cm^{-1}) $\tilde{\nu}$ = 3322 (w), 3282 (w), 3228 (w), 3209 (w), 3155 (w), 3135 (m), 1603 (m), 1583 (m), 1560 (m), 1545 (m), 1536 (m), 1522 (m), 1474 (s), 1460 (m), 1427 (s), 1374 (m), 1351 (m), 1280 (s), 1227 (s), 1171 (s), 1142 (s), 1133 (s), 1100 (s), 1085 (vs), 1043 (s), 984 (s), 972 (s), 954 (s), 938 (s), 914 (m), 899 (m), 826 (m), 793 (s), 779 (s), 736 (m), 705 (vs), 684 (s), 631 (s), 623 (s); UV-Vis spectrum: λ_{max} = 408, 711 nm; EA: ($C_{10}H_9CuN_{11}O_8$, 474.80): calcd: C 25.30, H 1.91, N 32.45 %; found: C 25.19, H 2.09, N 31.43 %; BAM drophammer: 3 J; friction tester: 60 N; ESD: 50 mJ (at grain size 100–500 μm).

General procedure for the preparation of metal(II) (Cu^{II}, Mn^{II}, Fe^{II}, Zn^{II}) 1-ATRI perchlorate complexes (10–13):

The nitrogen-rich ligand 1-ATRI (**10**: 84.1 mg, 1.00 mmol; **11**–**13**: 126 mg, 1.50 mmol) was dissolved in water (**10**, 2 mL) or ethanol (2 mL) and added dropwise to an aqueous (**10**) or

ethanolic solution (1 mL) of the corresponding metal(II) perchlorate (**10**: $Cu(ClO_4)_2 \cdot 6\ H_2O$ (92.6 mg, 0.25 mmol), **11**: $Mn(ClO_4)_2 \cdot 6\ H_2O$ (91.0 mg, 0.25 mmol), **12**: $Fe(ClO_4)_2 \cdot 6\ H_2O$ (63.7 mg, 0.25 mmol), **13**: $Zn(ClO_4)_2 \cdot 6\ H_2O$ (93.1 mg, 0.25 mmol)). The colored reaction mixtures were mechanically stirred for 1 min at room temperature and left for crystallization. The products were filtered off, washed and dried in air.

$[Cu(H_2O)_2(1\text{-ATRI})_4](ClO_4)_2$ (10)

The promising copper(II) perchlorate complex **10** was received within four days in the form of blue plates suitable for X-ray diffraction. Yield: 138 mg (0.22 mmol, 87 %).

DTA (5 °C min^{-1}): 167 °C (exothermic); IR (ATR, cm^{-1}): $\tilde{\nu}$ = 3347 (w), 3302 (m), 3218 (w), 3171 (m), 3155 (m), 1653 (vw), 1606 (w), 1506 (w), 1487 (w), 1474 (w), 1340 (vw), 1249 (w), 1224 (w), 1096 (s), 1063 (vs), 974 (s), 935 (m), 788 (s), 703 (w), 688 (w), 619 (s); UV-Vis spectrum: λ_{max} = 618 nm; EA: ($C_8H_{20}Cl_2CuN_{16}O_{10}$, 634.80): calcd: C 15.14, H 3.18, N 35.30 %; found: C 15.29, H 3.11, N 35.35 %; ball drop impact tester: < 4 mJ; BAM drophammer: 1 J; friction tester: 0.45 N; ESD: 100 mJ (at grain size 500–1000 μm).

$[Mn(1\text{-ATRI})_6](ClO_4)_2$ (11)

Complex **11** was isolated after one day in the form of a colorless solid. Yield: 43.2 mg (0.06 mmol, 23 %).

DTA (5 °C min^{-1}) onset: 161 °C (endothermic), 194 °C (exothermic); IR (ATR, cm^{-1}): $\tilde{\nu}$ = 3351 (m), 3285 (w), 3171 (w), 2001 (w), 1668 (w), 1612 (m), 1503 (w), 1486 (w), 1474 (m), 1225 (m), 1126 (m), 1093 (s), 1073 (vs), 1041 (s), 971 (s), 956 (m), 788 (s), 623 (s); EA ($C_{12}H_{24}Cl_2MnN_{24}O_8$, 758.32): calcd: C 19.01, H 3.19, N 44.33 %; found: C 19.01, H 3.23, N 43.21 %; ball drop impact tester: > 100 mJ; BAM drophammer: 3 J; friction tester: 10 N; ESD: 60 mJ (at grain size 100–500 μm).

[Fe(1-ATRI)$_6$](ClO$_4$)$_2$ (12)

[Fe(1-ATRI)$_6$](ClO$_4$)$_2$ (**12**) was isolated after one day in the form of colorless blocks suitable for X-ray diffraction. Yield: 118 mg (0.16 mmol, 62 %).

DTA (5 °C min^{-1}) onset: 166 °C (exothermic); IR (ATR, cm^{-1}): $\tilde{\nu}$ = 3353 (m), 3286 (w), 3209 (w), 3174 (w), 3158 (w), 1611 (w), 1504 (w), 1487 (w), 1473 (w), 1225 (m), 1128 (m), 1094 (s), 1073 (vs), 1041 (s), 969 (m), 954 (m), 877 (w), 788 (s), 704 (w), 622 (s); UV-Vis spectrum: λ_{max} = 950 nm; EA ($C_{12}H_{24}Cl_2FeN_{24}O_8$, 759.23): calcd: C 18.98, H 3.19, N 44.28 %; found: C 19.27, H 3.34, N 42.92 %; ball drop impact tester: 29 mJ; BAM drophammer: 1.5 J; friction tester: 2 N; ESD: 36 mJ (at grain size 100–500 µm).

[Zn(1-ATRI)$_6$](ClO$_4$)$_2$ (13)

The zinc(II) perchlorate complex **13** was obtained within several hours in the form of colorless single crystals suitable for X-ray diffraction. Yield: 99.3 mg (0.13 mmol, 52 %).

DTA (5 °C min^{-1}) onset: 91 °C (endothermic), 188 °C (exothermic); IR (ATR, cm^{-1}): $\tilde{\nu}$ = 3353 (w), 3334 (w), 3283 (w), 3207 (vw), 3169 (w), 3136 (w), 1610 (m), 1504 (w), 1472 (w), 1243 (w), 1228 (m), 1144 (w), 1123 (m), 1095 (s), 1070 (vs), 1042 (s), 982 (m), 967 (s), 955 (m), 893 (w), 879 (w), 789 (s), 705 (w), 693 (w), 622 (s); EA ($C_{12}H_{24}Cl_2N_{24}O_8Zn$, 768.77): calcd: C 18.75, H 3.15, N 43.73 %; found: C 18.73, H 3.11, N 42.47 %; ball drop impact tester: 53 mJ; BAM drophammer: 3 J; friction tester: 6.75 N; ESD: 65 mJ (at grain size 100–500 µm).

[Zn(1-ATRI)$_4$](NO$_3$)$_2$ (14)

The zinc(II) nitrate complex **14** was prepared through slow addition of an ethanolic solution (2 mL) of 1-amino-1,2,3-triazole (**1**, 84.1 mg, 1.00 mmol) to Zn(NO$_3$)$_2$ · 6 H$_2$O (74.4 mg, 0.25 mmol) dissolved in ethanol (1 mL) followed by 1 minute of stirring mechanically. The synthesized complex **14** was obtained after three days in the form of colorless blocks suitable for X-ray diffraction. Yield: 59.0 mg (0.11 mmol, 45 %).

DTA (5 °C min^{-1}) onset: 134 °C (endothermic), 188 °C (exothermic); IR (ATR, cm^{-1}): $\tilde{\nu}$ = 3350 (w), 3292 (m), 3154 (m), 3119 (m), 1615 (m), 1494 (w), 1470 (m), 1379 (s), 1339 (s),

1308 (vs), 1251 (m), 1226 (s), 1145 (s), 1102 (m), 1085 (m), 1051 (m), 1044 (m), 1005 (s), 912 (w), 828 (m), 800 (s), 704 (w), 694 (w), 636 (w), 623 (w); EA ($C_8H_{16}N_{18}O_6Zn$, 525.72): calcd: C 18.28, H 3.07, N 47.96 %; found: C 18.39, H 3.14, N 47.97 %; BAM drophammer: 6 J; friction tester: 45 N; ESD: 700 mJ (at grain size 100–500 μm).

[Cu(μ-TNR)(1-A-1,2,4-TRI)$_2$] (15)

Styphnic acid (49.0 mg, 0.20 mmol) and copper(II) carbonate (24.7 mg, 0.20 mmol) were stirred at 70 °C until all starting materials dissolved. 1-Amino-1,2,4-triazole (33.6 mg, 0.40 mmol) was dissolved in a small amount of water, added dropwise to the stirring solution and subsequently left for crystallization. The copper(II) complex **15** was yielded after two days in the form of green blocks suitable for X-ray diffraction. The product was filtered off, washed and dried in air. Yield: 63.6 mg (0.13 mmol, 67 %).

DTA (5 °C min^{-1}) onset: 237 °C (exothermic); IR (ATR, cm^{-1}): $\tilde{\nu}$ = 3325 (w), 3220 (w), 3130 (w), 1771 (w), 1610 (s), 1581 (m), 1544 (s), 1518 (s), 1491 (m), 1483 (m), 1438 (s), 1379 (m), 1359 (m), 1277 (vs), 1232 (vs), 1207 (vs), 1172 (s), 1124 (s), 1097 (s), 1016 (s), 993 (s), 909 (m), 884 (m), 826 (w), 780 (s), 735 (w), 708 (vs), 670 (vs), 632 (m), 624 (m), 577 (w); UV-Vis spectrum: λ_{max} = 410, 732 nm; EA ($C_{10}H_9CuN_{11}O_8$, 474.80): calcd: C 25.30, H 1.91, N 32.45 %; found: C 25.33, H 2.17, N 31.87 %; BAM drophammer: 30 J; friction tester: 240 N; ESD: 90 mJ (at grain size 100–500 μm).

[Cu(ClO$_3$)$_2$(1-A-1,2,4-TRI)$_4$] (16)

Complex **16** was synthesized through slow combination of an ethanolic solution (2 mL) of 1-amino-1,2,4-triazole (**2**, 168 mg, 2.00 mmol) and copper(II) chlorate (115 mg, 0.50 mmol) dissolved in ethanol (1 mL). The desired complex precipitated in form of a purple microcrystalline powder suitable for X-ray diffraction and the resulting mixture was stirred overnight. After filtration of the product, the complex has been washed and dried in air. Yield: 232 mg (0.41 mmol, 82 %).

DTA (5 °C min^{-1}) onset: 132 °C (exothermic); IR (ATR, cm^{-1}): $\tilde{\nu}$ = 3300 (w), 3218 (w), 3134 (w), 1638 (w), 1538 (w), 1486 (w), 1346 (vw), 1292 (m), 1220 (m), 1130 (m), 1013 (m), 945

(vs), 932 (vs), 893 (s), 886 (s), 711 (w), 674 (vs), 631 (m), 604 (m), 528 (vw), 483 (m), 473 (s), 460 (m), 442 (m), 410 (w); UV-Vis spectrum: λ_{max} = 565 nm; EA ($C_8H_{16}Cl_2CuN_{16}O_6$, 566.77): calcd: C 16.95, H 2.85, N 39.54 %; found: C 16.97, H 2.66, N 39.85 %; ball drop impact tester: 8 mJ; BAM drophammer: < 1 J; friction tester: 23 N; ESD: 14 mJ (at grain size < 100 µm).

19.12.10 References

[S1] *CrysAlisPro*, Oxford Diffraction Ltd., version 171.33.41, **2009**.

[S2] A. Altomare, G. Cascarano, C. Giacovazzo, A. Guagliardi, *J. Appl. Crystallogr.*, **1992**, *26*, 343–350.

[S3] a) A. Altomare, G. Cascarano, C. Giacovazzo, A. Guagliardi, A. G. G. Moliterni, M. C. Burla, G. Polidori, M. Camalli, R. Spagna, *SIR97*, **1997**; b) A. Altomare, M. C. Burla, M. Camalli, G. L. Cascarano, C. Giacovazzo, A. Guagliardi, A. G. G. Moliterni, G. Polidori, R. Spagna, *J. Appl. Crystallogr.*, **1999**, *32*, 115–119.

[S4] a) G. M. Sheldrick, *SHELXL-97*, *Program for the Refinement of Crystal Structures*, University of Göttingen, Germany, **1997**; b) G. M. Sheldrick, *Acta Crystallogr. Sect. A*, **2008**, *64*, 112–122.

[S5] A. L. Spek, *PLATON*, *A Multipurpose Crystallographic Tool*, Utrecht University, The Netherlands, **1999**.

[S6] L. J. Farrugia, *J. Appl. Cryst.*, **2012**, *45*, 849–854.

[S7] Empirical absorption correction using spherical harmonics, implemented in SCALE3 ABSPACK scaling algorithm (CrysAlisPro Oxford Diffraction Ltd., Version 171.33.41, **2009**).

[S8] *APEX3*. Bruker AXS Inc., Madison, Wisconsin, USA.

[S9] M. H. H. Wurzenberger, N. Szimhardt, J. Stierstorfer, *J. Am. Chem. Soc.* **2018**, *140*, 3206–3209.

[S10] NATO standardization agreement (STANAG) on explosives, impact sensitivity tests, no. 4489, 1st ed., Sept. 17, **1999**.

[S11] WIWEB-Standardarbeitsanweisung 4-5.1.02, Ermittlung der Explosionsgefährlichkeit, hier der Schlagempfindlichkeit mit dem Fallhammer, Nov. 8, **2002**.

[S12] http://www.ozm.cz, Accessed May 2018.

[S13] http://www.bam.de, Accessed May 2018.

[S14] Military Standard 1751A (MIL-STD-1751A): safety and performance tests for qualification of explosives (high explosives, propellants and pyrotechnics), method 1016, Dec. 11, **2001**.

[S15] UN Model Regulation: Recommendations on the Transport of Dangerous Goods – Manual of Tests and Criteria, section 13.4.2.3.3, **2015**.

[S16] NATO standardization agreement (STANAG) on explosive, friction sensitivity tests, no. 4487, 1st ed., Aug. 22, **2002**.

[S17] WIWEB-Standardarbeitsanweisung 4-5.1.03, Ermittlung der Explosionsgefährlichkeit oder der Reibeempfindlichkeit mit dem Reibeapparat, Nov. 8, **2002**.

[S18] Impact: insensitive > 40 J, less sensitive ≥ 35 J, sensitive ≥ 4 J, very sensitive ≤ 3 J; Friction: insensitive > 360 N, less sensitive = 360 N, sensitive < 360 N and > 80 N, very sensitive ≤ 80 N, extremely sensitive ≤ 10 N. According to the UN Recommendations on the Transport of Dangerous Goods, (+) indicates not safe for transport.

[S19] R. Scharf, PhD thesis, Ludwig-Maximilians Universität München, **2016**.

[S20] K. Shigeno, T. Ono, M. Tanaka, S. Yamada, T. Asao, *EP0727418B1* **1999**.

[S21] G. Kaplan, G. Drake, K. Tollison, L. Hall, T. Hawkins, *J. Heterocyclic Chem.* **2005**, *42*, 19–27.

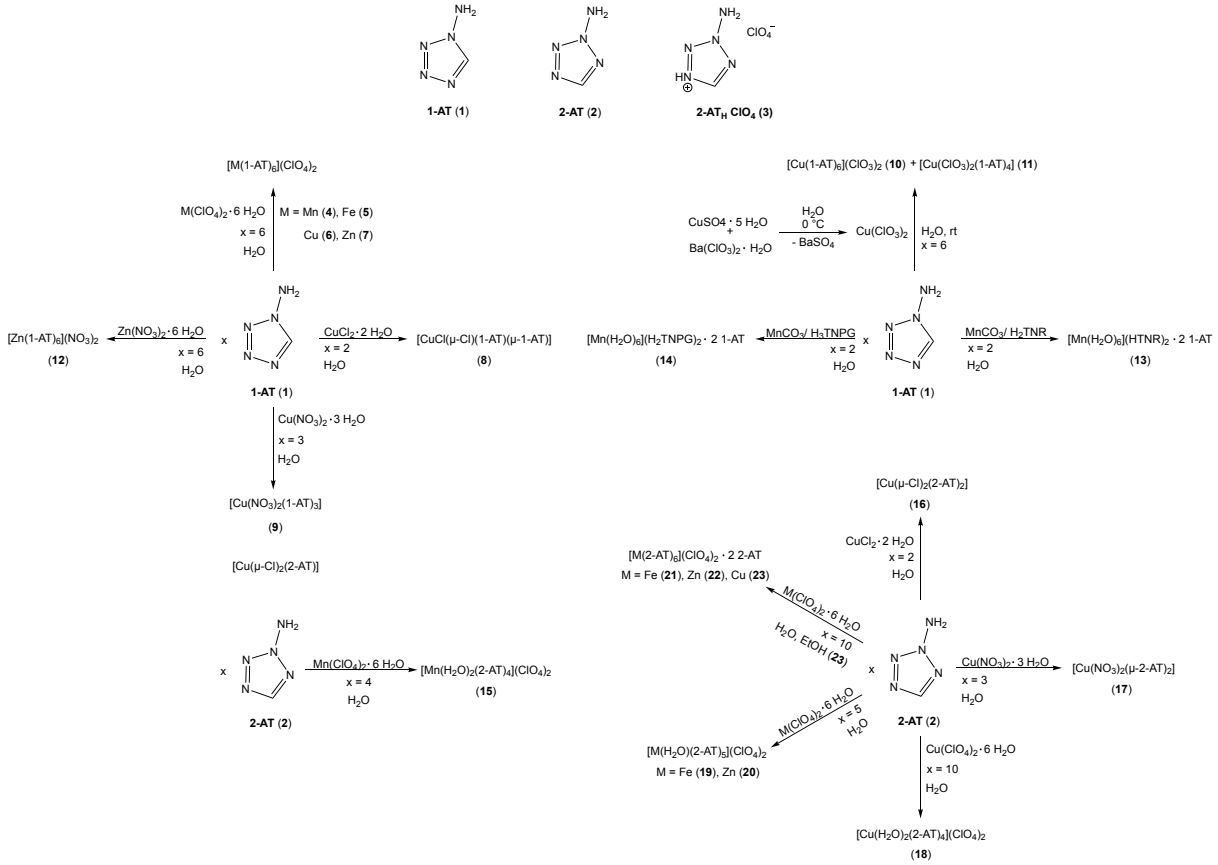
[S22] J. Attenburrow, A. F. B. Cameron, J. H. Chapman, R. M. Evans, B. A. Hems, A. B. A. Jansen, T. Walker, *J. Chem. Soc.* **1952**, 1094–1111.

[S23] H-X. Hu, H-X Niu, Y. Wang, Y-C. Li, S-P. Pang, *Mater. Res. Innovations* **2014**, *18*, 1127–1131.

[S24] G. Laus, W. Kloetzer, *Synthesis* **1989**, 269–272.

19.13 Supplementary Information: Maximization of the Energy Capability Level in Transition Metal Complexes through Application of 1-Amino- and 2-Amino-5*H*-tetrazole Ligands

19.13.1 Compounds Overview



19.13.2 IR Spectroscopy of 1–9, 12 and 16–23

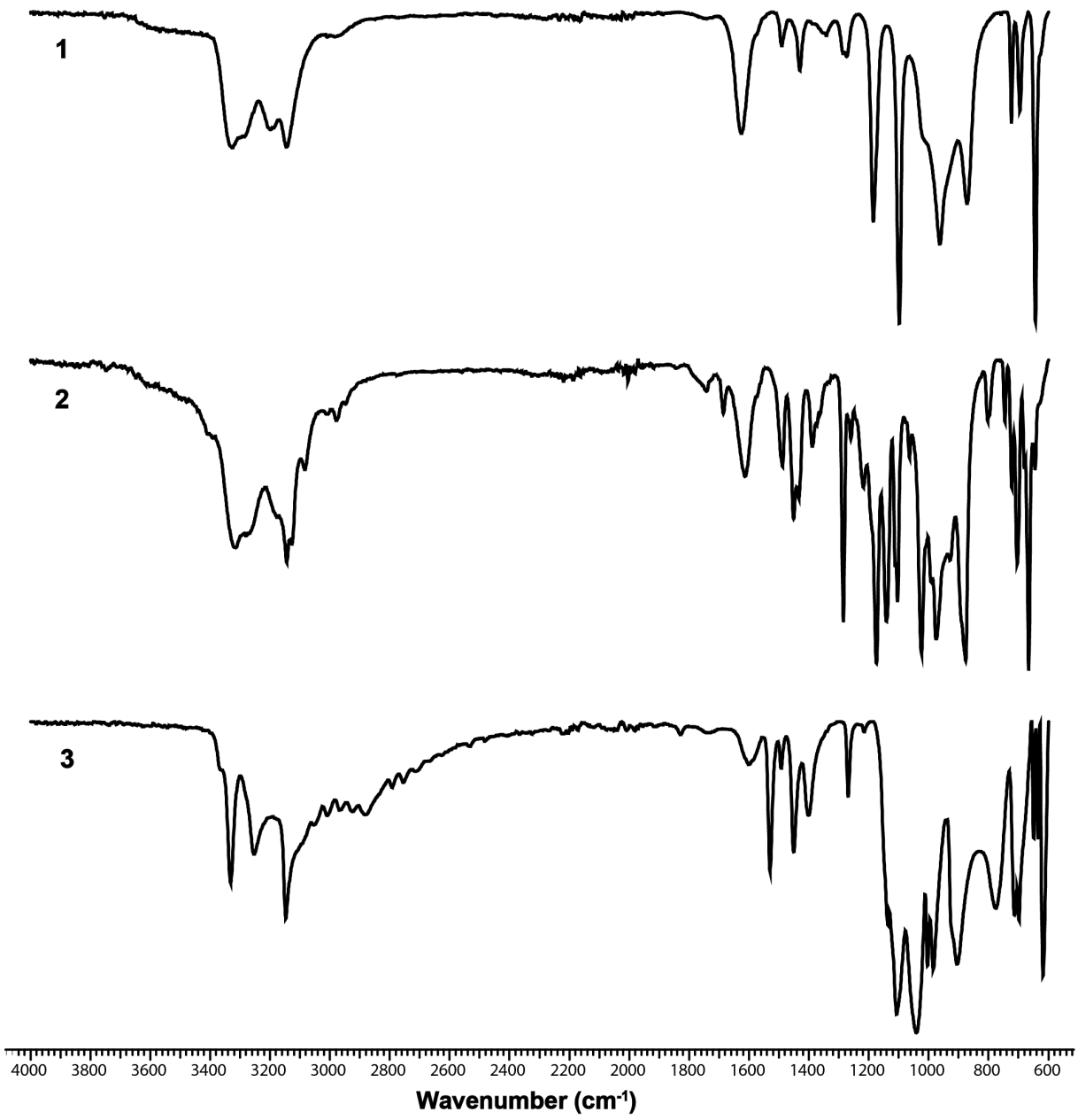


Figure S1. Infrared spectra of nitrogen-rich compounds **1**–**3**.

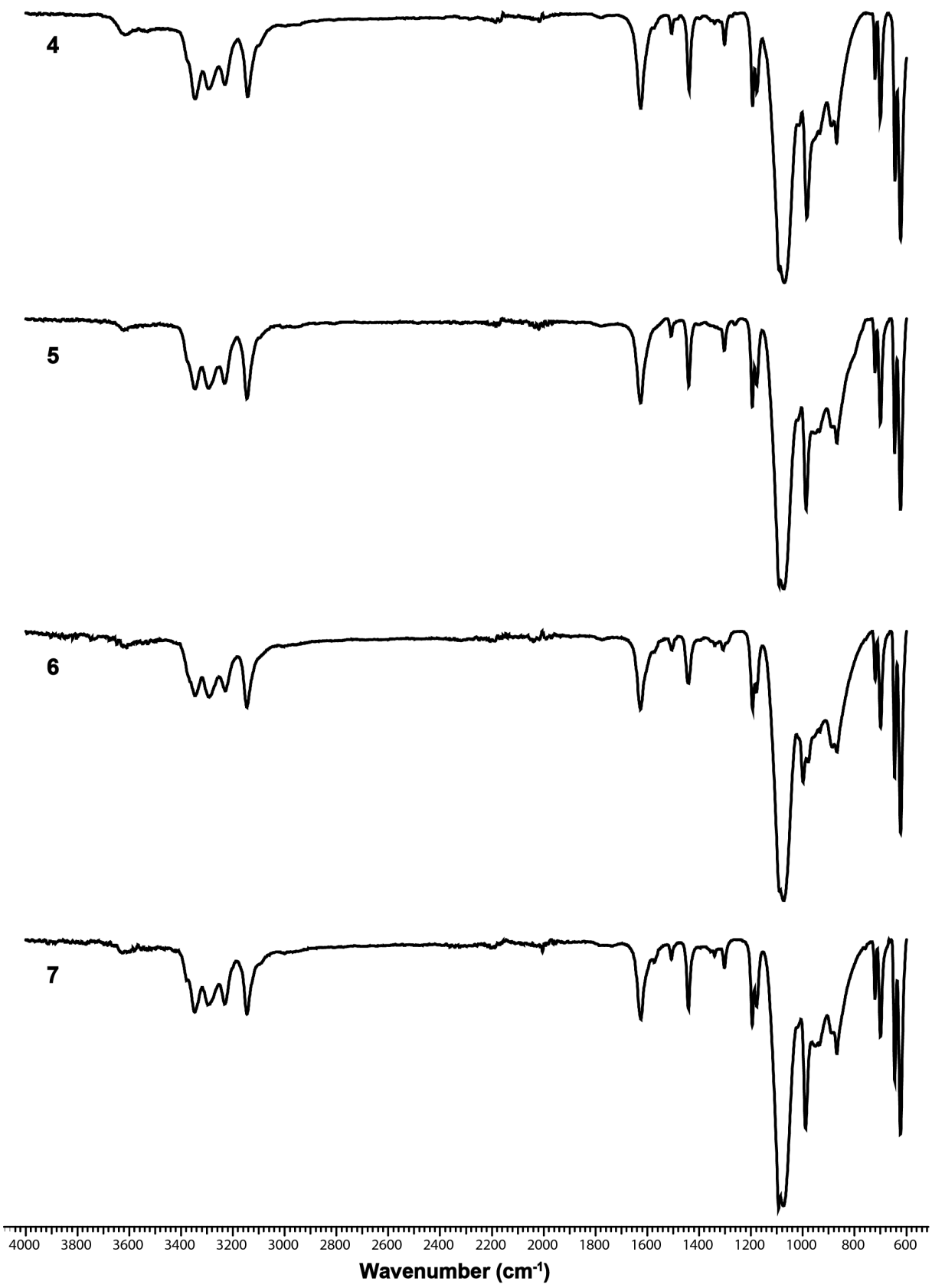


Figure S2. IR spectra of **4**–**7**.

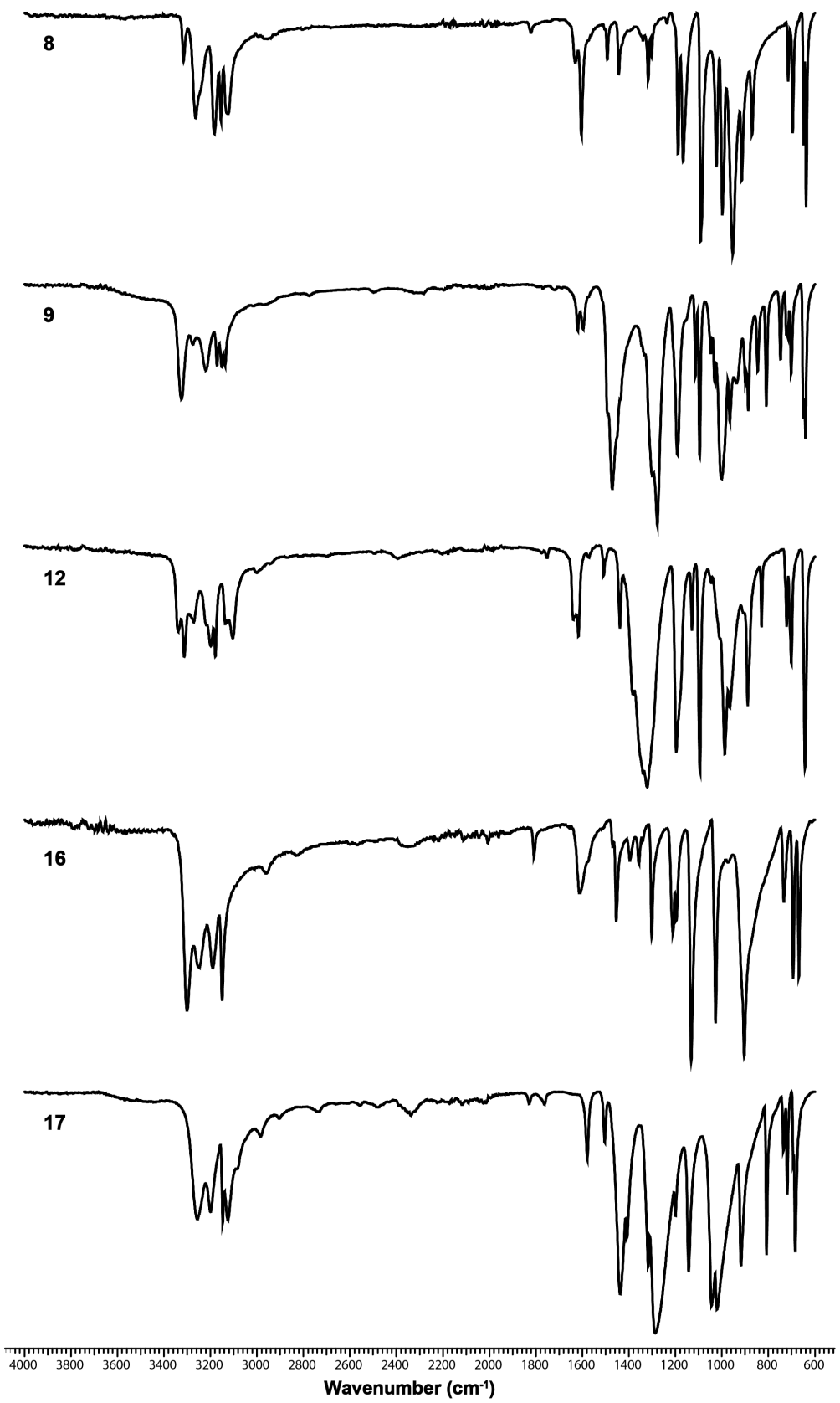


Figure S3. Infrared spectra of **8**, **9**, **12**, **16**, and **17**.

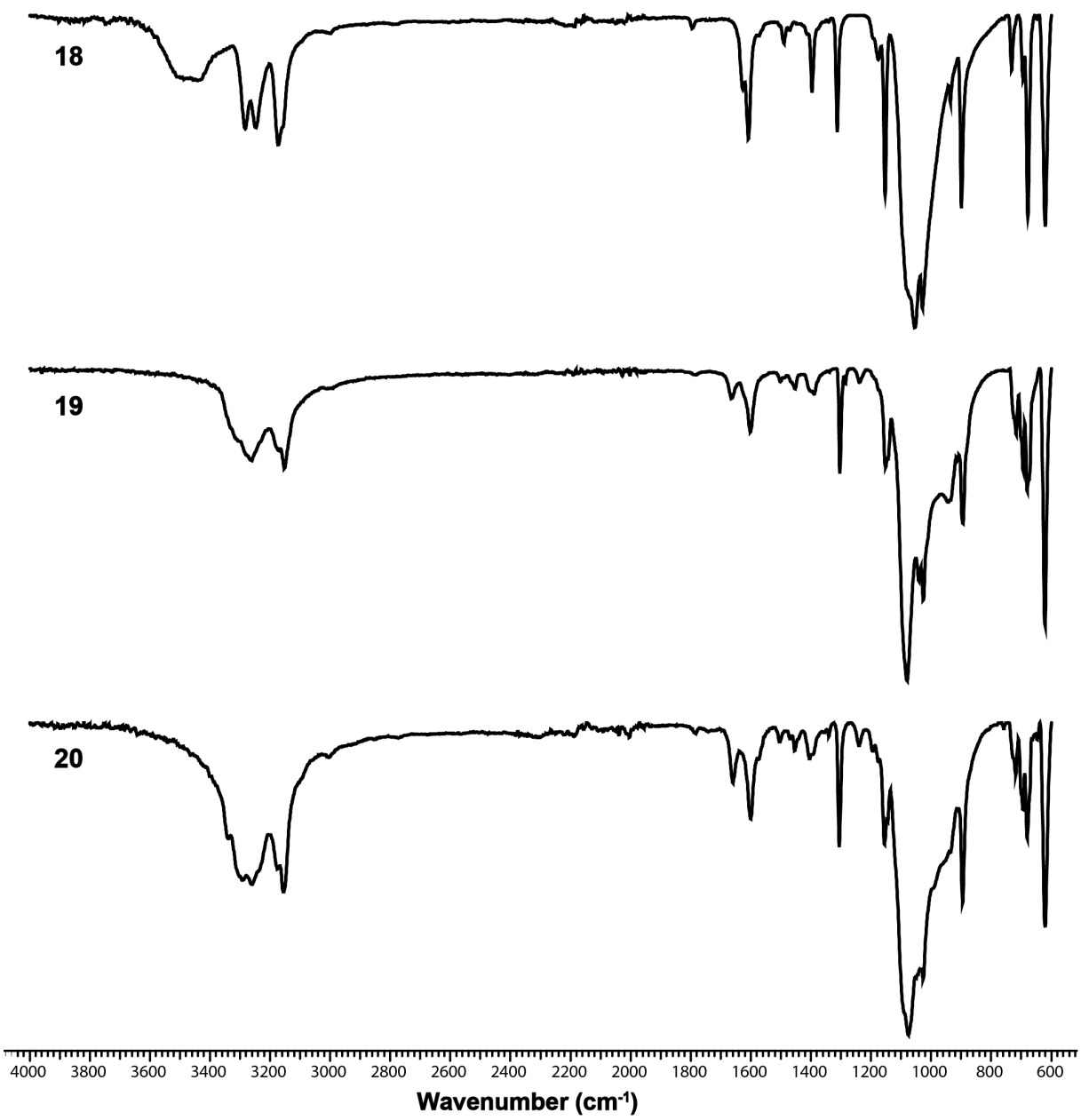


Figure S4. Infrared spectra of coordination compounds **18**–**20**.

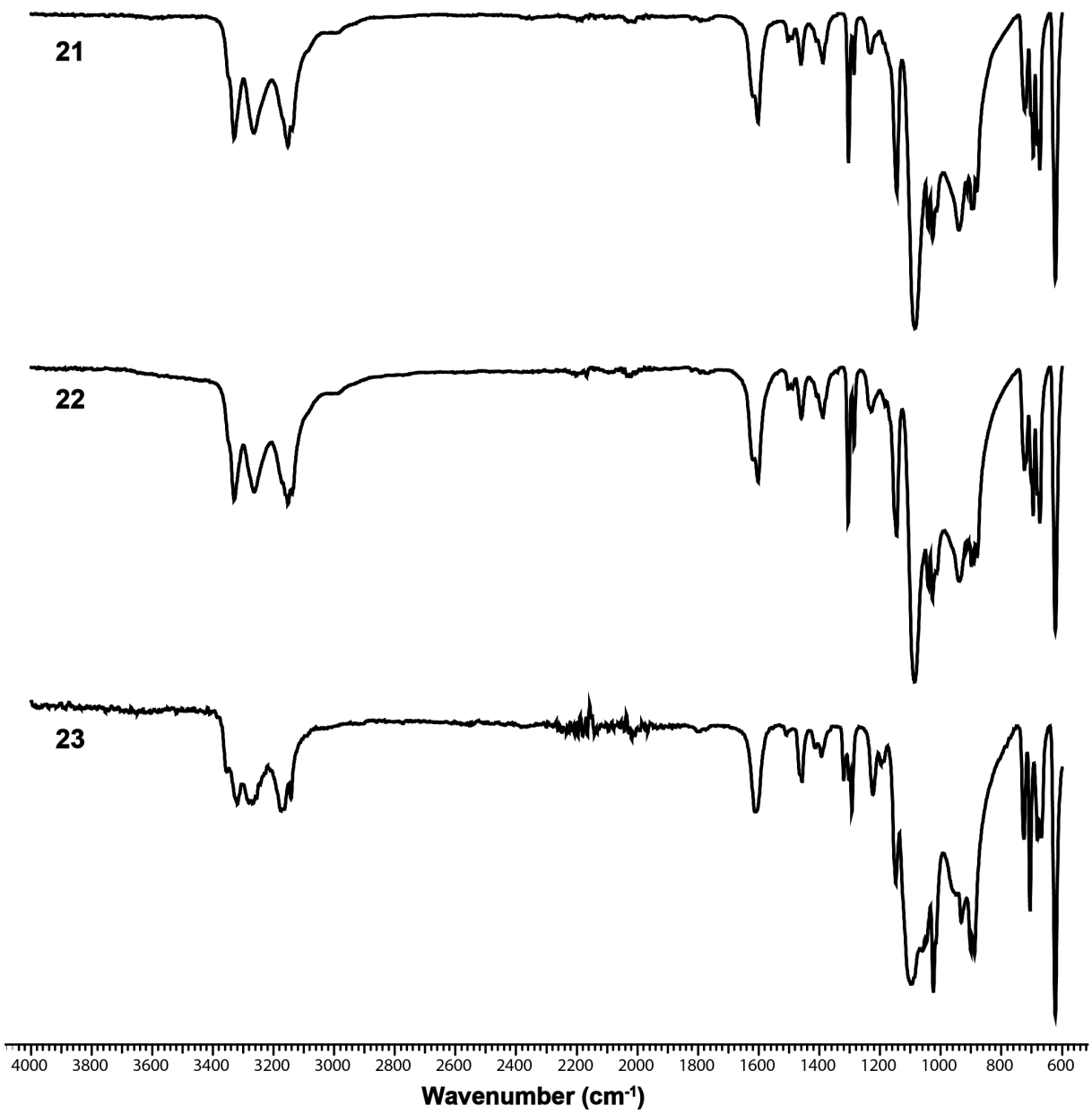


Figure S5. Infrared spectra of complexes **21**–**23**.

19.13.3 X-ray Diffraction

For all crystalline compounds, an Oxford Xcalibur3 diffractometer with a CCD area detector or Bruker D8 Venture TXS diffractometer equipped with a multilayer monochromator, a Photon 2 detector and a rotating-anode generator were employed for data collection using Mo-*K*α radiation (λ = 0.7107 Å). On the Oxford device, data collection and reduction were carried out using the Crysalispro software.[S1] On the Bruker diffractometer, the data were collected with the Bruker Instrument Service v3.0.21, the data reduction was performed using the SAINT V8.18C software (Bruker AXS Inc., 2011). The structures were solved by direct methods (Sir-92[S2], Sir-97[S3] or Shelxs-97[S4]) and refined by full-matrix least-squares on *F*2 (ShelxL[S4]) and finally checked using the platon software[S5] integrated in the WinGX[S6] software suite. The non-hydrogen atoms were refined anisotropically and the hydrogen atoms were located and freely refined. The absorptions were corrected by a Scale3 Abspack or Sadabs Bruker Apex3 multiscan method.[S7,8] All Diamond2 plots are shown with thermal ellipsoids at the 50% probability level and hydrogen atoms are shown as small spheres of arbitrary radius. X-ray powder experiments were performed on a Gunier diffractometer (Huber G644) with Mo-*K*α1 radiation (λ = 0.7093 Å, quartz monochromator) in Lindemann capillaries (0.7 mm diameter). The angle calibration was performed with electronic grade germanium. In the 2θ range between 4 and 34° with an increment of 0.04°, 750 data points were collected with a counting rate of 10 s for each increment. The Rietveld parameters were analyzed with the program FullProf.[S9]

Table S1. Crystallographic data of **1** and **3**–**5**.

	1	**3**	**4**	**5**
Formula	CH_3N_5	$CH_4ClN_5O_4$	$C_6H_{18}Cl_2MnN_{30}O_8$	$C_6H_{18}Cl_2FeN_{30}O_8$
FW [g mol^{-1}]	85.08	185.54	764.34	765.25
Crystal system	Orthorhombic	Monoclinic	Trigonal	Trigonal
Space Group	$P2_12_12_1$	$P2_1/n$	$P\bar{3}$	$P\bar{3}$
Color / Habit	Colorless block	Colorless block	Light-rose block	Colorless block
Size [mm]	0.20 x 0.40 x 0.50	0.13 x 0.19 x 0.42	0.15 x 0.15 x 0.15	0.23 x 0.30 x 0.50
a [Å]	5.0889(3)	5.5236(4)	10.9978(13)	18.8934(4)
b [Å]	6.5662(5)	8.3025(7)	10.9978(13)	18.8934(4)
c [Å]	11.1652(8)	13.6929(11)	6.9815(11)	6.9830(2)
α [°]	90	90	90	90
β [°]	90	90.247(5)	90	90
γ [°]	90	90	120	120
V [Å^3]	373.08(4)	627.95(9)	731.3(2)	2158.70(13)
Z	4	4	1	3
$\rho_{calc.}$ [g cm^{-3}]	1.515	1.963	1.736	1.766
μ [mm^{-1}]	0.119	0.586	0.725	0.802
F(000)	176	376	387	1164
$\lambda_{MoK\alpha}$ [Å]	0.71073	0.71073	0.71073	0.71073
T [K]	173	173	143	173
θ Min–Max [°]	4.4, 26.0	4.4, 26.0	4.3, 27.5	4.3, 26.2
Dataset	−5: 6; −7: 8; −13: 13	−6: 6; −10: 10; −16: 10	−13: 14; −12: 14; −9: 8	−23: 22; −20: 23; −8: 8
Reflections collected	2753	4330	5123	16975
Independent refl.	730	1228	1085	2898
Rint	0.017	0.027	0.079	0.024
Observed reflections	701	1098	703	2492
Parameters	67	117	104	286
R_1 (obs)[a]	0.0208	0.0272	0.1197	0.0637
wR_2 (all data)[b]	0.0504	0.0732	0.3420	0.1923
GooF[c]	1.13	1.07	1.19	1.06
Resd. Dens. [e Å^{-3}]	−0.13, 0.12	−0.42, 0.20	−0.74, 1.07	−1.13, 1.58
Absorption correction	multi-scan	multi-scan	multi-scan	multi-scan
CCDC	1834855	1834849	—	1834847

a) $R_1 = \Sigma||F_0|- |F_c||/ \Sigma|F_0|$; b) $wR_2 = [\Sigma[w(F_0^2-F_c^2)^2]/\Sigma[w(F_0)^2]]^{1/2}$; $w = [\sigma c^2(F_0^2)+(xP)^2+yP]^{-1}$ and $P=(F_0^2+2F_c^2)/3$; c) GooF = $\{\Sigma[w(F_o^2-F_c^2)^2]/(n-p)\}^{1/2}$ (n = number of reflections; p = total number of parameters).

Table S2. Crystallographic data of **6**–**9**.

	6	**7**	**8**	**9**
Formula	$C_6H_{18}Cl_2CuN_{30}O_8$	$C_6H_{18}Cl_2N_{30}O_8Zn$	$C_2H_6Cl_2CuN_{10}$	$C_3H_9CuN_{17}O_6$
FW [g mol^{-1}]	772.94	774.77	304.61	442.81
Crystal system	Trigonal	Trigonal	Monoclinic	Monoclinic
Space Group	*P*–3	*P*–3	$P2_1/n$	*Cc*
Color / Habit	Blue block	Colorless block	Green block	Blue block
Size [mm]	0.14 x 0.20 x 0.28	0.10 x 0.32 x 0.38	0.09 x 0.13 x 0.20	0.11 x 0.12 x 0.34
a [Å]	21.8207(4)	18.908(5)	7.4976(2)	15.301(5)
b [Å]	21.8207(4)	18.908(5)	12.2023(5)	6.684(5)
c [Å]	6.9043(5)	6.992(5)	10.3115(4)	15.203(5)
α [°]	90	90	90	90
β [°]	90	90	91.719	106.027(5)
γ [°]	120	120	90	90
V [Å^3]	2847.00(19)	2165(2)	942.95(6)	1494.4(13)
Z	4	3	4	4
$\rho_{calc.}$ [g cm^{-3}]	1.803	1.783	2.146	1.968
μ [mm^{-1}]	1.049	1.129	2.867	1.539
F(000)	1564	1176	604	892
$\lambda_{MoK\alpha}$ [Å]	0.71073	0.71073	0.71073	0.71073
T [K]	173	173	173	173
θ Min–Max [°]	4.3, 27.0	4.3, 26.5	4.3, 26.0	4.1, 28.0
Dataset	−25: 27; −27: 27; −8: 8	−15: 23; −23: 22; −8: 8	−9: 9; −14:15; −12: 12	−20: 19; −7: 8; −16: 20
Reflections collected	15966	17769	6823	6665
Independent refl.	4111	2987	1846	2808
*R*int	0.035	0.026	0.027	0.041
Observed reflections	2713	2571	1625	2567
Parameters	347	262	160	269
R_1 (obs)[a]	0.0628	0.0661	0.0224	0.0328
wR_2 (all data)[b]	0.1925	0.2024	0.0564	0.0575
GooF[c]	1.04	1.04	1.09	1.03
Resd. Dens. [e Å^{-3}]	−1.01, 1.47	−0.66, 3.07	−0.33, 0.34	−0.32, 0.31
Absorption correction	multi-scan	multi-scan	multi-scan	multi-scan
CCDC	1834859	1834851	1834845	1834844

a) $R_1 = \Sigma||F_0|- |F_c||/ \Sigma|F_0|$; b) $wR_2 = [\Sigma[w(F_0^2-F_c^2)^2]/\Sigma[w(F_0)^2]]^{1/2}$; $w = [\sigma c^2(F_0^2)+(xP)^2+yP]^{-1}$ and $P=(F_0^2+2F_c^2)/3$; c) GooF = $\{\Sigma[w(F_o^2-F_c^2)^2]/(n-p)\}^{1/2}$ (n = number of reflections; p = total number of parameters).

Table S3. Crystallographic data of **10** and **12**–**14**.

	10	**12**	**13**	**14**
Formula	$C_6H_{18}Cl_2CuN_{30}O_6$	$C_6H_{18}N_{32}O_6Zn$	$C_{14}H_{22}MnN_{16}O_{22}$	$C_{14}H_{22}MnN_{16}O_{24}$
FW [g mol^{-1}]	740.94	699.89	821.41	853.41
Crystal system	Monoclinic	Monoclinic	Monoclinic	Monoclinic
Space Group	$P2_1/c$	$P2_1/n$	$P2_1/c$	$P2_1/c$
Color / Habit	Blue block	Colorless block	Yellow block	Colorless block
Size [mm]	0.11 x 0.23 x 0.32	0.20 x 0.30 x 0.40	0.20 x 0.40 x 0.42	0.16 x 0.22 x 0.28
a [Å]	9.6517(3)	9.4477(10)	14.7040(6)	14.8973(9)
b [Å]	7.8880(3)	7.9116(9)	5.0490(2)	5.0185(2)
c [Å]	17.1904(5)	17.279(2)	20.4680(9)	20.4159(10)
α [°]	90	90	90	90
β [°]	93.923(2)	90.610(11)	103.858(4)	103.628(5)
γ [°]	90	90	90	90
V [Å^3]	1305.68(7)	1291.5(3)	1475.32(11)	1483.36(13)
Z	2	2	2	2
$\rho_{calc.}$ [g cm^{-3}]	1.885	1.800	1.849	1.911
μ [mm^{-1}]	1.133	1.047	0.573	0.578
F(000)	750	712	838	870
$\lambda_{MoK\alpha}$ [Å]	0.71073	0.71073	0.71069	0.71073
T [K]	173	173	143	143
θ Min–Max [°]	4.2, 26.0	4.2, 26.0	4.2, 26.0	4.2, 26.5
Dataset	−11: 11; −9: 6; −21: 21	−11: 11; −9: 9; −21: 20	−18: 18; −4:6; −25: 24	−18: 18; −6:6; −21: 25
Reflections collected	9613	9361	10483	11409
Independent refl.	2549	2524	2885	3029
*R*int	0.033	0.080	0.028	0.052
Observed reflections	2372	1856	2540	2410
Parameters	229	229	274	294
R_1 (obs)[a]	0.0647	0.0667	0.0278	0.0377
wR_2 (all data)[b]	0.1425	0.1725	0.0722	0.0794
GooF[c]	1.35	1.09	1.05	1.05
Resd. Dens. [e Å^{-3}]	−0.89, 0.81	−0.93, 1.12	−0.22, 0.30	−0.30, 0.35
Absorption correction	multi-scan	multi-scan	multi-scan	multi-scan
CCDC	1834853	1834852	1834858	1834857

a) $R_1 = \Sigma||F_0|- |F_c||/ \Sigma|F_0|$; b) $wR_2 = [\Sigma[w(F_0^2-F_c^2)^2]/\Sigma[w(F_0)^2]]^{1/2}$; $w = [\sigma c^2(F_0^2)+(xP)^2+yP]^{-1}$ and $P=(F_0^2+2F_c^2)/3$; c) GooF = $\{\Sigma[w(F_o^2-F_c^2)^2]/(n-p)\}^{1/2}$ (n = number of reflections; p = total number of parameters).

Table S4. Crystallographic data of **15**–**18**.

	15	**16**	**17**	**18**
Formula	$C_4H_{16}MnN_{20}Cl_2O_{10}$	$C_2H_6Cl_2CuN_{10}$	$C_2H_6CuN_{12}O_6$	$C_4H_{16}Cl_2CuN_{20}O_{10}$
FW [g mol^{-1}]	630.21	304.61	357.73	638.82
Crystal system	Triclinic	Monoclinic	Monoclinic	Tetragonal
Space Group	*P*–1	$P2_1/c$	$P2_1/n$	$P4_2/n$
Color / Habit	Colorless block	Green block	Blue plate	Blue block
Size [mm]	0.22 x 0.71 x 0.96	0.12 x 0.17 x 0.34	0.12 x 0.36 x 0.44	0.10 x 0.15 x 0.40
a [Å]	7.8980(5)	6.8468(5)	7.9953(8)	10.3883(3)
b [Å]	9.6180(6)	3.6679(2)	8.9746(8)	10.3883(3)
c [Å]	15.7710(7)	18.5122(12)	8.0033(9)	10.0967(8)
α [°]	78.554(4)	90	90	90
β [°]	76.267(4)	91.579(6)	107.469(12)	90
γ [°]	73.230(5)	90	90	90
V [Å^3]	1103.34(11)	464.73(5)	547.79(10)	1089.60(11)
Z	2	2	2	2
$\rho_{calc.}$ [g cm^{-3}]	1.897	2.177	2.169	1.947
μ [mm^{-1}]	0.933	2.909	2.058	1.342
F(000)	638	302	358	646
$\lambda_{MoK\alpha}$ [Å]	0.710769	0.71073	0.71073	0.71073
T [K]	173	173	173	173
θ Min–Max [°]	4.3, 26.0	4.4, 26.0	4.3, 26.5	4.4, 26.0
Dataset	−9: 9; −11: 11; −19: 17	−8: 8; −4: 4; −22: 22	−9: 10; −7: 11; −10: 10	−12: 11; −12:8; −12: 12
Reflections collected	8333	2907	4198	8313
Independent refl.	4311	920	1121	1067
*R*int	0.018	0.031	0.027	0.053
Observed reflections	3820	831	1024	879
Parameters	386	82	109	113
R_1 (obs)[a]	0.0378	0.0246	0.0229	0.0389
wR_2 (all data)[b]	0.0974	0.0596	0.0635	0.1049
GooF[c]	1.04	1.07	1.05	1.06
Resd. Dens. [e Å^{-3}]	−0.95, 1.39	−0.44, 0.40	−0.34, 0.30	−0.64, 0.74
Absorption correction	multi-scan	multi-scan	multi-scan	multi-scan
CCDC	1834854	1834842	1834843	1834841

a) $R_1 = \Sigma||F_0|- |F_c||/ \Sigma|F_0|$; b) $wR_2 = [\Sigma[w(F_0^2-F_c^2)^2]/\Sigma[w(F_0)^2]]^{1/2}$; $w = [\sigma c^2(F_0^2)+(xP)^2+yP]^{-1}$ and $P=(F_0^2+2F_c^2)/3$; c) GooF = $\{\Sigma[w(F_o^2-F_c^2)^2]/(n-p)\}^{1/2}$ (n = number of reflections; p = total number of parameters).

Table S5. Crystallographic data of **19**–**23**.

	19	**20**	**21**	**22**	**23**
Formula	$C_5H_{17}Cl_2FeN_{25}O_9$	$C_5H_{17}Cl_2N_{25}O_9Zn$	$C_8H_{24}Cl_2FeN_{40}O_8$	$C_8H_{24}Cl_2N_{40}O_8Zn$	$C_8H_{24}Cl_2CuN_{40}O_8$
FW [g mol^{-1}]	698.19	707.71	935.42	944.94	943.11
Crystal system	Triclinic	Triclinic	Triclinic	Triclinic	Triclinic
Space Group	*P*−1	*P*−1	*P*−1	*P*−1	*P*−1
Color / Habit	Colorless block	Colorless block	Colorless block	Colorless plate	Blue block
Size [mm]	0.23 x 0.35 x 0.64	0.17 x 0.31 x 0.51	0.26 x 0.32 x 0.42	0.07 x 0.17 x 0.27	0.10 x 0.10 x 0.40
a [Å]	9.4770(6)	9.4977(6)	8.5130(3)	8.5016(2)	10.3015(7)
b [Å]	9.9109(6)	9.9017(5)	10.8300(5)	10.8035(3)	10.8660(7)
c [Å]	15.4054(8)	15.3665(8)	19.3050(8)	19.2662(6)	16.4236(11)
α [°]	75.695(5)	75.918(5)	79.072(4)	79.175(3)	80.433(6)
β [°]	89.058(5)	89.336(5)	86.098(3)	86.100(2)	73.574(6)
γ [°]	63.694(6)	63.594(6)	86.476(3)	86.315(2)	80.646(5)
V [Å^3]	1249.66(15)	1247.54(14)	1741.78(13)	1731.63(8)	1725.8(2)
Z	2	2	2	2	2
$\rho_{calc.}$ [g cm^{-3}]	1.855	1.884	1.784	1.812	1.815
μ [mm^{-1}]	0.912	1.293	0.689	0.966	0.891
F(000)	708	716	952	960	958
$\lambda_{MoK\alpha}$ [Å]	0.71073	0.71073	0.71073	0.71073	0.71073
T [K]	173	173	173	173	143
θ Min–Max [°]	4.1, 26.0	4.3, 26.0	4.3, 26.0	4.3, 26.0	4.1, 26.0
Dataset	−11: 10; −12:11; −17: 19	−11: 8; −12: 12; −18: 18	−9: 10; −13: 13; −23: 23	−10: 10; −13: 13; −23: 22	−10: 12; −13:13; −20: 20
Reflections collected	10053	9906	13629	14327	13551
Independent refl.	4884	4875	6835	6784	6759
*R*int	0.023	0.028	0.023	0.033	0.039
Observed reflections	4136	4264	5770	5317	5061
Parameters	484	475	628	628	599
R_1 (obs)[a]	0.0473	0.0474	0.0317	0.0369	0.0403
wR_2 (all data)[b]	0.1369	0.1348	0.0821	0.0874	0.0951
GooF[c]	1.04	1.05	1.03	1.03	1.03
Resd. Dens. [e Å^{-3}]	−1.33, 2.49	−1.18, 2.75	−0.40, 0.45	−0.40, 0.39	−0.46, 0.36
Absorption correction	multi-scan	multi-scan	multi-scan	multi-scan	multi-scan
CCDC	1834856	1834846	1834848	1834850	1838980

a) $R_1 = \Sigma||F_0|- |F_c||/ \Sigma|F_0|$; b) $wR_2 = [\Sigma[w(F_0^2-F_c^2)^2]/\Sigma[w(F_0)^2]]^{1/2}$; $w = [\sigma c^2(F_0^2)+(xP)^2+yP]^{-1}$ and $P=(F_0^2+2F_c^2)/3$; c) GooF = $\{\Sigma[w(F_o^2-F_c^2)^2]/(n-p)\}^{1/2}$ (n = number of reflections; p = total number of parameters).

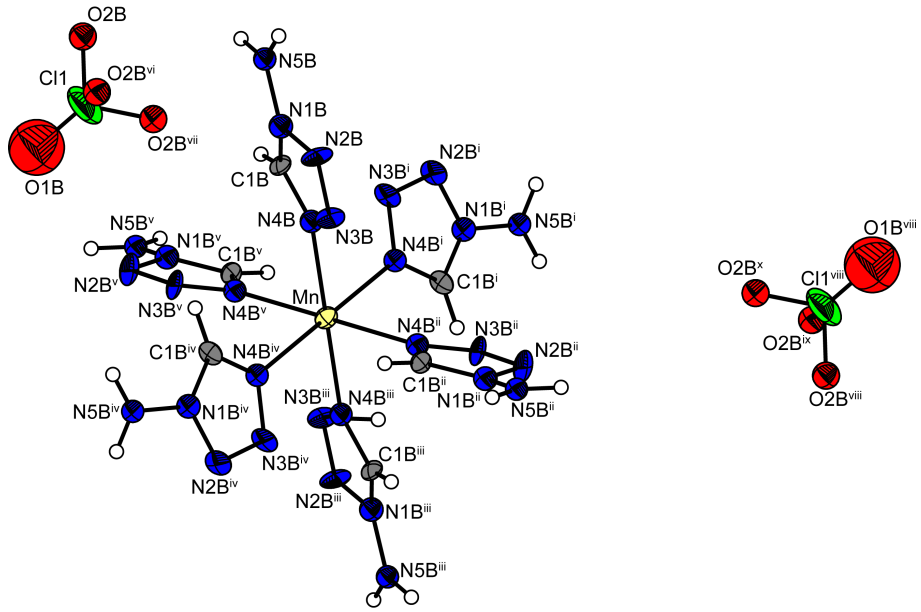


Figure S6. Molecular unit of $[Mn(1\text{-}AT)_6](ClO_4)_2$ (**4**). Selected bond length (Å): Mn–N4B 2.28(2); selected bond angles (°): N4B–Mn–N4B^{iv} 89.9(8), N4B–Mn–N4B^{i} 90.2(8i), and N4B–Mn–N4B^{iii} 180.00. Symmetry codes: (i) 1+y, 1−x+y, 2−z; (ii) x−y, −1+x, 2−z; (iii) 2–x, −y, 2−z; (iv) 1−y, −1+x−y, z; (v) 2–x+y, 1−x, z; (vi) 2−x, −y, 1−z; (vii) 2+y, 1−x+y, 1−z; (viii) 1+x−y, x, 1−z; (ix) 1−x+y, −x, z; (x) −y, −1+x−y, z.

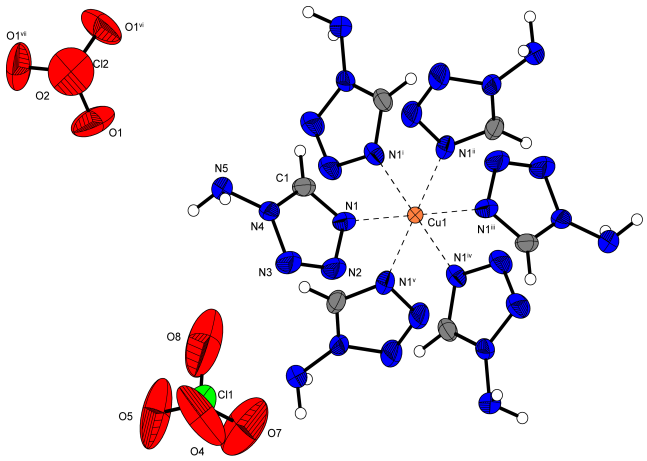


Figure S7. Molecular unit of $[Cu(1\text{-}AT)_6](ClO_4)_2$ (**6**). Selected bond length (Å): Cu1–N1 2.127(4); selected bond angles (°): N1–Cu1–N1^{iii} 91.79(17), N1–Cu1–N1^{vi} 88.21(17), N1^{iii}–Cu1–N1^{iv} 91.8(2), N1^{iii}–Cu1–N1^{vii} 88.2(2). Symmetry codes: (i) −x, −y, −z; (ii) x−y, x, −z; (iii) −x+y, −x, z; (iv) −y, x−y, z; (v) y, −x+y, −z; (vi) −x, 1−y, −z; (vii) 1−x+y, 1−x, z.

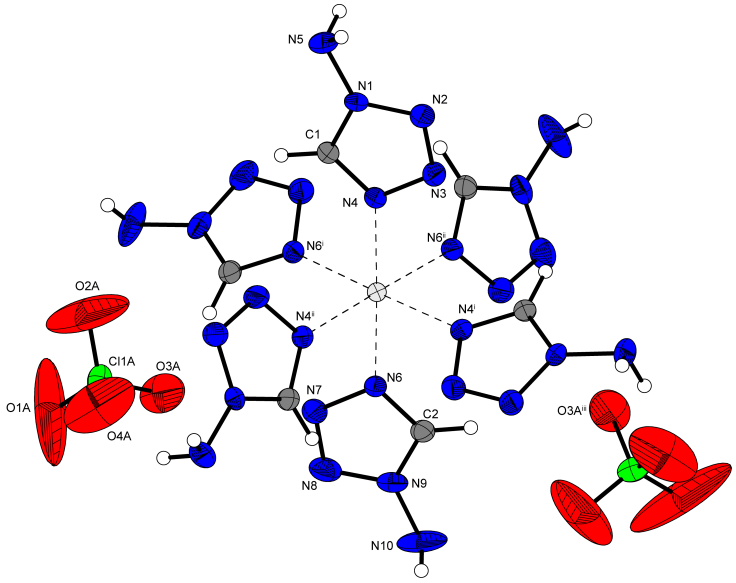


Figure S8. Molecular unit of $[Zn(1\text{-}AT)_6](ClO_4)_2$ (**7**). Selected bond lengths (Å): Zn1–N4 2.167(4), Zn1–N6 2.167(4), Zn2–N14 2.167(4); selected bond angles (°): N14–Zn2–$N14^{vii}$ 88.78(13), $N14^{iii}$–Zn2–$N14^{iv}$ 91.23(18), N4–Zn1–N6 178.62(15), N4–Zn1–$N4^{i}$ 91.07(16), N4–Zn1–$N6^{i}$ 89.98(16), N4–Zn1–$N6^{ii}$ 88.01(14), N6–Zn1–$N6^{i}$ 90.96(16). Symmetry codes: (i) 1−y, x−y, z; (ii) 1−x+y, 1−x, z; (iii) −x, −y, −z.

The unmanageable, extremely sensitive copper(II) chlorate coordination compounds **10** and **11** crystallize both in the form of blue blocks in the monoclinic space group $P2_1/n$ and the triclinic space group $P\bar{1}$, respectively. The calculated densities vary only slightly, with 1.885 g cm^{-3} (173 K) (**10**) and 1.959 g cm^{-3} (143 K) (**11**) from each other. Both complexes consist of closed octahedral coordination spheres with six and four coordinated 1-AT ligands. While in compound **10** the chlorate counter-anions are non-coordinating (Figure S9), they act as chlorato ligands in complex **11**. Similar to complex **4**, a high degree of disorder can be observed for the coordinating heterocycles and anions in the X-ray structure of the tetrakis(1-amino-5*H*-tetrazolyl) compound **11**, which unfortunately only allows an isotropic refinement of its data set (Figure S10).

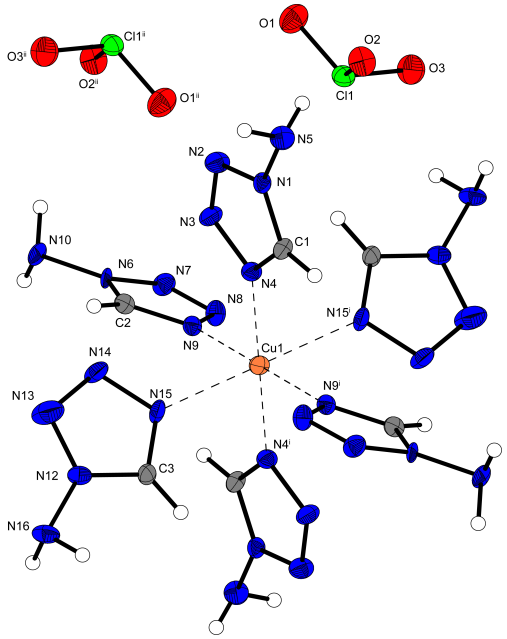


Figure S9. Molecular unit of $[Cu(1\text{-}AT)_6](ClO_3)_2$ (**10**). Selected bond lengths (Å): Cu1–N4 2.054(4), Cu1–N9 2.012(4), Cu1–N15 2.403(5); selected bond angles (°): N4–Cu1–N9 89.46(16), N4–Cu1–N15 90.15(16), N4–Cu1–$N4^i$ 180.00. Symmetry codes: (i) 1−x, −y, 2−z; (ii) 2−x, 1−y, 2−z.

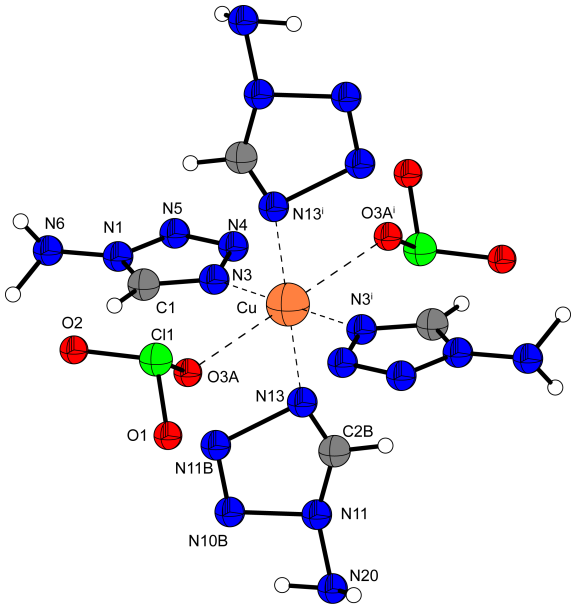


Figure S10. Isotropic illustration of the molecular unit of $[Cu(ClO_3)_2(1\text{-}AT)_4]$ (**11**).

$[Zn(1\text{-}AT)_6](NO_3)_2$ (**12**) crystallizes in the form of colorless blocks in the monoclinic space group $P2_1/n$ with two formula units per unit cell and a calculated density of 1.800 g cm^{-3} at 173 K. The metal(II) center is coordinated by six tetrazole ligands with Zn–N bonds in the range of 2.165(4)-2.175(4) Å and therefore forms an almost perfect octahedral structure with bond angles close to 90° (Figure S11).

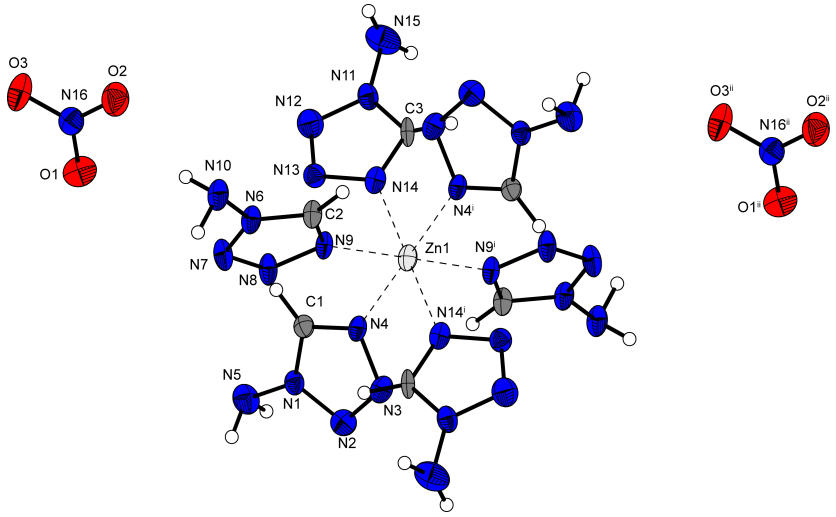


Figure S11. Molecular unit of $[Zn(1\text{-}AT)_6](NO_3)_2$ (**12**). Selected bond lengths (Å): Zn1–N4 2.165(4), Zn1–N9 2.171(4), Zn1–N14 2.175(4); selected bond angles (°): N4–Zn1–N9 90.42(14), N4–Zn1–N14 90.24(14), N9–Zn1–N14 90.29(14). Symmetry codes: (i) 2−x, −y, −z; (ii) 1+x, −2+y, z.

$[Mn(H_2O)_6](HTNR)_2 \cdot 2$ 2-AT (**13**) as well as $[Mn(H_2O)_6](H_2TNPG)_2 \cdot 2$ 2-AT (**14**) both did not form coordination compounds with 1-AT but crystallized as hexaaqua complexes with either $HTNR^-$ or H_2TNPG^- as counter-anions and cocrystallizing 1-AT molecules. Both compounds crystallize in the monoclinic space group $P2_1/c$ with two formula units per unit cell and calculated densities of 1.849 g cm^{-3} and 1.911 g cm^{-3} at 143 K, respectively. The Mn–O bonds differ only slightly in both compounds (**13**: 2.1355(12)-2.2037(13) Å; **14**: 2.140(2)-2.1874(18) Å) forming octahedral structures with negligible deformations (Figure S13 and S14).

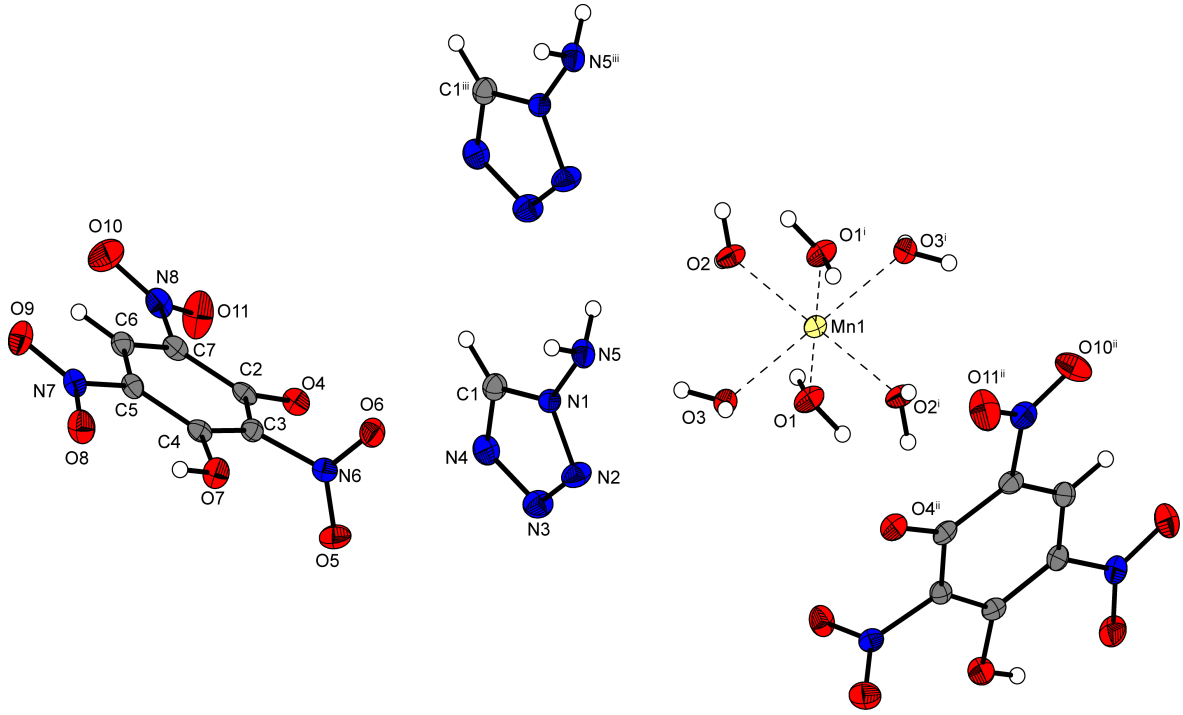


Figure S12. Molecular unit of $[Mn(H_2O)_6](HTNR)_2 \cdot 2$ 2-AT (**13**). Selected bond length (Å): Mn1–O1 2.1925(14), Mn1–O2 2.1355(12), Mn1–O3 2.2037(13); selected bond angles (°): O1–Mn1–O2 95.90(5), O1–Mn1–O3 92.27(5), O2–Mn1–O3 89.57(5). Symmetry codes: (i) 1−x, −y, −z; (ii) 1−x, 0.5+y, 0.5−z; (iii) x, −1+y, z.

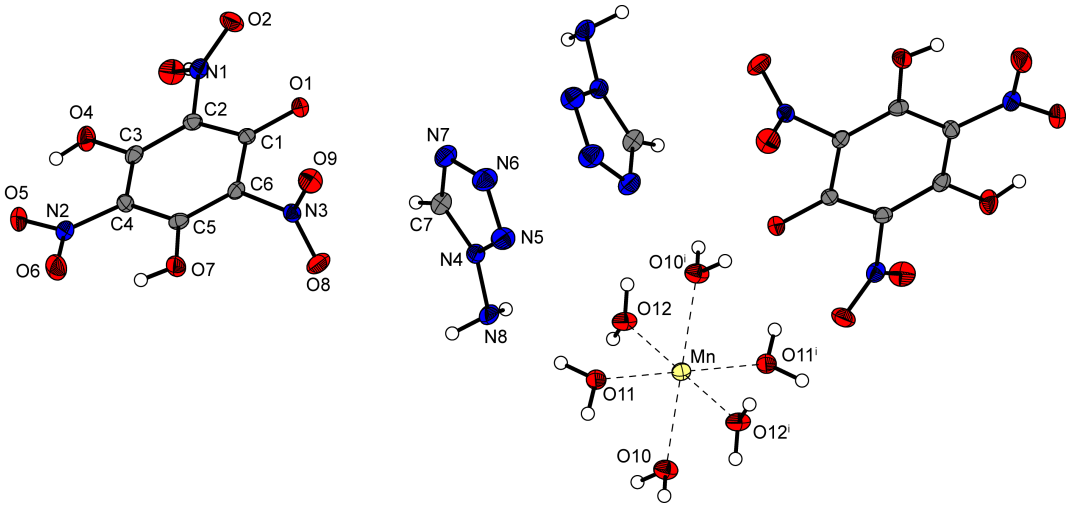


Figure S13. Molecular unit of $[Mn(H_2O)_6](H_2TNPG)_2 \cdot 2$ 2-AT (**14**). Selected bond lengths (Å): Mn–O10 2.1861(18), Mn–O11 2.1874(18), Mn–O12 2.140(2); selected bond angles (°): O10–Mn–O11 88.78(7), O10–Mn–O12 83.00(7). Symmetry code: (i) 1−x, 1−y, −z.

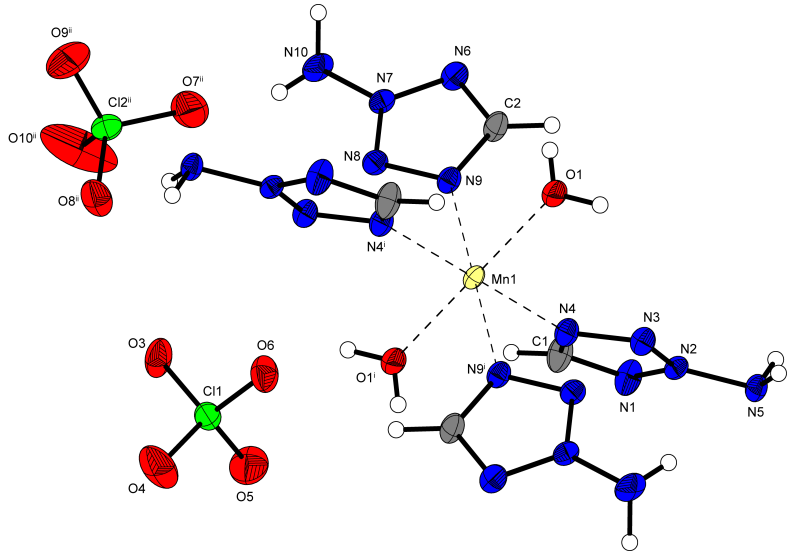


Figure S14. Molecular unit of $[Mn(H_2O)_2(2\text{-AT})_4](ClO_4)_2$ (**15**). Selected bond lengths (Å): Mn1–O1 2.142(2), Mn1–N4 2.245(2), Mn1–N9 2.268(2); selected bond angles (°): O1–Mn1–N4 85.86(8), O1–Mn1–N9 92.28(7). Symmetry codes: (i) −x, 1−y, 1−z; (ii) −1+x, y, z.

The exceptionality of the structure of **17** becomes clear when viewing along the *a*-axis (Figure S15). Brought about by the previously mentioned bridging 2-AT, a grid pattern, consisting of crosswise arranged one dimensional chains of **17**, can be observed. The distance between the copper(II) centers of adjacent chains of the same alignment is 8.975 Å, a value that resembles the lattice parameter b of the unit cell. The metal(II) centers in between the chains themselves are 6.521 Å apart from each other. The complete topology is revealed regarding the compound's crystal structure along the *b*-axis (Figure S16): The two-dimensional grid patterns that have been mentioned beforehand form a layer structure whose components are held together by several hydrogen bonds (Table S7). The respective layers are aligned parallel to the plane built up by the unit cell's b-axis and the diagonal through the a-c-plane.

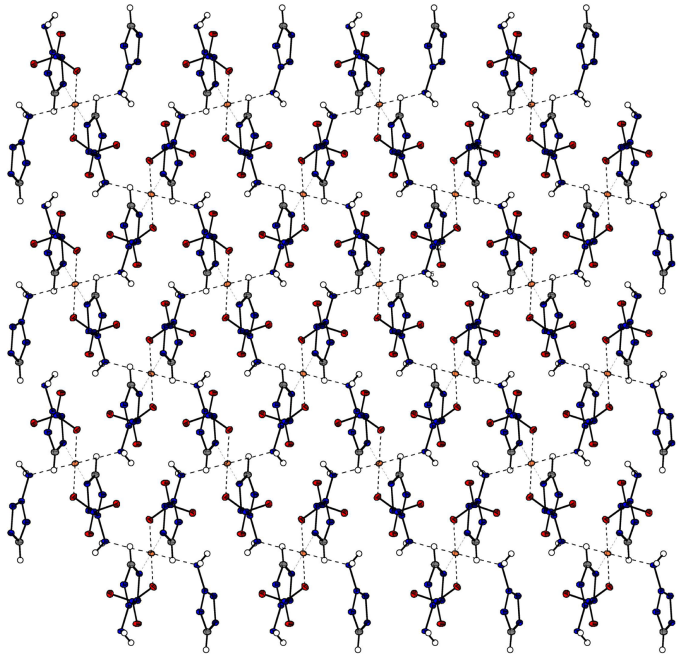


Figure S15. Grid pattern of **17** by viewing along the *a*-axis.

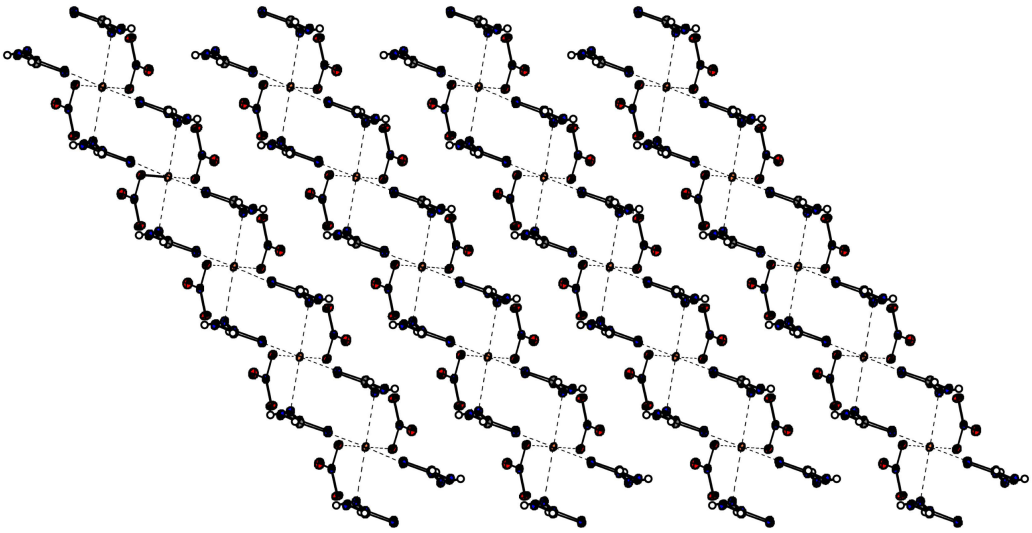


Figure S16. Structure of **17** with the direction of view along the *b*-axis.

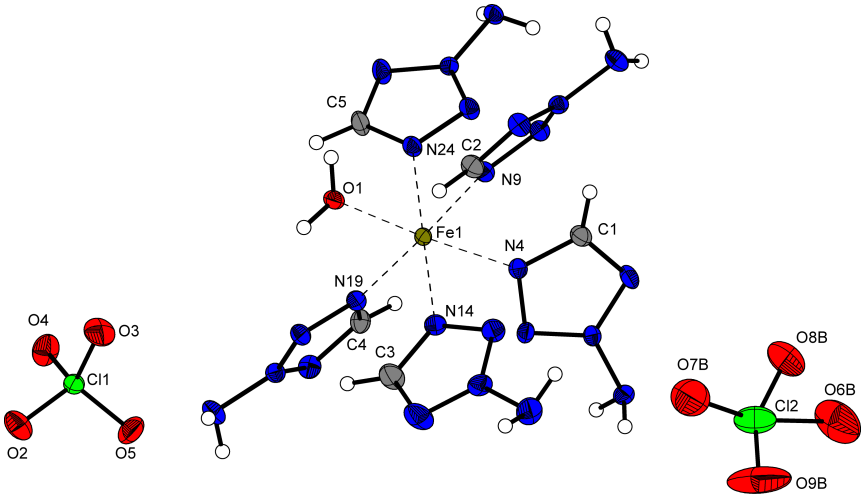


Figure S17. Molecular unit of $[Fe(H_2O)(2\text{-}AT)_5](ClO_4)_2$ (**19**). Selected bond lengths (Å): Fe1–O1 2.070(3), Fe1–N4 2.185(3), Fe1–N9 2.212(3), Fe1–N14 2.175(3), Fe1–N19 2.192(3), Fe1–N24 2.181(3); selected bond angles (°): O1–Fe1–N4 176.31(10), N9–Fe1–N19 176.18(12), N14–Fe1–N24 178.61(11), O1–Fe1–N9 86.02(11), O1–Fe1–N14 92.34(11), O1–Fe1–N24 87.60(11), N4–Fe1–N9 92.63(11), N4–Fe1–N14 91.03(11), N9–Fe1–N14 87.54(10), N9–Fe1–N24 91.06(10), N14–Fe1–N19 91.21(10).

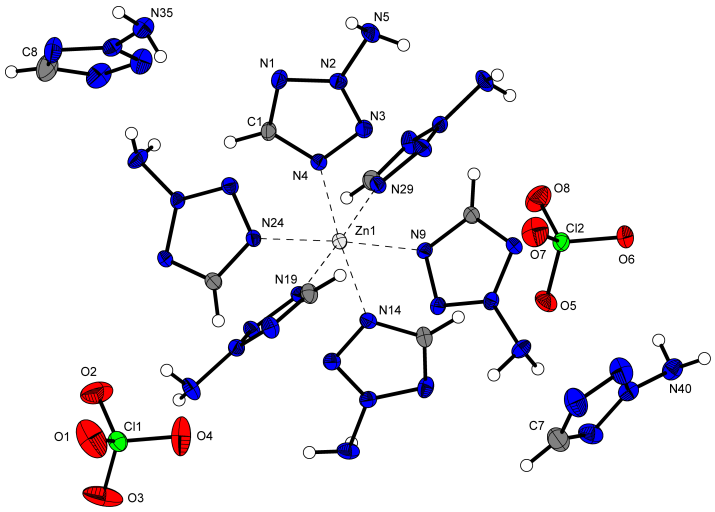


Figure S18. Molecular unit of $[Zn(2\text{-}AT)_6](ClO_4)_2 \cdot 2$ 2-AT (**22**). Selected bond lengths (Å): Zn1–N4 2.159(2), Zn1–N9 2.200(2), Zn1–N14 2.210(2), Zn1–N19 2.1303(18), Zn1–N24 2.206(2), Zn1–N29 2.1218(18); selected bond angles (°): N4–Zn1–N14 175.56(8), N9–Zn1–N24 176.19(8), N19–Zn1–N29 177.56(8), N4–Zn1–N9 89.61(8), N4–Zn1–N19 88.35(7), N4–Zn1–N24 93.16(8), N4–Zn1–N29 89.30(7), N9–Zn1–N14 86.38(7), N9–Zn1–N19 87.49(7), N9–Zn1–N29 93.17(7), N14–Zn1–N19 93.36(7), N14–Zn1–N24 90.93(7), N14–Zn1–N29 89.03(7), N19–Zn1–N24 89.98(7), N24–Zn1–N29 89.49(7).

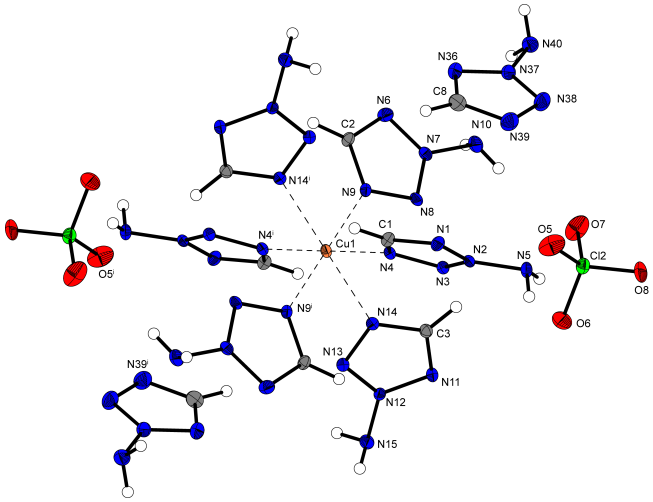


Figure S19. Molecular unit of $[Cu(2\text{-}AT)_6](ClO_4)_2 \cdot 2$ 2-AT (**23**). Selected bond lengths (Å): Cu1–N4 2.059(2), Cu1–N9 2.001(2), Cu1–N14 2.430(2); selected bond angles (°): N4–Cu1–N9 90.75(9), N4–Cu1–N14 90.65(8), N4–Cu1–$N4^i$ 180.00. Symmetry code: (i) −x, 2−y, −z.

Table S6. Selected hydrogen bonds in $[Fe(1\text{-}AT)_6](ClO_4)_2$ (**5**).

D–H··A	d(D–H) (Å)	d(H··A) (Å)	d(D··A) (Å)	<D–H··A (°)
N5–H5A··N15	0.80(3)	2.43(3)	3.143(5)	151(4)
N5–H5B··O3B	0.80(3)	2.42(5)	3.090(17)	142(4)
N10–H10A··O2B	0.80(7)	2.39(6)	3.107(14)	151(6)
N10–H10B··O3B	0.79(3)	2.36(5)	3.086(14)	153(6)
N15–H15A··N7	0.84(5)	2.48(5)	3.236(5)	151(5)
C1–H1··O1B	0.88(6)	2.60(6)	3.42(2)	156(4)

Table S7. Selected hydrogen bonds in $[Cu(NO_3)_2(\mu\text{-}2\text{-}AT)_4]$ (**17**).

D–H··A	d(D–H) (Å)	d(H··A) (Å)	d(D··A) (Å)	<D–H··A (°)
N5–H5A··N15	0.80(3)	2.43(3)	3.143(5)	151(4)
N5–H5B··O3B	0.80(3)	2.42(5)	3.090(17)	142(4)
N10–H10A··O2B	0.80(7)	2.39(6)	3.107(14)	151(6)
N10–H10B··O3B	0.79(3)	2.36(5)	3.086(14)	153(6)
N15–H15A··N7	0.84(5)	2.48(5)	3.236(5)	151(5)
C1–H1··O1B	0.88(6)	2.60(6)	3.42(2)	156(4)

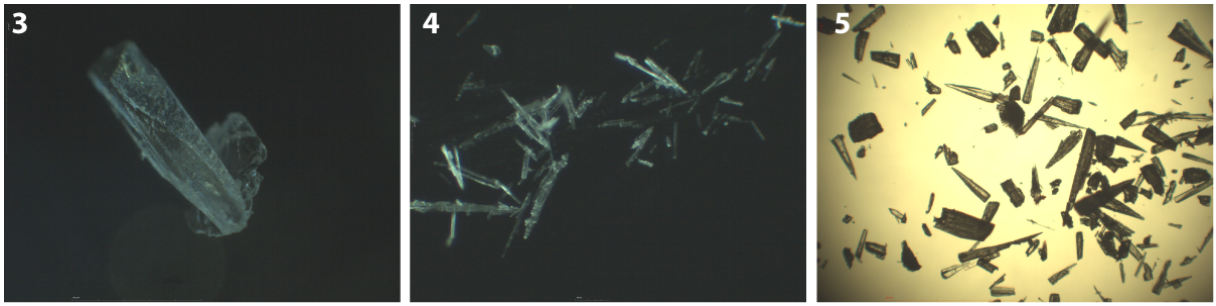


Figure S20. Microscope images of **3**–**5** (fourfold magnitude).

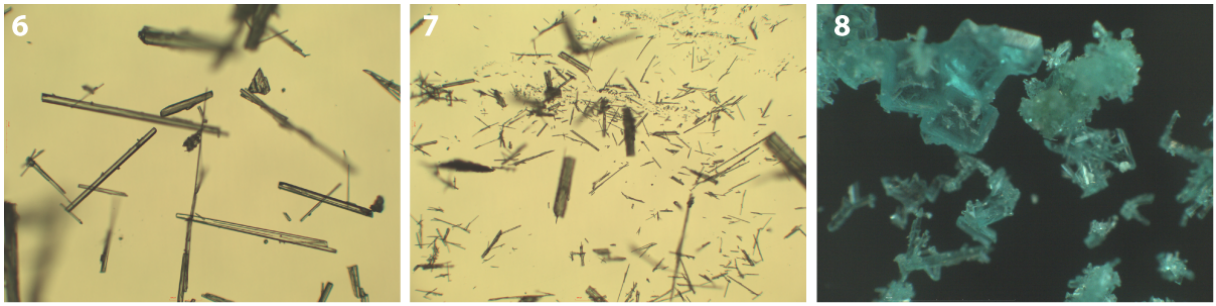


Figure S21. Microscope images of **6**–**8** (**6** and **7**: tenfold magnitude; **8**: fourfold magnitude).

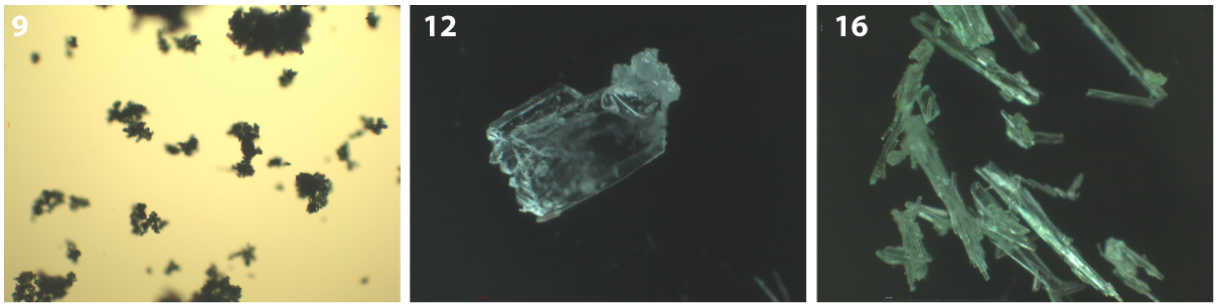


Figure S22. Microscope images of **9**, **12**, and **16** (**9**: tenfold magnitude; **12** and **16**: fourfold magnitude).

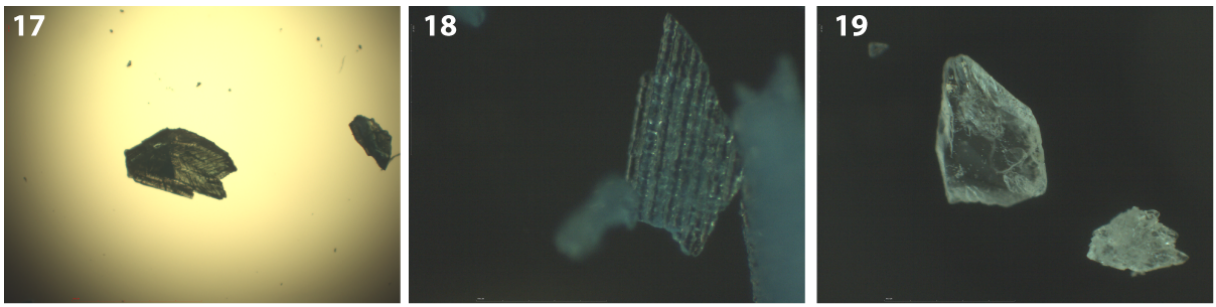


Figure S23. Microscope images of **17**–**19** (fourfold magnitude).

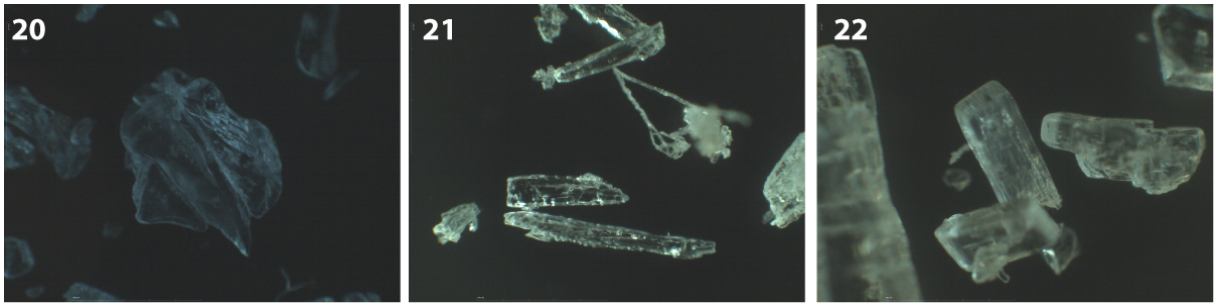


Figure S24. Microscope images of **20**–**22** (fourfold magnitude).

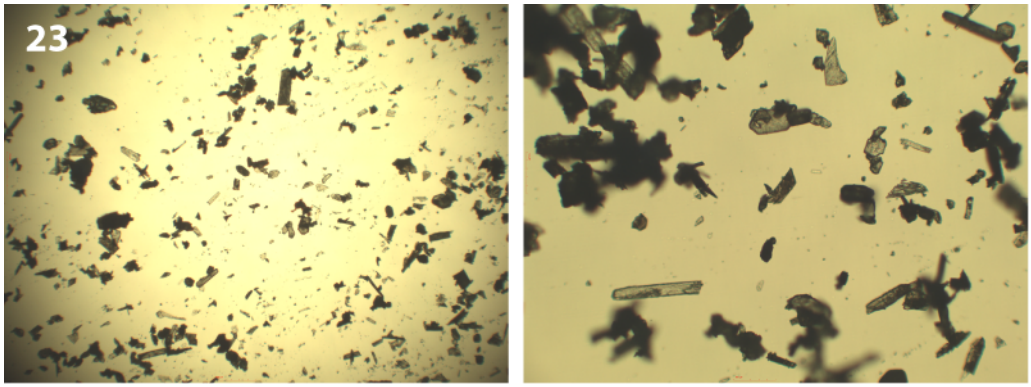


Figure S25. Microscope images of **23** (left: fourfold magnitude; right: tenfold magnitude).

19.13.4 TGA Plots of 1 and 2

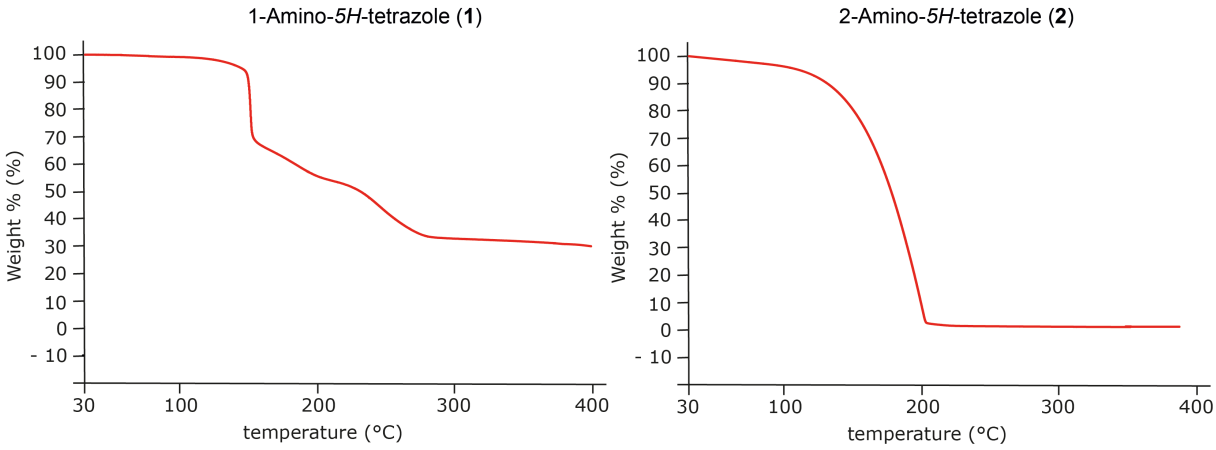


Figure S26. TGA plots of **1** and **2**.

19.13.5 DTA Plots of 1–3, 8, 9, 12 and 16–23

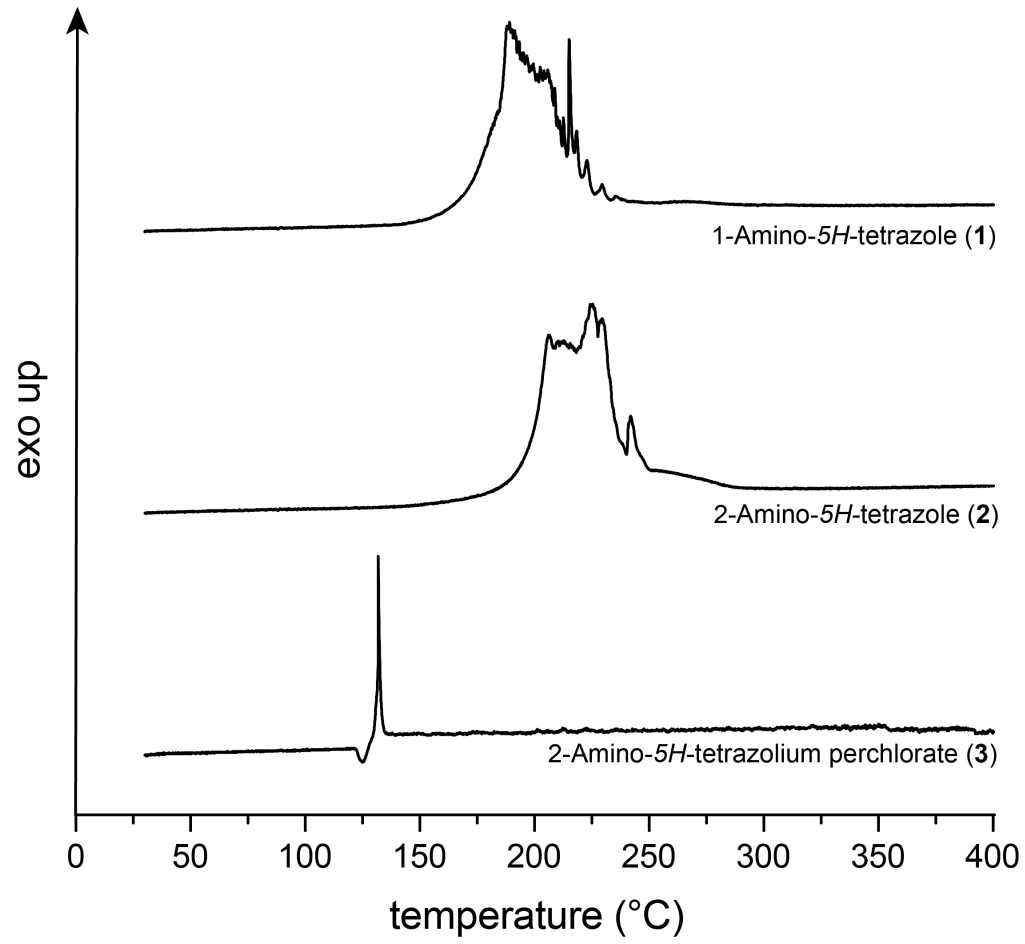


Figure S27. DTA plots of **1**–**3**.

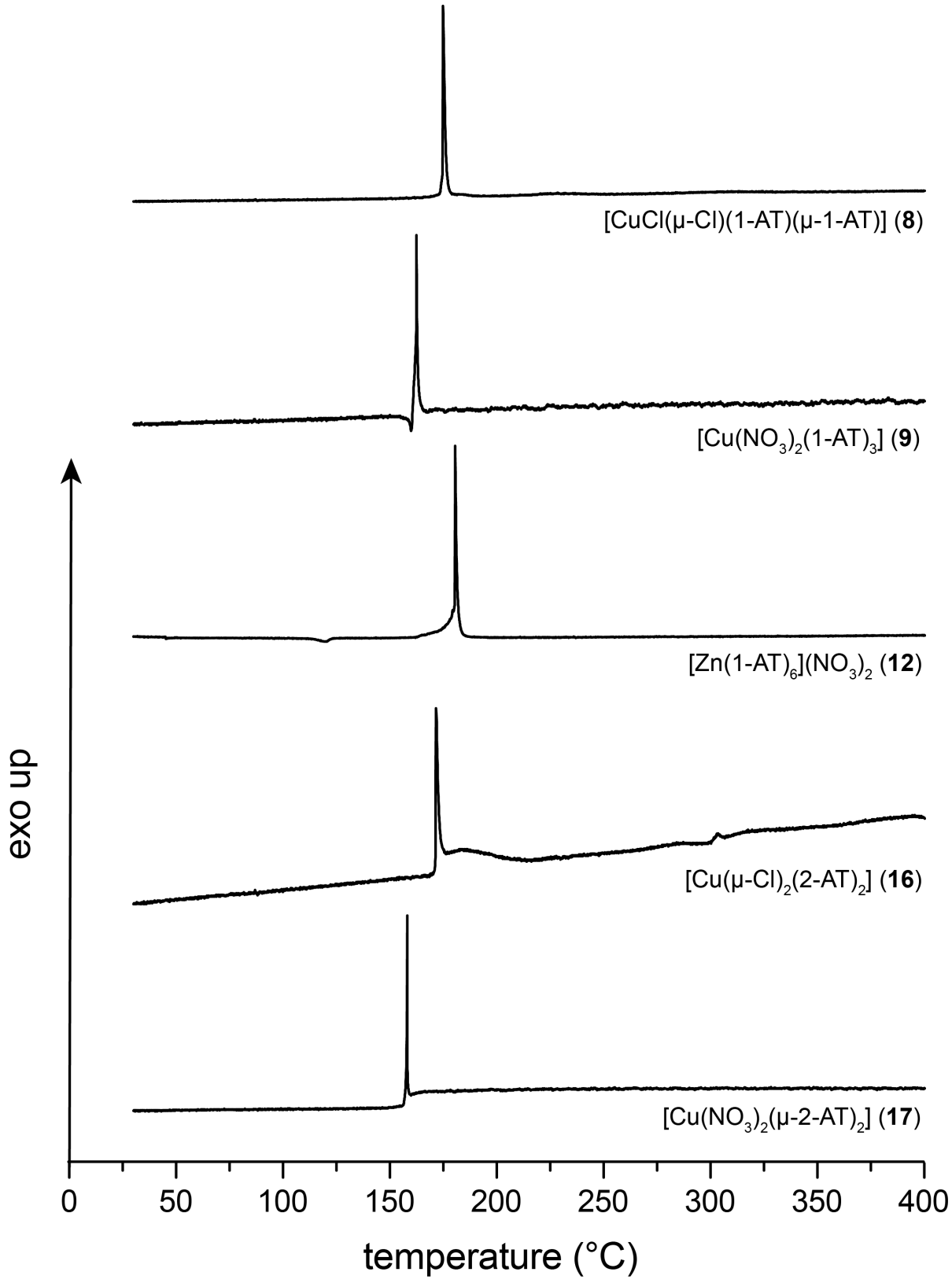


Figure S28. Different thermal analysis plots of **8**, **9**, **12**, **16**, and **17**.

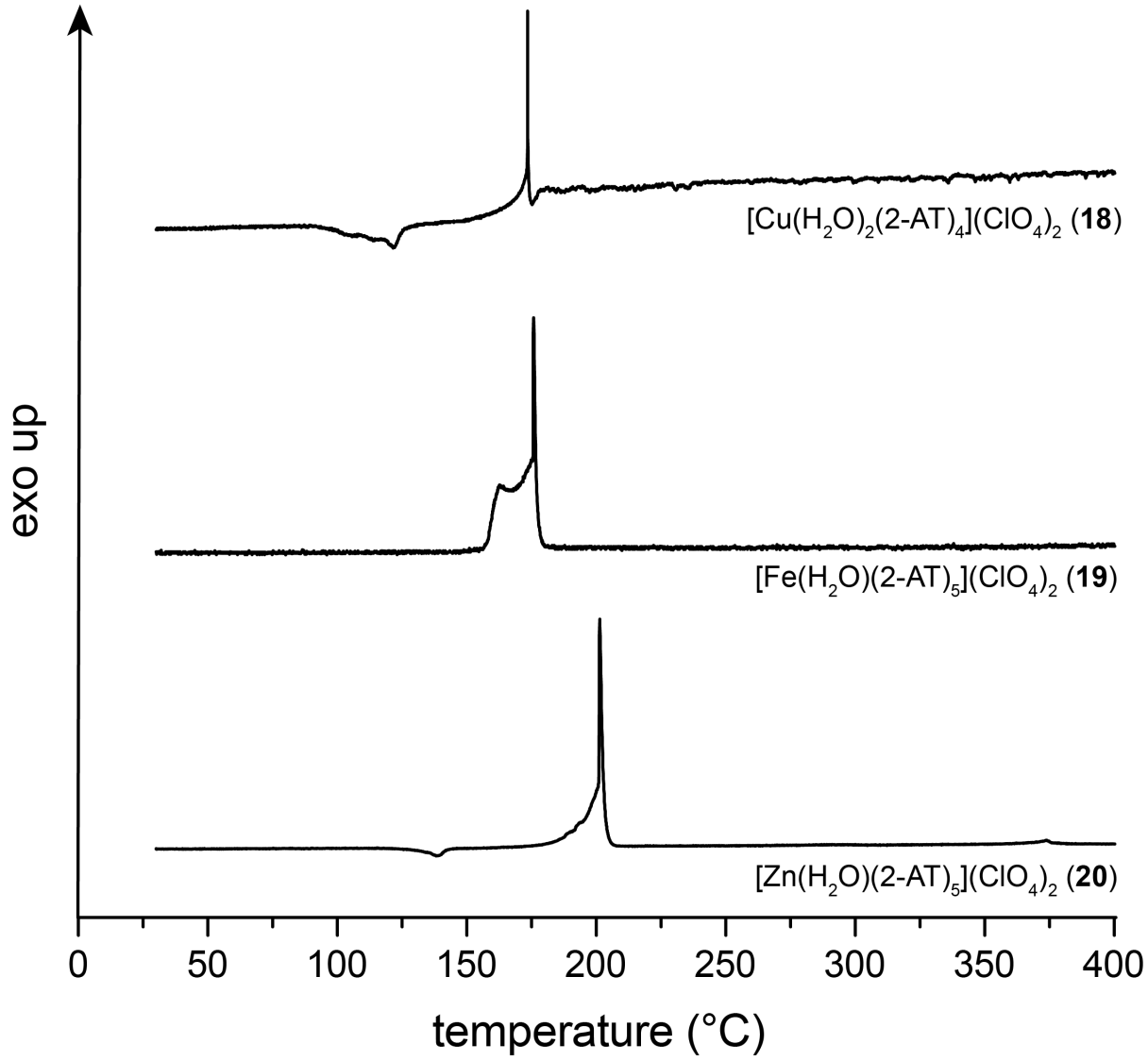


Figure S29. DTA plots of **18**–**20**.

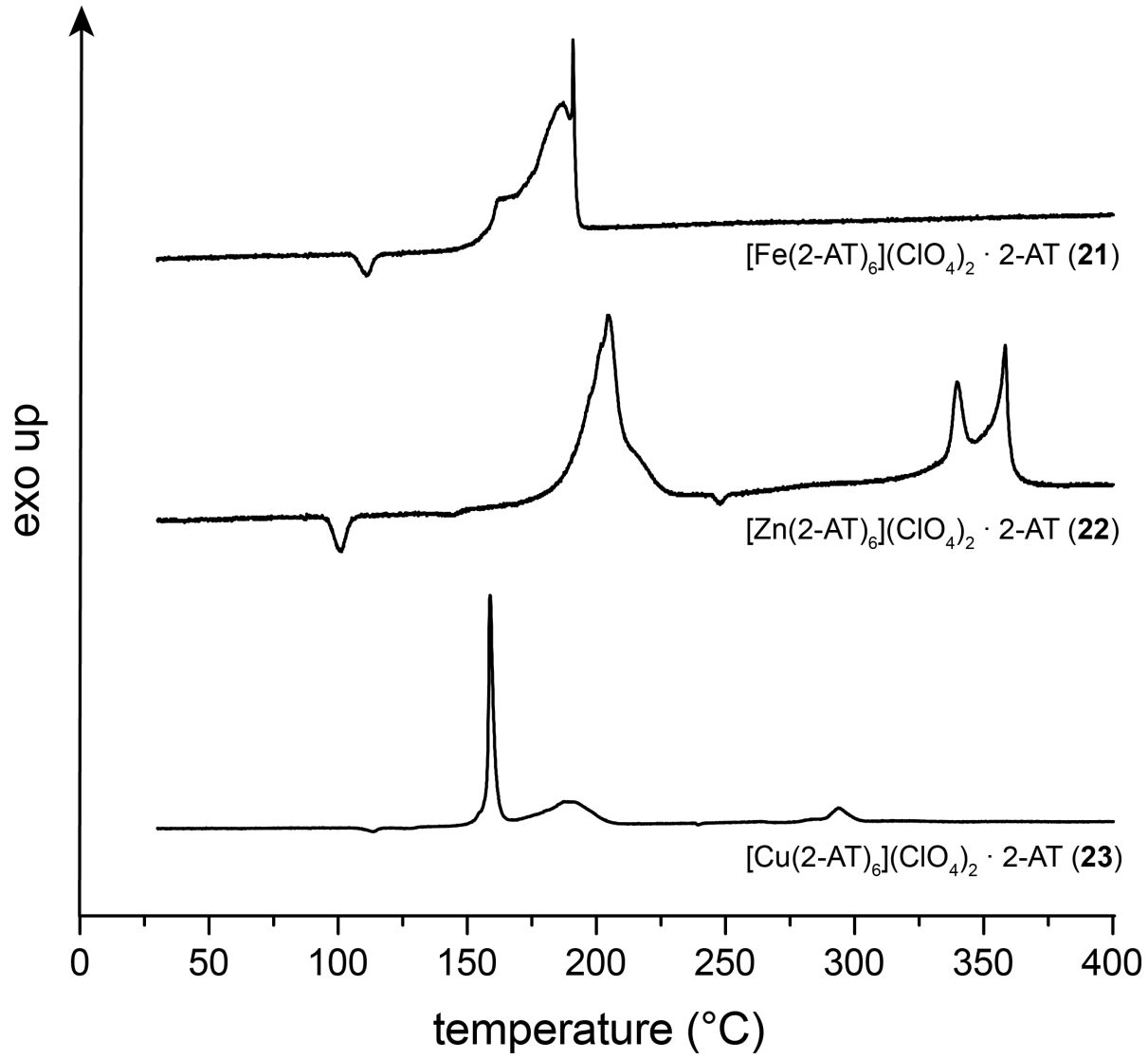


Figure S30. DTA plots of **21**–**23**.

19.13.6 Column Diagrams of the Complexes of 18–23

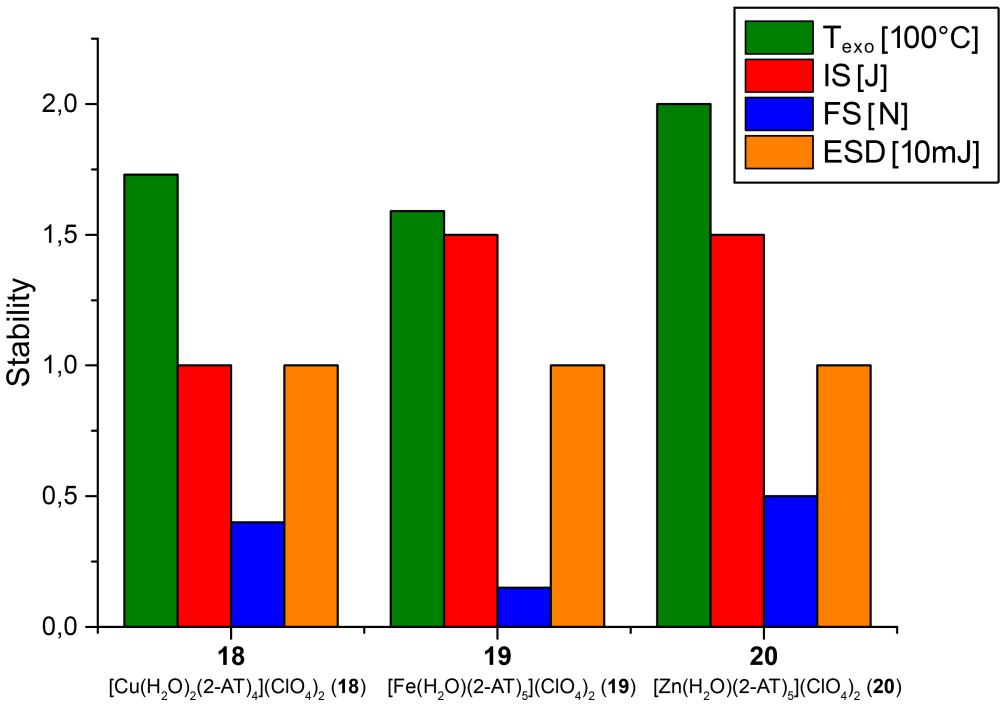


Figure S31. Stabilities of the aqua ligand containing metal(II) perchlorate complexes **18**–**20**.

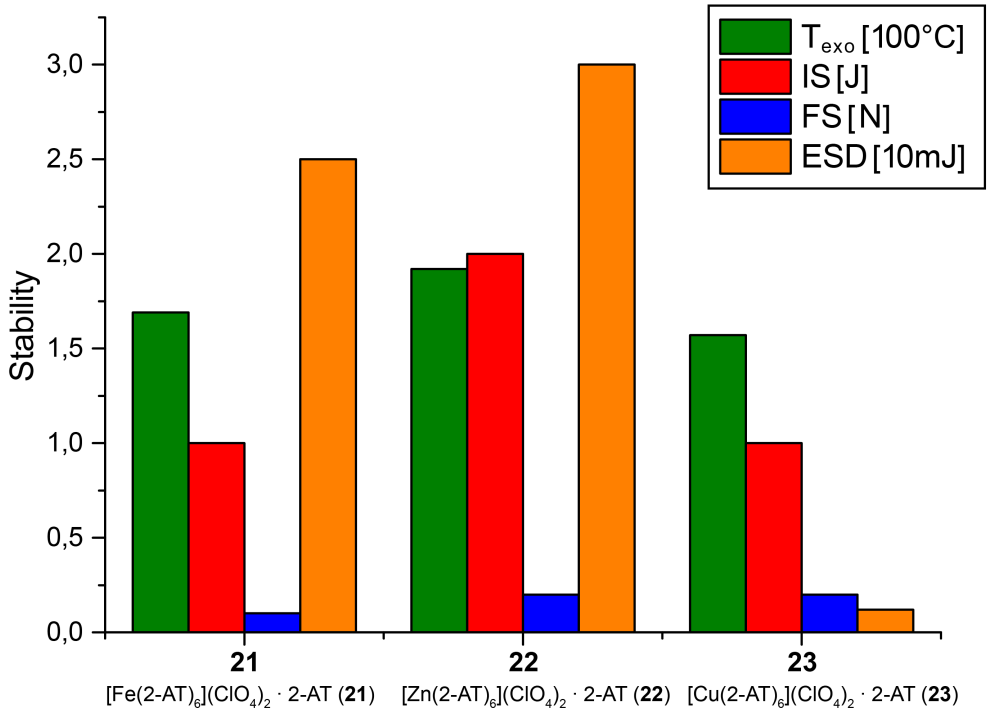


Figure S32. Stabilities of the 2-AT cocrystallized metal(II) perchlorate complexes **21**–**23**.

19.13.7 Hot Plate and Hot Needle Tests

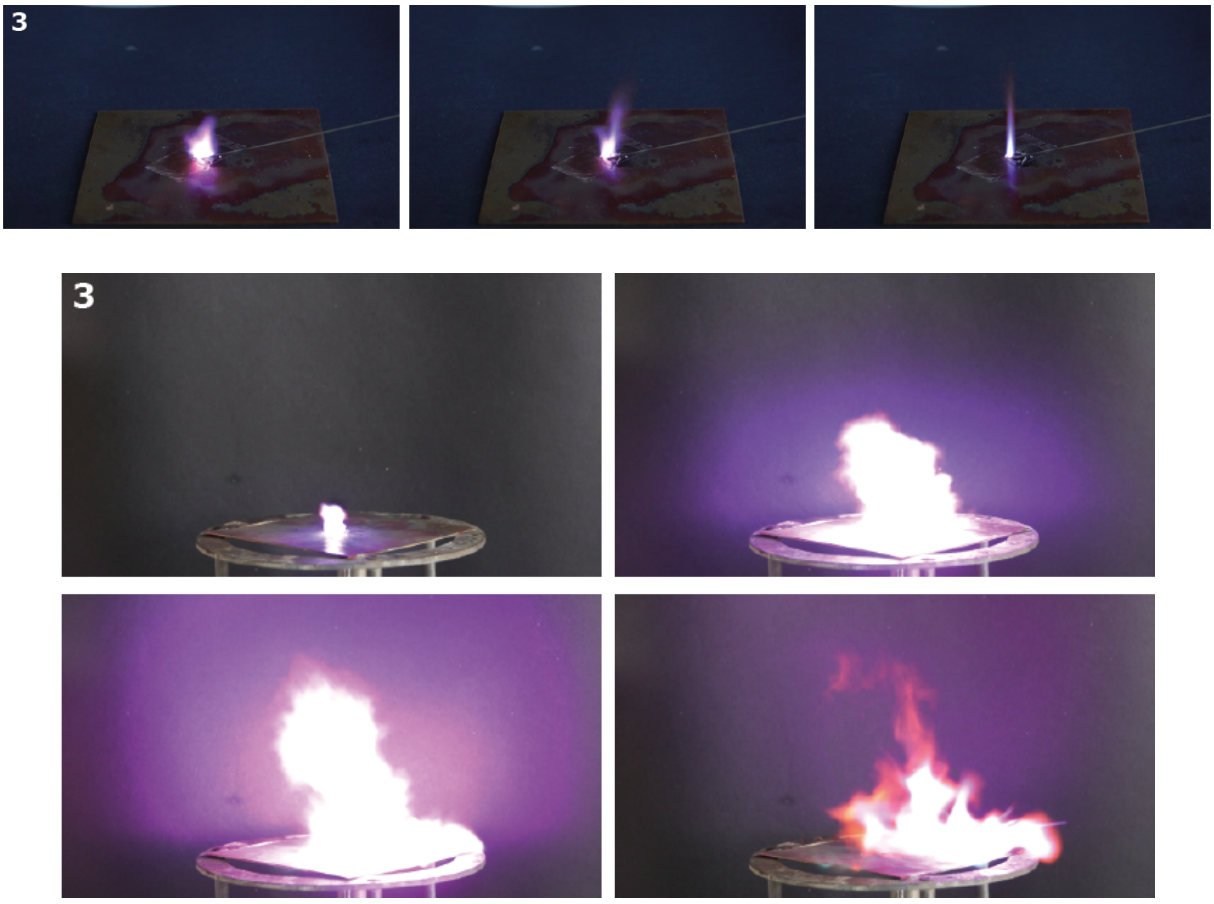


Figure S33. Hot needle and hot plate tests of complex **3** shown as a sequence.

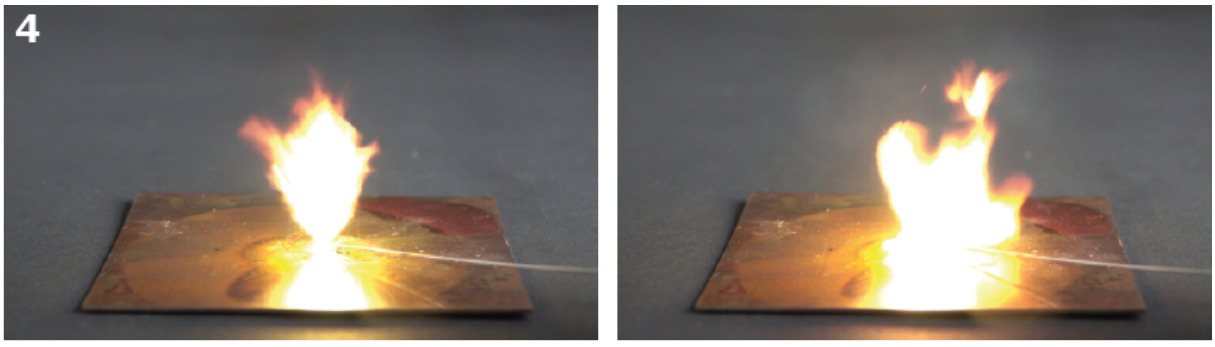


Figure S34. Hot needle test of coordination compound **4** shown as a sequence.



Figure S35. Hot plate test of coordination compound **4** shown as a sequence.

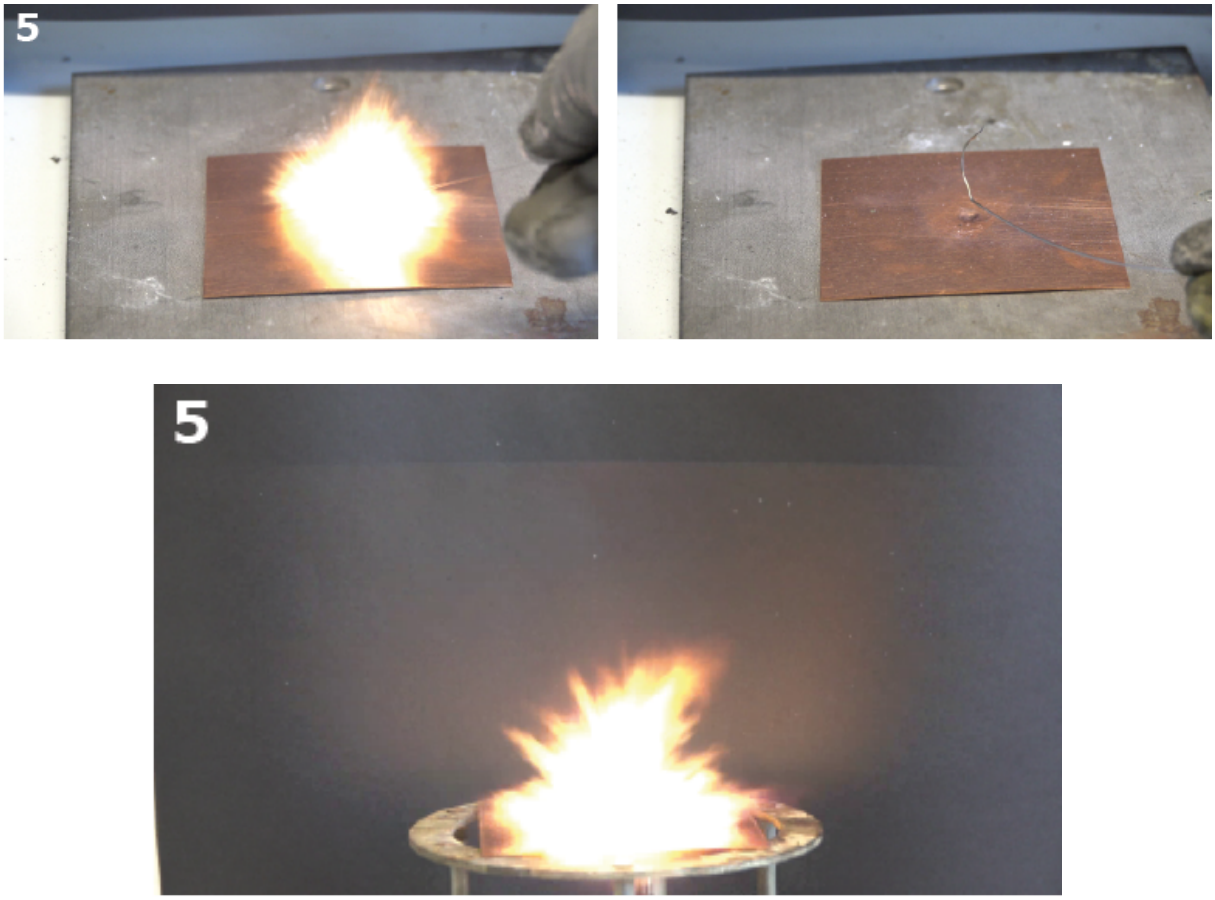


Figure S36. Detonation of coordination compound **5** during the hot needle and hot plate tests, partly shown as a sequence.

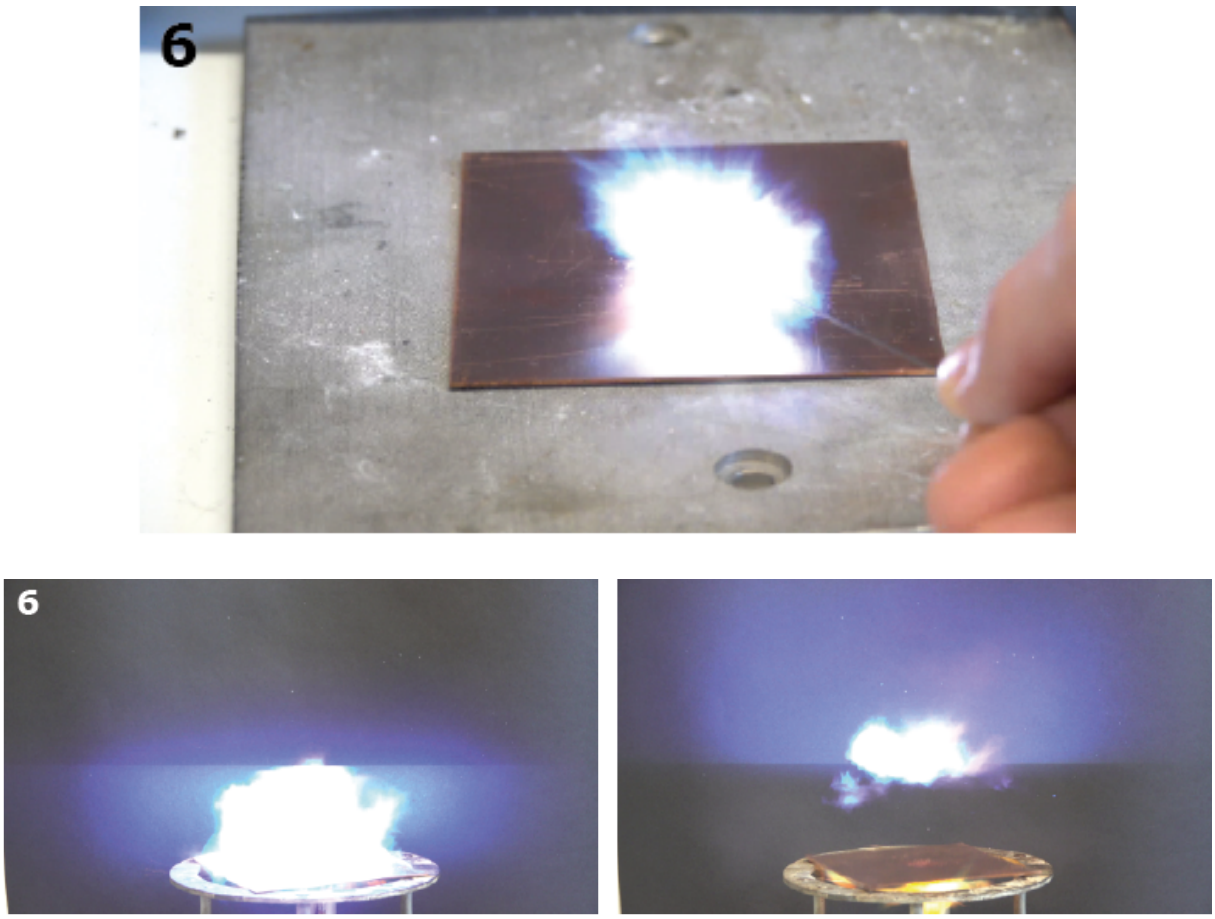


Figure S37. Detonation of coordination compound **6** during the hot needle and hot plate tests, partly shown as a sequence.

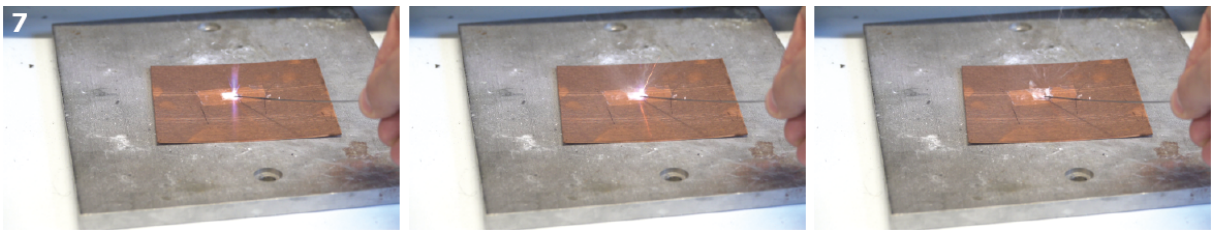


Figure S38. Initiation of complex **7** shown as a sequence during the hot needle test.

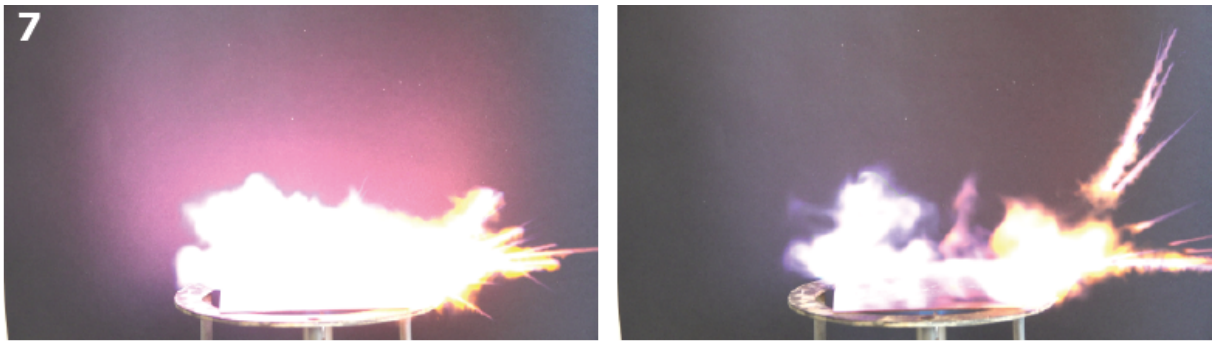


Figure S39. Hot plate test of complex **7** shown as a sequence.

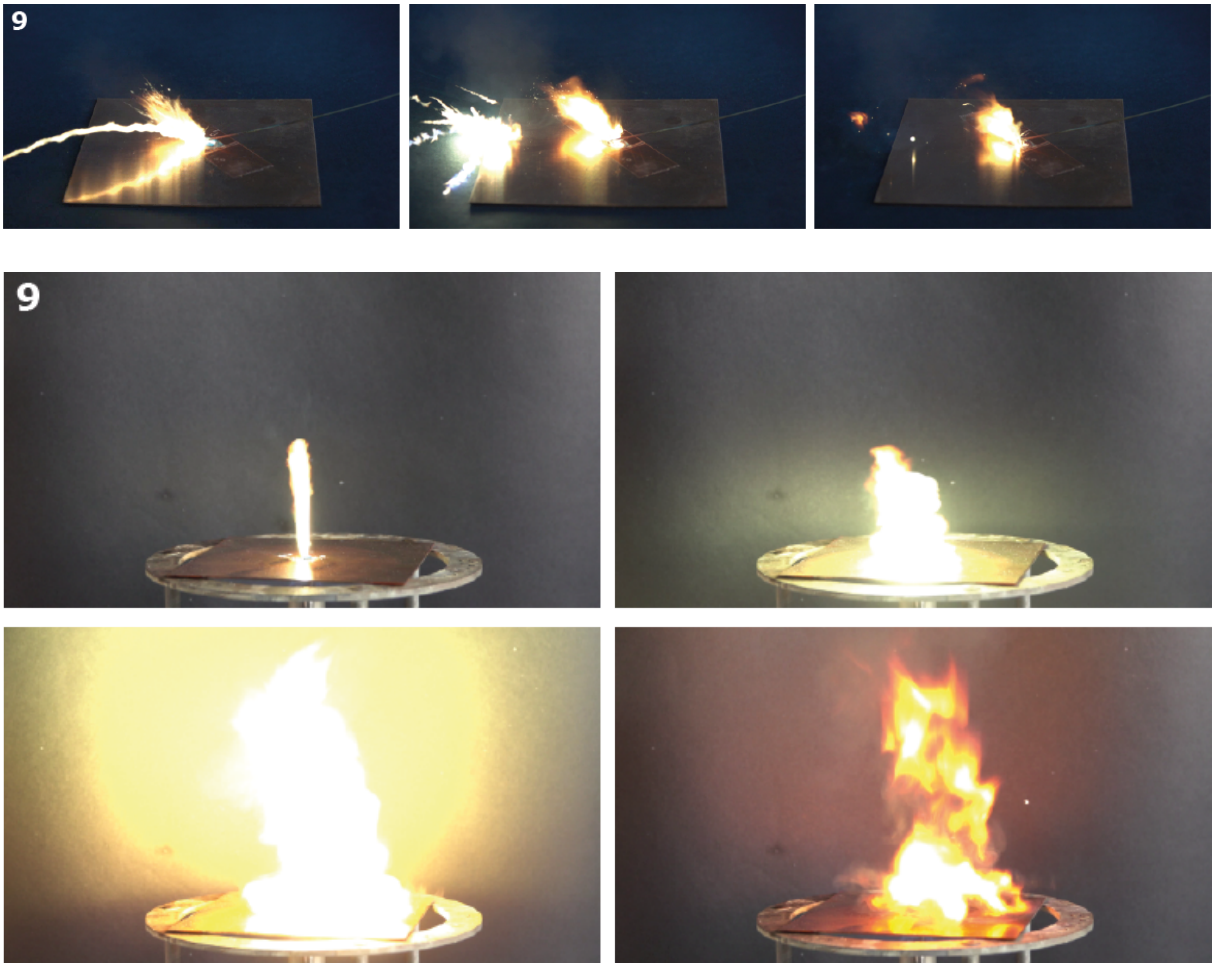


Figure S40. Hot needle and hot plate tests of the copper(II) nitrate complex **9** shown as sequences.

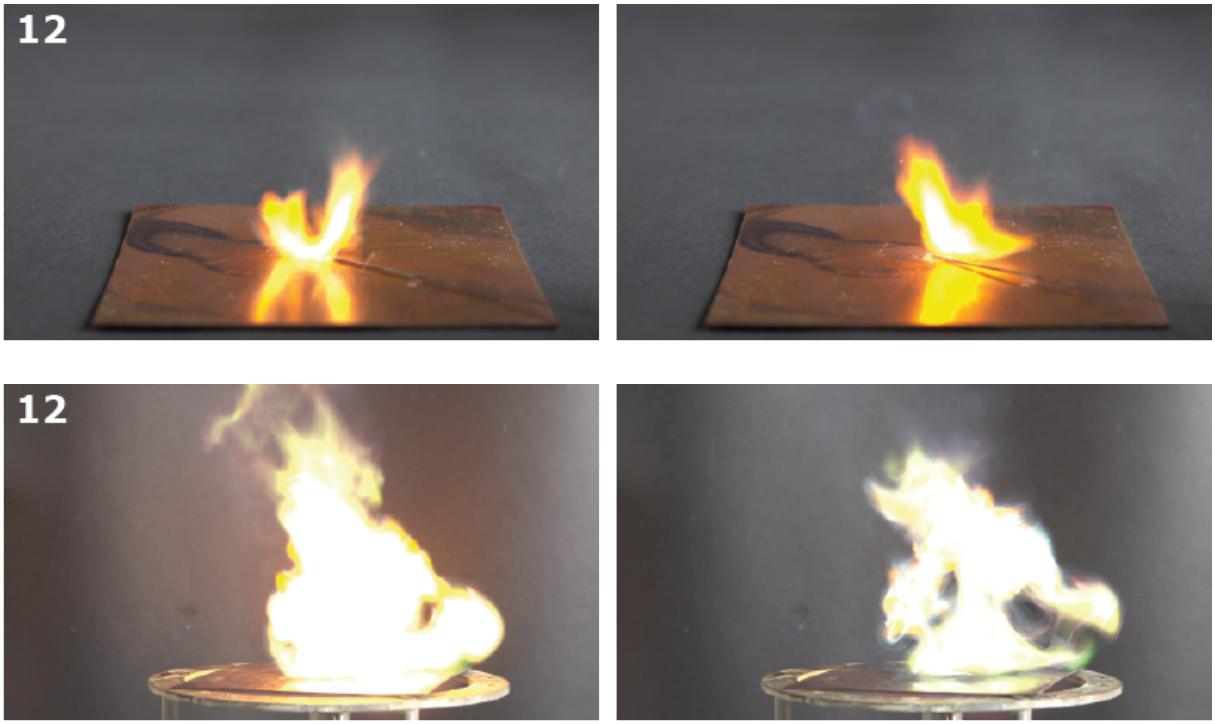


Figure S41. Initiation of the zinc(II) nitrate complex **12** shown as sequences during the hot needle and hot plate tests.

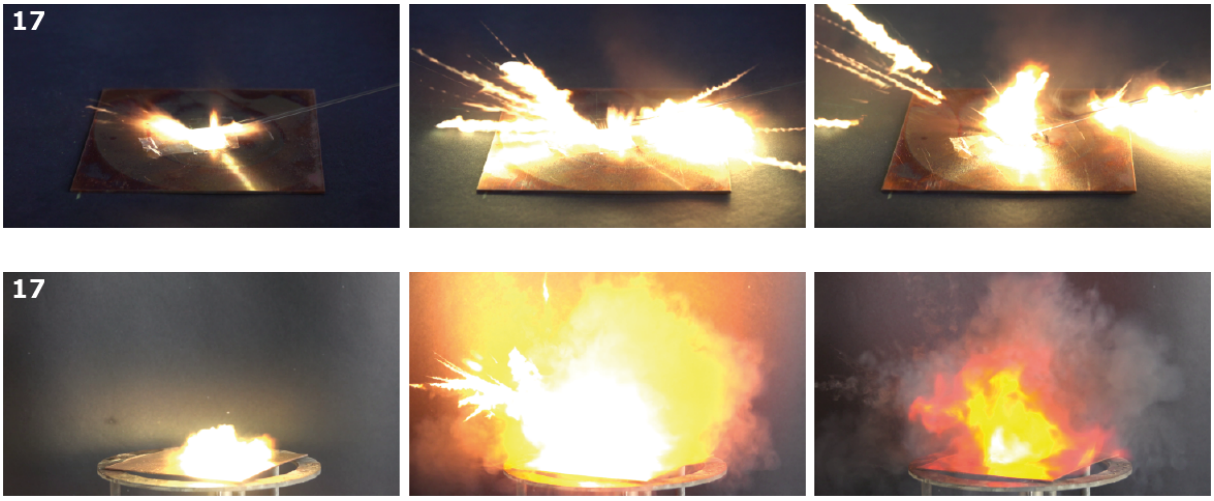


Figure S42. Initations of the coordination compound **17** shown as sequences during the hot needle and hot plate tests.

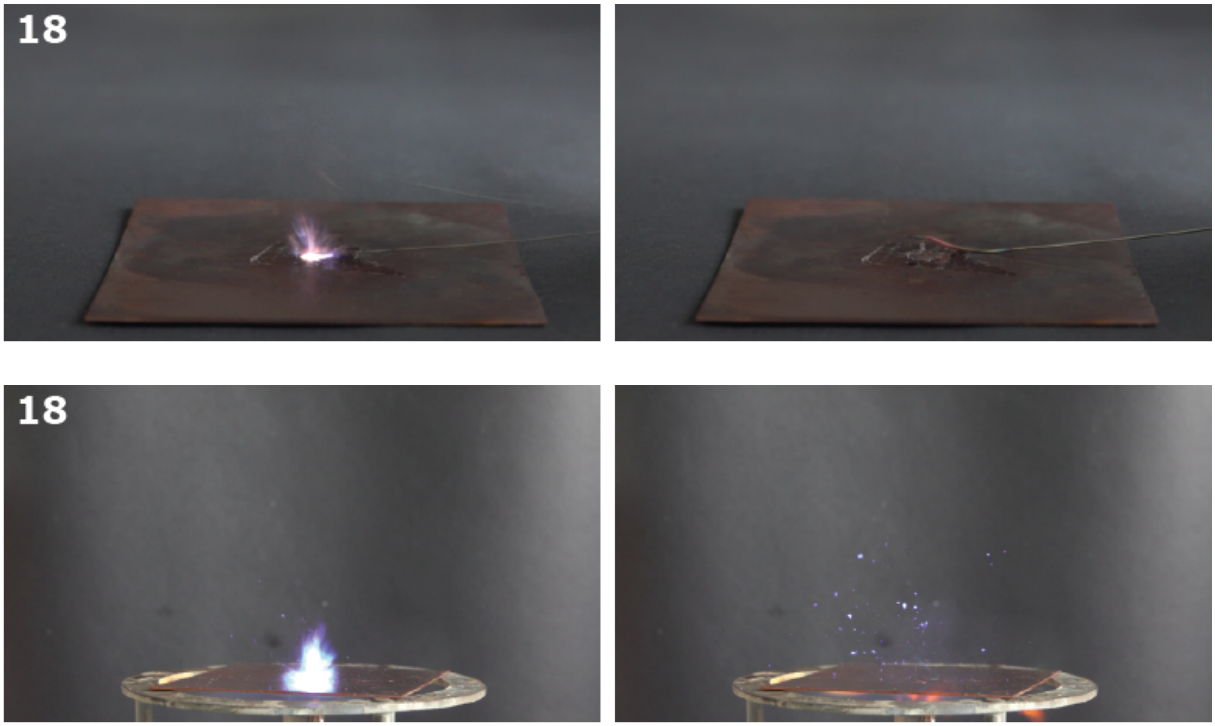


Figure S43. Detonations of the coordination compound **18** shown as sequences during the hot needle and hot plate tests.



Figure S44. Moment of detonation of complex **19** during the hot needle test.



Figure S45. Moment of detonation of complex **19** during the hot plate test.



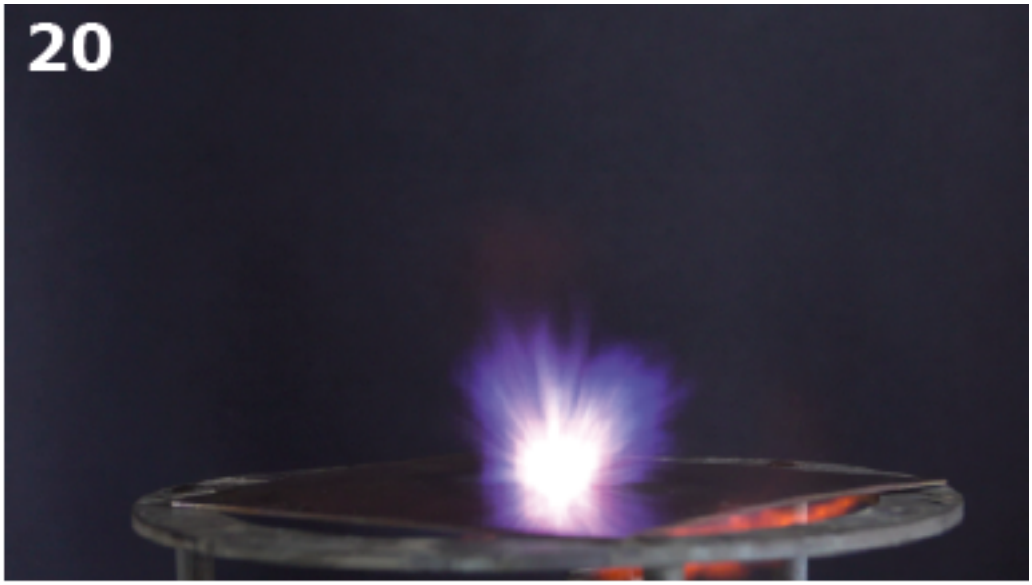


Figure S46. Detonation of complex **20** during the hot needle and hot plate tests, partly shown as a sequence.

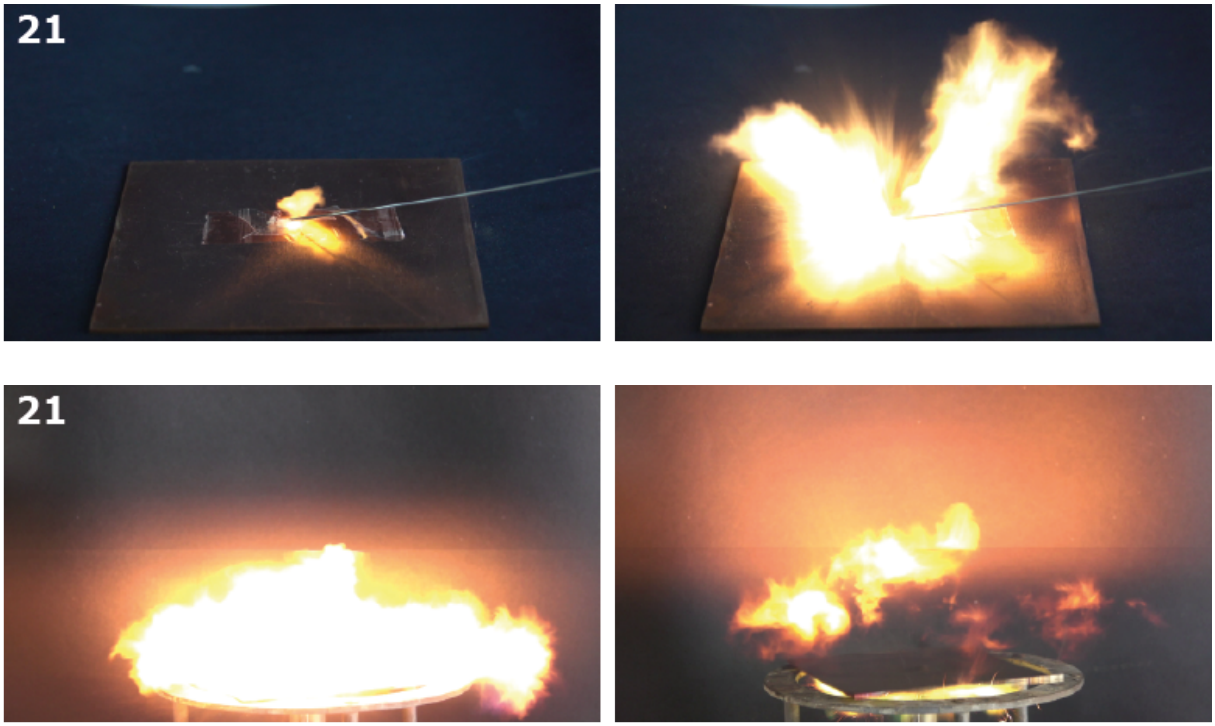


Figure S47. Detonations of coordination compound **21** during the hot needle and hot plate tests, partly shown as sequences.

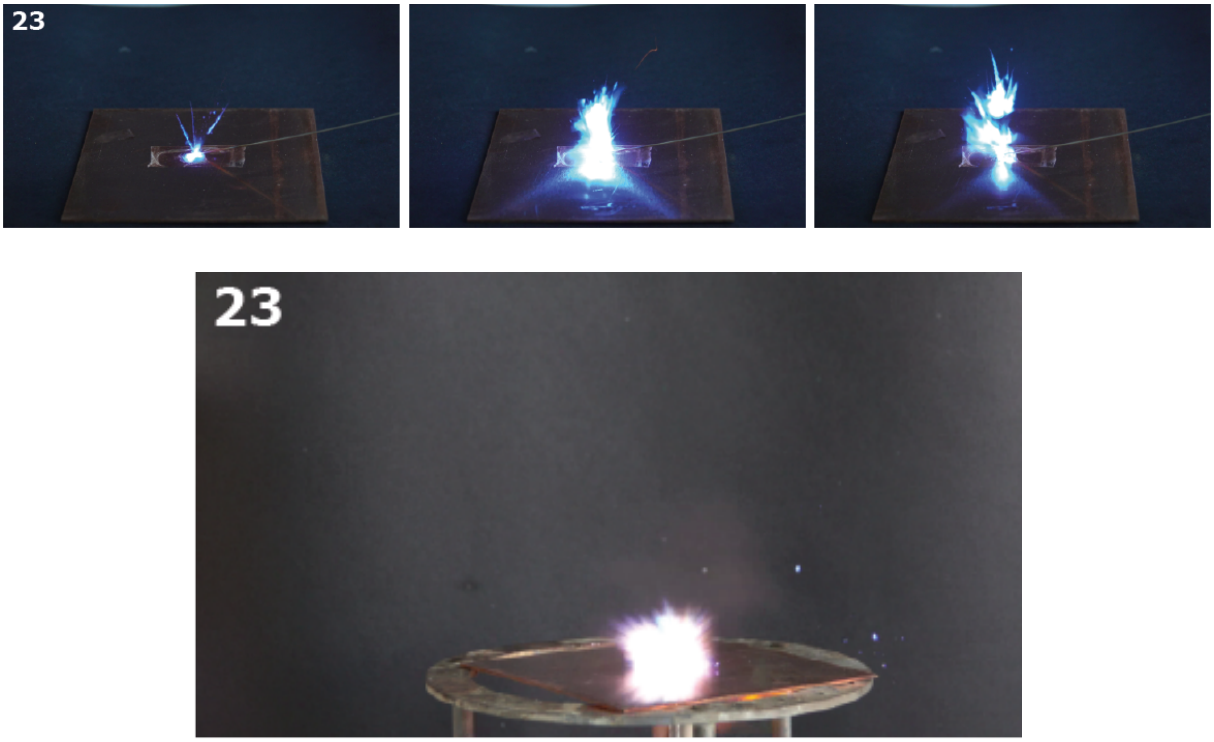


Figure S48. Behavior of complex **23** during the hot needle and hot plate tests, partly shown as a sequence.

19.13.8 Initiation Capability Tests



Figure S49. Positive PETN initiation test of 2-amino-5*H*-tetrazolium perchlorate salt **3**.

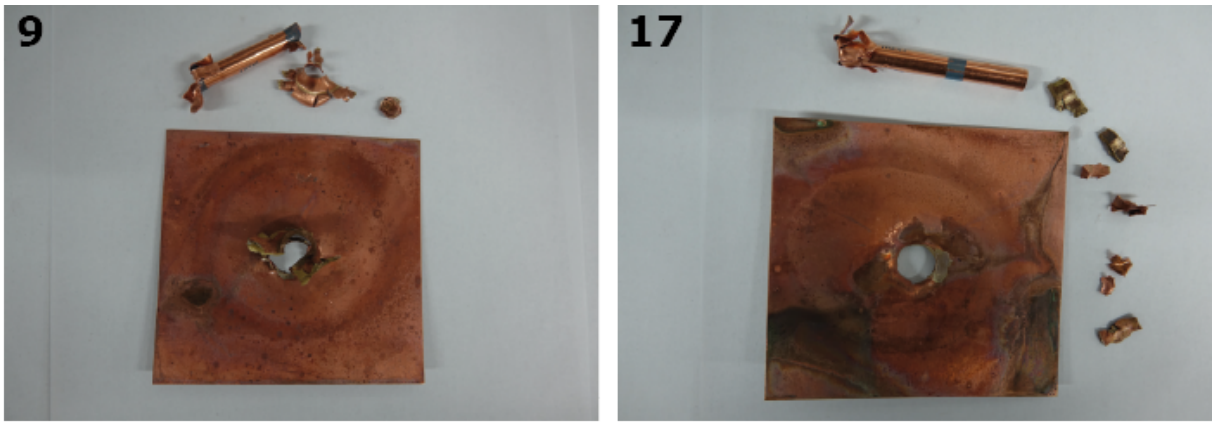


Figure S50. Positive PETN initiation tests of the copper(II) nitrate complexes **9** and **17**.

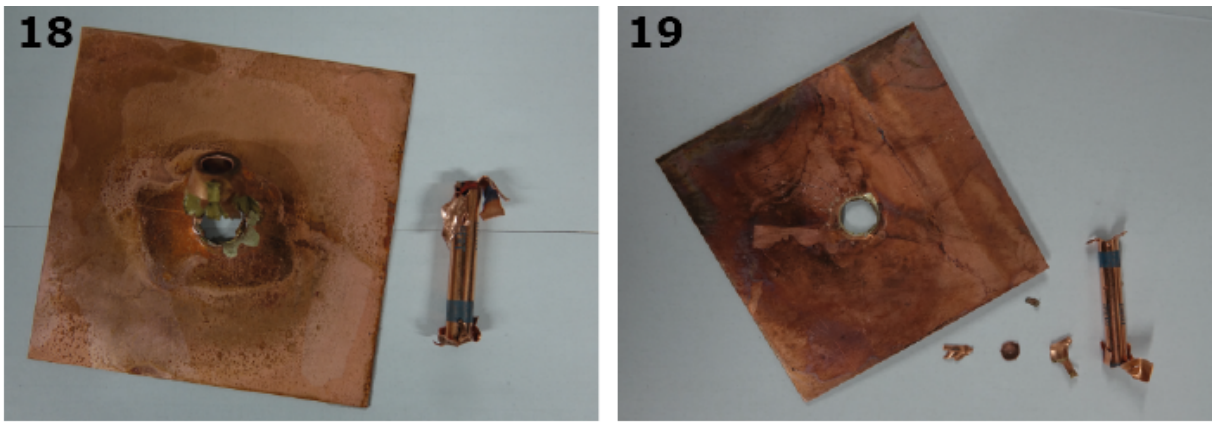


Figure S51. Positive PETN initiation tests of the metal(II) 2-AT perchlorate complexes **18** and **19**.

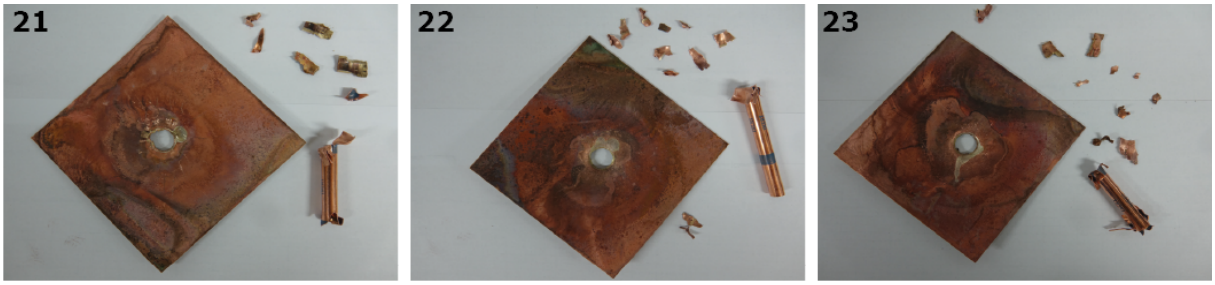


Figure S52. Positive PETN initiation tests of the 2-AT cocrystallized metal(II) perchlorate complexes **21**–**23**.

19.13.9 Laser Ignition Tests

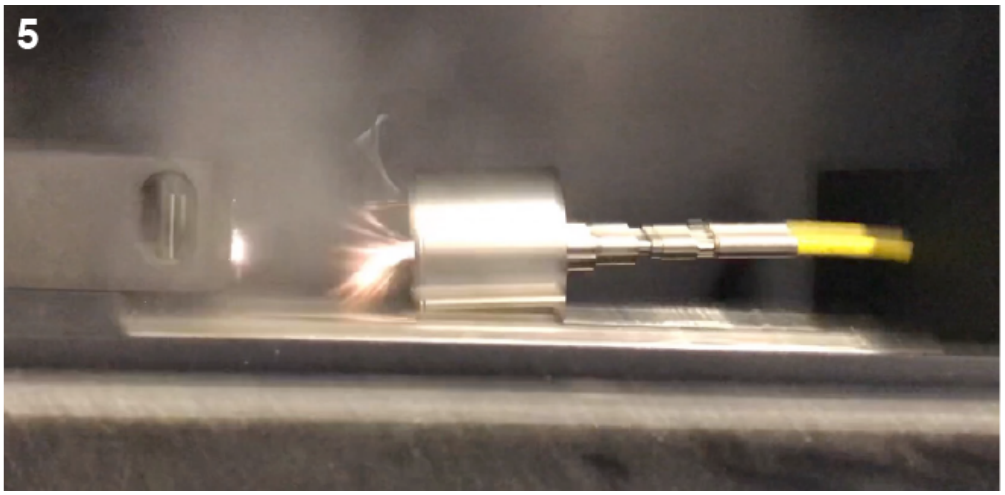


Figure S53. Detonation of **5** during the laser initiation test.

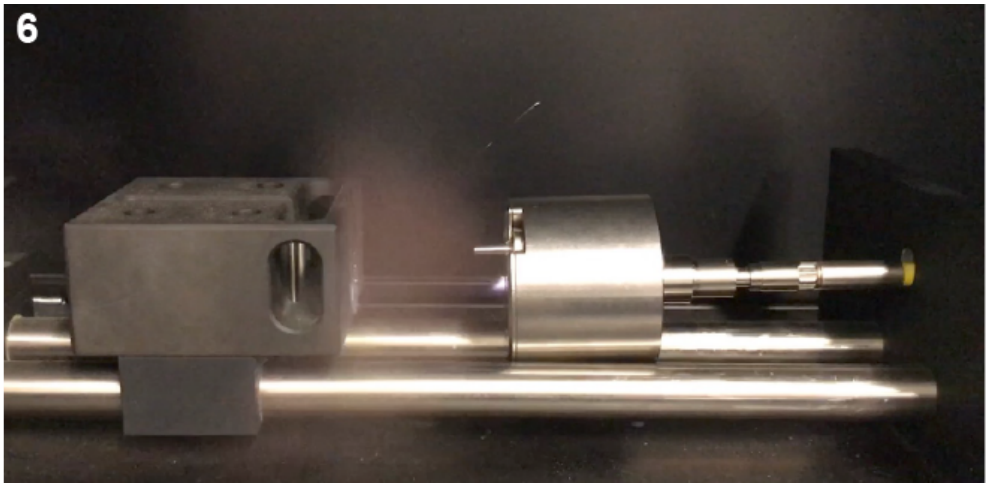


Figure S54. Detonation of **6** as reaction to laser irradiation.

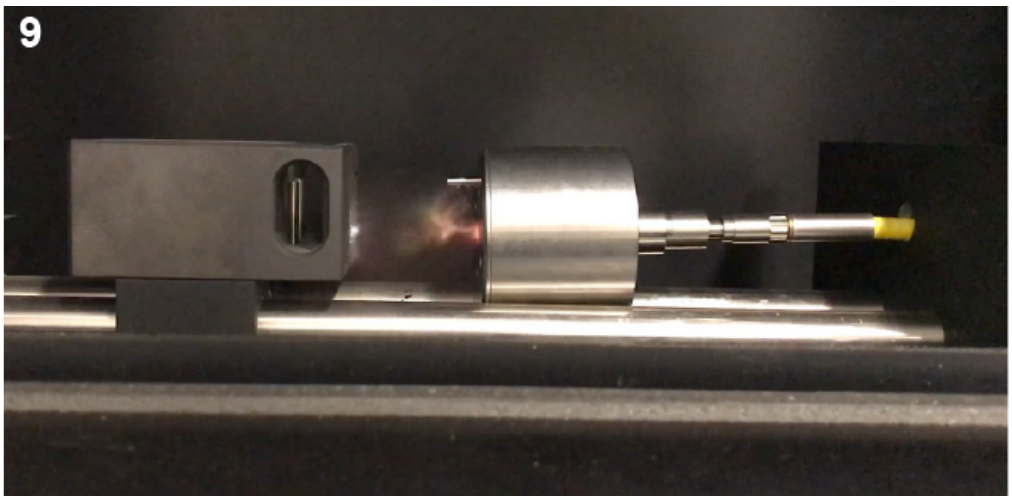


Figure S55. Moment of detonation of the copper(II) nitrate complex **9**.

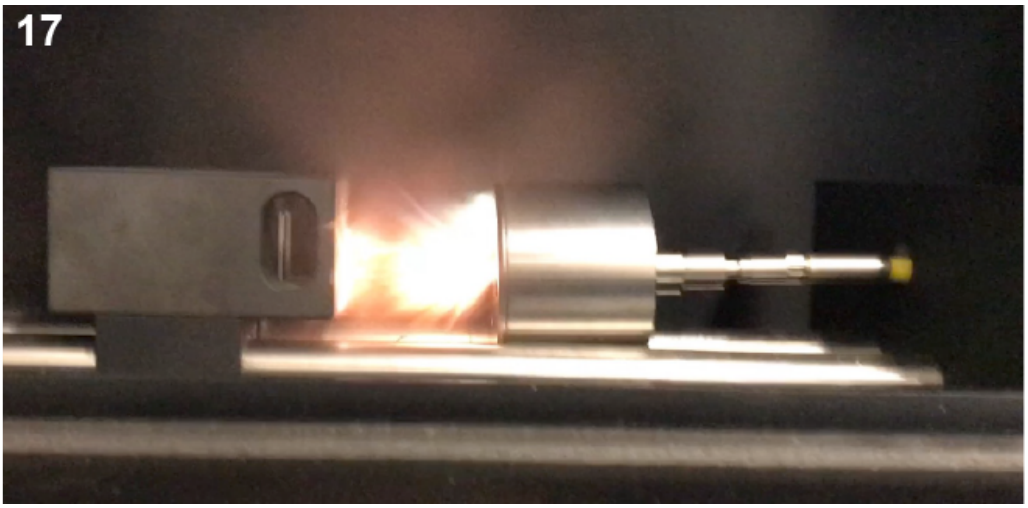


Figure S56. Detonation reaction of complex **17** during the laser initiation experiment.

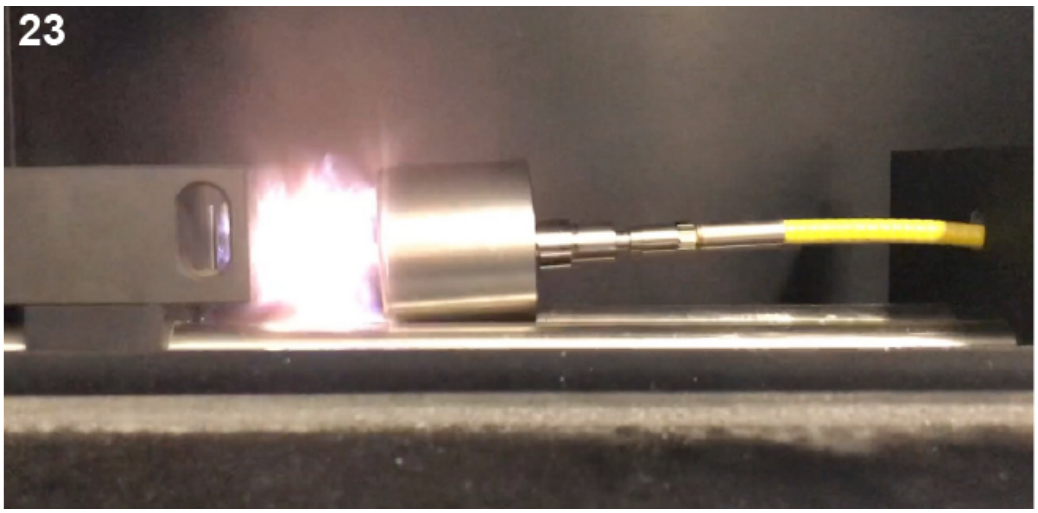


Figure S57. Moment of detonation of the copper(II) perchlorate complex **23**.

19.13.10 UV-Vis Spectra of 18, 19, 21 and 23

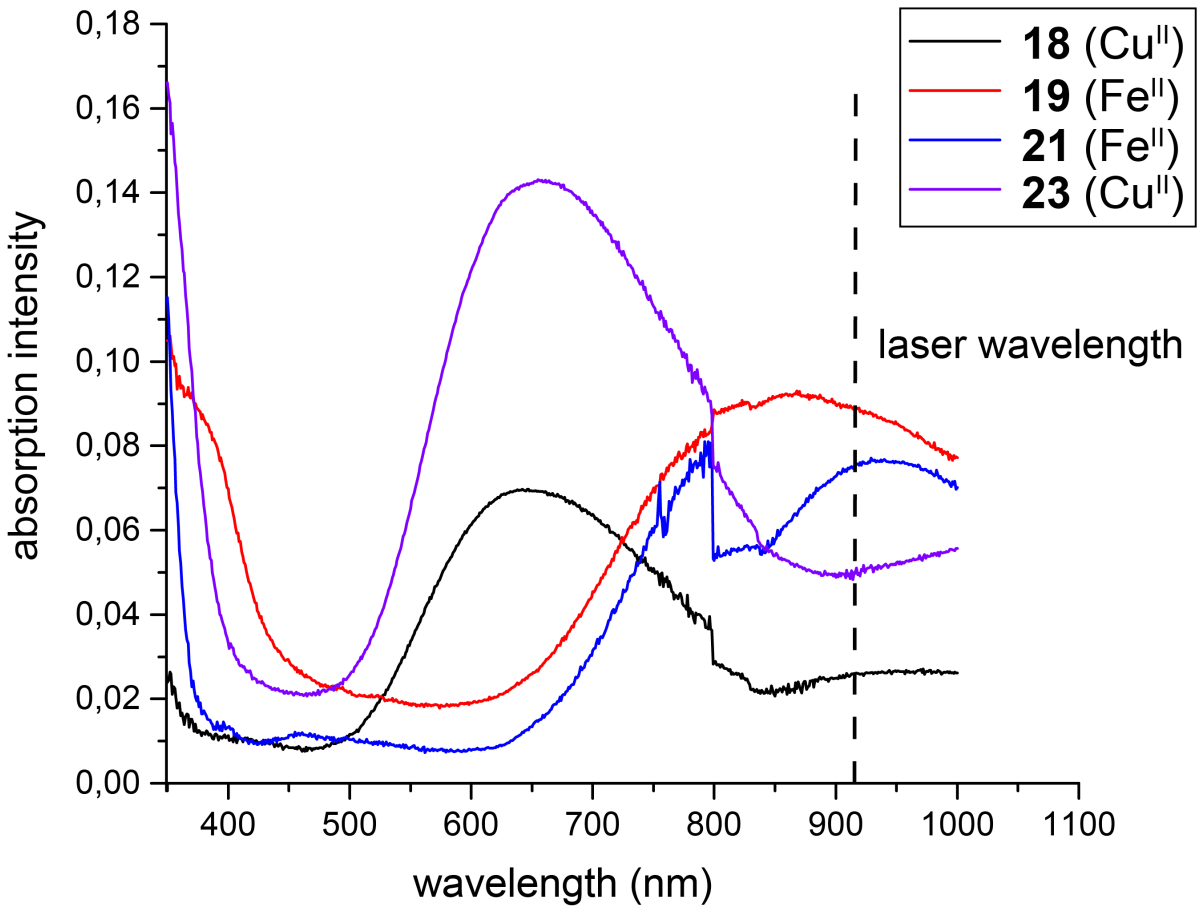


Figure S58. UV-Vis spectra in the solid state of coordination compounds **18**, **19**, **21**, and **23**.

19.13.11 Experimental Part and General Methods

All chemicals and solvents were employed as received (Sigma-Aldrich, Fluka, Acros, ABCR). The chemical composition and morphology of selected samples were investigated with a scanning electron microscope (SEM) NanoLab G3 (Helios). The samples were carbon-coated (BAL-TEC MED 020, Bal Tec AG) to prevent electrostatic charging and to increase the conductivity. Energy dispersive X-ray spectroscopy (EDX) was carried out with an acceleration voltage of 20 kV using an X-Max 80 SDD detector (Oxford Instruments). ^{1}H, ^{13}C and ^{15}N spectra were recorded at ambient temperature using a JEOL Bruker 400, Eclipse 270, JEOL EX 400 or a JEOL Eclipse 400 instrument. The chemical shifts quoted in ppm in the text refer to typical standards such as tetramethylsilane (^{1}H, ^{13}C) and nitromethane (^{15}N) in d_6-DMSO, d-$CHCl_3$ or d_3-MeCN as the solvents. The ^{1}H,^{15}N-HMBC NMR spectrum was measured with a

data matrix of 1024 x 256, an applied zero filling of 2048 x 4096, 32 scans per round, a relaxation delay of 1 second, an acquisition time of 0.3 second at a concentration of 140 mg/mL and an overall measurement time of approx. 3 h. Endothermic and exothermic events of the described compounds, which indicate melting, evaporation or decomposition, are given as the extrapolated onset temperatures. The samples were measured in a range of 25–400 °C at a heating rate of 5 °C min^{-1} through differential thermal analysis (DTA) with an OZM Research DTA 552-Ex instrument and partly by thermal gravimetric analysis (TGA) with a PerkinElmer TGA4000. Infrared spectra were measured with pure samples on a Perkin-Elmer BXII FT-IR system with a Smith DuraSampler IR II diamond ATR. Determination of the carbon, hydrogen and nitrogen contents was carried out by combustion analysis using an Elementar Vario El (nitrogen values determined are often lower than those calculated due to their explosive behavior). UV-Vis spectra were recorded in the solid state using a Varian Cary 500 spectrometer in the wavelength range of 350–1000 nm. The step in the absorption intensity at 800 nm is caused by a detector change. Impact sensitivity tests were carried out according to STANAG 4489[S10] with a modified instruction[S11] using a BAM (Bundesanstalt für Materialforschung) drophammer.[S12,13] Ball drop impact sensitivities were determined for selected compounds on an OZM ball drop machine (BIT-132) following MIL-STD-1751A (method 1016) by dropping a free-falling steel ball onto the explosive compound.[S14] A sample of approximately 30 mg was placed on a steel block and spread into a 0.33 mm layer of substance. The steel ball guide was set to the desired height and the loaded impact block positioned underneath. By releasing the ball shield, a 0.500-inch steel ball, weighing 8.35 g, was allowed to fall onto the sample. Any visual observation of decomposition was regarded as a positive result. If no reaction occurred, the remaining substance was disposed, and the impact block loaded with a freshly prepared sample. The limiting impact energy was determined in conformity with the recommended UN method for testing impact and friction sensitivities (1-in-6 approach), according to ST/SG/AC.10/11/Rev.6 (s. 13.4.2.3.3).[S15] The impact energy was calculated as the product of the weight of the steel ball and its fall height. An initial drop height was chosen, at which an explosion of the sample could be ensured. The impact energy level (ball guide height) was now stepwise decreased until no reaction was observed. At this point, testing was continued up to a total of six trials at that certain energy level. If an explosion occurred, the procedure was repeated by decreasing the drop height. As soon as six trials at a fixed energy level emerged as negative, the next higher energy level, where at least one out of at least six trials resulted in an explosion, is determined as the limiting impact energy. Friction

sensitivity tests were carried out according to STANAG 4487[S16] with a modified instruction[S17] using the BAM friction tester. The classification of the tested compounds results from the "UN Recommendations on the Transport of Dangerous Goods".[S18] Additionally all compounds were tested to determine the sensitivity toward electrical discharge using the OZM Electric Spark Tester ESD 2010 EN or OZM Electric Spark XSpark10 device.[S11] Hot plate and hot needle tests were performed in order to classify the initiation capability of selected complexes. The samples were fixed on a copper plate underneath adhesive tape and initiated by a red hot needle. Strong deflagration or detonation of the compound usually indicates a valuable primary explosive. The safe and straightforward hot plate test only shows the behavior of the unconfined sample toward fast heating on a copper plate. It does not necessarily allow any conclusions on a compound´s capability as a suitable primary explosive. Initiation capability tests of the newly investigated complexes toward pentaerythritol tetranitrate (PETN) were carried out in a copper shell with a diameter of 7 mm and length of 88 mm filled with 200 mg of sieved secondary explosive (grain size < 100 µm). First, the secondary explosive was pressed with a weight of 8 kg, then the primary explosive to be investigated was subsequently filled on top of the main charge and pressed with the same pressure force. The shell was sealed by an insulator, placed in a retaining ring, which was soldered to a copper witness plate with a thickness of 1 mm and finally initiated by a type A electric igniter. A positive test is indicated by a hole in the copper plate and fragmentation of the shell caused by a deflagration-to-detonation transition (DDT) of PETN. Liquid-dried luminescent bacteria of the strain *Vibrio fischeri* NRRL-B-11177 provided by the HACH LANGE GmbH were used for the luminescent bacteria inhibition test to determine their toxicity toward aquatic organisms according to a modified procedure.[S19] The laser initiation experiments were performed with a 45 W InGaAs laser diode operating in the single-pulsed mode. The diode is attached to an optical fiber with a core diameter of 400 µm and a cladding diameter of 480 µm. The optical fiber is connected via a SMA type connecter directly to the laser and to a collimator. This collimator is coupled to an optical lens, which was positioned in its focal distance (f = 29.9 mm) to the sample. The lens is shielded from the explosive by a sapphire glass. Approximately 15 mg of the carefully pestled complex to be investigated was filled into a transparent plastic cap (PC), pressed with a pressure force of 1 kN and sealed by a UV-curing adhesive. The confined samples were irradiated at a wavelength of 915 nm, a voltage of 4 V, currents of 6–8 A and varying pulse lengths (0.1 ms or 15 ms). The combined currents and pulse lengths result in an energy output of about 0.15 mJ up to 27 mJ.

The obtained coordination compounds were washed with cold ethanol when stated, dried overnight in air and used for analytics without further purification.

CAUTION! *All investigated compounds are potentially explosive energetic materials (the majority of the compounds lie in the range of primary explosives), which show partly increased sensitivities toward various stimuli (e.g. elevated temperatures, impact, friction or electrostatic discharge). Therefore, proper security precautions (safety glasses, face shield, earthed equipment and shoes, leather jacket, Kevlar gloves, Kevlar sleeves and ear plugs) have to be worn while synthesizing and handling the described compounds. Especially the very sensitive compounds **4**–**7** and **18**–**23** must be handled with great care! An excess of ligand **2** has to be applied during the synthesis of complex **18** in order to prevent the formation of unisolable side species (most likely a diperchlorato or hexacoordinated tetrazole complex), which tends to spontaneous violent decomposition during crystallization.*

Procedure for the preparation of 1-amino-5*H*-tetrazole (1) and 2-amino-5*H*-tetrazole (2):

Selective 1-amino-5*H*-tetrazole (1) synthesis:

Hydrazine monohydrate (46.2 mL, 940 mmol) was dissolved in 200 ml ethanol and the mixture cooled to 0 °C with an ice bath. Under vigorous stirring benzaldehyde (24 mL, 236 mmol) was added dropwise over a time period of 5 minutes. After complete addition, the resulting mixture was further stirred for 1 min at this temperature before quenching with water (300 mL). The milky white aqueous phase was extracted with dichloromethane (3 x 300 mL) and the combined organic phases dried over $MgSO_4$. The solvent was removed under reduced pressure yielding benzhydrazone in form of a yellow, odorous oil (20.8 g, 193 mmol, 82 %). ^{1}H NMR ($CHCl_3$-*d*, 25 °C, ppm) δ: 7.71 (s, 1H, NC-*H*), 7.54–7.49 (m, 2H, C_{aromat}-*H*), 7.36–7.23 (m, 3H, C_{aromat}-*H*), 5.48 (s, 2H, -N*H*$_2$). Benzhydrazone (20.8 g, 193 mmol) was dissolved in triethyl orthoformate (60 mL, 364 mmol) and subsequently further reacted with sodium azide (16.0 g, 246 mmol). While stirring, glacial acetic acid (100 mL) was added dropwise and the resulting reaction mixture heated to 80 °C for 2.5 h. During the reaction, a color change from yellow to orange and finally red could be observed. After complete reaction, the warm mixture was poured into water (200 mL) and stirred overnight. The yellow precipitate formed was filtrated, washed with a small amount of water and dried overnight in air yielding 1-benzylideneaminotetrazole (13.2 g, 76.2 mmol, 40 %). ^{1}H NMR ($CHCl_3$-*d*, 25 °C, ppm) δ: 9.37

(s, 1H, N_4C-*H*), 8.87 (s, 1H, NC-*H*), 7.96–7.84 (m, 2H, C_{aromat}-*H*), 7.67–7.47 (m, 3H, C_{aromat}-*H*). Under vigorous stirring, concentrated hydrochloric acid (150 mL) was added to 1-benzylideneaminotetrazole (13.2 g, 76.2 mmol) and water (200 mL). The suspension obtained was refluxed for 30 min resulting in a clear yellow solution. The cleaved benzaldehyde was removed together with the solvent in vacuo at 80 °C and the residues checked by TLC upon reaction completion. The received yellow-white residue was neutralized with a saturated solution of $NaHCO_3$ and extracted with EtOAc (3 x 400 mL). The combined organic phases were dried over $MgSO_4$ and the solvent removed under reduced pressure, yielding 1-amino-5*H*-tetrazole (**1**, 6.40 g, 75.2 mmol, 99 %) in form of a yellow liquid.

Amination of 1,5*H*-tetrazole:

The performed synthesis of the two isomers was carried out analogous to a modified literature procedure.[S20] 1,5-*H*-Tetrazole (14.0 g, 200 mmol) was dissolved in water (150 mL) and treated with Na_2CO_3 (23.2 g, 219 mmol). The resulting solution was heated to 75 °C, followed by the dropwise addition of hydroxylamine-*O*-sulfonic acid (27.2 g, 240 mmol) in water (120 mL). In the meantime, the pH value of the solution was maintained between 7 and 8 by periodic addition of a saturated solution of $NaHCO_3$. The reaction mixture was refluxed for 30 minutes followed by the evaporation of approximately half of the solvent under reduced pressure. After continuously extracting the remaining solution with ethyl acetate for two days, the evaporation of the extract gave a viscous oil containing both isomers **1** and **2**. The isomers were separated by column chromatography (SiO_2, ethyl acetate/ dichloromethane 5:1, R_f = 0.71, 0.47) yielding highly pure 2-amino-5*H*-tetrazole (**2**, 3.17 g, 37.2 mmol, 19 %) and 1-amino-5*H*-tetrazole (**1**, 4.54 g, 53.4 mmol, 27 %) as colorless liquids.

1-Amino-5*H*-tetrazole (1)

DTA (5 °C min^{-1}): 182 °C (exothermic); IR (ATR, cm^{-1}): $\tilde{\nu}$ = 3326 (m), 3197 (m), 3144 (m), 1626 (m), 1491 (w), 1430 (w), 1342 (w), 1273 (w), 1185 (s), 1098 (vs), 962 (s), 871 (s), 723 (m), 695 (m), 643 (vs); ^{1}H NMR (DMSO-d_6, 25 °C, ppm) δ: 9.24 (s, 1H, C-*H*), 7.10 (s, 2H, -NH_2); ^{13}C NMR (DMSO-d_6, 25 °C, ppm) δ: 143.4 (-CN$_4$); ^{15}N NMR (MeCN-d_3, 25 °C, ppm) δ: 6.8 (N3), −10.0 (N2), −53.8 (N4, d, $^2J_{N\text{-}H}$ = 11.2 Hz), −138.0 (N1, d, $^2J_{N\text{-}H}$ = 8.4 Hz), −308.4

(N5, t, $J_{N\text{-}H}$ = 73.1 Hz); EA: (CH_3N_5, 85.07) calcd: C 14.12, H 3.55, N 82.33 %; found: C 14.60, H 3.63, N 82.16 %.

2-Amino-5*H*-tetrazole (2)

DTA (5 °C min^{-1}): 197 °C (exothermic); IR (ATR, cm^{-1}): $\tilde{\nu}$ = 3314 (m), 3144 (m), 3128 (m), 3083 (w), 3012 (w), 2978 (w), 1685 (w), 1613 (m), 1488 (m),1451 (m), 1434 (m), 1388 (w), 1374 (w), 1361 (w), 1285 (s), 1259 (w), 1218 (m), 1174 (s), 1141 (s), 1111 (s), 1103 (s), 1064 (m), 1024 (s), 992 (s), 975 (s), 928 (s), 876 (s), 803 (w), 797 (w), 745 (m), 722 (m), 704 (s), 680 (m), 666 (vs), 644 (m); ^{1}H NMR (DMSO-d_6, 25 °C, ppm) δ: 8.72 (s, 1H, C-*H*), 8.03 (s, 2H, -NH_2); ^{13}C NMR (DMSO-d_6, 25 °C, ppm) δ: 151.8 (-CN$_4$); ^{15}N NMR (MeCN-d_3, 25 °C, ppm) δ: −11.2 (N3), −53.9 (N4, d, $^2J_{N\text{-}H}$ = 12.2 Hz), −78.9 (N1, d, $^2J_{N\text{-}H}$ = 14.5 Hz), −92.6 (N2, d, $^2J_{N\text{-}H}$ = 7.9 Hz), −289.6 (N5, t, $J_{N\text{-}H}$ = 72.5 Hz); EA: (CH_3N_5, 85.07) calcd: C 14.12, H 3.55, N 82.33 %; found: C 14.45, H 3.58, N 82.26 %.

2-Amino-5*H*-tetrazolium perchlorate (3)

2-Aminotetrazole (**2,** 255 mg, 3.00 mmol) was added to perchloric acid (1 M, 3 mL, 3.00 mmol) and mechanically stirred for 30 minutes. The obtained solution was left for crystallization at room temperature. After five days, the received colorless crystals were filtered and washed with diethyl ether to stoichiometrically yield 2-amino-5*H*-tetrazolium perchlorate (**3**).

DTA (5 °C min^{-1}): 122 °C (endothermic, followed by exothermic); IR (ATR, cm^{-1}): $\tilde{\nu}$ = 3332 (m), 3253 (m), 3147 (m), 3009 (w), 2967 (w), 2924 (w), 2883 (w), 2792 (w), 2755 (w), 1600 (w), 1530 (m), 1493 (w), 1451 (m), 1401 (w), 1269 (w), 1136 (m), 1107 (s), 1040 (s), 1004 (s), 984 (s), 904 (s), 775 (s), 713 (s), 698 (s), 649 (s), 635 (s), 617 (vs); EA: ($CH_4ClN_5O_4$, 185.52): calcd: C 6.47, H 2.17, N 37.45 %; found: C 6.47, H 2.37, N 37.45 %; BAM drophammer: < 1 J; friction tester: 0.2 N; ESD: 10 mJ (at grain size < 100 μm).

General procedure for the preparation of metal(II) (Mn^{II}, Fe^{II}, Cu^{II}, Zn^{II}) 1-AT perchlorate complexes (4–7):

1-Amino-5*H*-tetrazole (**1**, 128 mg, 1.50 mmol) was dissolved in water (2 mL) and added dropwise to an aqueous solution (1 mL) of the corresponding metal(II) perchlorate (**4**: $Mn(ClO_4)_2 \cdot 6\ H_2O$ (91.0 mg, 0.25 mmol), **5**: $Fe(ClO_4)_2 \cdot 6\ H_2O$ (63.7 mg, 0.25 mmol) **6**: $Cu(ClO_4)_2 \cdot 6\ H_2O$ (92.6 mg, 0.25 mmol), **7**: $Zn(ClO_4)_2 \cdot 6\ H_2O$ (93.1 mg, 0.25 mmol)). The colored reaction mixtures were mechanically stirred for one minute at ambient temperature and left for crystallization. After crystallization, the products were filtered off, washed (except complex **4**, due to its good solubility in ethanol) and dried in air.

$[Mn(1\text{-}AT)_6](ClO_4)_2$ (4)

The manganese(II) complex **4** crystallized within 4 days in the form of colorless rods suitable for X-ray determination. Yield: 142 mg (0.18 mmol, 72 %).

DTA (5 °C min^{-1}): 195 °C (exothermic); IR (ATR, cm^{-1}): $\tilde{\nu}$ = 3617 (vw), 3345 (m), 3293 (w), 3231 (w), 3142 (m), 1626 (m), 1506 (vw), 1439 (w), 1302 (w), 1194 (m), 1177 (w), 1092(vs), 1071 (vs), 984 (s), 934 (m), 869 (m), 721 (w), 700 (m), 644 (s), 622 (s); EA: ($C_6H_6Cl_2MnN_{30}O_8$, 764.25): calcd: C 9.43, H 2.37, N 54.98 %; found: C 9.85, H 2.35, N 54.39 %; ball drop impact tester: 14 mJ; BAM drophammer: < 1 J; friction tester: 0.5 N; ESD: 11 mJ (at grain size 100–500 μm).

$[Fe(1\text{-}AT)_6](ClO_4)_2$ (5)

Coordination compound **5** was obtained within three days in the form of colorless blocks suitable for X-ray diffraction. Yield: 117 mg (0.15 mmol, 60 %).

DTA (5 °C min^{-1}): 187 °C (exothermic); IR (ATR, cm^{-1}): $\tilde{\nu}$ = 3347 (w), 3295 (w), 3232 (w), 3145 (w), 1626 (m), 1508 (vw), 1440 (w), 1303 (w), 1195 (m), 1178 (w), 1092 (vs), 1074 (vs), 987 (s), 935 (m), 868 (m), 721 (w), 700 (m), 645 (m), 622 (s); UV-Vis spectrum: λ_{max} = 871 nm; EA: ($C_6H_{18}Cl_2FeN_{30}O_8$, 765.16): calcd: C 9.42, H 2.37, N 54.92 %; found: C 9.99, H 2.42, N

54.27 %; ball drop impact tester: 25 mJ; BAM drophammer: < 1 J; friction tester: < 0.1 N; ESD: 12 mJ (at grain size 100–500 µm).

$[Cu(1\text{-}AT)_6](ClO_4)_2$ (6)

Within a few hours, the very promising copper(II) complex **6** could be isolated in the form of blue blocks suitable for X-ray determination. Yield: 66.1 mg (0.09 mmol, 36 %).

DTA (5 °C min^{-1}): 174 °C (exothermic); IR (ATR, cm^{-1}): $\tilde{\nu}$ = 3346 (w), 3293 (w), 3229 (w), 3146 (w), 3010 (vw), 1626 (w), 1506 (vw), 1441 (w), 1340 (vw), 1308 (vw), 1194 (w), 1179 (w), 1090 (vs), 1074 (vs), 999 (m), 978 (m), 934 (m), 868 (m), 720 (w), 699 (m), 645 (s), 622 (s); UV-Vis spectrum: λ_{max} = 677 nm; EA: ($C_6H_{18}Cl_2CuN_{30}O_8$, 772.86): calcd: C 9.32, H 2.35, N 54.37 %; found: C 9.95, H 2.40, N 53.38 %; ball drop impact tester: < 4 mJ; BAM drophammer: < 1 J; friction tester: < 0.1 N; ESD: 5 mJ (at grain size < 100 µm).

$[Zn(1\text{-}AT)_6](ClO_4)_2$ (7)

After three days, the zinc perchlorate complex **7** was isolated in the form of colorless blocks suitable for X-ray diffraction. Yield: 64.2 mg (0.08 mmol, 32 %).

DTA (5 °C min^{-1}): 189 °C (exothermic); IR (ATR, cm^{-1}): $\tilde{\nu}$ = 3378 (w), 3347 (w), 3296 (w), 3231 (w), 3145 (w), 1625 (w), 1507 (vw), 1441 (w), 1340 (vw), 1302 (w), 1195 (m), 1178 (w), 1093 (vs), 1075 (vs), 989 (s), 935 (m), 868 (m), 758 (vw), 721 (w), 700 (m), 663 (vw), 645 (m), 623 (s); EA: ($C_6H_{18}Cl_2ZnN_{30}O_8$, 774.69): calcd: C 9.30, H 2.34, N 54.24 %; found: C 10.07, H 2.37, N 53.49 %; ball drop impact tester: 16 mJ; BAM drophammer: < 1 J; friction tester: 0.5 N; ESD: 12 mJ (at grain size 100–500 µm).

[CuCl(µ-Cl)(1-AT)(µ-1-AT)] (8)

1-Amino-5*H*-tetrazole (**1**, 42.5 mg, 0.50 mmol) was dissolved in ethanol (2 mL) and slowly added to an ethanolic solution (1 mL) of $CuCl_2 \cdot 2\ H_2O$ (42.6 mg, 0.25 mmol) while stirring mechanically. The obtained reaction mixture began to cloud leading to a green precipitate. The

addition of 2 m HCl (1 mL) caused the precipitate to dissolve while stirring for 10 minutes. After only one day, [CuCl(μ-Cl)(1-AT)(μ-1-AT)] (**8**) was received in the form of green single crystals suitable for X-ray diffraction. Yield: 55.1 mg (0.18 mmol, 72 %).

DTA (5 °C min^{-1}) onset: 175 °C (exothermic); IR (ATR, cm^{-1}): $\tilde{\nu}$ = 3316 (w), 3263 (m), 3183 (m), 3155 (m), 3125 (m), 2956 (w), 1630 (w), 1604 (m), 1493 (w), 1443 (w), 1317 (w), 1302 (w), 1189 (m), 1167 (s), 1091 (vs), 1023 (s), 998 (s), 953 (vs), 914 (s), 870 (m), 715 (m), 695 (m), 648 (m), 638 (s); UV-Vis spectrum: λ_{max} = 768 nm; EA: ($C_2H_6Cl_2CuN_{10}$, 304.59): calcd: C 7.89, H 1.99, N 45.99 %; found: C 8.13, H 2.17, N 45.75 %; BAM drophammer: 3 J; friction tester: 60 N; ESD: 50 mJ (at grain size < 100 μm).

[Cu(NO$_3$)$_2$(1-AT)$_3$] (9)

A solution of ligand **1** (63.8 mg, 0.75 mmol) in water (2 mL) was slowly added to an aqueous solution (1 mL) of $Cu(NO_3)_2 \cdot 3\ H_2O$ (60.4 mg, 0.25 mmol). Within five days, **9** was obtained in the form of dark blue single crystals suitable for X-ray diffraction. Yield: 88.1 mg (0.20 mmol, 79 %).

DTA (5 °C min^{-1}) onset: 161 °C (exothermic); IR (ATR, cm^{-1}) $\tilde{\nu}$ = 3324 (m), 3275 (w), 3219 (m), 3172 (m), 3151 (m), 3137 (m), 1620 (w), 1597 (w), 1491 (m), 1472 (s), 1436 (m), 1299 (s), 1278 (vs), 1192 (s), 1114 (m), 1095 (s), 1046 (m), 1031 (m), 1001 (s), 966 (s), 936 (m), 898 (m), 886 (m), 846 (m), 809 (m), 748 (m), 722 (w), 717 (w), 702 (m), 649 (s), 641 (s); UV-Vis spectrum: λ_{max} = 686 nm; EA: ($C_3H_9CuN_{17}O_6$, 442.77): calcd: C 8.14, H 2.05, N 53.78 %; found: C 8.48, H 2.09, N 50.95 %; ball drop impact tester: 6 mJ; BAM drophammer: 3 J; friction tester: 2.25 N; ESD: 10 mJ (at grain size < 100 μm).

[Zn(1-AT)$_6$](NO$_3$)$_2$ (12)

An ethanolic solution (0.5 mL) of zinc(II) nitrate hexahydrate (37.2 mg, 125 μmol) was treated with the nitrogen-rich ligand **1** (63.5 mg, 0.75 mmol) dissolved in ethanol (0.5 mL) and mechanically stirred at room temperature for several minutes. After leaving the reaction mixture for crystallization, colorless blocks of **12** suitable for X-ray determination could be collected

within three days. The product was filtered off, washed and dried in air. Yield: 34.0 mg (0.05 mmol, 39 %).

DTA (5 °C min^{-1}) onset: 115 °C (endothermic), 180 °C (exothermic); TGA (5 °C min^{-1}): 115–180 °C (loss of coordinating 1-AT ligands), 180 °C (dec.); IR (ATR, cm^{-1}): $\tilde{\nu}$ = 3339 (m), 3312 (m), 3272 (m), 3198 (m), 3179 (m), 3136 (m), 3126 (m), 3104 (m), 3000 (w), 1639 (m), 1617 (m), 1508 (w), 1438 (m), 1383 (s), 1339 (vs), 1321 (vs), 1196 (s), 1129 (m), 1094 (vs), 1045 (w), 988 (s), 966 (s), 889 (s), 829 (m), 721 (m), 701 (m), 643 (vs); EA ($C_6H_{18}N_{32}O_6Zn$, 699.89): calcd: C 10.30, H 2.59, N 64.05 %; found: C 10.80, H 2.57, N 64.67 %; BAM drophammer: < 1 J; friction tester: 6 N; ESD: 620 mJ (at grain size 100–500 µm).

[Cu(µ-Cl)$_2$(2-AT)$_2$] (16)

The copper(II) chloride complex **16** was synthesized through slow addition of an aqueous solution (2 mL) of 2-amino-5*H*-tetrazole (**2**, 42.5 mg, 0.50 mmol) to $CuCl_2 \cdot 2\ H_2O$ (42.6 mg, 0.25 mmol) dissolved in water (1 mL) followed by 10 minutes of stirring mechanically. The desired compound [Cu(µ-Cl)$_2$(2-AT)$_2$] (**16**) was isolated after two days in the form of green blocks suitable for X-ray diffraction. Yield: 31.1 mg (0.10 mmol, 40 %).

DTA (5 °C min^{-1}) onset: 171 °C (exothermic); IR (ATR, cm^{-1}): $\tilde{\nu}$ = 3300 (s), 3248 (m), 3190 (m), 3150 (s), 3011 (w), 2959 (w), 1808 (w), 1611 (m), 1576 (w), 1455 (m), 1395 (w), 1357 (w), 1302 (m), 1210 (m), 1196 (m), 1132 (vs), 1027 (s), 904 (vs), 733 (m), 693 (s), 669 (s); UV-Vis spectrum: λ_{max} = 796 nm; EA ($C_2H_6Cl_2CuN_{10}$, 304.59): calcd: C 7.89, H 1.99, N 45.99 %; found: C 8.16, H 2.04, N 45.90 %; BAM drophammer: < 2 J; friction tester: 40 N; ESD: 10 mJ (at grain size < 100 µm).

[Cu(NO$_3$)$_2$(µ-2-AT)$_2$] (17)

Copper(II) nitrate trihydrate (60.4 mg, 0.25 mmol) was dissolved in water (1 mL). While stirring mechanically, an aqueous solution (2 mL) of the *N*2-subsituted ligand **2** (42.5 mg, 0.50 mmol) was added slowly. The very sensitive nitrate complex **17** was obtained over a period of three days in the form of blue plates suitable for X-ray diffraction. Yield: 65.3 mg (0.18 mmol, 72 %).

DTA (5 °C min^{-1}) onset: 157 °C (exothermic); IR (ATR, cm^{-1}): $\tilde{\nu}$ = 3255 (m), 3200 (m), 3148 (m), 3125 (m), 2985 (w), 2905 (w), 1579 (w), 1505 (w), 1438 (s), 1408 (m), 1317 (s), 1291 (vs), 1200 (m), 1144 (s), 1045 (s), 1022 (s), 918 (s), 828 (w), 808 (s), 735 (w), 719 (m), 693 (m), 685 (s); UV-Vis spectrum: λ_{max} = 689 nm; EA ($C_2H_6CuN_{12}O_6$, 357.70): calcd: C 6.72, H 1.69, N 46.99 %; found: C 6.89, H 1.76, N 47.03 %; BAM drophammer: < 1 J; friction tester: 2 N; ESD: 10 mJ (at grain size < 100 μm).

$[Cu(H_2O)_2(2\text{-}AT)_4](ClO_4)_2$ (18)

To an aqueous solution (1 mL) of the nitrogen-rich compound **2** (213 mg, 2.50 mmol), a solution of copper(II) perchlorate hexahydrate was added dropwise (92.6 mg, 0.25 mmol). After three days, coordination compound **18**, an extremely sensitive complex, was isolated in the form of blue blocks suitable for X-ray diffraction. Yield: 82.1 mg (0.13 mmol, 52 %).

DTA (5 °C min^{-1}) onset: 110 °C (endothermic), 173 °C (exothermic); IR (ATR, cm^{-1}): $\tilde{\nu}$ = 3485 (w), 3443 (w), 3283 (m), 3248 (m), 3173 (m), 3000 (vw), 1626 (w), 1608 (m), 1572 (vw), 1490 (vw), 1396 (w), 1312 (m), 1176 (w), 1153 (m), 1054 (vs), 1029 (vs), 936 (m), 899 (s), 732 (w), 693 (w), 678 (s), 620 (s); UV-Vis spectrum: λ_{max} = 647 nm; EA ($C_4H_{16}Cl_2CuN_{20}O_{10}$, 638.75): calcd: C 7.52, H 2.52, N 43.86 %; found: C 8.10, H 2.39, N 43.78 %; BAM drophammer: 1 J; friction tester: 0.4 N; ESD: 10 mJ (at grain size 100–500 μm).

General procedure for the preparation of the metal(II) (Fe^{II}, Zn^{II}) 2-AT perchlorate coordination compounds (19/20):

While stirring mechanically, a solution of 2-amino-5*H*-tetrazole (**2**, 106 mg, 1.25 mmol) in water (2 mL) was slowly added to an aqueous solution (1 mL) of the corresponding metal(II) perchlorate (**19**: $Fe(ClO_4)_2 \cdot 6\ H_2O$ (63.7 mg, 0.25 mmol), **20**: $Zn(ClO_4)_2 \cdot 6\ H_2O$ (93.1 mg, 0.25 mmol)) at room temperature. The reaction mixtures were left for crystallization until a crystalline material appeared. The products obtained were filtered off, washed and dried in air.

$[Fe(H_2O)(2\text{-}AT)_5](ClO_4)_2$ (19)

Colorless blocks of **19**, which were suitable for X-ray analysis started to crystallize within two days. Yield: 82.0 mg (0.12 mmol, 48 %).

DTA (5 °C min^{-1}) onset: 159 °C (exothermic); IR (ATR, cm^{-1}): $\tilde{\nu}$ = 3262 (w), 3152 (m), 1664 (w), 1601 (w), 1502 (vw), 1453 (vw), 1389 (w), 1304 (m), 1285 (vw), 1238 (vw), 1151 (m), 1144 (m), 1080 (vs), 1041 (s), 1026 (s), 944 (m), 935 (m), 912 (m), 894 (m), 717 (w), 694 (m), 680 (m), 674 (m), 621 (vs); UV-Vis spectrum: λ_{max} = 868 nm; EA ($C_5H_{17}Cl_2FeN_{25}O_9$, 698.10): calcd: C 8.60, H 2.45, N 50.16 %; found: C 9.10, H 2.52, N 49.55 %; BAM drophammer: 1.5 J; friction tester: 0.15 N; ESD: 10 mJ (at grain size 100–500 μm).

$[Zn(H_2O)(2\text{-}AT)_5](ClO_4)_2$ (20)

After two days, **20** was obtained in the form of colorless blocks suitable for X-ray diffraction. Yield: 110 mg (0.16 mmol, 64 %).

DTA (5 °C min^{-1}) onset: 132 °C (endothermic), 200 °C (exothermic); IR (ATR, cm−1): $\tilde{\nu}$ = 3340 (m), 3261 (m), 3175 (m), 3156 (m), 3004 (w), 1660 (w), 1634 (w), 1600 (m), 1573 (w), 1505 (vw), 1454 (w), 1404 (w), 1340 (vw), 1306 (m), 1240 (w), 1194 (w), 1176 (w), 1155 (m), 1145 (m), 1076 (vs), 1050 (s), 1034 (s), 1026 (s), 935 (m), 895 (s), 758 (vw), 718 (w), 694 (m), 680 (m), 646 (m), 620 (s); EA: ($C_5H_{17}Cl_2N_{25}O_9Zn$, 707.64): calcd: C 8.49, H 2.42, N 49.49 %; found: C 8.99, H 2.67, N 49.15 %; BAM drophammer: 1.5 J; friction tester: 0.5 N; ESD: 10 mJ (at grain size < 100 μm).

General procedure for the preparation of the metal(II) (Fe^{II}, Zn^{II}, Cu^{II}) 2-AT perchlorate coordination compounds (21–23) with cocrystallized 2-ATs:

The relevant metal(II) perchlorate salt (**21**: iron(II) perchlorate hexahydrate (63.7 mg, 0.25 mmol), **22**: zinc(II) perchlorate hexahydrate (93.1 mg, 0.25 mmol), **23**: copper(II) perchlorate hexahydrate (92.6 mg, 0.25 mmol)) were dissolved in the minimum amount of distilled water or ethanol in the case of complex **23**. An aqueous or ethanolic (in case of **23**) solution (1 mL) of the energetic tetrazole ligand **2** (213 mg, 2.50 mmol) was added, the reaction

mixture mechanically stirred for one minute and finally left for crystallization. After crystallization, the cocrystallized species were filtered off, washed with cold ethanol and dried in air.

$[Fe(2\text{-}AT)_6](ClO_4)_2 \cdot 2\text{-}AT$ (21)

Product **21** was obtained after four days in the form of colorless blocks suitable for X-ray diffraction. Yield: 41.1 mg (0.04 mmol, 16 %).

DTA (5 °C min^{-1}) onset: 106 °C (endothermic), 169 °C (exothermic); IR (ATR, cm^{-1}): $\tilde{\nu}$ = 3329 (m), 3265 (m), 3152 (m), 3139 (m), 1602 (m), 1503 (vw), 1461 (w), 1388 (w), 1304 (m), 1286 (w), 1231 (w), 1145 (m), 1084 (vs), 1041 (s), 1026 (s), 1014 (s), 940 (s), 913 (m), 897 (s), 891 (s), 881 (m), 724 (m), 703 (m), 695 (m), 682 (m), 673 (m), 622 (s); UV-Vis spectrum: λ_{max} = 795 nm; EA: ($C_8H_{24}Cl_2FeN_{40}O_8$, 935.30): calcd: C 10.27, H 2.59, N 59.90 %; found: C 10.84, H 2.62, N 59.71 %; BAM drophammer: < 1 J; friction tester: 0.1 N; ESD: 25 mJ (at grain size 100–500 μm).

$[Zn(2\text{-}AT)_6](ClO_4)_2 \cdot 2\text{-}AT$ (22)

Within four days, complex **22** crystallized in the form of colorless plates suitable for X-ray diffraction. Yield: 46.0 mg (0.05 mmol, 20 %).

DTA (5 °C min^{-1}) onset: 96 °C (endothermic), 192 °C (exothermic); IR (ATR, cm^{-1}): $\tilde{\nu}$ = 3329 (m), 3263 (m), 3171 (m), 3152 (m), 3139 (m), 3005 (vw), 1602 (m), 1503 (vw), 1460 (w), 1409 (w), 1388 (w), 1305 (m), 1286 (w), 1228 (w), 1182 (w), 1145 (m), 1086 (vs), 1041 (s), 1027 (s), 1013 (s), 940 (s), 912 (s), 898 (s), 890 (s), 880 (s), 724 (m), 718 (m), 703 (m), 695 (m), 680 (m), 673 (m), 622 (s); EA: ($C_8H_{24}Cl_2N_{40}O_8Zn$, 944.83): calcd: C 10.17, H 2.56, N 59.30 %; found: C 10.42, H 2.57, N 59.10 %; BAM drophammer: 2 J; friction tester: 0.2 N; ESD: 30 mJ (at grain size 100–500 μm).

$[Cu(2\text{-}AT)_6](ClO_4)_2 \cdot 2\text{-}AT$ (23)

Within one hour, complex **23** appeared in the form of blue blocks suitable for X-ray diffraction. Yield: 30.0 mg (0.03 mmol, 13 %).

DTA (5 °C min^{-1}) onset: 108 °C (endothermic), 157 °C (exothermic); IR (ATR, cm^{-1}): $\tilde{\nu}$ = 3354 (m), 3319 (m), 3281 (m), 3268 (m), 3256 (m), 3244 (m), 3227 (m), 3176 (m), 3142 (m), 1612 (m), 1458 (w), 1393 (w), 1320 (w), 1302 (w), 1293 (m), 1223 (m), 1197 (w), 1188 (w), 1148 (m), 1098 (vs), 1060 (s), 1047 (s), 1024 (vs), 1015 (s), 948 (s), 932 (s), 901 (s), 889 (s), 726 (m), 705 (s), 681 (m), 674 (m), 668 (m), 622 (vs), 473 (w), 454 (m); UV-Vis spectrum: λ_{max} = 655 nm; EA: ($C_8H_{24}Cl_2CuN_{40}O_8$, 943.00): calcd: C 10.19, H 2.57, N 59.41 %; found: C 10.23, H 2.51, N 59.41 %; BAM drophammer: 1 J; friction tester: < 0.2 N; ESD: 1.2 mJ (at grain size 100–500 µm).

19.13.12 References

[S1] CrysAlisPRO (Version 171.33.41), Oxford Diffraction Ltd., 2009.

[S2] A. Altomare, G. Cascarano, C. Giacovazzo, and A. Guagliardi, *J. Appl. Crystallogr.*, 1992, **26**, 343.

[S3] a) A. Altomare, G. Cascarano, C. Giacovazzo, A. Guagliardi, A. G. G. Moliterni, M. C. Burla, G. Polidori, M. Camalli and R. Spagna, SIR97, 2003; b) A. Altomare, M. C. Burla, M. Camalli, G. L. Cascarano, C. Giacovazzo, A. Guagliardi, A. G. G. Moliterni, G. Polidori and R. Spagna, *J. Appl. Crystallogr.*, 1999, **32**, 115.

[S4] a) G. M. Sheldrick, SHELXL-97, University of Göttingen, Germany, 1997; b) G. M. Sheldrick, *Acta Crystallogr. Sect. A*, 2008, **64**, 112.

[S5] A. L. Spek, PLATON, Utrecht University, The Netherlands, 1999.

[S6] L.J. Farrugia, *J. Appl. Cryst.*, 2012, **45**, 849.

[S7] Empirical absorption correction using spherical harmonics, implemented in SCALE3 ABSPACK scaling algorithm (CrysAlisPro Oxford Diffraction Ltd., Version 171.33.41, 2009).

[S8] APEX3, Bruker AXS Inc., Madison, Wisconsin, USA.

[S9] J. R. Rodriguez-Carvajal, Abstracts of the Satellite Meeting on Powder Diffration of XV Congress of the IUCr, Toulouse, France, 1990, 127.

[S10] NATO standardization agreement (STANAG) on explosives, impact sensitivity tests, no. 4489, 1st ed., Sept. 17, 1999.

[S11] WIWEB-Standardarbeitsanweisung 4-5.1.02, Ermittlung der Explosionsgefährlichkeit, hier der Schlagempfindlichkeit mit dem Fallhammer, Nov. 8, 2002.

[S12] OZM, http://www.ozm.cz, (accessed April 2018).

[S13] BAM, http://www.bam.de, (accessed April 2018).

[S14] Military Standard 1751A (MIL-STD-1751A): safety and performance tests for qualification of explosives (high explosives, propellants and pyrotechnics), method 1016, Dec. 11, 2001.

[S15] UN Model Regulation: Recommendations on the Transport of Dangerous Goods – Manual of Tests and Criteria, section 13.4.2.3.3, 2015.

[S16] NATO standardization agreement (STANAG) on explosive, friction sensitivity tests, no. 4487, 1st ed., Aug. 22, 2002.

[S17] WIWEB-Standardarbeitsanweisung 4-5.1.03, Ermittlung der Explosionsgefährlichkeit oder der Reibeempfindlichkeit mit dem Reibeapparat, Nov. 8, 2002.

[S18] Impact: insensitive > 40 J, less sensitive ≥ 35 J, sensitive ≥ 4 J, very sensitive ≤ 3 J; Friction: insensitive > 360 N, less sensitive = 360 N, sensitive < 360 N and > 80 N, very sensitive ≤ 80 N, extremely sensitive ≤ 10 N. According to the UN Recommendations on the Transport of Dangerous Goods, (+) indicates not safe for transport.

[S19] R. Scharf, PhD thesis, Ludwig-Maximilians Universität München, 2016.

[S20] T. M. Klapötke, D. G. Piercey, J. Stierstorfer, *Dalton Trans.* 2012, **41**, 9451.

19.14 Supplementary Information: Use of a Copper(II) Azide Complex as a Primary Explosive

19.14.1 Crystal Structures and X-ray Powder Diffraction

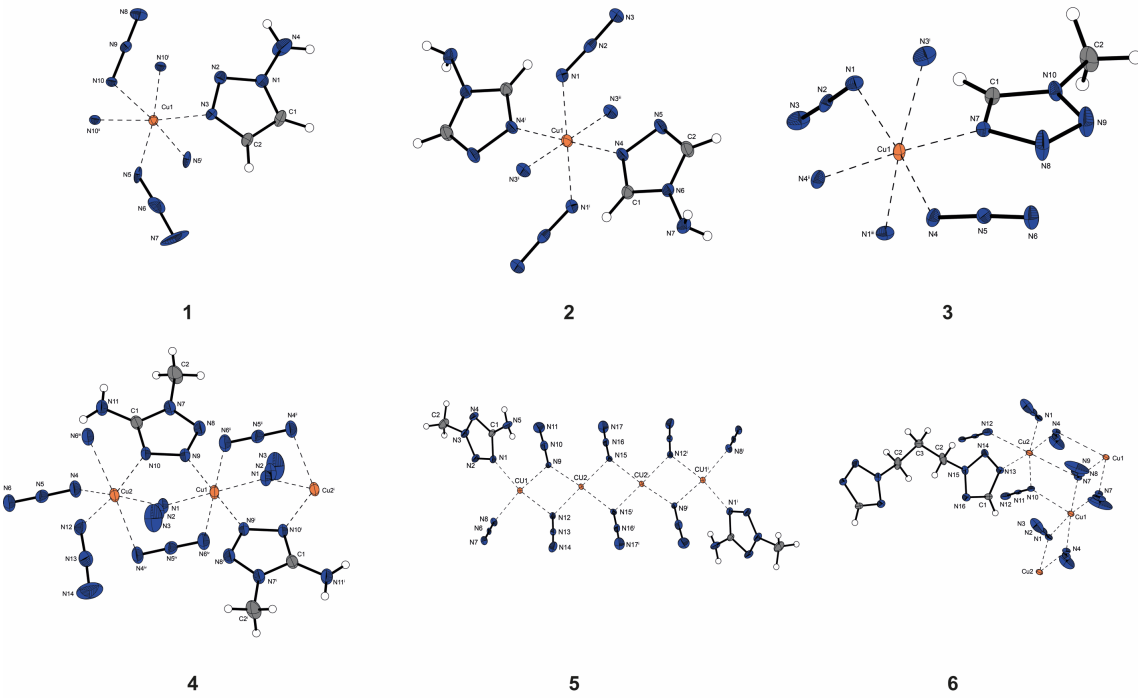


Figure 1. Crystal structures of the copper(II) azide complexes **1**-**6**.

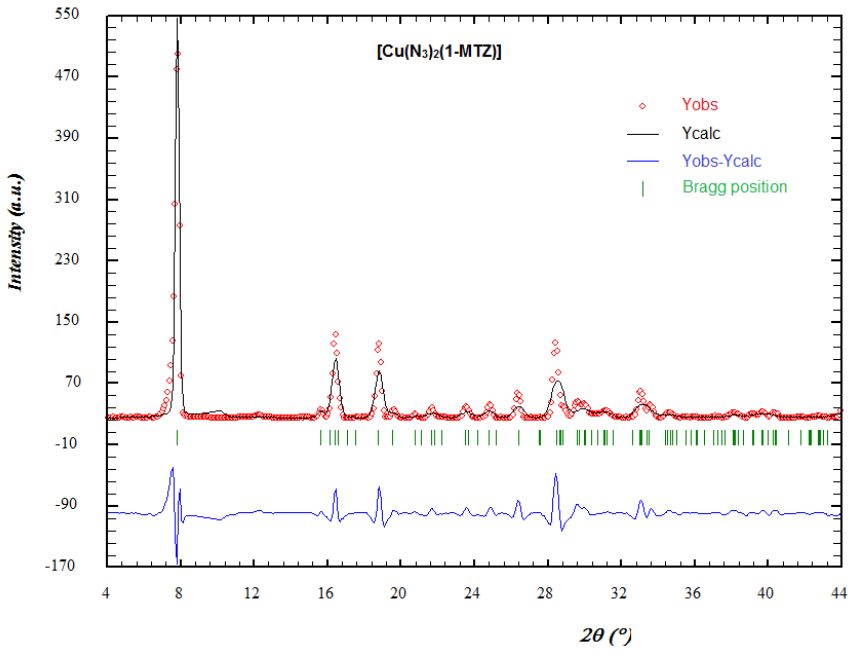


Figure 2. X-ray powder diffraction pattern of coordination compound **3**.

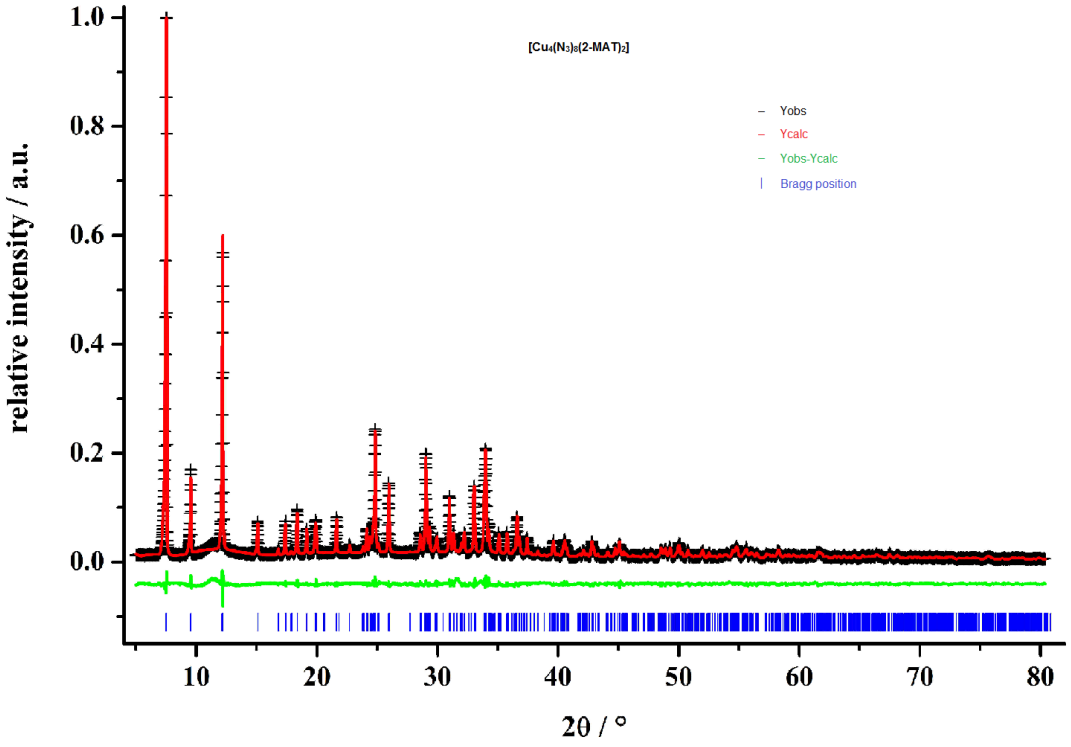


Figure 3. Powder diffraction pattern of complex **5**.

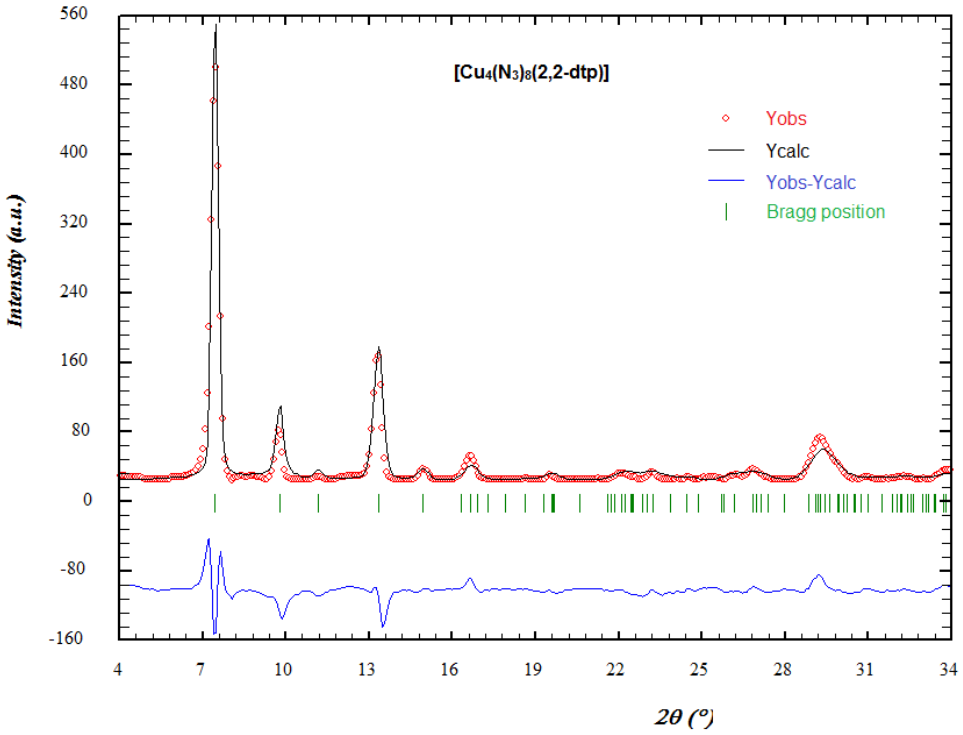


Figure 4. X-ray powder diffraction pattern of copper(II) azide complex **6**.

Table S1. Crystallographic data of **1**–**6.**

	1	**2**	**3**	**4**	**5**	**6**
Formula	$C_2H_4CuN_{10}$	$C_4H_8CuN_{14}$	$C_2H_4CuN_{10}$	$C_2H_{10}Cu_3N_{28}$	$C_2H_5Cu_2N_{17}$	$C_5H_8Cu_4N_{32}$
FW [g mol^{-1}]	231.67	315.75	231.67	641.02	394.28	770.59
Crystal system	Monoclinic	Triclinic	Monoclinic	Triclinic	Monoclinic	Monoclinic
Space Group	$P2_1/c$	$P\bar{1}$	$P2_1/c$	$P\bar{1}$	$P2_1/n$	$C2/c$
Color / Habit	Brown rod	Green needle	Red-brown plate	Red-platelet	Red rod	Brown needle
Size [mm]	0.02 x 0.03 x 0.10	0.08 x 0.14 x 0.39	0.05 x 0.16 x 0.21	0.01 x 0.05 x 0.08	0.01 x 0.02 x 0.10	0.02 x 0.25 x 0.50
a [Å]	3.4264(1)	5.3987(4)	11.4746(7)	6.2454(4)	14.7855(6)	18.2752(11)
b [Å]	14.7560(5)	6.9250(6)	6.1867(3)	8.5723(5)	5.6009(2)	5.5456(3)
c [Å]	14.5974(5)	7.9095(5)	10.8165(5)	10.1416(6)	14.8579(6)	24.0470(13)
α [°]	90	114.207(7)	90	91.435(2)	90	90
β [°]	95.029(1)	92.421(5)	100.078(5)	8.5723(5)	103.424(2)	100.556(5)
γ [°]	90	93.172(7)	90	102.203(6)	90	90
V [Å^3]	735.20(4)	268.61(4)	756.02(7)	506.20(5)	1196.80(8)	2395.9(2)
Z	4	1	4	1	4	4
$\rho_{calc.}$ [g cm^{-3}]	2.093	1.952	2.036	2.103	2.188	2.136
μ [mm^{-1}]	2.939	2.050	2.858	3.189	3.583	3.574
F(000)	460	159	460	317	776	1512
$\lambda_{MoK\alpha}$ [Å]	0.71073	0.71073	0.71073	0.71073	0.71073	0.71073
T [K]	100	143	123	293	100	123
θ Min–Max [°]	2.8, 26.3	4.6, 26.0	4.4, 26.0	3.1, 26.0	2.2, 26.0	4.3, 26.0
Dataset	−4:4; 0:18; 0:18	−6:6; −8:6; −9:9	−13:14; −7:7; −13:13	−7:7; −10:10; −12:12	−18:18; −6:6; −18:18	−15:22; −6:6; −29:29
Reflections collected	1517	1934	5633	8877	11334	9212
Independent refl.	1517	1057	1477	1989	2350	2347
R_{int}	0.038	0.021	0.043	0.027	0.044	0.045
Observed reflections	1456	1007	1277	1801	2018	1894
Parameters	119	96	119	161	199	186
R_1 (obs)[a]	0.0324	0.0269	0.0663	0.0203	0.0263	0.0329
wR_2 (all data)[b]	0.0950	0.0694	0.1734	0.0524	0.0910	0.0829
GooF[c]	1.27	1.12	1.07	1.06	1.22	1.08
Resd. Dens. [e Å^{-3}]	−0.49, 0.46	−0.40, 0.53	−1.44, 4.49	−0.28, 0.26	−0.45, 0.48	−0.72, 0.77
Absorption correction	multi-scan	multi-scan	multi-scan	multi-scan	multi-scan	multi-scan
CCDC						

a) $R_1 = \Sigma||F_0|-|F_c||/\Sigma|F_0|$; b) $wR_2 = [\Sigma[w(F_0^2-F_c^2)^2]/\Sigma[w(F_0)^2]]^{1/2}$; $w = [\sigma c^2(F_0^2)+(xP)^2+yP]^{-1}$ and $P=(F_0^2+2F_c^2)/3$; c) GooF = $\{\Sigma[w(F_o^2-F_c^2)^2]/(n-p)\}^{1/2}$ (n = number of reflections; p = total number of parameters).

19.14.2 Vacuum Stability Tests (VST)

Testing the stability of a material ensures that no unexpected decomposition occurs over time. In particular, the long-term storage life can be simulated by measuring the gas pressure in an evacuated glass tube, that is built up by the compound at elevated temperatures. The VST measurement for compound **1** was performed twice for 48 h at 100 °C. The corresponding results can be found in Table 2 and Figure 5.

Table 2. Results of VST measurement for compound **1**.

compound	decomposition speed
(1) #1	0.9832 mL·day^{-1} g^{-1}
(1) #2	0.9985 mL·day^{-1} g^{-1}

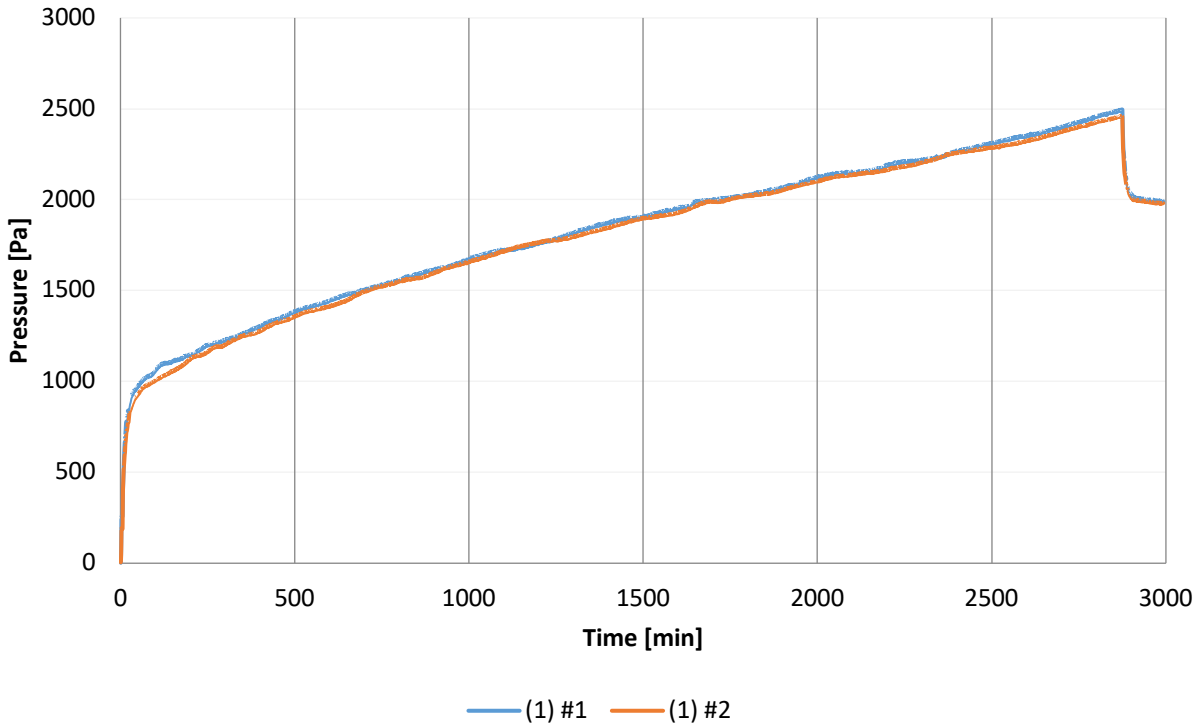


Figure. 5 Vacuum stability tests of compound **1** at 100 °C at a time period of 48 h.

Publications

1. M. Joas, T. M. Klapötke, J. Stierstorfer, N. Szimhardt, Synthesis and Characterization of Various Photosensitive Copper(II) Complexes with 5-(1-Methylhydrazinyl)-1*H*-tetrazole as Ligand and Perchlorate, Nitrate, Dinitramide, and Chloride as Anions, *Chem. Eur. J.*, **2013**, *19*, 9995–10003.

2. M. Joas, T. M. Klapötke, N. Szimhardt, Photosensitive Metal(II) Perchlorates with 1,2-Bis[5-(1-methylhydrazinyl)tetrazol-1-yl]ethane as Ligand: Synthesis, Characterization and Laser Ignition, *Eur. J. Inorg. Chem.*, **2014**, *2014*, 493–498.

3. T. M. Klapötke, P. C. Schmid, J. Stierstorfer, N. Szimhardt, Synthesis and Characterization of Tetrahedral Zinc(II) Complexes with 3,6,7-Triamino-*7H*-[1,2,4]triazolo[4,3-b][1,2,4]triazole as Nitrogen-Rich Ligand, *Z. Anorg. Allg. Chem.*, **2016**, *642*, 383–389.

4. D. Fischer, T. M. Klapötke, J. Stierstorfer, N. Szimhardt, 1,1'-Nitramino-5,5'-bitetrazoles, *Chem. Eur. J.*, **2016**, *22*, 4966–4970.

5. N. Szimhardt, M. F. Bölter, M Born, T. M. Klapötke, J. Stierstorfer, Metal salts and complexes of 1,1'-dinitramino-5,5'-bitetrazole, *Dalton Trans*., **2017**, *46*, 5033–5040.

6. M. Freis, T. M. Klapötke, J. Stierstorfer, N. Szimhardt, Di(1*H*-tetrazol-5-yl)methane as Neutral Ligand in Energetic Transition Metal Complexes, *Inorg. Chem.*, **2017**, *56*, 7936–7947.

7. G. Belanger-Chabot, S. M. Kaplan, P. Deokar, N. Szimhardt, R. Haiges, K. O. Christe, Synthesis and Characterization of Nitro-, Trinitromethyl-, and Fluorodinitromethyl-Substituted Triazolyl- and Tetrazolyl-trihydridoborate Anions, *Chem. Eur. J.*, **2017**, *23*, 13087–13099.

8. N. Szimhardt, M. H. H. Wurzenberger, A. Beringer, L. J. Daumann, J. Stierstorfer, Coordination chemistry with 1-methyl-5*H*-tetrazole: cocrystallization, laser-ignition, lead-free primary explosives - one ligand, three goals, *J. Mater. Chem. A*, **2017**, *5*, 23753–23765.

9. N. Szimhardt, J. Stierstorfer, Methylsemicarbazide as a Ligand in Late 3d Transition Metal Complexes, *Chem. Eur. J.*, **2018**, *24,* 2687–2698.

10. N. Szimhardt, M. H. H. Wurzenberger, T. M. Klapötke, J. T. Lechner, H. Reichherzer, C. C. Unger, J. Stierstorfer, Highly functional energetic complexes: stability tuning through coordination diversity of isomeric propyl-linked ditetrazoles, *J. Mater. Chem. A*, **2018**, *6*, 6565–6577.

11. M. H. H. Wurzenberger, N. Szimhardt, J. Stierstorfer, Copper(II) Chlorate Complexes: The Renaissance of a Forgotten and Misjudged Energetic Anion*, J. Am. Chem. Soc.*, **2018**, *140*, 3206–3209.

12. M. H. H. Wurzenberger, N. Szimhardt, J. Stierstorfer, Nitrogen-Rich Copper(II) Bromate Complexes: an Exotic Class of Primary Explosives*, Inorg. Chem.*, **2018**, *57*, 7940–7949.

13. N. Szimhardt, M. H. H. Wurzenberger, L. Zeisel, M. S. Gruhne, M. Lommel, J. Stierstorfer, Maximization of the Energy Capability Level in Transition Metal Complexes through Application of 1-Amino- and 2-Amino-5*H*-tetrazole Ligands, *J. Mater. Chem. A*, **2018**, *6*,16257–16272.

14. N. Szimhardt, M. H. H. Wurzenberger, L. Zeisel, M. S. Gruhne, M. Lommel, T. M. Klapötke, J. Stierstorfer, 1-Amino-triazole Transition Metal Complexes as Laser Ignitable and Lead-free Primary Explosives, *Chem. Eur. J.*, **2018**, DOI: 10.1002/chem.201803372.

15. N. Szimhardt, M. S. Gruhne, M. Lommel, A. Hess, M. H. H. Wurzenberger, T. M. Klapötke, J. Stierstorfer, 2,2-Bis(5-tetrazolyl)propane as Ligand in Energetic 3d Transition Metal Complexes, *Z. Anorg. Allg. Chem.*, **2018**, DOI: 10.1002/zaac.201800288.

16. N. Szimhardt, M. H. H. Wurzenberger, P. Spieß, T. M. Klapötke, J. Stierstorfer, Potassium *N*-Nitramino-5*H*-tetrazolates — Powerful Green Alternatives to Lead Containing Primary Explosives with High Initiation Capabilities, *Propellants Explos. Pyrotech.*, **2018**, (in press).

17. L. Zeisel, N. Szimhardt, M. H. H. Wurzenberger, T. M. Klapötke, J. Stierstorfer, 2-Methyl-substituted monotetrazoles in copper(II) perchlorate complexes: manipulating coordination chemistry and derived energetic properties, *Dalton Trans*., **2018**, (submitted).

Patents

1. T. M. Klapötke, J. Stierstorfer, N. Szimhardt, M. H. H. Wurzenberger, EP 18150491.1 and EP 18151497.7, application date: 12.01.2018.

Poster Presentations

1. New Trends in Research of Energetic Materials (NTREM) 2015, Czech Republic: Synthesis and investigation of energetic transition metal complexes using di(1H-tetrazol-5- yl)methane as nitrogen-rich ligand.
2. New Trends in Research of Energetic Materials (NTREM) 2016, Czech Republic: Highly energetic 1,1′-dinitramino-5,5′- bitetrazoles.
3. Gordon Research Seminar 2018, USA: Pushing the Boundaries-Maximization of the Energy Capability Level in Transition Metal Complexes through Application of 1-Amino- and 2-Amino-5*H*-tetrazole Ligands.
4. Gordon Research Conference 2018, USA: 1-Amino-triazole Ligands in Laser Ignitable and Lead-free Primary Explosive Complexes.

Oral Presentations

1. New Energetics Workshop 2016, FOI, Sweden: Approaches Toward the Replacement of Lead Containing Primary Explosives - A Challenge.
2. International Annual Conference 2017, ICT Karlsruhe, Germany: One Concept, Two Goals - Synthesis of Highly Energetic Transition Metal Complexes using 1-methyl-5*H*-tetrazole as ligand and their investigation as laser-ignitable primary explosives.